Nikos Hadjichristidis · Akira Hirao

Editors

Anionic Polymerization

Principles, Practice, Strength, Consequences and Applications

Springer

Anionic Polymerization

Nikos Hadjichristidis • Akira Hirao
Editors

Anionic Polymerization

Principles, Practice, Strength, Consequences and Applications

Editors
Nikos Hadjichristidis
King Abdullah University of Science
    and Technology (KAUST)
Thuwal, Saudi Arabia

Akira Hirao
Tokyo Institute of Technology
Tokyo, Japan

Printed on acid-free paper

Preface

Anionic polymerization, discovered by M. Schwarz in the 1950s and developed to its current level by a number of excellent chemists (M. Morton, S. Bywater, L. Fetters, J. Roovers, P. Rempp, and many others), is a powerful tool for the controlled manipulation of macromolecular architectures. Moreover, it is still unique for the capability to synthesize a huge variety of model polymeric materials with a high degree of molecular, structural, and compositional homogeneity. The uniqueness of anionic polymerization is due to the complete absence of a termination step, which is present with a very few exceptions, to a lower or higher degree in all other controlled/living polymerizations. For these reasons we have prepared this book to describe the principles, practice, strengths, consequences, and applications of this powerful chemistry.

A great polymer chemist, who shall remain nameless, said that "what is the past for anionic polymerization is the future of controlled/living polymerizations", since almost all structures (star, cyclic, comb, pom-pom, etc.) have been synthesized many years ago by anionic polymerization and the appropriate linking chemistry. In addition, polyethylene and polypropylene have also been synthesized by anionic polymerization of butadiene or 2,4-dimethyl pentadiene1,3, respectively, followed by hydrogenation.

High vacuum techniques have to be used in order to avoid premature termination of the initiator or living chains or destruction of the linking agents due to contaminants introduced from the air (humidity, carbon dioxide, oxygen) or from the chemicals involved (solvents, monomers, etc.). These techniques are very demanding in the need for glass blowing techniques, consume a great deal of time and usually produce just a few grams of model polymeric materials. Nevertheless, these limitations are a small price to pay given the tremendous potential of high vacuum techniques to generate model polymeric materials using anionic polymerization.

The availability of model polymers has facilitated studies in many fields of polymer physics and polymer theory. The Division of Polymer Physics of the American Physical Society recognized the importance of anionic polymerization

for the advancement of polymer science when it awarded the Polymer Physics Prize for 2000 to Dr. Lewis Fetters, an anionic polymerization chemist "For transforming the art of anionic polymerization into a powerful tool of polymer physics, creating and using polymers with precisely defined molecular architecture to advance our understanding of entanglement, miscibility, and phase separation". Not only have these model polymers been essential for the progress of polymer science, but they have also been very important technologically. A number of advances in the commercial use of polymers (including polystyrene, polyolefins, and others) have resulted from the improved understanding of the behavior of polymeric materials derived from model anionically produced macromolecules.

We should also point out that we have not covered the controversial topic of the mechanisms and kinetics of anionic polymerization. This topic by itself deserves an extensive discussion that is beyond the scope of this book.

Thuwal, Saudi Arabia   Nikos Hadjichristidis
Tokyo, Japan   Akira Hirao

Contents

Part I
Principles and Practice

Schlenk Techniques for Anionic Polymerization

Kedar Ratkanthwar, Junpeng Zhao, Hefeng Zhang, Nikos Hadjichristidis, and Jimmy W. Mays

Abstract Anionic polymerization-high vacuum techniques (HVTs) are doubtlessly the most prominent and reliable experimental tools to prepare polymer samples with well-defined and, in many cases, complex macromolecular architectures. Due to the high demands for time and skilled technical personnel, HVTs are currently used in only a few research laboratories worldwide. Instead, most researchers in this filed are attracted to more facile Schlenk techniques. The basic principle of this technique followed in all laboratories is substantially the same, i.e. the use of alternate vacuum and inert gas atmosphere in glass apparatus for the purification/charging of monomer, solvents, additives, and for the manipulation of air-sensitive compounds such as alkyl metal initiators, organometallic or organic catalysts. However, it is executed quite differently in each research group in terms of the structure of Schlenk apparatus (manifolds, connections, purification/storage flasks, reactors, etc.), the use of small supplementary devices (soft tubing, cannulas, stopcocks, etc.) and experimental procedures. The operational methods are partly purpose-oriented while also featured by a high flexibility, which makes it impossible to describe in detail each specific one. In this chapter we will briefly exemplify the application of Schlenk techniques for anionic polymerization by describing the performance of a few experiments from our own work.

Keywords Schlenk techniques • Vacuum gas manifold • Anionic polymerization • Living polymerization

K. Ratkanthwar • H. Zhang • N. Hadjichristidis (✉)
Division of Physical Sciences and Engineering, KAUST Catalysis Center (KCC), Polymer Synthesis Laboratory, King Abdullah University of Science and Technology (KAUST), Thuwal, Saudi Arabia
e-mail: Kedar.ratkanthwar@kaust.edu.sa; Hefeng.Zhang@kaust.edu.sa; Nikolaos.Hadjichristidis@kaust.edu.sa

J. Zhao
Faculty of Materials Science and Engineering, South China University of Technology, Guangzhou 510641, People's Republic of China
e-mail: msjpzhao@scut.edu.cn

J.W. Mays
Department of Chemistry, University of Tennessee, Knoxville, TN 37996, USA

Chemical Sciences Division, Oak Ridge National Laboratory, Oak Ridge, TN 37831, USA
e-mail: jimmymays@utk.edu

1 Introduction

Wilhelm Johann Schlenk (22 March 1879 – 29 April 1943) was a German organic chemist who discovered organolithium compounds around 1917 [1]. He was born and studied chemistry in Munich and later in 1919 he succeeded Hermann Emil Fischer at the University of Berlin. He also discovered (together with his son) that organo-magnesium halides are capable of participating in a complex chemical equilibrium, now known as "Schlenk equilibrium" [2]. The name Wilhelm Schlenk is familiar to many chemists also because of the techniques he developed and the widespread use of the "Schlenk flask" to handle air-sensitive compounds (Fig. 1) [3]. He also designed a double manifold known as the "Schlenk line" which incorporates an inert gas line and a vacuum system joined by three-way glass taps that allows the user to switch between gas and vacuum for the manipulation of air-sensitive substances.

Although anionic polymerization-high vacuum techniques (HVTs) [4] are the most reliable experimental tools for preparing polymer samples with well-defined and complex macromolecular architectures [5–11], they require mastery of glass-blowing and highly demanding experimental techniques in order to make and utilize specially designed reactors. Due to time consuming nature of HVTs and the requirement for skilled technical personnel, most researchers in the anionic polymerization field employ the more facile "Schlenk technique". This technique is attractive due to its convenience and acceptable performance for many applications.
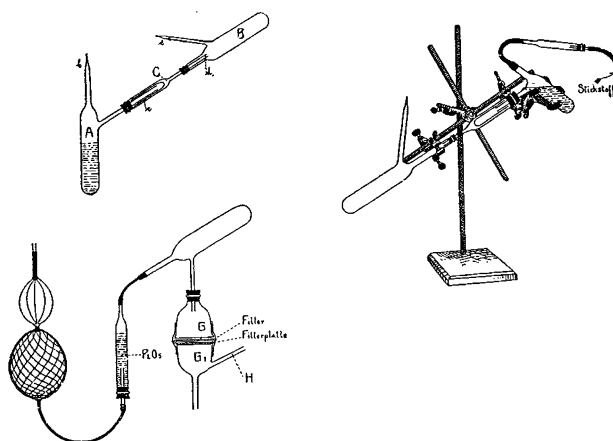
Fig. 1 Examples of Schlenk's glassware from his paper (from reference [3])

2 Different Component of Schlenk Techniques

To work with Schlenk techniques, the basic requirements are a good oil vacuum pump (secured with a liquid nitrogen trap), inert gas with an associated purification system, different types of Schlenk flasks, and a Schlenk line which is a dual manifold with several ports (Fig. 2).

2.1 Vacuum Pump

One manifold of the Schlenk line is connected to an oil vacuum pump with a capacity of 10^{-2}–10^{-4} mbar through a liquid nitrogen or dry ice/acetone cold trap, used to condense any volatile substances such as solvent vapors or gaseous reaction products and prevent contamination of the vacuum pump oil (Fig. 2).

2.2 Inert Gases-Nitrogen (N₂) or Argon (Ar)

The inert gas line is vented through an oil bubbler and/or purification system before being connected to the Schlenk line. Depending upon the reaction sensitivity, UHP (Ultra High Purity) grade nitrogen (N_2) or argon (Ar) is used with or without further purification. There are different methods for purification of inert gases to remove moisture which is deleterious to sensitive compounds and living polymers. In some cases inert gases are purified by passing through a column containing molecular
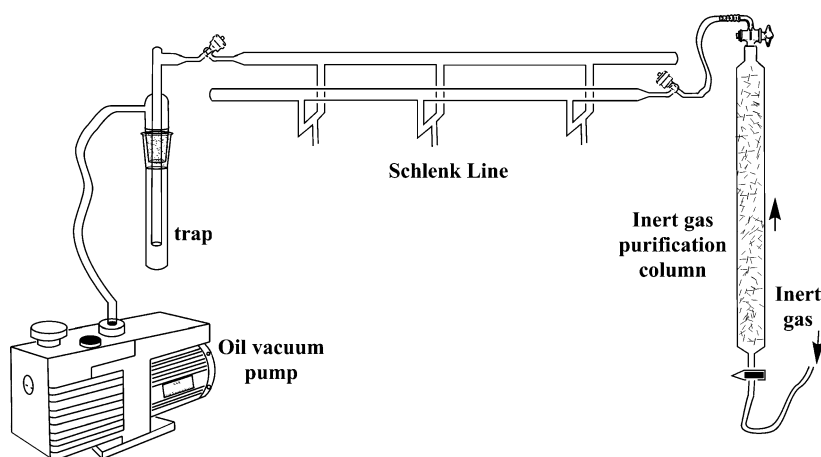
Fig. 2 General representation of a Schlenk line
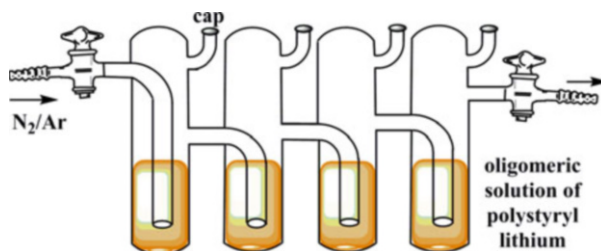
Fig. 3 Use of bubblers for purification of inert gases

sieves or silica gel with a color indicator (Fig. 2). This purified inert gas is then fed to the manifold through rubber tubing for use in reactions.

In another method, commercial nitrogen gas containing traces of moisture and oxygen is passed through columns (2 or 3) containing activated 4 Å molecular sieves and another (2 or 3) columns containing activated copper (Cu) deposited on kieselguhr kept at ~200 °C. This purified N_2 is then again passed through a bubbler containing a dark red solution of oligomers of poly(styryl) lithium in toluene (Fig. 3). The moisture in N_2, if present, quenches the living oligomers while passing through this bubbler, rendering the gas free of moisture. On regular basis, activation of molecular sieves and Cu columns is performed. Molecular sieves are activated by heating at ~200 °C under vacuum for 6 h and cooled under nitrogen, whereas Cu columns are activated by passing hydrogen (H_2) gas at 180 °C for 7–8 h and the water formed by the reaction of H_2 and Copper(II) oxide or cupric oxide (CuO) is removed under vacuum. There is a visual indication for determining the appropriate time for reactivation of Cu columns. Before activation the copper catalyst looks pale green in color, but it turns to dark brown after activation.

2.3   Schlenk Line

The Schlenk line, also called a vacuum gas manifold, is a double manifold incorporating a vacuum system and a gas line joined by double oblique taps that allow the user to switch between vacuum and gas for the manipulation of living polymerization systems or air-sensitive compounds. One manifold is connected to a source of purified inert gas, while the other is connected to an oil vacuum pump secured with liquid nitrogen trap. Special three-way glass stopcocks or Teflon taps are used for these ports on manifolds. They allow for vacuum or inert gas to be selected without the need for placing the sample on a separate line.

Different types of Schlenk lines can be designed as per user's requirements. Ports can be made of glass or high vacuum "o" ring stopcocks with only ground joints or only hoses (rubber tubing) or both (called a hybrid system), as shown in Fig. 4a–c.
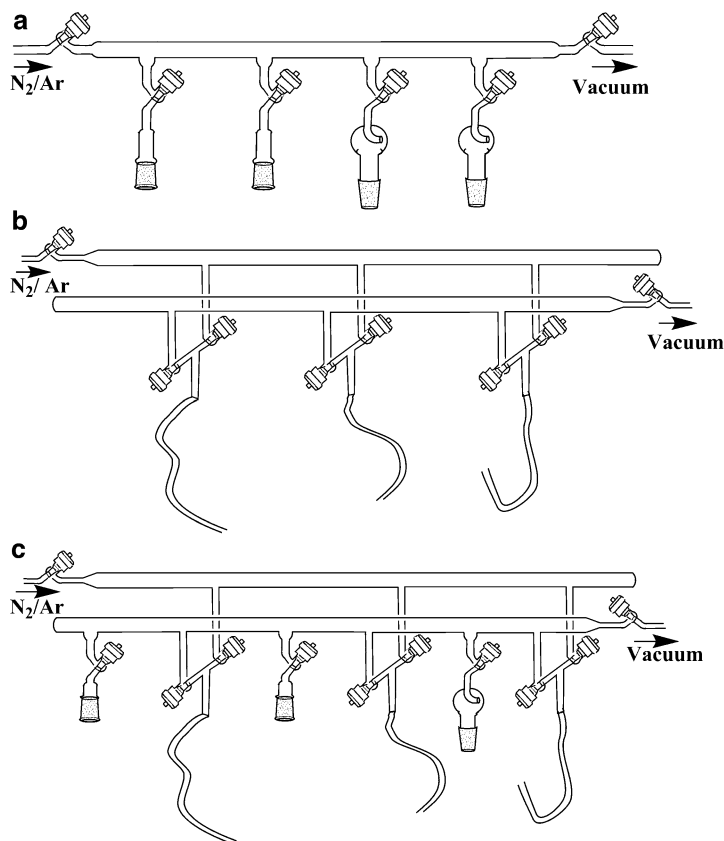
Fig. 4 (**a**) Schlenk line with ground joints. (**b**) Schlenk line with rubber tubes. (**c**) Schlenk line with ground joint and rubber tubes

2.4 Schlenk Flasks and Tubes

2.4.1 Specially Designed Schlenk Flasks and Storage Ampoules Using Septum Adaptors

For purification and storage of monomers, and solvents, as well as to perform polymerization, there are different types of Schlenk flasks. Initially these flasks were specially designed using three-way stopcocks with rubber septa. Addition of reagents and removal of aliquots using syringe techniques is possible through the septa. Using same three-way stopcocks, small and big storage ampoules are also made, as shown in Fig. 5. These types of Schlenk flasks can be connected to the Schlenk line through rubber tubing to have either gas or vacuum in it. Addition of

Fig. 5 Schlenk round bottom (*RB*) flask and ampoules
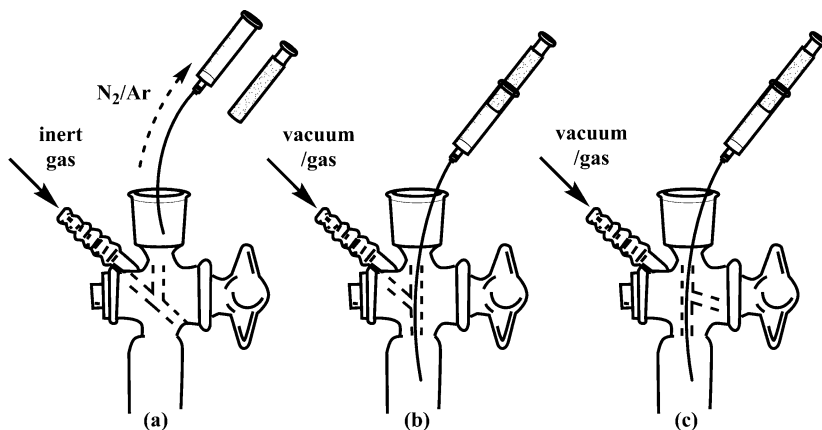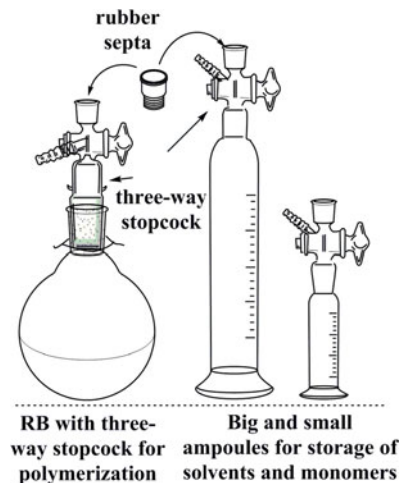
Fig. 6 Syringe flushes with inert gas (**a**) and addition of reagents (or removal of aliquots) in presence (**b**) or absence (**c**) of vacuum/gas

reagents by syringe through septa, in presence or absence of gas/vacuum, can be controlled by three-way stopcock positions (Fig. 6).

2.4.2 Commercially Available Different Types of Schlenk Flasks and Tubes

Later, reaction vessels with a Teflon tap/stopcock for the addition and removal of gases were made available commercially, and are known as Schlenk flasks (Fig. 7a) or Schlenk tubes (Fig. 7b) [12].
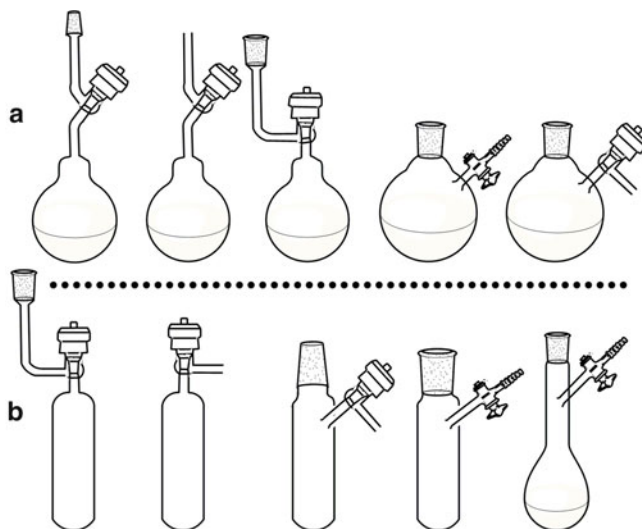
Fig. 7 Schlenk flasks (**a**) and tubes (**b**)

3 Procedures

3.1 Degassing

In anionic polymerization, in order to avoid termination of living anions from air (oxygen, carbon dioxide, moisture) every reagent needs to be purified before use. A degassing procedure is the first step of purification which helps to remove oxygen and other dissolved gasses from a liquid. The Schlenk flask containing the liquid is connected to the Schlenk line directly through a ground joint or via rubber tubing (Fig. 8). The stopcock (glass or Teflon) is opened two or three times to vacuum for a few seconds until bubbles are produced. With the stopcock closed, the liquid is frozen using a Dewar flask containing liquid nitrogen, and then the stopcock is opened to vacuum for a sufficient time so that the entire system can be pumped down. After some time the stopcock is closed and the liquid is thawed. This freeze-degas-thaw cycle is repeated two or three times to adequately remove dissolved gases.

3.2 Distillation

3.2.1 Simple Distillation of Solvents and Monomers

Under static vacuum, distillation of liquids (solvents, monomers, etc.) becomes simple by slightly heating the source flask and freezing the receiving flask (Fig. 9).
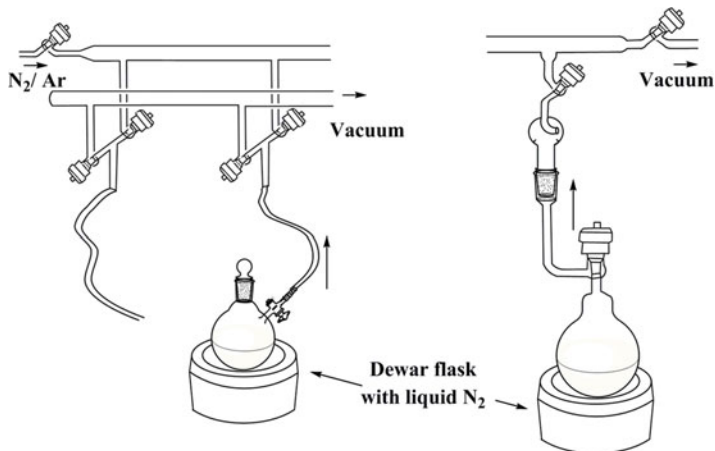
Fig. 8 Degassing of liquids

Fig. 9 Simple vacuum
distillation of solvent or
monomer
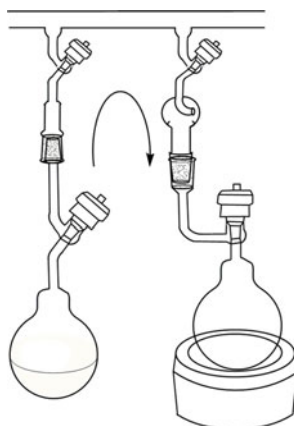
Before the beginning of the distillation the liquid is degassed two or three times.
After completion of the distillation process, the receiving flask is opened to
dynamic vacuum and the frozen liquid is degassed again. At the end of degassing
the stopcock is closed and the liquid is thawed and stirred.

3.2.2 Short Path Distillation

On a Schlenk line having rubber tubing, high boiling liquids (usually monomers)
are distilled using a specially designed glass apparatus, as shown in Fig. 10. From
two sides (A and B) the apparatus is connected to the Schlenk line through rubber
tubing and flame dried under vacuum. Then the liquid to be distilled is transferred

Fig. 10 Short-path
distillation apparatus for
high-boiling liquids
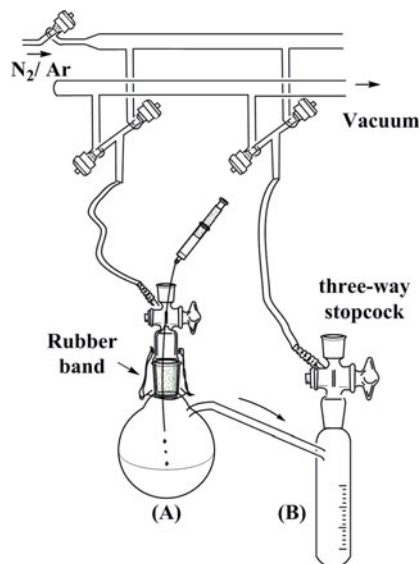
into flask (A) (with some purifying reagent, if necessary) using a dry syringe (after
flushing with inert gas; Fig. 6a), degassed two times, and then distilled into a
calibrated ampoule (B). Source flask (A) is round bottom flask fitted with a three-
way stopcock and secured with rubber bands under inert gas pressure. After
distillation, the required amount of purified liquid is taken by syringe from ampoule
(B) in presence of inert gas. Under inert gas pressure, after closing both of the
stopcocks, the apparatus is removed from the Schlenk line by detaching the rubber
tubing. The remaining amount of purified reagent is stored until further use by
keeping entire apparatus in the refrigerator.

3.3   Purification

In this section the purification of the most commonly used solvents and monomers
for anionic polymerization is described.

3.3.1   Solvents

Toluene is fractionally distilled over CaH_2 (freshly ground chunks is recommended,
rather than powdered CaH_2 which is rapidly deactivated on storage) and stored over
hot activated molecular sieves. The fractionated solvent is refluxed over K or Na
metal and then distilled. Benzophenone is added to show the distinct blue color as
an indication of dryness and purity. Alternatively, toluene distilled over CaH_2 is
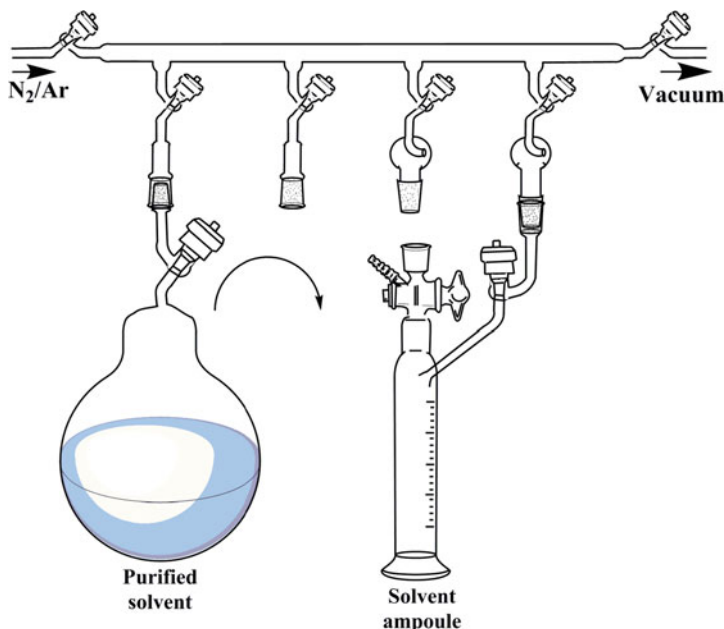
Fig. 11 Distillation of solvent to ampoule

stored (after proper degassing) in solvent storage flasks containing Na/K (1/3) alloy under high vacuum and kept continuously stirred. The required amount of solvent is distilled out into specially designed Schlenk ampoules (as shown in Fig. 11) just before the polymerization reactions. This type of solvent ampoule is used on all types of Schlenk lines.

Alternatively, toluene is stirred over CaH_2 overnight and distilled in a reservoir containing *n*-butyllithium and 1,1-diphenyl-ethylene (DPE) as an indicator of dryness (by showing a distinct red color). It is then directly distilled into a reactor before polymerization. A*lkanes such as n-hexane, cyclohexane, heptane* etc. are purified similarly with CaH_2 and then *n*-BuLi/DPE

Tetrahydrofuran (THF) is left to stir with CaH_2 overnight to react with moisture and then distilled. It is then refluxed over small pieces of sodium metal and distilled. The solvent is then degassed and distilled in a flask containing a Na/K (1/3) alloy. After stirring for some time it gives the blue color, which indicates that the solvent is free from impurities.

Benzene is also purified with CaH_2 and stored over mixture of *n*-BuLi and styrene or *n*-BuLi and DPE so as to give orange or red color, respectively, which indicates the purity of solvent.

3.3.2 Monomers

In this section the purification of the most commonly used monomers in anionic polymerization is discussed.

Styrene and other styrenic monomers [tert-butylstyrene, p-methylstyrene, α-methylstyrene, etc.] are purified using the same method. The monomer is dried overnight with freshly ground CaH_2 and distilled into a flask containing dibutylmagnesium (DBMg) [1 M solution in heptane]. DBMg, having one *n*-butyl and one *sec*-butyl group, shows higher solubility in hydrocarbon solvents. The monomer is allowed to stand overnight with continuous stirring and distilled in a Schlenk flask. The purified monomer develops a light yellow-green color indicative of high purity.

Isopene monomer is dried over finely grounded CaH_2 overnight followed by distillation into a flask containing *n*-BuLi where it remains with continuous stirring for 20–30 min at 0 °C (note that it is critical to use the less efficient initiator, *n*-BuLi *not sec*-BuLi, and keep the monomer at 0 °C for not more than 30 min in order to avoid potential exothermic polymerization of the isoprene). It is then further distilled in to a Schlenk flask and stored at low temperature.

Butadiene and ethylene oxide are gaseous monomers at room temperature. First the monomer is condensed into a round bottom flask containing CaH_2 at −78 °C (dry ice/isopropanol bath), stirred for 30 min at −10 °C (ice/salt bath). Then it is distilled into another flask with *n*-BuLi, stirred there for 20–30 min at −10 °C. With butadiene it is critical, as with isoprene (see above), to use only the *n*-BuLi isomer and keep the temperature low and duration to <30 min in order to avoid a violent exotherm. Finally the monomer is distilled into a calibrated Schlenk tube. In a few cases the monomer is diluted with purified solvent in a ratio of [monomer]/[solvent] lower than 0.2, which reduced the vapor pressure for storage.

Commercially available *acrylates and methacrylates* monomers may contain considerable amounts of residual alcoholic impurities. These monomers are first dried over CaH_2 overnight to remove traces of water, but CaH_2 does not react appreciably with alcohols. Therefore before polymerization these monomers are purified with trioctylaluminum (TOA). The treatment with TOA removes the residual alcohol present in alkyl(meth)acrylates, and the excess alkylaluminium then forms a complex with the carbonyl groups of (meth)acrylate monomer. The aklylaluminum-monomer complex has a characteristic bright yellow color indicating the end point of impurity titration. Immediate distillation under high vacuum affords extremely pure (meth)acrylate monomer.

Solid monomer such as *hexamethylcyclotrisiloxane (D3)* is purified by dissolution in a solvent like toluene or benzene. After 1 h stirring, the azeotropic mixture of solvent and moisture is removed on the vacuum line. This step is repeated two or three times in order to obtain pure moisture-free solid monomer.

1,1-Diphenylethylene (DPE) is stirred over CaH_2 for 5–6 h and then distilled using a short path distillation apparatus in vacuum. It is then stored in an ampoule under nitrogen or argon. Alternatively, DPE is distilled over a small amount of *n*-

BuLi (1.6 M solution in *n*-hexane). The desired amount of DPE is transferred into a flame dried distillation unit by syringe, and *n*-BuLi is added drop-wise to the DPE under stirring at room temperature. *n*-BuLi reacts with traces of impurities and residual benzophenone in DPE. After reacting with impurities, the excess of *n*-BuLi then adds to the double bond of DPE to form the 1,1-diphenylhexyllithium (DPHLi) anion. This DPHLi is red in color, which indicates the end point of impurity titration. The excess DPE is distilled over DPHLi under dynamic vacuum at 120 °C.

Despite the fact that DPE cannot homopolymerize (living terminator), it is included in this section due to double bond.

3.4 Initiators Synthesis

3.4.1 Commercially Available

Many initiators are used in anionic polymerization such as benzyl lithium (BzLi), potassium alkoxides, trityl potassium and *n*- or *sec*-butyl lithium (*n*- or *sec*-BuLi). *sec*-BuLi, available commercially, is the most commonly used initiator for anionic polymerization. Under inert atmosphere, a known amount of initiator solution is transferred into the polymerization apparatus by syringe (as shown in Fig. 12) and allowed to polymerize a known amount of styrene. The molecular weight of formed polystyrene is determined by size exclusion chromatography [SEC; calibrated with polystyrene (PS) standards] and the initiator concentration is back calculated using

Fig. 12 Use of commercial grade *sec*-BuLi as an initiator for polymerization
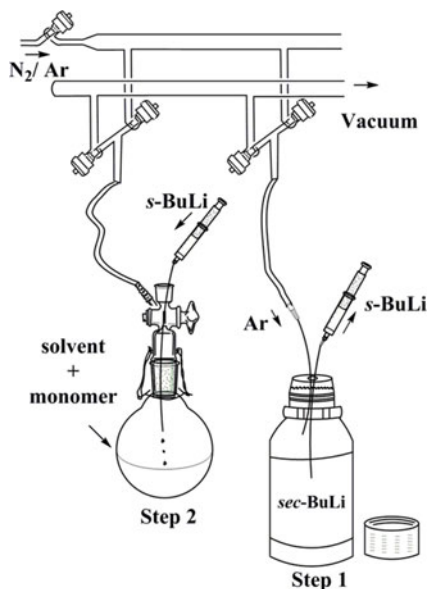
the relationship: moles of initiator $=$ g of styrene/$M_{n\ (PS)}$. Once the concentration is known, it is used for other polymerizations.

3.4.2 Triphenylmethylpotassium (TPMK) or Trityl potassium (Ph₃CK) or Potasiumtriphenyl Methanide

It is prepared in the laboratory from triphenylmethane and potassium metal in THF as described below.

- Triphenylmethane is dried under vacuum for 2 days at room temperature, and purified THF is added into the same flask under inert atmosphere.
- At room temperature, the above THF solution of triphenylmethane (A) is transferred through a cannula (hollow steel needle with two sharp ends) into another flask (B) containing a potassium mirror, as shown in Fig. 13. If the pressure in the flask (A) is greater than flask (B), the solution will be pushed from (A) to (B). This pressure difference is achieved by placing flask (A) under inert gas pressure and partially evacuating flask (B).
- Red color indicates the formation of triphenylpotassium.
- The reaction is kept stirring under vacuum for 6–7 h.
- The excess metal is filtered off, and the concentration of the TPMK solution is determined by double titration.

3.4.3 1,1′-Diphenylhexyllithium (DPHLi)

It is prepared from DPE and *n*-BuLi. A known amount of purified DPE in dry THF is added into the equimolar amount of *n*-BuLi at 40 °C under inert atmosphere. The solution immediately turns red, indicating the formation of DPHLi. The reaction mixture is slowly cooled to room temperature, stirred for 1 h and stored under inert gas at low temperature.

Fig. 13 Synthesis of TPMK initiator
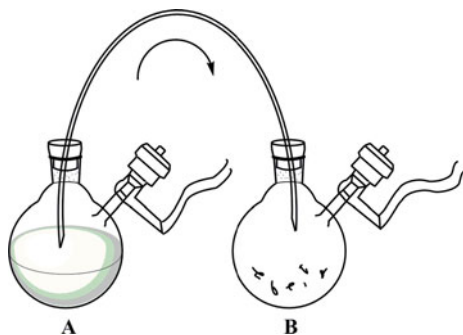
3.5 Examples of Polymerization

3.5.1 (Meth)acrylate Esters

Anionic polymerizations of alkyl(meth)acrylate [methyl methacrylate (MMA), *n*- or *tert*-butylacrylate (*n*-BA or *tert*-BA), Methacrylate (MA)] using DPHLi or BzLi are performed by adding neat monomer, or the solution of the monomer, into the initiator solution at the desired temperature.

An experimental procedure for the anionic polymerization of MMA using DPHLi as initiator is given below:

- To a flame-dried flask with a septum adapter, the required amount of dry solvent (toluene or THF) is transferred by a cannula (double-tipped stainless steel needle) under inert atmosphere (Fig. 14).
- The DPHLi initiator solution is added drop-wise by a syringe until a red color remained. After quenching all impurities, the calculated amount of initiator for polymerization is added.
- The temperature of the flask is brought to −78 °C using a dry ice (solid CO_2)-acetone (or dry ice/isopropyl alcohol) cold bath.
- The purified monomer is added to the cold initiator solution and allowed to polymerize for 15–20 min.
- The reaction is terminated with degassed methanol, and the polymer is precipitated into *n*-hexane or methanol.

3.5.2 Synthesis of Polystyrene-b-Polyisoprene Block Copolymer (PS-b-PI)

- By following a similar experimental procedure, as discussed above, styrene monomer (liquid) is polymerized using commercial grade *sec*-BuLi in benzene.
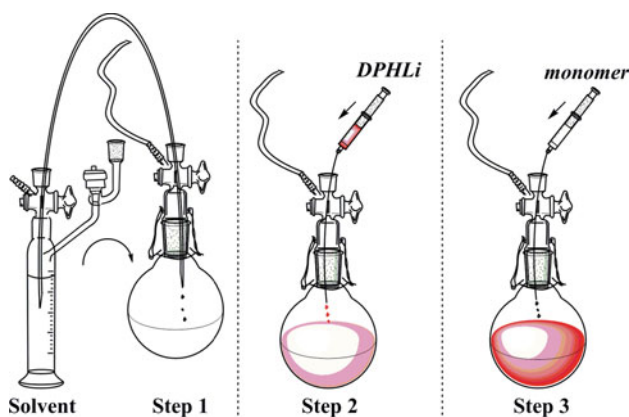
Fig. 14 Polymerization of (meth)acrylate liquid monomer

- After complete polymerization, a small aliquot is taken out by syringe for molecular weight determination.
- Pre-purified isoprene (liquid) monomer is added to the same flask containing living polystyryllithium to form PS-*b*-PI copolymer.
- The reaction is terminated by addition of degassed methanol.

3.5.3 Polymerization Solid and Gaseous Monomers

Solid monomers, such as hexamethylcyclotrisiloxane (D3) and lactides are polymerized by adding the initiators and/or catalysts to their solutions. Also in a few cases, especially when the solid monomer needs to be added as a second or third monomer, the polymerization is started by adding its solution in an inert gas flow into the solution containing the initiator or the precursor (co)polymer and the catalyst [13].

The polymerizations of gaseous monomers, such as butadiene and ethylene oxide, are conducted similarly. For example, a desired volume of purified butadiene is cryo-condensed on the Schlenk line into a reaction flask containing the solvent and the initiator (*sec*-BuLi). The solution is stirred at room temperature (in non-polar solvents such as benzene and cyclohexane) or −78 °C (in tetrahydrofuran) until the polymerization is completed. Recently developed phosphazene-catalysed metal-free ring-opening polymerization of ethylene oxide requires the premix of the protic compound (a small molecule or macromolecule containing a protic moiety) and the phosphazene catalyst for the deprotonation of the initiator and the generation of anionic initiating species [14, 15]. The purified ethylene oxide is then introduced in the reaction flask by cryo-condensation, and then allowed to polymerize at an elevated temperature.

References

1. Tidwell TT (2001) Wilhelm Schlenk: the man behind the flask. Angew Chem Int Ed Engl 40:331–337
2. Schlenk W, Schlenk J (1929) Uber die Konsti- tution der Grignard schen Magnesiumverbindungen. Aus d Chem Inst d Univ Berlin 62:920–924
3. Schlenk W, Thal A (1913) Uber Metallketyle, eine grobe Klasee von Verbindungen mit dreiwertigem Kohlenstoff. Aus dern Chem Lab der Univ Jena 46:2840–2854
4. Hadjichristidis N, Iatrou H, Pispas S, Pitsikalis M (2000) Anionic polymerization: high vacuum techniques. J Polym Sci Part A Polym Chem 38:3211–3234
5. Pitsikalis M, Pispas S, Mays JW, Hadjichristidisi N (1998) Nonlinear block copolymer architectures. Adv Polym Sci 135:1–137
6. Hadjichristidis N (1999) Synthesis of miktoarm star (μ-star) polymers. J Polym Sci Part A Polym Chem 37:857–871
7. Hadjichristidis N, Pispas S, Pitsikalis M, Iatrou H, Vlahos C (1999) Asymmetric star polymers: synthesis and properties. Adv Polym Sci 142:71–127

8. Hadjichristidis N, Pitsikalis M, Pispas S, Iatrou H (2001) Polymers with complex architecture by living anionic polymerization. Chem Rev 101:3747–3792

9. Hadjichristidis N, Iatrou H, Pitsikalis M, Mays J (2006) Macromolecular architectures by living and controlled/living polymerizations. Prog Polym Sci 31:1068–1132.

10. Ratkanthwar K, Hadjichristidis N, Lee S, Chang T, Pudukulathan Z, Vlassopoulos D (2013) Synthesis and characterization of an exact comb polyisoprene with three branches having the middle branch the molecular weight of the other two identical external branches. Polym Chem 4:5645–5655

11. Ratkanthwar KR, Hadjichristidis N, Pudukulathan Z (2013) Synthesis and characterization of well-defined regular star polyisoprenes with 3, 4, 6 and 8 arms. Chem J 03:1–11

12. Shriver DF, Drezdzon MA (1986) The manipulation of air-sensitive compounds, 2nd edn. John Wiley & Sons, New York

13. Zhao J, Pahovnik D, Gnanou Y, Hadjichristidis N (2014) Sequential polymerization of ethylene oxide, ε-caprolactone and l-lactide: a one-pot metal-free route to tri- and pentablock terpolymers. Polym Chem 5:3750–3753

14. Zhao J, Alamri H, Hadjichristidis N (2013) A facile metal-free "grafting-from" route from acrylamide-based substrate toward complex macromolecular combs. Chem Commun 49:7079–7081.

15. Zhao J, Pahovnik D, Gnanou Y, Hadjichristidis N (2014) Phosphazene-promoted metal-free ring-opening polymerization of ethylene oxide initiated by carboxylic acid. Macromolecules 47:1693–1698.

High Vacuum Techniques for Anionic Polymerization

Kedar Ratkanthwar, Nikos Hadjichristidis, and Jimmy W. Mays

Abstract Anionic polymerization high vacuum techniques (HVTs) are the most suitable for the preparation of polymer samples with well-defined complex macromolecular architectures. Though HVTs require glassblowing skill for designing and making polymerization reactor, it is the best way to avoid any termination of living polymers during the number of steps for the synthesis of polymers with complex structure. In this chapter, we describe the different polymerization reactors and HVTs for the purification of monomers, solvents, and other reagents for anionic polymerization as well as few model reactions for the synthesis of polymers with simple to complex structure.

Keywords High vacuum techniques (HVT) • Anionic polymerization • Living polymerization

1 Introduction

1.1 *Anionic Polymerization*

Anionic polymerization is a chain reaction which, under appropriate conditions, proceeds without chain termination and chain transfer reactions; hence, it is called a "living polymerization" [1–4]. The term living polymerization is used to describe systems in which active centers remain at the end of each chain after complete polymerization. If additional monomer is added to these living polymers, it will add to the existing polymeric chains and increase their degree of polymerization [5, 6]. For such living polymerizations, where chain initiation is rapid and quantitative, the

K. Ratkanthwar • N. Hadjichristidis (✉)

Division of Physical Sciences and Engineering, KAUST Catalysis Center (KCC), Polymer Synthesis Laboratory, King Abdullah University of Science and Technology (KAUST), Thuwal, Saudi Arabia
e-mail: Kedar.ratkanthwar@kaust.edu.sa; Nikolaos.Hadjichristidis@kaust.edu.sa

J.W. Mays
Department of Chemistry, University of Tennessee, Knoxville, TN 37996, USA

Chemical Sciences Division, Oak Ridge National Laboratory, Oak Ridge, TN 37831, USA
e-mail: jimmymays@utk.edu

molecular weights of the polymers obtained are accurately controlled by the amounts of monomer and initiator used and the polymers obtained will exhibit very narrow Poisson molecular weight distributions [7].

Anionic polymerization is thus most appropriate for the synthesis of polymers with predictable and well-defined structures, including polymers having complex architectures. Alkyllithium-initiated living polymerization of styrene and diene monomers provides the most versatile methodology of the synthesis of polymers with well-defined structures. With suitable monomer/initiator/solvent systems, one can prepare polymers with control on molecular weight, molecular weight distribution, microstructure, copolymer composition, chain-end and in-chain functional groups, architecture, and morphology.

The control variables that affect the polymer properties and the synthetic applications of living polymerization are as follows.

1.1.1 Molecular Weight

Molecular weight is one of the most important variables that affect polymer properties. Under living polymerization conditions, for a mono-functional initiator, one polymer chain is formed for each initiating molecule. Thus, the expected number-average molecular weight (M_n) can be calculated as

$$M_n = g \text{ of monomer/moles of initiator}$$

When using a difunctional initiator, the predicted molecular weight at complete monomer conversion is doubled based on moles of initiator, as shown below:

$$M_n = g \text{ of monomer/}(1/2) \text{ moles of difunctional initiator}$$

At less than quantitative degrees of conversion, the molecular weight is related to the grams of monomer consumed:

$$M_n = g \text{ of monomer consumed/moles of initiator}$$

So, for a living polymerization, M_n and the number-average degree of polymerization (X_n) are linear functions of conversion.

1.1.2 Molecular Weight Distribution

In a living polymerization, when the rate of initiation is competitive with the rate of propagation, all chains grow for approximately the same period of time; therefore, it is possible to make a polymer with a narrow molecular weight distribution (Poisson distribution) [7]. The relationship between the polydispersity and the degree of polymerization for a living polymerization is:

$$M_w/M_n \text{ or } X_w/X_n = 1 + \left[X_n/(X_n + 1)^2\right] \approx 1 + [1/X_n]$$

where M_w and X_w are weight-average molecular weight and weight-average degree of polymerization, respectively, and the ratios M_w/M_n and X_w/X_n are the polydispersity index (PDI). The approximation is valid for high molecular weight polymers, and thus it is predicted theoretically that the PDI decreases with increasing molecular weight. Experimentally PDI values for anionically synthesized polymers as determined by size exclusion chromatography (SEC) are in the range of 1.01–1.10, much larger than the theoretically predicted values. However, SEC suffers from significant band broadening effects, and recently, Chang and coworkers have shown that the PDIs of anionically synthesized polystyrenes approach the Poisson distribution in the late stages of polymerization, with PDIs <1.01 [8].

1.1.3 Block Copolymers

As mentioned earlier, when all of the monomer (A) has been consumed and a second monomer (B) is added, it will add to the existing polymeric chains to form diblock copolymer (A-B). Such sequential additions of monomer can also be used to generate triblock co-/terpolymers such as A-B-A, A-B-C, and even more complex multi-block multi-component structures.

1.1.4 Chain-End Functionalized Polymers

After complete polymerization, living polymers can be terminated with appropriate electrophilic reagents leading to chain-end functionalized polymers, as shown below.

$$P^- + X - Y \text{ (electrophilic reagent)} \rightarrow P - X + Y^-$$

Alternatively, initiators with functional groups, which may require protection, also give α-functionalized polymers.

$$
\begin{aligned}
X - I^* + M &\rightarrow X - I - M^* &\quad \text{Initiation} \\
X - I - M^* + nM &\rightarrow X - I - [M]_n - M^* &\quad \text{Propagation} \\
X - I - [M]_n - M^* &\rightarrow X - P &\quad \text{Termination}
\end{aligned}
$$
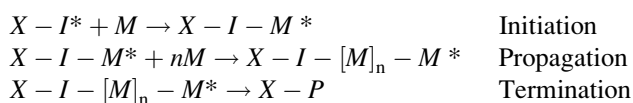
where X is the functional group in the initiating species $X - I^*$ and $X - P$ is the α-functionalized polymer.

1.1.5   Star-Branched Polymers

By controlled termination of living polymer with multifunctional linking reagents, star-branched polymers can be prepared as shown below.

$$nP^* + L \rightarrow (P)_n L$$
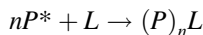
where L is a linking agent having functionality "n". For example, termination of the living polybutadienyllithium (PBLi) with a tetrafunctional electrophile such as silicon tetrachloride produces four-armed star polybutadiene.

$$4\,PBLi + SiCl_4 \rightarrow (PB)_4 Si + 4LiCl$$
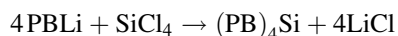
1.2   General Aspects of Anionic Polymerization

1.2.1   Monomers

Monomers that form stable carbanionic species under the polymerization conditions are amenable to anionic polymerization. Among the most widely utilized monomers are conjugated dienes, such as 1,3-butadiene and isoprene, styrenic monomers, such as styrene and α-methylstyrene, and cyclic monomers, such as ethylene oxide, that undergo nucleophilic ring opening. In general, the monomer must have substituents that can stabilize the propagating negative charge, either inductively or through resonance. Consequently, inductively electron-donating groups or relatively acidic proton-donating groups, such as amino-, carboxyl-, hydroxyl, or acetylene functional groups will interfere during anionic polymerization and thus must be excluded from the monomer unit or be suitably protected. On the other hand, aromatic rings, double bonds, carbonyl, ester, and cyano groups, stabilize the negative charge and promote the anionic polymerization of such monomers. Polar substituents, such as carbonyl, cyano, or nitro groups, may react with the initiator or with the propagating anionic species, and thus the living polymerization of monomers bearing polar substituents is possible only under specific reaction conditions (e.g., low polymerization temperature, use of bulky initiators, specific counterion). With such monomers, often termination reactions occur, leading to poor control over the molecular weight and PDI. For example, the anionic polymerization of acrylonitrile, vinyl silanes, halogenated monomers, and nitroalkenes does not proceed in a living manner.

Monomers that undergo living anionic polymerization include styrene and styrene derivatives (α-methylstyrene, p-methylstyrene, *tert*-butylstyrene, etc.), dienes (e.g., isoprene, butadiene, etc.), (meth)acrylates (at low temperatures, using bulky initiators to avoid side reactions with the carbonyl group), 2- and 4-vinylpyridines (at low temperatures, due to the reactivity of the pyridine ring), epoxides, lactones, and cyclic siloxanes.

1.2.2 Initiators

Commercially available alkyllithium compounds, specially the isomers of butyllithium, are the most useful anionic initiators. Alternatively, they can be prepared by the reaction of the corresponding alkyl chloride with Li metal. Alkyllithiums are soluble in a wide range of solvents, including hydrocarbon solvents. Organolithium compounds are unique, among organic compounds with alkali metals, in that the C-Li bond exhibits properties of both covalent and ionic bonds. This is because lithium, as compared to the other alkali metals, has the smallest radius, the highest electronegativity, and the highest ionization potential. Furthermore, low-energy unoccupied p orbitals are available for bonding. The covalent character of the C-Li bond and strong aggregation of the ionic pairs account for the higher solubility of organolithium compounds in hydrocarbon solvents, as compared to alkali metal-organic compounds. These compounds aggregate in both the solid state and in solution. The bulkiness of the organic moiety greatly impacts the extent of aggregation. Unhindered alkyllithium compounds, for example, n-butyllithium, form hexameric aggregates in hydrocarbon solvents, but when the alkyl group is branched at the α- or β-carbon the aggregates are tetrameric in nature. The extent of aggregation is also influenced by the nature of the solvent, solution concentration, and temperature. As a general rule, the degree of association is decreased by decreasing concentration, by using a more strongly solvating solvent (aromatic solvents are more strongly solvating agents than aliphatic solvents), by increasing temperature, and by the presence organic groups capable of delocalizing electrons. The reactivity of alkyllithium initiators directly reflects their degree of association; the lower the degree of association the higher is their reactivity. This trend is observed in the data below on relative reactivity of various alkyllithium initiators versus the degree of association (in parenthesis) in hydrocarbon solution for styrene and diene polymerizations:

$$\text{Methyl lithium} (2) > sec-\text{BuLi} (4) > i-\text{PrLi} (4-6) > t-\text{BuLi} (4)$$

$$> n-\text{BuLi} (6)$$
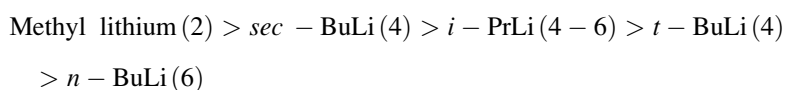
Alkyllithiums are usually the initiators of choice for polymerization of dienes and styrene, but they are not well suitable for methacrylate polymerization, due to their tendency for nucleophilic attack on the carbonyl group. In methacrylate polymerization, sterically hindered and thus less reactive initiators are commonly used, for example, diphenylhexyllithium (DPHLi), prepared by the reaction of n-BuLi with 1, 1-diphenylethylene, DPE (Scheme 1):

Scheme 1 Preparation of DPHLi initiator for polymerization of methacrylates
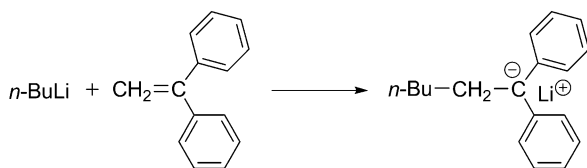
Scheme 2 Formation of naphthalene radical anion
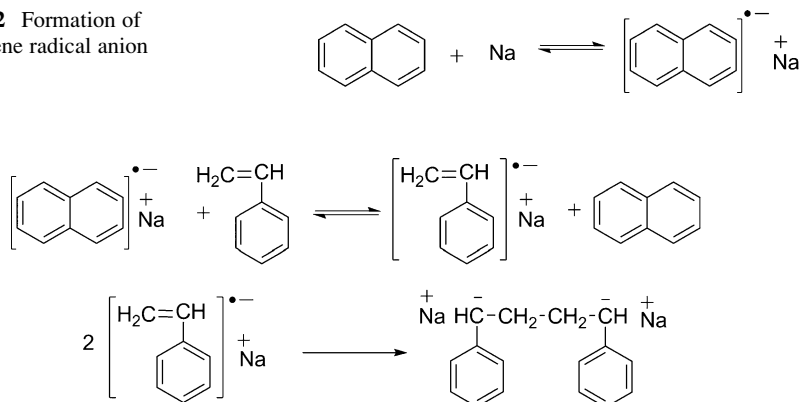
Scheme 3 Preparation of monomer radical anions and subsequently difunctional initiator

Radical anions formed by the reaction of alkali metals with aromatic hydrocarbons in polar aprotic solvents constitute another important class of anionic initiators. The best example is the reaction product of naphthalene with sodium metal (Na) in THF (Scheme 2), as used by Szwarc [2–4] in his pioneering work on living anionic polymerization:

These deep green naphthalene radical anions react with monomers such as styrene by reversible electron transfer to form the corresponding monomer radical anions. The example with styrene, cherry red in color, is given below in Scheme 3.

The radical anions couple, leading to α,ω-difunctional growing chains, useful for the synthesis of triblock copolymers, cyclic polymers, telechelics, and branched structures as the H-, super H-, and π-shaped polymers. Difunctional initiators can be conveniently prepared at ambient temperature by reaction of alkali metals with monomers having low ceiling temperatures, such as α-methylstyrene. Tetrameric dianions are the primary products formed by the reaction of α-methylstyrene with sodium metal whereas dimeric dianions are formed by its reaction with Na/K alloy. The fact that these initiators are formed only in polar solvents strongly limits their utility for the diene polymerization, since the polar solvent prevents the formation of the desirable 1,4 microstructure of the polydienes, attainable in hydrocarbon solvents and which result in low glass transition temperatures and excellent elastomeric properties. To address this problem difunctional, probably lithium-based, initiators soluble in hydrocarbon solvents are needed. Unfortunately such initiators become highly associated in hydrocarbon solvents, leading to the formation of gelled or insoluble products, which are not efficient initiators. Perhaps the most effective difunctional initiators, soluble in hydrocarbon media, is the one formed by the addition reaction of *sec*-BuLi to 1,3-bis(1-phenyl-ethenyl)benzene (Scheme 4).

A major advantage of this initiator is that an excess of *sec*-BuLi may be used in order to be certain of activating all the DPE double bonds [9]. The excess *sec*-BuLi
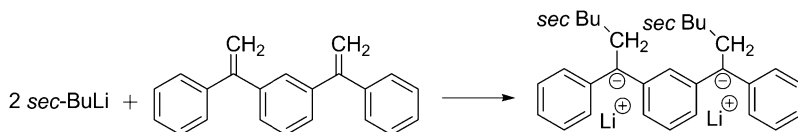
Scheme 4 Synthesis of difunctional initiator from 1,3-bis(1-phenyl-ethenyl)benzene

may be washed out using hexanes, which readily dissolve the alkyllithium but in which the dilithium initiator has very limited solubility. The perfectly difunctional initiator is then dissolved in benzene, and in the presence of lithium butoxide it is a highly efficient difunctional initiator for synthesis of high 1,4-PI [9].

1.3 High Vacuum Techniques for Anionic Polymerization

Model macromolecules having low degrees of structural, compositional, and molecular weight heterogeneity are required to elucidate structure–property relationships, which are critical for clarifying/improving the behavior of industrially important polymeric materials. In addition, the understanding of these relationships will be useful for the development of future materials tailored for high-tech applications. The anionic polymerization high vacuum technique is the best method for the synthesis of model macromolecules. These methods date back to the pioneering work of Szwarc [2, 3], and several prior reviews on these techniques are available [10–13]. In spite of the fact that high vacuum techniques are demanding, time consuming, and lead to a limited quantity of products, they have tremendous potential for synthesis of the appropriate structures needed for specific applications.

In comparison with the high vacuum techniques, the Schlenk technique is simple to perform, allowing anionic polymerization reactions to be carried out under inert gas condition in a commercially available Schlenk flask. The Schlenk method also is more amenable to carrying out reactions on a larger scale, whereas polymerizations carried out under high vacuum conditions with break seal techniques are usually conducted on the scale of about 10 g or less. However, the Schlenk method is most useful only for simple structures such as block copolymer or simple star polymers, and it is very difficult to synthesize complex macromolecular architectures using Schlenk techniques. Therefore, anionic polymerization high vacuum techniques are the most efficient method for the synthesis of well-defined complex macromolecular architectures [14–20]. Furthermore, when working with new monomers or initiators, it is best to carry out initial experiments using high vacuum line techniques, where the presence of impurities can be eliminated in assessing polymerizability of the monomer or initiator efficiency.

2 High Vacuum Techniques

2.1 *Components*

2.1.1 Vacuum Pump

With pressure requirements for different processes, vacuum science is necessarily subcategorized into a number of *vacuum regimes*. The following chart shows these regimes: rough vacuum, process vacuum, high vacuum, and ultra-high vacuum.

Vacuum Regimes

1. *Rough Vacuum: Atm (1,000 mbar) – 10^{-2} mbar*
   Rough vacuum is concerned with the removal of the bulk gas from the system. Gas molecules in the chamber interact with each other according to the laws of thermodynamics in the manner of a viscous fluid. The gases are said to be in "viscous flow"; therefore, rough vacuum pumps are called fluid flow pumps.
2. *Process Vacuum: 10^{-2}–10^{-4} mbar*
3. *High Vacuum: 10^{-5}–10^{-9} mbar*
   High vacuum pumps are statistical capture pumps. High vacuum pumps cannot pump atmospheric pressure gas and cannot be exhausted to atmosphere. Rather, they are secondary pumps and require either "backing" or periodic "regeneration" by a rough vacuum pump.
4. *Ultra-high Vacuum: $<10^{-9}$ mbar*

2.1.2 High Vacuum Line

In anionic polymerization, purification of the reagents is critical as impurities such as moisture, oxygen, etc., are capable of deactivating the initiator and the propagating living chain ends. To remove these impurities, the use of a high vacuum line is the usual choice (Fig. 1). The main parts of a high vacuum line are the following:

A. Mechanical vacuum pump
B. Mercury or oil diffusion pump
C. Liquid nitrogen trap
D. Upper glass tube rig
E. Lower glass tube rig and stopcocks

A high-quality mechanical pump is used in order to reduce the pressure in the system down to 10^{-2}–10^{-3} and mercury or oil in the diffusion pump is brought to reflux by heating it with a heating mantle. As mercury/oil distillation is started, the mercury/oil diffusion pump brings the pressure down to 10^{-5} mmHg (according to the Bernoulli principle, Fig. 2). The mercury or oil diffusion pump is connected to the vacuum line through a liquid nitrogen trap that condenses any volatile substances, such as solvent vapors or gaseous reaction products, and prevents
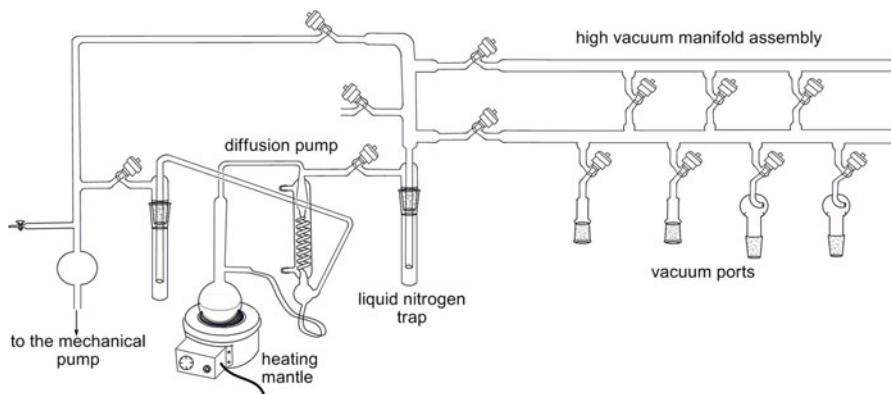
Fig. 1 High vacuum line

Fig. 2 Mercury or oil diffusion pump
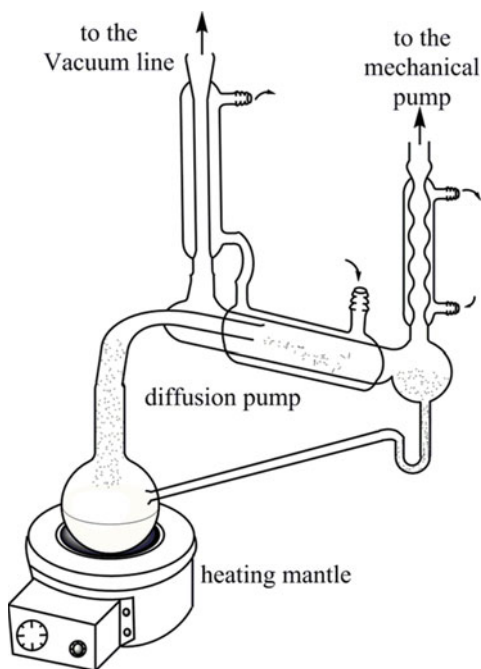
contamination of the pumps. The upper rig of the vacuum line is separated from the lower rig by special grade high-vacuum Teflon stopcocks. In this way, it is possible to isolate smaller parts of the lower rig in order to perform different procedures (e. g., distillations, degassing) simultaneously. Reaction and purification apparatuses are joined to the lower rig of the vacuum line through stopcocks and ground joints.

2.1.3 Diffusion Pump

Mercury is the historical choice as a fluid for diffusion pumps because mercury is a heavy metal (low vapor pressure) and a stream of its vapor has a large momentum. Moreover, mercury is inert to most of organic compounds that may be allowed to sweep through the pump. However, mercury is highly toxic and the use of large amounts of boiling mercury in diffusion pumps poses a major health risk. This fact, combined with continued improvements in the design of silicone oil-based diffusion pumps, has led us to recommend oil-based diffusion pumps, which can work just as well as mercury-based ones.

The mechanical pump and mercury/oil diffusion pumps work in series to achieve very high vacuum, as depicted in Fig. 1. In the 1700s, Bernoulli understood that particles in flow exert a lower pressure than particles in a stationary state. The diffusion pump sets up a stream of vapor (the diffusion pump fluid, i.e., mercury or silicon oil). As volatile liquids or gases come from the manifold into the diffusion pump, they encounter the stream of diffusion pump fluid, in its vapor state, and the vapors are swept towards the mechanical pump. The diffusion pump fluid has a high boiling point and it is continuously recycled within the diffusion pump using water condensers, as shown in Fig. 2.

2.1.4 Glass Cutter and Hand Torch

A glass cutter and a hand torch (Fig. 3a, b) are necessary tools for making simple to complicated glass reactors. The torch operates efficiently on a variety of fuel gases (natural gas, propane, or butane) combined with oxygen air. The selection of an
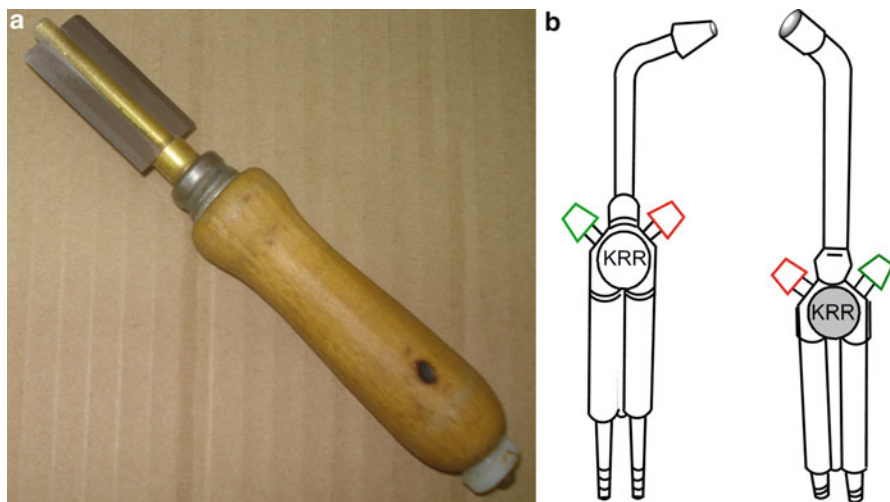
Fig. 3 (**a**) Glass cutter. (**b**) Hand torch

Fig. 4 Break seal with breaker and constriction
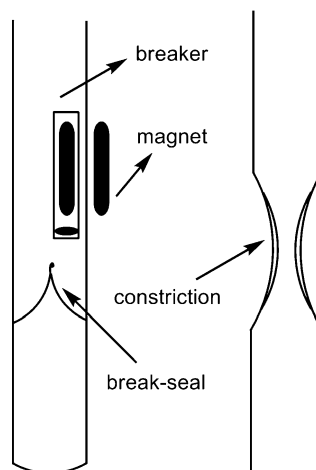
appropriate tip for the torch is based on the diameter and thickness of the glass tubing to be worked with and the application. The hand torch is useful in the practice of high vacuum techniques for the following:

- Custom glassblowing
- Flame drying of reaction apparatuses using a soft flame, under continuous pumping to remove moisture and other volatile impurities
- Sealing off constrictions
- Melting alkali metals using a soft flame, such as to form a Na mirror or Na/K alloy

2.1.5 Constrictions and Break Seals

Break seals (Fig. 4) are used for the introduction of reagents under vacuum conditions, and they can completely eliminate the need for septa or stockcocks on a polymerization apparatus. Break seals are constructed to have a thin glass tip (or bulb), which is easily ruptured with a cylindrical magnet encapsulated in an evacuated Pyrex glass tube (called a "breaker"). Breakers inside a sealed apparatus can be manipulated from outside the apparatus by moving magnets. Removal of the spent ampoules or separation of units is performed by heat sealing of constrictions (Fig. 4). Constrictions are regions of tubing that have been necked down in diameter but built up in wall thickness so as to allow for easy sealing with the torch.

2.1.6 Tesla Coil

The Tesla coil is very useful for checking the level of the vacuum and the existence of pinholes in the vacuum line. Initially, at a pressure achieved by the mechanical

pump only, the Tesla coil is noisy when it is close to the vacuum manifold (Fig. 1). Afterwards, when diffusion pump is working well, the coil is less noisy on the high vacuum side of the diffusion pump. The Tesla coil is noisy again when an apparatus is connected and allows gases and volatile compounds into the vacuum line. Later, the Tesla coil becomes quiet again as molecules are pumped out of the line by the diffusion pump. It is possible to distinguish whether these molecules are gases or volatile organic compounds by listening to coil noise on both sides of the liquid nitrogen trap. Gas molecules pass through the trap and are thus evidenced by noise from the Tesla coil on both sides of the trap. Solvent molecules are captured there and produce noise only in the vacuum line on the near side of the trap. After some time, if the coil is still noisy, it is possible there are pinholes in the apparatus, which can be checked. In the case of pinhole the tesla rays are induced showing blue color at pinhole.

2.1.7 Liquid Nitrogen

Liquid nitrogen (LN) is nitrogen in a liquid state at a very low temperature, and it is produced industrially by fractional distillation of liquid air. It is a colorless clear liquid with a density of 0.807 g/mL at its boiling point and a dielectric constant of 1.43. At atmospheric pressure, liquid nitrogen boils at $-196\ ^\circ$C and is a cryogenic fluid which is very useful in high vacuum techniques, as described below.

- A liquid nitrogen trap, as a part of the high vacuum line, is used to condense any volatile substances incorporated in the system and to protect the oil and the diffusion pumps from contamination.
- During degassing of solvents or other liquids, the liquid is frozen on the high vacuum line, with the stopcock closed, using liquid nitrogen and then the stopcock is opened and sufficient time is allowed for the whole system to be pumped down.
- Liquid nitrogen (LN) with different solvents is used as cooling mixture to obtain different temperatures, such as cyclopentane/LN ($-93\ ^\circ$C), hexane/LN ($-94\ ^\circ$C), toluene/LN ($-95\ ^\circ$C), methanol/LN ($-98\ ^\circ$C), and cyclohexane/LN ($-104\ ^\circ$C).
- During vacuum distillation, while the liquid in the source flask is thawed, the receiving flask is pumped down thoroughly and cooled by liquid nitrogen.
- While dealing with polar solvents [such as tetrahydrofuran (THF)] for polymerization, before the polymerization, the solvent is distilled into the polymerization flask, frozen using liquid nitrogen, and the purge section is removed by heat sealing.
- Before polymerization, to rinse the apparatus wall from inside, a towel strip is dipped in liquid nitrogen and briefly wrapped around the side arm. This causes the blanketing solvent (e.g., hexane) to reflux quite easily at room temperature, because the system is under reduced pressure, and washes the apparatus wall.

Caution When flasks and traps are frozen with liquid nitrogen, they cannot remain open to the atmosphere for an extended period (of even several minutes) because oxygen can condense inside the container which can result in an explosion.

2.2   Procedures

2.2.1   Degassing

The degassing procedure is helpful for removing oxygen and other gases from a liquid system. Liquid is degassed by connecting the flask to the vacuum line through a stopcock and the stopcocks is opened two or three times for very short time until bubbles are produced. With the stopcock closed, the liquid is then frozen with liquid nitrogen in a Dewar flask (depending on the melting point of the liquid, other cold baths such as dry ice/isopropyl alcohol or dry ice/acetone may be used). Then the stopcock is opened and sufficient time is allowed for the entire system to be pumped down. After high vacuum is attained as it is evidenced from the sound of the Tesla coil, the stopcock is closed and the liquid is thawed. This freeze-thaw cycle is repeated two or three times in order to thoroughly remove dissolved gases, mainly oxygen which reacts with initiators at propagating macroanions.

2.2.2   Vacuum Distillation

Simple Distillation

Because of the high vacuum in the vacuum line, distillation of liquids (solvents, monomers, etc.) becomes facile by heating (or even only maintaining at room temperature) the source flask containing the liquid and cooling the receiving flask. These two flasks are usually connected to neighboring stopcocks on the same part of the lower rig in order to minimize the distillation pathway (Fig. 5).

   The liquid is degassed completely before the beginning of the distillation. While the liquid is thawed, the receiving flask is pumped down thoroughly and brought to the desired temperature using a cold bath or LN. The part of the lower rig is isolated from the high vacuum by closing the appropriate stopcocks, and distillation begins by carefully opening the stopcock to the source flask while the liquid is rapidly stirred to prevent bumping. After the whole volume of the liquid has been collected in the receiving flask, this flask is connected to the vacuum by opening the appropriate stopcock, and the frozen liquid is degassed. After degassing, the stopcock connecting the flask to the lower rig is closed and the liquid is thawed and allowed to be stirred.

Fig. 5 Simple vacuum distillation
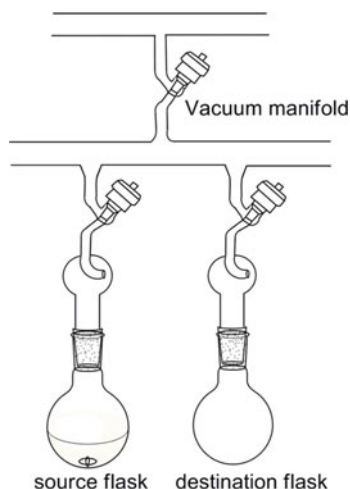
Fig. 6 Apparatus for short path distillation of high boiling point liquids
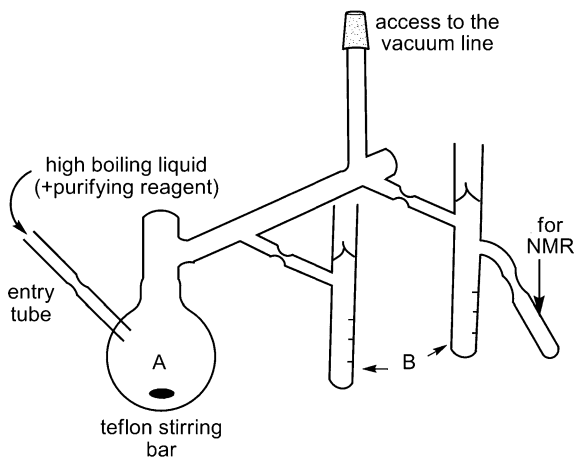
Short Path Distillation

For the distillation of high boiling liquids, a special glass apparatus is constructed (Fig. 6). The apparatus is connected to the vacuum line, checked for pin holes, and flame dried. Then the liquid to be distilled is transferred into flask (A) (with some purifying reagent, as desired), degassed on the vacuum line, and then distilled into calibrated ampoules (B). These ampoules can have a small side arm where a tiny amount of liquid can be transferred and removed for a purity checking before the ampoule is used.

Sometimes, as a final purification step, the reagent is further purified with a purifying agent such as an organometallic solution. In this case, the apparatus is constructed as shown in Fig. 7, docked to the vacuum line, evacuated, verified for integrity using the Tesla coil, and flame dried. Through the side arm while under a

Fig. 7 Short path
distillations: final
purification apparatus
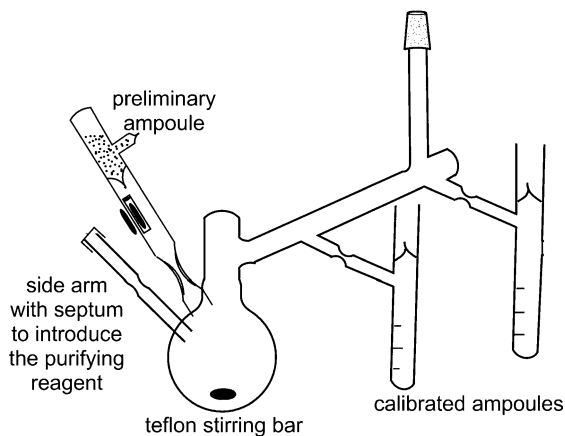
Fig. 8 Dilution apparatus
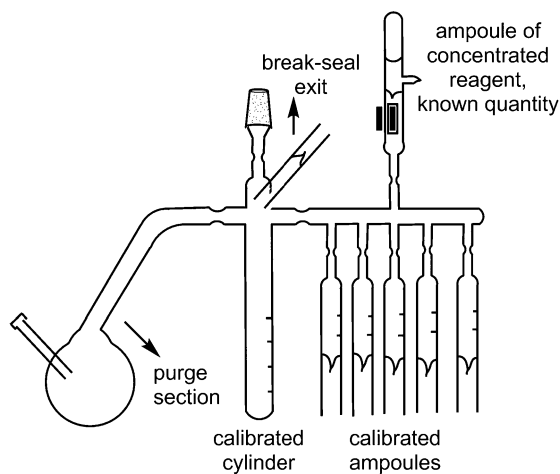
nitrogen blanket, a small quantity of an organometallic solution is injected into the apparatus with a syringe and long needle (e.g., the purification of styrene requires the use of dibutyl magnesium, Bu_2Mg). Using a towel strip dipped in liquid nitrogen, the constriction is rinsed with solvent and the side arm is then sealed with the hand torch. After removing the solvent, the break seal of the preliminary ampoule is ruptured and liquid is allowed to stir with purifying reagent. Subsequently, the monomer is collected to the final calibrated ampoules using freeze-ampulization techniques, and the ampoules are detached for further use.

2.2.3 Dilution

An ampoule of a concentrated reagent is diluted with purified solvent obtained from a reservoir using a typical dilution apparatus as shown in Fig. 8. The apparatus is

purged with *n*-BuLi solution using an appropriate purge section. After washing and rinsing the apparatus, an appropriate amount of solvent is distilled in calibrated cylinder from the purge section and then the purge section is removed by heat sealing the constriction. The break seal of the concentrated ampoule is ruptured using a breaker, the reagent is diluted in the cylinder, and the washed ampoule is removed. This diluted solution can be taken in calibrated ampoules as per reaction requirements.

2.2.4 Ampoulization

Simple or Basic Ampoulization

The apparatus shown in Fig. 9 is useful for the collection of small quantities of solvent additives or alcohols. The stepwise sequence to be used is as follows.

- The apparatus is connected to the vacuum line, evacuated, checked for pinholes, and flame dried.
- The required amount of reagent is distilled into the ampoules through the manifold by cooling with a small cloth towel strip dipped in liquid nitrogen or an alternative cooling bath.
- The ampoules are detached from the apparatus by heat sealing at the constrictions.

Fig. 9 Simple ampoulization apparatus
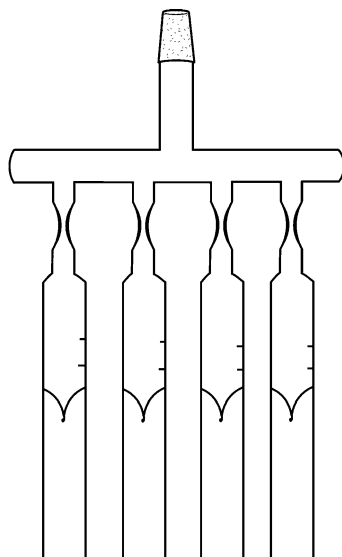
Fig. 10 Large-scale
ampoulization
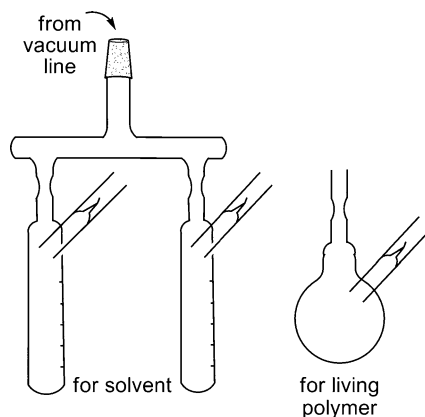
Large-Scale Ampoulization

Some time, it is necessary to ampoulize a large quantity of a compound for a single use. For example, during polymerization of hexamethylcyclotrisiloxane (D3), THF is added in a second propagation step, to make a 1/1 (v/v) mixture with benzene. In this case, it is necessary to have a large ampoule of THF connected to the reaction apparatus. This type of ampoulization can be done with the apparatus shown in Fig. 10. This technique is also useful for ampoulization of living polymers for further use.

Freeze Ampoulization

An ampoulization apparatus of alternative geometry is represented in Fig. 11. It permits the freezing of a volatile compound before it is detached and sealed into an ampoule. This technique is particularly advantageous in the collection of monomers but can be used for the collection of any volatile compound that is unstable in the presence of heat. A general stepwise experimental procedure is given below.

- The apparatus is attached to the vacuum line, flame dried, and pumped until high vacuum is achieved.
- The compound is collected in the ampoules, one after another, by simple distillation through the manifold.
- The source is closed. The ampoule is frozen at $-196\,^{\circ}$C by liquid nitrogen (or another suitable cold bath) and the apparatus is opened to the main vacuum for degassing.
- The ampoules are taken by heat sealing at the constrictions and detached from the apparatus.
- Thaw the ampoules and let them come to rest at $20\,^{\circ}$C before taking a volumetric measurement.

Fig. 11 Freeze
ampoulization apparatus
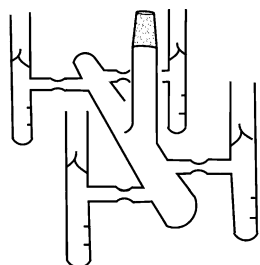
ampoules are calibrated
with a scratch on
the glass

Fig. 12 Apparatus for
split-down the ampoule

styrene or
isoprene
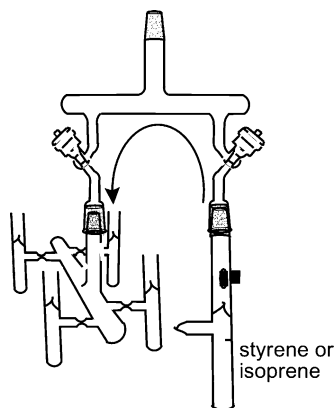
Volatile monomers (e.g., isoprene, bp 35 °C; cyclohexadiene, bp 80 °C) are easily collected through the vacuum manifold. Exceedingly volatile monomers (e. g., butadiene, bp −5 °C) may be ampoulized; however, they must be diluted in the ampoule to reduce their vapor pressure and prevent explosions.

Further use of the freeze ampoulization apparatus, as shown in Fig. 12, is suitable for "splitting down" the monomer ampoule into smaller ampoules.

2.3 Polymerization

2.3.1 Initiator

sec-Butyllithium (*sec*-BuLi) is the most commonly used initiator in anionic polymerization. This initiator is commercially available, but it is far less thermally stable than *n*-BuLi. The reported rate of decomposition is 1.4 % per month at 20 °C, and usually the presence of degradation products is visually apparent (cloudy rather than clear solution). Thus, it is preferable to synthesize this initiator and keep it

Fig. 13 Reactor for synthesis of *sec*-BuLi initiator
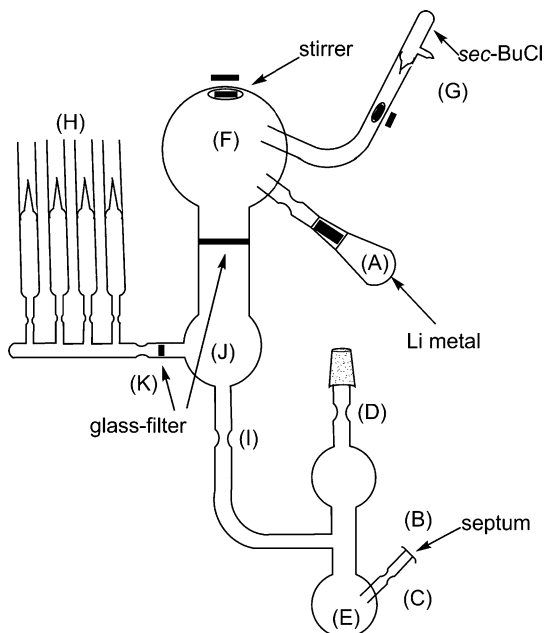
stored in solution at low temperatures. Under proper storage conditions, the concentration does not change appreciably over a period of months. *sec*-BuLi is prepared by the reaction of *sec*-BuCl with Li metal:

$$sec - \text{BuCl} + 2\text{Li} \rightarrow sec - \text{BuLi} + \text{LiCl}$$
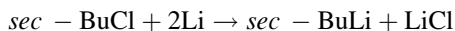
sec-BuCl is dried over CaH_2 on the vacuum line, degassed thoroughly and distilled into a calibrated ampoule, which is attached to the main apparatus used for the synthesis of the initiator, as shown in Fig. 13. The reactor is attached to the vacuum line, checked for pinholes, and flame dried. After pumping down lithium dispersion in hexane (containing 2 % sodium) is placed in ampoule (A) by breaking the vacuum with inert gas for a short time. Usually a seven- to tenfold excess of Li metal over *sec*-BuCl is used. The hexane is evaporated, removed through the vacuum line. 3–5 mL of *n*-BuLi solution (1.6 M in hexane) is introduced through septum (B) by a syringe, for purging of the reactor. After removal of the hexane, constriction (C) is heat sealed. The required amount of purified hexane is distilled from the vacuum line into flask (E) and the reactor is sealed at (D). The ampoule (A) is washed with *n*-BuLi solution in order to transfer the Li metal quantitatively to flask (F) and is sealed. The entire reactor is purged with *n*-BuLi solution, in order to react with the impurities on the glass and is rinsed thoroughly to remove the excess *n*-BuLi, by condensing hexane on the walls. The hexane is distilled from flask (E) to flask (F) and the purge section is heat sealed at (I).

Fig. 14 Filtration of the
sec-BuLi solution
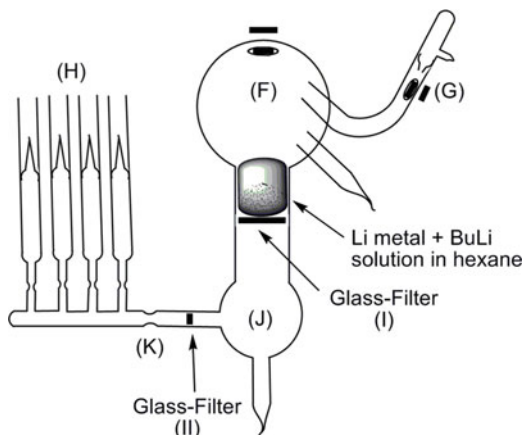
Flask (F) is immersed in an ice–water bath. Afterwards, the break seal (G) is broken and *sec*-BuCl is allowed to slowly distill into flask (F) containing the Li dispersion in hexane under stirring. After the distillation is complete, the reaction is allowed to continue for another 4 h under stirring and then flask (F) is left overnight in an ice–water bath at 0 °C.

The reaction mixture is filtered through a glass filter (Fig. 14) from flask (F) to (J) in order to remove unreacted Li and the (*sec*-Bu)$_2$ by-product (Wurtz reaction) which is insoluble in hexane, and the *sec*-BuLi solution in hexane is collected in ampoules (H) for use. The ampoule part is detached from the main reactor by heat sealing at constriction (K).

Dilution of the Initiator with Hexane

The concentration of the *sec*-BuLi solution obtained from the synthesis is usually too high for use, so it must be diluted to the desired concentration and split-down into calibrated ampoules. The apparatus used for dilution and split-down of initiator is shown in Fig. 15. This apparatus, having an ampoule containing the concentrated *sec*-BuLi solution, is connected to the vacuum line, pumped down, checked for pinholes, and flame dried. 3–5 mL of 1.6 M *n*-BuLi solution in hexane is introduced into the purge section through a septum via a syringe, and the side arm is removed by heat sealing the constriction. The required amount of purified *n*-hexane is distilled from the vacuum line into purge section, and the reactor is removed by heat sealing at (A). The apparatus is washed with the *n*-BuLi solution, and then it is rinsed thoroughly by condensing hexane onto the apparatus walls. The hexane is distilled from the purge section into the calibrated cylinder, and the purge section is removed at (B). The break seal of the *sec*-BuLi ampoule is broken, and the concentrated *sec*-BuLi solution is diluted with *n*-hexane and separated into the calibrated cylinder. This ampoule is rinsed several times and removed from the

Fig. 15 Dilution apparatus for *sec*-BuLi
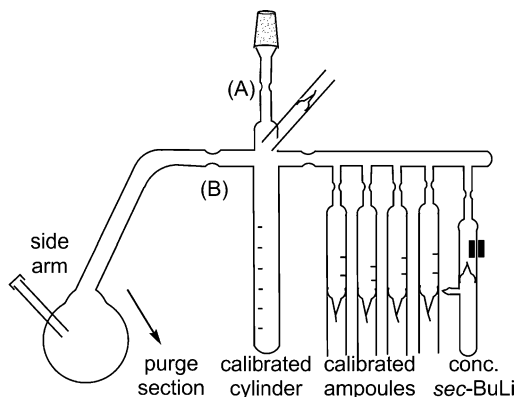
apparatus by heat sealing. The desired amount of dilute initiator solution is transferred into the ampoules. After rinsing the constrictions, the ampoules are removed by heat sealing, and the apparatus containing the rest of the initiator solution is stored at $-20\,^\circ$C for future use.

2.3.2 Solvents

Solvent Storage

Solvents may be stored on the vacuum line for several weeks in flasks attached through greased ground glass joints. A calibrated cylinder shown in Fig. 16a is very convenient as known amounts of solvent can be distilled from it with good accuracy. Generally, a greased vacuum joint will last with integrity for 1–3 weeks, depending on the nature of the solvent. As solvent migrates into the grease and compromises the seal, alternatively, a specialty cylinder can be used as shown in Fig. 16b. The side arm allows the introduction of purifying reagent and is subsequently sealed. Because this cylinder is fitted with a Teflon stopcock, it may be safely removed from the vacuum line by closing the stopcock and more vacuum grease can be applied.

Solvent Purification

Benzene This common solvent is purified by stirring over concentrated sulfuric acid for a week in a conical flask inside a fume hood. This procedure removes thiophenes, which may alter the microstructure of polydienes or otherwise participate in the polymerization. Then the benzene is transferred carefully into a round-bottom flask containing finely grounded CaH_2 and a magnetic stir bar, attached to the vacuum line, and degassed. It is left for reaction of CaH_2 with and water present overnight. Then the benzene is again degassed and distilled into a calibrated cylinder containing polystyryllithium (PSLi) made from *n*-BuLi and styrene. The
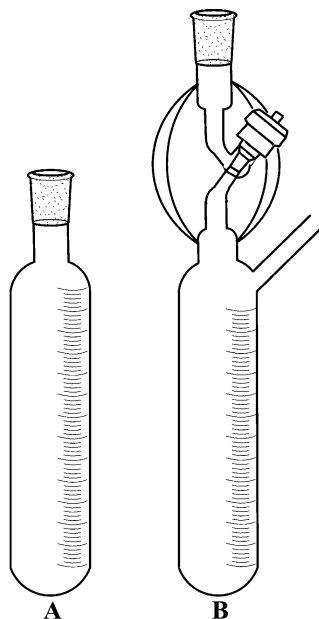
persistence of the bright orange color of PSLi produced after the thawing of benzene indicates the purity of the solvent (Fig. 17).

Toluene Toluene is purified in a manner similar to that used for benzene except for omitting the exposure to sulfuric acid.

Alkanes Alkanes (*n*-hexane, cyclohexane, heptane etc.) are purified with CaH_2 and then stored over *n*-BuLi as shown in Fig. 18.

Tetrahydrofuran (THF) THF is collected into a round-bottom flask containing fresh finely grounded CaH_2 and stirred overnight. This flask is then connected to the vacuum line, the solvent is degassed and distilled over Na metal dispersion. After stirring and degassing, the purified THF is distilled into a flask containing a Na/K (1/3) alloy. The bright blue color, which develops after stirring for some time, indicates that the solvent is free from impurities.

Ethers Other ethers such as dioxane are purified in a manner similar to that for THF. Usually, stirring over CaH_2 followed by exposure to Na mirrors is a procedure that ensures pure compounds.

Amines Purification of amines (usually tertiary amines like triethylamine, tetramethylethylene diamine, or dipiperidinoethane) presents some problems. Fortunately, these compounds are used in small amounts as modifiers of the kinetics of polymerization or the microstructure of polydienes. The procedure usually employed is composed of thorough drying over CaH_2, exposure to several sodium mirrors, and final distillation into ampoules. The use of BuLi should be avoided because it reacts with amines.

Fig. 17 Purification of benzene
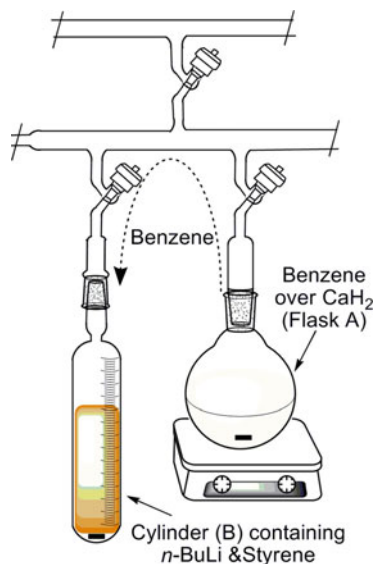
Fig. 18 Purification of *n*-hexane
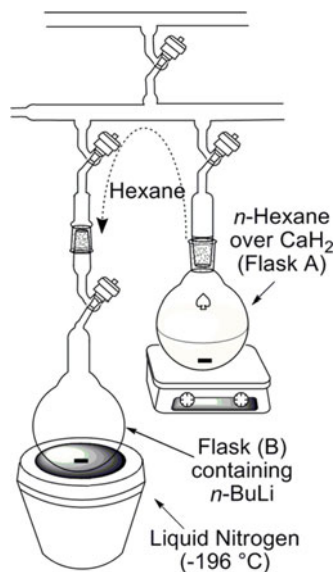
2.3.3 Monomers

Styrene (bp: 145 °C/760 mmHg) This high boiling monomer is dried overnight on the vacuum line over CaH_2 by using an apparatus as shown in Fig. 19, *step 1*. Then it is distilled into a flask containing dibutylmagnesium (DBMg) [1 M solution in heptane]. The magnesium compound having one *n*-butyl and one *iso*-butyl group is preferred due to its higher solubility in hydrocarbon solvents. The monomer is
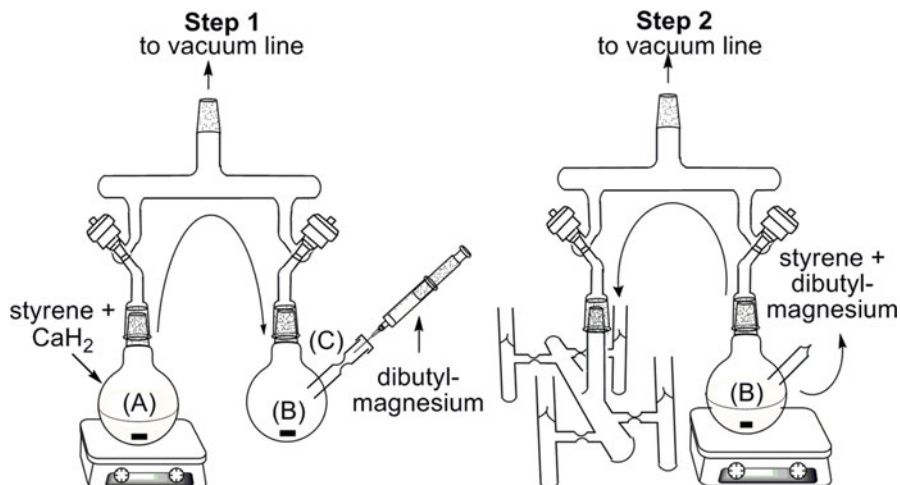
Fig. 19 Purification of styrene

allowed to stand overnight with continuous stirring. A bright yellow-green color develops as the pure monomer starts to polymerize. Polymerization of styrene with DBMg compounds proceeds very slowly. The next day the pure monomer can be distilled into the precalibrated ampoules (Fig. 19, *step 2*).

Other Styrenic Monomers Other styrenic monomers [*tert*-butylstyrene (bp: 91 °C/9 mmHg), *p*-methylstyrene (bp: 170 °C), α-methylstyrene (bp: 167 °C), etc.] can be purified in the same way as styrene. A short path distillation apparatus is used in all cases. In the case of α-methylstyrene, *n*-BuLi can be used, alternatively to DBMg, since this monomer has a low ceiling polymerization temperature and no polymerization occurs at room temperature. The purity of the monomer is determined from the red color of the anions formed.

1,1-Diphenylethylene (DPE; bp: 270 °C/760 mmHg) The apparatus (as shown in Fig. 20) used for the purification of DPE is checked for pinholes, a small amount of DPE (in hexane) is loaded into the flask through a ground joint (a) and the flask is evacuated slightly by connecting to the vacuum line. *n*-BuLi is introduced through septum (b) and sealed off at (c) and (d). Then, DPE is titrated with a solution of *n*-BuLi in hexane until a deep red color is permanently formed. The remaining *n*-BuLi is removed by sealing constriction (e). Again the apparatus is connected to the vacuum line by ground joint (f), and break seal (g) is ruptured. After the whole hexane has been distilled off, the flask is immersed in an oil bath and the temperature is set at 85 °C. DPE starts to distill and when the appropriate amount is collected in ampoule (h), the ampoule is removed by heat sealing the constriction (i). This DPE is further diluted with purified solvent by using a dilution assembly and stored at −20 °C.

Fig. 20 Purification and distillation apparatus for DPE
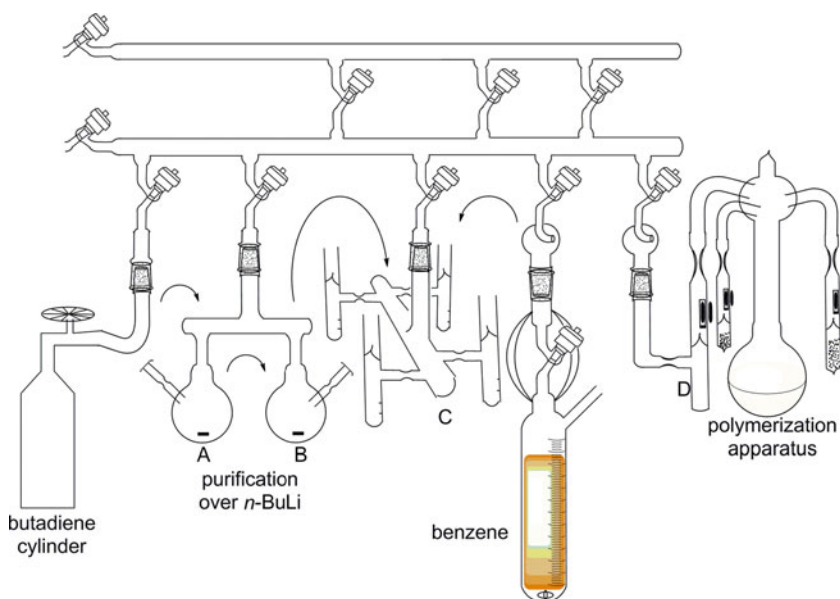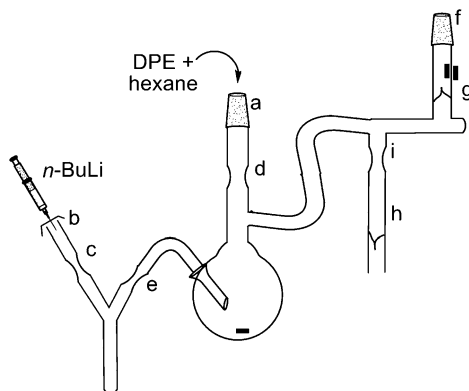
Fig. 21 Butadiene purification and ampoulization

Note *DPE is not really a monomer since does not homopolymerized. It is living terminator.*

Butadiene (bp: −4 °C/760 mmHg) This monomer is a gas at room temperature so it is condensed into a flask (A) that contains *n*-BuLi at −78 °C (dry ice/isopropanol bath) as shown in Fig. 21. The monomer is stirred for 20–30 min at −10 °C (ice/salt bath). Then it is distilled into another flask (B) containing fresh *n*-BuLi and it is allowed to stand for another 20–30 min at −10 °C until the viscosity is slightly increased (polymerization) indicating the absence of active impurities.

Note *Use only* n-*BuLi as it is a slow initiator of butadiene and never exceed 30 min of exposure in order to avoid potential violent exotherms!*

The butadiene is finally distilled at −78 °C into a calibrated ampoule (C) and the monomer is diluted with purified solvent (benzene) in a ratio of [monomer]/[solvent] lower than 0.2. Alternatively, purified butadiene monomer is directly distilled into the calibrated ampoule (D) of reaction apparatus as shown in Fig. 21.

Isoprene (bp: 34 °C/760 mmHg) This diene monomer is dried over finely grounded CaH_2 on the vacuum line overnight and degassed. It is then distilled into a flask containing *n*-BuLi where it remains with continuous stirring for 20–30 min at 0 °C. This step is repeated twice, before the pure monomer is distilled in precalibrated ampoules equipped with break seals. It can be stored at −20 °C for 6 months.

Note *Use only* n-*BuLi as it is a slow initiator of isoprene and never exceed 30 min of exposure in order to avoid potential violent exotherms!*

2-Vinylpyridine (bp: 158 °C/760 mmHg) This high boiling monomer is dried over CaH_2 in a short path apparatus overnight, degassed, and then it is distilled into ampoules as shown in Fig. 22, *Step 1*. The monomer, free from stabilizer, can be stored at −20 °C for about a week. The final purification steps involve exposure to sodium mirror for a few minutes in an apparatus similar to the one shown in Fig. 22 (*Step 2*) and subsequent distillation in another ampoule. The ampoule is then connected to a new short path apparatus with a side arm for the introduction of trioctylaluminum (*Step 3*). After stirring for a few minutes over trioctylaluminum, the purified 2-vinylpyridine is distilled into a precalibrated ampoule, which is then attached to the polymerization reactor. Polymerization of this monomer should be carried out the same day, following the final two purification steps, since the monomer obtained is so pure that it polymerizes by standing overnight, even at −20 °C.

Methacrylates and Acrylates These monomers are commercially available (usually in ~98–99 % purity) and are dried over CaH_2 overnight in a short path apparatus attached to the vacuum line. The monomer is degassed and distilled into calibrated ampoules. The purified monomer can be stored at −20 °C for up to a week. Just prior to polymerization, it undergoes a final purification involving a short exposure to triethylamine (TEA) or trioctylaluminum (TOA) in a short path distillation apparatus. When a yellow-green color persists in the monomer, it is distilled in a precalibrated ampoule, which may then be used in polymerization. Low levels of alcohols remaining from the synthesis of these monomers are removed during this last exposure to aluminum compounds. TOA is preferred with higher boiling monomers of the family (i.e., *tert*-butylmethacrylate) since TEA can be sublimed under high vacuum and contaminate the monomer ampoules. TOA is also considered more efficient in removing secondary or tertiary alcohols. The yellow-green color reflects the complex formed between the aluminum compound and the carbonyl of the monomer and may be misleading since complexation can occur before complete reaction with residual alcohol.

Fig. 22 Three-step
purification of 2-
vinylpyridine

a) Step 1

heavy wall
glass tube

2-vinylpyridine
+ CaH$_2$

(A)

b) Step 2

(A)

(B)

Na metal   Na mirror

c) Step 3

trioctylaluminum

(B)

(C)
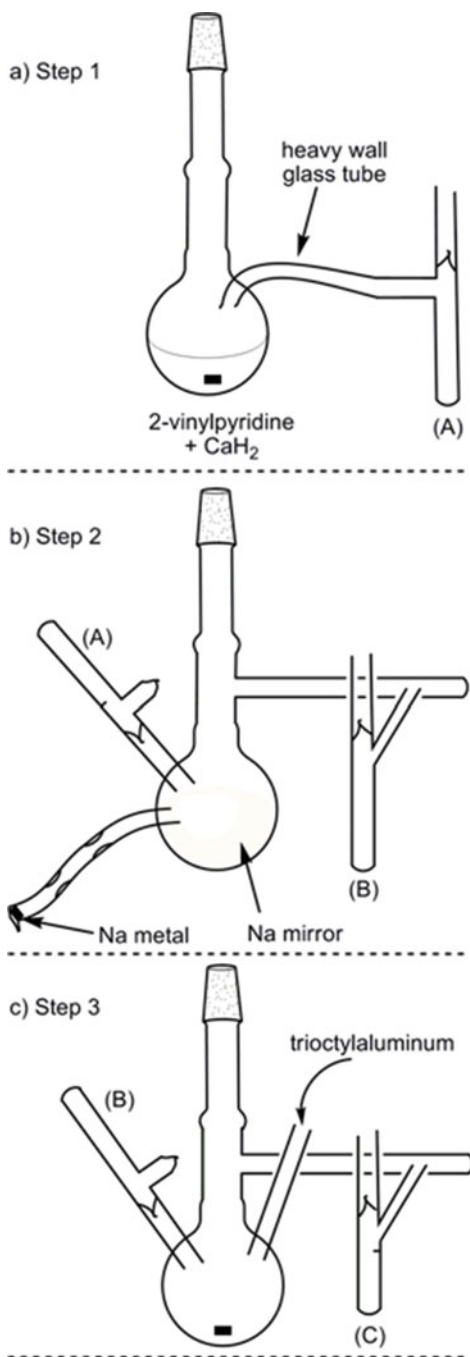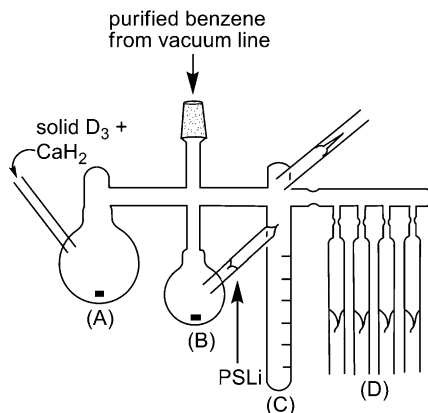
Fig. 23 Hexamethylcyclotrisiloxane (D3) monomer purification apparatus

Ethylene Oxide (EO; bp: 10 °C) EO is low boiling monomer and it is initially condensed into a cylinder containing freshly ground calcium hydride. It is stirred over CaH$_2$ on the vacuum line for about 30 min at 0 °C, degassed, and distilled over *n*-BuLi. During its exposure to *n*-BuLi, EO is kept at 0 °C with stirring (for 30 min). This step is repeated twice and finally the pure monomer is distilled into graduated ampoules and stored at −20 °C until use.

Hexamethylcyclotrisiloxane (D3) D3 is solid monomer having melting point at 70 °C. It is diluted with purified benzene and stirred over CaH$_2$ overnight in a specially designed short path distillation apparatus, as shown in Fig. 23 (*A*). By heating at around 40 °C, the solvent along with the monomer are sublimed into another flask (*B*) which contains PSLi. The monomer is allowed to stand in contact with PSLi for about 2 h at room temperature, and then it is distilled along with the solvent into the cylinder (*C*) where it can be split-down in precalibrated ampoules (*D*).

2.3.4 Terminating (Deactivating) Agents

The compounds used for deactivation of the living polymer chains are usually alcohols. Methanol is most widely used as the terminating agent. Methanol is degassed on the vacuum line several times and it is distilled into ampoules, as shown in Fig. 24. Other terminating agents used in special cases, that is, silanes – (CH$_3$)$_3$SiCl, CH$_3$SiCl$_3$ can be purified by simple degassing since they are used in large excess compared to the concentration of the living ends. Degassing the terminating agents is necessary since the air can contaminate the desired polymer with the double molecular weight polymer.

Ampoule containing known amount of chlorosilane (e.g., methyltrichlorosilane; MeSiCl$_3$) can be diluted with *n*-hexane or benzene using dilution apparatus, as shown in Fig. 25. With regular dilution procedure, *n*-BuLi is used as purging

Fig. 24 Ampoulization of
terminating agents

terminating agent,
methanol or silanes
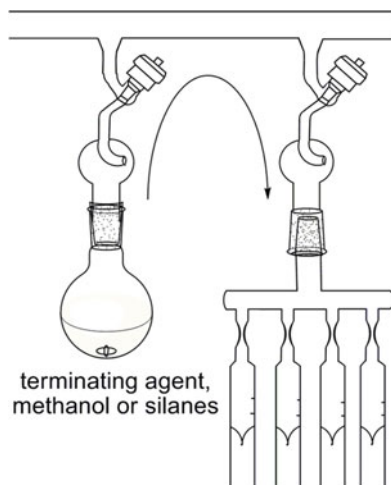
Fig. 25 Dilution of
methyltrichlorosilane

MeSiCl$_3$

Me$_3$SiCl

solvent
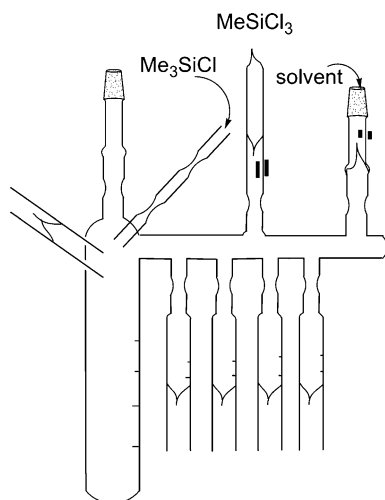
reagent. Silanization is an alternative for purging and is sometimes practical when multifunctional chlorosilanes are used. (CH$_3$)$_3$SiCl is the chlorosilane used for this purpose. Any impurities that are deleterious to the Si-Cl bond, including glass surface contaminants such as Si-OH, are deactivated with a small quantity of methyltrichlorosilane. Experimentally, a small quantity of (CH$_3$)$_3$SiCl is introduced to the apparatus; it is removed from vacuum line by heat sealing and the silane is allowed to completely wash the inner glass surface (liquid nitrogen/towel strip). The contents are then pumped off using another ground joint, without flame drying the apparatus, until high vacuum is achieved. After distilling in the appropriate

Fig. 26 (Step 1) Apparatus
for the preparation of linear
homo- and copolymers
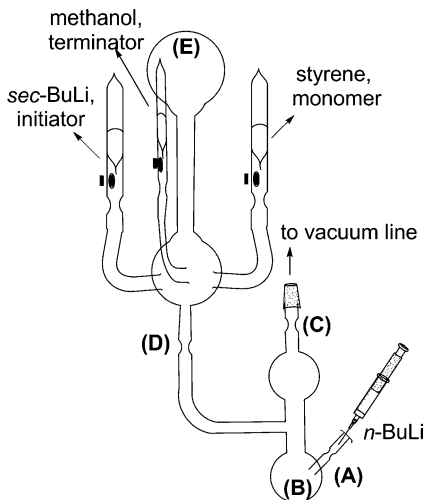
amount of purified solvent from vacuum line, the ampoule containing methyltri-
chlorosilane is ruptured for dilution.

2.3.5 Polymerization Procedures in Nonpolar Solvents

Canadian Technique for the Synthesis of Linear Homopolymers, Block
Copolymers, Star Homopolymers, and Star-Block Copolymers

The Canadian-style glass apparatus used for the synthesis of linear homopolymers,
block copolymers, star homopolymers, and star-block copolymers is shown in
Fig. 26. This apparatus was developed by the Canadian school of anionic polymer-
ization (S. Bywater, J. Worsfold, J. Roovers), during the 1960s and 1970s and then
improved by the Athens School (N. Hadhichristidis, H. Iatrou, M. Pitsikalis). The
ampoules containing the initiator, monomer, and terminator are attached to the
main reactor. The apparatus is connected to the vacuum line through ground joint,
checked for pinholes, and flame dried. Then, 2–3 mL of concentrated solution of *n*-
BuLi in hexane is introduced in flask (B) through the septum, and the tube holding
the septum is removed by heat sealing at (A).

   The apparatus is pumped for another ½ h in order to remove the hexane and air
inserted in the apparatus during inject, followed by distillation of the appropriate
amount of solvent into flask (B). Usually benzene is used as the solvent for the
polymerization of styrene and hexane or benzene for the polymerization of isoprene
or butadiene. For a typical polymerization, the amount of solvent is chosen such
that the final polymer concentration is 5–10 %, depending on the molecular weight
of the polymer. After degassing, the reactor is removed from the vacuum line by
heat sealing at (C). The inner wall of the reactor is purged by the solution of *n*-BuLi;
this solution is transferred back to flask (B) and placed in a 50 °C water bath.

Fig. 27 (Step 2)
Intermediate step involving
distillation of the solvent
from the purge section to
the main reactor

warmer (water) bath   ice bath
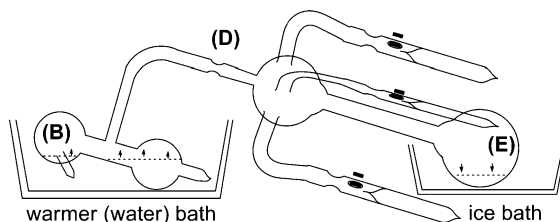
Fig. 28 (Step 3) The final
clean polymerization
apparatus
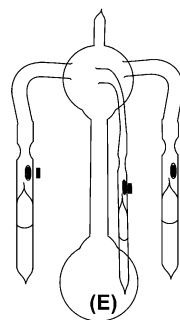
Because of the vacuum inside the apparatus, benzene refluxes and condenses over the whole reactor, rinsing traces of *n*-BuLi from the glass walls. As a consequence, all *n*-BuLi inserted along with the products of reaction impurities are collected in flask (B) of the purge section. The apparatus is tilted in a way shown in Fig. 27. A water bath at 25 °C is placed under the purge section and an ice–water bath under flask (E). Due to vacuum in the apparatus, the solvent is distilled into the main reactor but the nonvolatile species, that is, *n*-BuLi and its reaction products with impurities, remain in flask (B). The purge section is removed by heat sealing of constriction (D) leaving a clean reactor filled with an appropriate amount of pure solvent. First, the break seal of the monomer is ruptured, by moving the pair of magnets. The monomer is poured (or distilled in the case of isoprene or butadiene) into flask (E), followed by addition of the initiator and the ampoule is rinsed with solvent (Fig. 28). The polymerization is left to proceed until all monomer is consumed. The polymerization terminated by addition of degassed methanol to afford linear homopolymer.

Before termination, the living ends of the polymeric chains can initiate the polymerization of another monomer leading to block copolymers. Also the reaction of living chains with linking agent, such as multifunctional chlorosilane, affords star homopolymer. The living block copolymer can also be reacted with linking agent to form star-block copolymers.

Using the polymerization reactor shown in Fig. 29, two of the same (with different molecular weight) or different living homopolymers are prepared. After distilling solvent from the purge section into the main reactor, it is divided into two calibrated cylinders, and they are sealed off from the main reactor. By rupturing the break seals of respective monomer and initiator ampoules, two polymerization

Fig. 29 Apparatus for the preparation of two homopolymers
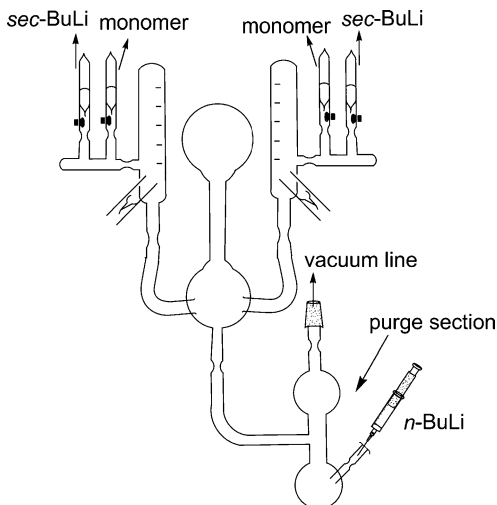
Fig. 30 Simple polymerization apparatus
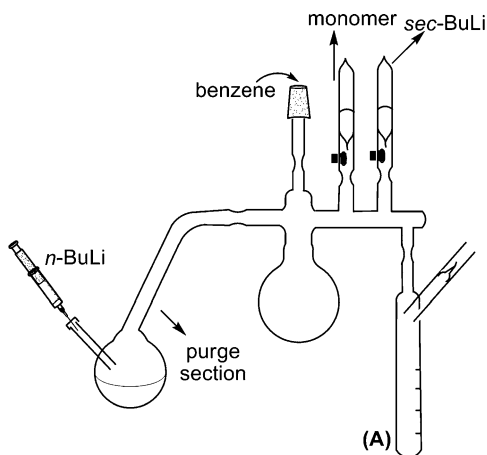
reactions are started. After polymerization, the calibrated cylinders are used as reservoir of living polymer for further use.

Simple Technique

Another type of polymerization apparatus can be used for the synthesis of homo, block, and star polymer, as shown in Fig. 30. All reaction steps are similar to those described above. After polymerization, the calibrated cylinder (A) is used as a reservoir for the solution of living polymer which can be served for the preparation of molecules with more complex architectures.

$$ALi + (CH_3)SiCl_3 \longrightarrow ASi(CH_3)Cl_2 + LiCl + (CH_3)SiCl_3 \uparrow$$

excess

$$ASi(CH_3)Cl_2 + BLi \longrightarrow ASi(CH_3)B_2 + 2LiCl$$

excess

or

$$ALi + SiCl_4 \longrightarrow ASiCl_3 + LiCl + SiCl_4 \uparrow$$

excess

$$ASiCl_3 + BLi \longrightarrow ASiB_3 + 3LiCl$$

excess
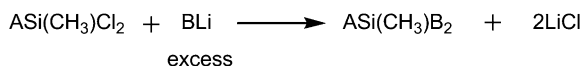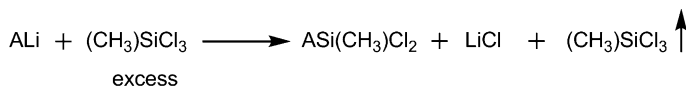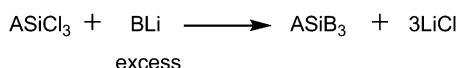
Scheme 5 Synthesis of 3 μ-star and 4 μ-star copolymer

Fig. 31 Reaction apparatus for the preparation of 3 μ-star and 4 μ-star copolymers
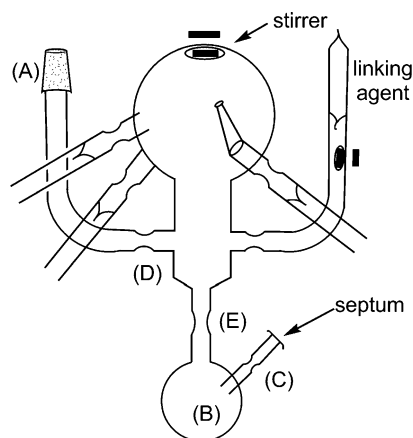
Synthesis of AB$_2$ and AB$_3$ Type 3- and 4-Miktoarm Star (μ-Star) Copolymers

The reaction sequences used for the preparation of 3- and 4-μ-arm star copolymers are given in Scheme 5.

The reaction apparatus used for this synthesis is shown in Fig. 31. The reactor is connected to the vacuum line through the ground joint (A), checked for pinholes, and flame dried very well. After 1 h of pumping, 4–5 mL of concentrated solution of *n*-BuLi is injected through the septum, the side tube is rinsed and removed by heat sealing at (C). 30–40 mL of benzene is distilled into flask (B), degassed and the apparatus is removed from the vacuum line by heat sealing the constriction (D). The reactor is purged with the *n*-BuLi solution to react with impurities and moisture.

Fig. 32 Intermediate step:
addition of the living arm
(ALi) to the excess of the
linking agent
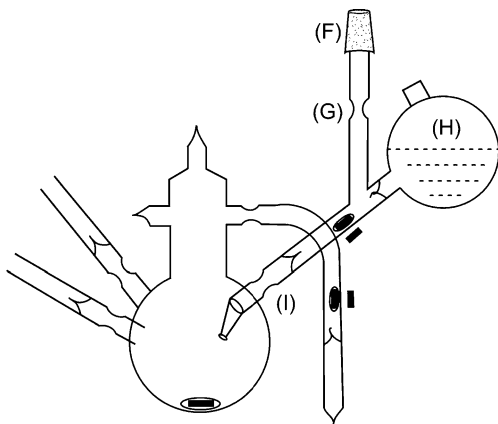
Fig. 33 Intermediate step:
removing the excess of the
volatile linking agent
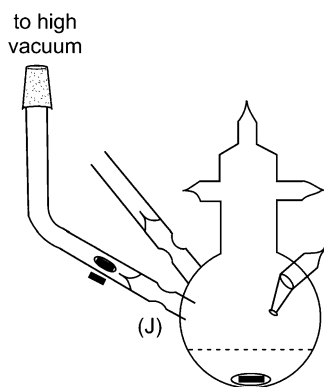
Then a water bath of 50 °C is placed under flask (B) and benzene starts to reflux rinsing the walls of the apparatus and is finally collected into flask (B). Subsequently traces of *n*-BuLi along with reaction products of impurities are collected in this flask. The purge section containing the solution of *n*-BuLi is removed by heat sealing constriction (E).

An ampoule (H) of living arm ALi (~5 % solution in benzene) is attached to the main reactor as shown in Fig. 32. The area between the two break seals is evacuated by attaching the reactor to the vacuum line via ground joint (F), followed by removal of the apparatus by heat sealing the constriction (G). Following distillation of the linking agent in the main flask, the flask is placed in an ice–water bath and a hot towel is placed simultaneously on ampoule (H). At the same time, the living polymer is added by rupturing the two break seals. During the addition, the mixture of the inserted solution and linking agent is vigorously stirred. The hot towel increases the vapor pressure of ampoule (H), and addition of the living arm to the silane solution is ensured. The ampoule is removed from the reactor by heat sealing of constriction (I).

Fig. 34 Final step: excess
addition of the living arm
BLi to ASi(CH$_3$)Cl$_2$ or
ASiCl$_3$
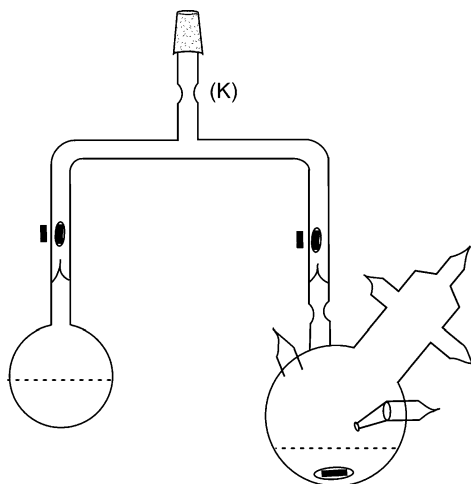
A ground joint is connected to one of the two remaining break seals and the apparatus is attached to the vacuum line (Fig. 33). The solvent and excess linking agent are removed by pumping on the vacuum line and also by redissolving the polymer in benzene and removing the solvent several times. After that 50–100 mL solvent is distilled into the main flask, followed by removal of the apparatus from the vacuum line by heat sealing at (J). After the preparation of an ampoule containing excess of living arm B (BLi), the two solutions are connected as shown in Fig. 34. The air between the two break seal is pumped, and after heat sealing at (K) the solution of living polymer (BLi) is added to the solution of the macromolecular linking agent ASi(CH$_3$)Cl$_2$ or ASiCl$_3$. After the completion of the linking reaction, the star copolymer is separated from the parent material by fractionation.

Synthesis of Exact Comb Polymers

A schematic representation of the reaction sequences for the synthesis of an exact comb homopolymer is given in Scheme 6, where A is polybutadiene or polyisoprene end capped with 2–3 units of butadiene:

The synthesis of double-tailed DPE (dtDPE) is based on the selective reaction of the living polymer (ALi) with the two chlorines of 4-(Dichloromethylsilyl) diphenylethylene (DCMSDPE), rather than with the non-homopolymerizable double bond [21]. Ampoules containing DCMSDPE and ALi are connected to specially designed homemade apparatus, as shown in Fig. 35.

After flame drying the apparatus on the vacuum line, 5 mL of *n*-BuLi is injected into the purge section through a septum and heat sealed at (A). Prepurified benzene is distilled into the purge section and frozen in liquid nitrogen. After degassing, the apparatus is removed from the vacuum line by heat sealing at (B). The apparatus is
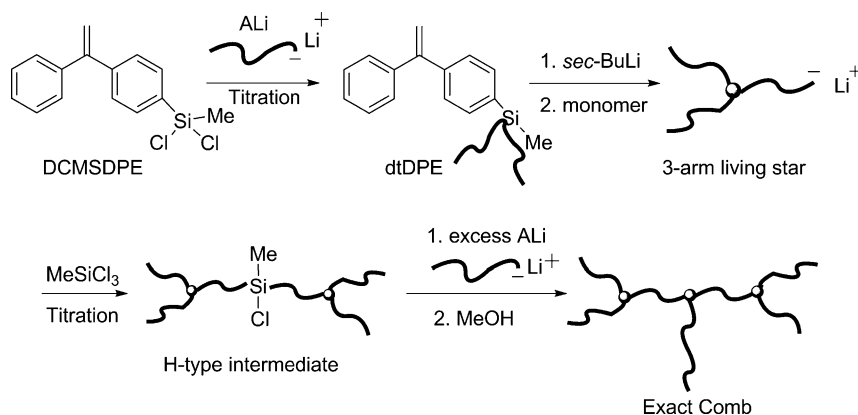
Scheme 6 Synthesis of exact comb polymer

Fig. 35 Glass apparatus for the synthesis of dtDPE
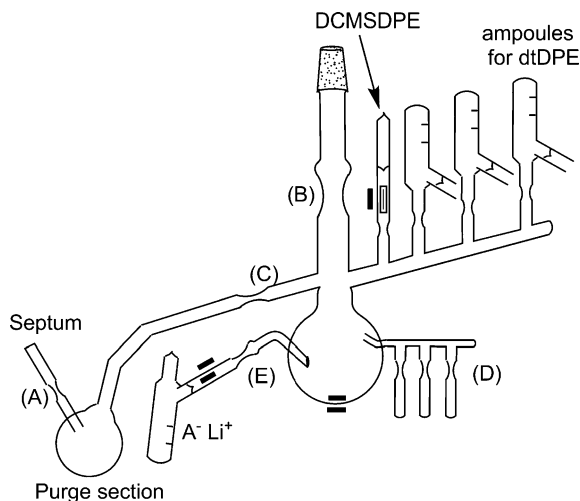
purged with *n*-BuLi solution and rinsed with benzene. Benzene is distilled very slowly from the purge section into the reaction flask, and the purge section is removed by heat sealing at (C). DCMSDPE is introduced into the main reactor by breaking the corresponding break seal. Approximately 10 % solution of A^-Li^+ is added dropwise into the solution of DCMSDPE. The reaction is monitored by removing small aliquot (D) tubes, and analyzing them by size exclusion chromatography (SEC). After the addition of two equivalents of A^-Li^+ relative to DCMSDPE, and more importantly when the end point is confirmed by SEC, the titration is stopped. The flask containing the excess living A^-Li^+ solution is

Fig. 36 Reactor for the synthesis of living 3-arm star
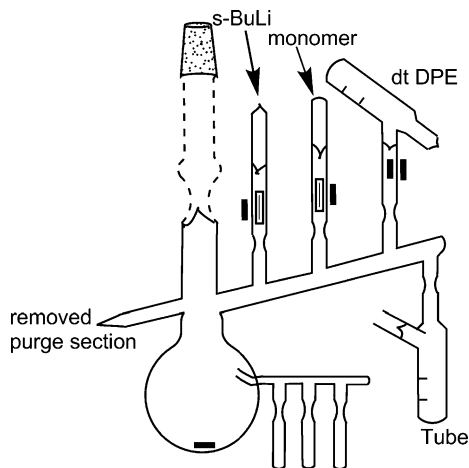
removed by heat sealing (constriction E). The resulting dtDPE is subsequently divided into tubes, equipped with break seals, for further reactions.

The reactor given in Fig. 36 is used for the synthesis of the living 3-arm star. Double-tailed DPE and *sec*-BuLi are introduced into the main reactor by breaking the corresponding break seals. The solution immediately turns to a deep red color (activation of the DPE double bond) and is left to stir for 48 h. Another fresh monomer is then introduced into the main reactor, and the polymerization is allowed to proceed for 24 h. The deep yellow colored polymer solution produced is transferred into a tube and removed from the apparatus.

Exact comb polymer with three branches is synthesized by titration of trichlorosilane with living 3-arm star followed by addition of living linear polymer (A^-Li^+) in excess. Trichloromethylsilane is introduced into the main reactor (Fig. 37) by breaking the corresponding break seal. The 3-arm living PI star is then added dropwise into the reactor. The reaction is monitored by removing small aliquots and analyzing them by SEC. After the addition of two equivalents of living star relative to $MeSiCl_3$, followed by SEC confirmation, the titration is stopped. The flask containing the excess living star is removed by heat sealing at constriction (B). Then another A^-Li^+ is introduced into the main flask and left to react with the remaining chlorine for 2 days. The final product mixture is terminated with degassed methanol, fractionated, precipitated into an excess of methanol, and dried under vacuum.

2.3.6 Polymerization Procedures in Polar Solvents

The polymerization of several monomers, such as methacrylates or 2-vinyl pyridine (2VP), is conducted in THF at low temperatures. The principles of the polymerization procedure are the same as in the case of the polymerizations that take place in

Fig. 37 Reaction apparatus for exact comb polymer
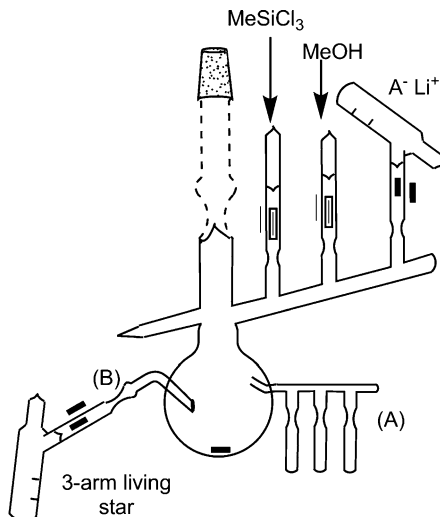
benzene. However, a different apparatus is used, as shown in Fig. 38. A characteristic example for the polymerization of 2VP in THF at $-78\ ^{\circ}$C is given below.

- The ampoules containing the initiator, *sec*-BuLi, and terminating agent MeOH are attached to the main reactor. The apparatus is connected to the vacuum line through a ground glass joint, checked for pinholes, flame dried, and pumped for 30 min in order to remove the volatile species such as air and humidity.
- Then 4 mL of a concentrated solution of *n*-BuLi in hexane and 2 mL of DPE are injected into the purge section through the septum, and the tube holding the septum is removed by heat sealing at (A). The apparatus is pumped for another ½ h in order to remove hexane and air inserted in the apparatus during the injection, followed by distillation of the required amount of purified THF solvent into purge section through the vacuum line.
- The reactor is removed from the vacuum line by heat sealing at (B). The inner walls of the reactor are washed by the red solution of *n*-BuLi and DPE; this solution is transferred back to purge section and placed in a 50 $^{\circ}$C water bath. Because of the vacuum inside the apparatus, THF refluxes and condenses over the whole reactor, rinsing traces of *n*-BuLi + DPE from the glass walls.
- Again by transferring solution to the purge section manually, as a consequence, all *n*-BuLi + DPE inserted along with the products of reaction impurities are collected in the purge section.
- A water bath at 30 $^{\circ}$C is placed under the purge section and an ice–water bath is placed under the reactor flask. Due to the vacuum in the apparatus, the solvent is distilled into the main reactor but the nonvolatile species, that is, *n*-BuLi, DPE, and its reaction products with impurities, remain in purge section.
- The purge section is removed by heat sealing at constriction (C) leaving a clean reactor filled with an appropriate amount of pure solvent. The complete cleaned apparatus is kept at $-20\ ^{\circ}$C.
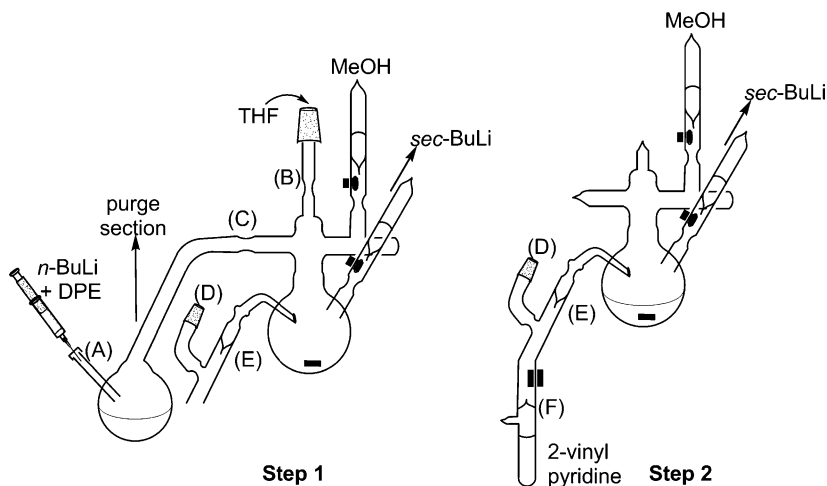
Fig. 38 Apparatus for the polymerization of 2-vinylpyridine

- Prepurified 2-VP over CaH_2 is again purified over Na metal mirror and trioctylaluminum and the final ampoule is connected to the reaction apparatus as shown in Fig. 38 *Step 2*.
- The reaction apparatus is again connected to vacuum line through ground joint D. The area between break seal E and F is flame dried and evacuated very well for longer time.
- The reaction apparatus is removed from the vacuum line by heat sealing.
- The reaction flask is cooled at −78 °C by the cooling mixture of dry ice and isopropanol (cooling mixture is kept below the solvent level).
- The ampoule containing 2-VP is kept in boiling water, and break seal of *sec*-BuLi ampoule is ruptured. Immediately, break seals E and F are ruptured using a double breaker (a breaker with a heavy collection of glass at both ends).
- 2VP is distilled slowly into the reaction flask, and the reaction is carried out with stirring for 20–30 min at −78 °C.
- The ampoule containing MeOH is ruptured, and the reaction is terminated to obtain linear poly(2-vinylpyridine).
- After opening the reaction apparatus, the reaction mixture is poured into *n*-hexane to precipitate the final linear homopolymer.

List of Abbreviations and Symbols

2VP	2-Vinyl pyridine
Bd	1,3-Butadiene
CaH_2	Calcium hydride
D3	Hexamethylcyclotrisiloxane

DBMg	Dibutylmagnesium
DCMSDPE	4-(Dichloromethylsilyl)diphenylethylene
DLI	Dilithium initiator
DPE	1,1-Diphenylethylene
EO	Ethylene oxide
GPC	Gel permeation chromatography
HVTs	High Vacuum Techniques
LN	Liquid nitrogen
M_n	Number-average molecular weight
n-BuLi	*n*-Butyl Lithium
P2VP	Poly(2-vinylpyridine)
PBd	Polybutadiene
PDI	Polydispersity Index
PDMS	Polydimethylsiloxane
PEB	1,3-bis(1-Phenylethenyl)benzene
PI	Polyisoprene
PSLi	Polystyryllithium
SEC	Size exclusion chromatography
sec-BuLi	*sec*-Butyl Lithium
TEA	Triethylamine
THF	Tetrahydrofuran
TOA	Trioctyl aluminum

References

1. Quirk RP, Hsieh H (1996) Anionic polymerization – principles and practical application. Marcel Dekker, Inc, New York
2. Szwarc M (1956) "Living" polymers. Nature 178:1168–1169. doi:10.1038/1781168a0
3. Szwarc M, Levy M, Milkovich R (1956) Polymerization initiated by electron transfer to monomer. A new method of formation of block polymers. J Am Chem Soc 78:2656–2657. doi:10.1021/ja01592a101
4. Szwarc M (1968) Carbanions, living polymers, and electron transfer processes. Interscience, New York
5. Quirk RP, Lee B (1992) Experimental criteria for living polymerizations. Polym Int 27:359–367. doi:10.1002/pi.4990270412
6. Penczek S, Kubisa P (1989) In: Kroschwitz JI (ed) Encyclopedia of polymer science and engineering, Supplemental volume. Wiley-Interscience, New York, p 380
7. Flory PJ (1940) Molecular size distribution in ethylene oxide polymers. J Am Chem Soc 62:1561–1565. doi:10.1021/ja01863a066
8. Lee W, Lee H, Cha J, Chang T, Hanley KJ, Lodge TP (2000) Molecular weight distribution of polystyrene made by anionic polymerization. Macromolecules 33:5111–5115. doi:10.1021/ma992121t
9. Iatrou H, Mays JW, Hadjichristidis N (1998) Regular comb polystyrenes and graft polyisoprene/polystyrene copolymers with double branches ("centipedes"). Quality of (1,3-

pheynylene)bis(3-methyl-1-phenylpentylidene)dilithum initiator in the presence of polar additives. Macromolecules 31:6697–6701

10. Fetters LJ (1966) Procedures for homogeneous anionic polymerization. J Res Natl Bur Stand Part A Phys Chem 70:421–433. dx.doi.org/10.6028/jres.070A.035

11. Morton M, Fetters LJ (1975) Anionic polymerization of vinyl monomers. Rubber Chem Technol 48:359–409. doi:10.5254/1.3547458

12. Hadjichristidis N, Iatrou H, Pispas S, Pitsikalis M (2000) Anionic polymerization: high vacuum techniques. J Polym Sci Part A Polym Chem 38:3211–3234

13. Uhrig D, Mays JW (2005) Experimental techniques in high-vacuum anionic polymerization. J Polym Sci Part A Polym Chem 43:6179–6222. doi:10.1002/pola.21016

14. Hadjichristidis N, Fetters LJ (1980) Start-branched polymers 4. Synthesis of 18-arm polyisoprenes. Macromolecules 13:191–194

15. Aliferis T, Iatrou H, Hadjichristidis N (2005) Well-defined linear multiblock and branched polypeptides by linking chemistry. J Polym Sci Part A Polym Chem 43:4670–4673. doi:10.1002/pola.20926

16. Hadjichristidis N, Pispas S, Pitsikalis M, Iatrou H, Vlahos C (1999) Asymmetric star polymers: synthesis and properties. Adv Polym Sci 142:71–127

17. Paraskeva S, Hadjichristidis N (2000) Synthesis of an exact graft copolymer of isoprene and styrene. J Polym Sci Part A Polym Chem 38:931–935

18. Lee C, Gido SP, Poulos Y, Hadjichristidisi N, Tan NB, Trevino SF, Mays JW (1997) H-shaped double graft copolymers: effect of molecular architecture on morphology. J Chem Phys 107:6460–6469

19. Fragouli PG, Iatrou H, Hadjichristidis N (2004) Synthesis and characterization of linear tetrablock quarterpolymers of styrene, isoprene, dimethylsiloxane, and 2-vinylpyridine. J Polym Sci Part A Polym Chem 42:514–519. doi:10.1002/pola.10856

20. Ratkanthwar KR, Hadjichristidis N, Pudukulathan Z (2013) Synthesis and characterization of well-defined regular star polyisoprenes with 3, 4, 6 and 8 arms. Chem J 03:1–11

21. Ratkanthwar K, Hadjichristidis N, Lee S, Chang T, Pudukulathan Z, Vlassopoulos D (2013) Synthesis and characterization of an exact comb polyisoprene with three branches having the middle branch twice the molecular weight of the other two identical external branches. Polym Chem 4:5645. doi:10.1039/c3py00848g

Nonpolar Monomers: Styrene and 1,3-Butadiene Derivatives

Akira Hirao and Katsuhiko Takenaka

Abstract This chapter reviews the living anionic polymerization of styrene, 1,3-butadiene, and their functional derivatives mainly achieved since the mid-1980s. Attention is first focused on the living anionic polymerization of functional styrene derivatives. With the finding of anion-stable functionalities and the successful development of two strategies using protective groups to mask the reactive functionalities and electron-withdrawing functional groups to change the reactivities of monomers and their chain-end anions, a large number of styrene derivatives carrying almost all the useful functionalities acquire the ability to undergo the living anionic polymerization. Secondly, the anionic polymerization of several functional 1,3-butadiene derivatives and the stereochemistry of the resulting polymers will be described. Finally, a variety of chain-functionalization reactions using functional 1,1-diphenylethylene derivatives via a 1:1 addition reaction will be introduced.

Keywords Living anionic polymerization • Functional styrene derivatives • Functional 1,3-diene derivatives • Functional 1,1-diphenylethylene derivatives • Stereochemistry

A. Hirao
Polymeric and Organic Materials Department, Graduate School of Science and Engineering, Tokyo Institute of Technology, 2-12-1, Ohokayama, Meguro-ku, Tokyo 152-8552, Japan

Institute of Polymer Science and Engineering, National Taiwan University, No.1, Sec.4, Roosevelt Road, Taipei 10617, Taiwan

College of Chemistry, Chemical Engineering and Materials Science, Soochow University, 199 Ren Ai Road, Suzhou Industrial Park, Suzhou 215123, China

K. Takenaka (✉)
Department of Materials Science and Technology, Nagaoka University of Technology, 1603-1, Kamitomioka, Nagaoka, Niigata 940-2188, Japan
e-mail: ahirao@email.plala.or.jp; ktakenak@vos.nagaokaut.ac.jp

1 Introduction

The major monomers capable of undergoing anionic polymerization are (1) conjugated hydrocarbon monomers like styrene, 1,3-butadiene, isoprene, and their derivatives, (2) electron-deficient polar monomers, such as 2- and 4-vinylpyridines, alkyl acrylates, alkyl methacrylates, alkyl vinyl ketones, *N,N*-dialkylacrylamides, phenyl vinyl sulfoxide, acrylonitrile, methacrylonitrile, nitroethylene, vinylidene cyanides, and α-cyanoacrylate, and (3) cyclic monomers including alkylene oxides, alkylene sulfides, hexamethylcyclotrisiloxane, lactones, lactide, lactams, cyclic carbonates, and α-amino acid *N*-carboxyanhydrides (NCA)s. Among the vinyl monomers listed in (1) and (2), α-substituted vinyl monomers are usually anionically polymerized, while the anionic polymerization of α,α-disubstituted vinyl monomers is possible only when the size of one substituent is small at low polymerization temperatures. The polymerizability of α,β-substituted vinyl monomers is very low due to steric hindrance between a monomer and the chain-end anion. Both α,α,β-trisubstituted and α,α,β,β-tetrasubstituted vinyl monomers usually do not undergo anionic polymerization under normal conditions, since these monomers and their chain-end anions are highly sterically hindered.

In general, the anionic polymerizability of vinyl monomers strongly depends on the electron density on the vinyl group and becomes higher as the electron density on the vinyl group decreases. Accordingly, substituents that have electron-withdrawing characters to reduce the electron density are preferred in order to promote the anionic polymerization. Substituents that stabilize the growing chain-end anions by anion charge delocalization are also preferable in order to render the vinyl monomer polymerizable by an anionic route. Such substituents typically include phenyl, vinyl, imino, carbonyl (ketone and ester), sulfonyl, cyano, and nitro groups. They all have multiple bonds, which are conjugated to the growing chain-end anions to delocalize the anion charges, and most of them belong to electron-withdrawing groups.

As shown in Fig. 1, vinyl monomers carrying these substituents can be roughly categorized into four groups from **A** to **D** according to the degree of electron density on the vinyl group, which is well related to the *e*-value determined by crossover copolymerization. The degree of electron density can also be estimated by the *σ*-value used in the Hammett rule, which reflects the electronic character of the substituent. As can be seen, styrene, α-methylstyrene, 1,3-butadiene, and isoprene belong to group **A** as the least reactive monomers in the anionic polymerization. Monomers in groups **B** and **C** correspond to 2-, 4-vinylpyridine, alkyl acrylates, methacrylates, *N,N*-dialkylacrylamides, vinyl phenyl sulfoxide, and vinyl alkyl (or aryl) ketone, vinyl alkyl sulfone, acrylonitrile, and methacrylonitrile. The most reactive monomers categorized in **D** group involve nitroethylene, α-cyanoacrylates, and vinylidene cyanide.

Highly reactive anionic initiators are required to polymerize the least reactive group **A** monomers, while the most reactive monomers in **D** group can be polymerized with very weak bases or nucleophiles, even water and alcohols. Based on
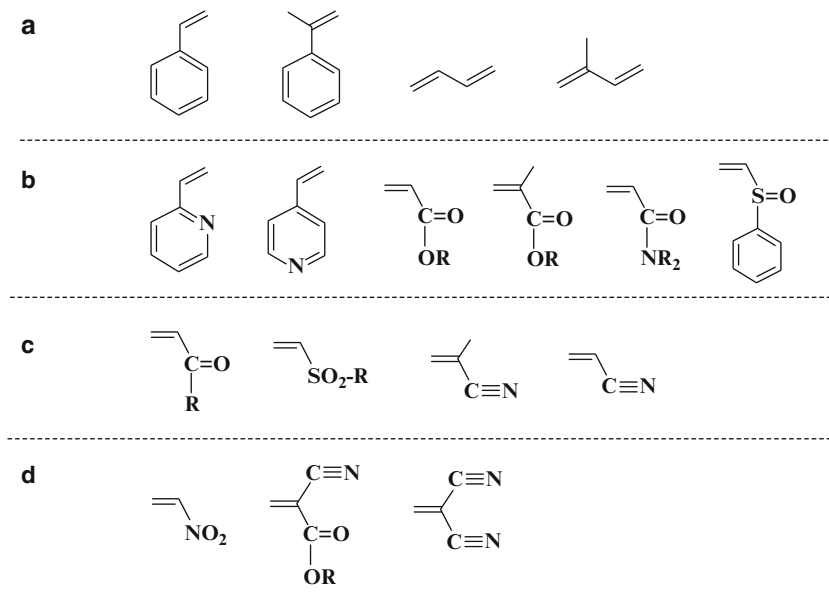
Fig. 1 Monomers in groups **a**, **b**, **c**, and **d**

the nucleophilicity and basicity, anionic initiators can also be roughly divided into four classes from **a** to **d**, as shown in Fig. 2. Alkali-metals, alkali-metal naphthalenides, organolithium (RLi), sodium, and potassium compounds correspond to the most reactive class **a** initiators, which readily and quantitatively initiate the polymerization of the least reactive group **A** monomers. It is a matter of course that all the monomers in groups **B**, **C**, and **D** can be polymerized with each initiator belonging to class **a**. The initiators in the second class **b** involve triphenyl-methyllithium, Grignard reagents, alkali-metal hydrides, alkali-metal dialkylamides, the anion radical complexes of aromatic ketones and alkali-metals, flurorenyllithium, conjugated anions derived from active methyl or methylene compounds, ate complexes such as $LiAlR_4$ and $NaZnR_3$, and $LiAlH_4$. These initiators cannot polymerize the **A** group monomers, but can possibly initiate the polymerization of the monomers in the **B** as well as **C** and **D** groups. Alkali-metal hydroxides and alkoxides, ZnR_2, and certain strong amines like sparteine and 1,4-diazabicyclo-[2,2,2]octane are the initiators for class **c** and can polymerize the monomers in **C** and **D** groups. The least reactive class **d** initiators are ammonia, amines, phosphines, ethers, and even alcohols and water having lone pairs. They can polymerize only the most reactive group **D** monomers, but are too weak to initiate the polymerization of any of the monomers belonging to group **A**, **B**, and **C**. Thus, there seems to be a distinct relationship between the monomer and initiator for the anionic polymerization shown in Fig. 3. Accordingly, it is very important and critical for selecting the correct combination of initiator and monomer for the polymerization.

a   Alkali-metals (Li, Na, K) $\left[\text{naphthalene}\right]^{\ominus}\overset{\cdot}{}M^{\oplus}$

RLi, RNa, RK

(R = Alkyl, Aryl)   (M = Li, Na, K)

Ph_3CLi, RMgX, MH and MNR_2 (M = Li, Na, K), $LiAlR_4$, $NaAlR_4$, $NaZnR_3$

b $[Ph_2C=O]^{\overset{\cdot}{\ominus}}M^{\oplus}$ (fluorenyl) $R\,M^{\oplus}$ $\ominus$ $R\text{-}\overset{\ominus}{CH}\text{-}C(=O)\text{-}OR'$ $M^{\oplus}$ $R\text{-}\overset{\ominus}{CH}\text{-}C{\equiv}N$ $M^{\oplus}$ $LiAlH_4$

(M = Li, Na, K)

---

c   MOH and MOR (M = Li, Na, K), Et_2Zn (sparteine structure)   (DABCO-type structure)

---

d NH_3, NH_2R, NHR_2, NR_3, PR_3, R-O-R', R-OH, H-O-H
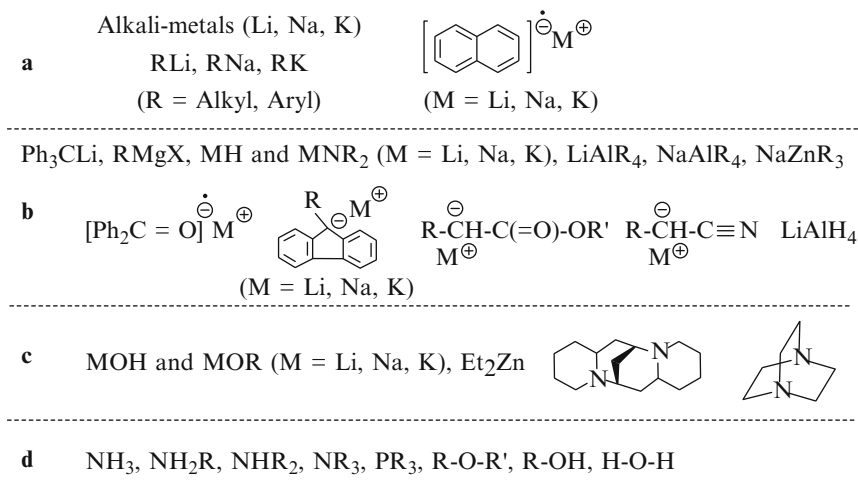
Fig. 2 Initiators in class **a**, **b**, **c**, and **d**

Fig. 3 Relationships among initiator and monomer in the polymerization

Initiator   *Monomer*

a ──────────────────────────► **A**

b ──────────────────────────► **B**

c ──────────────────────────► **C**

d ──────────────────────────► **D**
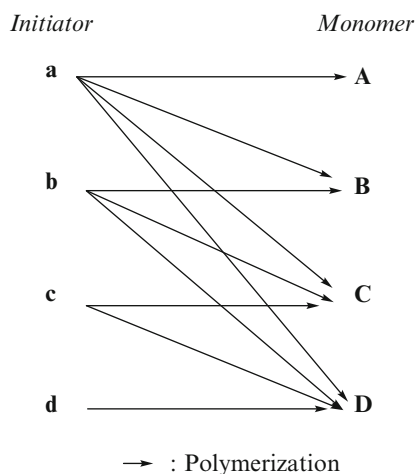
──► : Polymerization

Furthermore, the careful choice of an initiator is needed in some cases. For example, highly reactive **a** class initiators can polymerize not only the group **A** monomers but also monomers in the **B**, **C**, and **D** groups, as already mentioned. However, such initiators can also react with polar substituents in the monomers belonging to the **B**, **C**, and **D** groups. For example, the anionic polymerization of methyl acrylate (**B** group) with *sec*-BuLi (**a** class) proceeds with significant termination and/or transfer reactions due to the reactions of the ester carbonyl with *sec*-BuLi and the propagating chain-end anion. Moreover, α-proton abstraction of the vinyl group can occur with these carbanionic species (see Scheme 1).
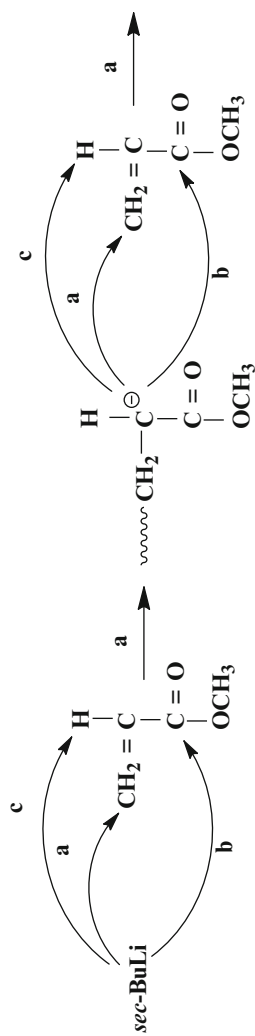
Scheme 1 Reactions of *sec*-BuLi or chain-end anion with methyl acrylate

One more important aspect of the anionic polymerization is the relationship between the monomer reactivity and the reactivity of the propagating chain-end anion. Since a monomer corresponds to the conjugate acid of the chain-end anion, the less reactive monomer basically produces the more reactive chain-end anion and vice versa. This is readily estimated by the pK_a value of the methyl derivative of the corresponding substituent. This relation is especially important for the synthesis of random as well as block polymers with the use of different monomers. For instance, styrene of the group **A** monomers produces a reactive propagating chain-end anion that polymerizes methyl methacrylate (MMA) of the more reactive group **B** monomer, resulting in the expected diblock copolymer of polystyrene (PS)-*b*-PMMA. On the other hand, the chain-end anion derived from MMA is less reactive and incapable of polymerizing styrene. Consequently, only the MMA homopolymer was recovered in this case. Thus, block polymers can be synthesized only by sequential addition of monomers in the order of decreasing reactivity of the chain-end anion. Similarly, the random copolymerization of styrene and MMA resulted in the formation of the almost homopolymer of MMA including a small amount of the styrene unit, which was incorporated during the very early stage of the copolymerization. Thus, the reactivities of both the monomer and the propagating chain-end anion should be kept in mind whenever anionic polymerization and copolymerization are carried out. These described subjects are also well summarized in books previously published [1–4].

One of the most important and advantageous features of the anionic polymerization is the establishment of the living anionic polymerization system of several monomers, since this system enables the precise synthesis of polymers with well-controlled molecular weights and nearly monodisperse molecular weight distributions and the tailored synthesis of block polymers and macromolecular architectures, such as graft, star-branched, and hyperbranched polymers. The first successful example of the living polymerization system was the anionic polymerization of styrene with sodium naphthalenide in THF reported in 1956 by Szwarc et al. [5]. Soon after, it was reported by Morton et al. that 1,3-butadiene and isoprene underwent the living anionic polymerization [6–8]. Monomers carrying polar substituents, that is, more reactive monomers in the **B**, **C**, and **D** groups, usually competitively polymerize with side reactions of such substituents with initiators and the propagating chain-end anions. Accordingly, the living anionic polymerization of these monomers was initially thought to be difficult. However, with the careful selection of the polymerization variables and conditions and the use of suitable additives, the living anionic polymerizations of 2-vinylpyridine (2VP), alkyl methacrylates, *N,N*-dialkylacrylamides, phenyl vinyl sulfoxide, methacrylonitrile, alkyl isocyanates, and several cyclic monomers, such as alkylene oxides, alkylene sulfides, hexamethylcyclotrisiloxane, lactones, lactides, silicon-bridged [1] ferrocenophanes, and NCAs, are successfully achieved (see Fig. 4).

Among these polymerizations, the most ideal system is undoubtedly the living anionic polymerization of styrene, 1,3-butadiene, and isoprene. However, it has
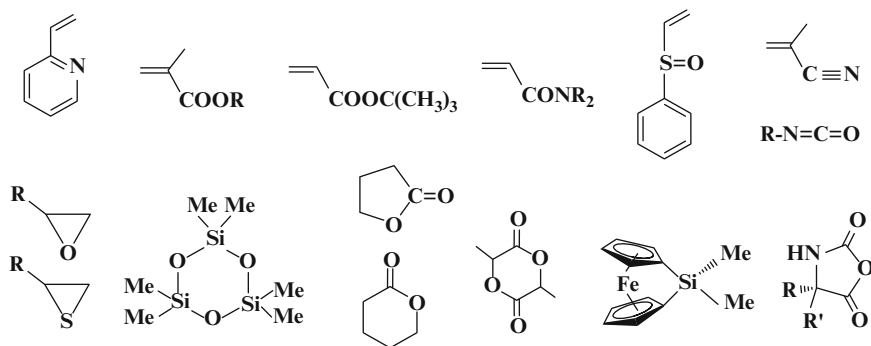
Fig. 4 Monomers capable of undergoing the living anionic polymerization

long been believed that the styrene or 1,3-butadiene derivatives carrying most of the useful functional groups cannot be used in this living polymerization system because such functionalities are not compatible with the highly reactive anionic initiators and propagating chain-end anion. Nevertheless, some functional styrene derivatives were previously reported to undergo the living anionic polymerization. Furthermore, new synthetic strategies have been successfully developed since the early 1980s in order to overcome this problem. With these strategies, the range of monomers feasible for the living anionic polymerization is significantly broadened. In this chapter, attention is focused on the advances in the living anionic polymerization of functional styrene and 1,3-butadiene derivatives mainly achieved during the past 30 years. The living anionic polymerization of the more reactive group **B** monomers with polar substituents will be introduced in the next chapter.

2 Styrene Derivatives

2.1 Living Anionic Polymerization of Functional Styrene Derivatives

The anionic polymerization of styrene has been widely studied from the viewpoints of academic interests and industrial production. As already mentioned, the anionic polymerization of styrene requires highly reactive initiators like RLi compounds and alkali-metal naphthalenides, because styrene belongs to the **A** group of the least reactive monomers. Furthermore, the propagating chain-end anion is also the highly reactive carbanionic species which is similar in reactivity to the above-mentioned anionic initiators. Since styrene is a conjugated hydrocarbon monomer and all the moieties except for the vinyl group are stable toward such highly reactive carbanionic species, it readily undergoes anionic polymerization to produce a stable

Table 1 Molecular weights and molecular weight distributions of PS samples by SEC and TGIC analyses

Sample	M_w(g/mol)		M_w/M_n		
	SEC	TGIC	SEC	TGIC	Poisson distribution
PS-1	35,000	34,400	1.05	1.02	1.002
PS-2	42,900	43,400	1.05	1.01	1.002
PS-3	50,400	50,200	1.05	1.008	1.002
PS-4	56,000	55,200	1.05	1.006	1.002
PS-5	62,000	62,000	1.05	1.005	1.002

PS samples were synthesized with *sec*-butyllithium in cyclohexane at 45 °C.

living anionic polymer and does not have any propensity to undergo either a chain transfer reaction or termination reaction during the course of the anionic polymerization.

The living anionic polymerization of styrene completely fulfills all the criteria of the living polymerization that are proposed by Quirk [9]. Furthermore, there are the following synthetic advantages: first, the molecular weight can be precisely controlled in a wide range from a few 10^3 to even up to the order of 10^6 g/mol. Second, nearly monodispersed molecular weight distributions are realized, the M_w/M_n value being 1.05 or even lower, approaching 1.0. Chang and Lodge et al. reported that size exclusion chromatography (SEC) and temperature gradient interaction chromatography (TGIC) analyses were performed on a set of polystyrene (PS) samples synthesized anionically with *sec*-butyllithium in cyclohexane at 45 °C, in order to investigate their true molecular weight distributions and to compare the Poisson distribution [10]. They confirmed that the molecular weight distribution of the PS samples determined by TGIC is close to the true value of less than 1.01, while the same samples exhibited their M_w/M_n values of 1.05 by SEC analyses, as shown in Table 1. Finally, the chain-end anion is highly reactive as mentioned above, but very stable under the appropriate conditions. Such characteristics are ideally suited for the tailored synthesis of block polymers and other macromolecular architectures, such as graft, star-branched, hyperbranched polymers, and more complex architectural polymers. Several examples of such polymers have been introduced in other chapters of this book.

Since the initiators used in the anionic polymerization of styrene and the resulting propagating chain-end anion are highly reactive carbanionic species, with which most functional groups are considered to be incompatible, it has long been believed that the living anionic polymerization of functional styrene derivatives is difficult or almost impossible. However, it was found that certain functional groups were stable under the living anionic polymerization conditions and the living anionic polymerization of styrene derivatives substituted with such functional groups was successfully achieved. In this section, these examples will be described.
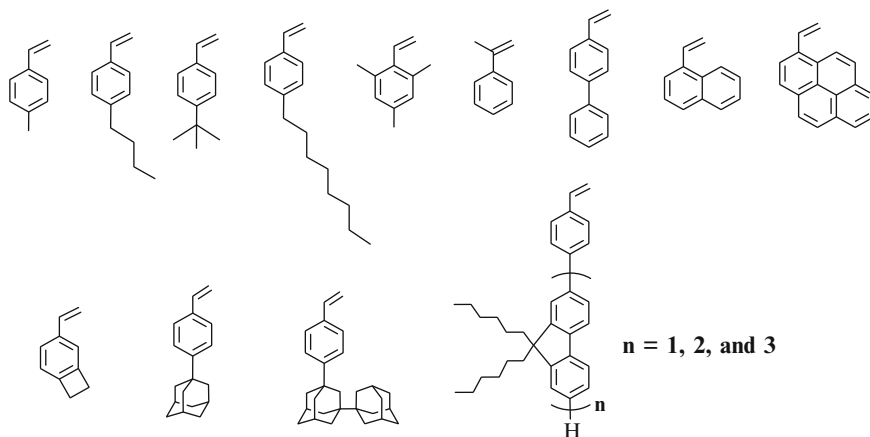
Fig. 5 Alkyl- and aryl-substituted styrene derivatives

2.1.1 Alkyl- and Aryl-Substituted Styrene Derivatives

Soon after the discovery of the living anionic polymerization of styrene in 1956, it was reported from 1960 to 1980 that a variety of styrene derivatives substituted with alkyl or aryl groups underwent the living anionic polymerization. As shown in Fig. 5, they are 4-methylstyrene, 4-butylstyrene, 4-*tert*-butylstyrene, 4-octylstyrene, 2,4,6-trimethylstyrene, α-methylstyrene, 4-vinylbiphenyl, 1-vinylnapthalene, and 1-vinylpyrene. As the styrene derivatives of this class, several new functional styrenes substituted with cyclobutane [11], π-conjugated oligo(fluorene)s [12], or adamantanes [13, 14] have recently been reported. Indeed, the resulting polymers possess interesting functionalities, such as a cross-linking ability at high temperatures, excellent electronic/optoelectronic properties, and high thermal stabilities with T_gs of over 230 °C. Interestingly, the T_g of polystyrene can be dramatically varied in a wide range from −36 °C to over 230 °C by changing the *para*-substituent from 7-octenyl [15] to adamantane.

The success of the living anionic polymerizations of alkyl- and aryl-substituted styrene derivatives can certainly be predicted because alkanes and aromatic compounds are usually stable and compatible with highly reactive carbanionic species.

2.1.2 Alkenyl- and Alkynyl-Substituted Styrene Derivatives

Followed by the living anionic polymerization of alkyl- and aryl-substituted styrenes, the living anionic polymerization of several styrene derivatives substituted with alkenes and alkynes was reported. Normal alkenes nonconjugated via the benzene ring are usually stable toward carbanionic species except for the following specific cases: PhLi adds the highly strained C=C bonds of norbornene and cyclopropene [16]. The intramolecular addition of the organolithium moieties to
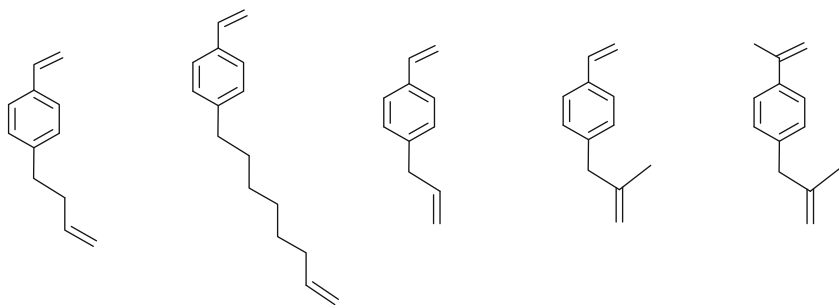
Fig. 6 Alkenyl-substituted styrene derivatives
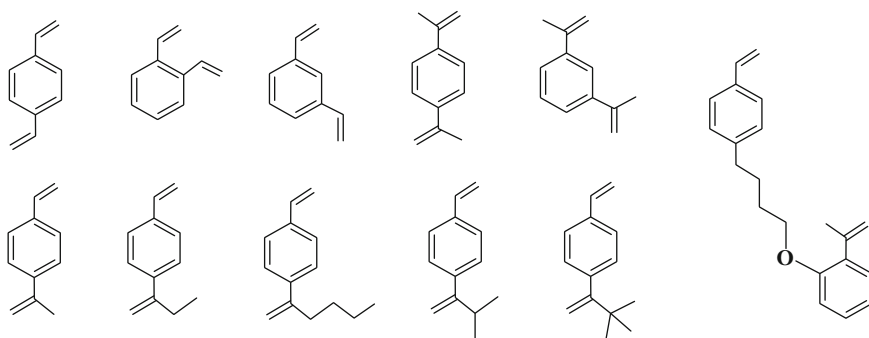
Fig. 7 Divinylbenzene derivatives

the C=C bonds often occurs in ω-alkenyllithium compounds even at lower temperatures [17]. As expected, general alkenyl-substituted styrene monomers like 4-(3-butenyl)styrene [18] and 4-(7-octenyl)styrene [19] shown in Fig. 6 readily underwent the living anionic polymerization. On the other hand, the anionic polymerization of 4-allylstyrene was problematic under the same conditions, resulting in the formation of polymers with multimodal molecular weight distributions [19]. This was possibly due to the allyl proton abstraction, but could be completely suppressed by introducing a methyl group at the 2-position. Indeed, two monomers, 4-(2-methyl-2-propenyl)styrene and 4-(2-methyl-2-propenyl)-α-methylstyrene, were successful in undergoing the living anionic polymerization [19]. The pendant C=C bonds are especially useful for post-functionalizations such as oxidative cleavage to aldehydes and carboxylic acids, hydrosilylation, hydroformylation, hydroboration, and epoxidation reactions.

In contrast, activated alkenes by aryl conjugation can readily react with carbanionic species under typical conditions. 1,4-Divinylbenzene (DVB) and its derivatives of the typical activated alkene-substituted monomers (see Fig. 7) normally underwent the competitive anionic polymerization with the addition reaction of the propagating chain-end anion to the pendant vinyl group to afford cross-linked

materials insoluble in solvents. Both 1,3- and 1,4-diisopropenylbenzenes were anionically polymerized to give soluble polymers with relatively narrow molecular weight distributions ($M_w/M_n \sim 1.3$) during the early stage of polymerization (~50 % conversion) [20]. As expected, branching gradually occurred as the polymerization proceeded, and insoluble polymers by cross-linking were obtained at the conclusion of the polymerization.

With the introduction of an alkyl group at the α-position of a pair of $C = C$ bonds in 1,4-divinylbenzene to provide steric hindrance as well as to increase the electron density on the double bond, the living anionic polymerization became feasible. The anionic polymerization of a series of 4-(α-alkylvinyl)styrene derivatives thus designed smoothly proceeded in a living manner with the use of the anionic initiators bearing K^+ to afford polymers with predictable molecular weights ($M_n = 5,000–82,000$ g/mol) and narrow molecular weight distributions ($M_w/M_n = 1.02–1.06$) [21–23]. The stability of the resulting living polymer strongly depended on the bulkiness of the alkyl substituent. The living polymers derived from 4-(α-methylvinyl)styrene and 4-(α-ethylvinyl)styrene were stable for 10 min in THF at $-78\ °C$, while the living anionic polymer of the corresponding isopropyl-substituent monomer was stable for at least 1 h. Moreover, the living polymer of 4-(α-*tert*-butylvinyl)styrene was very stable even after 48 h and found to retain the narrowness of the molecular weight distribution. It was also stable in benzene at room temperature for at least a few hours.

It was also possible to suppress the unwanted addition reaction of the chain-end anion to the pendant double bond by introducing an electron-donating alkoxy group into the benzene ring in α-methylstyrene. A new specially designed dual-functionalized styrene having the α-methylstyrene moiety, 4-(4-(2-isoprope-nylphenoxy)butyl)styrene, successfully underwent the living anionic polymerization to afford the polymers with predictable molecular weights ($M_n = 5,000–65,000$ g/mol) and narrow molecular weight distributions ($M_w/M_n = 1.02–1.04$) [24, 25].

As already mentioned, the cross-linked polymers insoluble in solvents were always obtained by the anionic polymerization of DVB. Very recently, Hirao et al. demonstrated for the first time that one of the two vinyl groups of DVB exclusively and selectively polymerized in a living manner in THF at $-78\ °C$ with an initiator system prepared from *sec*-BuLi or oligo(α-methylstyryl)lithium and a 10-fold excess of KOBu^t [26]. As shown in Fig. 8, a soluble linear poly(DVB) with a predictable M_n value and a nearly monodisperse distribution was quantitatively obtained. The resulting living polymer was stable for a few minutes at $-78\ °C$, but stable even after 30 min at $-95\ °C$. Under such conditions, any unwanted addition reaction was almost suppressed and the polymers with controlled M_n values (11,000–60,500 g/mol) and narrow molecular weight distributions ($M_w/M_n = 1.02–1.04$) were obtained. The living nature of the polymerization was also supported by the successful synthesis of the well-defined block copolymers of poly (DVB)-*b*-poly(2VP) and poly(DVB)-*b*-poly(*tert*-butyl methacrylate) [27, 28].

The suppression of the unwanted addition reaction, which essentially occurred during the polymerization, may be explained as follows: it is considered that the

Fig. 8 SEC profile of poly
(DVB) ($M_n = 26{,}400$, $M_w/M_n = 1.04$)
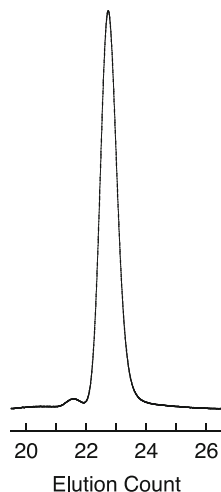
counter cation is completely replaced by K^+ and the chain-end anion is significantly shifted to the less reactive ion pair by the presence of a large excess of $KOBu^t$. Some $KOBu^t$ molecules may coordinate to the chain-end anion by an ionic interaction to provide a steric bulkiness around the chain-end anion. The two vinyl groups of DVB are activated by a long conjugation from the vinyl group to the other vinyl one via the benzene ring. After the polymerization, the pendant vinyl group becomes much less reactive due to the disappearance of the long conjugation and the electron-donating effect of the main chain alkyl ($-CH_2-CH-$) formed by the polymerization. Accordingly, the resulting less reactive and sterically bulkier chain-end anion may very slowly add to the less reactive pendant vinyl group, while one of the activated double bond of the monomer can be preferentially reacted with the chain-end anion to allow the polymerization as illustrated in Scheme 2.

It is known that carbanionic species react with the $C \equiv C$ bonds that are activated by aryl conjugation. Furthermore, the hydrogen directly attached to the $C \equiv C$ bond and methyl and methylene protons next to the $C \equiv C$ bond are acidic enough to react with the carbanionic species. Nonetheless, the living anionic polymerization of both 4-(3,3-dimethyl-1-butynyl)styrene and 4-phenylethynylstyrene shown in Fig. 9 was successfully carried out at $-78\ °C$ [29]. The living anionic polymerization of 4-(1-hexynyl)styrene having active methylene protons was also feasible under the same conditions. The success of the living anionic polymerization of such styrenes may be attributed to the stabilization of the chain-end anions by charge delocalization via the conjugation systems from the benzene rings to the $C \equiv C$ bonds. As would be expected, the polymerization of 4-(1-hexynyl)styrene either in THF at $0\ °C$ or in benzene at $20\ °C$ gave the polymers with multimodal distributions of molecular weight, possibly due to proton abstraction of the methylene chain next to the $C \equiv C$ bond during the polymerization. Since 4-ethynylstyrene cannot be anionically polymerized possibly due to the proton abstraction of the anionic

Scheme 2 Polymerization of DVB with a less reactive and bulkier chain-end anion
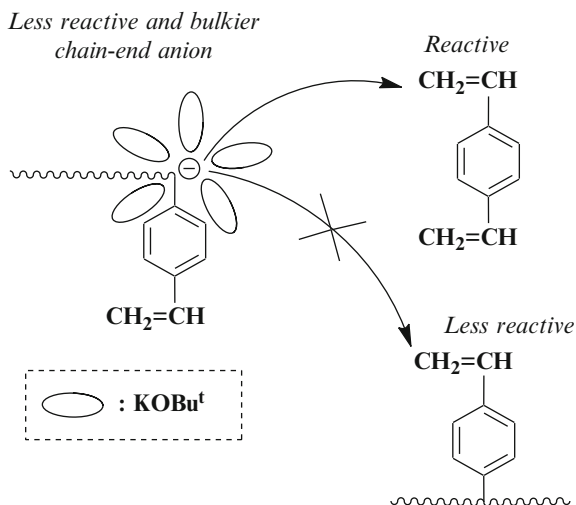
Fig. 9 Alkynyl-substituted styrene derivatives
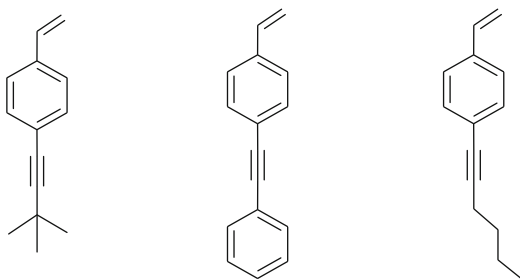
initiator with the acidic proton attached to the $C \equiv C$ bond, protection is needed prior to the polymerization. This will be discussed in the next section.

2.1.3 Ether-, *tert*-Amine-, and Sulfide-Substituted Styrene Derivatives

Ethers and *tert*-amines are often used as solvents or additives in the living anionic polymerization of styrene. This indicates that the living anionic polymerization of styrene derivatives substituted with ethers and *tert*-amines is possible. In practice, the living anionic polymerizations of 2- and 4-methoxystyrenes, 4-*tert*-butoxystyrene [30], 4-dimethylaminostyrene [31], 4-dimethylaminomethylstyrene [31], and 4-(2-dimethylaminoethyl)styrene [31] were successfully demonstrated. Interestingly, the specific styrenes substituted with crown ethers were reported to undergo the living anionic polymerization [32]. The resulting living polymers were stable in THF at below −50 °C. Recently, the living anionic polymerization of 4-diphenylaminostyrene [33] and a similar analog [34] was reported to yield
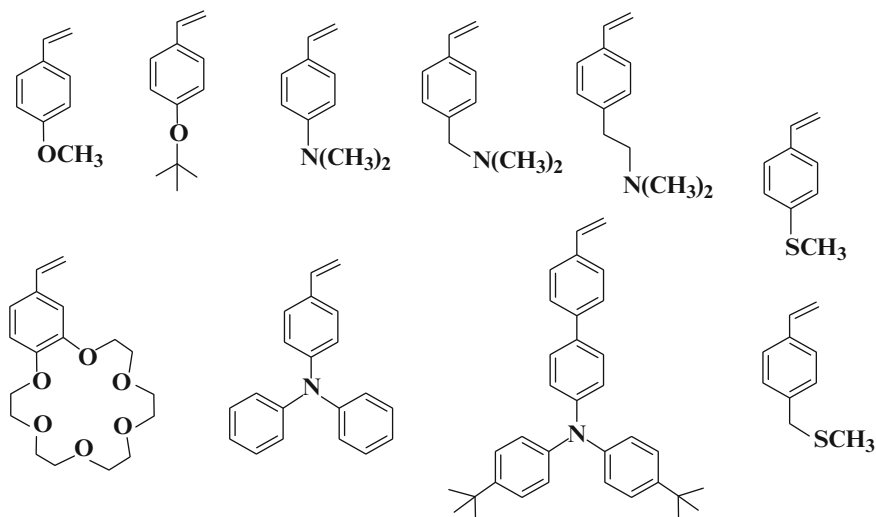
Fig. 10 Ether-, *tert*-amine-, and sulfide-substituted styrene derivatives

interesting functional polymers and block polymers with chromophore and hole-transporting characteristics.

Thioethers (or sulfides) are known to be more reactive toward the carbanions than the corresponding ethers, since the cleavage of the C-S bonds and proton abstraction of the methyl or methylene next to the sulfur atom by carbanions were previously reported. However, it was demonstrated that the living anionic polymerizations of both 4-vinylphenyl methyl sulfide and 2-(4-vinylphenyl)ethyl methyl sulfide were successful in THF at −78 °C [35]. The resulting polymers were observed to possess well-controlled predictable molecular weights and narrow molecular weight distributions ($M_n = 11,000$–$59,000$ g/mol, $M_w/M_n = 1.02$–1.05). On the hand, the anionic polymerization of 4-vinylphenyl methyl sulfide with *sec*-BuLi in benzene at 20 or even 0 °C was problematic. The polymers with broad molecular weight distributions were obtained in low yields, indicating that the above-mentioned reactions occurred during the course of the polymerization. Figure 10 shows all the substituted styrene derivatives capable of undergoing the living anionic polymerization.

2.1.4 Halostyrene Derivatives

The living anionic polymerizations of 4-chlorostyrene and 4-bromostyrene were reported in 1976 (Shima et al.) and 1983 (Königsberg et al.), respectively. In contrast to these results, it was also reported that serious side reactions occurred in the same polymerization systems to give polymers with broad or multimodal molecular weight distributions. The repeated polymerization of both monomers under the same conditions by our group also yielded similar polymers whose

Fig. 11 2- and
4-fluorostyrenes
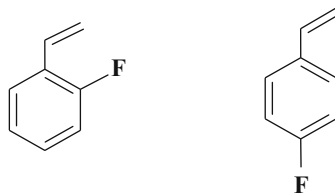
molecular weight distributions were multimodal in all cases. Thus, the above polymerization results appear extremely doubtful. On the other hand, both 2- and 4-fluorostyrenes shown in Fig. 11 were observed to quantitatively polymerize in a living manner in THF at $-78\ ^\circ$C to afford polymers with predictable molecular weights ($M_n = 13,000-47,000$ g/mol) and narrow molecular weight distributions ($M_w/M_n = 1.07-1.10$) [36]. The stability of the C-F bond toward carbanion is thus obvious.

2.1.5 Metal-Containing Styrene Derivatives

Since the silicon atom is situated next to the carbon atom in periodic table, the C-Si bond is considered to be relatively stable to both nucleophilic and electrophilic attacks. In fact, the C-Si bond is compatible with carbanionic species often used as anionic initiators and many RLi compounds containing C-Si bonds are practically synthesized. The living anionic polymerization of 4-trimethylsilylstyrene was reported in 1982 as the first successful example [37]. Soon after, 4-dimethylvinylsilylstyrene [30] and 4-dimethylallylsilyl-α-methylstyrene [38] were reported to undergo the living anionic polymerization. This success is somewhat surprising because these styrenes involve the reactive vinyl silyl and allyl silyl functions. At almost the same time, Hirao and Nakahama successfully demonstrated that the anionic polymerization of a variety of styrene derivatives with labile Si-O, Si-N, Si-H, Si-Si, and even Si-Si-Si bonds smoothly proceeded in a living manner to afford stable living polymers in THF at $-78\ ^\circ$C [3, 39, 40]. The typical monomers are 4-methoxydimethylsilyl-, 4-ethoxydimethylsilyl-, 4-isopropoxydimethylsilyl-, 4-diethoxymethylsilyl-, 4-triethoxysilyl-, 4-dimethylsilyl-, 4-methylsilyl-, 4-(diethylamino)dimethylsilyl-, 4-pentamethyldisilyl-, and 4-heptamethyltrisilylstyrenes [41] (see Fig. 12). The success of the living anionic polymerization of such styrene derivatives is particularly surprising considering the facts that all the above Si-X (X = O, H, and Si) bonds except for the Si-N bond readily react with RLi compounds and similar reactive carbanionic species. Indeed, the choice of the polymerization conditions proves the critical importance of achieving their living anionic polymerizations. The resulting polymers were all precisely controlled in M_n values up to 100,000 g/mol, narrowly distributed in molecular weight distributions ($M_w/M_n < 1.1$) and possessed valuable functional polymers with reactive silyl groups useful for the post-functionalization.
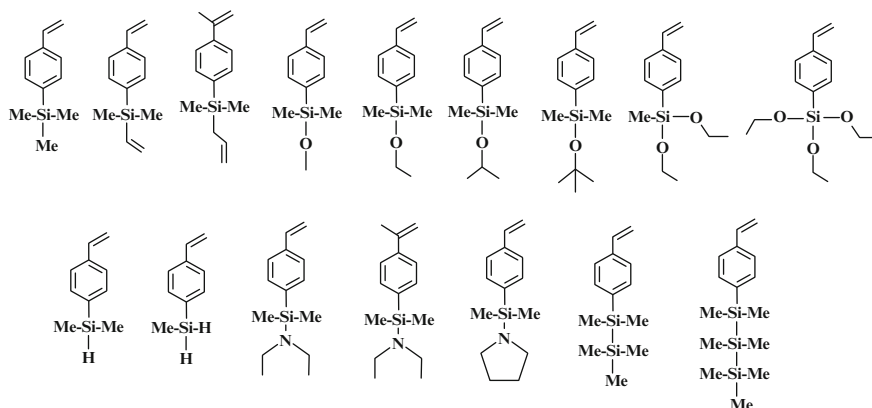
Fig. 12 Styrene derivatives substituted with functional silyl groups
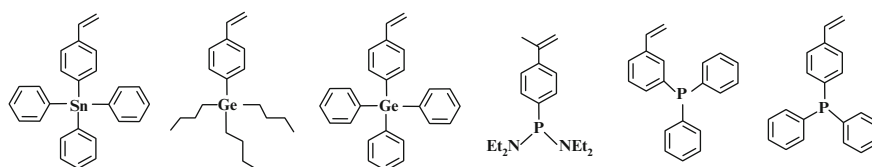
Fig. 13 Metal-containing styrene derivatives

Although germanium and tin atoms also belong to the same family as carbon, C-Ge and C-Sn bonds are more reactive with nucleophilic reagents than the C-Si bond. However, the living anionic polymerization of 4-tributylgermyl- and 4-triphenylgermylstyrenes and 4-triphenyltinstyrene shown in Fig. 13 was realized in THF at −78 °C [42, 43]. Fujimoto et al. reported the living anionic polymerization of 4-bis(diethylamino)phosphio-α-methylstyrene to yield the polymers with predictable molecular weights and narrow molecular weight distributions [44]. Thus, the P-N as well as P-C bonds were sufficiently stable below −30 °C under the living anionic polymerization condition. The (diethylamino)phosphio group was readily hydrolyzed and converted to either the HP(O)(OH) or P(O) (OH)$_2$ group. The living anionic polymerizations of both 3- and 4-diphenylphosphinostyrenes with *tert*-BuLi in THF at −85 °C were also reported [45]. The stability of the P-C bond toward the carbanionic species was again demonstrated. The resulting polymers are expected to be polymeric ligands that can complex with transition-metal catalysts or stabilize metal nanoparticles.

In this Sect. 2.1, the living anionic polymerizations of several functional styrene derivatives were introduced. It was found that the number of functional groups amenable to the living anionic polymerization was more than that might be expected. The chain-end anions derived from such functional styrene derivatives are roughly comparable in reactivity to the chain-end anion of polystyrene from the observation that crossover block copolymerization of each monomer with styrene is
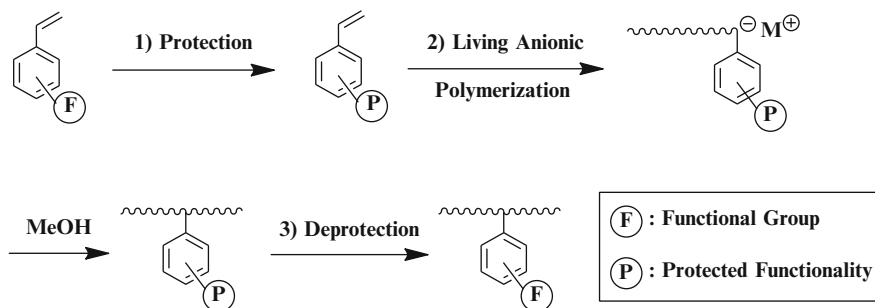
Scheme 3 Protection and living anionic polymerization of functional styrene

possible. The molecular weights of the resulting polymers can be precisely controlled in the range from a few thousands to 10^5 g/mol and their M_w/M_n values are usually less than 1.1. It should be mentioned that most of the living anionic polymers described herein are stable enough at -78 °C in THF, but gradually deactivated at elevated temperature. On the other hand, styrene derivatives substituted with alkyl, aryl, *tert*-amino, and trimethylsilyl groups undergo the living anionic polymerization with RLi compounds in hydrocarbon solvents at room temperature or higher temperatures, thus affording stable living polymers.

2.2 Protection and Living Anionic Polymerization of Functional Styrene Derivatives

2.2.1 Protective Strategy

Functional groups having active hydrogen(s) and/or carbonyl groups, such as OH, SH, SiOH, NH_2, $C \equiv CH$, CHO, COR, and COOH, are not compatible with the anionic initiators used for the polymerization of styrene and the chain-end anion, thus rendering the living anionic polymerization of styrene derivatives substituted with such functionalities very difficult or probably impossible. As one of the solutions to overcome this difficulty, the strategy of introducing the concept of protection into living anionic polymerization was proposed by Hirao and Nakahama in the 1980s [3, 4, 40, 46–49]. It involves the following three reaction steps, as illustrated in Scheme 3: first, the functional group is suitably masked by an appropriate protective group to convert it to a stable form under the living anionic polymerization conditions. Second, the resulting styrene carrying the protected functionality is subjected to the living anionic polymerization. Finally, the protective group is removed to regenerate the original functional group after the polymerization. Important in this strategy is that the protected functionality is required to be completely stable during the course of the living anionic polymerization. Otherwise, the polymerization cannot be controlled due to the termination and/or
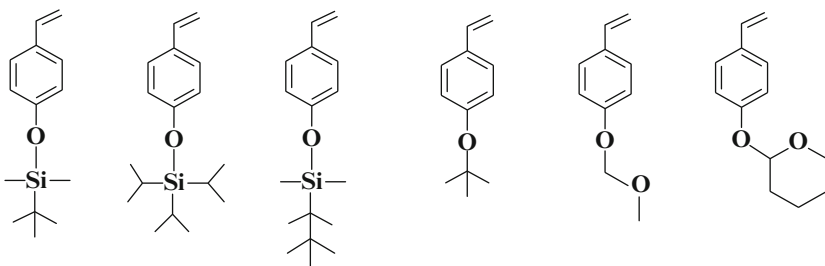
Fig. 14 Silyl-, ether-, and acetal-protected 4-vinylphenol derivatives
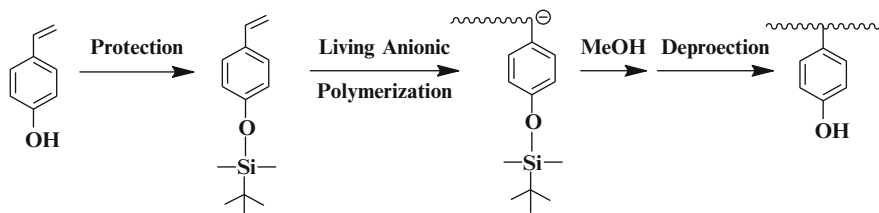
Scheme 4 Synthesis of well-defined poly(4-vinylphenol) by the living anionic polymerization of TBDMSOS, followed by deprotection

transfer reactions. One more requirement is the quantitative removal of the protective group after polymerization without damaging the resulting polymers. The reason is that, unlike low-molecular-weight compounds, the residual protected functionality and/or unwanted byproducts cannot be separated from the regenerated original functional group on the same polymer chain. If this strategy indeed works, the resulting polymer should have a functional group in each monomer unit and retain all the advantageous features of the living anionic polymerization.

The first successful example of this strategy using a protective group is the synthesis of poly(4-vinylphenol)s with well-controlled and nearly monodispersed chain lengths by the living anionic polymerization of 4-*tert*-butyldimethylsilyloxystyrene (TBDMSOS) shown in Fig. 14, a protected form of 4-vinylphenol with the *tert*-butyldimethylsilyl (TBDMS) group, and the subsequent removal of the silyl protective group to regenerate the phenolic hydroxyl group [50]. As shown in Scheme 4, the phenolic hydroxyl group of 4-vinylphenol is first masked by a TBDMS protective group and the resulting monomer, TBDMSOS, is subjected to the anionic polymerization in THF at −78 °C with *sec*-BuLi as the initiator. After mixing the initiator with the monomer, a reddish orange color, similar to living polystyrene, immediately appeared and remained unchanged even after 24 h. The polymerization efficiently proceeded to quantitatively yield the poly(TBDMSOS). The resulting polymer exhibited a sharp monomodal SEC peak ($M_w/M_n = 1.04$) and possessed an M_n value of 54,000 g/mol in good agreement with the predictable value of 52,000 g/mol. This protected monomer, TBDMSOS, was also polymerized with each of the various initiators, such as BuLi, lithium, sodium, or potassium

Table 2 Anionic polymerization of TBDMSOS in THF at -78 °C for 1 h

Initiator	M_n(g/mol)		M_w/M_n	
	Calculated	SEC-RALLS	SEC	SEC-RALLS
sec-BuLi	10,500	11,100	1.04	1.02
sec-BuLi	27,200	28,400	1.02	1.01
sec-BuLi	110,000	114,000	1.02	1.01
sec-BuLi/αMS[a]	45,000	51,000	1.03	1.01
Li-Naph	10,000	11,000	1.05	1.02
K-Naph	20,000	20,000	1.07	1.03
K-Naph/αMS[b]	43,300	48,400	1.05	1.02

[a]Oligo(α-methylstyryl)lithium
[b]Oligo(α-methylstyryl)dipotassium

naphthalenide, oligo(α-methylstyryl)lithium or potassium, and cumylpotassium. The results are listed in Table 2. Similar to the case of styrene, no polymerization occurred with the less reactive anionic initiators like RMgX, LiAlH$_4$, NaH, NaNH$_2$, and KOBu^t.

The TBDMS protective group was readily and quantitatively removed by treatment with 2 N HCl in a mixture of THF and water (5/1, *v/v*) or (C$_4$H$_9$)$_4$NF in THF at room temperature. The resulting poly(4-vinylphenol)s showed narrow monomodal molecular weight distributions almost identical to those of the parent poly (TBDMSOS)s. They were soluble in methanol, ethanol, THF, 1,4-dioxane, acetone, and pyridine, but insoluble in hexane, benzene, toluene, carbon tetrachloride, and chloroform. As expected, they were insoluble in water, but soluble in a 2 N NaOH aqueous solution. Thus, the poly(4-vinylphenol)s are considerably different in solubility from polystyrene.

Similar or sterically bulkier triisopropylsilyl, *tert*-butyldiphenylsilyl, and *tert*-hexyldimethylsilyl protective groups were effective for protection during the course of the living anionic polymerization of their silyl-protected monomers (see Fig. 14) [51, 52]. On the other hand, the protection of the phenolic hydroxyl function of 4-vinylphenol by a less bulky trimethylsilyl, trimethylsilyl, or isopropyldimethylsilyl group was not successful. Thus, a certain steric hindrance of the silyl protective groups is essential for the protection in order to achieve the living anionic polymerization.

As also shown in Fig. 14, the phenolic hydroxyl group could also be protected by converting it to the methoxymethyl, tetrahydropyranyl, or *tert*-butyl ether forms [30, 53]. The resulting styrenes with acetal- or ether-protected hydroxyl functionality underwent the living anionic polymerization to yield stable living polymers in THF at -78 °C. However, small amounts of dimeric or higher molecular weight polymer fractions were often byproducts of their deprotection steps even with very careful treatments.

In addition to the protection of the phenolic hydroxyl group, the TBDMS group was effective for the protection of alcoholic hydroxyl and mercapto groups [54–56]. The TBDMS-protected styrene derivatives shown in Fig. 15 smoothly
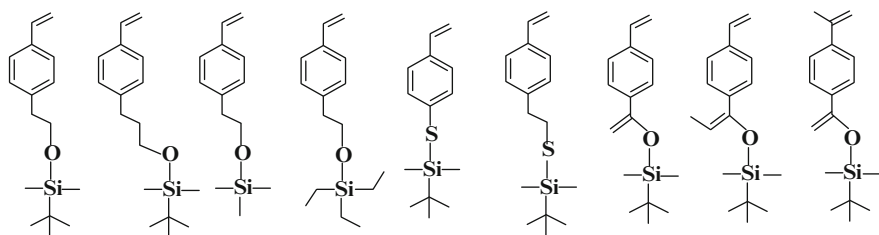
Fig. 15 *tert*-Butyldimethylsilyl-protected hydroxystyrene, mercaptostyrene, and vinylacetophenone derivatives
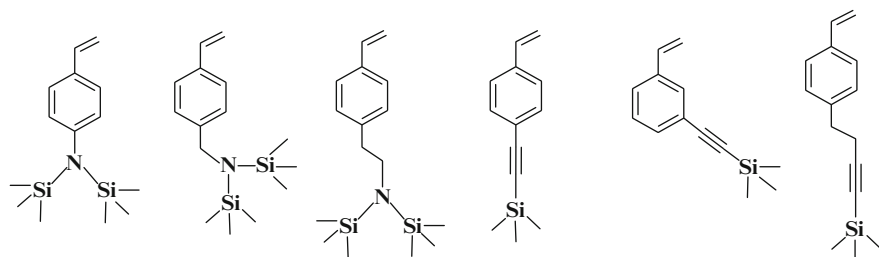
Fig. 16 Trimethylsilyl-protected amino and ethynyl styrene derivatives

underwent the living anionic polymerization. Interestingly, the protection of the alcoholic hydroxyl group by the less bulky trimethylsilyl or triethylsilyl group was possible in order to achieve the living anionic polymerization of such silyl-protected monomers without difficulty.

The TBDMS group was also successful for the protection of the acetyl group of 4-vinylacetophenone by converting it to the TBDMS enol ether form, followed by the living anionic polymerization of this protected monomer (see Fig. 15) [57]. The TBDMS-protected functionality was readily and quantitatively removed by treatment with $(C_4H_9)_4NF$ in THF at room temperature. Similarly, the TBDMS enol ethers of 4-vinylpropiophenone and 4-isopropenylacetophene were observed to undergo the living anionic polymerization ($M_n = 11,000–54,000$ g/mol, $M_w/M_n = 1.02–1.06$). Unfortunately, the trimethylsilyl enol ethers of the three monomers were not stable under the anionic polymerization conditions.

The active hydrogens of 4-aminostyrene could be protected by the trimethylsilyl (TMS) group for the same purpose and the living anionic polymerization of the resulting silyl-protected monomers shown in Fig. 16 was indeed successful [58].

Deprotection of the silyl group was readily achieved by mild acidic hydrolysis or the use of $(C_4H_9)_4NF$ in THF if anhydrous conditions were required. Similarly, two more aminostyrene derivatives were successfully protected by the TMS group [59, 60]. The resulting polymers possessed well-controlled molecular weights and narrow molecular weight distributions ($M_n = 13,000–53,000$ g/mol and $M_w/M_n = 1.04–1.15$).

Table 3 Living anionic polymerization of 4-trimethylsilylethynylstyrene (1), 3-trimethylsilylethynylstyrene (2), and 4-(4-trimethylsilyl-3-butynyl)styrene in THF at −78 °C for 10–60 min

Monomer	Initiator	M_n g/mol		M_w/M_n	
		Calculated	Observed (VPO)	SEC	LS
(1)	K-Naph/αMS[a]	12,000	10,000	1.04	1.02
(1)	K-Naph/αMS	25,000	25,000	1.04	1.02
(1)	sec-BuLi/αMS[b]	42,000	40,000	1.08	1.05
(2)	K-Naph/αMS	23,000	19,000	1.10	1.07
(3)	K-Naph/αMS	12,000	11,000	1.09	1.06
(3)	sec-BuLi/αMS	21,000	20,000	1.07	1.03

[a]Potassium naphthalenide capped with α-methylstyrene
[b]sec-BuLi capped with α-methylstyrene.

No Polymerization
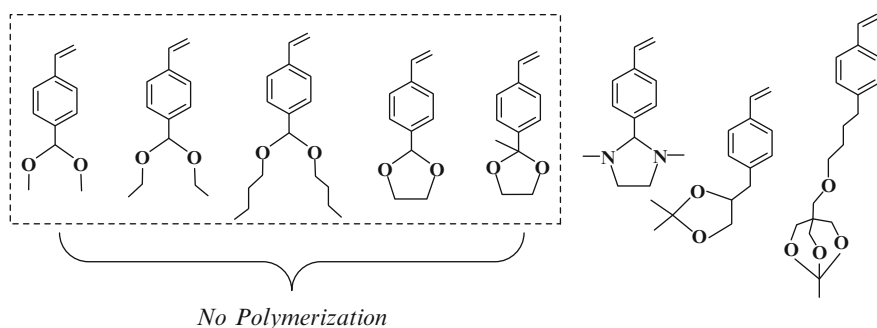
Fig. 17 Acetal-, *N,N*-acetal, and orthoester-protected styrene derivatives

The same TMS protection of the acidic hydrogen of 4-ethynylstyrene is also possible. The resulting protected monomer, 4-trimethylsilylethynylstyrene, underwent the living anionic polymerization in THF at −78 °C [61] (also see Fig. 16). The TMS group was quantitatively removed with $(C_4H_9)_4NF$ in THF at room temperature. The living anionic polymerization could also be achieved under the same conditions by protecting the acidic proton of the C≡C bonds of 3-ethynylstyrene and 4-(3-butynyl)styrene [62, 63]. These results are listed in Table 3.

In organic synthesis, acetals are often used for the protection of aldehydes and ketones and quantitatively deprotected under mild acidic conditions. Acetals are well known to be stable toward RLi and similar reactive carbanionic species. The formyl group of 4-vinylbenzaldehyde was converted to the several acetal forms shown in Fig. 17 and the resulting acetal-protected monomers were subjected to the anionic polymerization. Very surprisingly, no polymerization took place in all cases under various conditions (sec-BuLi, lithium, sodium or potassium naphthalenide, oligo(α-methylstyryl)lithium, or cumylpotassium in THF at −78 °C and sec-BuLi in benzene at 0 or 20 °C). Similarly, the anionic polymerization of the acetal-protected

4-vinylacetophenone was not successful. As compared to the above results, the
N,N-acetal-protected 4-vinylbenzaldehyde (also see Fig. 17) was able to undergo
the living anionic polymerization in THF at −78 °C (M_n = 12,000–40,000 g/mol,
M_w/M_n = 1.05–1.07) [64]. The resulting living polymer was stable after 24 h and
polymerized styrene, isoprene, or MMA to yield the corresponding well-defined
block copolymers.

The hydroxyl groups of the diol and triol can be simultaneously protected as the
anion-stable acetal and structurally similar orthoester forms. The living anionic
polymerization of the acetal- and orthoester-protected styrene derivatives (also see
Fig. 17) was observed to successfully proceed without any problems [65]. As
mentioned before, the acetal protection of the phenolic hydroxyl group of
4-vinylphenol was successful in the living anionic polymerization. Thus, these
results clearly show the sufficient stability of the acetal- and orthoester-protected
functionalities toward the anionic initiators and chain-end anions. Accordingly, the
instability of the acetal-protected functionalities of both 4-vinylbenzaldehyde and
4-vinylacetophenone seems to be peculiar. This will be discussed later.

Silanols were successfully protected as the silyl alkyl ether and silylamine
forms, which were stable under the conditions of the living anionic polymerization
of styrene. These were already discussed in the preceding Sect. 2.1.5. The protec-
tive groups can be quantitatively removed under mild acidic conditions and the
regenerated silanols are generally unstable and immediately form the
corresponding Si-O-Si bonds by dehydration or react with metallic and inorganic
materials via the Si-O-M bonds.

2.2.2   Living Anionic Polymerization of Styrene Derivatives Including Benzyl Ether Skeletons

The ether, silyl ether, acetal, or orthoester form is often used as suitable protective
group for the hydroxyl groups as well as aldehydes, ketones, and carboxylic acids.
In practice, the phenol, alcohol, diol, and triol functions were protected by
converting them to ether, silyl ether, acetal, and orthoester forms and the resulting
protected styrene derivatives successfully underwent the living anionic polymeri-
zation without any difficulty. This success clearly demonstrates that such protected
functionalities are basically stable toward the anionic initiators and their chain-end
anions produced during the polymerization. As mentioned in Sect. 2.2.1, however,
the anionic polymerization of the acetal-protected 4-vinylbenzaldehyde and
4-vinylacetophenone was not successful under various conditions. In addition, the
TBDMS-protected   4-vinylphenol   and   4-(2-hydroxyethyl)-   and
4-(3-hydroxypropyl)styrenes could be anionically polymerized in a living manner,
while   the   anionic   polymerization   of   the   TBDMS-protected
4-hydroxymethylstyrene (or 4-vinylbenzyl alcohol) failed under exactly the iden-
tical conditions [52]. Furthermore, both methyl and tert-butyl 4-vinylbenzyl ethers,
regarded as the ether-protected 4-vinylbenzyl alcohol, were not polymerized with
either sec-BuLi, oligo(α-methylstyryl)lithium, lithium naphthalenide, potassium
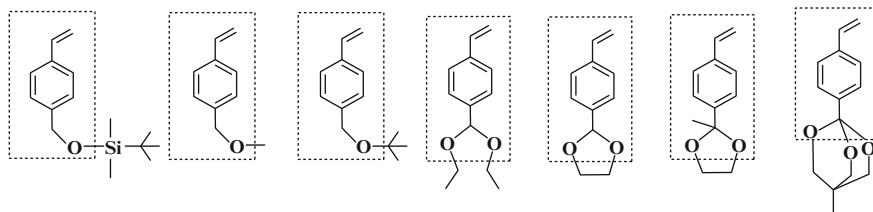
Fig. 18 Silyl ether-,ether-, acetal, and orthoester-protected styrene derivatives
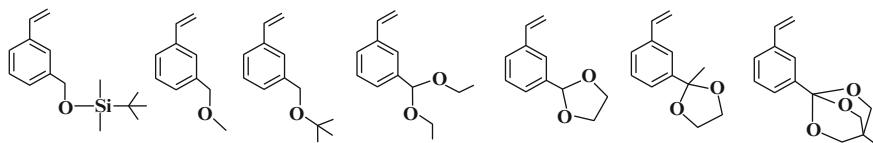
Fig. 19 *meta*-Substituted styrene derivatives with silyl ether, ether, acetal, and orthoester functionalities

naphthalenides, or cumylpotassium in THF at −78 °C as well as with *sec*-BuLi in benzene at 0 or 20 °C [66]. Based on these results, it has been observed that a series of styrene derivatives including both the benzyl silyl ether and benzyl ether skeletons shown in Fig. 18 exhibit anomalous anionic polymerization behaviors. Furthermore, in the polymerization of the acetal- or orthoester-protected monomers listed in Fig. 18, the red color characteristic of oligo(α-methylstyryl)lithium used as the initiator almost instantly disappeared upon mixing with each monomer and no polymer or only small amounts of insoluble polymers were obtained under the conditions in THF at −78 °C [52, 67, 68]. When the difunctional living polystyrene was added to each monomer under the same conditions, gel-like insoluble materials immediately formed in place of the expected block copolymers. IR analyses of such materials showed that they were cross-linked polystyrenes containing a few monomer units used.

In contrast, it was observed that all of the corresponding *meta*-substituted styrene derivatives with the same protected functionalities, as shown in Fig. 19, were successfully polymerized in a living manner in THF at −78 °C to quantitatively afford the polymers with predictable molecular weights ($M_n = 5,000$–50,000 g/mol) and narrow molecular weight distributions ($M_w/M_n < 1.1$) [52, 67, 68]. Both the ABA and BAB triblock copolymers were obtained by the sequential addition of styrene and each monomer to oligo(α-methylstyryl)dilithium or vice versa. Thus, a stable living anionic polymer was obviously obtained from each of the *meta*-substituted monomers. Accordingly, it was proved that the ether, silyl ether, acetal, and orthoester linkages are essentially stable toward the anionic initiators and the chain-end anions derived from these monomers. In a separate experiment, benzyl methyl ether, benzyl TBDMS ether, phenyl-1,3-dioxolane, and benzaldehyde diethylacetal were observed to be completely stable to polystyryllithium (PSLi) in THF at −78 °C even after 24 h. Accordingly, the termination reactions that
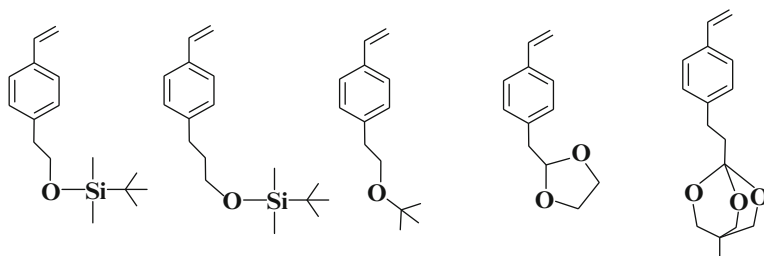
Fig. 20 *para*-Substituted styrene derivatives with silyl ether, ether, acetal, and orthoester functionalities not including the *para*-benzyl ether skeletons
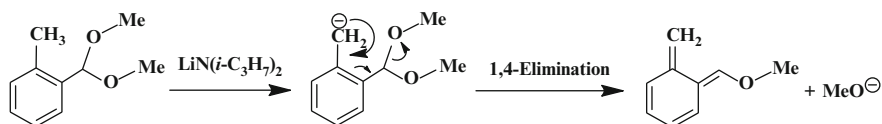
Scheme 5 Reaction of o-tolualdehyde dimethyl acetal with lithium diisopropylamide

occurred during the polymerization of the *para*-substituted styrene derivatives were found to not result from the direct attack on the (silyl)ether, acetal, and orthoester moieties used as protected functionalities by the anionic initiators and/or their chain-end anions if produced.

More importantly and indicatively, the *para*-substituted styrene derivatives shown in Fig. 20, in which their protected functionalities are separated from the benzene rings by one or two methylene chains, successfully undergo the living anionic polymerization under the same conditions [52, 67–69]. Again, these results clearly demonstrated that the silyl ether, ether, acetal, and orthoester functionalities were compatible with the anionic initiators and their chain-end anions. Thus, the anomalous polymerization behavior of the *para*-substituted styrene derivatives may possibly be attributed to the *para*-benzyl ether skeletons included as common structural frameworks, as shown in Fig. 18.

A suggested reaction was previously reported by Rickborn et al. [70, 71]. As shown in Scheme 5, *o*-tolualdehyde dimethyl acetal underwent an anion rearrangement, followed by a 1,4-elimination of the alkoxide anion upon treatment with $LiN(Pr^i)_2$, thus generating the very reactive α-methoxy-*o*-xylylene intermediate. This reaction pathway may also be adaptable to the *para*-isomer, whose carbanion generated by methyl proton abstraction looks very similar to the chain-end anion produced during the anionic polymerization of 4-vinylbenzaldehyde diethyl acetal. As expected, the corresponding *meta*-isomer cannot occur because the compound showing the chemical formula of *m*-xylylene is not present. Thus, the following reaction pathway shown in Scheme 6 was proposed to account for the anomalous polymerization behavior of all the *para*-substituted styrene derivatives including the *para*-benzyl ether skeletons.
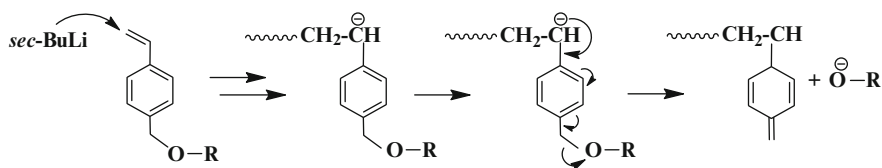
Scheme 6 Proposed reaction pathway occurred in the anionic polymerization
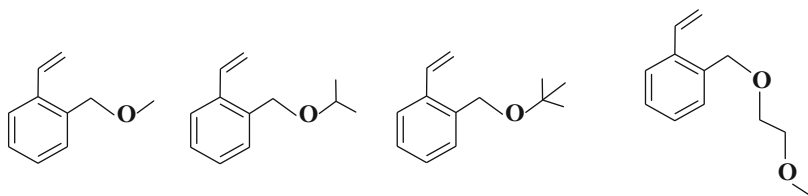
Fig. 21 2-Alkoxymethylstyrene derivatives

As can be seen, a few monomers are polymerized with *sec*-BuLi and the subsequent chain-end anion rearrangement occurs to generate a very reactive *p*-xylylene intermediate via a 1,6-elimination reaction of the alkoxide anion. The coupling reaction between the reactive *p*-xylylene intermediates and/or the addition of the carbanion to the tetraene moiety of the xylylene would then occur during the early stage of the polymerization. Consequently, the corresponding polymer was not produced and most of the unreacted monomer was recovered. With the use of difunctional living polystyrene, the xylylene intermediates may be generated at both chain ends via the same reaction pathway, followed by occurrence of the above unwanted coupling and/or addition reactions, resulting in the formation of the cross-linked polymer.

In order to further ascertain the reaction pathway, 2-methyl-2-(2-vinylphenyl)-1,3-dioxolane of the *ortho*-substituted monomer was subjected to the anionic polymerization [67]. As would be expected, no polymerization took place under the same conditions. The reaction of the difunctional living polystyrene with this monomer yielded an insoluble cross-linked material. Thus, the anionic polymerization of the *ortho*-substituted styrene showed exactly the same behavior as the case using the *para*-isomeric monomer. As already mentioned, 4-methoxymethylstyrene could not be polymerized, while somewhat surprisingly, 2-methoxymethylstyrene of the *ortho*-isomer was observed to polymerize in a living manner in THF at −78 °C [72]. Furthermore, the living anionic polymerization of three other 2-alkoxymethystyrenes shown in Fig. 21 was feasible under the same conditions.

The resulting polymers possessed predictable molecular weights ($M_n = 10,000–33,000$ g/mol) and narrow molecular weight distributions ($M_w/M_n = 1.03–1.09$). However, it was observed that their living anionic polymers were sensitive to temperature and unstable by raising the temperature. The molecular weight distributions became broader and/or multimodal by storing the polymerization mixture at
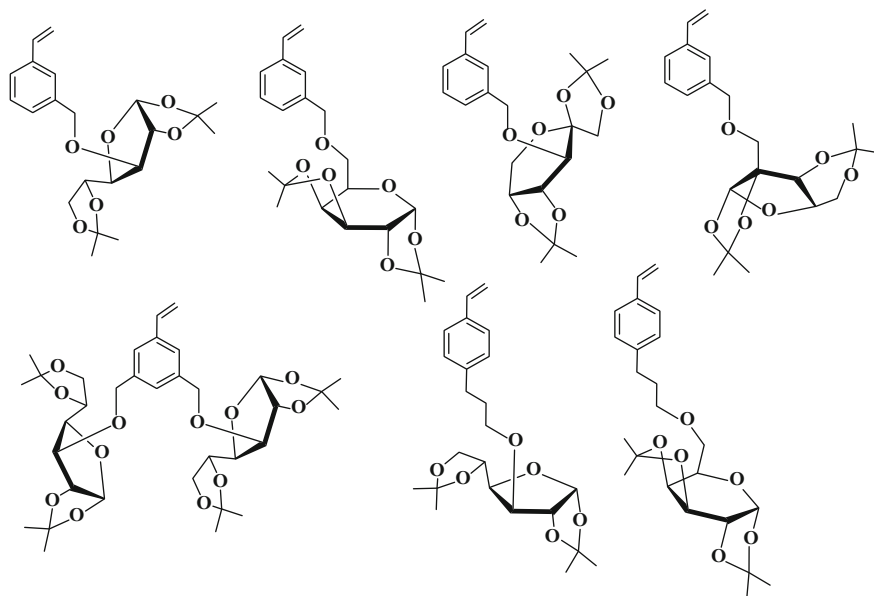
Fig. 22 Styrene derivatives substituted with acetal-protected monosaccharide residues

−30 °C for a few hours, possibly due to occurrence of the above-mentioned
unwanted reaction.

It should be emphasized that the success of the living anionic polymerization of
the protected monomers shown in Figs. 19 and 20 allows access to a variety of new
polystyrenes functionalized with OH, CHO, COR, and COOH groups in each
monomer unit. An advantageous application of this polymerization strategy is the
synthesis of well-defined polystyrene derivatives substituted with various mono-
saccharide moieties. The synthesis was carried out by the living anionic polymer-
ization of several styrene derivatives carrying monosaccharide moieties, whose OH
groups were acetal-protected, followed by removal of the acetal protective group
after the polymerization. The monomers used for this purpose are *meta*-substituted
styrenes or *para*-substituted styrenes except for the monomers containing the
benzyl ether skeletons, as shown in Fig. 22. All the protected styrenes underwent
the living anionic polymerization in THF at −78 °C to afford the polymers with
precisely controlled molecular weights (M_n = 10,000–82,000 g/mol) and narrow
molecular weight distributions (M_w/M_n = 1.04–1.13) [73–76]. Well-defined AB,
ABA, and BAB-type block copolymers of styrene with each monomer could also be
synthesized. After mild acidic hydrolysis, their acetal linkages were readily and
quantitatively removed to regenerate the original monosaccharides such as
D-glucose, D-galactose, D-fructose, and L-sorbose. The resulting well-defined
polymers are attractive water-soluble functional polymers, which have many chiral
centers and ability to recognize specific compounds.
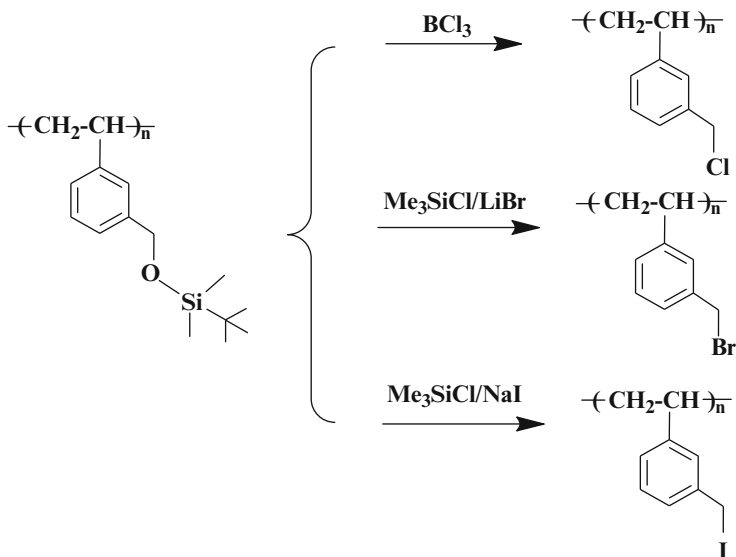
Fig. 23 Synthesis of well-defined poly(*m*-halomethylstyrene)s

One more advantage is the synthesis of poly(*m*-halomethylstyrene)s with well-defined structures. Needless to say, the direct anionic polymerization of *m*-halomethylstyrenes is not possible due to the reaction of the highly reactive benzyl halide moieties with the anionic initiators. Hirao and Hayashi successfully developed the synthesis of poly(*m*-chloromethylstyrene) by the living anionic polymerization of 3-*tert*-butyldimethylsilyloxymethylstyrene and the subsequent transformation of the TBDMS-protected functionality to the *m*-benzyl chloride function by treatment with BCl₃ [77] (see Fig. 23). The complete conversion was achieved in CH₂Cl₂ at 0 °C for 30 min. SEC profiles of the polymers before and after the transformation reaction exhibited almost identical sharp monomodal peaks.

Similarly, both poly(*m*-bromomethylstyrene)s and poly(*m*-iodomethylstyrene)s were synthesized by treatment of the same TBDMS-protected polystyrene with (CH₃)₃SiCl/LiBr and (CH₃)₃SiCl/NaI, respectively [78]. A series of comb-like polystyrenes were successfully prepared by the coupling reaction of poly(*m*-chloro (or bromo)methylstyrene) with living anionic polystyrene end-capped with 1,1-diphenylethylene [79]. These prepared polymers were highly dense comb-like polystyrenes, in which one branch chain per each repeating unit was present and both the branch and main chains were precisely controlled.

In this section, the anionic polymerizations of a series of styrene derivatives composed of benzyl ether skeletons have been examined. The *meta*-substituted styrenes underwent the living anionic polymerization in THF at −78 °C without difficulty, while no appreciable polymerization of the corresponding *para*- and

ortho-isomeric monomers, except for the 2-alkoxymethylstyrenes, occurred under the same conditions. In order to account for this anomalous polymerization behavior depending on the position of the protected functionalities, the reaction pathway involving the generation of the reactive *para*- or *ortho*-xylylene intermediate, via the anion rearrangement and 1,6- or 1,4-elimination reaction of the alkoxide anion, was proposed. For the *para*-substituted styrene derivatives, it was found that the living anionic polymerization made it possible by separating the protected functionalities from the benzene rings by one or two methylene chains. The resulting living anionic polymers are roughly similar in both reactivity and stability to the living polystyrene as well as the living polymers of the styrene derivatives carrying other protected functionalities introduced in Sect. 2.1.
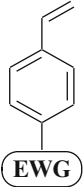
2.3   Living Anionic Polymerization of Functional Styrene Derivatives Substituted with Electron-Withdrawing Groups

As another effective strategy to achieve the living anionic polymerization of functional styrene derivatives, Ishizone et al. introduced a series of electron-withdrawing groups (EWGs) into the styrene frameworks to significantly change the reactivities of the monomers and their chain-end anions [80, 81]. Such EWGs used for this purpose involve *N*-alkyl- and arylimines, *N*,*N*-dialkylamides, 2-oxazoline, alkyl and aryl esters, *N*,*N*-dialkylsulfonamides, and nitrile. Indeed, the anionic reactivities of the styrene derivatives *para*-substituted with these EWGs were remarkably enhanced by their strong electron-withdrawing effects to reduce electron densities on the vinyl groups. This is evidenced by the lower ^{13}C NMR chemical shifts of the vinyl β-carbons of these monomers, as compared to the value of styrene shown in Table 4. These lower values demonstrate that the π-electron densities on the vinyl group decreased to various extents by introducing the above-listed EWGs.

On the other hand, the reactivities of the resulting chain-end anions were significantly lowered by reducing the electron densities on the anions through the same electron-withdrawing effects. These reactivity changes of the monomers and chain-end anions were also confirmed by the crossover block copolymerization of other monomers [82]. Thus, the well-balanced combination between the enhanced monomer reactivities and the reduced reactivities of their chain-end anions made it possible to achieve the living anionic polymerization of EWG-*para*-substituted styrene derivatives. In particular, the reduced chain-end anion reactivities may be attributed to the compatibility of such electron-withdrawing functional groups with the living anionic polymers because these functional groups generally react with the living polystyrene.

Table 4 ^{13}C NMR vinyl β-carbon chemical shift values of *para*-EWG-substituted styrene derivatives
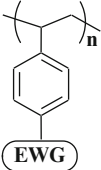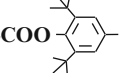
EWG	C_β (ppm)
-H(styrene)	113.8
-CON($^iC_3H_7$)$_2$	114.8
-CH=N-C$_6$H$_{11}$	114.9
(2-oxazoline structure)	115.3
-COOC(C$_4$H$_9$)$_3$	116.0
-SO$_2$N(C$_2$H$_5$)$_2$	117.0
-C≡N	117.6

R = Me, Et, Pr, ^{i}Pr, Allyl   R = Me, Et, ^{i}Pr, ^{t}Bu, Cyclohexyl
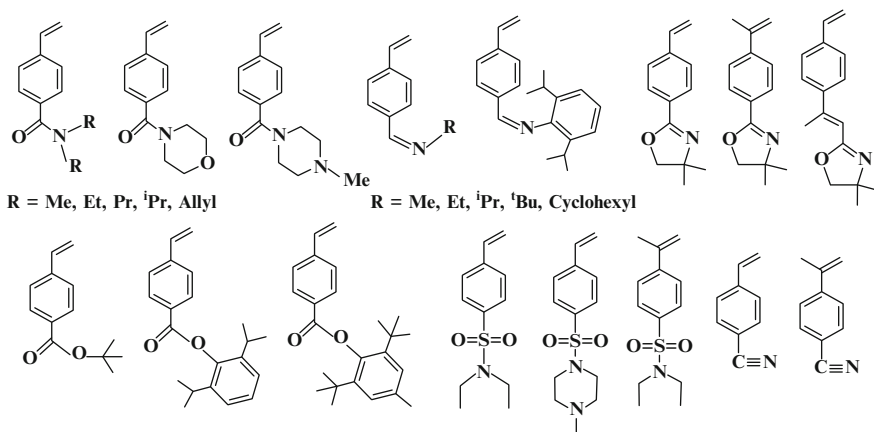
Fig. 24 *para*-EWB-substituted styrene derivatives

All of the successful EWG-substituted styrene derivatives in the living anionic polymerization are shown in Fig. 24. The resulting polymers possessed well-controlled molecular weights ($M_n = 10,000–100,000$ g/mol) and narrow molecular weight distributions ($M_w/M_n = 1.03–1.12$) [83–99]. The typical characterization results are listed in Table 5.

Based on the crossover block copolymerization results, all of the styrene derivatives were found to be more reactive than styrene, while their chain-end anions were less reactive than the living polystyrene [86]. The substituted styrenes with imines, 2-oxazoline, or *N,N*-dialkylamides were similar to 2-vinylpyridine with

Table 5 Living anionic polymerization of *para*-EWG-substituted styrene derivatives

EWG	Mn (g/mol)		Mw/Mn
	calcd	SLS	SEC
$-CO(C_2H_5)_2$	29,000	34,000	1.05
$-CON(^iC_3H_7)_2$	21,000	20,000	1.06
$-CON(CH_2CH=CH_2)$	26,000	23,000	1.08
$-CH=N-C_6H_{11}$	33,000	29,000	1.07
$-CH=N-^iC_3H_7$	22,000	24,000	1.06
(oxazoline)	15,000	13,000	1.06
	67,000	75,000	1.07
$-COO$ (di-tert-butylphenyl)	26,000	32,000	1.04
$-SO_2N(C_2H_5)_2$	33,000	38,000	1.09
	45,000	59,000	1.08
$-C\equiv N$	13,000	14,000	1.05
	99,000	122,000	1.09

Polymerizations were carried out in THF at $-78\ °C$ for 1–24 h.

respect to the reactivities of the monomer and chain-end anion, while the styrenes carrying esters and *N,N*-dialkylsulfonamides were almost comparable to methyl and *tert*-butyl methacrylates in anionic polymerization behavior. Surprisingly, 4-cyanostyrene appears more reactive than *tert*-butyl methacrylate, although it is a styrene derivative. Therefore, a careful addition order of monomers is needed for the synthesis of block copolymers among these EWG-substituted styrenes and other monomers, such as styrene, 2VP, and alkyl methacrylates, by the sequential addition polymerization.

As an additional advantage, some EWGs can be transformed into other functionalities. As shown in Scheme 7, the hydrolysis of polystyrenes *para*-substituted with esters, 2-oxazoline, and *N*-alkyl-, *N*-aryl imines yielded poly(4-vinylbenzoic acid)s and poly(4-vinylbenzaldehyde)s, respectively. These functional polymers were observed to still possess well-controlled molecular weights and narrow molecular weight distributions. Both well-defined poly(4-aminomethylstyrene) and poly(4-vinylbenzoic acid) were obtained in high yields by the reduction and oxidation of poly(4-vinylbenzonitrile). Thus, the proposed strategy using the electron-withdrawing character of the functional groups satisfactorily works and opens a promising route for providing new living anionic polystyrenes carrying polar functional groups.
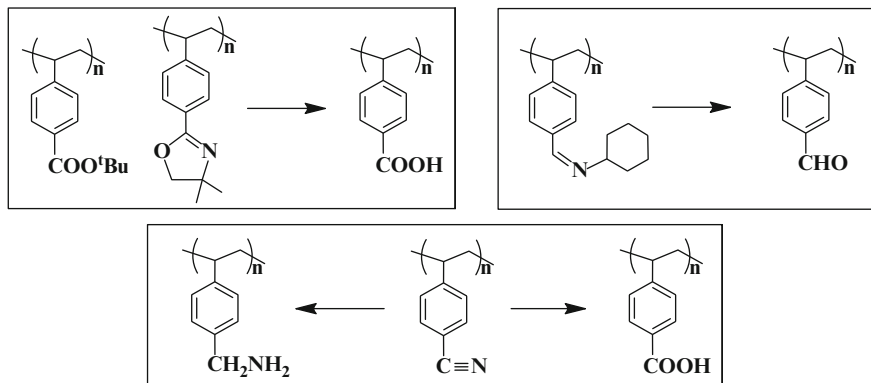
Scheme 7 Synthesis of well-defined poly(4-vinylbenzoic acid)s, poly(4-vinylbenzaldehyde), and poly(4-aminomethylstyrene)

3 1,3-Butadiene Derivatives

The living anionic polymerization with stereochemistry of 1,3-butadiene and isoprene has been widely investigated from the viewpoint of the industrial production of synthetic elastomers. Among the synthesized polymers, highly *cis*-1,4-regulated polymers are of special importance, because they are very similar in elastic property to natural rubber and industrially produced roughly comparable in amount to natural rubber. In addition to such *cis*-1,4 polymers, several copolymers of styrene and 1,3-butadine and/or isoprene, their hydrogenated polymers, and ABA triblock copolymers of PS-*b*-PB-*b*-PS and PS-*b*-PI-*b*-PS, known as thermoplastic elastomers, are also industrially produced as important synthetic elastomers used in various fields.

Since the elastic properties of the 1,3-diene polymers significantly depend on the microstructure of the repeating units shown in Fig. 25, most of the studies have focused on controlling the *cis*-1,4 microstructures by changing the reaction variables, such as initiator, solvent, additive, temperature, and substituent. For the synthesis of highly *cis*-1,4-regulated PB and PI by anionic polymerization, it has been almost established that the use of RLi compounds as initiators in aliphatic hydrocarbon media is essential. In practice, 96 % *cis*-1,4-PI with 4 % 3,4-content was obtained in heptane with BuLi at $-10\,^{\circ}$C. Under somewhat specific conditions, the highest *cis*-1,4 regulation up to 98 % was achieved in bulk at a low initiator concentration (ca. 10^{-6} M). The synthesis of a high percent *cis*-1,4 PB is rather difficult and the polymers consisting of 50–86 % *cis*-1,4 contents are generally obtained under similar conditions, although a total of 1,4 microstructures of over 90 % is achieved. It is also well known that their *cis*-1,4 and even *trans*-1,4 contents are drastically reduced by changing either the initiator from RLi to initiators bearing Na$^+$ or K$^+$ or solvents from aliphatic hydrocarbons to polar media such as THF, ethers, and *tert*-amines. Such subjects regarding the microstructures of the
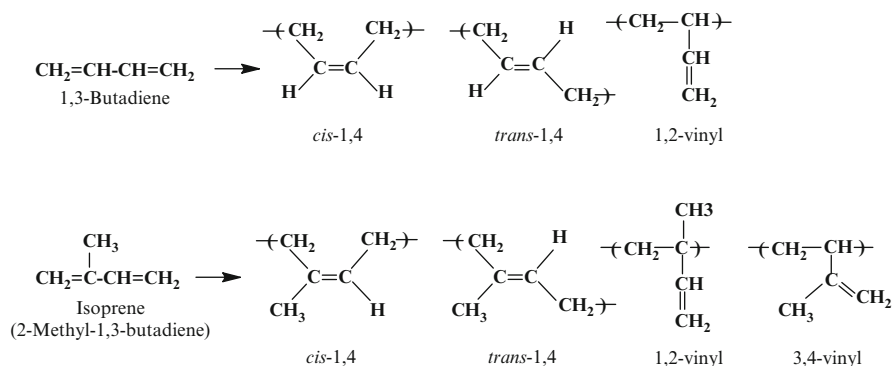
Fig. 25 Possible microstructures of PB and PI

polymers obtained under various conditions were described in more detail in the book previously published by Quirk and Hsieh [3, 9]. As related references are also cited in the book, they are not listed in this chapter to avoid duplication.

Although the living anionic polymerization and stereochemistry of 1,3-butadiene and isoprene have been widely investigated as already mentioned, examples of the anionic polymerization of functional 1,3-butadiene derivatives are rather limited because of their synthetic difficulties and high susceptibility to the Diels-Alder reaction. In this section, the anionic polymerization of functional butadiene derivatives will be introduced. In addition, the stereochemistry of the resulting polymers, that is, how the microstructure is affected by the functional substituent, will also be described.

3.1 Alkyl- and Aryl-Substituted 1,3-Butadiene Derivatives

Soon after a number of studies on the anionic polymerization of 1,3-butadiene and isoprene, the anionic polymerizations of several 2-alkyl-1,3-butadiene derivatives with (RLi)s as initiators were examined under the conditions using hydrocarbon media such as heptane and benzene as well as polar solvents like THF and ethers. The alkyl substituents used for this purpose involved ethyl, propyl, isopropyl, butyl, and *ter*t-butyl groups (see Fig. 26). Although the characterization results of the molecular weights and their distributions were not carried out in detail, it is considered that these 2-alkyl-substituted monomers basically all undergo the living anionic polymerization under carefully selected conditions similar to the cases using 1,3-butadiene and isoprene. Fetters and Mays et al. reported the details of the anionic polymerization of several alkyl-substituted dine monomers, such as 1,3-butadiene, 2,3-dimethyl-1,3-butadiene, 2-ethyl-1,3-butadiene, and 3-methylene-7-methyl-1,6-octadiene (β-myrcene) (see Fig. 27), in cyclohexane or *tert*-amine/aliphatic
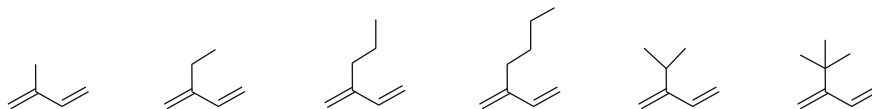
Fig. 26 2-Alkyl-1,3-butadiene derivatives
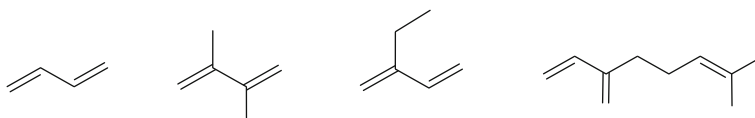
Fig. 27 1,3-Butadiene, 2,3-dimethyl-1,3-butadiene, 2-ethyl-1,3-butadiene, and 3-methylene-7-methyl-1,6-octadiene (β-myrcene)

Table 6 Anionic polymerization of 1,3-butadiene (98–99 % 1,2-addition, 1–2 % 1,4-addition)

M_w (g/mol)[a]	M_w/M_n (SEC)
27,000	1.03
44,000	1.05
71,000	1.05
104,000	1.05
273,000	1.06
489,000	1.07

[a]Low-angle laser light scattering

Table 7 Anionic polymerization of 2,3-dimethyl-1,3-butadiene (97 % 1,4-addition and 3 % 1,2-addition)

M_n (g/mol)[a]	M_w (g/mol)[b]	M_w/M_n (SEC)
14,700	16,200	1.05
76,900	81,700	1.06
145,000	152,000	1.10
176,000	189,000	1.09
197,000	240,000	1.10
386,000	425,000	1.17

[a]Membrane osmometry
[b]Low-angle laser light scattering

hydrocarbon mixtures with *sec*-BuLi or *tert*-BuLi at 0 or 30 °C [100]. The results are summarized in Tables 6, 7, 8, 9 and 10.

Regarding the stereochemistry of the resulting polymers, there appeared to be a general trend that higher *cis*-1,4 microstructures were obtained using the sterically bulkier alkyl-substituted 1,3-butadiene as listed in Table 11. Similar trends were observed even for the polymers obtained in polar ethereal media. Indeed, the microstructure was predominantly regulated up to 81 % in the 1,4-addition mode with the use of 2-isopropyl-1,3-butadiene, while 1,4-content of 35 % was observed in poly(2-methyl-1,3-butadiene) (polyisoprene) obtained under similar conditions. Somewhat surprisingly, the polymer with the 1,4-content of 50 % was produced by the polymerization of 2-*tert*-butyl-1,3-butadiene with sodium naphthalenide even

Table 8 Anionic polymerization of 2,3-dimethyl-1,3-butadiene (55 % 1,4-addition and 45 % 1,2-addition)

M_n (g/mol)[a]	M_w (g/mol)[b]	M_w/M_n (SEC)
21,100	25,100	1.05
59,500	62,100	1.05
77,600	83,000	1.06
120,000	124,000	1.07
172,000	180,000	1.07
213,000	238,000	1.11

[a]Membrane osmometry
[b]Low-angle laser light scattering

Table 9 Anionic polymerization of 2-ethyl-1,3-butadiene (90 % 1,4-addition and 10 % 1,2-addition)

M_w (g/mol)[a]	M_w/M_n (SEC)
15,800	1.02
42,800	1.03
51,800	1.03
136,000	1.05
304,000	1.06
407,000	1.07
666,000	1.07

[a]Low-angle laser light scattering

Table 10 Anionic polymerization of 3-methylene-7-methyl-1,6-octadiene (64 % 1,4-addition and 36 % 1,2-addition)

M_n (g/mol)[a]	M_w (g/mol)[b]	M_w/M_n (SEC)
53,700	63,000	1.04
109,000	119,000	1.05
127,000	135,000	1.05
222,000	251,000	1.05
372,000	442,000	1.06
461,000	557,000	1.07

[a]Membrane osmometry
[b]Low-angle laser light scattering

in THF. Thus, the effect of the steric bulkiness of the 2-alkyl substituent is obvious [101–103].

1,3-Cyclohexadiene (CHD) shown in Fig. 28 was long known as a cyclic monomer with a fixed cisoid 1,3-diene structure, which could polymerize using an anionic initiator. In 1997, Natori et al. reported the first successful living anionic polymerization of this interesting cyclic monomer with BuLi in the presence of *N,N,N′,N′*-tetramethylethylenediamine (TMEDA) in cyclohexane at 40 °C for 2 h to yield a polymer composed of 48 % 1,4 and 52 % 1,2 repeating units [104] (see Fig. 29).

Under such conditions, the polymers with well-controlled M_n values up to 19,000 g/mol and narrow molecular weight distributions (M_w/M_n <1.09) were

Table 11 Microstructures of poly(2-alkyl-1,3-butadiene)s

Alkyl substituent	Solvent	°C	Microstructure			
			cis-1,4	trans-1,4	1,2-vinyl	3,4-vinyl
H	Hexane	20	30	60	10	0
Me	Hexane	20	70	25	0	5
Et	Heptane	40	78	14	0	8
Pr	Heptane	40	91	4	0	5
i-Pr	Heptane	40	86	10	0	4
Bu	Heptane	40	62	33	0	5
			Microstructure			
Alkyl substituent	Solvent	°C	1,4 (cis + trans)		1,2-vinyl	3,4-vinyl
H	Ether	0	25 (8 + 17)		75	0
Me	Ether	20	35		13	52
Et	Ether	25	58		0	42
Pr	Ether	25	57		0	43
i-Pr	Ether	25	81		0	19
Bu	Ether	25	56		0	44
t-Bu	THF[a]	25	50		0	50

BuLi was used as an initiator in each case

[a]Sodium naphthalenide was used as an initiator
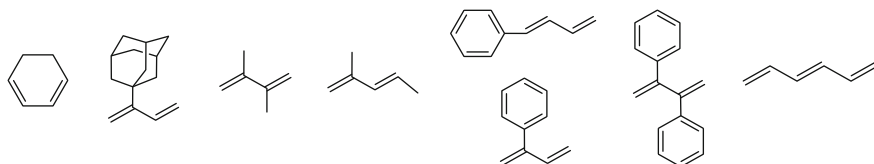
Fig. 28 Alkyl- and aryl-substituted 1,3-butadiene derivatives

Fig. 29 Microstructure of poly(CHD)
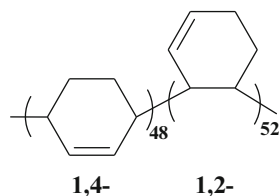
quantitatively obtained. Furthermore, well-defined triblock copolymers of poly (CHD)-b-PS-b-poly(CHD) and poly(CHD)-b-poly(1,3-butadiene)-b-poly(CHD) were also synthesized by sequentially adding the corresponding three monomers [105]. Soon after their reports, three-arm star poly(CHD)s and high-molecular-weight multiarmed star poly(CHD)s were synthesized by the linking reaction of the living poly(CHD)s with $MeSiCl_3$ or with divinylbenzenes [106, 107]. The well-

defined poly(CHD)s thus synthesized are potentially attractive precursor polymers, which can be transformed into thermally and chemically stable poly(cyclohexane)s with high T_g values and conductive π-conjugated poly(phenylene)s.

Later, Quirk et al. reported the occurrence of termination by chain transfer to monomer to a certain extent during the polymerization of CHD under the above conditions based on characterization of the products from ethylene oxide termination. The degree of termination was estimated to be around 10 % of the original living chain-end anion by the yield of ω-hydroxy-functionalized poly(CHD) and the MALDI-TOS MS analysis [108].

Recently, Ishizone et al. reported that an extremely sterically hindered 2-(1-adamantyl)-1,3-butadiene (see Fig. 28) was anionically polymerized in a living manner using either *sec*-BuLi in cyclohexane at 40 °C or potassium naphthalenide in THF at −78 °C [109, 110]. The polymers with well-controlled molecular weights ($M_n = 6,000$–21,000 g/mol (cyclohexane) and 4,300–16,000 g/mol (THF)) and narrow molecular weight distributions ($M_w/M_n = 1.08$–1.38 (cyclohexane) and 1.08–1.12 (THF)) were quantitatively obtained. As expected, the microstructure was affected by both the initiator and solvent and the 1,4-contents of the resulting polymers with *sec*-BuLi in cyclohexane, *sec*-BuLi in THF, and potassium naphthalenide in THF were 96 % (*cis/trans* = 93/7), 88 % (*cis/trans* = 82/18), and 79 % (*cis/trans* = 72/28), respectively. Small amounts of both the 1,2- and 3,4-vinyl structures were also present. Even in THF, the microstructures were predominantly regulated in the 1,4-structure of 79–88 %. Thus, perfect stereospecific control cannot be achieved with the use of this particular 1,3-butadiene monomer.

2,3-Dimethyl-1,3-butadiene was anionically polymerized in nearly 100 % yields with BuLi, Na, or K metal in THF and with BuLi, EtLi, or K metal in benzene [111]. The ratio of the 1,4- to 1,2-contents was found to be around 85/15 in the polymers obtained in benzene, while both the 1,2- and 1,4-addition reactions equally occurred in THF. The *cis:trans* ratio was not clear. As mentioned above, Fetters and Mays et al. reported the living anionic polymerization of 2,3-dimethyl-1,3-butadiene in cyclohexane and cyclohexane-triethylamine (7/3, v/v) to afford almost 1,4-polymers (97 %) and a mixture of 1,4-polymer (55 %) and 1,2-polymer (45 %) with controllable molecular weights and narrow molecular weight distributions, as shown in Tables 7 and 8 [100].

Hadjichristidis and Fetters et al. reported that the anionic polymerization of 2-methyl-1,3-pentadiene (see Fig. 28) proceeded in a living manner with *sec*-BuLi in benzene at 40 °C. As listed in Table 12, the resulting polymers possess well-controlled molecular weights and narrow molecular weight distributions [112]. Very interestingly, the resulting polymer was indicated to have an exclusively regulated 1,4-microstructure with a *cis:trans* ratio of 64:36. No indication of a 1,2- or 3,4-addition was observed by ^{13}C NMR. Thus, the polymerization completely proceeded regioselectively under the above conditions. The hydrogenation of the resulting polymer yielded a narrowly distributed atactic polypropylene.

Table 12 Anionic polymerization of 2-methyl-1,3-pentadiene

M_n (g/mol)[a]	M_w (g/mol)[b]	M_w/M_n
41,500	44,500	1.07
55,000	58,700	1.05
117,000	125,000	1.07
346,000	377,000	1.09

[a]Membrane osmometry
[b]Low-angle laser light scattering

Table 13 Anionic polymerization of 2-phenyl-1,3-butadiene

Initiator	Solvent	°C	M_n (g/mol)	M_w/M_n
sec-BuLi	Benzene	25	15,000	1.04
sec-BuLi	Benzene	25	80,000	1.04
sec-BuLi	Benzene	25	164,000	1.03
BuLi	THF	−78	17,000	1.06
BuLi	THF/TMEDA[a]	−78	48,000	1.05

[a]98.6/1.4, *v/v*-%

1-Phenyl- and 2-phenyl-1,3-butadienes are typical aryl-substituted 1,3-butadienes used for the anionic polymerization. The polymerization of 1-phenyl-1,3-butadiene in benzene or hexane with BuLi gave polymers composed of *cis*-1,4 (25–28 %), *trans*-1,4 (49–59 %), and 3,4-vinyl (16–23 %) contents [113]. Although the anionic polymerization of 1-phenyl-1,3-butadiene was suggested to proceed in a living manner (sodium naphthalenide/THF and BuLi/toluene, benzene, or hexane), no detailed characterization was available. On the other hand, the polymers with a high *cis*-1,4 microstructure of over 90 % were obtained by the polymerization of 2-phenyl-1,3-butadiene in hydrocarbon media like toluene and benzene at 25–30 °C [114]. Small amounts of the 1,2-vinyl structures were present in addition to *cis*-1,4. Interestingly, the high *cis*-1,4 structure (93 %) was not influenced by adding polar TMEDA. More interestingly, the highest *cis*-1,4 content was obtained in THF at 57 °C and gradually decreased from 98 to 72 % by lowering the polymerization temperature to −100 °C.

Fujimoto et al. reported the living anionic polymerization of 2-phenyl-1,3-butadiene with *sec*-BuLi in benzene at 25 °C as well as with BuLi in THF at −78 °C. The predictable molecular weights up to 164,000 g/mol with narrow molecular weight distributions (M_w/M_n <1.06) were attained in the resulting polymers [115] (see Table 13). From the viewpoint of stereochemistry, the terms of *E* and *Z* in place of *cis* and *trans* should be employed in all the polymers of the substituted 1,3-butadiene derivatives, but the *cis* and *trans* configurations to the main chains are herein used for convenience throughout this section in order to compare the *cis*-1,4 and *trans* 1,4-polyisoprenes.

Hirao et al. reported the living anionic polymerization of 2,3-diphenyl-1,3-butadiene in THF at −78 °C with cumylpotassium, potassium naphthalenide, or *sec*-BuLi [116]. The polymers with well-controlled molecular weights (M_n = 10,500–44,000 g/mol) and narrow distributions (M_w/M_n = 1.05–1.11) were

$$-(CH_2-CH)- \qquad -(CH_2-CH=CH-CH)- \qquad -(CH_2-CH=CH-CH=CH-CH_2)-$$
$$\quad\ CH=CH-CH=CH_2 \qquad\qquad\quad CH=CH_2$$
$$\qquad 1,2- \qquad\qquad\qquad\qquad 1,4- \qquad\qquad\qquad\qquad\qquad 1,6-$$
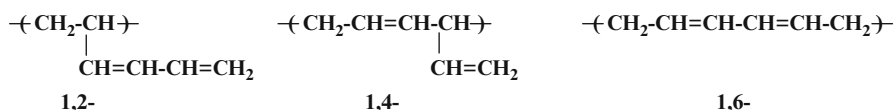
Fig. 30 Microstructure of poly(1,3,5-hexatriene)
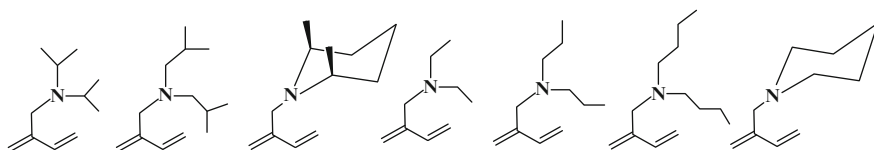
Fig. 31 2-Dialkylaminomethyl-1,3-butadiene derivatives

quantitatively obtained. Under each of the above conditions, the polymers that exclusively consisted of 1,4-contents were produced and their geometries of *cis/ trans* (that is, *Z/E* in this case) were estimated to be 9/1 based on the ^{13}C NMR spectra. Interestingly, the resulting polymers usually became insoluble in THF and benzene during isolation of the polymers by reprecipitation or upon standing for a few hours, due to the crystallization by their highly stereoregulated structures and the π-π interaction among the phenyl rings. This behavior seems not to be due to the cross-linking, since the polymers are still soluble in hot *o*-dichlorobenzene.

Unlike the living PB and PI, the living anionic polymer of 2,3-diphenyl-1,3-butadiene cannot initiate the polymerization of styrene, possibly due to the stabilization of the chain-end anion by a long conjugation system via the two phenyl groups. On the other hand, the more reactive MMA was readily and quantitatively polymerized with this living polymer, resulting in an expected poly(2,3-diphenyl-1,3-butadiene)-*b*-PMMA with well-defined structures.

Quirk et al. reported that 1,3,5-hexatriene (see Fig. 28) was polymerized with BuLi in THF at 0 °C for 30 min [117]. However, the structure of the resulting polymer was indicated by the SEC analysis to be branched and complicated. Approximately equal amounts of all three types of microstructures (1,2-, 1,4-, and 1,6-enchainments), as shown in Fig. 30, were observed in the resulting polymer.

3.2 Amine-Substituted 1,3-Butadiene Derivatives

A series of 2-dialkylaminomethyl-1,3-butadiene derivatives shown in Fig. 31 were newly synthesized and their anionic polymerizations were carried out under various conditions [118]. All these monomers could be polymerized with *sec*-BuLi in benzene at room temperature. A 4,1 addition manner of the monomer to the chain-end anion was suggested based on the NMR analysis. However, the polymerization of each monomer was not controlled and far from quantitative (13–55 %) even after 48 h. The resulting polymers were always lower in M_n value than
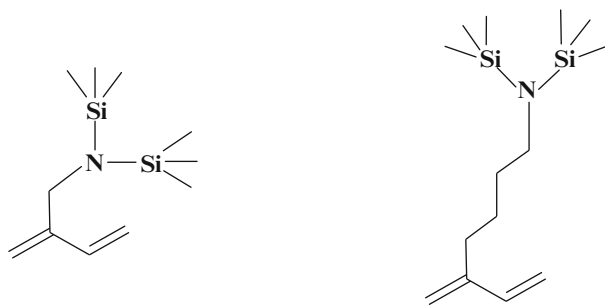
Fig. 32 2-Trimethylsilyl-protected aminoalkyl-1,3-butadiene derivatives

those expected and possessed rather broad molecular weight distributions ($M_n = 2,500$–$8,000$ g/mol, $M_w/M_n \sim 1.5$). On the other hand, the polymer was not obtained under the conditions with *sec*-BuLi either in THF at -78 °C, or 1,4-dioxane at room temperature. Thus obviously, serious side reactions indeed occurred in all of the polymerization systems.

Although the obtained polymers all consisted of high 1,4-contents (>90 %), the ratio of *cis:trans* was observed to be dependent on the bulkiness of the alkyl substituent in the *tert*-amino group. The polymers having more than 95 % *cis*-4,1-repeating units were produced by the polymerization of 1,3-butadiene derivatives 2-substituted with bulky and branched di(isopropyl)aminomethyl-, di(isobutyl) aminomethyl-, and 2,6-*cis*-dimethylpiperidylmethyl groups. Thus, the polymerization of such monomers regioselectively proceeded as well as stereoselectively. The polymers obtained from other monomers contained a mixture of *cis*- and *trans*-4,1-units (24–52 % *cis* and 43–68 % *trans*) in addition to small amounts of the 3,4 content (5–13 %).

As new trimethylsilyl-protected amine-2-substituted 1,3-butadienes, 2-bis (trimethylsilyl)aminomethyl-1,3-butadiene (SAMB) and 2-(4-bis(trimethylsilyl) amino)butyl-1,3-butadiene (SABB) were synthesized and their anionic polymerizations were carried out [119] (see Fig. 32). Although a sufficient stability of the Si-N bond toward *sec*-BuLi and carbanionic species was confirmed by the successful living anionic polymerization of 4-bis(trimethylsilyl)aminoalkylstyrene derivatives, as mentioned before [39], SAMB could not undergo the polymerization in cyclohexane with *sec*-BuLi or PSLi at 20–40 °C. The MALDI-TOF-MS analysis of the PS recovered by the reaction of PSLi with SAMB revealed that the PS contains one isoprene unit at the chain end. This strongly suggests that the isomerization of the chain-end anion with elimination of the bis(trimethylsilyl)amide anion might occur, as shown in Scheme 8.

In contrast, SABB was found to be polymerized with *sec*-BuLi in toluene at 40 °C to yield a polymer in 100 % yield. However, the resulting polymer possessed a bimodal distribution and a higher M_n value of 17,900 g/ml than the calculated value ($M_n = 6,200$ g/mol), indicating the occurrence of side reactions. The microstructure was determined to be a mixture of 86 % 1,4- and 14 % 3,4-contents,
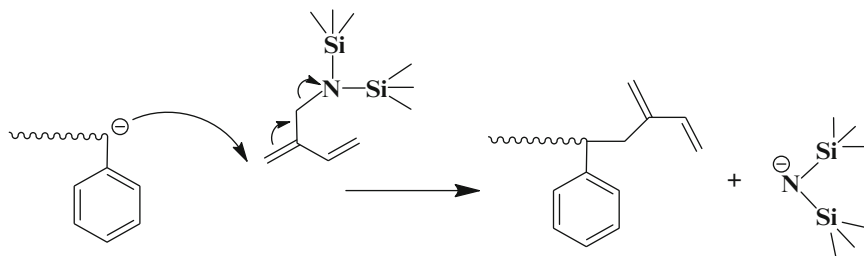
Scheme 8 Possible reaction between living PS and SAMB
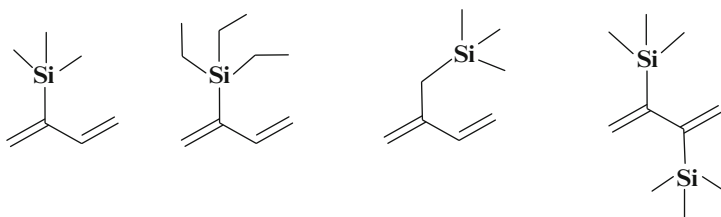
Fig. 33 Trialkylsilyl-substituted 1,3-butadiene derivatives

although the *cis/trans* geometry was not determined yet. On the other hand, PSLi quantitatively initiated the polymerization of SABB to afford the expected diblock copolymer of PS-*b*-poly(SABB) ($M_n = 10{,}200$ g/mol and $M_w/M_n = 1.09$). Therefore, the polymerization conditions should be optimized in order to discuss the anionic polymerizability and the polymerization control in detail.

3.3 Silyl-Substituted 1,3-Butadiene Derivatives

The anionic polymerizations of 2-trimethylsilyl-1,3-butadiene (TMSB) [120], 2-triethylsilyl-1,3-butadiene (TESB) [121], 2-(trimethylsilyl)methyl-1,3-butadiene [122] (TMSMB), and 2,3-bis(trimethylsilyl)-1,3-butadiene ((TMS)₂B) [123] shown in Fig. 33 were previously reported. It was observed that TMSB underwent the anionic polymerization in a living manner to yield the polymers with predictable molecular weights ($M_n \sim 16{,}300$ g/mol) and relatively narrow molecular weight distributions ($M_w/M_n \sim 1.15$) with oligo(α-methylstyryl)lithium, sodium, or potassium in THF at $-78\ ^\circ$C. Although the polymer was obtained with *sec*-BuLi in hexane at $20\ ^\circ$C, the polymerization was not controlled under such conditions. The addition of TMEDA to the above polymerization system rendered the polymerization rate slower and the conversion of 59 % was obtained even after 48 h.

Under the conditions in THF that provide polyisoprene with 12 % 1,4-, 29 % 1,2-vinyl, and 59 % 3,4-vinyl microstructures, poly(TMSB)s of high 1,4-contents

(~70 %) (*cis/trans* = ca. 6/4) with 1,2-vinyl structures (~30 %) were obtained. As expected, the microstructure of the polymer produced in hexane was predominantly the *cis*-1,4 unit (84 %) in addition to small amounts of the *trans*-1,4 (4 %) and 1,2-vinyl (12 %) structures. The *cis* 1,4 content decreased to 67 % with the addition of TMEDA.

TESB was anionically polymerized under various conditions (BuLi in hexane at 25 °C, BuLi in hexane/*N,N,N′,N′,N″,N″*-hexamethylphosphortriamide (HMPT) (20/1) at −25 °C, and THF at −78 °C). However, the polymerization was far from under control for each of these conditions. Interestingly, the polymerization with BuLi in hexane regioselectively and stereoselectively proceeded to yield only a *cis*-1,4-regulated polymer. On the other hand, the polymer obtained in THF/HMPT consisted of a mixture of *cis*-1,4 and *trans*-1,4 contents (*cis/trans* = 56/44). In this polymer, neither 1,2- nor 3,4-vinyl structures were found. Thus, high *cis*-1,4-microstructures in both poly(TMSB) and poly(TESB) obtained in hydrocarbon media were similar to those of the polymers of the 2-alkyl-1,3-butadienes and 2-phenyl-1,3-butadiene obtained in hydrocarbon media.

TMSMB was also anionically polymerized with BuLi in hexane at room temperature to yield a low-molecular-weight polymer (M_n = 7,050 g/mol and M_w/M_n = 1.4) that consisted of *cis*-1,4 (47 %), *trans*-1,4 (23 %), and 3,4-vinyl (30 %) units. Very recently, it was reported that a well-defined diblock copolymer of PS-*b*-poly(TMSMB) was synthesized by sequentially adding styrene and TMSMB with *sec*-BuLi in cyclohexane at 40 °C [124]. Both blocks were 54,200 and 14,100 g/mol in M_n value, respectively, and the M_w/M_n value was 1.02. Since this result suggests the possibility of the living anionic polymerization of TMSMB, the polymerization seems worthwhile to be reexamined.

The anionic polymerization of (TMS)$_2$B proceeded with BuLi either in THF or hexane/HMPT (10/1) at −25 °C. Somehow unexpectedly, this monomer cannot be polymerized with only BuLi in hexane and HMPT is an essential additive to promote the polymerization. Although the polymerization control was not satisfactory under both conditions, the resulting polymers were observed to exclusively consist of the *trans*-1,4 structure, which was special for the anionic polymerization of the 1,3-butadiene derivatives.

As mentioned for the anionic polymerization of alkoxysilyl-substituted styrene derivatives [39], the alkoxysilyl substituents were found to be compatible with the anionic initiators and the chain-end anions. Indeed, both 2-trimethoxysilyl-1,3-butadiene (TMOSB) and 2-triisopropoxysilyl-1,3-butadiene (TIPOSB) (see Fig. 34) were reported by Takenaka et al. to undergo the living anionic polymerization in THF at −78 °C with alkali-metal naphthalenides to yield the polymers with predictable molecular weights (M_n = 8,000–46,000 g/mol) and narrow molecular weight distributions (M_w/M_n = 1.07–1.14) [125, 126]. Very surprisingly, the anionic polymerization of both monomers was observed to proceed in a complete 1,4-addition mode even with the initiators bearing Na$^+$ and K$^+$ in THF. More surprisingly, the geometry of the repeating unit in the poly(TIPOSB)s obtained under such conditions was exclusively regulated to the *cis* configuration (*E* configuration in this case), while the *cis/trans*, that is, the *E/Z* ratios of 9/1
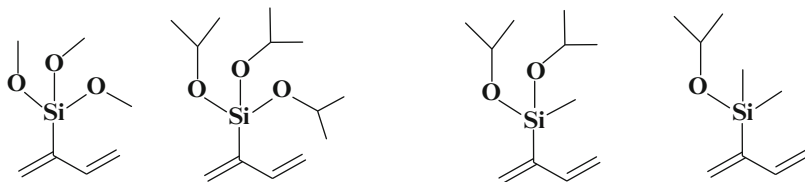
Fig. 34 2-Alkoxysilyl-substituted 1,3-butadiene derivatives
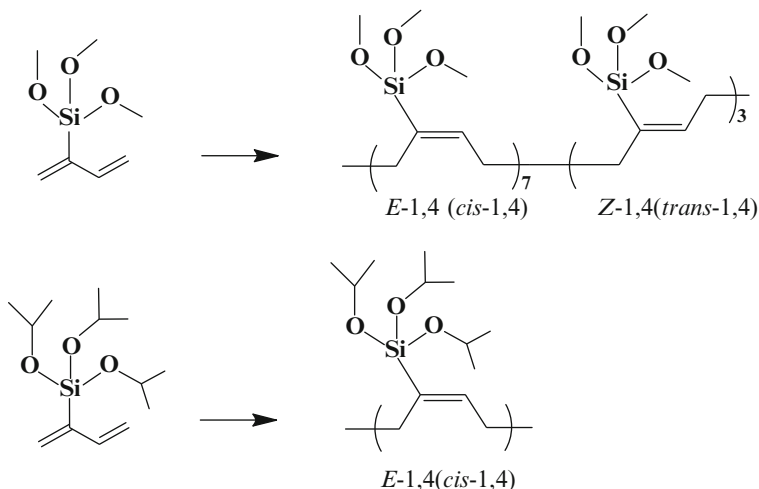
Fig. 35 Microstructures of poly(TMOSB) and poly(TIPOSB)

(Li^+) and 7/3 (Na^+ and K^+) were observed in the polymers of TMOB (see Fig. 35). Thus, the anionic polymerization of TIPOSB was the first successful polymerization system that proceeded not only in a living manner, but also regioselectively as well as stereoselectively. Although the reason could still not be understood, steric hindrance of the isopropoxy substituent on the Si atom and stabilization of the chain-end anion by the Si atom through a $p\pi$-$d\pi$ interaction might play important roles to facilitate the stereoregularity, as shown in Fig. 36.

Both 2-diisopropoxymethylsilyl-1,3-butadiene and 2-isopropoxydimethylsilyl-1,3-butadiene were also synthesized and subjected to the anionic polymerization for comparison with that using TIPOSB as already mentioned. The polymerization was observed to proceed in a living manner to afford the polymers with predictable molecular weights ($M_n \sim 17,000$ g/mol) and relatively narrow molecular weight distributions ($M_w/M_n < 1.2$) [120]. Although the resulting polymers consisted of high 1,4 structures, the complete *cis*-1,4 stereoregularity observed in the poly (TIPOSB)s was lost and the *trans*-1,4 and 1,2-vinyl contents gradually increased with progressive replacement by a methyl group (see Table 14).

Hirao et al. reported the synthesis and anionic polymerization of a series of 2-dialkylaminodimethylsilyl-1,3-butadiene derivatives shown in Fig. 37
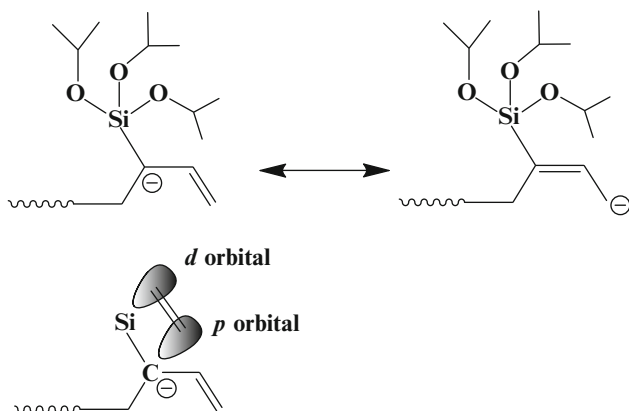
Fig. 36 Anion stabilization through interaction between chain-end anion and Si atom

Table 14 Microstructures of poly(2-alkoxysilyl-substituted 1,3-butadiene)s produced in THF

-SiR$_3$			Counter ion	cis-1,4	trans-1,4	1,2-vinyl	3,4-vinyl
OMe	OMe	OMe	Li$^+$	90	10	0	0
OMe	OMe	OMe	Na$^+$	75	25	0	0
OMe	OMe	OMe	K$^+$	73	27	0	0
OPr^i	OPr^i	OPr^i	Li$^+$	100	0	0	0
OPr^i	OPr^i	OPr^i	Na$^+$	100	0	0	0
OPr^i	OPr^i	OPr^i	K$^+$	100	0	0	0
OPr^i	OPr^i	Me	Li$^+$	91	3	6	0
OPr^i	OPr^i	Me	Na$^+$	67	17	16	0
OPr^i	OPr^i	Me	K$^+$	62	19	19	0
OPr^i	Me	Me	Li$^+$	65	15	20	0
OPr^i	Me	Me	Na$^+$	45	30	23	0
OPr^i	Me	Me	K$^+$	43	23	34	0
Me	Me	Me	Li$^+$	43	23	34	0
Me	Me	Me	Na$^+$	44	28	28	0
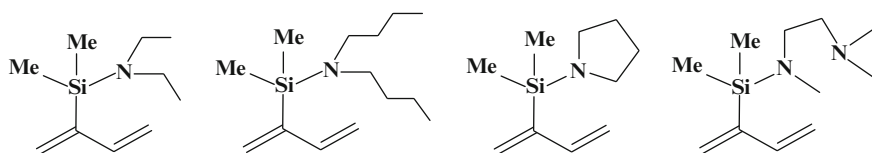
Fig. 37 2-Dialkylaminodimethylsilyl-1,3-butadiene derivatives

[127]. Like the alkoxysilyl group, dialkylaminosilyl groups are also regarded as the protected functionality for silanol and readily removed under mild acidic conditions. All these monomers were observed to undergo the living anionic polymerization in THF at −78 °C to yield polymers with predicable molecular weights

Fig. 38 *N,N*-diethyl-2-
methylene-3-buteamide
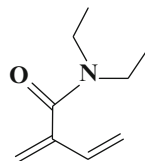
($M_n = 6,000$–20,000 g/mol) and narrow molecular weight distributions ($M_w/M_n = 1.06$–1.09). On the other hand, unwanted side reactions occurred to some extents during the anionic polymerization in heptane at 40 °C, since polymers with higher molecular weights than those expected and multimodal distributions were obtained.

The polymers obtained in THF mainly consisted of 1,4-microstructures (83–91 %) (*cis/trans* = ca. 1/2) containing small amounts of 1,2-vinyl units (9–17 %), while the polymers obtained in heptane were exclusive 1,4-addition products, which were mixtures of *cis*-1,4 (16–32 %) and *trans*-1,4 (68–84 %). Interestingly, the polymer of 2-(2-dimethylaminoethyl)methylaminosilyl-1,3-butadiene was found to have a microstructure totally composed of the *cis*-1,4 unit without any other structures. Thus, high 1,4-microstructures and, in some cases, exclusive *cis*-1,4 contents were observed in the polymers of the 2-alkoxysilyl- and 2-dialkylaminosilyl-1,3-butadiene derivatives obtained in THF. These results were in sharp contrast to the microstructures of poly(1,3-butadiene) and polyisoprene produced under the same conditions.

3.4 Dialkylamide-Substituted 1,3-Butadiene Derivatives

In general, 1,3-butadiene is significantly activated to become unstable by directly introducing the electron-withdrawing group (EWG) into the butadiene skeleton and occasionally undergoes dimerization by the Diels-Alder reaction. In fact, 2-ethoxycarbonyl-1,3-butadiene cannot exist at ambient temperature. Likewise, the synthesis and isolation of 2-formyl-, 2-acetyl, and 2-cyano-1,3-butadienes have not yet been reported, because of the instability at room temperature. Among such 2-EWG-substituted 1,3-butadiene derivatives, the 2-dialkylamide-substituted 1,3-butadiene derivatives are exceptionally stable and isolated even at room temperature. As the amide-substituted butadiene, *N,N*-diethyl-2-methylene-3-buteamide shown in Fig. 38 was synthesized and anionically polymerized [128]. The polymerization was observed to proceed using either potassium naphthalenide or Ph₂CHK in THF at −78 °C. However, the polymerization rate very slowly reached an 80 % conversion even after 30 days. Under such conditions, only a low-molecular-weight polymer ($M_n = 5,100$ g/mol and $M_w/M_n = 1.09$) was obtained. Raising the polymerization temperature with the use of the initiator bearing Li⁺, like lithium naphthalenide and Ph₂CHK/LiCl, increased the polymerization rate and the polymers with M_n values of around 10,000 g/mol and narrow

OMe
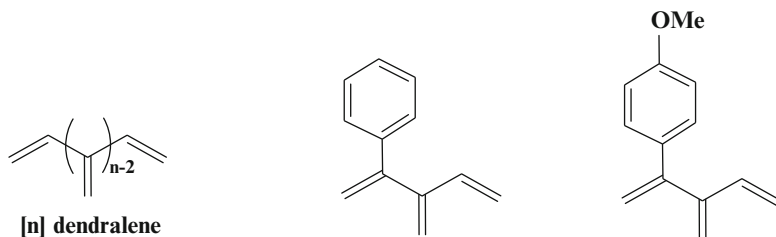
[n] dendralene

Fig. 39 [n]Dendralenes and 2-phenyl-substituted[3]dendralenes

molecular weight distributions ($M_w/M_n = 1.03$–1.09) were obtained in 75–92 % at 0–20 °C for 24 h. The microstructure of the polymer obtained with Ph$_2$CHK at -78 °C was a 1:1 mixture of *cis*-1,4 and 1,2-vinyl contents, while the 1,4-content (*cis/trans* = ca. 1/1) slightly increased to 68 % in the polymers produced using the initiators bearing Li$^+$.

For the polymerization of other dialkyl amide-substituted monomers, similar slow polymerization rates and microstructures were observed. A higher molecular weight polymer of over 12,000 g/mol could not be obtained even after longer polymerization times to 240 h.

3.5 [3]Dendralene Derivatives

Acyclic branched polyene compounds having cross-conjugated diene structures are called [n]dendralenes, in which "n" is the number of $C = C$ bonds in a molecule, as shown in Fig. 39. The lowest dendralene of the family, namely [3]dendralene, was first synthesized in 1955. Since then, a variety of dendralene derivatives up to [8] dendralene has been systematically synthesized [129]. On the other hand, the polymerization behavior of these interesting polyene molecules has not yet been reported.

Very recently, the synthesis and anionic polymerization of 2-phenyl[3] dendralene (P3D) and 2-(4-methoxyphenyl)[3]dendralene (MOP3D) were first reported by Takenaka et al. [130]. The anionic polymerization of both monomers with potassium naphthalenide in THF at -78 °C for 1–2 h proceeded in a living manner to quantitatively afford the polymers with predictable molecular weights ($M_n = 4,500$–$12,700$ g/mol) and narrow molecular weight distributions ($M_w/M_n = 1.04$–1.07). An additional proof for the living character of the polymerization of P3D and MOP3D was provided by the successful synthesis of the expected triblock copolymers of P2VP-*b*-poly(P3D)-*b*-P2VP and P2VP-*b*-poly(MOP3D)-*b*-P2VP by sequentially adding P3D or MOP3D and 2VP to potassium naphthalenide in THF at -78 °C. Broadening of the molecular weight distribution to the higher molecular weight side was observed by allowing the polymerization mixture for a longer time up to 20 h or raising the temperature even to -40 °C. This may possibly
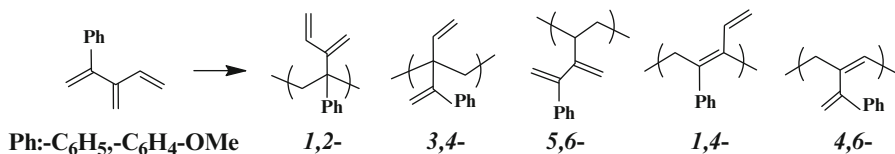
Fig. 40 Possible microstructures of phenyl-substituted [3]dendralenes
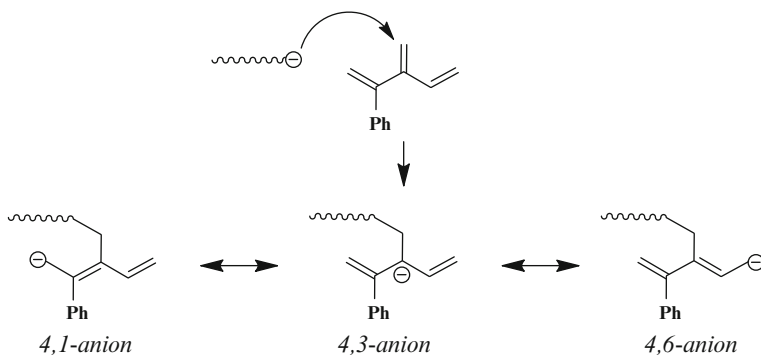
Scheme 9 Formation of 4,1- and 4,6-anions via 4,3-anion

be attributed to the addition reaction between the chain-end anion and the conjugated diene structure(s) in the polymer chain.

As shown in Fig. 40, five possible microstructures of the resulting poly(P3D) and poly(MOP3D) can be considered. Based on the careful ^{1}H and ^{13}C NMR analyses, the microstructure of the poly(MOP3D) was determined to be an almost 1:1 mixture of 1,4- and 4,6-units via the 4,1 and 4,6 anions as illustrated in Scheme 9, since no vinyl groups present in the 1,2- and 5,6 structures were detected. A similar microstructure was observed in the poly(P3D).

It is surprising that such specific triene monomers successfully undergo anionic polymerization in a living manner to afford well-defined linear polymers, although their molecular weights are not sufficiently high. This success strongly suggests the anionic polymerization possibility of other [n]dendralene derivatives with higher numbers of conjugated C=C bond units. It is of special interest to know the stereochemistry of the resulting polymers under various conditions, especially in hydrocarbon media, if the polymerization can be possible. Furthermore, the resulting polymers are regarded as quite new and unique functional polymers, since they possess highly reactive conjugated diene structures incorporated in each monomer unit, which can undergo a variety of characteristic reactions for conjugated diene compounds like the Diels-Alder reaction.

In this section, functional 1,3-butadiene derivatives capable of undergoing anionic polymerization and the stereochemistry of the resulting polymers were introduced. The number of functional groups introduced into the 1,3-butadiene

framework has been so far limited as compared to the significant number of functional styrene derivatives. Unfortunately, the anionic polymerization of several functional 1,3-butadienes could not be satisfactorily controlled, especially in hydrocarbon media, except for 2-phenyl-1,3-butadiene and 2-methyl-1,3-pentadiene. On the other hand, a certain number of functional 1,3-butadienes were reported to undergo the living anionic polymerization in polar media like THF. However, molecular weights of the resulting polymers were often around 10,000 g/mol or even smaller, which were not sufficiently high to conclude whether the living anionic polymerization practically occurred. Furthermore, the block copolymerization of styrene, 1,3-butadiene, or isoprene with such functional monomers were not carried out in many cases. Since the chain-end anions derived from 1,3-butadiene and isoprene are roughly similar in reactivity to the living polystyrene and the sophisticated living anionic polymerizations of 1,3-butadiene and isoprene are well established in both hydrocarbon and polar media, the anionic polymerization of functional 1,3-butadiene derivatives should be further optimized to achieve the living polymerization. After that, the protective strategy successful for the living anionic polymerization of functional styrene derivatives may be applied to 1,3-butadienes carrying the same protected functionalities. Consequently, the range of functionalities amenable to the living anionic polymerization of 1,3-butadiene derivatives can significantly expand.

Regarding the stereochemistry of the resulting polymers, certain interesting and valuable anionic polymerization systems that proceeded regioselectively or stereoselectively have been reported. Furthermore, the achievement of both selectivities was found in the anionic polymerizations of 2-triethyl-1,3-butadiene, three 1,3-butadiene derivatives 2-substituted with di(isopropyl)aminomethyl-, di(isobutyl)aminomethyl-, and 2,6-*cis*-dimethylpiperidylmethyl groups, 2-triisopropoxysilyl-1,3-butadiene, and (2-(2- dimethylamino)ethyl)methylaminosilyl-1,3-butadiene.

There seems to be a general trend that high 1,4-, especially the *cis*-1,4 microstructures, are obtained using the 2-substituted 1,3-butadiene derivatives with structurally bulky groups in hydrocarbon media. However, understanding the structural effect of the substituent on the microstructure seems very difficult at the present time, because various polymerization conditions have so far been employed and the resulting microstructures cannot be directly compared. Therefore, it is essential that the consistent polymerization conditions including initiator, solvent, temperature, and concentration are adjusted.

4 Functional 1,1-Diphenylethylene Derivatives

Although 1,1-diphenylethylene (DPE) is a member of the styrene family, highly reactive anionic initiators used for the polymerization of styrene, 1,3-butadiene, or isoprene, such as BuLi, *sec*-BuLi, and cumylpotassium, quantitatively react with DPE in a 1:1 addition manner (Scheme 10). Neither the polymerization nor even
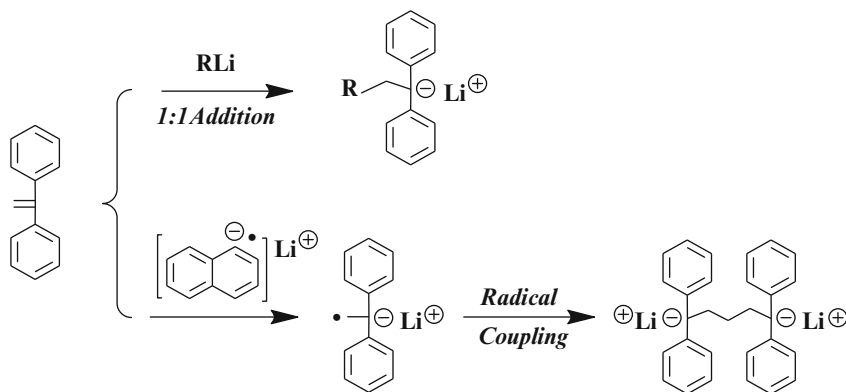
Scheme 10 Reaction of DPE with either RLi or lithium naphthalenide

oligomerization takes place under normal conditions due to the steric hindrance of the α-phenyl substituent and a very low ceiling temperature. The reaction of lithium or other alkali-metal naphthalenides with DPE produces an anion radical intermediate via an electron transfer pathway, followed by coupling to each other, to produce a dimeric dianion product (see also Scheme 10). Again, no further addition reaction of DPE to the dimeric dianion occurs by the same reason. Accordingly, DPE is not usually used as the polymerizable monomer.

The anion derived from DPE polymerizes not only styrene and 1,3-butadiene but also more reactive monomers such as 2VP, alkyl methacrylates, *tert*-butyl acrylate, *N,N*-dialkylacrylamides, and some cyclic monomers like ethylene oxide and cyclic siloxanes. Many functionalized anions can be prepared by the 1:1 addition reaction of RLi to the functional DPE derivatives and used as the initiators in the living anionic polymerization of such monomers. Almost all the functionalities used for the living polystyrene can be employed for this purpose, because the anion derived from DPE is somewhat less reactive than the living chain-end anion of styrene due to the stabilization via the anion delocalization through the two phenyl group. Thus, many functional DPE derivatives have now been used as the general agents for the chain-end functionalization of living anionic polymers, as shown in Scheme 11 [131–136]. With this reaction, the functional groups can quantitatively be introduced at the initiating chain end, that is, α-terminus.

The functional DPE derivative also readily and quantitatively reacts with the highly reactive living anionic polymer of styrene, 1,3-butadiene, or isoprene in a 1:1 addition manner, resulting in the introduction of the functional group at the terminating chain end (ω-terminus in this case). If the α-chain-end-functionalized living PS is used in place of the living PS and subsequently reacts with another functional DPE, an α,ω-asymmetric difunctional PS can be obtained, as shown in Scheme 12.

With the use of a living polymer with the anion at both ends, the functional group can be introduced at both ends. The reaction of the functional DPE with lithium naphthalenide, followed by polymerization of an appropriate monomer, resulted in the chain-end-di-functionalized polymer, in which the two functional groups were placed exactly at the middle of the polymer chain, as shown in Scheme 13.
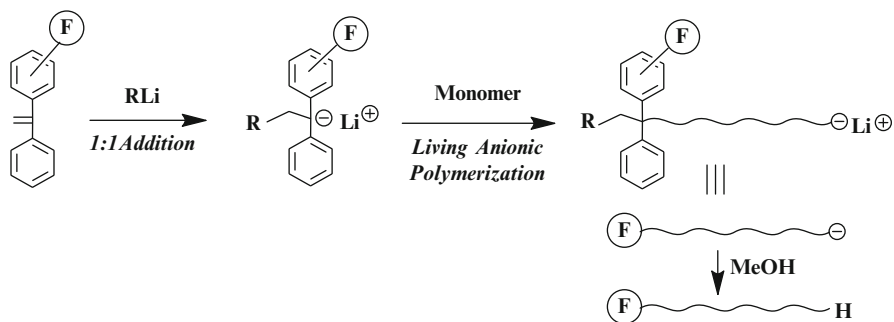
Scheme 11 α-Chain-end functionalization by living anionic polymerization with functionalized anion from RLi and functional DPE
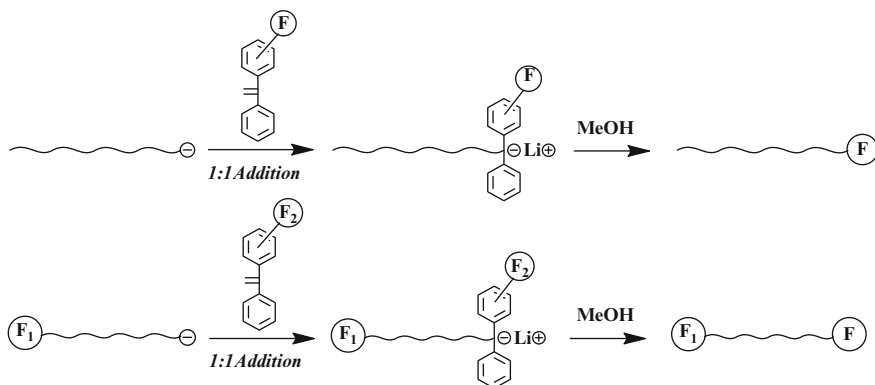
Scheme 12 Synthesis of ω-chain-end-functionalized PS and α,ω-chain-end-di-functionalized PS by the addition reaction of living anionic PS with functional DPE

Scheme 13 Synthesis of α,ω-chain-end-di-functionalized PS and in-chain-di-functionalized PS using functional DPE
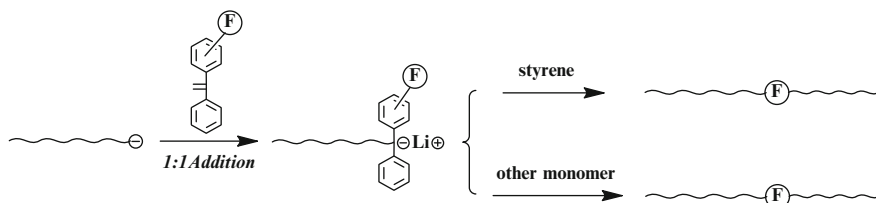
Scheme 14 Synthesis of in-chain-functionalized PS and block copolymer in-chain-functionalized between the two blocks
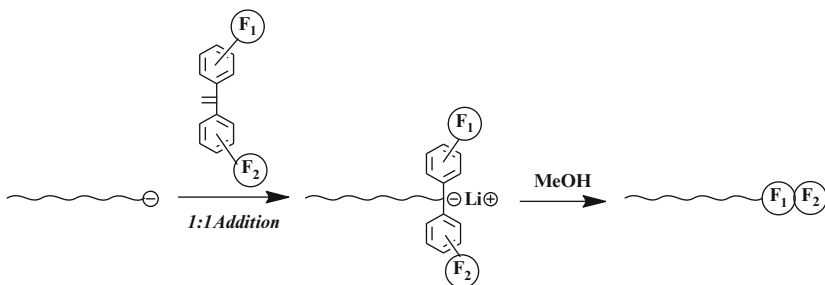
Scheme 15 Synthesis of chain-end-di-functionalized polymer with different functional groups

The addition reaction of the living PS with the functional DPE derivative is not a simple termination reaction. After the reaction, a new chain-end anion derived from the DPE is generated. The subsequent addition of styrene or another monomer results in an in-chain-functionalized PS or a block copolymer with the functional group introduced between the two blocks, as shown in Scheme 14. The position of the introduced functional group can be intentionally placed by changing the molecular weight of the polymer formed during the first or second stage.

As illustrated in Scheme 15, two or more functional groups can also be introduced at the α- or ω-terminal chain end simply by the addition reaction of the highly reactive living polymer of styrene, 1,3-butadiene, or isoprene with a DPE derivative substituted with multiples of the same or even different functional groups. A more general and versatile iterative strategy was developed by Hirao et al., as illustrated in Scheme 16 [137]. For example, PSLi reacts with 1,1-bis(3-*tert*-butyldimethylsilyloxymethylphenyl)ethylene (TBSOM-DPE) and the two introduced 3-*tert*-butyldimethylsilyloxymethylphenyl (TBSOMP) groups are subsequently transformed into two BnBr functions by treatment with $Me_3SiCl/LiBr$. The reaction was observed to cleanly and quantitatively proceed to afford a chain-end-$(BnBr)_2$-functionalized PS. Thus, the highly reactive two BnBr functions were successfully introduced at the PS ω-chain-end. In the next step, the functionalized anion prepared from TBSOM-DPE and *sec*-BuLi reacted with the above PS with two BnBr termini. As a result, four TBSOMP groups transformable into four BnBr termini could be quantitatively introduced at the ω-chain-end. By repeating the two reaction steps four more times, the BnBr termini successively increased from 4 to 8, 16, 32, and even a large number of 64 in number. The almost quantitative introduction
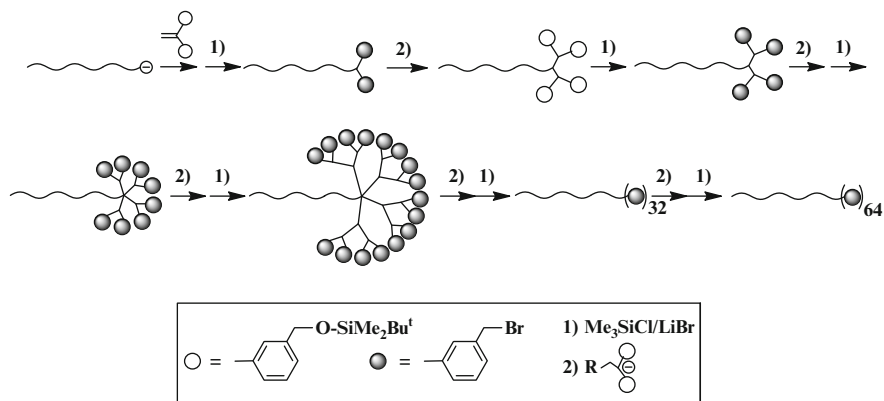
Scheme 16 Synthesis of chain-end-(BnBr)$_n$-multi-functionalized PS by a new iterative strategy ($n = 2, 4, 8, 16, 32,$ and 64)

Table 15 Synthesis of chain-end-(BnBr)$_n$-multi-functionalized PSs

Polymer	M_n (g/mol)		M_w/M_n	BnBr	
	Calculated	^{1}H NMR	SEC	Calculated	Observed
PS-(BnBr)$_2$	4,790	4,800	1.03	2	2.0$_0$
PS-(BnBr)$_4$	5,470	5,420	1.03	4	3.9$_2$
PS-(BnBr)$_8$	6,850	6,780	1.03	8	8.0$_8$
PS-(BnBr)$_{16}$	9,590	9,640	1.03	16	15.9
PS-(BnBr)$_{32}$	15,000	14,800	1.03	32	32.0
PS-(BnBr)$_{64}$	25,600	24,700	1.03	64	64.2

of many BnBr termini in each stage is confirmed by the characterization results listed in Table 15. In each step, the same number of other functional groups can be introduced by the reaction of the chain-end-(BnBr)$_n$-functionalized polymer with the anion prepared from another functional DPE and *sec*-BuLi, as illustrated in Scheme 17.

The functional anion prepared from TBSOM-DPE and *sec*-BuLi could also be used as the initiator in the living anionic polymerization of MMA [138]. In such a case, the number of BnBr functions was introduced from 2, 4, 8, 16, etc., at the α-chain-end. The synthesis of in-chain-(BnBr)$_n$-functionalized PS is also possible using the same iterative strategy starting from an in-chain-(BnBr)$_2$-functionalized PS, which is prepared by the reaction of the TBSOM-DPE end-capped PSLi with the chain-end-BnBr-functionalized PS, followed by transformation to two BnBr functions, as shown in Scheme 18 [139].

The typical functional DPE derivatives used for the chain functionalization are shown in Fig. 41 [137–159]. Among them, the following functional groups are appropriately masked by the same protective groups as those used in the living

Scheme 17 Synthesis of
chain-end-multi-
functionalized PSs
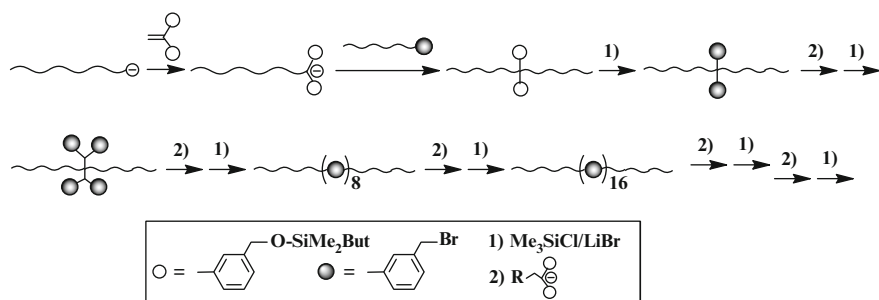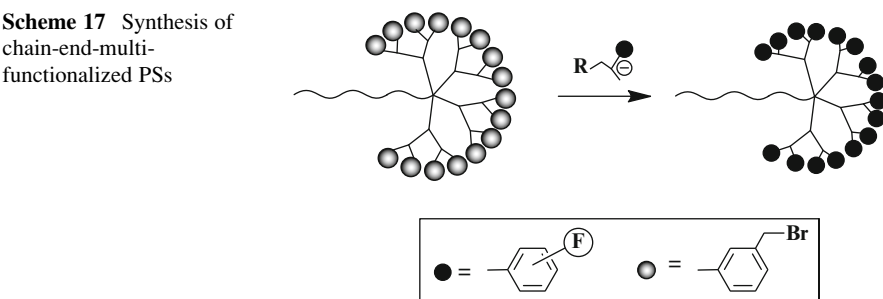
Scheme 18 Synthesis of in-chain-(BnBr)$_n$-multi-functionalized PSs
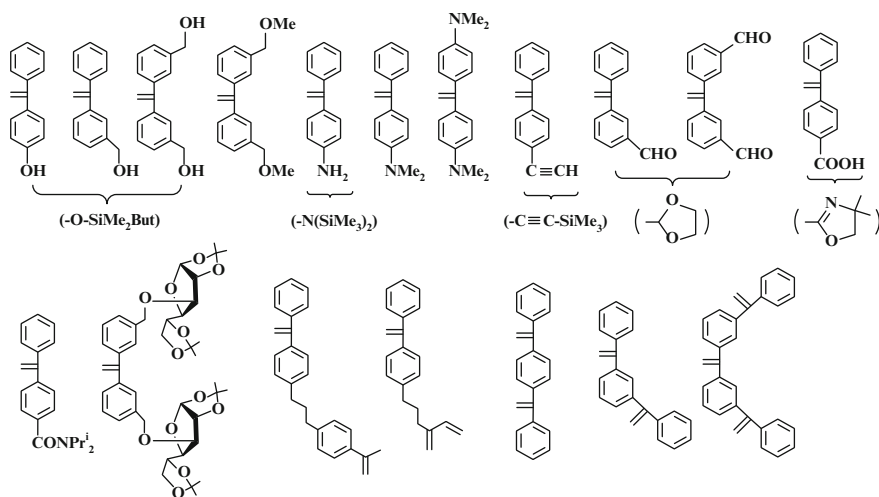
Fig. 41 Functional DPE derivatives

anionic polymerization of functional styrenes: OH, CH$_2$OH, NH$_2$, C$\equiv$CH, CHO, and COOH groups.

The 2-alkyl-1,3-butadienyl and α-methylstyryl groups can be used for the same purpose because the anions derived from their DPEs are compatible with such functionalities.

Moreover, DPE itself is also used as a functional group, because the anion derived from DPE cannot further react with DPE. Thus, the chain functionalization of living anionic polymers has now been well-established, with which the desired number of almost all the functional groups can be introduced at the α- or ω-chain-end and at any in-chain position. The resulting polymers are used as not only chain-functionalized polymers applicable in various fields, but also highly versatile precursor polymers for the synthesis of well-defined multiblock, exactly defined graft, multiarmed and multicomponent star-branched, and dendrimer-like star-branched polymers. These topics are described in some review articles [160–162].

5 Living Anionic Polymerization of Styrene and MMA: Purification and Practice

In this section, we describe the practical synthetic aspects of the living anionic polymerizations of styrene and MMA. In our laboratory, the polymerizations (and subsequent reactions) are performed under high vacuum conditions (10^{-6} Torr) using an all-glass hand-made apparatus equipped with break seals. Although skilled glass-blowing techniques are required to make the apparatus with careful handling during small-scale experiments (0.1–10 g), the polymerization results are highly reproducible and reliable. On the other hand, large-scale experiments (10 g or more) can be carried out under a nitrogen or argon atmosphere with the usual care. Many researchers believe that the living anionic polymerization is very difficult to be carried out due to the extremely rigorous purification of the monomers, solvents, and other reagents to be used as well as complete removal of oxygen, water, and some impurities from the polymerization system. This is true, but there are certain convenient and useful techniques under a nitrogen atmosphere.

For the anionic polymerization of styrene, 1,3-diene monomers, or their derivatives, the polymerization rate is slow in hydrocarbon media, such as cyclohexane, hexane, benzene, and toluene, with RLi. An induction period is also present prior to initiating the polymerization. If impurities including water and oxygen are relatively low, they usually react with RLi during the mixing of the monomer and RLi before the polymerization. As a consequence, the living anionic polymerization smoothly proceeds to quantitatively afford a polymer with a narrow MWD. The molecular weight is slightly shifted to a higher value than that expected because a small amount of RLi is lost due to the presence of impurities. For example, even commercially available styrene, after only drying over molecular sieves without distillation, smoothly undergoes the anionic polymerization with *sec*-BuLi in

commercially available dry benzene at 40 °C for a few hours. A series of polymerizations with different molar ratios of styrene and *sec*-BuLi were carried out under the same conditions. In each case, PS was quantitatively obtained. The resulting PSs showed nearly monodisperse distributions (M_w/M_n <1.05) with the SEC-observed M_n values of 11,000, 27,000, and 60,000 g/mol. Their calculated M_n values were 10,000, 25,000, and 52,000 g/mol, respectively. Thus, well-controlled polystyrenes could readily be prepared by the simple treatment of a commercially available styrene monomer without distillation.

In contrast, the polymerization of styrene is very fast and completed within a few seconds in THF with *sec*-BuLi even at −78 °C. PSs with relatively broad MWDs (M_w/M_n = 1.1–1.3) were obtained using the above treated styrene because the propagation and termination with impurities simultaneously occurred. In this system, the addition of a small amount of Bu_2Mg (commercially available from Aldrich) to the same treated styrene, before mixing the initiator, is very effective in achieving the living anionic polymerization. The presence of Bu_2Mg during the polymerization had no influence at all. For instance, the PSs (M_w/M_n <1.05) of the observed M_n values of 54,000 and 110,000 g/mol were quantitatively obtained and the M_n values were in good agreement with the calculated values.

For the living anionic polymerization of (meth)acrylate and *N,N*-dialkylacrylamide monomers, the addition of a small amount of Et_2Zn to either of the monomers, after drying over molecular sieves, is effective prior to the polymerization. Water, oxygen, and other impurities in each monomer react with Et_2Zn and then the resulting purified monomer is mixed with an initiator to start the polymerization. The presence of excess Et_2Zn does not interfere with the polymerization, but is instead a benefit to narrow the MWD of the resulting polymer. In practice, the low M_w/M_n values (<1.05) along with the good agreement between the M_n values calculated ($M_n \sim 50,000$ g/mol) and those observed by RALLS in the resulting polymers indicate that the living anionic polymerization proceeds as desired.

6   Conclusions

In this chapter, the anionic polymerization behavior of styrene, 1,3-butadiene, DPE, and their functional derivatives was described. In addition, ethylene and trimethylvinylsilane also belong to the group of nonpolar monomers. Ethylene can be anionically polymerized with the *tert*-BuLi-TMEDA complex in hydrocarbon media, but the resulting polyethylene is always precipitated during the early stage of the polymerization to yield a low-molecular-weight polymer ($M_n \sim$ a few thousands g/mol) [163, 164]. The anionic polymerization of trimethylvinylsilane with *sec*-BuLi in hexane was also reported. As shown in Scheme 19, the polymerization was observed to proceed in a normal manner with the occurrence of the isomerization. The ratio of the isomerization reaction was significantly increased by the addition of TMEDA [165].
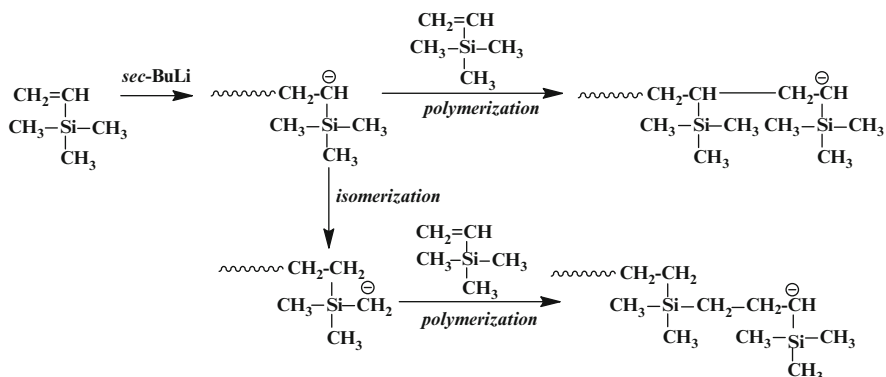
Scheme 19 Polymerization of trimethylvinylsilane, followed by isomerization
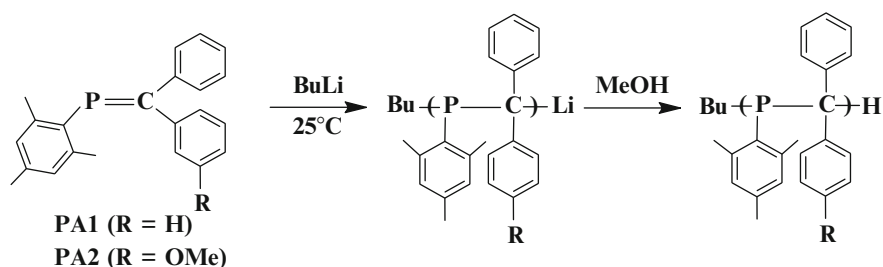
Scheme 20 Living anionic polymerization of phospaalkenes

Recently, two interesting monomers in this category have been reported. The first example is a $P=C$ bond containing phosphaalkene monomer. Gates et al. demonstrated that treating phosphaalkene (PA1 or PA2) with BuLi in dimethoxyethane at 25 °C gives a quite new living anionic poly(methylene-phosphine) composed of a P-C main chain, as shown in Scheme 20 [166–168]. Under such conditions, polymers with controllable molecular weights and narrow molecular weight distributions were obtained, as listed in Table 16. A further evidence for the living polymerization is provided by a linear plot of M_n value versus conversion as well as the successful formation of PS$_{100}$-b-poly(**PA1**)$_{50}$ ($M_{n\ Calculated} = 26,300$ g/mol, $M_{n\ GPC} = 29,600$ g/mol, and $M_w/M_n = 1.06$).

Thus, living anionic polymerization systems common for $C=C$ bonds have been extended to $P=C$ bonds. This chemistry further illustrates the remarkable parallel between $P=C$ and $C=C$ bond to construct new P-C main chain homo-polymers and block copolymers.

The second example is benzofulvene (BF, α-methyleneindene), an exomethylene monomer having a fixed transoid 1,3-diene moiety. Ishizone et al. successfully polymerized BF in a living manner with *sec*-BuLi or Ph$_2$CHK

Table 16 Anionic polymerization of PA1 and PA2 in dimethoxyethane at 25 °C

	M_n (g/mol)		M_w/M_n
Monomer	Calculated	laser-LS	SEC
PA1	8,000	8,900	1.08
PA1	10,500	10,500	1.08
PA1	15,900	14,800	1.04
PA1	31,700	29,600	1.15
PA2	11,500	11,500	1.09
PA2	17,400	14,600	1.11
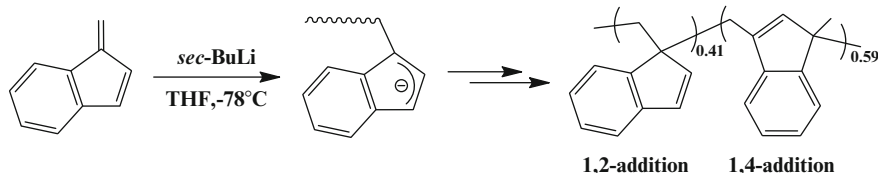
Scheme 21 Living anionic polymerization of **BF**

Table 17 Anionic polymerization of BF in THF at −78 °C

	M_n (g/mol)		M_w/M_n
Initiator	Calculated	laser-LS	SEC
sec-BuLi	8,900	8,900	1.11
sec-BuLi	16,000	18,000	1.03
sec-BuLi	27,000	28,000	1.11
Ph$_2$CHK	11,000	13,000	1.05

in THF at −78 °C for 1 h, as illustrated in Scheme 21 [169]. The resulting polymers were observed to possess the predictable M_n values and narrow molecular weight distributions (see Table 17).

Thus, BF acted as a novel polymerizable transoid 1,3-diene in the anionic polymerization. A remarkable high anionic polymerizability of BF was realized by the fact that a well-defined PMMA-*b*-poly(BF) could be synthesized by the sequential polymerization of BF with a low nucleophilic living PMMA in quantitative efficiency.

Throughout this chapter, we have emphasized the living anionic polymerization of functional styrene derivatives. With the finding of anion-stable functionalities and the development of two strategies using protective and EWG groups, many styrene derivatives carrying almost all the useful functionalities now acquire the ability to undergo the living anionic polymerization. Most of such functionalities were believed to be incompatible with highly reactive anionic initiators like RLi and alkali-metal naphthalenides and living polystyrenes until the 1980s. Most importantly, anion-stable functionalities and two successful strategies for the living anionic polymerization of styrene may possibly be applied to the living anionic polymerization systems of other functional monomers, whose monomer frameworks are 1,3-butadiene, 2VP, alkyl methacrylates, *tert*-butyl acrylate, *N,N*-

dialkylacrylamides, and several cyclic monomers, since their living chain-end anions are similar to or lower in reactivity than the living polystyrene. This will enable the synthetic range of available living anionic polymers with functional groups to be significantly broadened. The success of the living anionic polymerization of functional monomers can lead to the precise synthesis of block polymers and macromolecular architectures carrying such functional groups.

Abbreviations

(NCA)s	α-Amino acid *N*-carboxyanhydrides
(TMS)$_2$B	2,3-Bis(trimethylsilyl)-1,3-butadiene
2VP	2-Vinylpyridine
BF	Benzofulvene
CHD	1,3-Cyclohexadiene
DPE	1,1-Diphenylethylene
DVB	1,4-Divinylbenzene
EWGs	Electron-withdrawing groups
HMPT	*N,N,N′,N′,N″,N″*-hexamethylphosphortriamide
KOBu^t	Potassium *tert*-butoxide
MMA	Methyl methacrylate
MOP3D	2-(4-Methoxyphenyl)[3]dendralene
MWD	Molecular weight distribution
P3D	2-Phenyl[3]dendralene
PA	Phosphaalkene
PB	Poly(1,3-butadiene)
PI	Polyisoprene
PS	Polystyrene
PSLi	Poly(styryl)lithium
RLi	Organolithium
SABB	2-(4-Bis(trimethylsilyl)amino)butyl-1,3-butadiene
SAMB	2-Bis(trimethylsilyl)aminomethyl-1,3-butadiene
SEC	Size exclusion chromatography
sec-BuLi	*sec*-Butyllithium
TBDMS	*tert*-Butyldimethylsilyl
TBDMSOS	4-*tert*-Butyldimethylsilyloxystyrene
TBSOM-DPE	1,1-Bis(3-*tert*-butyldimethylsilyloxymethylphenyl)ethylene
TBSOMP	3-*tert*-Butyldimethylsilyloxymethylphenyl
TESB	2-Triethylsilyl-1,3-butadiene
TGIC	Temperature gradient interaction chromatography
TIPOSB	2-Triisopropoxysilyl-1,3-butadiene
TMEDA	*N,N,N′,N′*-Tetramethylethylenediamine
TMOSB	2-Trimethoxysilyl-1,3-butadiene
TMS	Trimethylsilyl

| TMSB | 2-Trimethylsilyl-1,3-butadiene |
| TMSMB | 2-(Trimethylsilyl)methyl-1,3-butadiene |

References

1. Quirk RP (1996) General aspect of anionic polymerization. In: Hsieh HL, Quirk RP (eds) Anionic polymerization: principles and practical applications. Marcel Dekker, New York, pp 93–127
2. Ishizone T, Sugiyama K, Hirao A (2012) Anionic polymerization of protected functional monomers. In: Matyjaszewski K, Möller M (eds) Polymer science: a comprehensive reference, vol 3. Elsevier BV, Amsterdam, pp 591–621
3. Quirk RP, Pickel DL (2012) Anionic polymerization of nonpolar monomers. In: Matyjaszewski K, Möller M (eds) Polymer science: a comprehensive reference, vol 3. Elsevier BV, Amsterdam, pp 559–590
4. Ishizone T, Hirao A (2012) Anionic polymerization: recent advances. In: Schlüter D, Hawker CJ, Sakamoto J (eds) Synthesis of polymers: new structures and methods, vol 1. Wiley-VCH, Singapore, pp 81–133
5. Szwarc M (1956) 'Living' polymers. Nature 178:1168–1169
6. Morton M, Bostick EE, Clarke RG (1963) Homogeneous anionic polymerization. III. Molecular weight of polyisoprene initiated by butyllthiums. J Polym Sci A 1:475–482
7. Morton M, Bostick EE, Livingni RA, Fetters LJ (1963) Homogeneous anionic polymerization. IV. Kinetics of butadiene and isoprene polymerization with butyllithium. J Polym Sci A 1:1735–1742
8. Morton M, Fetters LJ (1975) Anionic polymerization of vinyl monomers. Rubber Chem Technol 48:359–409
9. Quirk RP (1996) Living polymerizations: definitions, consequences, and criteria. In: Hsieh HL, Quirk RP (eds) Anionic polymerization: principles and practical applications. Marcel Dekker, New York, pp 71–92
10. Lee W, Lee H, Cha J, Chang T, Hanley KJ, Lodge TP (2000) Molecular weight distribution of polystyrene made by anionic polymerization. Macromolecules 33:5111–5115
11. Sakellariou G, Baskaran D, Hadjichristidis N, Mays JW (2006) Well-defined poly (4-vinylbenzocyclobutene): synthesis by living anionic polymerization and characterization. Macromolecules 39:3525–3530
12. Kobayashi S, Matsuzawa T, Matsuoka S, Tajima H, Ishizone T (2006) Living anionic polymerizations of 4-(1-adamantyl)styrene and 3-(4-vinylphenyl)-1,1'-biadamantane. Macromolecules 39:5979–5986
13. Kobayashi S, Kataoka H, Ishizone T, Kato T, Ono T, Kobutaka S, Ogi H (2008) Synthesis and properties of new thermoplastic elastomers containing poly[4-(1-adamantyl)styrene] hard Segments. Macromolecules 41:5502–5508
14. Sugiyama K, Hirao A, Hsu JC, Tung YC, Chen WC (2009) Living anionic polymerization of styrene derivatives *para*-substituted with π-conjugated oligo(fluorine) moieties. Macromolecules 42:4053–4062
15. Senshu K, Kobayashi M, Ikawa N, Yamashita S, Hirao A, Nakahama S (1999) Relationship between morphology of microphase-separated structure and phase restructuring at the surface. Langmuir 15:1763–1769
16. Whiteham GH (1979) Comprehensive organic chemistry. In: Stoddart JF (ed) vol 1. Pergamon Press, Oxford, pp 154–155

17. Baily WF, Patricia JJ (1988) The mechanism of the lithium-halogen interchange reaction. J Organomet Chem 352:1–46
18. Zhang H, Ruckenstein E (1999) Selective living anionic polymerization of a novel bifunctional monomer 4-(vinylphenyl)-1-butene. Macromolecules 32:5495–5500
19. Hirao A, Kubota S, Sueyoshi T, Sugiyama K (2001) Living anionic polymerization of functionalized monomers. 2. Macromol Chem Phys 202:1044–1052
20. Lutz P, Beinert G, Rempp P (1982) Anionic polymerization and copolymerization of 1,3- and 1,4-diisoprepenylbenzenes. Makromol Chem 183:2787–2797
21. Hirao A, Imai T, Watanabe K, Hayashi M, Sugiyama K (2006) Living anionic polymerization of 4-(α-alkylvinyl)styrene derivatives. Chem Mon 137:855–867
22. Hayashi M, Inagaki K, Sugiyama K, Hirao A (2006) Synthesis of well-defined poly (4-isopropenylstyrene) by living anionic polymerization and its application to graft copolymers using styrene-butadiene copolymer anions. Kautsch Gummi Kunstst 7(8):396–398
23. Sugiyama K, Watanabe K, Hirao A, Hayashi M (2008) Living anionic polymerization of 4-(α-alkylvinyl)styrene derivatives. Macromolecules 41:4235–4244
24. Hirao A, Kitamura M, Loykulnant S (2004) Living anionic polymerization of 4-(4-(2-isopropylphenoxy)butyl)styrene, A new dual functionalized styrene derivatives having α-methylstyrene functionality. Macromolecules 37:4770–4775
25. Hirao A, Kitamura M, Hayashi M, Loykulnant S, Sugiyama K (2005) Anionic polymerization of new dual-functionalized styrene and α-methylstyrene derivatives having styrene and α-methylstyrene moiety. Macromol Symp 226:35–50
26. Hirao A, Tanaka S, Goseki G, Ishizone T (2011) Living anionic polymerization of 1,4-divinylbenzene. Macromolecules 44:4579–4582
27. Tanaka S, Matsumoto M, Goseki R, Ishizone T, Hirao A (2013) Living anionic polymerization of 1,4-divinylbenzene and its isomers. Macromolecules 46:146–154
28. Tanaka S, Goseki R, Ishizone T, Hirao A (2014) Synthesis of well-defined novel reactive block polymers containing a poly(1,4-divinylbenzene) segment by living anionic polymerization. Macromolecules 47:2333–2339. doi:10.1021/ma402657t
29. Ishizone T, Uehara G, Hirao A, Nakahama S (1998) Anionic polymerizations of 2-, 3-, and 4-(3,3-dimethyl-1-butynyl)styrenes, 2-, 3-, and 4-(1-hexynyl)styrenes, and 4-(phenylethynyl) styrene. Macromolecules 31:3764–3774
30. Se K, Watanabe O, Isono Y, Fujimoto T (1989) Synthesis and characterization of model block-graft copolymers via anionic polymerization. Macromol Symp 25:249–261
31. Se K, Kijima M, Fujimoto T (1988) Anionic polymerization of tertiary aminostyrenes and characterization of the polymers. Polym J 20:791–799
32. Kopolow S, Hogen-Esch TE, Smid J (1973) Poly(vinyl macrocyclic polyethers). Macromolecules 6:133–142
33. Higashihara T, Ueda M (2009) Living anionic polymerization of 4-vinyltriphenylamine for synthesis of novel block copolymers containing low-polydisperse poly(4-vinyltriphenylamine) and regioregular poly(3-hexylthiophene) segments. Macromolecules 42:8794–8800
34. Kang BG, Kang NG, Lee JS (2010) Living anionic polymerization of styrene derivatives containing triphenylamine moieties through introduction of protecting group. Macromolecules 43:8400–8408
35. Hirao A, Shione H, Ishizone T, Nakahama S (1997) Anionic polymerization of monomers containing functional groups 9. Anionic polymerization of 4-vinylphenyl methyl sulfide and 2-(4-vinylphenyl)ethyl methyl sulfide. Macromolecules 30:3728–3731
36. Sugiyama K, Ishizone T, Hirao A, Nakahama S (1995) Anionic polymerization of fluorostyrenes. Acta Polym 46:424–431
37. Chaumont P, Bernert G, Herz JE, Rempp P (1982) Synthesis and properties of poly(p-trimethylsilylstyrene). Makromol Chem 183:1181–1190
38. Saigo K, Watanabe F (1989) Synthesis of nearly monodisperse poly(α-methylstyrene)s containing two Si atoms and an allyl group. J Polym Sci A Polym Chem 27:2611–2624

39. Hirao A, Nakahama S (1992) Anionic living polymerization of monomers with functional silyl groups. Prog Polym Sci 17:283–317
40. Hirao A, Loykulnant S, Ishizone T (2002) Recent advance in living anionic polymerization of functionalized styrene derivatives. Prog Polym Sci 27:1399–1471
41. Hirao A, Ando Y, Ishizone T, Nakahama S (2003) Anionic polymerization of *p*-pentamethyldisilyl-, *p*-heptamethyltrisilyl-, and *p*-nonamethyltetrasilylstyrenes. Macromolecules 36:5081–5087
42. Yamazaki N, Nakahama S, Hirao A, Goto J, Shiraishi Y, Martinez F, Phung HM (1981) Anionic polymerization of *p*-triphenyltinstyrene. J Macromol Sci Chem A16:1129–1144
43. Hirao A, Shiraishi Y, Martinez F, Phung HM, Nakahama S, Yamazaki N (1983) Anionic and radical polymerizations of *p*-triphenyl- and *p*-tributylgermylstyrenes. Makromol Chem 184:961–967
44. Kase T, Imahori M, Kazama T, Isono Y, Fujimoto T (1991) Anionic living polymerization of an α-methylstyrene derivative containing the bis(diethylamino)phosphino group. Macromolecules 21:1714–1719
45. Börner HG, Heitz W (2000) Anionic block copolymerization of vinyl functionalized triphenylphosphines with styrene. Macromol Chem Phys 201:740–746
46. Nakahama S, Hirao A (1990) Protection and polymerization of functional monomers: anionic living polymerization of protected monomers. Prog Polym Sci 15:299–335
47. Hirao A, Nakahama S (1994) Recent developments in anionic living polymerization. Trends Polym Sci 2:267–271
48. Hirao A, Nakahama S (1996) Anionic polymerization. In: Archady R (ed) Desk reference of functional polymers. ACS, Washington, DC, pp 19–34
49. Hirao A, Nakahama S (1998) Anionic living polymerization of functionalized monomers. Acta Polym 49:133–144
50. Hirao A, Yamaguchi K, Takenaka K, Suzuki K, Nakahama S, Yamazaki N (1982) Synthesis of poly(4-vinylphenol) by means of anionic living polymerization. Makromol Chem Rapid Commun 3:941–946
51. Hirao A, Takenaka K, Packirisamy S, Yamaguchi K, Nakahama S (1985) Studies on anionic living polymerization of 4-(*tert*-butyldimethylsilyloxy)styrene. Makromol Chem 186:1157–1166
52. Hirao A, Kitamura K, Takenaka K, Nakahama S (1993) Syntheses of well-defined poly (vinylphenol), poly((vinylphenyl)methanol), and poly(2-(vinylphenyl)ethanol) by means of anionic living polymerization of styrene derivatives containing *tert*-butyldimethylsilyl ethers. Macromolecules 26:4995–5003
53. The living anionic polymerization of the protected 4-vinylphenols with methoxymethoxy and tetrahydropyranyl ethers quantitatively proceeded with oligo(α-methylstyryl)potassium in THF at −78°C for 1 h to afford polymers with predictable molecular weights and narrow molecular weight distributions ($M_n = 35,000$ g/mol and 14,000 g/mol, $M_w/M_n = 1.05$ and 1.09)
54. Hirao A, Takenaka K, Yamaguchi K, Nakahama S, Yamazaki N (1983) Synthesis of poly (2-(4-vinylphenyl)ethanol) by anionic living polymerization. Polymer 24:339–341
55. Hirao A, Yamamoto A, Takenaka K, Yamaguchi K, Nakahama S (1987) Anionic living polymerization of 4-(2-trialkylsilyloxyethyl)styrene as protected 4-(2-hydroxyethyl)styrene. Polymer 28:303–310
56. Hirao A, Shione H, Wakabayashi S, Nakahama S (1994) Anionic polymerization of 4-vinylphenyl *tert*-butyldimethylsilyl sulfide and 2-(4-vinylphenyl)ethyl *tert*-butyldimethylsilyl sulfide. Macromolecules 22:2607–2611
57. Hirao A, Kato K, Nakahama S (1992) Synthesis of well-defined poly(vinylacetophenone)s by means of anionic living polymerization of *tert*-butyldimethylsilyl enol ethers of vinylacetophenones. Macromolecules 25:535–540

58. Yamaguchi K, Hirao A, Suzuki K, Takenaka K, Nakahama S, Yamazaki N (1983) Anionic living polymerization of p-N, N-bis(trimethylsilyl)aminostyrene. J Polym Sci Polym Lett Ed 21:395–401

59. Suzuki K, Hirao A, Yamaguchi K, Nakahama S (1989) Synthesis of well-defined poly (4-aminostyrene) by means of anionic living polymerization of p-N, N-bis(trimethylsilyl) aminostyrene. Macromolecules 22:2607–2611

60. Suzuki K, Hirao A, Nakahama S (1989) Anionic living polymerization of 4-N, N-bis (trimethylsilyl)aminomethylstyrene and 4-(2-N, N-bis(trimethylsilyl)amino)ethylstyrene. Makromol Chem 190:2893–2901

61. Ishizone T, Hirao A, Nakahama S, Kakuchi T, Yokota K, Tsuda K (1991) Anionic living polymerization of 4-trimethylsilylethynylstyrene. Macromolecules 24:5230–5231

62. Tsuda K, Ishizone T, Hirao A, Nakahama S, Kakuchi T, Yokota K (1993) Synthesis of well-defined poly(ethynylstyrene)s by means of anionic living polymerization of trimethylsilyl-lethynylstyrenes. Macromolecules 26:6985–6991

63. Ishizone T, Hirao A, Nakahama S, Tsuda K (1996) Synthesis of well-defined poly (4-(3-butynylstyrene)s) by means of anionic living polymerization of 4-(4-trimethylsilyl-3-butynyl) styrene. Macromol Chem Phys 197:1781–1791

64. Hirao A, Ishino Y, Nakahama S (1986) Synthesis of linear poly(4-vinylbenzaldehyde) by means of anionic living polymerization of 1,3-dimethyl-2-(4-vinylphenyl)imidazolidine and subsequent hydrolysis. Makromol Chem 187:141–147

65. Ishizone T, Tominaga T, Kitamura K, Hirao A, Nakahama S (1995) Synthesis of well-defined polystyrene bearing a triol functionality by means of anionic living polymerization of 4-(4-(4-vinylphenyl)butoxy)methyl-1-methyl-2,6,7-trioxabicyclo[2.2.2]octane. Macromole-cules 28:4829–4836

66. Hirao A (1989) Unpublished results

67. Ishizone T, Kato R, Ishino Y, Hirao A, Nakahama S (1991) Anionic living polymerization of 2-(3-vinylphenyl)-1,3-dioxolane and related monomers. Macromolecules 24:1449–1454

68. Ishizone T, Okamoto K, Hirao A, Nakahama S (1999) Syntheses of well-defined poly ((4-vinylphenyl)acetic acid), poly(3-(4-vinylphenyl)propionic acid), and poly (3-vinylbenzoic acid) by means of anionic living polymerization of protected monomers bearing bicyclic ortho ester moieties. Macromolecules 32:1453–1462

69. Hirao A (1990) Unpublished results. The *tert*-butyl ether- and acetal-protected monomers were observed to undergo living anionic polymerization in THF at $-78°$C with oligo (α-methylstyryl)lithium for 1 h to quantitatively yield the polymers with predictable molecular weights ($M_n = 26,700$ g/mol and 20,500 g/mol) and narrow molecular weight distributions ($M_w/M_n = 1.03$ and 1.04), respectively

70. Moss RJ, Rickborn B (1984) α-Methoxy-*o*-xylylene: formation by LiNR$_2$-induced 1,4-elimination of *o*-tolualdehyde dimethyl acetal. J Org Chem 49:3694–3701

71. Moss RJ, White RO, Rickborn B (1984) α, α-Dimethoxy-o-xylylene: formation by 1,4-elimination and electrocyclic routes and reactions. Org Chem 50:5132–5139

72. Hirao A, Negishi Y, Hayashi M, Seko K, Ryu SW, Loykulnant S, Matsuo A, Sugiyama K (2001) Anionic polymerization and reaction of styrene and DPE derivatives substituted with alkoxymethyl groups. Macromol Chem Phys 202:3590–3605

73. Loykulnant S, Hayashi M, Hirao A (1998) Anionic living polymerization of styrene derivatives containing acetal-protected monosaccharide residues. Macromolecules 31:9121–9126

74. Hirao A, Hayashi M, Loykulnant S (2000) Precise synthesis of various functionalized polystyrenes with monosaccharide residues by anionic living polymerization and living functionalization. Macromol Symp 161:45–52

75. Loykulnant S, Yamashiro M, Hirao A (2001) Living anionic polymerization of styrene derivatives m, m'-disubstituted with acetal-protected monosaccharide residues. Macromol Chem Phys 202:1791–1798

76. Loykulnant S, Hirao A (2000) Living anionic polymerization of 4-alkylstyrenes containing acetal-protected monosaccharide residues. Macromolecules 33:4757–4764

77. Hirao A, Hayashi M (1999) Synthesis of well-defined functionalized PSs with a definite number of chloromethylphenyl groups at chain-end or in-chains by means of living anionic polymerization in conjunction with functional group transformation. Macromolecules 32:6450–6460

78. Ryu SW, Hirao A (2000) Anionic synthesis of well-defined poly(*m*-halomethylstyrene)s and branched polymers via graft-onto methodology. Macromolecules 33:4765–4771

79. Ryu SW, Hirao A (2001) Synthesis of well-defined highly branched polymers and graft copolymers having one branch per repeating unit using poly(*m*-halomethylstyrene)s as backbone polymers. Macromol Chem Phys 202:1727–1736

80. Nakahama S, Ishizone T, Hirao A (1993) Anionic living polymerization of styrenes containing electron-withdrawing groups. Macromol Symp 67:223–236

81. Ishizone T, Hirao A, Nakahama S (1996) Anionic living polymerization of styrenes substituted with electron-withdrawing groups. Kobunshi Ronbunshu 54:829–842

82. Ishizone T, Hirao A, Nakahama S (1993) Anionic block copolymerization of styrenes derivatives *para*-substituted with electron-withdrawing groups. Macromolecules 26:6964–6975

83. Hirao A, Nakahama S (1986) Anionic living polymerization of 4-vinyl(N, N-diisopropyl-benzamide). Polymer 27:309–312

84. Ishino Y, Hirao A, Nakahama S (1986) Anionic living polymerization of 2-(4-vinylphenyl)-4,4-dimethyl-2-oxazoline. Macromolecules 19:2307–2309

85. Hirao A, Nakahama S (1987) Synthesis of well-defined poly(4-vinylbenzaldehyde) by the anionic living polymerization of *N*-((4-ethenylphenyl)methylene)cyclohexamine. Macromolecules 20:2968–2972

86. Hirao A, Ishino Y, Nakahama S (1988) Synthesis of well-defined poly(4-vinylbenzoic acid) by means of anionic living polymerization of 2-(4-vinylphenyl)-4,4-dimethyl-2-oxazoline. Macromolecules 21:561–565

87. Ishizone T, Hirao A, Nakahama S (1989) Anionic living polymerization of *tert*-butyl 4-vinylbenzoate. Macromolecules 22:2895–2901

88. Ishizone T, Wakabayashi S, Hirao A, Nakahama S (1991) Anionic living polymerization of N, N-dialkyl 4-vinylbenzamides. Macromolecules 24:5015–5022

89. Ishizone T, Hirao A, Nakahama S (1991) Anionic living polymerization of 4-cyanostyrene. Macromolecules 24:625–626

90. Ishizone T, Tsuchiya J, Hirao A, Nakahama S (1992) Anionic living polymerization of N, N-dialkyl-4-vinylbenzenesulfonamides. Macromolecules 25:4840–4847

91. Ishizone T, Sugiyama K, Hirao A, Nakahama S (1993) Anionic polymerization of 2-, 3-, and 4-cyanostyrenes. Macromolecules 26:3009–3018

92. Ishizone T, Sueyasu N, Sugiyama K, Hirao A, Nakahama S (1993) Anionic polymerization of *N*-alkyl-*N*-(4-vinylbenzylidene)amines. Macromolecules 26:6976–6984

93. Ishizone T, Kurosawa H, Hirao A, Nakahama S (1994) Synthesis of well-defined poly (4-vinylbenzoic acid) by means of anionic living polymerization of *N*-(4-vinylbenzoyl)-*N'*-methylpiperazine, followed by deprotection. Macromol Chem Phys 195:3173–3187

94. Ishizone T, Utaka T, Ishino Y, Hirao A, Nakahama S (1997) Anionic polymerization of *N*-aryl-*N*-(4-vinylbenzylidene)amines. Macromolecules 30:6458–6466

95. Ishizone T, Okazawa Y, Ohnuma K, Hirao A, Nakahama S (1997) Anionic living polymerization of 4-cyano-α-methylstyrene. Macromolecules 30:757–763

96. Ishizone T, Tsuchiya J, Hirao A, Nakahama S (1998) Synthesis of well-defined poly (4-vinyl-α-methylcinnamic acid) by means of anionic living polymerization of 2-(1-methyl-2-(4-ethenylphenyl)ethenyl)-4,4-dimethyl-2-oxazoline. Macromolecules 31:5598–5608

97. Ishizone T, Ohnuma K, Okazawa Y, Hirao A, Nakahama S (1998) Anionic equilibrium polymerization of 4-cyano-α-methylstyrene. Macromolecules 31:2797–2803

98. Ishizone T, Kato H, Yamazaki D, Hirao A, Nakahama S (2000) Anionic polymerization of aryl 4-vinylbenzoate. Macromol Chem Phys 201:1077–1087

99. Driva P, Pickel DL, Mays JW, Baskaran D (2010) A new approach to the living anionic polymerization of 4-cyanostyrene. Macromolecules 43:6915–6918

100. Hattam P, Gauntlett S, Mays JW, Hadjichristidis N, Young RN, Fetters LJ (1991) Conformational characteristics of some model polydienes and polyolefins. Macromolecules 24:6199–6209

101. Ohno R, Tanaka Y, Kawakami M (1973) Synthesis and characterization of 2-alkylbtadiene polymers. Polym J 4:56–60

102. Asami R, Higaki T (1970) Anionic polymerization of 1-*tert*-butyl- and 2-*tert*-butyl-1,3-butadiene. Polym Prepr Jpn 19:8

103. Asami R, Higaki T (1971) Substituent effect in the anionic polymerization of *tert*-butyl- and phenyl-substituent butadienes. Polym Prepr Jpn 20:261–264

104. Natori I (1997) Synthesis of polymers with an alicyclic structure in the main chain. Living anionic polymerization of 1,3-cyclohexadiene with the n-BuLi/TMEDA system. Macromolecules 30:3696–3697

105. Natori I, Inoue S (1998) Living anionic polymerization of 1,3-cyclohexadiene with the n-BuLi/TMEDA system. Copolymerization and block copolymerization with styrene, butadiene, and isoprene. Macromolecules 31:982–987

106. Hong K, Wan Y, Mays JW (2001) Near monodisperse star and star-block polymers based on poly(1,3-cyclohexadiene). Macromolecules 34:2482–2487

107. Williamson DT, Elman JF, Madison PH, Pasquale AJ, Long TE (2001) Synthesis and characterization of poly(1,3-cyclohexadiene) homopolymers and star-shaped polymers. Macromolecules 34:2108–2114

108. Quirk RP, You F, Wesdemiotis C, Arnould MA (2004) Anionic synthesis and characterization of ω-hydroxy-functionalized poly(1,3-cycloheadiene). Macromolecules 37:1234–1242

109. Kobayashi S, Kataoka H, Ishizone T (2009) Synthesis of well-defined poly(ethylene-*alt*-vinyladamantane) via living anionic polymerization of 2-(1-adamantyl)-1,3-buadiene, followed by hydrogenation. Macromolecules 42:5017–5026

110. Kobayashi S, Kataoka H, Ishizone T, Kato T, Ono T, Kubotaka S, Arimoto K, Ogi H (2009) Synthesis of well-defined random and block copolymers of 2-(1-adamantyl)-1,3-buadiene with isoprene via anionic polymerization. React Funct Polym 69:409–415

111. Yuki H, Okamoto Y, Takano H (1971) Anionic polymerization of 2,3-dimethylbutadiene. Polym J 2:663–669

112. Xu Z, Mays JW, Chen X, Hadjichristidis N, Schilling FC, Bair HE, Pearson DS, Fetters LJ (1985) Molecular characterization of poly(2-methyl-1,3-pentadiene) and its hydrogenated derivative, atactic polypropylene. Macromolecules 18:2560–2566

113. Suzuki T, Tsuji Y, Takegami Y (1978) Microstructure of poly(1-phenylbutadiene) prepared by anionic initiator. Macromolecules 11:639–644

114. Suzuki T, Tsuji Y, Takegami Y, Harwood HJ (1979) Microstructure of poly(2-phenylbutadiene) prepared by anionic initiators. Macromolecules 12:234–239

115. Kase T, Imahori M, Komiyatani T, Ito K, Isono Y, Fujimoto T (1990) Molecular characterization of poly(2-phenyl-1,3-butadiene) prepared by anionic living polymerization. Kobunshi Ronbunshu 47:17–24

116. Hirao A, Sakano Y, Takenaka K, Nakahama S (1998) Anionic living polymerization of 2,3-diphenyl-1,3-buadiene. Macromolecules 31:9141–9145

117. Quirk RP, Bhatia R (1989) Alkyllithium-initiated polymerization of trans-1,3,5-hexatriene and copolymerization with styrene. Rubber Chem Technol 62:332–342

118. Petzhold C, Morschhäuser R, Kolshorn H, Stadler R (1994) On the anionic polymerization of (dialkylamino)isoprenes. 2. Macromolecules 27:3707–3713

119. Takenaka K, Nakashima D, Miya M, Takeshita H, Shiomi T (2013) Anionic polymerization of 2-(N, N-bistrimethylsilylaminomethyl)-1,3-butadiene and 2-(4-(N, N-bistrimethylsilylamino)butyl)-1,3-butadiene. E-J Soft Mater 9:14–19

120. Takenaka K, Hattori T, Hirao A, Nakahama S (1992) Anionic polymerization of 2-silyl-substituted 1,3-butadienes with mixed substituents. Macromolecules 25:96–101

121. Ding YX, Weber WP (1988) Regio- and stereospecific 1,4-polymerization of 2-(triethylsilyl)-1,3-butadiene. Macromolecules 21:530–532
122. Ding YX, Weber WP (1988) Stereoregularity in Ziegler-Natta and anionic polymerization of 2-(trimethylsilyl)methyl-1,3-butadiene. Macromolecules 21:2672–2674
123. Ding YX, Weber WP (1988) Stereospecific 1,4-polymerization of 2,3-bis(trimethylsilyl)-1,3-butaidene. J Organomet Chem 341:267–271
124. Bates CM, Pantoja MAB, Strahan JR, Dean LM, Mueller BK, Ellison CJ, Wealey PF, Willson CG (2013) Synthesis and thin-film orientation of poly(styrene-*block*-trimethylsilylisoprene). J Polym Sci A Polym Chem 51:290–297
125. Takenaka K, Hirao A, Hattori T, Nakahama S (1987) Anionic polymerization of 2-trimethoxysilyl-substituted 1,3-butadiene. Macromolecules 20:2035–2037
126. Takenaka K, Hattori T, Hirao A, Nakahama S (1989) Anionic polymerization of 2-trialkoxysilyl-substituted 1,3-butadiene. Macromolecules 22:1563–1567
127. Hirao A, Hiraishi Y, Nakahama S (1998) Anionic polymerization of 2-(N, N-dialkylamino) dimethylsilyl-1,3-butadiene. Macromolecules 31:281–287
128. Takenaka K, Shibata N, Tsuchida S, Takeshita H, Miya M, Shiomi T (2008) Anionic polymerization of N, N-diethyl-2-methylene-3-butenamide. E-J Soft Mater 4:23–29
129. Payne AD, Bojase G, Paddon-Row MN, Sherburn MS (2009) Practical synthesis of the dendralene family reveals alternation in behavior. Angew Chem Int Ed 48:4836–4839
130. Takenaka K, Amamoto S, Kishi H, Takeshita H, Miya M, Shiomi T (2013) Anionic polymerization of 2-phenyl[3]dendralene and 2-(4-methoxyphenyl)[3]dendralene. Macromolecules 46:7282–7289
131. Quirk RP, Yin J, Guo SH, Hu XW, Summers G, Kim J, Zhu LF, Schock LE (1990) Anionic synthesis of chain-end functionalized polymers. Macromol Symp 32:47–599
132. Quirk RP, Kim J, Rodrigues K, Mattice WL (1991) Anionic synthesis and characterization of PS-*b*-PEO polymers with fluorescent probes at the block junctions. Macromol Symp 42/43:463–473
133. Quirk RP, Yin J, Guo SH, Hu XW, Summers G, Kim J, Zhu LF, Ma JJ, Takizawa T, Lynch T (1991) Recent advances in anionic synthesis of functionalized polymers. Rubber Chem Technol 64:648–660
134. Quirk RP (1992) Scope and limitation of 1,1-diphenylethylene chemistry in anionic polymer synthesis. Macromol Symp 63:259–269
135. Quirk RP (1996) Functionalized polymers and macromonomers. In: Hsieh HL, Quirk RP (eds) Anionic polymerization: principles and practical applications. Marcel Dekker, New York, pp 261–306
136. Quirk RP (2012) Controlled end-group functionalization. In: Matyjaszewski K, Möller M (eds) Polymer science: a comprehensive reference, vol 6. Elsevier BV, Amsterdam, pp 351–412
137. Hirao A, Haraguchi N (2002) Anionic synthesis of well-defined star-branched polymers by using chain-end-functionalized PSs with dendritic BnBr moieties. Macromolecules 35:7224–7231
138. Hirao A, Matsuo A (2003) Synthesis of chain-end-functionalized PMMAs with a definite number of BnBr moieties and their application to star-branched polymers. Macromolecules 36:9742–9751
139. Haraguchi N, Hirao A (2003) Synthesis of well-defined star-linear block polymers by coupling reactions of chain-functionalized polystyrenes with a definite number of benzyl bromide moieties with PSLis. Macromolecules 36:9364–9372
140. Heitz T, Höcker H (1988) Synthesis of PS macromonomers for use in polycondensation reactions. Makromol Chem 189:777–789
141. Quirk RP, Perry S, Mendicuti F, Mattice WL (1988) New method for quantitative functionalization of the terminus in PS. Naphthalene functional Macromol 21:2294–2295
142. Quirk RP, Zhu L (1989) Anionic synthesis of chain-end-functionalized polymers using DPE derivertives. Makromol Chem 190:487–493

143. Quirk RP, Zhu L (1989) Anionic synthesis of dimethylamino-functionalized PSs and PMMAs using 1-(4-dimethylaminophenyl)-1-phenylethylene. Br Polym J 23:47–54

144. Al-Takrity ETB, Jenkins AD, Walton DRM (1990) The synthesis of polymers bearing terminal fluorescent and fluorescent-quenching groups, 1. Makromol Chem 191:3059–3067

145. Quirk RP, Wang Y (1993) Anionic difunctionalization with 1,1-bis(4-*tert*-butyldimethylsilyloxyphenyl)ethylene. Polym Int 31:51–59

146. Quirk RP, Lynch T (1993) Anionic synthesis of primary amine-functionalized PSs using 1-(4-(N, N-bis(trimethylsilyl)amino)phenyl)-1-phenylethylene. Macromolecules 26:1206–1212

147. Quirk RP, Yoo T, Lee B (1994) Anionic synthesis of heteroarm star branched polymers. J Macromol Sci Pure Appl Chem A31:911–926

148. Summers GJ, Quirk RP (1996) Anionic synthesis of aromatic carboxy functionalized polymers. Polym Int 40:79–83

149. Summers GJ, Quirk RP (1998) Anionic synthesis of aromatic amide and carboxy-functionalized polymers. J Polym Scit A Polym Chem 36:1233–1241

150. Hirao A (1998) Unpublished results. The addition reaction of PSLi to 1-(4-trimethylethynylphenyl)-1-phenylethylene proceeded quantitatively in THF at -78°C for 1 h. The resulting polymer was quantitatively end-functionalized with ethynyl group ($M_n = 10,000$ g/mol, $M_w/M_n = 1.03$)

151. Hayashi M, Loykulnant S, Hirao A (1998) Synthesis of well-defined end-functionalized polymers with one, two, three, or four monosaccharide residues. Macromolecules 31:2057–2063

152. Kim J, Kwak S, Kim KU, Kim KH, Cho JC, Lim D, Kim D (1998) Synthesis of a DPE derivative carrying aromatic *tert*-amine groups and its use in chain end functionalization of RLi-initiated polymerizations. Macromol Chem Phys 199:2185–2191

153. Hirao A, Haraguchi N, Sugiyama K (1999) Synthesis of functionalized polymers with α-methylstyryl groups by anionic reaction with use of 1-(4-(3-(4-isopropenylphnyl)propyl) phenyl)-1-phenylethylene. Macromolecules 32:48–54

154. Hirao A, Hayashi M (1999) Synthesis of well-defined functionalized PSs with a definite number of chloromethylphenyl groups at chain-ends or in-chains by means of anionic living polymerization in conjunction with functional group transformation. Macromolecules 32:6450–6460

155. Hayashi M, Kojima K, Hirao A (1999) Synthesis of star-branched polymers by means of living anionic polymerization coupled with functional group transformation. Macromolecules 32:2425–2433

156. Hirao A, Hayashi M, Loykulnant S (2000) Precise synthesis of various functionalized polystyrenes with monosaccharide residues by anionic living polymerization and living functionalization. Macromol Symp 161:45–52

157. Hirao A, Negishi Y, Hayashi M, Sako K, Ryu SW, Loykulnant S, Matsuo A (2001) Anionic polymerization and reaction of styrene and DPE derivatives substituted with alkoxymethyl groups. Macromol Chem Phys 202:3590–3605

158. Haraguchi N, Sakaguchi Y, Sugiyama K, Hirao A (2001) Synthesis of well-defined chain-end and in-chain functionalized polymers with 1,3-butadienyl groups. Macromol Chem Phys 202:2221–2230

159. Reutenauer S, Hurtres G, Dumas P (2001) A new route to model (A_2B) and regular graft copolymers. Macromolecules 34:755–760

160. Higashihara T, Sugiyama K, Yoo HS, Hayashi M, Hirao A (2010) Combining living anionic polymerization with branching reactions in an iterative fashion to design branched polymers. Macromol Rapid Commun 31:1031–1059

161. Hirao A, Murano K, Oie T, Uematsu M, Goseki R, Matsuo Y (2011) Chain-end- and in-chain-functionalized AB diblock copolymers as key building blocks in the synthesis of well-defined architectural polymers. Polym Chem 2:1219–1233

162. Hirao A, Goseki R, Ishizone T (2014) Advance in living anionic polymerization. Macromolecules 47:1883–1905
163. Aldissi M, Schue F, Geckeler K, Abadie M (1980) Oligomérisation anionique de l'éthylène, 5. Fonctionalisation des oligomères vivants par action directe de l'oxygène. Makromol Chem 181:1425–1434
164. Bergbreiter DE, Blanton JR, Chandran R, Hein MD, Huang KJ, Treadwell DR, Walker SA (1989) Anionic syntheses of terminally functionalized ethylene oligomers. J Polym Sci Polym Chem Ed 27:4205–4226
165. Oku J, Hasegawa T, Takeuchi T, Takaki M (1991) Polymerization behavior of trimethylvinylsilane. Polym J 23:1377–1382
166. Tsang C-W, Yam M, Gates DP (2003) The addition polymerization of a P═C bond: a route to new phosphine polymers. J Am Chem Soc 125:1480–1481
167. Noonan KJT, Gates DP (2006) Ambient-temperature living anionic polymerization of phospaalkenes: homopolymers and block copolymers with controlled chain lengths. Angew Chem Int Ed 45:7271–7274
168. Noonan KJT, Gillon BH, Cappello V, Gates DP (2008) Phosphorus-containing block copolymer templetes can control the size and shape of gold nanostructure. J Am Chem Soc 130:12876–12877
169. Kosaka Y, Kitazawa K, Inomata S, Ishizone T (2013) Living anionic polymerization of benzofulvene: highly reactive fixed transoid 1,3-diene. ACS Macro Lett 2:164–167

Anionic Polymerization of Polar Vinyl Monomers: Vinylpyridines, (Meth)acrylates, (Meth)acrylamides, (Meth)acrylonitrile, Phenyl Vinyl Sulfoxide, Benzofulvene, and Other Monomers

Takashi Ishizone, Yuki Kosaka, and Raita Goseki

Abstract The living anionic polymerizations of various polar vinyl monomers, such as vinylpyridines, acrylates, methacrylates, *N*,*N*-dialkylacrylamides, *N*,*N*-dialkylmethacrylamides, *N*-isopropylacrylamide, α-methylene-*N*-methylpyrrolidone, methacrylonitrile, vinyl sulfoxide, and benzofulvene, quantitatively proceeded and gave the polymers having predicted molecular weights and narrow molecular weight distributions. The effective anionic initiator systems were newly developed to prevent the inherent side reactions derived from the polar substituents during the polymerizations of these monomers. The stereospecific anionic polymerizations were realized for several monomers including methacrylates and *N*,*N*-dialkyl(meth)acrylamides by choosing the suitable initiator systems. The polar monomers possessing electron-withdrawing groups showed high anionic polymerizabilities, and the resulting living polymers had low nucleophilicities because of the stabilization effects of the substituents.

Keywords Polar monomer • Electron-withdrawing group • Methacrylates • Acrylates • Acrylamides • Vinylpyridines • *N*-Isopropylacrylamide • Methacrylonitrile • Benzofulvene • Backbiting • Dormant species • Anionic polymerizability

1 Introduction

In this chapter, the anionic polymerization behaviors of polar vinyl monomers [1–4], such as (meth)acrylates, *N*,*N*-dialkylacrylamides, (meth)acrylonitriles, and vinylpyridines, are described. These polar monomers possess electron-withdrawing substituents including COOR, CONR$_2$, and CN groups and pyridine rings, and the

T. Ishizone (✉) • Y. Kosaka • R. Goseki
Department of Organic and Polymeric Materials, Tokyo Institute of Technology, 2-12-1-S1-13 Ohokayama, Meguro-ku, Tokyo 152-8552, Japan
e-mail: tishizon@polymer.titech.ac.jp

127
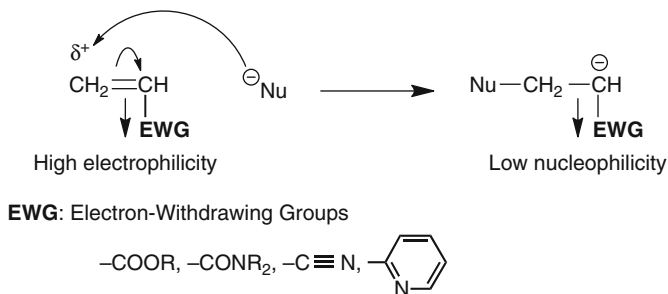
Scheme 1 Anionic polymerization of polar vinyl monomers carrying electron-withdrawing groups

electron densities of their vinyl (isopropenyl) groups are remarkably reduced by the substituent effects. This means that the vinyl groups in the polar monomers are fairly electrophilic and easily attacked by the nucleophiles to initiate the polymerization (Scheme 1). In other words, these polar monomers carrying electron-withdrawing groups show high anionic polymerizabilities. In fact, the anionic polymerizations of most polar monomers dealt with in this chapter can be initiated using relatively weak bases or nucleophiles, such as Grignard reagents and enolate anions, which are known to be entirely ineffective with hydrocarbon monomers including styrene and 1,3-butadiene.

The relationship between a monomer and its growing chain-end anion is also very important in order to understand the anionic polymerization behavior of polar vinyl monomers. In general, the less reactive chain-end anions are derived from the more reactive monomers and vice versa, because they are the conjugated bases and the corresponding acids to each other [5]. A typical example is the anionic copolymerization behavior of methyl methacrylate (MMA) and styrene. MMA is a typical polar monomer and much more reactive than styrene because the electron density on the $C=C$ bond of MMA is considerably reduced by the electron-withdrawing ester carbonyl group, while that on the $C=C$ bond of styrene is not as significantly influenced by the phenyl group. This means that the $C=C$ bond of MMA is more electrophilic than that of styrene. On the other hand, the electron density of the propagating carbanion (enolate anion) derived from MMA is remarkably reduced by the similar electron-withdrawing effect of the COOMe group, thus the poly(MMA) anion becomes much less reactive than that derived from styrene. In fact, the chain-end enolate anion from MMA ($pK_a = 25$, ethyl acetate) [6, 7] has no ability to polymerize styrene, while the chain-end anion from styrene ($pK_a = 41$, toluene) [6, 7] can polymerize styrene and the more reactive MMA, as shown in Scheme 2. This polymerization behavior can be correlated to the relative acidity (pK_a values) of the conjugate acids of the propagating chain ends. From more acidic compounds, less nucleophilic (or less basic) anions form and vice versa.

Thus, these relationships are very important when one considers the synthesis of block copolymers by the sequential anionic copolymerizations [5]. The addition order of comonomers is essential for the success of block copolymerization in
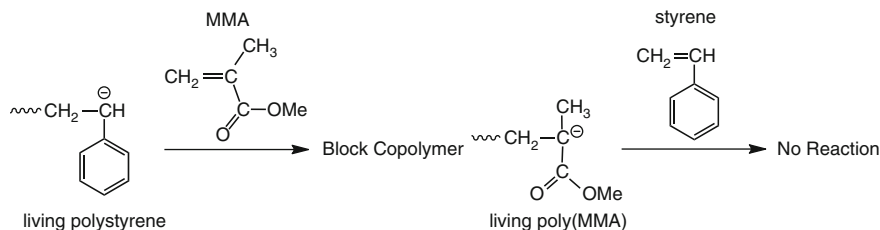
Scheme 2 Crossover reaction between MMA and styrene

Fig. 1 Vinylpyridine derivatives
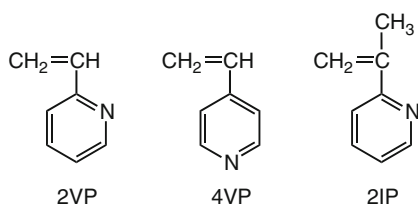
addition to the livingness of the polymerization system. From a synthetic viewpoint, styrene can be used as the first monomer, but MMA is not suitable as the first monomer due to the low nucleophilicity of the propagating carbanion for the synthesis of block copolymer of styrene and MMA by the sequential anionic copolymerization. Thus, the anionic polymerizations of polar vinyl monomers include interesting features on the polymerizability. This chapter mainly focuses on the living anionic polymerization of polar vinyl monomers from the viewpoints of molecular weight control and molecular design of the block copolymers.

2   Anionic Polymerization of Vinylpyridines

It is well known that both 2-vinylpyridine (2VP) and 4-vinylpyridine (4VP) have higher anionic polymerizability than those of styrene and 1,3-diene monomers, because the electron-deficient pyridine ring significantly reduces the π-electron densities of their vinyl groups (Fig. 1) [1–4]. In fact, their relative anionic polymerizabilities are roughly categorized between hydrocarbon monomers and alkyl (meth)acrylates [8]. The resulting poly(2-vinylpyridine) (P2VP) and poly (4-vinylpyridine) (P4VP) have attracted considerable attention, since they are hydrophilic and soluble in polar solvents, such as methanol. Furthermore, they possess reactive pyridine rings in the repeating units. The basic and nucleophilic pyridine rings of polymers can be readily quaternarized by the reactions with acids or alkyl halides, and the resulting quaternarized pyridinium salts show higher polarities than those of the starting polymers and are even soluble in water. It is noteworthy that the cross-linking of poly(vinylpyridine)s is possible, when difunctional alkyl halides, such as 1,4-dibromobutane, are used for the formation of quaternary ammonium salts [9].

Scheme 3 Preparation of DPHLi from *n*-BuLi and DPE

The anionic polymerizations of 2VP and 4VP have been investigated under various conditions [1–4, 10–24], in particular, for the preparation of block copolymers with other comonomers. The choice of a polar solvent, such as THF, DMF, and HMPT, is important for the anionic polymerizations of vinylpyridines to realize homogeneous reaction systems [20, 21, 24], since the resulting polymers are insoluble in hydrocarbons, such as hexane, cyclohexane, and benzene. It is noteworthy that the purification of 2VP and 4VP is rather difficult because of their high anionic polymerizability and hygroscopic property. Although Grignard reagents and dialkylmagnesiums are effective for the purification of hydrocarbon monomers, such as styrene and 1,3-dienes, 2VP and 4VP are readily polymerized by these nucleophiles. In practice, 2VP and 4VP are usually dried over calcium hydride powder and repeatedly distilled under vacuum prior to the polymerization [5]. The pretreatment with trialkylaluminum is more effective to remove the protonic impurities from the monomers due to the homogeneity of the system similarly to the purification of (meth)acrylates [25].

2VP readily undergoes anionic polymerization in THF at –78 °C with π-stabilized bulky initiators, such as 1,1-diphenylhexyllithium (DPHLi, 1:1 addition product of 1,1-diphenylethylene (DPE) and *n*-BuLi, Scheme 3), 1,1-diphenyl-3-methylpentyllithium (DMPLi, 1:1-addition product of DPE and *sec*-BuLi), (1,1,4,4-tetraphenyl)butanedilyldilithium (TPBLi$_2$, dianion of DPE dimer, produced from lithium naphthalenide and DPE, Scheme 4), fluorenyllithium (FlLi), diphenylmethyllithium (Ph$_2$CHLi), and diphenylmethylpotassium (Ph$_2$CHK) (Fig. 2) [1–5]. The reaction systems initiated by these initiators in THF are homogeneous and show the typical red to orange coloration due to the presence of the π-conjugated propagating carbanions derived from 2VP. The resulting P2VPs possess predicted molecular weights based on the molar ratios between the monomer and initiator and narrow molecular weight distributions ($M_w/M_n = 1.1$). It should be noted that the molecular weights of P2VPs estimated by polystyrene standards based on size exclusion chromatography (SEC) measurements in THF are always underestimated compared to the true molecular weights. The estimated M_n values (estimated from polystyrene standards) of P2VP are roughly two thirds of the true values, since the hydrodynamic volume of P2VP in THF is considerably smaller than that of polystyrene. Stronger nucleophilic initiators including *n*-BuLi or *sec*-BuLi in THF also allow the control of the molecular weights. Although several reports in organic chemistry suggest that the nucleophilic

Scheme 4 Preparation of (1,1,4,4-tetraphenyl)butanedilyldilithium from lithium naphthalenide and DPE

Fig. 2 π-Stabilized bulky anionic initiators for 2VP

addition of *n*-BuLi occurs with a pyridine molecule, the pyridine ring of 2VP seems inert to these anionic initiators and the propagating chain ends at low temperature such as –78 °C. However, the addition reactions of living polystyrene and polyisoprene to P2VP backbone form the graft copolymers at elevated temperature at 0 °C [26]. Interestingly, even Grignard reagents showing a lower nucleophilicity can induce the living anionic polymerization of 2VP in a quantitative manner, while Grignard reagents cannot generally initiate the polymerization of styrene at all [27]. Hogen-Esch and his coworkers reported that the anionic polymerization of 2-isopropenylpyridine (2IP), a pyridine analog of α-methylstyrene, also proceeded in a controlled fashion [28–30].

Since the polymerization systems of 2VP show the typical living characters, the living P2VP can be used as a macromolecular initiator to synthesize block copolymers. In fact, block copolymers, such as P2VP-*b*-PMMA and P2VP-*b*-PtBMA [17], have been synthesized by the sequential anionic copolymerization of 2VP with other comonomers showing a high anionic polymerizability. However, since the propagating carbanion of P2VP shows a low nucleophilicity, the addition of hydrocarbon monomers, such as isoprene or styrene, to the living P2VP results in the recovery of the homopolymer of 2VP or the insufficient initiation of the crossover reaction [5]. The latter case means the formation of a block copolymer with ill-defined chain structures. On the other hand, 2VP can be employed as a second monomer for the sequential anionic copolymerization with styrene, 1,3-butadiene, and isoprene because of the high anionic polymerizability [5, 12–16]. In these cases, well-defined PS-*b*-P2VP, PBd-*b*-P2VP, and PIsp-*b*-P2VP were successfully synthesized, and the micelle formation properties in selective solvents and the characteristic morphologies in bulk were investigated.

In contrast to the polymerization behaviors of 2VP, the anionic polymerization of 4VP often suffers from extremely rapid propagation and poor polymer-solubility. Even in polar THF at the low temperature of –78 °C, the red-colored precipitates instantaneously formed upon the addition of 4VP to the anionic initiators, indicating the very rapid polymerization. This causes poor control of the molecular weight of the resulting polymer and the difficulty in the subsequent sequential copolymerization due to the heterogeneous system. An improved procedure for the anionic polymerization of 4VP has been proposed to prevent polymer precipitation using a mixed solvent of pyridine and THF (9/1) [20, 21]. At 0 °C, the polymerization homogeneously proceeded to yield P4VP with well-defined chain structures. On the other hand, a macromolecular initiator, such as living polystyrene, also provides a homogeneous polymerization system of 4VP in THF to afford a tailored block copolymer, PS-b-P4VP [23].

The anionic polymerization of 4-(2-pyridiyl)styrene, a pyridine analog of 4-vinylbiphenyl, was also performed with Ph$_2$CHK in THF at –78 °C [31]. The *para*-substituted 2-pyridinyl group acts as an electron-withdrawing group and provides an extended π-conjugation system. Both the monomer and the resulting living polymer showed a reactivity similar to those of 2VP and the living P2VP, but not styrene and the living polystyrene.

3 Anionic Polymerization of (Meth)acrylates

3.1 Anionic Polymerization Behavior of (Meth)acrylates

The esters of (meth)acrylic acids, (meth)acrylates, are well known as typical α,-β-unsaturated carbonyl compounds, which readily allow the nucleophilic conjugate addition, that is, the 1,4-addition. It has been demonstrated that the (meth)acrylate monomers are highly electrophilic and show a higher anionic polymerizability than
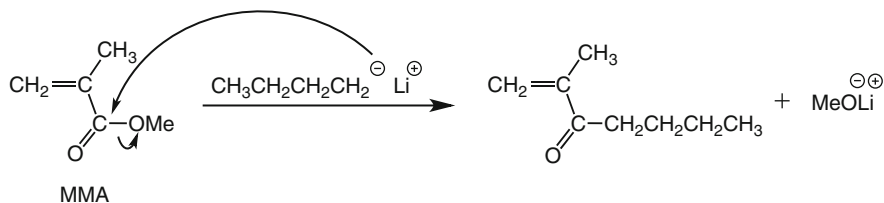
Scheme 5 Reactions of (meth)acrylates with n-BuLi

those of styrene, 1,3-dienes, and vinylpyridines [1–4, 32–35]. In fact, the anionic polymerizations of the (meth)acrylates can be initiated not only with organolithium and organopotassium reagents, but also with organomagnesium compounds, such as R_2Mg and $RMgX$, $LiAlH_4$, $NaAlEt_4$, amide anions (R_2N^-) [36, 37], and enolates derived from carbonyl compounds. The latter initiators are usually inert to the polymerization of hydrocarbon monomers, such as styrene and 1,3-butadienes, because of the low nucleophilicity or basicity. However, the living anionic polymerization of the (meth)acrylate monomers is not so straightforward, since the ester carbonyl attack and α-proton abstraction (in the case of acrylate monomers) with anionic initiators and growing chain-end enolate anions occasionally occur during the polymerization [38–43]. For example, a strong nucleophile, such as n-BuLi, directly attacks the $C=O$ moieties of (meth)acrylates to a considerable extent and not the $C=C$ bonds to decrease the concentration of the anionic initiators (Scheme 5). These acyl substitution reactions between (meth)acrylates and n-BuLi are considered as the termination reactions, since the resulting lithium alkoxides are usually unreactive to reinitiate the polymerization of the residual (meth)acrylate monomers. Furthermore, it is well known that the intramolecular Claisen-type condensation between the propagating enolate anion and the carbonyl group at the antepenultimate monomer unit, the so-called backbiting reaction, occasionally occurs to form the six-membered β-ketoester at the polymer terminal during the anionic polymerization of the (meth)acrylate monomers (Scheme 6) [39–43]. This reaction is not negligible during the final stage of polymerization and is also recognized as a unimolecular termination reaction, since the resulting alkoxides cannot usually reinitiate the polymerization of the (meth)acrylates. In addition, this side reaction should be more significant for acrylates because of the reduced steric hindrance around the propagating chain ends and the antepenultimate ester moieties compared to the methacrylates. Furthermore, for the acrylates, another propagating anion is immediately deactivated by the proton abstraction, since the resulting cyclic β-ketoester possesses a highly acidic hydrogen ($pK_a \sim 11$, similar to acetylacetonate), as shown in Scheme 6 [39–43]. This means that two polymer chains are successively deactivated during the polymerization of the acrylates once this backbiting reaction occurs. In fact, the molecular weight control during the anionic polymerizations for acrylates are much more difficult compared to those for the methacrylates.
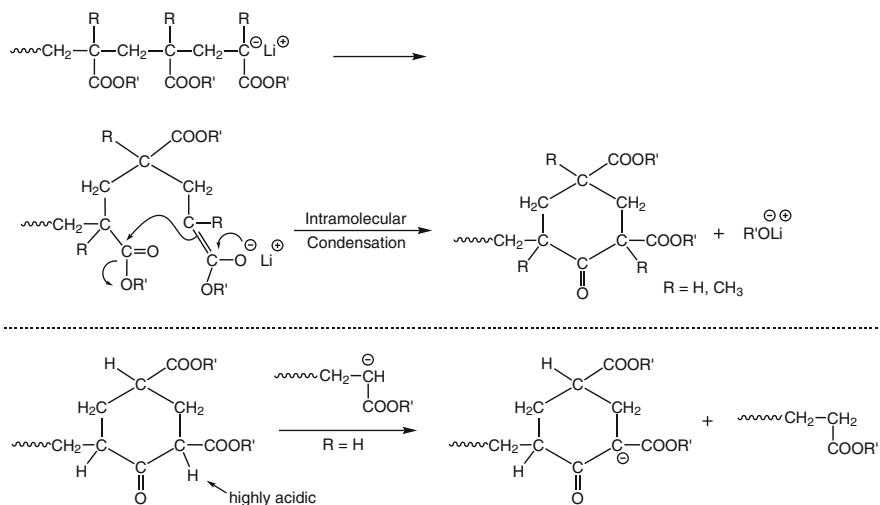
Scheme 6 Backbiting reaction during anionic polymerization of (meth)acrylates [39–43]

It is also noted that the exothermic rapid propagation and the partially aggregated propagating species often cause broadening of the molecular weight distribution of the poly(meth)acrylates. Furthermore, in practice, the purification of (meth)acrylate monomers is quite difficult due to their high anionic polymerizability. (Meth) acrylate monomers are rather hygroscopic and may contain a trace amount of starting materials, such as the corresponding alcohols and carboxylic acids. Vacuum distillation over calcium hydride is not sufficient to thoroughly remove such impurities from the monomers. A more effective purification of the (meth)acrylates has been achieved by the distillation in the presence of Lewis acidic trialkyla-luminums to eliminate the protonic impurities from the monomers [25].

3.2 Living Anionic Polymerization of (Meth)acrylates

As described above, the anionic polymerization of alkyl (meth)acrylates has occasionally encountered the above-described serious problems on the yields and the molecular characteristics, such as molecular weights and the molecular weight distributions. Therefore, a number of novel polymerization systems for the (meth)acrylate monomers have been developed to overcome such drawbacks by suitably modifying the initiator, counter ion, solvent, additive, and polymerization temperature [44–61]. This important issue has been reviewed in detail in several articles [32–35].

The most established system so far developed is the polymerization with bulky π-stabilized organolithium compounds, such as DPHLi, DMPLi, and Ph$_2$CHLi, in THF at a temperature lower than –40 °C [44, 45, 49] (Fig. 3). A very low
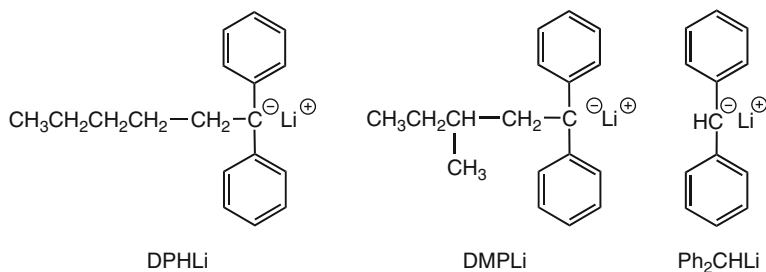
Fig. 3 Effective anionic initiator systems for (meth)acrylates [44, 45, 49]

polymerization temperature, such as –78 °C, is more preferable to suppress the above-mentioned intramolecular backbiting termination. It is noteworthy that these anionic initiators are also effective for the living polymerizations of vinylpyridines, as already described. In fact, these bulky π-stabilized carbanions exclusively attack the C=C double bonds of MMA not the C=O bonds to initiate the polymerization. In these cases, poly(MMA)s having the predicted molecular weights were quantitatively obtained, indicating the quantitative initiation efficiency of the polymerizations. The polydispersity indices, M_w/M_n, were between 1.1 and 1.2, indicating the rather narrow molecular weight distributions. Very interestingly, the addition of 3- or more-fold of LiCl to the initiator system drastically reduces the M_w/M_n values of poly(MMA) from 1.2 to 1.05, in particular, less than 1.02 [49]. It is considered that the added LiCl acts as a common salt to dissociate the aggregated propagating chain ends in THF. In the presence of common salts, the dissociated unimolecular propagating species allow the slow propagation of the active species to achieve a uniform polymer chain length. With this system, similar to MMA, isopropyl, *tert*-butyl, and other alkyl methacrylate monomers underwent the living anionic polymerization to yield well-defined polymers up to 10^5 g/mol in M_n values with extremely narrow molecular weight distributions ($M_w/M_n < 1.05$). Very interestingly, the addition of LiCl also induces the living anionic polymerization of *tert*-butyl acrylate (tBA) in THF at –78 °C [45]. Although the M_w/M_n values of the poly (tBA)s produced in the absence of LiCl were around 2, they were drastically reduced to within 1.2 for the polymerization of tBA in the presence of LiCl.

Similar additive effects have been observed for LiClO$_4$ [52, 53], LiOC(CH$_3$)$_3$ [54], KOC(CH$_3$)$_3$, and lithium 2-(2-methoxyethoxy)ethoxide [51] during the anionic polymerizations for MMA. The bulkiness around the chain-end anions provided by the coordination of such metal salts may prevent the above-mentioned backbiting termination reaction and ester carbonyl attacks. The chain-end enolate anion is stabilized in order to avoid side reactions by shifting the equilibrium to a less reactive species via the common salt effect.

Another effective initiator system is to add weak Lewis acids, such as R$_3$Al, R$_{3-n}$(R'O)$_n$Al, diethylzinc (Et$_2$Zn), and trialkylborane (R$_3$B), to the anionic polymerization system to stabilize the propagating chain-end anions [55–61]. For instance, the simple addition of Et$_2$Zn to the organopotassiums including Ph$_2$CHK and K
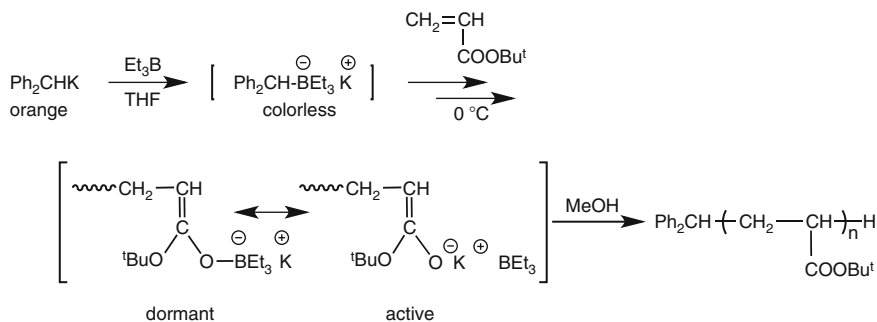
Scheme 7 Anionic polymerization of tBA in the presence of Et_3B [57]

$(C_6H_5)_2C(CH_2)_2C(C_6H_5)_2 K$ (dianion of DPE dimer, produced from potassium naphthalenide and DPE) in polar THF allowed the living anionic polymerization of various polar monomers including tBA [56], alkyl methacrylates [55], and *N,N*-dialkylacrylamides [62]. It is believed that the added Et_2Zn acts as a Lewis acid to dissociate the aggregated propagating carbanions and to form the single active species after shifting the equilibrium state. The undesirable backbiting might be eliminated upon the formation of stable and less-nucleophilic active chain ends. In addition to the precise molecular weight control of the resulting polymers, retardation of the propagation was apparently observed in the presence of Et_2Zn even in the polar basic solvent of THF. These results indicated that the Lewis acidic Et_2Zn may predominantly coordinate with the propagating chain-end enolate anions rather than other Lewis bases, such as the carbonyl groups of the monomers and THF.

A more drastic retarding effect of Lewis acidic organoboranes, such as triethylborane (Et_3B) and triphenylborane (Ph_3B), was first observed in the anionic polymerizations of tBA [57]. In this system, added organoboranes strongly coordinate to the anionic initiator and/or the propagating chain-end anion and no appreciable polymerization occurs at –78 °C even after 24 h. In contrast, the coordinated species, so-called dormant species, barely dissociates at a higher temperature around 0 °C to afford the active chain ends (Scheme 7). The polymerization then slowly proceeded at 0 °C to give poly(tBA)s with predictable molecular weights and narrow molecular weight distributions ($M_n = 24,000$ g/mol, $M_w/M_n = 1.07$) (Table 1) [57]. In other words, tBA smoothly undergoes the living anionic polymerization initiated with Ph_2CHK/Et_3B in THF at 0 °C. Similar drastic additive effects of R_3B were also observed in the polymerizations of *N,N*-dialkylacrylamides [63] and methacrylonitrile [64].

The polymerization systems of (meth)acrylate monomers initiated with organolithiums in the presence of Lewis acidic R_3Al and $R_{3-n}(R'O)_nAl$ also afforded well-defined polymers [65–67]. In these polymerization systems, the polymerization rate often increased in nonpolar solvent, such as toluene, by the monomer activation, since the electron density of $C=C$ group might be reduced by the coordination of added Lewis acids with the carbonyl groups of the (meth) acrylate monomers (Fig. 4).

Table 1 Anionic polymerization of tBA with Ph_2CHK in THF in the presence of Et_3B [57]

Initiator	Et_3B/M^+	Temp. °C	Time h	Yield %	$M_n \times 10^{-3}$ calcd.[b]	obsd.[c]	M_w/M_n[a]
Ph_2CHK		–78	0.08	100	17	49	2.64
Ph_2CHK/Et_3B	2.8	–78	24	Trace[d]	–	–	–
Ph_2CHK/Et_3B	2.4	0	1	57	5.4	4.1	1.05
Ph_2CHK/Et_3B	2.7	0	6	100	8.7	9.8	1.08
Ph_2CHK/Et_3B	2.5	0	24	100	19	24	1.07
Ph_2CHK/Et_3B	17	0	6	32	3.1	2.7	1.06
Ph_2CHK/Et_3B	19	0	72	96	12	11	1.04

[a]M_w/M_n was determined by the SEC calibration using PMMA standards
[b]M_n(calcd) = (MW of monomer) × yield/100 × [monomer]/[initiator] + (MW of initiator)
[c]M_n(obsd) was determined by the ^{1}H NMR
[d]Less than 4 %

tert-BuLi /   /Toluene   sec-BuLi /   /Toluene
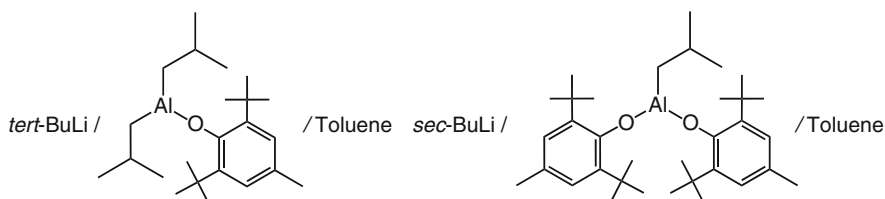
Fig. 4 Anionic initiator systems for (meth)acrylates in hydrocarbons [68, 69]

These polymerization systems in hydrocarbon solvents are very attractive for producing new materials based on poly((meth)acrylate)s from an industrial viewpoint, since these systems allow the polymer production under milder conditions compared to those in polar solvents carried out at very low temperatures. Recently, Kuraray Co., Ltd., in Japan, successfully developed the living anionic polymerization system for (meth)acrylate monomers at ambient temperature on an industrial scale by designing the above initiator system containing the bulky Lewis acidic diphenoxyalkylaluminum reagent [68, 69]. This is actually the first example in which polyacrylates and polymethacrylates are industrially produced by the living anionic polymerization. More interestingly, all (meth)acrylic ABA type triblock copolymers, for instance, poly(MMA)-b-poly(n-butyl acrylate)-b-poly(MMA), were synthesized as a promising thermoplastic elastomer showing an elasticity and process ability. In this case, the poly(MMA) terminals are hard segments showing a high T_g, and poly(n-butyl acrylate) is a soft middle segment showing a low T_g. It should be emphasized that the anionic polymerization of acrylates carrying a primary alkyl group can be controlled by this initiator system.

The significant effects of counter cations in the anionic polymerization have been observed in the metal-free anionic polymerizations [70–73]. Reetz and coworkers first used metal-free anionic initiators for the polymerization of primary acrylates at room temperature (Scheme 8). The tetrabutylammonium malonate derivative as an initiator produced poly(n-butyl acrylate) with a relatively
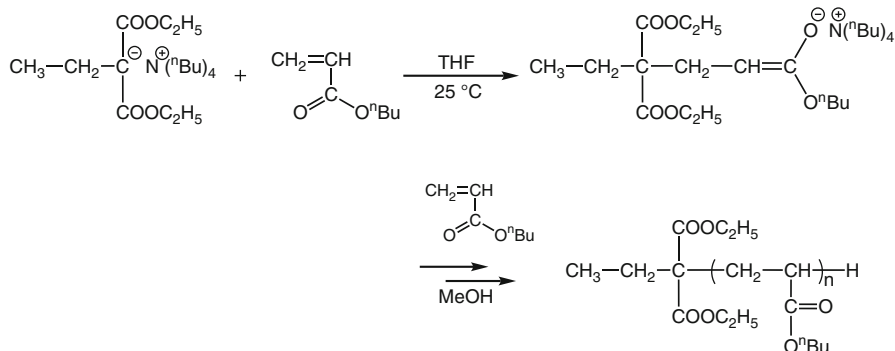
Scheme 8 Metal-free anionic polymerization [71]

narrow molecular weight distribution ($M_w/M_n \sim 1.20$) even at room temperature [71]. Similarly, the quaternary ammonium salts of thiolate anions induced the controlled anionic polymerization of alkyl acrylates at ambient temperature [72]. Seebach reported that the polymerization of MMA proceeds in THF at 60 °C with 1-*tert*-butyl-4,4,4-tris(dimethylamino)-2,2-bis(tris(dimethylamino) phosphoranylidenamino)-$2\Lambda^5,4\Lambda^4$-catenadi(phosphazene), P_4-*t*-Bu phosphazene base, to give a poly(MMA) with an M_n value of 15,200 g/mol and an M_w/M_n value of 1.11 [74].

The living anionic polymerization of MMA was also attained by Hogen-Esch and his coworkers using a bulky tetraphenylphosphonium cation (Ph_4P^+) under mild conditions [75–79]. The reaction of Ph_3CK and $Ph_4P^+Cl^-$ provided a triphenylmethyl anion possessing the Ph_4P^+ cation, $Ph_3C^- Ph_4P^+$, in situ (Scheme 9). The resulting $Ph_3C^- Ph_4P^+$ can initiate the anionic polymerization of MMA in THF at ambient temperature around 20 °C to afford poly(MMA)s with predictable molecular weights ($M_n = 8,500–29,100$ g/mol) and narrow molecular weight distributions ($M_w/M_n = 1.04–1.20$). The bulky and conjugated Ph_4P^+ cation may play important roles to attain the controlled molecular weight probably by reducing the rate of the side reactions.

The polymerization of alkyl (meth)acrylates using silyl ketene acetal as the initiator is well known as the group transfer polymerization (GTP) developed by Webster at DuPont [80–89]. Since the GTP is a repeating Michael addition reaction of silyl ketene acetal (silyl enolate) with α,β-unsaturated carbonyl compounds in the presence of a nucleophilic or Lewis acidic catalyst, it can be categorized as one of the related anionic polymerizations. In this polymerization, the trialkylsilyl group act as a counter cation for the propagating enolate anion derived from the (meth) acrylates (Scheme 10). From a synthetic viewpoint, the GTP is a very attractive method, since it can produce various poly((meth)acrylate)s with relatively narrow molecular weight distributions ($M_w/M_n = 1.2$) at ambient temperature. However, the controllable range of molecular weights of polymers produced by the GTP has been usually less than 10 kg/mol and rather limited.

A significant improvement in the GTP system has been recently reported using 1-triisopropylsiloxy-1-methoxy-2-methyl-1-propene in conjunction with
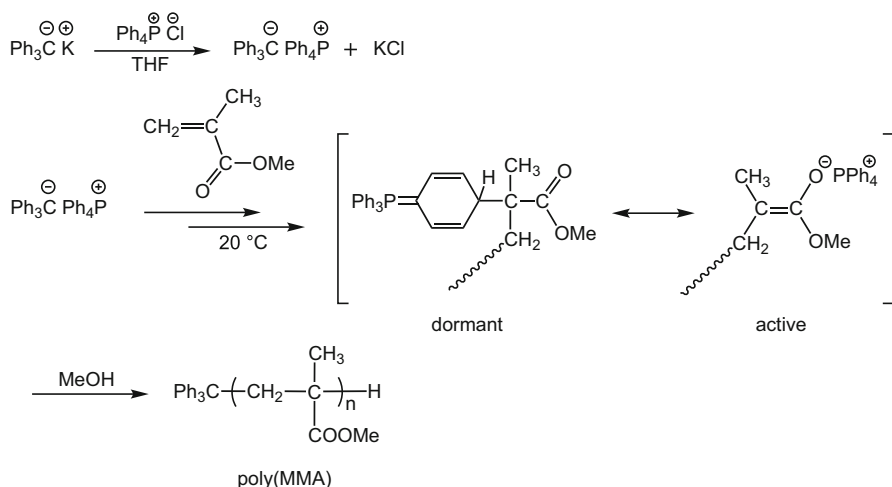
Scheme 9 Anionic polymerization of MMA with Ph_3C^- Ph_4P^+ [75, 76]
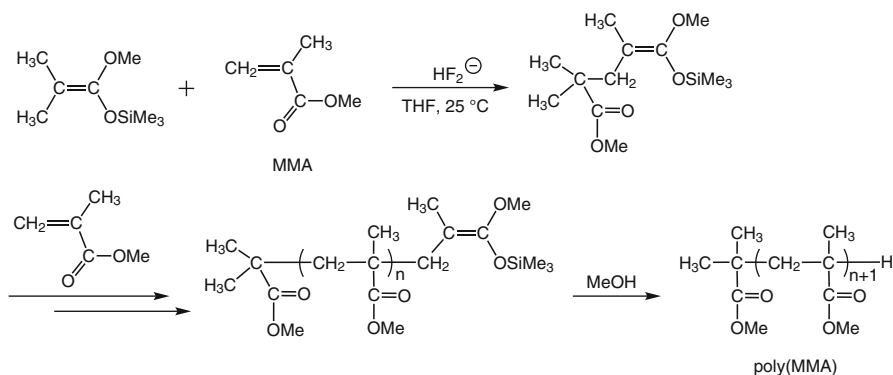
Scheme 10 GTP of MMA [83]

pentafluorophenylbis(triflyl)methane ($C_6F_5CHTf_2$) as the organocatalyst (Scheme 11). With this system, the polymerization of methyl acrylate (MA) rapidly and quantitatively proceeded to afford a well-defined poly(MA) ($M_n = 108,000$ g/mol, $M_w/M_n = 1.07$) at room temperature in toluene [90]. The use of the bulky triisopropylsilyl group in the silyl ketene acetal initiator may play an important role in precisely controlling the polymerization of the alkyl acrylate monomer. The GTP of MMA using either trifluoromethanesulfonimide ($HNTf_2$) as a strong Brønsted acid [91] or P_4-t-Bu [92] as an organic superbase catalyst afforded the poly(MMA)s with predicted M_n values higher than 50 kg/mol and narrow molecular weight distributions ($M_w/M_n \sim 1.1$).

It is thus demonstrated that the metal-free anionic polymerization and GTP of polar monomers are versatile for controlling the polymer architectures including the molecular weights and end-functionalities. In particular, these polymerization
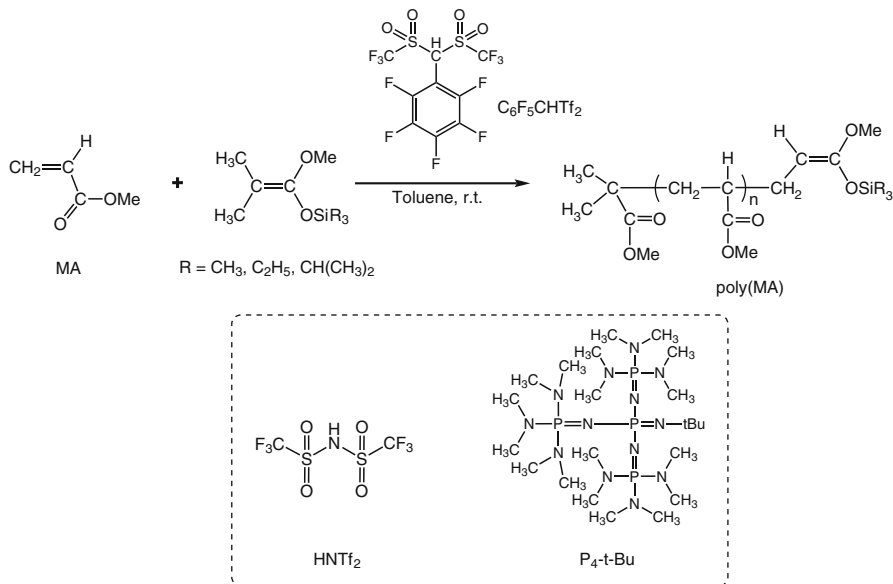
Scheme 11 New initiator systems for GTP [90–92]

methods allow milder reaction conditions, such as ambient temperature and wide solvent range, compared to the conventional anionic polymerizations with organolithium initiators. However, the advantages of the metal-free anionic polymerization and GTP are not true for the synthesis of block copolymers, since these polymerization systems are not applicable for the polymerization of hydrocarbon monomers, such as styrene and 1,3-butadiene. On the other hand, the sequential copolymerization using binary initiator systems including RLi/LiCl, RLi/Et$_2$Zn, and RK/Et$_2$Zn readily allows the synthesis of well-defined block copolymers of (meth)acrylates and other comonomers, such as styrene, 1,3-dienes, and 2VP in the proper addition order. In fact, a number of well-defined block copolymers have already been synthesized by the RLi/LiCl, RLi/Et$_2$Zn, and RK/Et$_2$Zn initiator systems. Furthermore, these binary initiator systems can be utilized for the living anionic polymerizations of methacrylates carrying a variety of functional groups, also indicating their superiority compared to other initiator systems.

3.3 Stereospecific Anionic Polymerization of Methacrylate Monomers

Needless to say, the stereoregularity or configuration of the vinyl polymer is very important to determine the thermal and/or mechanical properties of the final materials. One of the important features of the anionic polymerization is the potential to vary the stereoregularity of the resulting polymers. In the anionic polymerization, a variety of factors, such as solvent, counter cation, additive, and
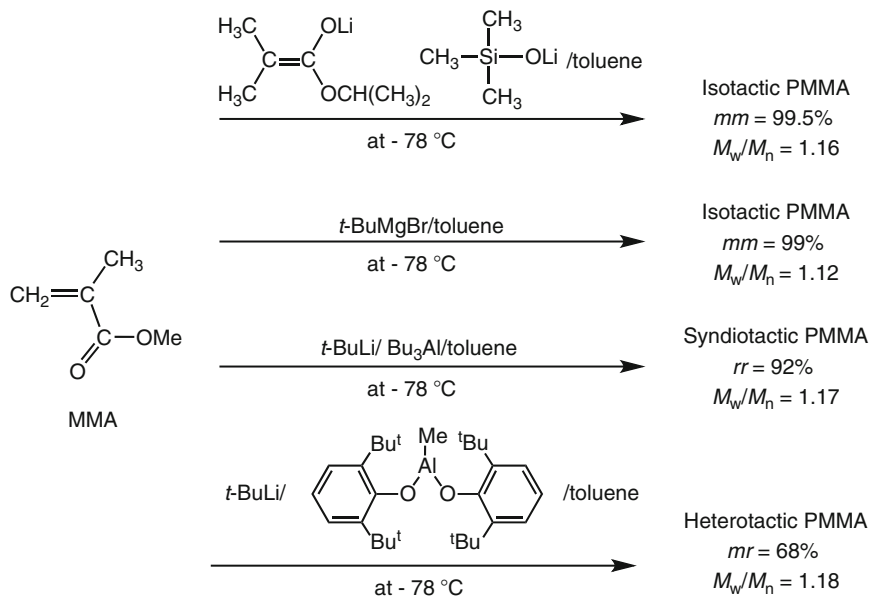
Scheme 12 Stereospecific anionic polymerization of MMA [58–60, 93]

temperature, can change the states of the propagating species and tend to affect the stereoregularity of the resulting polymers.

As the most reliable and established example, Hatada and Kitayama have succeeded in the stereospecific living anionic polymerizations of MMA under the specific conditions. In fact, a series of well-defined poly(MMA)s with highly isotactic, syndiotactic, and heterotactic configurations were successfully obtained by choosing the appropriate initiator systems and solvents (Scheme 12) [58–60, 93]. In these cases, organolithium or the Grignard reagent was used as the initiator in nonpolar hydrocarbon media, and the Lewis acidic compounds were added to optimize the stereoregularity and to narrow the molecular weight distribution. Control of the primary structures of the resulting polymers, such as molecular weights, molecular weight distributions, and high stereoregularities of the repeating units, was simultaneously attained in the resulting poly(MMA)s. In particular, an almost perfect isotactic poly(MMA) with the *mm* triad content higher than 99.5 % could be synthesized with a novel binary initiator system consisting of α-lithioisobutyrate (lithium ester enolate) and lithium trimethylsilanolate (Me₃SiOLi) in toluene [93]. These well-defined stereoregular poly(MMA)s are recognized as ideal model polymers to clarify the basic properties and characters. In fact, the differences in the glass transition temperatures (T_g) and the hydrodynamic volumes were discussed by changing the stereoregularity [34, 35]. In addition, these poly (MMA)s with a high stereoregularity might also be useful to study the stereocomplex formation behavior, since a mixture of isotactic and syndiotactic poly(MMA)s has been known to intermolecularly form a stereocomplex [94–96]. Not only MMA, but
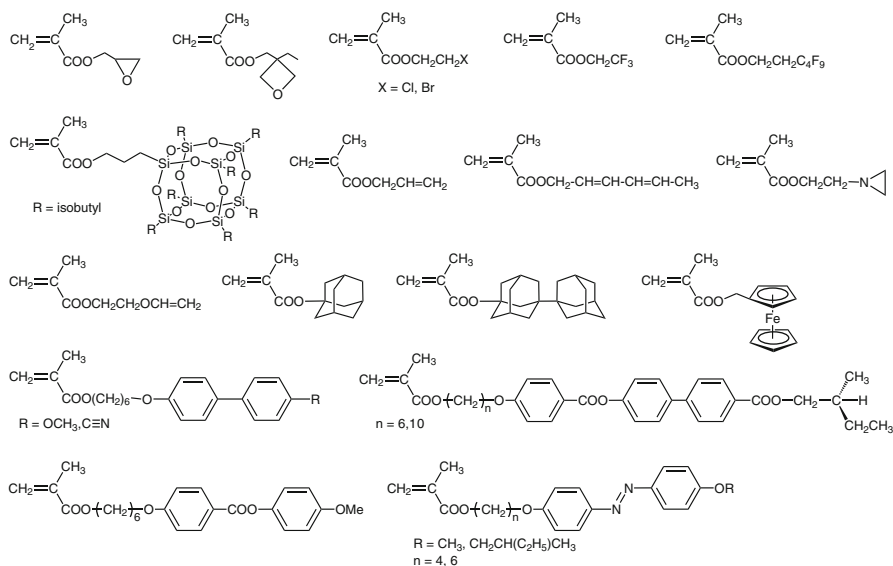
Fig. 5 Functional methacrylate monomers capable of living anionic polymerization [97–120]

also various alkyl methacrylate monomers could be converted into highly stereoregulated polymers by specific initiator systems and/or solvents.

3.4 Anionic Polymerization of Functional Methacrylates

It should be noted that chain-end enolate anions derived from methacrylates are less reactive and less basic than chain-end carbanions generated from styrene and 1,3-butadiene derivatives. Therefore, methacrylates bearing a variety of functional groups can tolerate the anionic polymerization to form polymers without serious side reactions. This means that many monomer designs are possible for the methacrylate monomers carrying functional groups compared to the functional styrenes. In fact, the functional methacrylate monomers shown in Fig. 5 undergo the living anionic polymerization by the above-mentioned initiator systems (organolithium/LiCl and organopotassium/Et$_2$Zn) in THF at −78 °C. The monomers included glycidyl, 3-oxetanylmethyl, 2-chloroethyl, 2-bromoethyl, 2,2,2-trifluoroethyl, 2-(perfluorobutyl)ethyl, 3-(3,5,7,9,11,13,15-heptaisobutyl-pentacyclo-[9.5.1.^{3,9}1^{5,15}17,^{13}]octasiloxan-1-yl)propyl (POSS), allyl, 2,4-hexadienyl-, 2-(1-aziridinyl)ethyl, 2-(vinyloxy)ethyl, 1-adamantyl, 3-(1,1'-biadamantyl), and ferrocenylmethyl methacrylates, and methacrylate monomers bearing several mesogenic moieties [97–120].

Some of these functional groups, such as epoxide, alkyl halides, perfluoroalkyl, conjugated 1,3-diene, and ferroceny moieties, are usually incompatible with the anionic polymerization of styrene monomers because of their high reactivities. On
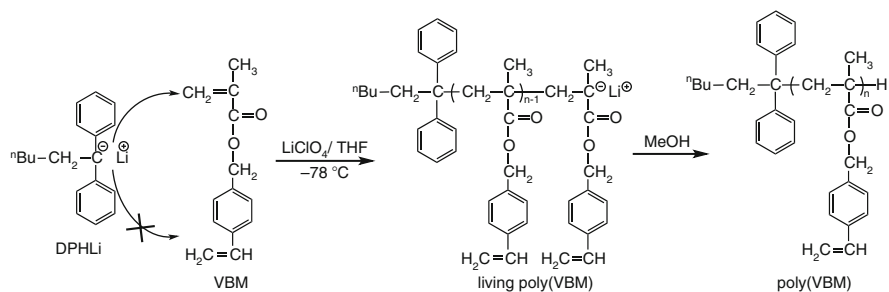
Scheme 13 Selective living anionic polymerization of 4-vinylbenzyl methacrylate [121]

the other hand, the methacrylates possessing these functional groups can tolerate the anionic polymerization, since the propagating enolate anions of the methacrylates are much less reactive or nucleophilic than those of the styrene monomers. The typical polymerization behavior was found in the anionic polymerization of 4-vinylbenzyl methacrylate (VBM) carrying a styrene framework in the side chain (Scheme 13) [121]. When the anionic polymerization of VBM was initiated with DPHLi in the presence of $LiClO_4$ in THF at –40 °C, the initiation and propagation exclusively proceeds on the methacrylate framework to give a polymer with a predicted molecular weight and a narrow molecular weight distribution ($M_w/M_n = 1.1$). The ^1H NMR of the poly(VBM) showed the presence of styrene moieties in every repeating unit. These results indicated that the styrene skeleton in the side chain is stable during the anionic polymerization of the methacrylate framework of VBM. However, at a higher temperature around –20 °C, the molecular weight distribution of the resulting polymer became fairly broad ($M_w/M_n \sim 1.8$), indicating the occurrence of some side reactions. It is suggested that the careful choice of the polymerization conditions is necessary to achieve the living anionic polymerization of functional methacrylate monomers.

3.5 Anionic Polymerization of Methacrylates Carrying Protected Functional Groups

It has been described in chapter "Nonpolar Monomers: Styrene and 1,3-Butadiene Derivatives" that the protection of functional groups is essential for the achievement of the anionic polymerization of several functional styrene derivatives, such as 4-hydroxystyrene, 4-vinylbenzoic acid, and 4-formylstyrene [122, 123]. This protective strategy is also applicable to methacrylate monomers carrying acidic functional groups, such as OH, $C \equiv CH$, and $\equiv SiOH$ groups [124–133] (Fig. 6).

As the most established example, the hydroxyl group of 2-hydroxyethyl methacrylate (HEMA) could be masked with various protective groups, such as trimethylsilyl [124], *tert*-butyldimethylsilyl [125], and methoxymethyl groups [125], and the resulting protected monomers were subjected to the anionic polymerization. Scheme 14 shows a successful example of the precise synthesis of poly
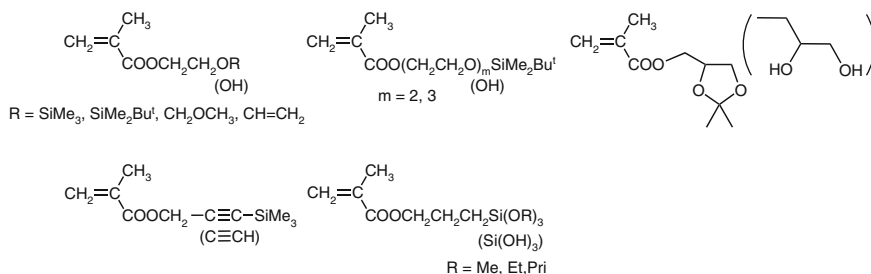
Fig. 6 Methacrylate monomers carrying protected functional groups capable of living anionic polymerization [124–133]
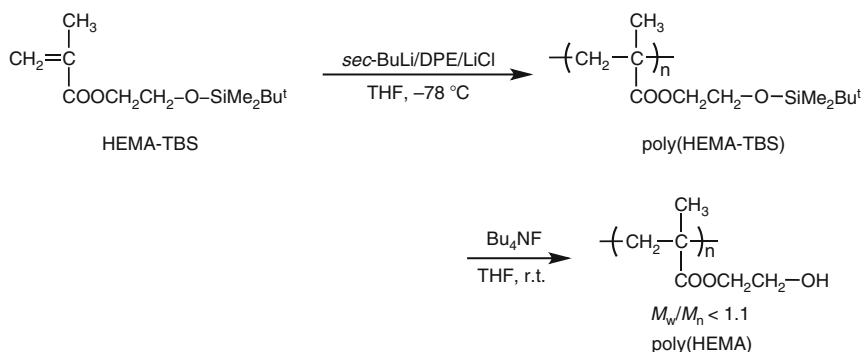
Scheme 14 Precise synthesis of poly(2-hydroxyethyl methacrylate) by living anionic polymerization [125]

(2-hydroxyethyl methacrylate), poly(HEMA), by the living anionic polymerization of 2-(*tert*-butyldimethylsilyloxy)ethyl methacrylate and the following deprotection. An acidic alcoholic OH group of 2-hydroxyethyl methacrylate (HEMA) was initially protected with a bulky *tert*-butyldimethylsilyl (TBS) group, and the resulting trialkylsilyl ether monomer (HEMA-TBS) was employed for the polymerization under anionic conditions [125]. The polymerization of the protected HEMA-TBS was initiated with DPHLi or DMPLi in the presence of LiCl in THF at −78 °C. The polymerization of HEMA-TBS quantitatively proceeded at −78 ° C within 10 min. After termination with methanol, the poly(HEMA-TBS) with the predicted molecular weight based on the molar ratio between the monomer and initiator and narrow molecular weight distribution ($M_w/M_n < 1.1$) was obtained in quantitative yield. The propagating carbanion derived from the trialkylsilyl ether monomer was stable in the presence of protective groups, and showed a reactivity similar to that of the living poly(MMA). After the termination with methanol, the TBS protective groups were completely removed from the resulting polymers to give a poly(HEMA) by treating with aqueous hydrochloric acid or tetrabutylammonium fluoride. After complete removal of the protective groups, the resulting poly(HEMA) still maintained the predicted molecular weight and narrow molecular weight
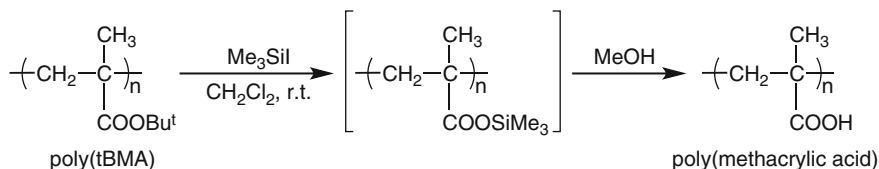
Scheme 15 Deprotection of poly(tBMA) with trimethylsilyl iodide [134, 135]

distribution. The SEC curve of the deprotected polymer maintained a unimodal and narrow distribution after the deprotection ($M_w/M_n < 1.1$). It was clearly demonstrated that a well-defined poly(HEMA) was obtained by the quantitative deprotection of poly(HEMA-TBS). Thus, the protective strategy is very effective to synthesize the tailored polymethacrylates bearing functional groups.

It is evident that there are two significant requirements for the protective groups in the monomers. One requirement is that they must be stable toward the basic and nucleophilic propagating enolate anions, and the other is that they must be completely removable without any chain degradation and cross-linking reaction under the suitable deprotection conditions. In addition, since the resulting polymethacrylates possess the ester linkage in each repeating unit, the deprotection must proceed without cleavage (hydrolysis) of the ester linkage. In fact, the 1,2-diol moiety of 2,3-dihydroxypropyl methacrylate was effectively masked with a cyclic acetal (1,3-dioxolane) form prior to the anionic polymerization [129, 130]. The cyclic acetal protective groups could be quantitatively hydrolyzed to give a tailored poly(2,3-dihydroxypropyl methacrylate) under acidic conditions without interfering ester moieties. In the case of the $C \equiv CH$ function of propargyl methacrylate, a trimethylsilyl protective group was employed to mask the acidic acetylene proton ($pK_a = 25$) [132]. The $C \equiv CSiMe_3$ moiety in the polymer was quantitatively converted into a $C \equiv CH$ group by treating with tetrabutylammonium fluoride. The SiOR groups in 3-(trialkoxysilyl)propyl methacrylate were stable under the basic conditions of the anionic polymerization, but those in the resulting polymers were readily hydrolyzed under acidic conditions to form an insoluble gel by cross-linking [133]. The reaction proceeded by the formation of SiOH groups and the subsequent intermolecular condensation resulting in the SiOSi linkages.

On the other hand, it is well known that esters themselves are often used as protective groups for carboxylic acids. This means that the esters of (meth)acrylic acids are considered as precursors for (meth)acrylic acids. In fact, a well-defined poly(acrylic acid) and a poly(methacrylic acid) were obtained by the living anionic polymerization of tBA and tBMA, followed by their acid hydrolyses. It is noted that poly(tBMA) was also readily transformed into the poly(methacrylic acid) by treating with trimethylsilyl iodide under neutral conditions (Scheme 15) [134, 135]. The living anionic polymerizations of trimethylsilyl ester [136, 137] and 1-alkoxyethyl ester [138–140] of methacrylic acid, shown in Fig. 7, and the subsequent deprotections of the resulting polymers were successfully conducted for the preparation of the well-defined poly(methacrylic acid).

Fig. 7 Protected forms of methacrylic acid [136–140]

$$CH_2=C\begin{smallmatrix}CH_3\\COOSiMe_3\end{smallmatrix}$$

$$CH_2=C\begin{smallmatrix}CH_3\\COO\end{smallmatrix}\begin{smallmatrix}CH_3\\CH\\O-R\end{smallmatrix}$$

R = Et, Bu, Bu^t

$-(CH_2-C)_n-$
CH$_3$
COOCH$_2$CH$-$CH$_2$
OH OH
T_c = 32- 47 °C [pH dependent]

$-(CH_2-C)_n-$
CH$_3$
COOCH$_2$CH$_2$NMe$_2$

$-(CH_2-C)_n-$
CH$_3$
COO$-(CH_2CH_2O)_m-$H
m = 2,3

$-(CH_2-C)_n-$
CH$_3$
COO$-(CH_2CH_2O)_m-$R

R = Me, m = 2: T_c = 26 °C
R = Me, m = 3: T_c = 52 °C
R = Me, m = 4: T_c = 68 °C
R = Et, m = 2: T_c = 4 °C
R = Et, m = 3: T_c = 27 °C
R = Et, m = 4: T_c = 42 °C
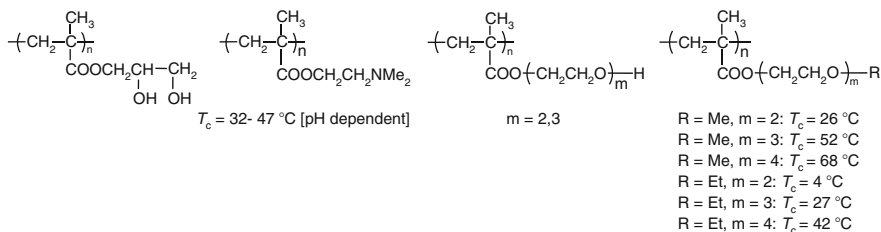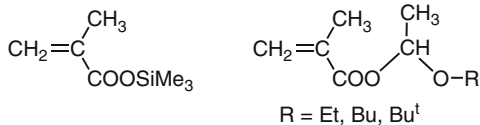
Fig. 8 Structures of water-soluble polymethacrylates obtained by living anionic polymerization [129, 130, 141–150]

3.6 Synthesis of Water-Soluble Thermoresponsive Polymethacrylates by Anionic Polymerization

Water-soluble polymers have attracted significant attention due to the wide potentials in industrial and medical applications. In the cases of polymethacrylates, the water-solubility is dependent on the polar functionalities in the side chains, which can be widely designed [141–150] (Fig. 8). Interestingly, several water-soluble polymethacrylates are known to show a thermoresponsive character in their aqueous solutions along with the reversible sol-gel transitions. In order to clarify the relationship between the macromolecular structures and water-solubility or thermoresponsive property, the synthesis of well-defined polymethacrylates has been intensively examined by the anionic polymerizations of the corresponding methacrylate monomers.

It is well known that the OH functional group is hydrophilic and provides a strong polarity to the molecules. As described in Sect. 3.5, the well-defined poly (HEMA), an ester of ethylene glycol, carrying an OH group in the side chain can be synthesized by the living anionic polymerization of the protected HEMA and the following deprotection [124–128]. Poly(HEMA) is highly hydrophilic because of the polar OH functions, but it is hardly soluble in water. On the other hand, the anionically synthesized poly(2,3-dihydroxypropyl methacrylate) [129, 130], an ester of glycerin, possesses two OH groups in each monomer unit and shows a water-solubility. This indicates that the number of OH groups in the monomer unit is important to realize the water-soluble polymethacrylates. The living anionic
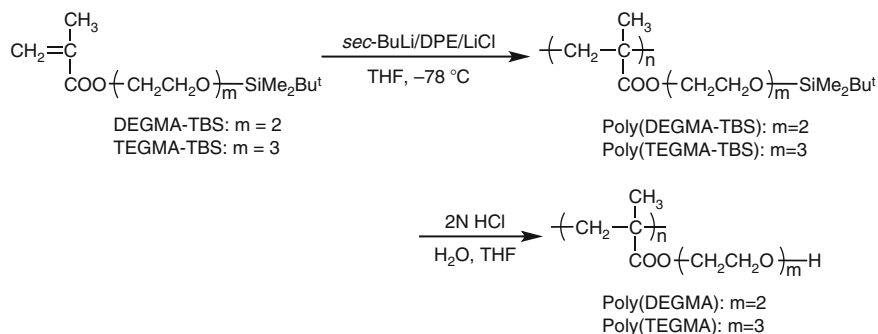
Scheme 16 Synthesis of poly(oligo(ethylene glycol) methacrylate)s by anionic polymerization and deprotection [131]

polymerization of 2-(dimethylamino)ethyl methacrylate having a polar tertiary amino group smoothly proceeds to produce a polymer in quantitative yield [141–143]. Poly(2-(dimethylamino)ethyl methacrylate) is a water-soluble polymer and shows an inverse temperature solubility behavior with the cloud point (T_c) in an aqueous solution.

In the past decade, polymethacrylates having oligo(ethylene glycol) side chains attracted great attention [131, 144–150], as they are water-soluble and often undergo a reversible sol-gel transition in water. Ishizone and his coworkers succeeded in the living anionic polymerization of a series of oligo(ethylene glycol) alkyl and *tert*-butyldimethylsilyl ether methacrylates with the above-mentioned initiator systems (organolithium/LiCl and organopotassium/Et$_2$Zn) in THF at – 78 °C [131]. In the cases of vinyl and *tert*-butyldimethylsilyl ethers, the resulting polymers could be converted into the corresponding poly(oligo(ethylene glycol) methacrylate)s possessing OH groups in the side chains by the subsequent deprotection reactions (Scheme 16). The obtained poly(oligo(ethylene glycol) methacrylate)s, poly(OEGMA), were soluble in water at any temperature from 0 to 95 °C. On the other hand, the corresponding methyl and ethyl ethers had a water-solubility and reversible thermosensitivity depending on the molecular structures of the repeating units including the side chain lengths and ω-functionalities (Fig. 9) [144, 145]. In fact, the T_c values in water ranged from 4 to 68 °C, and a clear relationship between the T_c and molecular structures of the repeating units is observed. The anionically produced polymers having narrow molecular weight distributions are considered to be good candidates for understanding the polymer properties. Polymers possessing longer side chains show higher T_c values than the shorter ones, and the T_cs of the methyl ethers are ca. 25 °C higher than those of the corresponding ethyl ethers with the same side chain length, indicating the significant effect of the ω-functions. The ω-functionality effect is clear from the fact that the poly(OEGMA)s possessing OH terminal groups are completely soluble in water. In addition, the effect of the ω-functions is also observed in that the vinyl ethers are not soluble in water, while the corresponding ethyl ethers are soluble in
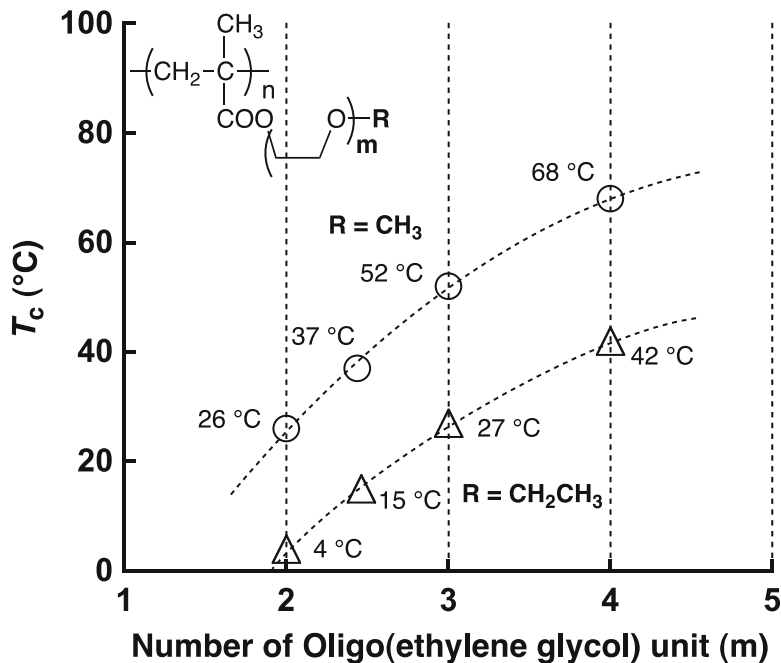
Fig. 9 Relationship between T_c and side chain length [144, 145]

water [146]. Thus, the introduction of hydrophilic oligo(ethylene glycol) units is also very effective to attain the water-solubility of polymethacrylates as well as the introduction of several OH groups. It should be emphasized that significant effects of the side chain length of the oligo(ethylene glycol) unit and the ω-functionality on the water-solubility and the thermosensitivity of the polymethacrylates are observed.

3.7 Anionic Block Copolymerization of (Meth)acrylates

The most important advantage of the living anionic polymerization is that a well-defined block copolymer can be synthesized by the sequential addition of comonomers. In fact, a number of block copolymers containing polymethacrylate segments have been synthesized by the sequential anionic polymerization of methacrylates and used for the fundamental research of the solution property, micelle structure, microphase separation in the bulk and at the surface, and mechanical property.

From a synthetic viewpoint, the anionic living polymers derived from hydrocarbon monomers, such as styrene, α-methylstyrene, 1,3-butadiene, and isoprene, are known to be excellent macroinitiators (initiators with high molecular weights) for (meth)acrylates. Usually, these living polymers were reacted (or masked) with
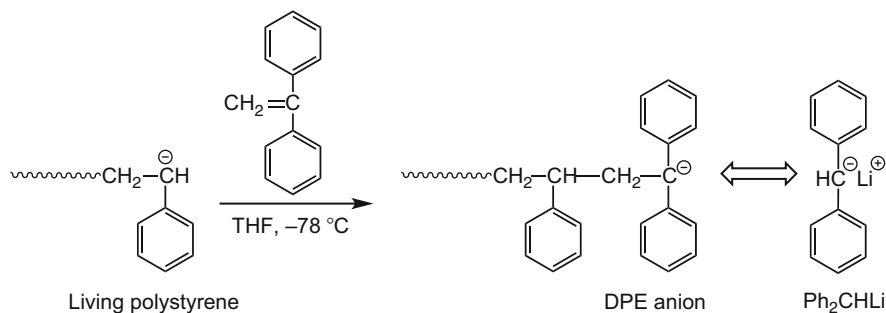
Scheme 17 Reaction of living polystyrene with 1,1-diphenylethylene

nonpolymerizable DPE derivatives prior to the addition of the (meth)acrylate monomers to reduce their nucleophilicities, since the resulting sterically hindered π-stabilized 1,1-diphenylalkyl anions (Scheme 17), similar to DPHLi and Ph$_2$CHLi, did not cause any serious side reactions with the carbonyl groups in the (meth) acrylates during the crossover reactions. On the other hand, the (meth)acrylate monomers can be directly added to the anionic living P2VP to form well-defined block copolymers, because the nucleophilicity is lower than those of styrene and 1,3-dienes. The block copolymers containing polymethacrylate and P2VP segments usually show amphiphilic properties, since the latter P2VP segment is hydrophilic and basic in character. Very interestingly, a series of well-defined block copolymers, AB (BA), ABA, and BAB, were synthesized by the sequential copolymerization of *tert*-butyl methacrylate (tBMA) and ethylene oxide by organopotassium initiators irrespective of addition order of monomers [151].

In principle, a block copolymer possessing a predictable composition and a molecular weight will be quantitatively produced by the sequential addition of comonomers, if a polymerization system of a monomer is living and the propagating chain end is stable. This is true for the monomers showing comparable anionic polymerizabilities. However, there is a strict limitation in the addition order of comonomers for the formation of block copolymer via the sequential anionic copolymerization, if the anionic polymerizabilities are significantly different from each other. One must polymerize a less (or least) reactive monomer first and add a more (or most) reactive monomer later for a successful block copolymerization. For example, only an ABC triblock terpolymer, polystyrene-*b*-P2VP-*b*-poly(MMA), can been synthesized by the sequential anionic copolymerization of three monomers with largely different polymerizabilities. Other triblock terpolymers, such as polystyrene-*b*-poly(MMA)-*b*-P2VP and P2VP-*b*-polystyrene-*b*-poly(MMA), are difficult to synthesize under similar conditions, although three types of copolymers, ABC, ACB, and BAC, can be considered in the three component block copolymers. The low nucleophilicity of the living polymers of 2VP and MMA prohibits the effective crossover reaction with other comonomers to prepare other block copolymers (Scheme 18) [5].

Scheme 18 Crossover reactions of living polymers of 2VP and MMA with other monomers [5]
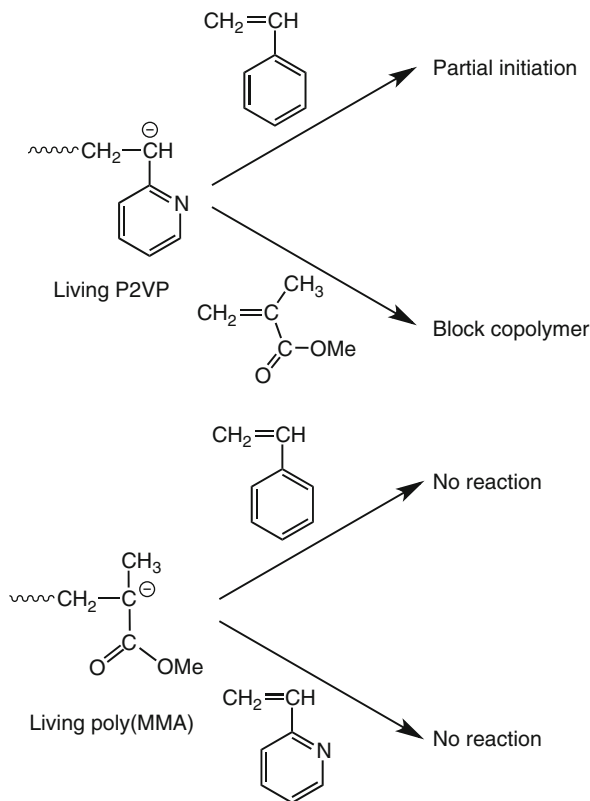
Very recently, Hirao and his coworkers have succeeded in the systematic synthesis of other two ACB and BAC block copolymers with different sequences and well-defined structures by the novel effective coupling reactions of anionic living polymers (Scheme 19) [152]. In this method, a 1:1 addition reaction between low nucleophilic poly(MMA) anions and the highly electrophilic α-phenylacrylate (PA) moiety in the end-functionalized polymers is used to link the polymer segments. This linkage reaction can be used for the precise synthesis of a series of architectural polymers, such as multiblock copolymers [153], multiarm star polymers [154], and exact graft copolymers [155], as described in the other chapters. For example, a series of multiblock copolymers composed of polystyrene (A) and poly(MMA) (C), ACA, ACAC, ACACAC, ACACACAC, and ACACACACAC, have been synthesized by the 1:1 addition reaction of PA-end-functionalized polymers and anionic living poly(MMA) [153].

On the other hand, the sequential anionic copolymerizations between methacrylate monomers smoothly proceed in any addition order, since the methacrylate monomers usually have comparable polymerizabilities regardless of the alkyl substituents. The anionic copolymerizations of the various methacrylates shown in Figs. 5, 6, and 8 afforded a number of well-defined block copolymers containing
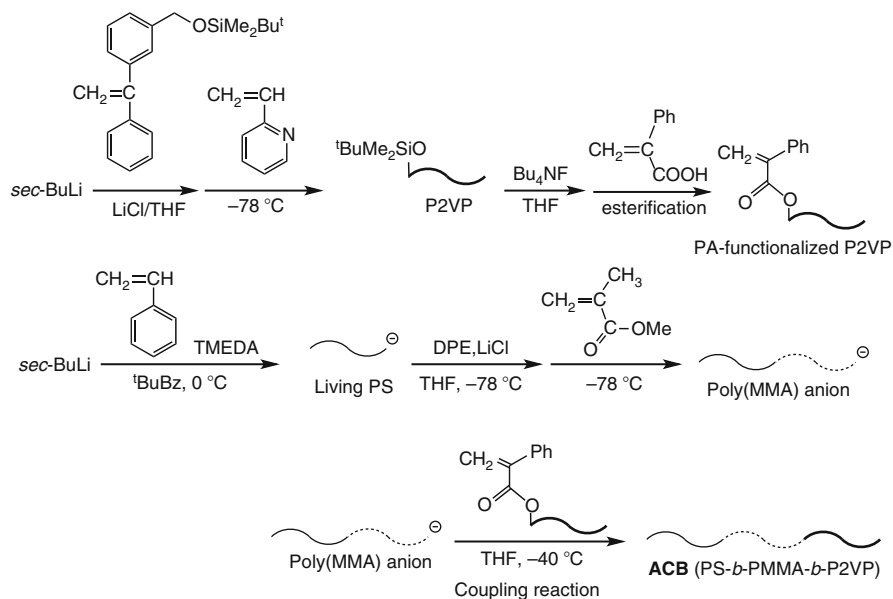
Scheme 19 Synthesis of ACB block copolymer via coupling reaction of living poly(MMA) with PA-end-functionalized polymer [152]

functional polymethacrylate segments with attractive properties, such as electrophilicity, basicity, hydrophilicity, hydrophobicity, high T_g, redox activity, and liquid crystallinity. For example, the anionic copolymerizations of 2-(perfluorobutyl)ethyl methacrylate (FMA), *tert*-butyl methacrylate (tBMA), and 2-(trimethylsilyloxy)ethyl methacrylate (HEMA-TMS) and the subsequent deprotection of the trimethylsilyl group successfully afforded a series of well-defined ABC triblock terpolymers, such as poly(FMA)-*b*-poly(tBMA)-*b*-poly(HEMA), poly(FMA)-*b*-poly(HEMA)-*b*-poly(tBMA), and poly(tBMA)-*b*-poly(FMA)-*b*-poly(HEMA), by changing the addition order of the three comonomers [102, 103] (Fig. 10). The poly(FMA) segment containing a hydrophobic and lipophobic perfluoroalkyl side chain was introduced in the ABC triblock terpolymers, since it was incompatible with the hydrophilic poly(HEMA) and lipophilic poly(tBMA) segments. In fact, the ¹H NMR spectra of the resulting triblock terpolymers suggested the formation of their micelles in selective solvents. The contact angle and X-ray photoelectron spectroscopic (XPS) measurements of the triblock terpolymer films confirmed the enrichment of the poly(FMA) segment at the film surface in the dry state. On the other hand, the surface rearrangement was also observed by changing the environmental conditions to the hydrophilic state. It was suggested that the segmental sequence in the ABC triblock terpolymers affected the structures in solution and at the surface due to the strong character of the poly(FMA) segment in the copolymers. The surface nanostructures and their reconstruction behavior of the polymer film were also investigated by altering the
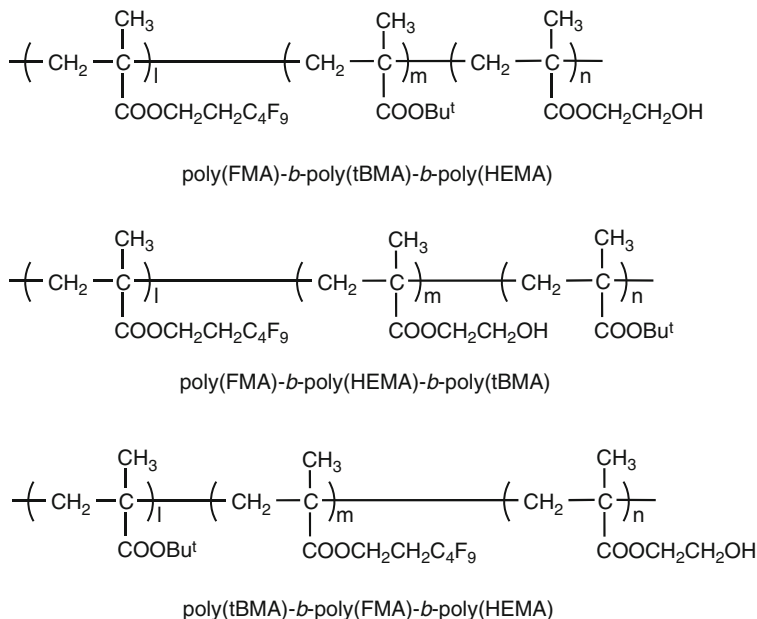
Fig. 10 Structures of ABC type triblock terpolymers derived from FMA, HEMA, and tBMA [102, 103]

outer environment. A series of amphiphilic ABC triblock terpolymers were also synthesized by GTP of the methacrylate monomers in order to investigate their solution properties [88, 156].

Various well-defined amphiphilic block copolymers composed of hydrophilic polymethacrylate segments have been synthesized by the sequential anionic block copolymerization with RLi/LiCl or RK/Et$_2$Zn initiator systems [126–128, 130]. Typical examples are polystyrene-b-poly(HEMA) [126, 127], polyisoprene-b-poly(HEMA) [128], and polystyrene-b-poly(2,3-dihydroxypropyl methacrylate) [130]. The outermost surface of the as-cast film of various amphiphilic block copolymers under dry conditions was usually covered with the hydrophobic polymer segments, and the restructuring of the surface occurred in response to the environment change [126–128, 130]. These reconstructed surfaces of the amphiphilic block copolymers containing hydrophilic poly(HEMA) segments often showed an excellent nonthrombogenic activity [157].

Similarly, a series of well-defined amphiphilic block copolymers containing water-soluble poly(OEGMA) segments with pendant OH groups were synthesized by the sequential anionic copolymerization of styrene and trialkylsilyl-protected oligo(ethylene glycol) methacrylates followed by deprotection [147–150] (Scheme 20). The corresponding methyl ethers of the oligo(ethylene glycol) methacrylates (MOEGMA) were also used to synthesize the amphiphilic block copolymers of styrene and MOEGMA, polystyrene-b-poly(MOEGMA). A small-angle
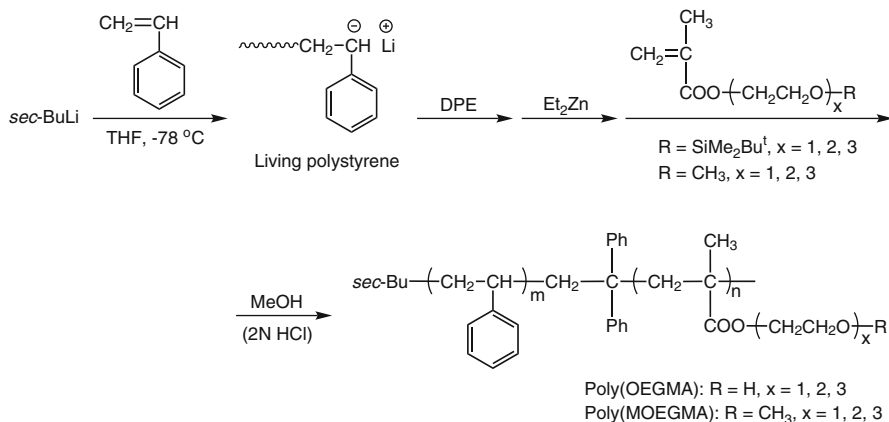
Scheme 20 Synthesis of polystyrene-*b*-poly(OEGMA) and polystyrene-*b*-poly(MOEGMA) by anionic polymerization [147–150]

X-ray scattering (SAXS) analysis indicated that the block copolymers containing poly(OEGMA) segments displayed a strongly segregated lamellar structure with sharp interfaces. On the other hand, the poly(MOEGMA) counterparts showed either weakly segregated lamellar or disorder structures. The angle-dependent XPS measurement of the films of block copolymers with poly(OEGMA) segments revealed that hydrophobic polystyrene segments exclusively covered the outermost surfaces, as expected. In contrast, enrichment of the oligo(ethylene glycol) units at the film surface was unexpectedly observed in the XPS measurement of polystyrene-*b*-poly(MOEGMA). The contact angle measurement also indicated that the film surface was covered with hydrophilic poly(MOEGMA) segments rather than hydrophobic polystyrene segments in contrast to the case for polystyrene-*b*-poly(OEGMA). Interestingly, the as-cast and annealed films of polystyrene-*b*-poly(MOEGMA) presented hydrophilic properties and showed a good biocompatibility including blood-compatibility [148]. The nature of the terminal moiety on the oligo(ethylene glycol) side chain, OH or OCH_3, played a very important role in determining the surface structure of the amphiphilic block copolymer films. Yokoyama and Ishizone reported that the hydrophobic terminal methyl groups of the hydrophilic oligo(ethylene glycol) side chain of the poly(MOEGMA) segment predominantly covered the surface to reduce the free energy of the system by the increased configurational entropy by exposing many chain ends to the surface [147, 149–150].

4 Polymerization of (Meth)acrylamides

4.1 Polymerization of N,N-Dialkylacrylamides

The anionic polymerizability of *N,N*-dialkylacrylamides is fairly high and roughly categorized into the same level as the (meth)acrylate monomers, since they are also electrophilic α,β-unsaturated carbonyl compounds activated by the electron-withdrawing amide substituents. Historically, although it has been reported that *N,N*-dialkylacrylamides readily undergo the anionic polymerization with strong nucleophiles, such as *n*-BuLi and *sec*-BuLi, these reports have mainly focused on the stereoregularity of the resulting polymers [158, 159]. Later studies have revealed that the π-stabilized bulky anionic initiators, such as DPHLi, DMPLi, Ph₂CHLi, and Ph₂CHK, are effective to realize the quantitative initiation efficiency in the anionic polymerization of *N,N*-dialkylacrylamides, similar to the (meth)acrylate monomers. As a first reliable study of the molecular weight control, Hogen-Esch reported the living anionic polymerization of *N,N*-dimethylacrylamide (DMA) with π-stabilized bulky organocesium initiators, such as triphenylmethylcesium (Ph₃CCs) and (1,1,4,4-tetraphenyl)butanediyldicesium in THF [160]. The resulting poly(DMA) is an attractive polymer because of its solubility in water.

On the other hand, Nakahama and Ishizone first succeeded in the stereospecific living anionic polymerization of *N,N*-diethylacrylamide (DEA) with binary initiator systems [62, 63, 161, 162]. Interestingly, poly(DEA)s possessing syndiotactic-rich ($rr = 88$ %, $M_w/M_n = 1.12$) and isotactic-rich ($mm = 88$ %, $M_w/M_n = 3.00$) configurations were produced in THF with π-conjugated organolithium initiator systems, RLi/Et₂Zn and RLi/LiCl, respectively (Scheme 21). The isotactic poly
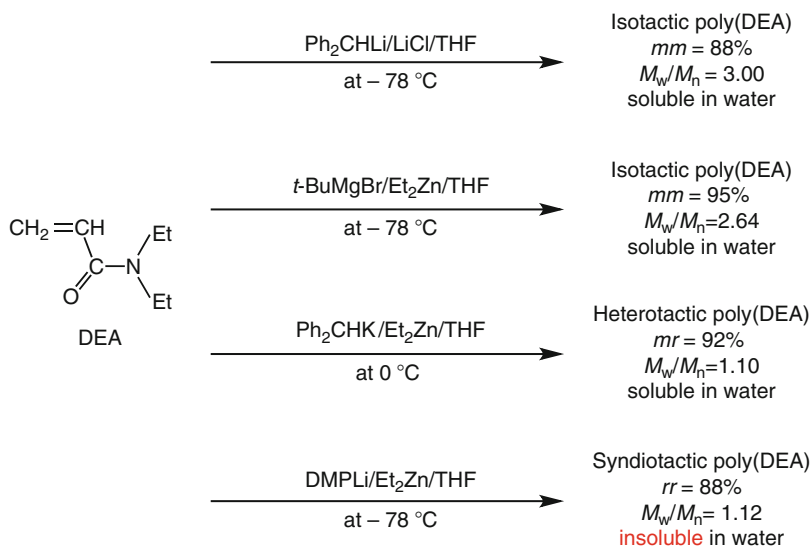
Scheme 21 Stereospecific anionic polymerization of DEA [62, 63, 161, 162]

Table 2 Anionic Polymerization of *N,N*-Dialkylacrylamides with Ph$_2$CHK or SiPK[a] in THF [62]

Initiator	Monomer	Et$_2$Zn/ K$^+$	Temp. °C	Time H	Yield %	$M_n \times 10^{-3}$ calcd.[b]	$M_n \times 10^{-3}$ obsd.[c]	M_w/ M_n[d]
SiPK	DMA		−78	1	100	11	14	2.85
SiPK	DEA		−78	1	100	10	15	2.37
SiPK	DEA		−78	15 s	97	21	23	1.63
SiPK	**A5**		−78	15 min	100	7.9	8.0	3.03
SiPK	**A6**		−78	0.5	100	9.9	11	1.60
SiPK/Et$_2$Zn	DMA	15	−78	1	60	8.5	5.6	1.07
SiPK/Et$_2$Zn	DMA	18	0	0.5	100	11	9.8	1.07
SiPK/Et$_2$Zn	DEA	15	−78	1	57	10	7.8	1.12
SiPK/Et$_2$Zn	DEA	15	−40	1	100	10	8.6	1.09
SiPK/Et$_2$Zn	DEA	17	0	20 min	100	41	45	1.05
SiPK/Et$_2$Zn	EMA	17	0	0.5	100	10	8.0	1.12
Ph$_2$CHK/ Et$_2$Zn	**A3**	11	−78	1	85	6.0	6.9	1.18
Ph$_2$CHK/ Et$_2$Zn	**A4**	14	−78	2	100	5.4	7.0	1.08
SiPK/Et$_2$Zn	**A5**	16	0	15 min	100	9.6	8.2	1.10
SiPK/Et$_2$Zn	**A6**	19	0	0.5	100	10	10	1.07
SiPK/Et$_2$Zn	AMO	16	0	1	100	10	10	1.09

[a]1,1-Bis[(4'-trimethylsilyl)phenyl]-3,3-diphenylpropylpotassium
[b]M_n(calcd) = (MW of monomer) × yield/100 × [monomer]/[initiator] + (MW of initiator)
[c]M_n(obsd) was determined by the ^{1}H NMR
[d]M_w/M_n was determined by the SEC calibration using PMMA standards

(DEA) (*mm* = 95 %) was also obtained with the organomagnesium initiator system, *t*-BuMgBr/Et$_2$Zn, in THF at −78 °C, while the molecular weight distribution was still very broad (M_w/M_n = 2.64). On the other hand, the addition of Et$_2$Zn to Ph$_2$CHK in THF at 0 °C induced the heterotactic-specific anionic polymerization of DEA (*mr* = 92 %). Similar to Ph$_2$CHK, 1,1-bis[(4'-trimethylsilyl)phenyl]-3,3-diphenylpropylpotassium (SiPK, 1:1-addition product of Ph$_2$CHK and 1,1-bis [4-(trimethylsilyl)phenyl]ethylene) was used for the polymerization of DEA as a monofunctional organopotassium initiator in THF (Table 2). The resulting *mr*-rich poly(DEA)s possessed the predicted molecular weights, and the SEC curves of the polymers showed sharp unimodal shapes, indicating their narrow molecular weight distributions (M_w/M_n = 1.10). The addition of Et$_2$Zn (11–19 equivalents) to the polymerization systems significantly lowered the polymerization rate and drastically reduced the polydispersity indices of the polymers [62]. The persistence of the propagating carbanion derived from DEA was also confirmed by the quantitative efficiency of the postpolymerization (monomer addition experiment) using Ph$_2$CHK/Et$_2$Zn. The results confirmed that the propagating species of poly(DEA) maintained the living character for at least 1 min even at 0 °C in THF, strongly indicating the tolerance of the amide carbonyl groups.
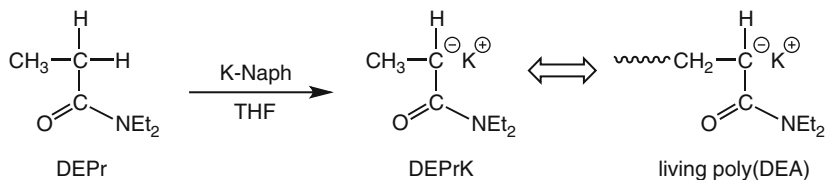
Scheme 22 Synthesis of amide enolate (DEPrK) [164]

Similar to DEA, the living polymerizations of DMA, *N*-ethyl-*N*-methylacrylamide (EMA), *N*-acryloyl-2-methylaziridine (A3), *N*-acryloylazetidine (A4), *N*-acryloylpyrrolidine (A5), *N*-acryloylpiperidine (A6), and *N*-acryloyl-morpholine (AMO) were achieved by the binary initiator system of Ph$_2$CHK/Et$_2$Zn in THF at 0 to –78 °C [62] (Table 2). In particular, the polymers derived from DMA, DEA, EMA, A5, A6, and AMO formed at 0 °C possessed narrow molecular weight distributions ($M_w/M_n < 1.12$), as well as the predicted molecular weights. In addition to the attainment of the livingness of the polymerization system, the stereospecific anionic polymerizations of several acrylamide monomers were achieved in the presence of Et$_2$Zn even in a polar Lewis basic solvent, such as THF.

The anionic polymerization of the *N*,*N*-dialkylacrylamides can be initiated using low nucleophilic enolate anions. For example, the polymerization of DEA with ethyl α-lithioisobutyrate (ester enolate) in the presence of the Lewis acidic AlEt$_3$ afforded a well-defined *mr*-rich poly(DEA) in THF at –78 °C ($M_n = 30,800$ g/mol, $M_w/M_n = 1.05$) [163]. On the other hand, Ishizone and his coworkers prepared a novel α-potassio-enolate (DEPrK) by the proton abstraction reaction from *N*,*N*-diethylpropionamide (DEPr) with potassium naphthalenide, as shown in Scheme 22 [164].

Since DEPrK can be recognized as a model for the active chain end of poly (DEA), the polymerization results provide useful information on the stability and the reactivity of the propagating chain ends of poly(DEA). It is generally known that the amide-derived enolates have a greater stability than the enolates of esters, indicating the tolerance of the amide moiety toward nucleophilic attack compared to the labile ester function. In fact, the resulting DEPrK can be stored in THF at least 1 year without degradation. The anionic polymerization of a series of mono-mers, such as styrene, 2VP, MMA, and DEA was performed with DEPrK in THF to confirm the initiation ability of the potassium amide enolate, as shown in Table 3 [164]. Interestingly, the polymerizations of all monomers could be directly initiated with DEPrK to give polymers in 100 % yields in THF at –78 °C within 1 h, while the molecular weight controls were not achieved in most cases. The high nucleo-philicity of DEPrK was thus demonstrated, since even styrene, having a low reactivity in the anionic polymerization, could be polymerized regardless of the

Table 3 Anionic Polymerization of Styrene, 2VP, MMA, and DEA with DEPrK in THF at $-78\,^\circ$C for 1h [164]

Initiator	Additive[a]	Monomer	Yield %	$10^{-3}M_n$ calcd[b]	$10^{-3}M_n$ obsd[c]	M_w/M_n[c]	Initiator efficiency[d] %	Tacticity (%) mm	Tacticity (%) mr	Tacticity (%) rr
DEPrK		Styrene	100	7.7	490	1.31	2			
DEPrK		2VP	100	9.4	14	1.27	67			
DEPrK		MMA	100	3.5	3.3	1.67	Quantitative			
DEPrK		DEA	100	8.6	12	1.92	Quantitative	40	54	6
DEPrK	Et$_2$Zn	Styrene	~0	–	–	–	–			
DEPrK	Et$_2$Zn	2VP	100	9.3	34	1.48	27			
DEPrK	Et$_2$Zn	MMA	100	3.5	3.3	1.09	Quantitative			
DEPrK	Et$_2$Zn	MMA	100	13	14	1.08	Quantitative			
DEPrK[e]	Et$_2$Zn	DEA	64	4.8	5.5	1.12	Quantitative	28	65	7
DEPrK[e]	Et$_2$Zn	DEA	100	8.4	8.2	1.23	Quantitative	39	45	16
DEPrK[e]	Et$_2$Zn	DEA	100	9.8	11	1.10	Quantitative	11	83	6
DEPrK[e]	Et$_2$Zn	DEA	100	32	28	1.04	Quantitative	6	89	5
Ph$_2$CHK		Styrene	100	11	68	1.36	16			
Ph$_2$CHK		2VP	100	10	9.6	1.06	Quantitative			
Ph$_2$CHK		MMA	100	10	11	1.99	Quantitative			
Ph$_2$CHK		DEA	100	10	14	2.07	Quantitative	52	32	16
Ph$_2$CHK	Et$_2$Zn	Styrene	<10	–	Oligomers	–	–			
Ph$_2$CHK	Et$_2$Zn	2VP	100	10	11	1.09	Quantitative			
Ph$_2$CHK[e]	Et$_2$Zn	MMA	100	4.2	4.4	1.07	Quantitative			
Ph$_2$CHK	Et$_2$Zn	DEA	100	10	10	1.19	Quantitative	33	48	19
Ph$_2$CHK[e]	Et$_2$Zn	DEA	100	9.3	8.6	1.08	Quantitative	21	71	8

[a][Et$_2$Zn]/[initiator] = 12~16
[b]M_n(calcd) = (MW of monomer) × yield/100 × [monomer]/[initiator] + (MW of initiator)
[c]M_n(obsd) and M_w/M_n were determined by the SEC calibration using standard polymer samples
[d]M_n(calcd)/M_n(obsd) × 100
[e]Polymerized at 0 °C for 1h

Table 4 Anionic polymerization of *N,N*-dialkylacrylamides in THF in the presence of Et$_3$B [63]

Initiator	Monomer	Et$_3$B/M$^+$	Temp. °C	Time h	Yield %	$M_n \times 10^{-3}$ calcd.[a]	obsd.[b]	M_w/M_n[c]
DMPLi	DMA		−78	0.02	100	5.3	6.5	3.41
DMPLi/Et$_3$B	DMA	5.9	−78	1	0	–	–	–
DMPLi/Et$_3$B	DMA	2.1	0	4	100	16	16	1.13
Ph$_2$CHK	DEA		−78	0.02	100	12	11	1.51
Ph$_2$CHK/Et$_3$B	DEA	2.4	−78	1	0	–	–	–
Ph$_2$CHK/Et$_3$B	DEA	2.3	0	24	56	6.5	4.7	1.07
Ph$_2$CHK/Et$_3$B	DEA	2.3	0	96	100	11	8.9	1.08
Ph$_2$CHK/Et$_3$B	DEA	3.4	30	6	100	28	30	1.06

[a]M_n(calcd) = (MW of monomer) × yield/100 × [monomer]/[initiator] + (MW of initiator)
[b]M_n(obsd) was determined by the ^{1}H NMR
[c]M_w/M_n was determined by the SEC calibration using PMMA standards

low initiation efficiency (~2 %) [165]. On the other hand, the initiation efficiency (nucleophilicity) of DEPrK apparently decreased in the presence of Et$_2$Zn (12–16 equivalents). No polymerization of styrene virtually occurred with DEPrK/Et$_2$Zn in THF at −78 °C. Although 2VP could be polymerized with DEPrK/Et$_2$Zn at −78 °C, the initiation efficiency decreased from 67 to 27 % after the addition of Et$_2$Zn. In contrast, this novel binary initiator system of DEPrK/Et$_2$Zn could initiate the anionic polymerizations of MMA and DEA with quantitative efficiencies in THF at −78 °C resulting in the formations of the tailored poly(MMA) and poly(DEA). In particular, significant narrowing of the molecular weight distribution and increasing of the triad *mr* values were achieved in the poly(DEA)s produced with DEPrK/ Et$_2$Zn at 0 °C, in addition to the molecular weight control.

It is thus demonstrated that the ability of the DEPrK/Et$_2$Zn system as the anionic initiator is almost comparable to that of the Ph$_2$CHK/Et$_2$Zn system. In addition, the nucleophilicity of the amide enolate is found to be higher than that of the ester enolate based on the polymerization result of styrene.

Compared to the initiator system in the presence of Et$_2$Zn, the additive effect of Et$_3$B is more drastic in the polymerization systems of DMA and DEA, as shown in Table 4 [63]. No apparent polymerization was observed at −78 °C within 1 h after the addition of Et$_3$B (2–6 equivalents) to DMPLi or Ph$_2$CHK. At the higher temperatures of 0 or 30 °C, the polymerization of DMA and DEA certainly proceeded in the presence of Et$_3$B to form polymers with controlled molecular characteristics ($M_w/M_n < 1.13$). The most significant effect was observed in retarding the polymerization. The rate of polymerization for DEA was very slow even at 0 °C, since only 56 % of DEA was consumed with Ph$_2$CHK/Et$_3$B after 24 h. A prolonged polymerization time of 96 h was required for the completion of the polymerization of DEA at 0 °C, while a quantitative propagation was achieved within 6 h at 30 °C. Similar to the polymerization systems of tBA [57] and methacrylonitrile [64], a possible dormant species like the borate complex might form at −78 °C by the strong coordination of the Lewis acidic Et$_3$B and the amide enolate anion, as shown in Scheme 23. At higher temperatures over 0 °C, the
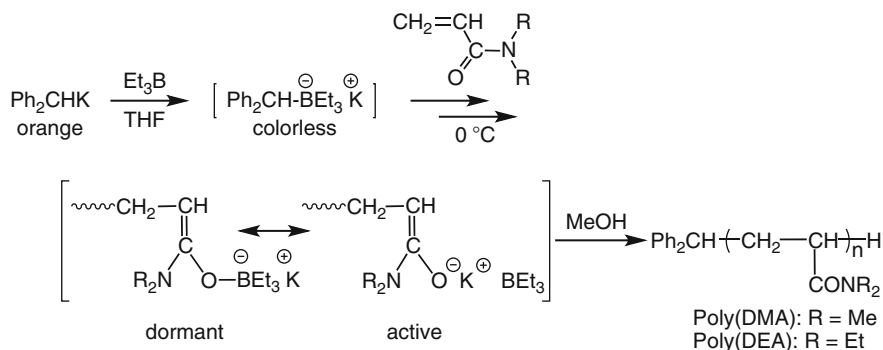
Scheme 23 Anionic polymerization of DMA and DEA in the presence of Et_3B [63]

equilibrium shifts from the dormant species toward the active amide enolate to propagate the polymerization rather slowly. It is considered that the coordinated Et_3B also prevents the undesirable side reactions, such as α-proton abstraction and carbonyl attack, and effectively stabilizes the propagating amide enolate anions. The poly(DEA) obtained with Ph_2CHK/Et_3B at 0 °C was highly heterotactic (rich in *mr* triads).

In addition to the molecular weight control, the added common salts (LiCl) or Lewis acids (Et_2Zn and Et_3B) apparently play important roles in varying the stereo-regularity of the poly(*N,N*-dialkylacrylamide)s during the course of the anionic polymerization. In contrast, in the polymerizations of (meth)acrylates in THF, their additive effects on the stereoregularity are rather limited or even negligible [45, 49, 55–57]. This is probably due to the difference between the ester and amide moieties in the coordination ability toward the acidic additives and the counter cations. The ester moieties might not coordinate enough with the additives, while the more polar amide groups coordinate to the additives as well as the counter cations of the chain-end anions, resulting in inducing the stereospecific polymerization.

Very importantly, it is evident that the stereoregularity of the poly(DEA) strongly affects its water-solubility and the T_c value in an aqueous solution. Although poly(DEA) has been believed to be a representative water-soluble poly-mer, the syndiotactic poly(DEA) ($rr = 88$ %) produced with $DMPLi/Et_2Zn$ is insoluble in water at any temperature [62]. On the other hand, both the heterotactic ($mr = 92$ %) and isotactic ($mm = 88$–95 %) polymers are soluble in water and show T_c values of 28 and 38 °C for the heating processes, respectively. This indicates that the water-solubility of poly(DEA) tended to increase with the *m* content in the repeating units. On the other hand, the poly(DMA)s with a higher polarity were always soluble in water at any temperature, while their stereoregularities were also varied by the initiator systems.

Related to the anionic polymerization, several *N,N*-dialkylacrylamides, such as DMA and DEA, can also undergo the GTP to provide polymers in good to quantitative yields. Although the polymerization condition was rather mild, the molecular weight control in GTP was difficult compared to the conventional
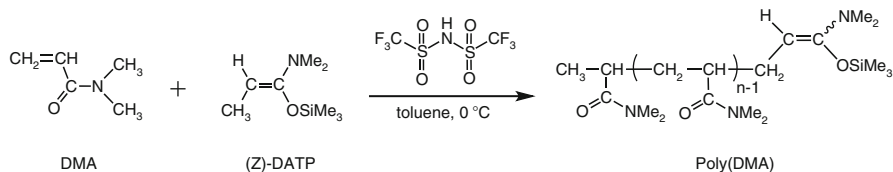
Scheme 24 GTP of DMA catalyzed by $(CF_3SO_2)_2NH$ [169]

anionic polymerization. For example, although poly(DMA) was quantitatively obtained with dimethylketene methyl trimethylsilyl acetal (DMTA) in the presence of a nucleophilic catalyst in THF, the number-average molecular weight was apparently lower than the theoretical one and the molecular weight distribution was broad ($M_w/M_n = 1.62$) [80]. The GTP of DEA similarly proceeded with DMTA in THF at 0 °C to afford poly(DEA) with a relatively narrow molecular weight distribution ($M_w/M_n = 1.2$) in 50–70 % yields [166–168]. Recently, Kakuchi and his coworkers newly synthesized (Z)-1-(dimethylamino)-1-trimethylsiloxy-1-propene, (Z)-DATP, the silyl enolate of N,N-dimethylpropionamide, as the new GTP initiator [169] (Scheme 24). The GTP of DMA quantitatively proceeded with (Z)-DATP in the presence of an organocatalyst, $(CF_3SO_2)_2NH$, to afford a tailored polymer with a high molecular weight ($M_n = 53,900$ g/mol, $M_w/M_n = 1.07$) in toluene at 0 °C. The living character of the new GTP system for DMA was clearly demonstrated by the monomer addition experiment and the detailed analysis based on MAIDI-TOF MS measurements.

4.2 Anionic Polymerization of Protected N-Isopropylacrylamide

In contrast to the N,N-dialkylacrylamides, both acrylamide and the N-alkylacrylamides were difficult to anionically polymerize due to the presence of the acidic amide protons [7] ($pK_a = 25$–26). Only under drastic basic conditions, the hydrogen-transfer polymerizations of these acrylamide monomers proceeded along with vinyl polymerization to give a complicated polymer consisting of 1,2-addition and 1,4-addition modes [170, 171] (Scheme 25). Needless to say, the molecular architectures of the resulting polymers are far from controlled.

Evidently, the protection of the amide protons of acrylamide and N-alkylacrylamides is required for the exclusive vinyl polymerization and the molecular weight control. Among such acrylamide monomers carrying acidic hydrogen, N-isopropylacrylamide (NIPAM) is the most popular monomer because of the strong interest in its polymer, poly(NIPAM). Poly(NIPAM) obtained by the free-radical polymerization has been well known as a water-soluble and thermoresponsive polymer, since the aqueous solution showed a typical reversible cloud point at around 32 °C. Therefore, the hydrophilic thermoresponsive poly(NIPAM)
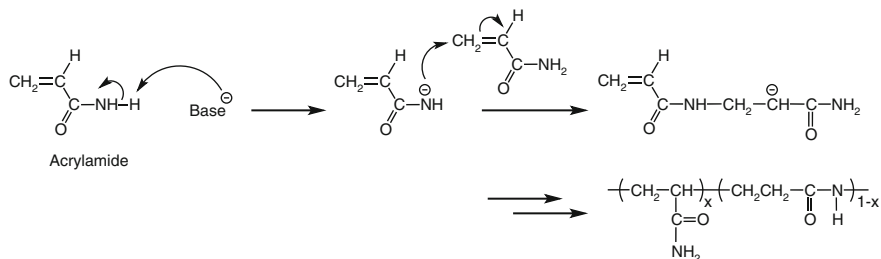
Scheme 25 Hydrogen-transfer polymerization of acrylamide [170, 171]
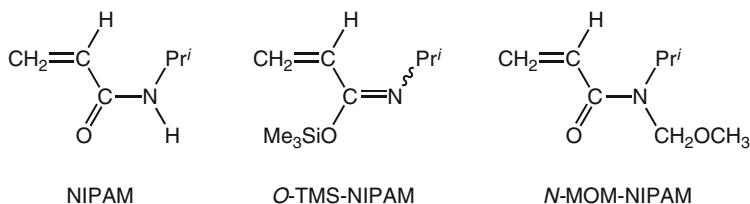
Fig. 11 Protected NIPAM monomers [177, 179–181]

has attracted significant attention for various applications due to its promising potentials as hydrogels [172, 173], biomedical uses, drug delivery devices [174], polymer-bound catalyst [175], and permeation membranes [176].

Two protected NIPAM monomers have been synthesized in order to realize the anionic polymerization (Fig. 11). Kitayama and his coworkers designed *O*-trimethylsilyl-*N*-isopropylacrylamide (TMS-NIPAM), whose amide proton is protected by the trimethylsilyl group [177]. The conjugation system of C=C-C=O in NIPAM is transformed into a C=C-C=N system in TMS-NIPAM. The anionic polymerization of TMS-NIPAM smoothly proceeded with *tert*-BuLi in the presence of trialkylaluminum in toluene, and a highly isotactic poly(NIPAM) ($m = 97$ %) was quantitatively obtained after quenching with methanol because of the labile trimethylsilyl protecting group. In this case, the molecular weight of the resulting poly(NIPAM) was not regulated probably due to the serious side reactions. Interestingly, the resulting isotactic poly(NIPAM) was completely insoluble in water, as described below. This is consistent with the previous finding regarding the solubility of the isotactic poly(NIPAM) ($m = 92$ %) obtained by the radical polymerization of NIPAM in the presence of rare earth metal triflates [178].

The second protected NIPAM, *N*-methoxymethyl-*N*-isopropylacrylamide (MOM-NIPAM), was specifically synthesized by Ishizone and Ito to prevent termination and chain transfer reactions [179–181] (Scheme 26). This acetal-protected NIPAM still kept the structure of the acrylamide derivative and readily underwent the anionic polymerization in THF at –78 °C with either DMPLi, Ph$_2$CHM (M = Li, K, and Cs), and Ph$_3$CK in combination with Et$_2$Zn. The resulting
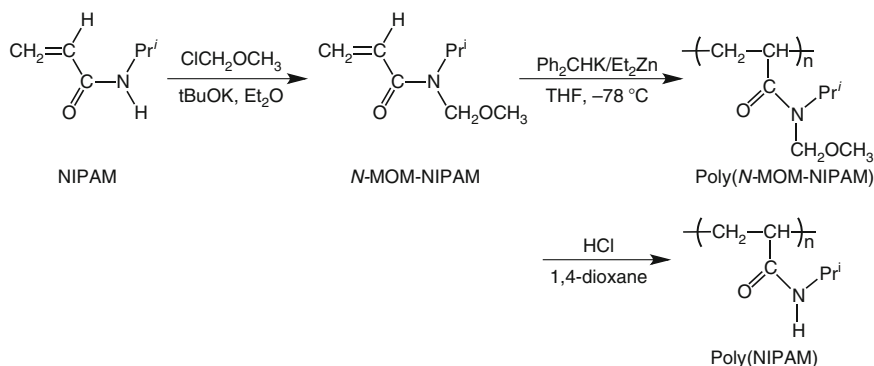
Scheme 26 Anionic polymerization of MOM-NIPAM [179–181]

Table 5 Anionic Polymerization of MOM-NIPAM in THF at −78 °C[a] [179–181]

Initiator	LiCl/Li$^+$	Et$_2$Zn/M$^+$	Time h	$M_n \times 10^{-3}$ calcd.[b]	obsd.[c]	M_w/M_n[d]	Tacticity (%)[e] m/r
DMPLi			1	11	15	2.06	57/43
DMPLi/LiCl	8.3		1	14	13	1.31	78/22
DMPLi/LiCl	26		1	11	14	1.19	85/15
DMPLi/Et$_2$Zn		17	1.5	11	12	1.11	23/77
DMPLi/Et$_2$Zn		43	1	10	12	1.10	20/80
DMPLi/Et$_2$Zn		54	3	16	18	1.13	17/83
Ph$_2$CHK			2	10	11	1.25	69/31
Ph$_2$CHK/Et$_2$Zn		15	5 min	12	12	1.12	52/48
Ph$_2$CHK/Et$_2$Zn		17	2	12	13	1.12	50/50
Ph$_2$CHK/Et$_2$Zn		18	20	23	23	1.10	50/50
Ph$_2$CHK/Et$_2$Zn		18	3	32	30	1.08	47/53
Ph$_2$CHK/Et$_2$Zn		20	6	52	67	1.06	48/52

[a]Yield ~ 100 %
[b]M_n(calcd) = (MW of monomer) × [monomer]/[initiator] + (MW of initiator)
[c]M_n(obsd) was determined by the ^{1}H NMR
[d]M_w/M_n was determined by the SEC calibration using polystyrene standards
[e]By ^{1}H NMR

poly(MOM-NIPAM)s always had well-defined chain structures including controlled molecular weights and narrow molecular weight distributions (M_w/M_n = 1.1), as shown in Table 5. In contrast, the molecular weight distribution was very broad (M_w/M_n = 2.06) when the polymerization of MOM-NIPAM was performed with DMPLi in the absence of Et$_2$Zn. The addition of LiCl to the polymerization system remarkably narrowed the molecular weight distribution (M_w/M_n = 1.19–1.31), while the additive effect of Et$_2$Zn was more significant.

The methoxymethyl (MOM) protective groups in the polymer were robust under the polymerization conditions but readily removable under the acidic condition. The quantitative hydrolysis of the MOM group was attained by treating the polymer with aqueous hydrochloric acid in 1,4-dioxane at room temperature for 20 h, as shown in Scheme 26. The ^{1}H and ^{13}C NMR and IR spectra of the deprotected polymer were consistent with those of the authentic poly(NIPAM) obtained by the free-radical polymerization of NIPAM. The SEC curve of the deprotected poly (NIPAM) still maintained the unimodal and narrow shape ($M_w/M_n = 1.08$) and shifted toward a lower molecular weight region from the original poly (MOM-NIPAM) ($M_w/M_n = 1.06$). These results indicated that the complete deprotection of poly(MOM-NIPAM) proceeds to give a well-defined poly (NIPAM) without side reactions, such as cross-linking and/or main chain degradation.

The stereoregularity of poly(NIPAM) in the diad level (m or r content) can be estimated from the integral ratio of the splitting methine proton signals of the main chain in the ^{1}H NMR spectroscopy. It is noted that the free-radical polymerization of NIPAM provides an atactic poly(NIPAM) ($m = 50$ %). From the polymerization system of MOM-NIPAM, syndiotactic-rich, isotactic-rich, and atactic poly (NIPAM)s could be obtained by selecting the initiator system (Table 5). The r diad content in poly(NIPAM)s can be significantly changed from 15 to 83 % by choosing the anionic initiator systems. The Li$^+$/Et$_2$Zn initiator system induced syndiotactic configurations ($r = 75$–83 %), while the K$^+$/Et$_2$Zn or Li$^+$/LiCl initiator system gave either an atactic ($r = 50$ %) or an isotactic poly(NIPAM) ($r = 15$–22 %), respectively. The highest r content (83 %) of poly(NIPAM) was achieved using organolithium at –95 °C in the presence of 54-fold Et$_2$Zn, indicating the effects of the polymerization temperature and the concentration of the Lewis acidic Et$_2$Zn.

Very interestingly, the stereoregularity of poly(NIPAM) strongly affects the solubility in water and the thermoresponsive property. In summary, although both atactic and syndiotactic-rich poly(NIPAM)s were soluble in water as expected, the isotactic-rich polymers ($m > 69$ %) were insoluble in water. The configuration of poly(NIPAM) evidently played a very important role to determine the solubility in water. The isotactic-rich poly(NIPAM) is no longer a water-soluble polymer regardless of the presence of highly polar CONH moieties in the repeating units. On the other hand, the atactic polymers ($r = 50$ %) produced with RK/Et$_2$Zn showed T_c values at around 32 °C, similar to the polymers obtained by the conventional radical polymerization. It should be noted that the T_c value slightly, but certainly increased with the r content and the highest T_c at 37 °C was observed in a syndiotactic-rich poly(NIPAM) ($r = 83$ %). This tendency in solubility on the stereoregularity is completely opposite to that of a series of stereoregulated poly (DEA)s, as described above. Thus, the living anionic polymerization evidently contributed to the fundamental research on the solution property of the water-soluble polymer via the precise synthesis of polymers with well-defined chain structures.

4.3 Anionic Polymerization of N,N-*Dialkylmethacrylamides*

As described above, it is well known that *N,N*-dialkylacrylamides readily undergo the radical and anionic polymerizations to produce vinyl polymers. In particular, they act as typical α,β-unsaturated carbonyl compounds and show high anionic polymerizabilities derived from the electron-withdrawing $CONR_2$ substituents. Their anionic polymerizations usually quantitatively proceed, and even stable living polymers form under the suitable polymerization conditions. In contrast, the corresponding *N,N*-dialkylmethacrylamides, such as *N,N*-dimethylmethacrylamide (DMMA) and *N,N*-dibutylmethacrylamide, could not be polymerized at all under similar anionic polymerization conditions. It has also been reported that no polymeric product of the *N,N*-dialkylmethacrylamides was obtained using the radical initiators [182–184]. Although the observed polymerizability significantly differs between *N,N*-dialkylacrylamides and *N,N*-dialkylmethacrylamides, the difference in the chemical structures of the α,β-unsaturated amides is only α-CH_3 groups in the latter monomers. Needless to say, the α,β-unsaturated esters (acrylates and methacrylates) and α,β-unsaturated nitriles (acrylonitrile and methacrylonitrile) can be converted into their vinyl polymers under radical and anionic conditions. This lack of polymerizability of the *N,N*-dialkylmethacrylamides is therefore a long-standing question in polymer chemistry.

Based on several studies using ^{1}H and ^{13}C NMR spectroscopies and molecular structure calculations of the *N,N*-dialkylmethacrylamides, a twisted conformation is estimated between the $C=C$ and $C=O$ groups due to the intramolecular steric repulsion between the α-CH_3 or $CH_2=$ group and *N*-alkyl substituents [160, 185, 186]. The partially conjugated planar structure of the $O=C$-NR_2 moiety in DMMA should also play an important role in reducing the π-conjugation between the $C=C$ and $C=O$ double bonds. Accordingly, it is considered that these structural demands and the unfavorable electronic environments lead to the observed nonpolymerizability of the monomers. In addition, the *N,N*-dialkylmethacrylamides might have an extremely low ceiling temperature, which also hinders their homopolymerizations.

As an exception, the vinyl polymerization of *N*-methacryloylaziridine (MAz), a cyclic analog of DMMA, has been reported [187, 188] (Fig. 12). MAz carrying a highly strained three-membered aziridine ring can be polymerized with either *n*-BuLi or AIBN, but the detailed results have not been reported. It is noted that plausible side reactions including the ring-opening reaction of the aziridine ring are suggested in the anionic polymerization due to the formation of insoluble polymeric products.

In order to clarify the polymerizability in detail, Ishizone and his coworkers have synthesized a series of *N,N*-dialkylmethacrylamides carrying cyclic substituents, such as 2-methylaziridine (M3), azetidine (M4), pyrrolidine (M5), and piperidine
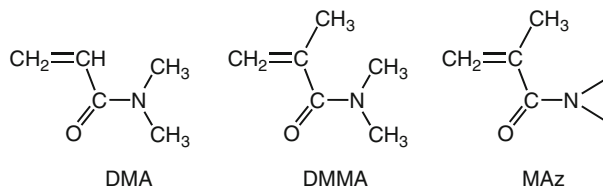
Fig. 12 *N,N*-Dialkylmethacrylamides [188].

(M6) rings, and subjected them to the anionic polymerization [189, 190] (Table 6). Interestingly, the polymerization behavior was significantly influenced by the ring size of the substituent. The anionic polymerizations of monomers with three- and four-membered rings, M3 and M4, proceeded with DMPLi or Ph_2CHLi in THF at –78 °C to afford polymers with well-controlled primary structures ($M_n \sim 50{,}000$ g/mol, $M_w/M_n < 1.1$) in quantitative yields either in the absence or presence of LiCl. Even at 0 °C, the tailored poly(M3) and poly(M4) were similarly produced with organolithiums in the presence of LiCl. The binary initiator systems of DMPLi/Et_2Zn and Ph_2CHLi/Et_2Zn also led to the controlled polymerization of M3 and M4, respectively. The addition of Et_2Zn markedly retarded the polymerization of M4 with an organopotassium initiator at –78 °C, and no polymerization proceeded even after 72 h. Interestingly, at the higher temperature of 0 °C, M4 was completely consumed by Ph_2CHK/Et_2Zn within 24 h to afford a polymer with a tailored chain length. On the other hand, the anionic polymerization of M5 having a five-membered ring afforded polymers in 44–77 % yields under the same conditions, but the polymerization was not completed under the various reaction conditions. Furthermore, M6 carrying a six-membered ring could not be polymerized at all even under drastic conditions, similar to the polymerization behavior of the *N,N*-dialkylmethacrylamides including DMMA.

From a kinetic viewpoint, the relative polymerizability of M3 and M4 has been compared in the polymerization systems using DMPLi/LiCl in THF [189, 190]. The k_p^{ap} values for the polymerization of M3 and M4 at –40 °C were estimated to be 0.165 and 0.0157 L mol^{-1} s^{-1}, respectively. The observed k_p^{ap} value of M3 was approximately 10 times greater than that of M4 under similar conditions. From the Arrhenius plots of the k_p^{ap} values, the activation energy of the polymerization, ΔE_a^{ap}, of M3 and M4 were determined to be 49 ± 4 and 51 ± 5 kJ mol^{-1}, respectively. Although these ΔE_a^{ap} values were rather comparable, the slightly larger ΔE_a^{ap} value of M4 supported the lower polymerizability compared to M3. The ΔE_a^{ap} values of both M3 and M4 were remarkably larger than the reported values of the anionic polymerization of MMA ($\Delta E_a^{ap} = 20$–25 kJ mol^{-1}) under similar conditions [53, 54]. The relative anionic polymerizability among M3, M4, and MMA is thus estimated as follows: M4 < M3 << MMA. Besides anionic polymerization, the radical polymerization of M3 and M4 certainly occurred with AIBN in toluene to give polymers in 77 and 40 % yields, respectively. M3 also underwent

Table 6 Anionic polymerization of M3, M4, and M5 in THF [189, 190]

Monomer	Initiator	Additive/M^+	Temp. °C	Time h	Yield %	$10^{-3}M_n$ calcd[a]	obsd[b]	M_w/M_n[c]	Tacticity (%)[d] mm	mr	rr
M3	DMPLi		−78	15	90	6.1	7.0	1.14			
M3	DMPLi/LiCl	3.8	−78	72	100	6.1	7.2	1.05			
M3	DMPLi/LiCl	5.2	−40	24	100	47	50	1.09			
M3	DMPLi/LiCl	4.3	0	15 min	100	15	16	1.05			
M3	DMPLi/Et₂Zn	11	−78	72	100	12	15	1.08			
M3	Ph₂CHK		−78	15	100	15	16	1.20			
M3	Ph₂CHK/Et₂Zn	12	−78	17	82	13	6.2	1.29			
M4	Ph₂CHLi		−40	16	100	18	23	1.08	60	33	7
M4	Ph₂CHLi/LiCl	4.6	−78	96	72	11	14	1.14	93	7	<1
M4	Ph₂CHLi/LiCl	4.1	−40	24	100	18	19	1.05	70	25	5
M4	Ph₂CHLi/LiCl	6.5	0	2	100	15	18	1.05	68	27	5
M4	Ph₂CHLi/Et₂Zn	17	−40	36	85	26	39	1.06	27	54	19
M4	Ph₂CHNa		−40	13	100	17	19	1.13	52	42	6
M4	Ph₂CHNa/Et₂Zn	16	−40	72	69	9.2	6.9	1.06	11	57	32
M4	Ph₂CHK		0	16	100	12	16	1.17	12	54	34
M4	Ph₂CHK/Et₂Zn	12	−78	72	0	–	–				
M4	Ph₂CHK/Et₂Zn	13	0	24	100	17	19	1.07	13	62	25
M5	Ph₂CHLi		0	72	69	6.2	8.7	1.07			
M5	DMPLi/LiCl	4.5	−40	72	44	3.8	1.6	1.06			
M5	DMPLi/LiCl	5.1	0	168	65	6.3	8.1	1.28			
M5	Ph₂CHK		0	168	77	6.5	7.8	2.51			
M5	Ph₂CHK/Et₂Zn	11	0	168	68	6.7	7.7	1.14			

[a]M_n(calcd) = (MW of monomer) × yield/100 × [monomer]/[initiator] + (MW of initiator)
[b]M_n(obsd) was determined by the ^{1}H NMR
[c]M_w/M_n was determined by the SEC calibration using polystyrene standards
[d]By ^{13}C NMR
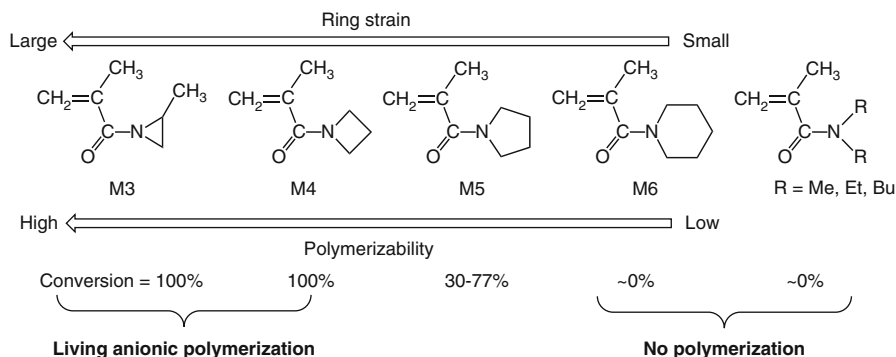
Fig. 13 Relative polymerizability of *N,N*-dialkylmethacrylamides [189, 190]

the coordination addition polymerization using a transition metal catalyst [191], further indicating the positive polymerizability.

Thus, the anionic polymerizability of the *N,N*-dialkylmethacrylamides with cyclic substituents drastically decreases by increasing the ring size from three to six members (M3 > M4 > M5 > M6 = DMMA) (Fig. 13). It is noted that M3 smoothly underwent the living anionic polymerization, while some side reactions were suggested for the polymerization of MAz [188]. As described above, all the acryloyl counterparts, A3, A4, A5, A6, and DMA, showed high anionic polymerizabilities, as expected for polar monomers. The positive polymerizability of M3 and M4 can be explained by the effective π-conjugation between the $C = C$ and $C = O$ double bonds estimated from the molecular structure calculations. In the stable molecular structures for M3 and M4, the planar amide conjugation between the $C = O$ and NR_2 groups was prohibited and the pyramidal structures of the highly strained small rings were maintained. In contrast, the $C = C$ and $C = O$ double bonds of M6 may not be on the same plane, since the amide conjugation between the $C = O$ and NR_2 group is predominant, similar to the cases in the other *N,N*-dialkylmethacrylamides lacking polymerizability.

The varied polymerizability of the *N,N*-dialkylmethacrylamides can be also correlated with the β-carbon chemical shifts in the ^{13}C NMR spectra, which reasonably reflect the electron densities of the $C = C$ bonds accepting the nucleophilic attack of the initiator and the propagating carbanion [5]. In fact, the ^{13}C NMR chemical shifts of the vinyl β-carbons of M3, M4, M5, M6, and DMMA are observed at 124.5, 119.1, 116.0, 114.6, and 115.4 ppm, respectively (Fig. 14). The upfield chemical shifts for M5, M6, and DMMA are far from the downfield values of typical polar monomers, such as methyl acrylate (130.6 ppm), MMA (125.3 ppm), and DMA (125.8 ppm), but rather comparable to that of styrene (113.8 ppm).

The stereoregularity of poly(M4) could be estimated from the relative ^{13}C NMR signal intensity of the α-methyl carbon at around 18.0–21.7 ppm, as shown in Table 6. Figure 15 illustrates a series of expanded ^{13}C NMR spectra of poly (M4) measured in DMSO-d_6 at 75 °C. It is evident that the tacticity of poly
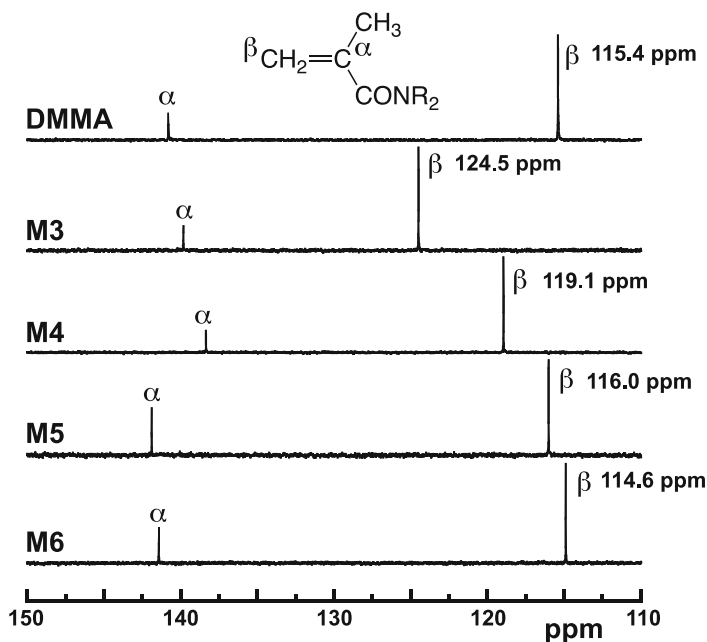
Fig. 14 ^{13}C NMR spectra of vinyl group region for DMMA, M3, M4, M5, and M6 measured in CDCl$_3$ at room temperature [190]

(M4) is definitely changed by the polymerization conditions. The *mm* content of the poly(M4)s produced with Ph$_2$CHLi, Ph$_2$CHNa, and Ph$_2$CHK at 0 or –40 °C was 60, 52, and 12 %, respectively, indicating that the smaller cation induced the isotactic configurations of the polymer. In the presence of Et$_2$Zn, the *mr* content of poly(M4) became predominant regardless of the counter cation. In contrast, in the presence of LiCl, the *mm* content tended to increase by lowering the polymerization temperature and reached 93 % at –78 °C. The addition of LiCl or Et$_2$Zn to the organolithium initiator allows the isotactic-specific or atactic polymerization of M4, respectively. It should be noted that the stereoregulation using LiCl as the additive is quite exceptional for the anionic polymerization of vinyl monomers. On the other hand, the tacticities of poly(M3) and poly(M5) were difficult to determine, since suitable signals in the ^{1}H and ^{13}C NMR spectra were overlapped with other signals or not well split.

The anionically obtained poly(M4) was readily soluble in water due to its high polarity, and no thermosensitivity was observed for aqueous solutions between 0 and 95 °C. On the other hand, an aqueous solution of poly(M5) showed a typical cloud point at 26–28 °C, while poly(M3) was insoluble in water. The exothermic cross-linking of poly(M3) readily started at around 120 °C due to the ring-opening reaction of the highly strained aziridine ring, indicating the potential of poly(M3) as a new thermosetting resin.

Fig. 15 ^{13}C NMR spectra of α-methyl carbon of poly (M4)s measured in DMSO-d_6 at 75 °C. (A) DMPLi/LiCl at –78 °C, *mm/mr/rr* = 93/7/<1; (B) Ph$_2$CHLi/LiCl at –40 °C, *mm/mr/rr* = 70/25/5; (C) Ph$_2$CHLi/LiCl at 0 °C, *mm/mr/rr* = 68/27/5; (D) Ph$_2$CHLi at –40 °C, *mm/mr/rr* = 60/33/7; (E) Ph$_2$CHNa at –40 °C, *mm/mr/rr* = 52/42/6; (F) Ph$_2$CHLi/Et$_2$Zn at –40 °C, *mm/mr/rr* = 27/54/19; (G) Ph$_2$CHK/Et$_2$Zn at 0 °C, *mm/mr/rr* = 13/62/25; (H) Ph$_2$CHK at 0 °C, *mm/mr/rr* = 12/54/34 [190]
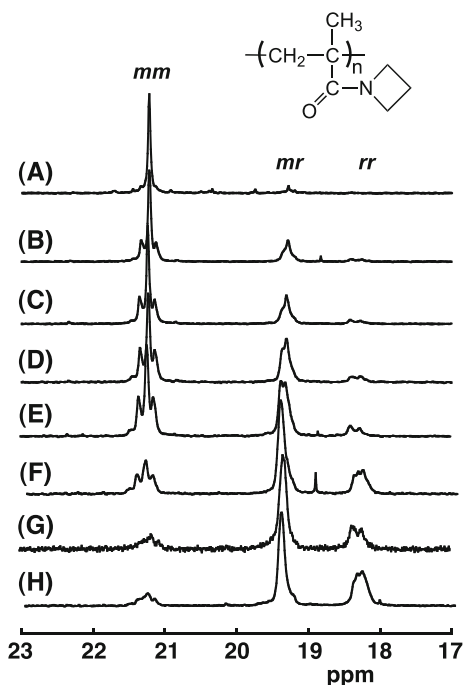
4.4 Anionic Polymerization of α-Methylene-N-Methylpyrrolidone

When the addition (or vinyl) polymerization of exomethylene compounds occurs, the resulting polymers should possess unique ring structures perpendicular to the main chain (Scheme 27). α-Methylene-*N*-methylpyrrolidone (MMP) is a typical exomethylene compound containing a polar *N*-methylpyrrolidone (NMP) ring in the molecule. Interestingly, MMP is considered to be a cyclic analog of the nonpolymerizable DMMA based on the chemical structure, but shows a radical polymerizability under the normal reaction conditions [184]. The C = C bond and the adjacent C = O bond in MMP should be almost flat and effectively conjugate with each other because of the restricted conformation derived from the cyclic structure. Therefore, the electronic environment of the C = C bond in MMP significantly differs from that of the nonpolymerizable DMMA possessing a less conjugated conformation.

Ishizone and his coworkers recently reported that the living anionic polymerization of MMP proceeded with either Ph$_2$CHK or Ph$_2$CHLi in the presence of Et$_2$Zn in THF at –78 ~ 0 °C [192] (Scheme 28). The resulting poly(MMP)s possessed predicted molecular weights based on the molar ratios between MMP and the initiator. Furthermore, the sharp unimodal SEC curves of poly(MMP)s indicated narrow molecular weight distributions ($M_w/M_n < 1.1$). From the polymerizations at
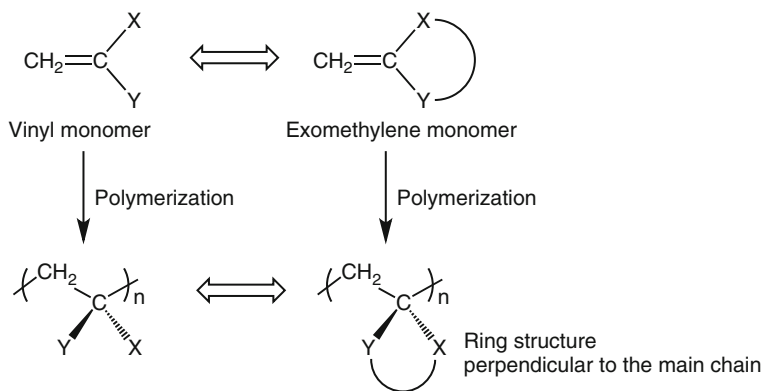
Scheme 27 Polymerization of exomethylene monomers
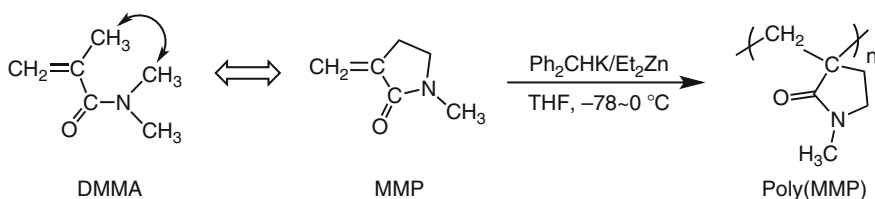
Scheme 28 Anionic polymerization of MMP [192]

various temperatures ranging from –50 to –30 °C, a slow polymerization rate of MMP and high activation energy of the polymerization ($\Delta E_a^{ap} = 57 \pm 5$ kJ mol^{-1}) were observed, while the complete consumptions of MMP were finally realized. Thus, another molecular design, by introducing the exomethylene group to the monomer in order to attain an effective π-conjugation between the C=C and C=O bonds, successfully leads to the anionic polymerizability of the *N,N*-dialkylmethacrylamides. It should be noted that the resulting poly(MMP) was highly hydrophilic and water-soluble between 0 and 95 °C due to the polar *N*-methylpyrrolidone (NMP) ring in the molecule.

5 Polymerization of (Meth)acrylonitrile

Acrylonitrile (AN) and methacrylonitrile (MAN) carrying strong electron-withdrawing cyano groups (Hammett sigma parameter: $\sigma_p = 0.66$) [193] are conventional polar vinyl monomers showing an anionic polymerizability. It is well known that their anionic polymerizability is significantly higher than those of the (meth)acrylate and *N,N*-dialkylacrylamide monomers. Although the anionic polymerizations of AN and MAN can be initiated with initiators of low reactivities, the polymerizations often suffer from inherent side reactions based on nucleophilic
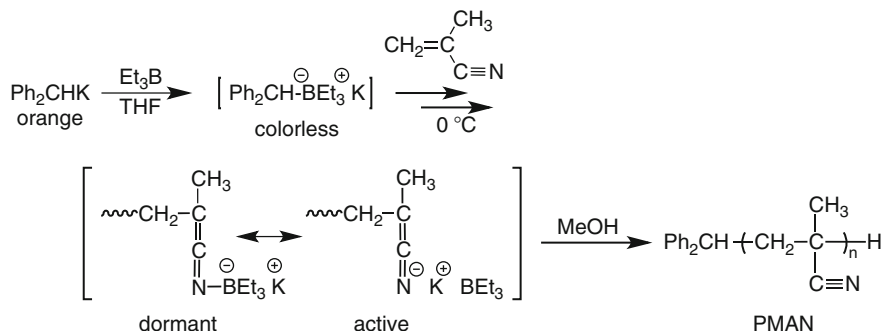
Scheme 29 Anionic polymerization of MAN in the presence of Et$_3$B [64]

attack of the anionic initiator or the propagating chain-end anion toward the electrophilic cyano group. In addition, the rapid polymerization of AN and MAN and low solubility of the poly(acrylonitrile) (PAN) and poly(methacrylonitrile) (PMAN) resulted in the heterogeneous polymerization systems. Consequently, for the anionic polymerizations of AN and MAN, low initiator efficiencies, poorly controlled molecular weights, and broad molecular weight distributions were observed in the resulting polymers.

Nakahama and Ishizone first succeeded in the living anionic polymerization of MAN by the addition of Lewis acidic Et$_3$B to the conventional polymerization system [64]. They confirmed that PMAN with a poorly controlled molecular weight and a very broad molecular weight distribution ($M_w/M_n = 3$) was quantitatively obtained with Ph$_2$CHK at –78 °C in THF. On the other hand, no apparent polymerization of MAN occurred with the binary initiator system of Ph$_2$CHK/Et$_3$B at –78 °C even after 28 h. However, the polymerization immediately took place and was completed within 1 min by raising the temperature from –78 °C to 0 °C. Interestingly, PMANs with predicted molecular weights ($M_n \sim 32{,}000$ g/mol) and narrow molecular weight distributions ($M_w/M_n < 1.1$) were produced in 100 % yields. The precise controls of the molecular weights indicate that the side reactions are effectively suppressed in the presence of Et$_3$B. The coordination of Et$_3$B to the initiator and/or the propagating anion stabilizes the anionic species even in polar THF, as shown in Scheme 29.

Based on the polymerization behavior at different temperatures, the so-called dormant species, borate anion, between the propagating polymer anion and Lewis acidic Et$_3$B might form in the polymerization system. The observed polymerization behaviors of MAN are similar to those of tBA [57] and the N,N-dialkylacrylamides [63] in the presence of Et$_3$B. It is noteworthy that Et$_2$Zn does not show any additive effect on the polymerization of MAN regardless of its Lewis acidity. The polymerization of MAN proceeds with Ph$_2$CHK/Et$_2$Zn even at –78 °C to afford PMAN with a very broad molecular weight distribution ($M_w/M_n = 2.5$).

On the other hand, even the binary initiator system of Ph$_2$CHK/Et$_3$B could not attain any degree of molecular weight control of PAN during the polymerization of

AN [194]. The highly acidic α-hydrogen on the resulting PAN main chain and extremely low solubility of PAN might prohibit the living anionic polymerization. A more effective initiation system might be necessary to achieve the living anionic polymerization of AN.

6   Polymerization of Phenyl Vinyl Sulfoxides

Phenyl vinyl sulfoxide (PVS) shows a remarkably high anionic polymerizability similar to other polar monomers, since PVS possesses an electron-withdrawing $S=O$ group and extended π-conjugation system including the $C=C-S=O$ linkage. Interestingly, a poly(phenyl vinyl sulfoxide), poly(PVS), has been known as a soluble precursor of polyacetylene. It has been demonstrated that the thermal degradation of the side chain of poly(PVS) produces a π-conjugated conductive polyacetylene showing a very low solubility.

It is reported that the anionic polymerization of PVS in THF at –78 °C afforded polymers with relatively narrow molecular weight distributions ($M_w/M_n = 1.1$–1.5) [195–200]. AB type diblock and BAB type triblock copolymers, polystyrene-b-poly(PVS) and poly(PVS)-b-polystyrene-b-poly(PVS), were also synthesized by the sequential addition of styrene (A monomer), followed by PVS (B monomer) using suitable monofunctional and difunctional initiators. For the anionic polymerization of 4-methylphenyl vinyl sulfoxide (MPVS), the molecular weight control of the resulting polymer was attained with DMPLi in the presence of a 20-fold amount of LiCl in THF at –78 °C [201]. The addition of the common ion was effective to narrow the molecular weight distribution of the polymer similar to the polymerizations of alkyl (meth)acrylates. Poly(MPVS)s with well-controlled molecular weights and narrow molecular weight distributions ($M_w/M_n \sim 1.1$) were always obtained. Although the polyacetylene segment is difficult to directly introduce into the polymer structures via the anionic polymerization of acetylene, both poly(PVS) and poly(MPVS) could be quantitatively converted into polyacetylenes by a thermal treatment at around 150 °C, as shown in Scheme 30.

Thus, the success of this methodology provides a new synthetic route to incorporate the polyacetylene segment into elaborate polymer structures accessible through anionic polymerization. For instance, a 5-armed star copolymer was successfully synthesized by the linking reaction of the propagating anion of poly (MPVS) [201]. The introduced poly(MPVS) segment in the star copolymer was smoothly converted into the attractive polyacetylene segment. The resulting polymers containing immiscible polyacetylene segments are of significant interest, since they should be well phase-separated at the molecular level via the strong segregation derived from rigid rod-coil polyacetylene segments.
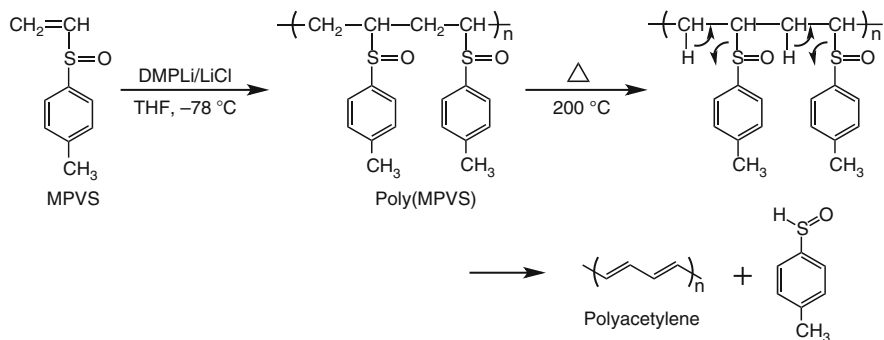
Scheme 30 Anionic polymerization of MPVS and thermal degradation of poly(MPVS) [201]

7 Anionic Polymerization of Dibenzofulvene and Benzofulvene

As described in Sect. 4, it has been clearly shown that the introduction of an exomethylene group of MMP can allow the nonpolymerizable N,N-dialkylmethacrylamide to be polymerized. In other words, the exomethylene monomer, MMP, shows a significantly higher polymerizability compared to the corresponding vinyl counterpart, DMMA. A similar relationship between the structure and polymerizability is observed in the cases of DPE and dibenzofulvene (DBF, α-methylenefluorene), as illustrated in Fig. 16. Although the $C=C$ bonds in the DPE derivatives show a high reactivity in the addition reaction and readily allows the 1:1 addition with either carbanions or carbocations, the DPE derivatives do not undergo homopolymerizations under various reaction conditions probably due to their very low ceiling temperatures. In fact, this particular reactivity of the DPE derivatives has enabled the quantitative end-functionalizations of anionic living polymers in numerous reports [202, 203]. However, it is noteworthy that the anionic copolymerization of DPE and styrene is possible to form a copolymer possessing alternating sequences [204–206].

On the other hand, DBF, a cyclic analog of DPE, exclusively allowed the radical, cationic, and anionic homopolymerizations on the exomethylene group [207, 208]. The polymerizations proceeded in a 1,2-addition mode to form a vinyl polymer possessing fluorene rings vertical to the main chain (Scheme 31). It is reported that the anionic polymerizations of DBF can be initiated with anionic initiators with a low nucleophilicity, such as CH_3MgBr and t-BuOK, indicating that the anionic polymerizability of DBF is fairly high. Unfortunately, since the anionic polymerization of DBF suffered from the low solubility of the resulting poly(DBF)s the molecular weight controls of the polymers have not been realized. Thus, the exomethylene monomer, DBF, again shows a higher polymerizability compared to the acyclic counterpart. In other words, the connection of two phenyl groups converts DPE into a planar molecule, DBF, and induces the homopolymerizability.
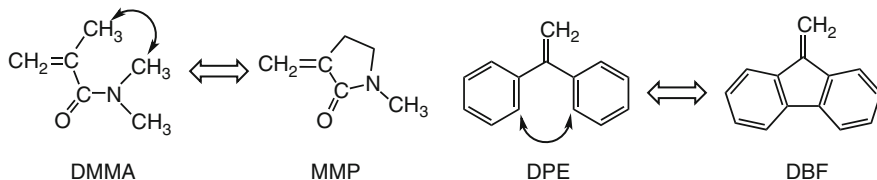
Fig. 16 Relationship between DPE and DBF
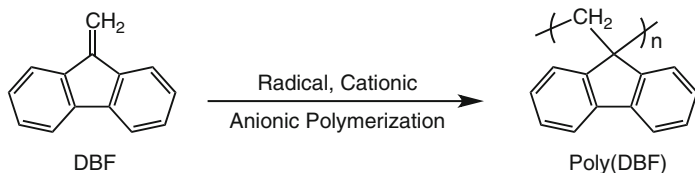
Scheme 31 Polymerization of DBF [207, 208]

Very recently, Ishizone and his coworkers succeeded in polymerizing a novel exomethylene monomer, benzofulvene (BF, α-methyleneindene) [209]. Although BF possesses a very simple structure, the polymerization behaviors have not yet been clarified probably due to the extremely high polymerizability. BF indeed shows a high spontaneous polymerizability after the isolation, but is stable after dilution with THF. Based on its chemical structure, BF is categorized as a cyclic analog of 2-phenyl-1,3-butadiene (2PhBd) and possesses a planar fixed transoid 1,3-diene framework including an exomethylene group. In fact, the anionic polymerization of BF quantitatively proceeded with *sec*-BuLi or Ph_2CHK in THF at –78 °C for 1 h to give polymers with predicted molecular weights ($M_n \sim 28{,}000$ g/mol) and narrow molecular weight distributions ($M_w/M_n < 1.1$). The detailed ^{13}C NMR analysis of the resulting poly(BF) indicated that the repeating units only consisted of 1,2-addition units (41 %) and 1,4-addition units (59 %) without 3,4-addition units. It has been substantiated that BF acts as a polymerizable transoid 1,3-diene and the exomethylene group always participates in the propagation (Scheme 32). The anionic polymerization of BF similarly occurred with *sec*-BuLi in benzene at 0 °C to give a well-defined polymer in 100 % yield. The microstructure of poly(BF) obtained in benzene possessed 24 % of the 1,2-structure and 76 % of the 1,4-structure, indicating the small effect of the solvent polarity on the addition mode of the polymerization. Interestingly, BF exhibited an unexpectedly high anionic polymerizability, while it seems to be a nonpolar hydrocarbon. Similar to DBF, the anionic polymerization of BF could be initiated with Grignard reagents and alkoxides to afford polymers in 100 % yields, although the initiation efficiencies are far from quantitative. Furthermore, a low nucleophilic enolate anion of poly (MMA) initiated the polymerization of BF in a quantitative efficiency to afford a well-defined diblock copolymer, poly(MMA)-*b*-poly(BF). As can be seen in Fig. 17, the SEC curve of the block copolymer shifts toward the higher molecular weight side while maintaining a narrow molecular weight distribution without a
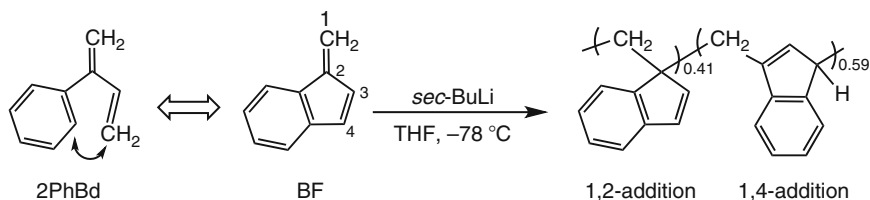
Scheme 32 Anionic polymerization of BF in THF [209]

Fig. 17 SEC curves of block copolymerization of MMA (1st monomer) and BF (2nd monomer). (A) Poly(MMA), M_n(calcd) = 4700, M_n(obsd) = 4400, M_w/M_n = 1.05; (B) Poly (MMA)-*block*-poly(BF), M_n(calcd) = 18,000, M_n(obsd) = 22,000, M_w/M_n = 1.09 [209]
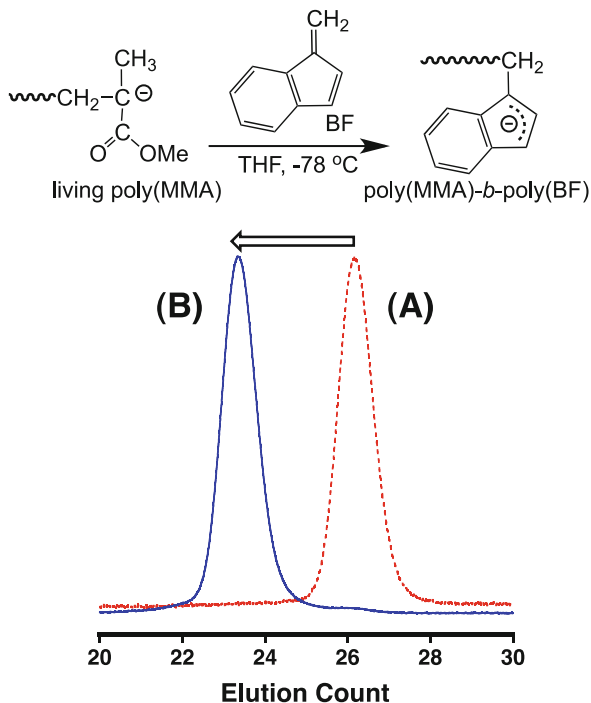
shoulder at the elution count of poly(MMA). Since 2PhBd could not be polymerized at all with Grignard reagents, alkoxides, and anionic living poly(MMA), the higher polymerizability of BF was again substantiated by changing the monomer structure to the corresponding exomethylene type.

8 Polymerization of Other Polar Monomers

As other polar vinyl monomers, vinyl methyl ketone and related monomers are considered as candidates for the anionic polymerization, since they are typical Michael acceptors showing a high electrophilicity in organic chemistry. In fact,
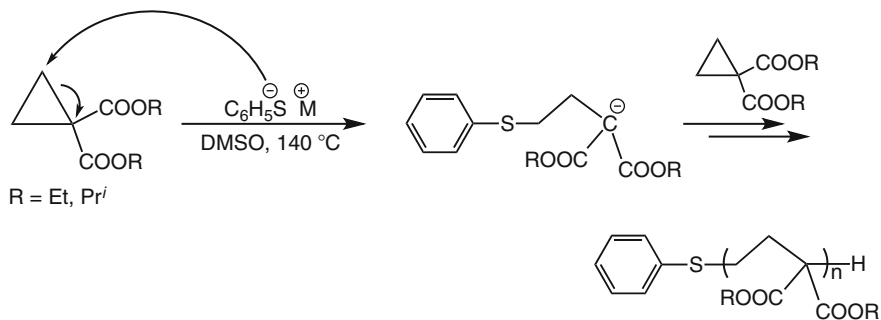
Scheme 33 Anionic polymerization of dialkyl cyclopropane-1,1-dicarboxylates [210, 211]

although the anionic polymerizations of these α,β-unsaturated compounds occurred using conventional anionic initiators or under the conditions of group transfer polymerization, such polymerizations cannot be controlled at the moment. Furthermore, the extremely high electrophilicity of α-cyanoacrylates is well known, since two electron-withdrawing COOR and CN groups are substituted on the $C=C$ double bonds. The electron density of the $C=C$ double bond of the monomer is remarkably reduced, and the propagating chain ends should be highly stabilized by these substituents. It is believed that the anionic polymerization of α-cyanoacrylates is readily initiated with weak basic compounds or weak nucleophiles, such as a tertiary amine and water. The polymerization behaviors are rather violent due to the high polymerizability and far from controlled.

Related to the anionic addition polymerization of these highly reactive polar monomers, highly strained cyclic alkanes carrying electron-withdrawing groups, that is, dialkyl cyclopropane-1,1-dicarboxylates and alkyl 1-cyanocyclopropanecarboxylates, are found to undergo the anionic ring-opening polymerization [210, 211] (Scheme 33). A nucleophilic thiophenolate initiator induces the ring-opening polymerization of these cyclic monomers to give carbon-chain polymers substituted by two electron-withdrawing groups on every third atom. The propagating species should be enolate anions highly stabilized by the electron-withdrawing groups, similar to the propagating anions derived from methylenemalonates and α-cyanoacrylates. In fact, the polymerizations certainly proceeded in DMSO at elevated temperatures (60–140 °C) to afford polymers with controlled molecular weights and relatively narrow molecular weight distributions ($M_n = 15,000$, $M_w/M_n = 1.06$).

As a new class of monomers capable of anionic addition polymerization, several phosphaalkenes containing the $C=P$ bond (PAE) have recently been synthesized and attempted to be anionically polymerized. Interestingly, the addition polymerization of phosphaalkenes exclusively proceeded with *n*-BuLi to yield a well-defined poly(methylenephosphine) possessing P-C linkages in a regioselective addition fashion [212–215] (Scheme 34). It is reported that a red-colored diphenylmethyl carbanion always formed via a nucleophilic attack on the phosphorus atom during the course of the polymerization. The anionic polymerizability of these phosphaalkenes is of great interest for the future design of functional
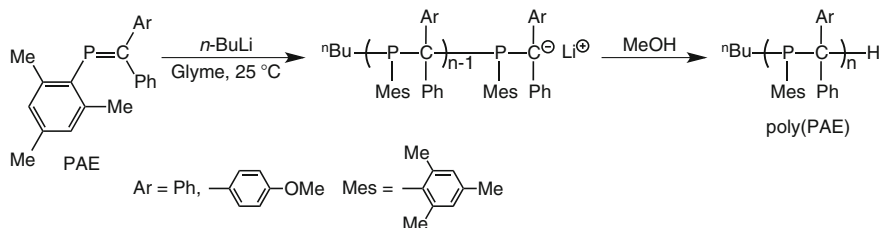
Scheme 34 Anionic polymerization of phosphaalkenes [212–215]

polymers. In fact, the resulting polymer containing the trivalent phosphorus atom could be oxidized to an air- and moisture-stable poly(methylenephosphine oxide) containing the pentavalent phosphorus atom by treating it with H_2O_2. The trivalent dialkylarylphosphine moieties in the poly(PAE) segment are typical Lewis bases and show the intrinsic binding ability to transition metals. Novel block copolymers, polystyrene-*b*-poly(PAE) and polyisoprene-*b*-poly(PAE), were also successfully synthesized by the sequential anionic copolymerization.

9 Conclusions

This chapter describes the living anionic polymerization of a series of polar vinyl monomers including vinylpyridines, acrylates, methacrylates, *N,N*-dialkyla-crylamides, *N,N*-dialkylmethacrylamides, *N*-isopropylacrylamide, α-methylene-*N*-methylpyrrolidone, methacrylonitrile, vinyl sulfoxides, and benzofulvene. All these polar monomers possess reduced π-electron densities on the $C=C$ double bonds and show an anionic polymerizability significantly higher than hydrocarbon mono-mers, such as styrene and 1,3-butadiene. In most cases, the combinations of π-conjugated bulky anionic initiators, such as DPHLi, DMPLi, Ph$_2$CHLi, and Ph$_2$CHK, and suitable additives, such as LiCl, Et$_2$Zn, and Et$_3$B, are very effective for the success of the living anionic polymerizations of these monomers preventing the inherent side reactions. These binary initiator systems including organolithium/LiCl, organolithium/Et$_2$Zn, organopotassium/Et$_2$Zn, and organopotassium/Et$_3$B indeed allow the living anionic polymerization of various (meth)acrylates carrying functional groups and produce homopolymers with predictable molecular weights based on the molar ratios between the monomers and initiators and narrow molec-ular weight distributions ($M_w/M_n < 1.1$) as well as the well-defined block copoly-mers. Among them, Lewis acidic Et$_3$B shows the most drastic effect on the anionic polymerization to form the so-called dormant species at low temperature. A higher temperature is necessary for the apparent propagation via the dissociation of the dormant species. It is noteworthy that the additive effect of Lewis acidic com-pounds on the stereoregularity is observed only for the anionic polymerizations of several *N,N*-dialkyl(meth)acrylamides and not for (meth)acrylates. The polar amide

moieties in the monomers and the resulting polymers may play a very important role in regulating the tacticity through possible coordination with the counter cations and the Lewis acidic additives. Thus, the newly established living anionic polymerization systems for polar monomers enable further molecular designs and tailored synthesis of a variety of architectural polymers in addition to the well-defined homopolymers. These tailored polymers are very important to clarify the fundamental structure-property relationship of polymers and for the future development of functional polymeric materials.

References

1. Morton M (1983) Anionic polymerization: principles and practice. Academic Press Inc., London
2. Hsieh HL, Quirk RP (1996) Anionic polymerization: principles and practical applications. Marcel Dekker Inc., New York
3. Ishizone T, Hirao A, Ishizone T, Hirao A (2012) Anionic polymerization: recent advances. In: Schlüter D, Hawker CJ, Sakamoto J (eds) Synthesis of polymers: new structures and methods, vol 1. Wiley-VCH, Singapore, pp 81–133
4. Hirao A, Goseki R, Ishizone T (2014) Advances in living anionic polymerization: from functional monomers, polymerization systems, to macromolecular architectures. Macromolecules 47:1883–1905
5. Ishizone T, Hirao A, Nakahama S (1993) Anionic polymerization of monomers containing functional groups. 6. Anionic block copolymerization of styrene derivatives para-substituted with electron-withdrawing groups. Macromolecules 26:6964–6975
6. Negishi E (1980) Organometallics in organic synthesis. Wiley, New York, p 506
7. Bordwell FG (1988) Equilibrium acidities in dimethyl sulfoxide solution. Acc Chem Res 21:456–463
8. Tsuruta Schluter Ref 3. Tsuruta T (1973) Polymerization reactions 4: anionic polymerization. Kagaku-Dojin, Tokyo
9. Ishizu K, Atsushi M, Fukutomi T (1986) Charge mosaic membranes: microdomain fixing of polystyrene-poly(4-vinylpyridine) sequential copolymers prepared by macromonomer methods. J Polym Sci Part A Polym Chem 24:1441–1454
10. Soum A, Fontanille M (1981) Living anionic stereospecific polymerization of 2-vinylpyridine, 2. Kinetics of polymerization and nature of active centres. Makromol Chem 182:1743–1750
11. Takaki M, Asami R, Tanaka S, Hayashi H, Hogen-Esch TE (1986) Preparation of (p-Vinylbenzyl)poly(2-vinylpyridine) macromers. Macromolecules 19:2900–2903
12. Ekizoglou N, Hadjichristidis N (2001) Benzyl potassium: an efficient one-pot initiator for the synthesis of block co- and terpolymers of ethyleneoxide. J Polym Sci Part A Polym Chem 39:1198–1202
13. Watanabe H, Shimura T, Kotaka T, Tirrell M (1993) Synthesis, characterization, and surface structures of styrene-2-vinylpyridine-butadiene three-block polymers. Macromolecules 26:6338–6345
14. Watanabe H, Tirrell M (1989) Force measurement between self-assembled layers of poly-isoprene-poly-2-vinylpyridine block copolymers in solution and in the melt. ACS Preprints 30:387–388
15. Shull KR, Kramer EJ, Hadziioannou G, Tang W (1990) Segregation of block copolymers to interfaces between immiscible homopolymers. Macromolecules 23:4780–4787

16. Creton C, Kramer EJ, Hui C-Y, Brown HR (1992) Failure mechanisms of polymer interfaces reinforced with block copolymers. Macromolecules 25:3075–3088
17. Yin R, Hogen-Esch TE (1994) Synthesis and characterization of poly(2-vinylpyridine)-*b*-poly(*t*-butyl methacrylate). J Polym Sci Part A Polym Chem 32:363–368
18. Spiegelman PP, Parravano G (1964) Heterophase polymerization of 4-vinylpyridine with butyllithium. J Polym Sci Part A 2:2245–2273
19. Antonietti M, Heinz S, Schmidt M, Rosenauer C (1994) Determination of the micelle architecture of polystyrene/poly(4-vinylpyridine) block copolymers in dilute solution. Macromolecules 27:3276–3281
20. Creutz S, Teyssié P, Jérôme R (1997) Living anionic homopolymerization and block copolymerization of 4-vinylpyridine at "elevated" temperature and its characterization by size exclusion chromatography. Macromolecules 30:1–5
21. Creutz S, Teyssié P, Jérôme R (1997) Anionic block copolymerization of 4-vinylpyridine and *tert*-butyl methacrylate at "elevated" temperatures: influence of various additives on the molecular parameters. Macromolecules 30:5596–5601
22. Nugay N, Kücükyavuz Z, Kücükyavuz S (1993) Anionic synthesis and characterization of poly(4-vinylpyridine)-poly(dimethylsiloxane) block copolymers. Polym Int 32:93–96
23. Nagano S, Matsushita Y, Shinma S, Ishiozne T, Seki T (2009) Two dimensional nano-dot array engineering of block copolymer surface micelles on water surface. Thin Solid Films 518:724–728
24. Varshney SK, Zhong XF, Eisenberg A (1993) Anionic homopolymerization and block copolymerization of 4-vinylpyridine and its investigation by high-temperature size-exclusion chromatography in *N*-methyl-2-pyrrolidinone. Macromolecules 26:701–706
25. Allen RD, Long TE, McGrath JE (1986) Preparation of high purity, anionic polymerization grade alkyl methacrylate monomers. Polym Bull 15:127–134
26. Watanabe H, Amemiya T, Shimura T, Kotaka T (1994) Anionic synthesis of graft block copolymers with poly(2-vinylpyridine) trunks: effects of trunk and branch molecular weights. Macromolecules 27:2336–2338
27. Soum A, Fontanille M, Sigwalt P (1977) Anionic polymerization of 2-vinylpyridine initiated by symmetrical organomagnesium compounds in tetrahydrofuran. J Polym Sci Polym Chem 15:659–673
28. Soum A, Tien C-F, Hogen-Esch TE (1983) Stereoregular anionic polymerization of 2-isopropenylpyridine. Makromol Chem Rapid Commun 4:243–248
29. Aboudalle A, Soum A, Fontanille M, Hogen-Esch TE (1986) Equilibrium anionic polymerization of 2-isopropenylpyridine: kinetic and thermodynamic aspects. Makromol Chem Rapid Commun 7:671–678
30. Soum A, Fontanille M, Aboudalle A (1988) Synthesis and characterization of new block copolymers of butadiene and 2-isopropenylpyridine. Polymer 29:1528–1534
31. Kang NG, Changez M, Lee JS (2007) Living anionic polymerization of the amphiphilic monomer 2-(4-vinylphenyl)pyridine. Macromolecules 40:8553–8559
32. Davis TP, Haddleton DM, Richards SN (1994) Controlled polymerization of acrylates and methacrylates. J Macromol Sci Rev Macromol Chem Phys C34(2):243–324
33. Baskaran D (2003) Strategic developments in living anionic polymerization of alkyl (meth) acrylate. Prog Polym Sci 28:521–581
34. Hatada K, Kitayama T, Ute K (1988) Stereoregular polymerization of α-substituted acrylates. Prog Polym Sci 13:189–276
35. Hatada K, Kitayama T (2000) Structurally controlled polymerizations of methacrylates and acrylates. Polym Int 49:11–47
36. Antoun S, Teyssié P, Jérôme R (1997) Lithium diisopropylamide as initiator for the anionic polymerization of methacrylates. Macromolecules 30:1556–1561
37. Long TE, Guistina RA, Schell BA, McGrath JE (1994) Hindered lithium dialkylamide initiators for the living anionic polymerization of methacrylic esters. J Polym Sci Part A Polym Chem 32:2425–2430

38. Kawabata N, Tsuruta T (1965) Elementary reactions of metal alkyl in anionic polymerization. I. Reaction mode of *n*-butyllithium in the initiation step of methyl acrylate and methyl methacrylate polymerization. Makromol Chem 86:231–252

39. Janata M, Lochmann L, Müller AHE (1990) Mechanism and kinetics of the anionic polymerization of acrylates, 1. Oligomerization of tert-butyl acrylate and characterization of products. Makromol Chem 191:2253–2260

40. Janata M, Lochmann L, Vlček P, Dybal J, Müller AHE (1992) Mechanism and kinetics of the anionic polymerization of acrylates, 2. Polymerization of *tert*-butyl acrylate in a flow tube reactor and effect of lithium chloride and lithium *tert*-butoxide. Makromol Chem 193:101–112

41. Janata M, Lochmann L, Müller AHE (1993) Mechanism and kinetics of the anionic polymerization of acrylates, 3. Effect of lithium chloride and lithium *tert*-butoxide on oligomerization of *tert*-butyl acrylate. Makromol Chem 194:625–636

42. Vlček P, Kříž J (1992) Anionic polymerization of acrylates. II. Polymerization of 2-ethylhexyl acrylate initiated by butyllithium/lithium-*tert*-butoxide system in tetrahydrofuran and its mixtures with toluene. J Polym Sci Part A Polym Chem 30:1511–1518

43. Jacobs C, Varshney SK, Hautekeer J-P, Fayt R, Jérôme R, Teyssié P (1990) Termination mechanism in the anionic copolymerization of methyl methacrylate and *tert*-butyl acrylate. Macromolecules 23:4024–4025

44. Anderson BC, Andrews GD, Arthur P Jr, Jacobson HW, Melby LR, Playtis AJ, Sharkey WH (1981) Anionic polymerization of methacrylates. Novel functional polymers and copolymers. Macromolecules 14:1599–1601

45. Fayt R, Forte R, Jacobs C, Jérôme R, Ouhadi T, Tessié P, Varshney SK (1987) New initiator system for the living anionic polymerization of *tert*-alkyl acrylates. Macromolecules 23:1442–1444

46. Klein JW, Gnanou Y, Rempp P (1990) Synthesis and characterization of high molecular weight poly(*tert*-butyl acrylate). Polym Bull 24:39–43

47. Antolin K, Lamps J-P, Rempp P, Gnanou Y (1990) Synthesis of poly(*t*-butyl acrylate) macromonomers. Polymer 31:967–970

48. Kubo M, Mollberg WC, Padias AB, Hall HK Jr (1995) Solubilization of peptides in water and hexane: synthesis of peptide-terminated poly(*tert*-butyl acrylate) and poly(acrylic acid) via living anionic polymerization. Macromolecules 28:838–843

49. Varshney SK, Hautekeer JP, Fayt R, Jérôme R, Teyssié P (1990) Anionic polymerization of (meth)acrylic monomers. 4. Effect of lithium salts as ligands on the "living" polymerization of methyl methacrylate using monofunctional initiators. Macromolecules 23:2618–2622

50. Varshney SK, Jérôme R, Bayard P, Jacobs C, Fayt R, Teyssié P (1992) Anionic polymerization of (meth)acrylic monomers. 7. Macrocyclic crown ethers as promoters of the living polymerization of methyl methacrylate using monofunctional initiators. Macromolecules 25:4457–4463

51. Wang J-S, Jérôme R, Bayard P, Patin M, Teyssié P (1994) Anionic polymerization of (meth) acrylic monomers. 16. Living anionic copolymerization of methyl methacrylate and *tert*-butyl acrylate as promoted by lithium 2-(2-methoxyethoxy)ethoxide. Macromolecules 27:4635–4638

52. Baskaran D, Sivaram S (1997) Specific salt effect of lithium perchlorate in living anionic polymerization of methyl methacrylate and *tert*-butyl acrylate. Macromolecules 30:1550–1555

53. Baskaran D, Müller AHE, Sivaram S (1999) Effect of lithium perchlorate on the kinetics of the anionic polymerization of methyl methacrylate in tetrahydrofuran. Macromolecules 32:1356–1361

54. Kunkel D, Müller AHE, Janata M, Lochmann L (1992) The role of association/complexation equilibria in the anionic polymerization of (meth)acrylates. Macromol Chem Macromol Symp 60:315–326

55. Ozaki H, Hirao A, Nakahama S (1995) Anionic polymerization of alkyl methacrylates in the presence of diethylzinc. Macromol Chem Phys 196:2099–2111
56. Ishizone T, Yoshimura K, Hirao A, Nakahama S (1998) Controlled anionic polymerization of *tert*-butyl acrylate with diphenylmethyl anions in the presence of dialkylzinc. Macromolecules 31:8706–8712
57. Ishizone T, Yoshimura K, Yanase E, Nakahama S (1999) Controlled anionic polymerization of *tert*-butyl acrylate with diphenylmethylpotassium in the presence of triethylborane. Macromolecules 32:955–957
58. Hatada K, Ute K, Tanaka K, Kitayama T, Okamoto Y (1985) Preparation of highly isotactic poly(methyl methacrylate) of low polydispersity. Polym J 17:977–980
59. Kitayama T, Shinozaki T, Masuda E, Yamamoto M, Hatada K (1988) Highly syndiotactic poly(methyl methacrylate) with narrow molecular weight distribution formed by *tert*-butyllithium-trialkylaluminum in toluene. Polym Bull 20:505–510
60. Hirano T, Yamaguchi H, Kitayama T, Hatada K (1998) Heterotactic polymerization of methacrylates having C-3 ester group. Polym J 30:767–769
61. Ballard DGH, Bowles RJ, Haddleton DM, Richards SN, Sellens R, Twose DL (1992) Controlled polymerization of methyl methacrylate using lithium aluminum alkyls. Macromolecules 25:5907–5913
62. Kobayashi M, Okuyama S, Ishizone T, Nakahama S (1999) Stereospecific anionic polymerization of N, N-dialkylacrylamides. Macromolecules 32:6466–6477
63. Kobayashi M, Ishizone T, Nakahama S (2000) Additive effect of triethylborane on anionic polymerization of N, N-dimethylacrylamide and N, N-diethylacrylamide. Macromolecules 33:4411–4416
64. Ishizone T, Yanase E, Matsushita T, Nakahama S (2001) Controlled anionic polymerization of methacrylonitrile with diphenylmethylpotassium in the presence of triethylborane. Macromolecules 34:6551–6553
65. Tabuchi M, Kawauchi T, Kitayama T, Hatada K (2002) Living polymerization of primary alkyl acrylates with *t*-butyllithium/bulky aluminum Lewis acids. Polymer 43:7185–7190
66. Schlaad H, Müller AHE (1998) Anionic polymerization of (meth)acrylates in the presence of tetraalkylammonium halide-trialkyl aluminum complexes in toluene, 1. Kinetic investigations with methyl methacrylate. Macromolecules 31:7127–7132
67. Schmitt B, Stauf W, Müller AHE (2001) Anionic polymerization of (meth)acrylates in the presence of cesium halide-trialkylaluminum complexes in toluene. Macromolecules 34:1551–1557
68. Uchiumi N, Harada K, Kato M, Ono T, Yaginuma S, Ishiura K (2001) Preparation process of acrylic acid ester polymer. U.S. Patent 6,329,480, 11 Dec 2001
69. Harada K, Ishiura K, Kato M, Yaginuma S (2003) Anionic polymerization process, and process for producing a polymer by the anionic polymerization process. U.S. Patent 6,555,637, 29 Apr 2003
70. Reetz MT (1988) New methods for the anionic polymerization of α-activated olefins. Angew Chem Int Ed Engl 27:994–998
71. Reetz MT, Knauf T (1988) Metal-free carbanion salts as initiators for the anionic polymerization of acrylic and methacrylic acid esters. Angew Chem Int Ed Engl 27:1373–1374
72. Reetz MT, Ostarek R (1988) Polymerization of acrylic acid esters initiated by tetrabutylammonium alkyl- and aryl-thiolates. J Chem Soc, Chem Commun 213–215
73. Baskaran D, Chakrapani S, Sivaram S, Hogen-Esch TE, Müller AHE (1999) Anionic polymerization of alkyl (meth)acrylates using metal-free initiators: effect of ion pairing on initiation equilibria. Macromolecules 32:2865–2871
74. Pietzonka T, Seebach D (1993) The P4-phosphazene base as part of a new metal-free initiator system for the anionic polymerization of methyl methacrylate. Angew Chem Int Ed Engl 32:716–717

75. Zagala AP, Hogen-Esch TE (1996) Living anionic polymerization of methyl methacrylate at ambient temperatures in the presence of the tetraphenylphosphonium cation. Macromolecules 29:3038–3039
76. Baskaran D, Müller AHE, Kolshorn H, Zagala AP, Hogen-Esch TE (1997) Polymerization of methacrylates in the presence of tetraphenylphosphonium cation. 2. Evidence for phosphorylide-mediated polymerizations. Macromolecules 30:6695–6697
77. Dimov DK, Warner WN, Hogen-Esch TE, Juengling S, Warzelham V (2000) Synthesis of PMMA and PMMA block copolymers at elevated temperatures by phosphor ylide-mediated polymerizations. Macromol Symp 157:171–182
78. Ling J, Hogen-Esch TE (2006) Mechanism of phosphor ylide-mediated living polymerizations of MMA. Nature of side reactions in the formation of initiators. Macromolecules 39:9665–9667
79. Ling J, Hogen-Esch TE (2007) Alkylation and coupling of living poly(methyl methacrylate) ylides at ambient conditions. Macromolecules 40:5706–5709
80. Webster OW, Hertler WR, Sogah DY, Farnham WB, RajanBabu TV (1983) Group transfer polymerization. 1. A new concept for addition polymerization with organosilicon initiators. J Am Chem Soc 105:5706–5708
81. Sogah DY, Hertler WR, Webster OW, Cohen GM (1987) Group transfer polymerization – polymerization of acrylic monomers. Macromolecules 20:1473–1488
82. Hertler WR (1987) Chain transfer in group-transfer polymerization. Macromolecules 20:2976–2982
83. Posner GH, Shulman-Roskes EM (1989) Interrupted polymerization of acrylates: sequential Michael-Michael-Dieckmann cyclizations for easy, one-pot, 2+2+2 construction of polyfunctionalized cyclohexanones. J Org Chem 54:3514–3515
84. Brittain WJ, Dicker IB (1989) Termination in group-transfer polymerization. Macromolecules 22:1054–1057
85. Dicker IB, Cohen GM, Farnham WB, Hertler WR, Laganis ED, Sgah DY (1990) Oxyanions catalyze group-transfer polymerization to give living polymers. Macromolecules 23:4034–4041
86. Quirk RP, Ren J (1992) Mechanistic studies of group transfer polymerization. Silyl group exchange studies. Macromolecules 25:6612–6620
87. Müller AHE (1994) Kinetic discrimination between various mechanisms in group-transfer polymerization. Macromolecules 27:1685–1690
88. Patrickios CS, Hertler WR, Abbott NL, Hatton TA (1994) Diblock, ABC triblock, and random methacrylic polyampholytes: synthesis by group transfer polymerization and solution behavior. Macromolecules 27:930–937
89. Webster OW (2000) The discovery and commercialization of group-transfer polymerization. J Polym Sci Part A Polym Chem 38:2855–2860
90. Takada K, Fuchise K, Chen Y, Satoh T, Kakuchi T (2012) Controlled polymerization of methyl acrylate for high-molecular-weight polymers by pentafluorophenylbis(triflyl)methane-promoted group transfer polymerization using triisopropylsilyl ketene acetal. J Polym Sci Part A Polym Chem 50:3560–3566
91. Kakuchi R, Chiba K, Fuchise K, Sakai R, Satoh T, Kakuchi T (2009) Strong brønsted acid as a highly efficient promoter for group transfer polymerization of methyl methacrylate. Macromolecules 42:8747–8750
92. Kakuchi T, Chen Y, Kitakado J, Mori K, Fuchise K, Satoh T (2011) Organic superbase as an efficient catalyst for group transfer polymerization of methyl methacrylate. Macromolecules 44:4641–4647
93. Kitaura T, Kitayama T (2007) Anionic polymerization of methyl methacrylate with the aid of lithium trimethylsilanolate (Me_3SiOLi)-superior control of isotacticity and molecular weight. Macromol Rapid Commun 28:1889–1893

94. Kawauchi T, Kumaki J, Okoshi K, Yashima E (2005) Stereocomplex formation of isotactic and syndiotactic poly(methyl methacrylate)s in ionic liquids leading to thermoreversible ion gels. Macromolecules 38:9155–9160

95. Kumaki J, Kawauchi T, Okoshi K, Kusanagi H, Yashima E (2007) Supramolecular helical structure of the stereocomplex composed of complementary isotactic and syndiotactic poly (methyl methacrylate)s as revealed by atomic force microscopy. Angew Chem Int Ed 46:5348–5351

96. Kumaki J, Kawauchi T, Ute K, Kitayama T, Yashima E (2008) Molecular weight recognition in the multiple-stranded helix of a synthetic polymer without specific monomer-monomer interaction. J Am Chem Soc 130:6373–6380

97. Leemans L, Fayt R, Teyssié P, Uytterhoeven H, De Winter W (1990) Controlled "living" anionic polymerization of glycidyl methacrylate. J Polym Sci Part A Polym Chem 28:2187–2193

98. Leemans L, Fayt R, Teyssié P, de Jaeger NC (1990) Poly(alkyl methacrylate-b-sulfonated glycidyl methacrylate). A new amphiphilic polymeric surfactant for the preparation and stabilization of polymer acrylic latices in aqueous medium. Macromolecules 24:5922–5925

99. Hild G, Lamps JP, Rempp P (1993) Synthesis and characterization of anionic 2,3-epoxypropyl methacrylate polymers and of related random and block copolymers with methyl methacrylate. Polymer 34:2875–2882

100. Zhang H, Ruckenstein E (1998) Graft, block-graft and star-shaped copolymers by an in situ coupling reaction. Macromolecules 31:4753–4759

101. Sugiyama K, Azuma H, Watanabe T, Ishizone T, Hirao A (2003) Anionic polymerization of 2-haloethyl methacrylates. Polymer 44:4157–4164

102. Ishizone T, Sugiyama K, Sakano Y, Mori H, Hirao A, Nakahama S (1999) Anionic polymerizations of perfluoroalkyl methacrylates and synthesis of well-defined ABC triblock copolymers of methacrylates containing hydrophilic, hydrophobic, and perfluoroalkyl groups. Polym J 31:983–988

103. Tanaka Y, Hasegawa H, Hashimoto T, Ribbe A, Sugiyama K, Hirao A, Nakahama S (1999) A study of three-phase structures in ABC triblock copolymers. Polym J 31:989–994

104. Hirai T, Leolukman M, Jin S, Goseki R, Ishida Y, Kakimoto M, Hayakawa T, Ree M, Gopalan P (2009) Hierachical self-assembled structures from POSS-containing block copolymers synthesized by living anionic polymerization. Macromolecules 42:8835–8843

105. Zhang H, Ruckenstein E (2000) A novel successive route to well-defined water-soluble poly (2,3-dihydroxypropyl methacrylate) and amphiphilic block copolymers based on an osmylation reaction. Macromolecules 33:4738–4744

106. Zhang H, Ruckenstein E (2001) Novel monodisperse functional (co)polymers based on the selective living anionic polymerization of a new bifunctional monomer, trans, trans-1-methacryloyloxy-2,4-hexadiene. Macromolecules 34:3587–3593

107. Ishizone T, Takata T, Kobayashi M (2003) Synthesis of new crosslinkable polymers by chemoselective polymerizations of 2-(1-aziridinyl)ethyl methacrylate. J Polym Sci Part A Polym Chem 41:1335–1340

108. Zhang H, Ruckenstein E (1998) Graft copolymers by combined anionic and cationic polymerizations based on the homopolymerization of a bifunctional monomer. Macromolecules 31:746–752

109. Ruckenstein E, Zhang H (2001) Well-defined poly(2-hydroxyethyl methacrylate) and its amphiphilic block copolymers via acidolysis of anionically synthesized poly(2-vinyloxyethyl methacrylate). Polym Bull 47:113–119

110. Ishizone T, Tajima H, Torimae H, Nakahama S (2002) Anionic polymerizations of 1-adamantyl methacrylate and 3-methacryloyloxy-1,1'-biadamantane. Macromol Chem Phys 203:2375–2384

111. Gallei M, Schmidt BVKJ, Klein R, Rehahn M (2009) Defined poly[styrene-*block*-(ferrocenylmethyl methacrylate)] diblock copolymers via living anionic polymerization. Macromol Rapid Commun 30:1463–1469

112. Yamada M, Iguchi T, Hirao A, Nakahama S, Watanabe J (1995) Synthesis of side-chain liquid crystalline homopolymers and block copolymers with well-defined structures by living anionic polymerization and their thermotropic phase behavior. Macromolecules 28:50–58
113. Yamada M, Itoh T, Nakagawa R, Hirao A, Nakahama S, Watanabe J (1999) Synthesis of side-chain liquid crystalline homopolymers and block copolymers with cyanobiphenyl moieties as the mesogen by living anionic polymerization and their thermotropic phase behavior. Macromolecules 32:282–289
114. Hammand PT, Zheng WY (1996) Synthesis of new smectic C* liquid-crystalline block copolymers. Macromol Rapid Commun 17:813–824
115. Zheng W-Y, Albalak RJ, Hammond PT (1998) Mesogen orientation within smectic C* side chain liquid crystalline diblock copolymers. Macromolecules 31:2686–2689
116. Zheng WY, Hammond PT (1998) Phase behavior of new side chain smectic C* liquid crystalline block copolymers. Macromolecules 31:711–721
117. Anthamatten M, Wu J-S, Hammond PT (2001) Direct observation of a smectic bilayer microstructure in side-chain liquid crystalline diblock copolymers. Macromolecules 34:8574–8579
118. Schneider A, Zanna J-J, Yamada M, Finkelmann H, Thomann R (2000) Competition between liquid crystalline phase symmetry and microphase morphology in a chiral smectic liquid crystalline-isotropic block copolymer. Macromolecules 33:649–651
119. Bohnert R, Finkelmann H, Lutz P (1993) Liquid-crystalline side-chain polymers by living anionic polymerization of mesogenic methacrylate. Makromol Chem Rapid Commun 14:139–146
120. Bohnert R, Finkelmann H (1994) Liquid-crystalline side-chain AB block copolymers by direct anionic polymerization of a mesogenic methacrylate. Macromol Chem Phys 195:689–700
121. Murali Mohan Y, Raghunadh V, Sivaram S, Baskaran D (2012) Reactive polymers bearing styrene pendants through selective anionic polymerization of 4-vinylbenzyl methacrylate. Macromolecules 45:3387–3393
122. Nakahama S, Hirao A (1990) Protection and polymerization of functional monomers: anionic living polymerization of protected monomers. Prog Polym Sci 15:299–335
123. Hirao A, Loykulnant S, Ishizone T (2002) Recent advance in living anionic polymerization of functionalized styrene derivatives. Prog Polym Sci 27:1399–1471
124. Hirao A, Kato H, Yamaguchi K, Nakahama S (1986) Polymerization of monomers containing functional groups protected by trialkylsilyl groups. 5. Synthesis of poly(2-hydroxyethyl methacrylate) with a narrow molecular weight distribution by means of anionic living polymerization. Macromolecules 19:1294–1299
125. Mori H, Wakisaka O, Hirao A, Nakahama S (1994) Protection and polymerization of functional monomers, 23. Synthesis of well-defined poly(2-hydroxyethyl methacrylate) by means of anionic living polymerization of protected monomers. Macromol Chem Phys 195:3213–3224
126. Senshu K, Yamashita S, Ito M, Hirao A, Nakahama S (1995) Surface characterization of 2-hydroxyethyl methacrylate/styrene block copolymers by transmission electron microscopic observation and contact angle measurement. Langmuir 11:2293–2300
127. Senshu K, Kobayashi M, Ikawa N, Yamashita S, Hirao A, Nakahama S (1999) Relationship between morphology of microphase-separated structure and phase restructuring at the surface of poly[2-hydroxyethyl methacrylate-*block*-4-(7'-octenyl)styrene] diblock copolymers corresponding to environmental change. Langmuir 15:1763–1769
128. Senshu K, Yamashita S, Mori H, Ito M, Hirao A, Nakahama S (1999) Time-resolved surface rearrangements of poly(2-hydroxyethyl methacrylate-*block*-isoprene) in response to environmental changes. Langmuir 15:1754–1762
129. Mori H, Hirao A, Nakahama S (1994) Protection and polymerization of functional monomers. 21. Anionic living polymerization of (2,2-dimethyl-1,3-dioxolan-4-yl)methyl methacrylate. Macromolecules 27:35–39

130. Mori H, Hirao A, Nakahama S, Senshu K (1994) Synthesis and surface characterization of hydrophilic-hydrophobic block copolymers containing poly(2,3-dihydroxypropyl methacrylate). Macromolecules 27:4093–4100
131. Ishizone T, Han S, Okuyama S, Nakahama S (2003) Synthesis of water-soluble polymethacrylates by living anionic polymerization of trialkylsilyl-protected oligo(ethylene glycol) methacrylates. Macromolecules 36:42–49
132. Ishizone T, Uehara G, Hirao A, Nakahama S, Tsuda K (1998) Anionic polymerization of monomers containing functional groups, 11. Anionic polymerizations of alkynyl methacrylates. Macromol Chem Phys 199:1827–1834
133. Ozaki H, Hirao A, Nakahama S (1992) Polymerization of monomers containing functional silyl groups. 11. Anionic living polymerization of 3-(tri-2-propoxysilyl)propyl methacrylate. Macromolecules 25:1391–1395
134. Bugner D E (1988) Chapter 20 AB block Copolymers Containing Methacrylic Acid and/or Metal Methacrylate Blocks. Benham JL, Kinstle JF Chemical Reactions on Polymers. ACS Symposium Series 276–288.
135. Bugner DE (1986) The preparation of ab block copolymers containing methacrylic acid and/or metal methacrylate blocks by selective cleavage of methacrylic esters. ACS Prep 27:57–58
136. Liu G, Guillet JE, Emad Taha Bakir Al-Takrity, Jenkins AD, Walton DRM (1991) Dimensions of polyelectrolytes using the "spectroscopic ruler". 2. Conformational changes of poly (methacrylic acid) chains with variation in pH. Macromolecules 24:68–74
137. Kawauchi T, Kawauchi M, Takeichi T (2011) Facile synthesis of highly syndiotactic and isotactic polymethacrylates via esterification of stereoregular poly(methacrylic acid)s. Macromolecules 44:1066–1071
138. Zhang H, Ruckenstein E (1998) Living anionic polymerization of 1-(alkoxy)ethyl methacrylates and the preparation of well-defined poly(methacrylic acid). Macromolecules 31:7575–7580
139. Ruckenstein E, Zhang H (1998) Living anionic copolymerization of 1-(alkoxy)ethyl methacrylates with polar and/or nonpolar monomers and the preparation of amphiphilic block copolymers containing poly(methacrylic acid) hydrophilic segments at higher temperatures than usually employed. Macromolecules 31:9127–9133
140. Zhang H, Ruckenstein E (2000) One-pot, three-step synthesis of amphiphilic comblike copolymers with hydrophilic backbone and hydrophobic side chains. Macromolecules 33:814–819
141. Creutz S, Teyssié P, Jérôme R (1997) Living anionic homopolymerization and block copolymerization of (dimethylamino)ethyl methacrylate. Macromolecules 30:6–9
142. Creutz S, van Stam J, Antoun S, De Schryver FC, Jérôme R (1997) Exchange of polymer molecules between block copolyme micelles studied by emission spectroscopy. A method for the quantification of unimer exchange rates. Macromolecules 30:4078–4083
143. Creutz S, van Stam J, De Schryver FC, Jérôme R (1998) Dynamics of poly(dimethylamino) alkyl methacrylate-block-sodium methacrylate) micelles. Influence of hydrophobicity and molecular architecture on the exchange rate of copolymer molecules. Macromolecules 31:681–689
144. Han S, Hagiwara M, Ishizone T (2003) Synthesis of thermally sensitive water-soluble polymethacrylates by living anionic polymerizations of oligo(ethylene glycol) methyl ether methacrylates. Macromolecules 36:8312–8319
145. Ishizone T, Seki A, Hagiwara M, Yokoyama H, Oyane A, Deffieux A, Carlotti S (2008) Anionic polymerization of oligo (ethylene glycol) alkyl ether methacrylates: effect of side chain length and ω-alkyl group of side chain on cloud point in water. Macromolecules 41:2963–2967
146. Yamanaka J, Kayasuga T, Ito M, Yokoyama H, Ishizone T (2011) Synthesis of water-soluble poly[oligo(ethylene glycol) methacrylate]s by living anionic polymerization of oligo(ethylene glycol) vinyl ether methacrylates. Polym Chem 2:1837–1848

147. Yokoyama H, Miyamae T, Han S, Ishizone T, Tanaka K, Takahara A, Torikai N (2005) Spontaneously formed hydrophilic surfaces by segregation of block copolymers with water-soluble blocks. Macromolecules 38:5180–5189

148. Oyane A, Ishizone T, Uchida M, Furukawa K, Ushida T, Yokoyama H (2005) Spontaneous formation of blood-compatible surface on hydrophobic polymers: surface enrichment of a block copolymer with a water-soluble block. Adv Mater 17:2329–2332

149. Ishizone T, Han S, Hagiwara M, Yokoyama H (2006) Synthesis and surface characterization of well-defined amphiphilic block copolymers containing poly[oligo(ethylene glycol) meth-acrylate] segments. Macromolecules 39:962–970

150. Zhang R, Seki A, Ishizone T, Yokoyama H (2008) Reduced hydrophobic interaction of polystyrene surfaces by spontaneous segregation of block copolymers with oligo(ethylene glycol) methyl ether methacrylate blocks: force measurements in water using atomic force microscope with hydrophobic probes. Langmuir 24:5527–5533

151. Wang J, Varshney SK, Jérôme R, Teyssié P (1992) Synthesis of AB(BA), ABA and BAB block copolymers of *tert*-butyl methacrylate (A) and ethylene oxide (B). J Polym Sci Part A Polym Chem 30:2251–2261

152. Hirao A, Matsuo Y, Oie T, Goseki R, Ishizone T (2011) Facile synthesis of triblock Co- and terpolymers of styrene, 2-vinylpyridine, and methyl methacrylate by a new methodology combining living anionic diblock copolymers with a specially designed linking reaction. Macromolecules 44:6345–6355

153. Sugiyama K, Oie T, El-Magd A, Hirao A (2010) Synthesis of well-defined (AB)$_n$ multiblock copolymers composed of polystyrene and poly(methyl methacrylate) segments using spe-cially designed living AB diblock copolymer anion. Macromolecules 43:1403–1410

154. Ito S, Goseki R, Ishizone T, Senda S, Hirao A (2013) Successive synthesis of miktoarm star polymers having up to seven arms by a new iterative methodology based on living anionic polymerization using a trifunctional lithium reagent. Macromolecules 46:819–827

155. Hirao A, Murano K, Abouelmagd A, Uematsu M, Ito S, Goseki R, Ishizone T (2011) General and facile approach to exact graft copolymers by iterative methodology using living anionic in-chain-functionalized AB diblock copolymers as key building blocks. Macromolecules 44:3302–3311

156. Patrickios CS, Lowe AB, Armes SP, Billingham NC (1998) ABC triblock polymethacrylates: group transfer polymerization synthesis of the ABC, ACB, and BAC topological isomers and solution characterization. J Polym Sci Part A Polym Chem 36:617–631

157. Nojiri C, Okano T, Koyanagi H, Nakahama S, Park KD, Kim SW (1993) In vivo protein adsorption on polymers: visualization of adsorbed proteins on vascular implants in dogs. J Biomater Sci Polym Ed 4:75–88

158. Butler K, Thomas PR, Tyler GJ (1960) Stereospecific polymerization of some polar vinyl monomers. J Polym Sci 48:357–366

159. Gia H-B, McGrath JE (1980) High resolution NMR spectra of poly N, N-dimethylacrylamide in CDCl3 solution. Polym Bull 2:837–840

160. Xie X, Hogen-Esch TE (1996) Anionic synthesis of narrow molecular weight distribution water-soluble poly(N, N-dimethylacrylamide) and poly(N-acryloyl-N'-methylpiperazine). Macromolecules 29:1746–1752

161. Nakahama S, Kobayashi M, Ishizone T (1997) Polymerization of N, N-dialkylacrylamides with anionic initiators modified by diethylzinc. J Macromol Sci Part A Pure and Appl Chem A34:1845–1855

162. Kobayashi M, Ishizone T, Nakahama S (2000) Synthesis of highly isotactic poly(N, N-diethylacrylamide) by anionic polymerization with Grignard reagents and diethylzinc. J Polym Sci Part A Polym Chem 38:4677–4685

163. André X, Bremohamed K, Yakimansky AV, Litvinenko GI, Müller AHE (2006) Anionic polymerization and block copolymerization of *N*, *N*-diethylacrylamide in the presence of triethylaluminum. Kinetic investigation using in-line FT-NIR spectroscopy. Macromolecules 39:2773–2787

164. Ishizone T, Yashiki D, Kobayashi M, Szuki T, Ito M, Nakahama S (2007) Potassium enolates of N, N-dialkylamides as initiators of anionic polymerization. J Polym Sci Part A Polym Chem 45:1260–1271
165. Nakhmanovich BI, Prudskova TN, Arest-Yakubovich AA, Müller AHE (2001) Copolymerization of N, N-dimethylacrylamide with styrene and butadiene: the first example of polar growing chain End/nonpolar monomer cross-initiation. Macromol Rapid Commun 22:1243–1248
166. Eggert M, Freitag R (1994) Poly-N, N-diethylacrylamide prepared by group transfer polymerization: synthesis, characterization and solution properties. J Polym Sci Part A Polym Chem 32:803–813
167. Freitag R, Baltes T, Eggert M (1994) A comparison of thermoreactive water-soluble poly-N, N-diethylacrylamide prepared by anionic and by group transfer polymerization. J Polym Sci Part A Polym Chem 32:3019–3030
168. Baltes T, Garret-Flaudy F, Freitag R (1999) Investigation of the LCST of polyacrylamides as a function of molecular parameters and the solvent composition. J Polym Sci Part A Polym Chem 37:2977–2989
169. Fuchise K, Sakai R, Satoh T, Sato S, Narumi A, Kawaguchi S, Kakuchi T (2010) Group transfer polymerization of N, N-dimethylacrylamide using Nobel efficient system consisting of dialkylamino silyl enol ether as an initiator and strong brønsted acid as an organocatalyst. Macromolecules 43:5589–5594
170. Breslow DS, Hulse GE, Matlack AS (1957) Snthesis of poly-β-alanine from acrylamide. A novel synthesis of β-alanine. J Am Chem Soc 79:3760–3763
171. Kennedy JP, Otsu T (1972) Hydrogen transfer polymerization with anionic catalysts and the problem of anionic isomerization polymerization. J Macromol Sci Rev Macromol Chem C6:237–283
172. Wu XS, Hoffman AS, Yager P (1992) Synthesis and characterization of thermally reversible macroporous poly(N-isopropylacrylamide) hydrogels. J Polym Sci Part A Polym Chem 30:2121–2129
173. Kokufuta E, Zhang Y-Q, Tanaka T, Mamada A (1993) Effects of surfactants on the phase transition of poly(N-isopropylacrylamide) gel. Macromolecules 26:1053–1059
174. Bae YH, Okano T, Kim SW (1990) Temperature dependence of swelling of crosslinked poly (N, N'-aklkyl substituted acrylamides) in water. J Polym Sci Part B Polym Phys 28:923–936
175. Bergbreiter DE, Osburn PL, Wilson A, Sink EM (2000) Palladium-catalyzed C-C coupling under thermomorphic conditions. J Am Chem Soc 122:9058–9064
176. Park YS, Ito Y, Imanishi Y (1998) Permeation control through porous membranes immobilized with thermosensitive polymer. Langmuir 14:910–914
177. Kitayama T, Shibuya W, Katsukawa K (2002) Synthesis of highly isotactic poly(N-isopropylacrylamide) by anionic polymerization of a protected monomer. Polym J 34:405–409
178. Isobe Y, Fujioka D, Habaue S, Okamoto Y (2001) Efficient Lewis acid-catalyzed stereocontrolled radical polymerization of acrylamides. J Am Chem Soc 123:7180–7181
179. Ishizone T, Ito M (2002) Synthesis of poly(N-isopropylacrylamide) by the anionic polymerization of N-methoxymethyl-N-isopropylacrylamide. J Polym Sci Part A Polym Chem 40:4328–4332
180. Ito M, Ishizone T (2004) Synthesis of well-defined block copolymers containing poly(N-isopropylacrylamide) segment by anionic block copolymerization of N-methoxymethyl-N-isopropylacrylamide. Des Monomer Polym 7:11–24
181. Ito M, Ishizone T (2006) Living anionic polymerization of N-methoxymethyl-N-isopropylacrylamide: synthesis of well-defined poly(N-isopropylacrylamide) having various stereoregularity. J Polym Sci Part A Polym Chem 44:4832–4845
182. Yokota K, Oda J (1970) Radical copolymerizability of N-substituted- and N, N-disubstituted-methacrylamides. Kogyo Kagaku Zasshi 70:224–228

183. Otsu T, Inoue M, Yamada B, Mori T (1975) Structure and reactivity of vinyl monomers radical reactivites of N-substituted acrylamides and methacrylamides. J Polym Sci Polym Lett Ed 13:505–510
184. Ueda M, Takahashi M, Suzuki T, Imai Y, Pittman CU (1983) Polymerization of α-Methylene-N-methylpyrrolidone. J Polym Sci Polym Phys Ed 20:1139–1149
185. Hobson RF, Reeves LW (1973) Hindered rotation about the N-C bond in some vinylogous amides. J Magn Res 10:243–252
186. Kodaira T, Tanahashi H, Hara K (1990) Cyclopolymerization XVII. Anionic cyclopolymerization tendency of N-methyldiacrylamide and N-substituted dimethacrylamides. Polym J 22:649–659
187. Watanabe N, Sakai M, Sakakibara Y, Uchino N (1970) Polymerization and copolymerization of aziridine derivatives possessing carbon-carbon double bond. Kogyo Kagaku Zasshi 73:1056–1058
188. Okamoto Y, Yuki H (1981) Anionic polymerization of N-methacryloylaziridine. J Polym Sci Polym Chem Ed 19:2647–2650
189. Suzuki T, Kusakabe J, Ishizone T (2008) Living anionic polymerization of N-methacryloyl-2-methylaziridine: polymerizable N, N-dialkylmethacrylamide. Macromolecules 41:1929–1936
190. Suzuki T, Kusakabe J, Kitazawa K, Nakagawa T, Kawauchi S, Ishizone T (2010) Living anionic polymerization of N-methacryloylazetidine: anionic polymerizabillity of N, N-dialkylmethacrylamides. Macromolecules 43:107–116
191. Miyake G, Caporaso L, Cavallo L, Chen EY-X (2009) Coordination-addition polymerization and kinetic resolution of methacrylamides by chiral metallocene catalyst. Macromolecules 42:1462–1471
192. Ishizone T, Kitazawa K, Suzuki T, Kawauchi S (2013) Anionic polymerization behavior of α-methylene-N-methylpyrrolidone. Macromol Symp 323:86–91
193. Hansch C, Leo A, Taft RW (1991) A survey of Hammett substituent constants and resonance and field parameters. Chem Rev 44:165–195
194. Sivaram S, Dhal PK, Kashikar SP, Khisti RS, Shinde BM, Baskaran D (1991) Tailoring carbanion structures for controlled anionic polymerization of acrylonitrile. Macromolecules 24:1697–1698
195. Müller AHE, Hogen-Esch TE (1988) Sterechemistry of anionic vinyl polymerization. Effects of Ion pair prochirality on chain statistics. Macromolecules 21:2336–2339
196. Kanga RS, Hogen-Esch TE, Randrianalimanana E, Soum A, Fontanille M (1990) Studies of the anionic polymerization of phenylvinylsulfoxide and its copolymer with styrene. Macromolecules 23:4235–4240
197. Kanga RS, Hogen-Esch TE, Randrianalimanana E, Soum A, Fontanille M (1990) Thermal elimination of poly(phenyl vinyl sulfoxide) and its polystyrene block copolymers. Macromolecules 23:4241–4246
198. Reibel D, Nuffer R, Mathis C (1992) Synthesis of polyacetylene by chemical modification of poly(phenyl vinyl sulfoxide). Macromolecules 25:7090–7095
199. Bader A, Wünsch JR (1995) Synthesis and polymerization of substituted aryl vinyl sulfoxides. On-line monitoring and kinetics of the thermal degradation of polymeric sulfoxides into trans-polyacetylene. Macromolecules 28:3794–3800
200. Sugiyama K, Karasawa Y, Higashihara T, Zhao Y, Hirao A (2006) Synthesis of block copolymers and asymmetric star-branched polymers comprised of polyacetylene and polystyrene segments via ionic bond formation. Chem Mon 137:869–880
201. Zhao Y, Higashihara T, Sugiyama K, Hirao A (2005) Synthesis of functionalized asymmetric star polymers containing conductive polyacetylene segments by living anionic polymerization. J Am Chem Soc 127:14158–14159
202. Quirk RP, Yoo T, Lee Y, Kim J, Lee B (2003) Application of 1,1-diphenylethylene chemistry in anionic synthesis of polymers with controlled structures. Adv Polym Sci 153:69–153

203. Hirao A, Hayashi M, Loykulnant S, Sugiyama K, Ryu SW, Haraguchi N, Matuo A, Higashihara T (2005) Precise syntheses of chain-multi-functionalized polymers, star-branched polymers, star-linear block copolymers, densely branched polymers, and dendritic branched polymers based on iterative approach using functionalized 1,1-diphenylethylene derivatives. Prog Polym Sci 30:111–182
204. Yuki H, Hotta J, Okamoto Y, Murahashi S (1967) Anionic copolymerization of styrene and 1,1-diphenylethylene. Bull Chem Soc Jpn 40:2659–2663
205. Ott C, Pavlov GM, Guerrero-Sanchez C, Schubert US (2009) Alternating terpyridine-endfunctionalized copolymers of styrene and diphenylethylene via anionic copolymerization techniques: a detailed characterization study. J Polym Sci Part A Polym Chem 47:3691–3701
206. Natalello A, Hall JN, Eccles NAL, Kimani SM, Hutchings LR (2011) Kinetic control of monomer sequence distribution in living anionic copolymerisation. Macromol Rapid Commun 32:233–237
207. Nakano T, Takewaki K, Yade T, Okamoto Y (2001) Dibenzofulvene, a 1,1-diphenylethylene analogue, gives a π-stacked polymer by anionic, free-radical and cationic catalysts. J Am Chem Soc 123:9182–9183
208. Nakano T, Yade T (2003) Synthesis, structure, and photophysical and electrochemical properties of a π-stacked polymer. J Am Chem Soc 125:15474–15484
209. Kosaka Y, Kitazawa K, Inomata S, Ishizone T (2013) Living anionic polymerization of benzofulvene: highly reactive fixed transoid 1,3-diene. ACS Macro Lett 2:164–167
210. Kagumba LC, Penelle J (2005) Anionic ring-opening polymerization of alkyl 1-cyanocyclopropanecarboxylates. Macromolecules 38:4588–4594
211. Penelle J, Xie T (2000) Ring-opening polymerization of diisopropyl cyclopropane-1,1-dicarboxylate under living anionic conditions: a kinetic and mechanistic study. Macromolecules 33:4667–4672
212. Tsang C-W, Yam M, Gates DP (2003) The addition polymerization of a P=C bond: a route to new phosphine polymers. J Am Chem Soc 17:1480–1481
213. Noonan KJT, Gates DP (2006) Ambient-temperature living anionic polymerization of phosphaalkenes: homopolymers and block copolymers with controlled chain lengths. Angew Chem Int Ed 45:7271–7274
214. Noonan KJT, Gates DP (2008) Studying a slow polymerization: a kinetic investigation of the living anionic polymerization of P=C bonds. Macromolecules 41:1961–1965
215. Noonan KJT, Gillon BH, Gappello V, Gates DP (2008) Phosphorous-containing block copolymer templates can control the size and shape of gold nanostructures. J Am Chem Soc 130:12876–12877

Cyclic Monomers: Epoxides, Lactide, Lactones, Lactams, Cyclic Silicon-Containing Monomers, Cyclic Carbonates, and Others

Stéphane Carlotti and Frédéric Peruch

Abstract Cyclic monomers constitute a broad family of monomers which are able to be polymerized by anionic ring-opening polymerization or related nucleophilic ring-opening mechanism. This chapter presents successively the polymerization of cyclic ethers, cyclic esters, cyclic amides, cyclosiloxanes and other cyclic silicon-based compounds, cyclic carbonates, and other cyclic monomers, i.e., cycloalkanes, cyclic sulfides, cyclic amines, cyclic ureas, depsipeptides, and cyclic phosphorus monomers. The main synthetic strategies are reviewed in terms of monomer reactivity, side reactions, and control of macromolecular architectures. Ring-opening polymerization of cyclic monomers utilizing alkali metal derivatives or other initiating systems in conjunction or not with activating systems is described. Emphasis is also put on the use of organic initiators or catalysts to trigger the metal-free ring-opening polymerization.

Keywords Anionic ring-opening polymerization • Epoxides • Lactones • Lactams • Cyclosiloxanes

1 Introduction

For many years, efforts in polymer science were directed toward the control of polymerization methods, a precise control of the structure, topology, and functionality of polymeric chains enabling the design of macromolecular scaffolds that may find applications in high added value domains. For polymers bearing heteroatoms in their backbone, two pathways are generally possible: step-growth polymerization and ring-opening polymerization (ROP). The main advantage of step-growth polymerization is the easy accessibility of a wide range of monomers of various structures. Nevertheless, it suffers from limitations. Indeed, high conversions are needed to get high molar mass polymers, often not controlled, and high polymerization temperatures are generally required. These drawbacks are overcome by the

S. Carlotti (✉) • F. Peruch
University of Bordeaux, LCPO, UMR 5629, Pessac F-33600, France

CNRS, LCPO, UMR 5629, Pessac F-33600, France
e-mail: carlotti@enscbp.fr
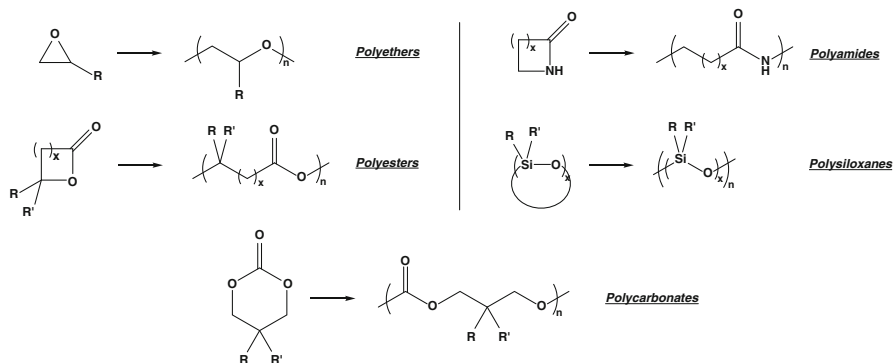
Scheme 1 Ring-opening polymerization of main cyclic monomers

implementation of ROP, which has become a powerful tool for the synthesis of various polymers, mainly polyethers, polyesters, polyamides, polysiloxanes, and polycarbonates (Scheme 1).

The ring strain, coming from distortion of the ring angles and stretching bonds, is generally responsible for conversion of monomer into polymer units. The ROP can be performed according to several mechanisms, namely, anionic, cationic, and coordination-insertion. In this chapter, we will focus on polymerization for which the propagating species is an anion. Few exceptions, where the propagating species are not fully charged, will also be presented. This chapter will be divided into several sub-chapters, each one focusing on one type of cyclic monomer. It will be presented successively the anionic ring-opening polymerization of cyclic ethers, cyclic esters, cyclic amides, cyclic silicon-containing monomers, cyclic carbonates, and other cyclic monomers, i.e., cycloalkanes, cyclic sulfides, cyclic amines, cyclic ureas, depsipeptides and cyclic phosphorus monomers. When well established, the elementary steps involved in the polymerization are given. Recent developments concerning the synthesis of controlled macromolecular architectures are also presented.

2 Cyclic Ethers

2.1 Introduction

The anionic ring-opening polymerization (AROP) of cyclic ethers enables the synthesis of polyethers like poly(ethylene oxide) (PEO) and poly(propylene oxide) (PPO), often referred to as poly(ethylene glycol) and poly(propylene glycol), respectively. The worldwide production of these polymers attains several million tons per year for commodity (precursors for polyurethanes, surfactants, and lubricants) or high-performance (biomedical or cosmetic domains) applications. Nucleophiles can initiate the polymerization leading to alkoxides able to attack a

new monomer enabling the propagation step. Cyclic ethers reactivity and polymerization kinetics are predominantly influenced by their polymerization enthalpy and ring strain but also by electronic and steric factors associated with the nature of the ring substituent as well as reaction conditions like temperature and solvent. An anionic-related mechanism can be considered after preliminary complexation of the monomer by specific additives (an *electrophile*), which strongly facilitate nucleophilic attack and ring-opening. Based on this chemistry, as well as organic synthetic tools, many substituted epoxide monomers are able to be polymerized, opening pathways for well-defined polyether structures and functionalities and allowing the preparation of materials with various properties.

2.2   Conventional Anionic Polymerization of Epoxides

Propagation may proceed without side reaction in anionic polymerization of ethylene oxide [1]. Alkali metal derivatives like hydrides, alkyls, aryls, and amides and mainly alkoxides of sodium, potassium, and cesium represent the most common initiators used for the AROP of epoxides [2, 3]. Lithium alkoxides do not lead to the polymerization of such monomers due to strong aggregation between lithium species after insertion of the first epoxide unit. Polymerizations initiated by alkali metal alkoxides are generally carried out in aprotic and apolar media or in coordinative solvents like dimethylsulfoxide (DMSO) or dimethylformamide (DMF) in order to dissociate active species. The driving force for the ring-opening reaction is the relief of the strain energy of the epoxide ring. High temperatures are usually needed for the AROP of long-chain alkylene oxides.

The different steps of conventional AROP of epoxides are shown in Scheme 2. The initiation step consists of a nucleophilic substitution – S_N2 type – of the alkoxide species leading to the formation of new alkoxide species able to further attack monomer molecules resulting in polyether chains with an atactic structure. The termination step is achieved by addition of an acidic compound with labile hydrogen. Alcohols and water are the most commonly used termination agents in order to obtain hydroxyl end groups. The transfer to monomer is observed with most of the initiating systems when substituted epoxides are polymerized.

2.2.1   Ethylene Oxide

Alkali metal salts of carbanions [4–6] and nitranions [7] are efficient initiators for the polymerization of ethylene oxide (EO). Alkali metal alkoxides were also investigated in detail due to the fact that the structure of these derivatives is similar to the one of propagating species. In aprotic solvents with low to medium polarity, i.e., ethers, alkali metal alkoxides exhibit a strong tendency to aggregate leading to complex reaction kinetics. This is particularly significant for small-sized metals such as lithium or sodium. If the reaction follows a monomer order of 1, the order in

Initiation

Mt = Na, K, Cs
R = H, alkyl, polymer,...
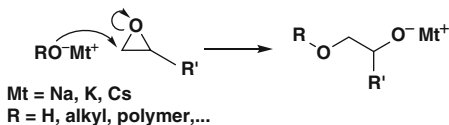
Propagation

Termination

R'' = HO–, RO–, R₂N–, RCOO–,...
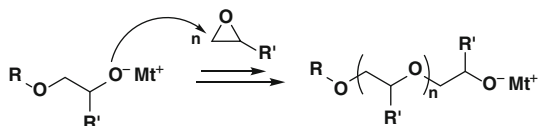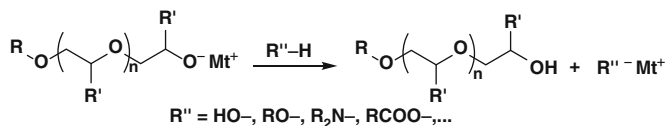
Transfer
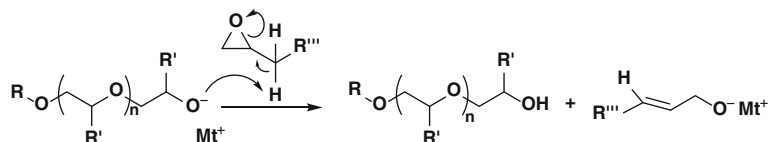
Scheme 2 Anionic ring-opening polymerization (AROP) of epoxides initiated by alkali metal alkoxides

alkoxide propagating species varies according to counterion and solvent. This can be related to the presence of aggregates, ion pairs, and free ions of different intrinsic reactivity (Scheme 3). EO polymerization with alkoxide aggregates is extremely slow and does not even proceed in most cases.

The combination of alkoxide with its parent hydroxy compound was used to limit aggregation and preserve solubility [8–10], allowing a better control of the initiation and propagation, to the detriment of reaction kinetics [11, 12]. This would be referred today as a "degenerative transfer," already reported by Flory in the 1940s.

The use of potassium *tert*-butoxide as initiator was reported to yield living PEO in DMSO with molar masses controlled by the ratio [monomer]/[initiator] [13–15]. With K^+ and Cs^+ salts, EO polymerization in DMSO proceeds almost exclusively by free ions in agreement with a higher dissociation constant in this solvent in line with a high DMSO permittivity ($\varepsilon = 48$ at 20 °C). With Na^+ as counterion, both ion pairs in equilibrium with a small proportion of free ions contribute to the propagation. In tetrahydrofuran (THF) ($\varepsilon = 7.6$ at 25 °C) and in the presence of sodium, potassium, and cesium naphthalene as initiators, a living polymerization takes place, the rate of propagation increasing with the size of the counterion [16, 17]. However, kinetics are complicated due to the strong association of alkoxide end groups.
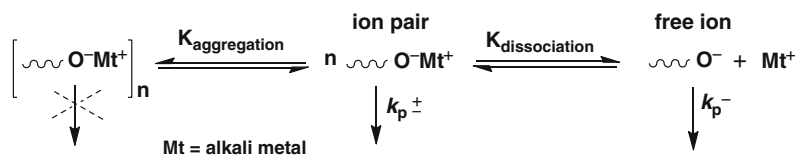
Scheme 3 Aggregates, ion pairs, and free ions in EO polymerization and their capacity to contribute to propagation

2.2.2 Monosubstituted Epoxides

Although alkali metal derivatives are efficient initiators for AROP of ethylene oxide, they are much less efficient for monosubstituted epoxides, e.g., propylene oxide (PO), glycidyl ethers, etc. Indeed, as alkoxide species are relatively strong bases, the abstraction of monomer substituent proton can take place. This side reaction leads to the formation of polyether chains, initiated by an allyloxy group, limiting the molar masses of polyethers (Scheme 2) [14, 18].

Similarly to ethylene oxide, the size of the counterion and the temperature were shown to influence the polymerization rate of monosubstituted epoxides. Increasing the size of the counterion leads to more dissociated active species and thus to higher polymerization rate, faster polymerizations being observed with cesium counterion. Higher temperatures increase the polymerization rate [18, 19] with the time frame being generally in the magnitude of several hours or days to reach high yields. In the presence of potassium as counterion (*t*-BuOK as initiator), the reactivity of racemic propylene oxide in hexamethylphosphoramide (HMPA) at 40 °C is about four times lower than that of EO on the basis of overall polymerization rates [20]. The reactivity of other monosubstituted epoxides depends on both electronic and steric factors induced by the substituent attached to the epoxide ring [21]. For instance, the reactivity of 2,2-dimethyloxirane (DMO) is ten times lower than that of PO, whereas glycidyl ethers such as *tert*-butyl glycidyl ether (*t*-BuGE) are more readily polymerized than PO [20].

Conventional anionic ring-opening polymerization suffers in general from slow kinetics and, more particularly for substituted epoxides, of transfer reactions. Other systems were therefore developed.

2.3 Systems for Activated Epoxide Polymerization

2.3.1 Alkali Metal Derivatives Associated to Crown Ether

Addition of complexing agents to alkali metal cations, such as crown ethers or cryptands (Scheme 4), was shown to drastically increase ethylene oxide propagation rate in ethereal solvents [8, 22, 23], reducing the aggregation of alkoxide polymer ends and increasing the proportion of free ions. For example, the dissociation constant of PEO$^-$ K$^+$ at 20 °C in THF is 1,700 times higher when K$^+$ is
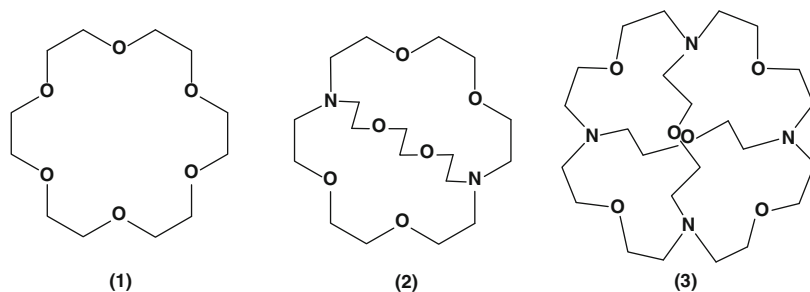
Scheme 4 Crown ether 18C6 (*1*), cryptand 222 (*2*) and sphere (*3*) used to complex alkali metal cations in ethylene oxide polymerization

complexed by cryptand 222. In this system, the reactivity of free ions is about 60 times higher than that of cryptated ion pairs.

For monosubstituted epoxides, 18-crown-6 was also shown to increase the reactivity, the propagation rate constant being up to 14 times at 25 °C [10, 24–26]. In line with the acidic character of hydrogen on the α-carbon of the monomer, the nature of epoxide substituent plays an important role in the chain transfer process. For instance, the anionic polymerization of long-chain alkylene oxides initiated by potassium and cesium alkoxides is much less subjected to chain transfer processes than alkoxides deriving from PO. However, relatively high temperatures were needed to reach reasonable polymerization times, which caused residual side reactions limiting molar masses. The breakthrough of using the additive 18C6 was associated with a decrease of polymerization temperatures, minimizing transfer reaction to monomer. This is reflected by the production of poly(2-butyloxirane) of higher molar masses at 20 °C (Table 1) [19]. The polymerization temperature of 2-butyloxirane and of higher 2-alkyloxiranes like 2-hexyloxirane and 2-octyloxirane could even be reduced below 0 °C, which almost eliminate completely all side reactions. However, very long reaction times were required, i.e., 4–8 days, and conversion did not go to completion [19]. Alkali metal hydrides were also associated to 18C6 for the AROP of glycidyl butyl ether [21, 27]. Polyethers with molar masses lower than 5,000 g/mol and low dispersity were obtained. For this range of molar masses, polymerization time was considerably reduced, from several days to a few hours, as well as transfer reactions.

2.3.2 Aluminum Systems: From Bulky to Simpler Compounds

In the 1980s, Inoue and coll. used metalloporphyrin as catalyst, in particular aluminum-based porphyrin, for the polymerization of methacrylates [28, 29], lactones [30], and epoxides [31] and, in some extent, oxetane [32] which is usually polymerized by a cationic route. The equimolar combination between diethylaluminum chloride and α, β, γ, δ-tetraphenylporphyrin (TPPAlCl) led to a high catalytic activity in the polymerization of propylene oxide. The covalent nature of the Al-Cl bond suggests a

Table 1 Polymerization conditions and characteristics of poly(2-butyloxirane) synthesized in presence of K or Cs *tert*-butoxide in toluene with or without crown ether 18C6 (molar ratio 18C6/metal = 3)

Counterion	T (°C)	Time (h)	Conv. (%)	$\overline{M}_n$ th. (g/mol)	$\overline{M}_n$ exp. (g/mol)	D
K	80	40	96	14,700	11,200	1.15
Cs	80	18	97	14,800	11,700	1.11
K/18C6	20	19	92	47,000	43,600	1.11
Cs/18C6	20	68	81	39,600	28,000	1.13

X = Cl, OCOR', OAr, OR'
R = alkyl or phenyl
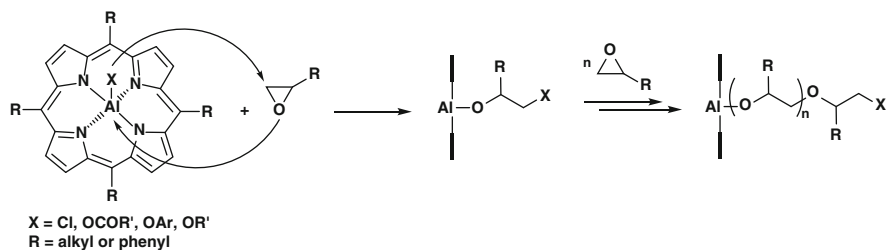
Scheme 5 Polymerization mechanism of epoxides initiated by an aluminum porphyrin

polymerization via a coordination mechanism. Synthesized polyethers, by the so-called "immortal" polymerization, reached molar masses up to 70,000 g/mol with a narrow distribution [33]. A monomer molecule is first inserted between the Al-Cl bond of the initiator (Scheme 5). Aluminum porphyrin, due to its nucleophilic character, was used as initiator enabling coordination with epoxide. Under such conditions, transfer reactions were considerably decreased, allowing the synthesis of a series of block copolymers, including poly(PO-*b*-EO), poly(1,2-butene oxide-*b*-PO), poly(PO-*b*-epichlorohydrin), poly(lactones-*b*-PO), poly(lactones-*b*-EO), etc. [34, 35]. Although EO polymerization could be achieved rapidly (half-time reaction is about 30 min at room temperature for [EO]/[TPPAlCl] = 400 in dichloromethane), other epoxides exhibited a lower reactivity. In similar conditions, several hours were required for the polymerization of PO and 1,2-epoxybutane [31] in order to reach complete conversion, whereas for styrene oxide or 1,2-epoxy-2-methylpropane conversions did not exceed 15 % after 8 days of reaction [33].

In order to increase polymerization rate of propylene oxide, aluminum porphyrin was used in association with a bulky Lewis acid [36–38]. For instance, methylaluminum bis(2,4,6-tri-*tert*-butylphenolate) (MAlBP) was used to coordinate the epoxide and to activate the monomer substrate toward a nucleophilic attack. As compared to the previous system, the catalytic species and the initiator are independent, i.e., employed as a bi-component initiating/activating system. There is no interaction between these two aluminum derivatives due to their bulkiness. Polymerization rates of propylene oxide and 1,2-butene oxide were strongly enhanced due to the presence of the bulky Lewis acid [36]. Only 0.25 %

of MAlBP, with respect to propylene oxide concentration, was added to increase the polymerization rate by a factor of 460. With a [MAlBP]/[TPPAlCl] ratio equal to 0.5, 3 min was enough for propylene oxide to be polymerized with 86 % conversion, leading to a PPO with a molar mass up to 12,000 g/mol. Without MAlBP, in 7 h, the conversion is around 20 % and molar mass reached 3,300 g/mol. The Lewis acid alone did not initiate the polymerization under similar conditions. The "living" nature of the polymerization could be demonstrated by the successful formation of block copolymers based on propylene oxide and 1,2-butene oxide, though complete conversions could not be obtained.

Using relatively similar systems based on quaternary ammonium and quaternary phosphonium halides associated to sterically hindered methyl(diphenoxy)aluminum, poorly reactive four-membered ring oxetane, e.g., 1,3-propylene oxide, was polymerized according to a coordinated-anionic mechanism, as a result of strong monomer activation by complexation with the aluminum derivative [39].

Braune and Okuda used porphyrin-free aluminate complexes for the polymerization of propylene oxide activated by their neutral Lewis acid precursors [40]. The nucleophilic species were easily obtained by reaction of a bulky Lewis acid based on diphenoxyaluminum compounds, with a cesium alkoxide or an ammonium salt. The ring-opening polymerization proceeds under the synergic interaction of a phenolate-aluminum-oxirane complex forming an activated monomer with the corresponding "ate" complex which initiates the reaction (Scheme 6). Ring-opening takes place by transfer of an alkoxy group from the "ate" complex, regenerating an aluminate able to activate a new monomer. The synthesis of poly (propylene oxide)s with molar masses up to 4,000 g/mol was reported following an anionic (or coordinative) mechanism because of exclusive head-to-tail linkages.

Tsvetanov reported in 1985 the polymerization of ethylene oxide initiated by sodium tetrabutylaluminate [41]. PEO were prepared in toluene in the range 15–
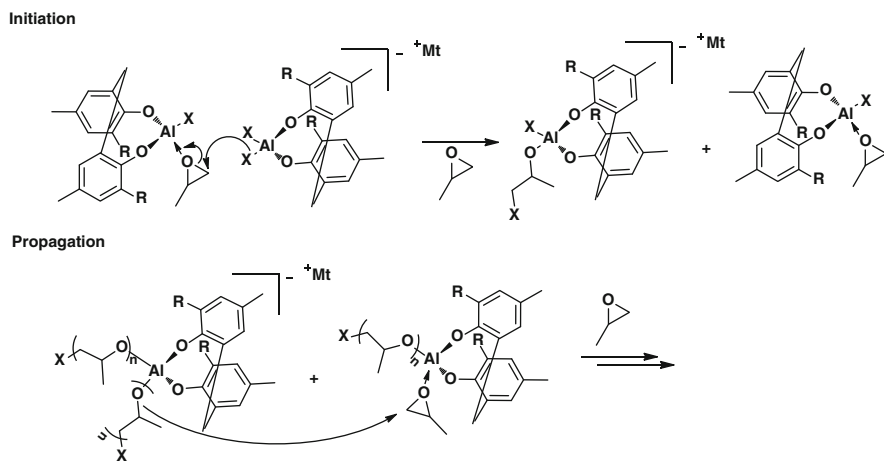
Scheme 6 Initiation and propagation steps of propylene oxide polymerization initiated by bulky aluminum complexes
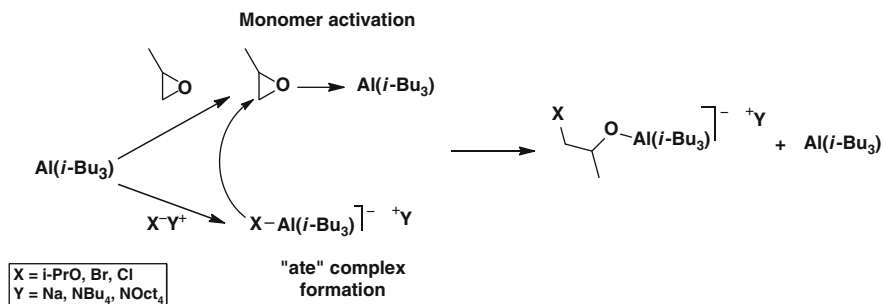
Scheme 7 Nucleophilic attack of sodium alkoxide or ammonium salts/triisobutylaluminum on activated propylene oxide

70 °C with a high kinetic order with respect to the initiator. The polymer chain growth was explained by the presence of aggregates of NaAlBu$_4$, predominantly trimers of the "ate" complex. Interaction between the oxygen atom of EO and the alkali metal, as well as EO and aluminum to a lesser degree, was shown, in line with some activation of the epoxide.

Using epoxide monomers and combinations of a Lewis acid – typically a trialkylaluminum – and alkali metal alkoxides or onium salts [42–47], Carlotti and Deffieux developed efficient synthesis of various polyethers. An excess of Lewis acid with respect to the initiator was required. The formation of an "ate" complex, which was able to ring-open the activated epoxide by the excess of activator, was observed (Scheme 7).

Propylene oxide polymerization, based on a monomer-activated anionic polymerization, occurs at room or lower temperature. Control over the polymerization strongly depends on the nature of the counterion. Sodium and potassium enable the polymerization, whereas lithium does not. In few hours, controlled poly(propylene oxide) chains, up to 20,000 g/mol, were obtained with nevertheless the presence of some residual transfer reactions, i.e., transfer to monomer leading to allyloxy groups in the α-position and transfer to triisobutylaluminum (i-Bu$_3$Al), which generates initiation by a hydride coming from an isobutyl group. Ammonium salts were more successful as much higher molar masses could be achieved in a controlled manner, especially at -30 °C, yielding polyethers of low dispersity (e.g., $Đ = 1.34$ for $\overline{M_n} = 170,000$ g/mol) [45]. The strong decrease of transfer reactions was explained by the decrease of basicity of the active bi-component complex. The exclusive preparation of regioregular polymers (head-to-tail) was indicative of an anionic/coordination type mechanism. Polymerization proceeds at [Al]/[Initiator] ratio higher than unity, indicating that only complexed PO molecules are susceptible to ring-open, thanks to significant electron-withdrawing effect that makes the ring carbon atoms much more electrophilic. Increasing trialkylaluminum concentration, at constant monomer and initiator concentrations, was shown to yield a drastic increase in polymerization rate, whereas the number of PPO chains remained unchanged.

These initiating systems were also applied to the polymerization of a broad variety of epoxides including several alkylene oxides and glycidyl ethers, epichlorohydrin (ECH), etc. Compared to conventional alkali metal initiators, the tetraoctylammonium bromide/i-Bu$_3$Al-initiating system strongly enhanced the rate of ethylene oxide polymerization while retaining the living character of the reaction [48]. At a ratio [i-Bu$_3$Al]/[NOct$_4$Br] = 1.5, the synthesis of PEO of 20,000 g/mol was completed within 2 h at room temperature in dichloromethane. By changing the ammonium salt by an alkyllithium, a PEO of 10,000 g/mol was synthesized at low temperature and in nonpolar media, e.g., toluene [49]. The presence of trialkylaluminum used in excess with respect to the lithium initiator permits disaggregation of lithium alkoxide species by forming lithium/aluminate complexes which are able to ring-open the AlR$_3$-complexed EO molecules. However, ligand exchanges in the lithium/aluminate complex lead to slow deactivation of the propagating species during the polymerization which limits the access to high molar mass PEO.

Monomer-activated anionic polymerization of epichlorohydrin utilizing similar conditions was also described. In contrast to conventional anionic polymerization, aluminate species that ensures propagation in AlR$_3$/onium systems selectively react with activated ECH ring, keeping the chloromethyl function [50]. Syntheses of poly (glycidyl methyl ether) (PGME) [51], linear poly(2-ethoxyethyl glycidyl ether) (PEEGE), and poly(*tert*-butyl glycidyl ether) (P*t*BuGE) [52] with narrow chain distribution and controlled molar masses were also reported. The amount of Lewis acid required to trigger the reaction and achieve quantitative monomer conversions was shown to increase with the number of oxygen atoms in the monomer.

This anionic living/controlled polymerization, employing onium salt/triisobutylaluminum systems and involving a monomer-activated mechanism, was applied to the synthesis of a series of random and block copolymers. For instance, EO/PO random copolymers with a gradient structure, molar masses up to 70,000 g/mol, and narrow dispersity were prepared [48]. PPO-*co*-PECH [50] and amphiphilic poly (alkylene oxide-*co*-glycidol) were also synthesized via the synthesis of PPOx-*co*-PEEGE and PBO-*co*-P*t*BuGE copolymers [52], followed by the deprotection of hydroxyl groups under acidic conditions. Despite the determining role of the monomer complexation in this polymerization process, the copolymerization ratios remain close to those reported for conventional anionic copolymerization. Different diblock and triblock copolymers of various compositions and lengths were also prepared by sequential monomer addition. Synthesis of PEO-*b*-PPO-*b*-PEO triblock copolymers with NOct$_4$Br/i-Bu$_3$Al initiating system was first achieved [48]. PPO-*b*-PECH block copolymers with molar masses ranging from 6,000 to 30,000 g/mol and with various PPO and PECH block lengths were also prepared by sequential addition of the two monomers [50]. The re-initiation efficiency was shown to be quantitative, no matter the order of addition of the two monomers. Finally, block copolymerization of EO initiated with lithium derivatives was also lately described [49]. Although it is known that EO polymerization could not proceed properly when lithium alkoxide species are involved [53, 54], it was shown that living polystyryllithium and polyisoprenyllithium chains can play the

role of a macroinitiator for EO polymerization in presence of trialkylaluminum. Block copolymers polystyrene(or polyisoprene)-*b*-poly(ethylene oxide)s were obtained in hydrocarbon within a few hours with a PEO block molar mass up to 10,000 g/mol and a re-initiation efficiency of about 80 %.

2.3.3 Calcium-Based Systems

The association of two metals was also proposed in 1980 to polymerize ethylene oxide [55]. A calcium amide/alkali metal alkoxide initiating system was used at high temperature in order to produce poly(ethylene oxide)s with high molar masses. EO polymerization involves monomer coordination at the catalyst active site via σ bond formation between the monomer heteroatom and the catalyst metal atom. It is followed by a nucleophilic attack of the alkoxide active group [56]. Tsvetanov and coworkers investigated this combination for the synthesis of poly(propylene oxide) and miscellaneous copolyethers [57–61]. The authors explained that calcium derivatives are much weaker than other metals, like aluminum or zinc, in the formation of oxiranes complexes. As a result, Ca-EO complexes are more readily formed in comparison with substituted epoxides where low-rate polymerizations are observed. In addition, the polymerization takes place under heterogeneous condition as the calcium-based initiator is not soluble in the solvents used. As an example, the synthesis of an amphiphilic poly(ethylene oxide)-*b*-poly(alkylglycidyl ether) copolymer with a molar mass up to 10^6 g/mol and a high dispersity (5–8) was achieved in relatively short times (several hours, but not days) at 97 °C [59].

In summary, various systems such as metals associated to crown ethers or metallic activators as well as combinations or organic initiators associated to organometallic compounds were used to polymerize epoxides affording control and fast kinetics. Nowadays, complementary challenges concerns metal-free systems which are able to fulfill all criteria so far discussed.

2.4 Toward Organic Initiating Systems

2.4.1 Tertiary Amines

Amines were essentially used for the anionic polymerization of di- and polyepoxides, mainly diglycidyl ether of bisphenol A and its derivatives as well as glycidyl phenyl ether [62]. Reaction with amines leads to slow polymerization rates, to long induction periods, and to the formation of short chains due to transfer reactions. Benzyldimethylamine, pyridine, triethylamine, 4-dimethylaminopyridine (DMAP), and 1,8-diazabicyclo[5.4.0]undec-7-ene (DBU) are the most common amines used as initiators. Ammonium salts and imidazoles are also employed to open epoxides by anionic polymerization. The main drawback of all these compounds is the limitation in terms of molar masses. Although the initiation mechanism is not well established,

Scheme 8 Possible initiation steps for the epoxide polymerization in the presence of tertiary amines
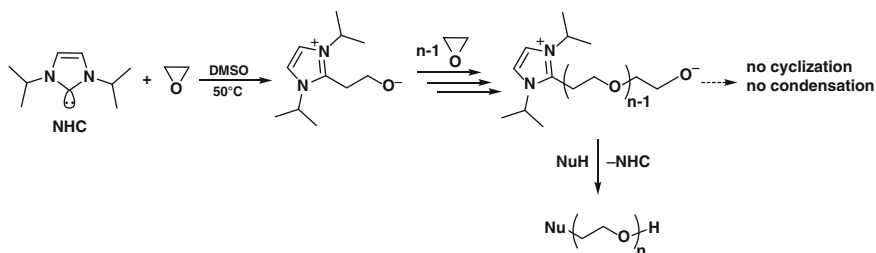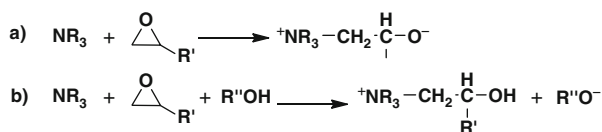
Scheme 9 Proposed mechanism for ethylene oxide polymerization initiated by N-heterocyclic carbenes

two pathways are generally considered (Scheme 8) [63, 64]. The addition of alcohol decreases induction periods and increases polymerization rates but limits molar masses [62]. The alkoxide formed by the second way (Scheme 8b) is more reactive than species resulting from usual initiation step (Scheme 8a). Williams and coll. succeeded to decrease the time of initiating step by using DMAP thanks to its conjugated structure with a negative charge on the nitrogen atom of the cycle and a positive charge on the tertiary amine [64]. The molar masses were about 1,000 g/mol at 80 °C.

2.4.2 *N*-Heterocyclic Carbenes

N-Heterocyclic carbenes (NHCs) can be used as ligands of transition metallic complexes [65] but also as organic catalysts for various metal-free reactions [66, 67]. Ring-opening polymerization of some epoxides was triggered by NHCs [68–70]. Taton and coll. showed that 1,3-bis-(diisopropyl)imidazole-2-ylidene is able to initiate ethylene oxide polymerization according to a zwitterionic mechanism (Scheme 9) [68]. NHC plays in this case the role of initiator controlling PEO molar masses and forming zwitterionic imidazolium. It can be released by attack of functionalizing terminators added to the medium. Polymerizations were performed at 50 °C in DMSO and required long times, i.e., several days. Molar masses up to 13,000 g/mol were obtained with narrow distribution and good agreement between theoretical and experimental molar masses, in line with a good control of the polymerization. This approach was less effective for the polymerization of propylene oxide due probably to transfer reactions to monomer. Poly(propylene oxide) oligomers with a relative low dispersity were nevertheless prepared [70].
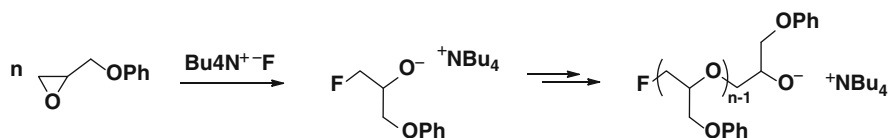
Scheme 10 Polymerization of glycidyl phenyl ether initiated with tetrabutylammonium fluoride

Controlled EO polymerization was found to proceed also with a catalytic amount of NHC, in DMSO at 50 °C, and in presence of a variety of chain regulators, e.g., benzyl alcohol, propargyl alcohol, or trimethylsilyl azide. They possess a nucleophilic part and an electrophilic one (Nu-E). In this case PEO molar masses match the [EO]/[Nu-E] ratio, typically in molar proportions [NHC]/[Nu-E]/[EO] = 0.1/1/ 100 [69]. Reversible exchanges with Nu-E molecules, involving the formation of active and dormant chains, yield α-Nu-ω-E-poly(ethylene oxide) opening a way for chain-end functionalization.

2.4.3 Ammonium, Phosphonium, and Phosphazene Bases

Ammonium salts were first used by Hemery, Ganachaud and coll. for the AROP of glycidyl phenyl ether (GPE) in miniemulsion [71]. Didodecyldimethylammonium hydroxide was used as an inisurf (initiator-surfactant) exhibiting both surface-active properties and the ability to initiate polymerization. Average molar masses increased with conversion and were dependent on the initiator concentration. A critical polymerization degree of 8 was reached. Using a similar initiator, i.e., tetrabutylammonium fluoride, in solution polymerization, endo achieved the synthesis of poly(glycidyl phenyl ether) oligomers with controlled molar masses up to 4,000 g/mol (Scheme 10) [72] and the synthesis of poly(ethylene oxide-b-glycidyl phenyl ether) when the polymerization of glycidyl phenyl ether was performed in the presence of poly(ethylene glycol) monomethyl ether [73].

As already mentioned, the size of the counterion plays a preponderant role in epoxide polymerization, in particular on the kinetics. As a result of their bulky size, some phosphonium and phosphazenium derivatives arising from strong Brönsted phosphazene bases, developed by Schwesinger, revealed potential interesting counterions in order to limit aggregation phenomena [74, 75]. Several of these commercially available bases were used as organic deprotonating agents of –OH (−CH, −SH, −NH, or –COOH) containing initiators, to polymerize epoxides like ethylene oxide [76–84], propylene oxide [85–87], butene oxide [82, 88, 89], styrene oxide [90], as well as ethoxy ethyl glycidyl ether [88, 91, 92] and other protected form of glycidol [93], affording homopolymers, copolymers [94–96], grafted or block copolymers [81, 84, 93, 97–100], and star-shaped structures [89].

Phosphonium and phosphazene bases can be used with an alcohol to form a protonated counterion. The use of t-BuP$_4$H$^+$ enables an increase of the polymerization rate of propylene oxide, but transfer reactions still occur. Polymerization
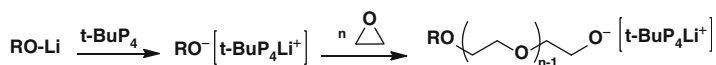
Scheme 11 Ethylene oxide polymerization initiated by lithium alkoxide in the presence of phosphazene base

rates increase when the positive charge is delocalized into the molecule, which is due to better ion separation [80, 81]. Phosphazene bases were also utilized in order to complex lithium alkoxides allowing the (co)polymerization of ethylene oxide and ethoxyethyl glycidyl ether with lithium derivatives (Scheme 11) [76, 79, 88, 91, 92, 101], which is generally not possible because of strong aggregation between lithium alkoxides except when a trialkylaluminum is added [49]. The base behaves as a cryptand for Li^+ ions via polar amino and imino groups located inside the globular molecule, and the outer shell is formed by alkyl substituents. The equilibrium between complexed lithium alkoxide ion pairs and reactive free anions is thus shifted toward the latter species allowing polymerization. Copolymers based on polystyrene and polyethers were prepared without the need of cation exchange. However, the presence of residual transfer reactions and an induction period resulting from the slow disaggregation of the lithium alkoxide ends still complicated the epoxide polymerization [79].

A broad range of polyethers can be synthesized leading to an important class of materials used in many applications. Controlled structures and dimensions as well as easy, inexpensive, and rapid polymerizations remain the major challenges to be addressed. Preparation of functional polyethers used as reactive precursors, by an anionic route, is also of major interest.

2.5 Functionalization of Polyethers Prepared by Anionic Ring-Opening Polymerization

Functionalization of polyether chains can occur either to chain ends or along the polymer backbone. In the first case, a functional initiator and/or a termination agent is employed. Further polymerization or other reactions can be conducted from the as-introduced functional groups. The functionalization into the chains is carried out by the use of functional monomers. Hydroxy, amine, epoxide, carbonate, thiol, azide, as well as double and triple bonds are the most commonly used functions in order to obtain a versatile range of functional polymers for many applications. Carlotti and coll. [102], Frey and coll. [103, 104], and Riffle and coll. [105] have reviewed main syntheses, properties, and applications of various functional polyethers. This part will focus on the functions introduced into polyethers prepared by AROP.
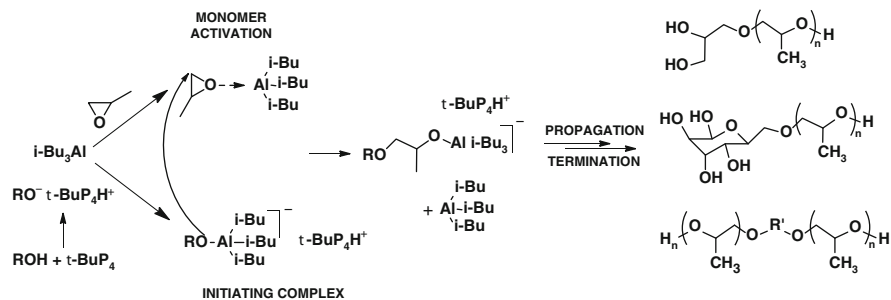
Scheme 12 Combination of phosphazene base and *i*-Bu₃Al for the synthesis of polyhydroxy telechelic PPO

2.5.1 Polyethers with Hydroxyl Functions

Low molar masses polyether polyols are mainly used as precursors of polyurethanes [106]. The majority of hydroxy telechelic polyethers are synthesized by AROP initiated by potassium or cesium hydroxide [18]. Initiation by a hydroxy group followed by termination reaction using water or an alcohol yields α-, ω-dihydroxy polyethers. As shown previously, this approach is efficient for ethylene oxide but much less with monosubstituted epoxides. Branched and star polyethers were synthesized from tri-, tetra-, penta-, and octa-alkoxides of potassium with molar masses close to 5,000 g/mol and a relatively broad dispersity [107–114]. With a similar approach and using hyperbranched polyglycerol initiators, Lutz, Frey and coll. prepared functional multiarm star PEO [9].

Bulkier counterion like phosphazene bases was used as deprotonating agents with dipropylene glycol as initiator showing some decrease of usual transfer reactions [86]. Using the monomer activation methodology [45], di-, tri-, and penta-hydroxy telechelic poly(propylene oxide)s were obtained in very short times (hours) at room temperature in hydrocarbon solvents with molar masses up to 80,000 g/mol with a relatively low dispersity (Scheme 12) [115].

Using an organo-catalysis approach described previously (Scheme 9), Taton and coll. reported that *N*-heterocyclic carbenes (NHC) could lead to α-,ω-dihydroxy poly(ethylene oxide) using water as terminating agent. Hydroxide (OH⁻) was shown to behave as a nucleophile that displaces the α-imidazolium moiety from PEO chains, thus releasing the NHC, whereas the terminal alkoxide was transformed into a ω-hydroxy function [69].

Hydroxyl functions can also be introduced after post-modification of other reactive functions introduced via initiation. An amino function can lead to an OH group after reaction with a molecule of ethylene oxide [116]. The use of tetrabutylammonium acetate as initiator proved efficient to introduce acetate-end groups to poly(glycidyl phenyl ether) [117]. Hydroxyl functions were obtained after hydrolysis with an acidic treatment. A narrow molar mass distribution and molar masses up to 4,000 g/mol were thus obtained.
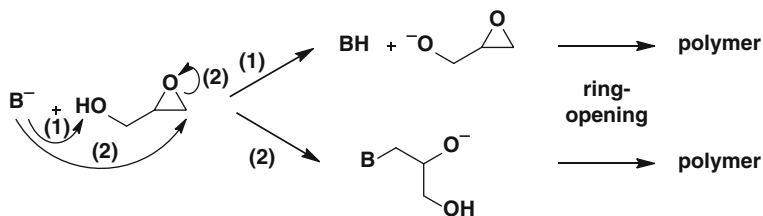
Scheme 13 Initiation mechanisms of glycidol in presence of a base

The introduction of pendant hydroxyl functions is predominantly obtained from anionic polymerization of glycidol and its derivatives. These polymers are very attractive for biological and medical applications [118]. Direct reaction of glycidol with bases such as triethylamine, pyridine, alkali metal hydroxide, and sodium methoxide leads to two distinct initiation steps at room temperature (Scheme 13) [119–123]. The first way corresponds to a basic attack toward the hydrogen atom of the hydroxyl group, and thus an oxyanion bearing an epoxy group is formed. The second way is the attack of the base over the methylene of the epoxide leading to ring-opening. Hyperbranched polyethers with a high functionality in hydroxyl groups were achieved [103, 124–126].

In order to access to well-defined linear polyols derived from glycidol, hydroxyl functions of that monomer had to be protected. Dworak, Tsvetanov and coll. [114, 127–131], and Möller and coll. [132–134] investigated the AROP of ethoxyethyl glycidyl ether using metal alkali alkoxides such as KOH, CsOH, and t-BuOK. These systems enabled the synthesis of linear polyols up to 30,000 g/mol. Quantitative conversion was obtained between 17 and 48 h, depending on targeted molar masses, and required high temperatures (up to 120 °C). Due to the initiating systems used, residual transfer reactions were observed, limiting somehow the control over the structures [91]. Linear polyglycidols with molar masses up to 85,000 g/mol, starting from ethoxyethyl glycidyl ether (EEGE), were obtained using NOct$_4$Br/ triisobutylaluminum as initiating system at room temperature in a few hours [52]. The formation of an initiating and propagating "ate" complex of weak basicity was proposed to explain the decrease of side reactions. Allyl glycidyl ether or isopropylidene glyceryl glycidyl ether was also used as a protected form of glycidol to obtain polyethers polyols [114, 133, 135, 136].

Taking advantages of the anionic route, various well-defined functional block copolymers were prepared [128, 133, 137–141].

2.5.2 Polyethers with Amine Functions

Jeffamines® represent the most industrially produced polyetheramines. Such polyamino telechelic polyethers cannot be directly obtained by initiation and termination steps. They are synthesized from hydroxytelechelic random copolymers of ethylene oxide and propylene oxide via reaction between hydroxyl

functions and ammoniac gas at 300 °C. Considering the nature of the polymerization, only polyetheramines with low molar masses can be prepared. They are thermoresponsive polymers possessing a lower critical solubility temperature around 30 °C in water. Amino end groups are mainly used as curing agents in epoxy resins [142, 143] and as chain extenders for polyurethane applications [144, 145].

The introduction of amino groups at the head of polyether chains is generally carried out using an initiator bearing a primary amine function and another more reactive function, i.e., an alcohol, which enables the initiation. Aminoalcohols can be thus used to polymerize ethylene oxide by an anionic mechanism [116]. In basic media, both metal alkoxide and amide are formed, and the equilibrium is driven toward the formation of alkoxide by increasing the size of the counterion. Molar masses of α-amino-ω-hydroxy functional polyethers reached 1,000 g/mol. Transfer and termination reactions occur due to the hydrogen of amino groups. Protection of the primary amino group by a tertiary one was considered to overcome those limitations [96, 100, 116, 135]. Molar masses increased up to 6,000 g/mol and required long times, i.e., 150 h [146]. Schlaad used α-methylbenzyl cyanide as a CH-acidic compound to obtain α-cyano, ω-hydroxy poly(ethylene oxide) with controlled molar masses up to 2,500 g/mol with narrow distributions [78]. The cyanide function was then reduced in –NH$_2$ group by LiAlH$_4$.

Polyethers bearing primary amino groups are also generated by using epoxide monomers with protected amines such as *N,N*-dibenzyl amino glycidol or *N,N*-diallylglycidylamine prepared from epichlorohydrin and *N,N*-dibenzylamine or *N,N*-diallylamine, respectively [147, 148]. The synthesis of copolymers with EO was next performed using cesium alkoxide as initiator giving controlled copolyethers with molar masses up to 10,000 g/mol. Pendant amine functions can also be introduced from chlorine atoms. Statistical or block copolyethers, made by NOct$_4$Br/i-Bu$_3$Al systems and having both hydroxy and amine pendant groups, were brought, respectively, by ethoxyethyl glycidyl ether (protected glycidol) and epichlorohydrin monomers (Scheme 14) [149]. Chlorine atoms were subsequently transformed into azido groups using sodium azide. Consequent reaction with
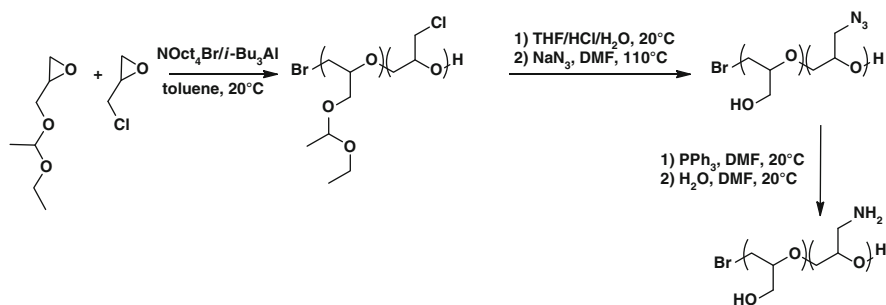
Scheme 14 Synthesis of poly(glycidol-co-glycidyl amine) from protected glycidol and epichlorohydrin units

triphenylphosphine enables quantitative formation of amino groups. Such type of copolymers was proposed to enable selective electrophilic reactions due to the difference of reactivity between –OH and –NH$_2$ functions.

2.5.3 Polyethers with Alcene Functions

Double bonds are known to be stable toward anionic ring-opening polymerization conditions but can be further easily modified into various functions which make them attractive. They can be introduced via initiation with an alcohol bearing such a function [96, 150–152]. Allyl alcohol and 10-undecen-1-ol can be deprotonated, for instance, by naphthalene potassium or by sodium hydride, respectively. However, during polymerization, double bonds can be isomerized into propenyl group to form $CH_3CH = CHO^-$ as initiating species. To avoid this side reaction, polymerization has to occur between 15 and 20 °C, rather than at high temperatures [151]. As one example, thiol-ene reactions were applied to PEO oligomers initiated by 10-undecen-1-ol [152]. The synthesis of α,ω-diallyl PEO was achieved by reaction between α,ω-dihydroxy PEO, deprotonated with diphenylmethyl potassium, and allyl bromide. Hydrogels were obtained by their post-reaction with octafunctional silsesquioxanes via hydrosilylation [153, 154].

Monomers bearing allyl functions, like allyl glycidyl ether (AGE), can be directly used to synthesize polyethers with pendant double bonds through AROP with alkali metal alkoxides as initiators [21, 133, 155]. Generally, molar masses lower than 10,000 g/mol and long polymerization times are required. Ammonium salts/trialkylaluminum systems [156] allowed controlled and high molar mass structures in a few hours. With potassium alkoxide/naphthalenide initiators, Lynd and Hawker could also obtain molar masses up to 100,000 g/mol with low dispersity within 20–144 h [157]. Similarly, ethoxy vinyl glycidyl ether (EVGE) was shown to be selectively polymerized and copolymerized with ethylene oxide to give functional polyethers able to be post-modified [158].

2.5.4 Polyethers with Azide Functions

Most of the PEO azidation routes reported in the literature involve the chemical modification of previously formed hydroxyl-terminated PEO [159–162]. Kataoka achieved the synthesis of azido-terminated heterobifunctional poly(ethylene oxide) s in a multistep process, involving ring-opening polymerization of ethylene oxide initiated by allyl alcohol and subsequent transformation of R-allyloxy and ω-hydroxy PEO end groups by a series of chemical reactions [163]. The azide group was introduced by mesylation of the hydroxyl terminus, followed by its subsequent substitution with sodium azide [164, 165].

The monomer-activated approach allowed the direct synthesis of a broad series of heterofunctional polyethers bearing an azido head group, and a hydroxy-terminated chain end, starting from tetrabutylammonium azide in the presence of
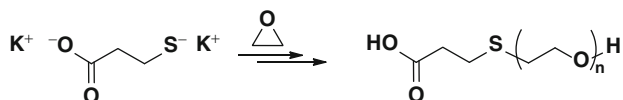
Scheme 15 Thiolate-initiated polymerization of ethylene oxide

triisobutylaluminum [166]. Poly(alkylene oxide)s, protected polyglycidol, and polyepichlorohydrin were obtained in this way with a high functionalization efficiency. Reduction reactions can lead to amine functionalization, or Huisgen's coupling reaction with alkyne moieties can be applied [167].

2.5.5 Polyethers with Other Functions

Carboxylic acid groups were, for instance, introduced from the initiation step. The use of dipotassium-3-mercaptopropionate synthesized from 3-mercaptopropionic acid and two equivalents of potassium naphthalide allowed the direct synthesis of α-carboxy, ω-hydroxy poly(ethylene oxide) up to 25,000 g/mol with narrow distribution [168]. Only the thiolate was shown to react; the carboxylate did not participate in the polymerization (Scheme 15), but the usual way to introduce such a function is post-modification of chain ends [152, 169–171].

Aldehyde functions in α-position can also be introduced by using an initiator bearing a protecting group, i.e., 4-(diethoxymethyl)benzyl alcohol [172].

As a last example, polyethers with pendant methacrylate functions were achieved by selective ring-opening polymerization of glycidyl methacrylate using a monomer-activated anionic approach affording cross-linkable low Tg polymers [173].

The method based on chemical modification of previously and anionically formed polyethers is the most common way to get various functionalized and reactive structures. In many cases a simple chemistry can be used which makes this way very attractive. But, in the other cases, the interest is much more limited particularly for an industrial application. The recent advances in the control of the anionic polymerization of epoxide offer nowadays direct routes to prepare reactive and new polymers. The research and development of novel technologies will certainly contribute to an increasing use of such recent methods.

3 Cyclic Esters

3.1 Introduction

The biodegradability and biocompatibility of aliphatic polyesters render them very attractive for a wide range of applications as environmental friendly thermoplastics and biomaterials [174]. Moreover, many of them could be obtained from renewable resources, which is one of the great challenges for polymer chemists. Three

different polymerization mechanisms can be implemented to synthesize aliphatic polyesters: the step-growth polymerization through esterification reaction of hydroxyl acids or diacids/diols, the ring-opening polymerization (ROP) of cyclic ketene acetals, and the ROP of cyclic esters. The step-growth polymerization is highly used as its main advantage is the easy availability of a very wide range of acid and alcohol precursors. Nevertheless, this polymerization suffers from severe limitations: extremely high conversion has to be reached to get high molar masses, high temperatures are generally needed, control of the molar masses is very difficult, and dispersity is quite large. The ROP of cyclic ketene acetals could proceed through cationic and radical processes [175]. Even if this polymerization is known for long, its development remains limited due to many drawbacks: there is competition between direct vinyl polymerization and indirect ring-opening of the cycle depending on the ring size, substituents, and temperature; monomers are not readily accessible; and branching reactions could occur. All these limitations can be overcome by implementing the ROP of cyclic esters either by ionic (cationic or anionic) or coordination-insertion mechanisms. Indeed, this technique allows living and/or controlled polymerization with fast initiation and high molar masses with low dispersity. Availability of the monomers occupies an intermediate position between step-growth polymerization and ROP of ketene acetals. The question of polymerizability of cyclic esters arises since the polymerization rate is highly dependent on the ring size and the substituents. Moreover, in the case of anionic mechanism, the active species varies with the ring size. Many recent reviews could give other details than those presented in this subchapter [175–183].

3.2 Thermodynamics of Cyclic Esters Ring-Opening Polymerization

The ability of a cyclic ester to be polymerized by the ring-opening mechanism has to be allowed both thermodynamically and kinetically. Indeed, the monomer-polymer equilibrium has to be shifted to the polymer formation, and the polymerization time has to be reasonable. ROP of cyclic esters could be sometimes limited by the presence of a relatively high concentration of the unreacted monomer when at the equilibrium. This is typically the case for γ-butyrolactone which is hardly polymerizable. The driving force for the polymerization of the majority of cyclic esters is their ring strain. As a consequence, large-ring lactones are more difficult to polymerize than small ones.

3.3 Lactide

The AROP of lactide was not as extensively studied as its coordination-insertion polymerization, this latter being most investigating because it could enable

stereoselective polymerization [179, 182, 184–186]. Nevertheless, several types of initiators were able to perform polymerization of lactide.

3.3.1 Initiators with Alkali Metals

Studies concerning the AROP of lactide with alkali metals initiators were essentially conducted in the 1990s [187–202]. It was shown that strong bases were needed as carboxylates and phenolates were not able to initiate the polymerization [192]. On the contrary, potassium *tert*-butoxide and butyllithium allowed the polymerization of lactide with yields below 80 % and with the presence of racemization, transesterification reactions, and macrocyclics formation whatever the polymerization conditions [192]. Moreover, it was demonstrated that the initiation did not proceed through a nucleophilic attack of the strong base but through a proton abstraction from lactide to give an enolate which was the actual initiator of the polymerization (Scheme 16). After the nucleophilic attack of the enolate onto a lactide molecule yielding acyl cleavage, the active species responsible of the propagation was an alkoxide. Better results were obtained with primary and secondary lithium and potassium alkoxides as in this case the initiation proceeded mainly through the nucleophilic attack, but still uncontrolled molar masses were achieved (Scheme 16) [194, 201]. With potassium methoxide as the initiator, polymerizations were completed in less than 2 h in THF at room temperature allowing a good control of the molar masses with dispersities around 1.3 and low extent of racemization [188–190].

The addition of a crown ether onto potassium *tert*-butoxide or naphthalenide potassium revealed beneficial for the dispersity that dropped below 1.2 and for the reduction of racemization reactions but detrimental for the polymerization rate that slowed down dramatically [191, 196, 197]. Finally, it was demonstrated that the AROP of *rac*-lactide initiated by lithium *tert*-butoxide could yield to the synthesis of disyndiotactic polylactide (PLA), provided that yield remained quite low (below 35 %) [199, 200].
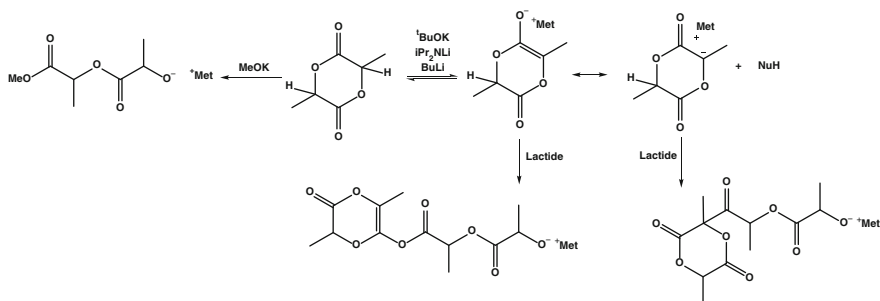
Scheme 16 Mechanism of AROP of lactide

In spite of some side reactions, many studies described the synthesis of block copolymers with at least one PLA block via AROP of lactide. For example, poly (ethylene oxide)-*b*-polylactide synthesis was highly investigated as these copolymers could be used in the biomedical field. They were either synthesized through the sequential AROP of ethylene oxide and lactide [203–212] or by the AROP of lactide using commercial poly(ethylene oxide)s [213–217]. Starting from a difunctional (macro)initiator, tri- [218, 219] and penta-blocks [220] copolymers were also produced. The sequential polymerization allowed also the synthesis of poly(ethylene oxide)-*b*-polyglycidol-*b*-polylactide copolymer [221]. Finally, the synthesis of polysaccharides-*g*-polylactide was described [222, 223].

3.3.2 Organocatalyzed Polymerization

Since 2001 and the description of the first nucleophilic organocatalyzed ROP of lactide [224], this field was highly investigated [225–228], with the use of imidazole [229], amines [224, 230], amidines [231], phosphines [232], phosphazene [233, 234], or *N*-heterocyclic carbenes (NHC) [235–250].

Tertiary amines and phosphines are among the simplest metal-free catalysts. The controlled ROP of lactide was thus performed in the presence of 4-dimethylaminopyridine (DMAP) or 4-pyrrolidinopyridine (PPY) in dichloromethane at 35 °C or in the melt at 135 and 185 °C yielding PLA with controlled molar masses and low dispersities [224]. The polymerization was proposed to proceed through a monomer-activated mechanism with a nucleophilic attack of the amine onto the lactide monomer resulting in a zwitterionic species that was attacked by the initiating or propagating alcohol chain end (Path A, Scheme 17). Nevertheless, computational calculation suggested that the propagation occurred preferentially through an alcohol-activated mechanism (Path B, Scheme 17).

Phosphazenes were described to also induce such an alcohol-activated mechanism to produce polylactides with predictable molar masses, low dispersities, and high chain-end fidelity [233, 234]. By analogy with cyclic ethers, one can ask about the mechanism implying the deprotonation of an alcohol by a phosphazene base and propagation through a phosphazenium alkoxide. With phosphines, polymerizations
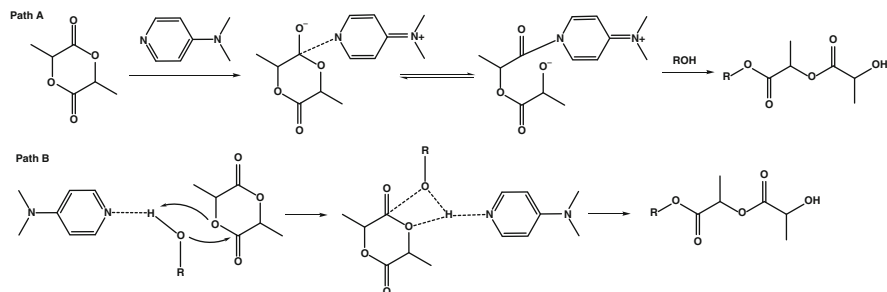
Scheme 17 ROP of lactide with tertiary amines
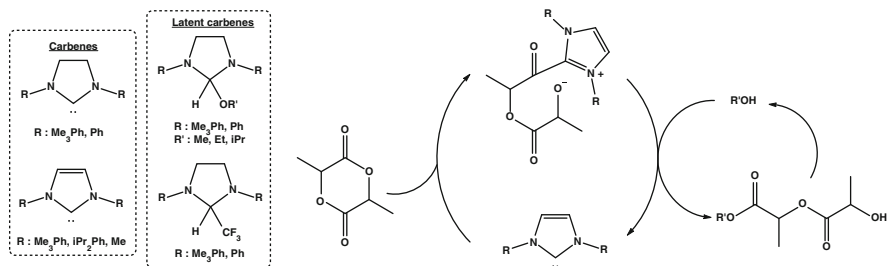
Scheme 18 Representative carbenes and mechanism of AROP of lactide

had to be conducted in bulk at high temperature to proceed with at least one equivalent of phosphine compared to initiator in order to control the polymerization [232]. A monomer-activated ROP mechanism comparable to that of tertiary amine was proposed for these catalysts. In the absence of any alcohol, it was shown that imidazoles [229] and amidines [231] were able to polymerize lactide in bulk at high temperature or in solution at room temperature, respectively. In both cases, it was shown that the catalyst was capable of nucleophilic attack onto lactide and that cyclic polylactides were almost exclusively obtained.

NHCs were also investigated as organocatalysts for lactide ROP. They proved to be active, with complete monomer conversion in a few hours at room temperature to afford PLAs with high and controlled molar masses and low dispersities [237, 242]. The mechanism is supposed to be an activated monomer mechanism (Scheme 18). NHCs can be obtained from ionic liquids, with the advantage that the use of a biphasic system (THF/ionic liquid) allowed an easy polymer and catalyst recovery [240, 242]. NHCs can also be produced in situ from thermally activated NHC adducts, but in this case, lactide racemization occurred [247]. Alcohol adducts of NHCs proved to act as single-component catalyst/initiators with various alcohols as initiators. Some of them are stable solids and readily release the alcohol and the carbene in solution at room temperature [248], whereas for some others, polymerization could only take place at 90 °C [236, 238]. In the absence of an alcohol, NHCs promoted the polymerization of lactide, and the propagating species was demonstrated to be a zwitterion [241, 245]. Under these conditions, exclusively cyclic PLAs with rather low dispersities and a good degree of control were obtained at room temperature. The presence of both even and odd numbers of lactate units deduced from Maldi-Tof analyses indicated the presence of transesterification reactions. Very recently, carbene carboxylates were able to perform the polymerization of lactide [235]. Finally, the use of bulky NHCs allowed the synthesis of highly isotactic and heterotactic polylactides from *rac*-lactide and *meso*-lactide, respectively, at low temperatures [244]. In aprotic conditions (absence of exogenous alcohol), it was shown that sparteine was able to perform the zwitterionic ROP of L-lactide from both nitrogen atom to end up with macrocyclic polylactide [251].
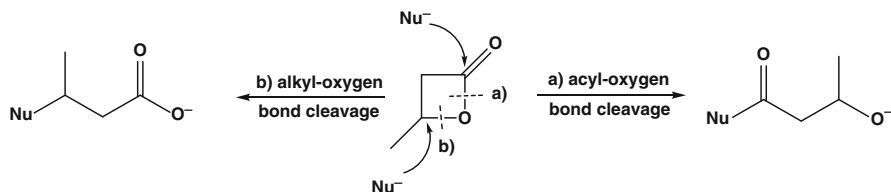
Scheme 19 AROP of four-membered lactones
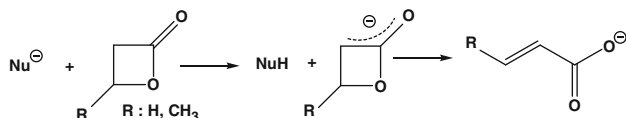
Scheme 20 Side reaction occurring during β-lactones polymerization

Finally, the ROP of *O*-carboxyanhydride catalyzed by NHCs yielded to the formation of polylactide with controlled molar masses and chain ends when the polymerization was performed at room temperature in THF [252]. Star-shaped structures were also successfully obtained.

3.4 *β-Lactones*

As polymer chemists would like to be able to synthesize polyesters that would resemble polyhydroxyalkanoates (PHA) that are natural polyesters produced by many bacteria [253], AROP of *β*-lactones was by far the most studied ROP of cyclic esters [188, 189, 193, 254–261]. Besides, *β*-lactones behave differently than other larger lactones due to their high polarity and high internal strain. Their polymerization can occur through the nucleophilic attack onto the carbonyl carbon or onto the carbon adjacent to the endocyclic oxygen atom (Scheme 19).

Another important difference from other lactones is the easy α-proton abstraction as a side reaction that would produce acrylate or crotonate ions that are also able to initiate the polymerization (Scheme 20). As a consequence, the control over the molar masses and chain-end fidelity could be problematic.

3.4.1 *β*-Propio- or *β*-Butyrolactone

Alkali Metal-Based Initiators

From the 1960s, the AROP of *β*-propiolactone (PL) was shown to be easily initiated by weak bases like alkali metal carboxylates but also by stronger bases such as alkali metal alkoxides. On the contrary, *β*-butyrolactone (BL) was shown to be
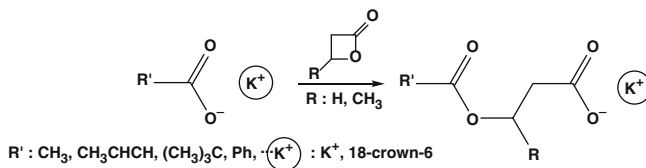
R' : CH₃, CH₃CHCH, (CH₃)₃C, Ph, ·(·K⁺) : K⁺, 18-crown-6

Scheme 21 AROP of β-lactones initiated by alkali metal carboxylates

(K⁺) : K⁺, 18-crown-6
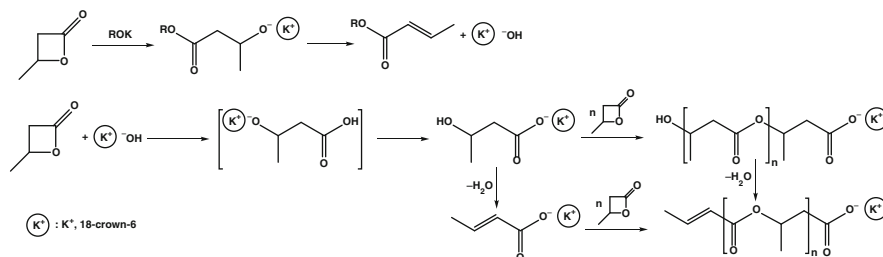
Scheme 22 AROP of β-butyrolactone initiated by metal alkoxides

polymerized by such bases only if they are activated by the addition of macrocyclic ligands (crown ethers or cryptands) [262]. When carboxylates salts were employed as initiating species, the polymerization of PL was not living as transfer reactions to the monomer occurred leading to side initiation by acrylate ions (Scheme 20). It was shown independently in 1976 by Penczek [263] and Boileau [264] that the introduction of crown ethers or cryptand could enable the living polymerization of PL (Scheme 21). Since then, many carboxylate salts were utilized as initiators [262, 265–275]. Polymerizations were generally performed in THF at room temperature with long reaction times (generally more than 100 h for BL).

When the polymerization of β-lactones was initiated by strong bases such as alkali metal alkoxides, active species involved in the propagation were highly debated in the literature [259, 274, 276–283]. Penczek and coll. suggested that, when polymerization of PL was initiated by potassium methoxide in DMF at room temperature, both acyl-oxygen and alkyl-oxygen bond could occur yielding alkoxide or carboxylate propagating species, as indicated in Scheme 19 [274, 276]. Nevertheless, as alkyl-oxygen bond cleavage is preferred, after few monomers addition, the only propagating species are carboxylates. Later, as double bonds were observed as chain ends, some other authors showed that initiation occurred through a nucleophilic attack at the carbonyl carbon atom of a monomer by the alkoxide anion of the initiator, cleaving the acyl-oxygen bond to yield the corresponding potassium alkoxide of the β-hydroxycarboxylic acid esters, followed by the formation of an unsaturated ester due to KOH elimination (Scheme 22) [259, 278–281]. Finally, KOH acts as the actual initiator of the polymerization, and block copolymers were obtained with this type of initiator [284].
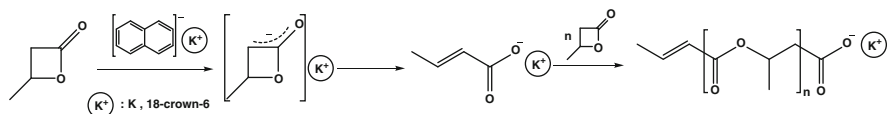
Scheme 23 AROP of β-butyrolactone initiated by naphthalenide potassium

In few examples, naphthalenide potassium was used as the initiator for the polymerization of β-lactones (BL, PL) in THF at 20 °C [262, 285, 286]. The initiation only occurred in the presence of a crown ether (18C6) or a cryptand ([222]), but even in this case, polymerization rate was very slow as more than 100 h or 10 h were needed to rich a conversion higher than 90 % for BL and PL, respectively, yielding polyesters with molar masses up to 10,000 g/mol with dispersities around 1.3. Concerning the mechanism involved with this type of initiator, as indicated on Scheme 23, it was demonstrated first the α-deprotonation of β-lactones followed by the ring-opening of the monomer yielding potassium crotonate for BL (or acrylate for PL) which is the actual initiator. Again, the active species are carboxylates. It is thus possible to produce macromonomer of BL or PL with a good control as the molar masses are in good agreement with the theoretical ones, and each chain bears a double bond at one chain end coming from the initiation step. In the same vein, very similar results were obtained with potassium hydride as the initiator in the same conditions [287].

Finally, potassium solutions (obtained from 18C6 THF solution in the presence of a potassium mirror) revealed also powerful initiators for the polymerization of β-lactones [285, 288–293]. When polymerizations were performed in THF at 20 °C, the polymerization rate was quite high (at least higher than with other anionic initiators) as PPL with 12,000 g/mol was obtained in 3 h. Very high molar mass PPL could also be obtained. For BL again, polymerization rate was much slower yielding atactic PBL with molar masses up to 6,000 g/mol in more than 100 h. As the polymerization is living, block copolymers of BL and PL were also achieved [291]. Again, concerning the mechanism and more specifically the initiation step, controversy can be found in the literature. The last suggested mechanism is depicted in Scheme 24. The initiation proceeds through a $2e^-$ transfer in two steps. After the first e^- transfer, an anion radical is formed, and after the second e^- transfer, the resulting dianion lactone is decomposed with the heterolytic cleavage of the acyl-oxygen bond. This compound deprotonates the monomer giving potassium enolate and potassium β-alkoxide aldehyde, this latter being unstable, it decomposes into crotonaldehyde and potassium hydroxide. Both potassium enolate and potassium hydroxide are able to generate initiators as indicated on Scheme 24. As a side reaction, the β-lactone anion radical can undergo a homolytic alkyl-oxygen bond cleavage yielding finally potassium butyrate that can also initiate the polymerization.

Few studies investigated the tacticity of PBL through anionic polymerization. Starting from racemic butyrolactone, mainly atactic PBL were obtained, whatever the initiating system [262, 270, 281, 287, 293, 294]. Nevertheless, it was also
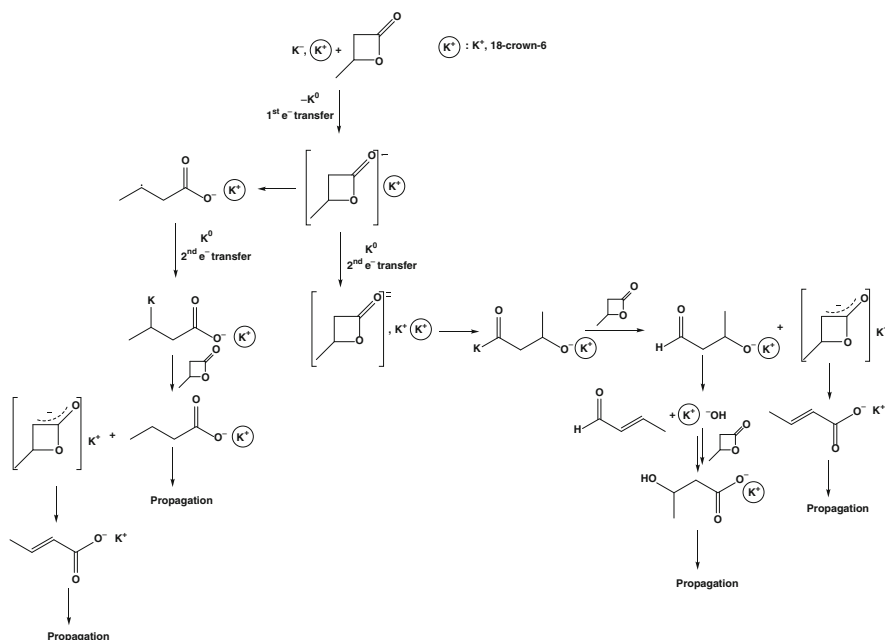
Scheme 24 AROP of β-butyrolactone initiated by potassium solution[288]

demonstrated that reducing polymerization temperature or adding tartrate esters could induce the synthesis of partially syndiotactic PBL (up to 60–65 %) starting from racemic butyrolactone [295, 296]. Finally, isotactic PBL were also synthesized efficiently using R-butyrolactone [295] (around 80–85 %) or S-butyrolactone [270, 273] (up to 95 %).

Organic Initiators

Organic bases, like phosphines, pyridines, tertiary amines, and betains, were among the first to be used for the initiation of β-lactones [259, 297–302]. It was first suggested that the initiation step involved the formation of betain species that are the actual initiator with active species being carboxylates. The propagation would then proceed via alkyl-oxygen bond cleavage yielding macrozwitterions [297, 298, 300]. Nevertheless, this was inconsistent with the respective nucleophilicity/basicity ratio of the engaged initiators, at least for amines. It was thus demonstrated that after the betain formation, the protonated base was released yielding acrylate or crotonate ions that were the actual initiators (Scheme 25) [299]. Eventually, PPL or PBL can be produced with unsaturated chain ends. In the case of phosphine, both phosphonium and unsaturated chain end were detected indicating the concomitance of both types of initiation [299]. These side reactions proved to be a limiting factor in the control over molar mass and molar mass distribution.
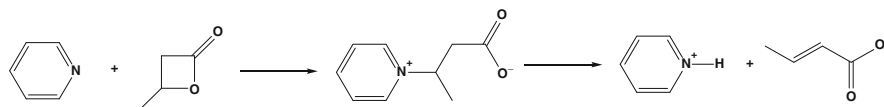
Scheme 25 Polymerization of β-butyrolactone initiated by organic bases
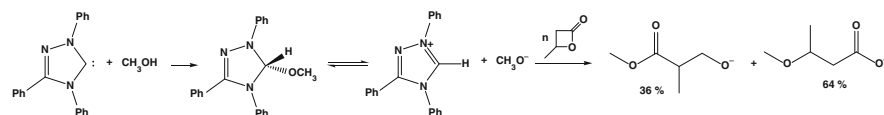
Scheme 26 AROP of β-butyrolactone initiated by triazole carbene
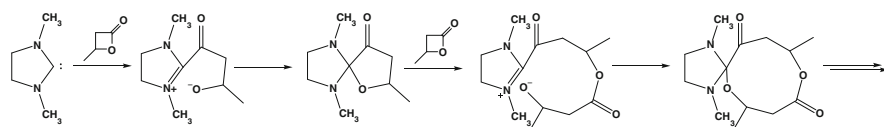
Scheme 27 Zwitterionic polymerization of β-butyrolactone initiated by a saturated carbene

More recently, other organic (co-)initiators, like carbenes [235, 236, 303], guanidine [304], amidine [304], and phosphazenes [304, 305], revealed powerful for the polymerization of β-lactones. Polymerizations initiated by a carboxylic acid/phosphazene base led to atactic PBL with good control over the molar masses, the polymerization rate being dependent on the basicity of the phosphazene used. With triazole carbenes, it was demonstrated that the polymerization of BL in toluene at 80 °C with methanol as the initiator was controlled for DP up to 200 with good chain-end fidelity (few crotonate chain end detected) in the presence of tert-butanol as the co-solvent [236, 303]. Concerning the initiation mechanism, it was shown that the initiator was deprotonated by the carbene, and it was thus an alkoxide that was the actual initiator (Scheme 26). Moreover, the propagation proceeded both via alkyl-oxygen or acyl-oxygen bond cleavage, yielding concomitantly alkoxides and carboxylates as active species. Nevertheless, the acyl bond cleavage being less favored, after a couple of monomer additions, carboxylates were the only active species.

Besides, with some other carbenes, the polymerization mechanism revealed different, yielding only cyclic polymers with a good control of the molar masses [306]. As spirocycles were formed all along the polymerization, it was proposed that 1,3-dimesitylimidazol-2-ylidene was able to perform a nucleophilic attack onto the carbon of the carbonyl group of BL yielding a zwitterion that ring-closed after each monomer addition (Scheme 27).
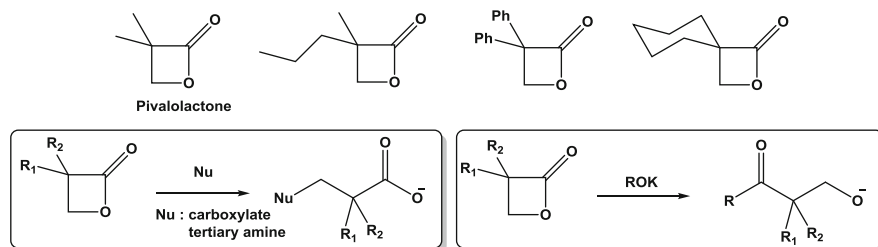
Scheme 28 Examples of α,α-disubstituted-β-propiolactones and propagating species depending on the initiating system

3.4.2 Other β-Lactones

α,α-Disubstituted-β-Propiolactones

The AROP of α,α-disubstituted-β-propiolactones (Scheme 28) was highly investigated, pivalolactone (α,α-dimethyl-β-propiolactone, PVL) being the most studied monomer [307–316]. Due to the absence of proton in α position compared to other β-lactones, the polymerization of α,α-disubstituted-β-propiolactones could be easily controlled, especially the chain ends, as the side reactions yielding crotonate or acrylate groups (Scheme 20) could not occur with these monomers.

In most of the studies, potassium or ammonium carboxylates were used as the initiating species, the propagating species being carboxylates in this case. When tertiary amines were the initiating species, again carboxylates were the propagating species [316]. On the contrary, when the initiator was a metal alkoxide, the propagation proceeded through an alkoxide, and the formation of macrocyclic structures was noticed [311, 312].

β-Substituted-β-Lactones

The AROP of β-substituted-β-lactones was also highly studied (Scheme 29) [317–345]. More specifically, researchers were interested in the monomers that could be precursors for the synthesis of poly(β-malic acid), which is a water-soluble, biodegradable, and biocompatible polymer that exhibits biological properties (proteinase inhibitor, for instance). Whereas this polymer is available from natural and/or bacterial resources, many studies deal with its chemical synthesis, especially since the first description of the synthesis of β-malolactonate in 1979 [346]. The racemic or the optically active versions of benzyl-β-malolactonate were the most studied monomers. Optically active polymers could be obtained (no racemization) with an inversion of the configuration [320].

Several types of initiators were able to polymerize β-substituted-β-lactones. With triethylamine, only low molar masses were obtained with poor control [337]. Great enhancement was achieved when tetraalkylammonium benzoate was
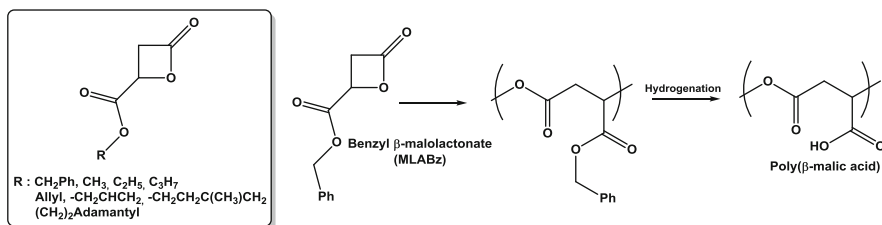
Scheme 29 Examples of β-substituted-β-lactones investigated in the literature

employed as the initiator. Polymerizations were generally performed in bulk at temperature ranging from 30 to 70 °C, but like for BL and PL, transfer reactions occurred through proton abstraction, preventing a good control over the molar masses and the chain-end fidelity [317, 318, 330, 340]. Transfer reactions were shown to be highly reduced when polymerizations were performed in THF at 0 °C, at low reactant concentration [330], or when monomers were highly purified [327]. Another possibility to suppress transfer reactions is to start from an α,1;α-disubstituted-β-substituted-β-lactones instead of β-substituted-β-lactones; as for pivalolactone, proton abstraction is no more possible in this case [319, 336, 343]. More recently, carbenes [236], phosphazenes [336, 344, 345], amidines [344, 345], and guanidine [344, 345] were described as efficient initiators for the polymerization of β-substituted-β-lactones. Nevertheless, the transfer reactions were still present. Despite the presence of transfer reactions, the synthesis of macromolecular architecture was possible since it was described the synthesis of block copolymers with the first block constituted of β-substituted-β-lactones and the second block constituted of another β-substituted-β-lactones [328], butyrolactone [317], lactide [334, 335], or caprolactone (CL) [330, 331, 334], these two latter being polymerized through organometallic catalyzed ROP. The synthesis of random copolymers was also performed [317, 322, 323, 326, 329, 332, 343], as well as the synthesis of graft copolymers [329, 332].

3.5 Larger-Ring Lactones

3.5.1 ε-Caprolactone and δ-Valerolactone

Polymerization Initiated with Alkali Metal Compounds

The AROP of other lactones was by far less investigated than that of β-lactones. The polymerization of CL could be initiated by metal alkoxides [264, 274, 279, 347–356], cyclopentadienyl sodium [357], phenyllithium [358], carbazole potassium [359], lithium diisopropyl amide [360], or sodium hydride [361]. Depending on the initiator, the initiation proceeded via monomer deprotonation (Path A, Scheme 30) or via nucleophilic attack, the monomer being opened at the acyl-oxygen bond and
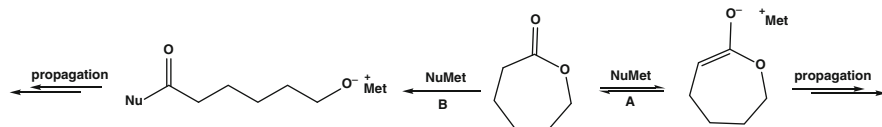
Scheme 30 Initiation step in the AROP of ε-caprolactone

the growing species being an alkoxide (Path B, Scheme 30). For example, using cyclopentadienyl sodium as the initiator, no cyclopentadienyl groups were present on the polymeric chain ends, and the polymerization is said to proceed through deprotonation of the monomer [357].

The main drawback of this method is the occurrence of significant intramolecular transesterification reactions, also called "back-biting," which were very dependent on the polymerization conditions and the initiator and resulted in the formation of generally low molar mass polymers and in cyclic polymers. For instance, it was demonstrated that with *tert*-butoxide potassium as the initiator, high dilution favored the formation of cyclics (less than 6–7 CL units) to the detriment of polymer formation [351, 352]. With cyclopentadienyl sodium as the initiator, in bulk and in nonpolar solvents, molar masses up to 130,000 g/mol were obtained, whereas in polar solvents, only oligomers were produced [357]. When the polymerization of CL was initiated with lithium diisopropylamide, medium molar mass polymers were obtained [360]. The polymerization of CL initiated by phenyl lithium in bulk at 170 °C led to high molar mass polymers (50–70,000 g/mol) [358]. Polymerizations performed in supercritical carbon dioxide exhibited low yields probably because of the occurrence of side reactions between the anionic species and carbon dioxide [350]. It was also demonstrated that alkali graphitides allowed the synthesis of very high molar mass polylactones with nevertheless the presence of a low molar mass fraction [362–368].

In spite of many possible side reactions and like for the other cyclic esters, the possible synthesis of poly(δ-valerolactone)-*b*-polylactide [188, 189, 369], poly (ethylene oxide)-*b*-poly(ε-caprolactone) [370], and polyglycidol-*b*-poly(-ε-caprolactone) [371] was described in the literature.

Organocatalyzed Polymerization

Few organocatalysts were shown to be able to perform the polymerization of lactones compared to lactide. Indeed, most of the studies employed carbenes [237, 242, 372–379], with few examples using phosphazenes [234, 380] or TBD [381]. With tBuP$_1$ or BEMP, in the presence of alcohols, only δ-valerolactone (δ-VL) was polymerized with high conversion in 2–4 days, whereas for ε-caprolactone only 15 % conversion was obtained after 10 days. On the contrary, with tBuP$_2$, CL was polymerized in few hours to yield PCL with controlled molar masses. NHCs were shown to polymerize both δ-valerolactone and ε-caprolactone giving access not only to linear but also to cyclic aliphatic polyesters. While the
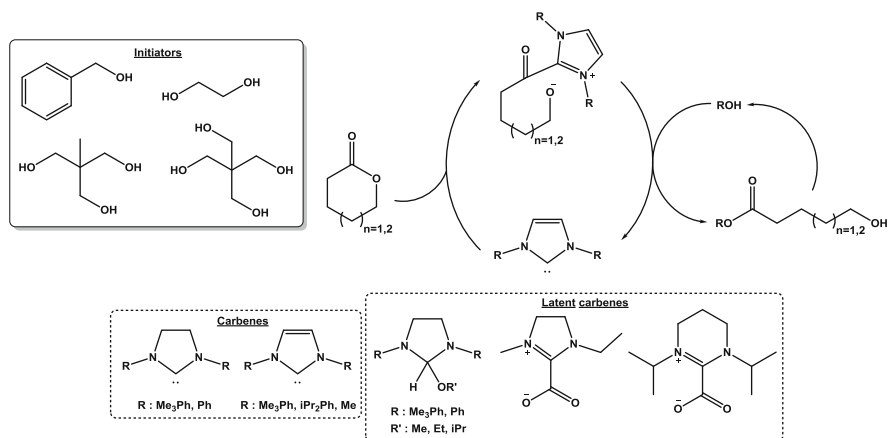
Scheme 31 Examples of initiators and carbenes employed for lactone ROP

NHCs were generally highly active in the polymerization of lactide, less efficiency was observed toward the ROP of CL. The mechanism is supposed to be an activated monomer mechanism, and several NHCs, either in their "bare" or masked form, were shown to perform the polymerization of lactones (Scheme 31).

The ROP of CL was generally performed at room temperature in THF solution (0.5–2.0 M), in the presence of monofunctional initiators or multihydroxylated initiators such as ethylene glycol, 1,1,1-tris(hydroxymethyl)propane, pentaerythritol, or a six-arm poly(propylene glycol) (Scheme 31), yielding well-defined linear or star polycaprolactone (PCL). Catalytic activity was sensitive to steric and electronic properties of the carbene, as more electron-rich and less bulky substituted carbenes were more active for the synthesis of well-defined PCL [242, 374]. A so-called "abnormal" NHC, in which the carbene center is no longer located between the two nitrogen atoms but between a nitrogen and a carbon atom, was reported to exhibit a high catalytic activity in the ROP of CL [376]. Again, like for lactide ROP, in the absence of alcohol, the polymerization was shown to be zwitterionic, and it was thus synthesized cyclic polycaprolactones at room temperature with relatively high dispersity (between 1.4 and 2.1) for a wide range of molar masses (41,000–114,000 g/mol) [372, 377, 378]. Copolymerization of CL and δ-VL led to the formation of cyclic copolyesters with a gradient microstructure due to the difference in the reactivity ratios between the two monomers, which is usually not observed with metal-based alkoxides [375].

3.5.2   Other Lactones

Some other lactones were shown to be polymerizable through AROP. For instance, bicyclic oxalactone (Scheme 32) could be polymerized with butyllithium to afford polymers of moderate molar mass and high dispersity [382]. The polymerization of
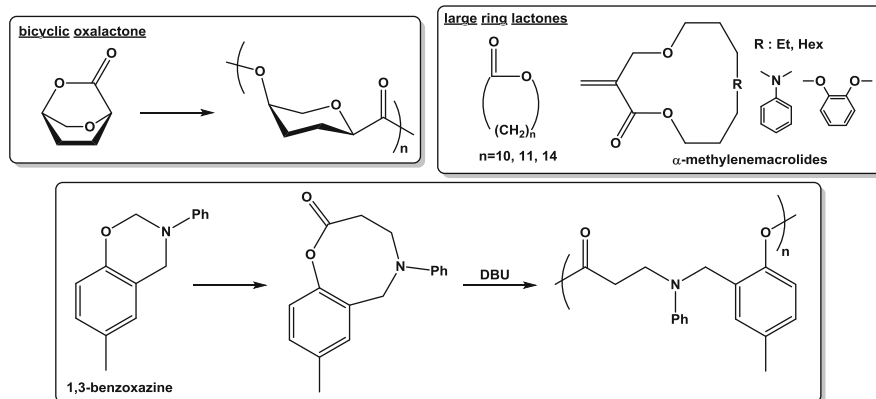
Scheme 32 Other lactones polymerized by AROP
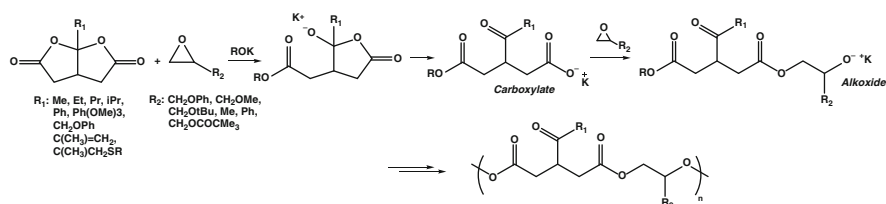
Scheme 33 Bis(γ-lactones) and epoxides for the synthesis of alternated copolymers

large-ring lactones (undecanolide, λ-lauryllactone, and pentadecanolide) was also performed in bulk at high temperature or in solution at moderate temperature in the presence of metal alkoxides [383, 384]. The presence of back-biting reactions leading to the formation of macrocycles was still detected. α-Methylenemacrolides were successfully polymerized with butyllithium at low temperature [385]. PEG-containing macrolactones were also successfully polymerized using thiols and tBuP$_4$ [386]. More recently, 8-membered lactones obtained from 1,3-benzoxazine were polymerized in bulk at high temperature in the presence of 1,8-diazabicyclo [5.4.0]undec-7-ene (DBU) yielding low molar mass polymers with high dispersity due to intensive back-biting reactions [387].

5-Membered γ-butyrolactones do not generally afford polymers because the rate of ring closure is faster than that of ring-opening, and therefore only insufficient formation of the corresponding polyesters was achieved. On the contrary, Endo et coll. showed that copolymerizations of bis(γ-lactones) with epoxides led to the synthesis of alternated copolymers (Scheme 33) [388–398]. This was possible due to the presence of an isomerizable structure onto the monomer that prevents backward ring closure. Concerning the mechanism, the bislactone reacts with alkoxide-type propagating chain end exclusively, to undergo double ring-opening reaction. The formed acyclic carboxylate is thermodynamically stable and thus does not undergo backward ring closure. At the same time, the nucleophilicity of
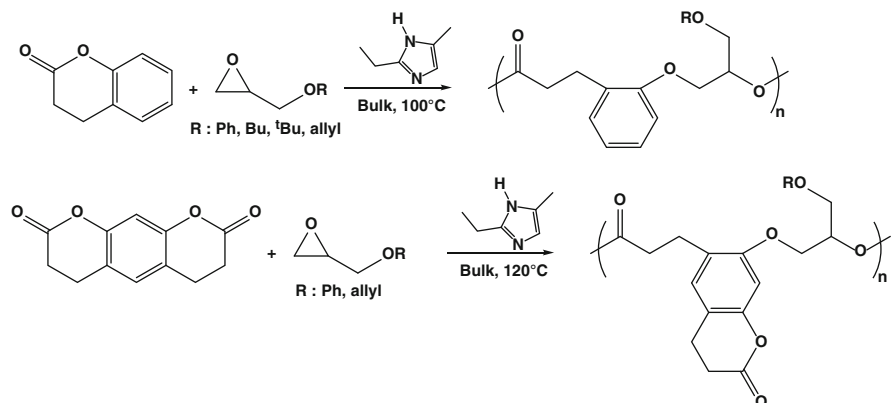
Scheme 34 6-Membered lactones and epoxides for the synthesis of alternated copolymers

the carboxylate is not high enough to react with the bislactone but is reactive with epoxide to regenerate an alkoxide. Moreover, as the formation of the copolyester synthesis was accompanied by low volume shrinkage during polymerization, such polymers are useful for network formation when bisepoxides were used. It was also shown that phosphines could replace alkali metal alkoxide to perform a zwitterionic polymerization.

The AROP of 3,4-dihydrocoumarin (DHCM, an aromatic lactone, Scheme 34) was also studied with an imidazole as the initiator in bulk at high temperatures (100–120 °C) [399–405]. Whereas DHCM is a 6-membered ring like δ-valerolactone, its homopolymerization was not possible. On the contrary, it was shown that DHCM was easily copolymerized with an epoxide to yield alternated copolymers. When the bislactone was copolymerized with epoxides, only one of the two lactones participated in the copolymerization yielding only linear polymers. Networks were only obtained by post-reaction of the remaining lactone with a diamine, for example.

4 Cyclic Amides (Lactams)

4.1 Introduction

Polyamides are well-known polymers that are present in markets such as fibers, engineering plastics, and specialties, due to specific and various properties depending on their structures. Ring-opening polymerization of lactams (cyclic amides) initiated by water, referred to hydrolytic polymerization (i.e., reactions between the amine chain-end group and the lactam and/or carboxylic group of its hydrolyzed derivative), is carried out for industrial polymerization of ε-caprolactam (ε-CL) to form polyamide 6 (PA6, Nylon 6), though nylon 6–6, 4–6, and 6–10 are

synthesized by stepwise reactions of a diacid monomer with a diamine monomer. Cationic initiation is also possible, but not useful because of the low conversion and molar mass of the resulting polyamides [406]. Anionic initiation following an activated monomer mechanism is mainly used for polymerization in molds in order to prepare polyamides (PA6, 10, 12) directly from the corresponding lactams [407]. Polymerization mechanism of lactams, their polymerizability, and the properties of the resulting polymers were largely investigated. Reviews published by Reimschuessel [408, 409], Šebenda [410], Sekiguchi [406], Hashimoto [411], Roda [412], and Russo and Casazza [413] can precise this presented overview.

The anionic route is the fastest method for producing polyamides due to the low activation energy needed. This fast kinetic makes nowadays this route of high interest for industrial processes producing lightweight composite materials for automotive and wind energy. The anionic polymerization of lactams may be accomplished in solution or in the bulk either below or above the melting point of the polymer for the latter.

4.2 Mechanism of the Anionic Polymerization of Lactams

The mechanism differs from the anionic polymerization of most of the unsaturated and heterocyclic monomers because the growth center is not an anionically activated end group but is represented by an N-acyllated neutral chain. The anionic polymerization of lactams is initiated, under anhydrous conditions, by formation of the lactamate anion. Strong bases are able to deprotonate lactams and produce N anion of lactam effective for initiating the polymerization.

4.2.1 Initiating and Activating Systems

The anionically activated species is the monomer in the form of lactamate anion which is a very strong nucleophile (Scheme 35). The negative charge is delocalized on the amide group due to resonance stabilization by conjugation with the carbonyl group.

The lactamate anion is acylated by a lactam monomer, although the acylating ability of the latter is poor, with the amide group being stabilized by resonance. The lactamate anion reacts with the monomer by a ring-opening transamidation reaction forming N-acyl lactam structures carrying primary amine anions. Assuming a free ion mechanism [414], the imide anion is formed, in the first slow step, by nucleophilic attack of the lactamate on the carbonyl of the lactam molecule (Scheme 36). As it is not stabilized by resonance, rapid proton exchange undergoes with lactam monomer, yielding imide dimer (N-acyl lactam) and regenerating the lactamate. Result of these two combined reactions is the disproportionation between two amide groups (present in lactam monomer and in lactamate anion) to give amine
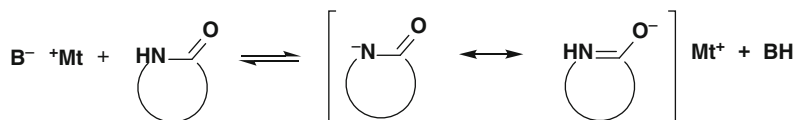
Scheme 35 Structures of the anionically activated monomer
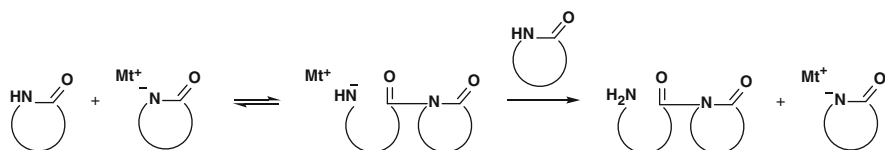
Scheme 36 Nucleophilic attack of lactamate to a lactam

and acyl lactam moieties (in the *N*-acyl lactam species) and the reaction rate dependent on factors like the nature of counterion and reaction medium, lactam ring size, substituents, and structure of the resulting linear monomeric unit. N-substituted lactams are observed to react with lactamate anion with a rate significantly higher than that of the initial reaction, depending on the size and the electrophilicity of the substituent, and are generally used as activators in the activated anionic polymerization. The use of high reaction temperatures (>250 °C) is required in the absence of activator, and only the more reactive lactams, such as ε-caprolactam, undergo polymerization in the presence of a strong base in a non-activated method.

The initiators, which are the monomers carrying the anionic charge able to attack the chain end, are prepared by reaction of a lactam with strong bases such as mainly metal alkoxide, metal halide, alkali metal, and Grignard reagent [406, 414, 415] but also pentamethylene guanidine [406], quaternary ammonium salts [416], phosphazene [417], bicyclic "superbase" protophosphatranes [418, 419], or carbenes [420, 421]. The association of a strong base (NaH, LiH, BuLi) with a reducing agent such metal dialkyl/dialkoxy aluminum hydrides [422–424] or metal dialkyl boron hydride [423] can also be used as precursors of lactamates. In this case, the nucleophilic species obtained, i.e., the activated monomer, is a metal salt of 2-(dialkyoxyaluminoxy)-1-azacycloheptan.

As usual in anionic polymerization, the nature and concentration of the initiator play a crucial role. The rate is directly related to the concentration of active species and in particular to the dissociation constant yielding free ions. It is known that the concentration of free lactam anion increases with temperature, starting to be predominant above 150 °C, alkali metal lactamates being considered completely dissociated at higher temperatures [425, 426]. The rate of polymerization becomes here independent of the nature of the cation. In general, the activity of alkali metals follows the order of electropositivity, except with Li and despite its highest ionization energy: $Na^+ < Li^+ < K^+ < Cs^+ = R_4N^+$. Lactamates of transition metals (e.g., Cr^{3+}) and other metals (e.g., Al^{3+}), exhibiting high electronegativity values and

having very low dissociation constants, hardly dissociate even at high temperatures. In the molten monomer medium, without solvating or complexing species, the lactamate dissociation depends on both the lactam properties (i.e., acidity, dielectric permittivity, donor-acceptor capability, substituents) and the electropositivity of the metal. For example, higher lactam permittivity, such as in ω-laurolactam as compared to ε-caprolactam, makes easier the salt dissociation [427].

An induction period and slow kinetics are observed with non-activated anionic polymerization of lactams, whereas opposite behaviors are obtained when an activator is added. The induction period is absent, and the AROP can be performed at much lower temperatures (130–180 °C for ε-CL) [410]. Poorly reactive lactams, such as 2-pyrrolidone and 2-piperidone, can be polymerized by initial reaction of monomers with an acylating agent. In this activated mechanism, the slow self-initiation step is strongly minimized to the detriment of a fast acylation reaction and propagation step. The interest to work with milder conditions for shorter times allows to strongly reducing side reactions, yielding more regular macromolecular chains. These observations are nevertheless dependent on structure and concentration of the activators. Many substances can be used such as N-substituted lactams (N-acyllactam (1) [428, 429] and carbamoyllactam (2) [430–434] with electronegative substituent (R) increasing the acylating ability of the cyclic acyl group), compounds capable of producing N-substituted lactams, under the conditions of the anionic polymerization (e.g., isocyanate (4), acid halides or esters (5), carbon dioxide (6)) [428, 435–437] and derivatives from side reactions (C-, N-, O-acylation) in low ring strain lactam monomers such as oxoamides type (8), N-acylamidine (3), and others (7) (Scheme 37).

4.2.2 Propagation Reaction

The slow formation of an N-acyllactam by reaction between monomer and lactamate ion ($k_i = 10^{-7}$ L·mol^{-1}·s^{-1} for sodium ε-caprolactamate at 160–190°C) [438] is followed by an extremely fast neutralization reaction, i.e., monomer deprotonation. For pyrrolidone at 35 °C and laurolactam at 160 °C, the rate constant of proton exchange (k_H) is 10^5 L·mol^{-1}·s^{-1} [439] and 10^2 L·mol^{-1}·s^{-1} [440], respectively, which prevent the process of ring-opening of lactam via an active chain-end (ACE) mechanism (i.e., $k_{p(ACE)} \sim k_i \sim 10^{-7}$ L·mol^{-1}·s^{-1}) (Scheme 38). The nucleophilic attack of the lactamate anion on the carbonyl group of the monomer is much slower than that of the carbonyl group in an N-acyllactam-type chain end ($10^{-1} < k_{p(AM)} < 10^3$ L·mol^{-1}·s^{-1}, $k_{p(AM)} = 68$ L·mol^{-1}·s^{-1} in the case of ε-caprolactam) [441], which refers to the process of ring-opening polymerization of lactam via activated monomer (AM) mechanism (Scheme 38).

The propagation step is therefore composed of a nucleophilic attack to the acyllactam-type growing chain end ($k_p < 10^3$ L·mol^{-1}·s^{-1}) and a subsequent very fast proton transfer from the monomer to the amidate ($k_H \sim 10^2$–10^5 L·mol^{-1}·s^{-1}) (Scheme 39). The neutral N-acyl lactam acts as the growth center at the chain end as the exocyclic carbonyl group in the N-acyl lactam increases the electron deficiency
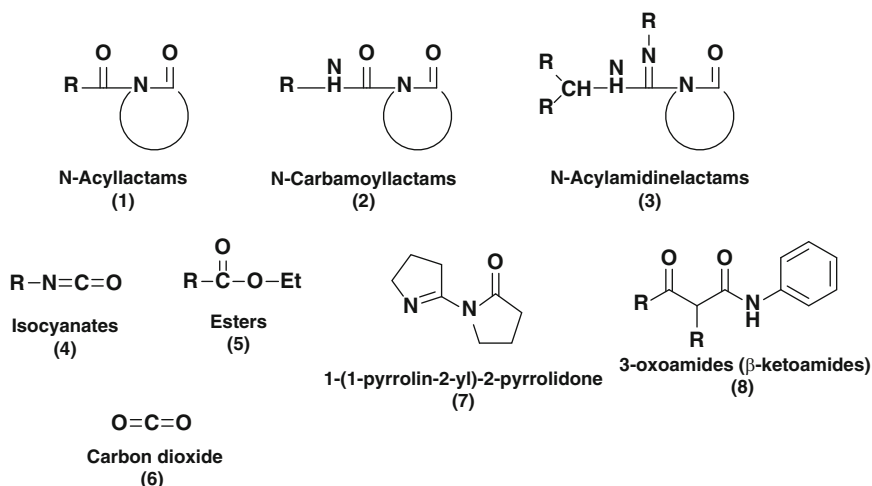
Scheme 37 Main activators in anionic lactam ring-opening polymerization
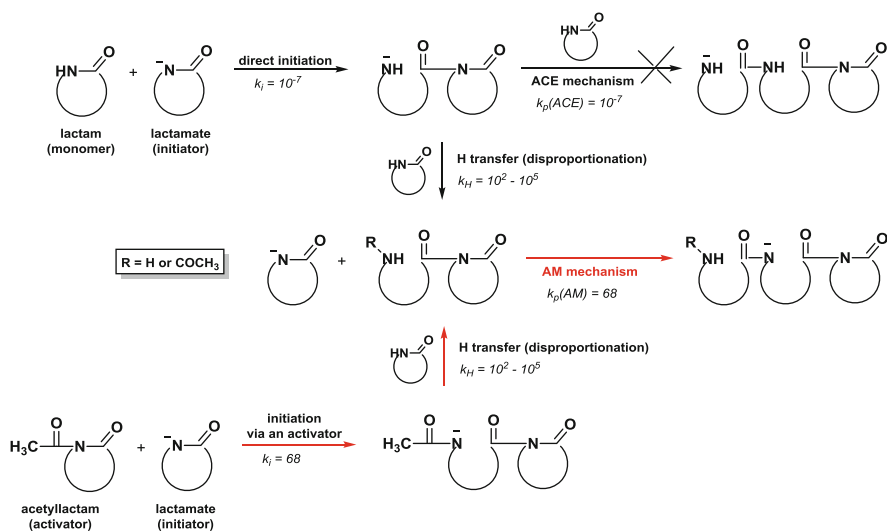
Scheme 38 Formation of active species in anionic ring-opening polymerization of ε-caprolactam: activated monomer (AM) mechanism vs. active chain-end (ACE) mechanism

of the amide group and, thus, the acylating ability. The polymerization rate is first order with respect to lactamate (L$^-$) and *N*-acyllactam (Act) concentrations and zero order with respect to lactam monomer (L) concentration [438] and can be written as follows .

$$-\frac{\mathrm{d}[L]}{\mathrm{d}t} = k_{\mathrm{p}}[\mathrm{Act}][\mathrm{L}^-]$$

N-acyllactam chain-end
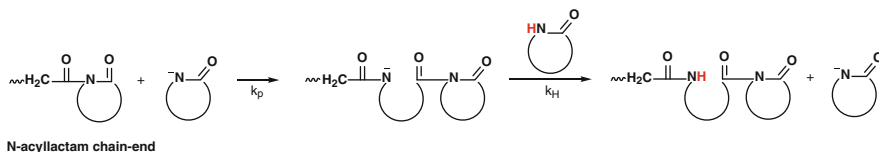
Scheme 39 Propagation step in anionic ring-opening polymerization of lactams via activated monomer mechanism

In the activated polymerization, the number average molar mass is determined by the concentration of the activator as compared to monomer concentration. Experimental values are generally higher than the theoretical ones. This is mainly due to the lowering of the number of growth centers due to the side reactions and to the cross-linking between polymer chains, for example, by Claisen-type condensation reactions, which are more and more relevant as the medium basicity and the polymerization temperature increase [442]. Such a polymerization is thus not living because of these side reactions. When the polymerization is run at temperatures below the melting point of the polyamide, side reactions are largely reduced, and, even at equimolar concentrations of initiator and activator, the polymerization proceeds essentially by the reaction of lactam anions with a constant number of growth centers, resulting in a narrower molar mass distribution ($D < 2$) [443] and the formation of high molar masses [434, 444]. In the non-activated polymerization where the growth centers are both formed at the very beginning and in the final stage, the molar mass distribution is expected to be broader than the ones observed with the use of an activator.

The structure of the activators, in particular the nature of the exocyclic acyl group in N-acyl lactam, was shown to play a crucial role on the polymerization rates [445]. "Very fast" activators, like of N-carbamoyl lactams in appropriate concentration, allowed to drastically reducing the polymerization time (less than a minute) [434, 446] to get high polymer yield, with the advantage to enable a decrease of polymerization temperature down to 140 °C, minimizing side reactions.

Concerning the mechanism, lactamolytic mechanism proposed by Sekiguchi [447–449] (Scheme 40a) assumes transfer of the alkali metal cation from the activated monomer species to the imide group at the end of the growing chain and its coordination to the carbonyls of the imide. A conductivity increase was attributed to a higher concentration of free ions. The reaction proceeds via formation of an alkoxide-type anion by nucleophilic attack of the lactam anion on the endocyclic carbonyl, proton exchange with monomer, and rearrangement with ring-opening. Alternatively, Frunze et al. [450, 451] proposed the participation of ion pairs of lactam salts in the propagation step and suggested an ion-coordination mechanism. According to this mechanism, complex between the lactamate and the two carbonyl groups of the growing center is formed (Scheme 40b). As already mentioned, side reactions are observed whatever the assumed mechanisms. In any case, free ions play a decisive role at high temperatures and in media of high
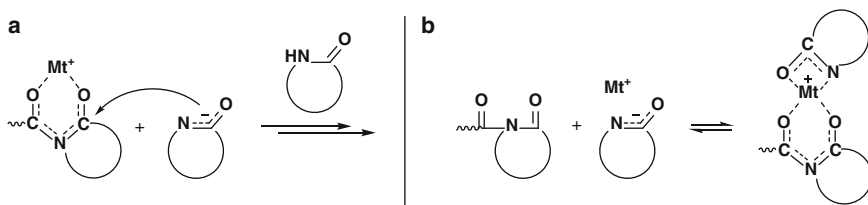
Scheme 40 Lactamolytic (**a**) and ion-coordinative (**b**) mechanisms

permittivity, while at low temperatures and in low polar media, the involvement of ion pairs is more expected.

4.2.3 Side Reactions

Species involved in anionic polymerization are generally highly reactive, leading to a series of side reactions, in particular at high temperatures for long polymerization times. Reversible and irreversible side reactions can occur, consuming both the growth centers and the monomer anions. The strongly basic conditions in AROP of lactams promote mainly polymer branching and β-keto compounds, yielding to side products and chain irregularities. UV spectrometry was shown to be a powerful tool for monitoring the occurrence of such side reactions [414, 442, 452].

Formation of Acyllactams, Amines, and Imides

The polymer amide groups may be involved in disproportionation reactions, forming acyl lactams and amine end groups (Scheme 41). The presence of amide N anions along the polymeric chain, derived from equilibrium reactions with lactam anions in strongly basic medium, may also produce imide groups and polymer branching (Scheme 41). Transacylation reactions between polymer amide anions and acyl lactams (N-acylations) (Scheme 42) may cause depolymerization or incorporation of a lactam unit when the exocyclic (Scheme 42a) or the endocyclic carbonyl groups (Scheme 42b) are involved. The nature of the counterion affects not only the degree of dissociation of the corresponding lactamates but also the whole polymerization rate [453].

Formation of β-Ketoimides and β-Ketoamides

The acidity of the hydrogen atoms in α position of the carbonyl of the imide group in the N-acyl lactam chain end is comparable to that of hydrogen in an amide group. As a consequence, in the presence of lactamate, deprotonation may occur, leading to the formation of two distinct carbanions (Scheme 43). The Claisen-type condensation reactions on exo- and endocarbonyls then happen, giving four different
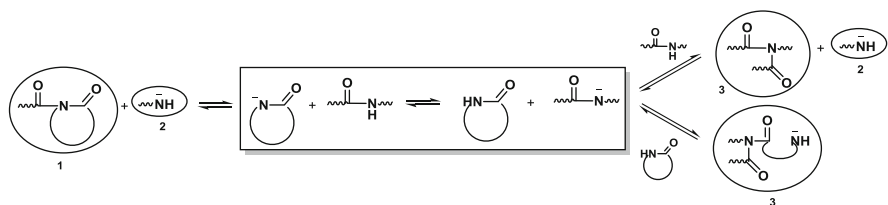
Scheme 41 Formation of acyllactam (*1*), amine (*2*), and imide (*3*) groups during AROP of lactams
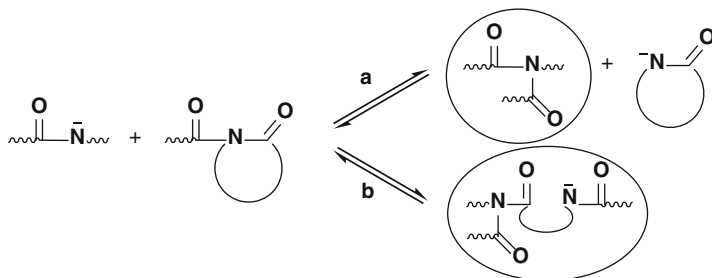
Scheme 42 Formation of imide groups by N-acylation
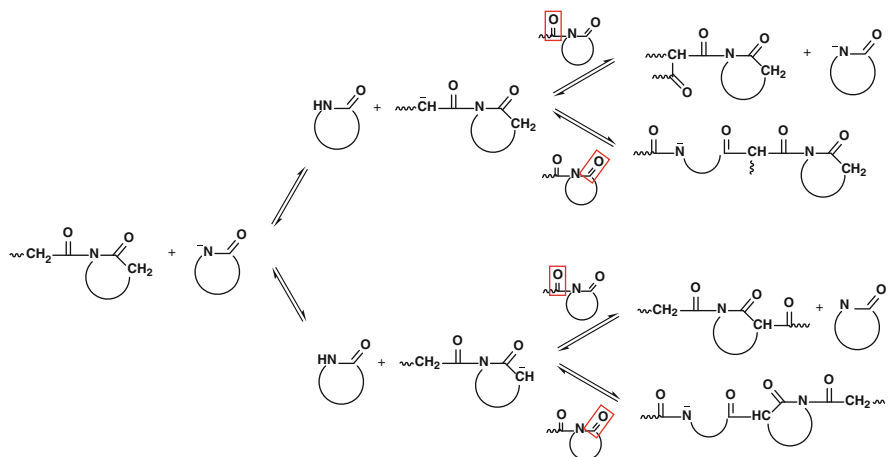
Scheme 43 Formation of carbanions followed by β-ketoimides during AROP of lactams

β-ketoimide structures. The concentration of these carbanions is generally low meaning that C-acylations and, only in some specific cases, O-acylations are competitive reactions with regard to the propagation step [454]. One can also consider the formation of carbanion in the α-position of the carbonyl of a branched structure. Reactivities are related to the lactam size and their substituents, the nature of the activator, the initial ratio of initiator and activator concentrations, the
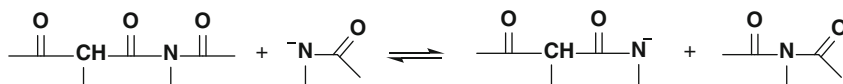
Scheme 44 Formation of a β-ketoamide from acylation of β-ketoimide
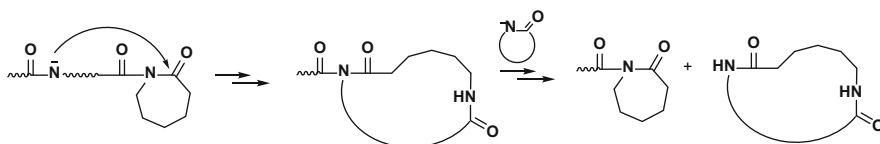
Scheme 45 Formation of cyclic oligomers by intramolecular reactions

permittivity of the reaction medium, and the reaction temperature as well as the nature of the counterion [454–456].

Neutral β-ketoimides are strong acylating agents and may be involved in reactions, acting as growth centers and leading to either linear or branched chains. β-Ketoimides may be converted to β-ketoamides (2-oxoamides) by nucleophilic attack of the N anion on the carbonyl of the imide group (Scheme 44). These keto derivatives decrease the concentration of active species and thus influence kinetics. They are also very reactive under basic conditions or at high temperatures and responsible for complex secondary reactions, i.e., formation of water, carbon dioxide, amines, and heterocyclic structures which are able to act as branching and cross-linking points [454]. The thermal or base-catalyzed decomposition of β-ketoamides can afford ketones and isocyanates. The latter reactive functions can also reform N-acyl lactams capable to react in the expected polymerization way. Formation of water can contribute to the deactivation of lactamate and to the hydrolysis of N-acyl lactams, β-keto compounds, and imide branching points leading to carboxylates, amine groups, ketones, carbon dioxide, or carbonates [410].

Formation of Cyclic Oligomers

The formation of cyclic oligomers was particularly investigated by Russo and coll. for ε-caprolactam [452, 457], their amount depending on the polymerization temperature (e.g., 3.5 % at 280 °C). The main reaction leading to cyclic oligomers is a back-biting reaction which is an intramolecular reaction of the neutral end groups with amidic groups inside the chain (Scheme 45). The counterion involved in the polymerization also directly influences the occurrence of such a side reaction [458]. With magnesium salts of ε-CL, cyclization reactions are strongly reduced both below and above the melting temperature of the polymer as compared to sodium systems, due probably to coordination between magnesium-based compounds and polyamides end groups. Cyclic structures can have a negative influence on processing or applications as they are able to modify the crystalline structure in the solid phase [459, 460].

4.3 Anionic (Co)polymerization of ε-Caprolactam and ω-Laurolactam

4.3.1 Homopolymerization of ε-Caprolactam and ω-Laurolactam

The polymerization of ε-caprolactam, a 7-membered ring, is usually conducted in bulk conditions, above the melting temperature of the monomer (80 °C) in the presence of initiator and activator. Initially liquid, the mixture turns turbid and then solidifies in the course of the polymerization which can be as fast as few tens of seconds for "very fast" systems. The beginning of solidification is considered as the moment at which the growing chains attain a critical length that enables their crystallization, forming spherulites insoluble in the monomer.

As discussed previously, playing with the structure and concentration of both activator and initiator allows tuning the polymerization rate of ε-CL. The initial polymerization temperature and isothermal, nonisothermal, or adiabatic conditions are also considered as tools to modify the time of reaction. "Very fast", "fast," or "slow" processes affect the structure and properties of the resultant anionic poly-amide 6. For a very fast bulk polymerization of ε-CL at 155 °C, conditions close to adiabatic ones are obtained due to high rate and poor heat exchange with the surroundings. A temperature increase of 50 °C is observed with a resultant polymer with high molar mass, low residual monomer content, and low cyclic oligomers [408, 434]. To decrease even more side reactions, quasi-isothermal conditions near 150–160 °C were proposed [433].

Similar polymerization systems and conditions were employed for the synthesis of polyamide 12 obtained by ring-opening of ω-laurolactam (ω-LL), a 13-membered ring. The polymer gained attention for its low level of absorbed moisture, easily removable during heating and melting of the monomer at 150 °C. Moreover, it possesses an excellent ductility, good electrical properties, and significant chemical resistance. However, due to the long methylene sequences between the amide linkages, it has a lower melting point (172 °C) compared to PA6 (210 °C). To get a low content of residual monomer due to favorable monomer-polymer equilibrium, temperatures above 150 °C are generally required [444, 461]. Some specific polymerization systems, based on alicyclic carbodiimide as activator and sodium caprolactamate as initiator, were also developed to allow, for instance, a long-term storage of the initiating species, an efficient control of the polymerization rate, and an accurate tailoring of polyamide molar masses [462]. As for ε-CL, initiation and activation influence also polymerization kinetics and thermodynamics but also the degree of crystallinity [463].

As discussed in the previous paragraph, the AROP of lactams suffers from numerous (ir)reversible side reactions, depending on the experimental conditions. The usual kinetic law depending on activator and initiator concentration ($R_p = -\mathrm{d}[M]/\mathrm{d}t = k_p \cdot f$ [Activator] [Initiator]$_0$) appears not efficient to get right values but might be sufficient to compare polymerization systems. The autocatalytic model of Malkin, based on a phenomenological approach, seems the most successful to

follow activated polymerization in bulk [464]. It describes the nonisothermal kinetics of both ε-caprolactam and ω-laurolactam, monitoring the temperature rise inside the reactor:

$$-\frac{d[\lambda]}{dt} = k\,\frac{[A]^2}{[M]_0}\,(1-\lambda)\left(1+\frac{b\lambda}{[A]}\right)\exp\left(-\frac{Ea}{RT}\right)$$

with λ the conversion, $[A]$ the activator concentration, $[M]_0$ the initial monomer concentration, k the reaction rate constant, Ea the activation energy, and b the autocatalytic term characterizing the intensity of the self-acceleration effect during chain growth. Both k and b depend on the chosen activator. The rate constant can be evaluated for low conversions where polymerization and crystallization are not overlapped.

4.3.2 Copolymerization of ε-Caprolactam and ω-Laurolactam

Anionic polymerization is well known and used for the synthesis of copolymers, in particular blocks, due to its living character. Despite the nonliving character of lactam polymerization, copolymers based on polyamide can be synthesized and offer interesting and specific properties. ω-Laurolactam is in general used as co-monomer of ε-caprolactam in order to extend the range of PA6 properties [429], in particular by increasing the notched Izod impact strength at low temperature, and the decrease of water absorption [465]. Roda and coworkers showed the influence of the initiator toward the copolymer structures and therefore properties [461, 466]. As compared to ε-caprolactam magnesium bromide, sodium caprolactamate exhibits higher polymerization activity especially in copolymerization with high content of ω-LL at high polymerization temperatures. The copolymers have only one melting endotherm in the whole range of monomer feed and one single crystalline form, when two melting endotherms (140 °C and 210 °C) and two types (α and β) of crystalline forms are observed from 30 to 70 mol% of ε-CL with the magnesium-based initiator. This is explained by a copolymer microstructure composed of PA6 blocks linked to sequences of ε-CL/ω-LL random copolymer. PA6 is preferentially formed at the beginning of the polymerization, due to the much higher reactivity of ε-CL as compared to ω-laurolactam. Random copolymers are then formed from the remaining ε-CL and slowly reacting with ω-LL. In the case of sodium caprolactamate which is a strong base as compared to the magnesium derivative, transamidation reactions cause full randomization of the sequences.

4.3.3 Copolymerization of Lactams and Lactones

Interesting degradable polyamides could be obtained through the synthesis of polyesteramides by copolymerizing lactams and lactones even if different anionic ring-opening mechanisms are involved in their homopolymers formation
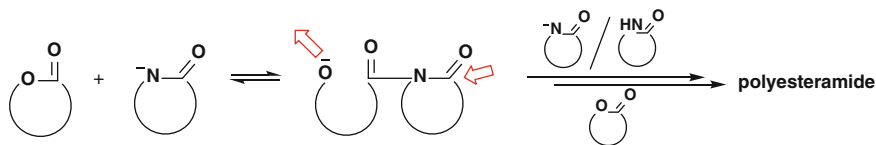
Scheme 46 Parallel initiation of lactams and lactones in the presence of lactamate

[412]. Some lactones were shown to act both as activator of lactam polymerization and as co-monomer for the synthesis of a polyester block [436, 467–469]. The initiation step corresponds to the acylation reaction between a lactamate and the reactive lactone (Scheme 46). The oxyanion formed is then able to initiate the rapid ring-opening polymerization of some cyclic esters such as ε-caprolactone or δ-valerolactone by usual chain growth mechanism (active chain end).

Playing with ε-caprolactam and ε-caprolactone ratios as well as experimental conditions, various random or multiblock copolymers were prepared. Fast transacylation reactions between ester and amide groups in the copolymer chains were proposed to be responsible for the observed copolymer randomness. Using reactive processing like a twin-screw extruder, diblock or triblock copolymers were prepared from various lactams and lactones using suitable sequential monomer feeding and specific temperature profiles [470–472]. The block lengths can be adjusted by controlling the feed rate. The use of poly(ε-caprolactone) (PCL) was also proposed as additive to the polymerization of ε-CL with ε-caprolactam magnesium bromide as initiator, with or without activator. PCL was shown to act as an activator, and random copolymers were prepared [473].

4.3.4 Polyamide-Based Copolymers with Non-polyamide Blocks

The use of macroactivators obtained from appropriately terminated prepolymers is the main route leading to lactam-based block copolymers. In general, hydroxy telechelic polymers are reacted with diisocyanates and then blocked with ε-CL. Combination of properties is the driving force of reacting various non-polyamide blocks as activators of anionic lactam polymerization. The toughness improvement of PA6 being a key issue, soft polymers such as polybutadiene [474–477], polyethers [478–483], and polysiloxanes [480, 484, 485] were particularly used. Following a similar approach, Styrene-Butadiene Rubber was also introduced into PA6 with the aim to tune the mechanical properties [486]. Graft copolymers were also designed for compatibilization purpose. Polypropylene or polystyrene grafted with polyamide-6 chains was easily obtained [430, 487–490].

4.3.5 Industrial Processes Using AROP of ε-Caprolactam and ω-Laurolactam

Ring-opening polymerization of ε-caprolactam initiated by water, i.e., the hydrolytic mechanism, is carried out for industrial cast nylon-6. Nowadays, due to fast kinetics of the "activated" anionic ring-opening polymerizations, this approach is more and more envisaged for the preparation of PA6 and PA6-co-PA12 in newly developed industrial applications using mainly powdered materials and molding or extrusion approaches.

Powdered Polyamides

As compared to techniques industrially utilized so far, i.e., low-temperature grinding and polymer dissolution/precipitation, AROP yielding PA6 and PA6-co-PA12 offers some advantages such as a much higher particle porosity, a total absence of irregular edges and sintered zones, and a controlled and narrow particle size. Dispersion [491–496], suspension [497], and miniemulsion [498] polymerizations are generally proposed. More recently, the use of phase inversion in PA6/PS blends allowed the preparation of microspheres with controlled diameters [499]. Fast polymerization systems have to be selected for such processes. The suspension method has the advantage to be the faster but suffers from difficult and expensive purification. Such materials are of great interest for cosmetic formulations, coating and graphic art applications, protein or enzyme immobilization techniques, rotational molding and sintering processes, chromatography applications, as well as filtration devices in food and beverage industry.

Molding and Extrusion

Reaction injection molding (RIM), resin transfer molding (RTM), rotational molding, and reactive extrusion are the main processes used with an in situ activated anionic polymerization of ε-CL [500, 501]. Due to its high crystallinity and high molar mass, anionic PA6 exhibits, for instance, better thermomechanical properties or lower water uptake as compared to the extruded or molded PA6. The short polymerization times in the order of minutes, as compared to hours for hydrolytic polymerization, the very low cyclic oligomer content, and the much lower initial polymerization temperature (130–170 °C vs. 230–280 °C) are the main advantages of this activated AROP.

Soft polymers bearing terminal *N*-acyl lactam groups are used in RIM processes as activators of ε-CL polymerization yielding PA6 with good impact strength. Usual initiators such as sodium ε-caprolactamate or magnesium bromide ε-caprolactamate are efficient in that process [502]. RTM enables the injection of the melted monomeric reactants of low viscosity into a mold filled with reinforcing

materials like fibers. Reactive extrusion processes regain also attention for the easy preparation of nanocomposites and nanoblends [501, 503–506]. Single- or multiwalled carbon nanotubes and nanosilica are also shown to be dispersed in PA6 modifying its initial properties [507, 508]. Nevertheless, it has to be mentioned that anhydrous conditions are required and may sometimes be considered as a limitation. Deactivation of the anionic groups is known to occur when some clays are used as reinforcing agents.

4.4 Anionic Polymerization of Other Lactams

β-Lactams, 2-pyrrolidone, and 2-piperidone are the three main unsubstituted lactams available and studied by AROP. They are, respectively, yielding polyamide-3, polyamide-4, and polyamide-5. It has to be noticed that N-substituted polyamide-1 as well as polyamide-2 (polypeptide) is not obtained from lactams but from oxadiazolinones and N-carboxyanhydride, respectively.

4.4.1 β-Lactams

Living anionic polymerization can be reached as substituted β-lactams (or -β-propiolactams) (Scheme 47) are highly reactive, due to high ring strain, enabling thus the use of low polymerization temperatures and times. The review of Hashimoto published in 2000 describes in detail the specificities of the ring-opening polymerization of such monomers [411].

Šebenda et al. showed first that the activated anionic polymerization of a bulky β-lactam, i.e., 3-butyl-3-methyl-2-azetidinone, has a living character giving a monodisperse polyamide of molar mass very close to the theoretical value [509, 510]. Other substituted monomers were also polymerized in a controlled manner in homogeneous solution, using aprotic and apolar solvents like N,N-dimethylacetamide, DMF, or DMSO in the presence of lithium salts [511–513]. Depolymerization and transamidation both at the acyl lactam chain end and on the polyamide chain are known to occur, therefore broadening the molar mass distribution [411]. Stopping the reaction before complete conversion minimizes the transamidation, enabling the preparation of block and graft copolymers or other structures taking advantage of the living character of the polymerization. The possibilities to play with substituents offer nowadays PA3 materials with amphiphilic character and possibly bioactivity, for instance [514].

Scheme 47 Structures of β-lactams
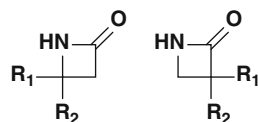
Scheme 48 Structure of
2-pyrrolidone
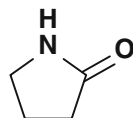
4.4.2 2-Pyrrolidone

The particularity of the polymerization of 2-pyrrolidone (Scheme 48), leading to polyamide-4, can be found in a rather low ceiling temperature (70 °C) limiting the reaction temperature to 50 °C [515]. In bulk conditions, economically more interesting than in solution, polymerization rate decreases with time, and partial conversion is obtained due to a phase separation, nucleation, and crystallization with occlusion of the growth centers in this solid phase [516–518]. Despite some potential industrial interests in textile for its good mechanical properties and hydrophilic behavior similar to cotton, synthesis difficulties are one main reason for its non-development.

Similar to ε-caprolactam polymerization, CO_2 was also proposed as activator to successfully prepare PA4 with an improved thermal stability [435, 519]. But depolymerization still remains a major drawback. Using quaternary ammonium salts of 2-pyrrolidone as initiator, instead of sodium or potassium ones, and *N*-acetyl-2-pyrrolidone as activator, yields up to 80 % could be obtained after 24 h at 30 °C [416]. It is assumed that bulky counterion allows the breaking of hydrogen bonds between polymer chains and creates local irregularities of the crystalline structure, enabling the contact between lactamates and reactive chain ends. Suspension polymerization can also be used [520], and whatever the process used, polyamide-4 was obtained free of structural irregularities thanks to the low polymerization temperature and limited conversions. Block copolymers containing PA4 segments could be obtained using the macroactivator approach [521]. The synthesis of PA4 with a terminal azide function [522] or with ε-CL as co-monomer above the ceiling temperature of 2-pyrrolidone was also performed [523, 524].

4.4.3 2-Piperidone

The ring-opening polymerization of 2-piperidone, also called 2-piperidinone or δ-valerolactam, is kinetically slow due to its stable 6-membered ring [406] (Scheme 49). Moreover, crystallization and side reactions contribute also to the slowness of the reaction. The use of activators is mandatory, and relatively high molar masses of PA5, with a melting temperature of 283 °C, were obtained with quaternary ammonium salts of monomers used as initiators [516, 525].

The use of bicyclic lactams is proposed as an alternative, the ring strain being favorable to a faster AROP.

Scheme 49 Structure of
2-piperidone
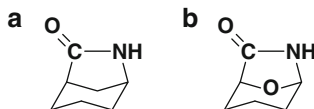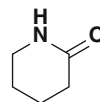
Scheme 50 Structures of a bicyclic lactam, i.e., 6-azabicyclo[3.2.1]octan-7-one (**a**) and of a bicyclic oxalactam, i.e., 8-oxa-6-azabicyclo[3.2.1]octan-7-one (**b**)

4.4.4 Bicyclic Lactams

The key point in the AROP of bicyclic lactams is indeed the ring strain, coming, for instance, from the repulsion of hydrogen atoms, and its release. At first, Hall reported in the 1960s the polymerization of a bicyclic lactam, i.e., the 6-azabicyclo[3.2.1]octan-7-one (Scheme 50a), in the presence of sodium hydride [526, 527]. Hashimoto proposed a detailed review in 2000 relative to bicyclic and heterobicyclic lactams [411]. High temperatures are generally required limiting the livingness of such polymerizations. For the case of bicyclic oxalactams (Scheme 50b), the polymerization could be run at 25 °C in DMSO due to a high kinetic polymerizability related to the high strain of internal bond angles [528, 529]. A living character was observed till 60 % of conversion.

5 Cyclosiloxanes and Other Cyclic Silicon-Based Compounds

5.1 Introduction

Cyclic silicon-containing monomers associated, or not, with oxygen, nitrogen, and carbon represent the main reactants toward the synthesis of silicon-based polymers by anionic polymerization. Their ring-opening leads to polysiloxanes and polycarbosiloxanes, polysilanes and polycarbosilanes, polysilazanes, and a few other silicon-containing polymers. The possibility to vary the molecular structure, of both the main chain and the side groups, enables the modulation of unique physicochemical properties which make them attractive in academic field as well as for industrial applications in some cases. Ring-opening polymerization (ROP) of cyclic oligomers allows in general a better precision in terms of chain lengths and molecular weight distributions than the polycondensation of functional precursors. Both cationic and anionic mechanisms can undergo polymerization of certain monomers, but a stringent control of the reaction conditions is required in order

to avoid the formation of by-products, such as short oligomers and rings [530]. Recent reviews [531–534] may add complementary information to this chapter focusing on silicon-containing polymers obtained by anionic polymerization. ROP of strained rings exploits the release of ring strain as the thermodynamic driving force [535]. It proceeds either by kinetic or thermodynamic control, which has noticeable consequences for the product distribution. Under kinetic control, the selective cleavage of the precursors and chain propagation occur almost exclusively, providing high molar mass polymers and barely any by-products. Under thermodynamic reaction control, equilibrium mixtures are obtained which generally consist of low molar mass polymers and high amounts of smaller oligomers and ring species.

5.2 Cyclosiloxanes

5.2.1 Polymerization Generalities

Anionic ring-opening polymerization (AROP) of cyclosiloxanes involves the cleavage of the Si-O bond in the monomer ring and the subsequent regeneration of this bond in a polymer chain. Among the various siloxane monomers, the two most important are hexamethylcyclotrisiloxane (D3) and octamethylcyclotetrasiloxane (D4) (Scheme 51).

Other cyclosiloxanes derived from these monomers are also available by substitution of methyl with various organic groups, such as vinyl, phenyl, fluoroalkyls, etc. Three-dimensional structures, i.e., silsesquioxanes or multicyclic siloxanes, are also available and attractive precursors. Cyclic organosiloxanes are usually prepared by hydrolytic polycondensation of dichlorodialkylsilane (R_2SiCl_2) or a mixture of α,ω-dichlorooligosiloxanes ($Cl(R_2SiO)_{n-1}R_2SiCl$) [536, 537]. Other routes are also proposed in the literature [538–540].

Initiation step requires strong bases (inorganic, organic, or organometallic), able to ring-open cyclosiloxanes and form silanolate anion, the active propagating species (Scheme 52). Alkali metals, ammonium, and phosphonium salts are the most used derivatives [533, 541]. The propagation is reversible leading to a back-biting reaction with the formation of cyclic structures of various ring sizes. Chain redistribution also occurs due to the nucleophilic attack of a silanolate to another growing polymer chain (Scheme 53). To get nonequilibrium AROP of

Scheme 51 Structure of hexamethylcyclotrisiloxane (D3) and octamethylcyclotetrasiloxane (D4)
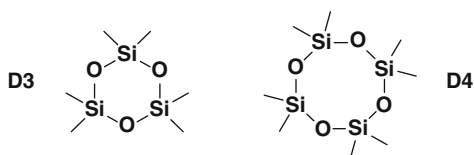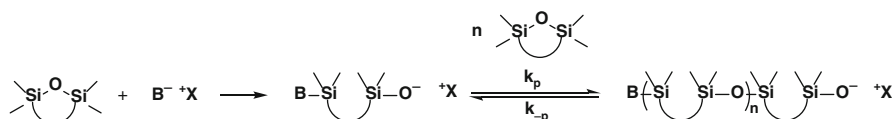
Scheme 52 Initiation and propagation/back-biting of cyclosiloxanes by AROP
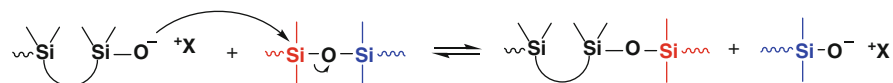
Scheme 53 Chain redistribution in AROP of cyclosiloxanes

cyclosiloxanes in order to minimize those re-equilibration reactions occurring during the final stage of the reaction, the polymerization must be quenched soon after a high monomer conversion is obtained [542].

Polymerization kinetic is dependent on monomer and initiator concentrations as well as experimental conditions. Ion pairs are the main active centers involved in the determination of the polymerization rate [533]. Free silanolate anions are not present in sufficient concentration to play a role, in contrary to aggregated species which are in equilibrium with ion pairs [533, 543, 544]. Fractional order in silanolate is introduced in the kinetic law of AROP of cyclosiloxanes due to the existence of less reactive or inactive aggregates.

The aggregation phenomenon can be minimized when bulky cations or additives are used. The polymerization of D3 initiated by trimethylammonium salts shows a first-order kinetic [545]. The rate of polymerization is directly related to the size of the counterion and increases in the series: $Li^+ < Na^+ < K^+ < Rb^+ < Cs^+ \sim {}^+NR_4 \sim {}^+PR_4$ [546]. Hexamethylphosphorous triamide, dimethylsulfoxide, dimethylformamide, N-methylpyrrolidone or cryptands, and crown ethers were shown to act as deaggregating agents [547–553]. Ring strain affects also the polymerization rate constants with the following order: D3 >> D4 > D5 > D6. Cyclotrisiloxanes show a remarkable high reactivity thanks to its ring strain and planar conformation [554]. Nevertheless, unexpected enhanced reactivity was observed with unstrained cyclodimethylsiloxanes in the order D4 < D5 < D6 < D7 < D8 when alkali metal were used in bulk or nonpolar solvents [533, 555, 556]. Multidentate interactions of siloxane units of the monomer with the counterion can explain this observation (Scheme 54). Lithium derivatives such as silazane lithium salts $((RMe_2Si)_2NLi)$, in the presence of promoters such as DMSO, were shown to initiate the AROP of D4 at elevated temperatures in high yields. The resulting polymers exhibited relatively narrow distribution which broaden gradually with time [557]. Propagation in this system is faster than the redistribution reactions, which lead to equilibration.

Organic initiators were more recently proposed for the AROP of cyclosiloxanes. Phosphazene bases, i.e., t-BuP$_4$, acts as a deprotonating agent of a proton donor
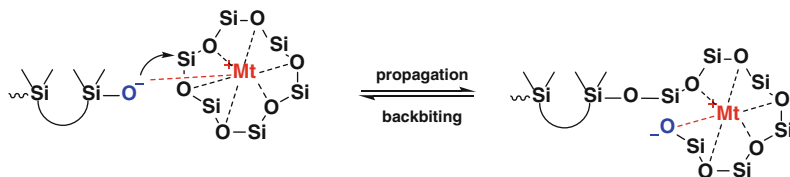
Scheme 54 Multidentate interactions of D6 with alkali metal in bulk
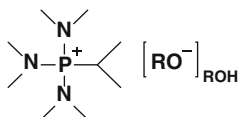
Scheme 55 Deprotonated alcohols by phosphorus ylides for the initiation of AROP of cyclosiloxanes

molecule such as an alcohol, leading to the formation in that case of an alkoxide of phosphazenium. Its bulkiness and stabilized positive charge, thanks to the resonance effect, enable an instantaneous polymerization of D4 [101, 558]. Similarly to the chemistry developed with cyclic ether monomers, the combination of lithium and phosphazene bases is also very efficient for the polymerization of cyclic siloxanes [559]. Within the same family, the direct use of amino-substituted oligophosphazenium hydroxides (P_5OH) enables to get polydimethylsiloxane in toluene with a first order both in monomer and base, and a faster rate than lithium cryptate systems [549, 560, 561]. Alcohols deprotonated by phosphorus ylides [562] were also proposed as initiators of D4 with the particularity to be thermolabile, facilitating its removal from the final polymer (Scheme 55). N-heterocyclic carbenes expressed also some interests thanks to the presence of alcohols as co-initiator and regulator of chain length [563].

Although polysiloxanes are not ordinarily considered stereoregular, some polymers enriched in stereoregularity are made from the cis-isomers of unsymmetrically substituted strained cyclosiloxanes. The monomers insert randomly at the reactive chain ends with equal probabilities of forming meso or racemic siloxane links while preserving the stereoconfiguration of the original monomer [564]. An advantage of stereoregularity was shown on the mechanical properties of a silicone elastomer [565].

5.2.2 AROP in Solid State and Emulsion

These two processes can be used both in anionic and cationic ROP of cyclosiloxanes. The discussion will focus on the parameters and consequences of the anionic route.

A simple approach based on crushed potassium hydroxide or potassium silanolates added onto a cyclosiloxane gives high molar mass polymers with high dispersity and high yields [566–569]. Polymerization proceeds inward from the surface of the monomer crystals, producing a highly crystalline material. The highly ordered crystalline state of hydroxycyclosiloxanes provides a possibility of solid-state synthesis of stereoregular polysiloxanes.

Polymerization in emulsion is also proposed to conduct anionic polymerization of cyclosiloxanes [532]. The synthesis of poly(dimethylsiloxane) from D4 in aqueous emulsion using an emulsifying agent acting also as initiator (benzyldimethyldodecylammonium hydroxide) gives controlled molar mass, a low dispersity and high yields [570, 571]. The amount of cyclics formed (essentially D4–D7) is lower than that observed in bulk. Polymerization proceeds by a combination of the addition and condensation mechanism involving redistribution reactions. The first stage of the anionic polymerization process occurs at the siloxane-water interface or in the siloxane phase close to the surface. Once the chains reach a critical degree of polymerization corresponding to their loss of surface tension activity, they penetrate into the particles where side reactions such as redistribution and condensation occur. The rate is strongly dependent on the size of the surface, which is function of the concentration of emulsifier. Polycondensation is responsible for a rapid increase in molar mass observed at high monomer conversions. Another α,ω-dihydroxy-terminated polysiloxane of low molar mass, issued from the polymerization of 2,4,6-trimethyl-2,4,6-tris(3,3,3-trifluoropropyl)cyclotrisiloxane with an anionic miniemulsion process, was also obtained [572]. The kinetic study showed that polymerization occurs in two stages. During the first stage, which corresponds to the nonequilibrium AROP, the maximum yield is close to 100 %, and the dispersity remains narrow (1.3). The second stage involves condensation and back-biting reactions leading to an increase of both molar masses, up to 60,000/mol, and dispersity (2.0). This approach was developed for other homopolymers [573] and copolymers [574].

5.2.3 Copolymerization and Functionalization

Anionic ring-opening polymerization offers possibilities in the controlled synthesis of functionalized polysiloxane polymers and copolymers. Functionalized initiators and terminators are currently used in nonequilibrium polymerization to introduce functional groups to one or both ends [548, 575–581]. The AROP allows the synthesis of block copolymers [550, 582–588], graft copolymers [589, 590], star polymers [544, 548, 591, 592], and polymeric networks [577, 581]. Alternating copolysiloxanes were also prepared by a regioselective polymerization of cyclosiloxanes containing different siloxane units. It depends strongly on the nature of counterion [593, 594]. Simultaneous polymerization of a mixture of cyclosiloxanes gives polymers with a composition depending on Mayo-Lewis reactivity ratios only when the propagation reactions are irreversible. Gradient copolysiloxanes can be obtained starting from cyclotrisiloxane monomers

[595]. Equilibrium copolymerization of cyclotetrasiloxanes leads to random structures [596, 597]. As usual, copolymers aim at broadening the scope of properties and applications. For instance, the introduction of methylphenyl or diphenylsiloxane units to PDMS helps to improve thermal, oxidation, or radiation stability, whereas fluoroalkyl groups enhance their resistance to fuel and oils.

5.3 Other Cyclic Organosilicon Monomers

5.3.1 Silsesquioxanes, Cyclic Carbosiloxanes, and Cyclic Silaethers

These three monomers are very similar to the cyclosiloxanes family as they can be polymerized anionically by breaking a siloxane bond.

Silsesquioxanes, of empirical formula $RSiO_{3/2}$, represent a wide class of more or less ordered three-dimensional structures (Scheme 56). They are intermediate structures between siloxanes (O/Si = 1) and silica (O/Si = 2). They are usually generated by hydrolytic condensation of trialkoxy- or trichlorosilanes. Numbers of reviews may give additional and detailed information about this compound and its properties and applications [598–601]. As an example, the anionic ring-opening copolymerization of D4 with polyhedral oligomeric silsesquioxanes (POSS) derivatives leads to cross-linked polysiloxanes exhibiting good thermal stability [602, 603].

Poly(carbosiloxane)s are obtained from high ring strain cyclic monomers, i.e., 1-oxa-2,5-disilacyclopentanes, having both carbosilane and silyloxy linkages (Scheme 57). Lithium or sodium silanolates were shown to initiate the polymerization in the presence of a polar solvating agent such as THF or dioxane to avoid aggregation of active centers [543, 604–606]. Strongly basic N-heterocyclic carbenes and guanidine derivatives in the presence of alcohols or other hydrogen bond donors were shown to allow the synthesis of poly(carbosiloxane)s with controlled molar masses [607] and also to cyclic poly(carbosiloxane)s in the

Scheme 56 Structure of an octaalkyl polyhedral oligomeric silsesquioxane
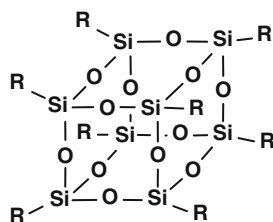
Scheme 57 Structure of cyclic carboxysiloxanes
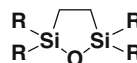
Scheme 58 AROP of cyclic silaethers at equilibrium
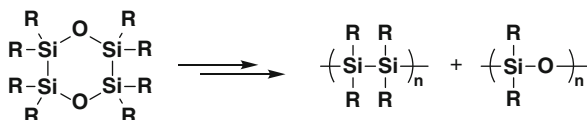
Scheme 59 AROP of cyclosilanes
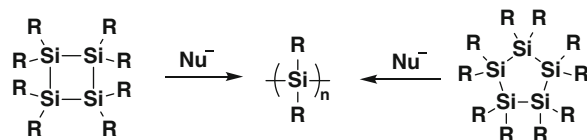
absence of alcohol [608]. Monomers bearing a chiral center could be synthesized and led to optically active polymers by AROP [609, 610].

The anionic polymerization of cyclic silaethers, or oxysilylenes, enables the cleavage of both the Si–Si and Si-O bonds, and lead to a polysilaether with an irregular structure and, at equilibrium, a mixture of polysiloxanes and polysilanes by rearrangement (Scheme 58) [611–613]. A silyl anion, as compared to a silanolate one, is a nucleophile able to initiate the polymerization of an ethylenic monomer. It was used for instance to change an alkoxide into a carbanion active center [613].

5.3.2 Cyclosilanes

Strained cyclosilanes were shown to ring-open anionically yielding high molar masses polysilanes (Scheme 59). Initiators such as butyllithium, silylpotassium, or lithium silyl cuprates were used with cyclotetrasilane [614–617] bearing methyl and/or phenyl groups. Diblock polystyrene-polysilane copolymers exhibiting a phase separation could be prepared using polystyryllithium to initiate the ROP of 1,2,3,4-tetramethyl-1,2,3,4-tetraphenylcyclotetrasilane in the presence of 12-crown-4 to enhance the polymerization [618]. Tetrabutylammonium fluoride and silyl potassium appeared efficient initiators for nonamethyl(phenyl)cyclopentasilane [619]. The strong affinity of fluoride anion to Si atom promoted the generation of silyl anion without any additives. The potassium initiator required the use of hexamethylphosphoramide or crown ethers promoters capable to solvate the potassium cation in order to enhance the reactivity of the silyl anion. Low temperature was needed ($-78\,^\circ$C) to reach high polymer yield (80 %), as well as quenching to prevent the back-biting reaction when temperature increases. Such a polymer is a kinetic product and cyclic oligosilanes are thermodynamically more stable.

5.3.3 Cyclocarbosilanes

Polycarbosilanes are attractive materials as they contain only Si-C bonds in the backbone making them of interest as silicon carbide precursors used for the

Scheme 60 AROP of silacyclobutanes
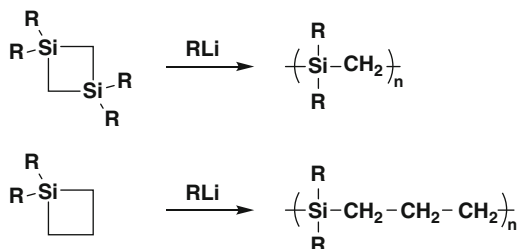
Scheme 61 Structures of cyclosilazanes
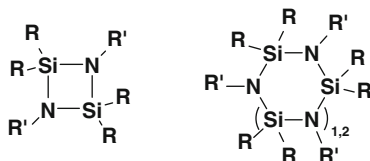
preparation of ceramic fibers. The anionic route offers an attractive way to ring-open strained silacyclobutane monomers using organolithium as initiators (Scheme 60) [620–625]. The polymerization yields high molar mass poly (silanediylmethylene)s with a strictly alternating SiR_2/CH_2 backbone structure. Depending on substituents in the ring and on the initiator, polymerizations may proceed in a controlled and living manner [626, 627]. Optically active polymers [628] as well as block copolymers based on silacyclobutane [629, 630] were also described. As cyclic silaethers, silacyclobutane may be used to transform a weak nucleophilic center into a more nucleophilic one. This makes possible the copolymerization of heterocyclics with vinylic monomers [631].

5.3.4 Cyclosilazanes

Despite the high reactivity with water, oxygen, etc., of Si-N bonds present in polysilazanes, obtained by ROP of cyclosilazanes (Scheme 61), these materials gained interest as precursors of Si-N and Si-CN ceramics through pyrolysis. Organolithium and organosodium are the typical initiators used in AROP leading to high molar masses in a living manner [632, 633]. The polymerization is kinetically controlled by the ring strain and by the steric hindrance around the nitrogen atom and/or the electronic effects of the R substituent on the Si-N bond [634, 635]. As a possible example, a pendant double bond could be introduced into a polystyrene-polysilazane block copolymer using 1,1,3,N,N'-pentamethyl-3-vinylcyclodisilazane as co-monomer added to living polystyryllithium [636]. Such a copolymer enabled the formation of cross-linked micelles and ceramic nanoparticles after pyrolysis.

Scheme 62 AROP of ferrocenylsilanes
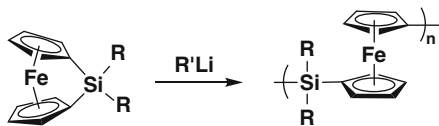
5.3.5 Ferrocenylsilanes

Polyferrocenylsilanes (PFS) and polyferrocenylsilane block copolymers, where iron and silicon are present in the main chain, are obtained from AROP of strained ferrocenylsilanes. The first report of living carbanionic ROP appeared in 1994, and this process permitted the synthesis of PFS with predictable molar masses and narrow dispersity [637]. The mechanism is based on a Cp-Si bond cleavage in the presence of lithium-based initiators (Scheme 62). Reviews published by Rider and Manners [638] and Bellas and Rehahn [639] propose details in their preparation as well as other polymerization routes or self-assembly toward nanostructured materials.

6 Cyclic Carbonates

6.1 Introduction

The polymerization of aliphatic or aromatic cyclic carbonates was highly investigated and recently reviewed [640–644]. Indeed, due to transparency, good heat resistance (up to 130 °C), high toughness, and excellent dimensional stability, polycarbonates (PC) are used in a broad range of applications like elastomers, sealants, foams, coatings, adhesives, etc. Aliphatic polycarbonates and copolycarbonates are also valuable biomaterials thanks to their biocompatibility and biodegradability.

6.2 5-Membered Cyclic Carbonates

The polymerization of 5-membered cyclic carbonates follows a peculiar behavior as their ceiling temperatures are below 25 °C. As a consequence, no ROP should be possible to yield poly(alkylene carbonate). Nevertheless, they can be polymerized at high temperatures (above 150 °C) resulting in poly(ether-carbonate)s (path A, Scheme 63), the repeating units being a mixture of alkylene carbonate (content generally lower than 50 mol%) and the corresponding alkylene oxide units coming from decarboxylation reactions during the polymerization with organometallics [645, 646], metal alkoxide [647–651], or organic initiating systems [96, 652]. Rokicki developed also the synthesis of poly(ether-carbonate)s through the

a

b
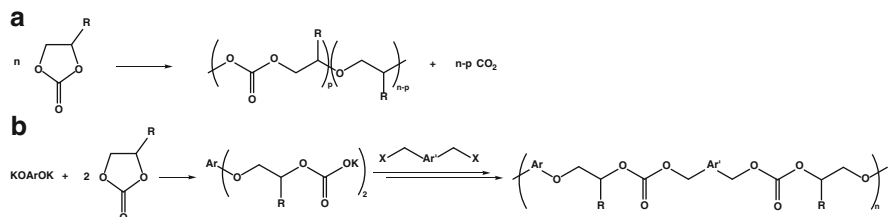
Scheme 63 Poly(ether-carbonate)s obtained from AROP of 5-membered cyclic carbonates
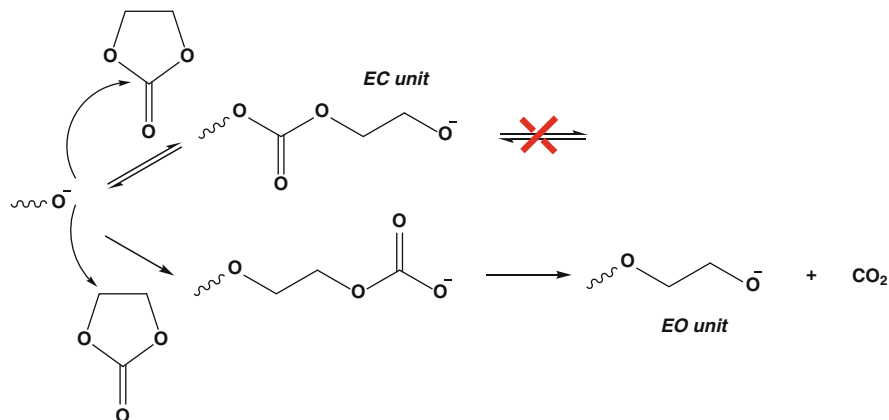
Scheme 64 Mechanism of the AROP of ethylene carbonate

combination of AROP of 5-membered cyclic carbonates initiated by bisphenolates leading to reactive difunctional species and their coupling reactions with dihalo compounds (path B, Scheme 63) [653, 654].

Detailed mechanistic studies of the polymerization of ethylene carbonate (EC) with KOH as the initiator performed at 150–200 °C in bulk suggested that, in the early stage of the polymerization, a major polymer structure comprises one EC unit per two ethylene oxide (EO) units (the content of EC units, even in the earliest stage of the reaction, was not higher than 32 mol-%). For longer reaction times, the content of EO units increases, through hydrolysis of the carbonate units [650]. Polymerization proceeded thus in two stages: during the first stage, EC conversion took place with an increase of molar masses, while in the second stage, when EC was completely consumed, a decrease of both the number of EC units and molar mass was noticed, indicating the occurrence of chain cleavage and decarboxylation reactions. During propagation, the alkoxide propagating species can attack the carbon atom of the carbonyl group. In this case, the reaction is reversible, but the new alkoxide is not able to attack again on the carbon atom of the carbonyl group of another EC monomer as it would yield an EC-EC sequence which is thermodynamically not possible. An alkoxide species can also attack the carbon atom of a methylene group, followed by decarboxylation and irreversible formation of an ethylene oxide unit (Scheme 64). The most probable EC
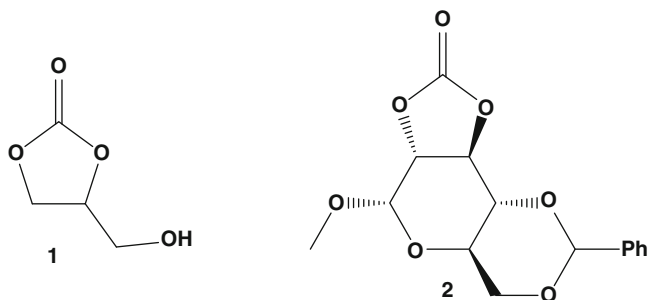
Scheme 65 Other 5-membered cyclic carbonates anionically polymerized

polymerization mechanism should thus be a combination of methylene and carbonyl carbon attack. Finally, after total monomer consumption, elimination reactions were detected, yielding vinyl end groups. Similar results were observed with other initiating systems for the AROP of EC. With butyllithium, the resulting polymers contained only 10 mol-% of carbonated units [645], and with potassium methoxide [647] and phosphazene [96], 28 and 20–25 mol-% of EC units were conserved, respectively. The AROP of propylenecarbonate yielded also poly(propylene carbonate-*co*-propylene oxide) copolymers whatever the initiating system [648, 649, 652].

Rokicki took advantage of these side decarboxylation reactions in order to produce hyperbranched aliphatic polyether through the AROP of glycerol carbonate (1, Scheme 65) conducted at 170 °C using trimethylolpropane/potassium methanolate as the initiating system [651]. Attempts to polymerize aromatic five-membered cyclic carbonate with *sec*-BuLi and potassium dihydronaphthalide revealed unsuccessful [655]. In contrast to other five-membered cyclic carbonates, five-membered cyclic carbonates obtained from methyl 4,6-*O*-benzylidene-glucopyranoside (2, Scheme 65) can be polymerized at relatively low temperatures (<60 °C) with alkali metal alkoxides or organic initiator, without elimination of carbon dioxide, to produce polycarbonates consisting exclusively of carbonate repeating units [656–658]. Such a behavior was suggested to be due to the ring strain which may result from the connection of two hydroxyl groups in E (trans) position by the carbonate linkage.

6.3   6-Membered Cyclic Carbonates

In contrast to thermodynamically unfavorable 5-membered cyclic carbonates, 6-membered cyclic carbonates easily polymerize with anionic initiators to afford PCs without ether sequences and generally high molar masses [659–663]. The AROP of trimethylene carbonate (TMC) was first reported in the 1930s using K_2CO_3 [664, 665]. Since then, many other initiators were able to polymerize
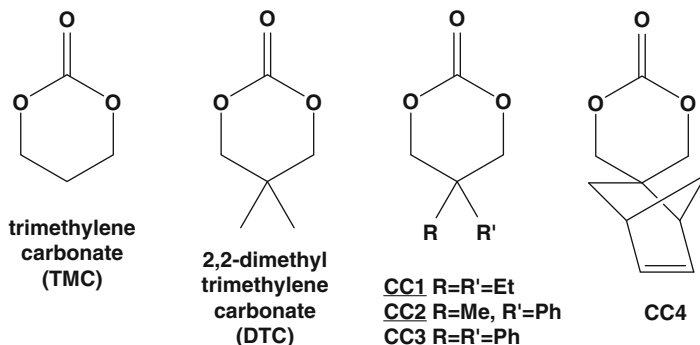
Scheme 66 Examples of 6-membered cyclic carbonates polymerized anionically

6-membered cyclic carbonates (Scheme 66), like butyllithium [666–672], alkali metal alkoxides [667, 672–676], naphthalene potassium [667], sodium hydride [673], and pure organic nucleophiles [379, 673, 677–688].

An important feature of AROP of 6-membered cyclic carbonates is its equilibrium character. Indeed, polymerization did not go to completion with the presence of residual monomer. Nevertheless, this drawback could be taken as an advantage as it allows polycarbonates recycling. It was shown that the monomer substitution had a strong effect on the equilibrium monomer concentration. For example, the AROP of TMC, 2,2-dimethyl trimethylene carbonate (DTC) and CC1–3 (Scheme 66) in THF solution using potassium *tert*-butoxide as the initiator exhibited an increasing monomer concentration at equilibrium, with an increasing bulkiness of the substituents, CC3 monomer being almost not polymerized [671, 675]. It was assessed that the decrease in polymerizability of the 6-membered cyclic carbonates with increasing bulkiness of the substituents was due to the conformational distortion of the polymer backbone, rather than in the change of conformation of the monomer caused by the substituents [641]. Several other parameters may also influence the polymerization rate. For example, the polymerization of DTC in toluene with lithium as a counterion was slower than that with potassium one due to the covalent character of the lithium-oxygen bond compared with the potassium-oxygen bond leading to a lower nucleophilicity of the lithium alkoxide. In the case of monomer CC4, the back-biting reaction was restricted due to the stiffness of the polymeric chain [670].

The AROP of 6-membered cyclic carbonates presents transesterification reactions, besides initiation and propagation reactions (Scheme 67). The initiation reaction comprises the nucleophilic attack of the initiator on the carbonyl carbon atom, followed by an acyl-oxygen cleavage and formation of the active species, an alkoxide. Peculiar initiation behaviors were also observed. When the ROP was initiated by naphthalene potassium, this latter did not act as an electron-transfer reagent (e.g., like for styrene polymerization) but as a nucleophile, naphthalene being incorporated in the polymeric chain [667]. Intramolecular nucleophilic attacks on carbonyl carbon atom (back-biting) lead to cyclic oligomers, while
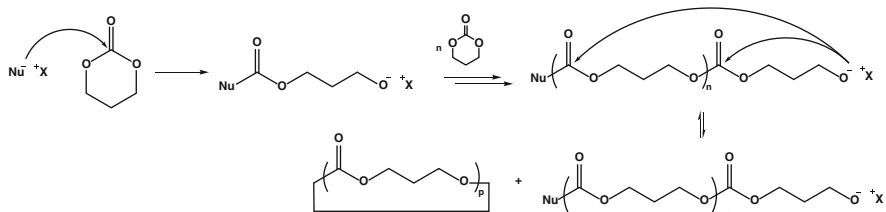
Scheme 67 Initiation, propagation, and transesterification reactions occurring in AROP of 6-membered cyclic carbonates
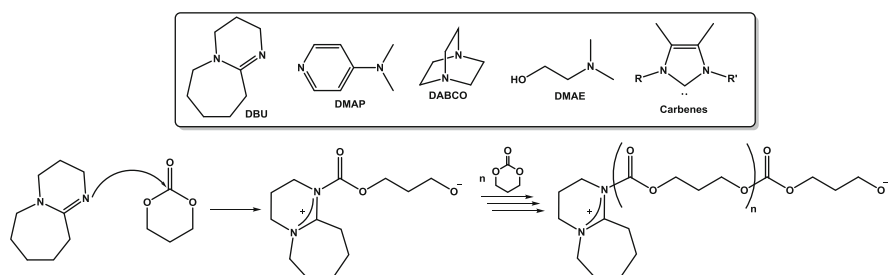
Scheme 68 Examples of organic initiators for the AROP of 6-membered cyclic carbonates and polymerization mechanism

intermolecular transesterification leads to a change of the macromolecule length. As a consequence, the control of the polymerization was poor, and bimodal distribution of molar masses was generally observed.

Instead of using metallic initiators, it is possible to use organic ones. Murayama et al. were the first to show that tertiary amines such as 1,8-diazabicyclo[5.4.0]undec-7-ene (DBU), 1,4-diazabicyclo[2.2.2]octane (DABCO), and 4-dimethylaminopyridine (DMAP) (Scheme 68) were able to achieve the AROP of a 6-membered cyclic carbonate (CC4, Scheme 66) in bulk at 120 °C, whereas no polymer was obtained with triethylamine, aniline, *N*,*N*-dimethylaniline, or pyridine [679]. It was suggested a zwitterionic polymerization mechanism, which was confirmed by mass spectrum analysis of the products. Tapered copolymers were also obtained when monomer CC4 was simultaneously polymerized with glycidyl naphthyl ether.

The ROP of TMC was also performed with *N*-heterocyclic carbenes, guanidine, and amidine bases in bulk at 65 °C with a good control, yielding well-defined polycarbonates with molar masses up to 50,000 g/mol, dispersity index below 1.08, and high end-group fidelity [680]. Similarly, the tertiary amine 2-(dimethylamino) ethanol (DMAE) was used as an efficient initiator/catalyst for the ROP of TMC in bulk at 50 °C leading to α,ω-heterotelechelic PTMC [682]. In this case, the mechanism could be either an activated monomer or an activated chain-end one. Phosphazenes revealed also efficient deprotonating agents of alcohols for the
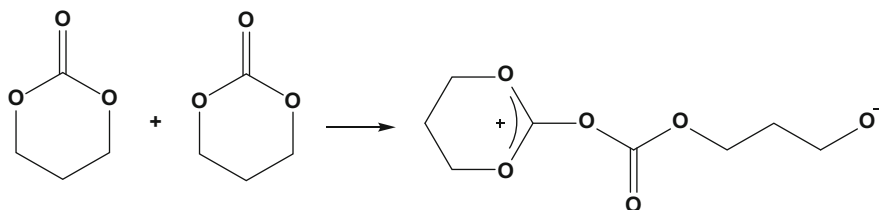
Scheme 69 Spontaneous ROP of TMC
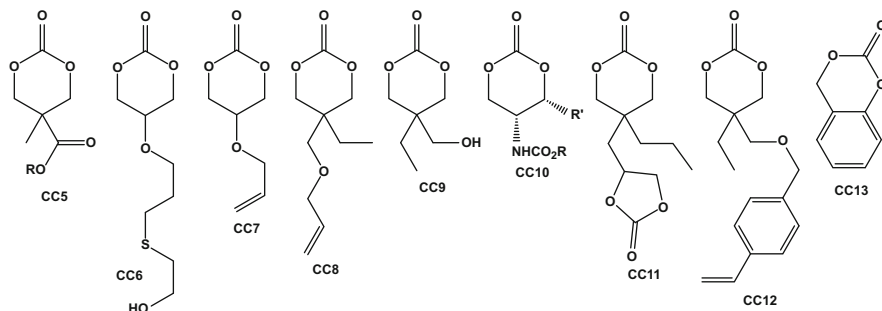
Scheme 70 Examples of functional 6-membered cyclic carbonates anionically polymerized

polymerization of TMC [688, 689]. Recently, several carbenes were used for the controlled polymerization of DTC [379, 685].

Some examples of initiator-free polymerization of cyclic carbonates were also described in the literature, assuming an anionic mechanism [690–693]. TMC can undergo spontaneous polymerization in bulk above 100 °C, with the formation of a zwitterion intermediate with a well-stabilized trialkoxycarbenium ion and on alkoxide (Scheme 69), whereas DTC cannot [691]. Initiator-free polymerizations were also observed for the thermal ROP of 5-benzyloxy-trimethylene carbonate (BTMC) in bulk at 150 °C or the microwave-assisted ROP of TMC. Molar masses were generally high.

In spite of some side reactions, the AROP of functional cyclic carbonates remains the preferable way to prepare functional polycarbonates. Several pathways permit functional monomer synthesis: from 2,2-bis(hydroxymethyl)propionic acid, glycerol, or alkyl malonates [640, 641, 643]. A number of functionalized PCs and copolycarbonates can be obtained by direct polymerization of cyclic monomers bearing functional groups. Functional side-chain groups introduced into PCs are carboxylic group and their derivatives, hydroxyl, allyl, acrylate, methacrylate, styrene, and stilbene derivatives, and even five-membered cyclic carbonates (Scheme 70).

Polycarbonates with carboxylic side groups could be synthesized through the ROP of CC5-type monomers (Scheme 70) with DBU [684] or *sec*-butyllithium [694] at room temperature in solution. With *sec*-butyllithium, bimodal distribution

of the molar masses was observed, whereas the polymers exhibited low dispersity with DBU. Aliphatic amines with different chain lengths were easily conjugated onto the polymer backbone in order to form nanoparticles [684].

6-Membered cyclic carbonate bearing free hydroxyl group attached to the ring via aliphatic spacer (CC6, Scheme 70) was polymerized with DBU in bulk or in solution at temperatures ranging from 60 to 110 °C to yield hyperbranched polycarbonates composed of carbonate and glycerol units [683]. The linear equivalent of poly(CC6) was obtained through the polymerization of CC7 followed by free radical addition of mercaptoethanol to the pendent allyl groups. Attempts to polymerize CC8 with *sec*-butyllithium in solution resulted in a mixture of polymers, cyclic oligomers, and unreacted monomer [668, 669]. The hydroxyl function of monomer CC9 was first protected by reaction with trimethylsilyl chloride and benzyl chloroformate of phenyl isocyanate and then polymerized with lithium alkoxide in solution at low temperature to yield bimodal distributions or even cross-linking [674]. After deprotection, polycarbonates with one hydroxyl group per repeating units were obtained. Amino acid functionalized polycarbonates were also synthesized through the ROP of CC10-type monomers with alkali metal alkoxides or *n*-butyllithium in solution at low temperature followed by deprotection [672]. Monomodal distributions were obtained, and the configuration of the monomer was inverted during the polymerization.

Bifunctional cyclic carbonate consisting of both 5- and 6-membered rings (CC11, Scheme 70) was polymerized with DBU at 60 °C in solution to afford a polycarbonate with remaining 5-membered cyclic carbonate group in the sidechain, as this latter did not polymerize in these conditions [677]. At such elevated temperature, conversion stopped around 50 % due to the equilibrium nature of the polymerization.

Styrene side groups were also introduced onto polycarbonates through the polymerization of monomer CC12 (Scheme 70) with potassium *tert*-butoxide as the initiator in THF at 0 °C [676]. Subsequent radical cross-linking of styrenic groups and anionic de-cross-linking of the carbonate units was performed. Aromatic cyclic carbonate CC13 (Scheme 70) was polymerized by *sec*-butyllithium or dihydronaphthalene potassium, but it was evidenced the presence of decarboxylation reactions to a great extent [655].

Macroinitiators such as polymeric Li, Na, and K alkoxides can also be used for the initiation of the 6-membered cyclic carbonate polymerization. Thus, living vinyl polymers [695], hydroxyl group-terminated polymers of poly(tetrahydrofuran) (PTHF) [696, 697], poly(ethylene oxide) (PEO) [697–699] and poly(dimethylsiloxane) (PDMS) [697, 700] were transformed to alkoxides by treatment with *sec*-BuLi or K-naphthalene and used as initiators for AROP of DTC allowing the synthesis of di- and triblocks copolymers. The polymerization initiated by PTHF alkoxides with different counterions was slower than that initiated by PEO alkoxides, because of the lower solvation ability of PTHF. It was also shown that the polymerization rate was highly dependent on the counterion, potassium alkoxides being more reactive than lithium alkoxides. Besides, higher molar mass PDMS macroinitiators exhibited lower polymerization rate. In the same vein, living poly

(methyl methacrylate) (PMMA) prepared by Group Transfer Polymerization (GTP) was used as a macroinitiator for the ROP of DTC after transformation of the silyl ketene acetal into an alkoxide [701]. PMMA-*b*-PDTC block copolymers were thus obtained.

The simultaneous or sequential polymerization of DTC with several cyclic esters or other cyclic carbonates (CC4, CC5, and CC8, Scheme 70), initiated with butyllithium, potassium dihydronaphthalene, or organic initiators, was performed in solution or in bulk [379, 668–670, 694, 702–704]. With ε-caprolactone (CL), tapered copolymers were obtained as DTC was more reactive than CL. Triblock copolymers with tapered DTC/CL outer blocks could also be obtained using macroinitiators (PEO or PTHF based) [699]. With pivalolactone, only block copolymers were synthesized; DTC was first reacted by alkoxide active species, followed by the reaction of pivalolactone through carboxylate active species. With the other cyclic carbonates, statistical or block copolymers were obtained from simultaneous or sequential polymerization, respectively.

6-Membered cyclic carbonates were also copolymerized with oxiranes [678, 705] and anhydride [706]. DTC was copolymerized with glycidyl phenyl ether (GPE) with DBU in bulk at 90 °C. An acceleration of GPE polymerization was observed, and quantitative yields were obtained. PGPE-*b*-PTMC copolymers were also successfully synthesized through the sequential polymerization of GPE and TMC with tetrabutylammonium fluoride. Attempts to copolymerize TMC and adipic anhydride with *sec*-butyllithium in several conditions revealed unfruitful as mixture of homopolymers were detected [706].

It was demonstrated that cyclic monothiocarbonate [707] and thiocarbonate [708, 709] (Scheme 71) could be polymerized by AROP. For the cyclic monothiocarbonate, potassium *tert*-butoxide revealed a good initiator yielding a polymer that precipitates during the course of the polymerization. It was shown that the propagating species was not an alkoxide but a thiolate as the monomer ring-opens exclusively through the carbonyl sulfur bond cleavage. Thiocarbonate was polymerized by n-butyllithium or potassium alkoxides in solution at room temperature or by DBU in bulk or in solution at 120 °C. Polymerization was pretty slow and proceeded with an isomerization of the thiocarbonate group.
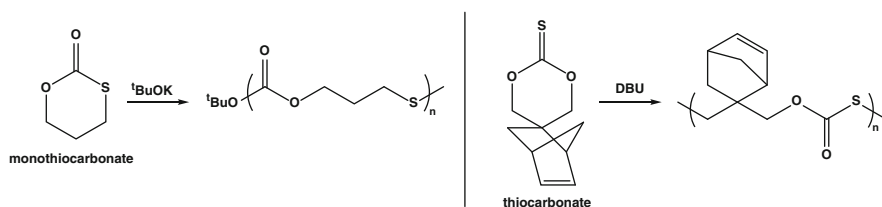
Scheme 71 Cyclic monothiocarbonate and thiocarbonate polymerized by AROP

6.4 Larger-Ring Cyclic Carbonates

The ROP of 7-membered cyclic carbonate (tetramethylene carbonate, TeMC, Scheme 72) is generally faster than that of the six-membered one due to relatively high ring strain. However, the polymerization of 7-membered cyclic carbonates was scarcely investigated because of the difficulty to synthesize the monomers. Indeed, TeMC is thermally unstable and difficult to isolate and purify. The polymerization of TeMC initiated with *sec*-butyllithium was carried out in THF to yield the corresponding polycarbonate in a relatively high yield in a short time [710]. Like for 6-membered cyclic carbonates, an important residual monomer concentration was observed with the formation of cyclic oligomers via back-biting reaction, which is characteristic for equilibrium polymerizations. However, the relative polymerization rate of TeMC is about 35 times faster than that of TMC.

Another 7-membered cyclic carbonate (β-Me7CC, Scheme 72) was polymerized in bulk at elevated temperature only (100 °C) with organic compounds (DMAP, phosphazene) with very good yields [711]. No regioselectivity was observed during ring-opening of the monomer.

The ROP of large-ring aromatic cyclic carbonates was also studied. It was shown that the polymerization of monomer CC14 with alkoxide or alkyllithium [712] or CC15 with *sec*-butyllithium or dihydronaphthalene lithium [713] failed, but CC15 was easily polymerized by dihydronaphthalene potassium or potassium *tert*-butoxide. Monomer CC16 was easily polymerized with potassium *tert*-butoxide in THF at room temperature to afford the corresponding polycarbonate in high yield [714]. Cyclic oligomeric carbonates of bisphenol A (CC17, Scheme 72) were polymerized by potassium dihydronaphthalene in THF [713] or in bulk at 250 °C [715]. The polymerization and copolymerization of cyclo bis(hexamethylene carbonate) and its fluorinated analog (CC18 and CC19, Scheme 72) were also successfully performed using *sec*-butyllithium in toluene [716].
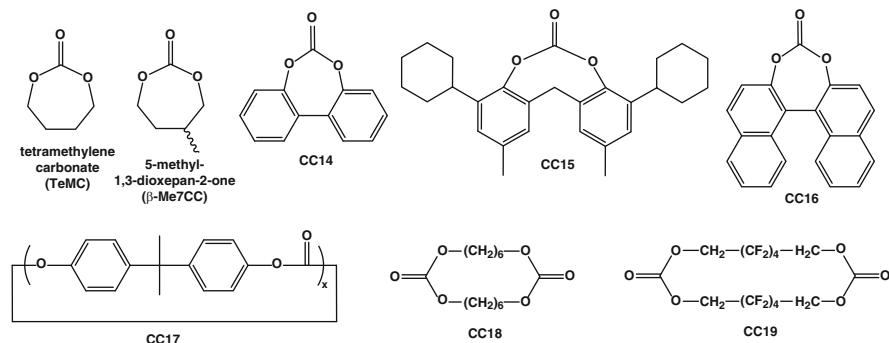
Scheme 72 7-Membered cyclic carbonates and larger-ring cyclic carbonates polymerized by AROP

7   Cycloalkanes, Cyclic Sulfides and Amines, Cyclic Ureas, Depsipeptides, and Cyclic Phosphorous Monomers

7.1   Introduction

The successful synthesis of polymers and copolymers issued from cyclic ethers, esters, lactams, carbonates, or siloxanes through anionic ring-opening polymerization triggered researches in cyclic monomers containing, or not, other heteroatoms or combination of several heteroatoms. New properties were expected for novel uses.

7.2   Cycloalkanes

Cycloalkanes are expected to polymerize by breaking a carbon-carbon single bond of a monomer ring. Such a bond does not generally react with free radicals and rarely participate in reactions with electrophiles and nucleophiles [717]. In addition, as the two atoms making the bond are identical, no polarization is introduced into the monomer, making ionic reactions with nucleophiles or electrophiles difficult. Reactivity can only be expected when monomer substituents are introduced on at least one of the two carbons, thereby increasing the bond polarity and introducing some zwitterionic nature into the bond, or when the overlap of atomic orbitals in the carbon-carbon bond is disturbed by geometric parameters, particularly observed with highly strained polycyclic systems [717, 718]. Cycloalkanes polymerized by anionic ring-opening polymerization are composed of functionalized cyclopropanes, cyclobutanes, and polycyclic molecules with high intrinsic polymerizabilities (e.g., bicycloalkanes and propellanes). Detailed reviews may give additional information in anionic polymerization as well as other polymerization methods used [719–723].

The AROP of cyclopropanes activated by various substituents (Scheme 73) was effective using mainly alkali metal derivatives as initiators. Two electron-withdrawing substituents on the same carbon are often needed for the polymerization to be efficient but still drastically less reactive than the corresponding vinyl monomers [724]. Sodium thiophenolate is shown to initiate the polymerization of cyclopropane-1,1-dicarboxylates with a living character in some cases [725–728]. Phosphazenium thiophenol or bisthiols were also proposed for the successful AROP of di-n-propyl cyclopropane-1,1-dicarboxylate [729, 730]. Well-defined monofunctional or difunctional polymers with a low dispersity were obtained through a living process in THF between 30 and 60 °C or in toluene between 30 and 100 °C. A much higher reactivity is noticed as compared to the alkali metal thiophenolate initiator used in DMSO at higher temperature. The polymerization of cyclopropanes bearing cyano [724, 731] or fluorine [732] groups initiated with sodium thiophenolate or fluorenyl lithium, respectively, was also observed. Sodium
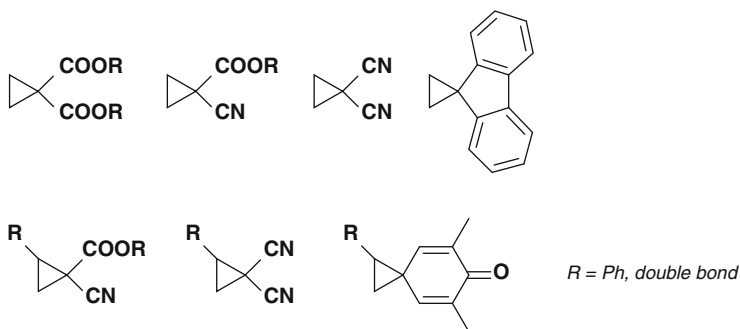
Scheme 73 Structure of cyclopropanes polymerized by AROP

Scheme 74 Structure of cyclobutanes polymerized by AROP
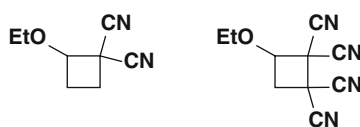
Scheme 75 Structure of polycyclic alkanes polymerized by AROP
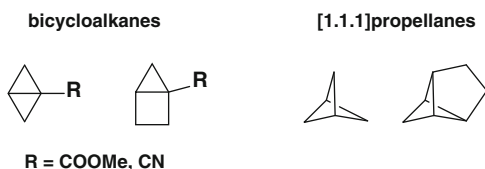
cyanide was particularly effective as anionic initiator of various trisubstituted cyclopropanes in DMF [733–737].

Cyclobutanes exhibit a much lower tendency to anionically ring-open as compared to cyclopropanes and as also observed for heterocyclic rings. Reasonable evidences for an AROP were only reported in highly activated monomers. The polymerizations of cyclobutanes substituted by nitrile groups on one or two carbons, and further substituted by an ether group on a neighboring carbon, are the most efficient (Scheme 74) [738, 739].

Activated bicyclobutanes [740–745] or other bicycloalkanes [746] and [1.1.1] propellanes [747–749] were observed to give oligomers or polymers using conventional anionic initiators, i.e., alkyllithium (Scheme 75).

7.3 Cyclic Sulfides and Amines

The anionic route is proposed, in addition to cationic and coordinative ones [750], as an efficient approach for the polymerization of cyclic sulfides (Scheme 76), in particular for thiirane (ethylene sulfide) and various substituted thiiranes. Thiolates

Scheme 76 Structure of cyclic sulfides polymerized by AROP

thiiranes ▽ | thiethanes ▢ | R = H, CH₃...
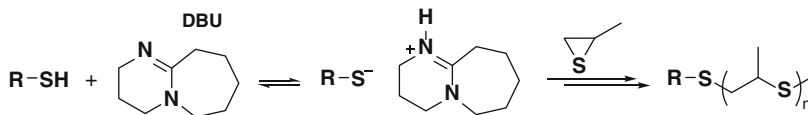
Scheme 77 Anionic polymerization of methylthiirane initiated by thiolates

are commonly used to attack the monomer, proceeding exclusively at the methylene carbon and leading to pure head-to-tail structures [751–753]. Naphthylsodium was found to act as a bifunctional initiator and to give a living character to the polymerization. The initiation reaction was proposed to consist of a desulfurization process producing ion radicals that combine to form dithiolates [754]. In a similar way to epoxide polymerization, Inoue experimented with success (N-methyl-5,10,15,20-tetraphenylporphinato)zinc propanethiolate as initiator of propylene sulfide (or methylthiirane MT) [755].

Organic initiators were also proposed. Tertiary amines such as 1,4-diazabicyclo [2.2.2]octane (DABCO) enable the polymerization of ethylene sulfide to high molar mass polymers through a zwitterionic mechanism [756]. In contrast, MT was only slowly polymerized by polyamines to give low molar mass materials. Nicol et al. described the living polymerization of MT initiated by various mono- and dithiolates [757]. The deprotonation of the thiols was carried out by addition of a strict stoichiometric amount of a bulky strong organic base such as 1,8-diazabicyclo [5,4,0]undec7-ene (DBU) (Scheme 77).

Advantages of thiols are based on low pKa values ranging from 7 to 11 in water, excluding substantially deactivation due to protonation in environments with pH ≥10. That allows a living character of the polymerization at not excessively basic pH and under non-anhydrous conditions, which is different from the structurally similar epoxide polymerization. It is possible to polymerize hydroxyl-containing monomers such as hydroxymethyl thiirane in a living manner [758] or to work in emulsion in water with restrictions, such as limited conversions producing polymers with molar masses lower than predicted ones due to physical reasons and not chemical [759]. On the other hand, the use of thiols is often complicated by the presence of disulfide impurities coming from oxidation of the initiating thiol, which results in transfer reactions [760]. Protected thiols which are deprotected right before polymerization may be proposed. Examples are the use of thioester, which is transformed into thiolate by the addition of sodium methanolate [761, 762] and the ring-opening of cyclic dithiocarbonates by an amine [763].

Thanks to the livingness of the polymerization of thiiranes, di- and triblock copolymers were prepared, marrying mainly polythiirane or poly(methylthiirane) (PMT) with polystyrene and derivatives, poly(methyl methacrylate), polyethers, and polydienes [762, 764–770]. A macromonomer approach was also helpful to
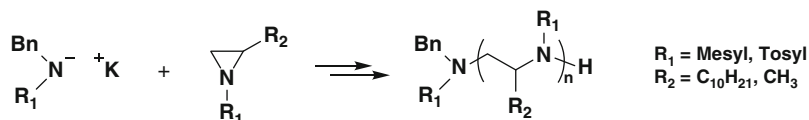
Scheme 78 AROP of sulfonylaziridines

obtain comb-like polymers with polythiirane main chains and various side chains [771–774]. The synthesis of star-shaped PMT by polymerization with tri- and tetrathiol initiators was also investigated [761–763, 775, 776].

The AROP of the four-membered rings family of cyclic sulfides (Scheme 76) is much more limited. Thiethane and 3,3-dimethylthietane were polymerized to high molar mass polymers by initiation with naphthylsodium or butyllithium [777–780]. The polymerizations were shown to occur with carbanions as active species instead of thiolates. The sulfur atom is attacked due to severe bond angle distortions forced upon the atom by the geometry of the molecule.

The conversion of cyclic amines into linear polyamines is much more limited by AROP, despite potential utilities, e.g., ion exchange chromatography or biomedicine [781, 782]. The polymerization of sulfonylaziridines was only effective in the presence of amide initiator, generated by the deprotonation of a primary sulfonamide (*N*-benzyl methanesulfonamide) by potassium bis(trimethylsilyl)amide (KHMDS), leading to polymers with a low dispersity (Scheme 78) [783].

7.4 *Cyclic Ureas and Depsipeptides*

The ROP of cyclic ureas has attracted only minor interest. Dimethylene urea and trimethylene urea can be successfully ring-open using sodium hydride as initiator leading to polyureas [784]. But the synthesis of polyurethanes, starting from tetramethylene urea (TeU) and cyclic carbonates, was particularly investigated by Keul and Höcker [785–788]. It was shown that first the cyclic carbonate polymerizes, and then TeU is formally inserted into the polycarbonate chain after deprotonation of the amine by dibutylmagnesium (Bu_2Mg) (Scheme 79).

Using γ-butyrolactone (γ-BL) instead of cyclic carbonates in the presence of Bu_2Mg, alternating poly(amide urethane)s were achieved [789]. The homopolymerizations of TeU and γ-BL were not observed. TeU reacts initially with Bu_2Mg to form the salt in which the nucleophilicity of the nitrogen is enhanced and the reaction between activated TeU and γ-BL is made possible. Ring-opening leads to the AB monomer. It is followed by the nucleophilic attack of the alkoxide at the endocyclic carbonyl carbon atom, resulting in polymer after ring-opening (Scheme 80).

Polydepsipeptides, alternated copolymers of α-hydroxy acids and α-amino acids, belong to the poly(ester-amide) family and are interesting for their degradable character. Ring-opening polymerization of morpholine-2,5-dione (MD) and its
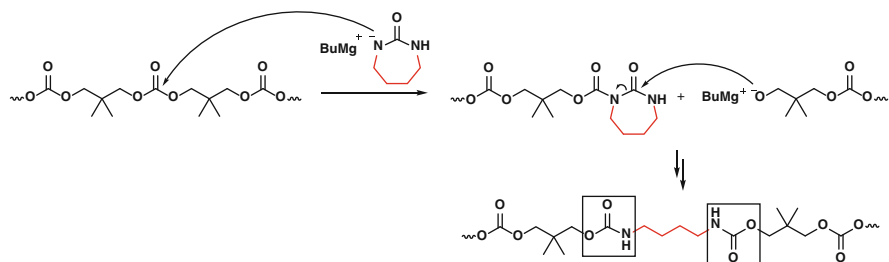
Scheme 79 Polyurethane synthesis by insertion and ROP of deprotonated tetramethylene urea in a polycarbonate
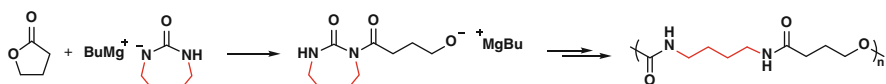
Scheme 80 Poly(amide urethane) synthesis by reaction between deprotonated tetramethylene urea and γ-BL
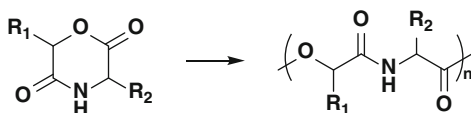
Scheme 81 Structure of cyclic depsipeptides (morpholine-2,5-dione) and corresponding polymers

derivatives (Scheme 81), in the presence of stannous catalyst, is the main way to obtain such polymers [790]. Detailed information can be found in the review of Dijkstra [791]. AROP using potassium alkoxides was also applied to provide polymers with limited conversions and molar masses [792]. The lack of control may be explained by the presence of a proton on the amine. Block copolymers such as polymorpholine-2,5-dione-*b*-polylactide were nevertheless prepared by a two-step procedure for surfactants applications [793, 794].

7.5 Cyclic Phosphorus Monomers

Cyclic phosphorus monomer family gives rise to polymers of interest in particular in biomedical field, due to biocompatibility, biodegradability, and structural similarities to naturally occurring nucleic acids, or in flame retardant applications. Lapienis reviewed recently all ring-opening polymerizations leading to polymers containing phosphorus atoms [795]. Only few monomers are polymerized by an
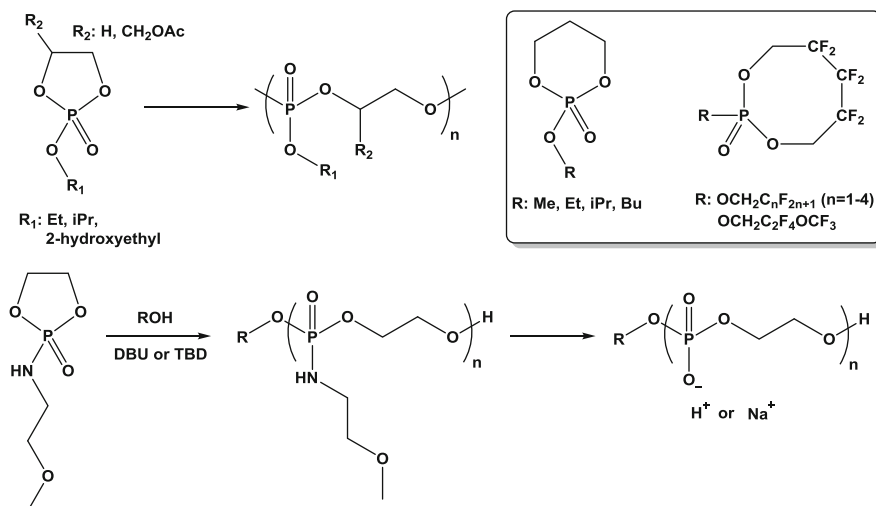
Scheme 82 Cyclic phosphoesters polymerized by AROP
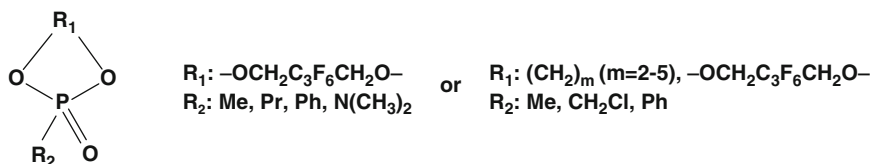
Scheme 83 Cyclic phosphonates polymerized by AROP

anionic route. Poly(phosphate esters) can be prepared from cyclic phosphoesters (Scheme 82) either with alkali metal initiators [796–800] or organic initiators (tertiary amines, TBD, or DBU) [801–805]. 5-Membered phosphoesters were by far the most studied monomers. The presence of a substituent on the ring decreases the polymerizability of the monomer as high polymerization temperatures are needed to get only oligomers. 6-Membered phosphoesters are also difficult to polymerize [799]. Fluorosubstituted phosphoesters (Scheme 82) can undergo AROP with KOH, butyllithium, or triethylamine, in bulk at 220–270 °C, giving rubber-like polymers, the molar mass being highly dependent on the initiator [800]. The presence of polar agents (e.g., THF, diethyl ether, and dimethyl-formamide (DMF)) considerably lowers the required polymerization temperature (100 °C). The polymerization presents a living character with organic initiators, enabling the formation of random and block copolymers [802, 803].

5-, 6-, 7-, and 8-Membered cyclic phosphonates (Scheme 83) can also undergo anionic polymerization at high temperatures [806]. Very recently, it was shown that DBU can perform the synthesis of poly(ethylene methylphosphonate) with an excellent control with molar masses up to 20,000 g/mol [807]. The polymerization
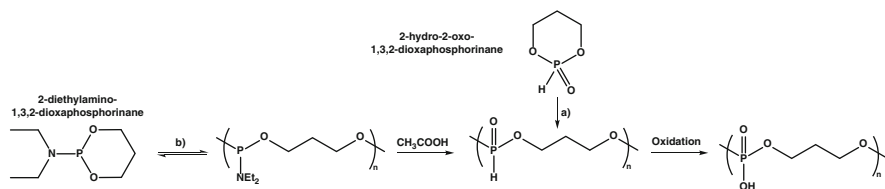
Scheme 84 Examples of other cyclic phosphorus containing monomers polymerized by AROP

of cyclic [808] or bicyclic [809] *H*-phosphonate was also performed with an alkyllithium. As an example, the polymerization of 2-hydro-2-oxo-1,3,2-dioxapho-sphorinane was achieved in bulk or in dichloromethane solution, initiated by n-BuLi, but also EtONa and t-BuOK, at 25–45 °C, to give a high molar mass polymer (route a, Scheme 84) [808]. Some trivalent phosphorus cyclic compounds were also polymerized by AROP with potassium or cesium alkoxides (no polymerization occurred with lithium or sodium) or potassium trimethylsi-lanolate (route b, Scheme 84) [810–812]. After acetolysis, poly(2-diethylamino-1,3,2-dioxaphosphorinane) gave the same polymer as the one obtained from 2-hydro-2-oxo-1,3,2-dioxaphosphorinane, which can be easily converted to polyacid after oxidation.

8   Conclusion

A large variety of cyclic monomers can be polymerized by anionic ring-opening polymerization. In spite of required rigorous experimental procedures as compared to some other polymerization routes, some industries and academic researchers used to play with such chemistry and already take advantages of some polymeric structures prepared by AROP. Indeed, thanks to the recent progress in the control of the polymerizations, functionalized polymers and copolymers (block in particular) are now available, broadening the scope of properties and thus opening many perspectives in various applications.

Abbreviations

18C6	1,4,7,10,13,16-Hexaoxacyclooctadecane (18-crown-6 ether)
ACE	Active chain end
AGE	Allyl glycidyl ether
AM	Activated monomer
AROP	Anionic ring-opening polymerization
BEMP	2-*tert*-butylimino-2-diethylamino-1,3-dimethylperhydro-1,3,2-diazaphosphorine

BL	β-butyrolactone
γ-BL	γ-butyrolactone
BO	Butylene oxide
BTMC	5-Benzyloxy-trimethylene carbonate
Bu$_2$Mg	Dibutylmagnesium
i-Bu$_3$Al	Triisobutylaluminum
BuLi	Butyllithium
CC	Cyclic carbonate
CL	ε-Caprolactone
ε-CL	ε-Caprolactam
Cp	Cyclopentadienyl
D3	Hexamethylcyclotrisiloxane
D4	Octamethylcyclotetrasiloxane
D5	Decamethylcyclopentasiloxane
D6	Dodecamethylcyclohexasiloxane
DABCO	1,4-Diazabicyclo[2.2.2]octane
DBU	1,8-Diazabicyclo[5.4.0]undec-7-ene
DHCM	3,4-Dihydrocoumarin
DMAE	2-(Dimethylamino)ethanol
DMAP	N,N-Dimethylamino pyridine
DMF	Dimethylformamide
DMO	2,2-Dimethyloxirane
DMSO	Dimethylsulfoxide
DP	Degree of polymerization
DTC	2,2-dimethyl trimethylene carbonate
EC	Ethylene carbonate
ECH	Epichlorohydrin
EEGE	2-Ethoxyethyl glycidyl ether
EO	Ethylene oxide
EtONa	Sodium ethoxide
EVGE	Ethoxy vinyl glycidyl ether
GME	Glycidyl methyl ether
GPE	Glycidyl phenyl ether
GTP	Group transfer polymerization
HMPA	Hexamethylphosphoramide
KHMDS	Potassium bis(trimethylsilyl)amide
LA	Lactide
ω-LL	ω-Lauryllactam
MAlBP	Methylaluminum bis(2,4,6-tri-$tert$-butylphenolate)
MD	Morpholine-2,5-dione
MLABz	Benzyl-β-malolactonate
MT	Methylthiirane
NHC	N-heterocyclic carbene
NOct$_4$Br	Tetraoctylammonium chloride

PA3	Polyamide 3
PA5	Polyamide 5
PA6	Polyamide 6
PA10	Polyamide 10
PA12	Polyamide 12
PBL	Poly(β-butyrolactone)
PBO	Poly(butylene oxide)
PC	Polycarbonate
PCL	Poly(ε-caprolactone)
PDMS	Poly(dimethyl siloxane)
PEEGE	Poly(2-ethoxyethyl glycidyl ether)
PEO	Poly(ethylene oxide)
PGME	Poly(glycidyl methyl ether)
PGPE	Poly(glycidyl phenyl ether)
PHA	Polyhydroxyalkanoate
PL	β-Propiolactone
PLA	Polylactide
PMMA	Poly(methyl methacrylate)
PMT	Polymethylthiirane
POSS	Oligomeric silsesquioxane
PO	Propylene oxide
PPL	Poly(β-propiolactone)
PPO	Poly(propylene oxide)
PPY	4-Pyrrolidinopyridine
PS	Polystyrene
PTHF	Polytetrahydrofuran
PTMC	Poly(trimethylene carbonate)
PVL	Pivalolactone (α,α-dimethyl-β-propiolactone)
P*t*BuGE	Poly(*tert*-butyl glycidyl ether)
RIM	Reaction injection molding
ROP	Ring-opening polymerization
RTM	Resin transfer molding
TBD	1,5,7-Triazabicyclo[4.4.0]dec-5-ene
t-BuGE	*tert*-butyl glycidyl ether
t-BuOK	Potassium *tert*-butoxide
tBuP$_1$	N'-*tert*-butyl-N,N,N',N',N'',N'''-hexamethylphosphorimidic triamide
tBuP$_2$	1-*tert*-Butyl-2,2,4,4,4-pentakis(dimethylamino)-2λ^5,4λ^5-catenadi (phosphazene)
tBuP$_4$	1-*tert*-Butyl-4,4,4-tris(dimethylamino)-2,2-bis[tris(dimethylamino)-phosphoranylidenamino]-2-λ^5,4-λ^5-catenadi (phosphazene) (phosphazene base)
TeMC	Tetramethylene carbonate
TeU	Tetramethylene urea
THF	Tetrahydrofuran

TMC   Trimethylene carbonate
TPPAlCl   α,β,γ,δ-Tetraphenylporphyrin aluminum chloride
δ-VL   δ-Valerolactone

References

1. Flory PJ (1940) Molecular size distribution in ethylene oxide polymers. J Am Chem Soc 62:1561–1565
2. Penczek S, Cypryk M, Duda A, Kubisa P, Slomkowski S (2007) Living ring-opening polymerizations of heterocyclic monomers. Prog Polym Sci 32:247–282
3. Boileau S (1989) 32 – anionic ring-opening polymerization: epoxides and episulfides. In: Allen G, Bevington JC (eds) Comprehensive polymer science and supplements. Pergamon, Amsterdam, pp 467–487
4. Lassalle D, Boileau S, Sigwalt P (1977) Reactivities of fluorenyl species as ethylene oxide polymerization initiators-II. Mechanisms of the ring opening of ethylene oxide by fluorenyl and 9-methylfluorenyl alkali salts. Eur Polym J 13:591–597
5. Lassalle D, Boileau S, Sigwalt P (1977) Reactivities of fluorenyl species as ethylene oxide polymerization initiators-I. Ultraviolet and visible absorption spectra of 9-methylfluorenyl alkali salts. Eur Polym J 13:587–589
6. Richards DH, Szwarc M (1959) Block polymers of ethylene oxide and its analogues with styrene. Trans Faraday Soc 55:1644–1650
7. Boileau S, Deffieux A, Lassalle D, Menezes F, Vidal B (1978) Reactivities of anionic species for the ring opening of ethylene oxide. Tetrahedron Lett 19:1767–1770
8. Szwarc M (1968) Carbanions, living polymers, and electron-transfer processes. Interscience Publishers, a division of John Wiley and Sons, Inc., New York
9. Knischka R, Lutz PJ, Sunder A, Mülhaupt R, Frey H (2000) Functional poly(ethylene oxide) multiarm star polymers: core-first synthesis using hyperbranched polyglycerol initiators. Macromolecules 33:315–320
10. Feng XS, Taton D, Chaikof EL, Gnanou Y (2005) Toward an easy access to dendrimer-like poly(ethylene oxide)s. J Am Chem Soc 127:10956–10966
11. Stolarzewicz A (1986) A new chain transfer-reaction in the anionic-polymerization of 2,3-epoxypropyl phenyl ether and other oxiranes. Makromol Chem Macromol Chem Phys 187:745–752
12. Stolarzewicz A, Grobelny Z, Kowalczuk M (1995) The unusual outcome of the reaction of potassium anions with phenyl glycidyl ether. J Organomet Chem 492:111–113
13. Nenna S, Figueruelo JE (1975) Caesium as counter-ion in the anionic polymerization of ethylene oxide-II. Kinetics in HMPT. Eur Polym J 11:511–513
14. Price CC, Carmelite DD (1966) Reactions of epoxides in dimethyl sulfoxide catalyzed by potassium t-butoxide. J Am Chem Soc 88:4039–4044
15. Solov'yanov AA, Kazanskii KS (1972) Polymerization of ethylene oxide in dimethyl sulphoxide (DMSO). Polym Sci USSR 14:1196–1206
16. Kazanskii KS, Solovyanov AA, Entelis SG (1971) Polymerization of ethylene oxide by alkali metal-naphthalene complexes in tetrahydrofuran. Eur Polym J 7:1421–1433
17. Solov'yanov AA, Kazanskii KS (1972) The kinetics and mechanism of anionic polymerization of ethylene oxide in ether solvents. Polym Sci USSR 14:1186–1195
18. Pierre LES, Price CC (1956) The room temperature polymerization of propylene oxide. J Am Chem Soc 78:3432–3436

19. Allgaier J, Willbold S, Taihyun C (2007) Synthesis of hydrophobic poly(alkylene oxide)s and amphiphilic poly(alkylene oxide) block copolymers. Macromolecules 40:518–525

20. Price CC, Akkapeddi MK (1972) Kinetics of base-catalyzed polymerization of epoxides in dimethyl sulfoxide and hexamethylphosphoric triamide. J Am Chem Soc 94:3972–3975

21. Stolarzewicz A, Neugebauer D (1999) Influence of substituent on the polymerization of oxiranes by potassium hydride. Macromol Chem Phys 200:2467–2470

22. Deffieux A, Boileau S (1977) Anionic polymerization of ethylene oxide with cryptates as counterions: 1. Polymer 18:1047–1050

23. Deffieux A, Graf E, Boileau S (1981) Anionic polymerization of ethylene oxide with cryptates as counterions: 2. Polymer 22:549–552

24. Ding J, Heatley F, Price C, Booth C (1991) Use of crown ether in the anionic polymerization of propylene oxide-2. Molecular weight and molecular weight distribution. Eur Polym J 27:895–899

25. Ding J, Price C, Booth C (1991) Use of crown ether in the anionic polymerization of propylene oxide-1. Rate of polymerization. Eur Polym J 27:891–894

26. Stolarzewicz A, Neugebauer D, Grobelny Z (1995) Influence of the crown-ether concentration and the addition of tert-butyl alcohol on anionic-polymerization of (butoxymethyl) oxirane initiated by potassium tert-butoxide. Macromol Chem Phys 196:1295–1300

27. Stolarzewicz A, Neugebauer D, Grobelny J (1996) Potassium hydride – the new initiator for anionic polymerization of oxiranes. Macromol Rapid Commun 17:787–793

28. Inoue S, Sugimoto H, Aida T (1996) Metalloporphyrin catalysts for living and immortal polymerizations. Macromol Symp 101:11–18

29. Kuroki M, Watanabe T, Aida T, Inoue S (1991) Steric separation of nucleophile and Lewis acid providing dramatically accelerated reaction. High-speed polymerization of methyl methacrylate with enolate-aluminum porphyrin/sterically crowded organoaluminum systems. J Am Chem Soc 113:5903–5904

30. Endo M, Aida T, Inoue S (1987) "Immortal" polymerization of ε-caprolactone initiated by aluminum porphyrin in the presence of alcohol. Macromolecules 20:2982–2988

31. Aida T, Inoue S (1981) Living polymerization of epoxides with metalloporphyrin and synthesis of block copolymers with controlled chain lengths. Macromolecules 14:1162–1166

32. Takeuchi D, Watanabe Y, Aida T, Inoue S (1995) Lewis acid-promoted anionic polymerization of a monomer with high cationic polymerizability. Synthesis of narrow molecular weight distribution polyoxetane and polyoxetane-poly(methyl methacrylate) block copolymer with aluminum porphyrin initiators. Macromolecules 28:651–652

33. Aida T, Mizuta R, Yoshida Y, Inoue S (1981) Polymerization of epoxides catalyzed by metalloporphine. Makromol Chem Macromol Chem Phys 182:1073–1079

34. Aida T, Wada K, Inoue S (1987) Copolymerization of epoxides by aluminum porphyrin. Reactivity of (porphinato) aluminum alkoxide as growing species. Macromolecules 20:237–241

35. Yasuda T, Aida T, Inoue S (1984) Synthesis of polyester-polyether block copolymer with controlled chain length from β-lactone and epoxide by aluminum porphyrin catalyst. Macromolecules 17:2217–2222

36. Aida T, Inoue S (1996) Metalloporphyrins as initiators for living and immortal polymerizations. Acc Chem Res 29:39–48

37. Sugimoto H, Inoue S (1999) Polymerization by metalloporphyrin and related complexes. In: Jacob S, Jiang M, Kennedy JP, Li M, Sugimoto H, Xiang M, Zhou H, Inoue S (eds) Polymer synthesis/polymer-polymer complexation. Springer, Berlin/Heidelberg, pp 39–119

38. Sugimoto H, Kawamura C, Kuroki M, Aida T, Inoue S (1994) Lewis acid-assisted anionic ring-opening polymerization of epoxide by the aluminum complexes of porphyrin, phthalocyanine, tetraazaannulene, and schiff-base as initiators. Macromolecules 27:2013–2018

39. Takeuchi D, Aida T (1996) Controlled coordinate anionic polymerization of oxetane by novel initiating systems: onium salts/bulky organoaluminum diphenolates. Macromolecules 29:8096–8100

40. Braune W, Okuda J (2003) An efficient method for controlled propylene oxide polymerization: the significance of bimetallic activation in aluminum Lewis acids. Angew Chem Int Ed 42:64–68

41. Tsvetanov CB, Petrova EB, Panayotov IM (1985) Polymerization of 1,2-epoxides initiated by tetraalkyl aluminates. 1. Polymerization of ethylene-oxide in the presence of sodium tetrabutyl aluminate. J Macromol Sci A Chem A22:1309–1324

42. Billouard C, Carlotti S, Desbois P, Deffieux A (2004) "Controlled" high-speed anionic polymerization of propylene oxide initiated by alkali metal alkoxide/trialkylaluminum systems. Macromolecules 37:4038–4043

43. Carlotti S, Billouard C, Gautriaud E, Desbois P, Deffieux A (2005) Activation mechanisms of trialkylaluminum in alkali metal alkoxides or tetraalkylammonium salts / propylene oxide controlled anionic polymerization. Macromol Symp 226:61–68

44. Carlotti S, Desbois P, Billouard C, Deffieux A (2006) Reactivity control in anionic polymerization of ethylenic and heterocyclic monomers through formation of 'ate' complexes. Polym Int 55:1126–1131

45. Labbé A, Carlotti S, Billouard C, Desbois P, Deffieux A (2007) Controlled high-speed anionic polymerization of propylene oxide initiated by onium salts in the presence of triisobutylaluminum. Macromolecules 40:7842–7847

46. Desbois P, Deffieux A, Carlotti S, Billouard C (2007) Method for the anionic polymerisation of oxiranes. US 2007100097, EP1629026

47. Desbois P, Deffieux A, Carlotti S, Billouard C (2007) Method for the anionic polymerization of oxirans. US 2007173576, EP1682603

48. Rejsek V, Sauvanier D, Billouard C, Desbois P, Deffieux A, Carlotti S (2007) Controlled anionic homo- and copolymerization of ethylene oxide and propylene oxide by monomer activation. Macromolecules 40:6510–6514

49. Rejsek V, Desbois P, Deffieux A, Carlotti S (2010) Polymerization of ethylene oxide initiated by lithium derivatives via the monomer-activated approach: application to the direct synthesis of PS-b-PEO and PI-b-PEO diblock copolymers. Polymer 51:5674–5679

50. Carlotti S, Labbé A, Rejsek V, Doutaz S, Gervais M, Deffieux A (2008) Living/controlled anionic polymerization and copolymerization of epichlorohydrin with tetraoctylammonium bromide-triisobutylaluminum initiating systems. Macromolecules 41:7058–7062

51. Labbé A, Carlotti S, Deffieux A, Hirao A (2007) Controlled polymerization of glycidyl methyl ether initiated by onium salt/triisobutylaluminum and investigation of the polymer LCST. Macromol Symp 249–250:392–397

52. Gervais M, Brocas AL, Cendejas G, Deffieux A, Carlotti S (2010) Synthesis of linear high molar mass glycidol-based polymers by monomer-activated anionic polymerization. Macromolecules 43:1778–1784

53. Quirk RP, Guo Y, Wesdemiotis C, Arnould MA (2004) Investigation of ethylene oxide oligomerization during functionalization of poly(butadienyl)lithium using MALDI-TOF MS and H-1 NMR analyses. Polymer 45:3423–3428

54. Quirk RP, Ma JJ (1988) Characterization of the functionalization reaction-product of poly (styryl)lithium with ethylene-oxide. J Polym Sci A Polym Chem 26:2031–2037

55. Goeke GL, Karol F (1980) Process for preparing olefin oxide polymerization catalysts by aging the catalysts. US 4193892

56. Dimitrov I, Tsvetanov CB (2012) 4.21 – high-molecular-weight poly(ethylene oxide). In: Matyjaszewski K, Möller M (eds) Polymer science: a comprehensive reference. Elsevier, Amsterdam, pp 551–569

57. Nelles G, Rosselli S, Miteva T, Yasuda A, Tsvetanov C, Stamenova R, Berlinova I, Petrov P (2010) Method of producing a poly (ethylene oxide) copolymerised with at least one other alkylene oxide. US 2010056753

58. Petrov P, Berlinova I, Tsvetanov CB, Rosselli S, Schmid A, Zilaei AB, Miteva T, Durr M, Yasuda A, Nelles G (2008) High-molecular-weight polyoxirane copolymers and their use in high-performance dye-sensitized solar cells. Macromol Mater Eng 293:598–604

59. Petrov P, Rangelov S, Novakov C, Brown W, Berlinova I, Tsvetanov CB (2002) Core-corona nanoparticles formed by high molecular weight poly(ethylene oxide)-b-poly(alkylglycidyl ether) diblock copolymers. Polymer 43:6641–6651

60. Dimitrov P, Hasan E, Rangejov S, Trzebicka B, Dworak A, Tsvetanov CB (2002) High molecular weight functionalized poly(ethylene oxide). Polymer 43:7171–7178

61. Hasan E, Jankova K, Samichkov V, Ivanov Y, Tsvetanov CB (2002) Graft copolymers composed of high molecular weight poly(ethylene oxide) backbone and poly (N-isopropylaerlylamide) side chains and their thermoassociating properties. Macromol Symp 177:125–138

62. Berger J, Lohse F (1985) Polymerization of para-cresyl glycidyl ether induced by benzyldimethylamine. Eur Polym J 21:435–444

63. Tanaka Y, Tomio M, Kakiuchi H (1967) Oligomerization of substituted phenyl glycidyl ethers with tertiary amine. J Macromol Sci A Chem 1:471–491

64. Dell'Erba IE, Williams RJJ (2006) Homopolymerization of epoxy monomers initiated by 4-(dimethylamino)pyridine. Polym Eng Sci 46:351–359

65. Herrmann WA (2002) N-heterocyclic carbenes: a new concept in organometallic catalysis. Angew Chem Int Ed 41:1290–1309

66. Bourissou D, Guerret O, Gabbai FP, Bertrand G (2000) Stable carbenes. Chem Rev 100:39–91

67. Naumann S, Buchmeiser MR (2014) Liberation of N-heterocyclic carbenes (NHCs) from thermally labile progenitors: protected NHCs as versatile tools in organo- and polymerization catalysis. Catal Sci Technol 4:2466–2479

68. Raynaud J, Absalon C, Gnanou Y, Taton D (2009) N-heterocyclic carbene-induced zwitterionic ring-opening polymerization of ethylene oxide and direct synthesis of α, ω-difunctionalized poly(ethylene oxide)s and poly(ethylene oxide)-b-poly(ε-caprolactone) block copolymers. J Am Chem Soc 131:3201–3209

69. Raynaud J, Absalon C, Gnanou Y, Taton D (2010) N-Heterocyclic carbene-organocatalyzed ring-opening polymerization of ethylene oxide in the presence of alcohols or trimethylsilyl nucleophiles as chain moderators for the synthesis of α, ω-heterodifunctionalized poly(ethylene oxide)s. Macromolecules 43:2814–2823

70. Raynaud J, Ottou WN, Gnanou Y, Taton D (2010) Metal-free and solvent-free access to α, ω-heterodifunctionalized poly(propylene oxide)s by N-heterocyclic carbene-induced ring opening polymerization. Chem Commun 46:3203–3205

71. Maitre C, Ganachaud F, Ferreira O, Lutz JF, Paintoux Y, Hemery P (2000) Anionic polymerization of phenyl glycidyl ether in miniemulsion. Macromolecules 33:7730–7736

72. Morinaga H, Ochiai B, Endo T (2007) Metal-free ring-opening polymerization of glycidyl phenyl ether by tetrabutylammonium fluoride. Macromolecules 40:6014–6016

73. Morinaga H, Ujihara Y, Endo T (2013) Synthesis of amphiphilic block copolymer by metal-free ring-opening oligomerization of glycidyl phenyl ether initiated with tetra-n-butylammonium fluoride in the presence of poly(ethylene glycol) monomethyl ether. J Polym Sci A Polym Chem 51:4451–4458

74. Boileau S, Illy N (2011) Activation in anionic polymerization: why phosphazene bases are very exciting promoters. Prog Polym Sci 36:1132–1151

75. Schwesinger R, Schlemper H (1987) Peralkylierte polyaminophosphazene -extrem Starke neutrale stickstoffbasen. Angew Chem 99:1212–1214

76. Esswein B, Moller M (1996) Polymerization of ethylene oxide with alkyllithium compounds and the phosphazene base "tBu-P-4". Angew Chem Int Ed 35:623–625

77. Esswein B, Steidl NM, Moller M (1996) Anionic polymerization of oxirane in the presence of the polyiminophosphazene base t-Bu-P-4. Macromol Rapid Commun 17:143–148

78. Schlaad H, Kukula H, Rudloff J, Below I (2001) Synthesis of alpha, omega-heterobifunctional poly(ethylene glycol)s by metal-free anionic ring-opening polymerization. Macromolecules 34:4302–4304

79. Schmalz H, Lanzendorfer MG, Abetz V, Muller AHE (2003) Anionic polymerization of ethylene oxide in the presence of the phosphazene base (BuP4)-P-t - Kinetic investigations using in-situ FT-NIR spectroscopy and MALDI-ToF MS. Macromol Chem Phys 204:1056–1071

80. Zhao JP, Schlaad H, Weidner S, Antonietti M (2012) Synthesis of terpene-poly(ethylene oxide)s by t-BuP4-promoted anionic ring-opening polymerization. Polym Chem 3:1763–1768

81. Zhao JP, Schlaad H (2011) Controlled anionic graft polymerization of ethylene oxide directly from poly(N-isopropylacrylamide). Macromolecules 44:5861–5864

82. Zhao J, Pahovnik D, Gnanou Y, Hadjichristidis N (2014) A "catalyst switch" strategy for the sequential metal-free polymerization of epoxides and cyclic esters/carbonate. Macromolecules 47:3814–3822

83. Zhao J, Pahovnik D, Gnanou Y, Hadjichristidis N (2014) Phosphazene-promoted metal-free ring-opening polymerization of ethylene oxide initiated by carboxylic acid. Macromolecules 47:1693–1698

84. Zhao J, Pahovnik D, Gnanou Y, Hadjichristidis N (2014) Sequential polymerization of ethylene oxide, epsilon-caprolactone and L-lactide: a one-pot metal-free route to tri- and pentablock terpolymers. Polym Chem 5:3750–3753

85. Nobori T, Hayashi T, Shibahara A, Saeki T, Yamasaki S, Ohkubo K (2010) Development of novel molecular catalysts "phosphazene catalysts" for commercial production of highly advanced polypropylene glycols. Catal Surv Asia 14:164–167

86. Rexin O, Mulhaupt R (2002) Anionic ring-opening polymerization of propylene oxide in the presence of phosphonium catalysts. J Polym Sci A Polym Chem 40:864–873

87. Rexin O, Mulhaupt R (2003) Anionic ring-opening polymerization of propylene oxide in the presence of phosphonium catalysts at various temperatures. Macromol Chem Phys 204:1102–1109

88. Misaka H, Tamura E, Makiguchi K, Kamoshida K, Sakai R, Satoh T, Kakuchi T (2012) Synthesis of end-functionalized polyethers by phosphazene base-catalyzed ring-opening polymerization of 1,2-butylene oxide and glycidyl ether. J Polym Sci A Polym Chem 50:1941–1952

89. Isono T, Kamoshida K, Satoh Y, Takaoka T, Sato S-I, Satoh T, Kakuchi T (2013) Synthesis of star- and figure-eight-shaped polyethers by t-Bu-P4-catalyzed ring-opening polymerization of butylene oxide. Macromolecules 46:3841–3849

90. Misaka H, Sakai R, Satoh T, Kakuchi T (2011) Synthesis of high molecular weight and end-functionalized poly(styrene oxide) by living ring-opening polymerization of styrene oxide using the alcohol/phosphazene base initiating system. Macromolecules 44:9099–9107

91. Hans M, Keul H, Moeller M (2009) Chain transfer reactions limit the molecular weight of polyglycidol prepared via alkali metal based initiating systems. Polymer 50:1103–1108

92. Toy AA, Reinicke S, Muller AHE, Schmalz H (2007) One-pot synthesis of polyglycidol-containing block copolymers with alkyllithium initiators using the phosphazene base t-BuP4. Macromolecules 40:5241–5244

93. Isono T, Satoh Y, Miyachi K, Chen Y, S-i S, Tajima K, Satoh T, Kakuchi T (2014) Synthesis of linear, cyclic, figure-eight-shaped, and tadpole-shaped amphiphilic block copolyethers via t-Bu-P4-catalyzed ring-opening polymerization of hydrophilic and hydrophobic glycidyl ethers. Macromolecules 47:2853–2863

94. Groenewolt M, Brezesinski T, Schlaad H, Antonietti M, Groh PW, Ivan B (2005) Polyisobutylene-block-poly(ethylene oxide) for robust templating of highly ordered mesoporous materials. Adv Mater 17:1158–1162

95. Thomas A, Schlaad H, Smarsly B, Antonietti M (2003) Replication of lyotropic block copolymer mesophases into porous silica by nanocasting: Learning about finer details of polymer self-assembly. Langmuir 19:4455–4459

96. Yang H, Yan M, Pispas S, Zhang G (2011) Synthesis of poly (ethylene carbonate)-co-(ethylene oxide) copolymer by phosphazene-catalyzed ROP. Macromol Chem Phys 212:2589–2593

97. Forster S, Kramer E (1999) Synthesis of PB-PEO and PI-PEO block copolymers with alkyllithium initiators and the phosphazene base t-BuP4. Macromolecules 32:2783–2785

98. Zhao J, Alamri H, Hadjichristidis N (2013) A facile metal-free "grafting-from" route from acrylamide-based substrate toward complex macromolecular combs. Chem Commun 49:7079–7081

99. Zhao JP, Mountrichas G, Zhang GX, Pispas S (2009) Amphiphilic polystyrene-b-poly (p-hydroxystyrene-g-ethylene oxide) block-graft copolymers via a combination of conventional and metal-free anionic polymerization. Macromolecules 42:8661–8668

100. Zhao JP, Zhang GZ, Pispas S (2010) Thermoresponsive brush copolymers with poly(propylene oxide-ran-ethylene oxide) side chains via metal-free anionic polymerization "grafting from" technique. J Polym Sci A Polym Chem 48:2320–2328

101. Esswein B, Molenberg A, Moller M (1996) Use of polyiminophosphazene bases for ring-opening polymerizations. Macromol Symp 107:331–340

102. Brocas AL, Mantzaridis C, Tunc D, Carlotti S (2013) Polyether synthesis: from activated or metal-free anionic ring-opening polymerization of epoxides to functionalization. Prog Polym Sci 38:845–873

103. Obermeier B, Wurm F, Mangold C, Frey H (2011) Multifunctional poly(ethylene glycol)s. Angew Chem Int Ed 50:7988–7997

104. Mangold C, Wurm F, Frey H (2012) Functional PEG-based polymers with reactive groups via anionic ROP of tailor-made epoxides. Polym Chem 3:1714–1721

105. Thompson MS, Vadala TP, Vadala ML, Lin Y, Riffle JS (2008) Synthesis and applications of heterobifunctional poly(ethylene oxide) oligomers. Polymer 49:345–373

106. Chattopadhyay DK, Raju K (2007) Structural engineering of polyurethane coatings for high performance applications. Prog Polym Sci 32:352–418

107. Gnanou Y, Lutz P, Rempp P (1988) Synthesis of star-shaped poly(ethylene oxide). Makromol Chem Macromol Chem Phys 189:2885–2892

108. Hou S, Chaikof EL, Taton D, Gnanou Y (2003) Synthesis of water-soluble star-block and dendrimer-like copolymers based on poly(ethylene oxide) and poly(acrylic acid). Macromolecules 36:3874–3881

109. Lapienis G (2009) Star-shaped polymers having PEO arms. Prog Polym Sci 34:852–892

110. Six JL, Gnanou Y (1995) From star-shaped to dendritic poly(ethylene oxide)s – toward increasingly branched architectures by anionic-polymerization. Macromol Symp 95:137–150

111. Taton D, Saule M, Logan J, Duran R, Sijian HOU, Chaikof EL, Gnanou Y (2003) Polymerization of ethylene oxide with a calixarene-based precursor: Synthesis of eight-arm poly (ethylene oxide) stars by the core-first methodology. J Polym Sci A Polym Chem 41:1669–1676

112. Choi YR, Bae YH, Kim SW (1998) Star-shaped poly(ether-ester) block copolymers: synthesis, characterization, and their physical properties. Macromolecules 31:8766–8774

113. Comanita B, Noren B, Roovers J (1999) Star poly(ethylene oxide)s from carbosilane dendrimers. Macromolecules 32:1069–1072

114. Dworak A, Walach W (2009) Synthesis, characterization and properties of functional star and dendritic block copolymers of ethylene oxide and glycidol with oligoglycidol branching units. Polymer 50:3440–3447

115. Brocas AL, Deffieux A, Le Malicot N, Carlotti S (2012) Combination of phosphazene base and triisobutylaluminum for the rapid synthesis of polyhydroxy telechelic poly(propylene oxide). Polym Chem 3:1189–1195

116. Mosquet M, Chevalier Y, LePerchec P, Guicquero JP (1997) Synthesis of poly(ethylene oxide) with a terminal amino group by anionic polymerization of ethylene oxide initiated by aminoalcoholates. Macromol Chem Phys 198:2457–2474

117. Morinaga H, Ujihara Y, Yuto N, Nagai D, Endo T (2011) Controlled polymerization of epoxides: metal-free ring-opening polymerization of glycidyl phenyl ether initiated by tetra-n-butylammonium fluoride in the presence of protic compounds. J Polym Sci A Polym Chem 49:5210–5216

118. Wong EWC (1981) Development of a biomedical polyurethane. In: Urethane chemistry and applications, vol 172, ACS Symposium Series of American Chemical Society., pp 489–504

119. Sandler SR, Berg F (1966) Room temperature polymerization of glycidol. J Polym Sci A Polym Chem 4:1253–1259

120. Sunder A, Hanselmann R, Frey H, Mulhaupt R (1999) Controlled synthesis of hyperbranched polyglycerols by ring-opening multibranching polymerization. Macromolecules 32:4240–4246

121. Sunder A, Heinemann J, Frey H (2000) Controlling the growth of polymer trees: concepts and perspectives for hyperbranched polymers. Chem Eur J 6:2499–2506

122. Sunder A, Mulhaupt R, Haag R, Frey H (2000) Hyperbranched polyether polyols: a modular approach to complex polymer architectures. Adv Mater 12:235–239

123. Vandenberg EJ (1985) Polymerization of glycidol and its derivatives – a new rearrangement polymerization. J Polym Sci A Polym Chem 23:915–949

124. Wilms D, Stiriba SE, Frey H (2010) Hyperbranched polyglycerols: from the controlled synthesis of biocompatible polyether polyols to multipurpose applications. Acc Chem Res 43:129–141

125. Wurm F, Frey H (2011) Linear-dendritic block copolymers: the state of the art and exciting perspectives. Prog Polym Sci 36:1–52

126. Schüll C, Wilms D, Frey H (2012) 4.22 – nonlinear macromolecules by ring-opening polymerization. In: Matyjaszewski K, Möller M (eds) Polymer science: a comprehensive reference. Elsevier, Amsterdam, pp 571–596

127. Dimitrov P, Rangelov S, Dworak A, Tsvetanov CB (2004) Synthesis and associating properties of poly(ethoxyethyl glycidyl ether)/poly(propylene oxide) triblock copolymers. Macromolecules 37:1000–1008

128. Libera M, Trzebicka B, Kowalczuk A, Walach W, Dworak A (2011) Synthesis and thermoresponsive properties of four arm, amphiphilic poly(tert-butyl-glycidylether)-block-polyglycidol stars. Polymer 52:250–257

129. Libera M, Walach W, Trzebicka B, Rangelov S, Dworak A (2011) Thermosensitive dendritic stars of tert-butyl-glycidylether and glycidol – synthesis and encapsulation properties. Polymer 52:3526–3536

130. Mendrek A, Mendrek S, Trzebicka B, Kuckling D, Walach J, Adler HJ, Dworak A (2005) Polyether core-shell cylinder-polymerization of polyglycidol macromonomers. Macromol Chem Phys 206:2018–2026

131. Walach W, Trzebicka B, Justynska J, Dworak A (2004) High molecular arborescent polyoxyethylene with hydroxyl containing shell. Polymer 45:1755–1762

132. Haamann D, Keul H, Klee D, Moller M (2010) Functionalization of linear and star-shaped polyglycidols with vinyl sulfonate groups and their reaction with different amines and alcohols. Macromolecules 43:6295–6301

133. Erberich M, Keul H, Moller M (2007) Polyglycidols with two orthogonal protective groups: preparation, selective deprotection, and functionalization. Macromolecules 40:3070–3079

134. Keul H, Moller M (2009) Synthesis and degradation of biomedical materials based on linear and star shaped polyglycidols. J Polym Sci A Polym Chem 47:3209–3231

135. Mangold C, Wurm F, Obermeier B, Frey H (2010) "Functional poly(ethylene glycol)": PEG-based random copolymers with 1,2-diol side chains and terminal amino functionality. Macromolecules 43:8511–8518

136. Wurm F, Nieberle J, Frey H (2008) Synthesis and characterization of poly(glyceryl glycerol) block copolymers. Macromolecules 41:1909–1911

137. Backes M, Messager L, Mourran A, Keul H, Moeller M (2010) Synthesis and thermal properties of well-defined amphiphilic block copolymers based on polyglycidol. Macromolecules 43:3238–3248
138. Halacheva S, Rangelov S, Tsvetanov C (2006) Poly(glycidol)-based analogues to pluronic block copolymers. Synthesis and aqueous solution properties. Macromolecules 39:6845–6852
139. Huang J, Li ZY, Xu XW, Ren Y, Huang JL (2006) Preparation of novel poly(ethyleneoxide-co-glycidol)-graft-poly(epsilon-caprolactone) copolymers and inclusion complexation of the grafted chains with alpha-cyclodextrin. J Polym Sci A Polym Chem 44:3684–3691
140. Kaluzynski K, Pretula J, Lapienis G, Basko M, Bartczak Z, Dworak A, Penczek S (2001) Dihydrophilic block copolymers with ionic and nonionic blocks. I. Poly(ethylene oxide)-b-polyglycidol with OP(O)(OH)(2) COOH, or SO₃H functions: synthesis and influence for CaCO₃ crystallization. J Polym Sci A Polym Chem 39:955–963
141. Li ZY, Chau Y (2009) Synthesis of linear polyether polyol derivatives as new materials for bioconjugation. Bioconjugate Chem 20:780–789
142. Kochergin YS, Pyrikov AV, Kulik TA, Grigorenko TI (2010) Investigation of epoxide adhesive compositions cured with polyoxypropylene triamine. Polym Sci Ser D 3:47–49
143. Morgan RJ, Kong FM, Walkup CM (1984) Structure property relations of polyethertriamine-cured bisphenol-A-diglycidyl ether epoxies. Polymer 25:375–386
144. Poellmann K, Muenter J (2007) Polyetheramine macromonomers comprising two neighboring hydroxyl groups and their use for producing polyurethanes. US 20070376273
145. Rowton LR (1971) Polyoxypropylenediamine chain extenders for polyurethane latices CA877362
146. Yokoyama M, Okano T, Sakurai Y, Kikuchi A, Ohsako N, Nagasaki Y, Kataoka K (1992) Synthesis of poly(ethylene oxide) with heterobifunctional reactive groups at its terminals by an anionic initiator. Bioconjugate Chem 3:275–276
147. Obermeier B, Wurm F, Frey H (2010) Amino functional poly(ethylene glycol) copolymers via protected amino glycidol. Macromolecules 43:2244–2251
148. Reuss VS, Obermeier B, Dingels C, Frey H (2012) N, N-diallylglycidylamine: a Key monomer for amino-functional poly(ethylene glycol) architectures. Macromolecules 45:4581–4589
149. Meyer J, Keul H, Moller M (2011) Poly(glycidyl amine) and copolymers with glycidol and glycidyl amine repeating units: synthesis and characterization. Macromolecules 44:4082–4091
150. Du J, Murakami Y, Senyo T, Adam IK, Yagci Y (2004) Synthesis of well-defined hybrid macromonomers of poly(ethylene oxide) and their reactivity in photoinitiated polymerization. Macromol Chem Phys 205:1471–1478
151. Studer P, Breton P, Riess G (2005) Allyl end-functionalized poly(ethylene oxide)-block-poly(methylidene malonate 2.1.2) block copolymers: synthesis, characterization, and chemical modification. Macromol Chem Phys 206:2461–2469
152. Herrwerth S, Rosendahl T, Feng C, Fick J, Eck W, Himmelhaus M, Dahint R, Grunze M (2003) Covalent coupling of antibodies to self-assembled monolayers of carboxy-functionalized poly(ethylene glycol): protein resistance and specific binding of biomolecules. Langmuir 19:1880–1887
153. Harris H, Lamy Y, Lutz PJ (2006) Macromonomers as well-defined building blocks in the synthesis of hybrid octafunctional star shaped or crosslinked poly(ethylene oxide)s. Polym Prepr 47:551–552
154. Harris H, Nohra B, Gavat O, Lutz PJ (2010) New trends in poly(ethylene oxide) or polystyrene macromonomer based networks exhibiting silsesquioxane cross-linking points. Macromol Symp 291–292:43–49

155. Lee BF, Wolffs M, Delaney KT, Sprafke JK, Leibfarth FA, Hawker CJ, Lynd NA (2012) Reactivity ratios and mechanistic insight for anionic ring-opening copolymerization of epoxides. Macromolecules 45:3722–3731

156. Brocas AL, Cendejas G, Caillol S, Deffieux A, Carlotti S (2011) Controlled synthesis of polyepichlorohydrin with pendant cyclic carbonate functions for isocyanate-free polyurethane networks. J Polym Sci A Polym Chem 49:2677–2684

157. Lee BF, Kade MJ, Chute JA, Gupta N, Campos LM, Fredrickson GH, Kramer EJ, Lynd NA, Hawker CJ (2011) Poly(allyl glycidyl ether) – a versatile and functional polyether platform. J Polym Sci A Polym Chem 49:4498–4504

158. Mangold C, Dingels C, Obermeier B, Frey H, Wurm F (2011) PEG-based multifunctional polyethers with highly reactive vinyl-ether side chains for click-type functionalization. Macromolecules 44:6326–6334

159. Cheng GW, Fan XD, Tian W, Liu YY, Kong JE (2010) Synthesis of three-arm poly(ethylene glycol) by combination of controlled anionic polymerization and 'click' chemistry. Polym Int 59:543–551

160. Hua C, Peng SM, Dong CM (2008) Synthesis and characterization of linear-dendron-like poly(epsilon-caprolactone)-b-poly(ethylene oxide) copolymers via the combination of ring-opening polymerization and click chemistry. Macromolecules 41:6686–6695

161. Stefanko MJ, Gun'ko YK, Rai DK, Evans P (2008) Synthesis of functionalised polyethylene glycol derivatives of naproxen for biomedical applications. Tetrahedron 64:10132–10139

162. Wang WJ, Li T, Yu T, Zhu FM (2008) Synthesis of Multiblock Copolymers by Coupling Reaction Based on Self-Assembly and Click Chemistry. Macromolecules 41:9750–9754

163. Hiki S, Kataoka K (2007) A facile synthesis of azido-terminated heterobifunctional poly (ethylene glycol)s for "click" conjugation. Bioconjugate Chem 18:2191–2196

164. Bertozzi CR, Bednarski MD (1991) The synthesis of heterobifunctional linkers for the conjugation of ligands to molecular probes. J Org Chem 56:4326–4329

165. Iyer SS, Anderson AS, Reed S, Swanson B, Schmidt JG (2004) Synthesis of orthogonal end functionalized oligoethylene glycols of defined lengths. Tetrahedron Lett 45:4285–4288

166. Gervais M, Labbé A, Carlotti S, Deffieux A (2009) Direct synthesis of α-Azido, ω-hydroxypolyethers by monomer-Activated anionic polymerization. Macromolecules 42:2395–2400

167. Huisgen R (1984) 1,3-Dipolar Cycloaddition Chemistry. In: Padwa A (ed) 1,3-Dipolar cycloaddition chemistry. Wiley, New York, pp 1–176

168. Zeng F, Allen C (2006) Synthesis of carboxy-functionalized heterobifunctional poly(ethylene glycol) by a thiol-anionic polymerization method. Macromolecules 39:6391–6398

169. Mizrahi DM, Omer-Mizrahi M, Goldshtein J, Askinadze N, Margel S (2010) Novel Poly (ethylene glycol) Monomers Bearing Diverse Functional Groups. J Polym Sci A, Polym Chem 48:5468–5478

170. Vadala ML, Thompson MS, Ashworth MA, Lin Y, Vadala TP, Ragheb R, Riffle JS (2008) Heterobifunctional poly(ethylene oxide) oligomers containing carboxylic acids. Biomacromolecules 9:1035–1043

171. Zhang S, Du H, Sun R, Li XP, Yang DJ, Zhang SG, Xiong CD, Peng YX (2003) Synthesis of heterobifunctional poly(ethylene glycol) with a primary amino group at one end and a carboxylate group at the other end. React Funct Polym 56:17–25

172. Akiyama Y, Nagasaki Y, Kataoka K (2004) Synthesis of heterotelechelic poly(ethylene glycol) derivatives having alpha-benzaldehyde and omega-pyridyl disulfide groups by ring opening polymerization of ethylene oxide using 4-(diethoxymethyl)benzyl alkoxide as a novel initiator. Bioconjugate Chem 15:424–427

173. Labbé A, Brocas AL, Ibarboure E, Ishizone T, Hirao A, Deffieux A, Carlotti S (2011) Selective ring-opening polymerization of glycidyl methacrylate: Toward the synthesis of cross-linked (co)polyethers with thermoresponsive properties. Macromolecules 44:6356–6364

174. Jerome C, Lecomte P (2008) Recent advances in the synthesis of aliphatic polyesters by ring-opening polymerization. Adv Drug Deliv Rev 60:1056–1076

175. Lecomte P, Jerome C (2012) Recent developments in ring-opening polymerization of lactones. In: Rieger B, Kunkel A, Coates GW, Reichardt R, Dinjus E, Zevaco TA (eds) Advances in polymer science. Synthetic biodegradable polymers, vol 245. pp 173–217

176. Albertsson A-C, Varma IK, Srivastava RK (2009) Polyesters from large lactones. In: Handbook of ring-opening polymerization. Wiley-VCH Verlag GmbH & Co. KGaA, pp 287–306

177. Coulembier O, Dubois P (2009) Polyesters from β-lactones. In: Handbook of ring-opening polymerization. Wiley-VCH Verlag GmbH & Co. KGaA, pp 227–254

178. Dechy-Cabaret O, Martin-Vaca B, Bourissou D (2009) Polyesters from dilactones. In: Handbook of ring-opening polymerization. Wiley-VCH Verlag GmbH & Co. KGaA, pp 255–286

179. Dechy-Cabaret O, Martin-Vaca B, Bourissou D (2004) Controlled ring-opening polymerization of lactide and glycolide. Chem Rev 104:6147–6176

180. Duda A (2012) 4.11 – ROP of cyclic esters. Mechanisms of ionic and coordination processes. In: Matyjaszewski K, Möller M (eds) Polymer science: a comprehensive reference. Elsevier, Amsterdam, pp 213–246

181. Labet M, Thielemans W (2009) Synthesis of polycaprolactone: a review. Chem Soc Rev 38:3484–3504

182. Platel RH, Hodgson LM, Williams CK (2008) Biocompatible initiators for lactide polymerization. Polymer Reviews 48:11–63

183. Slomkowski S (2012) 4.25 – Ring-opening dispersion polymerization. In: Matyjaszewski K, Möller M (eds) Polymer science: a comprehensive reference. Elsevier, Amsterdam, pp 645–660

184. Thomas CM (2010) Stereocontrolled ring-opening polymerization of cyclic esters: synthesis of new polyester microstructures. Chem Soc Rev 39:165–173

185. Wheaton CA, Hayes PG, Ireland BJ (2009) Complexes of Mg. Ca and Zn talyas homogeneous casts for lactide polymerization. Dalton Trans (25):4832–4846

186. Gupta AP, Kumar V (2007) New emerging trends in synthetic biodegradable polymers - Polylactide: A critique. Eur Polym J 43:4053–4074

187. Zhu ZX, Deng XM, Xiong CD (2001) Anionic ring-opening polymerization of D.L-lactide. Ind J Chem B - Org Chem Med Chem 40:108–112

188. Kurcok P, Matuslonicz A, Jedlinski Z (1995) Anionic-polymerization as a tool in the synthesis of biodegradable polymers. J Polym Mater 12:161–174

189. Jedlinski Z, Kurcok P, Lenz RW (1995) Synthesis of potentially biodegradable polymers. J Macromol Sci, Pure Appl Chem A32:797–810

190. Jedlinski Z, Walach W, Kurcok P, Adamus G (1991) Polymerization of lactones.12. Polymerization of L-dilactide and L, D-dilactide in the presence of potassium methoxide. Makromol Chem. Macromol Chem Phys 192:2051–2057

191. Sipos L, Zsuga M, Kelen T (1992) Living ring-opening polymerization of L, L-lactide initiated with potassium tert-butoxide and its 18-crown-6 complex. Polym Bull 27:495–502

192. Kricheldorf HR, Kreisersaunders I (1990) Polylactones.19. Anionic-polymerization of L-lactide in solution. Makromol Chem. Macromol Chem Phys 191:1057–1066

193. Kricheldorf HR, Kreisersaunders I, Scharnagl N (1990) Anionic and pseudoanionic polymerization of lactones - a comparison. Makromol Chem, Macromol Symp 32:285–298

194. Kricheldorf HR, Boettcher C (1993) Polylactones.27. Anionic-polymerization of L-lactide - variation of endgroups and synthesis of block-copolymers with poly(ethylene oxide). Makromol Chem. Macromol Symp 73:47–64

195. Kitamura T, Matsumoto A (2007) Synthesis of poly(lactic acid) with branched and network structures containing thermally degradable junctions. Macromolecules 40:509–517

196. Stere C, Iovu M, Boborodea A, Vasilescu DS, Fazakas-Anca IS (1998) Anionic and ionic coordinative polymerization of L-lactide. Polym Adv Technol 9:322–325

197. Sipos L, Gunda T, Zsuga M (1997) The role of complex formation in the anionic polymerization of L-lactide. Polym Bull 38:609–612
198. Sipos L, Zsuga M (1997) Anionic polymerization of L-lactide effect of lithium and potassium as counterions. J Macromol Sci, Pure Appl Chem A34:1269–1284
199. Kasperczyk JE (1995) Microstructure Analysis of Poly(lactic acid) Obtained by Lithium tert-Butoxide as Initiator. Macromolecules 28:3937–3939
200. Bero M, Dobrzyński P, Kasperczyk J (1999) Synthesis of disyndiotactic polylactide. J Polym Sci A Polym Chem 37:4038–4042
201. Kricheldorf HR, Boettcher C (1993) Polylactones 26. Lithium alkoxide-initiated polymerizations of L-lactide. Makromol Chem 194:1665–1669
202. Bhaw-Luximon A, Jhurry D, Spassky N, Pensec S, Belleney J (2001) Anionic polymerization of D, L-lactide initiated by lithium diisopropylamide. Polymer 42:9651–9656
203. Emoto K, Nagasaki Y, Iijima M, Kato M, Kataoka K (2000) Preparation of non-fouling surface through the coating with core-polymerized block copolymer micelles having aldehyde-ended PEG shell. Coll Surf B Biointerf 18:337–346
204. Jule E, Nagasaki Y, Kataoka K (2002) Surface plasmon resonance study on the interaction between lactose-installed poly(ethylene glycol)-poly(D, L-lactide) block copolymer micelles and lectins immobilized on a gold surface. Langmuir 18:10334–10339
205. Jule E, Yamamoto Y, Thouvenin M, Nagasaki Y, Kataoka K (2004) Thermal characterization of poly(ethylene glycol)-poly(D, L-lactide) block copolymer micelles based on pyrene excimer formation. J Control Rel 97:407–419
206. Kim JH, Emoto K, Iijima M, Nagasaki Y, Aoyagi T, Okano T, Sakurai Y, Kataoka K (1999) Core-stabilized polymeric micelle as potential drug carrier: Increased solubilization of taxol. Polym Adv Technol 10:647–654
207. Moroishi H, Yoshida C, Murakami Y (2013) A free-standing, sheet-shaped, "hydrophobic" biomaterial containing polymeric micelles formed from poly(ethylene glycol)-poly(lactic acid) block copolymer for possible incorporation/release of "hydrophilic" compounds. Coll Surf B Biointerf 102:597–603
208. Nagasaki Y, Okada T, Scholz C, Iijima M, Kato M, Kataoka K (1998) The reactive polymeric micelle based on an aldehyde-ended poly(ethylene glycol)/poly(lactide) block copolymer. Macromolecules 31:1473–1479
209. Tanodekaew S, Pannu R, Heatley F, Attwood D, Booth C (1997) Association and surface properties of diblock copolymers of ethylene oxide and DL-lactide in aqueous solution. Macromol Chem Phys 198:927–944
210. Yang X, Grailer JJ, Pilla S, Steeber DA, Gong S, Shuai X (2010) Multifunctional polymeric vesicles for targeted drug delivery and imaging. Biofabrication 2:025004
211. Yang X, Pilla S, Grailer JJ, Steeber DA, Gong S, Chen Y, Chen G (2009) Tumor-targeting, superparamagnetic polymeric vesicles as highly efficient MRI contrast probes. J Mater Chem 19:5812–5817
212. Yasugi K, Nagasaki Y, Kato M, Kataoka K (1999) Preparation and characterization of polymer micelles from poly(ethylene glycol)-poly(D, L-lactide) block copolymers as potential drug carrier. J Control Rel 62:89–100
213. Jedlinski Z, Kurcok P, Walach W, Janeczek H, Radecka I (1993) Polymerization of lactones.17. Synthesis of ethylene glycol-L-lactide block-copolymers. Makromol Chem. Macromol Chem Phys 194:1681–1689
214. Lemmouchi Y, Perry MC, Amass AJ, Chakraorty K, Schue F (2007) Novel synthesis of biodegradable poly(lactide-co-ethylene glycol) block copolymers. J Polym Sci A, Polym Chem 45:2235–2245
215. Stefani M, Coudane J, Vert M (2006) Effects of polymerization conditions on the in vitro hydrolytic degradation of plaques of poly(DL-lactic acid-block-ethylene glycol) diblock copolymers. Polym Degrad Stab 91:2853–2859
216. Stefani M, Coudane J, Vert M (2006) In vitro ageing and degradation of PEG – PLA diblock copolymer-based nanoparticles. Polym Degrad Stab 91:2554–2559

217. Zhu ZX, Xiong CD, Zhang LL, Yuan ML, Deng XM (1999) Preparation of biodegradable polylactide-co-poly(ethylene glycol) copolymer by lactide reacted poly(ethylene glycol). Eur Polym J 35:1821–1828

218. Pannu RK, Tanodekaew S, Li W, Collett JH, Attwood D, Booth C (1999) A DSC study of the miscibility of poly(ethylene oxide)-block-poly(DL-lactide) copolymers with poly (DL-lactide). Biomaterials 20:1381–1387

219. Sipos L, Zsuga M, Deak G (1995) Synthesis of poly(L-lactide)-block-polyisobutylene-block-poly(L-lactide), a new biodegradable thermoplastic elastomer. Macromol Rapid Commun 16:935–940

220. Deng XM, Zhu ZX, Xiong CD, Zhang LL (1997) Synthesis and characterization of biodegradable block copolymers of epsilon-caprolactone and D, L-lactide initiated by potassium poly(ethylene glycol)ate. J Polym Sci A, Polym Chem 35:703–708

221. Gadzinowski M, Sosnowski S (2003) Biodegradable/biocompatible ABC triblock copolymer bearing hydroxyl groups in the middle block. J Polym Sci A Polym Chem 41:3750–3760

222. Ohya Y, Maruhashi S, Ouchi T (1998) Preparation of poly(lactic acid)-grafted amylose through the trimethylsilyl protection method and its biodegradation. Macromol Chem Phys 199:2017–2022

223. Ouchi T, Saito T, Kontani T, Ohya Y (2004) Encapsulation and/or release behavior of bovine serum albumin within and from polylactide-grafted dextran microspheres. Macromol Biosci 4:458–463

224. Nederberg F, Connor EF, Möller M, Glauser T, Hedrick JL (2001) New paradigms for organic catalysts: the first organocatalytic living polymerization. Angew Chem Int Ed 40:2712–2715

225. Dove AP (2012) Organic catalysis for ring-opening polymerization. ACS Macro Lett 1:1409–1412

226. Fèvre M, Pinaud J, Gnanou Y, Vignolle J, Taton D (2013) N-Heterocyclic carbenes (NHCs) as organocatalysts and structural components in metal-free polymer synthesis. Chem Soc Rev 42:2142–2172

227. Kamber NE, Jeong W, Waymouth RM, Pratt RC, Lohmeijer BGG, Hedrick JL (2007) Organocatalytic ring-opening polymerization. Chem Rev 107:5813–5840

228. Kiesewetter MK, Shin EJ, Hedrick JL, Waymouth RM (2010) Organocatalysis: opportunities and challenges for polymer synthesis. Macromolecules 43:2093–2107

229. Kricheldorf HR, Lomadze N, Schwarz G (2008) Cyclic polylactides by imidazole-catalyzed polymerization of L-lactide. Macromolecules 41:7812–7816

230. Katiyar V, Nanavati H (2010) Ring-opening polymerization of L-lactide using N-heterocyclic molecules: mechanistic, kinetics and DFT studies. Polym Chem 1:1491–1500

231. Brown HA, De Crisci AG, Hedrick JL, Waymouth RM (2012) Amidine-mediated zwitterionic polymerization of lactide. ACS Macro Lett 1:1113–1115

232. Myers M, Connor EF, Glauser T, Möck A, Nyce GW, Hedrick JL (2002) Phosphines: nucleophilic organic catalysts for the controlled ring-opening polymerization of lactides. J Polym Sci A Polym Chem 40:844–851

233. Zhang L, Nederberg F, Messman JM, Pratt RC, Hedrick JL, Wade CG (2007) Organocatalytic stereoselective ring-opening polymerization of lactide with dimeric phosphazene bases. J Am Chem Soc 129:12610–12611

234. Zhang L, Nederberg F, Pratt RC, Waymouth RM, Hedrick JL, Wade C (2007) Phosphazene bases: a new category of organocatalysts for the living ring-opening polymerization of cyclic esters. Macromolecules 40:4154–4158

235. Brule E, Guerineau V, Vermaut P, Prima F, Balogh J, Maron L, Slawin AMZ, Nolan SP, Thomas CM (2013) Polymerization of cyclic esters using N-heterocyclic carbene carboxylate catalysts. Polym Chem 4:2414–2423

236. Coulembier O, Lohmeijer BGG, Dove AP, Pratt RC, Mespouille L, Culkin DA, Benight SJ, Dubois P, Waymouth RM, Hedrick JL (2006) Alcohol adducts of N-heterocyclic carbenes:

latent catalysts for the thermally-controlled living polymerization of cyclic esters. Macromolecules 39:5617–5628

237. Connor EF, Nyce GW, Myers M, Mock A, Hedrick JL (2002) First example of N-heterocyclic carbenes as catalysts for living polymerization: oganocatalytic ring-opening polymerization of cyclic esters. J Am Chem Soc 124:914–915

238. Coulembier O, Dove AP, Pratt RC, Sentman AC, Culkin DA, Mespouille L, Dubois P, Waymouth RM, Hedrick JL (2005) Latent, thermally activated organic catalysts for the on-demand living polymerization of lactide. Angew Chem Int Ed 44:4964–4968

239. Dorresteijn R, Haschick R, Klapper M, Mullen K (2012) Poly(l-lactide) nanoparticles via ring-opening polymerization in non-aqueous emulsion. Macromol Chem Phys 213:1996–2002

240. Dove AP, Pratt RC, Lohmeijer BGG, Culkin DA, Hagberg EC, Nyce GW, Waymouth RM, Hedrick JL (2006) N-Heterocyclic carbenes: effective organic catalysts for living polymerization. Polymer 47:4018–4025

241. Jeong W, Shin EJ, Culkin DA, Hedrick JL, Waymouth RM (2009) Zwitterionic polymerization: a kinetic strategy for the controlled synthesis of cyclic polylactide. J Am Chem Soc 131:4884–4891

242. Nyce GW, Glauser T, Connor EF, Mock A, Waymouth RM, Hedrick JL (2003) In situ generation of carbenes: a general and versatile platform for organocatalytic living polymerization. J Am Chem Soc 125:3046–3056

243. Wang Y, Zhang L, Guo X, Zhang R, Li J (2013) Characteristics and mechanism of L-lactide polymerization using N-heterocyclic carbene organocatalyst. J Polym Res 20:87

244. Dove AP, Li HB, Pratt RC, Lohmeijer BGG, Culkin DA, Waymouth RM, Hedrick JL (2006) Stereoselective polymerization of rac- and meso-lactide catalyzed by sterically encumbered N-heterocyclic carbenes. Chem Commun (27):2881–2883

245. Culkin DA, Jeong WH, Csihony S, Gomez ED, Balsara NR, Hedrick JL, Waymouth RM (2007) Zwitterionic polymerization of lactide to cyclic poly(lactide) by using N-heterocyclic carbene organocatalysts. Angew Chem Int Ed 46:2627–2630

246. Shin EJ, Jones AE, Waymouth RM (2012) Stereocomplexation in cyclic and linear polylactide blends. Macromolecules 45:595–598

247. Nyce GW, Csihony S, Waymouth RM, Hedrick JL (2004) A general and versatile approach to thermally generated N-heterocyclic carbenes. Chem Eur J 10:4073–4079

248. Csihony S, Culkin DA, Sentman AC, Dove AP, Waymouth RM, Hedrick JL (2005) Single-component catalyst/initiators for the organocatalytic ring-opening polymerization of lactide. J Am Chem Soc 127:9079–9084

249. Xiao Y, Coulembier O, Koning CE, Heise A, Dubois P (2009) Cumulated advantages of enzymatic and carbene chemistry for the non-organometallic synthesis of (co)polyesters. Chem Commun 2009:2472–2474

250. Csihony S, Beaudette TT, Sentman AC, Nyce GW, Waymouth RM, Hedrick JL (2004) Bredereck's reagent revisited: latent anionic ring-opening polymerization and transesterification reactions. Adv Synth Catal 346:1081–1086

251. Coulembier O, De Winter J, Josse T, Mespouille L, Gerbaux P, Dubois P (2014) One-step synthesis of polylactide macrocycles from sparteine-initiated ROP. Polym Chem 5:2103–2108

252. Xia H, Kan S, Li Z, Chen J, Cui S, Wu W, Ouyang P, Guo K (2014) N-heterocyclic carbenes as organocatalysts in controlled/living ring-opening polymerization of O-carboxyanhydrides derived from l-lactic acid and l-mandelic acid. J Polym Sci A, Polym Chem 52:2306–2315

253. Laycock B, Halley P, Pratt S, Werker A, Lant P (2013) The chemomechanical properties of microbial polyhydroxyalkanoates. Prog Polym Sci 38:536–583

254. Jedlinski Z (1993) Novel chemistry of beta-lactones anionic-polymerization. Makromol Chem Macromol Symp 73:65–76

255. Jedlinski Z (1993) Novel degradable engineering polyesters – synthesis and applications. J Macromol Sci Pure Appl Chem A30:689–701

256. Jedliński Z, Kowalczuk M, Kurcok P (1986) Anionic ring opening polymerization by alkali metal solutions. Makromol Chem Macromol Symp 3:277–293
257. Jedlinski Z, Kurcok P, Kowalczuk M (1995) Novel anionic-polymerization of beta-lactones mediated by alkali-metal supramolecular complexes. Polym Int 37:187–190
258. Jedlinski ZJ, Kowalczuk M, Kurcok P (1994) Novel evidence on the chemistry of beta-lactone anionic-polymerization. Macromol Symp 88:217–226
259. Kricheldorf HR, Scharnagl N (1989) Polyactones. 17. Anionic polymerization of β-D, L-butyrolactone. J Macromol Sci A Chem 26:951–968
260. Lenz RW, Jedlinski Z (1996) Anionic and coordination polymerization of 3-butyrolactone. Macromol Symp 107:149–161
261. Yamashita Y, Tsuda T, Ishida H, Uchikawa A, Kuriyama Y (1968) Anionic copolymerization of β-lactones in correlation with the mode of fission. studies on the syntheses of aliphatic polyesters. XI. Makromol Chem 113:139–146
262. Jedlinski Z, Kowalczuk M, Glowkowski W, Grobelny J, Szwarc M (1991) Novel polymerization of beta-butyrolactone initiated by potassium naphthalenide in the presence of a crown-ether or a cryptand. Macromolecules 24:349–352
263. Slomkowski S, Penczek S (1976) Influence of dibenzo-18-crown-6 ether on the kinetics of anionic polymerization of β-propiolactone. Macromolecules 9:367–369
264. Deffieux A, Boileau S (1976) Use of cryptates in anionic-polymerization of lactones. Macromolecules 9:369–371
265. Jedlinski Z, Kurcok P, Adamus G, Juzwa M (2000) Biomimetic polyesters and their role in ion transport across cell membranes. Acta Biochim Polon 47:79–85
266. Kawalec M, Smiga-Matuszowicz M, Kurcok P (2008) Counterion and solvent effects on the anionic polymerization of beta-butyrolactone initiated with acetic acid salts. Eur Polym J 44:3556–3563
267. Jedlinski Z, Kowalczuk M, Adamus G, Sikorska W, Rydz J (1999) Novel synthesis of functionalized poly(3-hydroxybutanoic acid) and its copolymers. Int J Biol Macromol 25:247–253
268. Arslan H, Hazer B, Kowalczuk M (2002) Synthesis and characterization of poly (RS)-3-hydroxybutyrate telechelics and their use in the synthesis of poly(methyl methacrylate)-b-poly(3-hydroxybutyrate) block copolymers. J Appl Polym Sci 85:965–973
269. Duda A (1992) Anionic-polymerization of 4-methyl-2-oxetanone (beta-butyrolactone). J Polym Sci A Polym Chem 30:21–29
270. Kurcok P, Smiga M, Jedlinski Z (2002) beta-butyrolactone polymerization initiated with tetrabutylammonium carboxylates: a novel approach to biomimetic polyester synthesis. J Polym Sci A. Polym Chem 40:2184–2189
271. Slomkowski S, Penczek S (1980) Macroions and macroion pairs in the anionic polymerization of β-propiolactone (β-PL). Macromolecules 13:229–233
272. Camps M, Ait-Hamouda R, Boileau S, Hemery P, Lenz RW (1988) Effect of water on the anionic polymerization of.alpha.-methyl-.alpha.-n-propyl-.beta.-propiolactone. Macromolecules 21:891–894
273. Jedliński Z, Kurcok P, Lenz RW (1998) First facile synthesis of biomimetic poly-(R)-3-hydroxybutyrate via regioselective anionic polymerization of (S)-β-butyrolactone. Macromolecules 31:6718–6720
274. Hofman A, Slomkowski S, Penczek S (1984) Structure of active-centers and mechanism of the anionic-polymerization of lactones. Makromol Chem Macromol Chem Phys 185:91–101
275. Słomkowski S (1986) Kinetics of the anionic polymerization of β-propiolactone in dimethyl-formamide. Polymer 27:71–75
276. Sosnowski S, Slomkowski S, Penczek S (1993) On the ambident reactivity of beta-lactones in their reactions with alcoholates initiating polymerization. Macromolecules 26:5526–5527
277. Kurcok P, Kowalczuk M, Jedlinski Z (1994) On the ambident reactivity of beta-lactones in their reactions with alcoholates initiating polymerization – response. Macromolecules 27:4833–4835

278. Kurcok P, Jedlinski Z, Kowalczuk M (1993) Reactions of β-lactones with potassium alkoxides and their complexes with 18-crown-6 in aprotic solvents. J Org Chem 58:4219–4220

279. Dale J, Schwartz JE (1986) Macrocyclic oligolactones by oligomerization of simple lactones. Acta Chem Scand Ser B Org Chem Biochem 40:559–567

280. Jedlinski Z, Kowalczuk M, Kurcok P (1991) What is the real mechanism of anionic-polymerization of beta-lactones by potassium alkoxides – a critical approach. Macromolecules 24:1218–1219

281. Kurcok P, Kowalczuk M, Hennek K, Jedlinski Z (1992) Anionic-polymerization of beta-lactones initiated with alkali-metal alkoxides – reinvestigation of the polymerization mechanism. Macromolecules 25:2017–2020

282. Jedlinski Z (1998) Regioselective ring-opening anionic polymerization of beta-lactones. Macromol Symp 132:377–383

283. Jedlinski Z, Adamus G, Kowalczuk M, Schubert R, Szewczuk Z, Stefanowicz P (1998) Electrospray tandem mass spectrometry of poly(3-hydroxybutanoic acid) end groups analysis and fragmentation mechanism. Rapid Commun Mass Spectrom 12:357–360

284. Scandola M, Focarete ML, Gazzano M, Matuszowicz A, Sikorska W, Adamus G, Kurcok P, Kowalczuk M, Jedlinski Z (1997) Crystallinity-induced biodegradation of novel (R, S)-beta-butyrolactone -b-pivalolactone copolymers. Macromolecules 30:7743–7748

285. Jedlinski Z (2002) Single-electron and two-electron transfer in the anionic polymerization of vinyl monomers and the ring-opening polymerization of lactones. J Polym Sci A, Polym Chem 40:2158–2165

286. Jedlinski Z, Kowalczuk M, Kurcok P (1992) Polymerization of beta-lactones initiated by alkali-metal naphthalenides – a convenient route to telechelic polymers. J Macromol Sci Pure Appl Chem A29:1223–1230

287. Kurcok P, Matuszowicz A, Jedlinski Z (1995) Anionic-polymerization of beta-lactones initiated with potassium hydride – a convenient route to polyester macromonomers. Macromol Rapid Commun 16:201–206

288. Grobelny Z, Stolarzewicz A, Morejko B, Pisarski W, Maercker A, Skibiński A, Krompiec S, Rzepa J (2006) C−O and Not C−C bond cleavage starts the polymerization of β-butyrolactone with potassium anions of alkalide. Macromolecules 39:6832–6837

289. Jedlinski Z, Kowalczuk M (1989) Nature of the active centers and the propagation mechanism of the polymerization of.beta.-propiolactones initiated by potassium anions. Macromolecules 22:3242–3244

290. Jedliński Z, Kowalczuk M, Grobelny Z, Stolarzewicz A (1983) Polymerization of 2-oxetanone initiated by alkali metal solutions. Makromol Chem Rapid Commun 4:355–358

291. Jedlinski Z, Kowalczuk M, Kurcok P, Brzoskowska L, Franek J (1987) Anionic block polymerization of beta-lactones initiated by potassium solutions.1. Synthesis of poly (4-methyl-2-oxetanone-block-2-oxetanone). Makromol Chem Macromol Chem Phys 188:1575–1582

292. Jedlinski Z, Kurcok P, Kowalczuk M (1985) Polymerization of.beta.-lactones initiated by potassium solutions. Macromolecules 18:2679–2683

293. Jedliński Z, Kurcok P, Kowalczuk M, Kasperczyk J (1986) Anionic polymerization of 4-methyl-2-oxetanone. Makromol Chem 187:1651–1656

294. Jedliński Z, Adamus G, Kowalczuk M (1995) Synthesis of novel functional poly[(R, S)-ß-hydroxybutyrate] containing phosphonoacetate end groups. Macromol Rapid Commun 16:59–65

295. Jedlinski Z, Kowalczuk M, Kurcok P, Adamus G, Matuszowicz A, Sikorska W, Gross RA, Xu J, Lenz RW (1996) Stereochemical control in the anionic polymerization of beta-butyrolactone initiated with alkali-metal alkoxides. Macromolecules 29:3773–3777

296. Kurcok P, Kowalczuk M, Adamus G, Jedliński Z, Lenz RW (1995) Degradability of poly (β-hydroxybutyrate)s. Correlation with chemical microstructure. J Macromol Sci A Chem 32:875–880

297. Corley LS, Vogl O, Biela T, Michalski J, Penczek S, Słombowski S (1980) Optically active zwitterions. Makromol Chem Rapid Commun 1:715–718

298. Jaacks V, Mathes N (1970) Formation of macrozwitterions in the polymerization of β-lactones initiated by tertiary amines. 2nd communication on macrozwitterions1. Makromol Chem 131:295–303

299. Kricheldorf HR, Scharnagl N, Jedlinski Z (1996) Polylactones.33. The role of deprotonation in the anionic polymerization of beta-propiolactone. Polymer 37:1405–1411

300. Mathes N, Jaacks V (1971) Formation of Macrozwitterions in the polymerization of β-propiolactone initiated by betaine. 4th Communication on Macrozwitterions. Makromol Chem 142:209–225

301. Yamashita Y, Ito K, Nakakita F (1969) Initiation mechanism for the anionic polymerization of β-propiolactone by pyridine. Makromol Chem 127:292–295

302. Etienne Y, Soulas R (1963) Suppression du Stade d'Initiation dans une polycondensation du second type: ouverture des β-lactones par les Bétaïnes. J Polym Sci C Polym Symp 4:1061–1074

303. Coulembier O, Delva X, Hedrick JL, Waymouth RM, Dubois P (2007) Synthesis of biomimetic poly(hydroxybutyrate): alkoxy- and carboxytriazolines as latent ionic initiator. Macromolecules 40:8560–8567

304. Jaffredo CG, Carpentier J-F, Guillaume SM (2012) Controlled ROP of β-butyrolactone simply mediated by amidine, guanidine, and phosphazene organocatalysts. Macromol Rapid Commun 33:1938–1944

305. Kawalec M, Coulembier O, Gerbaux P, Sobota M, De Winter J, Dubois P, Kowalczuk M, Kurcok P (2012) Traces do matter-Purity of 4-methyl-2-oxetanone and its effect on anionic ring-opening polymerization as evidenced by phosphazene superbase catalysis. React Funct Polym 72:509–520

306. Jeong W, Hedrick JL, Waymouth RM (2007) Organic spirocyclic initiators for the ring-expansion polymerization of beta-lactones. J Am Chem Soc 129:8414–8415

307. Bigdeli E, Lenz RW (1978) Polymerization of alpha, alpha-disubstituted beta-propiolactones and lactams.14. Substituent, solvent, and counterion effects in anionic-polymerization of lactones. Macromolecules 11:493–496

308. Cornibert J, Marchessault RH, Allegrezza AE, Lenz RW (1973) Crystalline, thermal, and mechanical properties of the polyester of α-methyl-α- n-propyl-β-propiolactone. Macromolecules 6:676–681

309. Haggiage J, Hémery P, Boileau S, Lenz RW (1983) Anionic polymerization of α, α-disubstituted β-propiolactones with cryptates as counterions. Polymer 24:578–582

310. Hall HK (1969) The Nucleophile-Initiated Polymerization of α, α-disubstituted β-Lactones. Macromolecules 2:488–497

311. Jedlinski Z, Kurcok P, Kowalczuk M, Matuszowicz A, Dubois P, Jerome R, Kricheldorf HR (1995) Anionic-polymerization of pivalolactone initiated by alkali-metal alkoxides. Macromolecules 28:7276–7280

312. Kurcok P, Matuszowicz A, Jedlinski Z, Kricheldorf HR, Dubois P, Jerome R (1995) Substituent effect in anionic-polymerization of beta-lactones initiated by alkali-metal alkoxides. Macromol Rapid Commun 16:513–519

313. Lenz RW, Dror M, Jorgensen R, Marchessault RH (1978) Polymerization of α, α-disubstituted-β-propiolactones and lactams. 9. ABA block copolymers of α-methyl-α-butyl-β-propiolactone and pivalolactone. Polym Eng Sci 18:937–942

314. Spassky N, Leborgne A, Reix M, Prud'homme RE, Bigdeli E, Lenz RW (1978) Preparation and properties of optically active poly(α-methyl-α-n-propyl-β-propiolactone). Macromolecules 11:716–719

315. Yamashita Y, Hane T (1973) Block copolymerization. VI. Polymerization of pivalolactone with macromolecular initiators from polystyrene and polytetrahydrofuran. J Polym Sci Polym Chem Ed 11:425–434

316. Kricheldorf HR, Garaleh M, Schwarz G (2005) Tertiary amine-initiated zwitterionic polymerization of pivalolactone – a reinvestigation by means of Maldi-Tof mass spectrometry. J Macromol Sci Pure Appl Chem A42:139–148
317. Adamus G (2009) Molecular level structure of (R, S)-3-hydroxybutyrate/(R, S)-3-hydroxy-4-ethoxybutyrate copolyesters with dissimilar architecture. Macromolecules 42:4547–4557
318. Adamus G, Kowalczuk M (2008) Anionic ring-opening polymerization of beta-alkoxymethyl-substituted beta-lactones. Biomacromolecules 9:696–703
319. Barbaud C, Fay F, Abdillah F, Randriamahefa S, Guerin P (2004) Synthesis of new homopolyester and copolyesters by anionic ring-opening polymerization of alpha, alpha', beta-trisubstituted beta-lactones. Macromol Chem Phys 205:199–207
320. Bear MM, Cammas S, Langlois V, Guerin P (1997) Chemoenzymatic synthesis of poly (2R,3S)-benzyl beta-3-methylmalate : beta-methylaspartase as a versatile enzyme in the preparation of the chiral precursor. CR Acad Sci Ser B Mecan Phys Chim Astron 325:165–172
321. Bear MM, Monne C, Robic D, Campion G, Langlois V, Rimbault A, Bourbouze R, Guerin P (1998) Synthesis and polymerization of benzyl (3R,4R)-3-methylmalolactonate via enzymatic preparation of the chiral precursor. Chirality 10:727–733
322. Bizzarri R, Chiellini F, Ober CK, Saltzman WM, Solaro R (2002) Influence of structural parameters on the ring-opening polymerization of new alkyl malolactonate monomers and on the biocompatibility of polymers therefrom. Macromol Chem Phys 203:1684–1693
323. Bizzarri R, Chiellini F, Solaro R, Chiellini E, Cammas-Marion S, Guerin P (2002) Synthesis and characterization of new malolactonate polymers and copolymers for biomedical applications. Macromolecules 35:1215–1223
324. Boutault K, Cammas S, Huet F, Guerin P (1995) Polystereoisomers with 2 stereogenic centers of malic-acid 2-methylbutyl ester configurational structure/properties relationship. Macromolecules 28:3516–3520
325. Brestaz M, Desilles N, Le G, Bunel C (2011) Polyester from dimethylketene and acetaldehyde: direct copolymerization and beta-lactone ring-opening polymerization. J Polym Sci A Polym Chem 49:4129–4138
326. Cammas S, Boutault K, Huet F, Guerin P (1994) 4-alkyloxycarbonyl-2-oxetanones with 2 stereogenic centers as precursors of malic-acid alkyl esters polystereoisomers. Tetrahedron Asym 5:1589–1597
327. Cammas S, Renard I, Langlois V, Guerin P (1996) Poly(beta-malic acid): obtaining high molecular weights by improvement of the synthesis route. Polymer 37:4215–4220
328. Cammas-Marion S, Bear MM, Harada A, Guerin P, Kataoka K (2000) New macromolecular micelles based on degradable amphiphilic block copolymers of malic acid and malic acid ester. Macromol Chem Phys 201:355–364
329. Coulembier O, Degee P, Barbaud C, Guerin P, Dubois P (2004) New amphiphilic graft copolymer based on poly(beta-malic acid): synthesis and characterization. Polym Bull 51:365–372
330. Coulembier O, Degee P, Cammas-Marion S, Guerin P, Dubois P (2002) New amphiphilie poly (R, S)-beta-malic acid-b-epsilon-caprolactone diblock copolymers by combining anionic and coordination-insertion ring-opening polymerization. Macromolecules 35:9896–9903
331. Coulembier O, Degee P, Dubois P (2006) Synthesis and micellization properties of novel symmetrical poly (epsilon-caprolactone-b-R, S beta-malic acid-b-epsilon-caprolactone) triblock copolymers. Macromol Chem Phys 207:484–491
332. Coulembier O, Degee P, Gerbaux P, Wantier P, Barbaud C, Flammang R, Guerin P, Dubois P (2005) Synthesis of amphiphilic poly((R, S)-beta-malic acid)-graft-poly(epsilon-caprolactone): "grafting from" and "grafting through" approaches. Macromolecules 38:3141–3150

333. Coulembier O, Degee P, Hedrick JL, Dubois P (2006) From controlled ring-opening poly-merization to biodegradable aliphatic polyester: especially poly(beta-malic acid) derivatives. Prog Polym Sci 31:723–747

334. Coulembier O, Ghisdal J, Degee P, Dubois P (2007) Benzyl beta-malolactonate: synthesis, copolymerization and design of novel biodegradable macromolecular surfactants. Arkivoc 2007:57–70

335. Coulembier O, Mespouille L, Hedrick JL, Waymouth RM, Dubois P (2006) Metal-free catalyzed ring-opening polymerization of, beta-lactones: synthesis of amphiphilic triblock copolymers based on poly(dimethylmalic acid). Macromolecules 39:4001–4008

336. De Winter J, Coulembier O, Gerbaux P, Dubois P (2010) High molecular weight poly(alpha, alpha', beta-trisubstituted beta-lactones) as generated by metal-free phosphazene catalysts. Macromolecules 43:10291–10296

337. Guerin P, Vert M, Braud C, Lenz RW (1985) Optically-active poly (beta-malic-acid). Polym Bull 14:187–192

338. LeboucherDurand MA, Langlois V, Guerin P (1996) Poly(beta-malic acid) derivatives with unsaturated lateral groups: epoxidation as model reaction of the double bonds reactivity. React Funct Polym 31:57–65

339. LeboucherDurand MA, Langlois V, Guerin P (1996) 4-carboxy-2-oxetanone as a new chiral precursor in the preparation of functionalized racemic or optically active poly(malic acid) derivatives. Polym Bull 36:35–41

340. Mabille C, Masure M, Hemery P, Guerin P (1998) Obvious complexity of the anionic polymerization of malolactonic acid esters. Polym Bull 40:381–387

341. Moine L, Cammas S, Amiel C, Guerin P, Sebille B (1997) Polymers of malic acid conjugated with the 1-adamantyl moiety as lipophilic pendant group. Polymer 38:3121–3127

342. Monne C, Robic D, Campion G, Bourbouze R, Rimbault A, Masure M, Langlois V, Hemery P, Guerin P (1996) Enantiospecific enzymatic preparation of (2S,3S)-3-alkylaspartic acids of current interest in the synthesis of stereoregular poly beta-(2S,3S)-3-alkylmalic acids as new optically active functional polyesters. Chirality 8:300–304

343. Ouhib F, Randriamahefa S, Guerin P, Barbaud C (2005) Synthesis of new statistical and block co-polyesters by ROP of alpha, alpha, beta-trisubstituted beta-lactones and their characterizations. Design Monom Polym 8:25–35

344. Jaffredo CG, Carpentier J-F, Guillaume SM (2013) Organocatalyzed controlled ROP of [small beta]-lactones towards poly(hydroxyalkanoate)s: from [small beta]-butyrolactone to benzyl [small beta]-malolactone polymers. Polym Chem 4:3837–3850

345. Jaffredo CG, Carpentier J-F, Guillaume SM (2013) Poly(hydroxyalkanoate) block or random copolymers of β-butyrolactone and benzyl β-malolactone: a matter of catalytic tuning. Macromolecules 46:6765–6776

346. Lenz RW, Vert M (1979) Preparation and properties of poly(b-malic acid): a functional polyester of potential biomedical importance. Polym Prepr 20:608–611

347. Sosnowski S, Slomkowski S, Penczek S (1991) Kinetics of the anionic-polymerization of epsilon-caprolactone with K+ (dibenzo-18-crown-6 ether) counterion – propagation via macroions and macroion pairs. Makromol Chem Macromol Chem Phys 192:735–744

348. Sosnowski S, Słomkowski S, Penczek S, Reibel L (1983) Kinetics of ε-caprolactone poly-merization and formation of cyclic oligomers. Makromol Chem 184:2159–2171

349. Sosnowski SS, Slomkowski SS, Penczek SS (1983) Kinetics of anionic polymerization of ε-caprolactone (εCL). Propagation of poly-ε=CL-K+ ion pairs. J Macromol Sci A Chem 20:979–988

350. Mingotaud AF, Cansell F, Gilbert N, Soum A (1999) Cationic and anionic ring-opening polymerization in supercritical CO_2. Preliminary results. Polym J 31:406–410

351. Ito K, Hashizuka Y, Yamashita Y (1977) Equilibrium cyclic oligomer formation in the anionic polymerization of iε-caprolactone. Macromolecules 10:821–824

352. Ito K, Yamashita Y (1978) Propagation and depropagnation rates in the anionic polymeriza-tion of ε-caprolactone cyclic oligomers. Macromolecules 11:68–72

353. Morton M, Wu M (1985) Organolithium polymerization of ?-caprolactone. In: Ring-opening polymerization, ACS Symposium Series of American Chemical Society., pp 175–182
354. Bero M, Adamus G, Kasperczyk J, Janeczek H (1993) Synthesis of block copolymers of ε-caprolactone and lactide in the presence of lithium *t*-butoxide. Polym Bull 31:9–14
355. Hofman A, Slomkowski S, Penczek S (1987) Polymerization of ε-caprolactone with kinetic suppression of macrocycles. Makromol Chem Rapid Commun 8:387–391
356. Perret R, Skoulios A (1972) Synthèse et caractérisation de quelques poly-ε-caprolactones. Makromol Chem 152:291–303
357. Yuan ML, Xiong CD, Deng XM (1998) Ring-opening polymerization of epsilon-caprolactone initiated by cyclopentadienyl sodium. J Appl Polym Sci 67:1273–1276
358. Deng X, Yuan M, Xiong C, Li X (1999) Polymerization of lactides and lactones. IV Ring-opening polymerization of ε-caprolactone by rare earth phenyl compounds. J Appl Polym Sci 73:1401–1408
359. Stere C, Iovu MC, Iovu H, Boborodea A, Vasilescu DS, Read SJ (2001) Anionic and ionic coordinative polymerization of epsilon-caprolactone. Polym Adv Technol 12:300–305
360. Bhaw-Luximon A, Jhurry D, Motala-Timol S, Lochee Y (2005) Polymerization of ε-caprolactone and its copolymerization with γ-butyrolactone using metal complexes. Macromol Symp 231:60–68
361. Gorrasi G, Pappalardo D, Pellecchia C (2012) Polymerization of epsilon-caprolactone by sodium hydride: from the synthesis of the polymer samples to their thermal, mechanical and barrier properties. React Funct Polym 72:752–756
362. Gitsov I, Rashkov IB, Panayotov IM (1990) Anionic-polymerization of lactones initiated by alkali graphitides.5. Initiation mechanism and nature of the active-centers. J Polym Sci A Polym Chem 28:2115–2126
363. Gitsov I, Rashkov IB, Panayotov IM, Golub A (1989) Anionic-polymerization of lactones initiated by alkali graphitides.4. Copolymerization of epsilon-caprolactone initiated by KC24. J Polym Sci A Polym Chem 27:639–646
364. Mazier C, Douillard C, Merle G, Pascault JP (1980) Anionic-polymerization of lactones initiated by KC 24 intercalation compounds – characterization of obtained polymers. Eur Polym J 16:773–777
365. Rashkov I, Panayotov I, Gitsov I (1981) Mechanism of the anionic-polymerization of lactones, initiated by intercalation graphite compounds. Polym Bull 4:97–103
366. Rashkov IB, Gitsov I (1984) Anionic-polymerization of lactones initiated by alkali graphitides.3. Polymerization of delta-valerolactone initiated by KC24. J Polym Sci A Polym Chem 22:905–910
367. Rashkov IB, Gitsov I, Panayotov IM (1983) Anionic-polymerization of lactones initiated by alkali graphitides.2. Changes in the KC24 structure during polymerization of lactones. J Polym Sci A Polym Chem 21:937–941
368. Rashkov IB, Gitsov I, Panayotov IM, Pascault JP (1983) Anionic-polymerization of lactones initiated by alkali graphitides.1. Polymerization of epsilon-caprolactone initiated by KC24. J Polym Sci A Polym Chem 21:923–936
369. Kurcok P, Penczek J, Franek J, Jedlinski Z (1992) Anionic-polymerization of lactones.14. Anionic block copolymerization of delta-valerolactone and L-lactide initiated with potassium methoxide. Macromolecules 25:2285–2289
370. Zhu ZX, Xiong CD, Zhang LL, Deng XM (1997) Synthesis and characterization of poly (epsilon-caprolactone) – poly(ethylene glycol) block copolymer. J Polym Sci A Polym Chem 35:709–714
371. Mao J, Gan Z (2009) The influence of pendant hydroxyl groups on enzymatic degradation and drug delivery of amphiphilic poly glycidol-block-(epsilon-caprolactone) copolymers. Macromol Biosci 9:1080–1089
372. Brown HA, Xiong S, Medvedev GA, Chang YA, Abu-Omar MM, Caruthers JM, Waymouth RM (2014) Zwitterionic ring-opening polymerization: models for kinetics of cyclic poly (caprolactone) synthesis. Macromolecules 47:2955–2963

373. Naumann S, Schmidt FG, Frey W, Buchmeiser MR (2013) Protected N-heterocyclic carbenes as latent pre-catalysts for the polymerization of epsilon-caprolactone. Polym Chem 4:4172–4181

374. Kamber NE, Jeong W, Gonzalez S, Hedrick JL, Waymouth RM (2009) N-heterocyclic carbenes for the organocatalytic ring-opening polymerization of epsilon-caprolactone. Macromolecules 42:1634–1639

375. Shin EJ, Brown HA, Gonzalez S, Jeong W, Hedrick JL, Waymouth RM (2011) Zwitterionic copolymerization: synthesis of cyclic gradient copolymers. Angew Chem Int Ed 50:6388–6391

376. Sen TK, Sau SC, Mukherjee A, Modak A, Mandal SK, Koley D (2011) Introduction of abnormal N-heterocyclic carbene as an efficient organocatalyst: ring opening polymerization of cyclic esters. Chem Commun 47:11972–11974

377. Prasad AV, Zhu Y (2013) Syntheses of cyclic poly(lactones) by zwitterionic ring opening polymerization catalyzed by N-heterocyclic carbene. J Appl Polym Sci 128:3411–3416

378. Shin EJ, Jeong W, Brown HA, Koo BJ, Hedrick JL, Waymouth RM (2011) Crystallization of cyclic polymers: synthesis and crystallization behavior of high molecular weight cyclic poly (epsilon-caprolactone)s. Macromolecules 44:2773–2779

379. Zhang R, Zhang L, Wang J, Guo X (2013) Ring-opening copolymerization of ε-caprolactone with 2,2-dimethyltrimethylene carbonate using N-heterocyclic carbene organocatalysts. Polym Bull 70:1289–1301

380. Alamri H, Zhao J, Pahovnik D, Hadjichristidis N (2014) Phosphazene-catalyzed ring-opening polymerization of [epsilon]-caprolactone: influence of solvents and initiators. Polym Chem. doi:10.1039/c1034py00493k

381. Guillerm B, Lemaur V, Ernould B, Cornil J, Lazzaroni R, Gohy J-F, Dubois P, Coulembier O (2014) A one-pot two-step efficient metal-free process for the generation of PEO-b-PCL-b-PLA amphiphilic triblock copolymers. RSC Adv 4:10028–10038

382. Okada M, Sumitomo H, Atsumi M, Hall HK (1991) Ring-opening polymerization of bicyclic oxalactones and oxalactams. Makromol Chem Macromol Symp 42–3:355–364

383. Jedlinski Z, Juzwa M, Adamus G, Kowalczuk M, Montaudo M (1996) Anionic polymerization of pentadecanolide. A new route to a potentially biodegradable aliphatic polyester. Macromol Chem Phys 197:2923–2929

384. Nomura R, Ueno A, Endo T (1994) Anionic ring-opening polymerization of macrocyclic esters. Macromolecules 27:620–621

385. Habaue S, Asai M, Morita M, Okamoto Y, Uyama H, Kobayashi S (2003) Chemospecific ring-opening polymerization of alpha-methylenemacrolides. Polymer 44:5195–5200

386. Illy N, Taylan E, Brissault B, Wojno J, Boileau S, Barbier V, Penelle J (2013) Synthesis and anionic ring-opening polymerization of crown-ether-like macrocyclic dilactones: an alternative route to peg-containing polyesters PEG-containing polyesters and related networks. Eur Polym J 49:4087–4097

387. Kudoh R, Sudo A, Endo T (2009) Synthesis of eight-membered lactone having tertiary amine moiety by ring-expansion reaction of 1,3-benzoxazine and its anionic ring-opening polymerization behavior. Macromolecules 42:2327–2329

388. Chung K, Takata T, Endo T (1995) Anionic ring-opening copolymerization of bicyclic bis (gamma-lactone)s with monofunctional and bifunctional epoxides via double ring-opening isomerization of the bis(gamma-lactone)s and volume change during copolymerization. Macromolecules 28:3048–3054

389. Chung K, Takata T, Endo T (1995) Anionic alternating ring-opening copolymerization of spirocyclic bis(gamma-lactone)s with bisepoxides and volume change during the copolymerization. Macromolecules 28:1711–1713

390. Chung KW, Takata T, Endo T (1995) Anionic copolymerization of bicyclic bis(gamma-lactone)s with poly(glycidyl methacrylate) and volume change during the copolymerization. Macromolecules 28:4044–4046

391. Endo T, Sanda F (1996) Molecular design of novel network polymers. Angew Makromol Chem 240:171–180

392. Ohsawa S, Morino K, Sudo A, Endo T (2010) Alternating copolymerization of bicyclic bis (gamma-butyrolactone) and epoxide through Zwitterion process by phosphines. Macromolecules 43:3585–3588

393. Ohsawa S, Morino K, Sudo A, Endo T (2011) Synthesis of a reactive polyester bearing alpha, beta-unsaturated ketone groups by anionic alternating copolymerization of epoxide and bicyclic bis(gamma-butyrolactone) bearing isopropenyl group. Macromolecules 44:1814–1820

394. Ohsawa S, Morino K, Sudo A, Endo T (2012) Synthesis of bicyclic bis(gamma-butyrolactone) derivatives bearing sulfide moieties and their alternating copolymers with epoxide. J Polym Sci A Polym Chem 50:4666–4673

395. Tadokoro A, Takata T, Endo T (1993) Anionic ring-opening alternating copolymerization of a bicyclic bis(gamma-lactone) with an epoxide – a novel ring-opening polymerization of a monomer containing a gamma-lactone structure. Macromolecules 26:4400–4406

396. Takata T, Tadokoro A, Chung K, Endo T (1995) Anionic ring-opening alternating copolymerizations of bicyclic and spirocyclic bis(gamma-lactone)s with epoxides via a tandem double ring-opening isomerization of the bislactones. Macromolecules 28:1340–1345

397. Zhang CX, Ochiai B, Endo T (2005) Matrix-assisted laser desorption/ionization time-of-flight mass spectrometry study on copolymers obtained by the alternating copolymerization of bis(gamma-lactone) and epoxide with potassium tert-butoxide. J Polym Sci A Polym Chem 43:2643–2649

398. Endo T, Sudo A (2009) Development and application of novel ring-opening polymerizations to functional networked polymers. J Polym Sci A Polym Chem 47:4847–4858

399. Sudo A, Uenishi K, Endo T (2008) Anionic copolymerization of epoxide with bifunctional aromatic lactone derived from 2-methylresorcinol. J Polym Sci A Polym Chem 46:3447–3451

400. Sudo A, Uenishi K, Endo T (2009) Anionic alternating copolymerization of epoxide and 3,4-dihydrocoumarin and its application to networked polymers. Polym Int 58:970–975

401. Sudo A, Zhang Y, Endo T (2011) Anionic alternating copolymerization of epoxide and six-membered lactone bearing naphthyl moiety. J Polym Sci A Polym Chem 49:619–624

402. Uenishi K, Sudo A, Endo T (2008) Anionic alternating copolymerization of 3,4-dihydrocoumarin and glycidyl ethers: a mew approach to myester synthesis. J Polym Sci A Polym Chem 46:4092–4102

403. Uenishi K, Sudo A, Endo T (2009) Synthesis of polyester having sequentially ordered two orthogonal reactive groups by anionic alternating copolymerization of epoxide and bislactone. J Polym Sci A Polym Chem 47:6750–6757

404. Uenishi K, Sudo A, Endo T (2009) Anionic alternating copolymerization of a bifunctional six-membered lactone and glycidyl phenyl ether: selective synthesis of a linear polyester having lactone moiety. J Polym Sci A Polym Chem 47:1661–1672

405. Sudo A, Uenishi K, Endo T (2007) Imidazole-promoted copolymerization of epoxide and 3,4-dihydrocoumarin and its application to a high-performance curing system. J Polym Sci A Polym Chem 45:3798–3802

406. Sekiguchi H (1984) Lactam and cyclic imides in ring-opening polymerization. In: Ivin J, Saegusa T (eds) Ring-opening polymerization. Elsevier, London, pp 809–818

407. Puffr R (1991) Lactam-based polyamides, vol 1, Puffr R, Kubánek V (eds). CRC Press, Boca Raton

408. Reimschuessel HK (1969) Kinetics and Mechanisms of polymerization. In: Frisch K, Reegen S (eds) Ring-opening polymerizations, vol 2. Marcel Dekker, New York, pp 303–326

409. Reimschuessel HK (1977) Nylon 6. Chemistry and mechanisms. J Polym Sci Macromol Rev 12:65–139

410. Šebenda J (1976) Chapter 6: Lactams. In: Bamford CH, Tipper CFH (eds) Comprehensive chemical kinetics. Elsevier, Amsterdam, pp 379–471

411. Hashimoto K (2000) Ring-opening polymerization of lactams. Living anionic polymerization and its applications. Prog Polym Sci 25:1411–1462
412. Roda J (2009) Polyamides. In: (ed) Handbook of ring-opening polymerization. Wiley-VCH Verlag GmbH & Co. KGaA, pp 165–195
413. Russo S, Casazza E (2012) 4.14 – Ring-opening polymerization of cyclic amides (lactams). In: Matyjaszewski K, Möller M (eds) Polymer science: a comprehensive reference. Elsevier, Amsterdam, pp 331–396
414. Sebenda J (1972) Lactam polymerization. J Macromol Sci A Chem A 6:1145–1199
415. Fiala F, Kralicek J (1978) Polymerization of lactams.15. Polymerization of lactames in presence of n-benzoyllactames and pentamethylguanidine. Angew Makromol Chem 71:29–41
416. Sekiguchi H, Tsourkas PR, Coutin B (1973) Anionic polymerization of alpha-pyrrolidone and alpha-piperidone using their quaternary ammonium salts as catalysts. J Polym Sci C Polym Symp 42:51–61
417. Huisgen R, Brade H, Walz H, Glogger I (1957) Mittlere ringe.7. Die eigenschaften aliphatischer lactame und die cis-trans-isomerie der saureamidgruppe. Chem Ber 90:1437–1447
418. Schwesinger R, Hasenfratz C, Schlemper H, Walz L, Peters EM, Peters K, Vonschnering HG (1993) How strong and how hindered can uncharged phosphazene bases be. Angew Chem Int Ed 32:1361–1363
419. Tang JS, Dopke J, Verkade JG (1993) Synthesis of new exceedingly strong nonionic bases – RN=P(MeNCH2CH2)3N. J Am Chem Soc 115:5015–5020
420. Naumann S, Epple S, Bonten C, Buchmeiser MR (2013) Polymerization of epsilon-caprolactam by latent precatalysts based on protected N-heterocyclic carbenes. ACS Macro Lett 2:609–612
421. Naumann S, Schmidt FG, Speiser M, Böhl M, Epple S, Bonten C, Buchmeiser MR (2013) Anionic ring-opening homo- and copolymerization of lactams by latent, protected N-heterocyclic carbenes for the preparation of PA 12 and PA 6/12. Macromolecules 46:8426–8433
422. Mougin N, Rempp P, Gnanou Y (1992) New activating agents for the anionic-polymerization of lactams. Macromolecules 25:6739–6743
423. Mougin N, Veith CA, Cohen RE, Gnanou Y (1992) Anionic-polymerization of lactams in the presence of metal dialkoxyaluminum hydrides - presentation of a new mechanism. Macromolecules 25:2004–2016
424. Mougin N, Rempp P, Gnanou Y (1993) Synthesis and characterization of polysiloxane-polyamide block and graft-copolymers. J Polym Sci A Polym Chem 31:1253–1260
425. Bolgov SA, Begishev VP, Malkin AY, Frolov VG (1981) Role of the functionality of activators during isothermal crystallization accompanying the activated anionic polymerization of ε-caprolactam. Polym Sci USSR 23:1485–1492
426. Sibal PW, Camargo RE, Macosko CW (1983) Designing nylon-6 polymerization systems for RIM. Polym Process Eng 1:147–169
427. Stehlicek J, Sebenda J (1987) Anionic-polymerization of episilon-caprolactam.60. Ionization and solvation changes in the initial-stage of the anionic-polymerization of lactams in tetrahydrofuran. Eur Polym J 23:237–242
428. Petit D, Jerome R, Teyssie P (1979) Anionic block co-polymerization of epsilon-caprolactam. J Polym Sci A Polym Chem 17:2903–2916
429. Ricco L, Russo S, Orefice G, Riva F (2001) Caprolactam-laurolactam copolymers: fast activated anionic synthesis, thermal properties and structural investigations. Macromol Chem Phys 202:2114–2121
430. Hu GH, Li HX, Feng LF (2006) Follow-up of the course of the anionic ring-opening polymerization of lactams onto an isocyanate-bearing polymer backbone in the melt. J Appl Polym Sci 102:4394–4403

431. Mateva R, Filyanova R, Velichkova R, Gancheva V (2003) Anionic copolymerization of hexanelactam with functionalized polyisoprene. J Polym Sci A Polym Chem 41:487–496
432. Petrov P, Mateva R, Dimitrov R, Rousseva S, Velichkova R, Bourssukova M (2002) Structure and thermal behavior of nylon-6/polytetrahydrofuran triblock copolymers obtained via anionic polymerization. J Appl Polym Sci 84:1448–1456
433. Ricco L, Russo S, Orefice G, Riva F (1999) Anionic poly(epsilon-caprolactam): relationships among conditions of synthesis, chain regularity, reticular order, and polymorphism. Macro-molecules 32:7726–7731
434. Russo S, Biagini E, Bonta G (1991) Novel synthetic approaches to poly(epsilon-caprolac-tam)-based materials. Makromol Chem Macromol Symp 48–9:31–46
435. Daniel L, Brozek J, Roda J, Kralicek J (1982) Polymerization of lactams.52. Anionic-polymerization of 2-pyrrolidone accelerated with CO_2.1. Makromol Chem Macromol Chem Phys 183:2719–2729
436. Merna J, Chromcova D, Brozek J, Roda J (2006) Polymerization of lactams: 97. Anionic polymerization of epsilon-caprolactam activated by esters. Eur Polym J 42:1569–1580
437. Roda J, Brozek J, Kralicek J (1980) Polymerization of lactams.37. Isolation and character-ization of alkali carboxylates of 2-pyrrolidone. Makromol Chem Rapid Commun 1:165–169
438. Sittler E, Sebenda J (1968) Alkaline polymerization of 6-caprolactam. 34. Kinetics of polymerization of caprolactam initiated by sodium caprolactam. Coll Czech Chem Commun 33:3182–3190
439. Barzakay S, Levy M, Vofsi D (1965) On mechanism of anionic polymerization of lactams. J Polym Sci B Polym Lett 3:601–605
440. Rached R, Hoppe S, Fonteix C, Schrauwen C, Pla F (2005) New developments for modelling and simulation of activated anionic polymerization of lauryllactam. Chem Eng Sci 60:2715–2727
441. Frunze TM, Kotelnikov VA, Kurashev VV, Arakyan YA, Danilevskaya LB, Davtyan SP (1983) IUPAC macro 83, Bucharest, p 233
442. Alfonso GC, Chiappori C, Razore S, Russo S (1985) Activated anionic polymerization of ε-caprolactam for RIM process. In: Krestan JE (University of Detroit) (ed) Reaction injection molding. ACS symposium series, vol 270. American Chemical Society, pp 163–179
443. Mendichi R, Russo S, Ricco L, Schieroni AG (2004) Hexafluoroisopropanol as size exclusion chromatography mobile phase for polyamide 6. J Separat Sci 27:637–644
444. Udipi K, Dave RS, Kruse RL, Stebbins LR (1997) Polyamides from lactams via anionic ring-opening polymerization.1. Chemistry and some recent findings. Polymer 38:927–938
445. Stehlicek J, Sebenda J (1986) Anionic-polymerization of 6-caprolactam.58. The relative rates of elementary reactions in the activated anionic-polymerization of epsilon-caprolactam in tetrahydrofuran. Eur Polym J 22:5–11
446. Russo S, Imperato A, Mariani A, Parodi F (1995) The fast activation of epsilon-caprolactam polymerization in quasi-adiabatic conditions. Macromol Chem Phys 196:3297–3303
447. Champetier G, Sekiguchi H (1960) Mécanisme réactionnel de la polymérisation anionique des lactames. J Polym Sci 48:309–319
448. Sekiguchi H (1960) Mécanisme réactionnel de la polymérisation catalytique alcaline de l'alpha-pyrrolidone (iii). Bull Soc Chim Fr 1835–1838
449. Sekiguchi H (1963) Mécanisme réactionnel de la polymérisation alcaline des lactames. J Polym Sci A, General Papers 1:1627–1633
450. Frunze TM, Kotel'nikov VA, Volkova TV, Kurašev VV, Davtjan SP, Stankevič IV (1981) The active centres in the anionically activated polymerization of ε-caprolactam. Acta Polym 32:31–35
451. Frunze TM, Kotelnikov VA, Volkova TV, Kurashov VV (1981) Ions and ion-pairs in anionic activated polymerization of epsilon-caprolactam. Eur Polym J 17:1079–1084
452. Bonta G, Ciferri A, Russo S (1977) Specific interactions of lithium chloride in the anionic polymerization of lactams. In: Saegusa T (Kyoto University), Goethals E (University of

Ghent) (eds) Ring-opening polymerization. ACS symposium series, vol 59. American Chemical Society, pp 216–232

453. Cefelin P, Stehlice J, Cefelin P, Sebenda J (1974) Alkaline polymerization of 6-caprolactam.54. Effect of cation on formation of keto structures during activated anionic-polymerization of lactams. Coll Czech Chem Commun 39:2212–2220

454. Šebenda J (1989) 35 – Anionic ring-opening polymerization: lactams. In: Allen G, Bevington JC (eds) Comprehensive polymer science and supplements. Pergamon, Amsterdam, pp 511–530

455. Cefelin P, Stehlice.J, Sebenda J (1973) Anionic polymerization of caprolactam. 47. Effect of polymerization conditions upon keto groups content in anionic polycaprolactam. J Polym Sci C Polym Symp 79–88

456. Coutin B, Sekiguchi H (1977) Dissociation of alkaline and quaternary ammonium-salts of 2-piperidone in polymerization of 2-piperidone. J Polym Sci A Polym Chem 15:2539–2541

457. Alfonso GC, Cirillo G, Russo S, Turturro A (1983) Adiabatic polymerization of epsilon-caprolactam in presence of calcium-chloride – thermodynamic and kinetic aspects. Eur Polym J 19:949–953

458. Greenberg A, Hsing HJ, Liebman JF (1995) Aziridinone and 2-azetidinone and their protonated structures – an ab-initio molecular-orbital study making comparisons with bridgehead bicyclic lactams and acetamide. J Molecul Struct Theochem 338:83–100

459. Dybal J, Schneider B, Doskocilova D, Baldrian J, Pavlikova H, Kvarda J, Prokopova I (1997) Spectral and structural characterization of a cyclic trimeric model of poly(6-hexanelactam). Polymer 38:2483–2491

460. Schneider B, Kvarda J, Dybal J, Schmidt P, Suchoparek M, Prokopova I (1993) Molecular-structure of a cyclic dimeric model of poly(6-hexanelactam). Coll Czech Chem Commun 58:2403–2414

461. Budin J, Brozek J, Roda J (2006) Polymerization of lactams, 96. anionic copolymerization of epsilon-caprolactam with omega-laurolactam. Polymer 47:140–147

462. Luisier A, Bourban PE, Manson JAE (2002) Initiation mechanisms of an anionic ring-opening polymerization of lactam-12. J Polym Sci A Polym Chem 40:3406–3415

463. Mateva R, Delev O, Rousseva S (1997) Structure of poly-omega-dodecalactam obtained in bulk by an anionic mechanism. Eur Polym J 33:1377–1382

464. Malkin AY, Ivanova SL, Frolov VG, Ivanova AN, Andrianova ZS (1982) Kinetics of anionic-polymerization of lactams – (solution of non-isothermal kinetic problems by the inverse method). Polymer 23:1791–1800

465. Rusu G, Ueda K, Rusu E, Rusu M (2001) Polyamides from lactams by centrifugal molding via anionic ring-opening polymerization. Polymer 42:5669–5678

466. Budin J, Roda J, Brozek J, Kriz J (2006) Anionic copolymerization of epsilon-caprolactam with omega-laurolactam. Macromol Symp 240:78–82

467. Chromcova D, Baslerova L, Roda J, Brozek J (2008) Polymerization of lactams. 99 Preparation of polyesteramides by the anionic copolymerization of epsilon-caprolactam and epsilon-caprolactone. Eur Polym J 44:1733–1742

468. Fang XM, Hutcheon R, Scola DA (2000) Microwave syntheses of poly(epsilon-caprolactam-co-epsilon-caprolactone). J Polym Sci A Polym Chem 38:1379–1390

469. Goodman I, Vachon RN (1984) Copolyesteramides.2. Anionic copolymers of epsilon-caprolactam with epsilon-caprolactone – preparation and general-properties. Eur Polym J 20:529–537

470. Kim BJ, White JL (2003) Continuous polymerization of lactam – lactone block copolymers in a twin-screw extruder. J Appl Polym Sci 88:1429–1437

471. Kim I, White JL (2003) Anionic copolymerization of lauryl lactam and polycaprolactone for the production of a poly(ester amide) triblock copolymer. J Appl Polym Sci 90:3797–3805

472. Kim I, White JL (2005) Reactive copolymerization of various monomers based on lactams and lactones in a twin-screw extruder. J Appl Polym Sci 96:1875–1887

473. Bernaskova A, Chromcova D, Brozek J, Roda J (2004) Polymerization of lactams, 95 – part 94 – preparation of polyesteramides by the anionic polymerization of epsilon-caprolactam in the presence of poly(epsilon-caprolactone). Polymer 45:2141–2148

474. Novakova V, Sobotik R, Matenova J, Roda J (1996) Polymerization of lactams.87. – Block copolymers of poly(epsilon-caprolactam) and polybutadiene prepared by anionic polymerization.1. Preparation and properties. Angew Makromol Chem 237:123–141

475. Petrov P, Jankova K, Mateva R (2003) Polyamide-6-b-polybutadiene block copolymers: synthesis and properties. J Appl Polym Sci 89:711–717

476. Roda J (2000). In: Baltá Calleja FJ, Roslaniec Z (eds) Block copolymers. Marcel Dekker, Basel, p 93

477. Sobotik R, Srubar R, Roda J (1997) Polymerization of lactams.88. Copolymers poly(epsilon-caprolactam)-block-polybutadiene prepared by anionic polymerization.3. Model polymerizations initiated with potassium salt of epsilon-caprolactam and accelerated with isocyanates and their derivatives. Macromol Chem Phys 198:1147–1163

478. Coutinho FMB, Sobrinho AAB (1991) Thermal and mechanical-properties of some caprolactam-poly(propylene oxide) block copolymers. Eur Polym J 27:105–108

479. Kim KJ, Hong DS, Tripathy AR, Kyu T (1999) Toughening and phase separation behavior of nylon 6-PEG block copolymers and in situ nylon 6-PEG blend via in situ anionic polymerization. J Appl Polym Sci 73:1285–1303

480. Maier S, Loontjens T, Scholtens B, Mulhaupt R (2003) Isocyanate-free route to caprolactam-blocked oligomeric isocyanates via carbonylbiscaprolactam- (CBC-) mediated end group conversion. Macromolecules 36:4727–4734

481. Stehlicek J, Chauhan GS, Znasikova M (1992) Preparation of polymeric initiators of the anionic-polymerization of lactams from polyetherdiols. J Appl Polym Sci 46:2169–2175

482. Yeh JL, Kuo JF, Chen CY (1993) Adiabatic anionic-polymerization of caprolactam in the presence of n-acylated caprolactam macroactivator – kinetic-study. J Appl Polym Sci 50:1671–1681

483. Zhilkova K, Mateva R (2008) Anionic block polymerization of hexanelactam and dodecalactam in the presence of a polymeric activator. J Univ Chem Technol Metal 43:291–296

484. Mateva R, Filyanova R, Dimitrov R, Velichkova R (2004) Structure, mechanical, and thermal behavior of nylon 6-polyisoprene block copolymers obtained via anionic polymerization. J Appl Polym Sci 91:3251–3258

485. Owen MJ, Thompson J (1972) Siloxane modification of polyamides. Brit Polym J 4:297–303

486. Allen WT, Eaves DE (1977) Caprolactam based block copolymers using polymeric activators. Angew Makromol Chem 58:321–343

487. Hu GH, Cartier H, Feng LF, Li BG (2004) Kinetics of the in situ polymerization and in situ compatibilization of poly(propylene) and polyamide 6 blends. J Appl Polym Sci 91:1498–1504

488. Hu G-H, Li H, Feng L-F (2005) Rate of the activated anionic polymerisation of ε-caprolactam onto an isocyanate bearing polypropylene in the melt. Polymer 46:4562–4570

489. Teng J, Otaigbe JU, Taylor EP (2004) Reactive blending of functionalized polypropylene and polyamide 6: in situ polymerization and in situ compatibilization. Polym Eng Sci 44:648–659

490. Zhang CL, Feng LF, Hoppe S, Hu GH (2008) Grafting of polyamide 6 by the anionic polymerization of epsilon-caprolactam from an isocyanate bearing polystyrene backbone. J Polym Sci A Polym Chem 46:4766–4776

491. Biernacki P, Chrzczon S, Wlodarcz M (1971) Molecular weight distribution of polycaproamide obtained by anionic polymerization of caprolactam in solvent. Eur Polym J 7:739–747

492. Biernacki P, Wlodarczyk M (1975) Study of molecular-weight of polycaproamide obtained by anionic-polymerization of caprolactam in solvent. Eur Polym J 11:107–109

493. Biernacki P, Wlodarczyk M (1980) Chemical-structure of polycaproamide obtained by anionic-polymerization of caprolactam in solvent. Eur Polym J 16:843–848

494. Dan F, Vasiliu-Oprea C (1998) On the relationship between synthesis parameters and morphology of the anionic polycaproamide obtained in organic media. III. Macroporous powders obtained using CO_2 and carbodiimides as activating compounds. J Appl Polym Sci 67:231–243

495. Vasiliu-Oprea C, Dan F (1996) On the relation between synthesis parameters and morphology of anionic polycaproamide obtained in organic media. I. Influence of the Na[O $(CH_2)_2OCH_3]_2AlH_2$/isophorone diisocyanate catalytic system. J Appl Polym Sci 62:1517–1527

496. Vasiliu-Oprea C, Dan F (1997) On the relation between synthesis parameters and morphology of anionic polycaproamide obtained in organic media. II. Influence of the Na[O $(CH_2)_2OCH_3]_2AlH_2$/aliphatic diisocyanates catalytic systems. J Appl Polym Sci 64:2575–2583

497. Ricco L, Monticelli O, Russo S, Paglianti A, Mariani A (2002) Fast-activated anionic polymerization of epsilon-caprolactam in suspension, 1 – role of the continuous phase on characteristics and properties of powdered PA6. Macromol Chem Phys 203:1436–1444

498. Crespy D, Landfester K (2005) Anionic polymerization of epsilon-caprolactam in miniemulsion: synthesis and characterization of polyamide-6 nanoparticles. Macromolecules 38:6882–6887

499. Pei AH, Liu AD, Xie TX, Yang GS (2006) A new strategy for the preparation of polyamide-6 microspheres with designed morphology. Macromolecules 39:7801–7804

500. Hedrick RM, Gabbert JD, Wohl MH (1985) Nylon 6 RIM. In: Kresta JE (University of Detroit) (ed) Reaction injection molding. ACS symposium series, vol 270. American Chemical Society, pp 135–162

501. Illing G (1969) Direct extrusion of nylon products from lactams. Mod Plast 46:70–76

502. Macosko CW (1989) RIM fundamentals of reaction injection molding. Hanser Publications, Munich

503. Du LB, Yang GS (2010) A super-toughened nylon 12 blends via anionic ring-opening polymerization of lauryllactam in a twin screw extruder. Preparation, morphology, and mechanical properties. Polym Eng Sci 50:1178–1185

504. Hu GH, Cartier H, Plummer C (1999) Reactive extrusion: toward nanoblends. Macromolecules 32:4713–4718

505. Rothe B, Elas A, Michaeli W (2009) In situ polymerisation of polyamide-6 nanocompounds from caprolactam and layered silicates. Macromol Mater Eng 294:54–58

506. Wollny A, Nitz H, Faulhammer H, Hoogen N, Mulhaupt R (2003) In situ formation and compounding of polyamide 12 by reactive extrusion. J Appl Polym Sci 90:344–351

507. Yan DG, Yang GS (2009) Synthesis and properties of homogeneously dispersed polyamide 6/MWNTs nanocomposites via simultaneous in situ anionic ring-opening polymerization and compatibilization. J Appl Polym Sci 112:3620–3626

508. Yang M, Gao Y, He JP, Li HM (2007) Preparation of polyamide 6/silica nanocomposites from silica surface initiated ring-opening anionic polymerization. Expr Polym Lett 1:433–442

509. Sebenda J, Hauer J (1981) Living polymerization of lactams and synthesis of monodisperse polyamides. Polym Bull 5:529–534

510. Sebenda J, Hauer J, Svetlik J (1986) An unusual kinetics of anionic-polymerization of 4-membered lactams. J Polym Sci Polym Symp 74(1):303–310

511. Hashimoto K, Hotta K, Okada M, Nagata S (1995) Synthesis of monodisperse polyamides by living anionic-polymerization of beta-lactams in the mixture of N, N-dimethylacetamide and lithium-chloride. J Polym Sci A Polym Chem 33:1995–1999

512. Hashimoto K, Oi T, Yasuda J, Hotta K, Okada M (1997) Molecular weight distribution of polyamides obtained in anionic polymerization of methyl-substituted beta-lactams and aminolysis of their N-benzoyl lactams. J Polym Sci A Polym Chem 35:1831–1838

513. Hashimoto K, Yasuda J, Kobayashi M (1999) Proton transfer-controlled anionic polymerization of methyl-substituted beta-lactams with potassium t-butoxide and subsequent coupling reaction with saccharides. J Polym Sci A Polym Chem 37:909–915

514. Zhang JH, Gellman SH, Stahl SS (2010) Kinetics of anionic ring-opening polymerization of variously substituted beta-lactams: homopolymerization and copolymerization. Macromolecules 43:5618–5626

515. Tachibana K, Hashimoto K, Tansho N, Okawa H (2011) Chemical modification of chain end in nylon 4 and improvement of its thermal stability. J Polym Sci A Polym Chem 49:2495–2503

516. Roda J, Votrubcova Z, Kralicek J, Stehlicek J, Pokorny S (1981) Polymerization of lactams.39. Condensation as side reaction in the anionic-polymerization of 2-pyrrolidone. Makromol Chem Macromol Chem Phys 182:2117–2126

517. Schirawski G (1972) Studies on anionic polymerization of pyrrolidone. Makromol Chem 161:57–68

518. Sekiguchi H (1960) Etude cinétique de la polymérisation catalytique de l'alpha-pyrrolidone (ii). Bull Soc Chim Fr 1831–1834

519. Roda J, Kralicek J (1982) Process for the anionic polymerization of 2-pyrrolidone with fast freezing step US 4,343,933

520. Costa G, Nencioni M, Russo S, Semeghini GL (1981) The anionic-polymerization of 2-pyrrolidone in bulk and in suspension. Makromol Chem Macromol Chem Phys 182:1399–1405

521. Hashimoto K, Sudo M, Sugimura T, Inagaki Y (2004) Synthesis of novel block copolymers containing polyamide4 segments and control of their biodegradability. J Appl Polym Sci 92:3492–3498

522. Kawasaki N, Yamano N, Takeda S, Ando H, Nakayama A (2012) Synthesis of an azo macromolecular initiator composed of polyamide 4 and its initiation activity for the radical polymerization of vinyl monomers. J Appl Polym Sci 126:E425–E432

523. Chuchma F, Trska P, Roda J, Kralicek J (1983) Polymerization of lactams.57. GLC and NMR analysis of the anionic co-polymers of 2-pyrrolidone with 6-caprolactam and 8-octanelactam. Polymer 24:1491–1494

524. Komoto H (1968) Anionic copolymerization of omega-lactams with omega-lactones. Makromol Chem, Macromol Chem Phys 115:33–42

525. Stehlicek J, Sebenda J (1986) Anionic-polymerization of epsilon-caprolactam.59. Effect of the ratio of reacting components, of the medium and of the ring size on the initial-stage of the anionic-polymerization of lactams. Eur Polym J 22:769–773

526. Hall HK (1958) Polymerization and ring strain in bridged bicyclic compounds. J Am Chem Soc 80:6412–6420

527. Hall HK (1960) Synthesis and polymerization of atom-bridged bicyclic lactams. J Am Chem Soc 82:1209–1215

528. Hashimoto K, Sugata T, Imanishi SI, Okada M (1994) Synthesis of saccharide-conjugated polyamides by quasi-living anionic-polymerization of a bicyclic lactam. J Polym Sci A Polym Chem 32:1619–1625

529. Hashimoto K, Sumitomo H, Washio A (1989) Preparation of monodisperse hydrophilic polyamide by anionic-polymerization of bicyclic oxalactam. J Polym Sci A Polym Chem 27:1915–1923

530. Clarson SJ, Semlyen JA (1993) Siloxane polymers. Prentice Hall, Englewood Cliffs

531. Cypryk M (2012) 4.17 – Polymerization of cyclic siloxanes, silanes, and related monomers. In: Matyjaszewski K, Möller M (eds) Polymer science: a comprehensive reference. Elsevier, Amsterdam, pp 451–476

532. Ganachaud F, Boileau S (2009) Siloxane-containing polymers. In: (ed) Handbook of ring-opening polymerization. Wiley-VCH Verlag GmbH & Co. KGaA, pp 65–95

533. Chojnowski J, Cypryk M (2000) Synthesis of linear polysiloxanes. In: Jones R, Ando W, Chojnowski J (eds) Silicon containing polymers. Kluwer Academic Publishers, Dordrecht, pp 3–42

534. Yilgor E, Yilgor I (2014) Silicone containing copolymers: synthesis, properties and applications. Prog Polym Sci. doi:10.1016/j.progpolymsci.2013.1011.1003

535. Sigwalt P (1981) Ring-opening polymerizations of heterocycles with organometallic catalysts. Angew Makromol Chem 94:161–180

536. Butts M, Cella J, Wood CD, Gillette G, Kerboua R, Leman J, Lewis L, Rajaraman S, Rubinsztajn S, Schattenmann F, Stein J, Wengrovius J, Wicht D (2004) Silicones. In: Encyclopedia of polymer science and technology. John Wiley & Sons, Inc, Hoboken, pp 765–841

537. Noll W (1968) Chemistry and technology of silicones. Academic, New York

538. Fortuniak W, Chojnowski J, Sauvet G (2001) Controlled synthesis of siloxane polymers and siloxane-siloxane block copolymers with 3-chloropropyl groups pendant to the siloxane chain. Macromol Chem Phys 202:2306–2313

539. Takiguchi T, Sakurai M, Kishi T, Ichimura J, Iizuka Y (1960) Preparation of hexaphenylcyclotrisiloxane by the reaction of diphenyldichlorosilane with zinc oxide. J Org Chem 25:310–311

540. Voronkov MG, Basenko SV (1995) From ephemers to monomers, oligomers and polymers - new methods for the generation and transformation of silanones. J Organomet Chem 500:325–329

541. Embery C, Clarke S, Matisons J (2003) Ring-opening polymerization of poly(siloxane) materials. In: Nalwa HS (ed) Handbook of organic–inorganic hybrid materials and nanocomposites, vol 2. American Scientific Publishers, Stevenson Ranch, pp 331–347

542. Bellas V, Iatrou H, Hadjichristidis N (2000) Controlled anionic polymerization of hexamethylcyclotrisiloxane. Model linear and miktoarm star co- and terpolymers of dimethylsiloxane with styrene and isoprene. Macromolecules 33:6993–6997

543. Chojnowski J, Mazurek M (1975) Anionic-polymerization of siloxanes - mechanism of initiation with triorganosilanolates. Makromol Chem, Macromol Chem Phys 176:2999–3023

544. Wilczek L, Kennedy JP (1987) Aggregation in the anionic-polymerization of hexamethylcyclotrisiloxane with lithium counterion. Polym J 19:531–538

545. Kopylov VM, Prokhodko PL, Kovyazin VA (1982) polymerization of hexamethylcyclotrisiloxane by alpha, omega-bis-(tetramethylammonium) oligodimethylsiloxanolate in the presence of trimethylsilanol. Vysokomol Soedin A 24:1751–1756

546. Wright P (1984). In: Ivin J, Saegusa T (ed) Ring-opening polymerization. Elsevier, London, p 1055

547. Boileau S (1981) Use of cryptates in anionic polymerization of heterocyclic compounds. In: James E. McGrath (Virginia Polytechnic Institute and State University) (ed) Anionic Polymerization Kinetics, Mechanisms, and Synthesis. ACS symposium series, vol 166. American Chemical Society, pp 283–305

548. Dickstein WH, Lillya CP (1989) Blocked amine functional initiator for anionic-polymerization. Macromolecules 22:3882–3885

549. Hubert S, Hemery P, Boileau S (1986) Anionic-polymerization of cyclosiloxanes with cryptates as counterions – new results. Makromol Chem Macromol Symp 6:247–252

550. Molenberg A, Siffrin S, Moller M, Boileau S, Teyssie D (1996) Well defined columnar liquid crystalline polydiethylsiloxane. Macromol Symp 102:199–207

551. Suzuki T (1989) Preparation of poly(dimethylsiloxane) macromonomers by the initiator method.2. Polymerization mechanism. Polymer 30:333–337

552. Veith CA, Cohen RE (1989) Kinetic modeling and optimization of the trifluoropropylmethylsiloxane polymerization. J Polym Sci A Polym Chem 27:1241–1258

553. Zhang Y, Zhang ZJ, Wang Q, Xie ZM (2007) Synthesis of well-defined difunctional polydimethylsiloxane with an efficient dianionic initiator for ABA triblock copolymer. J Appl Polym Sci 103:153–159

554. Beckmann J, Dakternieks D, Lim AEK, Lim KF, Jurkschat K (2006) Understanding ring strain and ring flexibility in six- and eight-membered cyclic organometallic group 14 oxides. J Molecul Struct Theochem 761:177–193

555. Mazurek M, Chojnowski J (1977) Anionic-polymerization of siloxanes.2. Internal multifunctional assistance of siloxane system to siloxane bond-cleavage by alkali-metal silanolates. Makromol Chem Macromol Chem Phys 178:1005–1017

556. Ritch JS, Chivers T (2007) Silicon analogues of crown ethers and cryptands: a new chapter in host-guest chemistry? Angew Chem Int Ed 46:4610–4613

557. Su SX, Zhang ZJ, Zheng ZM, Xie ZM (2004) Anionic non-equilibrium ring-opening poly-merization of octamethylcyclotetrasiloxane (D-4) initiated by silazyl-lithiums. Polym Int 53:149–152

558. Molenberg A, Moller M (1995) A fast catalyst system for the ring-opening polymerization of cyclosiloxanes. Macromol Rapid Commun 16:449–453

559. Molenberg A, Moller M (1997) Polymerization of cyclotrisiloxanes by organolithium com-pounds and P-2-Et base. Macromol Chem Phys 198:717–726

560. Grzelka A, Chojnowski J, Fortuniak W, Taylor RG, Hupfield PC (2004) Kinetics of the anionic ring opening polymerization of cyclosiloxanes initiated with a superbase. J Inorg Organomet Polym 14:85–99

561. Hupfield PC, Taylor RG (1999) Ring-opening polymerization of siloxanes using phosphazene base catalysts. J Inorg Organomet Polym 9:17–34

562. Bessmertnykh A, Ben F, Baceiredo A, Mignani G (2003) Anionic ring-opening polymeriza-tion of cyclic organosiloxanes using phosphorus ylides as strong non-ionic bases. J Organomet Chem 686:281–285

563. Rodriguez M, Marrot S, Kato T, Sterin S, Fleury E, Baceiredo A (2007) Catalytic activity of N-heterocyclic carbenes in ring opening polymerization of cyclic siloxanes. J Organomet Chem 692:705–708

564. Saam JC (1999) Stereoregular polysiloxanes via ring-opening polymerization, a review. J Inorg Organomet Polym 9:3–16

565. Clarson SJ (2000) Synthesis of linear polysiloxanes. In: Jones R, Ando W, Chojnowski J (eds) Silicon containing polymers. Kluwer Academic Publishers, Dordrecht, p 139

566. Andrianov KA, Godovskii IK, Svistunov VS, Papkov VS, Zhdanov AA, Slonimskii GL (1977) Polymerization of some organocyclosiloxanes in solid-phase. Dokl Akad Nauk Sssr 234:1326–1328

567. Andrianov KA, Temnikovskii VA, Khananashvili LM, Zavin BG, Kuznetsova AG, Golubtsov SA, Ivanov VI (1969) Solid-state polymerization of organocyclosiloxanes. Vysokomol Soedin B 11:637–638

568. Buzin MI, Gerasimov MV, Obolonkova ES, Papkov VS (1997) Solid-state polymerization of hexaphenylcyclotrisiloxane. J Polym Sci A Polym Chem 35:1973–1984

569. Unno M, Takada K, Kawaguchi Y, Matsumoto H (2005) Supramolecular aggregates of silanols and solid-state synthesis of siloxanes. Mol Cryst Liq Cryst 440:259–264

570. Barrere M, Ganachaud F, Bendejacq D, Dourges MA, Maitre C, Hemery P (2001) Anionic polymerization of octamethylcyclotetrasiloxane in miniemulsion II. Molar mass analyses and mechanism scheme. Polymer 42:7239–7246

571. Degunzbourg A, Favier JC, Hemery P (1994) Anionic-polymerization of octamethylcyclote-trasiloxane in aqueous emulsion.1. Preliminary-results and kinetic-study. Polym Int 35:179–188

572. Barrere M, Maitre C, Dourges MA, Hemery P (2001) Anionic polymerization of 1,3,5-tris (trifluoropropylmethyl)cyclotrisiloxane (F-3) in miniemulsion. Macromolecules 34:7276–7280

573. Caille JR, Teyssie D, Bouteiller L, Bischoff R, Boileau S (2000) Ring-opening polymeriza-tion in aqueous emulsion applied to the preparation of interpenetrating networks based on telechelic polysiloxanes. Macromol Symp 153:161–166

574. Ivanenko C, Maitre C, Ganachaud F, Hemery P (2003) Multiblock silicones, 1 – vinyl functionalized polydimethylsiloxane. e-Polymers 3:111–125
575. Aoyagi T, Tadenuma R, Nagase Y (1996) Novel silicones for transdermal therapeutic system.6. Preparation of oligodimethylsiloxane containing 2-pyrrolidone moiety as a terminal group and its enhancing effect on transdermal drug penetration. Macromol Chem Phys 197:677–686
576. Elkins CL, Long TE (2004) Living anionic polymerization of hexamethylcyclotrisiloxane (D-3) using functionalized initiation. Macromolecules 37:6657–6659
577. Kazama H, Tezuka Y, Imai K (1991) Synthesis and reactions of uniform-size poly(dimethylsiloxane)s having carboxylic-acid as a single end group and both end groups. Macromolecules 24:122–125
578. Kumar A, Eichinger BE (1990) Anionic polymerization of hexamethylcyclotrisiloxane with acetylacetone initiator to form telechelic polymer. Macromolecules 23:5358
579. Saxena A, Rajaraman S, Leatherman M (2007) Synthesis of narrowly dispersed bis-hydride-capped polydimethylsiloxane using difunctional anionic initiator based on 1,3-diisopropenylbenzene. Macromolecules 40:752–755
580. Suzuki T, Yamada S, Okawa T (1993) Synthesis of polydimethylsiloxanes containing aminosilyl or amidosilyl groups at one chain end. Polym J 25:411–416
581. Yin R, Hogenesch TE (1993) Synthesis and characterization of narrow molecular-weight distribution polystyrene poly(dimethylsiloxane) macrocyclic block-copolymers and their isobaric precursors. Macromolecules 26:6952–6957
582. Chang TC, Chen YC, Ho SY, Chiu YS (1996) The effect of silicon and phosphorus on the degradation of poly(methyl methacrylate). Polymer 37:2963–2968
583. Miura Y, Hirota K, Moto H, Yamada B (1999) High-yield synthesis of functionalized alkoxyamine initiators and approach to well-controlled block copolymers using them. Macromolecules 32:8356–8362
584. Miura Y, Miyake K (2005) Synthesis of poly(dimethylsiloxane)-containing diblock and triblock copolymers by the combination of anionic ring-opening polymerization of hexamethylcyclotrisiloxane and nitroxide-mediated radical polymerization of methyl acrylate, isoprene, and styrene. J Polym Sci A Polym Chem 43:6153–6165
585. Miura Y, Sakai Y, Taniguchi I (2003) Syntheses of well-defined poly(siloxane)-b-poly(styrene) and poly(norbomene)-b-poly(styrene) block copolymers using functional alkoxyamines. Polymer 44:603–611
586. Pollack SK, Singer DU, Morgan AM (1999) Siloxane/styrene copolymers via nitroxide-mediated radical polymerization. Polym Prepr 40:370
587. Rheingans O, Hugenberg N, Harris JR, Fischer K, Maskos M (2000) Nanoparticles built of cross-linked heterotelechelic, amphiphilic poly(dimethylsiloxane)-b-poly(ethylene oxide) diblock copolymers. Macromolecules 33:4780–4790
588. Tezuka Y, Nobe S, Shiomi T (1995) Synthesis and surface formation of 3-component copolymers having polystyrene-block-poly(dimethylsiloxane) graft segments. Macromolecules 28:8251–8258
589. Aoyagi T, Takamura Y, Nakamura T, Nagase Y (1992) Preparation of pyridyl-terminated oligodimethylsiloxane and siloxane-grafted copolymers containing pyridyl groups at the side-chain ends. Polymer 33:1530–1536
590. Suzuki T, Lo PY (1991) Preparation of poly(dimethylsiloxane) macromonomers having ethynylene functionality by the initiator method. Macromolecules 24:460–463
591. Fragouli P, Iatrou H, Hadichristidis N, Sakurai T, Matsunaga Y, Hirao A (2006) Synthesis of well-defined miktoarm star polymers of poly(dimethylsiloxane) by the combination of chlorosilane and benzyl chloride linking chemistry. J Polym Sci A Polym Chem 44:6587–6599
592. Hammouch SO, Beinert GJ, Zilliox JG, Herz JE (1995) Synthesis and characterization of monofunctional polydimethylsiloxanes with a narrow molecular-weight distribution. Polymer 36:421–426

593. Chojnowski J, Cypryk M, Fortuniak W, Rozga-Wijas K, Scibiorek M (2002) Controlled synthesis of vinylmethylsiloxane-dimethylsiloxane gradient, block and alternate copolymers by anionic ROP of cyclotrisiloxanes. Polymer 43:1993–2001

594. Cypryk M, Kazmierski K, Fortuniak W, Chojnowski J (2000) Microstructure of the copolymer chain generated by anionic ring-opening polymerization of a model cyclotrisiloxane with mixed siloxane units. Macromolecules 33:1536–1545

595. Cypryk M, Delczyk B, Juhari A, Koynov K (2009) Controlled synthesis of trifluoropropylmethylsiloxane-dimethylsiloxane gradient copolymers by anionic ROP of cyclotrisiloxanes. J Polym Sci A Polym Chem 47:1204–1216

596. Liu LH, Yang SY, Zhang ZJ, Wang Q, Xie ZM (2003) Synthesis and characterization of poly (diethylsiloxane) and its copolymers with different diorganosiloxane units. J Polym Sci A Polym Chem 41:2722–2730

597. Ziemelis MJ, Saam JC (1989) Sequence distribution in poly(dimethylsiloxane-co-methylvinylsiloxanes). Macromolecules 22:2111–2116

598. Abe Y, Gunji T (2004) Oligo- and polysiloxanes. Prog Polym Sci 29:149–182

599. Baney RH, Itoh M, Sakakibara A, Suzuki T (1995) Silsesquioxanes. Chem Rev 95:1409–1430

600. Cordes DB, Lickiss PD, Rataboul F (2010) Recent developments in the chemistry of cubic polyhedral oligosilsesquioxanes. Chem Rev 110:2081–2173

601. Loy DA, Shea KJ (1995) Bridged polysilsesquioxanes – highly porous hybrid organic–inorganic materials. Chem Rev 95:1431–1442

602. Li HY, Yu DS, Zhang JY (2005) A novel and facile method for direct synthesis of cross-linked polysiloxanes by anionic ring-opening copolymerization with Ph-12-POSS/D-4/Ph8D4. Polymer 46:5317–5323

603. Li HY, Zhang JY, Xu RW, Yu DS (2006) Direct synthesis and characterization of cross-linked polysiloxanes via anionic ring-opening copolymerization with octaisobutyl-polyhedral oligomeric silsesquioxane and octamethylcyclotetrasiloxane. J Appl Polym Sci 102:3848–3856

604. Suryanarayanan B, Peace BW, Mayhan KG (1974) Anionic-polymerization of 2,2,5,5-tetramethyl-1-oxa-2,5-disilacyclopentane. J Polym Sci A Polym Chem 12:1089–1107

605. Suryanarayanan B, Peace BW, Mayhan KG (1974) Anionic-polymerization of a series of 5-membered cyclocarbosiloxanes. J Polym Sci A Polym Chem 12:1109–1123

606. Ziatdinov VR, Cai GP, Weber WP (2002) Anionic ring-opening polymerization of trimethylsiloxy-substituted 1-oxa-2,5-disilacyclopentanes: synthesis of trimethylsiloxy-substituted poly 1-oxa-2,5-disila-1,5-pentanylene s. Macromolecules 35:2892–2897

607. Lohmeijer BGG, Dubois G, Leibfarth F, Pratt RC, Nederberg F, Nelson A, Waymouth RM, Wade C, Hedrick JL (2006) Organocatalytic living ring-opening polymerization of cyclic carbosiloxanes. Org Lett 8:4683–4686

608. Brown HA, Chang YA, Waymouth RM (2013) Zwitterionic polymerization to generate high molecular weight cyclic poly(carbosiloxane)s. J Am Chem Soc 135:18738–18741

609. Li YN, Kawakami Y (1999) Synthesis and polymerization of an optically active bifunctional disiloxane. 2. Preparation of optically active (S)-2-(1-naphthyl)-2-phenyl-5,5-dimethyl-1-oxa-2,5-disilacyclopentane and its ring-opening polymerization. Macromolecules 32:548–553

610. Li YN, Kawakami Y (2000) Stereoselective feature in anionic ring-opening polymerization of 2-(1-naphthyl)-2-phenyl-5,5-dimethyl-1-oxa-2,5-disilacyclopentane and influence of tacticity on the thermal property of polymers. Macromolecules 33:1560–1564

611. Chojnowski J, Kurjata J (1995) Selective anionic ring-opening polymerization of permethyl-tetrasila-1,4-dioxane, d-2(2) – transformation of poly(silaether) in polysiloxane and polysilylene. Macromolecules 28:2996–2999

612. Steward OW, Williams JL (1988) New mechanisms for the base-catalyzed cleavage of Si-Si bonds in organopolysilanes – the base-catalyzed solvolysis of pentaphenyldisilanecarboxylic acid and pentaphenyldisilanol in ethanol water media. J Organomet Chem 341:199–211

613. Zundel T, Baran J, Mazurek M, Wang JS, Jerome R, Teyssie P (1998) Climbing back up the nucleophilic reactivity scale. Use of cyclosila derivatives as reactivity boosters in anionic polymerization. Macromolecules 31:2724–2730
614. Cypryk M, Chrusciel J, Fossum E, Matyjaszewski K (1993) Ring-opening polymerization of strained cyclotetrasilanes as a new route towards well-defined polysilylenes. Makromol Chem Macromol Symp 73:167–176
615. Cypryk M, Gupta Y, Matyjaszewski K (1991) Anionic ring-opening polymerization of 1,2,3,4-tetramethyl-1,2,3,4-tetraphenylcyclotetrasilane. J Am Chem Soc 113:1046–1047
616. Fossum E, Gordonwylie SW, Matyjaszewski K (1994) Identification of the stereoisomers of 1,2,3,4-tetramethyl-1,2,3,4-tetraphenylcyclotetrasilane. Organometallics 13:1695–1698
617. Fossum E, Matyjaszewski K (1995) Ring-opening polymerization of cyclotetrasilanes – microstructure and mechanism. Macromolecules 28:1618–1625
618. Fossum E, Matyjaszewski K, Sheiko SS, Moller M (1997) Morphology of polystyrene-block-poly(methylphenylsilylene). Macromolecules 30:1765–1767
619. Suzuki M, Kotani J, Gyobu S, Kaneko T, Saegusa T (1994) Synthesis of sequence-ordered polysilane by anionic ring-opening polymerization of phenylnonamethylcyclopentasilane. Macromolecules 27:2360–2363
620. Koopmann F, Frey H (1996) Synthesis of poly(silylenemethylene)s symmetrically substituted with alkyl side groups containing 4–6 carbon atoms. Macromolecules 29:3701–3706
621. Matsumoto K, Nishimura M, Yamaoka H (2000) Organolithium-induced anionic polymerization of 1,1,3,3-tetramethyl-1,3-disilacyclobutane in the presence of hexamethylphosphoramide. Macromol Chem Phys 201:805–808
622. Matsumoto K, Shimazu H, Deguchi M, Yamaoka H (1997) Anionic ring-opening polymerization of silacyclobutane derivatives. J Polym Sci A Polym Chem 35:3207–3216
623. Matsumoto K, Shinohata M, Yamaoka H (2000) Anionic ring-opening polymerization of phenylsilacyclobutanes. Polym J 32:354–360
624. Ogawa T, Lee SD, Murakami M (2002) Synthesis of siloxane-crosslinked polysilyiene-methylenes by chlorodephenylation. J Polym Sci A Polym Chem 40:416–422
625. Theurig M, Weber WP (1992) Stereoselective anionic ring-opening polymerization of 1,1-dimethyl-1-silacyclobutene – characterization of poly(1,1-dimethyl-1-sila-cis-but-2-ene. Polym Bull 28:17–21
626. Finkelshtein ES, Ushakov NV, Krasheninnikov EG, Yampolskii YP (2004) New polysilalkylenes: synthesis and gas-separation properties. Russ Chem Bull 53:2604–2610
627. Kawahara S, Nagai A, Kazama T, Takano A, Isono Y (2004) Preparation of poly (1,1-dimethyl silabutane) by anionic polymerization and its crystallization. Macromolecules 37:315–321
628. Kakihana Y, Uenishi K, Imae I, Kawakami Y (2005) Anionic ring-opening polymerization of optically pure 1-methyl-1-(1-naphthyl)-2,3-benzosilacyclobut-2-ene. Macromolecules 38:6321–6326
629. Kloninger C, Rehahn M (2004) 1,1-dimethylsilacyclobutane-mediated living anionic block copolymerization of 1 dimethylsilaferrocenophane and methyl methacrylate. Macromolecules 37:1720–1727
630. Sheridan JB, Gomez P, Manners I (1996) Transition metal-catalyzed ring-opening copolymerization of silicon-bridged 1 ferrocenophanes and sila- or disilacyclobutanes: synthesis of poly(ferrocenylsilane)-poly(carbosilane) random copolymers. Macromol Rapid Commun 17:319–324
631. Sheikh MRK, Tharanikkarasu K, Imae I, Kawakami Y (2001) Silacyclobutane as "carbanion pump" in anionic polymerization. 2. Effective trapping of the initially formed carbanion by diphenylethylene. Macromolecules 34:4384–4389
632. Bruzaud S, Soum A (1996) Anionic ring-opening polymerization of cyclodisilazanes.1. General aspects. Macromol Chem Phys 197:2379–2391

633. Cazalis C, Mingotaud AF, Soum A (1997) Anionic ring-opening polymerization of cyclodisilazanes.3. Influence of the silicon substituent on the kinetics of polymerization. Macromol Chem Phys 198:3441–3450

634. Duguet E, Schappacher M, Soum A (1992) High molar mass polysilazane – a new polymer. Macromolecules 25:4835–4839

635. Soum A (2000) Polysilazanes in Silicon containing polymers: the science and technology of their synthesis and applications. In: Jones R, Ando W, Chojnowski J (eds) Silicon containing polymers. Kluwer Academic Publishers, Dordrecht, pp 323–349

636. Matsumoto K, Nakashita J, Matsuoka H (2006) Synthesis of silicon nitride based ceramic nanoparticles by the pyrolysis of silazane block copolymer micelles. J Polym Sci A Polym Chem 44:4696–4707

637. Rulkens R, Lough AJ, Manners I (1994) Anionic ring-opening oligomerization and polymerization of silicon-bridged 1 ferrocenophanes – characterization of short-chain models for poly (ferrocenylsilane) high polymers. J Am Chem Soc 116:797–798

638. Rider DA, Manners I (2007) Synthesis, self-assembly, and applications of polyferrocenylsilane block copolymers. Polym Rev 47:165–195

639. Bellas V, Rehahn M (2007) Polyferrocenylsilane-based polymer systems. Angew Chem Int Ed 46:5082–5104

640. Rokicki G (2000) Aliphatic cyclic carbonates and spiroorthocarbonates as monomers. Prog Polym Sci 25:259–342

641. Rokicki G, Parzuchowski PG (2012) 4.12 – ROP of cyclic carbonates and ROP of macrocycles. In: Matyjaszewski K, Möller M (eds) Polymer science: a comprehensive reference. Elsevier, Amsterdam, pp 247–308

642. Keul H (2009) Polycarbonates. In: (ed) Handbook of ring-opening polymerization. Wiley-VCH Verlag GmbH & Co. KGaA, pp 307–327

643. Tempelaar S, Mespouille L, Coulembier O, Dubois P, Dove AP (2013) Synthesis and post-polymerisation modifications of aliphatic poly(carbonate)s prepared by ring-opening polymerisation. Chem Soc Rev 42:1312–1336

644. Mespouille L, Coulembier O, Kawalec M, Dove AP, Dubois P (2014) Implementation of metal-free ring-opening polymerization in the preparation of aliphatic polycarbonate materials. Prog Polym Sci 39:1144–1164

645. Vogdanis L, Heitz W (1986) Carbon dioxide as a monomer, 3. The polymerization of ethylene carbonate. Makromol Chem Rapid Commun 7:543–547

646. Vogdanis L, Martens B, Uchtmann H, Hensel F, Heitz W (1990) Synthetic and thermodynamic investigations in the polymerization of ethylene carbonate. Makromol Chem 191:465–472

647. Elmer AM, Jannasch P (2006) Synthesis and characterization of poly(ethylene oxide-co-ethylene carbonate) macromonomers and their use in the preparation of crosslinked polymer electrolytes. J Polym Sci A Polym Chem 44:2195–2205

648. Keki S, Torok J, Deak G, Zsuga M (2004) Mechanism of the anionic ring-opening oligomerization of propylene carbonate initiated by the tert-butylphenol/KHCO$_3$ system. Macromol Symp 215:141–150

649. Kéki S, Török J, Deák G, Zsuga M (2001) Ring-opening oligomerization of propylene carbonate initiated by the bisphenol a/KHCO3 system: a matrix-assisted laser desorption/ ionization mass spectrometric study of the oligomers formed. Macromolecules 34:6850–6857

650. Lee J-C, Litt MH (2000) Ring-opening polymerization of ethylene carbonate and depolymerization of poly(ethylene oxide-co-ethylene carbonate). Macromolecules 33:1618–1627

651. Rokicki G, Rakoczy P, Parzuchowski P, Sobiecki M (2005) Hyperbranched aliphatic polyethers obtained from environmentally benign monomer: glycerol carbonate. Green Chem 7:529–539

652. Wu M, Guo J, Jing H (2008) Organic base catalyzed oligomerization of propylene carbonate and bisphenol A: unexpected polyether diol formation. Catal Commun 9:120–125

653. Rokicki G, Jezewski P (1988) Polycarbonates from cyclic carbonates, carbanions, and dihalo compounds. Polym J 20:499–509

654. Rokicki G, Pawlicki J, Kuran W (1985) Poly(ether-carbonate)s from diphenolates, cyclic carbonates, and dihalo compounds. Polym J 17:509–516

655. Bialas NJ, Kühling S, Keul H, Höcker H (1990) On the behaviour of benzo-1,3-dioxolan-2-one and benzo-1,3-dioxan-2-one versus carbanionic species. Makromol Chem 191:1165–1175

656. Azechi M, Matsumoto K, Endo T (2013) Anionic ring-opening polymerization of a five-membered cyclic carbonate having a glucopyranoside structure. J Polym Sci A Polym Chem 51:1651–1655

657. Haba O, Furuichi N, Akashika Y (2009) Anionic ring-opening copolymerization of L-lactide with a five-membered cyclic carbonate having a glucopyranoside structure. Polym J 41:702–708

658. Haba O, Tomizuka H, Endo T (2005) Anionic ring-opening polymerization of methyl 4,6-O-benzylidene-2,3-O-carbonyl-alpha-D-glucopyranoside: a first example of anionic ring-opening polymerization of five-membered cyclic carbonate without elimination of CO2. Macromolecules 38:3562–3563

659. Hocker H, Keul H (1992) Initiation and growth mechanisms of the ring-opening polymerization of cyclic carbonates. Makromol Chem Macromol Symp 54–5:9–11

660. Hocker H, Keul H (1994) Controlled copolymer structures via anionic insertion polymerization of cyclic carbonates. Macromol Symp 85:211–215

661. Hocker H, Keul H, Kuhling S, Hovestadt W (1991) Ring-opening polymerization and copolymerization of cyclic carbonates. Makromol Chem Macromol Symp 42–3:145–153

662. Hocker H, Keul H, Kuhling S, Hovestadt W, Muller A, Wurm B (1993) Ring-opening polymerization and copolymerization of cyclic carbonates with a variety of initiating systems. Makromol Chem Macromol Symp 73:1–5

663. Hocker H, Keul H, Kuhling S, Hovestadt W, Muller AJ (1991) The anionic ring-opening polymerization and copolymerization of cyclic carbonates. Makromol Chem Macromol Symp 44:239–245

664. Carothers WH, Dorough GH, Van Natta FJ (1932) Studies of polymerization and ring formation. X The reversible polymerization of six-membered cyclic esters. J Am Chem Soc 54:761–772

665. Carothers WH, Van Natta FJ (1930) Studies on polymerization and ring formation. III Glycol esters of carbonic acid. J Am Chem Soc 52:314–326

666. Keul H, Bacher R, Hocker H (1986) Anionic ring-opening polymerization of 2,2-dimethyltrimethylene carbonate. Makromol Chem Macromol Chem Phys 187:2579–2589

667. Kuhling S, Keul H, Hocker H (1989) Active species in the anionic ring-opening polymerization of cyclic carbonates. Makromol Chem Macromol Chem Phys 190:9–13

668. Kuhling S, Keul H, Hocker H (1990) Polymers from 2-allyloxymethyl-2-ethyltrimethylene carbonate and copolymers with 2,2-dimethyltrimethylene carbonate obtained by anionic ring-opening polymerization. Makromol Chem Macromol Chem Phys 191:1611–1622

669. Kühling S, Keul H, Höcker H (1992) Copolymerization of 2,2-dimethyltrimethylene carbonate with 2-allyloxymethyl-2-ethyltrimethylene carbonate and with ε-caprolactone using initiators on the basis of Li, Al, Zn and Sn. Makromol Chem 193:1207–1217

670. Kuhling S, Keul H, Hocker H, Buysch HJ, Schon N, Leitz E (1991) Polymerization of 5,5-(bicyclo 2.2.1 hept-2-en-5,5-ylidene)-1,3-dioxan-2-one and copolymerization with 5,5-dimethyl-1,3-dioxan-2-one. Macromolecules 24:4229–4235

671. Matsuo J, Sanda F, Endo T (1998) A novel observation in anionic ring-opening polymerization behavior of cyclic carbonates having aromatic substituents. Macromol Chem Phys 199:2489–2494

672. Sanda F, Kamatani J, Endo T (2001) Synthesis and anionic ring-opening polymerization behavior of amino acid-derived cyclic carbonates. Macromolecules 34:1564–1569

673. Albertsson AC, Sjoling M (1992) Homopolymerization of 1,3-dioxan-2-one to high-molecular-weight poly(trimethylene carbonate). J Macromol Sci Pure Appl Chem 29:43–54

674. Kuhling S, Keul H, Hocker H, Buysch HJ, Schon N (1991) Synthesis of poly(2-ethyl-2-hydroxymethyltrimethylene carbonate). Makromol Chem Macromol Chem Phys 192:1193–1205

675. Matsuo J, Aoki K, Sanda F, Endo T (1998) Substituent effect on the anionic equilibrium polymerization of six-membered cyclic carbonates. Macromolecules 31:4432–4438

676. Miyagawa T, Shimizu M, Sanda F, Endo T (2005) Six-membered cyclic carbonate having styrene moiety as a chemically recyclable monomer. Construction of novel cross-linking-de-cross-linking system of network polymers. Macromolecules 38:7944–7949

677. Endo T, Kakimoto K, Ochiai B, Nagai D (2005) Synthesis and chemical recycling of a polycarbonate obtained by anionic ring-opening polymerization of a bifunctional cyclic carbonate. Macromolecules 38:8177–8182

678. Morikawa H, Sudo A, Nishida H, Endo T (2005) Volume-expandable monomer 5,5-dimethyl-1,3-dioxolan-2-one: Its copolymerization behavior with epoxide and its applications to shrinkage-controlled epoxy-curing systems. J Appl Polym Sci 96:372–378

679. Murayama M, Sanda F, Endo T (1998) Anionic ring-opening polymerization of a cyclic carbonate having a norbornene structure with amine initiators. Macromolecules 31:919–923

680. Nederberg F, Lohmeijer BGG, Leibfarth F, Pratt RC, Choi J, Dove AP, Waymouth RM, Hedrick JL (2007) Organocatalytic ring opening polymerization of trimethylene carbonate. Biomacromolecules 8:153–160

681. Nederberg F, Trang V, Pratt RC, Mason AF, Frank CW, Waymouth RM, Hedrick JL (2007) New ground for organic catalysis: A ring-opening polymerization approach to hydrogels. Biomacromolecules 8:3294–3297

682. Mindemark J, Hilborn J, Bowden T (2007) End-group-catalyzed ring-opening polymerization of trimethylene carbonate. Macromolecules 40:3515–3517

683. Parzuchowski PG, Jaroch M, Tryznowski M, Rokicki G (2008) Synthesis of new glycerol-based hyperbranched polycarbonates. Macromolecules 41:3859–3865

684. Seow WY, Yang YY (2009) Functional polycarbonates and their self-assemblies as promising non-viral vectors. J Control Rel 139:40–47

685. Wang Z, Zhang L, Wang J, Wang Y, Guo X, Liu C (2012) Ring-opening polymerization of 2,2-dimethyltrimethylene carbonate using imidazol-2-ylidenes. Polym Bull 68:141–150

686. Brignou P, Carpentier JF, Guillaume SM (2011) Metal- and organo-catalyzed ring-opening polymerization of alpha-methyl-trimethylene carbonate: insights into the microstructure of the polycarbonate. Macromolecules 44:5127–5135

687. Helou M, Brusson J-M, Carpentier JF, Guillaume SM (2011) Functionalized polycarbonates from dihydroxyacetone: insights into the immortal ring-opening polymerization of 2,2-dimethoxytrimethylene carbonate. Polym Chem 2:2789–2795

688. Helou M, Miserque O, Brusson J-M, Carpentier J-F, Guillaume SM (2010) Organocatalysts for the controlled "immortal" ring-opening polymerization of six-membered ring cyclic carbonates: a metal-free, green process. Chem Eur J 16:13805–13813

689. Guerin W, Helou M, Slawinski M, Brusson J-M, Carpentier J-F, Guillaume SM (2014) Macromolecular engineering via ring-opening polymerization (3): trimethylene carbonate block copolymers derived from glycerol. Polym Chem 5:1229–1240

690. Feng J, Wang X-L, He F, Zhuo R-X (2007) Non-catalyst synthesis of functionalized biodegradable polycarbonate. Macromol Rapid Commun 28:754–758

691. Kricheldorf HR, Lee SR, WeegenSchulz B (1996) Polymers of carbonic acid.12. Spontaneous and hematin-initiated polymerizations of trimethylene carbonate and neopentylene carbonate. Macromol Chem Phys 197:1043–1054

692. Liao L, Zhang C, Gong S (2007) Rapid synthesis of poly(trimethylene carbonate) by microwave-assisted ring-opening polymerization. Eur Polym J 43:4289–4296

693. Pawlowski P, Szymanski A, Kozakiewicz J, Przybylski J, Rokicki G (2005) Poly(urethaneurea)s based on oligocarbonatediols comprising bis(carbamate)alkanes. Polym J 37:742–753

694. Weilandt KD, Keul H, Höcker H (1996) Synthesis and ring-opening polymerization of 2-acetoxymethyl-2-alkyltrimethylene carbonates and of 2-methoxycarbonyl-2-methyltri-methylene carbonate; a comparison with the polymerization of 2,2-dimethyltrimethylene carbonate. Macromol Chem Phys 197:3851–3868

695. Keul H, Hocker H (1986) Block polymers obtained by means of anionic-polymerization - polystyrene-block-poly(epsilon-caprolactone) and polystyrene-block-poly(2,3-dimethyltri-methylene carbonate). Makromol Chem Macromol Chem Phys 187:2833–2839

696. Muller AJ, Keul H, Hocker H (1993) Synthesis and thermal-properties of poly (2,2-dimethyltrimethylene carbonate)-block-poly(tetrahydrofurane)-block-poly(2,2-dimethyl-trimethyle ne carbonate). Eur Polym J 29:1171–1178

697. Keul H, Muller AJ, Hocker H, Sylvester G, Schon N (1993) Preparation of polymers with polycarbonate sequences and their depolymerization – an example of thermodynamic recycling. Makromol Chem Macromol Symp 67:289–298

698. Muller AJ, Keul H, Hocker H (1991) Lithium and potassium alcoholates of poly(ethylene glycol)s as initiators for the anionic-polymerization of 2,2-dimethyltrimethylene carbonate - synthesis of AB and ABA block copolymers. Eur Polym J 27:1323–1330

699. Gerhard-Abozari E, Keul H, Höcker H (1994) Copolymers with soft and hard segments based on 2,2-dimethyltrimethylene carbonate and ε-caprolactone. Macromol Chem Phys 195:2371–2380

700. Muller AJ, Keul H, Hocker H (1994) Poly(2,2-dimethyltrimethylene carbonate)-block-poly (dimethylsiloxane)-block-poly(2,2-dimethyltrimethyl ene carbonate) - synthesis and thermal-properties. Polym Int 33:197–204

701. Hovestadt W, Keul H, Hocker H (1991) Poly(methyl methacrylate)-block-poly(2,2-dimethyl-trimethylene carbonate) - site transformation from a group transfer polymerization to an anionic ring-opening polymerization. Makromol Chem Macromol Chem Phys 192:1409–1418

702. Keul H, Hocker H, Leitz E, Ott KH, Morbitzer L (1988) Copolymers obtained by means of anionic ring-opening polymerization - poly(2,2-dimethyltrimethylene carbonate-tapered-epsilon-caprolactone). Makromol Chem Macromol Chem Phys 189:2303–2321

703. Keul H, Hocker H, Leitz E, Ott KH, Morbitzer L (1990) Copolymers obtained by means of anionic ring-opening polymerization – poly(2,2-dimethyltrimethylene carbonate)-block-polypivalolactone. Makromol Chem Macromol Chem Phys 191:1975–1990

704. Keul H, Schmidt P, Robertz B, Hocker H (1995) Copolymerization of 2,2-dimethyltrimethylene carbonate and cyclic esters. Macromol Symp 95:243–253

705. Morinaga H, Ujihara Y, Endo T (2012) Metal-free ring-opening block copolymerization of glycidyl phenyl ether with trimethylene carbonate initiated by tetra-n-butylammonium fluoride. J Polym Sci A, Polym Chem 50:3461–3465

706. Edlund U, Albertsson A-C (1999) Copolymerization and polymer blending of trimethylene carbonate and adipic anhydride for tailored drug delivery. J Appl Polym Sci 72:227–239

707. Sanda F, Kamatani J, Endo T (1999) The first anionic ring-opening polymerization of cyclic monothiocarbonate via selective ring-opening with C-S bond cleavage. Macromolecules 32:5715–5717

708. Kakimoto K, Nemoto N, Sanda F, Endo T (2002) Anionic ring-opening polymerization of cyclic thiocarbonates containing norbornene and norbornane groups undergoing volume expansion on polymerization. Chem Lett 31:156–157

709. Kricheldorf HR, Damrau D-O (1998) Polymers of carbonic acid, 26. Synthesis and ionic polymerization of 1,3-dioxane-2-thione. Macromol Chem Phys 199:2589–2596

710. Matsuo J, Sanda F, Endo T (1997) Anionic ring-opening polymerization behavior of a seven-membered cyclic carbonate 1,3-dioxepan-2-one. J Polym Sci A Polym Chem 35:1375–1380

711. Brignou P, Gil MP, Casagrande O, Carpentier JF, Guillaume SM (2010) Polycarbonates derived from green acids: ring-opening polymerization of seven-membered cyclic carbonates. Macromolecules 43:8007–8017

712. Kricheldorf HR, Jenssen J (1989) Polymers of carbonic acid—2. synthesis and polymerization of 2,2'-dihydroxybiphenyl carbonate (4,5,6,7-dibenzo-2-oxo-1,3-dioxacycloheptane). Eur Polym J 25:1273–1279
713. Keul H, Deisel F, Höcker H, Leitz E, Ott K-H, Buysch H-J, Schön N (1991) Aromatic polycarbonates by means of anionic ring-opening polymerization: bisphenol-A-polycarbonate and poly(4,8-dicyclohexyl-2,10-dimethyl-6-oxo-12 H-dibenzo[d, g]-[1,3]dioxocin). Makromol Chem Rapid Commun 12:133–139
714. Takata T, Matsuoka H, Endo T (1991) Synthesis and anionic ring-opening polymerization of a novel aromatic cyclic carbonate having binaphthyl structure. Chem Lett 2091–2094
715. Brunelle DJ, Evans TL, Boden EP (1993) Preparation and ring-opening polymerization of cyclic oligomeric aromatic carbonates. Ind J Technol 31(4–6):234–246
716. Weilandt KD, Keul H, Höcker H (1996) Synthesis and polymerization of bis(hexamethylene carbonate) and bis(2,2,3,3,4,4,5,5-octafluorohexamethylene carbonate). Macromol Chem Phys 197:2539–2551
717. Mitsuhashi T (1989) Structure and reactivity. Wiley-VCH Verlag GmbH, Weinheim, pp 179–230
718. Chakrabarti P, Seiler P, Dunitz JD, Schluter AD, Szeimies G (1981) Experimental-evidence for the absence of bonding electron-density between inverted carbon-atoms. J Am Chem Soc 103:7378–7380
719. Cho I (2000) New ring-opening polymerizations for copolymers having controlled microstructures. Prog Polym Sci 25:1043–1087
720. Hall HK, Ykman P (1976) Addition polymerization of cyclobutene and bicyclobutane monomers. J Polym Sci Macromol Rev 11:1–45
721. Levin MD, Kaszynski P, Michl J (2000) Bicyclo 1.1.1 pentanes, n staffanes, 1.1.1 propellanes, and tricyclo 2.1.0.0(2,5) pentanes. Chem Rev 100:169–234
722. Penelle J (2000) Synthetic control over substituent location on carbon-chain polymers using ring-opening polymerization of small cycloalkanes. In: Boffa LS (Exxon Research & Engineering Company), Novak BM (North Carolina State University) (eds) Transition metal catalysis in macro-molecular design. ACS symposium series, vol 760. American Chemical Society, pp 59–76
723. Penelle J (2009) Polymerization of cycloalkanes. In: Handbook of ring-opening polymerization. Wiley-VCH Verlag GmbH & Co. KGaA, Weinheim, pp 329–357
724. Kagumba LC, Penelle J (2005) Anionic ring-opening polymerization of alkyl 1-cyanocyclopropanecarboxylates. Macromolecules 38:4588–4594
725. Penelle J, Herion H, Xie T, Gorissen P (1998) Synthesis and characterization of a model carbon-chain polymer substituted by two esters on every third atom via anionic ring-opening polymerization of a cyclopropane-1,1-dicarboxylate. Macromol Chem Phys 199:1329–1336
726. Penelle J, Xie T (2000) Ring-opening polymerization of diisopropyl cyclopropane-1,1-dicarboxylate under living anionic conditions: A kinetic and mechanistic study. Macromolecules 33:4667–4672
727. Penelle J, Xie T (2001) Synthesis, characterization, and thermal properties of poly(trimethylene-1,1-dicarboxylate) polyelectrolytes. Macromolecules 34:5083–5089
728. Xie T, Penelle J, Verraver M (2002) Experimental investigation on the reliability of routine SEC-MALLS for the determination of absolute molecular weights in the oligomeric range. Polymer 43:3973–3977
729. Illy N, Boileau S, Buchmann W, Penelle J, Barbier V (2010) Control of End groups in anionic polymerizations using phosphazene bases and protic precursors as initiating system (XH-^{t}BuP$_4$ approach): application to the Ring-opening polymerization of 1,1-dicyanocyclopropane. Macromolecules 43:8782–8789
730. Illy N, Boileau S, Penelle J, Barbier V (2009) Metal-free activation in the anionic ring-opening polymerization of cyclopropane derivatives. Macromol Rapid Commun 30:1731–1735

731. Kagumba LC, Penelle J (2000) Ring-opening polymerization of 1,1-dicyanocyclopropane. Polym Prepr 41:1290
732. Alder RW, Anderson KR, Benjes PA, Butts CP, Koutentis PA, Orpen AG (1998) Polymers and oligomers with transverse aromatic groups and tightly controlled chain conformations. Chem Commun 309–310
733. Cho I, Ahn KD (1979) Polymerizations of substituted cyclopropanes.2. Anionic-polymerization of 1,1-disubstituted 2-vinylcyclopropanes. J Polym Sci A Polym Chem 17:3183–3191
734. Cho I, Kim JB (1980) Polymerization of substituted cyclopropanes.3. Anionic polymerizations of 2-substituted cyclopropane-1,1-dicarbonitriles. J Polym Sci A Polym Chem 18:3053–3057
735. Cho I, Kim WT (1986) Exploratory ring-opening polymerization.12. Polymerization of substituted spiro 2,5 octa-4,7-diene-6-ones and spiro cyclopropane-1,4'-(1'-naphthalenone). J Polym Sci C Polym Lett 24:109–111
736. Cho I, Kim WT (1987) Polymerization systems driven by aromatization energy - anionic-polymerization of 4-allylidene-2,6-dimethyl-2,5-cyclohexadien-1-one and spiro 2,5 octadienone derivatives. J Polym Sci A Polym Chem 25:2791–2798
737. Kim JB, Cho IH (1997) Synthesis and electronic effect of the substituents on anionic ring-opening polymerization of para-substituted phenyl cyclopropanes. Tetrahedron 53:15157–15166
738. Lee JY, Cho I (1986) Synthesis and ring-opening polymerization of 1,2-disubstituted cyclobutanes. Bull Kor Chem Soc 7:210–213
739. Yokozawa T, Miyamoto Y, Futamura S (1993) Synthesis of alternating copolymer of tetracyanoethylene and ethyl vinyl ether by ring-opening polymerization. Makromol Chem Rapid Commun 14:245–249
740. Barfield M, Chan RJH, Hall HK, Mou YH (1986) C-13 NMR-studies of sequence distributions in polymers having all rings in the backbone - 1-substituted 1,3-poly(bicyclobutanes). Macromolecules 19:1343–1349
741. Hall HK, Blanchar EP, Cherkofs SC, Sieja JB, Sheppard WA (1971) Synthesis and polymerization of 1-bicyclobutanecarbonitriles. J Am Chem Soc 93:110–120
742. Hall HK, Padias AB (2003) Bicyclobutanes and cyclobutenes: unusual carbocyclic monomers. J Polym Sci A Polym Chem 41:625–635
743. Hall HK, Smith CD, Blanchar EP, Cherkofs SC, Sieja JB (1971) Synthesis and polymerization of bridgehead-substituted bicyclobutanes. J Am Chem Soc 93:121–130
744. Kawauchi T, Nakamura M, Kitayama T, Padias AB, Hall HK (2005) Structural analyses of methyl bicyclobutane-1-carboxylate oligomers formed with tert-butyllithium/aluminum bisphenoxide and mechanistic aspect of the polymerization. Polym J 37:439–448
745. Kitayama T, Kawauchi T, Chen XP, Padias AB, Hall HK (2002) Stereospecific anionic polymerization of methyl bicyclobutane-1-carboxylate. Macromolecules 35:3328–3330
746. Hall HK (1971) Synthesis and polymerization studies of bicyclo 2.1.0 pentene-1-carbonitrile and bicyclo 3.1.0 hexane-1-carbonitrile. Macromolecules 4:139–142
747. Kaszynski P, Michl J (1988) N staffanes - a molecular-size tinkertoy construction set for nanotechnology - preparation of end-functionalized telomers and a polymer of 1.1.1 propellane. J Am Chem Soc 110:5225–5226
748. Schluter AD (1988) Poly(1.1.1 propellane) - a novel rigid-rod polymer obtained by ring-opening polymerization breaking a carbon carbon sigma-bond. Macromolecules 21:1208–1211
749. Schluter AD (1988) The central propellane bond as polymerizable cc single bond – poly (tricyclo 4.2.0.02,7 octane-1,7-diyl) – a poly(1.1.1 propellane). Angew Chem Int Ed 27:296–298
750. Goethals EJ, Dervaux B (2012) 4.13 – ROP of cyclic amines and sulfides. In: Matyjaszewski K, Möller M (eds) Polymer science: a comprehensive reference. Elsevier, Amsterdam, pp 309–330

751. Boileau S, Champetier G, Sigwalt P (1963) Polymérisation anionique du sulfure de propylène. Makromol Chem 69:180–192
752. Boileau S, Raynal JM, Sigwalt P, Coste J (1962) Chimie macromoléculaire – hauts polymères du sulfure d'éthylène. CR Acad Sci 254:2774–2776
753. Sigwalt P, Spassky N (1984) In: Ivin J, Saegusa T (eds) Ring-opening polymerization. Elsevier, London, p 603
754. Favier JC, Boileau S, Sigwalt P (1968) Kinetics of anionic polymerization of propylene sulfide in tetrahydrofuran.i. Bifunctional polymers with a sodium counter-ion at −30 °C. Eur Polym J 4:3–12
755. Aida T, Kawaguchi K, Inoue S (1990) Zinc N-substituted porphyrins as novel initiators for the living and immortal polymerizations of episulfide. Macromolecules 23:3887–3892
756. Morgan DR, Williams GT, Wragg RT (1970) Polyamines as polymerization catalysts for alkylene sulphide. Eur Polym J 6:309–317
757. Nicol E, Bonnans-Plaisance C, Levesque G (1999) A new initiator system for the living thiiranes ring-opening polymerization: a way toward star-shaped polythiiranes. Macromolecules 32:4485–4487
758. Bonnans-Plaisance C, Levesque G (1989) Homo- and copolymerization of unprotected 2-(hydroxymethyl)thiirane initiated by quaternary ammonium salts of dithiocarboxylic acids. Macromolecules 22:2020–2023
759. Rehor A, Tirelli N, Hubbell JA (2002) A new living emulsion polymerization mechanism: episulfide anionic polymerization. Macromolecules 35:8688–8693
760. Kilcher G, Wang L, Tirelli N (2008) Role of thiol-disulfide polymerization exchange in episulfide polymerization. J Polym Sci A Polym Chem 46:2233–2249
761. Napoli A, Tirelli N, Kilcher G, Hubbell JA (2001) New synthetic methodologies for amphiphilic multiblock copolymers of ethylene glycol and propylene sulfide. Macromolecules 34:8913–8917
762. Wang L, Kilcher G, Tirelli N (2007) Synthesis and properties of amphiphilic star polysulfides. Macromol Biosci 7:987–998
763. Suzuki A, Nagai D, Ochiai B, Endo T (2004) Star-shaped polymer synthesis by anionic polymerization of propylene sulfide based on trifunctional initiator derived from trifunctional five-membered cyclic dithiocarbonate. Macromolecules 37:8823–8824
764. Boileau S, Sigwalt P (1965) Copolymères séquencés à partir des épisulfures. CR Acad Sci 261:132–134
765. Boileau S, Sigwalt P (1973) Block copolymers of epoxyethane with epithioalkanes. Makromol Chem Macromol Chem Phys 171:11–18
766. Bonnans-Plaisance C, Guerin P, Levesque G (1995) Preparation and characterization of poly (thiirane) block copolymers with pendent hydroxy groups. Polymer 36:201–208
767. Gourdenne A, Sigwalt P (1967) Stability of the living polymers of dienes in relation with the preparation of block copolymers. Eur Polym J 3:481–499
768. Morton M, Kammerec RF, Fetters LJ (1971) Synthesis and properties of block polymers. 2. Poly(alpha-methylstyrene)-poly(propylene sulfide)-poly(alpha-methylstyrene). Macromolecules 4:11–15
769. Nevin RS, Pearce EM (1965) Alkylene sulfide block copolymers. J Polym Sci B Polym Lett 3:487–490
770. Watanabe Y, Aida T, Inoue S (1990) Visible-light-mediated living and immortal polymerizations of epoxides initiated with zinc-complexes of N-substituted porphyrins. Macromolecules 23:2612–2617
771. Bonnans-Plaisance C, Corvazier L, Emery J, Nicol E (1998) Functional polythiiranes 9: stilbene mesogen side chain polythiirane. Polym Bull 41:525–532
772. Bonnans-Plaisance C, Corvazier L, Skoulios A (1997) Functional polythiiranes: 5. Side chain liquid crystalline polythiiranes. Polymer 38:3843–3854
773. Bonnans-Plaisance C, Retif P (1999) Functional polythiiranes 6: hydrolysis of side chains ester and monothioacetal functions of comb-like polythiiranes. React Funct Polym 39:9–18

774. Bonnans-Plaisance C, Rétif P, Levesque G (1995) Functional polythiiranes 4. Polym Bull 34:141–147
775. Hirata M, Ochiai B, Endo T (2010) Synthesis of refractive star-shaped polysulfide by anionic polymerization of phenoxy propylene sulfide using an initiating system consisting of trifunctional thiol derived from five-membered cyclic dithiocarbonate and amine. J Polym Sci A Polym Chem 48:525–531
776. Nicol E, Bonnans-Plaisance C, Dony P, Levesque G (2001) Synthesis of end-functionalized star-shaped poly(methylthiirane)s. Macromol Chem Phys 202:2843–2852
777. Lazcano S, Bello A, Marco C, Fatou JG (1989) Anionic synthesis and thermal-properties of poly(3,3-diethylthietane). Polym Bull 21:571–576
778. Lazcano S, Marco C, Fatou JG, Bello A (1989) Growth-rates and regime transitions in poly (3,3-dimethylthietane). Eur Polym J 25:1213–1218
779. Machon JP, Nicco A (1971) Synthesis of homopolymers of thietane of determined molecular mass. Eur Polym J 7:353–361
780. Morton M, Kammerec RF (1970) Nucleophilic substitution at bivalent sulfur - reaction of alkyllithium with cyclic sulfides. J Am Chem Soc 92:3217–3218
781. Saegusa T, Kobayashi S, Hayashi K, Yamada A (1978) Preparation and chelating properties of mercaptoethylated and dithiocarboxylated poly(styrene-g-ethylenimine)s. Polym J 10:403–408
782. Yingyongnarongkul B-E, Howarth M, Elliott T, Bradley M (2004) Solid-phase synthesis of 89 polyamine-based cationic lipids for DNA delivery to mammalian cells. Chem Eur J 10:463–473
783. Stewart IC, Lee CC, Bergman RG, Toste FD (2005) Living ring-opening polymerization of N-sulfonylaziridines: synthesis of high molecular weight linear polyamines. J Am Chem Soc 127:17616–17617
784. Hall HK, Schneider AK (1958) Polymerization of cyclic esters, urethans, ureas and imides. J Am Chem Soc 80:6409–6412
785. Keul H, Hocker H (2000) Expected and unexpected reactions in ring-opening (co)polymerization. Macromol Rapid Commun 21:869–883
786. Schmitz F, Keul H, Hocker H (1997) Alternating copolymers of tetramethylene urea with 2,2-dimethyltrimethylene carbonate and ethylene carbonate; preparation of the corresponding polyurethanes. Macromol Rapid Commun 18:699–706
787. Schmitz F, Keul H, Hocker H (1998) Copolymerization of 2,2-dimethyltrimethylene carbonate with tetramethylene urea: a new route to the polyurethane. Polymer 39:3179–3186
788. Ubaghs L, Novi C, Keul H, Hocker H (2004) Copolymerization of ethylene carbonate and 1,2-propylene carbonate with tetramethylene urea and characterization of the polyurethanes. Macromol Chem Phys 205:888–896
789. Ubaghs L, Waringo M, Keul H, Hocker H (2004) Copolymers and terpolymers of tetramethylene urea, gamma-butyrolactone, and ethylene carbonate or 1,2-propylene carbonate. Macromolecules 37:6755–6762
790. Jorres V, Keul H, Hocker H (1998) Polymerization of (3S,6S)-3-isopropyl-6-methyl-2,5-morpholinedione with tin octoate and tin acetylacetonate. Macromol Chem Phys 199:835–843
791. Dijkstra PJ (2009) Polymerization of cyclic depsipeptides, ureas and urethanes. In: Handbook of ring-opening polymerization. Wiley-VCH Verlag GmbH & Co. KGaA, Weinheim, pp 123–140
792. Ouchi T, Miyazaki H, Arimura H, Tasaka F, Hamada A, Ohya Y (2002) Synthesis of biodegradable amphiphilic AB-type diblock copolymers of lactide and depsipeptide with pendant reactive groups. J Polym Sci A Polym Chem 40:1218–1225
793. Ouchi T, Toyohara M, Arimura H, Ohya Y (2002) Preparation of poly(L-lactide)-based microspheres having a cationic or anionic surface using biodegradable surfactants. Biomacromolecules 3:885–888

794. Yongzhen L, Jidong H, Guozhen C, Weina H, Zheng P (2010) Synthesis of polymorpholine-2,5-dione-block-polylactide by two-step anionic ring-opening polymerization. J Appl Polym Sci 118:2005–2008

795. Lapienis G (2012) 4.18 - ring-opening polymerization of cyclic phosphorus monomers. In: Matyjaszewski K, Möller M (eds) Polymer science: a comprehensive reference. Elsevier, Amsterdam, pp 477–505

796. Łapienis G, Penczek S (1977) Kinetics and thermodynamics of anionic polymerization of 2-methoxy-2-oxo-1,3,2-dioxaphosphorinane. J Polym Sci Polym Chem Ed 15:371–382

797. Libiszowski J, Kałużynski K, Penczek S (1978) Polymerization of cyclic esters of phosphoric acid. VI. Poly(alkyl ethylene phosphates). Polymerization of 2-alkoxy-2-oxo-1,3,2-dioxaphospholans and structure of polymers. J Polym Sci Polym Chem Ed 16:1275–1283

798. Vogt W, Pflüger R (1975) Polymere ester von säuren des Phosphors, 3. Polymerisation des 2-Äthoxy-2-oxo-1,3,2-dioxaphospholans. Makromol Chem 1:97–110

799. Vogt W, Siegfried R (1976) Polymere ester von säuren des phosphors, 4. Polymerisation des 2-äthoxy-2-oxo-4,5-dihydro-1,3,2-dioxaphosphorins. Makromol Chem 177:1779–1789

800. Sharov VN, Sharov VN, Bartashe VA, Klebansk AL (1972) Polymers based on cyclic polyfluoroalkylene polyfluoroalkyl phosphates. Vysokomol Soedin A 14:653–661

801. Iwasaki Y, Yamaguchi E (2010) Synthesis of well-defined thermoresponsive polyphosphoester macroinitiators using organocatalysts. Macromolecules 43:2664–2666

802. Liu J, Pang Y, Huang W, Zhai X, Zhu X, Zhou Y, Yan D (2010) Controlled topological structure of copolyphosphates by adjusting pendant groups of cyclic phosphate monomers. Macromolecules 43:8416–8423

803. Steinbach T, Schroder R, Ritz S, Wurm FR (2013) Microstructure analysis of biocompatible phosphoester copolymers. Polym Chem 4:4469–4479

804. Zhang S, Wang H, Shen Y, Zhang F, Seetho K, Zou J, Taylor J-SA, Dove AP, Wooley KL (2013) A simple and efficient synthesis of an acid-labile polyphosphoramidate by organobase-catalyzed ring-opening polymerization and transformation to polyphosphoester Ionomers by acid treatment. Macromolecules 46:5141–5149

805. Yasuda H, Sumitani M, Lee K, Araki T, Nakamura A (1982) High molecular weight poly (2-methoxy-1,3,2-dioxaphospholane 2-oxide) by ring-opening catalysis of tertiary amines. Initiation and stepwise propagation mechanisms as studied by the stoichiometric reaction with triethylamine. Macromolecules 15:1231–1237

806. Sharov VN, Klebansk AL (1973) Polymers based on cyclic polyfluoroalkylene alkyl(aryl) phosphonates. Vysokomol Soedin A 15:2453–2457

807. Steinbach T, Ritz S, Wurm FR (2014) Water-soluble poly(phosphonate)s via living ring-opening polymerization. ACS Macro Lett 3:244–248

808. Kałuzynski K, Libiszowski J, Penczek S (1977) Poly(2-hydro-2-oxo-1,3,2-dioxaphosphorinane). Preparation and NMR spectra. Makromol Chem 178:2943–2947

809. Łapienis G, Penczek S (1990) Synthesis of poly(alkylene phosphate)s with n-containing bases in the side chains. III. N1-oxoethyleneuracil on the poly(trimethylene phosphate) chain. J Polym Sci A Polym Chem 28:1519–1526

810. Pretula J, Kałużyński K, Penczek S (1984) Living reversible anonic polymerization of N,N-diethylamine-1,3,2-dioxaphosphorinan. J Polym Sci Polym Chem Ed 22:1251–1258

811. Kałużyński K, Penczek S (1987) Polymerization of 2-diethylamino-1,3,2-dioxaphosphorinane, 2. Kinetics. Makromol Chem 188:1713–1721

812. Lapienis G, Penczek S, Pretula J (1983) Poly (dialkylphosphates) based on deoxyribose. Macromolecules 16:153–158

Ring-Opening Polymerization of *N*-Carboxyanhydrides for Preparation of Polypeptides and Polypeptide-Based Hybrid Materials with Various Molecular Architectures

David Pahovnik and Nikos Hadjichristidis

Abstract Different synthetic approaches utilizing ring-opening polymerization of *N*-carboxyanhydrides for preparation of polypeptide and polypeptide-based hybrid materials with various molecular architectures are described. An overview of polymerization mechanisms using conventional (various amines) as well as some recently developed initiators (hexamethyldisilazane, *N*-heterocyclic persistent carbenes, etc.) is presented, and their benefits and drawbacks for preparation of polypeptides with well-defined chain lengths and chain-end functionality are discussed. Recent examples from literature are used to illustrate different possibilities for synthesis of pure polypeptide materials with different molecular architectures bearing various functional groups, which are introduced either by modification of amino acids, before they are transformed into corresponding *N*-carboxyanhydrides, or by post-polymerization modifications using protective groups and/or orthogonal functional groups. Different approaches for preparation of polypeptide-based hybrid materials are discussed as well using examples from recent literature. Syntheses of simple block copolymers or copolymers with more complex molecular architectures (graft and star copolymers) as well as modifications of nanoparticles and other surfaces with polypeptides are described.

Keywords Polypeptides • *N*-carboxyanhydrides • Ring-opening polymerization • Hybrid materials • Molecular architectures

D. Pahovnik • N. Hadjichristidis (✉)
Division of Physical Sciences and Engineering, KAUST Catalysis Center (KCC), Polymer Synthesis Laboratory, King Abdullah University of Science and Technology (KAUST), Thuwal, Saudi Arabia
e-mail: Nikolaos.Hadjichristidis@kaust.edu.sa

307

1 Introduction

Polypeptide materials are of great interest due to the very broad functionalities that can be introduced into polypeptide chain as well as due to their ability to form different secondary structures (α-helix, β-sheets, etc.), which play a very important role in their self-assembly and have thus consequently a very significant effect on their chemical and mechanical properties. Recent developments in the field of polypeptide synthesis by ring-opening polymerization (ROP) of α-amino acid *N*-carboxyanhydrides (NCA) enabled us preparation of well-defined polypeptides with different molecular architectures. When polypeptides are combined with other polymers, hybrid materials are prepared, which combine the functionality and ability of self-organization of polypeptides with properties of more conventional polymers, this expanding the possible applications even further. Recently, there have been a number of excellent reviews published on the synthetic polypeptides and polypeptoids prepared by ROP of NCA and their potential applications focusing mainly on the mechanisms and synthesis of complex macromolecular architectures [1, 2], biomedical applications [3, 4], stimuli responsive polypeptides [5] and their self-assembly [6], or polypeptoids [7]. In this work we will present a general overview of a very fast developing field of synthetic polypeptides with regard to the mechanism of polymerization using different conventional as well as some more recently developed initiators for preparation of polypeptides with well-defined chain lengths and chain-end functionality. Using examples from recent literature, different possibilities for synthesis of pure polypeptide materials as well as polypeptide-based hybrid materials with different molecular architectures are described.

2 Polymerization Mechanisms

Due to the structure of the NCA molecule, bearing multiple possible sites for either nucleophilic or electrophilic attack (Fig. 1), there are several possible initiating systems that can be used for the ROP of NCAs, each following their own mechanism having various advantages as well as disadvantages.

High reactivity of the NCA monomers comes hand in hand with the necessity to have them as pure as possible, so that we are able to prepare well-defined polypeptides and avoid a large number of possible side reactions. In most cases, repeated crystallization is enough to obtain pure solid NCAs. On the other hand, oily NCAs can be purified by washing the reaction mixture with water and sodium bicarbonate [8]. Washing also proved efficient in cases where acid scavengers (triethylamine) had to be used with acid-labile protective groups on the amino acid [9]. However, washing has to be done at low temperature to avoid hydrolysis of NCAs, and water has to be completely removed afterwards since it can act as initiator as well. Another option for purification of NCAs is flash column

Fig. 1 NCA with possible reaction centers shown


Electrophilic centers

Nucleophilic centers
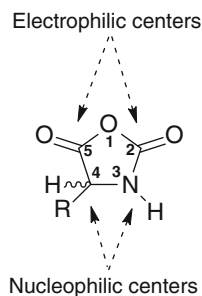
chromatography on silica. This procedure is especially useful for the preparation of highly functional and low-melting NCAs that are difficult to crystallize. However, it has to be done under anhydrous conditions in a glove box [10]. To ensure not only high purity of all reagents involved but also maintain the necessary conditions for the living polymerization of NCAs, high-vacuum technique for purification of the NCAs by crystallization and subsequent polymerization was developed [11]. The NCA monomer was introduced into a glass apparatus specially designed for crystallization (Fig. 2), which was then attached to the high-vacuum line. High molecular weight homopolypeptides with very low dispersities were obtained using primary amine initiators, and the livingness of the chains was confirmed by subsequent addition of other monomers to make diblock and triblock copolymer, which also had very low dispersities and expected molecular weights. The living-ness of the polypeptides under high-vacuum conditions can be preserved indefi-nitely, thus making possible the use of linking chemistry for the synthesis of a wide variety of macromolecular architectures. The high-vacuum technique for purifica-tion of NCAs and subsequent polymerization was shown to be very effective for preparation of highly reactive NCAs, e.g., L-prolin and well-defined poly(L-prolin) homopolypeptides as well as diblock and triblock hybrids with PEO, where poly (L-prolin) forms a hydrophilic helix independent of pH and temperature within the physiological range [12].

The most commonly used initiators for the NCA polymerization are primary amines, which follow the normal amine mechanism (NAM) of polymerization. The amino group attacks the carbonyl atom at position 5, which is followed by the opening of the ring, yielding a peptide bond and carbamic acid. Carbamic acid then undergoes decarboxylation to give a free primary amino group, which acts as a new initiator, thus enabling the chain growth (Fig. 3) [13, 14]. Other nonionic initiators like secondary amines, alcohols, water, etc., can follow the same mechanism, as long as they have a labile proton bound to the nucleophilic center.

If instead of a nucleophilic amine, we use a nonprotic base such as triethylamine, it will deprotonate the NCA by taking away the proton at the 3-N. This creates an NCA anion which then acts as an initiator, so this mechanism is called activated monomer mechanism (AMM) [15]. Since a proton is required at the position 3-N, this mechanism only works for *N*-unsubstituted NCAs. The NCA anion attacks the 5-carbonyl group of another NCA molecule opening the ring. The carbamate anion
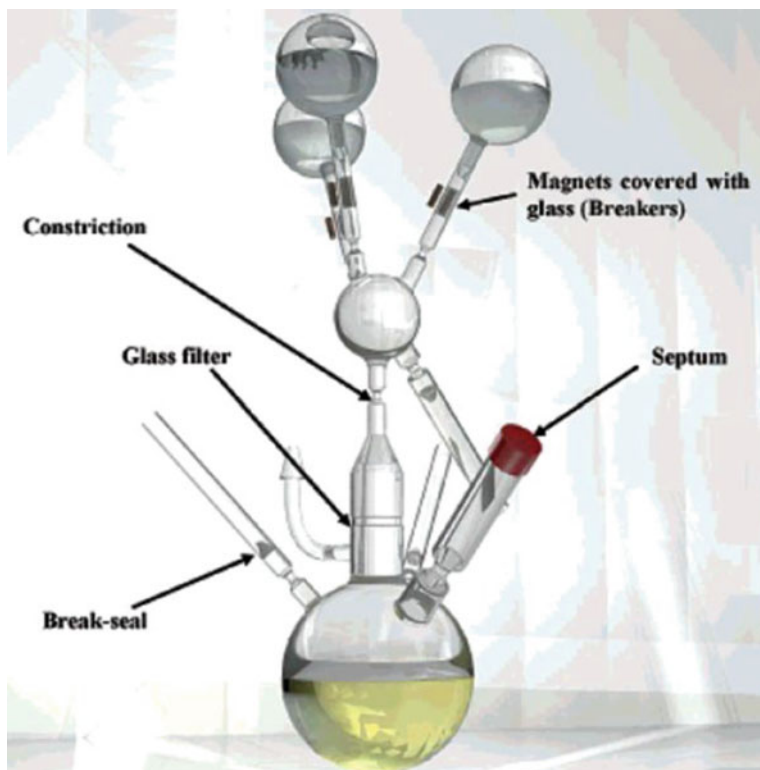
Fig. 2 Apparatus used for purification of NCAs by high-vacuum technique (Reprinted with permission from Aliferis et al. [11]. Copyright 2004 American Chemical Society)
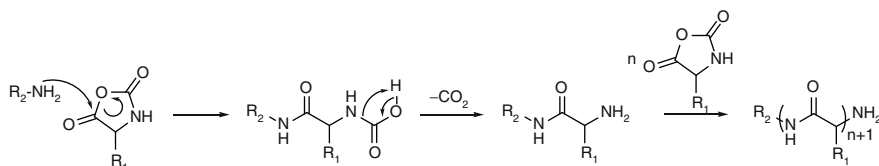
Fig. 3 Normal amine mechanism of NCA polymerization

then deprotonates a new NCA which forms an NCA anion, while the carbamic acid decarboxylates to give an amino group. The formed dimer now has two reactive centers capable of propagation. The new NCA anion can attack the 5-carbonyl group of the dimer, and a new carbamate is formed which deprotonates another NCA so it can decarboxylate, thus regenerating the NCA anion needed for propagation, which can however still act as a new initiator thus leading to poorly controlled polymerization. On the other side, the amino group can react with NCA to propagate via NAM (Fig. 4). Since most nucleophiles can act as a base,
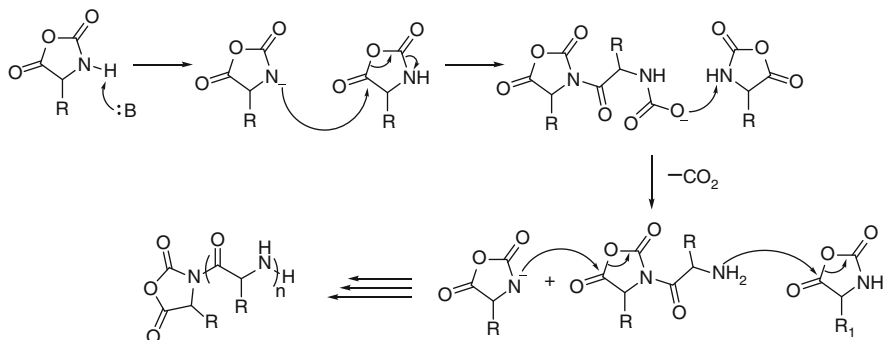
Fig. 4 Activated monomer mechanism of NCA polymerization

both NAM and AMM can coexist. This is especially true for sterically hindered secondary amines, which are stronger bases than the primary amines, and can deprotonate the NCA while still having the proton on the nucleophile so they can undergo the NAM.

To avoid the AMM when using primary amines, use of primary amine salts was proposed. The amine salt can neither initiate nor propagate the polymerization; however, at high temperatures the exchange between the free amino group (active) and protonated one (dormant) becomes faster, making it possible for the NCA to polymerize. The constant presence of protons in the reaction mixture ensures that the NCA stays protonated thus avoiding the AMM. Dimitrov and Schlaad [16] have used a polystyrene macroinitiator with primary amine hydrochloride end group as an initiator. The polymerization was run at 40–80 °C for 3 days. Polypeptides with significantly narrower molecular weight distributions were obtained as compared to polypeptide initiated by primary amine macroinitiator. Since chloride anion is known to be able to initiate the polymerization of NCA, a primary amine salt with a non-nucleophilic anion was used by Vicent et al. [17]. They have prepared a series of primary amine tetrafluoroborate salts ($R-NH_3^+ BF_4^-$) and tested them as initiators. They have managed to control the molecular weight of polymers up to a degree of polymerization of about 800 without the use of complex initiators or a demanding experimental setup. The derived polymers had low dispersities, below 1.2.

A special case of secondary amine used for the controlled polymerization of NCA was hexamethyldisilazane (HDMS) [18]. It was expected that HDMS, as a secondary amine with two bulky groups, will react by the AMM; however, it turns out that it follows a unique mechanism. HMDS, as expected, first deprotonates the NCA; however, a trimethylsilyl (TMS) group gets transferred to 2-CO from HMDS, and an intermediate is formed, which is rapidly attacked by the in situ-generated TMS amine causing ring to open, thus forming a TMS carbamate. The polypeptide chain then propagates through the transfer of the TMS group from the terminal TMS carbamate to the incoming monomer to form a new TMS carbamate terminal propagating group (Fig. 5). This mechanism is similar to the group transfer
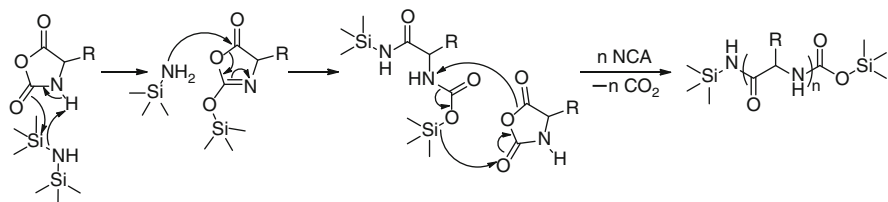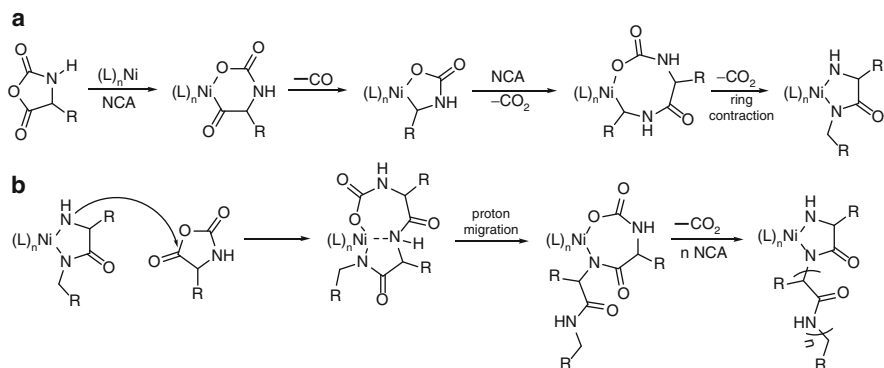
Fig. 5 Proposed mechanism of NCA polymerization using hexamethyldisilazane (HMDS)

polymerizations of acrylic monomers initiated by similar organosilicon compounds. Using HDMS polymerizations proceeded smoothly to yield PBLGs with good control over molecular weight and molecular weight distributions. Other N-TMS amines can be used as initiators as well, enabling functionalization at the C-terminus [19].

Deming [20–22] moved away from the amine-based initiators and developed a new class of initiators for NCA polymerization based on transition metal complexes of cobalt and nickel. By using the zerovalent nickel or cobalt complexes with the right ligands (2,2′-bipyridyl (bipy), 1,5-cyclooctadiene (COD), and trimethyl-phosphine (PMe$_3$)), he was able to prepare well-defined polypeptides. In the proposed mechanism [23], the metal reacts with the NCA by oxidative addition to the anhydride group, forming a metallacyclic complex, which reacts with another NCA to give a 6-membered cyclic intermediate. This intermediate upon further reaction with NCA followed by a ring contraction produce a 5-membered amido-amidate metallacycle, which is the active polymerization intermediate, through which the polymerization then proceeds (Fig. 6). The obtained polypeptides had narrow molecular weight distributions ($Đ_M < 1.3$), and good control over the molecular weight was achieved. However, this type of initiators does not work for the polymerization of N-substituted NCAs.

Besides cobalt and nickel, a number of other transition elements have proven to be efficient initiators for NCA polymerization, including platinum, where it was again shown that the choice of the right chelating groups plays the most important role in the activity of the metal complex [24]. It also determines the efficiency of the metal complex to keep the NCA polymerization living and to give polypeptides with narrow molecular weight distributions.

Recently, N-heterocyclic persistent carbenes (NHC) have been successfully used as initiators for polymerization of N-substituted NCAs to synthesize poly(α-peptoid)s [25]. This mechanism does not work for N-unsubstituted NCAs, since imidazolium-based persistent carbenes are not only good nucleophiles but are a strong base as well, easily deprotonating the N-unsubstituted NCAs. They are actually capable of deprotonating the methylene group of the monomer, which leads by yet unknown mechanism to the formation of a proposed Münchnone zwitterion-initiating species. This species is supposed to have an exocyclic carbamate group from which subsequent monomer addition may occur (Fig. 7a). NHC-mediated ring-opening polymerization can proceed through another

Fig. 6 Proposed mechanism of NCA polymerization using zerovalent nickel complex. Path (**a**) represents the creation of the initiating species, while path (**b**) shows the mechanism of propagation
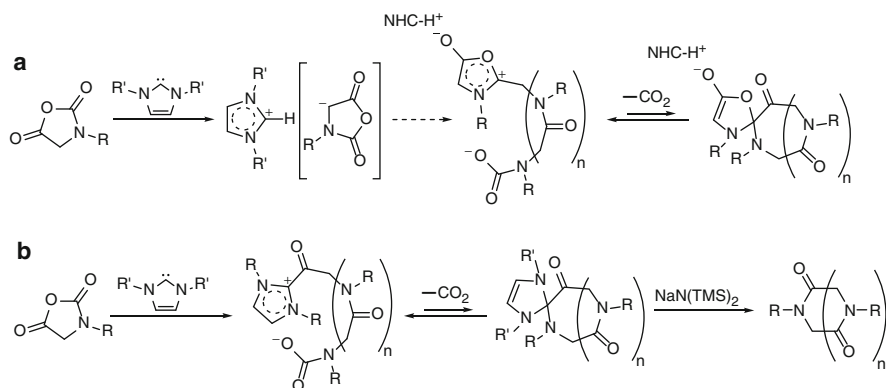
Fig. 7 Proposed mechanisms for NHC-mediated ring-opening polymerization of *N*-substituted NCAs proceeding through deprotonation of NCA (**a**) or nucleophilic attack of NHC on NCA (**b**) with formation of the spirocycles and subsequent cyclization with NaN(TMS)$_2$ to give cyclic poly (α-peptoid)s

mechanism, where after the attack of the carbene and ring opening of the NCA, a zwitterionic intermediate is formed that transforms into spirocyclic product, which upon treatment with NaN(TMS)$_2$, is turned into a free cyclic poly(α-peptoid) (Fig. 7b) [26]. The control over the polymer molecular weight strongly depends on the solvents and the NHC structure, since only low molecular weight polymers were obtained regardless of the initial monomer/initiator ratio when *N,N*-dimethyl-formamide was used. However, in tetrahydrofuran or toluene, very low dispersities were obtained ($Đ_M < 1.12$) even for high molecular weights with good control over the molecular weight. In solvents with low dielectric constant, zwitterionic inter-mediate species maintain cyclic architectures with two chain ends in close contact

through Coulombic interaction, which significantly suppresses the side reactions. The livingness of the system was tested with chain-extension experiment, and an increase of polymer molecular weight was observed with no low molecular weight species formed [25].

3 Polypeptide Materials with Various Molecular Architectures

Due to the large selection of possible amino acids and their readiness for further modifications, various different NCA monomers were successfully polymerized. A broad selection of protective groups for the side chains have been used that enable selective deprotection and post-polymerization modifications to afford polypeptides with desired functionality. A high grafting efficiency can usually be achieved, especially in the case of polypeptides that form α-helix since it can reduce steric hindrance and result in increased accessibility of the side chains for reaction [27]. Another method is to modify the amino acid prior to the cyclization to prepare the NCAs. Completely modified polypeptides can be prepared this way; however, complex substituents often require exotic protective groups and/or reaction conditions to survive the formation of the NCA as well as purification can be significantly harder, especially if the substituted NCAs do not crystallize.

Preparation of various well-defined biomimetic analogs shows a lot of promise for biomedical applications. Glycopolypeptides were so prepared by a transformation of ε-amino group on lysine to azido group using a diazotransfer reagent imidazole-1-sulfonyl-azide · HCl [28]. Modified amino acid was then cyclized to NCA, and homo- and copolymers with Cbz-lysine using $(PMe_3)_4Co$ initiator were prepared with narrow molecular weight distributions (Fig. 8). The azido functional polypeptides were then readily modified with alkyne functional glycoside by copper-catalyzed azide−alkyne cycloaddition to afford glycopolypeptides.

Formation of various secondary structures (α-helix, β-sheets, etc.) of the polypeptide chains plays a very important role in their self-assembly and have consequently a very significant effect on their chemical and mechanical properties. Hammond et al. [29] developed a set of hydrogels based on poly(-γ-propargylglutamate). Homopolymer was then grafted with diethylene glycol using copper-catalyzed azide–alkyne cycloaddition. Diethylene glycol grafted poly(γ-propargylglutamate) with only L-amino acids exists in predominantly α-helix conformation, while polypeptides prepared from a racemic mixture of amino acids adopt random coil conformation. To prepare the hydrogels, hydroxyl groups of diethylene glycol grafted to poly(γ-propargylglutamate) were reacted with 4-(maleimido)phenyl-isocyanate to transform them to maleimide functionality, followed by cross-linking with a thiol-functionalized poly(ethylene oxide) (PEO) star (Fig. 9). Both hydrogels with either helical or coil polypeptides exhibited similar swelling and permeability, but dramatically different stiffness due to rigidity of the polypeptide backbone.
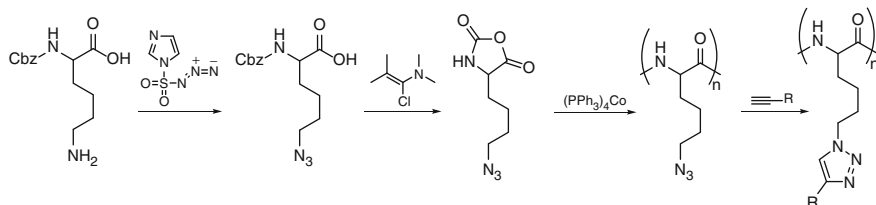
Fig. 8 Modification of lysine to prepare azide-containing polypeptides

Fig. 9 Preparation of hydrogels with either helical or coil polypeptides with the same formulation (Reproduced from Oelker et al. [29] with permission of The Royal Society of Chemistry)
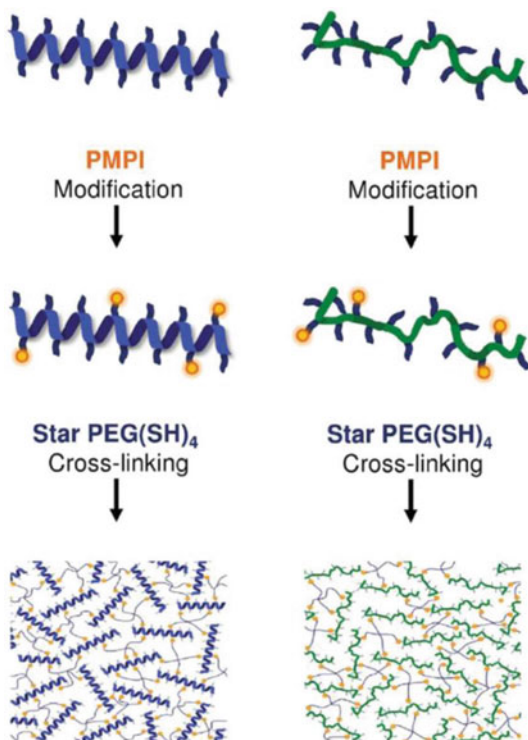
Glycopolypeptides were also prepared by Gupta et al. [30]; however, instead of post-polymerization modification, they have attached protected galactose, mannose, or lactose to L-lysine, which was then transformed to NCA, polymerized, and finally deprotected to afford water-soluble glycopolypeptides. Glycopolypeptides prepared from purely L-lysine-modified amino acid adopt an α-helix conformation in water, while glycopolypeptide prepared from racemic mixture of lysine showed no helicity. A self-assembly of such glycopolypeptides was studied and prepared by azide–amine-terminated bifunctional oligopeptide PEO to which a hydrophobic dendron of different generations were attached by copper-catalyzed azide–alkyne cycloaddition. The self-assembly was found to depend not only upon
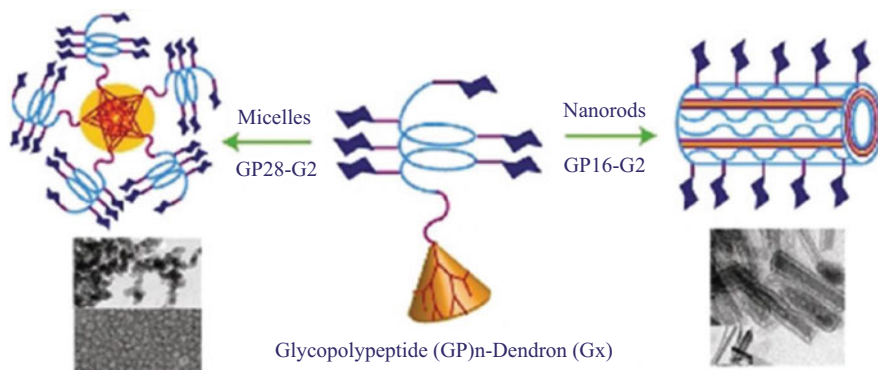
Fig. 10 Self-assembly of a hydrophilic glycopolypeptide chains with a wedge-like hydrophobic dendron attached to one end stiff (Reprinted with permission from Pati et al. [31]. Copyright 2012 American Chemical Society)

generation of the dendron and the length of the glycopeptide segment, but on extent of helicity of the polypeptide backbone as well. A range of one-dimensional to three-dimensional topologies were thus prepared (Fig. 10) [31].

Similarly, Gupta et al. [32] have prepared phosphopolypeptides by attaching a diethylphosphate or diethylphosphonate to L-cysteine thiol group by thiol–ene click reaction. A bifunctional alkyne–amine initiator was used for polymerization of phosphate containing NCAs (Fig. 11). Obtained molecular weights were close to the expected ones, and dispersities below 1.12 were achieved. An azide-functional PEO was then attached to the polypeptides by copper-catalyzed azide−alkyne cycloaddition to afford block copolymers. To make the polypeptides water soluble, the phosphoester groups had to be deprotected. Iodotrimethylsilane was used successfully for deprotection of phosphonate esters; however, in the case of phosphate ester, partial removal of the phosphorus from the polymer chain was unavoidable.

Chan-Park et al. [33] have prepared a series of random co- and terpolymers by polymerization of lysine NCA as hydrophilic and alanine, phenylalanine, or leucine NCAs as hydrophobic amino acids. Ni(COD)$_2$ was used as initiator, and number-average molecular weight of the peptides from around 5 to 35 kDa and narrow molecular weight dispersities of 1.1–1.3 were obtained. The hydrophobic amino acid content was varied from 0 to 100 %. Poly(lysine-*ran*-phenylalanine) and poly (lysine-*ran*-phenylalanine-*ran*-leucine) showed the best antimicrobial properties and even lower minimum inhibitory concentrations than values of many naturally occurring antimicrobial peptides. Optimal antimicrobial activity was achieved when the polypeptide was 25 units long with 60 % hydrophobic amino acid content. No distinct α-helix, β-sheet, or random coil structures were evident in all the peptides indicating that the lack of a distinct secondary structure in poly(lysine-*ran*-phenylalanine-*ran*-leucine) and poly(lysine-*ran*-phenylalanine) did not compromise the peptides' antimicrobial activity.
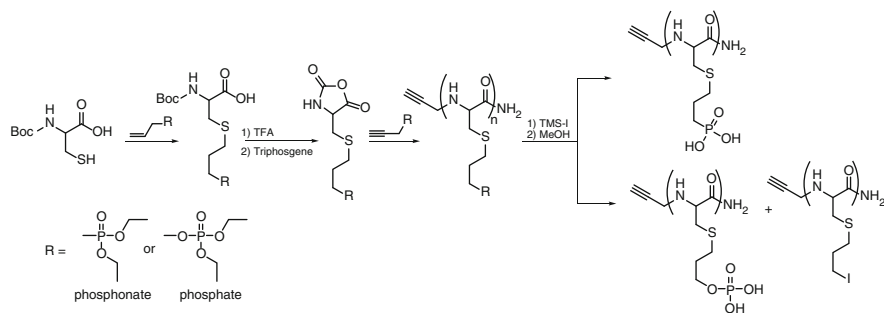
Fig. 11 Synthesis of phosphopolypeptides from L-cysteine
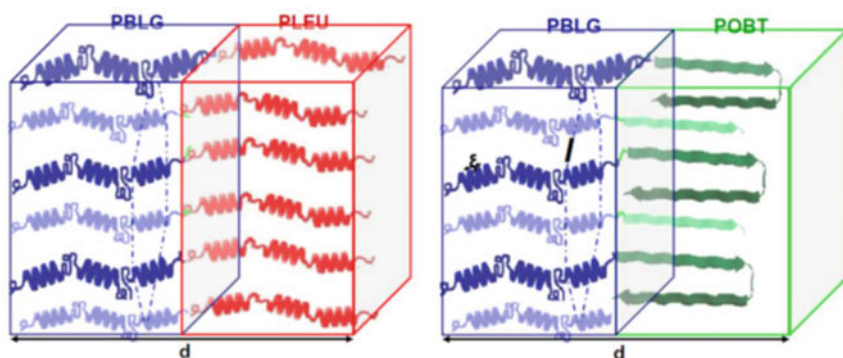
Fig. 12 Schematic representation of the self-assembly in the diblock copolypeptides showing PBLG α-helices that are hexagonally packed and relatively disordered α-helices within the PLEU domain or multiple-folded β-pleated sheets of POBT (Reprinted from Mondeshki et al. [34]. Copyright (2011), with permission from Elsevier)

Floudas et al. [34] prepared two types of poly(γ-benzyl-L-glutamate) (PBLG) diblock copolypeptides with either poly(L-leucine) (PLEU) or poly(*O*-benzyl-L-tyrosine) (POBT) as the second block. NCAs were purified by high-vacuum technique and polymerization was done using *n*-hexylamine as initiator. The first copolymer consists of two blocks that both form α-helix secondary structure, while the POBT block in the second copolymer forms β-strands. After the self-assembly of the diblock copolypeptides, it turns out that the nanoscale confinement in the copolymers preserves the main secondary motifs but affects their folding and lateral packing: β-pleated sheets are multiple folded, whereas the PBLG and PLEU α-helices are defected and of limited lateral coherence (Fig. 12).

The self-assembly of a diblock copolymer was studied for the case of poly (γ-benzyl-L-glutamate)-*b*-polyalanine as well. Block copolymers were prepared under high vacuum using *n*-hexylamine as initiator. Floudas et al. [35] discovered that although pure polyalanine (PAla) stabilizes both α-helices and β-sheets, in the
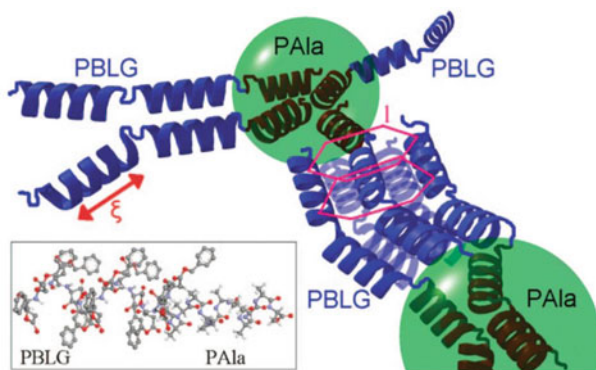
Fig. 13 Schematic representation of the diblock copolymer self-assembly showing PBLG and PAla α-helices that are hexagonally packed (Reprinted with permission from Mondeshki et al. [35]. Copyright 2008 American Chemical Society)
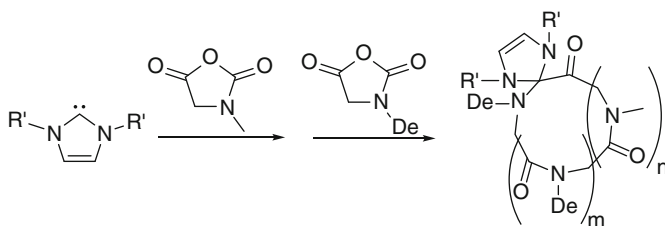
Fig. 14 Synthesis of amphiphilic cyclic diblock copolypeptoids by *N*-heterocyclic carbene-mediated ring-opening polymerization

copolypeptides the latter motif is suppressed due to the strong effects of the thermodynamic field on the peptide secondary structures (Fig. 13), indicating that the PAla β-sheets are less stable than α-helices and hence more prone to the thermodynamic restrictions imposed by the copolymers.

Cyclic block poly(α-peptoid)s were prepared by copolymerization of *N*-methyl and *N*-decyl-*N*-carboxyanhydride monomers by NHC-mediated ring-opening polymerization (Fig. 14) [36]. They have shown that adjusting the initial monomer to NHC molar ratio can readily control the block copolymer chain length and composition. A series of amphiphilic cyclic diblock copolypeptoids were thus prepared with variable molecular weight and composition that self-assemble into spherical micelles which reorganize into micrometer-long cylindrical micelles with uniform diameter in room temperature methanol. To prepare cyclic poly(α-peptoid)s that adopt helical conformations, a monomer with chiral side group, (S)/(R)-*N*-phenylethyl *N*-carboxyanhydrides, was polymerized by *N*-heterocyclic carbene-mediated ring-opening polymerization [37]. Polymers with the degree of polymerization up to 95 and low $Đ_M < 1.10$ were obtained; however, attempts to synthesize the polymers of higher molecular weight were unsuccessful.
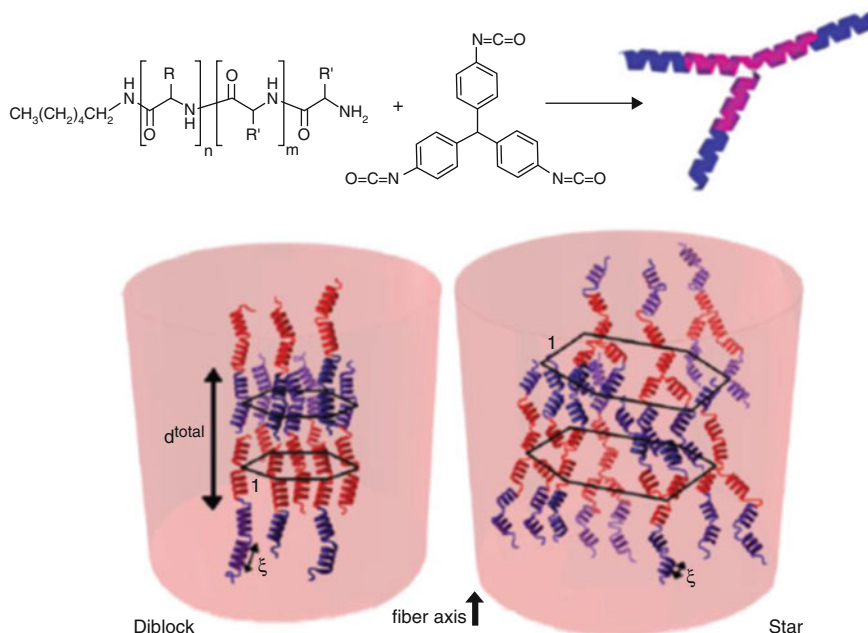
Fig. 15 Synthesis of three-arm star diblock copolymers of γ-benzyl-L-glutamate and ε-benzyloxycarbonyl-L-lysine (*left*) (Reprinted with permission from Aliferis et al. [38]. Copyright © 2005 Wiley Periodicals, Inc.) and a schematic representation of their self-assembly as compared to the diblock copolymers (*right*) (Reprinted with permission from Gitsas et al. [39]. Copyright 2008 American Chemical Society)

Three-arm star homopolymers and diblock copolymers of γ-benzyl-L-glutamate and ε-benzyloxycarbonyl-L-lysine were prepared by Hadjichristidis et al. [38]. The homopolymers and block copolymers were first prepared under high vacuum using *n*-hexylamine as initiator. The star copolymers were prepared by linking the living homo- and block copolypeptides carrying amine end groups with triphenylmethane-4,4′,4″-triisocyanate core (Fig. 15) using high-vacuum technique. For the efficient linking reaction, an excess of the arms was used, which were removed by the salting-out technique to afford pure stars as confirmed by SEC and membrane osmometry showing very narrow molecular weight distribution. Floudas et al. [39] discovered that the chain topology has a very strong influence on the self-assembly of complex copolypeptides. In the diblock copolymers, a lamellar nanostructures were found composed of poly(ε-benzyloxycarbonyl-L-lysine) PZLL and PBLG domains both consisting of α-helical segments that were hexagonally packed. The star topology on the other hand results in mixing of the PBLG and PZLL blocks, which still form α-helices, however, with a smaller persistence length, which are packed in a pseudohexagonal lattice (Fig. 15).

Liu et al. [40] reported on the synthesis of well-defined AB$_2$ miktoarm polypeptide stars. First, they have polymerized ε-benzyloxycarbonyl-L-lysine from a
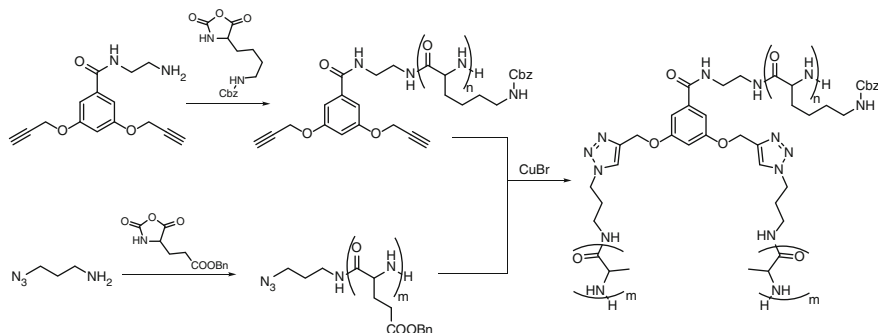
Fig. 16 Preparation of Y-shaped AB$_2$ miktoarm polypeptide stars

trifunctional initiator, which had one amino group and two alkyne groups and γ-benzyl-L-glutamate NCA from azide–amine difunctional initiator. Coupling of both homopolymers was achieved by copper-catalyzed cycloaddition reaction, and the excess azide-terminated homopolymer was removed by reaction with alkynyl-functionalized Wang resin. Purified miktoarm star copolymer had $Đ_M$ of 1.13; however, molecular weights determined by relative SEC with polystyrene standards were about three times overestimated when compared to the molecular weights determined by NMR. The deprotection of both protective groups was achieved by a one-pot acid hydrolysis to give a pH-responsive Y-shaped miktoarm star polypeptide copolymer (Fig. 16), which self-assemble into poly(L-glutamic acid) (PLGA)-core micelles at acidic pH and poly(L-lysine) (PLL)-core micelles at alkaline pH, accompanied with the coil-to-helix transition of PLGA and PLL sequences, respectively.

Heise et al. [41] prepared a series of star polypeptides based on poly(L-glutamic acid) using polypropylene imine dendrimers of various generations as initiators with a maximum number of arms from 8 to 64. By changing the dendrimer generation as well as the ratio of NCA/amino groups, they were able to prepare a broad range of different star polypeptides (Fig. 17). However, no details about the initiation efficiency were presented to show how many polypeptide arms there really are per dendrimer. SEC traces showed a lower molecular weight shoulder indicating a formation of linear homopolymer through activated monomer mechanism due to the tertiary amines in the dendrimer core. Star copolymers have been tested as drug delivery systems by using rhodamine B, and successful enzyme-responsive release was achieved. The same types of stars have been prepared with poly(L-lysine) to afford cationic star polymers which were tested as gene delivery vectors [42]. The complexation of siRNA as well as transfection of pDNA with star-shaped poly(L-lysine) was greatly superior as compared to linear poly (L-lysine).

Qiao et al. [43] prepared core cross-linked star polypeptides by sequential polymerization of NCAs with di-NCA L-cystine that acts as a cross-linker. γ-Benzyl-L-glutamate or ε-benzyloxycarbonyl-L-lysine was first polymerized
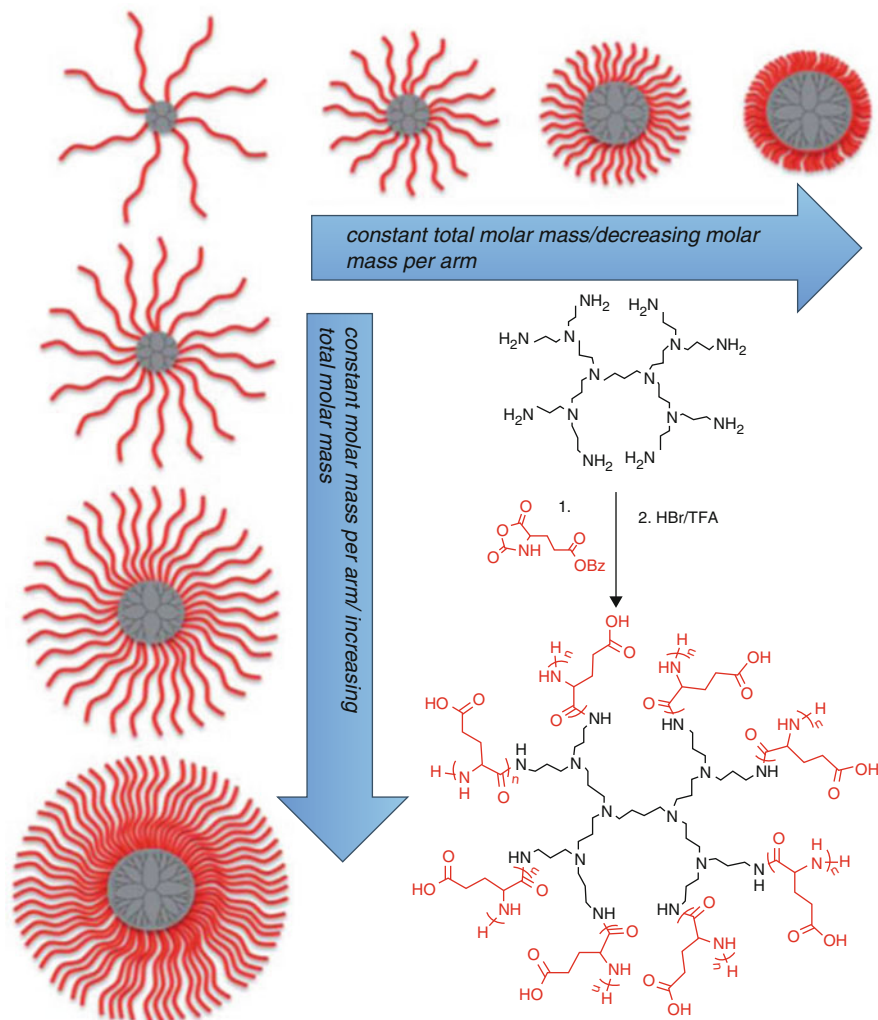
Fig. 17 Star polypeptides prepared from polypropylene imine dendrimers as initiators (Reproduced from Byrne et al. [42] with permission of The Royal Society of Chemistry)

using HDMS as initiator to prepare the arms, which was followed by the addition of L-cystine to afford core cross-linked stars (Fig. 18). The optimum cystine NCA/arm ratio for star formation was found to be highly dependent on the arm molecular weight. To obtain good stars, the ratio of cystine NCA to arms had to be controlled since higher ratios led to star–star coupling and gelation. The unreacted NCA groups in the core after the star formation were reacted with various amines bearing different functionalities for core functionalization. Deprotection of the arms afforded water-soluble core cross-linked stars, while reduction of the disulfide bonds with dithiothreitol (DTT) caused degradation of the stars to afford poly
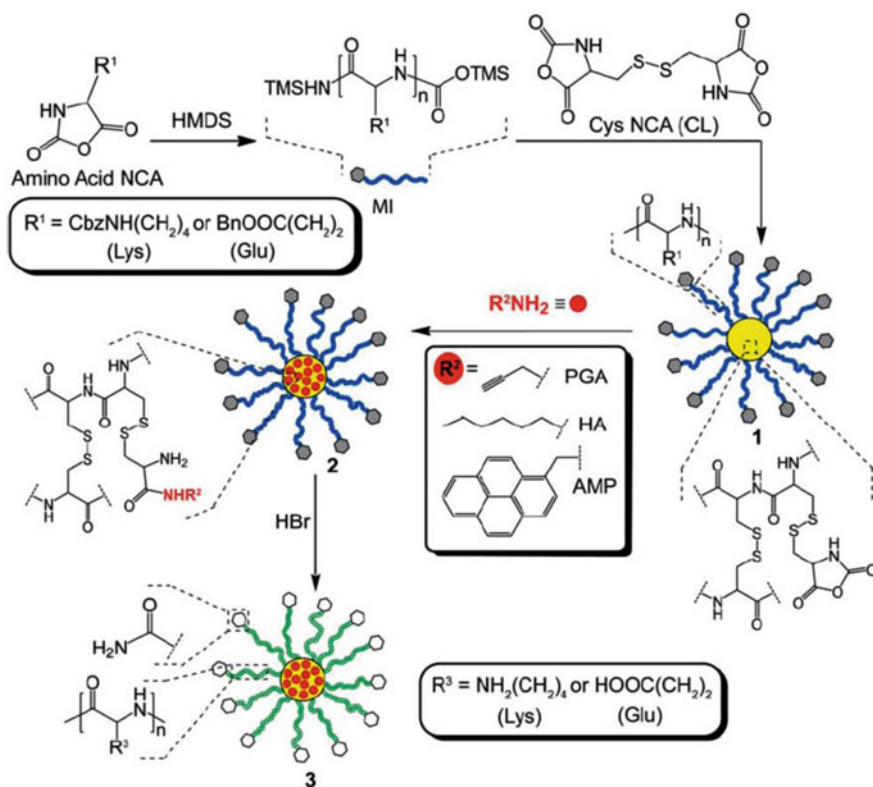
Fig. 18 Synthesis of core cross-linked polypeptide stars (Reproduced from Sulistio et al. [43] with permission of The Royal Society of Chemistry)

(ε-benzyloxycarbonyl-L-lysine-*b*-L-cysteine), which after exposure to oxygen formed organogels due to the random reformation of disulfide bonds.

4 Polypeptide-Based Hybrid Materials with Various Molecular Architectures

Polypeptides have been prepared in combination with various other polymers with either simple block structure or more complex molecular architectures to give rise to a number of new hybrid materials. The combination of highly self-organized polypeptide chains with other polymer chains with unique intrinsic properties led to a development of new materials with unprecedented properties that show a great potential in biomedical applications as well as other fields.

Block copolymer hybrid materials are usually prepared by using the first block with an amino end group as a macroinitiator for ROP of NCAs. An amine-
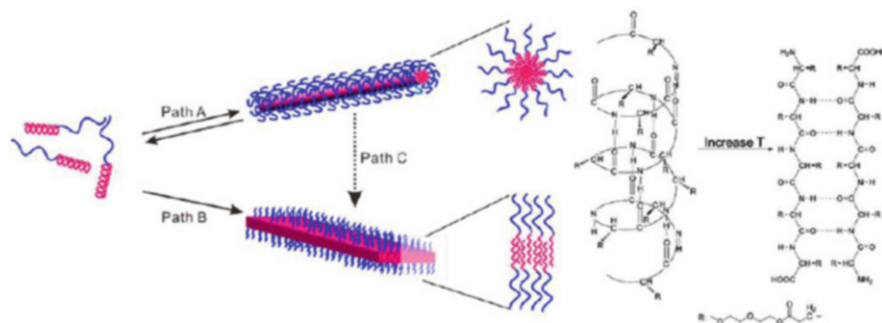
Fig. 19 Schematic representation of thermally induced self-assembly of PEO-*b*-poly(diethylene glycol-L-glutamate) copolymers (Reprinted with permission from Shen et al. [45]. Copyright 2013 American Chemical Society)

terminated PEO was used as a macroinitiator to prepare diblock PEO-poly(-β-benzyl-L-aspartate) copolymers, which were then coupled through amide bond formation, with *N*,*N*′-carbonyldiimidazole as coupling reagent, to eight pending carboxyl groups of the polyhedral oligomeric silsesquioxanes as a core to give star-shaped amphiphilic block copolymers, which self-assembled into micelles in aqueous medium [44]. Low dispersities ($Đ_M < 1.16$) were reported for the block copolymer; however, dispersities increased to 1.35–1.38 after the coupling to the core, indicating that coupling was not 100 % efficient. Micelles showed some potential as carriers for anticancer drug delivery.

An amine-terminated PEO was also used as a macroinitiator to prepare diblock copolymers with diethylene glycol-L-glutamate [45]. The second block shows thermoresponsive properties and adopts primarily helical conformation. The diblock copolymer upon increasing the temperature forms wormlike micelles, in which the poly(diethylene glycol-L-glutamate) formed the micelle core and maintained helical conformation. After prolonged thermal annealing, the helical conformation transforms to a β-sheet, which causes a rearrangement from wormlike micelles to nanoribbons, which is an irreversible process (Fig. 19).

Diethylene glycol-L-glutamate was used for preparation of star polypeptides as well [46]. Tetra(amine) compound with a disulfide bond was used as initiator core. The star polypeptides could self-assemble into micelles as well as hydrogels, which were reduction- and thermosensitive. The addition of DTT leads to a decrease of the size of the micelles due to the reduction of the disulfide bonds creating linear polypeptide chains with half the molecular weight instead of stars. The micelles exhibited LCST of about 40 °C which at higher temperatures leads to shrinking of the micelles as well (Fig. 20). Such a material shows great potential for triggered drug-release properties useful for on-demand drug delivery.

Chang et al. [47] prepared linear and comb-like terpolymers using amino-end-group functional PEO as macroinitiator for ROP to first prepare block copolymers with either poly(L-phenylalanine) or poly(L-serine) prepared from *O*-(*tert*-butyl)-L-serine NCA. Chain extension by polymerization of D,L-lactide in melt using Sn
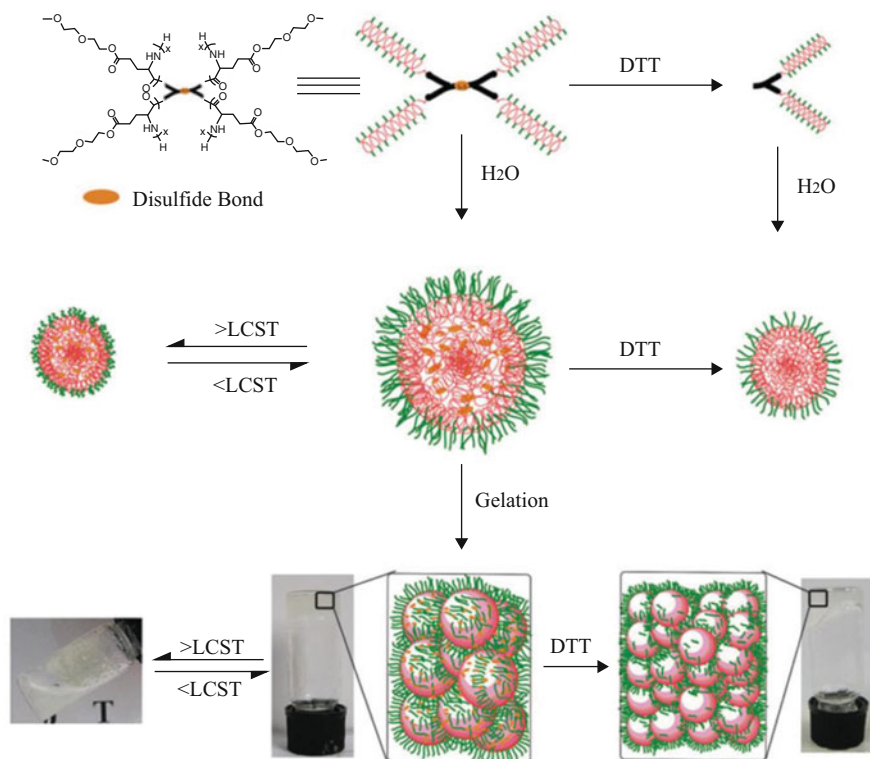
Fig. 20 Illustration of dual stimuli-sensitive micellization and hydrogelation process of diethylene glycol-L-glutamate-based star polypeptide (Reproduced from Liu et al. [46] with permission of The Royal Society of Chemistry)

(Oct)$_2$ afforded a linear terpolymer from block copolymer with poly (L-phenylalanine) and comb-like terpolymers when block copolymer with poly (L-serine) was used due to the hydroxyl group on each repeating unit of the poly (L-serine). Molecular weights were only determined from NMR, so no information on the dispersity was given. They have also prepared nanoparticles of the terpolymers by an emulsion-solvent evaporation method (Fig. 21).

Cheng et al. [48] prepared a series of PEO-cationic helical polypeptide copolymers with architectures ranging from diblock and triblock to 8-star and graft copolymers. Polymerization of γ-4-((2-(piperidin-1-yl)ethyl)aminomethyl)benzyl-L-glutamate was done using HDMS as initiator, while copolymers were obtained using mono-, di-, or 8-arm star PEO as initiator (Fig. 22), affording polymers with expected molecular weight and Đ$_M$ in range of 1.2, except for the star copolymer where obtained dispersity was a little higher. Polymers were tested for gene delivery, and diblock and triblock copolymers exhibited lower membrane activity and cytotoxicity and uncompromised gene transfection efficiencies compared to the
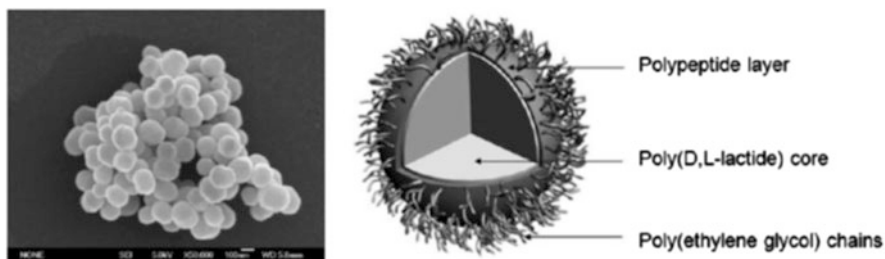
Fig. 21 Schematic representation of the PEO/polypeptide/poly(D,L-lactide) nanoparticle (*right*) and FE-SEM image of freeze-dried nanoparticles (*left*) (Reprinted with permission from Lee et al. [47]. Copyright © 2011 Wiley Periodicals, Inc.)

| AB block copolymer | BAB triblock copolymer | 8-arm star block copolymer | graft copolymer |
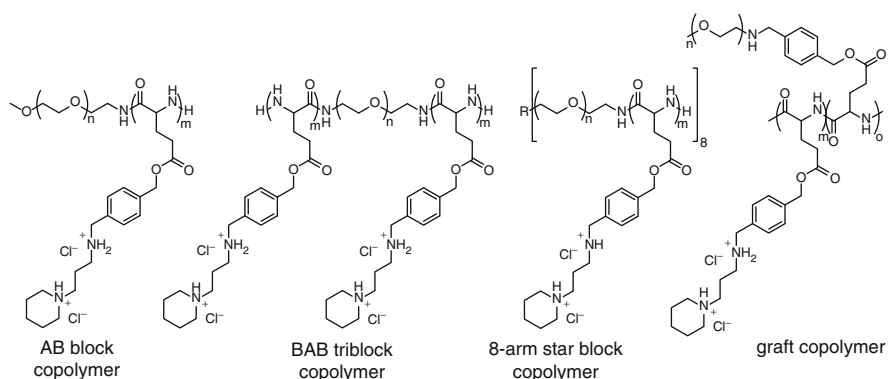
Fig. 22 Copolymers of PEO and cationic helical polypeptide poly(γ-4-((2-(piperidin-1-yl)ethyl) aminomethyl)benzyl-L-glutamate) with various macromolecular architectures

non-PEGylated homopolymer. Star copolymer displayed the highest membrane activity yet relatively low cytotoxicity.

After the polymerization of the first polymer block for hybrid materials, it is often necessary to prepare the macroinitiator by end-group transformation or deprotection reactions to afford the necessary amino functionality for ROP of NCAs. Diblock copolymers of highly branched polyethylene and γ-benzyl-L-glutamate were successfully prepared in this way. First, a highly branched polyethylene macroinitiator was synthesized by living polymerization of ethylene using an amine–imine nickel catalyst and a $ZnEt_2$ transfer agent. Hydroxyl end group was then transformed into amino group by end-capping reaction with Boc-protected valine. Such macroinitiator was then used for ROP of NCA (Fig. 23). $Đ_M$ of polyethylene macroinitiator was below 1.04; however, they were unable to determine the molecular weight characteristics of the diblock copolymer by size-exclusion chromatography. The diblock copolymer can form thermoreversible gels by self-assembled nanoribbons in toluene [49].
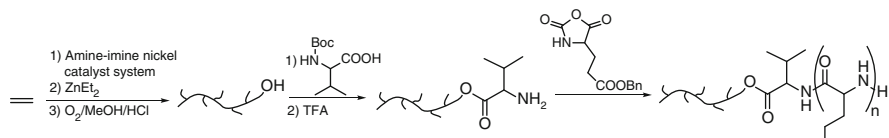
Fig. 23 Synthesis of diblock copolymer of highly branched polyethylene and γ-benzyl-L-glutamate
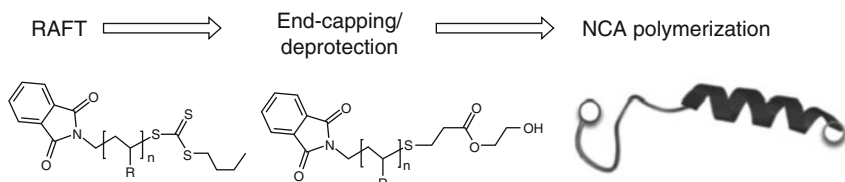
Fig. 24 Schematic representation of polypeptide hybrid materials synthesis using bifunctional RAFT agent (Reprinted with permission from Jacobs et al. [50]. Copyright © 2013 WILEY-VCH Verlag GmbH & Co. KGaA, Weinheim)

Polypeptide hybrid materials were prepared with poly(*n*-butyl acrylate), polystyrene, and poly(*N*-isopropyl acrylamide) as well, which were prepared by reversible addition–fragmentation chain transfer (RAFT) polymerization using bifunctional RAFT chain transfer agent with a phthalimide-protected amino group to afford well-defined polymers ($Đ_M < 1.1$) [50]. The trithiocarbonate group was first cleaved of with aminoethanol to form a thiolactone in the case of poly(*n*-butyl acrylate) or by simultaneous aminolysis/thiol–ene reaction with hydroxyethylacrylate for polystyrene and poly(*N*-isopropyl acrylamide). Effective cleavage of the trithiocarbonate group was essential since it can react with the amino groups. After purification, the phthalimide group was deprotected to afford amino-end-group functional macroinitiators, which were used for polymerization of γ-benzyl-L-glutamate or ε-benzyloxycarbonyl-L-lysine NCAs (Fig. 24). Block copolymers with expected molecular weight and low $Đ_M$ (<1.1) were obtained with poly(*n*-butyl acrylate) and polystyrene; however, in the case of poly(*N*-isopropyl acrylamide), a low molecular weight shoulder was observed indicating the presence of some starting material.

McCormick et al. [51] on the other hand used monofunctional RAFT chain transfer agent to polymerize the *N*-(2-hydroxypropyl)methacrylamide and transformed the trithiocarbonate end group by simultaneous aminolysis and thiol−ene Michael addition with *N*-(3-aminopropyl)methacrylamide to afford an amino-end-group functional macroinitiator. A chain extension was accomplished via ROP of γ-benzyl-L-glutamate NCA to afford block copolymers with different lengths and low dispersities (<1.2) (Fig. 25). The poly(L-glutamic acid) block shows a pH-responsive coil-to-helix transitions.
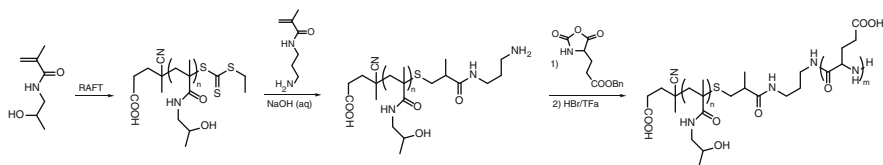
Fig. 25 Synthesis of poly(*N*-(2-hydroxypropyl)methacrylamide)-*b*-poly(L-glutamic acid)
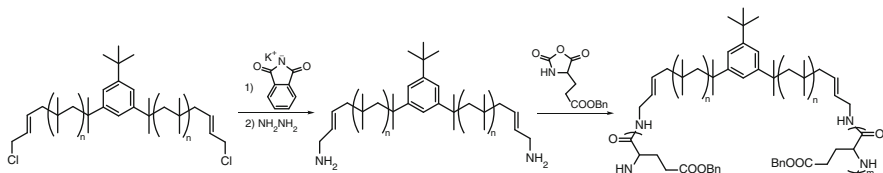
Fig. 26 Synthesis of poly(γ-benzyl-L-glutamate)-*b*-polyisobutylene-*b*-poly(γ-benzyl-L-gluta-mate) triblock copolymers

Faust et al. [52] prepared ABA triblock copolymers by polymerization of γ-benzyl-L-glutamate NCA from α,ω-primary amino-functional polyisobutylene. Polyisobutylene was prepared by cationic polymerization from a difunctional initiator, and the living cations were transformed to α,ω-chloroallyl polyisobutylene by reaction with 1,3-butadiene in hexanes/methylchloride. Nucleophilic substitution using phthalimide afforded after deprotection the α,ω-amino polyisobutylene, which was used for ammonium-mediated polymerization of γ-benzyl-L-glutamate NCA to obtain well-defined ABA copolymer with low $Đ_M$ (1.12) and molecular weights of about 5 kDa (Fig. 26). They have also performed a chain-extension experiment with 4,4′-methylene-bis(phenyldiisocyanate) to obtain (ABA)$_n$ multiblock copolymers; however, while they did obtain higher molecular weights, the $Đ_M$ increased to 2.80 with significant amount of what appeared to be unreacted ABA triblock copolymer as seen from SEC chromatogram.

Polypeptide-based amphiphilic graft terpolymers containing both hydrophilic PEO and hydrophobic poly(γ-benzyl-L-glutamate) attached to the acrylate backbone were synthesized by Huang et al. [53]. The pegylated backbone was first prepared by single-electron transfer-living radical polymerization (SET-LRP) of pegylated acrylic acid. The graft copolymer was then treated with lithium diisopropylamide followed by 2-bromoisobutyryl bromide to introduce bromide functional groups to the backbone, which were first transformed into azide groups by a nucleophilic substitution and then reduced to afford an amine-functionalized macroinitiator. The macroinitiator, with about 30 % of amino groups per repeating units, was then used for grafting from polymerization of γ-benzyl-L-glutamate NCA (Fig. 27). The macroinitiator had a very narrow molecular weight distribution ($Đ_M = 1.03$), which increased after grafting to $Đ_M < 1.21$ for the terpolymer. Amphiphilic graft terpolymers self-assembled into various micellar, which
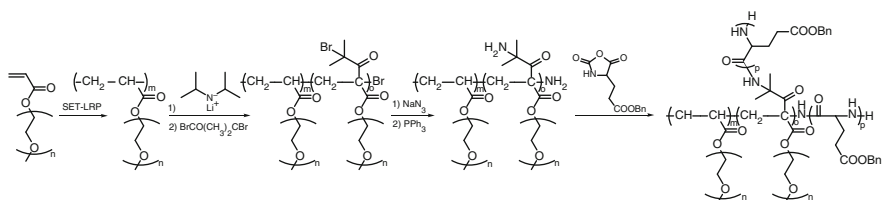
Fig. 27 Polypeptide-based amphiphilic graft copolymers prepared by successive SET-LRP of pegylated acrylic acid and ROP of γ-benzyl-L-glutamate NCA

morphologies depended on the initial water content, composition of the organic cosolvent, and length of the poly(γ-benzyl-L-glutamate) side chains.

Karatzas et al. [54] used unique features of anionic polymerization and the possibilities offered for the synthesis of end- or in-chain amino-functionalized polymers as well as of the living nature of the ROP of NCAs under high-vacuum conditions to prepare a variety of well-defined miktoarm star hybrids – macromolecular chimeras. The following structures were prepared: (PS)(PI)(PBLG or PBLL) (3 μ-stars), (PS)$_2$[P(α-MeS)](PBLG or PBLL), and (PS)$_2$(PBLG or PBLL)$_2$ (4 μ-stars), where PS is polystyrene, PI is polyisoprene, P(α-MeS) is poly (α-methylstyrene), PBLG is poly(γ-benzyl-L-glutamate), and PBLL is poly(ε-*tert*-butyloxycarbonyl-L-lysine) (Fig. 28). Diphenylethylene-functionalized polymers were first prepared and subsequently activated by reaction with a living polymer chain or *s*-BuLi followed by reaction with 1-(3-bromopropyl)-2,2,5,5-tetramethyl-aza-2,5-disilacyclopentane. The silyl-protected group was cleaved under acidic conditions to afford amine-functionalized macroinitiators for the polymerization of BLG and BLL NCAs to prepare the desired miktoarm stars (Fig. 28). Detailed characterization revealed the efficiency of this synthetic scheme and the homogeneity of prepared products; however, the miktoarm stars prepared from (PS)$_2$(NH$_2$)$_2$ showed broader molecular weight distributions, while (PS)$_4$(NH$_2$)$_2$ afforded multimodal distributions due to the significant steric hindrance of the in-chain functionalized macroinitiators.

(PS)(PI)(PBLL) miktoarm star terpolymer with two coil-like arms and an α-helical mesogenic polypeptide arm self-assemble in the solid state to form a hierarchical smectic self-assembly where the α-helical rod-like PBLL blocks stack to form pure polypeptide lamellae, while the PS and PI blocks form lamellae with an inner structure composed of rectangular cylinders (Fig. 29). This morphology is observed locally already after quick drop casting from chloroform solution, indicating the powerful driving force of the α-helical stacking in the formation of the structure; however, overall order is increased notably after thermal annealing even though partial thermal deprotection of PBLL block was observed [55].

ROP of NCA was employed to modify various nanoparticles and other surfaces with polypeptide chains as well. Materials prepared in such a way show a lot of promise for applications in the biomedical, electronic, or environmental fields.
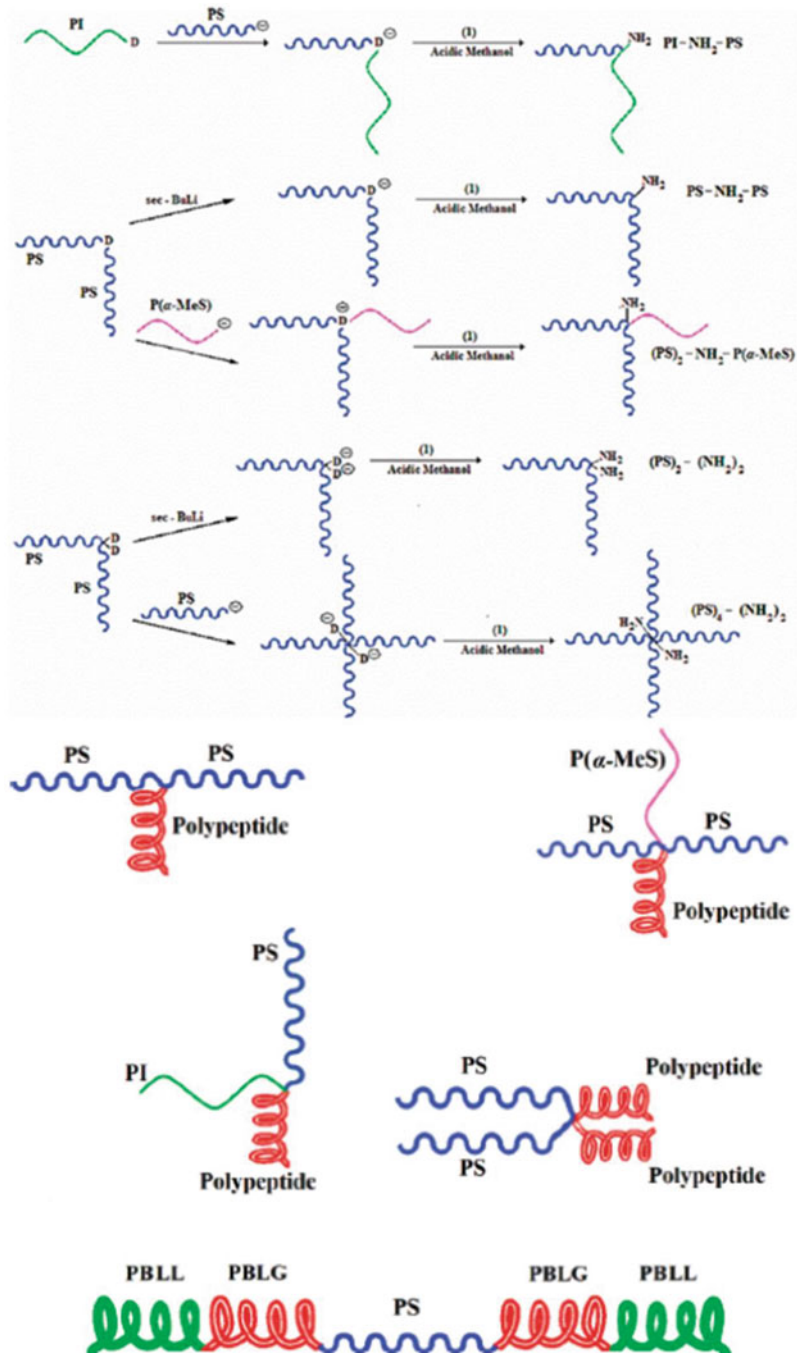
Fig. 28 Macromolecular chimeras based on polypeptides (Reprinted with permission from Karatzas et al. [54]. Copyright 2008 American Chemical Society)
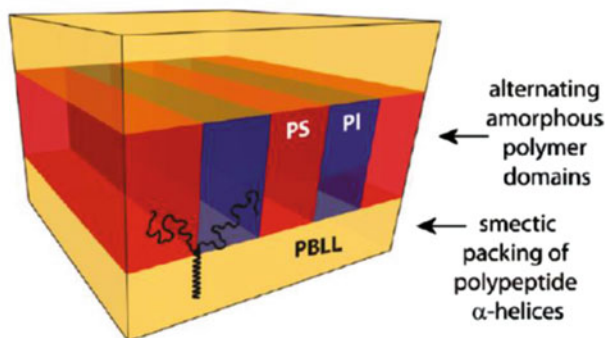
Fig. 29 Schematic illustration of the self-assembly of the (PS)(PI)(PBLL) miktoarm star terpolymer (Reprinted with permission from Junnila et al. [55]. Copyright 2010 American Chemical Society)

Chitin nanofibers have been successfully used for surface-initiated graft polymerization of γ-benzyl-L-glutamate NCA [56]. Chitin nanofibers were first partly deacetylated under very strong basic conditions to create amino groups, which were used as initiating sites. Grafted copolymer was then deprotected using milder basic conditions to afford carboxylic groups on the side chains. Carboxylic groups were then reacted with either remaining amino groups on the chitin backbone or with the amino group at the end of grafted polypeptides to produce a cross-linked biocompatible network film, which showed improved mechanical properties compared to the pure chitin nanofiber film.

Qiao et al. have prepared biodegradable hollow poly(L-glutamic acid) capsules by using silica nanoparticles as templates [57]. First hyperbranched poly(ethylene imine) macroinitiators were deposited on silica which enabled a highly dense polypeptide brush films to be formed after the γ-benzyl-L-glutamate NCA polymerization. High density of the growing chains leads to the cross-chain termination reactions between the propagating amine end groups of the growing polymer brushes and the side-chain benzyl ester protecting groups from neighboring polymer chains, to form stable cross-linked polypeptide films. Benzyl groups were then deprotected by acid hydrolysis, and the silica template was dissolved by HF/NH_4F solution to afford stable and dispersible hollow poly(L-glutamic acid) capsules (Fig. 30), which were successfully degraded using an endopeptidase papain.

Heise et al. [58] have prepared macroporous monoliths by polymerization of a high internal phase emulsion (HIPE) of a mixture of styrene, divinylbenzene, and 4-vinylbenzylphthalimide. After removal of the phthalimide, the free amino groups were used as initiators for ROP of γ-benzyl-L-glutamate or ε-*tert*-butyloxy-carbonyl-L-lysine NCA to afford dense homogeneous coating of polypeptides throughout the internal polyHIPE surfaces (Fig. 31). Both types of polypeptide-grafted monoliths responded to pH by changes in their hydrophilicity, and successful bioconjugation with proteins was achieved, thus showing potential for use in biosensor as well as in bioseparation applications.
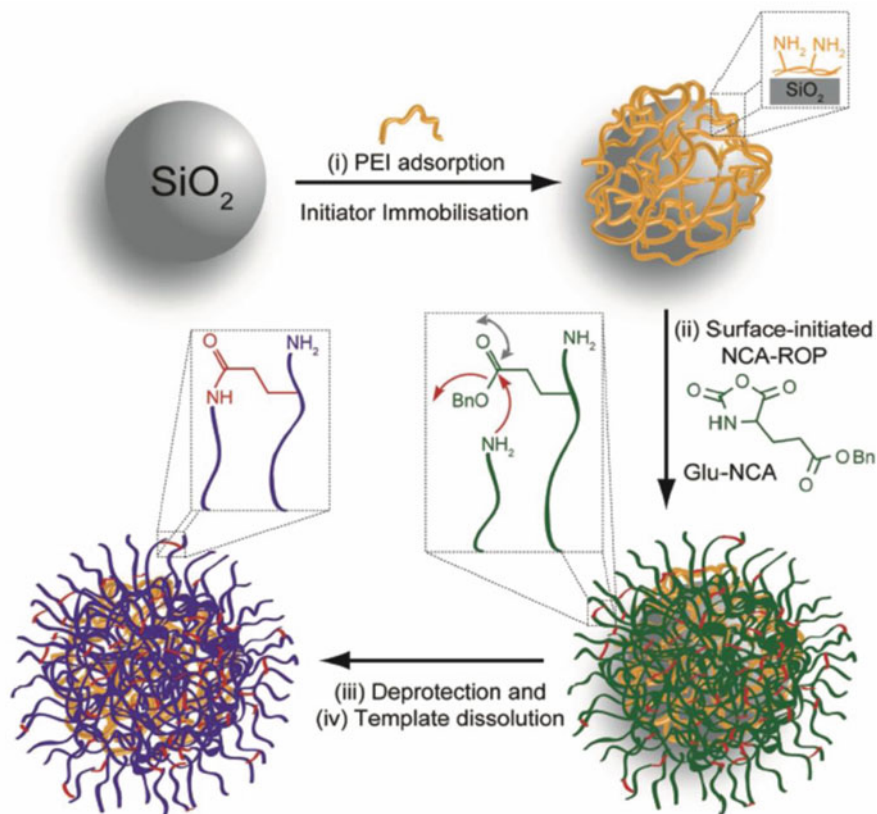
Fig. 30 Preparation of stable poly(L-glutamic acid) capsules using silica nanoparticles as template (Reprinted with permission from Harris et al. [57]. Copyright © 2013 WILEY-VCH Verlag GmbH & Co. KGaA, Weinheim)

Sakellariou et al. [59] grafted poly(L-proline) from an amine-modified surface of single-wall carbon nanotubes (SWNT) using high-vacuum technique. First, 1-benzocyclobutene-1′-phenylethylene was attached to the surface of carbon nanotubes by Diels–Alder cycloaddition. After reaction with *s*-butyl lithium, a carbanion was formed that reacted with 1-(3-bromopropyl)-2,2,5,5-tetramethyl-aza-2,5-disilacyclopentane which after the deprotection afforded an amine-functionalized carbon nanotubes with rather uniform polymer layer (Fig. 32). While grafted SWNTs are very well dispersed in CHCl$_3$, a small amount of trifluoroacetic acid causes aggregates to form due to the change in poly(L-proline) conformation from form I to form II, which is less soluble in organic solvents.

Brougham et al. [60] used surface-modified Fe$_3$O$_4$ nanoparticles bearing primary amino groups as initiators for ROP of γ-propargyl-L-glutamate to prepare
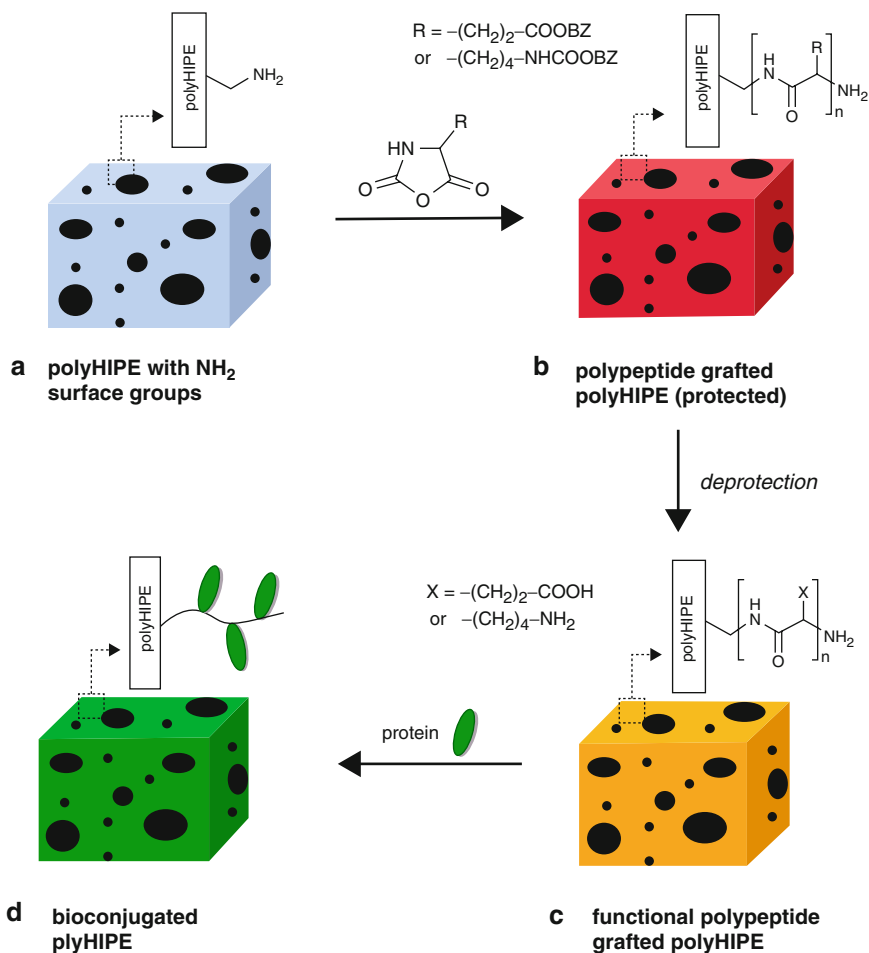
Fig. 31 (**a**) polyHIPE with NH2 surface groups (**b**) polypeptide grafted polyHIPE (protected). (**c**) Functional polypeptide grafted polyHIPE. (**d**) Bioconjugated polyHIPE

polypeptide-grafted magnetic nanoparticles. Polypeptide chains formed α-helix, and the pendant alkyne groups were reacted with azide-functionalized carbohydrate by copper-catalyzed cycloaddition reaction to afford biocompatible glycopeptide-grafted magnetic nanoparticles (Fig. 33). The grafted nanoparticles showed very low distribution of sizes suggesting that the stable suspensions are composed of fully dispersed grafted magnetic nanoparticles, which is critical for biological applications and were suitable for T_1-weighted magnetic resonance imaging as contrast agents.
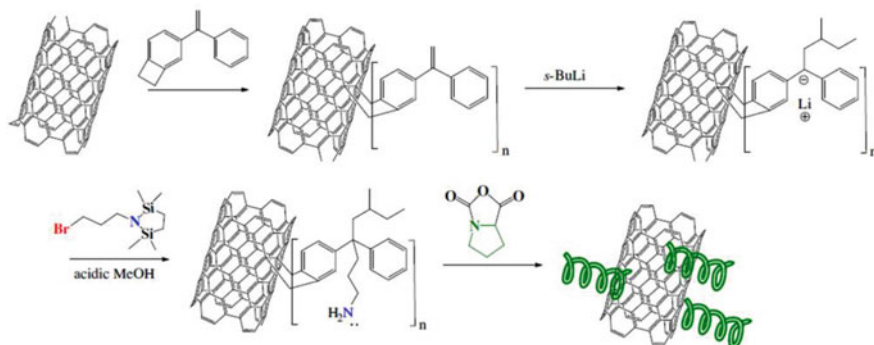
Fig. 32 Synthesis of the carbon nanotubes grafted with poly(L-prolin) (Reprinted from Gkikas et al. [59]. Copyright (2013), with permission from Elsevier)
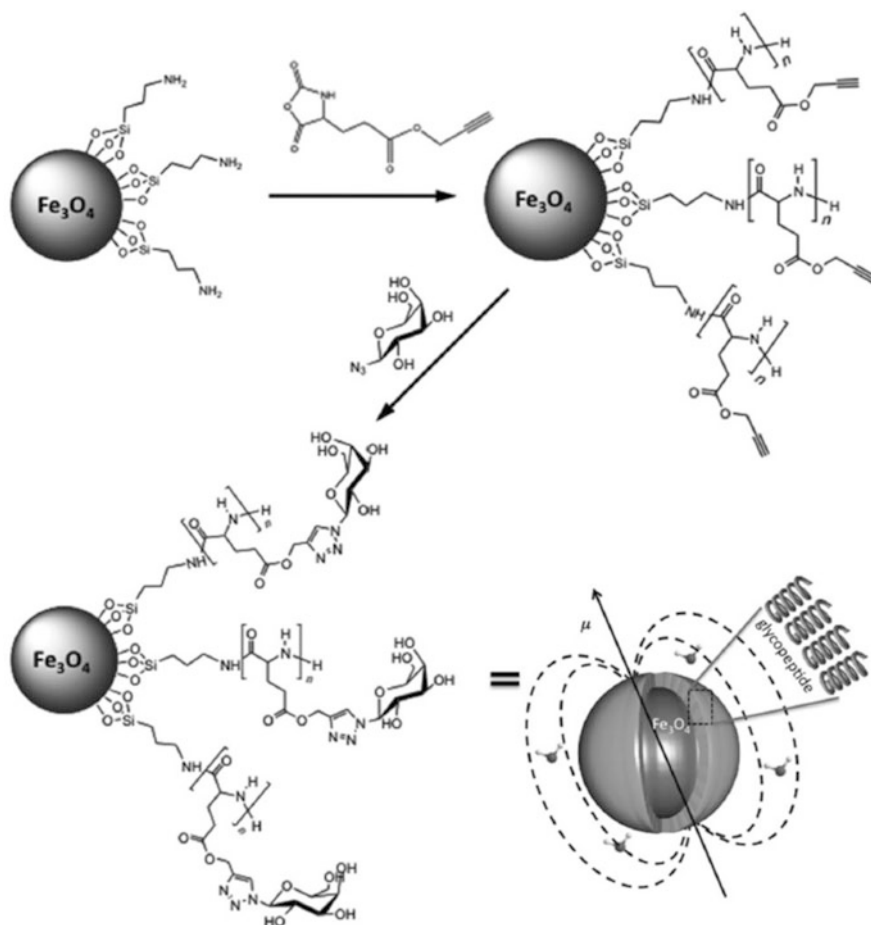
Fig. 33 Synthesis of glycopeptide-grafted magnetic nanoparticles (Reprinted with permission from Borase et al. [60]. Copyright © 2013 WILEY-VCH Verlag GmbH & Co. KGaA, Weinheim)

Abbreviations

AMM	Activated monomer mechanism
Bipy	2,2′-bipyridyl
COD	1,5-cyclooctadiene
$Đ_M$	Dispersity
DTT	Dithiothreitol
HMDS	Hexamethyldisilazane
HIPE	High internal phase emulsion
LCST	Lower critical solution temperature
NAM	Normal amine mechanism
NCA	*N*-carboxyanhydrides
NHC	*N*-heterocyclic persistent carbenes
P(α-MeS)	Poly(α-methylstyrene)
PAla	Polyalanine
PBLG	Poly(γ-benzyl-L-glutamate)
PBLL	Poly(ε-tert-butyloxycarbonyl-L-lysine)
pDNA	Plasmid deoxyribonucleic acid
PEO	Poly(ethylene oxide)
PI	Polyisoprene
PLEU	Poly(L-leucine)
PLGA	Poly(L-glutamic acid)
PLL	Poly(L-lysine)
POBT	Poly(*O*-benzyl-L-tyrosine)
PS	Polystyrene
PZLL	Poly(ε-benzyloxycarbonyl-L-lysine)
RAFT	Reversible addition–fragmentation chain transfer
ROP	Ring-opening polymerization
SET-LRP	Single-electron transfer-living radical polymerization
siRNA	Small interfering ribonucleic acid
SWNT	Single-wall carbon nanotubes
TMS	Trimethylsilyl

References

1. Hadjichristidis N, Iatrou H, Pitsikalis M, Sakellariou G (2009) Synthesis of well-defined polypeptide-based materials via the ring-opening polymerization of α-amino acid *N*-carboxyanhydrides. Chem Rev 109:5528–5578
2. Kricheldorf HR (2006) Polypeptides and 100 years of chemistry of α-amino acid *N*-carboxyanhydrides. Angew Chem Int Ed 45:5752–5784
3. Deming TJ (2007) Synthetic polypeptides for biomedical applications. Prog Polym Sci 32:858–875

4. Deng C, Wu J, Cheng R, Meng F, Klok HA, Zhong Z (2013) Functional polypeptide and hybrid materials: precision synthesis via α-amino acid *N*-carboxyanhydride polymerization and emerging biomedical applications. Prog Polym Sci 39:330–364

5. Huang J, Heise A (2013) Stimuli responsive synthetic polypeptides derived from *N*-carboxyanhydride (NCA) polymerisation. Chem Soc Rev 42:7373–7390

6. Ray JG, Johnson AJ, Savin DA (2013) Self-assembly and responsiveness of polypeptide-based block copolymers: how "smart" behavior and topological complexity yield unique assembly in aqueous media. J Polym Sci Part B Polym Phys 51:508–523

7. Luxenhofer R, Fetsch C, Grossmann A (2013) Polypeptoids: a perfect match for molecular definition and macromolecular engineering? J Polym Sci Part B Polym Phys 51:2731–2752

8. Poché DS, Moore MJ, Bowles JL (1999) An unconventional method for purifying the *N*-carboxyanhydride derivatives of γ-alkyl-L-glutamates. Synth Commun 29:843–854

9. Gibson MI, Cameron NR (2009) Experimentally facile controlled polymerization of *N*-carboxyanhydrides (NCAs), including *O*-benzyl-L-threonine NCA. J Polym Sci Part A Polym Chem 47:2882–2891

10. Kramer JR, Deming TJ (2010) General method for purification of α-amino acid-*N*-carboxyanhydrides using flash chromatography. Biomacromolecules 11:3668–3672

11. Aliferis T, Iatrou H, Hadjichristidis N (2004) Living polypeptides. Biomacromolecules 5:1653–1656

12. Gkikas M, Iatrou H, Thomaidis NS, Alexandridis P, Hadjichristidis N (2011) Well-defined homopolypeptides, copolypeptides, and hybrids of poly(L-proline). Biomacromolecules 12:2396–2406

13. Peggion E, Terbjevich M, Cosani A, Colombini C (1966) Mechanism of *N*-carboxyanhydride (NCA) polymerization in dioxane. Initiation by carbon-14-labeled amines. J Am Chem Soc 88:3630–3632

14. Goodman M, Hutchison J (1966) The mechanisms of polymerization of N-unsubstituted *N*-carboxyanhydrides. J Am Chem Soc 88:3627–3630

15. Ballard DGH, Bamford CH (1956) Reactions of *N*-carboxy-α-amino-acid anhydrides catalysed by tertiary bases. J Chem Soc 9:381–387

16. Dimitrov I, Schlaad H (2003) Synthesis of nearly monodisperse polystyrene–polypeptide block copolymers via polymerisation of *N*-carboxyanhydrides. Chem Commun 23:2944–2945

17. Conejos-Sanchez I, Duro-Castano A, Birke A, Barz M, Vicent MJ (2013) A controlled and versatile NCA polymerization method for the synthesis of polypeptides. Polym Chem 4:3182–3186

18. Lu H, Cheng J (2007) Hexamethyldisilazane-mediated controlled polymerization of α-amino acid *N*-carboxyanhydrides. J Am Chem Soc 129:14114–14115

19. Lu H, Cheng J (2008) *N*-trimethylsilyl amines for controlled ring-opening polymerization of amino acid *N*-carboxyanhydrides and facile end group functionalization of polypeptides. J Am Chem Soc 130:12562–12563

20. Deming TJ (1997) Facile synthesis of block copolypeptides of defined architecture. Nature 390:386–389

21. Deming TJ (1998) Amino acid derived nickelacycles: intermediates in nickel-mediated polypeptide synthesis. J Am Chem Soc 120:4240–4241

22. Deming TJ (1999) Cobalt and iron initiators for the controlled polymerization of α-amino acid-*N*-carboxyanhydrides. Macromolecules 32:4500–4502

23. Deming TJ, Curtin SA (2000) Chain initiation efficiency in cobalt- and nickel-mediated polypeptide synthesis. J Am Chem Soc 122:5710–5717

24. Peng YL, Lai SL, Lin CC (2008) Preparation of polypeptide via living polymerization of Z-Lys-NCA initiated by platinum complexes. Macromolecules 41:3455–3459

25. Guo L, Zhang D (2009) Cyclic poly(α-peptoid)s and their block copolymers from N-heterocyclic carbene-mediated ring-opening polymerizations of N-substituted *N*-Carboxylanhydrides. J Am Chem Soc 131:18072–18074

26. Guo L, Lahasky SH, Ghale K, Zhang D (2012) N-heterocyclic carbene-mediated zwitterionic polymerization of N-substituted N-carboxyanhydrides toward poly(α-peptoid)s: kinetic, mechanism, and architectural control. J Am Chem Soc 134:9163–9171
27. Engler AC, Lee H, Hammond PT (2009) Highly efficient "grafting onto" a polypeptide backbone using click chemistry. Angew Chem Int Ed 48:9334–9338
28. Rhodes AJ, Deming TJ (2013) Soluble, clickable polypeptides from azide-containing N-carboxyanhydride monomers. ACS Macro Lett 2:351–354
29. Oelker AM, Morey SM, Griffith LG, Hammond PT (2012) Helix versus coil polypeptide macromers: gel networks with decoupled stiffness and permeability. Soft Matter 8:10887–10895
30. Pati D, Shaikh AY, Das S, Nareddy PK, Swamy MJ, Hotha S, Gupta SS (2012) Controlled synthesis of O-glycopolypeptide polymers and their molecular recognition by lectins. Biomacromolecules 13:1287–1295
31. Pati D, Kalva N, Das S, Kumaraswamy G, Gupta SS, Ambade AV (2012) Multiple topologies from glycopolypeptide–dendron conjugate self-assembly: nanorods, micelles, and organogels. J Am Chem Soc 134:7796–7802
32. Das S, Kar M, Sen Gupta S (2013) Synthesis of end-functionalized phosphate and phosphonate-polypeptides by ring-opening polymerization of their corresponding N-carboxyanhydride. Polym Chem 4:4087–4091
33. Zhou C, Qi X, Li P, Ning Chen W, Mouad L, Chang MW, Su Jan Leong S, Chan-Park MB (2010) High potency and broad-spectrum antimicrobial peptides synthesized via ring-opening polymerization of α-aminoacid-N-carboxyanhydrides. Biomacromolecules 11:60–67
34. Mondeshki M, Spiess HW, Aliferis T, Iatrou H, Hadjichristidis N, Floudas G (2011) Hierarchical self-assembly in diblock copolypeptides of poly(γ-benzyl-L-glutamate) with poly poly (L-leucine) and poly(O-benzyl-L-tyrosine). Eur Polym J 47:668–674
35. Gitsas A, Floudas G, Mondeshki M, Spiess HW, Aliferis T, Iatrou H, Hadjichristidis N (2008) Control of peptide secondary structure and dynamics in poly(γ-benzyl-L-glutamate)-b-polyalanine peptides. Macromolecules 41:8072–8080
36. Lee CU, Smart TP, Guo L, Epps TH, Zhang D (2011) Synthesis and characterization of amphiphilic cyclic diblock copolypeptoids from N-heterocyclic carbene-nediated zwitterionic polymerization of N-substituted N-carboxyanhydride. Macromolecules 44:9574–9585
37. Guo L, Li J, Brown Z, Ghale K, Zhang D (2011) Synthesis and characterization of cyclic and linear helical poly(α-peptoid)s by N-heterocyclic carbene-mediated ring-opening polymerizations of N-substituted N-carboxyanhydrides. Biopolymers 96:596–603
38. Aliferis T, Iatrou H, Hadjichristidis N (2005) Well-defined linear multiblock and branched polypeptides by linking chemistry. J Polym Sci Part A Polym Chem 43:4670–4673
39. Gitsas A, Floudas G, Mondeshki M, Butt HJ, Spiess HW, Iatrou H, Hadjichristidis N (2008) Effect of chain topology on the self-organization and dynamics of block copolypeptides: from diblock copolymers to stars. Biomacromolecules 9:1959–1966
40. Rao J, Zhang Y, Zhang J, Liu S (2008) Facile preparation of well-defined AB₂ Y-shaped miktoarm star polypeptide copolymer via the combination of ring-opening polymerization and click chemistry. Biomacromolecules 9:2586–2593
41. Byrne M, Thornton PD, Cryan SA, Heise A (2012) Star polypeptides by NCA polymerisation from dendritic initiators: synthesis and enzyme controlled payload release. Polym Chem 3:2825–2831
42. Byrne M, Victory D, Hibbitts A, Lanigan M, Heise A, Cryan SA (2013) Molecular weight and architectural dependence of well-defined star-shaped poly(lysine) as a gene delivery vector. Biomater Sci 1:1223–1234
43. Sulistio A, Blencowe A, Widjaya A, Zhangb X, Qiao G (2012) Development of functional amino acid-based star polymers. Polym Chem 3:224–234
44. Pu Y, Zhang L, Zheng H, He B, Gu Z (2014) Synthesis and drug release of star-shaped poly (benzyl L-aspartate)-block-poly(ethylene glycol) copolymers with POSS cores. Macromol Biosci 14:289–297

45. Shen J, Chen C, Fu W, Shi L, Li Z (2013) Conformation-specific self-assembly of thermo-responsive poly(ethylene glycol)-*b*-polypeptide diblock copolymer. Langmuir 29:6271–6278
46. Liu DL, Chang X, Dong CM (2013) Reduction- and thermo-sensitive star polypeptide micelles and hydrogels for on-demand drug delivery. Chem Commun 49:1229–1231
47. Lee H, Park JB, Chang JY (2011) Synthesis of poly(ethylene glycol)/polypeptide/poly(D, L-lactide) copolymers and their nanoparticles. J Polym Sci Part A Polym Chem 49:2859–2865
48. Yin L, Song Z, Hoon Kim K, Zheng N, Tang H, Lu H, Gabrielson N, Cheng J (2013) Reconfiguring the architectures of cationic helical polypeptides to control non-viral gene delivery. Biomaterials 34:2340–2349
49. Gao H, Hu Z, Guan Q, Liu Y, Zhu F, Wu Q (2013) Synthesis and thermoreversible gelation of coil-helical polyethylene-block-poly(γ-benzyl-L-glutamate) diblock copolymer. Polymer 54:4923–4929
50. Jacobs J, Gathergood N, Heise A (2013) Synthesis of polypeptide block copolymer hybrids by the combination of *N*-carboxyanhydride polymerization and RAFT. Macromol Rapid Commun 34:1325–1329
51. Holley AC, Ray JG, Wan W, Savin DA, McCormick CL (2013) Endolytic, pH-responsive HPMA-b-(l-Glu) copolymers synthesized via sequential aqueous RAFT and ring-opening polymerizations. Biomacromolecules 14:3793–3799
52. Higashihara T, Faust R (2009) Synthesis of novel ABA triblock and (ABA)$_n$ multiblock copolymers comprised of polyisobutylene and poly(γ-benzyl-L-glutamate) segments. React Funct Polym 69:429–434
53. Zhai S, Song X, Feng C, Jiang X, Li Y, Lu G, Huang X (2013) Synthesis of α-helix-containing PPEGMEA-*g*-PBLG, well-defined amphiphilic graft copolymer, by sequential SET-LRP and ROP. Polym Chem 4:4134–4144
54. Karatzas A, Iatrou H, Hadjichristidis N, Inoue K, Sugiyama K, Hirao A (2008) Complex macromolecular chimeras. Biomacromolecules 9:2072–2080
55. Junnila S, Houbenov N, Hanski S, Iatrou H, Hirao A, Hadjichristidis N, Ikkala O (2010) Hierarchical smectic self-assembly of an ABC miktoarm star terpolymer with a helical polypeptide arm. Macromolecules 43:9071–9076
56. Kadokawa J, Setoguchi T, Yamamoto K (2013) Preparation of highly flexible chitin nanofiber-*graft*-poly(γ-L-glutamic acid) network film. Polym Bull 70:3279–3289
57. Harris Wibowo S, Wong EHH, Sulistio A, Guntari SN, Blencowe A, Caruso F, Qiao GG (2013) Assembly of free-standing polypeptide films via the synergistic combination of hyperbranched macroinitiators, the grafting-from approach, and cross-chain termination. Adv Mater 25:4619–4624
58. Audouin F, Fox M, Larragy R, Clarke P, Huang J, O'Connor B, Heise A (2012) Galactose-functionalized PolyHIPE scaffolds for use in routine three dimensional culture of mammalian hepatocytes. Macromolecules 45:6127–6135
59. Gkikas M, Das BP, Tsianou M, Iatrou H, Sakellariou G (2013) Surface initiated ring-opening polymerization of L-proline N-carboxy anhydride from single and multi walled carbon nanotubes. Eur Polym J 49:3095–3103
60. Borase T, Ninjbadgar T, Kapetanakis A, Roche S, O'Connor R, Kerskens C, Heise A, Brougham DF (2013) Stable aqueous dispersions of glycopeptide-grafted selectably functionalized magnetic nanoparticles. Angew Chem Int Ed 52:3164–3167

Living Anionic Polymerization of Isocyanates

Chang-Geun Chae, Ho-Bin Seo, and Jae-Suk Lee

Abstract Polyisocyanates are rodlike polymers with dynamic helical conformations likely to be synthesized using anionic polymerization. Although many scientists have tried to obtain polyisocyanates with a controlled molecular weight and a narrow weight distribution, the trimerization precluded controlled polyisocyanate formation. To overcome the lack of a living nature, special anionic polymerizations were invented. The use of effective additives and dual functional initiators stabilized the living chain end to prevent the trimerization. These polymerizations eventually achieved the living nature indicating quantitative yield and predictable molecular weight and narrow molecular weight distribution. The state of art of anionic polymerization of isocyanates and the effective functionalization techniques led to synthesis of well-defined linear, telechelic, chiral, star, rod-coil block, and graft polymers. From the controlled molecular architectures, a comprehensive understanding on helical properties and morphologies for polyisocyanates and their block copolymers has been accomplished.

Keywords Polyisocyanate • Helical conformation • Anionic polymerization • Trimerization • Additive • Dual functional initiator • Rod-coil block copolymer • Chirality • Morphology

1 Introduction

After the anionic polymerization of vinyl monomers without a termination and chain transfer reaction was discovered in the 1950s [1, 2], an addition mechanism was applied to the synthesis of polyisocyanates with high molecular weights by Shashoua et al. in 1959 [3, 4]. Unlike vinyl polymers with random coil conformations, polyisocyanates exhibit rigid rod structure with dynamic helical conformation because they have a stiff amide backbone and steric hindrance generated by the *N*-substituted side chains [5–10]. Owing to their functional architecture, polyisocyanates are potentially utilized in diverse applications, such as nano-

C.-G. Chae • H.-B. Seo • J.-S. Lee (✉)
School of Materials Science and Engineering, Gwangju Institute of Science and Technology (GIST), 123 Cheomdangwagi-ro, Buk-gu, Gwangju 500-712, Republic of Korea
e-mail: cgchae@gist.ac.kr; hbseo@gist.ac.kr; jslee@gist.ac.kr

structured carriers, lithography, liquid crystals, chiral recognition, optical sensing, and bioinspired models. Many researchers have tried to identify the helical properties of optically active polyisocyanates and the morphological behaviors of the rod-coil block copolymers composed of polyisocyanates.

The distinctive macromolecular properties of polyisocyanates emerge from their elaborately designed molecular architecture. Many investigations of polyisocyanates require precise control over the molecular weight and its distribution. Although anionic polymerization has become the most powerful method to obtain linear polyisocyanates, the initial polymerization system could not maintain a living nature due to the presence of depolymerization (specifically, trimerization) [2, 11–13]. Since then, special anionic polymerization techniques have been developed to safeguard the polymer's living nature; living polymers display quantitative yield and predictable molecular weight and narrow molecular weight distribution. In this chapter, the long-term history of anionically polymerized polyisocyanates and advanced living anionic polymerization techniques are described. Synthetic methods that produce well-defined polyisocyanates have significantly contributed to the elucidation of this helical polymer's properties.

2   Properties of Polyisocyanates

Polyisocyanate, or nylon-1, is composed of *N*-substituted amide repeating units in a polymeric backbone, and it exhibits stiff, rodlike structure. The amide bonds have partial double bond character, and therefore tend to be planar, stiffening the backbone [14]. Polyisocyanate is also a type of synthetic helical polymer, as illustrated in Fig. 1. The steric hindrance between the carbonyl group and the *N*-substituted side group rotates the polymer backbone to relieve the torsional strain, which brings about a stable helical conformation. The helical conformation of polyisocyanate is a racemic mixture of right- (P) and left-handed (M) helices [15–19]. Unless polyisocyanate has a chiral substituent, shorter P and M helical segments are equally populated with the occasional helical reversal occurring over a long chain [15]. Consequently, normal polyisocyanates are not optically active. Polyisocyanate has thermodynamically stable helical conformation [20]. The interconversion between the P and M helical senses is in a dynamic equilibrium related to variations in the thermodynamic conditions, such as temperature and solvent [21–23].

Optically active polyisocyanate possesses a one-handed helical sense over a long chain via chiral amplification. After Goodman and Chen first characterized an optically active polyisocyanate using circular dichroism (CD) [24, 25], various aspects of the helicity induction by the inclusion of a chiral moiety have been

Fig. 1 Chemical structure of polyisocyanate
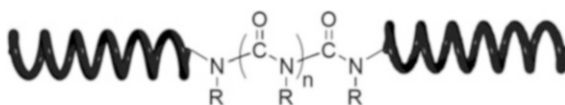
identified. Chiral components are separated into (R)- and (S)-enantiomers; each component contains at least one stereocenter chiral carbon which is non-superimposable with its mirror image. One-handed helical sense is driven by the cooperative amplification of the very small energy differences contributed by each chiral residue in a repeating unit, leading to the large energetic difference between the P- and M-helices ("cooperative effect") [21]. A small number of chiral repeating units (sergeants) in a copolymer with achiral monomers cause a large number of achiral units (soldiers) preferentially adopt a one-handed helical sense like a small number of sergeants command many soldiers ("sergeants and soldiers principle") [22, 26]. For isocyanate copolymers consisting of a mixture of opposing enantiomeric monomers, the inclination toward one-handed helical sense is determined by which enantiomer is in greater excess. The chirality of the minority is overshadowed, while the helical sense of the majority is revealed by reducing the perturbation energy between the two opposing helical senses ("majority rule") [27, 28]. Covalent introduction of a chiral moiety to the α-end of a polymer chain induces the preferred one-handed helical sense in a specific range of overall chain length ("covalent chiral domino effect", CCD effect) [29].

3 General Aspect of the Anionic Polymerization of Isocyanates

3.1 View on the Structural Tendency of Isocyanate Monomers

Isocyanate groups contain two cumulated double bonds ($N = C$ and $C = O$) on the same axis, and the π-electrons from the respective double bonds are situated in two different perpendicular planes, as illustrated in Fig. 2a [30]. Because nitrogen and oxygen atoms are highly electronegative, the electron density should be shifted toward these atoms. In the resonance structure, the carbon atom is located between the oxygen atom and the nitrogen atom with a stronger electronegativity. Nucleophiles add to the electrophilic carbon atom. Most isocyanates may be polymerized by nucleophilic addition, which occurs in the anionic mechanism. If an electron-withdrawing group is attached to the nitrogen atom, then the electron density of the carbon atom decreases, and its electrophilicity increases. Therefore, the addition of a nucleophile to the carbon is far easier. On the contrary, an electron-donating group connected to the nitrogen atom weakens the electrophilicity of the carbon.

During the anionic polymerization of isocyanate, two possible structures, an amidate anion and an acetal anion, may exist based on the resonance structure of isocyanate, as illustrated in Fig. 2b [30]. The nucleophilic addition to the $N = C$ and the $C = O$ bond may yield a mixed structure of amide and acetal backbones. Normally, the major structure of polyisocyanate is reported to be an amide backbone [5, 11, 14]. A combination of spectroscopic and chemical data demonstrates

(a)   (b)
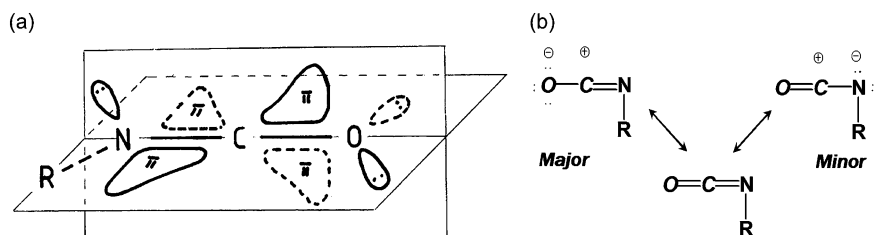
Fig. 2 (**a**) Spatial arrangement of the π and p orbitals in the –NCO group of an isocyanate and (**b**) resonance structures of isocyanate (Reproduced with permission from [30]. Copyright 2001 Elsevier.)
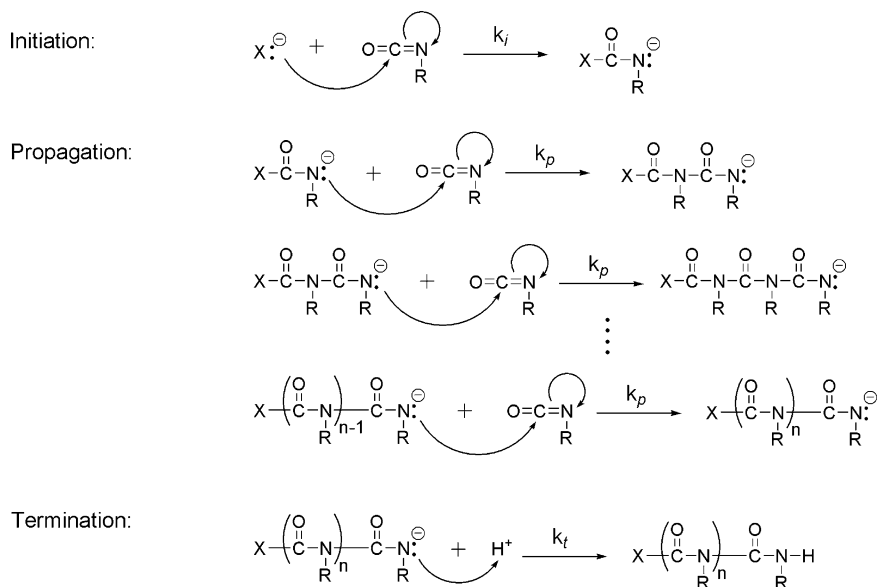
Scheme 1 General procedure for the anionic polymerization of isocyanate

that anionic polymerization initiators produce polyisocyanates with an amide backbone regardless of counterion or solvent [41]. In other words, the addition of a propagating chain end to the monomer mainly breaks the $N=C$ bond. However, the presence of a trace amount of the acetalic structure in these polyisocyanates is not excluded entirely [5].

3.2 Mechanism of the Anionic Polymerization of Isocyanates

Due to its chemical structure, polyisocyanate tends to be synthesized using anionic polymerization. The fundamental mechanism would be expected to proceed beginning with the addition of a nucleophile to a monomer, producing an amidate
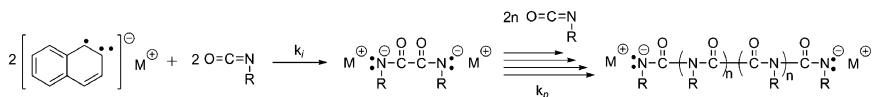
Scheme 2 Procedure for the anionic polymerization of isocyanate using an electron transfer initiator

anion [4]. This procedure is described in Scheme 1. During the initiation step, a nucleophilic anionic initiator, usually a cyanide anion, reacts with the carbonyl carbon of an isocyanate monomer and transfers an electron pair to the nitrogen atom after opening the $N=C$ π-bond. The reactive nitrogen anion, specifically the amidate anion, participates in the propagation step by successively reacting with monomers. As more monomers are added, the propagating polymeric anion continuously grows, extending its chain length. Polymerization is mostly terminated when the growing chain end dissipates and the reaction is neutralized with a proton source.

In addition to the nucleophilic anion initiator, an electron transfer initiator also initiates the polymerization of isocyanate [5]. As presented in Scheme 2, an aromatic anionic radical initiator, such as metal naphthalenide (M-Naph), reacts with an isocyanate monomer, leading to the formation of an isocyanate radical anion, followed by a *bis*-amidate anion through the immediate coupling of two molecules. This mechanism generates a bidirectional growing chain.

3.3 Main Cause of Degradation in Polyisocyanates

Interestingly, another reaction pathway is found during the anionic polymerization of isocyanates: intramolecular backbiting of the living end to the third carbonyl carbon close to chain end, which is called the trimerization. The trimerization occurring during or shortly after anionic polymerization generates a large amount of 1,3,5-tri-N-substituted isocyanurates, a thermodynamically stable cyclic trimer. It results in the formation of polyisocyanate with low yield and uncontrolled molecular weight and broad molecular weight distributions. The rate of trimerization increased with the increasing polymerization temperature [4, 31, 32].

The trimerization is a main reason of the degradation of polyisocyanates. It is boosted by basic chemicals or heat. When polyisocyanate stands in N,N-dimethylformamide (DMF) at room temperature with sodium cyanide, the polymer degrades [4]. It also degrades to monomers and trimers in DMF with a catalytic amount of di-n-butylamine as a base [12]. The thermal degradation of polyisocyanates is observed through thermal analysis and mass spectrometry [33, 34]. All of the degradation cases yield mostly trimers. The gradual decrease in the viscosity and mass of the polymers during degradation notes that the degradation of polyisocyanates is closely involved with successive unzipping of the polymer chain as occurs during trimerization rather than random chain scission. Afterward,
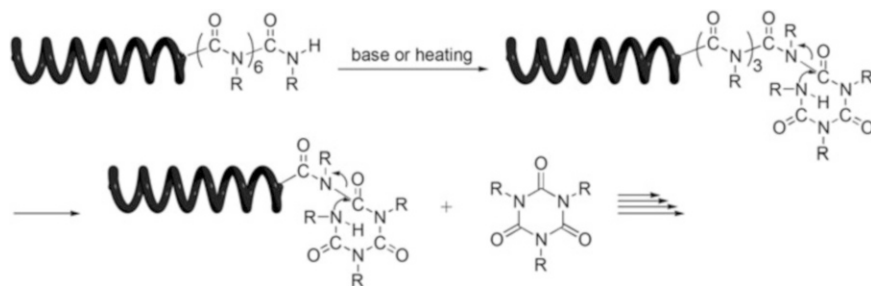
Scheme 3 Reaction mechanism for the degradation of polyisocyanate using a base or heating (Reproduced with permission from [36]. Copyright 2008 Nature Publishing Group.)

several kinetic and practical studies revealed the degradation mechanism of polyisocyanates. As shown in Scheme 3, the degradation process begins with backbiting reaction of the reactive anion regenerated by the abstraction of a proton at the –NH end group of polyisocyanates in the presence of the basic chemicals or heat [34, 35].

The chemical and thermal fragility at the end of polymer chain facilitates the degradation of polyisocyanates. Therefore, the polymer must be made more stable by endcapping with a suitable material. Kawaguchi et al. and Iwata et al. synthesized α, ω-end-functionalized telechelic poly(n-hexyl isocyanate) (PHIC) to probe its enhanced stability. The resulting endcapped PHIC displayed the significantly decreased degradation rate even in the presence of base or heating, whereas the polymer with the terminal –NH group rapidly degraded under the same conditions [35, 36].

3.4 Effect of Counter Cation on Anionic Polymerization of Isocyanates

In the anionic polymerization, the propagation rate is affected by the solvation of counter cation in the solvent. In polar solvents, such as tetrahydrofuran (THF), the degree of solvation of the counter cation is higher with increasing the ratio of the cation's charge to the size (or charge density). Specifically, a small counter cation forms a loose ion pair with anions due to its high solvation and eventually raises the propagation rate. For example, during the anionic polymerization of styrene as a nonpolar monomer in THF, the propagation rate constant and the dissociation constants of the ion pair were shown in the order of $Li^+ > Na^+ > K^+ > Rb^+ > Cs^+$ [37], which is in inverse order of the size of the counter cation.

During the anionic polymerization of isocyanate as a polar monomer in THF, the degree of propagation rate was revealed to be $Li^+ < Na^+ < K^+$ [32], which is opposed to results for the anionic polymerization of nonpolar monomers. This

Table 1 Anionic polymerization of HIC using M-Naph in THF at $-98\ ^\circ$C as a function of time (Data from [32])

Counter cation	$[HIC]_0/[M\text{-Naph}]_0$	Time (min)	M_n (kDa) calcd[a]	obsd[b]	M_w/M_n[b]	Yield (%)
Li$^+$	50.2	5	4.0	22.0	3.92	33 (67)[c]
Li$^+$	50.1	10	7.0	34.0	3.59	56 (44)[c]
Li$^+$	56.9	20	13.5	42.0	2.95	95 (4)[c]
Na$^+$	40.3	2	7.5	26.5	1.26	74 (26)[c]
Na$^+$	49.3	5	12.0	44.4	1.14	95 (5)[c]
Na$^+$	55.2	10	14.0	36.5	1.21	100
Na$^+$	44.3	20	10.5	29.6	1.26	92 (8)[d]
Na$^+$	52.3	30	12.0	39.0	1.19	89 (11)[d]
Na$^+$	48.2	60	10.5	72.8	1.24	86 (14)[d]
K$^+$	52.4	5	13.0	53.0	3.62	96 (4)[d]
K$^+$	57.6	10	12.3	49.8	2.43	87 (13)[d]
K$^+$	52.8	20	11.0	67.0	2.11	81 (18)[d]

[a]M_n is calculated using the expression $\{([HIC]/[M\text{-Naph}]) \times 2 \times \text{molecular weight of HIC}\} \times$ yield of polymer/100
[b]M_n and M_w/M_n were measured by size exclusion chromatography-multiangle laser light scattering (SEC-MALLS) in THF at 40 $^\circ$C
[c]The amount of unreacted monomer is presented in parentheses
[d]The yield of trimer is presented in parentheses

result indicates that the propagation rate increases as the size of counter cation increases. The same trend is generally observed during the polymerization of other polar monomers, such as methyl methacrylate and ethylene oxide, in polar solvents, which can be explained by the push-pull event [38]. The carbon atom of the isocyanate group is located between the negatively charged nitrogen and oxygen atoms. More reactive living anion might be more likely to repulse the negatively charged isocyanate group rather than to react with it in the polar solvent. In that case, the ion pair formed by a small counter cation might demonstrate a low propagation rate. However, this assumption was not clearly verified yet. The results of the polymerization of HIC using Li-, Na-, and K-Naph in THF at $-98\ ^\circ$C are summarized in Table 1.

The molecular weight distribution during the anionic polymerization of HIC in THF is affected by the initiation and propagation rate. The propagation rate is too slow with Li$^+$ and too fast with K$^+$. These conditions result in heterogeneous polymerization with a broad molecular weight distribution caused by the discordance between the propagation and initiation rates. For the polymerization using Na-Naph, the propagation rate displays intermediate properties compared to the above two cases. The molecular weight distribution is also relatively narrow. Therefore, Na$^+$ is generally accepted to be the best counter cation among three during the polymerization of isocyanate [32].

3.5 Effect of Temperature and Time on Anionic Polymerization of Isocyanates

The polymerization temperature and time are also important variables to influence the formation of polyisocyanates [4, 31, 32]. During the propagation step, the trimerization can also occur simultaneously. Concurrently, the degree of trimerization controls the amount of linear polymer. The presence of a large amount of trimer indicates a low yield of linear polymer. The trimerization is generally accelerated at higher temperatures. In addition, it proceeds continuously with increasing reaction time, even after all of the monomer is consumed. Therefore, the optimized polymerization time is determined at low temperatures to minimize the trimerization.

The anionic polymerization of 3-(triethoxysilyl)propyl isocyanate (TESPI) using a Na-Naph initiator in THF was carried out while varying the polymeriza- tion temperature and time [31]. When the polymerization was carried out at −50 °C, only trimer was observed, as shown in Fig. 3a, indicating that the trimerization of the growing oligomer chains proceeded without reacting with the monomer. The yield of the polymer increased with decreasing polymerization temperature. Quantitative yield of the polymer was obtained at −98 °C. The results of varying the polymerization time at −98 °C are described in Fig. 3b. The yield and molecular weight of the polymer increased with polymerization time for the initial 5 min. The polymerization was completed at 5 min to furnish a quantitative yield of the polymer. As the polymerization time increased beyond 5 min, yield of the polymer continuously decreased in tandem with increased trimer formation.
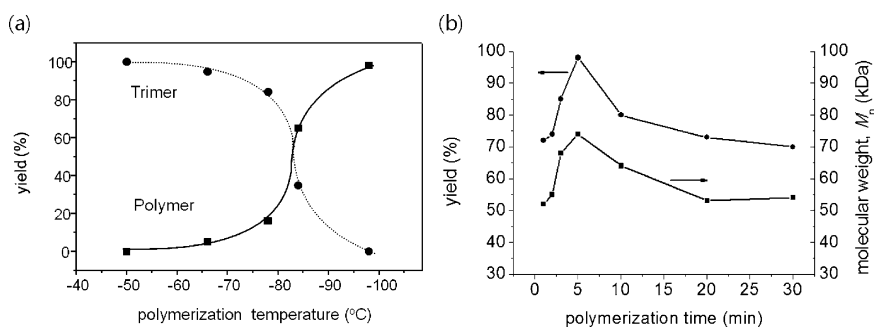
Fig. 3 (**a**) Yield of the polymer and the trimer as a function of polymerization temperature and (**b**) yield and molecular weight (M_n) of the polymer as a function of polymerization time during the anionic polymerization of TESPI using Na-Naph in THF (Reproduced with permission from [31]. Copyright 1999 American Chemical Society.)

4   Classical Anionic Polymerization of Isocyanates

Until the polymerization of isocyanates began, only the formation of cyclic dimer and trimers from isocyanates had been understood. Shashoua et al. reported the first anionic polymerization of isocyanates to achieve a high molecular weight [3, 4]. A wide variety of monomers, including aliphatic and aromatic isocyanates, was polymerized using anionic initiators, such as sodium in DMF, sodium benzophenone ketyl, and sodium cyanide in conditions of DMF at low polymerization temperatures (-20 to -100 °C), producing high molecular weight polyisocyanates. Goodman et al. and Green et al. adopted this polymerization method to prepare optically active polyisocyanates using chiral monomers [21, 22, 24, 25].

Sodium cyanide in DMF initially became a commonly used polymerization system, but it was disadvantageous to the polymerization of several aliphatic isocyanates due to the limited solubility of their growing polymeric chains in DMF. These precipitated from the DMF during propagation, leading to unpredictable molecular weight and broad molecular weight distributions and low yield. To overcome the solubility problems, Aharoni and Okamoto et al. used toluene/DMF mixtures and toluene at low temperatures [39, 40]. Their results demonstrated that changing the solvent from DMF to toluene offered increased solubility of the growing chains at low temperatures (-78 to -100 °C) and generated materials in high yield with relatively good control over the molecular weight corresponding to the ratio of the monomer to the initiator.

There have been attempts using various organolithium initiators. Natta et al. polymerized n-butyl and phenyl isocyante using ethyllithium initiator in toluene, but this system offered only ~50 % yield [11]. Fetters et al. reported the use of n-butyllithium during the anionic polymerization of several alkyl isocynates in toluene at -78 °C under vacuum [41, 42]. The resulting polymers possessed moderately narrow molecular weight distributions ($M_w/M_n \sim 1.2$), but the yield of polymer and the correlation between the observed molecular weight and feed ratio of monomer to the initiator were not revealed in detail. Okamoto et al. polymerized optically active alkyl isocyanates and phenyl isocyanates using the lithium amide of piperidine in THF at -98 °C under a nitrogen atmosphere [43–47]. In that case, the molecular weights were moderately controllable by modulating the feed ratio of the monomer to the initiator. However, the resulting polymers were still received in low yield, and the observed molecular weights were higher than calculated molecular weights.

Endo et al. introduced samarium iodide as a ligand-type additive to prevent backbiting during the anionic polymerization of isocyanates initiated by alkyllithiums in THF at -98 °C [48]. The ligand coordinating with the reactive anion end stabilized the anion and introduced the steric hindrance at the chain end. As a result, the formation of trimers was heavily suppressed, and this reaction yielded polymers with high molecular weight. However, the polymerization remained uncontrolled because the heterogeneous coordination of samarium iodide with reactive anion led to broader molecular weight distributions ($M_w/M_n \sim 2.4$–3.5).

Inoue et al. used a lanthanum isopropoxide as an anionic initiator for the polymerization of several isocyanates [49]. Lanthanum complexes formed during

the reaction with an isocyanate activated the electrophilic carbonyls, such as carbon dioxide. The anionic polymerization of HIC using lanthanum isopropoxide without solvent at $-78\,^{\circ}\mathrm{C}$ under argon atmosphere for 24 h produced a polymer with 90 % yield. However, the observed molecular weight of resulting polymer was higher than the theoretical value because the lanthanum isopropoxide aggregated. The molecular weight distribution of the produced polymer was much broader ($M_{\mathrm{w}}/M_{\mathrm{n}} \sim 2.45$).

5 Advanced Living Anionic Polymerization of Isocyanates

As described in the above section, anionic polymerization is a popular approach for the synthesis of polyisocyanates. However, it was difficult to maintain a living polymerization. Most ordinary polymerization systems could not suppress the trimerization and yielded polymers with undesired molecular weight and broad molecular weight distributions. In many cases, the observed molecular weights of polymers were much higher than the calculated molecular weights. Therefore, invention of a living anionic polymerization was required to overcome the synthetic limitations of well-defined polyisocyanates. Toward this purpose, several studies have focused on the following: (1) preventing the backbiting reaction by introducing the steric hindrance to the living chain end and (2) adjusting the reactivity of the living amidate anion. Lee et al. invented impressive techniques to control polymerization. Advanced anionic polymerizations, such as introducing the additional reagents and using dual functional initiators, successfully prevented trimerization and led to quantitative yield and predictable molecular weight and narrow molecular weight distributions. In this section, detailed mechanism of a living anionic polymerization of isocyanate is described.

5.1 Addition of a Ligand Reagent: 15-Crown-5 (First Generation)

Crown ethers are cyclic, oligomeric rings consisting of ethyleneoxy repeating units. The oxygen atoms on crown ethers have such a strong affinity toward metal cations that they pull a specific metal cation into the interior cavity of the ethereal ring. Therefore, crown ethers achieve specific complexation with a cation [50, 51]. Crown ethers were tested as reasonable additives to suppress backbiting during the anionic polymerization of isocyanates. Theoretically, a crown ether makes a cation-ligand complex by coordinating with the counter cation bound to growing chain end. The bulky complex at the living chain end inhibits the backbiting reaction by limiting the mobility of the amidate anion through steric hindrance

Table 2 Living anionic polymerization of TESPI using Na-Naph and 15-crown-5 in THF at various reaction times at -98 °C (Data from [31].)

Na-Naph (mmol)	15-crown-5 (mmol)	TESPI (mmol)	Time (min)	M_n (kDa) calcd[a]	obsd[b]	M_w/M_n[b]	Yield (%)
0.08	1.01	5.62	1	33.0	28.0	1.55	96
0.16	1.49	5.17	5	15.0	16.0	1.34	93
0.06	1.14	4.92	10	37.0	40.0	1.39	97
0.06	1.04	4.50	30	35.0	32.0	1.39	95
0.07	0.82	5.26	60	34.0	35.0	1.50	96
0.06	0.12	4.92	120	28.0	55.0	1.70	73 (26)[c]
0.07[d]	0.14	5.21	5	20.0	40.0	1.60	55 (45)[c]
0.07[e]	0.14	5.70	5	6.5	75.0	2.45	15 (85)[c]

[a]M_n is calculated using the expression $\{([\text{TESPI}]/[\text{Na-Naph}]) \times 2 \times \text{molecular weight of TESPI}\} \times \text{yield of polymer}/100$
[b]M_n and M_w/M_n were measured with size exclusion chromatography (SEC) using polystyrene (PS) standards in THF at 40 °C
[c]The yield of the trimer appears in parentheses
[d,e]Each polymerization was carried out at -84 °C (d) and -78 °C (e), respectively

introduced by the ligand. The additional bulk restricts nucleophilic addition into the carbonyls on the intramolecular chain.

Lee et al. synthesized poly((3-triethoxysilyl)propyl isocyanate) (PTESPI) by using Na-Naph and 15-crown-5 complex in THF at -98 °C under high vacuum (10^{-6} torr) [31]. The 15-crown-5 was chosen due to its specificity for sodium; the cavity size of 15-crown-5 is 1.7–2.2 Å, which fits the radius of the sodium cation (1.9 Å) [52]. The polymerization results are summarized in Table 2. The polymerization generated a ~97 % yield and this high yield was retained for up to 1 h. The bulky cation-ligand complex from 15-crown-5 effectively suppressed the trimerization, generating a living polymer as depicted in Scheme 4. Despite this advantage, this formulation was not stable. The bulky ligand formed a sterically hindered complex on the chain end, but increased the distance between the amidate anion and the counter cation, raising the anion's reactivity. This effect throws the initiation and propagation rates out of balance, resulting in a broad molecular weight distribution.

5.2 Addition of a Common Ion Salt: Sodium Tetraphenylborate (Second Generation)

To overcome the limitations of the ligand additive, a common ion salt, sodium tetraphenylborate (NaBPh$_4$), was utilized as an additive to prevent trimerization. When introducing NaBPh$_4$, the following effects are expected: (1) NaBPh$_4$ increases the counter ion concentration in the polymerization solution and shortens the distance between the amidate anion and the counter cation. The tight ion pair
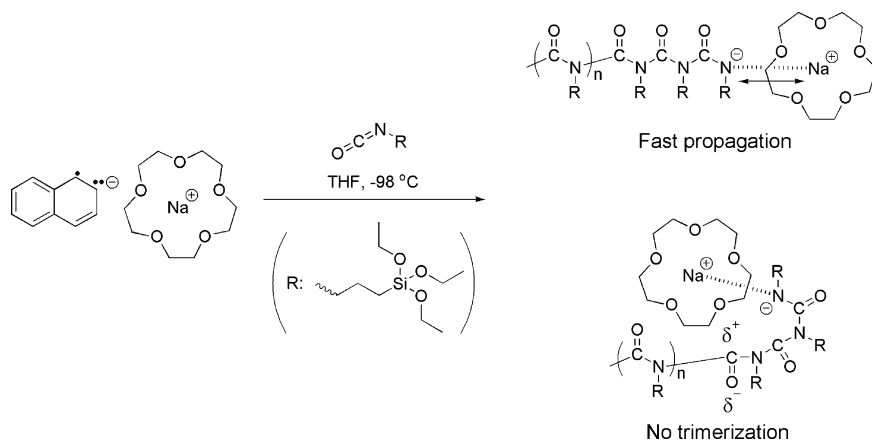
Scheme 4 Preventing trimerization by introducing 15-crown-5 as an additive in anionic polymerization of TESPI using Na-Naph in THF at −98 °C (Reproduced with permission from [31]. Copyright 1999 American Chemical Society.)

stabilizes the living amidate anion enough to suppress the trimerization and decreases the propagation rate [53–55]. (2) The bulky tetraphenylborate groups inducing steric hindrance at the chain end restrict the mobility of living chain end and therefore suppress the trimerization.

Lee et al. studied the effect of NaBPh$_4$ on the anionic polymerization of HIC using Na-Naph in THF at −98 °C under high vacuum (10^{-6} torr) [32, 56]. The polymerization results are summarized in Table 3. NaBPh$_4$ increased the efficiency of the Na-Naph because the tetraphenylborate groups coordinating a sodium cation promoted the activity of the naphthalene anion. When a 10-fold excess of NaBPh$_4$ was used relative to the initiator, the observed molecular weights of the polymers agreed with the calculated values and the molecular weight distribution became narrow. Furthermore, this concentration completely suppressed the trimerization during propagation. The polymerization yield reached ~100 % for 20 min and the growing chain end was stable for up to 40 min without backbiting. The results explain that the presence of NaBPh$_4$ causes the living chain anion to react exclusively with the monomer molecules rather than the carbonyl backbone as long as monomers are present. As the reaction time increased beyond 40 min, the yield of the polymer decreased and the trimer yield increased. Under the optimized conditions, the relationship between the molecular weight of the polymer and the molar ratio of the monomer to the initiator was linear. Successful postpolymerization and block copolymerization also supported living nature of this polymerization system by confirming the clear growth of whole chains.

Scheme 5 indicates that NaBPh$_4$ tightens the ion pair and stabilizes the living chain anion to block the backbiting reaction. Based on this additive system, Hadjichristidis et al. attempted an anionic polymerization of HIC using monodirectional initiators in THF at −98 °C while employing various additives

Table 3 Living anionic polymerization of HIC using Na-Naph in the presence of NaBPh$_4$ in THF at −98 °C (Data from [32, 56].)

[NaBPh$_4$]$_0$/[Na-Naph]$_0$	[HIC]$_0$/[Na-Naph]$_0$	Time (min)	M_n (kDa) calcd[a]	M_n (kDa) obsd[b]	M_w/M_n[b]	Yield (%)
9.7	48.9	10	11.0	12.8	1.08	89 (11)[c]
0	44.3	20	10.5	29.6	1.26	92 (8)[d]
2.8	59.2	20	14.4	23.4	1.22	96
4.7	54.5	20	13.3	17.5	1.17	96
9.6	45.3	20	11.5	11.7	1.09	99
14.5	84.3	20	11.8	18.5	1.10	55 (45)[c]
26.2	63.8	20	6.0	20.9	1.15	36 (64)[c]
10.0	56.4	20	13.9	14.6	1.06	97
10.0	88.1	20	21.5	22.2	1.11	96
10.3	138.3	20	34.4	31.0	1.07	97
9.7	163.4	20	40.3	42.7	1.12	97
10.0	200.4	20	50.9	54.5	1.11	97
9.9	48.0	40	11.8	12.8	1.12	96
9.5	49.6	60	11.5	10.8	1.13	93 (7)[d]
11.0	52.7	80	11.8	11.0	1.08	87 (13)[d]
10.0	55.2	120	11.4	10.6	1.05	81 (19)[d]
e	e	30				0

[a]M_n is calculated using the expression {([HIC]/[Na-Naph]) × 2 × molecular weight of HIC} × yield of polymer/100
[b]M_n and M_w/M_n were measured by SEC-MALLS in THF at 40 °C
[c]The amount of unreacted monomer is presented in parentheses
[d]The yield of the trimer is presented in parentheses
[e]Polymerization of HIC (5.24 mmol) was performed with NaBPh$_4$ (0.97 mmol) without Na-Naph

R = n-hexyl
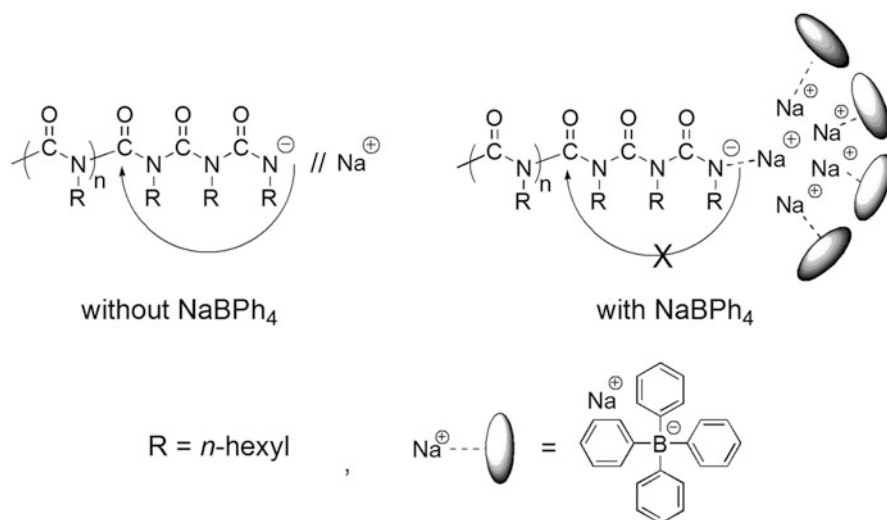
Scheme 5 Prevention of trimerization with NaBPh$_4$ (Reproduced with permission from [56]. Copyright 2001 American Chemical Society.)
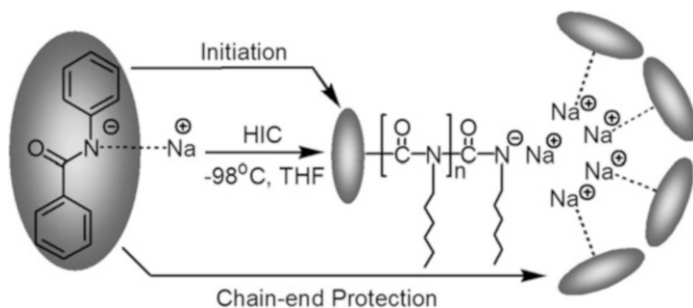
Scheme 6 Role of sodium benzanilide (Na-BA) as a dual functional initiator during the anionic polymerization of isocyanate (Reprinted with permission from [58]. Copyright 2005 American Chemical Society.)

[57]. Of the several initiation systems, using a benzyl sodium initiator under the presence of excess NaBPh$_4$ displayed the best results, including a high yield and predictable molecular weight and narrow molecular weight distributions.

5.3 Dual Functional Initiators (Third Generation)

The range of initiators for living anionic polymerization of isocyanate is limited. The polymerization of isocyanates using radical anion or carbanion initiators generates low yields of the polymer and unpredictable molecular weights. The high reactivity of these initiators cannot suppress the backbiting reaction during polymerization, unless the reactivity of growing chain end is properly adjusted and sterically hindered by the additives. Because of these problems, investigations of alternative anionic initiators have been encouraged. Lee et al. have discovered several initiators with low reactivity that effectively prevent the trimerization during polymerization without additives [58–60]. These initiators are called "dual functional initiators," because they initiate the anionic polymerization while protecting the living chain anion. The role of the dual functional initiator is visualized in Scheme 6 [58].

Sodium benzanilide (Na-BA) Various sodium amide initiators have been investigated to achieve living nature in anionic polymerization in HIC. Of them, sodium benzanilide (Na-BA) was the best initiator, resulting in high yield and controlled molecular weight and narrow molecular weight distributions [58]. On the other hand, sodium alkyl amides did not accomplish the initiation due to their low solubility in THF. The amidate anion structure of Na-BA is similar to the living chain end from the isocyanate polymer. The amidate anion of the initiator is relatively weak nucleophilic due to the charge delocalization generated by the phenyl ring and the carbonyl group. Therefore, this initiator was expected to be less reactive than Na-Naph or diphenylmethyl sodium (Na-DPM). The pK_a values

Table 4 Living anionic polymerization of HIC using Na-BA in THF at −98 °C (Data from [58].)

Na-BA (mmol)	HIC (mmol)	Time (min)	M_n (kDa) calcd[a]	obsd[b]	M_w/M_n[b]	Yield (%)
0.390	8.24	60	2.7	13.6	1.09	100
0.340	8.64	60	3.2	16.8	1.11	100
0.350	13.3	60	4.8	22.1	1.12	99
0.380	18.0	70	5.9	30.5	1.08	98
0.265	17.6	70	8.2	40.8	1.16	97

[a]M_n is calculated using the relation $\{([HIC]/[Na\text{-}BA]) \times$ molecular weight of HIC + molecular weight of BA$\} \times$ yield of polymer/100
[b]M_n and M_w/M_n were measured by SEC-MALLS in THF at 40 °C

of diphenylmethane and benzanilide in water are 32.2 and 20, respectively [61], indicating that the amidate anion of benzanilide is much less reactive than the carbanion from Na-DPM [62]. The results of the anionic polymerization using Na-BA are summarized in Table 4. Using Na-BA led to a slower propagation than using the Na-Naph initiator with NaBPh$_4$. A nearly quantitative yield of the polymer was obtained when reaction time reached 60 min. The molecular weight distribution of resulting polymer was narrow. Because Na-BA mimics the structure of the living chain end, it established a balance between the initiation and propagation rates, resulting in PHIC with a narrow molecular weight distribution.

Unexpectedly, the observed molecular weight was 5 times higher than the calculated molecular weight. This result indicates that the effective concentration of the initiator for polymerization is approximately 20 %. To confirm the discrepancy between the actual concentration and the initiation efficiency of Na-BA, the benzanilide anion content was estimated with a reaction of Na-BA and acetyl chloride. As a result, a quantitative yield of the *N*-acetyl benzanilide was observed. From this result and the molecular structure of the initiator, it was suggested that five Na-BA molecules form an aggregator and one of those molecules covalently reacts with the monomers. To confirm this event, a set of polymerization experiments using a mixture of Na-Naph as an initiator and Na-BA (2–3-fold excess) as an additive was carried out. Consequently, PHIC with a molecular weight corresponding to the concentration of Na-Naph resulted and backbiting was successfully prevented. Furthermore, the obtained polymer did not contain any aromatic residue derived from Na-BA. This result clearly demonstrates that Na-BA molecules efficiently protect the living chain end as an additive.

The dual function mechanism of Na-BA in polymerization was illustrated in Scheme 7. Five Na-BA molecules may aggregate to form a pentameric macrocycle using the weak interactions between the sodium cation of one molecule and the carbonyl oxygen of its neighbor. The cavity of the macrocycle has a nitrogen atom that is accessible to the monomer. The initiation process is visualized as follows: (1) A monomer molecule approaches a pentameric aggregate of Na-BA. (2) A monomer reacts with any one of Na-BA nitrogens with equal probability. (3) The
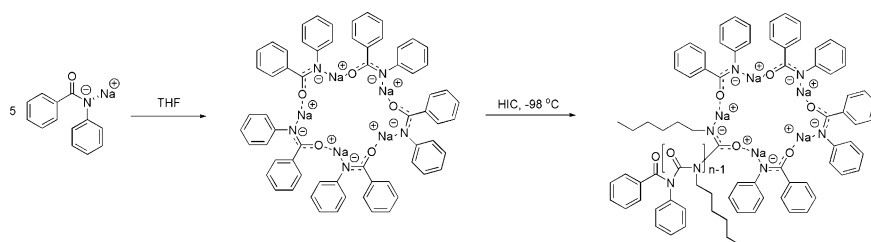
Scheme 7 Assumed dual function mechanism for the anionic polymerization of isocyanate using Na-BA (Reproduced with permission from [58]. Copyright 2005 American Chemical Society.)

Table 5 Living anionic polymerization of HIC using Na-DB in THF at −98 °C (Data from [59].)

| Na-DB (mmol) | HIC (mmol) | Time (min) | M_n (kDa) | | M_w/M_n[b] | Yield (%) |
			calcd[a]	obsd[b]		
0.271	5.45	10	2.75	8.71	1.09	100
0.272	8.64	10	4.24	11.5	1.08	100
0.253	12.3	10	6.33	19.1	1.03	99
0.270	17.8	10	8.39	24.5	1.05	98
0.231	22.4	10	12.3	35.3	1.07	98

[a]M_n is calculated using the relation {([HIC]/[Na-DB]) × molecular weight of HIC + molecular weight of DB} × yield of polymer/100
[b]M_n and M_w/M_n were measured by SEC-MALLS in THF at 40 °C

negative charge is transferred from nitrogen of Na-BA to the isocyanate nitrogen, and the monomer occupies the cavity of the macrocycle. (4) Negatively charged nitrogen from the monomer unit in the growing ring is more nucleophilic than the other nitrogen atoms from benzanilide. This nitrogen has the high probability of adding to monomer molecules and therefore leads to the chain growth of the polyisocyanate.

Sodium deoxybenzoin (Na-DB) Sodium deoxybenzoin (Na-DB) was investigated as an initiator for the living anionic polymerization of HIC [59]. The results are summarized in Table 5. Like Na-BA, this molecule also played a dual role as the initiator and protector of the living chain end, preventing trimerization. The difference between the two initiators was polymerization time. The time needed for complete polymerization of the HIC using Na-DB in THF at −98 °C was 10 min. This result indicates that the type of initiator influences the propagation conditions. Unlike the case of Na-DB, the initiation efficiency of Na-DB was 33 %. The observed molecular weight of the resulting polymer was 3 times higher than the calculated value. Therefore, 33 % of initiator molecules participate in the initiation, and the others act as additives to protect the growing chain ends.

Na-DB's dual function mechanism during polymerization is described in Scheme 8. Three Na-DB molecules may form a three-membered self-aggregate in THF at −98 °C. On that aggregate, one enolate anion initiates the anionic

Scheme 8 Assumed dual function mechanism for the anionic polymerization of isocyanate using Na-DB (Reproduced with permission from [59]. Copyright 2013 John Wiley and Sons.)

Table 6 Living anionic polymerization of HIC using Na-BH in THF at $-98\ ^{\circ}\text{C}$ (Data from [60].)

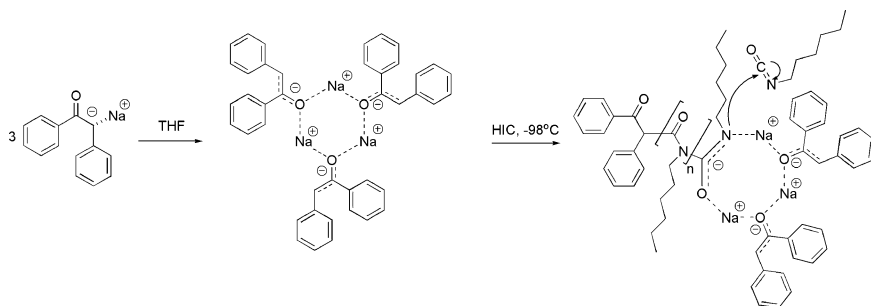| Na-BH (mmol) | HIC (mmol) | Time (min) | M_n (kDa) | | M_w/M_n[b] | Yield (%) |
			calcd[a]	obsd[b]		
0.194	4.29	10	2.9	8.4	1.11	96
0.195	9.45	10	6.2	14.6	1.04	97
0.181	14.5	10	10.2	26.6	1.10	98
0.205	27.0	10	16.4	38.2	1.14	97

[a]M_n is calculated using the relation $\{([\text{HIC}]/[\text{Na-BH}]) \times$ molecular weight of HIC + molecular weight of BH$\} \times$ yield of polymer/100

[b]M_n and M_w/M_n were measured by SEC-MALLS in THF at $40\ ^{\circ}\text{C}$

polymerization by reacting with HIC, and the other two initiator molecules protect living chain end, preventing trimerization.

Sodium benzhydroxide (Na-BH) Because carboxy anions were also considered relatively less reactive, various carboxylate initiators were investigated in the anionic polymerization of isocyanates. Among them, sodium benzhydroxide (Na-BH) was the most effective for the living polymerization of HIC [60]. The results are summarized in Table 6. Like Na-BA and Na-DB, Na-BH also initiated and protected the living chain and prevented trimerization. A quantitative yield was obtained in 10 min, and the molecular weight and narrow molecular weight distribution was also well controlled. The initiation efficiency of Na-BH was 40 %. The observed molecular weight of obtained polymer was 2.5 times higher than the calculated molecular weight. Like initiation trends of Na-BA and Na-DB, 40 % of the initiator molecules participate in the initiation, while the others act as protective additives.
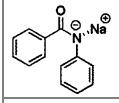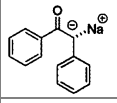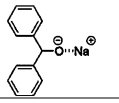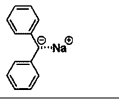
The dual function mechanism in polymerization initiated by Na-BH is also described based on their self-aggregation in Scheme 9. Na-BH molecules may form two- and three-membered self-aggregates in THF at $-98\ ^{\circ}\text{C}$. One carboxy anion per aggregate initiates the anionic polymerization by reacting with the HIC monomer, and the other initiator molecules protect living chain end and prevent
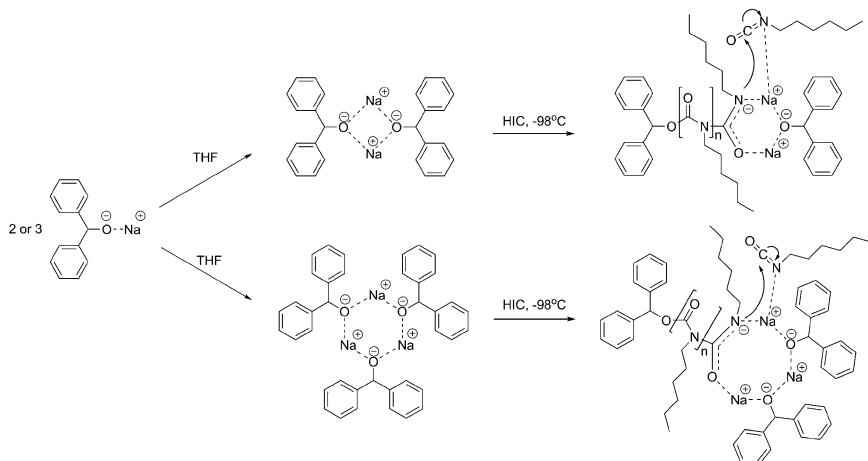
Scheme 9 Assumed dual function mechanism for the anionic polymerization of isocyanate using Na-BH (Reproduced with permission from [60]. Copyright 2011 American Chemical Society.)

Table 7 Efficiency and living nature of various anionic initiators used in the anionic polymerization of isocyanate in THF at −98 °C

	Na-BA [58]	Na-DB [59]	Na-BH [60]	Na-DPM [91]
Efficiency (%)	20	33	40	30–50
Living nature	○	○	○	×

trimerization. Each initiator displays the intrinsic initiation efficiency dependent on the molar ratio between the actual initiating molecules and the chain end protective molecules. The values of the initiation efficiency for the dual functional initiators are listed in Table 7.

6　Organotitanium(IV)-Catalyzed Coordination Polymerization of Isocyanates

Novak et al. discovered the living nature in coordination polymerization of iso-cyanates using organotitanium(IV) compounds as catalysts instead of living anionic polymerization [63–65]. As shown in Scheme 10, the mechanism of the polymer-ization using organotitanium(IV) was proposed to proceed using the coordination of the polarizable isocyanate monomer to the electron-deficient titanium metal
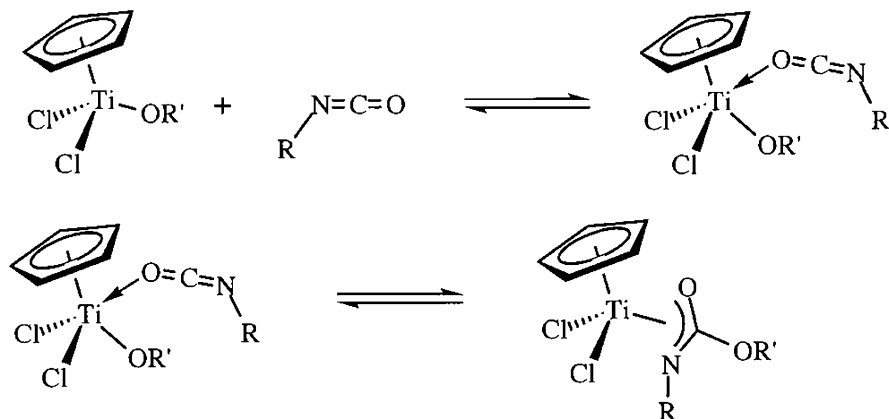
Scheme 10 Mechanism for the organotitanium(IV)-catalyzed coordination polymerization of isocyanate (Reprinted with permission from [70]. Copyright 2001 American Chemical Society.)

center, followed by the insertion of the monomer into the titanium-ligand bond to form the propagating titanium-amidate species. Several catalysts, including $TiCl_3OCH_2CF_3$ and $CpTiCl_2L$ ($Cp = \eta^5$-cyclophentadienyl, $L = -OCH_2CF_3$, $-N(CH_3)_2$, or $-CH_3$), were reported to be highly suitable for the polymerization of isocyanates at room temperature [65].

The following series contains the evidence supporting the living nature of the HIC polymerization applying the coordination mechanism. This polymerization in bulk provides a ~95 % yield (but not ~100 %, due to its equilibrium behavior), without cyclic trimers and with a narrow molecular weight distribution ($M_w/M_n \sim 1.05$–1.20). In addition, it demonstrates linear variation of molecular weight as functions of the feed ratio of monomer to initiator and conversion, as displayed in Fig. 4. Block copolymers of isocyanates with homogeneous molecular weight distribution are synthesized using sequential monomer addition in the coordination method, which implies that the titanium-amidate end species remains alive and termination does not occur. Because the catalyst is versatile, this coordination polymerization is suitable to prepare telechelic polyisocyanates. With this polymerization method, well-defined polyisocyanates with varying geometries, including block copolymers [66–69], star polymers [70], and graft polymers [71], were generated.

Despite the merits, the coordination polymerization is not superior to living anionic polymerization. Because the coordination polymerization is reversible, the conversion never reaches 100 %. In addition, the activity of the organotitanium(IV) catalyst and the polymerization kinetics are highly variable depending on the initiating ligand at the titanium center. Different ligands connecting titanium center exhibit different initiation efficiencies and make it hard to predict the molecular weight of the polymer [65, 69]. Therefore, living anionic polymerization is an easier method to prepare polyisocyanates with ~100 % yield and predictable molecular weights.

Fig. 4 (**a**) Molecular weight as a function of the monomer feed ratio to the initiator and (**b**) molecular weight (M_n) as a function of the percent conversion during the organotitanium (IV)-catalyzed coordination polymerization of isocyanate (Reproduced with permission from [63]. Copyright 1991 American Chemical Society.)

7 End Functionalization of Polyisocyanates
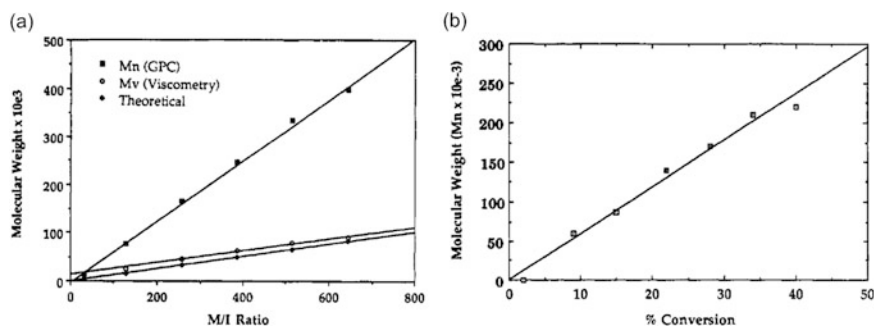
An interest in the synthesis of polyisocyanates with functionalized chain end for various purposes has increased. End-functionalized polymers are prepared for the chirally terminated polymer, block copolymer, nonlinear-shaped polymer formation, and so on. During the living anionic polymerization of isocyanate, two approaches were used to achieve end-functionalized polyisocyanates: α-end functionalization that uses a functionalized initiator and ω-end functionalization that uses a functional terminator. There are various structures available for end functionalization of the polyisocyanate that depends on the initiator and the terminator types. Mono- and bidirectional initiators, as well as mono- and difunctional terminators, form α,ω-end, α,α,-end, ω,ω-end functionalization as well as α-end and ω-end functionalization.

7.1 α-End Functionalization by Functional Initiators

Organolithium initiators with a chiral moiety Because chiral residues at the α-end of the polyisocyanate chain induces a preferential one-handed helical sense over a long chain length, optically active polyisocyanates have been prepared by attaching a chiral residue to the α-end of the polymer chain via anionic polymerization using chiral anionic initiators. Several chiral lithium alkoxides and lithium amides have been employed as optically active initiators. A list of these initiators is displayed in Fig. 5 [72–74]. The degree of the optical activity of the resulting polymers depends on the combination of the monomer and the initiator, as well as the molecular weight of the polymers. Anionic polymerizations using these initiators were carried out in THF at −98 °C. However, the resulting aliphatic and aromatic polyisocyanates did not show the living properties.
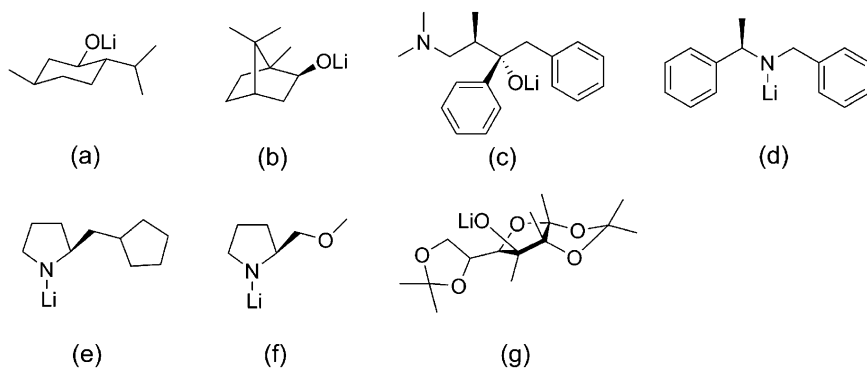
Fig. 5 Examples of chiral organolithium initiators: (**a**) Lithium (−)-menthoxide, (**b**) lithium (−)-borneoxide, (**c**) lithium (2S, 3R)-(+)-4-dimethylamino-1,2-diphenyl-3-methyl-2-butanolate, (**d**) lithium (R)-(+)-N-benzyl-α-methylbenzylamide, (**e**) lithium amide of (S)-(+)-1-(2-pyrrolidinylmethyl)pyrrolidine, (**f**) lithium amide of (S)-(−)-(2-methoxymethyl)pyrrolidine and (**g**) lithium oxide of 1,2,5,6-diisopropylidene-D-glucose [72–74]
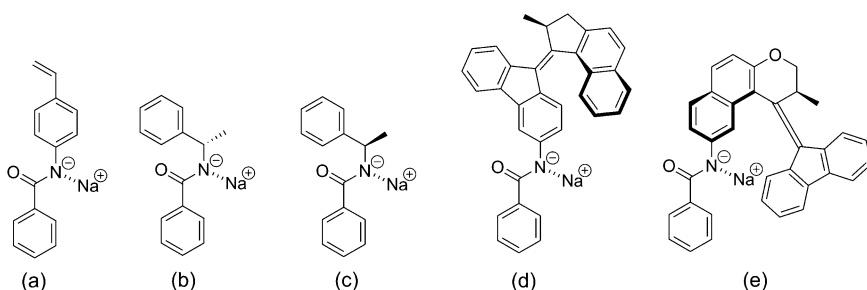
Fig. 6 Examples of sodium benzamide initiators with functionality: (**a**) Sodium N-(4-vinylphenyl)benzamide, (**b**) sodium (S)-N-(1-phenylethyl)benzamide, (**c**) sodium (R)-N-(1-phenylethyl)benzamide, (**d**) sodium (2'S)-(M)-cis-1-N-(9-(2-methyl-2,3-dihydrocyclopenta[a]naphthalen-1-ylidene)-9H-fluoren-2-yl)benzamide and (**e**) sodium (2'S)-(P)-N-(1-(9H-Fluoren-9-ylidene)-2-methyl-2,3-dihydro-1H-benzo[f]-chromen-9-yl)benzamide [58, 75–78]

Sodium benzamide initiators with a functional moiety Polymerization of isocyanate using sodium N-(4-vinylphenyl)benzamide generates macromonomers (Fig. 6a) [58, 75]. Because the amidate anions from this initiator and the living chain end do not react with the styryl group, the living nature is maintained during polymerization. Furthermore, the vinyl moiety does not disturb the pentameric aggregation of this initiator in THF. Therefore, the dual function of initiation and protection of the living chain end still proceeds well. Anionic polymerization of HIC using sodium N-(4-vinylphenyl)benzamide in THF at −98 °C generated well-defined PHICs with the molecular weight corresponding to 20 % initiation efficiency.

To synthesize optically active polyisocyanates, the sodium anionic initiators made from chiral benzamides have been used. Anionic polymerization of HIC using sodium (S)- or (R)-N-(1-phenylethyl)benzamide in THF at −98 °C offered the living polymerization like using Na-BA (Fig. 6b, c) [76]. These chiral initiators also formed pentameric

aggregates and both initiated and protected the living chain end, generating living polymer chains. The polymerizations generated chains with 5 times of the calculated molecular weight. Other sodium benzamide initiators containing photo- and thermal-isomerizable chiral units were also used in the anionic polymerization of HIC in THF at $-90\,°C$ under N_2 atmosphere (Fig. 6d, e) [77, 78]. In these cases, the initiation efficiency was not 20 %, most likely because the bulky substituents interrupted the self-aggregation. These bulky initiators might not protect the living chain ends.

7.2 ω-End Functionalization by Functional Terminators

Endcap installation reactions of living polymeric carbanion with electrophilic reagents such as benzyl halide [79] are effective to generate quantitative ω-end-functionalized vinyl polymers at low temperatures. However, an endcapping reaction of the living polyisocyanate requires a more electrophilic agent than a benzyl halide due to the low nucleophilicity of living amidate anions at $-98\,°C$. Increasing the temperature is counterproductive because doing so leads to rapid depolymerization. For quantitative termination, it is important to choose strong enough electrophilic reagents to react with all of the living polymeric amidate anions at $-98\,°C$ within a short time. Acyl chloride is an effective terminator for endcapping reactions of living polyisocyanate anions. The living chain end from the isocyanate quantitatively reacts with the acyl chloride in the presence of a pyridine catalyst in THF at $-98\,°C$. The typical procedure for an endcapping reaction of polyisocyanate is described in Scheme 11. The acylpyridinium ion-mediated reaction [80] raises the nucleophilicity of the living polyisocyanate anion and leads to the quantitative introduction of the terminal residue.

Acyl chloride residues are located at either one end or both ends of the polymer chain, depending on the type of initiator. For example, Na-Naph, which is a bidirectional initiator, generates a bidirectionally growing polyisocyanate. The termination reaction with acyl chloride leads to ω,ω-end functionalization. However, Na-BA, which is a monodirectional initiator, generates ω-end-functionalized polyisocyanates after endcapping.

ω-End functionalization of PHICs with various acyl chlorides has been reported by Lee et al. These polymers display ~100 % end-termination efficiency [29, 58, 75].
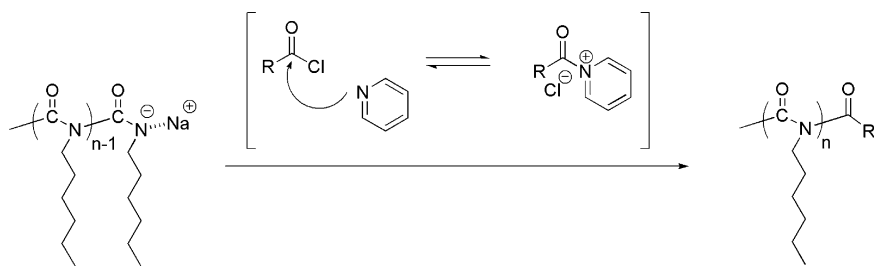
Scheme 11 Endcapping reaction using acyl chloride with the living PHIC end
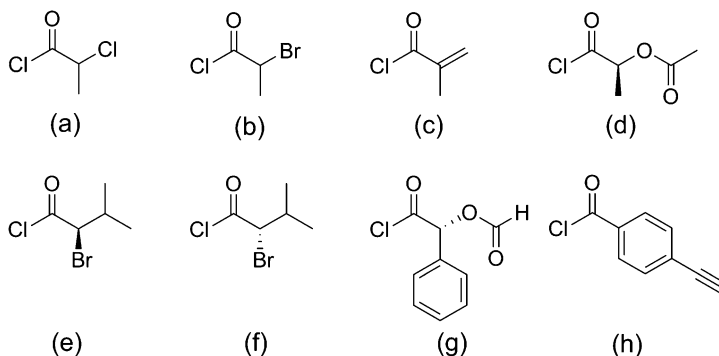
Fig. 7 Examples of acyl chloride terminator with functionality: (**a**) 2-Chloropropionyl chloride, (**b**) 2-bromopropionyl chloride, (**c**) methacryloyl chloride, (**d**) (S)-(−)-2-acetoxypropionyl chloride, (**e**) (S)-2-bromo-3-methylbutyryl chloride, (**f**) (R)-2-bromo-3-methylbutyryl chloride, (**g**) (R)-2-chloro-2-oxo-1-phenylethyl formate and (**h**) 4-ethynylbenzoyl chloride [29, 58, 75, 81]

This reaction method installs a variety of functionalities on the chain end. Several functionalities are suitable for further polymerization to prepare block copolymers (Fig. 7a, b) or graft polymers (Fig. 7c). A chiral residue at the α-position of a polymer chain end induces a one-handed helical sense (Fig. 7d–g). The endcapping of a living poly(phenyl isocyanate) with an aromatic acyl chloride to prepare a macromonomer has been reported by Maeda et al. (Fig. 7h) [81]. Because the aromatic acyl chloride is less reactive than the aliphatic acyl chlorides, the termination efficiency was low and the removal of non-terminated polymer chains was necessary.

7.3 Chain Middle-Functionalization by Difunctional Terminators

Diacyl chlorides have been considered as useful difunctional terminators that couple two living polyisocyanate chains in situ. The in situ coupling generates coil-rod-coil triblock copolymers that cannot be synthesized using the sequential polymerization of an isocyanate and a vinyl monomer. The coil-rod-coil triblock copolymer, poly(2-vinylpyridine)-*block*-poly(*n*-hexyl isocyanate)-*block*-poly(2-vinylpyridine) (P2VP-*b*-PHIC-*b*-P2VP), is synthesized by coupling two living diblock poly(2-vinylpyridine)-*block*-poly(*n*-hexyl isocyanate) (P2VP-*b*-PHIC) amidate anions with malonyl or suberoyl chloride [82]. The active methylene group from the malonyl residue becomes a functional site for further modification at the center of the rod block. For example, a Michael reaction of this coil-rod-coil triblock copolymer with 7-(4-trifuloromethyl) coumarin acrylamide generated a copolymer bearing a fluorescent group in the middle of a rod block with ~94 % conversion. Pendant fullerene (C_{60}) was also introduced to the middle of the rod block using a Bingel reaction with ~54 % conversion [83]. Two chain-centered functionalization reactions are illustrated in Scheme 12.
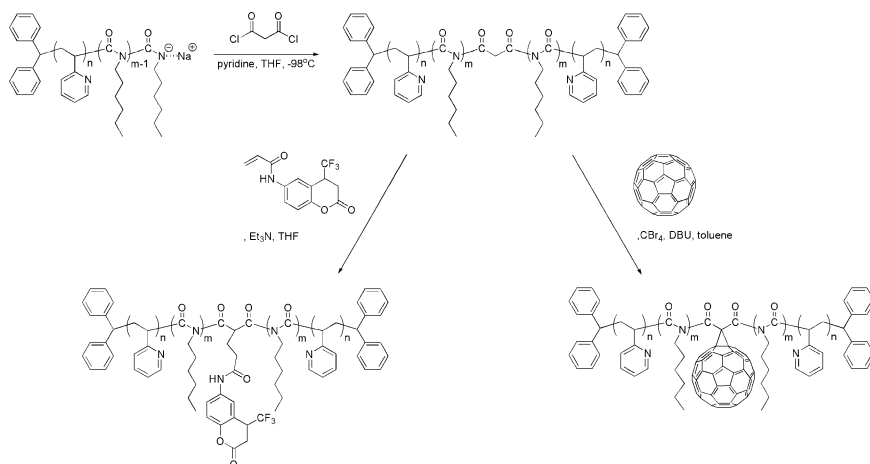
Scheme 12 Endcapping reaction of malonyl chloride and two living P2VP-*b*-PHIC ends, as well as the subsequent functionalization with a coumarin compound or C$_{60}$ in the middle of the rod block (Reproduced with permission from [83]. Copyright 2011 Elsevier.)

8 Synthesis of Side Chain-Functionalized Polyisocyanates

There have been difficulties with the anionic polymerization of vinyl monomers containing a functional moiety because the carbanion encounters competition between propagation reaction with monomers and a side reaction with the functional groups. However, the anionic polymerization of functionalized isocyanates is less restrictive compared to vinyl monomers. The amidate anion from an isocyanate monomer is less nucleophilic than carbanions, leaving a wider range of functional isocyanate monomers available for anionic polymerization. Polymer modification strategies, such as the protection/deprotection method and addition reaction, are also utilized for isocyanates containing protic side chains or other reactive functional groups. In that case, the endcapped polyisocyanate precursor should be used under mild reaction conditions to avoid trimerization during modification reactions.

8.1 Synthesis of Polyisocyanates with Heteroatom Bond

Many polyisocyanates with heteroatom bonds were synthesized using in situ anionic polymerization. Alkyl isocyanates bearing ether, ester, or ketone side groups were polymerized using sodium cyanide in toluene at −78 °C (Fig. 8a–c) [84]. Phenyl isocyanates bearing chiral ester groups (Fig. 8d, e) [45, 46] and chiral alkyl ether groups (Fig. 8f, g) [47] were polymerized using the lithium amide of piperidine in THF at −98 °C. Phenyl isocyanate bearing a crown ether was polymerized using methyl lithium and a lithium amide with a chiral moiety in THF at −78 °C (Fig. 8h) [85, 86]. In the similar method, a α,ω-diisocyanate
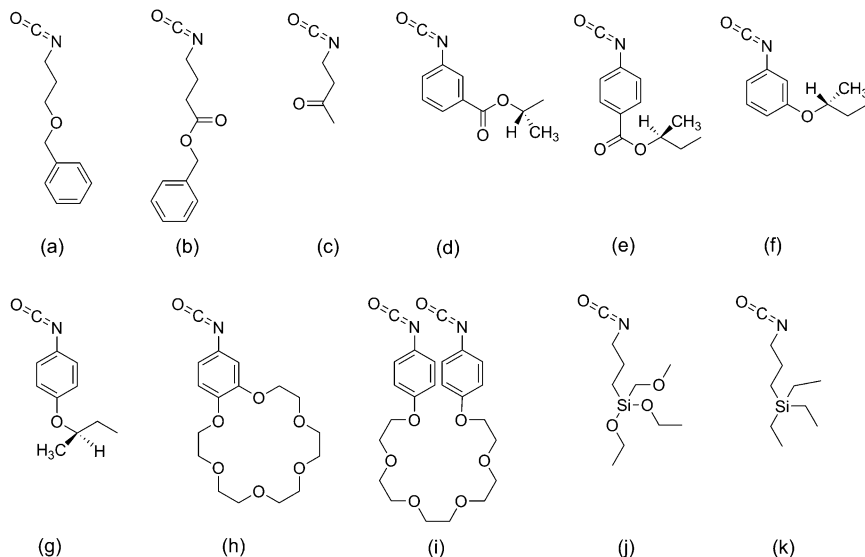
Fig. 8 Examples of isocyanate monomers with heteroatom bonds: (**a**) 3-(Benzyloxy)-*n*-propyl isocyanate, (**b**) 3-(benzyloxycarbonyl)-*n*-propyl isocyanate, (**c**) 4-isocyanato-2-butanone, (**d**) 3-((S)-*sec*-butoxycarbonyl)phenyl isocyanate, (**e**) 4-((S)-*sec*-butoxycarbonyl)phenyl isocyanate, (**f**) 3-((R)-*sec*-butoxy)phenyl isocyanate, (**g**) 4-((R)-*sec*-butoxy)phenyl isocyanate, (**h**) 4'-isocyanatobenzo-18-crown-6, (**i**) 1,14-*bis*(4-isocyanatophenoxy)-3,6,9,12-tetraoxatetradecane, (**j**) 3-(triethoxysilyl)propyl isocyanate and (**k**) 3-(triethylsilyl)propyl isocyanate [31, 45–47, 84–88]

monomer bearing a crown ether was polymerized according to an anionic cyclopolymerization mechanism, to yield the linear poly(phenyl isocyanate) without any insoluble portions (Fig. 8i) [87]. Alkyl isocyanates with a triethoxysilyl group (Fig. 8j) [31] and a triethylsilyl group (Fig. 8k) [88] were polymerized using Na-Naph in THF at −98 °C in the presence of a crown ether and NaBPh$_4$, respectively, generating well-defined polymers in quantitative yield. The bulky side chain on 3-(triethylsilyl)propyl isocyanate stabilized the living anion end, and therefore living polymerization successfully proceeded at −78 °C, which is a unique case [88]. Most of isocyanate monomers listed in Fig. 8 are expected to be polymerized by advanced anionic polymerization techniques (using additives or dual functional initiators) designed by Lee et al. in a living manner.

8.2 Synthesis of Polyisocyanates with Active Hydrogen Side Group

The synthesis of functional protic polyisocyanates bearing hydroxyl (–OH), amino (–NH$_2$), carboxyl (–COOH), amido (–NHCOR), and carbamate (–NHCOOR) side groups has attracted considerable attention. These functionalities can strongly influence the helical structure of the polymer and provide a chance for further
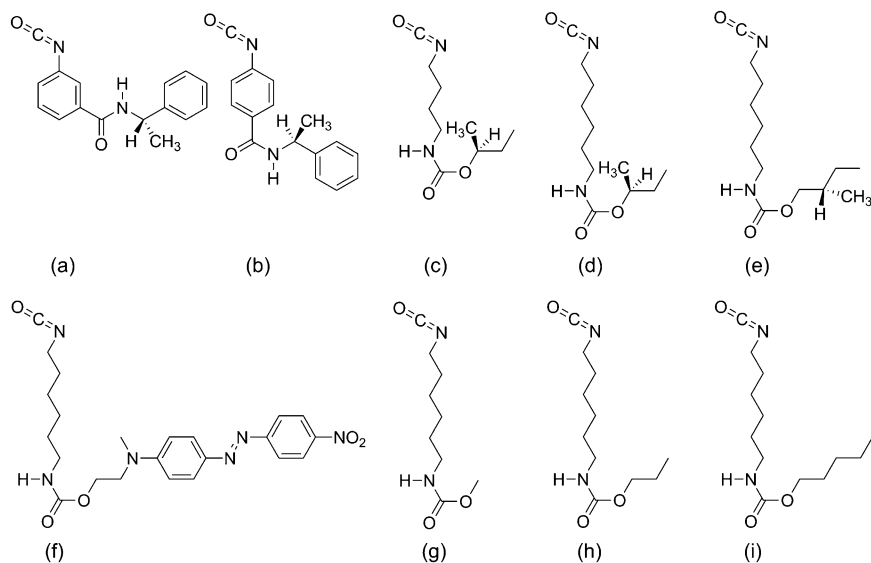
Fig. 9 Examples of isocyanate monomers with active hydrogen side groups: (**a**) 3-((S)-(a-Methylbenzyl)carbamoyl)phenyl isocyanate, (**b**) 4-((S)-(a-methylbenzyl)carbamoyl)phenyl isocyanate, (**c**) 4-((S)-(+)-s-butoxycarbonylamino)butyl isocyanate, (**d**) 6-((S)-(+)-s-butoxycarbonylamino)hexyl isocyanate, (**e**) 6-((S)-(−)-2-methylbutoxycarbonylamino)hexyl isocyanate, (**f**) 6-[2-(4-[4-nitrophenylazo]-N-ethylphenylamino)ethoxycarbonylamino]hexyl isocyanate, (**g**) methoxycarbonylaminohexyl isocyanate, (**h**) n-propyloxycarbonylaminohexyl isocyanate and (**i**) n-pentyloxycarbonylaminohexyl isocyanate [43, 44, 89–94]

functionalization with a variety of organic molecules. However, the construction of well-defined functional polyisocyanates via anionic polymerization has not been carried out in a living system due to inter- and intramolecular side reactions caused by proton abstraction by anionic species.

The anionic polymerization of isocyanates bearing amide groups (Fig. 9a, b) [44] and carbamate groups (Fig. 9c–i) [43, 89–94] using various initiators in THF at −98 °C has been reported. Okamoto et al. achieved moderately controlled polymers using this procedure, but insoluble portions were still obtained due to chain transfer during polymerization (Fig. 9a–d) [43, 44]. Lee et al. reported the anionic polymerization of carbamate isocyanates bearing an azo group and a chiral alkyl group on the side chain using a Na-Naph initiator with 15-crown-5 and NaBPh$_4$ in THF at −98 °C, respectively (Fig. 9e, f) [90, 91]. The resulting polymers were isolated in ~95 % yield and in narrow molecular weight distributions (M_w/M_n ~ 1.28). The bulky side groups and additives prevented chain transfer and led to a living system. Lee et al. also attempted the anionic polymerization of a carbamate isocyanate bearing a simple alkyl group using additives (Fig. 9g–i) [93]. The resulting polymer's molecular weight was uncontrolled and the molecular weight distribution was broad due to chain transfer, even in the presence of the additive.

This chain transfer was more effectively prevented when using Na-BA initiator [94]. Na-BA stabilized the amidate anion by protecting the propagating chain end, reducing the incidence of the chain transfer by proton abstraction. For anionic

Table 8 Anionic polymerization of MAHI, PAHI, and PEAHI using Na-BA in THF at $-98\ ^\circ$C (Data from [94].)

Monomer	Na-BA (mmol)	Monomer (mmol)	Time (mmol)	M_n (kDa) calcd[b]	obsd[c]	M_w/M_n[c]	Yield (%)
MAHI	0.11	6.50	40	10.7			
PAHI	0.12	6.92	60	14.5	16.4	1.18	98
	0.11	6.15	60	14.0	19.8	1.22	95
PEAHI	0.12	4.77	70	10.7	10.9	1.14.	98
	0.12	5.40	70	12.1	12.5	1.11	99
	0.13	9.66	70	19.9	19.1	1.13	98
	0.13	11.6	70	24.5	26.2	1.08	98

[a]The presented number of moles of Na-BA is 20 % of the actual number of moles because the initiation efficiency of Na-BA is 20 %
[b]Number-average molecular weight (M_n) was calculated using the relation {[monomer]/[Na-BA] × (molecular weight of monomer) + (molecular weight of benzanilide)} × yield of polymer/100
[c]M_n and M_w/M_n were measured by SEC-MALLS in THF at 40 $^\circ$C

polymerization using Na-BA, the effects of the alkyl side chain were clearly observed. The results are summarized in Table 8. Polymerization of methoxycarbonylaminohexyl isocyanate (MAHI) and *n*-propyloxycarbonylaminohexyl isocyanate (PAHI) underwent full cross-linkage and partial side reactions, respectively. However, the polymerization of *n*-pentyloxycarbonylaminohexyl isocyanate (PEAHI) maintained a living nature without chain transfer, leading to quantitative yield and predictable molecular weight and narrow molecular weight distributions. The results demonstrated that the steric hindrance provided by longer alkyl group protects the carbamate group and therefore perfectly supports the living polymerization without chain transfer. This situation is visualized in Fig. 10.

The protection/deprotection strategy is another method used for polyisocyanate with protic side groups. Protection/deprotection is carried out according to following procedure: (1) Polyisocyanate bearing protective side groups is synthesized using anionic polymerization, and (2) an endcapping reaction is sequentially carried out. (3) The protective side groups of the precursor polymer are completely removed with a deprotection reaction. Okamoto et al. utilized this method to prepare the poly(phenyl isocyanate) with carboxylic acids in the side chain. As shown in Scheme 13, poly(3-carboxyphenyl isocyanate) was synthesized using the anionic polymerization of 3-(*tert*-butoxycarbonyl)phenyl isocyanate with the lithium amide of piperidine in THF at $-98\ ^\circ$C, followed by the rapid hydrolysis of the *tert*-butyl ester using trifluoroacetic acid [95].

8.3 Synthesis of Polyisocyanates with Reactive Side Group and Its Modification

Polymer modification reactions are a facile and effective approach to functionalize polymers. The diverse reactions include alkyne-azide cycloaddition [96], thiol-ene
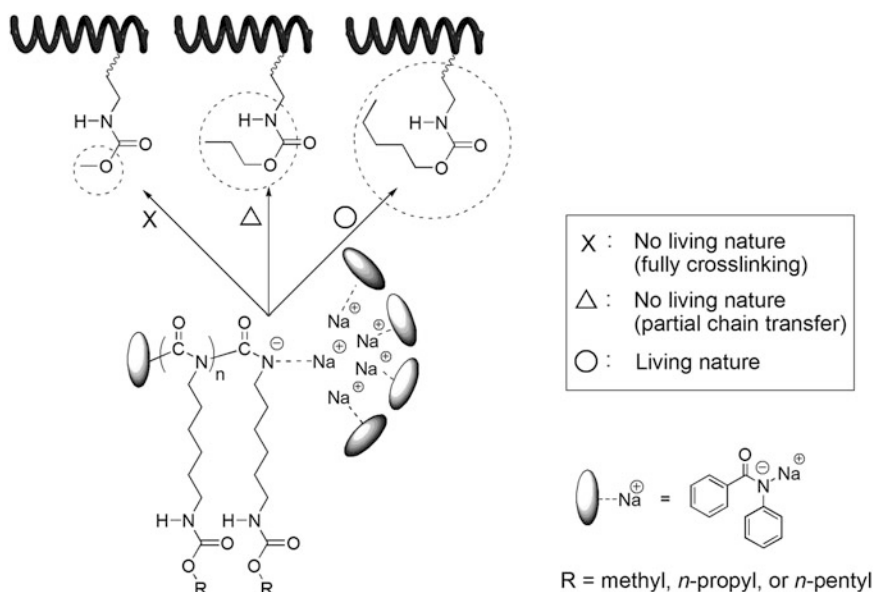
Fig. 10 Dependence on the length of the alkyl side chain in anionic polymerization of carbamate isocyanates (Reproduced with permission from [94]. Copyright 2009 American Chemical Society.)
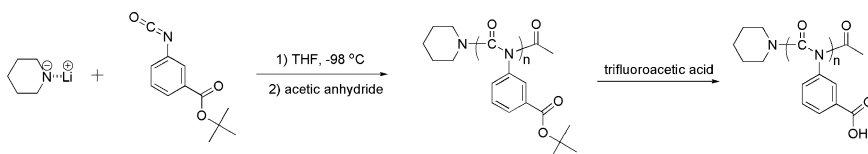
Scheme 13 Anionic polymerization of 3-(*tert*-butoxycarbonyl)phenyl isocyanate and hydrolysis of the protecting group [95]

click reaction [97], and Diels-Alder cycloaddition [98]; these reactions offer ~100 % conversion without degrading the polymers (by the mild reaction conditions) and compatibility with a wide range of functional groups (hydroxy, carboxyl acid, amine, etc.). These reactions have been frequently utilized with controlled polymerizations to prepare functionalized polymers. Until living anionic polymerization of isocyanate was established, however, polymer modification had not attracted an attention. Currently, living polymerization systems using additives or dual functional initiators can make well-defined polyisocyanate precursors for further modification.

Polyisocyanates with reactive furan side group have been investigated. Furan, which is a diene compound, is utilized in the Diels-Alder reaction. Furan undergoes [4 + 2] cycloadditions with the π bonds of various dienophiles, such as maleic anhydride, maleimide, C_{60}, alkene, and alkyne compounds. Gandini et al. attempted to synthesize poly(furfuryl isocyanate) (PFIC) via anionic polymerization, but the resulting polymers were generated in low yield and low molecular weight because
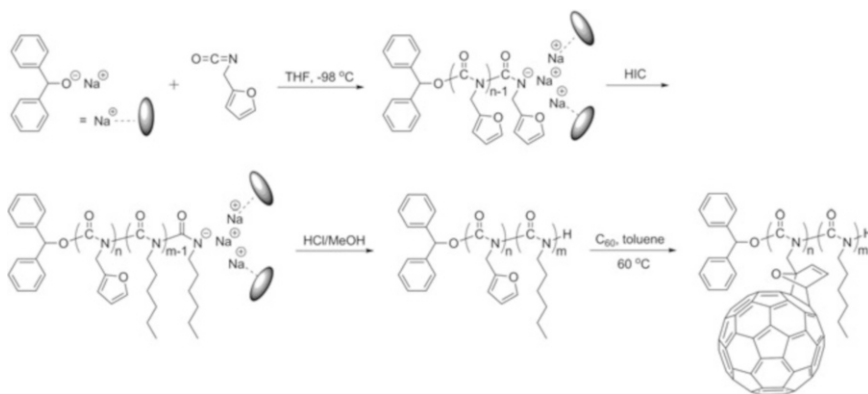
Scheme 14 Synthesis of PFIC-*b*-PHIC via sequential living anionic polymerization and a subsequent Diels-Alder reaction with C_{60} (Reproduced with permission from [100]. Copyright 2012 John Wiley and Sons.)

trimerization dominated [99]. Lee et al. synthesized well-defined PFIC with living anionic polymerization using Na-BH in THF at -98 °C [100]. The sequential addition of *n*-hexyl isocyanate provided poly(furfuryl isocyanate)-*block*-poly(*n*-hexyl isocyanate) (PFIC-*b*-PHIC) with a unimodal molecular weight distribution and the desired composition ratio. The addition of C_{60} with furan in the block copolymer with a Diels-Alder reaction resulted in ~50 % conversion. The procedure is shown in Scheme 14.

9 Synthesis of Rod-Coil Block Copolymers of Isocyanates

The inherent immiscibility between different blocks of a block copolymer raises the microphase separation, forming periodic arrangements, such as spheres, lamellas, cylinders, and gyroids. Block copolymers that contain a flexible coil block and a rigid rod block may form unexpected self-organized structures. The self-assembly of rod-coil block copolymers has potential applications for size-controlled nanoparticles, nanoporous membranes, and periodically patterned films. Because polyisocyanates have stiff and rodlike conformations in the solid and solution state, they exhibit unique self-assembly behaviors, such as liquid crystalline ordering and uniform nanostructure formation from the block copolymer [101, 102]. The supramolecular architectures are largely predicted depending on the relative volume fraction and molecular weight of each block [103], as well as the uniformity of polymer chain. Two synthetic routes for rod-coil block copolymers consisting of polyisocyanate blocks have been reported: (1) sequential addition of monomers in anionic polymerization and (2) combination of another controlled polymerization.

9.1 Block Copolymerization by Sequential Monomer Addition

In the living manner, the living chain end is reactive, even after the completion of polymerization. It can react with a second monomer, forming a well-defined block copolymer. The synthesis of a block copolymer via sequential anionic polymerization depends on the reactivity of the two feeding monomers [104]. A more reactive monomer toward a nucleophile forms a less nucleophilic anion after addition reaction. Generally, less reactive monomer is added first so that second monomer can be added to whole living chains homogeneously. Isocyanate is highly reactive compared to most common vinyl monomers. The living amidate anion is not nucleophilic enough to react with a vinyl monomer. For block copolymerization with a vinyl monomer, the vinyl monomers must be polymerized first so that the living carbanions can initiate the polymerization of the isocyanate monomers homogeneously. The reverse sequence is impossible [13].

Because the living anionic polymerizations of isocyanates were established, the synthesis of well-defined rod-coil block copolymers consisting polyisocyanates has progressed rapidly. The living carbanion generated by anionic polymerization of a vinyl monomer in THF at -78 °C undergoes sequential polymerization when an isocyanate is added as a second monomer in the presence of excess $NaBPh_4$ at -98 °C. In that case, $NaBPh_4$ replaces existing counter cations with Na^+ and prevents trimerization. The resultant block copolymers exhibit quantitative yield and predictable molecular weight and narrow molecular weight distributions.

Well-defined rod-coil-rod triblock copolymers of n-hexyl isocyante with vinyl monomers have been synthesized via living anionic polymerization using M-Naphs by Lee et al. Homopolymerization of vinyl monomers, such as styrene and isoprene, using the appropriate M-Naph forms *bis*-carbanions that grow bidirectionally, and the sequential polymerization with HIC yields rod-coil-rod triblock copolymers [32, 105]. An amphiphilic rod-coil-rod triblock copolymer, poly(n-hexyl isocyanate)-*block*-poly(2-vinylpyridine)-*block*-poly(n-hexyl isocyanate) (PHIC-*b*-P2VP-*b*-PHIC), is synthesized using the anionic polymerization of 2VP and HIC as illustrated in Scheme 15 [106]. Hadjichristidis et al. synthesized pentablock terpolymers of HIC with styrene and isoprene in the same manner [107].

Amphiphilic rod-coil diblock copolymers and rod-coil-rod triblock copolymers are synthesized by the following procedure shown in Scheme 16 [82, 108]. Living P2VP carbanions formed by the anionic polymerization of 2VP with diphenylmethyl potassium (DPM-K) extends the chain monodirectionally after the HIC is added. Termination by protonation of the growing chain end generates rod-coil diblock copolymers [108]. A coupling reaction using malonyl chloride as a difunctional terminator generates coil-rod-coil triblock copolymers [82]. Rod-coil-rod tri-, rod-coil di-, and coil-rod-coil triblock copolymers each exhibit different domain positions, significantly influencing self-assembly.
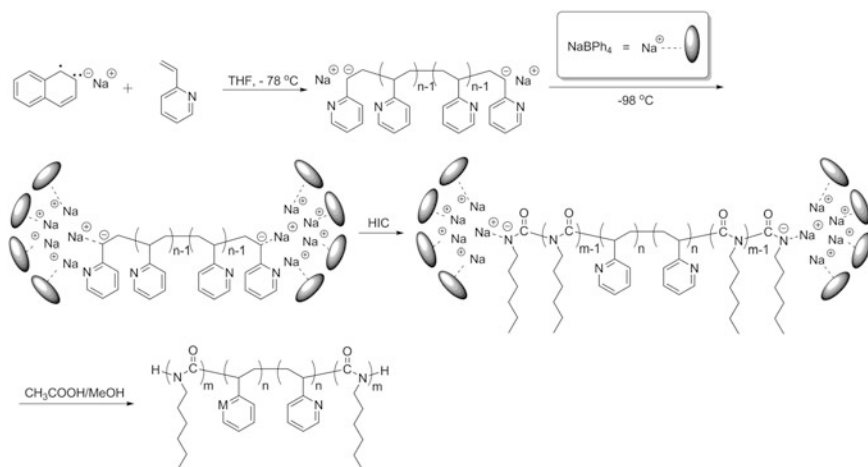
Scheme 15 Synthesis of PHIC-*b*-P2VP-*b*-PHIC rod-coil-rod triblock copolymer via sequential living anionic polymerization (Reproduced with permission from [106]. Copyright 2006 American Chemical Society.)
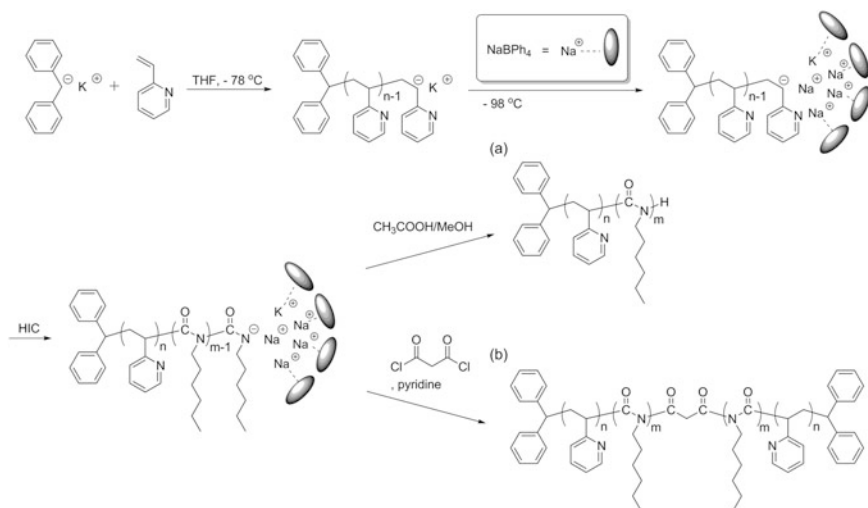
Scheme 16 Synthesis of (**a**) P2VP-*b*-PHIC coil-rod diblock copolymer and (**b**) P2VP-*b*-PHIC-*b*-P2VP coil-rod-coil triblock copolymer via sequential living anionic polymerizations (Reproduced with permission from [82, 108]. Copyright 2007 American Chemical society and 2004 John Wiley and Sons, respectively.)

9.2 Block Copolymerization in Combination with Another Controlled Polymerization

A variety of controlled polymerization methods are utilized to prepare controlled block copolymers. The monomer choice depends on each polymerization
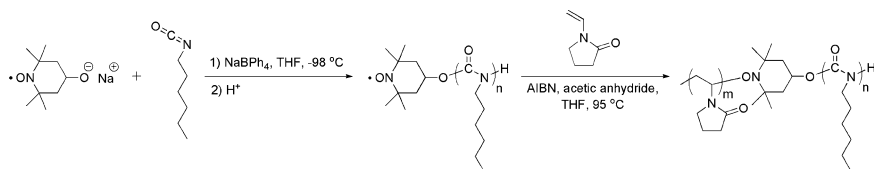
Scheme 17 Synthesis of PHIC-*b*-PVP rod-coil block copolymer via anionic polymerization and nitroxide-mediated radical polymerizations (Reproduced with permission from [109]. Copyright 2006 John Wiley and Sons)
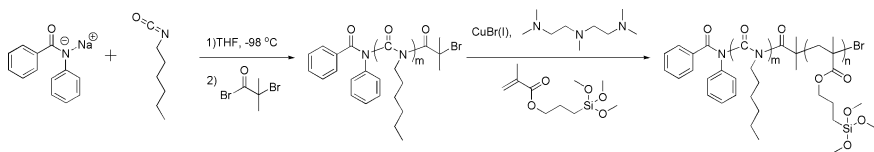
Scheme 18 Synthesis of PHIC-*b*-PTMSPMA via living anionic polymerization and atom transfer radical polymerization (Reproduced with permission from [110]. Copyright 2011 American Chemical Society)

mechanism. The range of monomers available for anionic polymerization is highly limited. It restricts the synthesis of block copolymers with a wide range of monomer combination. In some cases, block copolymerization by combining two different types of controlled polymerization is encouraged.

Hadjichristidis et al. reported switching the polymerization mechanism from one type to another by using a difunctional initiator compatible with two different polymerization methods. For example, poly(*n*-hexyl isocyanate)-*block*-poly(*N*-vinylpyrrolidone) (PHIC-*b*-PVP) was synthesized by combining anionic and nitroxide-mediated radical polymerization, as shown in Scheme 17 [109]. The used difunctional initiator contains both an anionic and radical species. In the detailed procedure, sodium-4-oxy-2,2,6,6-tetramethylpiperidinyloxy (TEMPO-ONa) initiated anionic polymerization of HIC in the presence of excess NaBPh₄ in THF at −98 °C to make the PHIC. The isolated homopolymer was used as a macroradical for the nitroxide-mediated radical polymerization of *N*-vinylpyrrolidone (VP) using 2,2′-azobisisobutyronitrile (AIBN). The resultant block copolymerization exhibited a shift to a higher molecular weight and a unimodal molecular weight distribution without a trace of macroradical. Therefore, the nitroxide radical end group of a homopolymer chain was proved to participate in a sequential radical polymerization with VP to generate a homogeneous block copolymer.

Lee et al. synthesized poly(*n*-hexyl isocyanate)-*block*-poly(3-(trimethoxysilyl) propyl methacrylate) (PHIC-*b*-PTMSPMA) via living anionic polymerization and atom transfer radical polymerization [110]. As shown in Scheme 18, a PHIC macroinitiator was synthesized using the living anionic polymerization of HIC with Na-BA in THF at −98 °C, followed by quantitative endcapping with 2-

bromoisobutanoyl bromide. ω-Functionalized PHIC was used for subsequent atom transfer radical polymerization with (3-trimethoxysilyl)propyl methacrylate (TMSPMA) in toluene at 35 °C to yield the diblock copolymer (coil fraction ~10 %) with a unimodal molecular weight distribution.

10 Synthesis of Nonlinear Polyisocyanates

Fundamental exploration of nonlinear polymers is an important research area. Architectures distinguishable from linear polymers contribute to the difference of properties, including segmental density, crystallinity, viscosity, and other physical properties. Living anionic polymerization is the most ideal method to prepare star polymers and graft copolymers with predictable molecular weights and narrow molecular weight distributions. The features of the non-dissipating living anion ends and quantitative end functionalization through reactions with linking reagents can precisely modify the structure of polymers. The synthesis of nonlinear polymers consisting of rodlike polyisocyanates has become more popular because living polymers are now available. Some reports describe efficient routes to synthesize star-branched (co)polymers, miktoarm star copolymers, and graft copolymers consisting of polyisocyanate chains.

10.1 Synthesis of Star Polymers with Polyisocyanates

The in situ methodology to synthesize star polymers is classified into three different techniques: the use of (1) a multifunctional initiator, (2) a divinyl monomer, and (3) a multifunctional linking reagent. With the two former techniques, star polymers are synthesized via living polymerization initiated by the multifunctional anionic cores ("core-first" approach). The rest involves the termination reaction of living polymer arms with linking reagents possessing the appropriate functionalities ("arm-first" approach). The in situ synthesis of star polymers containing polyisocyanate arms via arm-first approach remains a challenge. The in situ arm-first approach requires a rapid reaction of the living polyisocyanate anions and a multifunctional terminator to avoid trimerization. However, most multifunctional terminators require long reaction times due to steric effects. The effective multifunctional linking reagent may need to possess their ability of both in situ couplings of living polymers and sequential linking reaction with other polymers. Hadjichristidis et al. and Lee et al. reported well-defined star-shaped homopolymers, block copolymers, and miktoarm copolymers containing PHIC arms via anionic polymerization using the divinyl monomer and several linking reagents [111, 112].
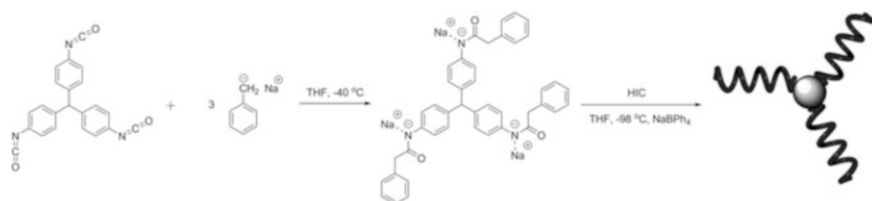
Scheme 19 Synthesis of a three-armed star polymer of PHIC via living anionic polymerization using a trifunctional initiator (Reproduced with permission from [111]. Copyright 2007 John Wiley and Sons)

Multifunctional initiators An anionic initiator with a specific number of functionalities is employed to initiate anionic polymerization, leading to formation of a growing star-shaped chain. Three-arm star-shaped PHIC was synthesized using the trifunctional initiator displayed in Scheme 19 [111]. The trifunctional initiator was prepared through a reaction of *tris*(4-isocyanatrophenyl)methane with a stoichiometric quantity of benzyl sodium in THF at −40 °C. The resulting initiator molecule possessed the three amidate anions. HIC was polymerized with this trifunctional initiator in the presence of NaBPh₄ in THF at −98 °C. After anionic polymerization, a relatively high yield and narrow molecular weight distribution were obtained. The structure of the three-armed star polymer was confirmed by contrasting its intrinsic viscosity between the resulting polymer and the linear polymer.

Divinyl monomers The reaction of a nucleophilic anionic initiator with a slightly large excess of divinyl monomer creates a tightly cross-linked core with a specific number of anions. The multifunctional anion core acts as an initiator for the synthesis of star polymers. Although the number of functionalities is not precisely predicted in this method, it is approximately adjusted by varying the molar ratio of divinyl monomer to initiator. The number of functionalities in the resulting star polymers is determined by differences between the observed degree of polymerization and the molar ratio of monomer to initiator.

The multiarmed star PHIC was synthesized by using 1,4-divinylbenzene (1,4-DVB) as shown in Scheme 20a [111]. The multifunctional initiator was prepared by reacting benzyl sodium initiator and a suitable amount of 1,4-DVB in THF at −40 °C. The anionic polymerization of HIC in the presence of NaBPh₄ in THF at −98 °C generated the multiarmed star PHIC. The star-shaped rod-coil block copolymers have been synthesized via sequential anionic polymerization of a vinyl monomer and an isocyanate using this multifunctional initiator as shown in Scheme 20b [111]. The multifunctional initiator formed from 1,4-DVB polymerized isoprene as a first monomer in THF at −60 °C, followed by HIC as a second monomer in the presence of NaBPh₄ at −98 °C, leading to multiarmed star block copolymers containing polyisoprene-*block*-poly(*n*-hexyl isocyanate) (PI-*b*-PHIC) arms.

The miktoarm star copolymers (A_nB_n) are frequently synthesized using 1,4-DVB. The linking reaction of linear living polymer with 1,4-DVB generates a
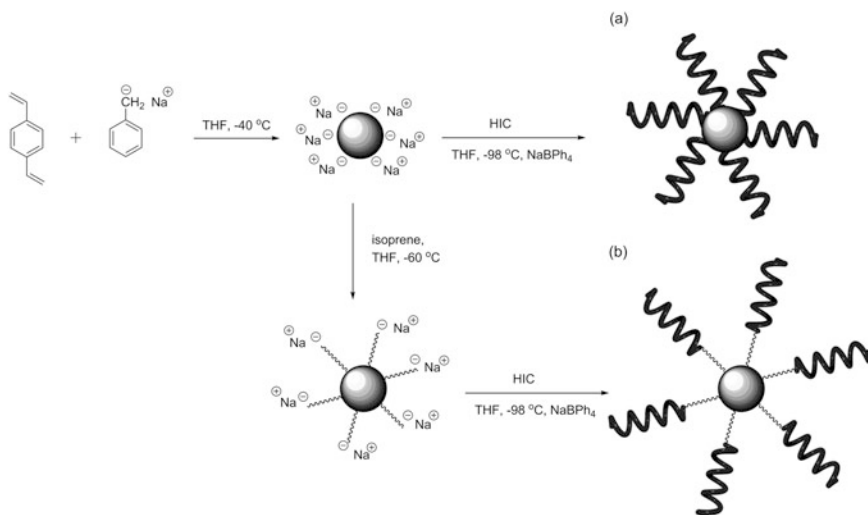
Scheme 20 Synthesis of (**a**) multiarmed star polymer of PHIC and (**b**) multiarmed star block copolymer of PI-*b*-PHIC via living anionic polymerization using 1,4-DVB (Reproduced with permission from [111]. Copyright 2007 John Wiley and Sons)

multifunctional initiator bearing polymer arms. The sequential addition of another monomer forms miktoarm star copolymers (A_nB_n). The miktoarm star copolymer of styrene and HIC was synthesized by linking a living PS anion with a suitable amount of 1,4-DVB to form the multifunctional PS core, followed by the sequential polymerization of HIC, as shown in Scheme 21 [111].

Multifunctional linking reagents Lee et al. synthesized a miktoarm star copolymers of PHIC and poly(ethylene glycol) (PEG), which are shown in Scheme 22 [112]. In this manner, malonyl chloride acts as a multifunctional linking reagent for both in situ coupling of two living PHIC chains and the linking reaction of PHIC and PEG via the Michael reaction. The coupling of two living PHICs using malonyl chloride proceeded after living anionic polymerization. The active methyl group of the malonyl residue in the middle of PHIC underwent the Michael reaction with monomethacrylate and dimethacrylate PEG under basic condition, leading to yield of well-defined miktoarm star copolymers with A_2B and A_2BA_2 structures, respectively.

10.2 Synthesis of Graft Copolymers with Polyisocyanates

Synthesis of graft copolymers is classified into "grafting through," "grafting from," and "grafting onto." "Grafting through" polymerizes a macromonomer. "Grafting from" initiates the polymerization of a second monomer at functional repeating
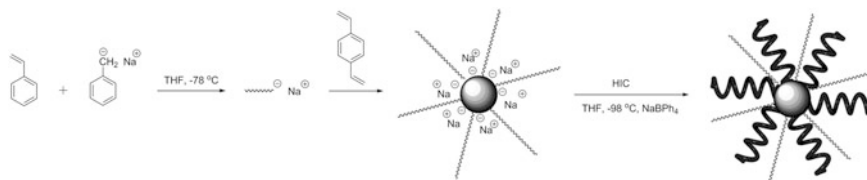
Scheme 21 Synthesis of miktoarm star copolymer of PS and PHIC via living anionic polymerization using 1,4-DVB (Reproduced with permission from [111]. Copyright 2007 John Wiley and Sons)
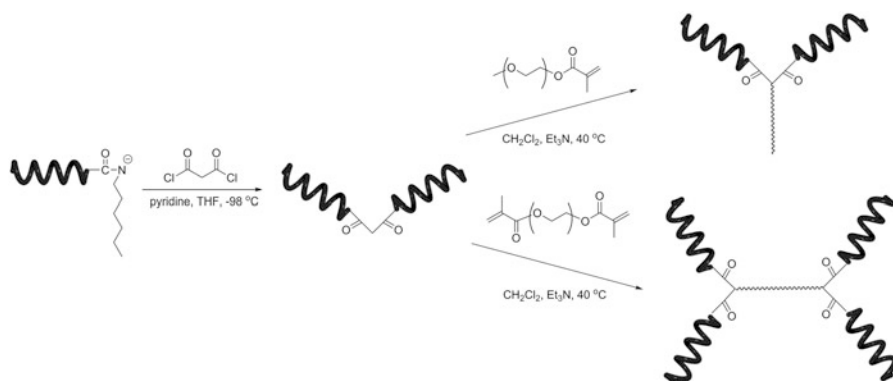
Scheme 22 Synthesis of miktoarm star copolymers PEG and PHIC via living anionic polymerization using malonyl chloride and Michael reaction (Reproduced with permission from [112]. Copyright 2008 American Chemical Society)

sites in the backbone to extend branches. "Grafting onto" involves the coupling reaction of the backbone polymer and branch polymers. The graft copolymers containing well-defined polyisocyanate branches have been mostly synthesized by the "graft through" method. The "graft through" process combines with the living polymerization to prepare macromonomers with predictable and homogeneous branch lengths. The methods to introduce a polymerizable group to the polymer chain end in living anionic polymerization use a functional initiator (α-end functionalization) or a functional terminator (ω-end functionalization).

An example of the graft copolymerization of the polyisocyanate macromonomer with a polymerizable group at α-end of polymer chain is described in Scheme 23 [75]. Chiral PHIC macromonomer was synthesized via living anionic polymerization using sodium N-(4-vinylphenyl)benzamide bearing a polymerizable styryl group and a chiral terminator. The resulting macromonomer was polymerized via free radical polymerization using AIBN initiator, leading to graft copolymers containing PS backbone and chiral PHIC side branches, polystyrene-*graft*-poly(*n*-hexyl isocyanate) (PS-*g*-PHIC).

The graft copolymerization of the polyisocyanate macromonomer with a polymerizable group at the ω-end has also been reported. As shown in Scheme 24,
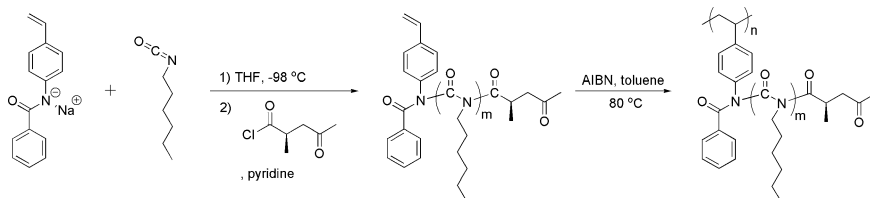
Scheme 23 Synthesis of PS-*g*-PHIC graft copolymer via living anionic polymerization and free radical polymerization (Reproduced with permission from [75]. Copyright 2011 American Chemical Society)
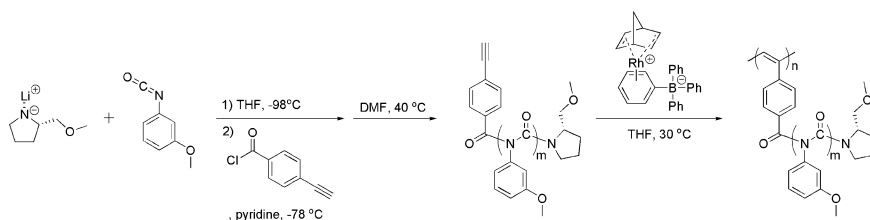
Scheme 24 Synthesis of PPA-*g*-P3MeOPI graft copolymer via anionic polymerization and rhodium-catalyzed polymerization (Reproduced with permission from [81]. Copyright 2012 Royal Society of Chemistry)

poly(phenyl isocyanate) macromonomers with a polymerizable phenylacetylene end group were synthesized by anionic polymerization of 3-methoxyphenyl isocyanate (3MeOPI) using chiral lithium amide initiator, followed by end capping with 4-ethynylbenzoyl chloride [81]. This polymerization was not living system, and the end-caption was also not quantitative due to insufficient reactivity of the living aromatic polyisocyanate end and aromatic acid chloride. Therefore, the uncapped polymer chains had to be completely removed by selective depolymerization. The prepared macromonomers were polymerized by using Rh^+(2,5-norbornadiene)[(η^6-C_6H_5)B^-(C_6H_5)$_3$] (Rh(nbd)BPh$_4$) catalyst, leading to the graft copolymers of poly (phenylacetylene) (PPA) bearing chiral poly(phenyl isocyanate) side branches, poly (phenyl acetylene)-*graft*-poly(3-methoxyphenyl isocyanate) (PPA-*g*-P3MeOPI).

11 Development of Structural Studies in Well-Defined Polyisocyanates

The rodlike and helical properties of polyisocyanates have been considered intriguing structural characteristic. Their macroscopic helical conformation is similar to structural features of biological macromolecules such as DNA, RNA, and proteins. Because the sophisticated control of helical conformation is an important key to determine physiological functions involving signal transmission and recognition,

polyisocyanate as bioinspired model material is worth investigating its helical properties. Interestingly, the introduction of the chirality in the polymers offers the long-range control of helical conformation in polyisocyanate. Polyisocyanate also exhibits the unique morphological aspect involving self-assembly and liquid crystalline ordering of rod-coil block copolymers containing polyisocyanates.

Past findings on the helicity and the morphology from homo- and rod-coil block copolymers with polyisocyanates were inconsistent, due to the absence of precise control of molecular architecture in polymer synthesis. Because these properties are highly dependent upon the molecular weight and molecular weight distribution, the preparation of well-defined polyisocyanates by living polymerization is essential for systematic investigation of these properties. Recent living anionic polymerization techniques have provided high-quality polyisocyanates. These have brought rapid development in the definition of the helical and morphological properties of polyisocyanates. Many examples of experiments using controlled polyisocyanates are briefly described in this section.

11.1 Chiroptical Properties of Polyisocyanates

The dynamic helical conformation of optically active polyisocyanate is a structural motif that mimics biopolymers and performs the translation of macromolecular stereochemistry. A number of studies related to polyisocyanates have focused on examining helical properties. Chiral attachment into the polymer to induce a preferred one-handed helical sense in polyisocyanate led to several discoveries, including the cooperative effect, the sergeants and soldiers principle, and the majority rules. Optical activity in polyisocyanate is highly dependent on the molecular weight of the polymer. Modular quantification of helicity through CD measurement requires sophisticated control of molecular weight of the polyisocyanate. In the past, there has been little consistency during the analysis of optical activity of polyisocyanates due to difficulties in controlling the molecular weight using classical anionic polymerization.

After the elaborate design of a molecular weight scale via living anionic polymerization became possible, new helicity induction phenomena have been discovered. Chiral benzamide initiators and chiral acyl chloride terminators offered quantitative attachment of chiral residues at the α- and ω-ends of the polymer chain. CD spectra of chirally terminated PHICs with varying molecular weights indicated that a terminal chiral moiety in the PHIC chain induced a one-handed helical sense of up to 36 monomer units (up to 5.0 kDa M_n). This outcome is the result of helicity induction corresponding to the CCD effect [29, 76].

Graft copolymerization of a PHIC macromonomer containing a styryl end and a chiral end yielded PS-g-PHIC. CD spectra showed that the graft copolymers possessed the opposite helical sense compared to the chiral macromonomer. This finding was attributed to the "double covalent chiral domino effect (DCCD effect)"

of the coupled PHIC chain containing chiral moieties at both ends and covalent linkage in the middle of the chain [75].

PHIC synthesized using a chiral benzamide initiator, in which a chiral residue is located in the α-position to an *N*-atom end of polymer chain, exhibited kinetically stable helical behavior (static helical conformation). On the other hand, PHIC synthesized using a chiral terminator, in which a chiral residue is located at the α-position to a *C*-atom end, showed thermodynamically stable helical behavior (dynamic helical conformation). When chirality was introduced to the polymer using both chiral initiator and chiral terminator, the resulting polymer showed an one-handed helical conformation up to 7.2 kDa M_n according to the DCCD effect. Furthermore, the overall helical sense was determined by the chirality of the initiator, and the chirality of the terminator only supported the helical sense ("governing initiation-supporting termination," the GIST effect) [76].

PHIC synthesized using Na-Naph and chiral terminator contains two chiral residues at both the *C*-atom ends of the polymer chain and the covalent linkage in the middle of the polymer chain. This polymer showed a dynamic helical conformation with the 12.0 kDa M_n according to the DCCD effect. As an effect of the covalent linkage, PHIC containing chiral moieties at both *C*-atom ends of the polymer chain possessed the opposite helical sense compared with PHIC containing a chiral moiety at one *C*-atom end of the polymer chain [113].

11.2 Morphology of Polyisocyanate-Based Rod-Coil Block Copolymers

Well-defined rod-coil block copolymers synthesized by living anionic polymerization were utilized for studies on the morphology of these block copolymers. To observe the transition of the microphase separation and self-assembly, the domain length and the volume fraction of each block were varied by controlling the molecular weight of each block based on the feed ratio of the monomer and initiator. Well-defined rod-coil-rod triblock copolymers of HIC with styrene, isoprene, or 2VP displayed periodic patterns such as lamellar and cylindrical in the film casting, which were strongly variable depending on the composition ratio of block copolymers [32, 105, 106]. The morphology in rod-coil diblock and coil-rod-coil triblock copolymers of 2VP and HIC was investigated to confirm the effect of composition type [82, 108].

Amphiphilic rod-coil block copolymers exhibit more complicated morphological aspects. The immiscibility between each block and the different affinity of each block to a certain solvent strongly promote the phase separation. Furthermore, the transition of self-assembly in these bock copolymers is induced by varying not only the molecular weight of each block but also the solvent composition. The amphiphilic rod-coil-rod PHIC-*b*-P2VP-*b*-PHIC triblock copolymer exhibited different micellar structures depending on the solvent type. The triblock copolymer formed

the solid micelle with a coil core in chloroform as a rod-selective solvent, whereas it formed the hollow micelles with a rod core in methanol as a coil-selective solvent [106]. The coil-rod P2VP-*b*-PHIC diblock copolymer formed intermicellar-chained and cylindrical micellar networks in a chloroform/THF mixed solvent. The addition of THF to the polymer in chloroform solution led to intermicellar fusion due to the thermodynamic instability of spherical micelles [114]. In the THF/water mixed solvent, P2VP-*b*-PHIC showed the transformation of the solid micelle into the bilayered vesicle, as water content increased. After the degradation of rod block under basic pH, a hollow vesicle remained intact [115]. In the rod-selective solvent, P2VP-*b*-PHIC showed a chain-wrapped micelle and vesicle, in which rod chains wrapped tangentially to the curved interface of the coil core [116].

The liquid crystalline nature of stiff and rodlike polyisocyanate influences the self-organization of the rod-coil block copolymer containing a polyisocyanate block. The several liquid crystalline morphology of the P2VP-*b*-PHIC emerged in the coil-attractive substrate. Vapor annealing using different solvents made a liquid crystalline monolayer or bilayer with long-range-ordered, smectic-on-nematic biphasic sheets [117, 118]. A monolayer of rod-coil PHIC-*b*-PTMSPMA self-organized in the substrate reactive with coil block, displaying nematic liquid crystalline ordering [110].

12 Summary

Since the first discovery of feasible synthesis of polyisocyanate via anionic polymerization in 1959, it was hard to find the living nature in anionic polymerization of isocyanate due to trimerization. After much effort, special anionic polymerization systems have been invented, finally resulting in an excellent living nature including quantitative yield and predictable molecular weight and narrow molecular weight distributions. The living mechanism is mainly related to stabilization of living chain end. Additives such as 15-crown-5 and NaBPh$_4$ protected the living chain end from trimerization by induction of the steric hindrance into living chain end. Several low reactive initiators that form intrinsic self-aggregates in solution played a dual function of both initiation and protection of living chain end. The quantitative endcapping reaction using acyl chloride and pyridine catalyst generated end-functionalized polyisocyanates. The living anionic polymerizations combined with the endcapping reaction and other functionalization techniques have led to synthesis of well-defined linear, telechelic, chiral, rod-coil block, star, and graft polyisocyanates. The elaborate molecular design of polyisocyanate has contributed to finding new properties on their helicity and morphology. From chiral polyisocyanate, various helicity phenomena with different effects depending on the type of chiral structures have been found. Self-assembly of amphiphilic rod-coil block copolymers containing polyisocyanate has led to formation of stable nanostructures such as micelles and vesicles in solution as well as the distinctive liquid crystalline ordering in mono- and bilayer film.

Abbreviations

1,4-DVB	1,4-Divinylbenzene
2VP	2-Vinylpyridine
3MeOPI	3-Methoxyphenyl isocyanate
AIBN	2,2′-Azobisisobutyronitrile
C_{60}	Fullerene
calcd	Calculated
CCD effect	Covalent chiral domino effect
CD	Circular dichroism
DCCD effect	Double covalent chiral domino effect
DMF	N,N-Dimethylformamide
DNA	Deoxyribonucleic acid
DPM-K	Diphenylmethyl potassium
GIST effect	Governing initiation-supporting termination effect
HIC	*n*-Hexyl isocyanate
K-Naph	Potassium naphthalenide
Li-Naph	Lithium naphthalenide
M helix	Left-handed helix
MAHI	Methoxycarbonylaminohexyl isocyanate
M_n	Number-average molecular weight
M-Naph	Metal naphthalenide
M_w/M	Molecular weight distribution
M_w	Weight-average molecular weight
Na-BA	Sodium benzanilide
Na-BH	Sodium benzhydroxide
$NaBPh_4$	Sodium tetraphenylborate
Na-DB	Sodium deoxybenzoin
Na-DPM	Diphenylmethyl sodium
Na-Naph	Sodium naphthalenide
obsd	Observed
P helix	Right-handed helix
P2VP	Poly(2-vinylpyridine)
P2VP-*b*-PHIC	Poly(2-vinylpyridine)-*block*-poly(*n*-hexyl isocyanate)
P2VP-*b*-PHIC-*b*-P2VP	Poly(2-vinylpyridine)-*block*-poly(*n*-hexyl isocyanate)-*block*-poly(2-vinylpyridine)
PAHI	*n*-Propyloxycarbonylaminohexyl isocyanate
PEAHI	*n*-Pentyloxycarbonylaminohexyl
PEG	Poly(ethylene glycol)
PFIC	Poly(furfuryl isocyanate)

PFIC-*b*-PHIC	Poly(furfuryl isocyanate)-*block*-poly(*n*-hexyl isocyanate)
PHIC	Poly(*n*-hexyl isocyanate)
PHIC-*b*-P2VP-*b*-PHIC	Poly(*n*-hexyl isocyanate)-*block*-poly(2-vinylpyridine)-*block*-poly(*n*-hexyl isocyanate)
PHIC-*b*-PTMSPMA	Poly(*n*-hexyl isocyanate)-*block*-poly(3-(trimethoxysilyl) propyl methacrylate)
PHIC-*b*-PVP	Poly(*n*-hexyl isocyanate)-*block*-poly(*N*-vinylpyrrolidone)
PI	Polyisoprene
PI-*b*-PHIC	Polyisoprene-*block*-poly(*n*-hexyl isocyanate)
PPA	Poly(phenylacetylene)
PPA-*g*-P3MeOPI	Poly(phenyl acetylene)-*graft*-poly(3-methoxyphenyl isocyanate)
PS	Polystyrene
PS-*g*-PHIC	Polystyrene-*graft*-poly(*n*-hexyl isocyanate)
PTESPI	Poly(3-(triethoxysilyl)propyl isocyanate)
PTMSPMA	Poly(3-(trimethoxysilyl)propyl methacrylate)
PVP	Poly(N-vinylpyrrolidone)
Rh(nbd)BPh$_4$	Rh$^+$(2,5-norbornadiene)[(η^6-C$_6$H$_5$)B$^-$(C$_6$H$_5$)$_3$]
RNA	Ribonucleic acid
SEC	Size exclusion chromatography
SEC-MALLS	Size exclusion chromatography-multiangle laser light scattering
TEMPO-ONa	Sodium-4-oxy-2,2,6,6-tetramethylpiperidinyloxy
TESPI	3-(Triethoxysilyl)propyl isocyanate
THF	Tetrahydrofuran
TMSPMA	3-(Trimethoxysilyl)propyl methacrylate
VP	*N*-Vinylpyrrolidone

References

1. Szwarc M, Levy M, Milkovich R (1956) Polymerization initiated by electron transfer to monomer. A new method of formation of block polymers. J Am Chem Soc 78:2656–2657
2. Szwarc M (1956) 'Living' polymers. Nature 176:1168–1169
3. Shashoua VE (1959) The homopolymerization of monoisocyanates. J Am Chem Soc 81:3156
4. Shashoua VE, Sweeny W, Tietz RF (1960) The homopolymerization of monoisocyanates. J Am Chem Soc 82:866–873
5. Bur AJ, Fetters LJ (1976) The chain structure, polymerization, and conformation of polyisocyanates. Chem Rev 76:727–746
6. Okamoto Y, Nakano T (1994) Asymmetric polymerization. Chem Rev 94:349–372
7. Green MM, Peterson NC, Sato T, Teramoto A, Cook R, Lifson S (1995) A helical polymer with a cooperative response to chiral information. Science 268:1860–1866

8. Okamoto Y (1996) Synthesis, characterization, and application of helical polymers. Macromol Symp 101:343–354
9. Mayer S, Zentel R (2001) Chiral polyisocyanates, a special class of helical polymers. Prog Polym Sci 26:1973–2013
10. Yashima E, Maeda K, Lida H, Furusho Y, Nagai K (2009) Helical polymers: synthesis, structures, and functions. Chem Rev 109:6102–6211
11. Natta G, Dipietro J, Cambini M (1962) Crystalline polymers of phenyl- and *n*-butyliso-cyanates. Makromol Chem 56:200–207
12. Iwakura Y, Uno K, Kobatashi N (1968) Polymerization of isocyanate. III. Chemical behavior and structure of polyisocyanates. J Polym Sci Part A Polym Chem 6:1087–1096
13. Godfrey RA, Miller GW (1969) Block polymers of isocyanates and vinyl monomers by homogeneous anionic polymerization. J Polym Sci Part A Poly Chem 7:2387–2404
14. Schneider NS, Furusaki S (1965) Chain stiffness in polyisocyanates. J Polym Sci Part A Gen Pap 3:933–948
15. Lifson S, Felder CE, Green MM (1992) Helical conformations, internal motion and helix sense reversal in polyisocyanates, and the preferred helix sense of an optically active polyisocyanate. Macromolecules 25:4142–4148
16. Troxell TC, Scheraga HA (1971) Electric dichroism and polymer conformation. II. Theory of electric dichroism, and measurements on poly(*n*-butyl isocyanate). Macromolecules 4:528–539
17. Toneli AE (1974) Conformational characteristics of the poly(*n*-alkyl isocyanates). Macro-molecules 7:628–631
18. Cook R (1987) Flexibility in rigid rod poly(*n*-alkyl isocyanates). Macromolecules 20:1961–1964
19. Cook R, Johnson RD, Wade CG, O'Leary DJ, Munoz B, Green MM (1990) Solvent dependence of the chain dimension of poly(*n*-hexyl isocyanate). Macromolecules 23:3454–3458
20. Ute K, Fukunishi Y, Jha SK, Cheon K-S, Muñoz B, Hatada K, Green MM (1999) Dynamic NMR determination of the barrier for interconversion of the left- and right-handed helical conformations in a polyisocyanate. Macromolecules 32:1304–1307
21. Green MM, Andreola C, Muñoz B, Reidy MP, Zero K (1988) Macromolecular stereochem-istry: a cooperative deuterium isotope effect leading to a large optical rotation. J Am Chem Soc 110:4063–4065
22. Green MM, Reidy MP, Johnson RD, Darling G, O'Leary DJ, Willson G (1989) Macromo-lecular stereochemistry: the out-of-proportion influence of optically active comonomers on the conformational characteristics of polyisocyanates. The sergeant and soldiers experiment. J Am Chem Soc 111:6452–6454
23. Khatri CA, Pavlova Y, Green MM, Morawetz H (1997) Chiral solvation as a means to quantitatively characterize preferential solvation of a helical polymer in mixed solvents. J Am Chem Soc 119:6991–6995
24. Goodman M, Chen S (1970) Optically active polyisocyanates. Macromolecules 3:398–402
25. Goodman M, Chen S (1971) Optically active polyisocyanates II. Macromolecules 4:625–629
26. Gu H, Nakamura Y, Sato T (1998) Optical rotation of random copolyisocyanates of chiral achiral monomers: sergeant and soldier copolymers. Macromolecules 31:6362–6368
27. Green MM, Garetz BA, Munoz B, Chang H (1995) Majority rules in the copolymerization of mirror image isomers. J Am Chem Soc 117:4181–4182
28. Jha SK, Cheon KS, Green MM, Selinger JV (1999) Chiral optical properties of a helical polymer synthesized from nearly racemic chiral monomers highly diluted with achiral mono-mers. J Am Chem Soc 121:1665–1673
29. Nath GY, Samal S, Park S-Y, Murthy CN, Lee J-S (2006) Induction of helicity in poly(*n*-hexyl isocyanate) with terminal chiral residues. Macromolecules 39:5965–5966
30. Caraculacu AA, Coseri S (2001) Isocyanates in polyaddition processes. Structure and reac-tion mechanism. Prog Polym Sci 26:799–851

31. Lee J-S, Ryu S-W (1999) Anionic living polymerization of 3-(triethoxysilyl)propyl isocyanate. Macromolecules 32:2085–2087
32. Ahn J-H, Shin Y-D, Kim S-Y, Lee J-S (2003) Synthesis of well-defined block copolymers of *n*-hexyl isocyanate with isoprene by living anionic polymerization. Polymer 44:3847–3854
33. Iwakura Y, Uno K, Kobayashi N (1968) Polymerization of isocyanates. V. Thermal degradation of polyisocyanates. J Polym Sci Part A Poly Chem 6:2611–2620
34. Durairaj B, Dimock AW, Samulski ET (1989) Investigation of the thermal degradation of alkyl isocyanate polymers by direct pyrolysis mass spectrometry. J Polym Sci Part A Poly Chem 27:3211–3225
35. Se K, Iwata T (2011) Selective complete decomposition of poly(*n*-hexylisocyanate) and its use in a new molecular design method. J Polym Sci Part A Polym Chem 49:3939–3950
36. Lien LTN, Kikuchi M, Narumi A, Nagai K, Kawaguchi S (2008) Preparation of α-, ω-end-functionalized poly(*n*-hexyl isocyanate) heterotelechelics. Polym J 40:1105–1112
37. Bhattacharyya DN, Lee CL, Szwarc M (1965) Reactivities and conductivities of ions and ion pairs in polymerization processes. J Phys Chem 69:612–623
38. Szwarc M (1983) Living polymers and mechanisms of anionic polymerization. Adv Polym Sci 49:1–177
39. Aharoni SM (1979) Rigid backbone polymers. 2. Polyisocyanates and their liquid-crystal behavior. Macromolecules 12:94–103
40. Okamoto Y, Nagamura Y, Hatada K, Khatri C, Green MM (1992) An unexpected chiral spiro tetramer offers mechanistic insight into an improved sodium cyanide initiated polymerization of *n*-hexyl isocyanate in toluene. Macromolecules 25:5536–5538
41. Fetters LJ, Yu H (1971) Equilibrium conformation and "worm-like coil" configuration of poly(*n*-alkyl isocyanates). Macromolecules 4:385–389
42. Bur AJ, Fetters LJ (1973) Intrinsic viscosity measurements on rodlike poly(*n*-butyl isocyanate) and poly(*n*-octyl isocyanate). Macromolecules 6:874–879
43. Maeda K, Matsunaga M, Yamada H, Okamoto Y (1997) Synthesis and anionic polymerization of isocyanates bearing a carbamate group. Polym J 29:333–338
44. Maeda K, Okamoto Y (1998) Synthesis and conformation of optically active poly(phenyl isocyanate)s bearing an ((S)-(α-methylbenzyl)carbamoyl) group. Macromolecules 31:1046–1052
45. Maeda K, Okamoto Y (1998) Unusual conformational change of optically active poly(3-((S)-*sec*-butoxycarbonyl)phenyl isocyanate). Macromolecules 31:5164–5166
46. Maeda K, Okamoto Y (1999) Synthesis and conformational characteristics of poly(phenyl isocyanate)s bearing an optically active ester group. Macromolecules 32:974–980
47. Hino K, Maeda K, Okamoto Y (2000) Synthesis and structure of poly(phenyl isocyanate)s bearing an optically active alkoxyl group. J Phys Org Chem 13:361–367
48. Wang J, Nomura R, Endo T (1996) Effect of samarium iodide on isocyanate-polymerization by alkyllithiums. Chem Lett 25:909–910
49. Fukuwatari N, Sugimoto H, Inoue S (1996) Lanthanoid isopropoxide as a novel initiator for anionic polymerization of isocyanates. Macromol Rapid Commun 17:1–7
50. Pedersen CJ (1967) Cyclic polyethers and their complexes with metal salts. J Am Chem Soc 89:2495–2496
51. Pedersen CJ (1967) Cyclic polyethers and their complexes with metal salts. J Am Chem Soc 89:7017–7036
52. Karkhaneei E, Afkhami A, Shamsipur M (1996) Nuclear magnetic resonance studies of sodium ion complexes with several crown ethers in binary acetonitrile-dimethylsulfoxide mixtures. Polyhedron 15:1989–1994
53. Schmitt VBJ, Schulz GV (1969) Über zwei formen des initiators Na-naphthalin und die bestimmung der „lebenden" kettenenden bei der anionischen polymerisation. Makromol Chem 121:184–204
54. Löhr G, Schulz GV (1974) Kinetics of anionic polymerization of methylmethacrylate with caesium and sodium as counterions in tetrahydrofuran. Eur Polym J 10:121–130

55. Jeuck H, Müller AHE (1982) Kinetics of the anionic polymerization of methyl methacrylate in tetrahydrofuran using lithium and potassium as counterions. Makromol Chem Rapid Commun 3:121–125

56. Shin Y-D, Kim S-Y, Ahn J-H, Lee J-S (2001) Synthesis of poly(n-hexyl isocyanate) by controlled anionic polymerization in the presence of NaBPh₄. Macromolecules 34:2408–2410

57. Zobra G, Vazaios A, Pitsikalis M, Hadjichristidis N (2005) Anionic polymerization of n-hexyl isocyanate with monofunctional initiators. Synthesis of well-defined diblock copolymers with styrene and isoprene. J Polym Sci Part A Polym Chem 43:3533–3542

58. Ahn J-H, Shin Y-D, Nath GY, Park S-Y, Rahman MS, Samal S, Lee J-S (2005) Unprecedented control over polymerization of n-hexyl isocyanate using an anionic initiator having synchronized function of chain-end protection. J Am Chem Soc 127:4132–4133

59. Min J, Yoo H-S, Shah PN, Chae C-G, Lee J-S (2013) Enolate anionic initiator, sodium deoxybenzoin, for leading living natures by formation of aggregators at the growth chain ends. J Polym Sci Part A Polym Chem 51:1742–1748

60. Min J, Shah PN, Ahn J-H, Lee J-S (2011) Effects of different reactive oxyanionic initiators on the anionic polymerization of n-hexyl isocyanate. Macromolecules 44:3211–3216

61. Norman ROC, Norman JM (1993) Principles of organic synthesis, 3rd edn. Sprinder-Verlag, New York

62. Hsieh HL, Quirk RP (1996) Anionic polymerization: principle and practical application. Marcel Dekker, New York

63. Pattern TE, Novak BM (1991) "Living" titanium(IV) catalyzed coordination polymerization of isocyanates. J Am Chem Soc 113:5065–5066

64. Pattern TE, Novak BM (1993) Organotitanium(IV) compounds as catalysts for the polymerization of isocyanates: the polymerization of isocyanates with functionalized side-chains. Macromolecules 26:436–439

65. Pattern TE, Novak BM (1996) Living organotitanium(IV)-catalyzed polymerizations of isocyanates. J Am Chem Soc 118:1906–1916

66. Mourmouris S, Kostakis K, Pitisikalis M, Hadjichristidis N (2005) Polymerization of n-hexyl isocyanate with CpTiCl₂(OR) (R = functional group or macromolecular chain): a route to ω-functionalized and block copolymers and terpolymers of n-hexyl isocyanate. J Polym Sci Part A Polym Chem 43:6503–6514

67. Ishizu K, Hatoyama N, Uchida S (2007) Novel synthesis of rod-coil block copolymers by combination of coordination polymerization and ATRP. J Polym Sci Part A Polym Chem 45:4037–4042

68. Liu X, Deng J, Wu Y, Zhang L (2012) Amphiphilic triblock terpolymers consisting of poly (n-hexyl isocyanate) and poly(ethylene glycol): preparation and characterization. Polymer 53:5717–5722

69. Satoh T, Ihara R, Kawato D, Nishikawa N, Suemasa D, Kondo Y, Fuchise K, Sakai R, Kakuchi T (2012) Precise synthesis of clickable poly(n-hexyl isocyanate). Macromolecules 45:3677–3686

70. Goodson SH, Novak BM (2001) Synthesis and characterization of wormlike three-arm poly (n-hexyl isocyanate) star polymers. Macromolecules 34:3849–3855

71. Miyake GM, Weitekamp RA, Piunova VA, Grubbs RH (2012) Synthesis of isocyanate-based brush block copolymers and their rapid self-assembly to infrared-reflecting photonic crystals. J Am Chem Soc 134:14249–14254

72. Okamoto Y, Matsuda M, Nakano T, Yashima E (1993) Asymmetric polymerization of isocyanates with optically active anionic initiators. Polym J 25:391–396

73. Okamoto Y, Matsuda M, Nakano T, Yashima E (1994) Asymmetric polymerization of aromatic isocyanates with optically active anionic initiators. J Polym Sci Part A Polym Chem 32:309–315

74. Maeda K, Matsuda M, Nakano T, Okamoto Y (1995) Chiroptical properties of oligomers of m-methylphenyl isocyanate bearing an optically active end-group. Polym J 27:141–146

75. Shah PN, Min J, Kim H-J, Park S-Y, Lee J-S (2011) Chiroptical properties of graft copolymers containing chiral poly(*n*-hexyl isocyanate) as a side chain. Macromolecules 44:7917–7925

76. Shah PN, Min J, Lee J-S (2012) "Governing initiation-supporting termination" in chiral poly (*n*-hexyl isocyanate). Chem Commun 48:826–828

77. Pijper D, Feringa BL (2007) Molecular transmission: controlling the twist sense of a helical polymer with a single light-driven molecular motor. Angew Chem Int Ed 46:3693–3696

78. Pijper D, Jongejan MGM, Meetsma A, Feringa BL (2008) Light-controlled supramolecular helicity of a liquid crystalline phase using a helical polymer functionalized with a single chiroptical molecular switch. J Am Chem Soc 130:4541–4552

79. Higashihara T, Hayashi M, Hirao A (2011) Synthesis of well-defined star-branched polymers by stepwise iterative methodology using living anionic polymerization. Prog Polym Sci 36:323–375

80. Kivinen A (1972) In: Patai S (ed) The chemistry of acyl halides. Mechanism of substitution at the COX group. Interscience, New York

81. Maeda K, Wakasone S, Shimomura K, Ikai T, Kanoh S (2012) Helical polymer brushes with a preferred-handed helix-sense triggered by a terminal optically active group in the pendant. Chem Commun 48:3342–3344

82. Rahman MS, Samal S, Lee J-S (2007) Quantitative in situ coupling of living diblock copolymers for the preparation of amphiphilic coil-rod-coil triblock copolymer poly (2-vinylpyridine)-*b*-poly(*n*-hexyl isocyanate)-*b*-poly(2-vinylpyridine). Macromolecules 40:9279–9283

83. Rahman MS, Chengez M, Min J, Shah PN, Samal S, Lee J-S (2011) Functionalization of amphiphilic coil-rod-coil triblock copolymer poly(2-vinylpyridine)-*b*-poly(*n*-hexyl isocyanate)-*b*-poly(2-vinylpyridine) with florescence moiety and C_{60}. Polymer 52:1925–1931

84. Khatri CA, Vaidya MM, Levon K, Jha SK, Green MM (1995) Synthesis and molecular composites of functionalized polyisocyanates. Macromolecules 28:4719–4728

85. Sakai R, Satoh T, Kakuchi R, Kaga H, Kakuchi T (2003) Macromolecular helicity induction for novel optically inactive poly(phenyl isocyanate) bearing crown ether based on the host-guest complexation. Macromolecules 36:3709–3713

86. Sakai R, Otsuka I, Satoh T, Kakuchi R, Kaga H, Kakuchi T (2006) Chiral discrimination of a helically organized crown ether array parallel to the helix axis of polyisocyanate. J Polym Sci Part A Polym Chem 44:325–334

87. Sakai R, Satoh T, Kakuchi R, Kaga H, Kakuchi T (2004) Helicity induction of polyisocyanate with a crown cavity on the main chain synthesized by cyclopolymerization of α, ω-diisocyanate. Macromolecules 37:3996–4003

88. Ahn J-H, Lee C-H, Shin Y-D, Lee J-S (2004) Generation of highly stable amidate anion in anionic polymerization of 3-(triethylsilyl)propyl isocyanate. J Polym Sci Part A Polym Chem 42:933–940

89. Han SH, Wu JW, Kang J-W, Shin Y-D, Lee J-S, Kim J-J (2001) Induced chirality in a polyisocyanate polymeric film and the change in polarization rotation under an external electric field. J Opt Soc Am B 18:298–301

90. Shin Y-D, Ahn J-H, Lee J-S (2001) Anionic polymerization of isocyanates with optical functionalities. Polymer 42:7979–7985

91. Shin Y-D, Ahn J-H, Lee J-S (2001) Anionic polymerization of chiral isocyanate and influence of the initiator on changes in the optical activity. Macromol Rapid Commun 22:1041–1045

92. Chun C, Seo E-M, Kim M-J, Shin Y-D, Lee J-S, Kim D-Y (2007) Photoinduced behaviors of isocyanate-based azo molecular glass and polymer. Opt Mater 29:970–974

93. Shin Y-D, Rahman MS, Samal S, Lee J-S (2006) The effect of alkyl side chain and additives on the anionic polymerization of isocyanates with carbamate group. Macromol Symp 240:151–156

94. Rahman MS, Yoo H-S, Changez M, Lee J-S (2009) Living anionic polymerization of isocyanate containing a reactive carbamate group. Macromolecules 42:3927–3932

95. Maeda K, Yamamoto N, Okamoto Y (1998) Helicity induction of poly(3-carboxyphenyl isocyanate) by chiral acid-base interaction. Macromolecules 31:5924–5926

96. Meldal M, Tornøe CW (2008) Cu-catalyzed azide-alkyne cycloaddition. Chem Rev 108:2952–3015

97. Holye CE, Bowman CN (2010) Thiol-ene click chemistry. Angew Chem Int Ed 49:1540–1573

98. Nicolaou KC, Snyder SA, Montagnon T, Vassilikogiannakis G (2002) The Diels-Alder reaction in total synthesis. Angew Chem Int Ed 49:1540–1573

99. Zuen H, Gandini A (1991) Crystalline furanic polyisocyanate. Polym Bull 26:383–390

100. Min J, Shah PN, Chae C-G, Lee J-S (2012) Arrangement of C60 via self-assembly of post-functionalizable polyisocyanate block copolymer. Macromol Rapid Commun 33:2029–2034

101. Stupp SI (1997) Supramolecular materials: self-organized nanostructures. Science 276:384–389

102. Lee M, Cho B-K, Zin W-C (2001) Supramolecular structures from rod-coil block copolymers. Chem Rev 101:3869–3892

103. Hadjichristidis N, Prispas S, Floudas GA (2003) Block copolymers. Wiley-VCH, New York

104. Fetters LJ (1969) Synthesis of block polymers by homogeneous anionic polymerization. J Polym Sci Part C Polym Symp 26:1–35

105. Ahn J-H, Lee J-S (2003) Synthesis of well-defined rod-coil-rod polyhexylisocyanate-*block*-polystyrene-*block*-polyhexylisocyanate via one-pot anionic polymerization. Macromol Rapid Commun 24:571–575

106. Rahman MS, Samal S, Lee J-S (2006) Synthesis and self-assembly studies of amphiphilic poly(*n*-hexyl isocyanate)-*block*-poly(2-vinylpyridine)-*block*-poly(*n*-hexyl isocyanate) rod-coil-rod triblock copolymer. Macromolecules 39:5009–5014

107. Vazaios A, Pitsikalis M, Hadjichristidis N (2003) Triblock copolymers and pentablock terpolymers of *n*-hexyl isocyanate with styrene and isoprene: synthesis, characterization, and thermal properties. J Polym Sci Part A Polym Chem 41:3094–3102

108. Shin Y-D, Han S-H, Samal S, Lee J-S (2005) Synthesis of poly(2-vinyl pyridine)-*b*-poly(*n*-hexyl isocyanate) amphiphilic coil-rod block copolymer by anionic polymerization. J Polym Sci Part A Polym Chem 43:607–615

109. Bilalis P, Zorba G, Pitsikalis M, Hadjichristidis N (2006) Synthesis of poly(*n*-hexyl isocyanate-*b*-*N*-vinylpyrrolidone) block copolymers by the combination of anionic and nitroxide-mediated radical polymerizations: micellization properties in aqueous solution. J Polym Sci Part A Polym Chem 44:5719–5728

110. Han M, Rahman MS, Lee J-S, Khim D, Kim D-Y, Park J-W (2011) Surface-grafted rodlike polymers: adaptive self-assembled monolayers and rapid photo-patterning of surfaces. Chem Mater 23:3517–3524

111. Zorba G, Pitsikalis M, Hadjichristidis N (2006) Novel well-defined star homopolymers and star-block copolymers of poly(*n*-hexyl isocyanate) by anionic polymerization. J Polym Sci Part A Polym Chem 45:2387–2399

112. Rahman MS, Changez M, Yoo J-W, Lee CH, Samal S, Lee J-S (2008) Synthesis of amphiphilic miktoarm star copolymers of poly(*n*-hexyl isocyanate) and poly(ethylene glycol) through reaction with the active methylene group. Macromolecules 41:7029–7032

113. Shah PN, Min J, Chae C-G, Nishikawa N, Suemasa D, Kakuchi T, Satoh T, Lee J-S (2012) "Helicity inversion": linkage effects of chiral poly(*n*-hexyl isocyanate)s. Macromolecules 45:8961–8969

114. Koh H-D, Changez M, Rahman MS, Lee J-S (2009) Formation of intermicellar-chained and cylindrical micellar networks from an amphiphilic rod-coil block copolymer: poly(*n*-hexyl isocyanate)-block-poly(2-vinylpyridine). Langmuir 25:7188–7192

115. Changez M, Kang N-G, Koh H-D, Lee J-S (2010) Effect of solvent composition on trans-formation of micelles to vesicles of rod-coil poly(*n*-hexyl isocyanate-*block*-2-vinylpyridine) diblock copolymers. Langmuir 26:9981–9985

116. Koh H-D, Park J-W, Rahman MS, Changez M, Lee J-S (2009) Reversibly interchangeable, chain-wrapped micelles and vesicles of an amphiphilic rod-coil block copolymer. Chem Commun 32:4824–4826
117. Kim J-H, Rahman MS, Lee J-S, Park J-W (2007) Liquid crystalline ordering in the self-assembled monolayers of tethered rodlike polymers. J Am Chem Soc 129:7756–7757
118. Kim J-H, Rahman MS, Lee J-S, Park J-W (2008) Self-organization of an amphiphilic rod-coil-rod block copolymer into liquid crystalline, substrate-supported monolayers and bilayers. Macromolecules 41:3181–3189

Poly(ferrocenylsilanes) with Controlled Macromolecular Architecture by Anionic Polymerization: Applications in Patterning and Lithography

Lionel Dos Ramos, Mark A. Hempenius, and G. Julius Vancso

Abstract In this chapter, the versatility of poly(ferrocenylsilanes) (PFSs) as resists in reactive ion etching (RIE) for nanofabrication is presented. PFSs, belonging to the class of organometallic polymers, possess skeletal ferrocene and alkylsilane units which provide these solution-processable materials with a very high RIE resistance. First, it is shown that among the different paths for synthesizing PFS, anionic polymerization creates an opportunity to produce well-defined PFSs with a targeted molar mass and low polydispersity. Block copolymers and more complex structures can also be realized, which leads to exciting openings in maskless self-assembly lithography for nanopatterning. Then, optimization of the etching process, aimed at maximizing aspect ratios for PFS-based resists, is discussed. Next, several micro- and nanofabrication processes, using PFS homopolymers to fabricate nanoscale structures, are demonstrated. Finally, phase separation of PFS block copolymers and their use as self-assembled resists with long-range guided order in nanolithography is discussed. With this technique, various nanopatterns useful for CMOS design could be obtained.

Keywords CMOS • Poly(ferrocenylsilane) • Anionic polymerization • Nanolithography • Microphase separation • Self-assembly • Epitaxy

1 Introduction

Complementary metal oxide semiconductor (CMOS) is a technology that was patented in 1967 by Frank Wanlass [1]. It is used to construct integrated circuits, such as microprocessors, microcontrollers, static RAM, and other digital logic circuits. CMOS technology is also used for analog circuits, such as image sensors, data converters, and highly integrated transceivers for many types of communication [2].

L. Dos Ramos • M.A. Hempenius • G.J. Vancso (✉)
Materials Science and Technology of Polymers, MESA+ Institute for Nanotechnology,
University of Twente, Enschede 7500 AE, The Netherlands
e-mail: g.j.vancso@utwente.nl

In the race to produce ever smaller, faster, and more economical electronic devices, the component density of integrated circuits needs to be ever greater, i.e., component sizes must decrease. One of the main limitations in the fabrication of integrated circuits is the difficulty to further scale down CMOS transistors [3]. Most of the patterning processes take place on the wafer in two steps: (1) the patterning of a resist film on top of the functional material, known as lithography, and (2) the transfer of the resist pattern into the functional material, termed etching. Current state-of-the-art photolithographic techniques, such as immersion lithography [4] and double patterning [5], combined with a 193-nm UV light source, allow the fabrication of 22-nm-node technology. Electron and ion beam lithography have allowed the creation of features with less than 10 nm wide and continue to be developed in laboratories. However, due to the limits implied by the use of these wavelengths and especially the high costs of implementing these new technologies, alternative techniques capable of producing sub-10-nm-node features must be introduced.

Non-radiation-based resist patterning techniques have been introduced and offer fascinating prospects [6, 7]. Compared with radiation-based nanopatterning, non-radiation-based patterning methods have major advantages due to the fundamentally different physical principles involved. These techniques have no diffraction limits to resolution; are easily applicable for 3D patterning; can directly pattern functional materials, thereby reducing fabrication steps; and eliminate the need for complicated and expensive equipments, such as particle sources and optical systems. These techniques are based on mechanical or chemical patterning processes, and recently the combination of both has attracted research interest.

Mechanical patterning uses a mechanical mold as a template to shape the resist on the substrate, for example, through nanoimprinting, or as a stamp to transfer an ink onto the surface, e.g., nanoprinting or soft lithography [8]. Chemical patterning methods are bottom-up processes and appear to be a viable alternative for the fabrication of nanoscale features. They exploit the ability of a system to settle at its minimum energy, forming polymeric patterns by self-organization [9]. Chemical patterning processes include the self-assembly of monolayers on a surface and the phase separation of block copolymers [10]. As shown in Fig. 1, several basic structures obtained with block copolymer (BCP) patterning which are useful for CMOS functions have already been achieved. These patterns include dense and isolated bends, jogs, spots, line terminations, and T-junctions. Nealey and his coworkers obtained these features [12, 13] by using a lithographically patterned self-assembled monolayer or polymer brushes. These monolayers were subsequently etched with oxygen plasma to define regions with distinct surface tension, which were used to guide the self-organization of a thermally annealed thin block copolymer film.

Mixed patterning techniques combine mechanical and chemical methods, such as guided self-assembly in which a larger mechanical or chemical pattern is used to guide the self-assembly of smaller patterns. This technique induces self-organization at predetermined locations with large domain sizes, possessing long-
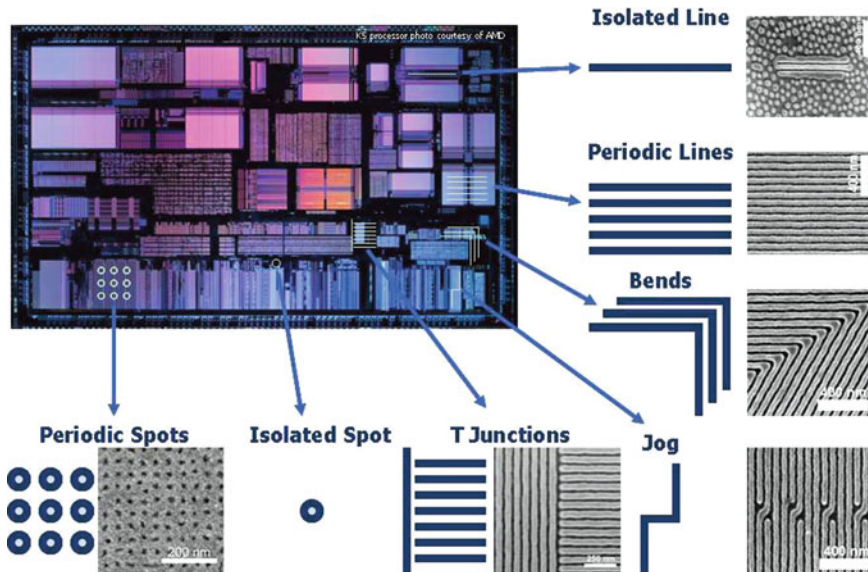
Fig. 1 Examples of structures obtained with BCP patterning which can have useful CMOS functions (Reprinted from Team ERM [11]. © 2007 International Technology Roadmap for Semiconductors)

range order, instead of the random order and small domain sizes typically resulting from unguided self-assembly [14].

Another challenge in CMOS fabrication and the scaling down of features is the need for high-performance resists that allow the obtaining of high-contrast features. In this chapter, we focus on poly(ferrocenylsilane) (PFS), an organometallic polymer, which has shown very promising properties as reactive ion etch barrier and, therefore, creates exciting opportunities in maskless self-assembly lithography for nanopatterning [15].

In the second part of this chapter, the synthesis of PFS will be presented, and it will be shown that anionic polymerization creates an opportunity to produce well-defined PFS homopolymers with targeted molar mass and low polydispersity, as well as block copolymers or more complex structures. In the third part, the reactive ion etching properties of PFS and the optimization of the etching process to achieve higher contrast will be discussed. The fourth part is dedicated to demonstrating the opportunities of using PFS in various mechanical lithography processes to fabricate nanoscale structures. Finally, in the fifth part, phase separation of PFS block copolymers and their use as self-assembled resists with long-range guided order in nanolithography will be discussed.

2 Poly(ferrocenylsilane) Synthesis

Poly(ferrocenylsilanes) are organometallic polymers composed of alternating ferrocene and silane units in the main chain. These materials were first obtained in 1962 by Rosenberg in a condensation polymerization between a biscyclopentadienide and iron(II) chloride, resulting in oligomers with degrees of polymerization ranging from 1 to 10 [16]. Manners and coworkers reported in 1992 a method for synthesizing high-molar-mass PFSs, involving thermal ring-opening polymerization (ROP) of strained silicon-bridged [1]ferrocenophanes [17]. The synthesis of polysilane-poly(ferrocenylsilane) random copolymers by thermal ROP was reported in 1995 by Manners and coworkers [18]. Enhanced control over the molar mass of PFSs was gained by polymerizing [1]silaferrocenophanes in solution using transition metal catalysts [19, 20]. Later, in 1998, transition metal-catalyzed ring-opening polymerization was used to synthesize PFSs with regioregular, comb, star, and block architectures [21]. Very well-defined PFSs with unprecedented control over molar mass are obtained by the anionic ring-opening polymerization of [1]silaferrocenophanes [22, 23]. This method allows one to synthesize near-monodisperse PFS homopolymers, block copolymers, and end-functional PFS chains. Interestingly, [1]silaferrocenophanes can also be polymerized in the solid state using a ^{60}C γ-ray source [24] (Fig. 2).

Several types of iron-containing macromolecules have been synthesized by polymerizing ferrocenophanes with varying numbers and types of bridging atoms [26] and substituents on the cyclopentadienyl rings [27, 28].

One of the main advantages of PFS compared to other organometallic polymers is the possibility to adjust the macromolecular characteristics by changing the substituents on the silicon atoms. Polymerization of asymmetrically substituted [1]silaferrocenophanes [29] yields amorphous polymers, while symmetrically substituted ferrocenophanes yield semicrystalline materials [30]. In addition, the glass transition temperature of PFSs can be tuned by varying the size and type of the substituents [31–33]. The synthesis of water-soluble PFS polyanions [34–36] and polycations [37, 38] and their layer-by-layer deposition [37, 39] to form multilayer thin films were also reported. The introduction of different reactive side groups allowed the synthesis of hyperbranched structures [40], PFS-based hydrogels [41], and recently the covalent fixation of PFS on a substrate [42].

Living anionic ring-opening polymerization of silicon-bridged [1] ferrocenophanes enabled the synthesis of well-defined and near-monodisperse poly(ferrocenylsilane)

Fig. 2 Ring-opening polymerization of strained dimethyl[1] silaferrocenophane (With kind permission from Springer Science and Business Media [25])
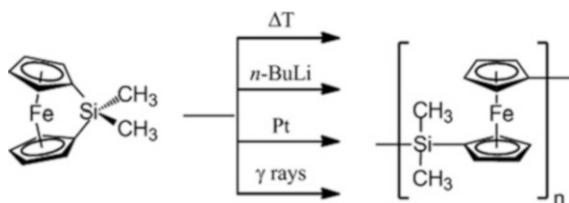
homo- and block copolymers. A variety of block copolymers with controlled molar masses and low polydispersity have been prepared (see Table 1). The polymerization mechanism, shown in Fig. 3, involves a nucleophilic attack by an alkyllithium initiator at the bridging silicon atom with a simultaneous cleavage of the ipso-carbon-silicon bond to create a metal-coordinated cyclopentadienyl anion. The propagation continues from the living anionic chain end until the monomer is consumed. Highly purified monomers, dry solvents, and an oxygen-free atmosphere are needed to avoid termination or chain transfer reactions. Under these conditions, predictable molecular weights and narrow molecular weight distributions (PDI < 1.2) are realized [44].

Later, in 2004, it was reported that PFS can also be synthesized by living photolytic anionic ring-opening polymerization [23, 58]. Dimethyl[1]silaferrocenophane was exposed to UV–vis radiation in the presence of an anionic initiator, sodium cyclopentadienylide ($Na[C_5H_5]$), leading to photocontrolled ring-opening polymerization. As shown in Fig. 4, under irradiation at 5 °C, some monomers (M) are photoexcited (M*) and react with the initiator to form a ring-opened monomer. The propagation proceeds via the opening of more Fe-η^5-cyclopentadienyl bonds in the photoexcited monomer (M*) via silyl-substituted cyclopentadienyl anions which are less basic than iron coordinated cyclopentadienyl anions. The chain is terminated with methanol and controlled molecular weights, and narrow polydispersities (PDI = 1.04–1.21) were obtained. Several block copolymers were obtained via this method (see Table 1), but this approach does not permit the synthesis of acrylate-, methacrylate-, or acrylamide-based block copolymers by sequential anionic polymerization as the uncoordinated cyclopentadienyl site is insufficiently reactive [59].

Figure 5 shows some examples of PFS-based block copolymers synthesized by traditional sequential anionic polymerization. For block copolymer synthesis, the monomers have to be added following a decrease of the end-group reactivity [59]. Nevertheless, sequential anionic polymerization has several drawbacks as it cannot be used with monomers containing either an acidic proton, e.g., acrylamide or N-alkylacrylamides, or reactive functional groups, such as acrylates or methacrylates. Moreover, some monomers which are suitable for anionic polymerization, e.g., 2-vinylpyridine or ethylene oxide, will not react and polymerize with the propagating PFS anion, and, conversely, a propagating poly(2-vinylpyridine) carbanion is not nucleophilic enough to initiate polymerization of dimethyl[1]silaferrocenophane. An elegant way to solve this problem, introduced by Rehahn and coworkers [49], involves the end-functionalization of the propagating PFS anion with a strained silacyclobutane to create a living end with enhanced basicity which can be end-capped with 1,1-diphenylethylene. The resulting living end is quite suitable as anionic initiator for acrylic monomers. Anionic ring-opening polymerization also allowed the introduction of functional end-groups, providing access to the synthesis of a broad range of PFS-based block copolymers [50]. For instance, alkyne-ended PFS chains could be connected to azide-ended poly(N-isopropylacrylamide) chains, using a Cu-catalyzed "click" reaction [45]. Table 1 gives an overview of PFS-based block copolymers synthesized by anionic polymerization methods.

Table 1 Recapitulative table of the different PFS-based block copolymers synthetized

Non-PFS block polymer	Synthesis method of PFS block	Synthesis method of non-PFS block	Attachment of the blocks	DP of non-PFS block	PDI of non-PFS block	Year	Reference
Poly(dimethylsiloxane)	Anionic	Anionic	Sequential anionic	40/95	1.13	1994	[43]
	Anionic	Anionic	Sequential anionic	39/99	1.13–1.15	1996	[44]
	Anionic	Commercial	Click reaction	80	1.10	2013	[45]
Polystyrene	Anionic	Anionic	Sequential anionic	100	1.08	1996	[44]
	Anionic	ATRP	Click reaction	29	1.14	2013	[45]
Poly(ethylene oxide)	Pt catalyzed	Commercial	Macromolecular condensation	68	1.13	1999	[46]
	Anionic	Commercial	Click reaction	113	1.16	2013	[45]
Polyisoprene	Anionic	Anionic	Sequential anionic	450	1.03	2000	[47]
Poly (ferrocenylphenylphosphine)	Anionic	Anionic	Sequential anionic	1–11	1.01–1.10	2002	[48]
Poly(aminoalkyl methacrylate)	Anionic	Oxyanionic	Sequential with deprotection of hydroxyl group	52	1.3	2002	[48]
Poly(methyl methacrylate)	Anionic	Anionic	DMSB-mediated end-capping	580	<1.1	2004	[49]
	Anionic	ATRP	ATRP macroinitiator end-functionalized	531	1.06	2004	[50]
	Anionic	ATRP	Click reaction	227	1.14	2013	[45]

Poly(γ-benzyl-L-glutamate)	Anionic	NCA ROP	Amino end-capping	95	1.13	2005	[51]
Gly-Ala-Gly-Ala	Anionic	SPPS	Amino end-capping	18	1.00	2006	[52]
Poly(ε-benzyloxycarbonyl-L-lysine)	Anionic	NCA ROP	Amino end-capping	75/180	1.25/1.16	2006	[53]
Poly(lactide)	Anionic	Zn catalyzed	Hydroxyl end-capping	472	1.41	2007	[54]
Poly(phosphazene)	Anionic	Cationic	Phosphorane end-capping	77	1.09	2008	[55]
Poly(ferrocenylmethyl(3,3,3-trifluoropropyl)silane)	PROP	PROP	Sequential anionic	78	1.02	2010	[56]
Poly(cobaltoceniumethylene)	PROP	PROP	Sequential anionic	50, 75	/	2011	[57]
Poly(N-isopropylacrylamide)	Anionic	ATRP	Click reaction	105	1.16	2013	[45]
Poly(2-(dimethylamino)ethyl methacrylate)	Anionic	ATRP	Click reaction	400	1.28	2013	[45]

NCA ROP α-amino acid *N*-carboxyanhydride ring-opening polymerization, *SPPS* solid-phase peptide synthesis, *PROP* photocontrolled living anionic ring-opening polymerization (ROP)
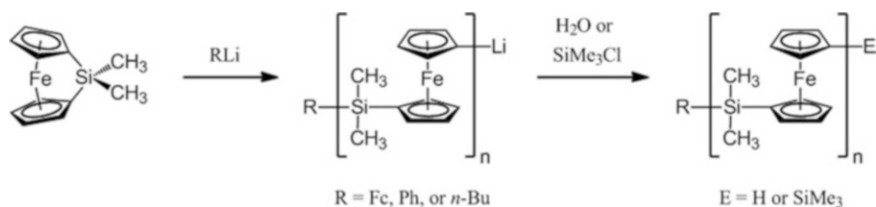
Fig. 3 Reaction scheme for the living anionic polymerization of dimethyl[1]silaferrocenophane (Reprinted with permission from Ni et al. [44]. Copyright 1996 American Chemical Society)
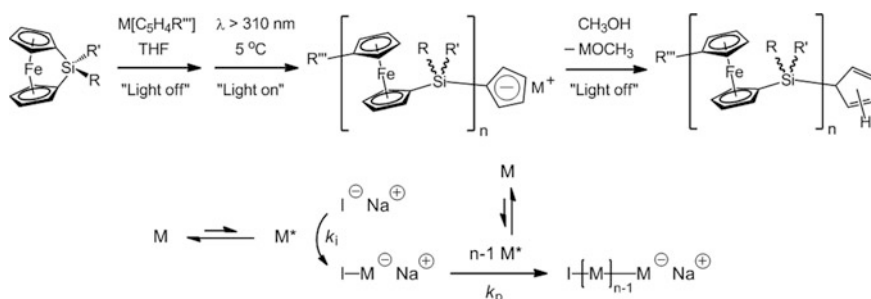
Fig. 4 Photocontrolled living anionic ring-opening polymerization reaction of [1]silaferrocenophane monomers and the photolytic living ring-opening polymerization mechanism (Reprinted by permission from Macmillan Publishers Ltd: Nature Materials, copyright (2006) [58])
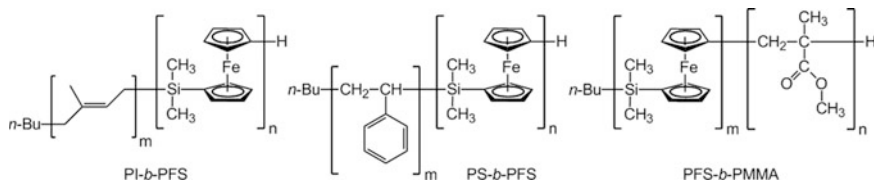
Fig. 5 Examples of poly(ferrocenylsilane)-based block copolymers (With kind permission from Springer Science and Business Media [25])

More complex architectures, such as pentablocks [44, 60], dendrimers [61], or block star terpolymers [62], have been synthesized recently.

3 Reactive Ion Etching Barrier Properties of Poly(ferrocenylsilanes)

In microfabrication, reactive ion etching using oxygen and oxygen-containing plasmas is a common dry etching technology used to selectively remove materials deposited on wafers [63]. Two mechanisms, chemical and physical etching,

Fig. 6 Comparison of the etched thickness by reactive ion etching for PS and PFS as a function of time
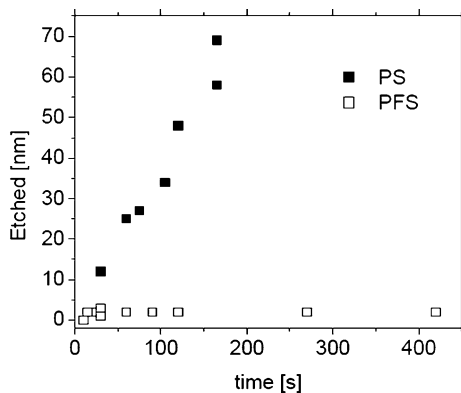
compete during this process [64]. In chemical etching, the active plasma reacts chemically with the substrate material. Etchant species are adsorbed on the surface and the reactions take place. Then the formed volatile products desorb from the surface and are pumped out. In physical etching, the positive ions are accelerated toward the surface and then mechanically eject substrate material after breaking bonds upon impact. The balance between these two etching mechanisms depends on different parameters, e.g., gas pressure and composition, reactor design, and temperature [65, 66]. Adjusting the relative contribution of these two etching processes is crucial for controlled nanofabrication as contrast is inversely proportional to the etching rate ratio of resist and substrate.

Organometallic compounds are known for their etching barrier properties in oxygen plasmas. Chemical etching products of these compounds are not volatile, contrary to common organic compounds, and therefore they are not desorbed from the surface. The behavior of poly(ferrocenylsilanes) under reactive ion etching conditions was studied [67]. Due to the presence of iron and silicon in the main chain, PFSs were found to be very efficient oxygen plasma etching barriers compared to common organic polymers. Figure 6 gives a comparison between the etched thickness of poly(styrene) (PS) and poly(ferrocenylsilane) (PFS) as a function of time. During etching, it was established by XPS that a thin iron and silicon oxide layer was formed at the surface, which decreased the etching rate considerably.

The composition in the depth of PFS films was investigated using Auger electron spectroscopy (AES). In the AES spectra (Fig. 7), the front part corresponds to the sample surface and the increase in sputtering cycles indicates a depth increase. The silicon signal around cycle 90 originates from the underlying silicon substrate. Compared to the film interior, on the surface little carbon and a significant amount of oxygen are present, revealing a thin oxide-rich layer of approximately 10 nm. Interestingly, more silicon is removed from the surface compared to iron during the oxygen plasma treatment. The presence of iron gives a higher resistance than silicon toward removal by oxygen plasma and also provides a high resistivity when fluorocarbon plasmas are applied.
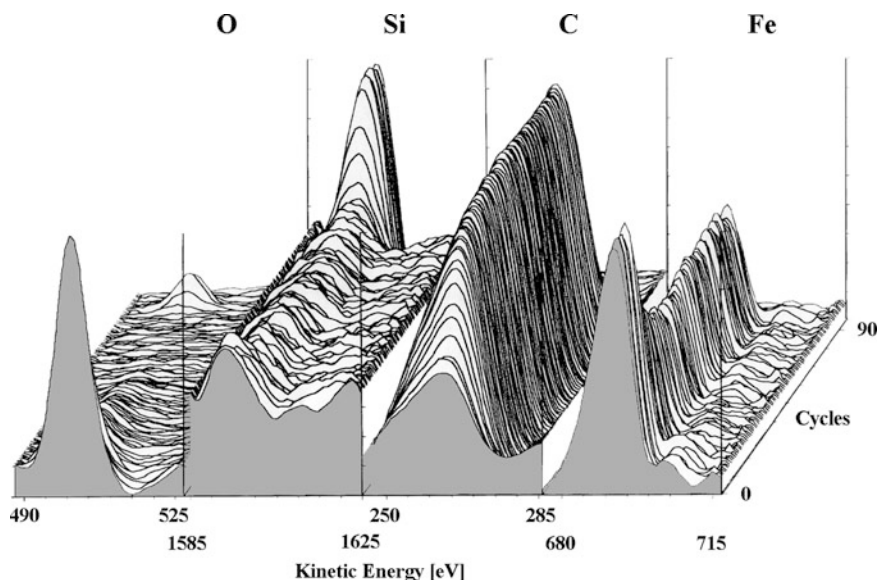
Fig. 7 Auger electron spectroscopy depth profile of an oxygen plasma etched film of poly (ferrocenyldimethylsilane) of 106 nm. Cycles start at the film surface and end at the substrate (Reprinted with permission from Lammertink et al. [67]. Copyright 2001 American Chemical Society)

Radio-frequency discharges in low-pressure fluorocarbon gases are frequently used for etching silicon, silicon oxide, and silicon nitride [68, 69]. CF_4, CHF_3, C_2F_6, and SF_6 are common gases used in reactive ion etching [70]. The nature of the plasma and its related etching characteristics can be radically changed by adjusting the composition of the gas [71]. For example, the C/F atomic ratio of the feed gas is a decisive parameter for the nature of the plasma [72]. An increase of the C/F ratio of the feed-in gas leads to an increase of the concentration of CF and CF_2 radicals which results in polymerization of the plasma. The concurrent deposition of a very thin fluorocarbon film on the substrate enhances the protection to etching, resulting in a significant reduction of the SiO_2 etch rate [73]. To overturn this etch stop, the fluorocarbon gases have been diluted with other gases like oxygen [74–76]. Oxygen atoms act as scavengers for carbon, and consequently the concentration of fluorine atoms [F] (the etching component) will be relatively higher than the concentration of fluorocarbons [CFX] (the polymerizing component). Figure 8 (left) shows an example of a structured silicon wafer produced by exposure to CF_4/O_2 reactive ion etching (RIE), using a PFS mask prepared by capillary force lithography [77]. Under the employed conditions, the etch rate contrast between PFS resist and silicon substrate is on the order of 10:1.

In order to fabricate structures with higher aspect ratios, the rate of the chemical etching of the substrate compared to the polymeric mask has to be increased without compromising the anisotropy of the etching process. This was reached by
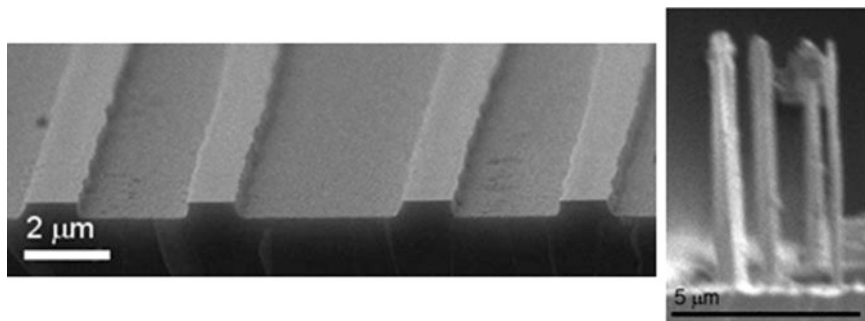
Fig. 8 (*left*) SEM image of a patterned silicon substrate after introduction of poly(ferrocenyl-methylphenylsilane) lines by capillary force lithography, followed by 10 min of CF_4/O_2 reactive ion etching. (*right*) SEM image of silicon nanopillars obtained using SF_6 (2 min) in a cryogenic reactive ion etcher with a poly(ferrocenyldimethylsilane) mask. In both cases, the polymer mask was subsequently removed using nitric acid (With kind permission from Springer Science and Business Media [25])

using SF_6 as the etching gas in a cryogenic reactive ion etcher. The physical and chemical etching parameters were varied independently, and conditions for the highest etch rate contrast were optimized [78]. The substrate temperature was kept at $-110\ °C$ during processing, resulting in an increase of the chemical etching rate for Si and a drastic decrease of the physical sputtering rate. Using this process, etch rates of 3,000 nm/min into Si and around 5 nm/min in the PFS layer were obtained, giving an etch rate contrast of 600:1. Such a high etch rate contrast enables the fabrication of high-aspect-ratio structures like silicon nanopillars with aspect ratios of 10 as shown in Fig. 8 (right).

The etch barrier potential of PFS has now been demonstrated. In the next part, we focus on pathways to generate patterns using this resist. The deposition of a very thin resist layer of high etch resistance is a determining step in the fabrication of defined high-aspect-ratio structures, as this minimizes pattern collapse.

4 Poly(ferrocenylsilane) Homopolymers in Lithography Applications

With the ongoing miniaturization, polymers have rapidly become crucial in the fabrication of submicron and nanoscale devices, most notably as highly tailorable resist materials. Indeed, their well-defined architecture, wide range of chemical functionalities, and ease of processing on micro- and nanoscale were extensively used to fabricate optical systems and microelectronics devices. Nanoimprint lithography, microcontact printing, micro-fluid-contact printing, lift-up, micromolding in capillaries, replica molding, solvent-assisted micromolding with its variations, and photolithography were the most used techniques in the past decades. Nevertheless,

most of the polymers have low resistivity to etching which is a large disadvantage when high-aspect-ratio patterns are to be obtained. Poly(ferrocenylsilanes), as seen in paragraph 3, were shown to be ideal materials for one-step resists. The etch barrier potential of poly(ferrocenyldimethylsilane) in O_2 and CF_4/O_2 plasmas was demonstrated for patterns made by micromolding in capillaries [67].

In the next sections, some examples of microfabrication will be presented, using poly(ferrocenylmethylphenylsilane) (PFMPS) as etch barrier in O_2 and CF_4/O_2 plasmas. The asymmetric substitution on the silicon atoms of PFMPS prevents crystallization of the polymer film, providing excellent homogeneity. The dependence of its glass transition temperature on the number average molar mass was studied [29, 77]. The extrapolated value of T_g of the polymer with infinite molar mass was found to be 92 °C. A low-molar-mass PFMPS of 3,700 g/mol, $M_w/M_n = 1.07$, was used for its liquid-like behavior above its T_g of 74 °C. At this molar mass, a favorable balance between T_g and viscosity was found, which permits processing at relatively low temperatures. Above its T_g, the polymer should be suitable to wet the stamp, while below T_g, the generated patterns retain their shape.

4.1 Solvent-Assisted Microcontact Printing

Microcontact printing, introduced by Whitesides and coworkers [79, 80], has become one of the most prominent methods for introducing patterns on flat and curved substrates with feature sizes ranging from micrometers to below 100 nm. Relief patterns on a master poly(dimethylsiloxane) (PDMS) stamp are used to transfer the "ink" to the surface of the substrate by physical contact printing. Usually, small molecules are used as ink and react with the surface, creating self-assembled monolayers (SAMs). When the stamp is removed, the pattern of ink, directed by the stamp shape, remains on the surface of the substrate. One application of the technique is the printing of etch-resistant polymer patterns.

Macromolecular "inks" have been used but poor wetting characteristics of PDMS surfaces by many polymers limit the process. Compared to common polymers, PDMS stamps have a low surface tension which is around 20 mN/m [81]. Indeed, the wetting properties of the ink polymer on the stamp surface will generate a continuous film or discontinuous islands on the substrate. A continuous thin layer of polymer on the surface of the stamp during inking is necessary for the transfer of a well-defined and continuous thin polymer film onto a substrate. In order to form a homogeneous polymer film, it is essential to increase the wettability of macromolecules by employing different surface oxidation techniques. For example, oxygen-based plasma treatments were used to increase the surface free energy of PDMS by creating a thin silica-like layer [82, 83]. However, this thin layer, formed during plasma treatment, thermally expands and generates mechanical stress on the stamp upon cooling. The relief of compressive stress by buckling of the silica-like thin film that was formed as a result of the plasma exposure induces a
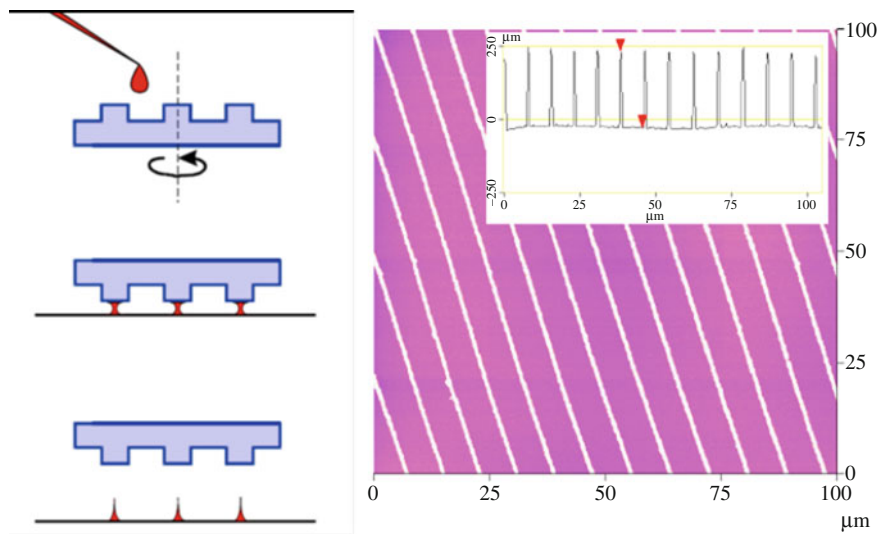
Fig. 9 Schematic diagram (*left*) and AFM height image with section analysis (*right*) of solvent-assisted dewetting of PFMPS confined between PDMS stamp and silicon substrate after 10 min of CF_6/O_2-RIE treatment (Adapted with permission from Korczagin et al. [77]. Copyright 2003 American Chemical Society)

periodic wavy structure perpendicular to the pattern of the stamp [84]. This submicron structure can also be replicated on the PFS ink [85, 86].

Nevertheless, less aggressive cleaning and oxidation techniques were found and the corrugation formation was eliminated. A mild ozone/UV environment can be used to clean the PDMS stamp, making the PDMS surface hydrophilic [87]. This treatment does not result in extensive heating and therefore stress related to thermal expansion is suppressed.

A solution of PFMPS (1 wt%) in toluene was spin coated on a PDMS stamp treated by the latter method. As shown in Fig. 9 (left), the patterns possessed a spacing corresponding to the periodicity of the stamp structure. During printing, the polymer solution dewets between the stamp and the silicon substrate, forming continuous lines in the middle of the protruding stamp contact areas. The lines, with a width on the order of 1 μm, were then etched into the underlying silicon substrate. As shown in Fig. 9 (right), after 10 min in O_2 and CF_4/O_2 plasmas, a direct pattern transfer into silicon resulted, with approximately 300 nm of silicon removed. The etch rate contrast between silicon substrate and PFMPS resist was estimated by AFM at 6:1.

4.2 Capillary Force Lithography

In capillary force lithography, a PDMS stamp is used to expel a thin polymer film from areas of contact between the substrate and the stamp. The polymer film was
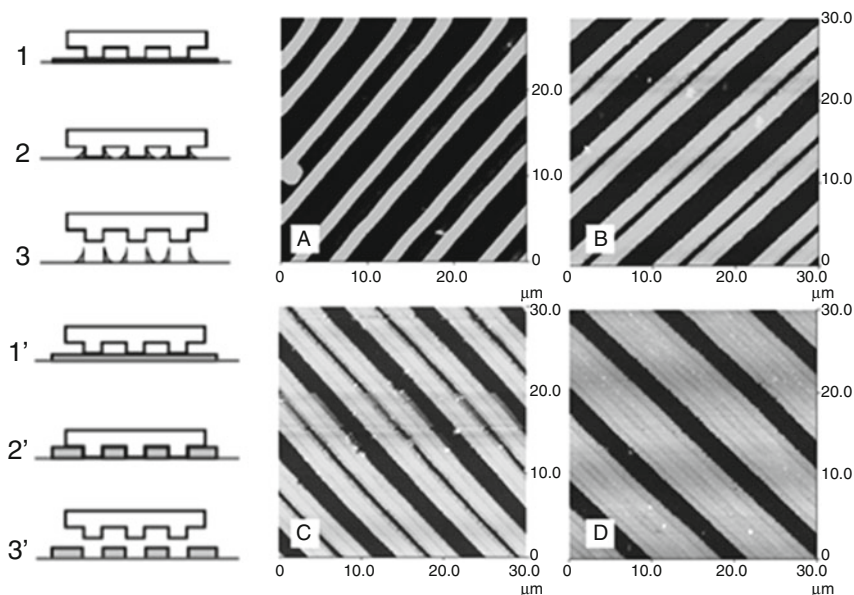
Fig. 10 Schematic diagram (*left*) and AFM height image (*right*) of capillary force lithography of PFMPS after etching and resist stripping for initial film thickness of (**a**) 30 nm, (**b**) 80 nm, (**c**) 100 nm, and (**d**) 150 nm (Adapted with permission from Korczagin et al. [77]. Copyright 2003 American Chemical Society)

previously deposited on the substrate and heated above its T_g (74 °C for PFMPS). As shown in Fig. 10 (left), the polymer diffuses into the grooves along the vertical walls of the stamp due to capillary forces, and structures are formed with a shape of a meniscus. A very thin film does not fill the grooves of the stamps completely; hence, a double line is formed per groove. An increase of the initial polymer film thickness results in thicker lines and a decrease of the space between the double lines. With a sufficiently high film thickness, the two lines merge and a single line with the dimensions of the groove (Fig. 10 (right)) is obtained.

Vancso and coworkers [77] used a PDMS stamp of 3-μm-wide cavity lines spaced by 2-μm-wide prominent lines, denoted as 2×3 μm. With a 27-nm thin PFMPS film, patterns with 110-nm-high and 500-nm-wide features were fabricated. It was observed from the section analysis of AFM height images that a meniscus of the capillary rise is formed in the grooves. The contact angle between PFMPS and PDMS was calculated to be 70° which is in agreement with microscopic measurements ($\theta_{PDMS/PFMPS} = 67°$). The receding contact angle between the silicon substrate and PDMS was also determined from AFM section analysis and was found to be 5°, whereas the static contact angle was 45°.

Using a 3×5 μm stamp, lines with widths of 1.1, 2.1, 2.4, and 5.4 μm corresponding to initial film thicknesses of 30, 80, 100, and 150 nm, respectively, were obtained. The gap between the lines can be adjusted from 2.5 μm for a 30-nm

film to 840 nm for a 100-nm film. With a film thickness higher than 140 nm, the two lines merge and a single line with the size of the groove is formed (Fig. 10 (right)).

The structures were developed by CF_4/O_2-RIE into silicon and the remaining PFMPS resist was stripped in HNO_3. The pattern transferred into the silicon was shown previously in Fig. 8 (left). In 10 min of CF_4/O_2-RIE etching, 300 nm of silicon was removed and the etch rate contrast between silicon substrate and PFMPS resist was determined to be 6:1.
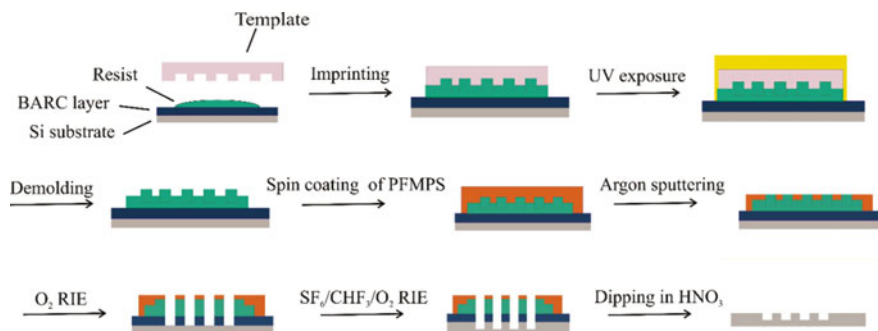
4.3 Thermal and UV-Assisted Nanoimprint Lithography

Nanoimprint lithography (NIL) allows the fabrication of nanostructures with high resolution and constitutes an alternative to traditional photolithography which uses masks. Thermal NIL [88, 89] and UV-light-assisted NIL [90, 91] are two techniques giving access to sub-10-nm features in a low-cost and high-throughput manner. The technique is based on a rigid template or mold with prefabricated topographic features which is used to replicate patterns within a resist layer that can then be employed as an etch mask for further pattern transfer. In thermal NIL, the template is replicated into a thermoplastic material by heating the polymer above its glass transition temperature and applying pressure on the mold. By contrast, in UV-light-assisted NIL, a transparent and rigid template is used to photocure a low-viscosity UV-curing resist material. The main challenge is to find an appropriate fast curable material that has a low adhesion to the mold, shows a good adhesion to the substrate, and has a high etch resistance.

Huskens, Vancso, and coworkers suggested the use of PFMPS for thermal NIL [92]. With this technique, small features below 100 nm were not precisely transferred on the substrate. Later, in order to obtain a higher contrast, they proposed a bilayer-type step-and-flash imprint lithography using a UV-curable resist [92] covered on the top by PFMPS. After patterning of the UV-curable resist, the template was demolded from the substrate, and PFMPS was spin coated on the top of the structures to form a bilayer structure with a distinctly different etch selectivity between the top layer and the underlying one. Argon sputtering was applied to homogeneously etch down the polymer until the organic imprint material became exposed. Subsequent treatment with oxygen plasma was performed to remove the exposed organic imprint material and keep the PFMPS lines on the substrate. Finally, pattern transfer into the silicon substrate was accomplished by the use of a $CHF_3/SF_6/O_2$ plasma and the resist was stripped off with nitric acid (Fig. 11).

With this technique, etch-resistant patterns of PFMS with sizes down to the nanometer range could be created. Nevertheless, because it is a bilayer process, the final pattern size is defined not only by the imprinting resist but also depends on the subsequent etch processes. PFMPS plays an important role here as it provides a very high selectivity over UV-curable resist.

The S-FIL^{TM} method [93] was used to create PFMPS patterns on a substrate. A template consisting of lines of 100-nm-wide pitches of 1:1, 1:2, and 1:3 and with a

Fig. 11 Fabrication process of UV-light-assisted nanoimprint lithography using a spin-coated top layer of PFMPS (Reprinted with permission from Acikgoz et al. [92]. Copyright 2009 American Chemical Society)

height of 100 nm was used. By SEM, the thickness of the transfer layer was determined to be 60 nm, the residual UV-curable resist layer after imprinting was about 40–50 nm, and the PFMPS after spin coating in toluene was 60 nm on the top of a line and 120 nm between two lines. The etch rate of PFMPS upon argon sputtering was determined to be 1.5 nm/min. Then the exposed organic imprint layer and the transfer layer material underneath were selectively etched by O_2 RIE. The O_2 RIE etch rates of PFMPS and the organic imprint material were found to be 1 and 60 nm/min, respectively, which results in an etch selectivity of 60. Because of the oxide layer formation, PFMPS lines stayed intact while the material between the lines was totally removed. PFMPS lines down to 30 nm were obtained after oxygen plasma treatment as shown in Fig. 12b. Patterning of the silicon substrate was then tested with CHF_3 and SF_6 plasma. The etch rates into Si and PFMPS were 300 and 1 nm/min, respectively, resulting in an etch contrast of 300. This process permitted Huskens, Vancso, and coworkers to combine the advantages of UV-NIL with the high etch resistance of PFS to realize the fabrication of feature sizes down to the sub-100-nm range.

4.4 Nanosphere-Assisted Lithography

A nanosphere lithography multilayer fabrication process for a freestanding poly (ethersulfone) (PES) membrane with well-defined pore size was proposed by Vancso, Huskens, and coworkers [94]. This procedure employed a self-assembled colloidal silica layer as template, embedded in a PFMPS matrix which acted as etch resist. As shown in Fig. 13, first, a sacrificial layer of cellulose acetate was spin coated on a silicon substrate, followed by spin coating of PES. Then a well-ordered and closely packed assembly of silica nanoparticles was deposited by the convective self-assembly method [95], and PFMPS was spin coated on the top to fill the pores between the silica particles. Subsequently, argon sputtering was used to
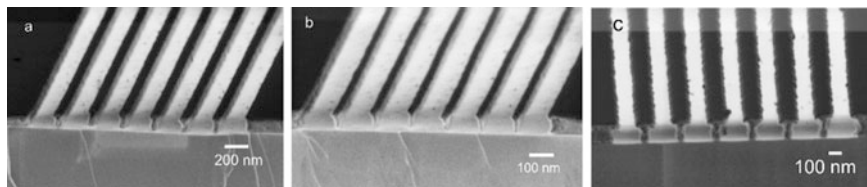
Fig. 12 SEM images of lines fabricated after oxygen RIE of (**a**) 80-nm PFMPS lines and (**b**) 30-nm PFMPS lines after 2 min of treatment. (**c**) 100-nm PFMS lines after 2.5 min treatment. The dark stripes in the images correspond to PFMPS lines (Reprinted with permission from Acikgoz et al. [92]. Copyright 2009 American Chemical Society)
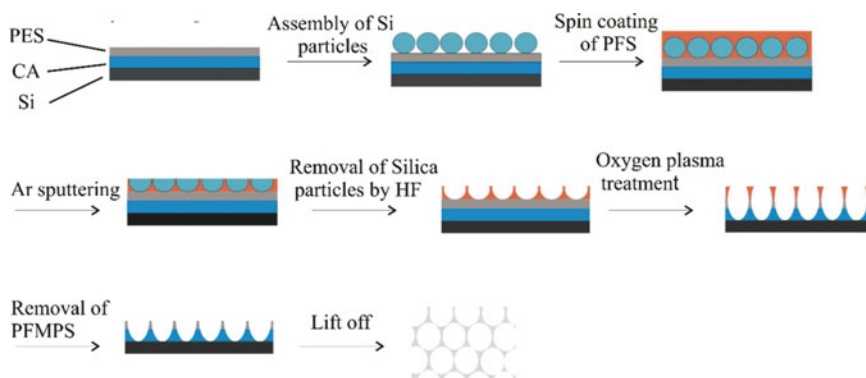
Fig. 13 Scheme of freestanding PES membranes by silica nanosphere-assisted lithography (Copyright © 2009 WILEY-VCH Verlag GmbH & Co. KGaA, Weinheim [94])

remove the top layer of PFMPS and silica particles, exposing a well-ordered surface of half nanospheres surrounded with PFMPS. The ordered hexagonal close-packed pattern was then transferred by oxygen plasma treatment into the PES layer and the sacrificial layer. Contrary to conventional nanosphere lithography, the silica particles are not used as an etch mask but as an inversion mask, PFMPS being the etch mask. Finally, the PFMPS layer was removed by nitric acid treatment, and the sacrificial layer of cellulose acetate was dissolved in acetone in order to obtain freestanding PES films.

The silica particles used were of a size of 300 nm and the PES membrane was shown to have a thickness of 500 nm and a pore size of about 230 nm. The pore size was less than the size of the particles used due to the difference in sputtering rate of PFMPS and silica nanoparticles in a stream of Ar$^+$ ions. Figure 14 shows the SEM, AFM images, and the AFM section profile of freestanding PES films at different stages of the process.
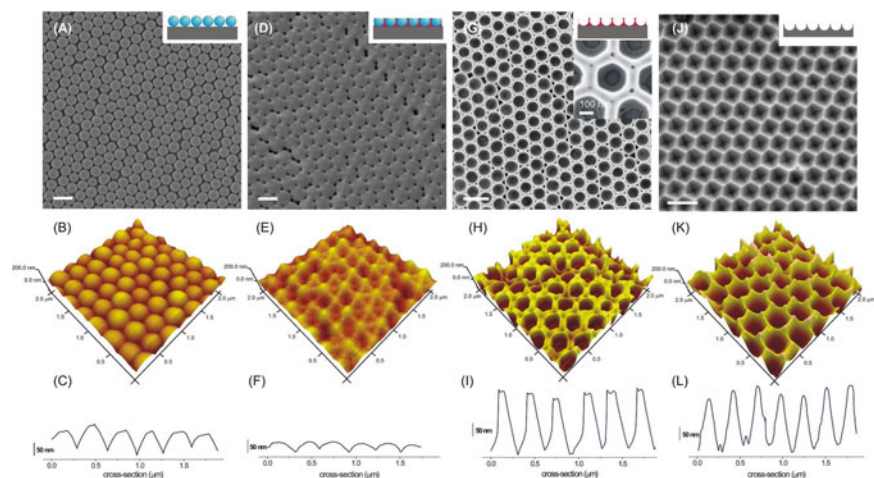
Fig. 14 SEM images of (**a**) a 300-nm silica particle array, (**d**) particles treated with argon sputtering after PFMPS spin coating, (**g**) the substrate after particle removal by HF, and (**j**) the substrate after oxygen plasma and PFMPS removal. (**b**), (**e**), (**h**), and (**k**) are the corresponding 3D AFM images and (**c**), (**f**), (**i**), and (**l**) show the corresponding height profile (Copyright © 2009 WILEY-VCH Verlag GmbH & Co. KGaA, Weinheim [94])

5 Poly(ferrocenylsilane)-Based Block Copolymers in "Maskless" Nanolithography Applications

5.1 Block Copolymer Microphase Separation

Block copolymers (BCPs) are macromolecules composed of two or more different polymeric segments. Due to this segmented structure, BCPs tend to phase-separate and order themselves into a range of complex periodic domains with a size of tens of nanometers. Figure 15 shows the classical morphologies in diblock copolymer systems depending on the volume fraction of the two phases; here the volume fraction of the black block increases from left to right. These include body-centered-cubic packed spheres, hexagonally packed cylinders, and alternating lamellae.

A complete study of microphase separation in block copolymers was done by Leibler in 1980 [96]. In the example of a pure diblock copolymer A-B, the driving force for phase separation is due to the free energy cost of contact between blocks A and B which is described by the Flory–Huggins interaction parameter χ_{AB}. Several experimental methods to determine this parameter exist, including light scattering [97–99], small-angle neutron scattering (SANS) [100–104], ellipsometry [105], melting point depression, and comparison of solubility parameters [106]. The equilibrium structure depends also significantly on the degree of polymerization, N, of each block. At large N, the minimization of A-B contacts

Fig. 15 The classical morphologies in block copolymer systems (With kind permission from Springer Science and Business Media [25])

and phase separation is thermodynamically more favorable even if there is a loss in translational and configurational entropy due to the separate domains of each block. The magnitude of χN determines whether a block copolymer will phase-separate into an ordered system or remain disordered. The order-disorder transition (ODT) is where the BCP phase-separates when χN exceeds a critical value denoted χN_{ODT}. The relative volume fraction φ of A and B defines the morphology that the block copolymer will reach at the equilibrium after phase separation, while the size of each domain is directed by the degree of polymerization N.

For a BCP system in the strong segregation limit ($\chi N \gg 10$), the width of the interfaces separating block A from block B can be described by $\alpha \chi^{-1/2}$ where α is the characteristic segment length of a monomer unit. Consequently, the creation of sharper interfaces between each block, allowing features with a smaller edge roughness, is possible with higher χ-values. Furthermore, the period of the phase-separated microdomains can be described as $D \sim \alpha N^{2/3} \chi^{1/6}$. This means that a reduction of N while maintaining χN over the critical value for phase separation would lead to smaller features with a smaller period [107]. Several organic BCP systems have been studied, e.g., PS-*b*-PMMA, PS-*b*-PI, and PS-*b*-PB, but their relatively low χ-values limit the definition of the domains and the scaling down of the features. Inorganic-organic BCPs, such as PFS-based BCPs, tend to have higher χ-values [108] and therefore allow the formation of sharp interfaces separating the domains. Anionic polymerization enabled the preparation of various PFS-based BCPs with narrow polydispersity and low N, permitting the formation of well-defined microdomains with small size.

The solubility of BCPs in various solvents allows their processing into thin films on solid substrates, for instance, by spin coating. The phase separation still occurs, and detailed studies on the influence of block copolymer composition, molar mass, and film thickness on microdomain morphology have been possible using AFM. Figure 16 shows the tapping mode AFM phase images of PI-*b*-PFS of 30-nm thin films with different volume fractions. The morphology of PI-*b*-PFS with a molar mass ratio PI/PFS of 29/15 (in kg.mol^{-1} for each block), corresponding to 28 vol.% of the organometallic phase, displays an in-plane wormlike cylindrical PFS microdomain structure with an average distance between domains of 32 nm (Fig. 16a). Parallel orientation is induced by preferential segregation of the lower surface energy PI phase at the surface. A thin film of 31/13, corresponding to 24 vol. % of PFS phase, displays a mixture of the previous wormlike cylindrical structures and also exhibits domains of hexagonally arranged dots. From the 2D Fourier
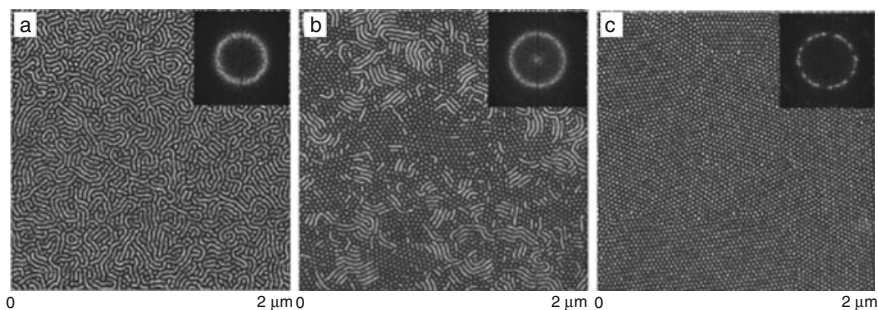
Fig. 16 Tapping mode AFM phase images of 30-nm PI-*b*-PFS thin spin-coated films. (**a**) PI/PFS = 29/15 (in kg.mol^{-1}), i.e., 28 vol.% of PFS. (**b**) PI/PFS = 31/13, i.e., 24 vol.% of PFS. (**c**) PI/PFS = 36/12, i.e., 20 vol.% of PFS. The insets (*top right*) show the 2D Fourier transform (Adapted with permission from Lammertink et al. [47]. Copyright 2000 American Chemical Society)

transform, the lattice spacing of these dots was determined to be 29 nm, resulting in a domain spacing of 33 nm (Fig. 16b). A thin film of 36/12, corresponding to 20 vol. % of PFS, shows a fully hexagonal microdomain morphology with a domain spacing of 30 nm (Fig. 16c).

Other PFS-based diblock copolymers have also been studied, such as PS-*b*-PFDMS [109], PS-*b*-PFEMS [110, 111], or poly(styrene)-*b*-poly(ferrocenylisopropylmethylsilane) (PS-*b*-PFiPMS) [112]. However, in order to obtain a larger variety of ordered structures with more complexity, different copolymer structures have been developed and their phase separation studied. Figure 17 shows, for example, a simple geometry prediction of the different morphologies that an ABC triblock terpolymer can adopt. These morphologies only take into account the possible combinations of lamellar, cylindrical, and spherical microdomains, but more complex microdomains have been observed [114, 115].

Blends of PFS-based diblock copolymer with the corresponding homopolymers also presented different morphologies [116]. As shown in Fig. 18, bicontinuous gyroidic morphologies of blends of PFS-*b*-PMMA in different volume fractions (percentage of each block in subscript) with PFS or PMMA homopolymers (hPFS and hPMMA) have been demonstrated. Annealing temperature was also found to be an important parameter. The influence of annealing temperature on the morphology of the triblock copolymer PS-*b*-PB-*b*-PMMA was presented earlier [117]. Solvent annealing is also possible and was studied as well. Later, pentablock copolymer PMMA-*b*-PFS-*b*-PS-*b*-PFS-*b*-PMMA systems [60] and recently PS/PI/PFS star terpolymer systems [62] have been studied and revealed more complex microdomains as shown in Figs. 19 and 20, respectively.

Anionic polymerization has given the opportunity to synthetize well-defined and sophisticated PFS-based structures which opened a broad research of PFS-based block copolymer microdomain phase separation in bulk and in thin films.

Fig. 17 Possible microdomain morphologies for three-phase structures of ABC triblock terpolymers composed of lamellar, cylindrical, and spherical microdomains (Reprinted from Yamauchi et al. [113], Copyright 2002, with permission from Elsevier)
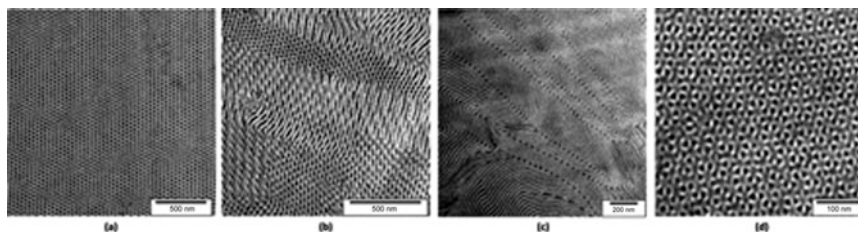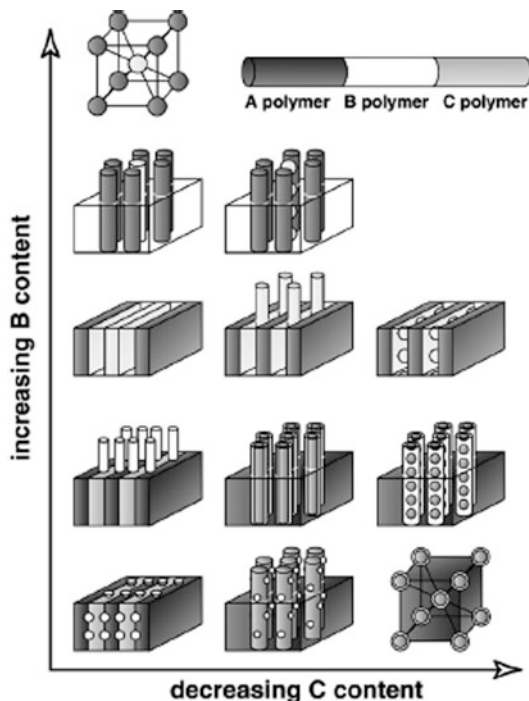
Fig. 18 TEM images of (**a**) PFS_{36}-b-$PMMA_{64}$ + 4 % hPFS annealed at 190 °C. (**b**) PFS_{37}-b-$PMMA_{63}$ + 2 % hPFS annealed at 190 °C. (**c**) PFS_{40}-b-$PMMA_{60}$ + 5 vol% hPFS annealed at 190 °C. (**d**) PFS_{45}-b-$PMMA_{55}$ + 6 % hPMMA annealed at 190 °C (Adapted with permission from Kloninger and Rehahn [116]. Copyright 2004 American Chemical Society)

5.2 Block Copolymer Thin Films as Nanolithographic Templates

The ability of block copolymer thin films to self-assemble into tunable and different morphologies makes them suitable candidates for bottom-up lithography processes. The nanoscale ordered structures formed by block copolymer self-assembly can be transferred into an underlying substrate via plasma etching. As traditional photoresists, they act as sacrificial templates but the bottom-up approach obviates the
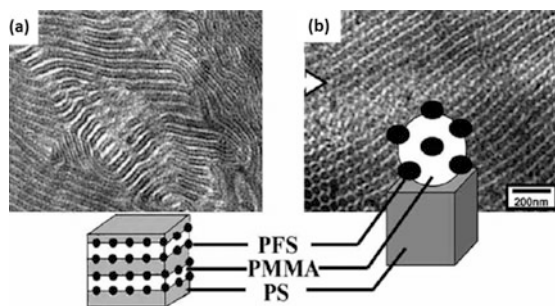
Fig. 19 TEM images and corresponding morphology schemes of a PMMA-*b*-PFS-*b*-PS-*b*-PFS-*b*-PMMA pentablock copolymer presenting different morphologies. (**a**) Lamellar morphology of PS and PMMA with PFS droplets at the interphase. (**b**) Spheres-on-spheres morphology. Thin films were cast from dichloromethane solution and annealed for 1 day at 180 °C (Copyright © 2004 WILEY-VCH Verlag GmbH & Co. KGaA, Weinheim [60])
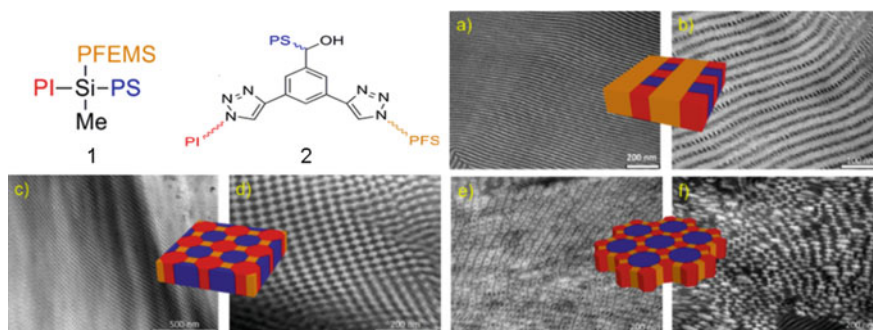
Fig. 20 TEM images of thin-sectioned bulk films of PFS star terpolymer with the corresponding morphology scheme. (**a**) Polymer 1 PS/PI/PFS = 12.7/15.5/71.8 wt%, no stain. (**b**) Same as (**a**) with OsO$_4$ stain. (**c**) Polymer 2 PS/PI/PFS = 42.5/29.7/27.7 wt%, no stain. (**d**) Same as (**c**) with OsO$_4$ stain. (**e**) Polymer 2 PS/PI/PFS = 36.3/35.5/28.1 wt%, no stain. (**f**) Same as (**e**) with OsO$_4$ stain (Adapted with permission from Manners [62]. Copyright 2013 American Chemical Society)

complicated template designs and expensive optical setups. In the late 1990s, Register, Chaikin, and coworkers used poly(styrene)-*b*-poly(butadiene) and poly(styrene)-*b*-poly(isoprene) for the fabrication of periodic arrays of densely packed holes [118, 119]. The self-assembly into a hexagonally packed array of PB cylinders and into body-centered-cubic ordered spheres of PI, both embedded in a PS matrix, allowed the etching of holes with sizes reaching approximately 13 nm and a lattice constant of 27 nm. Later, PS-*b*-PMMA was used for the fabrication of several microelectronic devices, e.g., semiconductor capacitors [120, 121], field effect transistors [122], and flash memory devices [123, 124]. But as mentioned previously (Sect. 5.1), these block copolymers present low χ-values. Other organic BCP systems with high χ-values exist, e.g., amphiphilic poly(styrene)-*b*-poly(4-vinylpyridine) and PS-*b*-PEO, but
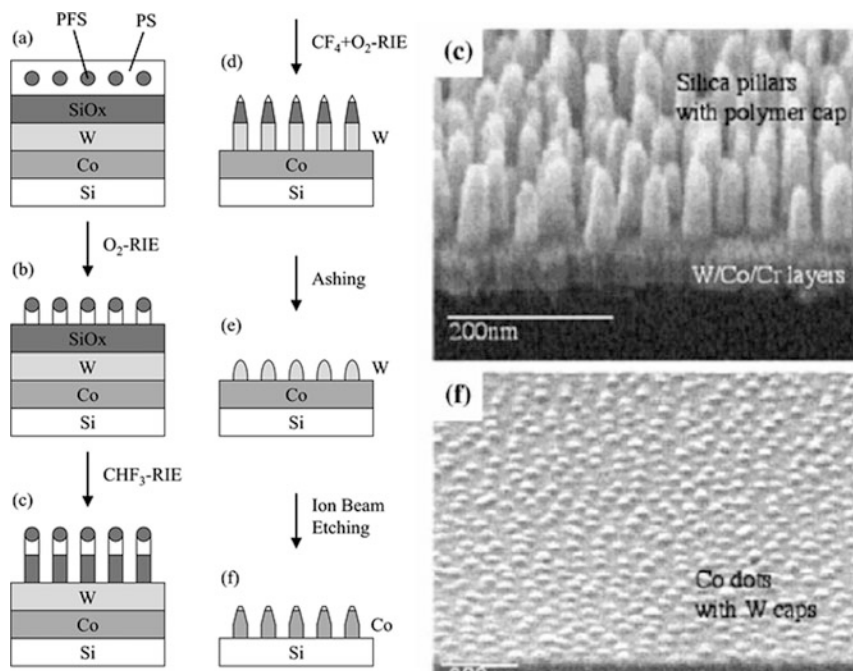
Fig. 21 Fabrication process of a cobalt magnetic dot array via block copolymer lithography. Tilted SEM images of the intermediate stages of cobalt magnetic dot array formation via block copolymer lithography (© 2001 WILEY-VCH Verlag GmbH, Weinheim, Fed. Rep. of Germany [125])

their low etch selectivity between the organic blocks reduces their potential in the fabrication of nanoscale features with high contrast.

PFS-based block copolymer lithography, because of the high χ-values which allow high contrast of the domains, as discussed in Sect. 5.1, and the good etch selectivity between the PFS block and the organic block, as shown in Sect. 3, appear to be an excellent system for pattern transfer. Vancso, Ross, and coworkers used PS-*b*-PFS for the fabrication of an ultrahigh-density cobalt magnetic dot array via BCP lithography [125]. Figure 21 shows the fabrication process of the cobalt magnetic dot array.

PS-*b*-PFS diblock copolymer with 20 vol.% of PFS was spin coated, using a 2 % solution, on a multilayer substrate of silica, tungsten, and cobalt. After annealing, the 60-nm thin films presented close-packed PFS spheres in a PS matrix. The spheres were found to be about 25 nm in diameter with a periodicity of 50 nm. The block copolymer lithographic mask was formed through an oxygen plasma reactive ion etching process (RIE). This step removes the PS block and leaves the PFS block with a thin layer of iron and silicon oxide on the top, giving a high etch resistance (see Sect. 3). Then the PFS pattern was transferred into the silicon film using CHF$_3$-RIE. The tungsten hard mask was patterned using CF$_4$ + O$_2$-RIE. The
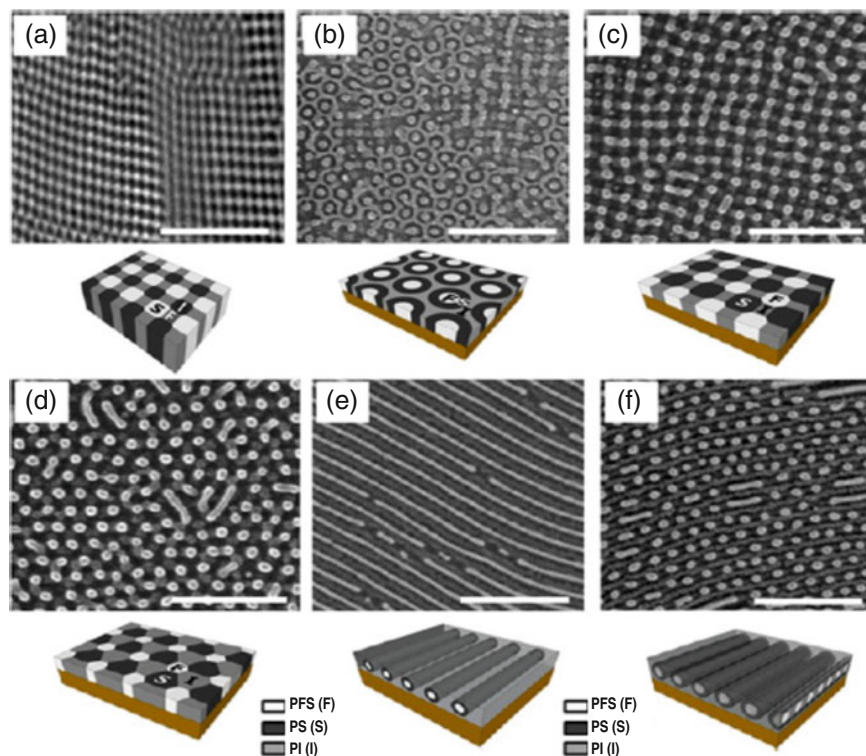
Fig. 22 (**a**) TEM and (**b–f**) SEM images and the corresponding morphology scheme of (**a**) unblended bulk 3 μ-ISF, (**b–d**) blended 3 μ-ISF with 15 vol.% of PS homopolymer on untreated Si wafer with chloroform annealing at (**b**) $0.7P_0$, (**c**) $0.75 P_0$, and (**d**) $0.85 P_0$. (**e–f**) Blended 3 μ-ISF with 15 vol.% of PS homopolymer on P2VP-coated surface with chloroform annealing at (**e**) $0.75P_0$ and (**f**) $0.8P_0$. Samples were stained with OsO$_4$. Thin films (**b–f**) were etched by O$_2$ RIE before SEM observation, so PFS appears bright and regions formerly occupied by PS appear dark. The film thicknesses were (**b–e**) 34 nm and (**f**) 42 nm. Scale bars are 200 nm (Reprinted with permission from Aissou et al. [126]. Copyright 2013 American Chemical Society)

silicon and residual polymer layers were then removed by high-pressure ashing. Finally, the cobalt dot array was formed using ion beam etching using the tungsten pattern as hard mask. The cobalt dots after etching had diameters of 20 nm.

Recently, Manners, Ross, and coworkers used the self-assembly of 3-miktoarm star terpolymer chains of polyisoprene-*arm*-polystyrene-*arm*-polyferrocenylethyl-methylsilane (3 μ-ISF) thin films to create novel microdomain structures [126]. Their use as nanolithographic masks was also demonstrated by the transfer of square and triangular hole arrays into a substrate. As shown in Fig. 22, a range of 2D Archimedean tiling was obtained after solvent annealing of 3 μ-ISF with PS homopolymer blends. The 3 μ-ISF consisted of PI/PS/PFS with a volume fraction of 39/35/26 vol.% and a polydispersity index (PDI) of 1.03, and the homo-PS had a molar mass of 10 kg.mol^{-1} with a PDI of 1.08. This narrow PDI was obtained by
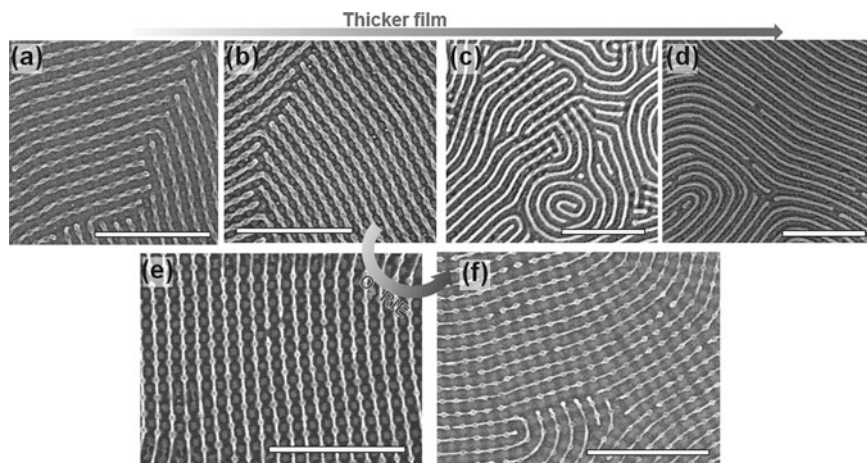
Fig. 23 SEM images of 3 μ-ISF thin films with different thickness and different RIE exposure times. The film thicknesses were (**a**) 28 nm, (**b, e, f**) 35 nm, (**c**) 40 nm, and (**d**) 43 nm. The films were etched in O2 RIE for (**a–d**) 15 s, (**e**) 20 s, and (**f**) 30 s. Samples were stained with OsO_4 before RIE treatment. Scale bars are 300 nm (Adapted with permission from Choi et al. [127]. © 2014 WILEY-VCH Verlag GmbH & Co. KGaA, Weinheim)

anionic polymerization (see Sect. 2). Furthermore, it was shown that thin films annealed on a substrate with P2VP brushes, which are preferentially wetted by PI, produced additional morphologies (see Fig. 22e–f). Thin films were then etched by O_2 RIE before SEM observation. PFS appears bright and regions formerly occupied by PS appear dark.

Later, they used solely a 3 μ-ISF, without adding homopolymer, consisting of PI/PS/PFS with a volume fraction of 34/43/23 vol.% and annealed in chloroform vapor to obtain a "knitting pattern" morphology [127]. This system allowed the formation of periodic structures consisting of undulating lamellae and alternating cylinders, and it was shown that the knitting morphologies could be tuned by varying the film thickness. Furthermore, 90° bends and T-junctions which are generally considered energetically unstable conformations in block copolymers were obtained, due to the unique microdomain structure of the films, as shown in Fig. 23.

5.3 Nanostructures with Long-Range Guided Order Using Block Copolymer Lithography

The use of the self-assembling properties of block copolymers for block copolymer lithography has been shown to yield nanoscale patterns over large areas. These patterns present good short-range order, but the order is reduced over longer ranges

Fig. 24 SEM images of
48 h annealed and plasma-
treated PS/PFS 50/12 spin-
coated films at 3,500 rpm on
a silica substrate with (**a**)
500-nm-wide, (**b**) 320-nm-
wide, and (**c**) 240-nm-wide
grooves (Reprinted with
permission from Cheng
et al. [129]. Copyright 2002
American Institute of
Physics)
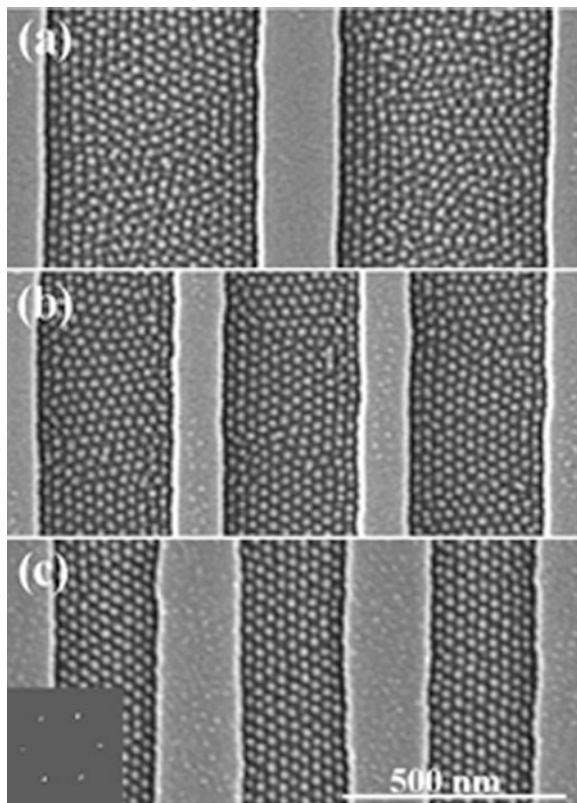
which can be a limitation for block copolymer lithography. The combination of
block copolymer self-assembly with long-range ordering methods could permit the
fabrication of nanostructures in precise positions on a substrate. Graphoepitaxy is a
method that uses surfaces patterned with shallow grooves to order nanostructures
formed by the phase separation of block copolymers [128]. Several examples of
graphoepitaxy using PFS-based copolymers are presented below.

Figure 24 shows how the long-range pattern order of a thin film of PS-*b*-PFS
diblock copolymer changes with the width of the grooves in which the film is
deposited [129]. Within the 500-nm-wide groove, about three rows of close-packed
PFS features are aligned parallel to the sidewall (Fig. 24a). In the 320-nm-wide
groove, alignment of the PFS features was observed across the groove, but a
significant amount of defects existed (Fig. 24b). However, in the 240-nm-wide
groove, the alignment was almost perfect with a sixfold symmetry, and the pattern
in each groove has the same orientation, as shown in the superposed fast Fourier
transform of the image in Fig. 24c. The rare domain-packing defects were appar-
ently caused by the edge roughness of the grooves. The patterns were then trans-
ferred to the silicon substrate by a single etching step, resulting in arrays of well-
ordered silica pillars with 20-nm diameters and aspect ratios above 3.

Fig. 25 SEM images of PS-*b*-PFS domains within channels of different confinement widths W, proportional to the equilibrium row spacing, d₀ (Reprinted with permission from Cheng et al. [130]. Copyright 2006 American Chemical Society)
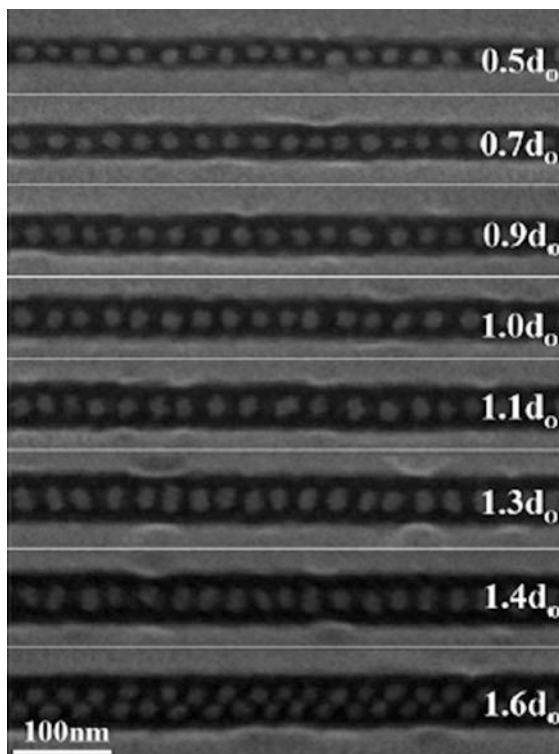
By using a similar PS-*b*-PFS diblock copolymer thin film, spin coated in etched channels of 30–80 nm wide, isolated 1D arrays of distorted PFS spheres were obtained [130]. In the confined channels of width W, approaching the row spacing of the spherical domains, d_0, a single row of ordered PFS domains was observed over the range $0.6 < W/d_0 < 1.5$ (Fig. 25). The ellipticity of the domains and the orientation of their major axis were controlled by W/d_0. At $W/d_0 \sim 1.0$, the domain projections were circular; for $W/d_0 > 1.0$, they were elongated perpendicular to the channel; and for $W/d_0 < 1.0$, they were elongated parallel to the channel. Below a W/d_0 of 0.6, the domains were found to be hemispheres, and above 1.5, regions consisted of two rows of domains. This method allowed the fabrication of a linear array of dots which is difficult to create by conventional lithography.

The influence of topographically patterned substrates on the spherical morphology and close-packing of PS-*b*-PFS domains was also studied by templating thin films within V-shaped grooves [130]. The V-grooves promoted the formation of a well-ordered face-centered cubic (fcc) close-packed sphere array with (100) planes of the array parallel to the groove walls (Fig. 26b), while it typically formed a body-centered-cubic (bcc) sphere array in bulk. The top surface of the close-packed array, parallel to the substrate, showed a square symmetry (see Fig. 26a), while a monolayer of spherical domains showed a hexagonal symmetry.
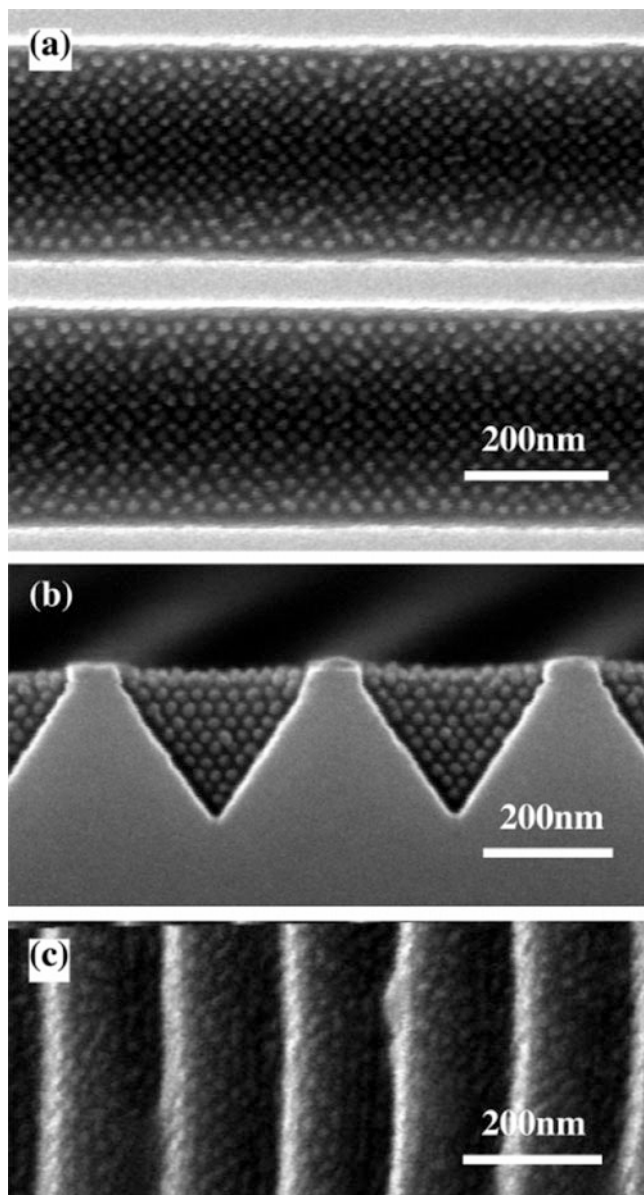
Fig. 26 SEM images of PS-*b*-PFS films in V-grooves after 72 h annealing and etching. (**a**) Square packing from the top view. (**b**) Cross section of the same groove showing a sphere array with 11 rows presenting a fcc packing (Reprinted with permission from Cheng et al. [130]. Copyright 2006 American Chemical Society)
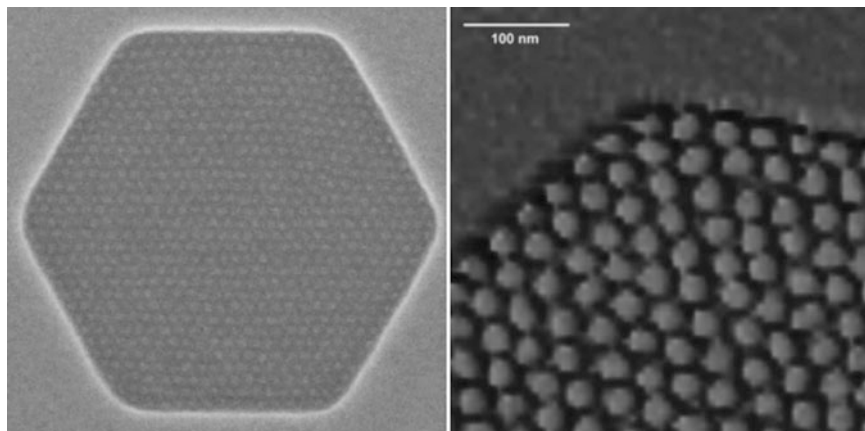
Fig. 27 SEM images of PI-*b*-PFS thin film self-assembly (**a**) in an 800-nm-wide hexagonal groove and (**b**) zoom on the corner showing single domain positioning (Copyright © 2007 WILEY-VCH Verlag GmbH & Co. KGaA, Weinheim [131])
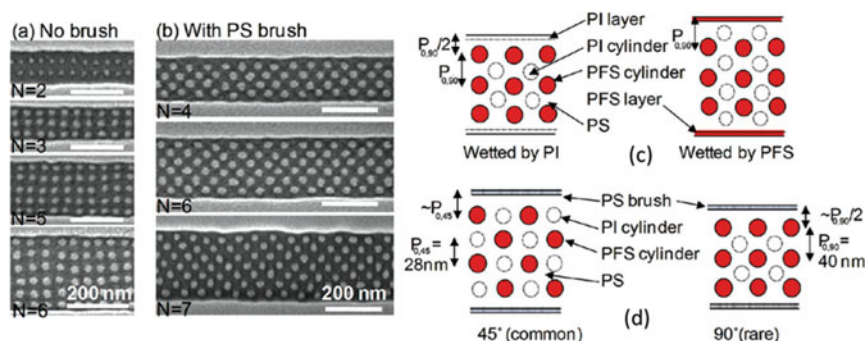
Fig. 28 (**a**, **b**) SEM images of ISF/PS blend self-assembly in shallow grooves after annealing in chloroform vapor for 2.5 h at room temperature, followed by etching with O_2-RIE to remove PI and PS domains, (**a**) with uncoated trenches and (**b**) with PS brush coated trenches. (**c**, **d**) Schematic of the options for packing the microdomains with (**c**) uncoated trenches and (**d**) PS brush coated trenches (Adapted with permission from Chuang et al. [132]. Copyright 2009 American Chemical Society)

Successful positioning of PI-*b*-PFS block copolymer spheres in hexagonal grooves was also achieved, and complete 2D alignment was demonstrated [131]. Figure 27 shows the alignment of the domains with respect to the six sidewalls over the entire 800-nm-diameter hexagonal groove. The hexagonal grooves open up the possibility of accurate positioning of the domains, since one single domain is located in each corner, as shown in Fig. 27b.

The block copolymer architecture and the wettability of the substrate also play a key role in the self-assembly of the domains. Figure 28 illustrates both factors combined with graphoepitaxy by showing the self-assembly of a triblock terpolymer
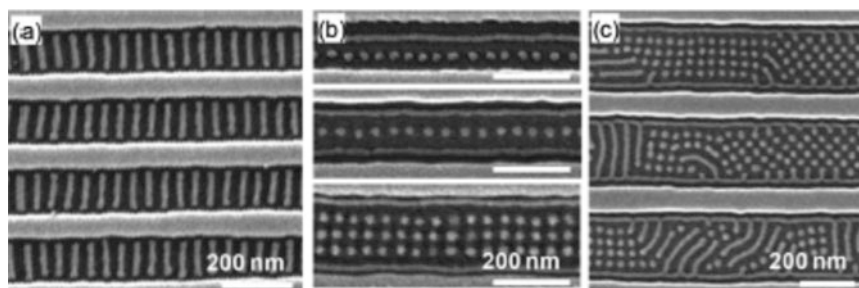
Fig. 29 SEM images of ~35 nm thick films of ISF/PS blend assembly in (**a**) a PS brush coated template and (**b**, **c**) uncoated silica substrates with (**b**) narrow and (**c**) wide grooves, after annealing and etching with oxygen RIE (Reprinted with permission from Chuang et al. [132]. Copyright 2009 American Chemical Society)

PI-*b*-PS-*b*-PFS blended with PS (ISF/PS), deposited as a thin film within shallow etched grooves in silica. As shown in Fig. 28a, thin films of the ISF/PS blend presented perfectly ordered cylinders with square-packed morphology, and the number of rows was controlled by the width of the grooves. The dots on the top view show PFS cylinders after etching of PS and PI blocks. The influence of the substrate surface chemistry was proved by coating the walls of the grooves with PS brushes. The difference in wettability of the various blocks leads to a different morphology during self-assembly. While an uncoated groove gave square-packed cylinders with the principal axis at 90° of the walls of the trench, PS brush coated grooves provided PFS microdomain arrays with 45° orientation, as shown in Fig. 28b.

The polymer film thickness of the previous system was investigated, and thicker films of ~35 nm presented different morphologies. As shown in Fig. 29a, for PS brush coated trenches, the PFS (and PI) cylinders lie in plane perpendicular to the trench walls without contacting the walls. Contrary to the previous examples of cylinders oriented perpendicular to the substrate surface, which was attributed to kinetic effects, the orientation in this case comes from the requirement for the middle PS block to contact the trench walls while maintaining its connectivity to the in-plane PI and PFS cylinders. In contrast, untreated grooves showed regions of mixed parallel and perpendicular cylinders (Fig. 29b, c). Figure 29b presents the case of narrow trenches containing in-plane PFS cylinders parallel to the trench walls and rows of cylinders oriented perpendicular to the substrate surface. Figure 29c shows wider grooves containing a variety of morphologies including branched cylinders and 90° and 45° oriented arrays. These results demonstrated that the cylinder microdomain orientation and the principal axes of the cylinder lattice can be controlled by tuning the film thickness and the relative affinity of the groove walls.

In order to gain more control on the positioning and ordering of the PFS cylindrical microdomains over larger surface areas, topographically guiding walls and posts were recently used by Ross, Manners, and coworkers [133]. Topographical ridge patterns with a rectangular layout and sparse arrays of posts were
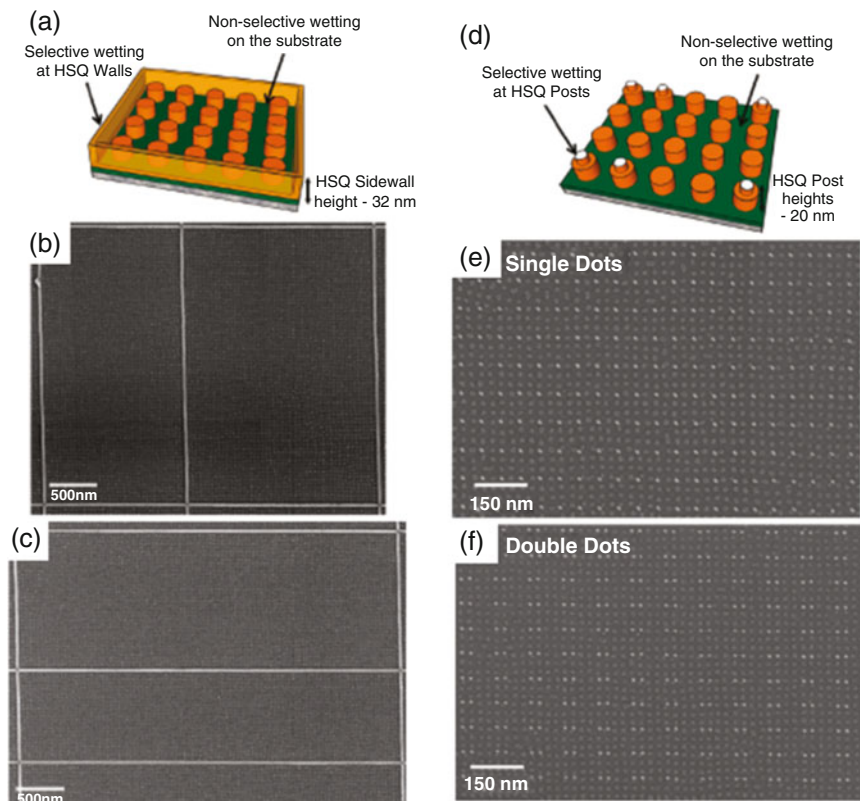
Fig. 30 (**a, d**) Schematics and (**b, c, e, f**) SEM images of highly ordered square arrays of ISF/PS blend self-assembly in HSQ templates consisting of (**b**) 1.5 and 2 μm × 3 μm topographical sidewalls; (**c**) 0.5 μm, 1 μm, and 1.5 μm × 4 μm topographical sidewalls; (**e**) 88 nm × 132 nm single posts; and (**f**) 44 nm spacing double posts (Adapted with permission from Lammertink et al. [133]. Copyright 2011 American Chemical Society)

prepared by electron-beam patterning of a negative tone inorganic hydrogen silsesquioxane (HSQ) resist (Fig. 30). To obtain preferential wetting on the sidewalls and nonpreferential wetting on the horizontal substrate surface, the substrate was functionalized with a PEO brush layer, and the sidewalls and posts were coated with a PFS brush layer. Highly ordered square patterns with a 44-nm period and an average grain size on the micrometer scale were produced. Topographical templates consisting of rectangular walls could produce "single grain" square symmetry patterns inside the template (Fig. 30a–c), while single and double HSQ post arrays allowed the authors to accurately align and register the PFS arrays (Fig. 30d–f). This method shows that a perfect control and positioning of the self-assembled block copolymer domains is possible, enabling the design of lithographic masks which can be used in the fabrication of complex CMOS.

6 Conclusion

In this chapter, the ability of anionic polymerization to synthesize various well-defined PFS-based copolymers with a narrow molar mass distribution, a low degree of polymerization, and complex architectures has been shown. The range of usable monomers was even expanded by the discovery of photoassisted anionic polymerization and the developments in the end-capping of living PFS chains, such as the use of a silacyclobutane which is acting as a "carbanion pump." Due to the possibility of varying the side groups of PFSs, a wide range of controllable properties has become accessible. Considering its exceptionally high resistance toward plasma etching, PFS may be of considerable value as an etch resist material in CMOS fabrication. The protective layer of silicon oxide and iron oxide formed on PFS features during reactive ion etching processes allows high contrasts to be achieved compared to common organic polymers. This contrast can be controlled by adjusting the conditions during the etching process, and one of the remaining challenges is to find the perfect parameter settings for etching, such as gas composition and pressure.

PFSs may be used as resists in soft lithography-based patterning approaches. Such patterning methods are both versatile and cost-effective and enable the generation of patterns at the micro- and submicrometer scales. PFSs have also been employed as resists in nanoimprint lithography processes, which offers advantages compared to conventional optical lithography techniques, due to the suppression of resolution limitations caused by diffraction. Several examples in which PFS was used as a resist in soft lithography, nanoimprint lithography, and nanosphere-assisted lithography have been presented. These examples demonstrate the utility of PFS in both micro- and nanofabrication.

Nevertheless, for sub-10-nm-node fabrication, challenging techniques remain to be developed and bottom-up lithography seems to hold the greatest potential. PFS-based BCPs are optimal candidates for bottom-up resists because of their low polydispersity, accurately controlled degrees of polymerization, high χ-value, high selectivity to etching, and long-range order of the microstructures. Polymer thin film physics differs from the bulk; therefore, properties, such as thermal transitions and surface viscoelasticity, need to be studied separately for each system. Precise and quantitative molar mass characterization is also required to obtain PDIs for both components and blocks. Edge roughness and defects must be reduced to improve pattern fidelity. The microphase separation patterns and the phase separation kinetics remain to be studied in detail. Long-range order has been induced using graphoepitaxy and several controlled geometries have been fabricated by this method. The ability to form ordered 3D arrangements makes BCPs attractive for the templated self-assembly of nanoscale periodic arrays. The coating of substrates by polymer brushes provides access to additional morphologies and constitutes an important tool in guided BCP self-assembly. Surfaces of underlying substrates and of topographic features in graphoepitaxy can be tailored to preferentially attract one block. Therefore, insight in creating both neutral and block-selective surfaces is needed. Substrate engineering

opens several new research avenues by giving opportunities to control grafting type, i.e., "to" or "from," grafting density and composition, and chain length. Furthermore, solvent and high-temperature annealing must be optimized to reduce both fabrication time and chemical costs and make these processes more feasible. In addition to BCP self-assembly, it would be of interest to create patterns of etch-resistant materials with thicknesses of 1 or 2 nm. The assembly of nanomaterials into such ultrathin barrier layers is expected to further improve resolution in the fabrication of nanoscale CMOS.

BCPs, soft matter, and inorganic materials, such as nanooptics and QD emitters, could also be integrated into complex systems with applications in areas, such as sensing and bionanomedicine. Resist development for CMOS fabrication, requiring ever smaller feature sizes and low defect densities, will continue to challenge polymer scientists in the years ahead.

Abbreviations

3 μ-ISF	PI-*arm*-PS-*arm*-PFS
AES	Auger electron spectroscopy
ATRP	Atom transfer radical polymerization
bcc	Body-centered cubic
BCP	Block copolymer
CMOS	Complementary metal oxide semiconductor
fcc	Face-centered cubic
HSQ	Hydrogen silsesquioxane
ISF	PI-*b*-PS-*b*-PFS
NCA	ROP α-amino acid N-carboxyanhydride ring-opening polymerization
NIL	Nanoimprint lithography
ODT	Order-disorder transition
PB	Poly(butadiene)
PDI	Polydispersity index
PDMS	Poly(dimethylsiloxane)
PEO	Poly(ethylene oxide)
PES	Poly(ethersulfone)
PFiPMS	Poly(ferrocenylisopropylmethylsilane)
PFMPS	Poly(ferrocenylmethylphenylsilane)
PFS	Poly(ferrocenylsilanes)
PI	Poly(isoprene)
PMMA	Poly(methyl methacrylate)
PROP	Photocontrolled living anionic ring-opening polymerization
PS	Poly(styrene)

RIE   Reactive ion etching
ROP   Ring-opening polymerization
SAM   Self-assembled monolayer
SANS   Small-angle neutron scattering
SPPS   Solid-phase peptide synthesis

References

1. Wanlass FM (1967) Low stand-by power complementary field effect circuitry. United States Patent US 3356858 A
2. Baker RJ (2011) CMOS: circuit design, layout, and simulation. John Wiley & Sons, Inc., hoboken, New Jersey
3. Haron NZ, Hamdioui S (2008) Why is CMOS scaling coming to an END? In: Design and Test Workshop, 2008. IDT 2008. 3rd International, 20–22 Dec 2008, pp 98–103. doi:10.1109/IDT.2008.4802475
4. Kusumoto S, Shima M, Wang Y, Shimokawa T, Sato H, Hieda K (2006) Advanced materials for 193 nm immersion lithography. Polymer Adv Tech 17(2):122–130. doi:10.1002/pat.677
5. Hori M, Nagai T, Nakamura A, Abe T, Wakamatsu G, Kakizawa T, Anno Y, Sugiura M, Kusumoto S, Yamaguchi Y, Shimokawa T (2008) Sub-40-nm half-pitch double patterning with resist freezing process. 69230H-69230H. doi:10.1117/12.772403
6. Pease RF, Chou SY (2008) Lithography and other patterning techniques for future electronics. Proc IEEE 96(2):248–270. doi:10.1109/JPROC.2007.911853
7. Acikgoz C, Hempenius MA, Huskens J, Vancso GJ (2011) Polymers in conventional and alternative lithography for the fabrication of nanostructures. Eur Polym J 47(11):2033–2052. http://dx.doi.org/10.1016/j.eurpolymj.2011.07.025
8. Kaufmann T, Ravoo BJ (2010) Stamps, inks and substrates: polymers in microcontact printing. Polym Chem 1(4):371–387. doi:10.1039/B9PY00281B
9. Hadjichristidis N, Pispas S, Floudas G (2003) Block copolymers: synthetic strategies, physical properties, and applications. John Wiley & Sons, Inc., hoboken, New Jersey
10. Hamley IW (2004) Developments in block copolymer science and technology. Wiley, Chichester
11. ERM Team (2007) International Technology Roadmap for Semiconductors: Emerging Research Materials, 2007 Edition. http://www.itrs.net/reports.html
12. Stoykovich MP, Nealey PF (2006) Block copolymers and conventional lithography. Mater Today 9(9):20–29. http://dx.doi.org/10.1016/S1369-7021(06)71619-4
13. Stoykovich MP, Müller M, Kim SO, Solak HH, Edwards EW, de Pablo JJ, Nealey PF (2005) Directed assembly of block copolymer blends into nonregular device-oriented structures. Science 308(5727):1442–1446. doi:10.1126/science.1111041
14. Chi L (2010) Nanotechnology: volume 8: nanostructured surfaces. Wiley-VCH Verlag GmbH & Co. KGaA, Weinheim
15. Nunns A, Gwyther J, Manners I (2013) Inorganic block copolymer lithography. Polymer 54(4):1269–1284. http://dx.doi.org/10.1016/j.polymer.2012.11.057
16. Rosenberg H, Rausch MD (1962) Silicon-containing dicyclopentadienylmetal compounds and polymers and methods for preparing same. US Patent 3060215
17. Foucher DA, Tang BZ, Manners I (1992) Ring-opening polymerization of strained, ring-tilted ferrocenophanes: a route to high-molecular-weight poly(ferrocenylsilanes). J Am Chem Soc 114(15):6246–6248. doi:10.1021/ja00041a053

18. Fossum E, Matyjaszewski K, Rulkens R, Manners I (1995) Polysilane-Poly(ferrocenylsilane) random copolymers. Macromolecules 28(1):401–402. doi:10.1021/ma00105a061

19. Gómez-Elipe P, Macdonald PM, Manners I (1997) Architectural control in the transition-metal-catalyzed ring-opening polymerization of silicon-bridged [1]ferrocenophanes. Angew Chem Int Ed Engl 36(7):762–764. doi:10.1002/anie.199707621

20. Ni Y, Rulkens R, Pudelski JK, Manners I (1995) Transition metal catalyzed ring-opening polymerization of silicon-bridged [1]ferrocenophanes at ambient temperature. Macromol Rapid Commun 16(9):637–641. doi:10.1002/marc.1995.030160901

21. Gómez-Elipe P, Resendes R, Macdonald PM, Manners I (1998) Transition metal catalyzed ring-opening polymerization (ROP) of silicon-bridged [1]ferrocenophanes: facile molecular weight control and the remarkably convenient synthesis of poly(ferrocenes) with regioregular, comb, star, and block architectures. J Am Chem Soc 120(33):8348–8356. doi:10.1021/ja981429h

22. Rulkens R, Lough AJ, Manners I (1994) Anionic ring-opening oligomerization and polymerization of silicon-bridged [1]ferrocenophanes: characterization of short-chain models for poly(ferrocenylsilane) high polymers. J Am Chem Soc 116(2):797–798. doi:10.1021/ja00081a062

23. Tanabe M, Manners I (2004) Photolytic living anionic ring-opening polymerization (ROP) of silicon-bridged [1]ferrocenophanes via an iron-cyclopentadienyl bond cleavage mechanism. J Am Chem Soc 126(37):11434–11435. doi:10.1021/ja046657s

24. Rasburn J, Petersen R, Jahr R, Rulkens R, Manners I, Vancso GJ (1995) Solid-state synthesis and morphology of poly(ferrocenyldimethylsilane). Chem Mater 7(5):871–877. doi:10.1021/cm00053a010

25. Korczagin I, Lammertink RH, Hempenius M, Golze S, Vancso GJ (2006) Surface nano- and microstructuring with organometallic polymers. In: Vancso GJ (ed) Ordered polymeric nanostructures at surfaces, vol 200. Advances in polymer science. Springer, Berlin Heidelberg, pp 91–117. doi:10.1007/12_038

26. Nelson JM, Rengel H, Manners I (1993) Ring-opening polymerization of [2]ferrocenophanes with a hydrocarbon bridge: synthesis of poly(ferrocenylethylenes). J Am Chem Soc 115(15): 7035–7036. doi:10.1021/ja00068a096

27. Nelson JM, Lough AJ, Manners I (1994) Synthesis and ring-opening polymerization of highly strained, ring-tilted [2]ruthenocenophanes. Angew Chem Int Ed Engl 33(9): 989–991. doi:10.1002/anie.199409891

28. Gallei M, Schmidt BVKJ, Klein R, Rehahn M (2009) Defined poly[styrene-block-(ferrocenylmethyl methacrylate)] diblock copolymers via living anionic polymerization. Macromol Rapid Commun 30(17):1463–1469. doi:10.1002/marc.200900177

29. Foucher D, Ziembinski R, Petersen R, Pudelski J, Edwards M, Ni Y, Massey J, Jaeger CR, Vancso GJ, Manners I (1994) Synthesis, characterization, and properties of high molecular weight unsymmetrically substituted poly(ferrocenylsilanes). Macromolecules 27(14): 3992–3999. doi:10.1021/ma00092a046

30. Foucher DA, Ziembinski R, Tang BZ, Macdonald PM, Massey J, Jaeger CR, Vancso GJ, Manners I (1993) Synthesis, characterization, glass transition behavior, and the electronic structure of high-molecular-weight, symmetrically substituted poly(ferrocenylsilanes) with alkyl or aryl side groups. Macromolecules 26(11):2878–2884. doi:10.1021/ma00063a037

31. Manners I (2003) Polymer science with main group elements and transition metals. Macromol Symp 196(1):57–62. doi:10.1002/masy.200390176

32. Kulbaba K, Manners I (2001) Polyferrocenylsilanes: metal-containing polymers for materials science, self-assembly and nanostructure applications. Macromol Rapid Commun 22(10): 711–724. doi:10.1002/1521-3927(20010701)22:10<711::AID-MARC711>3.0.CO;2-C

33. Manners I (1999) Poly(ferrocenylsilanes): novel organometallic plastics. Chem Commun 1999(10):857–865. doi:10.1039/A810043H

34. Hempenius MA, Brito FF, Vancso GJ (2003) Synthesis and characterization of anionic and cationic poly(ferrocenylsilane) polyelectrolytes. Macromolecules 36(17):6683–6688. doi:10.1021/ma034432g

35. Wang Z, Lough A, Manners I (2002) Synthesis and characterization of water-soluble cationic and anionic polyferrocenylsilane polyelectrolytes. Macromolecules 35(20):7669–7677. doi:10.1021/ma0203694

36. Hempenius MA, Vancso GJ (2002) Synthesis of a polyanionic water-soluble poly (ferrocenylsilane). Macromolecules 35(7):2445–2447. doi:10.1021/ma0119629

37. Hempenius MA, Robins NS, Lammertink RGH, Vancso GJ (2001) Organometallic poly-electrolytes: synthesis, characterization and layer-by-layer deposition of cationic poly (ferrocenyl(3-ammoniumpropyl)-methylsilane). Macromol Rapid Commun 22(1):30–33. doi:10.1002/1521-3927(20010101)22:1<30::AID-MARC30>3.0.CO;2-J

38. Power-Billard KN, Manners I (1999) Hydrophilic and water-soluble poly(ferrocenylsilanes). Macromolecules 33(1):26–31. doi:10.1021/ma991350c

39. Ginzburg M, Galloro J, Jäkle F, Power-Billard KN, Yang S, Sokolov I, Lam CNC, Neumann AW, Manners I, Ozin GA (2000) Layer-by-layer self-assembly of organic − organometallic polymer electrostatic superlattices using poly(ferrocenylsilanes). Langmuir 16(24): 9609–9614. doi:10.1021/la0012283

40. Wurm F, Hilf S, Frey H (2009) Electroactive linear–hyperbranched block copolymers based on linear poly(ferrocenylsilane)s and hyperbranched poly(carbosilane)s. Chem Eur J 15(36): 9068–9077. doi:10.1002/chem.200900666

41. Sui X, van Ingen L, Hempenius MA, Vancso GJ (2010) Preparation of a rapidly forming poly (ferrocenylsilane)-poly(ethylene glycol)-based hydrogel by a Thiol-Michael addition click reaction. Macromol Rapid Commun 31(23):2059–2063. doi:10.1002/marc.201000420

42. Sui X, Feng X, Song J, Hempenius MA, Vancso GJ (2012) Electrochemical sensing by surface-immobilized poly(ferrocenylsilane) grafts. J Mater Chem 22(22):11261–11267. doi:10.1039/C2JM30599B

43. Rulkens R, Ni Y, Manners I (1994) Living anionic ring-opening polymerization of silicon-bridged [1]ferrocenophanes: synthesis and characterization of poly(ferrocenylsilane)-polysiloxane block copolymers. J Am Chem Soc 116(26):12121–12122. doi:10.1021/ja00105a090

44. Ni Y, Rulkens R, Manners I (1996) Transition metal-based polymers with controlled archi-tectures: well-defined poly(ferrocenylsilane) homopolymers and multiblock copolymers via the living anionic ring-opening polymerization of silicon-bridged [1]ferrocenophanes. J Am Chem Soc 118(17):4102–4114. doi:10.1021/ja953805t

45. Zhang M, Rupar PA, Feng C, Lin K, Lunn DJ, Oliver A, Nunns A, Whittell GR, Manners I, Winnik MA (2013) Modular synthesis of polyferrocenylsilane block copolymers by Cu-Catalyzed Alkyne/Azide "Click" Reactions. Macromolecules 46(4):1296–1304. doi:10.1021/ma302054q

46. Resendes R, Massey J, Dorn H, Winnik MA, Manners I (1999) A convenient, transition metal-catalyzed route to water-soluble amphiphilic organometallic block copolymers: syn-thesis and aqueous self-assembly of poly(ethylene oxide)-block-poly(ferrocenylsilane). Macromolecules 33(1):8–10. doi:10.1021/ma991450i

47. Lammertink RGH, Hempenius MA, van den Enk JE, Chan VZH, Thomas EL, Vancso GJ (2000) Nanostructured thin films of organic–organometallic block copolymers: one-step lithography with poly(ferrocenylsilanes) by reactive ion etching. Adv Mater 12(2):98–103. doi:10.1002/(sici)1521-4095(200001)12:2<98::aid-adma98>3.0.co;2-5

48. Wang XS, Winnik MA, Manners I (2002) Synthesis and solution self-assembly of coil − crystalline − coil   polyferrocenylphosphine-b-polyferrocenylsilane-b-polysiloxane triblock copolymers. Macromolecules 35(24):9146–9150. doi:10.1021/ma020564i

49. Kloninger C, Rehahn M (2004) 1,1-dimethylsilacyclobutane-mediated living anionic block copolymerization of [1]dimethylsilaferrocenophane and methyl methacrylate. Macromole-cules 37(5):1720–1727. doi:10.1021/ma034909o

50. Korczagin I, Hempenius MA, Vancso GJ (2004) Poly(ferrocenylsilane-block-methacrylates) via sequential anionic and atom transfer radical polymerization. Macromolecules 37(5):1686–1690. doi:10.1021/ma0358172

51. Kim KT, Vandermeulen GWM, Winnik MA, Manners I (2005) Organometallic−polypeptide block copolymers: synthesis and properties of poly(ferrocenyldimethylsilane)-b-poly- (γ-benzyl-l-glutamate). Macromolecules 38(12):4958–4961. doi:10.1021/ma050336z

52. Vandermeulen GWM, Kim KT, Wang Z, Manners I (2006) Metallopolymer−peptide conjugates: synthesis and self-assembly of polyferrocenylsilane graft and block copolymers containing a β-sheet forming Gly-Ala-Gly-Ala tetrapeptide segment. Biomacromolecules 7(4):1005–1010. doi:10.1021/bm050732p

53. Wang Y, Zou S, Kim KT, Manners I, Winnik MA (2008) Organometallic–polypeptide block copolymers: synthesis and self-assembly of poly(ferrocenyldimethylsilane)-b-poly(-ε-benzyloxycarbonyl-L-lysine). Chem Eur J 14(28):8624–8631. doi:10.1002/chem.200800762

54. Roerdink M, van Zanten TS, Hempenius MA, Zhong Z, Feijen J, Vancso GJ (2007) Poly (ferrocenylsilane)-block-polylactide block copolymers. Macromol Rapid Commun 28(22): 2125–2130. doi:10.1002/marc.200700364

55. Soto AP, Manners I (2008) Poly(ferrocenylsilane-b-polyphosphazene) (PFS-b-PP): a new class of organometallic−inorganic block copolymers. Macromolecules 42(1):40–42. doi:10.1021/ma8016713

56. Smith GS, Patra SK, Vanderark L, Saithong S, Charmant JPH, Manners I (2010) Photocontrolled living anionic polymerization of silicon-bridged [1]ferrocenophanes with fluorinated substituents: synthesis and characterization of fluorinated polyferrocenylsilane (PFS) homopolymers and block copolymers. Macromol Chem Phys 211(3):303–312. doi:10.1002/macp.200900395

57. Gilroy JB, Patra SK, Mitchels JM, Winnik MA, Manners I (2011) Main-chain heterobimetallic block copolymers: synthesis and self-assembly of polyferrocenylsilane-b-poly (cobaltoceniummethylene). Angew Chem Int Ed 50(26):5851–5855. doi:10.1002/anie.201008184

58. Tanabe M, Vandermeulen GWM, Chan WY, Cyr PW, Vanderark L, Rider DA, Manners I (2006) Photocontrolled living polymerizations. Nat Mater 5(6):467–470. http://www.nature.com/nmat/journal/v5/n6/suppinfo/nmat1649_S1.html

59. Rider DA, Manners I (2007) Synthesis, self-assembly, and applications of polyferrocenylsilane block copolymers. Polym Rev 47(2):165–195

60. Datta U, Rehahn M (2004) Synthesis and self-assembly of styrene–[1]dimethylsilaferrocenophane–methyl methacrylate pentablock copolymers. Macromol Rapid Commun 25(18):1615–1622. doi:10.1002/marc.200400241

61. Kim KT, Han J, Ryu CY, Sun FC, Sheiko SS, Winnik MA, Manners I (2006) Synthesis, characterization, and AFM studies of dendronized polyferrocenylsilanes. Macromolecules 39(23):7922–7930. doi:10.1021/ma060607l

62. Nunns A, Ross CA, Manners I (2013) Synthesis and bulk self-assembly of ABC star terpolymers with a polyferrocenylsilane metalloblock. Macromolecules 46(7):2628–2635. doi:10.1021/ma302602u

63. d'Agostino R (1990) Plasma deposition, treatment, and etching of polymers. Ed. Academic Press, INC., London

64. Manos DM, Flamm DL (1989) Plasma etching: an introduction. Academic, Boston

65. van Roosmalen AJ, Baggerman JAG, Brader SJH (1991) Dry etching for VLSI. Springer Science+Business Media, New York

66. Flamm D, Donnelly V (1981) The design of plasma etchants. Plasma Chem Plasma Process 1(4):317–363. doi:10.1007/BF00565992

67. Lammertink RGH, Hempenius MA, Chan VZH, Thomas EL, Vancso GJ (2001) Poly (ferrocenyldimethylsilanes) for reactive ion etch barrier applications. Chem Mater 13(2):429–434. doi:10.1021/cm001052q

68. Knizikevičius R, Galdikas A, Grigonis A (2002) Real dimensional simulation of anisotropic etching of silicon in CF4 + O2 plasma. Vacuum 66(1):39–47. http://dx.doi.org/10.1016/S0042-207X(01)00418-3

69. Kokkoris G, Gogolides E, Boudouvis AG (2002) Etching of SiO[sub 2] features in fluorocarbon plasmas: explanation and prediction of gas-phase-composition effects on aspect ratio dependent phenomena in trenches. J Appl Phys 91(5):2697–2707

70. Henri J, Han G, de Meint B, Miko E, Jan F (1996) A survey on the reactive ion etching of silicon in microtechnology. J Micromech Microeng 6(1):14

71. Oehrlein GS, Williams HL (1987) Silicon etching mechanisms in a CF[sub 4]/H[sub 2] glow discharge. J Appl Phys 62(2):662–672

72. Coburn JW, Kay E (1979) Some chemical aspects of the fluorocarbon plasma etching of silicon and its compounds. Solid State Technol 22(4):117–124

73. Strobel M, Corn S, Lyons CS, Korba GA (1987) Plasma fluorination of polyolefins. J Polym Sci A Polym Chem 25(5):1295–1307. doi:10.1002/pola.1987.080250508

74. Mogab CJ, Adams AC, Flamm DL (1978) Plasma etching of Si and SiO[sub 2]–-the effect of oxygen additions to CF[sub 4] plasmas. J Appl Phys 49(7):3796–3803

75. Donnelly VM, Flamm DL, Dautremont-Smith WC, Werder DJ (1984) Anisotropic etching of SiO[sub 2] in low-frequency CF[sub 4]/O[sub 2] and NF[sub 3]/Ar plasmas. J Appl Phys 55(1):242–252

76. Egitto FD, Matienzo LJ, Schreyer HB (1992) Reactive ion etching of poly(tetrafluoroethylene) in O[sub 2]–CF[sub 4] plasmas. J Vac Sci Technol A (Vacuum, Surfaces, and Films) 10(5):3060–3064

77. Korczagin I, Golze S, Hempenius MA, Vancso GJ (2003) Surface micropatterning and lithography with poly(Ferrocenylmethylphenylsilane). Chem Mater 15(19):3663–3668. doi:10.1021/cm031024i

78. Legtenberg R, Jansen H, de Boer M, Elwenspoek M (1995) Anisotropic reactive ion etching of silicon using SF 6/O 2/CHF 3 gas mixtures. J Electrochem Soc 142(6):2020–2028. doi:10.1149/1.2044234

79. Xia Y, Whitesides GM (1998) Soft lithography. Angew Chem Int Ed 37(5):550–575. doi:10.1002/(SICI)1521-3773(19980316)37:5<550::AID-ANIE550>3.0.CO;2-G

80. Kumar A, Whitesides GM (1993) Features of gold having micrometer to centimeter dimensions can be formed through a combination of stamping with an elastomeric stamp and an alkanethiol "ink"' followed by chemical etching. Appl Phys Lett 63(14):2002–2004

81. Clarson SJ, Semlyen JA (1993) Siloxane polymers. PTR Prentice Hall, Englewood Cliffs

82. Donzel C, Geissler M, Bernard A, Wolf H, Michel B, Hilborn J, Delamarche E (2001) Hydrophilic poly(dimethylsiloxane) stamps for microcontact printing. Adv Mater 13(15):1164–1167. doi:10.1002/1521-4095(200108)13:15<1164::AID-ADMA1164>3.0.CO;2-S

83. Hillborg H, Gedde UW (1998) Hydrophobicity recovery of polydimethylsiloxane after exposure to corona discharges. Polymer 39(10):1991–1998. http://dx.doi.org/10.1016/S0032-3861(97)00484-9

84. Chua DBH, Ng HT, Li SFY (2000) Spontaneous formation of complex and ordered structures on oxygen-plasma-treated elastomeric polydimethylsiloxane. Appl Phys Lett 76(6):721–723

85. Lammertink RGH, Korczagin I, Hempenius MA, Vancso GJ (2003) Metal-containing polymers for high-performance resist applications. In: Macromolecules containing metal and metal-like elements. Wiley, pp 115–133. doi:10.1002/0471466573.ch7

86. Bowden N, Brittain S, Evans A, Hutchinson J, Whitesides G (1998) Spontaneous formation of ordered structures in thin films of metals supported on an elastomeric polymer. Nature 393(6681):146–149. citeulike-article-id:2885101. doi:10.1038/30193

87. Efimenko K, Wallace WE, Genzer J (2002) Surface modification of Sylgard-184 poly (dimethyl siloxane) networks by ultraviolet and ultraviolet/ozone treatment. J Colloid Interface Sci 254(2):306–315. http://dx.doi.org/10.1006/jcis.2002.8594

88. Chou SY, Krauss PR, Renstrom PJ (1995) Imprint of sub-25 nm vias and trenches in polymers. Appl Phys Lett 67(21):3114. doi:10.1063/1.114851

89. Chou SY, Krauss PR, Renstrom PJ (1996) Imprint lithography with 25-nanometer resolution. Science 272(5258):85–87. doi:10.1126/science.272.5258.85

90. Bender M, Otto M, Hadam B, Vratzov B, Spangenberg B, Kurz H (2000) Fabrication of nanostructures using a UV-based imprint technique. Microelectron Eng 53(1):233–236. doi:10.1016/S0167-9317(00)00304-X

91. Colburn M, Johnson SC, Stewart MD, Damle S, Bailey TC, Choi B, Wedlake M, Michaelson TB, Sreenivasan SV, Ekerdt JG, Willson CG (1999) Step and flash imprint lithography: a new approach to high-resolution patterning. Proc SPIE 3676:379–389. doi:10.1117/12.351155

92. Acikgoz C, Hempenius MA, Julius Vancso G, Huskens J (2009) Direct surface structuring of organometallic resists using nanoimprint lithography. Nanotechnology 20(13):135304. doi:10.1088/0957-4484/20/13/135304

93. Resnick DJ, Sreenivasan SV, Willson CG (2005) Step & flash imprint lithography. Mater Today 8(2):34–42. doi:10.1016/s1369-7021(05)00700-5

94. Acikgoz C, Ling XY, Phang IY, Hempenius MA, Reinhoudt DN, Huskens J, Vancso GJ (2009) Fabrication of freestanding nanoporous polyethersulfone membranes using organometallic polymer resists patterned by nanosphere lithography. Adv Mater 21(20):2064–2067. doi:10.1002/adma.200803647

95. Ling XY, Malaquin L, Reinhoudt DN, Wolf H, Huskens J (2007) An in situ study of the adsorption behavior of functionalized particles on self-assembled monolayers via different chemical interactions. Langmuir 23(20):9990–9999. doi:10.1021/la701671s

96. Leibler L (1980) Theory of microphase separation in block copolymers. Macromolecules 13(6):1602–1617. doi:10.1021/ma60078a047

97. Sun Z, Wang CH (1995) Determination of Flory–Huggins interaction parameter and self-diffusion coefficients in ternary polymer solutions by quasielastic light scattering. J Chem Phys 103(9):3762–3766

98. Posharnowa N, Schneider A, Wunsch M, Kuleznew V, Wolf BA (2001) Polymer–polymer interaction parameters for homopolymers and copolymers from light scattering and phase separation experiments in a common solvent. J Chem Phys 115(20):9536–9546

99. Fukuda T, Nagata M, Inagaki H (1984) Light scattering from ternary solutions. 1. Dilute solutions of polystyrene and poly(methyl methacrylate). Macromolecules 17(4):548–553. doi:10.1021/ma00134a007

100. Nedoma AJ, Robertson ML, Wanakule NS, Balsara NP (2008) Measurements of the composition and molecular weight dependence of the Flory – Huggins interaction parameter. Macromolecules 41(15):5773–5779. doi:10.1021/ma800698r

101. Lee JH, Balsara NP, Chakraborty AK, Krishnamoorti R, Hammouda B (2002) Thermodynamics and phase behavior of block copolymer/homopolymer blends with attractive and repulsive interactions. Macromolecules 35(20):7748–7757. doi:10.1021/ma020361u

102. Lefebvre AA, Balsara NP, Lee JH, Vaidyanathan C (2002) Determination of the phase boundary of high molecular weight polymer blends. Macromolecules 35(20):7758–7764. doi:10.1021/ma020552x

103. Zirkel A, Gruner SM, Urban V, Thiyagarajan P (2002) Small-angle neutron scattering investigation of the Q-dependence of the Flory – Huggins interaction parameter in a binary polymer blend. Macromolecules 35(19):7375–7386. doi:10.1021/ma010576o

104. Ryu DY, Jeong U, Lee DH, Kim J, Youn HS, Kim JK (2003) Phase behavior of deuterated polystyrene-block-poly(n-pentyl methacrylate) copolymers. Macromolecules 36(8):2894–2902. doi:10.1021/ma026002g

105. Elbs H, Krausch G (2004) Ellipsometric determination of Flory-Huggins interaction parameters in solution. Polymer 45(23):7935–7942. http://dx.doi.org/10.1016/j.polymer.2004.09.021

106. Marsac P, Li T, Taylor L (2009) Estimation of drug–polymer miscibility and solubility in amorphous solid dispersions using experimentally determined interaction parameters. Pharm Res 26(1):139–151. doi:10.1007/s11095-008-9721-1

107. Bates FS, Fredrickson GH (1990) Block copolymer thermodynamics: theory and experiment. Ann Rev Phys Chem 41(1):525–557. doi:10.1146/annurev.pc.41.100190.002521

108. Eitouni HB, Balsara NP, Hahn H, Pople JA, Hempenius MA (2002) Thermodynamic interactions in organometallic block copolymers: poly(styrene-block-ferrocenyldimethylsilane). Macromolecules 35(20):7765–7772. doi:10.1021/ma020647z

109. Xu J, Bellas V, Jungnickel B, Stühn B, Rehahn M (2010) A novel crystallization scheme in poly[styrene-block-(ferrocenyl dimethylsilane)] diblock copolymers. Macromol Chem Phys 211(21):2276–2285. doi:10.1002/macp.201000220

110. Rider DA, Cavicchi KA, Power-Billard KN, Russell TP, Manners I (2005) Diblock copolymers with amorphous atactic polyferrocenylsilane blocks: synthesis, characterization, and self-assembly of polystyrene-block-poly(ferrocenylethylmethylsilane) in the bulk state. Macromolecules 38(16):6931–6938. doi:10.1021/ma047410i

111. Gwyther J, Lotze G, Hamley I, Manners I (2011) Double-gyroid morphology of a polystyrene-block-poly(ferrocenylethylmethylsilane) diblock copolymer: a route to ordered bicontinuous nanoscale architectures. Macromol Chem Phys 212(2):198–201. doi:10.1002/macp.201000496

112. Gwyther J, Manners I (2009) Diblock copolymers with an amorphous, high glass transition temperature, organometallic block: synthesis, characterisation and self-assembly of polystyrene-b-poly(ferrocenylisopropylmethylsilane) in the bulk state. Polymer 50(23):5384–5389. http://dx.doi.org/10.1016/j.polymer.2009.08.041

113. Yamauchi K, Hasegawa H, Hashimoto T, Köhler N, Knoll K (2002) Synthesis and morphological studies of polyisoprene-block-polystyrene-block-poly(vinyl methyl ether) triblock terpolymer. Polymer 43(12):3563–3570. http://dx.doi.org/10.1016/S0032-3861(02)00112-X

114. Mogi Y, Mori K, Matsushita Y, Noda I (1992) Tricontinuous morphology of triblock copolymers of the ABC type. Macromolecules 25(20):5412–5415. doi:10.1021/ma00046a044

115. Breiner U, Krappe U, Thomas EL, Stadler R (1998) Structural characterization of the "knitting pattern" in polystyrene-block-poly(ethylene-co-butylene)-block-poly(methyl methacrylate) triblock copolymers. Macromolecules 31(1):135–141. doi:10.1021/ma961550d

116. Kloninger C, Rehahn M (2004) Bicontinuous gyroidic morphologies in ferrocenyldimethylsilane-b-methyl methacrylate diblock copolymer blends. Macromolecules 37(22):8319–8324. doi:10.1021/ma0489321

117. Corté L, Yamauchi K, Court F, Cloître M, Hashimoto T, Leibler L (2003) Annealing and defect trapping in lamellar phases of triblock terpolymers. Macromolecules 36(20):7695–7706. doi:10.1021/ma034169j

118. Park M, Harrison C, Chaikin PM, Register RA, Adamson DH (1997) Block copolymer lithography: periodic arrays of ~1011 holes in 1 square centimeter. Science 276(5317):1401–1404. doi:10.1126/science.276.5317.1401

119. Mansky P, Harrison CK, Chaikin PM, Register RA, Yao N (1996) Nanolithographic templates from diblock copolymer thin films. Appl Phys Lett 68(18):2586–2588

120. Black CT, Guarini KW, Milkove KR, Baker SM, Russell TP, Tuominen MT (2001) Integration of self-assembled diblock copolymers for semiconductor capacitor fabrication. Appl Phys Lett 79(3):409–411

121. Black CT, Guarini KW, Ying Z, Kim H, Benedict J, Sikorski E, Babich IV, Milkove KR (2004) High-capacity, self-assembled metal-oxide-semiconductor decoupling capacitors. Electron Device Lett IEEE 25(9):622–624. doi:10.1109/LED.2004.834637

122. Black CT (2005) Self-aligned self assembly of multi-nanowire silicon field effect transistors. Appl Phys Lett 87(16):163116

123. Black CT, Ruiz R, Breyta G, Cheng JY, Colburn ME, Guarini KW, Kim HC, Zhang Y (2007) Polymer self assembly in semiconductor microelectronics. IBM J Res Dev 51(5):605–633. doi:10.1147/rd.515.0605

124. Guarini KW, Black CT, Zhang Y, Babich IV, Sikorski EM, Gignac LM (2003) Low voltage, scalable nanocrystal FLASH memory fabricated by templated self assembly. Electronic devices meeting, 2003. IEDM '03 technical digest. IEEE International, pp 541–544

125. Cheng JY, Ross CA, Chan VZH, Thomas EL, Lammertink RGH, Vancso GJ (2001) Formation of a cobalt magnetic dot array via block copolymer lithography. Adv Mater 13(15):1174–1178. doi:10.1002/1521-4095(200108)13:15<1174::aid-adma1174>3.0.co;2-q

126. Aissou K, Choi HK, Nunns A, Manners I, Ross CA (2013) Ordered nanoscale Archimedean tilings of a templated 3-miktoarm star terpolymer. Nano Lett 13(2):835–839. doi:10.1021/nl400006c

127. Choi HK, Nunns A, Sun XY, Manners I, Ross CA (2014) Thin film knitting pattern morphology from a miktoarm star terpolymer. Adv Mater 26(16):2474–2479. doi:10.1002/adma.201305243

128. Segalman RA, Yokoyama H, Kramer EJ (2001) Graphoepitaxy of spherical domain block copolymer films. Adv Mater 13(15):1152–1155

129. Cheng JY, Ross CA, Thomas EL, Smith HI, Vancso GJ (2002) Fabrication of nanostructures with long-range order using block copolymer lithography. Appl Phys Lett 81(19):3657–3659

130. Cheng JY, Zhang F, Chuang VP, Mayes AM, Ross CA (2006) Self-assembled one-dimensional nanostructure arrays. Nano Lett 6(9):2099–2103. doi:10.1021/nl061563x

131. Roerdink M, Hempenius MA, Gunst U, Arlinghaus HF, Vancso GJ (2007) Substrate wetting and topographically induced ordering of amorphous PI-b-PFS block-copolymer domains. Small 3(8):1415–1423. doi:10.1002/smll.200700044

132. Chuang VP, Gwyther J, Mickiewicz RA, Manners I, Ross CA (2009) Templated self-assembly of square symmetry arrays from an ABC triblock terpolymer. Nano Lett 9(12):4364–4369. doi:10.1021/nl902646e

133. Son JG, Gwyther J, Chang J-B, Berggren KK, Manners I, Ross CA (2011) Highly ordered square arrays from a templated ABC triblock terpolymer. Nano Lett 11(7):2849–2855. doi:10.1021/nl201262f

Polymerization Using Phosphazene Bases

Junpeng Zhao, Nikos Hadjichristidis, and Helmut Schlaad

Abstract In the recent rise of metal-free polymerization techniques, organic phosphazene superbases have shown their remarkable strength as promoter/catalyst for the anionic polymerization of various types of monomers. Generally, the complexation of phosphazene base with the counterion (proton or lithium cation) significantly improves the nucleophilicity of the initiator/chain end resulting in highly enhanced polymerization rates, as compared with conventional metal-based initiating systems. In this chapter, the general features of phosphazene-promoted/catalyzed polymerizations and the applications in macromolecular engineering (synthesis of functionalized polymers, block copolymers, and macromolecular architectures) are discussed with challenges and perspectives being pointed out.

Keywords Metal-free polymerization • Organocatalytic polymerization • Phosphazene bases

J. Zhao
Faculty of Materials Science and Engineering, South China University of Technology, Guangzhou 510641, People's Republic of China
e-mail: msjpzhao@scut.edu.cn

N. Hadjichristidis
Division of Physical Sciences and Engineering, KAUST Catalysis Center (KCC), Polymer Synthesis Laboratory, King Abdullah University of Science and Technology (KAUST), Thuwal, Saudi Arabia
e-mail: Nikolaos.Hadjichristidis@kaust.edu.sa

H. Schlaad (✉)
Department of Colloid Chemistry, Max Planck Institute of Colloids and Interfaces, Potsdam 14424, Germany

Institute of Chemistry, University of Potsdam, Karl-Liebknecht-Str. 24-25, Potsdam 14476, Germany
e-mail: schlaad@uni-potsdam.de

1 Introduction

Organocatalytic, i.e., metal-free, polymerization/depolymerization techniques are among the most appealing topics in polymer chemistry, not only for the inherent merit that products are free of residual metal compounds but also for the powerful synthetic toolbox for sophisticated macromolecular engineering [1–3]. Through the activation of monomer, initiator/chain end, or simultaneous activation of both, polymerization (in most cases a ring-opening polymerization of heterocycles) from initiating sites on certain substrates can be conducted, usually in a controlled manner, giving rise to polymers with narrow molecular weight distribution, high-level chain-end functionality, and/or designated macromolecular architectures [1–4].

Organic phosphazene superbases (Fig. 1) [5] and corresponding phosphazenium cations (Fig. 2) [6], first introduced by Schwesinger et al., have been utilized as
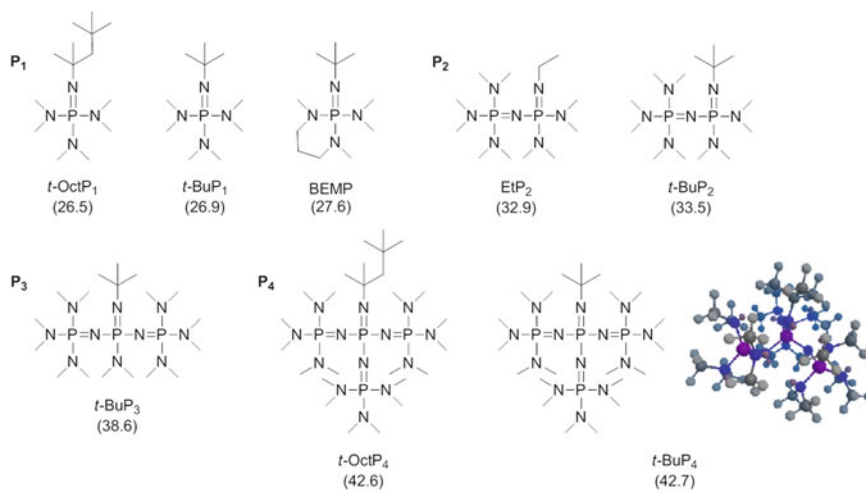
Fig. 1 Chemical structures of phosphazene bases P_x ($x = 1$–4, number of $P=N$ units) in the order of increasing basicity (pK_a values in acetonitrile in parentheses). BEMP, 2-*tert*-butylimino-2-diethylamino-1,3-dimethylperhydro-1,3,2-diazaphosphorine; *t*-BuP$_4$, 1-*tert*-butyl-4,4,4-tris(dimethylamino)-2,2-bis[tris(dimethylamino)phosphoranylidenamino]-$2\lambda^5,4\lambda^5$-catenadi(phosphazene)
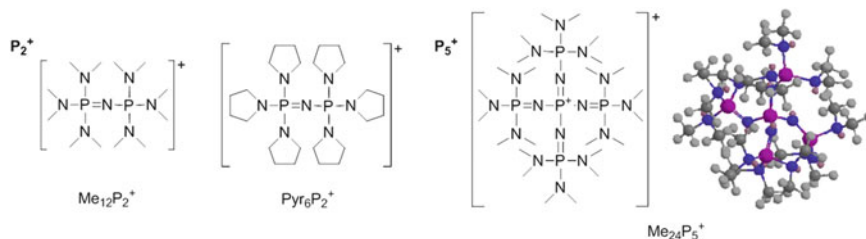
Fig. 2 Chemical structures of non-protonated phosphazenium cations P_x^+ ($x = 2, 5$)

effective catalysts or promoters for the polymerizations of heterocycles and also of vinyl monomers. The main feature of phosphazenes is, besides good solubility in many organic solvents and easy handling and work-up, the high basicity to generate a reactive anionic species associated to a very soft counterion. So far, the polymerizations of epoxides [7–13], cyclosiloxanes [14–18], lactams [19, 20], cyclopropane derivatives [21–23], cyclic esters [24–28], cyclic carbonates [29–31], alkyl (meth) acrylates [32–36], and dienes [37] have been reported. By intentionally employing different substrates, this synthetic strategy has also manifested the strength in facile achievement of end-functionalized polymers (the substrates being small molecules or biomolecules) [38, 39] and complex macromolecular architectures (the substrates being macromolecules) [40–42].

In the following sections, the general polymerization reactions and the advanced application of phosphazenes in macromolecular engineering will be described.

2   Polymerization Reactions

The main feature of the phosphazene bases P_{1-4} (Fig. 1) used in anionic polymerization is that they are bulky and extremely strong ($26 < pK_a < 43$ in acetonitrile, the pK_a is increasing from P_1 to P_4) but non-nucleophilic Brönsted bases, in contrast to the commonly employed alkali metal organic initiators [4]. Due to their basicity, they can readily generate reactive anions by the deprotonation of acidic or protic moieties, i.e., hydroxyl ($-OH$) [4], thiol ($-SH$) [21–23], secondary amide ($-CONH–$) [43], and alkyne ($-C \equiv CH$) [44], or by the complexation of lithium ions [12] (similar to the formation of cation inclusion complexes with crown ethers or cryptands [4]). However, deprotonation also involves polar CH acidic solvents like acetone, acetonitrile, or dimethyl sulfoxide, especially with P_4 but also P_2 [5, 45]; hence, phosphazenes are preferably used in non-acidic and aprotic solvents (hexane, tetrahydrofuran, etc.). The non-protonated phosphazenium cations P_2^+ or P_5^+ (Fig. 2) can replace metal ions of initiating species to promote a fast anionic polymerization [6]. In any case, an anionic species (alcoholate, ester enolate, etc.) with a large and very soft counterion is generated, which then exhibits higher reactivity because of the larger interionic distance and the lower tendency for ion-pair association.

2.1   Polymerization with Protonated Phosphazene Bases

Epoxides, mainly ethylene oxide and propylene oxide, were polymerized by the anionic species formed by deprotonation of an alcohol (methanol, octanol [7, 8], dipropylene glycol [46], terpene–OH [39], or polymer–OH [8, 47, 48]), phenol [38, 40, 41], or amide [43], usually with t-BuP$_4$ (Scheme 1).

Polymerizations were preferably performed in tetrahydrofuran solution at 25–50 °C but as well in toluene ($\leq$80 °C) or in bulk (propylene oxide, 100 °C). The propagating species were ion pairs with a protonated phosphazenium cation,

Scheme 1 Polymerization of epoxide, cyclosiloxane, or lactone by alkoxide-[t-BuP$_4$H$^+$] ion pair [38]

t-BuP$_4$H$^+$, with expected higher reactivity than for instance the commonly used potassium ion pairs (radii: t-BuP$_4$H$^+$ 7.0 Å [49] or 4.7 Å [50], K$^+$ 1.4 Å). However, kinetic data are not available. A poly(ethylene oxide) of 5.8 kDa and narrow molecular weight distribution (dispersity <1.1) at >90 % conversion could be prepared within 2 days at room temperature [7, 8]. In tetrahydrofuran at 45 °C, monomer conversion was quantitative within less than a day to give a polymer of 2.5 kDa [38]. With the less bulky t-BuP$_2$H$^+$ (radius: 3.3 Å [50]), higher temperature, higher monomer concentration, and longer polymerization time were needed to reach high conversion of ethylene oxide (target molecular weight: 5 kDa); polymerization of propylene oxide with t-BuP$_2$H$^+$ was not successful [51].

While the polymerization of ethylene oxide with t-BuP$_4$H$^+$ proceeds in the absence of side reactions [7], the polymerization of propylene oxide (bulk, 95–110 °C) was accompanied by transfer reactions [46]. The poly(propylene oxide)s contained unsaturated chain ends, 0.06 mol/kg, but had narrow molecular weight distribution with a dispersity of ~1.1 (see also Sect. 2.3).

Octamethyl- (D$_4$) and octaphenylcyclotetrasiloxane (P$_4$) have been polymerized with CH$_3$O$^-$[t-BuP$_4$H$^+$] in toluene solution or in bulk, respectively, at room temperature [7, 15]. The polymerization of D$_4$ was extremely fast, the equilibrium being reached within about 1 min, and homogeneous compared to the bulk polymerizations with alkali metal hydroxides. Polydiphenylsiloxanes with number-average molecular weight of >120 kDa and rather broad molecular weight distributions, dispersity index ~1.5, were obtained. Polymerizations of other cyclotetrasiloxane derivatives have been performed in the bulk at 80 °C to give linear polymers with broad molecular weight distributions, eventually contaminated with linear and cyclic oligomers [52–54].

The bulk polymerization of decamethylcyclopentasiloxane (D$_5$) was studied using different phosphazene bases (t-BuP$_1$, t-OctP$_1$, t-BuP$_2$, t-BuP$_4$, and t-OctP$_4$) in combination with water (250 ppm water in the monomer) [18]. The OH$^-$[t-BuP$_4$H$^+$] system, however, appeared to be more efficient than the OH$^-$[t-OctP$_4$H$^+$] and produced polymer within a few minutes at 90–130 °C (with 5 % monomer at equilibrium). The less bulky phosphazenes led to a slow polymerization (P$_2$H$^+$) or were ineffective (P$_1$H$^+$), similar to what was observed for the polymerization of ethylene oxide (see above).

Cyclic esters, such as lactide, δ-valerolactone, and ε-caprolactone, have been polymerized using alcohols, i.e., 1-pyrenebutanol, benzyl alcohol, or polymer–OH, associated with t-BuP$_1$ or BEMP as initiators in toluene or dichloromethane solution or in bulk at room temperature [25]. Polymerizations were very slow, reaching

monomer conversions of 47–97 % after several days. However, the rates with BEMP were little higher than with t-BuP$_1$, which correlates with the pK_a values. The polyesters prepared had predictable molecular weights, narrow molecular weight distributions (dispersity ~1.1), and high end-group fidelity, indicative of a living polymerization. The polymerization occurred through an activated alcohol mechanism (cf. Scheme 1) without activation of the ester group in the monomer. With the more bulky phosphazene base t-BuP$_2$, the polymerization of lactide in toluene was found to come to completion within 10 s at 20 °C and within 3 h at −75 °C [24]. The high reactivity and excellent stereocontrol of the polymerization were explained by the basicity of t-BuP$_2$ and steric hindrance suppressing transesterifications.

Other cyclic monomers that have been polymerized using t-BuP$_4$ included lactams (bulk, 220–270 °C) [19] and cyclopropane-1,1-dicarboxylates (tetrahydrofuran, 30–60 °C, toluene, 30–100 °C) [21, 22].

The poly(ethylene oxide)–OH/t-BuP$_4$ was used to initiate the anionic polymerization of 2-(dimethylamino)ethyl methacrylate in tetrahydrofuran at 5–20 °C (see also Sect. 2.2) [55]. The block copolymers had broad molecular weight distributions (1.6–1.7) and were contaminated with 20 % homopolymer, attributable to a slow initiation process. Methyl methacrylate, on the other hand, could be polymerized with ethyl acetate/t-BuP$_4$ as the initiator in tetrahydrofuran at 60 °C to give polymers with predictable molecular weight and narrow molecular weight distribution (dispersity <1.2) [32]. A controlled polymerization of n-butyl acrylate, however, could not be achieved with the methyl isobutyrate/t-BuP$_4$ initiating system [33].

2.2 Polymerization with Lithiated Phosphazene Bases

Organolithium compounds in the presence of phosphazene bases, usually t-BuP$_4$ but also EtP$_2$, have been used for the living anionic polymerization of epoxides and cyclosiloxanes (Scheme 2) and also of vinyl and diene monomers.

Ethylene oxide was first reacted with n-butyl lithium in tetrahydrofuran at −78 °C before the addition of an equimolar amount of t-BuP$_4$. Complexation of the Li$^+$ by t-BuP$_4$ produced the reactive alcoholate species shown in Scheme 2, which was able to add further monomer at room temperature to give poly(ethylene oxide) with predictable molecular weight and narrow molecular weight distribution (dispersity <1.3) [56]. Other organolithium species included sec-butyl lithium and lithium $tert$-butoxide [37, 57] as well as lithiated polymer chains [37, 58–60]. Importantly, it was noticed that the polymerization kinetics was considerably affected by the initiator preparation protocol (type of organolithium, amount of phosphazene base, sequence of addition of reactants, and temperature) due to the complex association equilibria of ionic species and possible occurrence of side reactions [57]. The polymerizations of ethylene oxide were usually conducted in benzene, toluene, or tetrahydrofuran solution at 20–60 °C and were finished within 2–3 days.

The 1-ethoxyethyl glycidyl ether has been polymerized using macroinitiators with terminal alkoxide-[t-BuP$_4$Li$^+$] end groups in tetrahydrofuran solution at
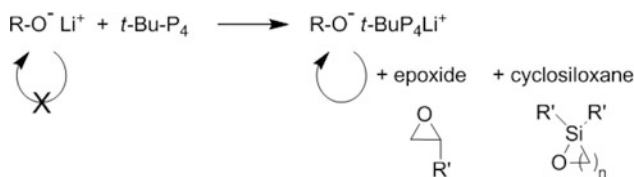
Scheme 2 Polymerization of epoxide or cyclosiloxane by alkoxide-[t-BuP$_4$Li$^+$] ion pair [12]

50 °C [61]. Polymerizations came to completion within 2–3 days (the rate constant being comparable to that of polymerization of ethylene oxide, ~0.01 L mol^{-1} s^{-1}) and proceeded in a living (i.e., in the absence of termination and transfer reactions) and controlled manner. The polymers had very narrow molecular weight distributions with dispersity index of 1.02. The same procedure could also be applied to statistical copolymers of glycidyl ethyl/methyl ether with tBuOLi/t-BuP$_4$ or polymer–OLi/t-BuP$_4$ as the initiators [62]. However, the molar ratio of monomer to initiator had to be kept below 80 to avoid significant side reactions.

It is noteworthy that the molecular weights of the polymers obtained by the polymerization of 1-ethoxyethyl glycidyl ether with sec-butyl lithium/t-BuP$_4$ (benzene, 20 °C, 5 days) were always lower than expected and that polymers contained 29–62 % allyl end groups [63]. The t-BuP$_4$ (but not the sec-butyl lithium) was able to abstract a proton from the monomer to form an allylic alcoholate initiating species, and the alkoxide-[t-BuP$_4$Li$^+$] was prone to chain transfer (even more than the alkoxide–K$^+$). Nevertheless, the dispersity of the polymers remained low (1.11–1.16).

Cyclosiloxanes, i.e., hexamethyl- and hexaethylcyclotrisiloxane (D$_3$), were polymerized in toluene or in bulk, respectively, at 25 °C [7, 64]. Lithium silanolates were formed by the addition of sec-butyl lithium to the cyclotrisiloxane, followed by the addition of EtP$_2$ to start the polymerization. The polymerization of the hexamethylcyclotrisiloxane was found to proceed in the absence of termination, backbiting, or transfer at low conversion (<10 %). Polymers with (apparent) number-average molecular weights of 13–274 kDa and narrow molecular weight distributions (dispersity of 1.05–1.27) could be obtained at monomer conversions of ≤80 %. At near quantitative conversions, i.e., >90 %, the molecular weight distributions were still monomodal but significantly broadened (dispersity >1.4).

Poly(ethylene oxide)–O$^-$[t-BuP$_4$Li$^+$] was used to initiate the anionic polymerization of 2-(dimethylamino)ethyl methacrylate in tetrahydrofuran at 10 °C [55]. The block copolymer had a rather broad molecular weight distribution (dispersity of 1.4), attributable to a slow initiation process, but contained much less homopolymer (<4 %) as compared to the sample prepared with poly(ethylene oxide)–O$^-$[t-BuP$_4$H$^+$] (see Sect. 2.1).

Butadiene and isoprene have been polymerized with sec-butyl lithium/t-BuP$_4$ as the initiator in tetrahydrofuran at −110 °C [37]. The very low temperature ensures that the initiation step is fast compared to the propagation to give narrow disperse polymers (dispersity <1.03). Monomer conversion was usually quantitative within a few hours (overnight) at −78 °C. The microstructures of polybutadiene

(89 % 1,2- and 11 % 1,4-addition) and polyisoprene (28 % 1,2-, 61 % 3,4-, and 11 % 1,4-addition) were little or not affected by the presence of the phosphazene base.

2.3 Polymerization with Non-protonated Phosphazenium Cations

Anionic initiating species, particularly alcoholates and ester enolates, with non-protonated phosphazenium cations were readily available by ion exchange from phosphazenium chlorides or tetrafluoroborates (Scheme 3) [34, 46].

The anionic bulk polymerization of propylene oxide at 95–110 °C was found to proceed more than 100 times faster with $Me_{12}P_2^+$ instead of K^+ as the counterion, reducing the reaction time from several days to a few hours, which can be rationalized in terms of cation size (radii: P_2^+ ~5 Å [65], K^+ 1.4 Å) and charge delocalization [46]. The polymer exhibited narrow molecular weight distribution, dispersity index <1.2, but contained a larger content of unsaturation (resulting from transfer reactions to monomer).

The polymerization of hexamethylcyclotrisiloxane (D_3) proceeded faster than that of the less strained octamethylcyclotetrasiloxane (D_4) using $Pyr_6P_2^+OH^-$ as the initiator in toluene–acetonitrile mixed solvent at room temperature [17]. The polymerization rate was even higher than with the cryptated Li^+ counterion in toluene, which could be attributed to cation size and also solvation effects (acetonitrile). The polysiloxanes contained lesser amounts of cyclic by-products and had narrower molecular weight distributions than those produced with conventional alkali metal-based systems. For silanolates with bulky phosphazenium counterions, however, the rate of monomer addition appeared to be faster than the intra- or intermolecular attack of the polysiloxane chain. Also, the $Pyr_6P_2^+OH^-$ was used for the polycondensation and disproportionation of oligosilanols in toluene at 25 °C [66].

The anionic polymerization of methyl methacrylate with $Me_{24}P_5^+$ as the counterion in tetrahydrofuran proceeded extremely fast, reaching full conversion within about 0.2 s at room temperature [34]. The very high polymerization rate, roughly corresponding to that observed with cryptated Na^+ but being lower than that of the free anion, could be attributed to the large size of $Me_{24}P_5^+$ (radius: ~6.0 Å [67]) and the absence of aggregates in tetrahydrofuran solution (as confirmed by small-angle neutron scattering and UV–visible spectroscopy [68]). Albeit the initiator efficiency was low, just about 20 %, the polymerization proceeded with little or no termination

$$CH_3O^-\,K^+ + Me_{12}P_2^+\,BF_4^- \longrightarrow CH_3O^-\,Me_{12}P_2^+ + KBF_4 \downarrow$$
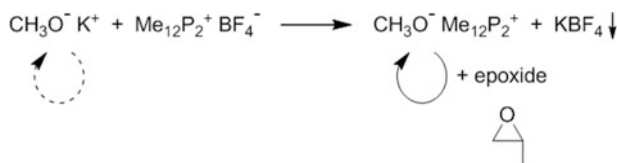
Scheme 3 Polymerization of epoxide by alcoholate-[$Me_{12}P_2^+$] ion pair [46]

and in the absence of transfer reactions even at room temperature. The polymers had a rather narrow molecular weight distribution with a dispersity of 1.2.

3 Macromolecular Engineering

Owing to the simplicity of the mechanism, i.e., activation of initiating sites on the substrate via deprotonation/delithiation followed by polymerization therefrom and the remarkably enhanced polymerization efficiency, phosphazene-promoted anionic polymerization techniques have been applied to enrich the toolbox for macromolecular engineering toward polymer chain-end functionality and architectures (i.e., block/star/graft/hyperbranched polymers). A few types of monomers have been used so far, however, the most common ones being epoxides.

3.1 Functional Polymers

End-functionalized polyethers could be easily obtained by the use of a bifunctional agent (Scheme 4), i.e., a small molecule containing a protic moiety acting as the initiating site and another chemical functionality which remains unreactive during the polymerization and can undergo further chemical modification ("click" chemistry, polymerization as macroinitiator or macromonomer, etc.). Due to the presence of two different functional groups at the two chain ends, such polyethers have also been referred to as α,ω-heterobifunctional or telechelic polymers.
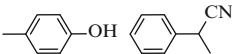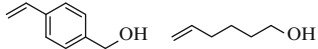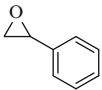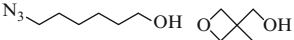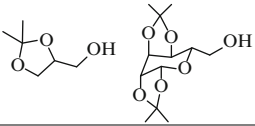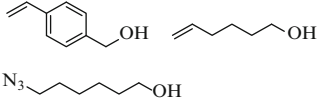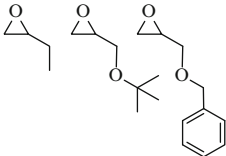
The heterobifunctional initiators used for different epoxide monomers are listed in Table 1. Usually, 1 equivalent of t-BuP$_4$ was used with regard to the initiator, leading to high polymerization rate as well as high chain-end functionality. However, some results have indicated that reducing the amount of t-BuP$_4$ to a certain extent (e.g., from 1 to 0.6) did not cause too much influence to the polymerization of 1,2-butylene oxide [11]. Further decrease (to 0.3) slowed down the polymerization, but initiation efficiency was still high owing to the rapid proton exchange between alkoxide and alcohol. Chain transfer to substituted epoxide monomers was believed
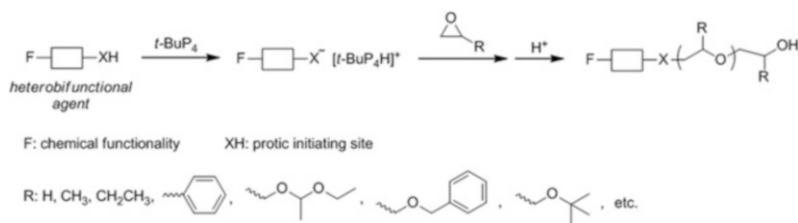
Scheme 4 General synthetic mechanism toward end-functionalized polyethers via t-BuP$_4$-promoted ring-opening polymerization [9, 11, 38, 69]

Table 1 Heterobifunctional initiators used for different epoxide monomers in t-BuP$_4$-promoted anionic ring-opening polymerization

Initiators	Monomers	Reference
		[38]
		[9]
		[69]
		[11]

to be suppressed in this case, probably due to the low reaction temperature and relatively low targeted degree of polymerization. With the help of a Lewis acid like triisobutylaluminum, which was to reduce the basicity of the alkoxide (suppressing chain transfer reactions) and to activate the monomer, it was possible to prepare high molecular weight poly(propylene oxide) with narrow molecular weight distribution and high chain-end functionality [69].

The same synthetic strategy has been used to control the chain end of poly (cyclopropane-1,1-dicarboxylates) [22]. Different types of initiators (thiol, alcohol, carbazole, and malonate) have been used to control the end group at α-position. The use of 1 equivalent of t-BuP$_4$ accelerated the polymerization, and high temperature ensured high monomer conversion, and finally halogenated capping agents were used to introduce a functional group, e.g., allyl or propargyl, to the ω-chain end. Excess of capping agent was employed for quantitative functionalization.

Terpene alcohols, including menthol, retinol, cholesterol, and betulin, have been used as initiators for the anionic ring-opening polymerization of ethylene oxide to introduce biological component at the end of poly(ethylene oxide) (Scheme 5) [39]. Very low amount of t-BuP$_4$ has been used ($[t$-BuP$_4]/[OH] = 0.01$–0.2) to achieve nearly complete initiation efficiency, as revealed by macromolecular characterization, indicating that the proton transfer between active and dormant chain ends during the polymerization is much faster than the chain growth. However, it is to be expected that a low amount of t-BuP$_4$ should lead to a reduced polymerization

$R-OH + x\ t\text{-BuP}_4 \xrightarrow[\text{2. H}^+]{\text{1. n}\ \triangle\ O,\ 45\ °C} R{-}O\text{-}\!\!\left(\!\!\begin{array}{c}\end{array}\!\!\right)\!\!O\!\!\left(\!\!\begin{array}{c}\end{array}\!\!\right)_{\!n}\!\!H$ $[t\text{-BuP}_4]_0/[\text{OH}]_0 = 0.01 \sim 0.2\ (x = 0.01 \sim 0.4)$

menthol retinol cholesterol betulin
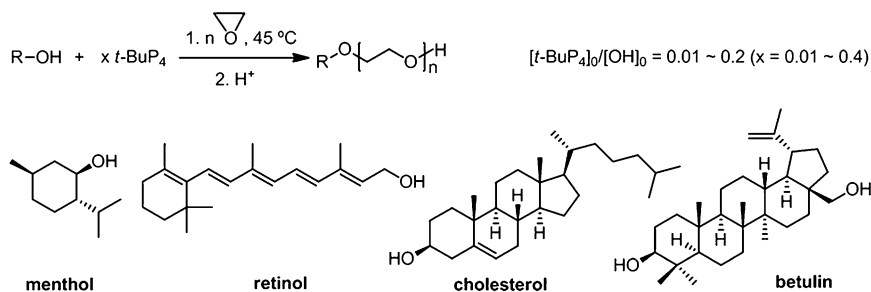
Scheme 5 Synthesis of terpene–poly(ethylene oxide)conjugates by t-BuP$_4$-promoted anionic ring-opening polymerization of ethylene oxide [39]

rate. In order to better reveal the influence of terpene entities, low molecular weights were targeted at in this study. However, on a chemical point of view, it would be interesting to examine the limitation of the achievable molecular weight with different amounts of t-BuP$_4$ or proportion of activated chain ends. The different terpene entities have been demonstrated to affect the thermal and solution properties of these terpene–poly(ethylene oxide) conjugates [70]. The successful synthesis of bioconjugate polymers in this manner should also be attributed to the simplicity of chemical structures of the involved terpene alcohols, which stay intact during the anionic polymerization process. It is also of interest to investigate the tolerance of such metal-free polymerization system toward other types of biological entities.

3.2 Block Copolymers

Polyether-based block copolymers have been synthesized by conducting anionic ring-opening polymerization of epoxide monomers from macroinitiators. The chain end of the macroinitiator was activated by t-BuP$_4$ via either delithiation (Scheme 6a, b) [37, 58–61, 71] or deprotonation (Scheme 6c) [47, 48]. The combination with butyl lithium-initiated anionic polymerization of dienes and styrene were the mostly employed. The t-BuP$_4$ was usually introduced after completion of the first block and addition of the epoxide monomer (Scheme 6b) [58–61, 71], but sequential polymerization with a sec-butyl lithium/t-BuP$_4$ complex has also been reported (Scheme 6a) [37]. No side reaction was caused between the active carbanion and t-BuP$_4$ probably due to the very low temperature (-110 to -78 °C) used. In all these studies, high ratio of [t-BuP$_4$]/[Li] (0.9–1.05) has been used, and quantitative blocking efficiency could be achieved. The polymerization of epoxides was conducted at elevated temperature (40–50 °C) for 2–4 days to ensure complete conversion. Triblock copolymers have been achieved by sequential polymerization of two diene monomers and an epoxide monomer [60] or styrene and two epoxide monomers [61].
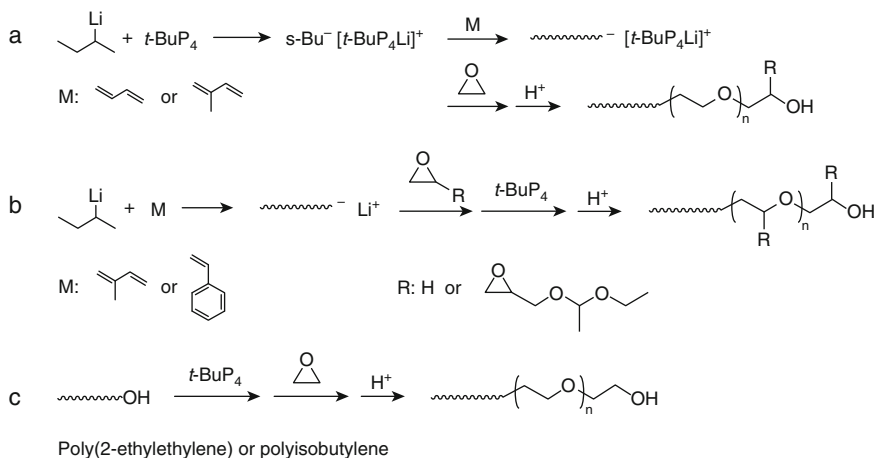
Scheme 6 Synthesis of polyether-based block copolymers via *t*-BuP$_4$-promoted anionic ring-opening polymerization [37, 47, 48, 58–61, 71]
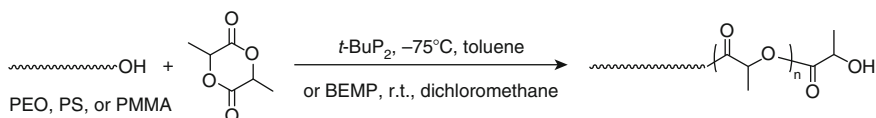
Scheme 7 Synthesis of polylactide-based block copolymers via phosphazene-catalyzed ring-opening polymerization from macroinitiators [24, 25]

Hydroxyl-terminated macroinitiators based on poly(2-ethylethylene) and polyisobutylene have been used in combination with *t*-BuP$_4$ to polymerize ethylene oxide toward the preparation of diblock copolymers (Scheme 6c) [47, 48]. The macroinitiators have been activated with 0.5 equivalents of *t*-BuP$_4$ to give the pure diblock copolymers without homopolymer contaminations.

A similar strategy has been applied on the preparation of polyester-based block copolymers, for which phosphazene bases with lower basicity are employed [24–26]. BEMP and *t*-BuP$_2$ have been used to catalyze the polymerization of *rac*-lactide from hydroxyl-terminated macroinitiators based on poly(ethylene oxide), polystyrene, and poly(methyl methacrylate), as shown in Scheme 7 [24, 25]. Despite of the high molecular weight of the macroinitiators and relatively low monomer concentrations, high yields could be achieved with quantitative initiation efficiency and low dispersity. Since *t*-BuP$_2$ exhibits a higher basicity than BEMP, low temperature has been used in the case of *t*-BuP$_2$ to suppress transesterification reactions on the polyester chains (thus preserving the narrow molecular weight distribution). Also, carboxyl-terminated poly(ethylene oxide) has been used as a macroinitiator for the polymerization of 4-benzyloxycarbonyl-3,3-dimethyl-2-oxetanone [26]. Phosphazene bases with different basicity (*t*-BuP$_1$, *t*-BuP$_2$, and *t*-BuP$_4$) have been used as
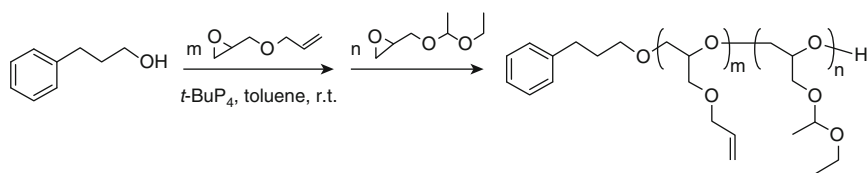
Scheme 8 Synthesis of poly(allyl glycidyl ether)-*block*-poly(1-ethoxyethyl glycidyl ether) by *t*-BuP$_4$-promoted sequential anionic ring-opening polymerization [10]

promoters, the polyesters with highest molecular weight ($>1.5 \times 10^6$ kDa) being produced with *t*-BuP$_4$.

Block copolymers were prepared by sequential polymerization of two functional epoxide monomers, allyl glycidyl ether and 1-ethoxyethyl glycidyl ether, from a primary alcohol initiator (Scheme 8) [10]. The homopolymerization of the 1-ethoxyethyl glycidyl ether was plagued by side reactions, i.e., chain transfer to monomer, while the sequential polymerization of allyl glycidyl ether followed by 1-ethoxyethyl glycidyl ether appeared to be a smooth reaction at room temperature. Selective deprotection of the two blocks allowed further chemical modification toward novel polyether-based materials.

A one-pot synthesis of a diblock copolymers has been attempted by polymerization of a methacrylate monomer, i.e., 2-(dimethylamino)ethyl methacrylate, using poly(ethylene oxide)–O$^-$[*t*-BuP$_4$Li]$^+$ as a macroinitiator [55]. High blocking efficiency has been achieved, but the block copolymer exhibited a relatively broad molecular weight distribution (dispersity of 1.4) (see Sect. 2.2).

As discussed above, the phosphazene-promoted polymerizations of epoxides, cyclic esters, and methacrylates benefit from high polymerization rates but sometimes suffer from side reactions due to the high basicity of the initiator/chain end, e.g., chain transfer to monomer (in the case of substituted epoxide) or to polymer chains (in the case of cyclic esters). Such side reactions might lead to some undesirable effect on synthesis of block copolymers, such as low initiation efficiency, broad molecular weight distribution, and contamination with homopolymer. As a matter of fact, every system requires specifically optimized synthetic reaction conditions.

3.3   Graft Copolymers

A multifunctional backbone, i.e., (co)polymer containing multiple protic groups as initiating sites, in combination with *t*-BuP$_4$ was used to promote the anionic graft (co)polymerization of epoxides. This *grafting from* technique enabled the generation of various comblike macromolecular architectures including graft copolymers with homopolymer [8, 40, 43], statistical [42], and block copolymer [41] side chains.

The first reported t-BuP$_4$-promoted graft polymerization of ethylene oxide was performed on a poly[ethylene-co-(vinyl alcohol)] backbone [8]. The poor solubility of the backbone copolymer did not affect the graft polymerization as the solution turned homogeneous after a certain reaction time (25 % monomer conversion). The number of hydroxyl groups grafted with poly(ethylene oxide) side chains, i.e., the grafting density, was found to correspond to the initial ratio of [t-BuP$_4$]/[OH], indicating that there was no effective proton exchange between active alkoxide and inactive hydroxyl sites left on the backbone. This behavior appears to be common for graft polymerizations, as will be discussed further below, but is substantially different to the case of mono- or di-alkoxide-initiated polymerizations (see above).

Amphiphilic graft block copolymers were prepared by graft polymerization of ethylene oxide from polystyrene-$block$-poly(p-hydroxystyrene) backbones [40]. Different ratios of t-BuP$_4$ to phenol were used. Direct analysis for the proportion of the incorporated phenol moieties on the backbone was not performed; however, the crystallinity of poly(ethylene oxide) side chains indicated that, at least qualitatively, the grafting density could be controlled. Sequential or statistical copolymerizations of ethylene oxide and propylene oxide from poly(p-hydroxystyrene) backbones allowed for the preparation of graft copolymers with densely grafted block copolymer or statistical copolymer side chains (Scheme 9) [41, 42]. The poor solubility of the highly charged backbone ([t-BuP$_4$]/[phenol] = 0.9) did not affect the results, i.e., low dispersity, as the solutions became homogeneous in the course of reaction.

Secondary amide moieties, in combination of t-BuP$_4$, have also been utilized to perform graft polymerizations. Thermoresponsive poly(N-isopropylacrylamide)-
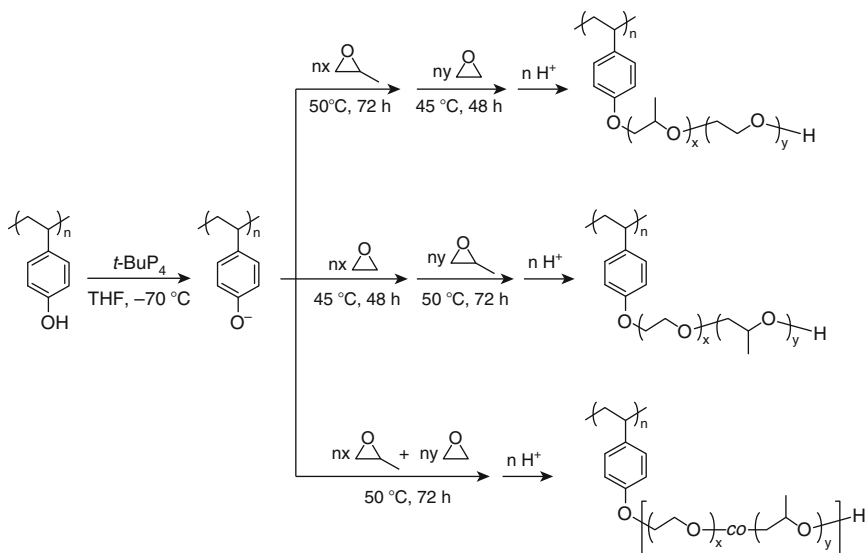
Scheme 9 Synthesis of graft copolymers by t-BuP$_4$-promoted graft (co)polymerization of propylene oxide and ethylene oxide from poly(p-hydroxystyrene) [41, 42]
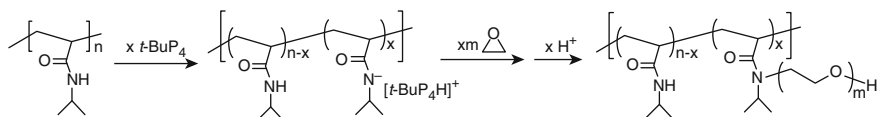
Scheme 10 Synthesis of graft copolymers by t-BuP$_4$-promoted graft polymerization of ethylene oxide directly from poly(N-isopropylacrylamide) [43]

graft-poly(ethylene oxide) copolymers have been prepared in this way (Scheme 10) [43]. It was found that the grafting density could be controlled by the initial ratio of t-BuP$_4$ to secondary amide moiety, consistent with the previously discussed results, probably due to steric hindrance, inhibiting the proton transfer from the unreacted protic moiety on the backbone to the growing side chain. However, more investigations need to be performed toward kinetic details.

This concept has also successfully been applied to high molecular weight acrylamide-based homo- and copolymers, i.e., primary amides, to yield complex macromolecular combs with one or two polyether chains per amide unit. The grafted polyether chains included poly(ethylene oxide), poly(propylene oxide)-*block*-poly(ethylene oxide), poly[(ethylene oxide)-*co*-(1,2-butylene oxide)], and poly[(ethylene oxide)-*co*-(*tert*-butyl glycidyl ether)] [72].

3.4 Star-Shaped Polymers

Synthesis of star-shaped polyether through t-BuP$_4$-promoted anionic ring-opening polymerization has scarcely been reported, which, however, can be predicted to be readily conductible via a *core-first* protocol. Pentaerythritol has been used to make four-armed star-shaped poly(ethylene oxide) [8]. Regardless of its poor solubility in the solvent, tetrahydrofuran, a homogeneous solution was obtained at about 30 % monomer conversion, and the final product had a low dispersity of 1.1. Narrowly distributed four-armed star-shaped poly(butylene oxide)s have been prepared in a similar manner [73]. The predicted number and molecular weight of the arms were confirmed by cleaving the (benzyl ether) linkage between the initiator residue and the arms and characterization of the arms. A polylithiated carbosilane dendrimer has been used to prepare multi-armed poly(ethylene oxide) star polymer [74], aided by the formation of t-BuP$_4$–Li complex. Such initiating system benefits from the dendritic structure, preventing the multiply charged species from intermolecular association and precipitation.

Group transfer polymerization (GTP) catalyzed by t-BuP$_4$ has been used to prepared star-shaped polymethacrylates (Scheme 11) [35]. Despite the fact that the ratio between t-BuP$_4$ and the silyl enolate initiating sites was usually kept below unity, star-shaped polymers with the desired number of arms were obtained in all cases. The polymerization/catalysis mechanisms are still awaiting further evidence and discussion; however, the utilization of silicon activation ability of phosphazene
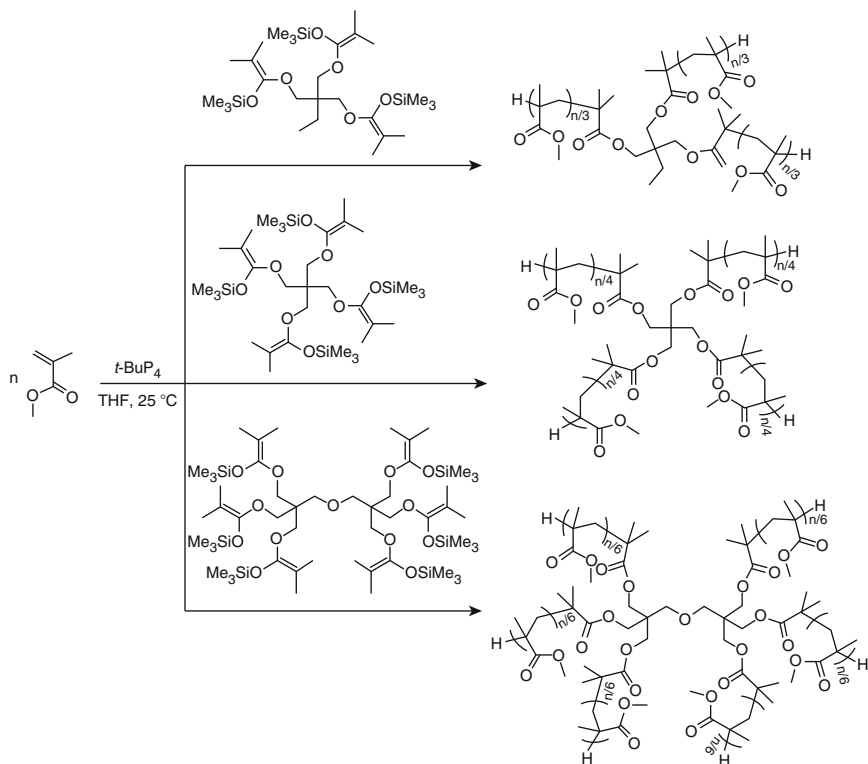
Scheme 11 Synthesis of three-, four-, and six-armed star-shaped poly(methyl methacrylate)s by *t*-BuP$_4$-catalyzed group transfer polymerization [35]

base toward star-shaped polymethacrylates has definitely opened a new pathway toward macromolecular engineering based on metal-free polymerization techniques.

3.5 Hyperbranched Polymers

Hyperbranched polysiloxanes have been prepared by *t*-BuP$_4$-promoted anionic ring-opening polymerization of hydroxyl-functionalized pentamethylcyclotrisiloxane monomers (Scheme 12) [75, 76]. Rapid proton transfer between deprotonated and protonated hydroxyl groups was believed to facilitate the formation of hyperbranched structure, since in this case the reaction with monomer can occur at any of the six silanolate/silanol centers. Low reaction temperature was also needed to suppress the occurrence of cross-linking (base-catalyzed silanol condensation).
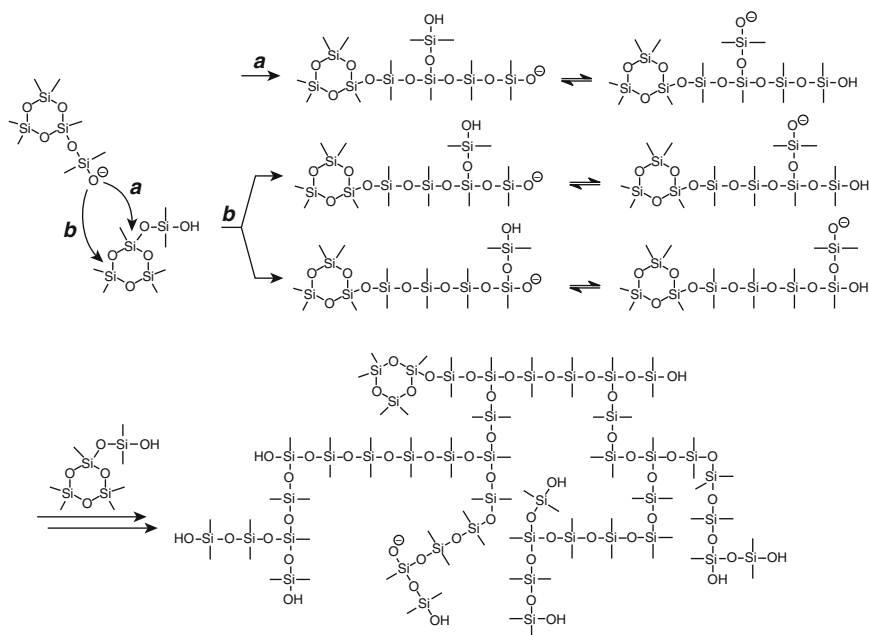
Scheme 12 Synthesis of hyperbranched polysiloxane by *t*-BuP$_4$-promoted anionic ring-opening polymerization of 1-(hydroxydimethylsiloxy)pentamethylcyclotrisiloxane [76]

4 Summary

Although still in the preliminary stage of employment and exploration, phosphazene bases have already manifested their remarkable strength as catalyst/promoter in metal-free anionic polymerization techniques for a wide range of monomer types, i.e., epoxides, cyclosiloxanes, lactones, cyclic carbonates, lactams, cyclopropane derivatives, and alkyl (meth)acrylates. By associating with the counterion (proton, lithium cation, etc.) and thus enhancing the nucleophilicity of the initiator, such organic superbases have allowed a significant increase of the polymerization rate and, in many cases, achievement of high molecular weight polymers with narrow molecular weight distribution. Moreover, the simplicity and efficiency of the catalysis/promotion allows in situ growth of (co)polymer chains from substrate containing initiating sites (mono- or multifunctional small molecules, biomolecules, and macromolecules), which provides a new strategic metal-free concept for sophisticated macromolecular engineering toward end-functionalized polymers, complex macromolecular architectures, and bioconjugates. But still a lot of work, concerning the understanding of the activation/polymerization mechanism and kinetics, remains to be done. It is also of great interest to further investigate the applicability of other monomer/initiator types; to optimize the conditions for each specific system in terms of basicity and the amount of phosphazene base, cocatalyst, polymerization solvent/concentration/temperature, etc.; and to exploit the strength of this technique for more

applications in macromolecular engineering such as surface modification of polymeric materials.

Abbreviations

BEMP	2-*tert*-Butylimino-2-diethylamino-1,3-dimethylperhydro-1,3,2-diazaphosphorine
t-BuP$_1$	*tert*-Butylimino-tris(dimethylamino)phosphorane
t-BuP$_2$	1-*tert*-Butyl-2,2,4,4,4-pentakis(dimethylamino)-2λ^5,4λ^5-catenadi(phosphazene)
t-BuP$_4$	1-*tert*-Butyl-4,4,4-tris(dimethylamino)-2,2-bis[tris(dimethylamino)phosphoranylidenamino]-2λ^5,4λ^5-catenadi(phosphazene)
EtP$_2$	1-Ethyl-2,2,4,4,4-pentakis(dimethylamino)-2λ^5,4λ^5-catenadi(phosphazene)
D$_3$	Hexamethylcyclotrisiloxane
D$_4$	Octamethylcyclotetrasiloxane
D$_5$	Decamethylcyclopentasiloxane
t-OctP$_1$	*tert*-Octylimino-tris(dimethylamino)phosphorane
t-OctP$_4$	1-*tert*-Octyl-4,4,4-tris(dimethylamino)-2,2-bis[tris(dimethylamino)phosphoranylidenamino]-2λ^5,4λ^5-catenadi(phosphazene)

References

1. Kamber NE, Jeong W, Waymouth RM, Pratt RC, Lohmeijer BGG, Hedrick JL (2007) Organocatalytic ring-opening polymerization. Chem Rev 107:5813–5840
2. Kiesewetter MK, Shin EJ, Hedrick JL, Waymouth RM (2010) Organocatalysis: opportunities and challenges for polymer synthesis. Macromolecules 43:2093–2107
3. Dove AP (2012) Organic catalysis for ring-opening polymerization. ACS Macro Lett 1:1409–1412
4. Boileau S, Illy N (2011) Activation in anionic polymerization: why phosphazene bases are very exciting promoters. Prog Polym Sci 36:1132–1151
5. Schwesinger R, Schlemper H (1987) Peralkylated polyaminophosphazenes – extremely strong, neutral nitrogen bases. Angew Chem Int Ed 26:1167–1169
6. Schwesinger R, Link R, Wenzl P, Kossek S, Keller M (2006) Extremely base-resistant organic phosphazenium cations. Chem Eur J 12:429–437
7. Eßwein B, Molenberg A, Möller M (1996) Use of polyiminophosphazene bases for ring-opening polymerizations. Macromol Symp 107:331–340
8. Eßwein B, Steidl NM, Möller M (1996) Anionic polymerization of oxirane in the presence of the polyiminophosphazene base *t*-Bu-P$_4$. Macromol Rapid Commun 17:143–148
9. Misaka H, Sakai R, Satoh T, Kakuchi T (2011) Synthesis of high molecular weight and end-functionalized poly(styrene oxide) by living ring-opening polymerization of styrene oxide using the alcohol/phosphazene base initiating system. Macromolecules 44:9099–9107

10. Kwon W, Rho Y, Kamoshida K, Kwon KH, Jeong YC, Kim J, Misaka H, Shin TJ, Kim J, Kim K-W, Jin KS, Chang T, Kim H, Satoh T, Kakuchi T, Ree M (2012) Well-defined functional linear aliphatic diblock copolyethers: a versatile linear aliphatic polyether platform for selective functionalizations and various nanostructures. Adv Funct Mater 22:5194–5208

11. Misaka H, Tamura E, Makiguchi K, Kamoshida K, Sakai R, Satoh T, Kakuchi T (2012) Synthesis of end-functionalized polyethers by phosphazene base-catalyzed ring-opening polymerization of 1,2-butylene oxide and glycidyl ether. J Polym Sci Part A Polym Chem 50:1941–1952

12. Eßwein B, Möller M (1996) Polymerisation von ethylenoxid mit alkyllithiumverbindungen und der phosphazenbase "tBu-P$_4$". Angew Chem 108:703–705

13. Zhao J, Pahovnik D, Gnanou Y, Hadjichristidis N (2014) Phosphazene-promoted metal-free ring-opening polymerization of ethylene oxide initiated by carboxylic acid. Macromolecules 47:1693–1698

14. Molenberg A, Möller M (1995) A fast catalyst system for the ring-opening polymerization of cyclosiloxanes. Macromol Rapid Commun 16:449–453

15. Van Dyke ME, Clarson SJ (1998) Reaction kinetics for the anionic ring-opening polymerization of tetraphenyltetramethylcyclotetrasiloxane using a fast initiator system. J Inorg Organomet Polym 8:111–117

16. Hupfield PC, Taylor RG (1999) Ring-opening polymerization of siloxanes using phosphazene base catalysts. J Inorg Organomet Polym 9:17–34

17. Grzelka A, Chojnowski J, Fortuniak W, Taylor RG, Hupfield PC (2004) Kinetics of the anionic ring opening polymerization of cyclosiloxanes initiated with a superbase. J Inorg Organomet Polym 14:85–99

18. Pibre G, Chaumont P, Fleury E, Cassagnau P (2008) Ring-opening polymerization of decamethylcyclopentasiloxane initiated by a superbase: kinetics and rheology. Polymer 49:234–240

19. Memeger W, Campbell GC, Davidson F (1996) Poly(aminophosphazene)s and protophosphatranes mimic classical strong anionic base catalysts in the anionic ring-opening polymerization of lactams. Macromolecules 29:6475–6480

20. Yang H, Zhao J, Yan M, Pispas S, Zhang G (2011) Nylon 3 synthesized by ring opening polymerization with a metal-free catalyst. Polym Chem 2:2888–2892

21. Illy N, Boileau S, Penelle J, Barbier V (2009) Metal-free activation in the anionic ring-opening polymerization of cyclopropane derivatives. Macromol Rapid Commun 30:1731–1735

22. Illy N, Boileau S, Buchmann W, Penelle J, Barbier V (2010) Control of end groups in anionic polymerizations using phosphazene bases and protic precursors as initiating system (XH-Bu^{t}P$_4$ approach): application to the ring-opening polymerization of cyclopropane-1,1-dicarboxylates. Macromolecules 43:8782–8789

23. Illy N, Boileau S, Winnik MA, Penelle J, Barbier V (2012) Thiol-ene "clickable" carbon-chain polymers based on diallyl cyclopropane-1,1-dicarboxylate. Polymer 53:903–912

24. Zhang L, Nederberg F, Messman JM, Pratt RC, Hedrick JL, Wade CG (2007) Organocatalytic stereoselective ring-opening polymerization of lactide with dimeric phosphazene bases. J Am Chem Soc 129:12610–12611

25. Zhang L, Nederberg F, Pratt RC, Waymouth RM, Hedrick JL, Wade CG (2007) Phosphazene bases: a new category of organocatalysts for the living ring-opening polymerization of cyclic esters. Macromolecules 40:4154–4158

26. De Winter J, Coulembier O, Gerbaux P, Dubois P (2010) High molecular weight poly(α, α', β-trisubstituted β-lactones) as generated by metal-free phosphazene catalysts. Macromolecules 43:10291–10296

27. Jaffredo CG, Carpentier J-F, Guillaume SM (2012) Controlled rop of *β*-butyrolactone simply mediated by amidine, guanidine, and phosphazene organocatalysts. Macromol Rapid Commun 33:1938–1944

28. Yang H, Xu J, Pispas S, Zhang G (2012) Hybrid copolymerization of *ε*-caprolactone and methyl methacrylate. Macromolecules 45:3312–3317

29. Helou M, Miserque O, Brusson J-M, Carpentier J-F, Guillaume SM (2010) Organocatalysts for the controlled "immortal" ring-opening polymerization of six-membered-ring cyclic carbonates: a metal-free, green process. Chem Eur J 16:13805–13813

30. Brignou P, Priebe Gil M, Casagrande O, J-Fo C, Guillaume SM (2010) Polycarbonates derived from green acids: ring-opening polymerization of seven-membered cyclic carbonates. Macromolecules 43:8007–8017

31. Yang H, Yan M, Pispas S, Zhang G (2011) Synthesis of poly (ethylene carbonate)-co-(ethylene oxide) copolymer by phosphazene-catalyzed ROP. Macromol Chem Phys 212:2589–2593

32. Pietzonka T, Seebach D (1993) The P4-phosphazene base as part of a new metal-free initiator system for the anionic polymerization of methyl methacrylate. Angew Chem Int Ed 32:716–717

33. Börner HG, Heitz W (1998) Anionic polymerization of butyl acrylate with metal free initiator systems containing [1-tert-butyl-4,4,4-tris(dimethylamino)-2,2-bis[tris(dimethylamino)-phosphor-anylidenamino]-2λ^5, 4λ^5-catenadi(phosphazene)] base (P$_4$-tert-butyl-phosphazene base). Macromol Chem Phys 199:1815–1820

34. Baskaran D, Müller AHE (2000) Anionic polymerization of methyl methacrylate using tetrakis tris(dimethyl amino)phosphoranylidenamino phosphonium (P$_5^+$) as counterion in tetrahydrofuran. Macromol Rapid Commun 21:390–395

35. Chen Y, Fuchise K, Narumi A, Kawaguchi S, Satoh T, Kakuchi T (2011) Core-first synthesis of three-, four-, and six-armed star-shaped poly(methyl methacrylate)s by group transfer polymerization using phosphazene base. Macromolecules 44:9091–9098

36. Kakuchi T, Chen Y, Kitakado J, Mori K, Fuchise K, Satoh T (2011) Organic superbase as an efficient catalyst for group transfer polymerization of methyl methacrylate. Macromolecules 44:4641–4647

37. Förster S, Krämer E (1999) Synthesis of PB − PEO and PI − PEO block copolymers with alkyllithium initiators and the phosphazene base t-BuP$_4$. Macromolecules 32:2783–2785

38. Schlaad H, Kukula H, Rudloff J, Below I (2001) Synthesis of α, ω-heterobifunctional poly (ethylene glycol)s by metal-free anionic ring-opening polymerization. Macromolecules 34:4302–4304

39. Zhao J, Schlaad H, Weidner S, Antonietti M (2012) Synthesis of terpene-poly(ethylene oxide)s by t-BuP$_4$-promoted anionic ring-opening polymerization. Polym Chem 3:1763–1768

40. Zhao J, Mountrichas G, Zhang G, Pispas S (2009) Amphiphilic polystyrene-b-poly(p-hydroxystyrene-g-ethylene oxide) block-graft copolymers via a combination of conventional and metal-free anionic polymerization. Macromolecules 42:8661–8668

41. Zhao J, Mountrichas G, Zhang G, Pispas S (2010) Thermoresponsive core-shell brush copolymers with poly(propylene oxide)-block-poly(ethylene oxide) side chains via a "grafting from" technique. Macromolecules 43:1771–1777

42. Zhao J, Zhang G, Pispas S (2010) Thermoresponsive brush copolymers with poly(propylene oxide-ran-ethylene oxide) side chains via metal-free anionic polymerization "grafting from" technique. J Polym Sci Part A Polym Chem 48:2320–2328

43. Zhao J, Schlaad H (2011) Controlled anionic graft polymerization of ethylene oxide directly from poly(N-isopropylacrylamide). Macromolecules 44:5861–5864

44. Tanaka Y, Arakawa M, Yamaguchi Y, Hori C, Ueno M, Tanaka T et al (2006) NMR spectroscopic observation of a metal-free acetylide anion. Chem Asian J 1:581–585

45. Kaljurand I, Kutt A, Soovali L, Rodima T, Maemets V, Leito I, Koppel IA (2005) Extension of the self-consistent spectrophotometric basicity scale in acetonitrile to a full span of 28 pKa units: unification of different basicity scales. J Org Chem 70:1019–1028

46. Rexin O, Mülhaupt R (2002) Anionic ring-opening polymerization of propylene oxide in the presence of phosphonium catalysts. J Polym Sci Part A Polym Chem 40:864–873

47. Thomas A, Schlaad H, Smarsly B, Antonietti M (2003) Replication of lyotropic block copolymer mesophases into porous silica by nanocasting: learning about finer details of polymer self-assembly. Langmuir 19:4455–4459

48. Groenewolt M, Brezesinski T, Schlaad H, Antonietti M, Groh PW, Iván B (2005) Polyisobutylene-block-poly(ethylene oxide) for robust templating of highly ordered mesoporous materials. Adv Mater 17:1158–1162

49. Leito I, Rodima T, Koppel IA, Schwesinger R, Vlasov VM (1997) Acid-base equilibria in nonpolar media. 1. a spectrophotometric method for acidity measurements in heptane. J Org Chem 62:8479–8483

50. Hinman JG, Lough AJ, Morris RH (2007) Properties of the polyhydride anions [WH$_5$(PMe$_2$Ph)$_3$]$^-$ and [ReH$_4$(PMePh$_2$)$_3$]$^-$ and periodic trends in the acidity of polyhydride complexes. Inorg Chem 46:4392–4401

51. Zhao J, Pahovnik D, Gnanou Y, Hadjichristidis N (2014) Sequential polymerization of ethylene oxide, ε-caprolactone and L-lactide: a one-pot metal-free route to tri- and pentablock terpolymers. Polym Chem 5:3750–3753

52. Cai G, Weber WP (2002) Synthesis and chemical modification of poly(divinylsiloxane). Polymer 43:1753–1759

53. Teng CJ, Weber WP, Cai G (2003) Anionic and cationic ring-opening polymerization of 2,2,4,4,6,6-hexamethyl-8,8-divinylcyclotetrasiloxane. Macromolecules 36:5126–5130

54. Teng CJ, Weber WP, Cai G (2003) Acid and base catalyzed ring-opening polymerization of 2,2,4,4,6,6-hexamethyl-8,8-diphenylcyclotetrasiloxane. Polymer 44:4149–4155

55. Schacher F, Müllner M, Schmalz H, Müller AHE (2009) New block copolymers with poly(N,N-dimethylaminoethyl methacrylate) as a double stimuli-responsive block. Macromol Chem Phys 210:256–262

56. Esswein B, Möller M (1996) Polymerization of ethylene oxide with alkyllithium compounds and the phosphazene base "tBu-P$_4$". Angew Chem Int Ed 35:623–625

57. Schmalz H, Lanzendörfer MG, Abetz V, Müller AHE (2003) Anionic polymerization of ethylene oxide in the presence of the phosphazene base Bu^{t}P$_4$ – kinetic investigations using in-situ FT-NIR spectroscopy and MALDI-TOF MS. Macromol Chem Phys 204:1056–1071

58. Floudas G, Vazaiou B, Schipper F, Ulrich R, Wiesner U, Iatrou H, Hadjichristidis N (2001) Poly(ethylene oxide-b-isoprene) diblock copolymer phase diagram. Macromolecules 34:2947–2957

59. Pispas S (2006) Double hydrophilic block copolymers of sodium(2-sulfamate-3-carboxylate) isoprene and ethylene oxide. J Polym Sci Part A Polym Chem 44:606–613

60. Schmalz H, Knoll A, Müller AJ, Abetz V (2002) Synthesis and characterization of ABC triblock copolymers with two different crystalline end blocks: influence of confinement on crystallization behavior and morphology. Macromolecules 35:10004–10013

61. Toy AA, Reinicke S, Müller AHE, Schmalz H (2007) One-pot synthesis of polyglycidol-containing block copolymers with alkyllithium initiators using the phosphazene base t-BuP$_4$. Macromolecules 40:5241–5244

62. Reinicke S, Schmelz J, Lapp A, Karg M, Hellweg T, Schmalz H (2009) Smart hydrogels based on double responsive triblock terpolymers. Soft Matter 5:2648–2657

63. Hans M, Keul H, Moeller M (2009) Chain transfer reactions limit the molecular weight of polyglycidol prepared via alkali metal based initiating systems. Polymer 50:1103–1108

64. Molenberg A, Möller M (1997) Polymerization of cyclotrisiloxanes by organolithium compounds and P$_2$-Et base. Macromol Chem Phys 198:717–726

65. Kaljurand I, Rodima T, Leito I, Koppel IA, Schwesinger R (2000) Self-consistent spectrophotometric basicity scale in acetonitrile covering the range between pyridine and DBU. J Org Chem 65:6202–6208

66. Grzelka A, Chojnowski J, Cypryk M, Fortuniak W, Hupfield PC, Taylor RG (2002) Polycondensation and disproportionation of an oligosiloxanol in the presence of a superbase. J Organomet Chem 660:14–26

67. Ishio M, Katsube M, Ouchi M, Sawamoto M, Inoue Y (2009) Active, versatile, and removable iron catalysts with phosphazenium salts for living radical polymerization of methacrylates. Macromolecules 42:188–193

68. Miyamoto N, Inoue Y, Koizumi S, Hashimoto T (2007) Living anionic polymerization of methyl methacrylate controlled by metal-free phosphazene catalyst as observed by small-angle neutron scattering, gel-permeation chromatography and UV-visible spectroscopy. J Appl Crystallogr 40:S568–S572

69. Brocas A-L, Deffieux A, Le Malicot N, Carlotti S (2012) Combination of phosphazene base and triisobutylaluminum for the rapid synthesis of polyhydroxy telechelic poly(propylene oxide). Polym Chem 3:1189–1195

70. Zhao J, Jeromenok J, Weber J, Schlaad H (2012) Thermoresponsive aggregation behavior of triterpene–poly(ethylene oxide) conjugates in water. Macromol Biosci 12:1272–1278

71. Siebert M, Keul H, Möller M (2010) Synthesis of well-defined polystyrene-block-polyglycidol (PS-*b*-PG) block co-polymers by anionic polymerization. Des Monomers Polym 13:547–563

72. Zhao J, Alamri H, Hadjichristidis N (2013) A facile metal-free "grafting-from" route from acrylamide-based substrate toward complex macromolecular combs. Chem Commun 49:7079–7081

73. Isono T, Kamoshida K, Satoh Y, Takaoka T, S-i S, Satoh T, Kakuchi T (2013) Synthesis of star- and figure-eight-shaped polyethers by *t*-Bu-P$_4$-catalyzed ring-opening polymerization of butylene oxide. Macromolecules 46:3841–3849

74. Vasilenko NG, Rebrov EA, Muzafarov AM, Eßwein B, Striegel B, Möller M (1998) Preparation of multi-arm star polymers with polylithiated carbosilane dendrimers. Macromol Chem Phys 199:889–895

75. Paulasaari JK, Weber WP (2000) Synthesis of hyperbranched polysiloxanes by base-catalyzed proton-transfer polymerization. Comparison of hyperbranched polymer microstructure and properties to those of linear analogues prepared by cationic or anionic ring-opening polymerization. Macromolecules 33:2005–2010

76. Paulasaari JK, Weber WP (2000) Base catalyzed proton transfer polymerization of 1-hydroxypentamethylcyclotrisiloxane. Comparison of hyperbranched polymer microstructure and properties to those of highly regular linear analogs. Macromol Chem Phys 201:1585–1592

Group Transfer Polymerization of Acrylic Monomers

Yougen Chen, Keita Fuchise, Toshifumi Satoh, and Toyoji Kakuchi

Abstract Group transfer polymerization (GTP) as one of the living polymerizations was put forward over 30 years ago by DuPont for the upscale and cost-reducing synthesis of acrylic polymers. In the GTP process, a silyl ketene acetal compound is used as an initiator and a Lewis base/acid as the catalysts, and polymerizations can be operated at advantageously moderate temperatures when compared with the conventional living anionic polymerizations of acrylic monomers. GTP using conventional catalysts, referred to as conventional GTP, had experienced a booming development during 1980–1990s. In retrospect, most of the studies in this field before 2007 had been focusing on the optimization of conventional catalysts, the exploration of applicable monomers, and the molecular design of polymeric architectures. In addition, debates on polymerization mechanisms involving associative and dissociative routes had also been discussed. In contrast to the conventional GTP, the recent progress (2007~) in this field has been mainly reflected on the significant and creative utilization of organocatalysts, such as strong organic Lewis acids/bases, which might be termed as organocatalytic GTP. This subchapter strives to provide a latest, systematic, and comprehensive summary throughout the over 30-year development, and in particular, the organocatalytic GTP will be emphatically described.

Keywords Group transfer polymerization • Silyl ketene acetal • Nucleophilicity/silicophilicity • Associative mechanism • Dissociative mechanism • Organocatalyst

1 Introduction

Group transfer polymerization (GTP) was first discovered by Webster et al. in 1983 as to find an alternative polymerization method of anionic polymerization for industrially practical and cost-reducing synthesis of acrylic polymers [1]. Immediately after the discovery, GTP had attracted great attention and was evaluated as

Y. Chen • K. Fuchise • T. Satoh • T. Kakuchi (✉)
Faculty of Engineering, Division of Biotechnology and Macromolecular Chemistry,
Hokkaido University, Sapporo 060-8628, Japan
e-mail: chen@poly-bm.eng.hokudai.ac.jp; fuchise@poly-bm.eng.hokudai.ac.jp;
satoh@poly-bm.eng.hokudai.ac.jp; kakuchi@poly-bm.eng.hokudai.ac.jp

"the first new approach to polymers to occur in several decades" from the academic viewpoint by polymer chemists, because of its excellent performance for "living control" under moderate polymerization conditions [2]. In principle, the initiation and propagation reactions during a GTP process are rooted on the iteration of an elementary organic reaction of the Mukaiyama-Michael reaction, which is a typical C–C formation reaction affording high yield and stereoselective control [3]. The term "group transfer polymerization" has been conferred based on the repetitive transfer of the silyl group from the propagating end to the incoming monomer, which becomes the new propagating end, during propagation, though it was later proven to be inappropriate according to its mechanistic studies. Except for some harsh conditions, such as superhigh pressure of thousands atms, polymerizations do not proceed at all only with silyl ketene acetals (SKAs) and without any catalysts, which strongly indicates that the Lewis base/acid plays a significant role during the polymerization process [4]. Similarly, polymerizations do not proceed only with a Lewis base/acid and without SKA, suggesting that the Lewis base/acid does not initiate any anionic/cationic polymerizations, though they are potentially an initiator or a catalyst in anionic/cationic polymerizations. Obviously, the coexistence of an SKA and a catalyst turns out to be indispensable. This finding, to some extent, supplementarily explains the concept that the polymerization proceeds through a "group transfer" mechanism. When compared with other living polymerizations, the most characteristic feature of GTP method is that the trialkylsilyl-capped end of a propagating polymer is electronically neutral. Therefore, GTP is free from recombination terminations, which is similar to an ionic polymerization. In addition, side reactions caused by impurities, such as chain transfer and termination reactions, can be suppressed to a minimum. For this reason, GTP method has been widely used to polymerize functional (meth)acrylates which bear reactive side groups such as epoxides, cyclic esters, dienes, vinyl, allylic, and styrenic groups; these functionalities are normally sensitive to the conditions of ionic and radical polymerizations [5].

Since its first discovery, GTP, which can actually be referred to as conventional GTP, had experienced a florescent development period from middle 1980s until early 1990s, basically covering all the aspects in terms of (1) the exploration of new efficient catalysts, (2) the broadening of applicable monomers, and (3) the efforts in elucidating polymerization mechanisms. During the middle 1990s–2007, the study of GTP had been a minor research field because of the emergence and rapid development of living radical polymerizations (LRPs). However, the application of organocatalysts to GTP after 2007 has made a breakthrough and significant progress in this field. Relative to the conventional one, Kakuchi et al. have proposed a new definition to the GTPs using organocatalysts as "organocatalytic GTP." Since 2007, many aspects in this field have much improved in terms of catalytic activity, applicable monomers, livingness of polymerization, and control of polymer architecture, owing to the use of organocatalysts.

This subchapter sequentially describes the introduction of catalysts and covers the contents in the following three sections:

1. A comprehensive overview on the Lewis-base-catalyzed GTP, including GTPs using conventional nucleophilic anions and organic strong bases
2. A comprehensive overview on the Lewis-acid-catalyzed GTP, including GTPs using conventional metallic catalysts and organic Lewis acids
3. A recapitulative introduction on the control of polymer architectures

It is worth mentioning that an overview on the scope of applicable monomers and polymerization mechanisms is also discussed throughout this subchapter.

2 Lewis-Base-Catalyzed GTP

2.1 Overview

The first GTP of methyl methacrylate (MMA) was realized using tris(dialkylamino) sulfonium (TAS) salts of nucleophilic anions, such as $SiMe_3F_2^-$ [1, 6, 7], HF_2^- [1, 6–8], CN^- [1, 6, 8, 9], and N_3^- [1, 8]. The catalytic activity of these nucleophilic anions was then extensively studied and widely used as catalysts for GTP. Meanwhile, a variety of other nucleophilic anions, such as F^- [6, 8, 9], oxyanions [10, 11], and hydrogen bioxyanions [11, 12], were also used to optimize the conditions for the GTPs of (meth)acrylates. These nucleophilic anions are now referred to as conventional Lewis base catalysts. For each of them, a bulky and sterically hindered counter cation is basically required to enhance its catalytic activity and solubility in organic solvents. In addition to TASs, much cheaper and readily available tetraalkylammoniums were commonly used later. Other cations, such as cesium ion (Cs^+) [13], bis(triphenylphosphoranylidene)ammonium ($Ph_3PNPPh_3^+$) [14], and 18-crown-6-complexed K^+ [15], were also reported to be suitable for the counter cations of the catalysts. Among all the used nucleophilic anions, the fluoride-based ones exhibited the highest activity, probably due to their extremely high affinity toward silyl groups. Oxyanions and hydrogen bioxyanions are more favorable for the polymerizations above ambient temperatures. The relative order of catalytic activity is as $F^- > HF_2^- >$ oxyanions $>$ hydrogen bioxyanions [16]. It has, for a long time, been considered that the catalytic activity of a nucleophilic anion is correlated to basicity. However, Hertler et al. found that too high basicity would cause side reactions, such as chain transfer, in the GTP of MMA [17]. In fact, the silicophilicity, rather than basicity, could be a much more suitable notion to account for the catalytic activity because Lewis base catalysts actually attack the silicon atom to activate the *Si–O* bond in an initiator or a propagating polymer end for the initiation reaction or the propagation reaction. The nucleophilic anions have been recognized to be suitable catalysts only for methacrylates because their catalytic activities are too high to control the polymerization of acrylates with much higher reactivity than methacrylates. Most of the GTPs of acrylates are out of control by nucleophilic anions.

Nucleophilic anions (featured a hindred counter cation)
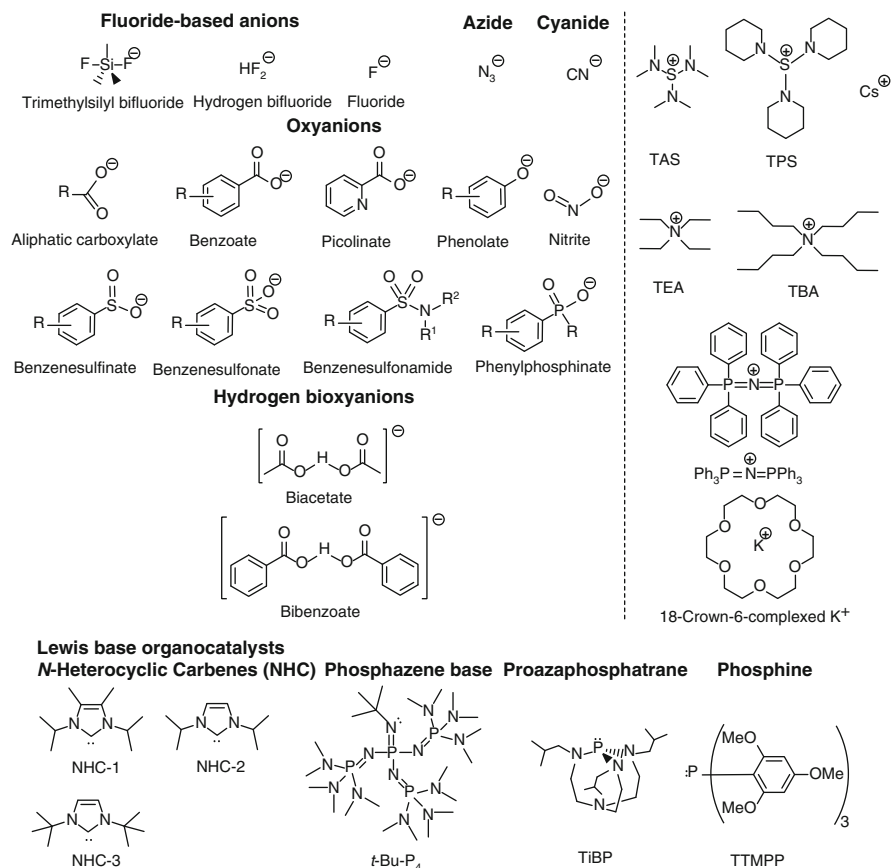
Scheme 1 Chemical structures of nucleophilic anions and Lewis base organocatalysts used in GTP

In addition to the conventionally used nucleophilic anions, the use of recently developed organocatalysts has opened a new avenue in the field of GTP. Lewis base organocatalysts, such as *N*-heterocyclic carbenes (NHCs) [18–24]; organic strong bases such as proazaphosphatranes and phosphazene bases [25–28]; and phosphines [29] have been used as catalysts for GTP since 2007. In comparison with the aforediscussed nucleophilic anions, the Lewis base organocatalysts are more advantageous because they are electronically neutral and much less nucleophilic, thus enabling to suppress side reactions between the catalyst and a monomer, a living polymer, or a solvent. Scheme 1 shows the structures of nucleophilic anions and Lewis base organocatalysts that have been used for GTP so far. The detailed discussion on each class of catalysts is separately implemented in the following sections.
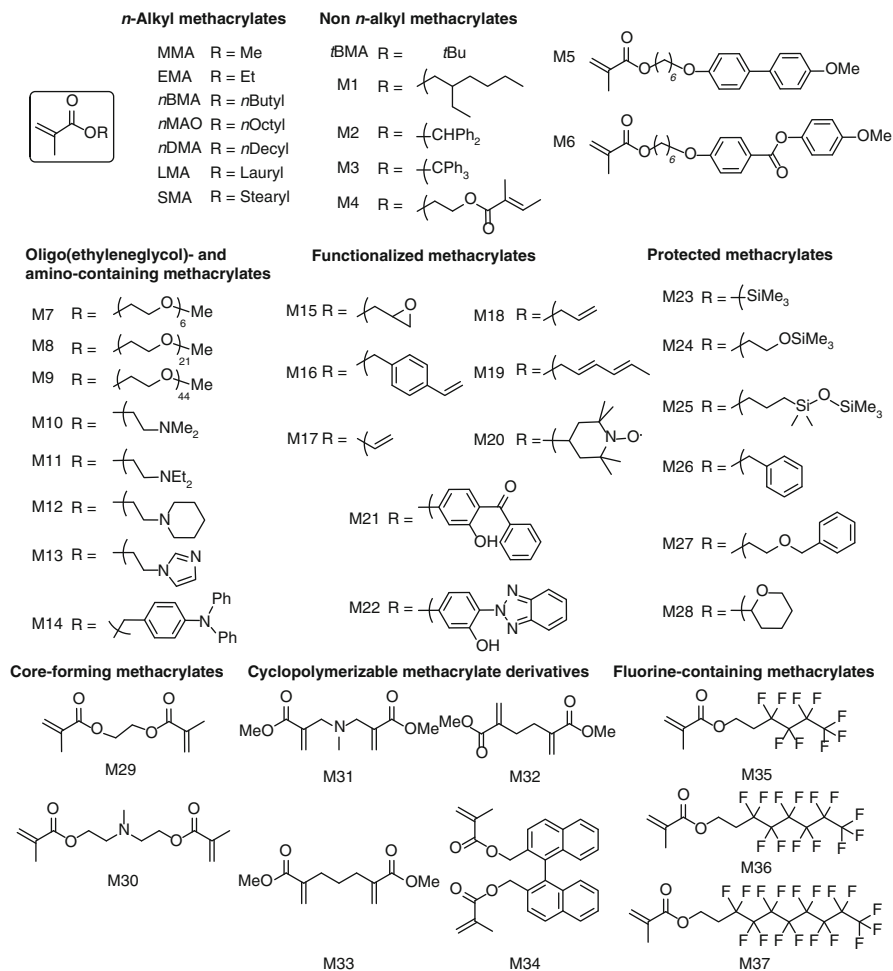
Scheme 2 Structures of methacrylic monomers used in Lewis-base-catalyzed GTP

The Lewis base catalysts are widely used for (co)polymerizing most of methacrylates to produce polymers with homo, random, block, or other architectures. The polymerizable methacrylates include n-alkyl, non-n-alkyl, oligo(ethylene glycol)-, and amino-containing, functionalized, protected, core-forming, cyclopolymerizable, and some fluorine-containing methacrylates, as shown in Scheme 2. The n-alkyl methacrylates include methyl (MMA), ethyl (EMA) [30, 31], n-butyl (nBMA) [1, 5, 8, 32–35], n-octyl (nOMA) [36], lauryl (LMA) [8, 36, 37], and stearyl methacrylate (SMA) [26], which are widely used to synthesize homopolymers or copolymers. Other methacrylates, such as non-n-alkyl methacrylates (tBMA and M1-6) [11, 38–45], oligo(ethylene glycol)- and amino-containing methacrylates (M7-14) [27, 46–53], functionalized methacrylates (M15-20) [1, 8,

Acrylates

MA   R = Me
EA   R = Et
*n*BA   R = *n*Bu
*t*BA   R = *t*Bu

M38   R =

M39   R =

M40   R =

M41   R =

M42   R =

Polyunsaturatedesters

	R^1	R^2	R^3
M43	$R^1 = H$	$R^2 = H$	$R^3 = Me$
M44	$R^1 = Me$	$R^2 = H$	$R^3 = Et$
M45	$R^1 = CO_2Et$	$R^2 = H$	$R^3 = Et$
M46	$R^1 = H$	$R^2 = Me$	$R^3 = Me$
M47	$R^1 = H$	$R^2 = Me$	$R^3 = Et$
M48	$R^1 = Me$	$R^2 = Me$	$R^3 = Me$

M49

Acrylamides

DMAAR = Me
DEAAR = Et

Acrylonitriles

AN   MAN
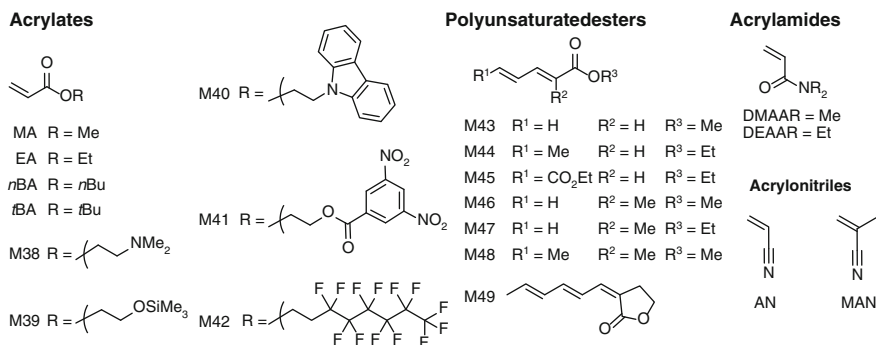
Scheme 3 Structures of acrylates and some vinyl monomers polymerized by Lewis-base-catalyzed GTP

54–59], protected methacrylates (M23-28) [36, 39, 46, 47, 55, 60–63], core-forming methacrylates (M29–30) [48–50, 52, 53, 64], cyclopolymerizable methacrylate derivatives (M31–34) [5, 35, 65, 66], and fluorine-containing methacrylates (M35–37) [67], can also be polymerized to afford corresponding (co)polymers as designed. Generally, the Lewis-base-catalyzed GTP is effective to polymerize most of methacrylates, though livingness of polymerization should be optimized by selecting an appropriate catalyst depending on the structure of a methacrylate.

In addition to methacrylates, acrylates, such as methyl (MA) [6, 7, 9], ethyl (EA) [1, 8], *n*-butyl (*n*BA) [8, 23, 26], *tert*-butyl (*t*BA) [21, 23], and functionalized (M38–42) acrylates [23, 67, 68], have been used to synthesize (co)polymers by the Lewis-base-catalyzed GTP, though most of their GTPs lack ideal control. Other vinyl monomers, such as polyunsaturated esters (M43–49) [69], some of acrylamides [1, 8, 24, 70–72], and acrylonitriles [8, 24, 73, 74], can also be polymerized by the GTP method. Their structures are shown in Scheme 3.

When it comes to GTP, initiators should be brought to discussion. It is recognized that a fast initiation can be achieved when the structure of a silyl ketene acetal has a similar structure with that of the propagating polymer chain end. Webster et al. gave a detailed summarization [75]. In order to precisely control the architectures of resulting polymers, many initiators have been designed, as shown in Scheme 4. 1-Methoxy-1-(trimethylsiloxy)-2-methylprop-1-ene (MeSKA) is undoubtedly the most commonly used one in GTP. Other monofunctional SKAs, such as EtSKA, Me2tBuSKA, Me2nC18H37SKA, Me2PhSKA, and SKA1-3 [1, 8, 69], have also been used to synthesize homopolymers and block copolymers. The bifunctional initiators (SKA4-13) are useful initiators for the synthesis of ABA-type block copolymers [5, 8, 51, 69, 76–78]. Other SKAs, such as functionalized and star-shaped SKAs, are discussed in Sect. 4.

Table 1 summarizes the ranges of molar mass (M_n) and dispersity (M_w/M_n) reported for poly(meth)acrylates synthesized by Lewis-base-catalyzed GTP. Generally, polymethacrylates with high molar mass can be hardly synthesized using the conventional Lewis base catalysts, probably due to their high nucleophilicity which
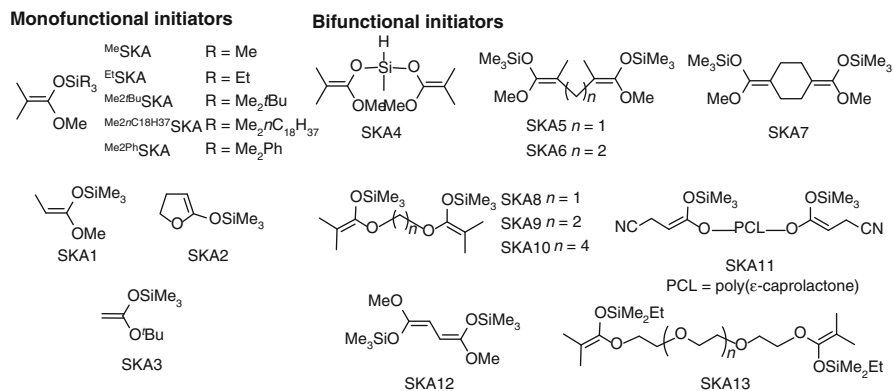
Scheme 4 Structures of monofunctional and bifunctional silyl ketene acetals (SKA) used in Lewis-base-catalyzed GTP

leads to side reactions to terminate living polymer ends. In contrast, the use of organocatalysts can advantageously overcome these limitations in a great extent to improve the livingness of polymerization and thus afford high molar mass polymers.

2.2 Mechanisms of Lewis-Base-Catalyzed GTP

For Lewis-base-catalyzed GTP, two mechanistic routes, i.e., associative [1, 79, 80] and dissociative mechanisms [13, 81–83], have been widely accepted so far. The associative mechanism was originally proposed by Webster et al. based on the fact that no intermolecular exchange of the silyl groups occurred between two propagating polymers labeled with an isotope of the silicon atom [1]. This mechanism involves the formation of a pentacoordinated siliconate by the addition of the catalyst to the electrophilic silyl group and a continuous intramolecular transfer of the silyl group along the same polymer chain end after each addition reaction of monomer, which was claimed to proceed in a "concerted" fashion, as shown in Scheme 5. Afterward, Müller et al. proposed a "two-step" associative mechanism based on their kinetic and stereocontrol studies, in which the formation of *C–C* bond between pentacoordinated SKA and monomer does not simply complete through a "concerted" fashion but through a two-step reaction [84, 85]. The formation of *C–C* bond first occurs via the formation of a hexacoordinated state from the pentacoordinated SKA and a monomer. The silyl group then migrates through the formation and rupture of the unstable eight-membered intermediate. However, the associative mechanism had been questioned by Quirk et al. They proposed the dissociative mechanism and believed that the dissociated enolate ions or anions, which are derived from the interaction between SKA and catalyst, are the true active species, as shown in Scheme 5 [81, 86, 87]. In the dissociative pathway,

Table 1 Ranges of M_n and M_w/M_n reported for poly(meth)acrylates synthesized by Lewis-base-catalyzed GTP

Catalyst	Monomer	Solvent	M_n(expt.) (kg mol^{-1})	M_w/M_n
TASHF$_2$	MMA	THF	$\leq$22.1	–
TBAF	MMA	THF	$\leq$62.3	–
TASN$_3$	MMA	MeCN	3.0	1.03
TASCN	MMA	DMF/THF (9/91)	10.5	1.14
Et$_4$NCN	MMA	DMF/THF (9/91)	11.5	1.06
Oxyanions	MMA	THF	$\leq$17.6	1.06–1.56
TBABA	MMA	THF	$\leq$57.9	–
TBABB	MMA	THF	$\leq$67.6	–
NHC-1	MMA	THF	$\leq$18.9	$\leq$1.35
	tBA	THF	$\leq$16.3	<1.20
NHC-2	MMA	THF	6.7–330	1.07–1.30
	MMA	Toluene	$\leq$31.0	$\leq$1.30
	nBA	THF	9.0–31.0	1.39–1.60
	nBA	Toluene	19.7	1.60
	tBA	THF	4.8–40.0	1.09–1.25
	tBA	Toluene	4.9–24.0	1.19–1.45
	M10	THF	6.5–34.0	1.10–1.15
	M38	THF	23.0	1.46
	DMAA	THF	$\leq$42.0	$\leq$1.15
	MAN	DMF	5.0–18.0	1.37–1.51
NHC-3	MMA	THF	2.6–110	1.10–1.30
	nBA	THF	$\leq$33.0	$\leq$1.40
	nBA	Toluene	21.4	1.50
	tBA	THF	4.8	1.30
	M10	THF	18.0	1.19
	DMAA	THF	37.0	1.17
t-Bu-P$_4$	MMA	THF	6.5–109.6	1.15–1.32
	M14	THF	6.2–34.0	1.06–1.26
TiBP	MMA	THF	6.5–55.9	1.05–1.14
TTMPP	MMA	THF	3.0–22.6	1.13–1.16
	MMA	Bulk	3.6–57.0	1.30–1.37
	tBA	THF	2.1–7.8	1.12–1.45

the active chain ends are true anionic species in equilibrium with dormant complexes. Due to the dissociation of silyl groups from enolates, the degenerative exchange of silyl groups between propagating polymers can readily take place. The dissociative mechanism may proceed through two possible routes, namely, the reversible dissociative mechanism and the irreversible dissociative mechanism. In the reversible dissociative mechanism, the dormant species are a propagating polymer not coordinated by a catalyst and a bis(enolate)siliconate, the adduct of an active enolate and a silyl enolate. On the contrary, the dormant species in the
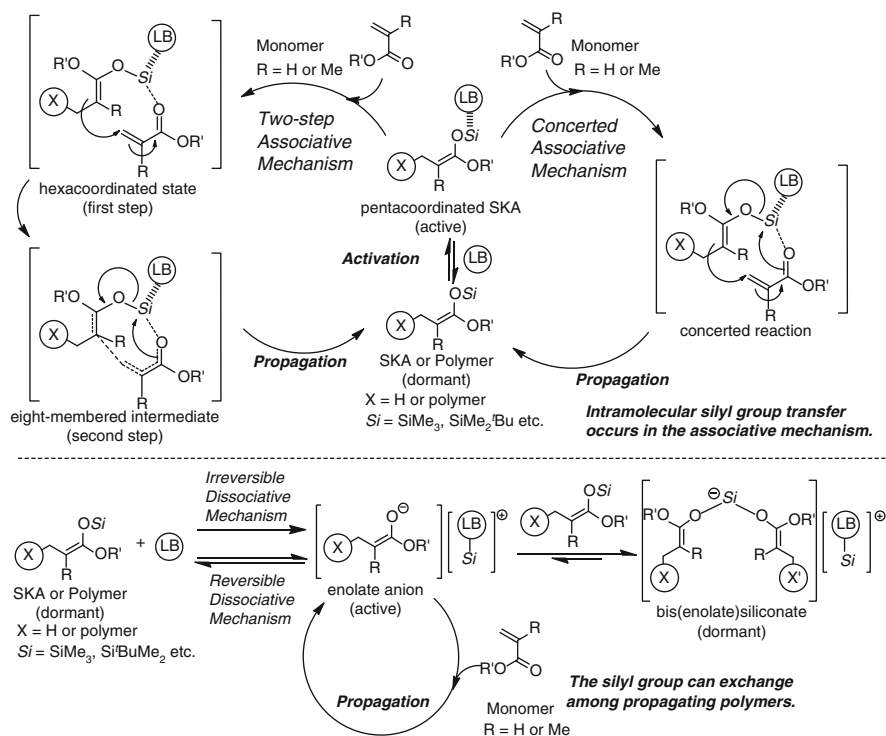
Scheme 5 Proposed associative (*top*) and dissociative (*bottom*) mechanisms of Lewis-base-catalyzed GTP

irreversible dissociative mechanism should be only a bis(enolate)siliconate. Both the associative and dissociative mechanisms are respectively supported by persuasive proofs, as discussed in ref. [75].

2.3 Trimethylsilyl Bifluoride, Hydrogen Bifluoride, and Fluoride

Fluoride-based catalysts, including TAS or tetra-*n*-butylammonium (TBA) salts of trimethylsilyl bifluoride (SiMe$_3$F$_2$$^-$) [1], hydrogen bifluoride (HF$_2$$^-$) [1, 6–8], and fluoride (F$^-$) [6, 8, 9], are most generally used in GTP and were studied since the development of GTP. The initial use of them might be attributed to their high silicophilicity, which has been well known in Mukaiyama aldol reaction and Mukaiyama-Michael reaction. As aforediscussed, they have the highest catalytic activity to promote the GTPs of methacrylates among the catalysts for the conventional GTP. A quite low loading of SiMe$_3$F$_2$$^-$ (0.1–1 mol% relative to an SKA) is

enough for the GTPs of (meth)acrylates to proceed fast. Due to its high catalytic activity, the $SiMe_3F_2^-$-catalyzed GTP is best to be implemented at low temperatures like $-78\,°C$. Any moisture in polymerization system causes the decomposition of $SiMe_3F_2^-$ to its hydrolyzed product, HF_2^-. $SiMe_3F_2^-$ has been less used than HF_2^- and F^- perhaps because of its lower stability. The catalytic activity of HF_2^- and F^- is not so high that realizes GTPs of (meth)acrylates at room temperature. Fluorine-based catalysts are effective in the GTPs of most methacrylates to produce corresponding polymers with moderately controlled molar masses and relatively low dispersities. However, side reactions, such as chain transfer and backbiting reactions, often accompany with the chain propagation because of the high nucleophilicity of these catalysts. Therefore, these fluoride-based catalysts are usually used at a low loading relative to initiator to minimize such side reactions. The F^--catalyzed GTP of MMA could afford a hydroxyl end-functionalized PMMA with a M_n of up to 64.7 kg mol^{-1} and a M_w/M_n of 1.14. To obtain a PMMA with M_n, more than 50–60 kg mol^{-1} has been difficult by the fluoride-based catalysts.

2.4 Azide and Cyanide

N_3^- and CN^- have been also used as catalysts with 3–15 mol% relative to an initiator for the polymerizations of methacrylates and acrylates [1, 6, 8, 9]. Due to their poor solubility in apolar solvents, they required the use of polar solvents like DMF and CH_3CN.

2.5 Oxyanions and Hydrogen Bioxyanions

Oxyanions, such as carboxylates, benzoates, phenoxides, phosphinates, sulfinates, sulfonates, sulfonamides, nitrite, and corresponding bioxyanions, can effectively activate SKAs, though they are not often used [10, 11]. All the oxyanions shown in Scheme 1 can catalyze the GTP of MMA to afford moderate control over molar mass and dispersities. Sogah et al. have provided a deep insight into the oxyanion-catalyzed GTP and found that the catalytic activity of an oxyanion strongly depended on the acidity (pK_a value) of its conjugated acid [11].

Hydrogen bioxyanions are the most effective conventional catalysts for methacrylates [11, 12]. The best examples of hydrogen bioxyanions are bibenzoates and biacetates. In most of cases, they afford better control over molar masses and dispersities than their homologous oxyanions. The reason for this phenomenon might be that the hydrogen bioxyanions have much lower nucleophilicity than corresponding oxyanions because the negative charges in hydrogen bioxyanions are more favorably delocalized than the homologous oxyanions. It has been reported that hydrogen bioxyanions could catalyze not only the GTP of MMA to

produce a PMMA with a M_n of up to 67.6 kg mol^{-1} and M_w/M_n of 1.13 but also catalyze the GTPs of other methacrylates. For instance, the biacetate-catalyzed GTP of nBMA can produce a PnBMA with an M_n of up to 67.6 kg mol^{-1} and a M_w/M_n as narrow as 1.13. The biacetate- and bibenzoate-catalyzed GTPs have also been used to polymerize methacrylates, such as M1, M10, M15, M24, and M28.

2.6   N-*Heterocyclic Carbenes*

The recent development of GTP catalyzed by Lewis base organocatalysts dates back to 2007–2008 when Waymouth and Hedrick et al. and Taton et al. independently reported the GTP of (meth)acrylates using *N*-heterocyclic carbenes (NHCs). Waymouth and Hedrick reported the GTPs of MMA and *t*BA using 1,3-diisopropyl-4,5-dimethylimidazol-2-ylidene (NHC-1) (0.026–3.2 mol% relative to initiator) in THF at room temperature, which afforded good control over polymerization to produce PMMAs with an M_n of up to 18.9 kg mol^{-1} and M_w/M_n narrower than 1.35 as well as P*t*BAs with an M_n of up to 16.3 kg mol^{-1} and M_w/M_n narrower than 1.20 [18, 20]. Taton et al. first reported the GTPs of MMA, *t*BA, and *n*BA using 1,3-diisopropylimidazol-2-ylidene (NHC-2) and 1,3-di-*tert*-butylimidazol-2-ylidene (NHC-3) (5–6 mol% relative to initiator for the polymerization of MMA and 1 mol% relative to initiator for the polymerization of *t*BA and *n*BA) both in THF and toluene at room temperature, which produced PMMAs with the M_n of 2.6–330 kg mol^{-1} and M_w/M_n of 1.07–1.3 as well as P*t*BAs with the M_n of 4.8–33.0 kg mol^{-1} and M_w/M_n of 1.15–1.6 [19, 21]. The polymers synthesized in toluene had relatively broader M_w/M_n than those obtained in THF. It is noteworthy that the PMMA with an M_n greater than 100 kg mol^{-1} has been obtained using NHCs, which can be hardly synthesized using a conventional catalyst. In addition to MMA, M10, *n*BA, M38, DMAA, and MAN can also be polymerized using NHC-2 and NHC-3 [21, 23].

2.7   *Organic Strong Bases*

Kakuchi et al. have recently used the organic strong bases, which have low nucleophilicity and high basicity, to catalyze GTP [25]. Their structures are shown in Scheme 6. Among the five bases, 2,8,9-triisobutyl-2,5,8,9-tetraaza-1-phosphabicyclo[3.3.3]undecane (TiBP) and 1-*tert*-butyl-4,4,4-tris(dimethylamino)-2,2-bis[tris(dimethylamino)-phosphoranylidenamino]-2Λ^5,4Λ^5-catenadi(phosphazene) (*t*-Bu-P$_4$) are the efficient ones to catalyze GTP of MMA. The polymerization using TiBP or *t*-Bu-P$_4$ rapidly proceeded with a [TiBP or *t*-Bu-P$_4$]$_0$/[^{Me}SKA]$_0$ = 0.01, which produced PMMAs with M_n of 6.5–55.9 kg mol^{-1} and 6.5–109.6 kg mol^{-1}, while the narrow M_w/M_n was kept in a range of 1.05–1.14 and 1.15–1.32, respectively. It is worth noting that the *t*-Bu-P$_4$ can catalyze the GTP of MMA to produce a PMMA with M_n
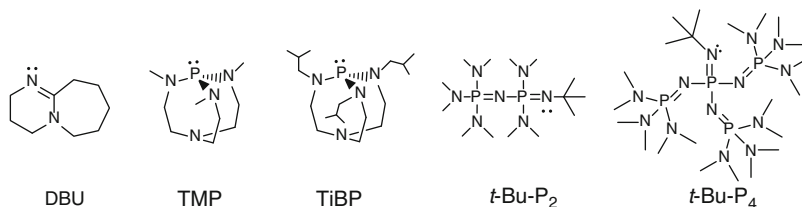
Scheme 6 Chemical structures of organic strong bases

greater than 100 kg mol^{-1}. On the contrary, the GTPs of MMA using 1,8-diazabicyclo [5.4.0]undec-7-ene (DBU), 2,8,9-trimethyl-2,5,8,9-tetraaza-1-phosphabicyclo[3.3.3] undecane (TMP) and 1-*tert*-butyl-2,2,4,4,4-pentakis(dimethylamino)-2Λ^5,4Λ^5-catenadi(phosphazene) (*t*-Bu-P$_2$) were very slow or did not proceed at all both in THF and toluene even when a large amount of the catalysts was used. Interestingly, TMP, TiBP, and *t*-Bu-P$_2$ showed different catalytic activity in the GTP of MMA though they have similar Brønsted basicity, indicating that ability to activate a silicon atom for the polymerization is crucially affected by the structure and silicophilicity of the strong bases, rather than by the Brønsted basicity.

2.8 Phosphines

Most recently, Taton et al. attempted to use phosphines, including tri-*n*-butylphosphine (Bu$_3$P), tricyclohexylphosphine (Cy$_3$P), triphenylphosphine (Ph$_3$P), and tris(2,4,6-trimethoxyphenyl)phosphine (TTMPP), as the catalysts of GTP [29]. Among these phosphines, only TTMPP showed high catalytic activity probably due to its higher Lewis basicity than others. TTMPP (10 mol% relative to initiator) promoted the GTP of MMA in THF in a living fashion to produce a PMMA with M_n of up to 22.6 kg mol^{-1} and M_w/M_n narrower than 1.16. However, in toluene or bulk, the GTP of MMA was out of control. The polymerization produced PMMAs with M_w/M_n broader than 1.3. In addition to MMA, the GTP of *t*BA has also been achieved using TTMPP. A low monomer concentration is more favorable for the GTP of *t*BA. For instance, the GTP of *t*BA in THF under the conditions of [*t*BA]$_0$/[^{Me}SKA]$_0$/[TTMPP]$_0$ = 22/1/0.01 and [*t*BA]$_0$ = 0.7 mol L^{-1} produced a P*t*BA with M_n of 2.1 kg mol^{-1} and M_w/M_n of 1.12, while the same polymerization under ten times condensed condition produced a P*t*BA with an M_n of 3.1 kg mol^{-1}, and an M_w/M_n = 1.4. 2 h induction period has been observed in the polymerization of MMA in THF at 25 °C under the condition of [MMA]$_0$/[^{Me}SKA]$_0$/[TTMPP]$_0$ = 30/1/0.1, though the polymerization rate followed the first order of the concentration of MMA after the induction period.

3 Lewis-Acid-Catalyzed GTP

3.1 Overview

Lewis-acid-catalyzed GTP is considered to proceed through the activation of a monomer by a Lewis acid (LA), as illustrated in Scheme 7. Scheme 8 summarizes catalysts, monomers, and initiators used in Lewis-acid-catalyzed GTP so far. Conventional Lewis acid catalysts, such as zinc halides and organoaluminums, are only suitable for the controlled polymerizations of acrylates because of the low catalytic activity, i.e., weak Lewis acidity [88]. Thus, several metallic Lewis acids with high acidity have been examined to develop controlled polymerizations of other monomers [8, 70, 89–99]. The controlled polymerization of alkyl crotonates has been achieved by the GTP catalyzed by the mixture of mercury(II) iodide (HgI_2) and trialkylsilyl iodide, even though it has been hardly achieved by radical polymerization and anionic polymerization. The emergence of highly Lewis acidic nonmetallic catalysts, namely, Lewis acid organocatalysts, has broken the limit of conventional Lewis-acid-catalyzed GTPs. The GTPs of alkyl methacrylates, DMAA, α-methylenebutyrolactone (MBL), and γ-methyl-α-methylenebutyrolactone (MMBL) have been newly achieved using Lewis acid organocatalysts, such as tris (pentafluorophenyl)borane ($B(C_6F_5)_3$) with a silylating agent, triphenylmethyl salts, and strong organic Brønsted acids. The Lewis acid organocatalysts are regularly used at a ratio of ca. 1–50 mol% relative to the initiator to obtain polymers with M_w/M_n narrower than 1.15. Apolar solvents, such as CH_2Cl_2 and toluene and cyclohexane, are more favorable for the Lewis-acid-catalyzed GTP. Generally, the polymerization rate increases with the increasing polarity of the solvent. However, polar and donating solvents, such as THF and DMF, inhibit the polymerization. The mechanism of each polymerization is described in detail in the following sections because it slightly varies depending on the used catalyst. Table 2 summarizes the ranges of M_n and M_w/M_n for the polymers obtained from the Lewis-acid-catalyzed GTP using respective catalyst.

Scheme 7 Plausible mechanism of the Lewis-acid-catalyzed GTP
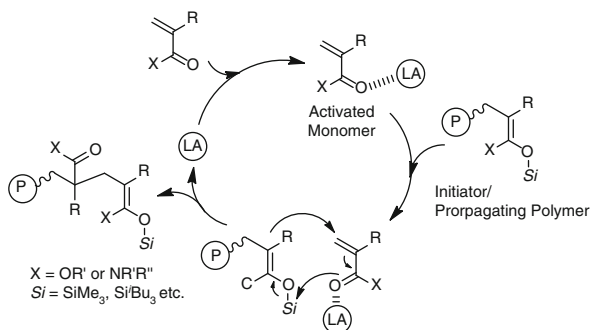
Conventional Lewis Acid Catalysts
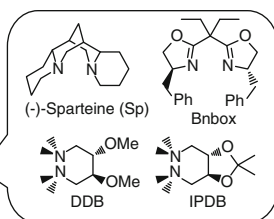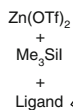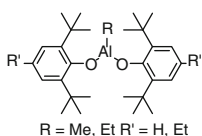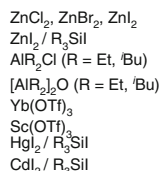
Lewis Acid Organocatalysts
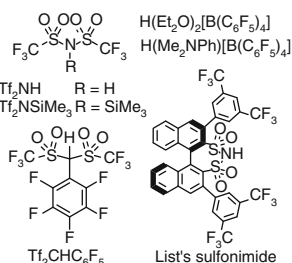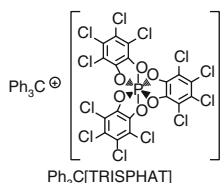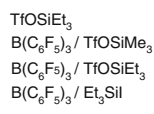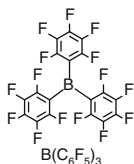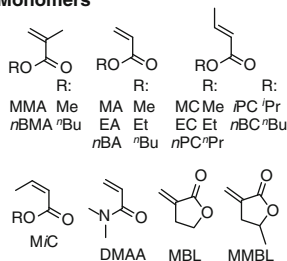
Monomers   **Initiators**
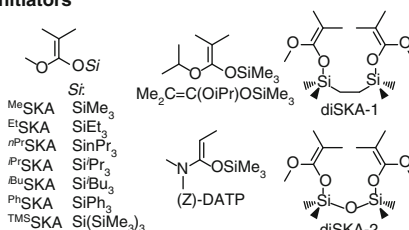
Scheme 8 Catalysts, monomers, and initiators used in the Lewis-acid-catalyzed GTP

3.2 Zinc Halides and Zinc Triflates

Hertler et al. first reported the Lewis-acid-catalyzed GTP of methacrylates and acrylates using zinc halides, such as zinc(II) iodide (ZnI_2), zinc(II) bromide ($ZnBr_2$), and zinc(II) chloride ($ZnCl_2$) [8, 88]. ZnI_2 has been the best catalyst for the polymerization of EA at ambient temperature in the conventional GTP. The GTPs of EA using 1-[2-(trimethylsiloxy)ethoxy]-1-(trimethylsiloxy)-2-methylprop-1-ene (SKA14) and ZnI_2 in CH_2Cl_2 or ethylene dichloride produced PEAs with M_n of 1.25–3.30 kg mol^{-1} and M_w/M_n of 1.03–1.10. The GTP of MMA using ^{Me}SKA and $ZnBr_2$ in ethylene dichloride produced a PMMA with M_n of 6.02 kg mol^{-1} and M_w/M_n of 1.20, though the M_n was almost 1.8 times greater than the calculated M_n. 10–20 mol% of the catalyst is required for the controlled polymerization of both EA and MMA. $ZnBr_2$ has been used for the GTP of 2-methacryloxyethyl acrylate and DEAA using ^{Me}SKA. In the former polymerization, the acryloyl group in the monomer was selectively polymerized to produce a polyacrylate-bearing methacryloyl groups on the side-chain [8]. The latter

Table 2 M_n and M_w/M_n scopes of Lewis-acid-catalyzed GTP

Catalyst	Monomer	Solvent	M_n(expt.) (kg mol^{-1})	M_w/M_n
ZnI$_2$	EA	CH$_2$Cl$_2$	1.25–3.30	1.03–1.10
	DEAA	CH$_2$Cl$_2$	–[a]	–[a]
ZnBr$_2$	MMA	CH$_2$Cl$_2$	6.02	1.20
Organoaluminums	EA or nBA	CH$_2$Cl$_2$	1.98–2.37	1.06–1.17
(^{i}BuO)$_2$Al	EA	Toluene	1.33	1.19
HgI$_2$ + R$_3$SiI	nBA	Toluene	≤3.7	1.08–1.15
	MC	CH$_2$Cl$_2$	5.2–13	1.12–1.22
	MiC	CH$_2$Cl$_2$	9.0	1.20
CdI$_2$ + Et$_3$SiI	MC	CH$_2$Cl$_2$	1.3–7.7	1.06–1.19
B(C$_6$F$_5$)$_3$ + silylating agents	MMA	CH$_2$Cl$_2$	12.1	1.06
	EA	CH$_2$Cl$_2$	5.3–21.7	1.14–1.26
	EA	Toluene	17.4	1.12
TTPB	MMA	CH$_2$Cl$_2$	20.8	1.07
	MMA	Toluene	21.6	1.07
	nBMA	CH$_2$Cl$_2$	42.1	1.07
	nBMA	Toluene	49.1	1.08
	nBA	Toluene	24.3	1.07
	MMBL	CH$_2$Cl$_2$	18.8–548	1.01–1.06
[Ph$_3$C][TRISPHAT]	MMA	–[b]	–[b]	–[b]
	MMBL	CH$_2$Cl$_2$	36.2	1.01
Tf$_2$NH	MMA	CH$_2$Cl$_2$	3.86–17.0	1.04–1.08
	DMAA	CH$_2$Cl$_2$	12.7	1.08
	DMAA	Toluene	3.24–53.9	1.06–1.16
Tf$_2$NSiMe$_3$	MMA	CH$_2$Cl$_2$	4.1–8.6	1.07–1.11
Tf$_2$CHC$_6$F$_5$	MA	Toluene	2.9–108	1.03–1.07
	DMAA	CH$_2$Cl$_2$	2.8–10.4	1.04–1.07
H(Et$_2$O)$_2$[B(C$_6$F$_5$)$_4$]	MMA	CH$_2$Cl$_2$	11.3–74.1	1.07–1.12
	MMA	Toluene	20.0	1.08
	BMA	CH$_2$Cl$_2$	44.3	1.07
	nBA	Toluene	23.2	1.08
	DMAA	CH$_2$Cl$_2$	102	1.09
	MMBL	CH$_2$Cl$_2$	40.0	1.07
H(Me$_2$NPh)[B(C$_6$F$_5$)$_4$]	MMA	CH$_2$Cl$_2$	18.5	1.07
List's sulfonimide	MMA	CH$_2$Cl$_2$	–[a]	–[a]
	DMAA	CH$_2$Cl$_2$	30.2	1.13

[a]Not polymerized
[b]Not mentioned in the original article [100]

polymerization in CH$_2$Cl$_2$ did not proceed [70]. The combined use of ZnI$_2$ and trialkylsilyl iodide has been found to be as effective as the catalytic system of HgI$_2$ and trialkylsilyl iodide for the controlled polymerization of methyl crotonate (MC) (see Sect. 3.4) [95].

3.3 Organoaluminums

The GTPs of EA and *n*BA using ^{Me}SKA and organoaluminum, such as chlorodiethylaluminum, chlorodiisobutylaluminum, and oxybis(diisobuty-laluminum), in CH_2Cl_2 or a mixture of CH_2Cl_2 and acetonitrile (1/2, v/v) produced corresponding polyacrylates with M_n of 1.98–2.37 kg mol^{-1} and M_w/M_n of 1.06–1.17, though it required low polymerization temperature as −78 °C. On the contrary, the GTP of EA using oxybis(diisobutylaluminum) and ^{Me}SKA in toluene quantitatively proceeded at ambient or higher temperatures (20–58 °C) to produce PEA with M_n of 1.33 kg mol^{-1} and M_w/M_n of 1.19 [8, 70]. The polymerization of MMA using chlorodiisobutylaluminum and ^{Me}SKA in CH_2Cl_2 was uncontrolled, which produced a PMMA with M_n of 3.0 kg mol^{-1} and M_w/M_n of 2.43. In contrast to zinc halides, the aluminum catalysts were used at 10 mol% relative to an initiator.

The combination of alkylaluminum bis(2,6-di-*tert*-butylphenoxide) and trimethylsilyl iodide was effective for the synthesis of highly syndiotactic PMMA using ^{Me}SKA in CH_2Cl_2 at 0 °C under the condition of $[M]_0/[I]_0/[Al]_0/[Si]_0 = 50/1/0.75/0.5$, though the resulting PMMA had bimodal and dispersity [89]. The high molar mass part was highly syndiotactic ($rr = 95.6$–98.7 %) and insoluble in acetone, THF, and toluene, while the solubility of the low molar mass part ($rr = 78.9$–88.6 %) was the same as conventional PMMA.

3.4 Mercury(II) Iodide with Trialkylsilyl Iodide

Conventionally, the most efficient catalytic system consisting of Lewis acids is a mixture of HgI_2 and trialkylsilyl iodide, which was effective for the controlled polymerization of acrylates in toluene, with 5.2 mol% of HgI_2 and 2.1 mol% of trimethylsilyl iodide relative to the initiator [90–93], as well as crotonates in CH_2Cl_2, with 8 mol% of HgI_2 and 24 mol% of triethylsilyl iodide relative to the initiator [94, 95]. Müller et al. proposed the mechanism of the GTP catalyzed by HgI_2 and trialkylsilyl iodide, as shown in Scheme 9, in order to elucidate the high catalytic activity of this catalytic system [92, 93]. The polymerization of *n*BA using HgI_2 itself as a catalyst required a maximum of 200 min of induction period, though the polymerization eventually proceeded with a first-order kinetics on monomer concentration [92]. Trimethylsilyl iodide (Me_3SiI) itself did not show any catalytic
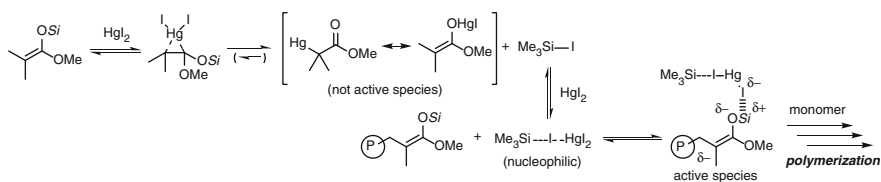
Scheme 9 Plausible mechanism of the GTP catalyzed by HgI_2 and trialkylsilyl iodide

activity for the polymerization. Thus, they proposed that Me_3SiI is generated from the reaction of a trimethylsilyl enolate and HgI_2 as a byproduct in the formation of α-mercuroester or O-mercuric enolate. The generated Me_3SiI forms a nucleophilic adduct with HgI_2, $Me_3SiI\text{-}HgI_2$, which can activate a silyl enolate of an initiator or the propagating end to catalyze the initiation/propagation reaction. The isolated mixture of α-mercuroester or O-mercuric enolate has been recognized to be not the active species in the polymerization, because they produced only a mixture of oligomer of nBA.

The controlled polymerization of alkyl crotonates has been achieved with the GTP catalyzed by HgI_2 and trialkylsilyl iodide for the first time [94–97]. The polymerization of methyl crotonate (MC) at $-20\ ^\circ$C using ^{Et}SKA/Et_3SiI, ^{nPr}SKA/^{n}Pr$_3$SiI, or ^{Me2tBu}SKA/Me_2tBuSiI in CH_2Cl_2 produced poly(methyl crotonate) (PMC) with M_n of 5.2–13 kg mol^{-1} and M_w/M_n of 1.12–1.22 [95, 97]. The PMC obtained using ^{Me2tBu}SKA/Me_2tBuSiI had the highest disyndiotacticity up to 94 % among them. The polymerizations of n-propyl crotonate (nPC), isopropyl crotonate (iPC), and n-butyl crotonate (nBC) using ^{Et}SKA and HgI_2/Et_3SiI were also controlled to produce corresponding polymers with M_n of 71–90 kg mol^{-1}, M_w/M_n of 1.07–1.16, and predominant disyndiotacticity [96]. In addition, the controlled polymerization of methyl isocrotonate (MiC) has been for the first time achieved by the GTP using ^{Me}SKA, HgI_2, and Me_3SiI at $-40\ ^\circ$C in CH_2Cl_2 to produce a poly(methyl isocrotonate), which has the same primary structure as PMC, with M_n of 9.0 kg mol^{-1} and M_w/M_n of 1.20. Interestingly, the stereoregularity of the resulting polymer was similar to the PMC obtained by the same polymerization condition, though the structures of the monomers are geometrically different. The unique mechanism of the GTP using HgI_2/trialkylsilyl iodide might be the reason why the controlled polymerizations of alkyl crotonates and methyl isocrotonate have been achieved.

3.5 Other Metallic Catalysts

Matyjaszewski et al. once reported that tris(trifluoromethanesulfonyl) lanthanides, such as $Yb(OTf)_3$ and $Sc(OTf)_3$, were effective for the GTP of acrylates [98]. Oishi et al. attempted the GTP of N-cyclohexylmaleimide catalyzed by the complexes of zinc(II) trifluoromethanesulfonate ($Zn(OTf)_2$) and chiral diamine ligands [99]. Kitayama et al. found that a catalytic system of cadmium(II) iodide and trialkylsilyl iodide was also effective for the polymerization of MC, which produced PMC with M_n of 1.3–7.7 kg mol^{-1} and M_w/M_n of 1.06–1.19 [95].

3.6 $B(C_6F_5)_3$ with Silylating Agents

The first example of the GTP catalyzed by a nonmetallic Lewis acid is the GTP of EA catalyzed by $B(C_6F_5)_3$ [101, 102] or triethylsilyl trifluoromethanesulfonimide (TfOSiEt$_3$) [103] reported in 2000, though it was not originally reported as an organocatalytic polymerization [104]. The former polymerization was carried out with [Et]SKA in CH_2Cl_2 at 20 °C for 1 h under the conditions of [EA]$_0$/[[Et]SKA]$_0$/[B$(C_6F_5)_3$]$_0$ = 100/1/0.1 and [EA]$_0$ = 2.5 mol L^{-1} to produce a PEA with an M_n of 7.5–12.6 kg mol^{-1} and an M_w/M_n of 1.13–1.52. The latter polymerization was carried out in CH_2Cl_2 at 0 °C for 24 h under the conditions of [EA]$_0$/[[Et]SKA]$_0$/[TfOSiEt$_3$]$_0$ = 50/1/0.5 and [EA]$_0$ = 2.5 mol L^{-1} to produce a PEA with an M_n of 3.2 kg mol^{-1} and an M_w/M_n of 2.35. However, the combined use of $B(C_6F_5)_3$ and TfOSiEt$_3$ improved the control of the polymerization; the GTP of EA catalyzed by $B(C_6F_5)_3$ and TfOSiEt$_3$ under the conditions of [[Et]SKA]$_0$/[$B(C_6F_5)_3$]$_0$/[TfOSiEt$_3$]$_0$ = 5–20/1/0.01 produced PEAs with M_n of 5.3–21.7 kg mol^{-1} and M_w/M_n of 1.14–1.18. The same catalytic system allowed the controlled block copolymerization of EA and nBA. It is noteworthy that the controlled polymerization of MMA by the GTP catalyzed by a Lewis acid has been for the first time achieved by the combined use of $B(C_6F_5)_3$ and Et$_3$SiI in the same report. The polymerization was carried out in CH_2Cl_2 at 0 °C under the conditions of [MMA]$_0$/[[Et]SKA]$_0$/[$B(C_6F_5)_3$]$_0$/[Et$_3$SiI]$_0$ = 100/1/2/0.5 and [MMA]$_0$ = 2.5 mol L^{-1} to produce PMMA with an M_n of 12.1 kg mol^{-1} and M_w/M_n of 1.06, though it required two equivalents of $B(C_6F_5)_3$ relative to the initiator. The triethylsilyl cation generated from $B(C_6F_5)_3$/TfOSiEt$_3$ and $B(C_6F_5)_3$/Et$_3$SiI was presumed to be the true catalyst in the polymerization, though a detailed mechanism of the polymerization had not been experimentally investigated.

3.7 Triphenylmethyl Salts

Since 2008, Chen et al. proposed and demonstrated the oxidative GTP catalyzed by triphenylmethyl salts, especially triphenylmethyl tetrakis(pentafluorophenyl)borate (TTPB), which can lead to the living polymerization of alkyl (meth)acrylates as well as MMBL [100, 105–107]. The controlled polymerization of MMA has been achieved by adding TTPB to a solution of MMA and [Me]SKA at ambient temperature both in CH_2Cl_2 and toluene, which produced PMMAs with an M_n greater than 100 kg mol^{-1} and narrow M_w/M_ns of 1.04–1.12 [105]. However, donating solvents, such as tetrahydrofuran (THF), inhibited the polymerization. The same initiating system consisting of [Me]SKA and TTPB allowed the quantitative polymerization of nBMA at room temperature (~25 °C) within 60 min to give poly(n-butyl methacrylate) (PnBMA) with an M_n of 54.4 kg mol^{-1}, an M_w/M_n of 1.06, and a high syndiotacticity (rr = 80 %). Scheme 10 depicts the proposed mechanism of the oxidative GTP promoted by triphenylmethyl salts, which postulates that in situ
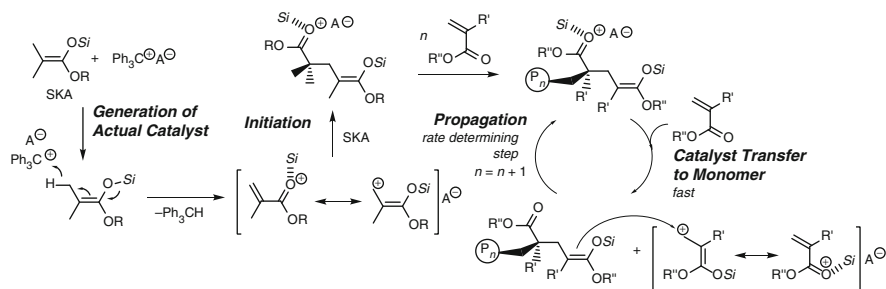
Scheme 10 Presumed mechanism of the GTP promoted by a triphenylmethyl salt

generated silylium cation is the actual catalyst for the polymerization. The triphenylmethyl cation abstracts a hydrogen atom from a SKA to generate a triphenylmethane and an alkyl methacrylate coordinated by a silylium cation, which has been proven from a ^{1}H NMR measurement at low temperature. Another silyl enolate reacts with the activated methacrylate to produce an adduct coordinated by the silylium cation. The catalyst transfer from the propagating polymer to the incoming monomer is much faster than the $C–C$ bond formation by intermolecular Michael addition between the propagating polymer and the monomer activated by the silylium cation because the kinetics of the polymerization is zero order on monomer concentration and first order on the concentrations of SKA and TTPB regardless of the $[M]_0/[SKA]_0/[TTPB]_0$ ratio. It has not been investigated whether the silyl groups of the propagating end and the catalyst exchanged through the propagation reaction.

The silyl group in the silyl enolate significantly affects the reactivity and stability of the propagating polymer [100]. This result is rational because the silyl group has been involved in whole polymerization step as the propagating end and the catalyst. For example, in the polymerization of MMA, the reactivity of the propagating PMMA decreased as the increasing bulkiness of the silyl group, which caused the deceleration of polymerization rate of MMA. The polymerization of MMA under the condition of $[MMA]_0/[^{Me}SKA]_0/[TTPB]_0 = 400/2/1$ at 25 °C in CH_2Cl_2 could complete within 25 min. Under the same condition, the polymerizations using ^{iBu}SKA with a triisobutylsilyl group and 1-tris(trimethylsilyl)siloxy-1-methoxy-2-methyl-1-propene (^{TMS}SKA) with a tris(trimethylsilyl)silyl group became 5 times and 175 times slower than that using ^{Me}SKA. Instead, the syndiotacticity of the resulting PMMA increased with the increasing bulkiness of the silyl group; the polymerization using ^{Me}SKA, ^{iBu}SKA, 1-triphenylsilyl-1-methoxy-2-methyl-1-propene (^{Ph}SKA), and ^{TMS}SKA produced PMMAs with rr triad content of 70 %, 73 %, 73 %, and 77 %, respectively. The stability of the propagating polymer also increased with the increasing bulkiness of the silyl group. Rapid and controlled polymerization of nBA has been achieved with ^{iBu}SKA in toluene at room temperature (~25 °C) under the condition of $[nBA]_0/[^{Me}SKA]_0/[TTPB]_0 = 200/1.1/0.1$ to produce a PnBA with an M_n of 24.3 kg mol^{-1} and an M_w/M_n of 1.06, though the polymerization with ^{Me}SKA under the condition of $[nBA]_0/[^{Me}SKA]_0/$

$[\text{TTPB}]_0 = 400/2/1$ at 25 °C in CH_2Cl_2 was terminated within 6 h at a conversion of 24.6 % to give a PnBA with an M_n of 15.5 kg mol^{-1} and a broad M_w/M_n of 1.63. The M_n of PnBA was controlled in a range of 23.1–73.1 kg mol^{-1} while keeping M_w/M_n narrower than 1.17, though attempts to synthesize PnBAs with M_n more than 100 kg mol^{-1} resulted in the formation of PnBA with M_w/M_n broader than 1.5. Even cyclohexane as a less polar solvent than toluene was available for the polymerization of nBA to give PnBA with an M_w/M_n of 1.06. In addition, ^{TMS}SKA was also effective for the polymerization of nBA.

For the TTPB-promoted GTP, the effectiveness of other dimethyl ketene group 14 (alkyl, germyl, and stannyl) acetals has been investigated [100]. Dialkyl dimethylketene acetal did not act as an initiator for the polymerization, though the oligomerization occurred in the presence of TTPB. The synthesis of germyl and stannyl dimethyl ketene acetal was unsuccessful because of exclusive formation of C-germyl/stannyl compounds, which was ineffective for the polymerization, in the reaction of lithium enolate and germyl/stannyl chlorides. On the contrary to the large effect of the silyl group on the polymerization behavior, the alkoxy group of the initiator did not show any appreciable effects on entire polymerization characteristics because the difference in the alkoxy group only affected the initiation reaction, which was similar to the result in the conventional GTP [8, 100].

The effect of the counter anion of triphenylmethyl salt on the polymerization was also reported [100]. $Ph_3C[BF_4]$ and $Ph_3C[(C_6F_5)_3Al\text{-}F\text{-}Al(C_6F_5)_3]$ led to the addition of the triphenylmethyl group to ^{Me}SKA rather than the polymerization of MMA because the silylium cation, which was supposed to be generated from the reaction between the triphenylmethyl salts and ^{Me}SKA, was trapped by the fluoride anion released from the counter anions. On the other hand, $[Ph_3C][rac\text{-}TRISPHAT]$ promoted the polymerization of MMA in CH_2Cl_2 at 25 °C to produce PMMA with rr triad content of 73 %, though the polymerization rate was three times slower than the polymerization using TTPB.

Applicable monomers for the TTPB-promoted GTP have been expanded to MMBL [106]. The GTP of MBL using either ^{Me}SKA or ^{iBu}SKA in CH_2Cl_2 was uncontrolled to produce poly(α-methylenebutyrolactone) (PMBL) with bimodal molar mass distribution due to the low solubility of resulting polymer. The polymerization in DMF was totally inhibited probably due to the exclusive coordination of the silylium cation to the solvent, even though a polar solvent was favorable for PMBL. On the other hand, the GTP of MMBL using ^{iBu}SKA and TTPB in CH_2Cl_2 at ~25 °C under the condition of $[\text{MMBL}]_0/[^{iBu}\text{SKA}]_0 = 200$ homogeneously proceeded within 10 min with a quantitative monomer conversion. The obtained poly(γ-methyl-α-methylenebutyrolactone) (PMMBL) had an M_n of 30.4 kg mol^{-1} and an M_w/M_n of 1.02 as determined by size exclusion chromatography (SEC) combined with a light-scattering detector. Kinetics of the polymerization in CH_2Cl_2 at ambient temperature (25 °C) showed zero-order dependence on monomer concentration regardless of the ratio of $[\text{MMBL}]_0/[^{iBu}\text{SKA}]_0/[\text{TTPB}]_0$, which implied that the polymerization mechanism of MMBL could be also expressed by Scheme 10. The M_n of the resulting PMMBL increased with the increasing monomer conversion while keeping M_w/M_n narrower than 1.09. $[Ph_3C][TRISPHAT]$ was

also effective for the polymerization, though the polymerization rate was slightly slower than that using TTPB. The resulting PMMBL had almost similar stereoregularity, $mm/mr/rr = 11.3/43.0/45.7$, in comparison with that obtained using TTPB, $mm/mr/rr = 14.3/39.9/45.8$.

Furthermore, the TTPB-promoted GTP of MMA was investigated using difunctional silyl enolates (diSKA), namely, 1,2-bis([(1-methoxy-2-methyl-1-propenyl) oxy](dimethyl)silyl)ethane (diSKA-1) and 1,3-bis([(1-methoxy-2-methyl-1-propenyl)oxy])-1,1,3,3-tetramethyldisiloxane (diSKA-2), to increase activity of the silylium catalyst and stereoregularity of the resulting PMMA [107]. The polymerization of MMA using diSKA-1 and TTPB in CH_2Cl_2 at ambient temperature (~25 °C) under the condition of $[MMA]_0 = 0.935$ mol L^{-1} and $[MMA]_0/[diSKA-1]_0/[TTPB]_0 = 400/1/1$ was 12 times more rapid than that using ^{Me}SKA in the early stage of the polymerization. However, a resulting PMMA had an M_n around 1.5 times smaller than M_n calculated from the polymerization condition and a broad M_w/M_n of 1.2–1.7, which indicated occurrence of side reactions, such as chain-transfer reaction. The polymerization of MMA using diSKA-2 under similar conditions reached completion within 1 min to give a PMMA with an M_n of 47.4 kg mol^{-1} and an M_w/M_n of 1.28, which was 3.7 times faster than that using diSKA-1 though the M_w/M_n was still broad. The presence of oxygen atom between two silicon atoms in diSKA-2 might have caused the increased reactivity of the silyl enolate. The polymerization with tenfold smaller amount of TTPB ($[MMA]_0/[diSKA-1]_0/[TTPB]_0 = 400/1/0.1$) produced PMMA with a broad M_w/M_n of 1.28, though the rate of polymerization significantly decreased (42.1 % conversion in 31 h). Opposite to the expectation of Chen et al., the stereoregularity of the PMMA synthesized with diSKAs was similar to that synthesized with ^{Me}SKA regardless of the polymerization condition and the employed triphenylmethyl salts, i.e., TTPB and $[Ph_3C][TRISPHAT]$; the polymerization in CH_2Cl_2 at 25 °C and −78 °C produced PMMA with $mm/mr/rr$ of 2/28/70 and 1/7/92.

Unlike the GTP using ^{Me}SKA and TTPB, the kinetics of the polymerization using diSKA-2 in CH_2Cl_2 at 25 °C under the condition of $[diSKA-2]_0/[TTPB]_0 = 1/1$ showed first-order dependence on monomer concentration, which implied that the mechanism of the propagation reaction differs in respective polymerizations. The mechanism of the polymerization using a diSKA was presumed as illustrated in Scheme 11. The reaction of TTPB and diSKA generates mono cationic adducts of the triphenylmethyl cation, which was proven by ^1H NMR measurements in deuterated CH_2Cl_2 at −78 °C. The propagation reaction proceeds with intramolecular Michael addition through the formation of the propagating polymer coordinating to MMA (**J**) as an intermediate, which was considered plausible because the polymerization rate must show second-order dependence on catalyst concentration and zero-order dependence on monomer concentration when two propagating polymers are involved in the reaction. The first-order dependence of the polymerization rate on monomer concentration also implied that the transfer of the silylium cation from the propagating polymer, i.e., intermediate **J′**, to the incoming monomer was the rate-determining step.
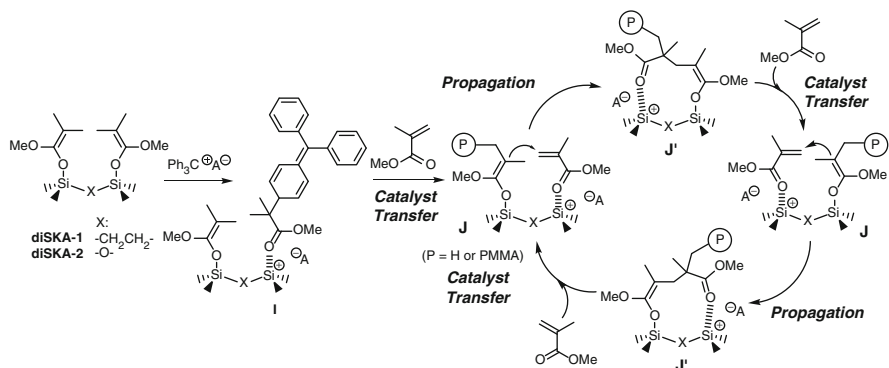
Scheme 11 Proposed mechanism for the GTP of MMA using a difunctional silyl enolate (diSKA)

The GTPs of MBL and MMBL were also examined with diSKAs and TTPB, though they were less controlled than the polymerization using $^{i\mathrm{Bu}}$SKA. The polymerization of MBL using TTPB in CH_2Cl_2 was uncontrolled because the resulting PMBL was insoluble in CH_2Cl_2. The polymerization in DMF did not proceed because the silylium cation dominantly coordinated to DMF rather than to the monomer. The polymerization of MMBL using diSKA-1 and TTPB terminated before reaching perfect monomer conversion and only produced PMMBLs with broad M_w/M_ns of around 1.4–1.5. The GTP of MMBL using diSKA-2 and TTPB was about 6.7 times faster than that using diSKA-1. The resulting PMMBL had broad M_w/M_ns of 1.64–2.07 regardless of the polymerization condition, though monomer conversion reached 78–98 %.

3.8 Organic Strong Acids

Not only triphenylmethyl salts but also Brønsted acids have been found to be effective for GTP. Kakuchi et al. first paid attention to the potential of strong Brønsted acids and applied them to GTP [108]. In advance of the series of study, Yamamoto et al. have reported that trifluoromethanesulfonimide (Tf$_2$NH), one of the strong Brønsted acids, can efficiently promote Mukaiyama aldol reaction of which reaction mechanism is similar to the propagation reaction of GTP [109, 110]. List et al. achieved the asymmetric Mukaiyama aldol reaction promoted by a chiral strong Brønsted, which showed a high reactivity and high enantioselectivity [111]. In these reactions, a strong Brønsted acid (A-H) was considered to first react with a silyl enolate to form silicon Lewis acid (A-SiR$_3$) as an actual catalyst with extremely high Lewis acidity.

The GTP of MMA was carried out using Tf$_2$NH and $^{\mathrm{Me}}$SKA in CH_2Cl_2 at 27 °C under the condition of $[\mathrm{MMA}]_0/[^{\mathrm{Me}}\mathrm{SKA}]_0/[\mathrm{Tf_2NH}]_0 = 100/1/0.05$ to produce PMMA with an M_n of 13.5 kg mol^{-1} and an M_w/M_n of 1.04 within 24 h of the
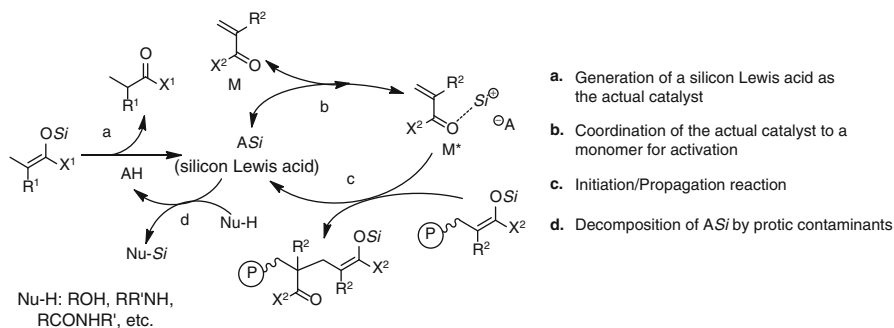
Fig. 1 Plausible mechanism of the GTP promoted by a strong Brønsted acid (AH)

polymerization time [108]. The kinetics of the polymerization showed first-order dependence between polymerization time and monomer conversion. The M_n of the resulting PMMA linearly increased with the increasing monomer conversion while retaining low M_w/M_n. The postpolymerization experiment directly proved the living nature of the polymerization. The matrix-assisted laser desorption ionization time-of-flight mass spectrometry (MALDI-TOF MS) spectrum of the resulting PMMA showed only one population of molecular ion peaks, which corresponded to the molar mass of PMMA bearing terminal structure originated from [Me]SKA. The polymerization allowed to synthesize PMMAs with various M_ns of 3.86–17.0 kg mol^{-1} and M_w/M_ns of 1.04–1.08 by changing initial feed ratio of MMA and [Me]SKA, [MMA]$_0$/[[Me]SKA]$_0$. Another feature of the polymerization was simultaneous control of molar mass and stereoregularity; the polymerization of MMA in CH$_2$Cl$_2$ at $-55\,^{\circ}$C afforded PMMA with M_n of 14.0 kg mol^{-1}, M_w/M_n of 1.04, and $mm/mr/rr$ of 0/10/90 after the 168 h of polymerization.

The polymerization mechanism was presumed based on an analogy with the mechanism of the strong Brønsted-acid-promoted Mukaiyama aldol reaction, as shown in Fig. 1 [111–113]. Five possible elemental reactions were considered as following: (a) the generation of the silicon Lewis acid (ASi) as the actual catalyst from the irreversible reaction between a strong Brønsted acid (AH) and the silyl enolate, (b) the reversible coordination of ASi to the monomer for the formation of an activated monomer (M*), (c and d) the initiation/propagation reaction between M* and the silyl enolate or the propagating polymer, and (e) the decomposition of ASi with protic impurities (Nu-H) accompanied by the regeneration of AH as a side reaction. Thus, the polymerization was considered to proceed through a similar mechanism to the conventional Lewis-acid-catalyzed GTP, though the generation and decomposition of ASi additionally occurred [88]. It has not been investigated whether the silyl groups of the propagating end and the catalyst exchange through the propagation reaction. Figure 2 depicts plausible structure of the reaction center on the propagation reaction for the formation of r diad and m diad. Highly selective formation of r diad in the polymerization of MMA was described by the fact that the structure on the left for the formation of r diad was considered more favorable

On the propagation reaction
r **diad formation**
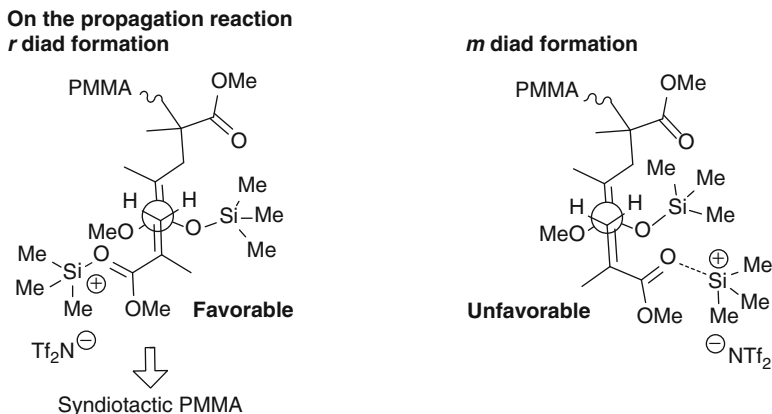
Fig. 2 Speculation of the syndiotactic control of the strong Brønsted acid-promoted GTP of MMA

because of the low steric repulsion between the propagating end and the MMA coordinated by Tf_2NSiMe_3.

Kakuchi et al. later investigated the GTP of MMA using the isolated Tf_2NSiMe_3 itself as the catalyst [114]. The polymerization in CH_2Cl_2 at 25 °C under the condition of $[MMA]_0/[^{Me}SKA]_0/[Tf_2NSiMe_3]_0 = 80/1/0.05$ and $[MMA]_0 = 2.0$ mol L^{-1} produced a PMMA with M_n of 8.6 kg mol^{-1} and M_w/M_n of 1.07 within 9 h. The initiation efficiency of the polymerization using Tf_2NSiMe_3 (94–100 %) improved from that using Tf_2NH (71–75 %). The kinetics of the polymerization using Tf_2NSiMe_3 also showed first-order relationship between polymerization time and monomer conversion. The M_n of the resulting PMMA linearly increased with increasing monomer conversion while retaining low M_w/M_n. The MALDI-TOF MS measurement proved that the product is PMMA-bearing terminal structure originated from ^{Me}SKA. The consumption of a silyl enolate can be avoided by the direct use of a silicon Lewis acid instead of a strong Brønsted acid. However, one must still be aware that contamination of protic impurities causes the decomposition of the silicon Lewis acid and the consumption of a silyl enolate by the regeneration of the silicon Lewis acid from the strong Brønsted acid.

Living polymerization of MA was achieved by the GTP using ^{iPr}SKA as the initiator and 2,3,4,5,6-pentafluorophenyl-1,1-bis(trifluoromethanesulfonyl)meth-ane ($Tf_2CHC_6F_5$) [115, 116] as the catalyst [117]. On analogy to the TTPB-promoted GTP of nBA, a silyl enolate with bulky silyl group was favorable for the polymerization. A PMA with an M_n of 108 kg mol^{-1} and an M_w/M_n of 1.07 was obtained from the polymerization in toluene at room temperature (23 °C ± 5 °C) under the condition of $[MA]_0/[^{iPr}SKA]_0/[Tf_2CHC_6F_5]_0 = 1000/1/0.02$ and $[MA]_0 = 1.0$ mol L^{-1} within 1 h of the polymerization time. Polymerization kinetics showed first-order relationship between monomer conversion and polymerization time. Unlike the polymerization of MMA, the stereoregularity of the resulting PMA was poor.

The Tf_2NH-promoted GTP of N,N-dimethylacrylamide (DMAA) initiated by (Z)-1-(dimethylamino)-1-trimethylsiloxyprop-1-ene ((Z)-DATP), an amino silyl enolate, proceeded in a living fashion, which is the first success for the controlled/living polymerization of acrylamide monomers in the chemistry of GTP [118]. The polymerization using ^{Me}SKA was uncontrolled and produced PDMAA with broad M_w/M_ns of 1.24–1.76 due to the slower initiation rate than the propagation rate. The analogous structure of (Z)-DATP to the propagating end of PDMAA was considered to increase the initiation rate, which led to the living nature of the polymerization. The Tf_2NH-promoted GTP of DMAA in CH_2Cl_2 was faster than that in toluene. The M_n of the resulting PDMAA was controlled in a range of 3.24–53.9 kg mol^{-1} while retaining narrow M_w/M_ns of 1.06–1.16. The MALDI-TOF MS analysis revealed that the resulting PDMAA had a terminal structure originated from (Z)-DATP initiator residue and desialylated propagating end, indicating that the Tf_2NH-catalyzed GTP of DMAA proceeded without any side reactions. Although the polymerization kinetics was originally regarded as first order of the monomer concentration [118], it was later revealed to be intermediate of zero order and first order by analytically deriving the polymerization rate equation and numerically analyzing the experimental polymerization rate [119]. The stereoregularity of the resulting PDMAA was moderately syndiotactic and controlled in a range of 56–73 % of r diad contents depending on the polymerization solvent and polymerization temperature. Only strong Brønsted acids, such as Tf_2NH and $Tf_2CHC_6F_5$, were effective for the GTP using (Z)-DATP; the polymerizations using other conventional catalysts, such as $TAS-HF_2$, tetra-n-butylammonium acetate (TBA-AcO), and ZnI_2, did not proceed or was uncontrolled.

Chen et al. have employed Brønsted acids, such as $H(Et_2O)_2[B(C_6F_5)_4]$, $H(Me_2NPh)[B(C_6F_5)_4]$, and (R)-3,3′-Bis[3,5-bis(trifluoromethyl)phenyl]-1,1binaphthyl-2,2′-disulfonimide (List's sulfonimide), for GTP [106, 107, 120]. Formation of silicon Lewis acids from the reaction of the Brønsted acids and ^{Me}SKA was carefully investigated by ^1H, ^{19}F, and ^{29}Si NMR measurements in CD_2Cl_2 [120]. The reaction of ^{Me}SKA and $H(Et_2O)_2[B(C_6F_5)_4]$ generated both trimethylsilyl cation coordinated by methyl isobutyrate and diethyl ether. On the other hand, the reaction of ^{Me}SKA with $H(Me_2NPh)[B(C_6F_5)_4]$ or the List's sulfonimide generated only trimethylsilyl cation coordinated by N,N-dimethylaniline or the sulfonimido group, which indicated coordinating nature of the nitrogen atom to the silylium cation. The GTP of MMA promoted by $H(Et_2O)_2[B(C_6F_5)_4]$ in CH_2Cl_2 at 25 °C under the conditions of $[MMA]_0 = 0.935$ mol L^{-1} and $[MMA]_0/[^{Me}SKA]_0/[H(Et_2O)_2[B(C_6F_5)_4]]_0 = 100/1/0.05$, 133/1/0.067, 200/1/0.10, 400/1/0.20, and 800/1/0.40 reached perfect monomer conversion within 3 h and produced PMMAs with M_ns of 11.3–74.7 kg mol^{-1}, M_w/M_ns of 1.07–1.12, and $mm/mr/rr$s of 2/26/72. Unlike the GTP of MMA promoted by Tf_2NH, the kinetics of the polymerization showed zero-order dependence on the monomer concentration, which was explained by the difference in coordinating nature of the counter anions, namely, Tf_2N^- and $B(C_6F_5)_4^-$ ($vide\ infra$). The polymerization rate was first order with respect to the concentration of both $H(Et_2O)_2[B(C_6F_5)_4]$ and ^{Me}SKA. The M_n of the resulting PMMA linearly increased with monomer conversion while keeping low M_w/M_n. The GTP of MMA promoted by $H(Me_2NPh)[B(C_6F_5)_4]$ in

CH$_2$Cl$_2$ at 25 °C under the condition of [MMA]$_0$/[^{Me}SKA]$_0$/[H(Me$_2$NPh)[B (C$_6$F$_5$)$_4$]]$_0$ = 200/1/0.10 reached only 97.6 % of monomer conversion after 15 h of polymerization, while the polymerization using H(Et$_2$O)$_2$[B(C$_6$F$_5$)$_4$] completed within 40 min under the similar polymerization condition. The GTP of MMA using the List's sulfonimide did not proceed due to exclusive coordination of the silylium cation to the sulfonamide as the counter anion. The result indicated that the presence of a nucleophilic counter anion or a nucleophilic compound inhibits the catalytic activity of the silicon Lewis acid. Chen et al. proposed that the polymerization mechanism for the GTP promoted by a strong Brønsted acid in a manner slightly differed from that shown in Fig. 1, in which the silicon Lewis acid was considered to always coordinate to a propagating polymer or a monomer as well as the mechanism shown in Scheme 10.

The controlled polymerization of DMAA, which has higher Lewis basicity than MMA, was also achieved by the GTP using ^{Me}SKA as the initiator and both H (Et$_2$O)$_2$[B(C$_6$F$_5$)$_4$] and List's sulfonimide as the precatalyst, which produced PDMAAs with M_ns of 30.2–102 kg mol^{-1} and M_w/M_ns of 1.09–1.13. The stereo-regularity of the resulting PDMAA was atactic ($mm/(mr + rr)$ = 38.5/61.5) in the latter polymerization even though the chiral catalyst was utilized. H(Et$_2$O)$_2$[B (C$_6$F$_5$)$_4$] was also effective for the polymerization of nBMA using ^{Me}SKA [120] as well as that of nBA and MMBL using ^{iBu}SKA [106, 120] to give corresponding polymers with narrow M_w/M_ns of 1.07–1.08. However, the polymerization rate of MMBL was four times slower than the polymerization using TTPB. Similarly, H (Et$_2$O)$_2$[B(C$_6$F$_5$)$_4$] was less effective than TTPB in the polymerization of MMA using diSKAs; the initiation efficiency was only 27 % [107].

4 Precise Synthesis of Polymer Architectures

4.1 End-Functionalized Polymers

Living/controlled polymerization methods have been utilized for the synthesis of end-functionalized polymers as precursors for intelligent materials and diverse polymer architectures, such as end-functionalized, block, star-shaped, dendritic, and cyclic polymers [121]. Synthesis of end-functionalized polymers has been attempted with GTP using both functional initiators [8, 69, 78, 122–126] and terminating agents [8, 127–129].

4.1.1 GTP Using Functional Initiators

Scheme 12 summarizes the functional initiators. SKA14 bearing a silylated hydroxyl group was used for the synthesis of hydroxyl end-functionalized polymers [8, 78]. SKA15 was used for the synthesis of 2,5-dihydroxyphenyl
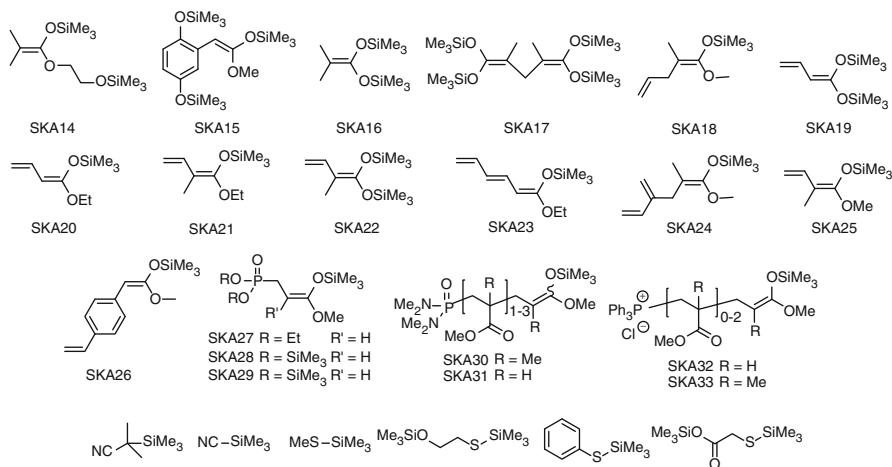
Scheme 12 Functional initiators used in the GTP

end-functionalized polymers, which were subsequently used for the polycondensation [126]. SKA16 and SKA17 were used for the synthesis of PMMA end functionalized with a carboxylic acid [4, 78]. For example, the polymerization of MMA using SKA17 produced PMMA end functionalized with a carboxylic acid with a M_n of 2.1 kg mol^{-1} and an M_w/M_n of 1.29. The polymerizations using SKA18-22 and SKA23-24 produced vinyl and dienyl end-functionalized polymers, respectively [69, 125]. The GTPs of MMA using SKA19 and SKA20 exclusively produced vinyl end-functionalized polymers, while the similar polymerizations using SKA21 and SKA22 produced 71–72 % of vinyl end-functionalized PMMA and 28–29 % of internal olefin end-functionalized polymers. Bandermann et al. later investigated the polymerization of MMA using other vinyl- and dienyl-functionalized initiators [124]. For example, The GTP using SKA25 produced vinyl end-functionalized PMMA with M_ns of 11.2–91.8 kg mol^{-1} and M_w/M_ns of 1.41–1.69. The polymerization of MMA using SKA26 produced 4-vinylphenyl end-functionalized PMMA with M_ns of 6.9–35.5 kg mol^{-1} and M_w/M_ns of 1.27–1.55. Silyl enolates bearing a phosphonate group (SKA27-31) were used to prepare phosphonate end-functionalized polymers. For instance, SKA27 and SKA29-30 were effective for the synthesis of narrowdispersed phosphonate end-functionalized PMMAs, though the M_n of the product when using SKA30 was 2–3 times higher than the calculated M_n. In contrast, the GTP of MMA using SKA28 and SKA31 was uncontrolled and produced PMMAs with broad M_w/M_ns. Shen et al. reported the GTP of MMA using triphenylphosphine and chlorotrimethylsilane [123]. In this case, trimethylsilyl chloride is the potential initiator and can add to a monomer to form a silyl enolate (SKA32-33) in accordance with the formation of a Wittig reagent. The triphenylmonoalkyl phosphonium cation is stable under the condition of GTP to produce a Wittig reagent end-functionalized polymer.

In addition, α-cyanosilyl compounds and silylated thiols were also applied for the GTP to develop stable initiator than silyl enolates, which eventually produced cyano end-functionalized polymers and sulfide end-functionalized polymers. Sogah et al. carried out the polymerization of MMA using α-trimethylsilylisobutyronitrile and TAS-HF$_2$ in THF, which resulted in an uncontrolled polymerization to produce a PMMA with a M_n of 47.5 kg mol^{-1} and an M_w/M_n of 3.96 [8]. Trimethylsilyl cyanide was also used for the polymerization of MMA in acetonitrile catalyzed by tetraethylammonium cyanide (TEACN) to produce a PMMA with a M_n of 6.91 kg mol^{-1} and an M_w/M_n of 1.49 [8]. Some of the silylated thiol initiators were designed to have a protected functional group and used for the synthesis of hydroxyl or carboxylic acid end-functionalized polymers [122]. Webster et al. carried out the polymerization of MMA using methyl trimethylsilyl sulfide and that of EA using phenyl trimethylsilyl sulfide catalyzed by TEACN in aceto-nitrile, which produced a PMMA with an M_n of 11.8 kg mol^{-1} and an M_w/M_n of 1.64 and a PEA with an M_n of 2.27 kg mol^{-1} and an M_w/M_n of 1.83 [8]. Reetz et al. carried out the polymerization of MA and nBA using four silylated thiol initiators [122]. The polymerization of nBA using methyl trimethylsilyl sulfide or 2-(trimethylsiloxy)ethyl trimethylsilyl sulfide catalyzed by TASHF$_2$ in THF or acetonitrile was uncontrolled and produced PnBAs with M_ns of 1.1–1.5 kg mol^{-1} and M_w/M_ns of 1.44–2.0. Lewis acids, such as ZnI$_2$ and chlorodiisobutylaluminum, were effective for the polymerization of MA and nBA using trimethylsilyl methyl sulfide and 2-(trimethylsiloxy)ethyl trimethylsilyl sulfide in toluene or CH$_2$Cl$_2$ to produce corresponding polymers with M_ns of 6.9–14.2 and M_w/M_ns of 1.08–1.16.

4.1.2 GTP Using Terminating Agents

The end-functionalization using terminating agents is based on the termination reaction of the silyl enolate in the propagating polymer. Scheme 13 summarizes the terminating agents employed so far. Sogah et al. synthesized bromine end-functionalized PMMA by the termination reaction of a living PMMA using molecular bromine or N-bromosuccinimide [78]. Difunctional alkylating and acyl-ating agents were used for the coupling reaction of two propagating polymers. Sogah et al. synthesized α,ω-end-functionalized polymers by the termination reac-tion of α-end-functionalized polymers synthesized using functional initiators, such as SKA14 and SKA15, and difunctional alkylating and acylating agents, which required equimolar fluoride anion relative to the propagating polymer [8, 78]. 4-Vinylphenyl end-functionalized PMMA was synthesized in the same
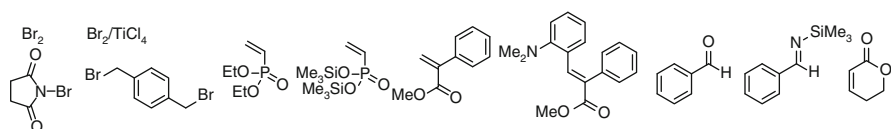
Scheme 13 Terminating agents used in the GTP

manner using 4-(bromomethyl)styrene [130, 131]. These reactions required equimolar fluoride anion [8]. The mixture of molecular bromine and titanium (IV) chloride was used for the direct coupling reaction of two living PMMAs based on the bromination of the living PMMA and the coupling reaction between the PMMA end functionalized with tertiary alkyl bromide and the PMMA bearing a silyl enolate, which was also used for the synthesis of α,ω-dihydroxyl and α,-ω-carboxylic acid PMMA [78]. Diethyl vinylphosphonate and bis(trimethylsilyl) vinylphosphonate were used as a terminating agent for the synthesis of phosphonate end-functionalized PMMAs synthesized using TAS-HF$_2$ in THF [127]. The phosphonic acid end-functionalized PMMA was obtained by treating the diethyl phosphonate end-functionalized PMMA with bromotrimethylsilane and the bis (trimethylsilyl) phosphonate end-functionalized PMMA with aqueous THF in the presence of catalytic amount of p-toluenesulfonic acid. Quirk et al. reported end-functionalization reaction using a monomer with high ceiling temperature, such as methyl 2-phenylmethacrylate and methyl (E)-3-(2-(dimethylamino)phe-nyl)-2-phenylacrylate [128]. The Mukaiyama-Michael reaction as the termination reaction using both of the terminating agent quantitatively proceeded in the presence of TAS-HF$_2$ to give corresponding end-functionalized PMMAs. The latter terminating agent produced the dimethylamino end-functionalized PMMA. Sivaram et al. performed the termination reaction of the PMMA synthesized using TBABB by treating with benzaldehyde, N-trimethylsilylbenzylideneimine, and 5,6-dihydro-2H-pyran-2-one to synthesize hydroxyl, amino, and δ-valerolactone end-functionalized PMMA, though the number-average degree of functionalization was in the range of 0.70–0.85 [129]. The termination reaction using N-trimethylsilylbenzylideneimine was carried out with additional ZnI$_2$ as a catalyst, which is only one method to synthesize primary amine end-functionalized polymer with GTP method.

4.2 Block Copolymers

Before the emergence of LRPs, conventional GTP was a universally used means to prepare block copolymers consisting of polymethacrylate and polyacrylate segments due to the living nature of the polymerization. The syntheses of block copolymers by GTP can be readily achieved by a sequential addition of monomer. For instance, an AB-type diblock copolymer with the simplest structure can be prepared by the following procedures: the synthesis of the first block possessing a living chain end with a quantitative consumption of the first monomer and the addition and polymerization of a second monomer. Similarly, a multiblock copolymer like ABC type can also be easily prepared by this method. In addition to AB- and ABC-type block copolymers, the syntheses of ABA-type block copolymers have been also reported by using difunctional initiators. The block copolymers consisting of similar sort of monomer units, such as two different alkyl methacrylates, generally have controlled molar masses (up to 204 kg mol^{-1}) and dispersities

Table 3 Ranges of M_n and M_w/M_n for star-shaped poly(meth)acrylates synthesized by GTP

Star-shaped polymer	SKA	Catalyst	Arm number	M_n(expt) (kg mol^{-1})	M_w/M_n
PEA[a]	SKA34	$(i\text{-}Bu_2Al)_2O$	3	2.19	1.39
	SKA35	$(i\text{-}Bu_2Al)_2O$	4	2.40	1.24
PMMA[b]	SKA36	TBA-OAc	4	6.3–50.9	1.21–1.30
P(M14)[b]	SKA37	$t\text{-}Bu\text{-}P_4$	3	11.1–41.6	1.09–1.10
PMMA[b]	SKA38	$t\text{-}Bu\text{-}P_4$	3	3.9–132.0[c]	1.07–1.14
PMMA[b]	SKA39	$t\text{-}Bu\text{-}P_4$	4	5.5–130.3[c]	1.07–1.17
P(M18)[b]	SKA39	$t\text{-}Bu\text{-}P_4$	4	13.6–21.2[c]	1.11–1.16
P(M10)[b]	SKA39	$t\text{-}Bu\text{-}P_4$	4	15.5–23.3[c]	1.10–1.16
PSMA[b]	SKA39	$t\text{-}Bu\text{-}P_4$	4	34.5–65.2[c]	1.06–1.08
PMMA[b]	SKA40	$t\text{-}Bu\text{-}P_4$	6	7.5–131.6[c]	1.06–1.15
PMMA[a]	SKA38	Tf_2NSiMe_3	3	12.9[c]	1.04
PMMA[a]	SKA39	Tf_2NSiMe_3	4	12.9[c]	1.04
PMMA[a]	SKA40	Tf_2NSiMe_3	6	13.4[c]	1.04

[a]The polymerizations were carried out in CH_2Cl_2
[b]The polymerizations were carried out in THF
[c]The molar masses are absolute molar masses determined by multi-angle laser light scattering (MALS) in THF

(lower than 1.64) by conventional GTP [1, 8, 30, 36, 40, 42, 45, 46, 61, 76, 132, 133]. On the other hand, the synthesis of (polymethacrylate-*b*-polyacrylate)-type block copolymers is proven to be difficult due to the big difference in the reactivities of methacrylate and acrylate as well as the lack of a suitable catalyst for both monomers [1, 76, 134–136]. Therefore, the conventional GTP has been actually unsuitable to prepare block copolymers consisting of different polymer segments. It is restricted to synthesize either all acrylic or all methacrylic block copolymers.

Fortunately, the organocatalytic GTP has realized the block copolymerization of structurally different monomers in some extent. As described before, NHCs are known to catalyze the GTP of (meth)acrylates, DMAA, and MAN under similar polymerization conditions, which has opened new doors for the synthesis of block copolymers consisting of different sort of polymer segments. The sequential block copolymerization of MMA and *t*BA was first achieved via the GTPs using NHC-1 by Waymouth et al. and using NHC-2 by Taton and Gnanou et al. [19, 20]. Taton and Gnanou et al. further succeeded in the synthesis of various di- and triblock copolymers by the sequential GTP of MMA, M10, *n*BA, *t*BA, M38, DMAA, and MAN catalyzed by NHC-2 or NHC-3 regardless of the addition order of monomers, as summarized in Table 3, though some of them had rather broad M_w/M_n [21, 24]. Notably, the synthesized PMMA-*b*-P*t*BA-*b*-PDMAA might have partially gradient structure because the monomer conversion in the second polymerization of *t*BA and the third polymerization of DMAA were not quantitative. They explained that the feature of the GTP catalyzed by NHC-2 or NHC-3, which plausibly proceeds with the associative mechanism, realized the synthesis of various block copolymers by the sequential polymerization. The GTP catalyzed by

TTMPP was also effective for the block copolymerization of MMA and tBA, which produced PMMA-b-PtBA with an M_n of 22.0 kg mol^{-1} and an M_w/M_n of 1.19 with quantitative conversions of monomers on both steps [29].

In contrast to the success in the Lewis-base-catalyzed GTP, the block copolymerization with the Lewis-acid-catalyzed GTP is still limited to the synthesis of polymethacrylate-b-polyacrylate and polymethacrylate-b-poly(-α-methylenebutyrolactone) because of the difference in the reactivity of monomers. Chen et al. have investigated the block copolymerization by the GTP promoted by triphenylmethyl salts and strong Brønsted acids. Sequential block copolymerization of MMA and nBA was attempted by the GTP using TTPB starting from both MMA and nBA [100]. The former polymerization produced a PMMA-b-PnBA with an M_n of 45 kg mol^{-1} and an M_w/M_n of 1.1 both in CH$_2$Cl$_2$ and toluene, while the latter polymerization only produced homo PnBA. Interestingly, statistical copolymerization of MMA and nBA also turned out to be a selective polymerization of nBA to produce only homo PnBA. There are two possible reasons: (1) the nucleophilicity of the propagating end derived from nBA is insufficient to attack MMA; (2) the silyl cation does not coordinate to the carbonyl group of MMA due to steric hindrance. More future work is needed for this interesting issue. Sequential GTP of MMA and MBL as well as MMA and MMBL using TTPB in CH$_2$Cl$_2$ successfully produced PMMA-b-PMBL and PMMA-b-PMMBL, even though the solubility of the PMBL segment in CH$_2$Cl$_2$ is low [106]. These block copolymerizations did not proceed when the polymerization was started from MBL or MMBL probably due to the similar reasons in the block copolymerization of nBA and MMA (*vide supra*). The block copolymerization of MMBL and MBL successfully produced well-defined diblock copolymer, PMMBL-b-PMBL ($M_n = 117$ kg mol^{-1} and $M_w/M_n = 1.02$), when the polymerization was initiated from MMBL. Unlike the statistical copolymerization of MMA and nBA, the statistical copolymerization of MBL and MMBL proceeded to give statistical copolymer, PMMBL-co-PMBL ($M_n = 123$ kg mol^{-1} and $M_w/M_n = 1.01$). The GTP using $^{i\text{Bu}}$SKA and H(Et$_2$O)$_2$[B(C$_6$F$_5$)$_4$] also allowed the block copolymerization of MMA and nBA in toluene in a controlled fashion to produce a PMMA-b-PnBA with an M_n of 42.5 kg mol^{-1} and an M_w/M_n of 1.08 [120].

4.3 Star-Shaped Polymers

A propagating end of polymer in GTP is stable and electronically neutral, which is advantageous for core-first synthesis of a star-shaped polymer in comparison with other living/controlled polymerizations. Unlike the LRPs, GTP is free from intermolecular termination reaction involved by two propagating polymers. In addition, the high solubility of multivalent initiator/propagating polymer in solvents assists the homogeneous growth of arm polymers, which is hard to achieve in anionic/cationic polymerizations. Several attempts to synthesize star-shaped polymers using the GTP have been revealed by several groups so far, as summarized in

Table 4 Block copolymers synthesized by sequential GTP using organocatalysts

Catalyst	Initiator	Solvent	Block copolymer	M_n (expt.)[a] (kg mol^{-1})	M_w/M_n[a]	Ref.
NHC-1	[Me]SKA	THF	PMMA-b-PtBA	11.8	1.14	[20]
NHC-2	[Me]SKA	Toluene	PMMA-b-PtBA	21.9	1.3	[19]
		THF	PMMA-b-PtBA-b-PMMA	12.6	1.4	[19]
		THF	PMMA-b-P(M38)	11.0[b]	1.3	[24]
		THF	PMMA-b-P(M10)	22.0[b]	1.1	[24]
		THF	PMMA-b-PDMAA	16.9[b]	1.09	[24]
		THF	PMMA-b-PMAN	71.0[b]	1.18	[24]
		THF	PMMA-b-PtBA-b-PDMAA	5.3[b]	1.09	[24]
		THF	P(M10)-b-PDMAA	13.0[b]	1.29	[24]
		THF	P(M10)-b-P(M38)	4.8[b]	1.21	[24]
		THF	PtBA-b-PMMA	12.0[b]	1.27	[24]
		THF	PtBA-b-PDMAA	21.3[b]	1.2	[24]
		THF	PtBA-b-P(M10)	36.7[b]	1.23	[24]
		THF	PDMAA-b-P(M10)	17.6[b]	1.4	[24]
		THF	PDMAA-b-PMMA	23.9[b]	1.3	[24]
NHC-3	[Me]SKA	THF	PMMA-b-PnBA	16.0	1.5	[21]
		Toluene	PMMA-b-PnBA	18.2	1.6	[21]
		THF	PnBA-b-PMMA	10.5[b]	1.4	[24]
		THF	PMMA-b-PnBA-b-PMMA	130	1.6	[21]
TTMPP	[Me]SKA	THF	PMMA-b-PtBA	22.0	1.19	[29]
TTPB	[iBu]SKA	CH$_2$Cl$_2$	PMMA-b-PnBA	44.8	1.09	[100]
		Toluene	PMMA-b-PnBA	45.3	1.13	[100]
		CH$_2$Cl$_2$	PMMA-b-PMBL	68.4[c]	1.01[c]	[106]
		CH$_2$Cl$_2$	PMMA-b-PMMBL	68.1[c]	1.03[c]	[106]
		CH$_2$Cl$_2$	PMMBL-b-PMBL	117[c]	1.02[c]	[106]
H(Et$_2$O)$_2$ [B(C$_6$F$_5$)$_4$]	[iBu]SKA	Toluene	PMMA-b-PnBA	42.5	1.08	[120]

[a]Determined with SEC measurements

[b]Determined by NMR measurements

[c]Determined by multi-angle laser light scattering (MALS)

Table 4. Webster and Sogah first reported the core-first synthesis of three- and four-armed star-shaped PEA through an in situ GTP using a conventional Lewis acid catalyst of (i-Bu$_2$Al)$_2$O. They first synthesized tri- and tetra-functional initiators (SKA34-35) by the Michael addition of trimethylolpropane triacrylate and pentaerythritol tetraacrylate with [Me]SKA, respectively. After a consequent addition of EA to the initiator solution, the (i-Bu$_2$Al)$_2$O-catalyzed GTP of EA proceeded with quantitative conversion to produce three- and four-armed star-shaped PEAs without cross-linking. The obtained star-shaped PEAs however had only low M_ns ($\leq$2.4 kg mol^{-1}) and broad dispersities above 1.24 [8]. Wnek et al. then reported the

core-first synthesis of the four-armed star-shaped PMMAs with M_n of 6.3–50.9 kg mol^{-1} and M_w/M_n of 1.21–1.30 using SKA36 and a Lewis base catalyst of TBAOAc [137]. Patrickios et al. reported the arm-first synthesis of various star-shaped poly(methacrylate)s or copolymers with undefined arm number using monofunctional monomers and bifunctional linking agents like M29-31 [44, 48–50, 53]. Most recently, our group first achieved the core-first synthesis of star-shaped polymers by organocatalytic GTP using star-shaped initiators with multiple SKA groups (SKA37-40) and either a Lewis base organocatalyst (t-Bu-P$_4$) or a Lewis acid organocatalyst (Tf$_2$NSiMe$_3$) [26–28, 114]. The t-Bu-P$_4$-catalyzed GTP favored in producing star-shaped polymers with high molar mass, while Tf$_2$NSiMe$_3$-catalyzed GTP was advantageous in producing star-shaped polymers with high stereoregularity. The t-Bu-P$_4$-catalyzed GTP of MMA using the SKA38-40 homogeneously proceeded to give the well-defined three-, four-, and six-armed star-shaped PMMAs with M_n of 3.6–118.0 kg mol^{-1} and M_w/M_n of 1.06–1.17. The homogeneous growth of each arm polymer was proven by cleavage experiments of the core linkage. It is noteworthy that the star-shaped PMMAs with definite arm number, high M_n, and narrow M_w/M_n were obtained with easy procedures under moderate conditions, which was absolutely different from the core-first synthesis of star-shaped PMMAs by LRPs and ionic polymerizations. In addition to MMA, t-Bu-P$_4$-catalyzed GTP was also suitable for other methacrylates, such as M10, M14, M18, and SMA. The t-Bu-P$_4$-catalyzed GTPs of M10, M18, and SMA using SKA39 in THF quantitatively produced corresponding four-armed star-shaped polymers with predetermined M_ns and M_w/M_ns narrower than 1.16 within 1 h. The polymerization of M14 using SKA37 produced three-armed polymers with M_ns of 11.1–41.6 kg mol^{-1} and M_w/M_ns of ~1.10 within 30 min. On the other hand, Tf$_2$NSiMe$_3$-catalyzed GTP of MMA using SKA38-40 could produce well-defined syndiotactic-rich star-shaped PMMAs (rr up to 89 %). The star-shaped SKAs are shown in Scheme 14.
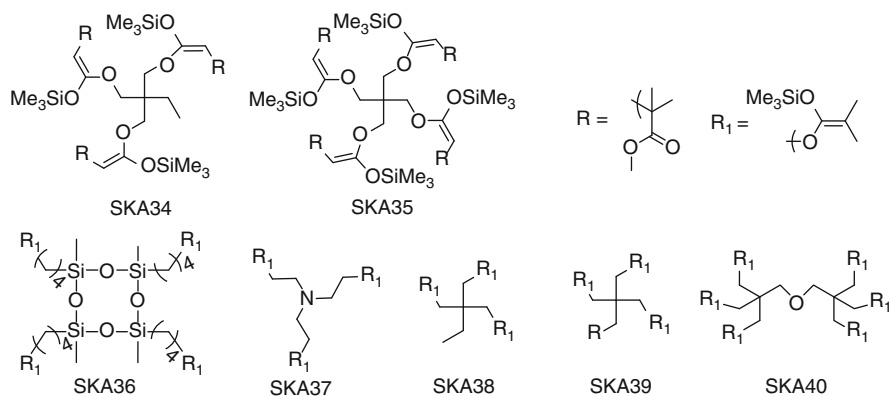
Scheme 14 Structures of star-shaped initiators used in GTP (SKA34-40)

4.4 Hyperbranched Polymers

The one-pot synthesis of hyperbranched polymethacrylates has been attempted by a creative design of an inimer composed of a methacrylate (A) and a SKA (B). B in a polymer is a latent propagating site. It becomes active (B*) when activated by a Lewis base catalyst. B* then intermolecularly reacts with A in another inimer to produce an adduct consisting of a reacted A (a), a reacted B (b), an inner B*, and an outer B, as shown in Scheme 15. After the first addition of an inimer, the inner B* may be deactivated due to the detachment of the catalyst in the associate mechanism or the silylation of the active enolate anion in the dissociate mechanism. Therefore, if the deactivation rate of the inner B* is much slower than that of its propagation, the polymerization will occur predominantly at the inner B*. A perfect hyperbranched polymethacrylate can be ideally obtained when the inner B*s are completely deactivated before propagation, and the reaction rates of the inner and outer B*s with the methacryloyl group are the same. Since propagations from the inner B* and the outer B* generate methyl- and dimethyl-substituted quaternary carbons (C_1 and C_2, respectively), the degree of branching (DB) can be estimated by ^{13}C NMR analyses.

Both Sakamoto et al. and Müller et al. reported the self-condensing GTP of 2-(2-methyl-1-triethylsiloxy-1-propenyloxy)ethyl methacrylate (SKA41). The self-condensing GTP of SKA41 using Lewis base catalyst of TASMe$_3$SiF$_2$ or TBABB by Sakamoto et al. produced hyperbranched polymers with M_ns of 5.7–11.0 kg mol^{-1} and M_w/M_ns of 1.10–1.70 within 5 min. In their studies, the extent of branching was evaluated by the ratio of C_1 and C_2 (C_1/C_2). A perfect hyperbranched polymethacrylate has a C_1/C_2 value of 1. The higher the C_1/C_2 value is, the more defective the hyperbranched polymethacrylate is. It has been
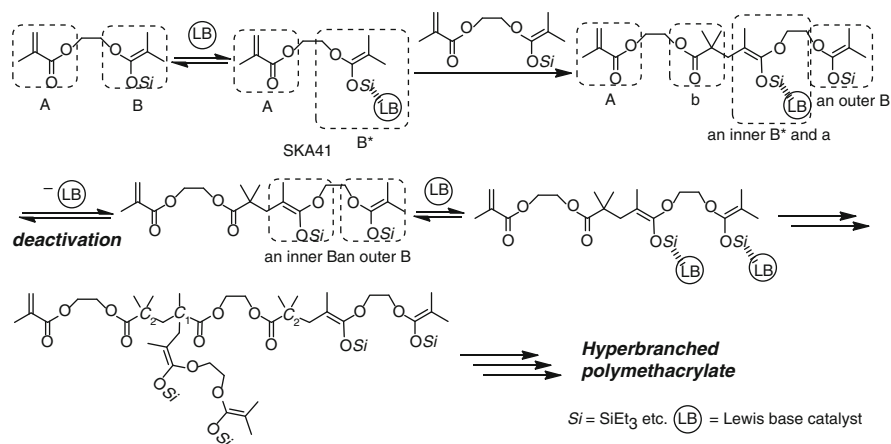
Scheme 15 One-pot synthesis of hyperbranched polymethacrylate by GTP catalyzed by a Lewis base catalyst

found that a less active catalyst tends to decrease the C_1/C_2 value because the deactivation of the inner active sites seemed to much easily take place [138]. The self-condensing GTP of SKA41 by Müller et al. produced hyperbranched polymethacrylates with an M_w up to 38.0 kg mol^{-1} at a dispersity of ca. 3.6. The resulting hyperbranched polymethacrylates in their study had a maximum DB of ≈ 0.4 on the basis of a standard calculation. In addition, they also reported the self-condensing group transfer copolymerization of SKA41 and MMA to afford highly branched polymethacrylates, the M_w of which could reach a maximum of 240 kg mol^{-1} at a dispersity of ca. 3.0. When MMA was replaced by tBMA, the self-condensing group transfer copolymerization of SKA41 and tBMA was also achieved, from which a water-soluble highly branched poly(methacrylic acid) was obtained by acid-catalyzed hydrolysis of the $tert$-butyl groups [139–143].

5 Conclusion and Outlook

The field of GTP is divided into two branches, i.e., the conventional and organocatalytic GTPs, on the basis of the employed catalysts. The conventional GTP catalyzed by traditional nucleophilic anions or metallic Lewis acids has been extensively studied, and their polymerization behavior and mechanisms were well understood though many debates have been lasting so far. On the contrary, the organocatalytic GTP has been flourishing since 2007. It is more advantageous than the conventional one and has made great progress in many aspects such as catalytic activity, applicable monomers, molar mass control, and control of polymer structures. In short, much more work should be conducted in this field. The future development in GTP is expected to achieve the following goals: (1) to realize controlled/living polymerizations of other vinyl monomers, such as α- or β-substituted acrylates, α- or β-substituted acrylamides, acrylonitrile, and vinylphosphonate; (2) to further develop chemically stable initiators as to greatly enhance the practical application of GTP because silyl enolates used nowadays are rather expensive and unstable; (3) to achieve new organocatalytic aldol GTP, which should further expand the scope of applicable monomer; (4) to design and synthesize polymers with functional groups and/or complicated architectures by GTP or by the combination of GTP and other controlled/living polymerization procedures; (5) to prepare stereospecific polymers, and so on. In conclusion, the GTP method still has much potential to bring about further development in polymer chemistry. The authors firmly believe that the aforementioned introduction would lead the readers to a comprehensive understanding on the methodology of GTP.

Abbreviations

AN	Acrylonitrile
*n*BA	*n*-Butyl acrylate
*t*BA	*t*-Butyl acrylate
*n*BMA	*n*-Butyl methacrylate
*t*BMA	*t*-Butyl methacrylate
t-Bu-P$_4$	1-*tert*-Butyl-4,4,4-tris(dimethylamino)-2,2-bis[tris(dimethylamino)-phosphoranylidenamino]-2Λ^5,4Λ^5-catenadi(phosphazene)
(*Z*)-DATP	(*Z*)-1-(Dimethylamino)-1-trimethylsiloxy-1-propene
DEAA	*N*,*N*-Diethyl acrylamide
*n*DMA	*n*-Dodecyl methacrylate
DMAA	*N*,*N*-Dimethyl acrylamide
EA	Ethyl acrylate
EMA	Ethyl methacrylate
LMA	Lauryl methacrylate
LRP	Living radical polymerization
MA	Methyl acrylate
MAN	Methacrylonitrile
MBL	α-Methylenebutyrolactone
MMA	Methyl methacrylate
MMBL	γ-Methyl-α-methylenebutyrolactone
M_n	Number average molar mass
M_w	Weight average molar mass
M_w/M_n	Dispersity
NHC	*N*-heterocyclic carbene
NHC-1	1,3-Diisopropyl-4,5-dimethylimidazol-2-ylidene
NHC-2	1,3-Diisopropylimidazol-2-ylidene
NHC-3	1,3-Di-*tert*-butylimidazol-2-ylidene
*n*OMA	*n*-Octyl methacrylate
^{Me}SKA	1-Methoxy-1-(trimethylsiloxy)-2-methylprop-1-ene
^{Et}SKA	1-Methoxy-1-(triethylsiloxy)-2-methylprop-1-ene
^{iBu}SKA	1-Methoxy-1-[tri(*iso*-butyl)siloxy]-2-methylprop-1-ene
^{iPr}SKA	1-Methoxy-1-[tri(*iso*-propyl)siloxy]-2-methylprop-1-ene
^{nPr}SKA	1-Methoxy-1-[tri(*n*-propyl)siloxy]-2-methylprop-1-ene
^{Ph}SKA	1-Methoxy-1-(triphenylsiloxy)-1-methylprop-1-ene
^{TMS}SKA	1-Methoxy-1-[tri(trimethylsilyl)siloxy]-2-methylprop-1-ene
SKA	Silyl ketene acetal
SMA	Stearyl methacrylate
TAS	Tris(dialkylamino)sulfonium
TBA	Tetra-*n*-butylammonium
TBABA	Tetra-*n*-butylammonium biacetate
TBABB	Tetra-*n*-butylammonium bibenzoate
TBAF	Tetra-*n*-butylammonium fluoride

Tf$_2$CHC$_6$F$_5$	2,3,4,5,6-Pentafluorophenyl-1,1-bis(trifluoromethanesulfonyl) methane
Tf$_2$NH	Trifluoromethanesulfonimide
TiBP	2,8,9-Triisobutyl-2,5,8,9-tetraaza-1-phosphabicyclo[3.3.3]undecane
TTMPP	Tris(2,4,6-trimethoxyphenyl)phosphine
TTPB	Triphenylmethyl tetrakis(pentafluorophenyl)borate

References

1. Webster OW, Hertler WR, Sogah DY, Farnham WB, RajanBabu TV (1983) Group-transfer polymerization. 1. A new concept for addition polymerization with organosilicon initiators. J Am Chem Soc 105:5706–5708
2. Maugh TH (1983) New way to catalyze polymerization: group transfer polymerization gives excellent control of molecular weight of acrylic polymers, allows introduction of functional groups. Science 222:39
3. Mukaiyama T (2004) Explorations into new reaction chemistry. Angew Chem Int Ed 43:5590–5614
4. Brittain WJ (1992) A review of group-transfer polymerization. Rubber Chem Technol 65:580–600
5. Hadjichristidis N, Pispas S, Floudas G (eds) (2003) Block copolymers: synthetic strategies, physical properties, and applications. Wiley, New York, pp 65–79
6. Schubert W, Bandermann F (1989) Group-transfer polymerization of methyl acrylate in acetonitrile. Makromol Chem 190:2161–2171
7. Schubert W, Sitz HD, Bandermann F (1989) Group-transfer polymerization of methyl methacrylate and methyl acrylate in tetrahydrofuran with tris(piperidino)sulfonium bifluoride as catalyst. Makromol Chem 190:2193–2201
8. Sogah DY, Hertler WR, Webster OW, Cohen GM (1987) Group transfer polymerization – polymerization of acrylic monomers. Macromolecules 20:1473–1488
9. Schubert W, Bandermann F (1989) Group transfer polymerization of methyl acrylate in tetrahydrofuran with tetrabutylammonium fluoride trihydrate and tetrabutylammonium cyanide as catalysts. Makromol Chem 190:2721–2726
10. Hellstern AM, DeSimone JM, McGrath JE (1988) Fundamental investigations of the group-transfer polymerization of various alkyl methacrylates using tetrabutylammonium benzoate as the catalyst. Polym Prepr (Am Chem Soc Div Polym Chem) 29:342–344
11. Dicker IB, Cohen GM, Farnham WB, Hertler WR, Laganis ED, Sogah DY (1990) Oxyanions catalyze group-transfer polymerization to give living polymers. Macromolecules 23:4034–4041
12. Patrickios CS, Hertler WR, Abbott NL, Hatton TA (1994) Diblock, ABC triblock, and random methacrylic polyampholytes: synthesis by group transfer polymerization and solution behavior. Macromolecules 27:930–937
13. Quick RP, Kim JS (1995) Mechanistic aspects of silicon-mediated polymerization (group transfer polymerization) of methyl methacrylate with ester enolate anions as nucleophilic catalysts. J Phy Org Chem 8:242–248
14. Martin DT, Bywater S (1992) Group transfer initiated polymerization of methyl methacrylate catalyzed by [((C$_6$H$_5$)$_3$P)$_2$N]$^+$HF$_2^-$. Makromol Chem 193:1011–1019

15. Miller J, Jenkins AD, Tsartolia E, Walton DRM, Stejskal J, Kratochvil P (1988) The participation of crown ethers in the initiation of group-transfer polymerization. Polym Bull 20:247–248

16. Brittain WJ (1988) Kinetics of the anion-catalyzed Michael reaction of silyl ketene acetals. Initiation and propagation steps of group transfer polymerization. J Am Chem Soc 110:7440–7444

17. Hertler WR (1987) Chain transfer in group-transfer polymerization. Macromolecules 20:2976–2982

18. Scholten MD, Hedrick JL, Waymouth RM (2007) Group transfer polymerization of acrylates and methacrylates using N-heterocyclic carbene catalysts. Polym Prepr (Am Chem Soc Div Polym Chem) 48:167–168

19. Raynaud J, Ciolino A, Baceiredo A, Destarac M, Bonnette F, Kato T, Gnanou Y, Taton D (2008) Harnessing the potential of N-heterocyclic carbenes for the rejuvenation of group-transfer polymerization of (meth)acrylics. Angew Chem Int Ed 47:5390–5393

20. Scholten MD, Hedrick JL, Waymouth RM (2008) Group transfer polymerization of acrylates catalyzed by N-heterocyclic carbenes. Macromolecules 41:7399–7404

21. Raynaud J, Gnanou Y, Taton D (2009) Group transfer polymerization of (meth)acrylic monomers catalyzed by N-heterocyclic carbenes and synthesis of all acrylic block copolymers: evidence for an associative mechanism. Macromolecules 42:5996–6005

22. Raynaud J, Gnanou Y, Taton D (2009) N-heterocyclic carbene-catalyzed group transfer polymerization of (meth)acrylic-based monomers. PMSE Prepr 101:1771–1772

23. Raynaud J, Liu N, Gnanou Y, Taton D (2010) Expanding the scope of group transfer polymerization using N-heterocyclic carbenes as catalysts: application to miscellaneous (meth)acrylic monomers and kinetic investigations. Macromolecules 43:8853–8861

24. Raynaud J, Liu N, Fèvre M, Gnanou Y, Taton D (2011) No matter the order of monomer addition for the synthesis of well-defined block copolymers by sequential group transfer polymerization using N-heterocyclic carbenes as catalysts. Polym Chem 2:1706–1712

25. Kakuchi T, Chen Y, Kitakado J, Mori K, Fuchise K, Satoh T (2011) Organic superbase as an efficient catalyst for group transfer polymerization of methyl methacrylate. Macromolecules 44:4641–4647

26. Chen Y, Fuchise K, Narumi A, Kawaguchi S, Satoh T, Kakuchi T (2011) Core-first synthesis of three-, four-, and six-armed star-shaped poly(methyl methacrylate)s by group transfer polymerization using phosphazene base. Macromolecules 44:9091–9098

27. Hsu J-C, Chen Y, Kakuchi T, Chen W-C (2011) Synthesis of linear and star-shaped poly [4-(diphenylamino)benzyl methacrylate]s by group transfer polymerization and their electrical memory device applications. Macromolecules 44:5168–5177

28. Chen Y, Satoh T, Kakuchi T (2012) Precise synthesis of star-shaped poly(methyl methacrylate)s by t-Bu-P$_4$-catalyzed group transfer polymerization. Polym Prepr (Am Chem Soc Div Polym Chem) 53:107–108

29. Fevre M, Vignolle J, Heroguez V, Taton D (2012) Tris(2,4,6-trimethoxyphenyl)phosphine (TTMPP) as potent organocatalyst for group transfer polymerization of alkyl (meth)acrylates. Macromolecules 45:7711–7718

30. Augenstein M, Müeller MA (1990) Gradient high-performance liquid chromatography of polymers. 2. Characterization of block copolymers of decyl and methyl methacrylate synthesized via group transfer polymerization. Makromol Chem 191:2151–2172

31. Catagil H, Jenkins AD (1991) "Group-transfer" copolymerization. Eur Polym J 27:651–652

32. Çatalgil-Giz H, Uyanik N, Erbil C (1992) Statistical group transfer copolymerization. monomer reactivity ratios for allyl methacrylate and n-butyl methacrylate. Polymer 33:655–656

33. Vamvakaki M, Billingham NC, Armes SP (1998) Synthesis of novel block and statistical methacrylate-based ionomers containing acidic, basic or betaine residues. Polymer 39:2331–2337

34. Choi WJ, Lim KT, Kwon SK, Choi SK (1993) Synthesis and characterization of ABA triblock copolymers of 2-hydroxyethyl methacrylate and *n*-butyl methacrylate by group transfer polymerization. Polym Bull 30:401–406

35. Kim YB, Choi WJ, Choi BS, Choi SK (1991) Cyclopolymerization of 2,6-dicarbomethoxy-1,6-heptadiene by group-transfer polymerization. Macromolecules 24:5006–5008

36. Lowe AB, Billingham NC, Armes SP (1999) Synthesis and properties of low-polydispersity poly(sulfopropylbetaine)s and their block copolymers. Macromolecules 32:2141–2148

37. Purcell A, Armes SP, Billingham NC (1997) ABA triblock copolymers via group transfer polymerization. Polym Prepr (Am Chem Soc Div Polym Chem) 38:502–503

38. Doherty MA, Müller AHE (1989) Kinetics of group transfer polymerization of *tert*-butyl methacrylate in tetrahydrofuran. Makromol Chem 190:527–539

39. Choi WJ, Kim YB, Kwon SK, Lim KT, Choi SK (1992) Synthesis, characterization, and modification of poly(*tert*-butyl methacrylate-b-alkyl methacrylate-b-*tert*-butyl methacrylate) by group-transfer polymerization. J Polym Sci Part A Polym Chem 30:2143–2148

40. Gabor AH, Ober CK (1996) Group-transfer polymerization of *tert*-butyl methacrylate and [3-(methacryloxy)propyl]pentamethyldisiloxane: synthesis and characterization of homopolymers and random and block copolymers. Chem Mater 8:2272–2281

41. Bannerjee KG, Hogen-Esch TE (1993) Stereochemistry of polymerization of triphenylmethyl and diphenylmethyl methacrylate under group-transfer conditions. Macromolecules 26:926–932

42. Hefft M, Springer J (1990) Liquid-crystalline AB block and graft copolymers via group-transfer polymerization. Makromol Chem Rapid Commun 11:397–401

43. Kreuder W, Webster OW (1986) Liquid-crystalline polymethacrylates by group-transfer polymerization. Makromol Chem Rapid Commun 7:5–13

44. Kassi E, Patrickios CS (2010) Well-defined polymers from biosourced monomers: the case of 2-(methacryloyloxy)ethyl tiglate. Macromolecules 43:1411–1415

45. Kassi E, Constantinou MS, Patrickios CS (2013) Group transfer polymerization of biobased monomers. Eur Polym J 49:761–767

46. Bütün V, Vamvakaki M, Billingham NC, Armes SP (2000) Synthesis and aqueous solution properties of novel neutral/acidic block copolymers. Polymer 41:3173–3182

47. Patrickios CS, Lowe AB, Armes SP, Billingham NC (1998) ABC triblock polymethacrylates: group transfer polymerization synthesis of the ABC, ACB, and BAC topological isomers and solution characterization. J Polym Sci Part A Polym Chem 36:617–631

48. Achilleos DS, Georgiou TK, Patrickios CS (2006) Amphiphilic model conetworks based on cross-linked star copolymers of benzyl methacrylate and 2-(dimethylamino)ethyl methacrylate: synthesis, characterization, and DNA adsorption studies. Biomacromolecules 7:3396–3405

49. Georgiou TK, Patrickios CS, Groh PW, Iván B (2007) Amphiphilic model conetworks of polyisobutylene methacrylate and 2-(dimethylamino)ethyl methacrylate prepared by the combination of quasiliving carbocationic and group transfer polymerizations. Macromolecules 40:2335–2343

50. Triftaridou AI, Vamvakaki M, Patrickios CS (2007) Cationic amphiphilic model networks based on symmetrical ABCBA pentablock terpolymers: synthesis, characterization, and modeling. Biomacromolecules 8:1615–1623

51. Budde H, Höering S (1998) Synthesis of ethylene oxide/methyl methacrylate diblock copolymers by group-transfer polymerization of methyl methacrylate with poly(ethylene oxide) macroinitiators. Macromol Chem Phys 199:2541–2546

52. Bütün V, Bannister I, Billingham NC, Sherrington DC, Armes SP (2005) Synthesis and characterization of branched water-soluble homopolymers and diblock copolymers using group transfer polymerization. Macromolecules 38:4977–4982

53. Kafouris DK, Themistou E, Patrickios CS (2006) Synthesis and characterization of star polymers and cross-linked star polymer model networks with cores based on an asymmetric, hydrolyzable dimethacrylate cross-linker. Chem Mater 18:85–93

54. Simms JA, Spinelli HJ (1987) Recent advances in group transfer polymerization and their applications in coatings. J Coat Technol 59:125–131
55. Pugh C, Percec V (1985) Synthesis and group transfer polymerization and copolymerization of *p*-vinylbenzyl methacrylate. Polym Bull 14:109–116
56. Lu Z, Lee SY, Goh SH (1997) Group transfer copolymerisation of vinyl methacrylate and methyl methacrylate. Polymer 38:5893–5895
57. Webster OW, Hertler WR, Sogah DY, Farnham WB, RajanBabu TV (1984) Synthesis of reactive-ended acrylic polymers by group transfer polymerization: initiation with silyl ketene acetals. J Macromol Sci Chem A21:943–960
58. Bugnon L, Morton CJH, Novak P, Vetter J, Nesvadba P (2007) Synthesis of poly (4-methacryloyloxy-TEMPO) via group-transfer polymerization and its evaluation in organic radical battery. Chem Mater 19:2910–2914
59. Gomez PM, Neidlinger HH (1987) Incorporation of ultraviolet light stabilizers into PMMA prepared by group transfer polymerization. Polym Prepr (Am Chem Soc Div Polym Chem) 28:209–210
60. Mykytiuk J, Armes SP, Billingham NC (1992) Group-transfer polymerization of benzyl methacrylate: a convenient method for synthesis of near-monodisperse poly(methacrylic acids). Poly Bull 29:139–145
61. Rannard SP, Billingham NC, Armes SP, Mykytiuk J (1993) Synthesis of monodisperse block copolymers containing methacrylic acid segments by group-transfer polymerization: choice of protecting group and catalyst. Eur Polym J 29:407–414
62. Dyakonov TA, Huang B, Hamoudi A, Burns DH, Liu Y, Stevenson WTK (2000) Poly (benzyloxy ethyl methacrylate): preparation by free radical polymerization and by group transfer polymerization; with subsequent debenzylation to form poly(2-hydroxyethyl methacrylate). Eur Polym J 36:1779–1793
63. Lowe AB, Billingham NC, Armes SP (1998) Synthesis and characterization of zwitterionic block copolymers. Macromolecules 31:5991–5998
64. Pafiti KS, Mastroyiannopoulos NP, Phylactou LA, Patrickios CS (2011) Hydrophilic cationic star homopolymers based on a novel diethanol-*N*-methylamine dimethacrylate cross-linker for siRNA transfection: synthesis, characterization, and evaluation. Biomacromolecules 12:1468–1479
65. Kim YB, Oh JM, Choi WJ, Choi SK (1993) Cyclopolymerization of 2,5-bis (methoxycarbonyl)-1,5-hexadiene by group-transfer polymerization. Macromolecules 26:2383–2385
66. Nakano T, Sogah DY (1995) Toward control of stereochemistry in GTP by a rational monomer design. cyclopolymerization of 2,2′-bis((methacryloyloxy)methyl)-1,1′-binaphthyl. J Am Chem Soc 117:534–535
67. Krupers MJ, Möller M (1997) Synthesis and characterization of semifluorinated polymers via group transfer polymerization. J Fluorine Chem 82:119–124
68. Epple U, Scheider HA (1990) The group transfer copolymerization of alkyl acrylates with acrylates containing electron-donor or -acceptor substituents. Polymer 31:961–966
69. Hertler WR, RajanBabu TV, Ovenall DW, Reddy GS, Sogah DY (1988) Group transfer polymerization with polyunsaturated esters and silyl polyenolates. J Am Chem Soc 110:5841–5853
70. Eggert M, Freitag R (1994) Poly-N, N-diethylacrylamide prepared by group transfer polymerization: synthesis, characterization, and solution properties. J Polym Sci Part A Polym Chem 32:803–813
71. Freitag R, Baltes T, Eggert M (1994) A comparison of thermoreactive water-soluble poly-N, N-diethylacrylamide prepared by anionic and by group transfer polymerization. J Polym Sci Part A Polym Chem 32:3019–3030
72. Baltes T, Garret-Flaudy F, Freitag R (1999) Investigation of the LCST of polyacrylamides as a function of molecular parameters and the solvent composition. J Polym Sci Part A Polym Chem 37:2977–2989

73. Hertler WR, Sogah DY, Boettcher FP (1990) Group-transfer polymerization on a polymeric support. Macromolecules 23:1264–1268
74. Zhang J, Wang M, Wang J, Shi Y, Tao J, Wang D (2005) Group transfer polymerization of acrylonitrile in bulk at ambient temperature. Polym Bull 54:157–161
75. Webster OW (2004) Group transfer polymerization: mechanism and comparison with other method. Adv Polym Sci 167:1–34
76. Yu H, Choi W, Lim KT, Choi SK (1988) Group transfer polymerization by bifunctional initiators: a simple method for ABA triblock copolymers. Macromolecules 21:2893–2894
77. Steinbrecht K, Bandermann F (1989) Bifunctional initiators for group-transfer polymerization. Makromol Chem 190:2183–2191
78. Sogah DY, Webster OW (1983) Telechelic polymers by group transfer polymerization. J Polym Sci Polym Lett Ed 21:927–931
79. Farnham WB, Sogah DY (1986) Group transfer polymerization. Mechanistic studies. Polym Prepr (Am Chem Soc Div Polym Chem) 27:167–168
80. Müller AHE (1990) Group transfer and anionic polymerization: a critical comparison. Makromol Chem Macromal Symp 32:87–104
81. Quirk RP, Bidinger GP (1989) Mechanistic role of enolate ions in "group transfer polymerization". Polym Bull 22:63–70
82. Sogah DY, Farnham WB (1985) In: Sakurai (ed) Organosilicon and biooganosilicon chemistry: structure, bonding, reactivity and synthetic application. Ellis Horwood, Chichester, chap 20, p 219
83. Müller AHE, Litvinenko G, Yan D (1996) Kinetic analysis of "living" polymerization systems exhibiting slow equilibria. 3. "Associative" mechanism of group transfer polymerization and Ion Pair Generation in Cationic Polymerization. Macromolecules 29:2339–2345
84. Mai PM, Müller AHE (1987) Kinetics of group transfer polymerization of methyl methacrylate in tetrahydrofuran. 1. Effect of concentrations of catalyst and initiator on reaction rates. Makromol Chem Rapid Commun 8:99–107
85. Mai PM, Müller AHE (1987) Kinetics of group transfer polymerization of methyl methacrylate in tetrahydrofuran. 2. Effect of monomer concentration and temperature on reaction rates. Makromol Chem Rapid Commun 8:247–253
86. Quirk RP, Ren J, Bidnger G (1993) Mechanistic aspects of group-transfer polymerization. Makromol Chem Macromol Symp 67:351–363
87. Quirk RP, Ren J (1992) Mechanistic studies of group transfer polymerization. Silyl group exchange studies. Macromolecules 25:6612–6620
88. Hertler WR, Sogah DY, Webster OW (1984) Group-transfer polymerization. 3. Lewis acid catalysis. Macromolecules 17:1415–1417
89. Ute K, Ohnuma H, Shimizu I, Kitayama T (2006) Stereospecific group transfer polymerization of methyl methacrylate with Lewis-acid catalysis-formation of highly syndiotactic poly (methyl methacrylate). Polym J 38:999–1003
90. Dicker IB (1988) Group transfer polymerization (GTP) of acrylates catalyzed by mercuric iodide. Polym Prep (Am Chem Soc Div Polym Chem) 29(2):114
91. Zhuang R, Müller AHE (1994) Kinetics and mechanism of group transfer polymerization of n-butyl acrylate catalyzed by HgI$_2$/(CH$_3$)$_3$SiI in toluene. Macromol Symp 85:379–392
92. Zhuang R, Müller AHE (1995) Group transfer polymerization of n-butyl acrylate with Lewis acid catalysts. 1. Kinetic investigation using HgI$_2$ as a catalyst in toluene. Macromolecules 28:8035–8042
93. Zhuang R, Müller AHE (1995) Group transfer polymerization of n-butyl acrylate with Lewis acid catalysts. 2. Kinetic investigation using the HgI$_2$/Me$_3$SiI catalyst system in toluene and methylene chloride. Macromolecules 28:8043–8050
94. Ute K, Tarao T, Hatada K (1997) Group transfer polymerization of methyl crotonate. Polym J 29:957–958

95. Ute K, Tarao T, Hongo S-Y, Ohnuma K, Hatada K, Kitayama T (1999) Preparation of disyndiotactic poly(methyl crotonate) by stereospecific group transfer polymerization. Polym J 31:177–183

96. Ute K, Tarao T, Nakao S, Kitayama T (2003) Preparation and properties of *disyndiotactic* poly(alkyl crotonate)s. Polymer 44:7869–7874

97. Ute K, Tarao T, Kitayama T (2005) Enhanced stereocontrol in disyndiotactic-specific group transfer polymerization of methyl crotonate-stereochemical evidence of group transfer. Polym J 37:578–583

98. White D, Matyjaszewski K (1995) Controlled polymerization of acrylates activated by lanthanoid triflates. Polym Prep (Am Chem Soc Div Polym Chem) 36(2):286

99. Oishi T, Onimura K, Sumida W, Zhou H, Tsutsumi H (2000) Asymmetric group transfer polymerization of *N*-cyclohexylmaleimide with Lewis acid and chiral ligand complexes. Polym J 32:722–728

100. Zhang Y, Chen EYX (2008) Structure-reactivity relationships in bimolecular-activated monomer polymerization of (meth)acrylates using oxidatively activated group 14 ketene acetals. Macromolecules 41:6353–6360

101. Ishihara K, Hanaki N, Yamamoto H (1993) Tris(pentafluorophenyl)boron as a new efficient, air stable, and water tolerant catalyst in the aldol-type and Michael reactions. Synlett 577–579

102. Ishihara K, Hanaki M, Funahashi M, Miyata M, Yamamoto H (1995) Tris(pentafluorophenyl) boron as an efficient, air stable, and water tolerant Lewis acid catalyst. Bull Chem Soc Jpn 68:1721–1730

103. Dilman AD, Ioffe SL (2003) Carbon-carbon bond forming reactions mediated by silicon Lewis acids. Chem Rev 103:733–772

104. Ute K, Ohnuma H, Kitayama T (2000) Combination of tris(pentafluorophenyl)borane and trialkylsilyl triflate as an efficient catalyst system for the group transfer polymerization of acrylates. Polym J 32:1060–1062

105. Zhang Y, Chen EYX (2008) Controlled polymerization of methacrylates to high molecular weight polymers using oxidatively activated group transfer polymerization initiators. Macromolecules 41:36–42

106. Miyake GM, Zhang Y (2010) Living polymerization of naturally renewable butyrolactone-based vinylidene monomers by ambiphilic silicon propagators. Macromolecules 43:4902–4908

107. Zhang Y, Gustafson LO, Chen EYX (2011) Dinuclear silylium-enolate bifunctional active species: remarkable activity and stereoselectivity toward polymerization of methacrylate and renewable methylene butyrolactone monomers. J Am Chem Soc 133:13674–13684

108. Kakuchi R, Chiba K, Fuchise K, Sakai T, Satoh T, Kakuchi T (2009) Strong brønsted acid as a highly efficient promoter for group transfer polymerization of methyl methacrylate. Macromolecules 42:8747–8750

109. Ishihara K, Hiraiwa Y, Yamamoto H (2001) A high yield procedure for the Me$_3$SiNTf$_2$-induced carbon-carbon bond-forming reactions of silyl nucleophiles with carbonyl compounds: the importance of addition order and solvent effects. Synlett 1851–1854

110. Boxer MB, Yamamoto H (2006) Tris(trimethylsilyl)silyl-governed aldehyde cross-aldol cascade reaction. J Am Chem Soc 128:48–49

111. García-García P, Lay F, García-García P, Rabalakos C, List B (2009) A powerful chiral counteranion motif for asymmetric catalyst. Angew Chem Int Ed 48:4363–4366

112. Ishihara K, Hiraiwa Y, Yamamoto H (2002) Crucial role of the ligand of silyl Lewis acid in the Mukaiyama aldol reaction. Chem Commun 1564–1565

113. Hiraiwa Y, Ishihara K, Yamamoto H (2006) Crucial role of the conjugate base for silyl Lewis acid induced Mukaiyama aldol reactions. Eur J Org Chem 1837–1844

114. Chen Y, Takada K, Fuchise K, Satoh T, Kakuchi T (2012) Synthesis of syndiotactic-rich star-shaped poly(methyl methacrylate) by core-first group transfer polymerization using *N*-(trimethylsilyl)bis(trifluoromethanesulfonyl)imide. J Polym Sci Part A Polym Chem 50:3277–3285

115. Ishihara K, Hasegawa A, Yamamoto H (2001) Polystyrene-bound tetrafluorophenylbis (triflyl)methane as an organic-solvent-swellable and strong brønsted acid catalyst. Angew Chem Int Ed 40:4077–4079
116. Hasegawa A, Ishihara K, Yamamoto H (2003) Trimethylsilyl pentafluorophenylbis(trifluoromethanesulfonyl)methide as a super Lewis acid catalyst for the condensation of trimethylhydroquinone with isophytol. Angew Chem Int Ed 42:5731–5733
117. Takada K, Fuchise K, Chen Y, Satoh T, Kakuchi T (2012) Controlled polymerization of methyl acrylate for high-molecular-weight polymers by pentafluorophenylbis(triflyl)methane-promoted group transfer polymerization using triisopropylsilyl ketene acetal. J Polym Sci Part A Polym Chem 50:3560–3566
118. Fuchise K, Sakai R, Satoh T, Sato S, Narumi A, Kawaguchi S, Kakuchi T (2010) Group transfer polymerization of N, N-dimethylacrylamide using nobel efficient system consisting of dialkylamino silyl enol ether as an initiator and strong brønsted acid as an organocatalyst. Macromolecules 43:5589–5594
119. Fuchise K, Chen Y, Takada K, Satoh T, Kakuchi T (2012) Effect of counter anions on kinetics and stereoregularity for the strong brønsted acid-promoted group transfer polymerization of N, N-dimethylacrylamide. Macromol Chem Phys 213:1604–1611
120. Zhang Y, Lay F, García-García P, List B (2010) High-speed living polymerization of polar vinyl monomers by self-healing silylium catalysts. Chem Eur J 16:10462–10473
121. Tasdelen MA, Kahveci MU, Yagci Y (2011) Telechelic polymers by living and controlled/living polymerization methods. Prog Polym Sci 36:455–567
122. Reetz MT, Ostarek R, Piejko K-E, Arlt D, Bömer B (1986) Group transfer polymerization of acrylic acid esters with alkylthio- or arylthiosilanes as initiators. Angew Chem Int Ed Engl Ed 25:1108–1109
123. Shen W-P, Zhu W-D, Yang M-F, Wang L (1989) New initiators for group transfer polymerization. Triphenylphosphonium-containing ketene silyl acetal. Makromol Chem 190:3061–3066
124. Speikamp H-D, Bandermann F (1988) Group transfer polymerization of methyl methacrylate in acetonitrile, 2. Initiation by trimethylsilyl cyanide. Makromol Chem 189:437–445
125. Witkowski R, Bandermann F (1989) Macromonomers of acrylates by group transfer polymerization. Makromol Chem 190:2173–2182
126. Heitz T, Webster OW (1991) Synthesis of poly(methyl methacrylate) macromonomers with phenolic functionality by group transfer polymerization and their use in polycondensation reactions. Makromol Chem 192:2463–2478
127. Hertler WR (1991) Vinylphosphonic ester as end-capping agents in group transfer polymerization. J Polym Sci Part A Polym Chem 29:869–873
128. Quirk RP, Ren J (1993) Living functionalization of polymethacrylates by group transfer polymerization (GTP)-using low ceiling-temperature monomers. Polym Int 32:205–212
129. Gnaneshwar R, Sivaram S (2007) End-functional poly(methyl methacrylate)s via group transfer polymerization. J Polym Sci Part A Polym Chem 45:2514–2531
130. Asami R, Kondo Y, Takaki M (1986) Synthesis of poly(methyl methacrylate) macromer by group transfer polymerization and polymerization of the macromer. ACS Polym Prepr 27:186–187
131. Cohen GM (1988) Alpha, omega-diols and macromonomers through new reactions of group transfer polymers. ACS Polym Prepr 29:46
132. Sannigrahi B, Wadgaonkar PP, Sehra JC, Sivaram S (1997) Copolymerization of methyl methacrylate with lauryl methacrylate using group transfer polymerization. J Polym Sci Part A Polym Chem 35:1999–2007
133. Bütün V, Billingham NC, Armes SP (1997) Synthesis and aqueous solution properties of novel hydrophilic-hydrophilic block copolymers based on tertiary amine methacrylates. Chem Commun 32:671–672

134. Masař B, Vlček P, Křiž J, Kovářová J (1994) Poly(methyl methacrylate)-*block*-poly(ethyl acrylate) by group transfer polymerization: synthesis and structural characterization. Macromol Chem Phys 195:289–302
135. Masař B, Vlček P (1994) Block copolymers by sequential group transfer polymerization: poly (methyl methacrylate)-*block*-poly(2-ethylhexyl acrylate) and poly(methyl methacrylate)-*block*-poly(tert-butyl acrylate). Macromol Chem Phys 195:671–678
136. Lim KT, Lee HJ, Choi SK (1996) Synthesis of ABA triblock copolymers of *N*-substituted maleimides and methacrylates by group transfer polymerization. Polym Bull 37:699–704
137. Zhu Z, Rider J, Yang C, Gilmartin ME, Wnek GE (1992) Synthesis of PMMA star polymers with siloxane cores via group-transfer polymerization using silyl ketene acetal functionalized cyclic siloxanes. Macromolecules 25:7330–7333
138. Sakamoto K, Aimiya T, Kira M (1997) Preparation of hyperbranched polymethacrylates by self-condensing group transfer polymerization. Chem Lett 26:1245–1246
139. Simon PFW, Müller AHE (2004) Kinetic investigation of self-condensing group transfer polymerization. Macromolecules 37:7548–7558
140. Simon PFW, Müller AHE, Pakula T (2001) Characterization of highly branched poly(methyl methacrylate) by solution viscosity and viscoelastic spectroscopy. Macromolecules 34:1677–1684
141. Simon PFW, Müller AHE (2001) Synthesis of hyperbranched and highly branched methacrylates by self-condensing group transfer copolymerization. Macromolecules 34:6206–6213
142. Simon PFW, Radke W, Müller AHE (1997) Hyperbranched methacrylates by self-condensing group transfer polymerization. Macromol Rapid Commun 18:865–873
143. Simon PFW, Müller AHE (2006) Kinetic investigations of self-condensing group transfer polymerization. Macromol Symp 240:83–92

Surface-Initiated Anionic Polymerization from Nanomaterials

Zhong Li and Durairaj Baskaran

Abstract Surface-initiated anionic polymerization is one of the many techniques used for the modification of organic and inorganic nanomaterials. Surface modification of nanomaterials using polymers is a unique way to reduce interface incompatibility of nanomaterials for applications in new technologies. The properties of nanomaterials strongly depend on their compatibility with organic phases either in bulk or in solution. This chapter focuses on surface grafting of polymers using living anionic polymerization from various nanomaterials and provides accounts on the developments in this area.

Keywords Surface-initiated polymerization • Carbon nanotubes • Graphene • "Grafting-from" • Anionic polymerization

1 Introduction

Unique polymers that are suitable for tailor-made applications in chemical, mechanical, and biomedical engineering are in high demand. Ultrahigh-strength polymeric materials and functional polymers that can reduce interfacial energy with other incompatible organic and inorganic materials are crucial in the development of efficient electronic devices and nanocomposites. Enhancement of strength in polymeric materials is often accomplished by blending with organic and inorganic fillers to form nanocomposites.

Since the establishment of polymer chemistry by Hermann Staudinger in the early twentieth century, polymer-based nanocomposites have been extensively studied and applied in usage to reshape modern civilization [1–3]. Nature is a great inspiration and exhibits unique composite structures everywhere [4, 5]. The development of polymer-reinforced porous ceramics is one such an example, which mimics the structural details of seashells [4, 5].

Nanocomposites based on modern carbon allotropes, such as carbon nanotubes, graphene, and graphene oxide, with polymers are expected to produce ultrahigh-

Z. Li • D. Baskaran (✉)
EMD Performance Materials Corp., 70 Meister Avenue, Somerville,
NJ 08876, USA
e-mail: zhong.li@emdgroup.com; durairaj.baskaran@emdgroup.com

strength and electrically conducting materials [6–8]. On the other hand, nanomaterials that are used in technologies, such as sensors, optoelectronics, and imaging, require specific functionality at their interface that is specially introduced by surface modification via covalent grafting or functionalization. Thus, polymer grafting onto the surfaces of organic and inorganic nanomaterials is very important to tailor-make materials that are suitable for niche applications.

1.1 Necessity for Surface Modification of Nanomaterials

Nanomaterials can be classified broadly into inorganic and organic, which can be further subdivided into various materials exhibiting unique dimensional, structural, and surface properties as shown in Scheme 1. The presence of polar and nonpolar secondary interactions in nanomaterials induces intermolecular interactions leading to aggregation, which prevents intermixing with polymers. Although there exist weak non-covalent interactions, including van der Waals, dipole-dipole, hydrogen bonding, CH-π, OH-π, and π-π, in between polymers and nanomaterials, they generally cannot overcome intermolecular interaction forces within the nanomaterials.

A low inherent incompatibility between organic polymers with fillers such as carbon nanotubes (CNTs), graphitic materials, and other inorganic components is due to a high interfacial energy that prohibits coexistence of these materials in a single phase [9, 10]. Thus, simply blending these nanomaterials with polymers often leads to macrophase separation and produces poor mechanical stability. To reduce interfacial energy and to improve compatibility, nanomaterials need to be surface modified. Even in the case of cross-linked polymeric nanoparticles, one has to choose a compatible polymer matrix to form nanocomposites.

Grafting technique is widely used to modify surfaces of nanomaterials and to enhance dispersion of nanomaterials in the polymer matrices. The surface of nanomaterial is, generally, grafted with compatible polymer or small molecule that reduces interfacial tension and enables dispersion in organic solvents and polymer matrices. For example, blending the clay, such as montmorillonite, into
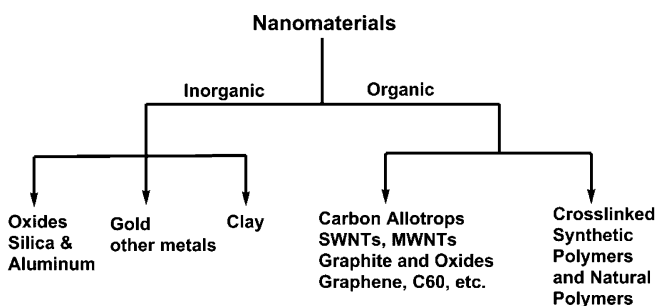
Scheme 1 Classification of nanomaterials that are used in surface-initiated anionic polymerization

a polymer can face a serious macrophase separation due to the difficulty in exfoliating the silicate layers bonded by ionic interactions. However, if montmorillonite is pretreated by intercalation of organoamines, nanoscale distribution can be achieved in polymer composites to largely enhance the mechanical properties, thermal stability, and gas barrier ability. Similar situations have also been known for CNT-based polymer composites. A strong aggregation of CNTs significantly affects the mechanical and electronic properties of the polymer composites due to inadequate tube debundling, inefficient load transfer, and limited percolation network formation. Therefore, organic and inorganic nanomaterials are, in general, require to be surface modified to improve organophilic character that suppresses aggregation and promotes molecular dispersion.

1.2 *Surface-Initiated Polymerization*

Several strategies have been used for the functionalization of nanomaterials through covalent and non-covalent reactions with polymers. Covalent functionalization through post chemical reactions and non-covalent functionalization through intermolecular interactions have been attempted to modify the surfaces of nanomaterials. Compared to non-covalent functionalization, which simply relies on either physisorbed or chemisorbed buffer layer to close the surface energy gap between nanomaterials and polymers, covalent chemical functionalization has been widely used to provide sophisticated surface manipulation. There are two basic functionalization strategies, namely, grafting-from and grafting-to, depending on whether the covalently attached polymer is initiated from, or performed functional polymer is reacted to the nanomaterial surfaces, respectively.

It is worth noting that the grafting ω-functionalized polymer via a grafting-to method usually is inefficient due to entropy penalty associated with the conformation of high molecular weight polymer. Thus, for grafting high molecular weight polymers, the grafting-to method is not a preferred one. The grafting-from strategy otherwise called surface-initiated polymerization (SIP) is the most promising one, since it provides a certain degree of control over polymer brush density, layer thickness, composition, and architecture of the brushes (Fig. 1). Depending on the grafting density (d), the polymer assumes different conformations, such as random-coil and extended-coil, leading to different layer or film thicknesses (LT or FT). By controlling the attachment of initiating groups on the surface and the polymerization to grow predetermined molecular weight, the surface energy can also be tuned.

The mechanism of polymer growth from solid surfaces is complex compared to the homogeneous solution polymerization and affects uniform initiation and propagation depending on the size of the surface and the interface interaction with medium of the polymerization. Thus, the reactivity, especially in the case of ionic initiators grafted at high concentration localized at the surface, may be different due to intimate ion-pair interactions leading to dormant aggregates. Moreover, the propagating centers confined in a quasi-two-dimensional area at the interface of
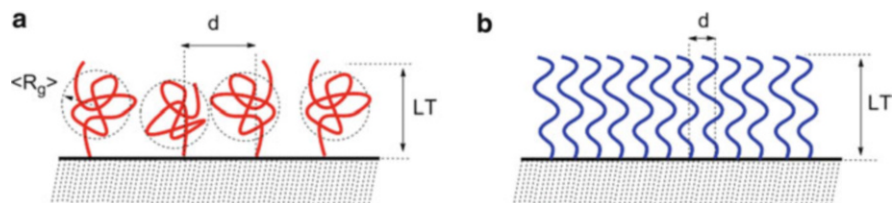
Fig. 1 Configuration of polymer brushes on surfaces with different graft density. (**a**) A low and disperse grafted brushes with coil-like conformation and (**b**) a high brush density with extended forest-like conformation

the surface to the monomer solution will change the surface properties that likely influence the monomer flux at the surface for the polymerization [11]. Therefore, the kinetic considerations are more complex and challenging to grow narrow distributed polymer chains from solid surfaces.

A successful surface-initiated polymerization involves three steps as shown in Scheme 2. An introduction of potential initiating functionality is the first step towards growing polymers from the surface of nanomaterials. The functional group is, then, activated using a catalyst or an external initiator for controlled polymerization (second-step). Subsequently, the polymerization is initiated from the nanomaterials to grow polymer brushes (third-step). Covalent attachment of the potential initiating functionality is generally performed via grafting-to method using appropriate organic reactions suitable for the chosen surface of nanomaterials. The initiators for SIP are aptly designed considering the nature and the availability of functionality on the surface of nanomaterials.

The advent of controlled or living polymerization techniques enables successful SIP from nanomaterials. In fact, the use of controlled or living polymerization is a prerequisite for grafting polymer from nanomaterials as the propagation of chains from the surfaces occurs without undergoing termination and transfer reactions. All known types of controlled and living polymerization techniques have been utilized for grafting polymers covalently from nanomaterials. Methods that have been employed are atom transfer radical polymerization (ATRP), reversible addition fragmentation chain transfer polymerization (RAFT), nitroxide-mediated radical polymerization (NMRP), living ionic polymerization, and ring-opening polymerization (ROP). Among these techniques, the living anionic polymerization provides several advantages over other methods such as control of molecular weight even at very low initiator concentration, transfer- and termination-free nature of propagation, and narrow distribution of polymer (MWD). These characteristics would allow one to control the grafting density and chain conformation of polymer brushes grown from nanomaterial surface [12]. However, the living anionic polymerization can only be performed from surfaces, which are not a deterrent to the propagation. Surfaces that contain acidic hydrogen cannot be used for surface-initiated anionic polymerization (SIAP). In this chapter, we intend to focus on the recent developments of SIAP from nanomaterials.

1) Covalent Co-initiator Attachment

Substrate Surface → Covalent functionalization (R) → Initiator Anchored Surface

2) Initiator Activation

R R R R R R R R R R → Activator / Catalyst → Reactive Surface

3) Surface initiated Polymerization

R R R R R R R R R R → n M / Polymerization → Polymer Brushed Surface
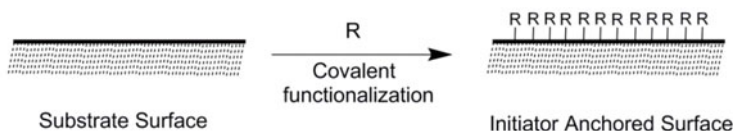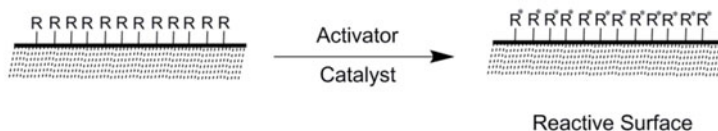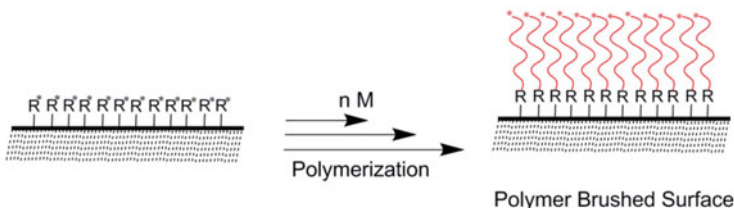
Scheme 2 Essential steps of surface-initiated anionic and other living/controlled polymerizations from theoretical surfaces of nanomaterials

2 Surface-Initiated Anionic Polymerization from Inorganic Surfaces

Inorganic materials have distinct chemical functionalities on their surfaces. They also vary in dimensions such as nanoparticles, nanoplatelets, and large flat surfaces (Scheme 3). In order to modify inorganic surfaces via SIAP, a precursor or co-initiator has to be attached on them using appropriate chemistries suitable for the surface. Specific connectivity for a particular surface, such as –S-Au– for gold, covalent –Si-O– bond for silicon wafer and silica nanoparticles, and ionic bond for layered aluminosilicates (clay), is chosen to link potential co-initiator moiety before subjecting the surface to the polymerization (Scheme 3).

Reactivity of carbanions toward the hydroxyl and carboxylic acid groups that are often found in these surfaces is very high, and hence protic functional groups have to be protected to sustain polymer growth. More importantly, the reactivity of anionic centers varies depending on the polarity of the medium in which the polymerization is conducted. Anionic polymerization in polar solvents such as tetrahydrofuran (THF) and dimethoxyethylene (DME) involves solvent-separation
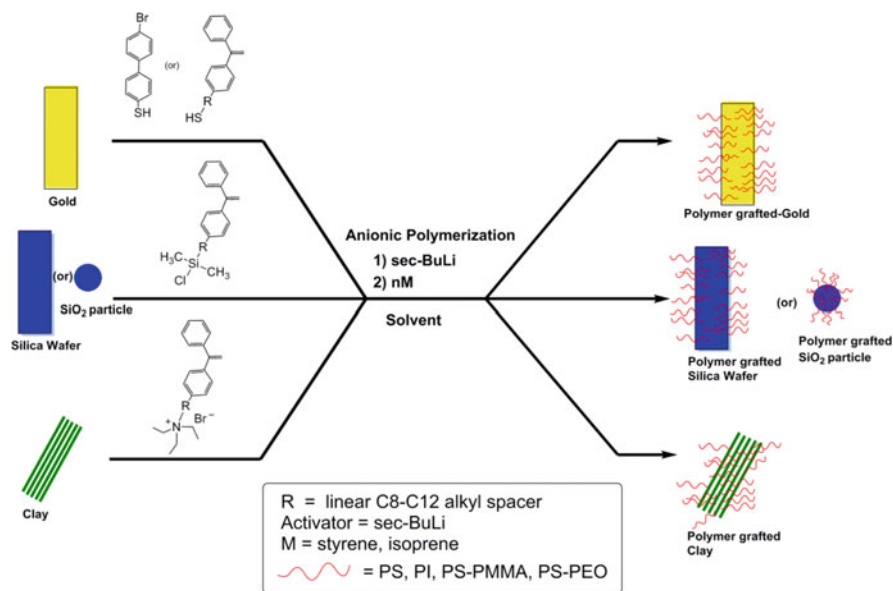
Scheme 3 Illustration of different strategies used in surface-initiated anionic polymerization from inorganic substrates

and even free ions, depending on the concentration, that are very reactive and can react with surfaces like Si-O-Si links. Thus, optimum reaction conditions should be chosen for SIAP.

Accordingly, researchers have selected 1, 1′-diphenylethylene (DPE) as a precursor co-initiator to functionalize various substrates [13–21]. The structure of DPE is unique with a sterically hindered diaryl substitution at α-carbon, and as a result, it will not undergo homopolymerization. However, the double bond of the DPE can be easily reacted by *n*- or *sec*-butyllithium (BuLi) to form an adduct with a resonance-stabilized carbanion. The resulting diphenylalkyl anion with lithium as counter cation is reactive for initiation of styrene, diene, and methacrylates [22–24]. Therefore, many of the approaches in the surface-initiated anionic polymerization involve the usage of DPE as a precursor co-initiator as shown in Scheme 3.

2.1 Anionic Polymerization from Gold Surface

It is well known that through a robust S-Au bonding, the gold surface can be easily functionalized by a self-assembled monolayer (SAM) of versatile thiol derivatives. Using S-Au bonding, a broad range of chemistries has been applied to attach precursor co-initiators on gold for surface-initiated anionic polymerization. The first example of SIAP on a flat gold surface was demonstrated by Ulman and coworkers [25]. They used 4′-bromo-4-mercaptobiphenyl thiol to functionalize
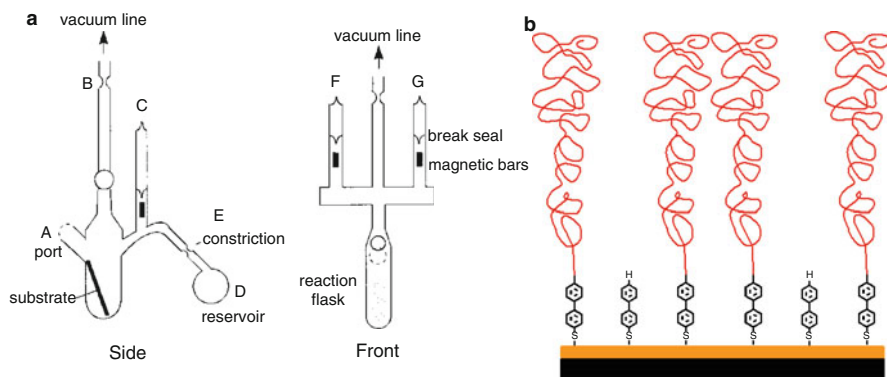
Fig. 2 (**a**) All-glass reactor used for SIAP of styrene (Reproduced with permission from Ref. [25], Copyright 1999 ACS) (**b**) The surface-induced living anionic polymerization by using the self-assembled monolayer of 4′-lithio-4-mercaptobiphenyl

the polycrystalline gold surface via SAM (Fig. 2a). The SAM-decorated gold substrate was then introduced into a sealed anhydrous reactor and reacted with *sec*-BuLi to form aryllithium initiator via halogen-metal exchange in a nonpolar medium. After a thorough washing of the aryllithium gold surface with a fresh solvent under high-vacuum condition, the monolayers of aryllithium were used to initiate styrene polymerization under vacuum (Fig. 2b).

The surface was thoroughly cleaned to remove any non-grafted polystyrene (PS) via Soxhlet extraction in toluene. The brush thickness probed by ellipsometry indicated that the PS film of 18 nm was the surface of gold in a collapsed state. It was found that the surface of the grafted PS brush contained defects such as dimples or holes corresponding to the film thickness. Upon swelling in toluene, the brush thickness increased to 29 nm. The authors used the thicknesses of the brush in the collapsed and the swollen states to estimate the degree of polymerization by applying the self-consistent mean field theory [26]. The calculated graft density based on R_g (50.6 Å) of the grafted PS chains was 7–8 chains/R_g^2, which corresponded to the area of 3.6 nm^2/chain (Table 1, entry 1) and suggested that the tethered polymer chains were adopting a stretched conformation. Although the SAM coverage indicated a dense packing of precursor mercaptobiphenyl molecules (0.2 nm^2/molecules), the numbers of grafted PS chains are relatively low, 1 in 18 molecules of SAM. This could be attributed to several factors as the efficiency of metal-halogen exchange reaction in self-assembled molecules and the reactivity of ion-pairs of the closely packed aryllithium monolayers are not known.

Advincula and coworkers later extended this technique to prepare SAM on gold using DPE-based thiol derivative as a precursor co-initiator [27]. They used *n*-BuLi to activate DPE SAMs and grafted polystyrene-*b*-poly(ethylene oxide) (PS-*b*-PEO) and polyisoprene-*b*-poly(meth methacrylate) (PI-*b*-PMMA) from gold-coated glass surface. They obtained inhomogeneous, thinner polymer brushes in the range 5–12 nm (Table 1, entry 2). One interesting aspect was to understand

Table 1 SIAP on different substrate surfaces

Entry	Type of surface	Attached initiator functionality[a]	Initiator activation[b]	Monomer[c]	Solvent/additive/temperature/time[d]	Grafted polymer	Reference
Inorganic surfaces							
1	Gold	BMBP	sec-BuLi	S	Cyclohexane:benzene 60:40/–/rt/3 days	3.2–3.6 nm²/chain	[25]
2	Gold	DPE	n-BuLi	S	THF/–/–78 °C/12 h	–	[27]
				EO	THF/t-BuP4/40 °C/8 days		
				S + EO	THF/–/–78 °C/4 h, then THF/t-BuP4/40 °C/8 days		
				I + MMA	THF/–/–78 °C/4 h, then THF/DPE/–78 °C/3 h		
3	Clay	DPE	n-BuLi	S	Benzene/–/rt/8 h	Up to 0.81 g/g of clay	[28]
4	SiO₂ (nanoparticles or glass slide)	S	t-BuLi	S, 2VP, MMA, I, CMS; S + I + S, S + MMA, S + 2VP	Homopolymers: Toluene/–/rt/–; Block copolymers: PMMA and P2VP blocks Toluene/–/–80 °C/–; Other blocks Toluene/–/rt/–	Up to 45 wt %	[29]
5	SiO₂ nanoparticles	DPE	n-BuLi or sec-BuLi	S	Benzene/THF/rt/2 days	–	[30]
6	Si/SiO₂	DPE	n-BuLi or sec-BuLi	S	Benzene/THF or TMEDA or BuOLi/rt/up to 5 days	Thickness up to 23.4 nm	[31]
				S + I, BD + S	Benzene/THF or TMEDA or BuOLi/rt/1 w		

7	Si/SiO$_2$	DPE	n-BuLi	I	Benzene/–/rt/	0.10–0.24 nm^2/chain	[22][a]
				S	Benzene/–/rt/4 days	Thickness up to 24 nm	[22][b]
				I + EO	Benzene/–/rt/87 + 40 h		
8	SiO$_2$ nanoparticles	CP-TES	n-BuLi	S	Cyclohexane/THF/rt/2 h	Up to 0.032 chains nm^{-2}	[32]
9	Si/SiO$_2$	Si-OH	MeONa	Glycidol	Methanol/–/110 °C/15 min	Thickness up to 70 nm	[33]
Organic surfaces							
10	Carbon whisker	Surface -OH	n-BuLi	S, MMA	Toluene/–/0 °C/1 h	39–100 wt %	[34]
11	Graphene nanoribbon	sp2 carbons	Li, Na or K	S	THF/naphthalene/–78 °C/1 d	9–22 wt %	[35]
12	Graphene oxide	Surface -OH	MDI	ε-CL	THF/50–150 °C/1 h	74 wt %	[36]
13	SWNTs	sp2 carbons	sec-BuLi	S	Cyclohexane/–/48 °C/2 h	10 wt %	[37]
14	SWNTs	sp2 carbons	sec-BuLi	t-BA	THF/–/–78 °C/3 h	29 wt %	[38]
				t-BA + MMA	THF/–/–78 °C/6 h	47 wt %	
15	SWNTs	sp2 carbons	Li/NH$_3$	MMA	NH$_3$/–/rt/overnight	45 wt %	[39]
16	MWNTs	DPE	sec-BuLi	S	Benzene/–/rt/0.75–1.5 h	86–98 wt %	[40]
				S + I	Benzene/–/rt/42 h	99 wt %	
17	SWNTs	Amino alcohol	Sn(Oct)$_2$	p-Dioxanone	Toluene/–/90 °C/72 h	40 wt %	[41]
18	MWNTs	2-azidoethanol	MeOK	Glycidol	Dioxane/–/95 °C/4 h	21–91 wt %	[42]
19	MWNTs	Surface -COOH, -OH	MeOK	Glycidol	bulk/100 °C/4 h	56 wt %	[43]
20	SWNTs	Diazonium benzyl alcohol	Sn(Oct)$_2$	ε-CL	DCB/–/130 °C/24 h	63 wt %	[44]
21	MWNTs	Glycol	Sn(Oct)$_2$	ε-CL	Bulk/120 °C/24 h	32–52 wt %	[45]
22	MWNTs	Surface -OH	Al(CH$_3$)$_3$	ε-CL	Toluene/–/rt/18 h	95–99 wt %	[46]

(continued)

Table 1 (continued)

Entry	Type of surface	Attached initiator functionality[a]	Initiator activation[b]	Monomer[c]	Solvent/additive/temperature/time[d]	Grafted polymer	Reference
23	MWNTs	Surface -NH2	Al(CH$_2$CH$_3$)$_3$	ε-CL	Toluene/–/40 °C/25 min	–	[47]
24	MWNTs		Sn(Oct)$_2$	ε-CL	DCB/–/130 °C/16 h	58 wt %	[48]
25	MWNTs	BCB-EO	Sn(Oct)$_2$	ε-CL	THF/–/120 °C/3 min-4 h	18–98 wt %	[49, 50]
26	MWNTs	Butanediol	Sn(Oct)$_2$	L-LA	DMF/–/140 °C/2–20 h	10–35 wt %	[51]
27	MWNTs	Surface -COOH	Sn(Oct)$_2$	ε-CL	DMF/–/140 °C/2–20 h	–	[52]
28	MWNTs	Surface -COOH	Sn(Oct)$_2$	α-Chloro-ε-CL	DMF/–/140 °C/2–20 h	–	[53]
29	SWNTs	BCB-EO	CpTiCl$_3$	L-LA	Toluene/–/135 °C/7.5–20 h	13–94 wt %	[54]
30	MWNTs	EG	Sn(Oct)$_2$	L-LA	Bulk/–/130 °C/48 h	26–34 wt %	[55]
31	MWNTs	EG	Sn(Oct)$_2$	L-LA, ε-CL	Toluene/–/130 °C/48 h	73 wt %	[56]
32	SWNTs	EDA	–	γ-BLG-NCA	DMF/–/rt/48 h	–	[57]
33	MWNTs	DAH	–	ε-Boc-L-Lys-NCA	THF/–/30 °C/48 h	27–54 wt %	[58]
34	SWNTs	APA	–	γ-BLG-NCA	DMF/–/rt/48 h	41 wt %	[59]
35	SWNTs	Surface -COOH	Na	ε-CL	Bulk/–/140 °C/24 h	30 wt %	[60]
36	MWNTs	Isocyanate	Na	ε-CL	Bulk/–/170 °C/2–10 h	40–65 wt %	[61]
37	MWNTs	S + MA	NaCL	ε-CL	Bulk/–/170 °C/6 h	–	[62]
38	MWNTs	Toluene 2, 4-diisocyanate	NaCL	ε-CL	Bulk/–/160 °C/10 min	–	[63]
39	Cross-linked PS beads	BIBA	SmI$_2$	MMA	THF/DEPA/–78 °C/12 h	–	[64]

40	Cross-linked PS beads	BIBA	SmI$_2$	AMA	THF/DEPA/−78 °C/8 h	–	[65]
41	Cross-linked PS beads	BIBA	SmI$_2$	Hydroxyethyl methacrylate	THF/DEPA/−78 °C/48 h	–	[66]

[a]BMBP 4′-bromo-4-mercaptobiphenyl, DPE 1,1-diphenylethylene, CP-TES (3-chloropropyl)triethoxysilane, BCB-EO 4-hydroxyethyl benzocyclobutene, EG ethylene glycol, EDA ethylene diamine, DAH 1,6-diaminohexane, APA 3-azidopropan-1-amine, MA maleic anhydride, BIBA 2-bromoisobutyric acid

[b]n-BuLi n-butyl lithium, sec-BuLi secondary-butyl lithium, t-BuLi tert-butyl lithium, MeONa sodium methoxide, MDI 4,4′-methylenebis(phenyl isocyanate), Sn(Oct)$_2$ tin(II) 2-ethylhexanoate, MeOK potassium methoxide, CpTiCl$_3$ cyclopentadienyltitanium(IV) trichloride, NaCL ε-caprolactam sodium salt, SmI$_2$ samarium(II) iodide

[c]S styrene, EO ethylene oxide, I isoprene, MMA methyl methacrylate, 2VP 2-vinylpyridine, CMS chloromethylstyrene, BD butadiene, t-BA tert-butyl acrylate, ε-CL ε-caprolactam, L-LA L-lactide, γ-BLG-NCA γ-benzyl-L-glutamate N-carboxyanhydride, ε-Boc-L-Lys-NCA ε-(benzyloxycarbonyl)-L-lysine N-carboxyanhydride, AMA allyl methacrylate, HEMA hydroxyethyl methacrylate

[d]THF tetrahydrofuran, TMEDA tetramethylethylenediamine, BuOLi lithium tert-butoxide, DCB dichlorobenzene, DMF dimethylformamide, DEPA N,N-diethylphenylacetamide
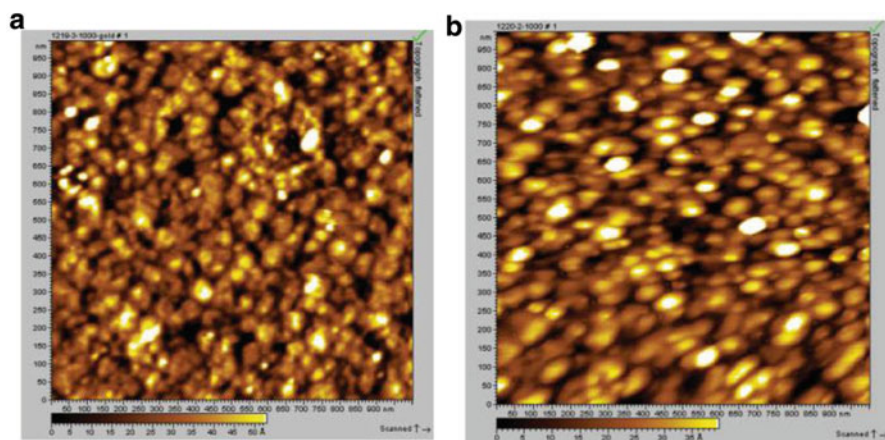
Fig. 3 (**a**) AFM images of PS-*b*-PEO diblock copolymer brush. The topological or height image before annealing. (**b**) AFM images of PS-*b*-PEO diblock copolymer brush. The topological or height image after annealing at 120 °C (Reproduced with permission from Ref. [27], Copyright 2006 Wiley)

the self-assembling behavior of the copolymer brushes. Microphase separation of the two blocks was expected; however, no self-assembling patterns were observed by atomic force microscopy (AFM) (Fig. 3), even though polymer reorganization can be induced by solvent treatment as detected by contact angle measurements. The authors attributed this observation to a small thickness of the polymer brushes and to a low molecular weight of the block segments.

2.2 Anionic Polymerization from Clay Surface

Owning to their unique layered structure and cheap availability of clays, they have been used extensively to strengthen polymer nanocomposites targeting for high thermal, environmental, and mechanical stability and to enhance the gas barrier properties. Generally, pristine clay needs to be modified by positively charged organic species via ion exchanging the metal cations like Li^+, Na^+, or Ca^{2+} in order to improve the organophilicity and to exfoliate the silicate layers for better compatibility with the polymer matrix through either a simple blending or an in situ polymerization. However, anionic polymerization involving clay is quite challenging because the hydrophilic nature of clay inevitably hosts moisture in it, which would terminate propagating living anions during grafting. As a result, reactions need to be conducted in a specially designed reactor to ensure a complete removal of moisture under high vacuum. Using high-vacuum and break-seal technique, Mays and coworkers [28] demonstrated the surface-initiated anionic polymerization of styrene from clay intercalated with DPE-functionalized triethylammonium bromide (Fig. 4).
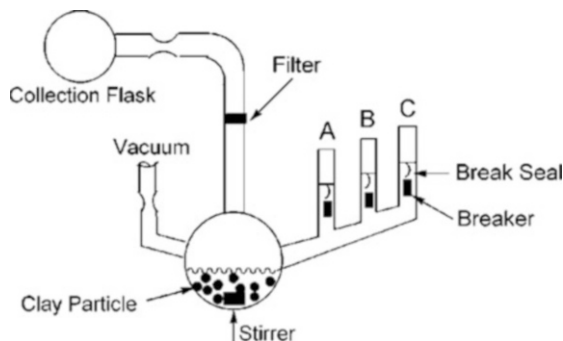
The elegance of such a reaction setup includes a feasibility to completely remove free initiators, which is known to compete severely with the immobilized initiators for monomer consumption, as well as a direct visual monitoring of the formation of living anions bound on the substrate surface. The DPE-based initiator is thermally stable over 300 °C, which allowed the organo-modified clay free from any trapped H_2O by extensive drying in vacuum at high temperature. After treated by *n*-BuLi, the DPE carbanions were generated and, consequently, initiated the living polymerization of styrene (Scheme 3). In spite of a thorough washing of excess BuLi with the solvent, the authors found that a small amount of the free initiator is present in the polymerization solution. It is worth noting that although the SIP was confirmed by Fourier transform infrared spectroscopy (FTIR), X-ray diffraction (XRD) and X-ray photoelectron spectroscopy (XPS), the thermal gravimetric analysis (TGA) of the PS-grafted clays, the AFM imaging of the clay nanoparticles, and the polymer weight analysis of the cleaved polymer; all indicated that a significant polymerization took place only at the outer layers of the DPE-modified clay, while most of the intercalated initiators inside the gallery did not participate in the anionic polymerization. Therefore, the expected exfoliation of the clay during the polymerization was not achieved, and the grafted PS showed a much larger polydispersity index than a typical living anionic polymerization process (Table 1, entry 3).

2.3 Anionic Polymerization from Silicon Oxide Particles and Substrates

Some early works exploring the living anionic SIP on silica surfaces appeared around the 1990s. Taking advantage of the hydroxyl groups commonly existing on the SiO_2 surface, Oosterling et al. [29] developed a technology for immobilizing styrene on the silica nanoparticle surfaces using *p*-vinylbenzyltrichlorosilane. The attached styrene monomer was activated by *t*-BuLi and used for the polymerization of styrene assuming that inter-/intramolecular reactions are insignificant. Several
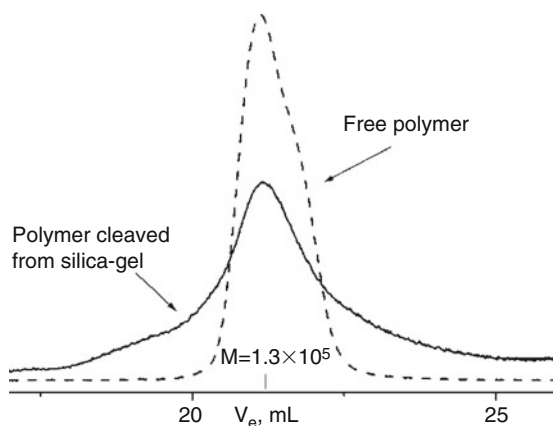
types of block copolymers such as PS-*b*-PI-*b*-PS, PS-*b*-PMMA, and polystyrene-b-poly(2-vinyl pyridine) (PS-*b*-PVP) were synthesized from the surface. In order to avoid a potential attack on Si-O-Si bonds by the highly reactive *t*-BuLi, the authors chose benzene as a nonpolar solvent for the polymerization. However, the molecular weight distributions were broader than the ones observed in a typical anionic polymerization, possibly due to the aggregation tendency of *t*-BuLi in hydrocarbon solvents (Table 1, entry 4).

In another study, Zhou et al. [30] connected DPE to the silica surface via silylether bond using dimethylsilylchloride-functionalized DPE. They used *n*-BuLi to activate the styrene polymerization and thus obtained PS-grafted silica nanoparticles in toluene. Although the same reactor shown in Fig. 4 was used to ensure the complete removal of nonattached free initiators through washing under vacuum, they found that some free DPE or *n*-BuLi residue was present in the polymerization solution and caused concurrent homopolymerization of styrene in small quantity. Thus, they obtained PS grafts with a broad molecular weight distribution (Fig. 5). They also reported problems associated with reproducibility and very low initiator efficiency. These results suggest that growing polymers from the silica surface is complicated due to dormancy of reaction sites, side reactions, and difficulty in the purification of surface (Table 1, entry 5).

The same group also applied the silylchloride-functionalized DPE to silicon wafer and formed SAM of DPE initiators on the surface [31]. However, a similar low grafting density was observed. On the other hand, Quirk and coworkers successfully grafted silicon wafers using both grafting-to and grafting-from approaches via anionic polymerization [22]. They used trichlorosilyl- and dimethylsilyl-substituted DPE to form SAM on the silicon wafer. The formation of a monolayer of DPE was confirmed based on the packing density (0.41 nm^2/DPE molecule) using X-ray reflectometry. The DPE monolayer was converted into 1,1-diphenylhexyllithium by reacting with *n*-BuLi and used to initiate styrene and diene monomers. The excess *n*-BuLi after activation of DPE monolayers was washed away by repeated back distillation of benzene using a high-vacuum

technique. In spite of such a treatment to remove excess *n*-BuLi from the surface, they observed 100–300 mg of free PS formed in the polymerization solution. Nevertheless, the PS grown from the silicon wafers had the highest brush thickness, 24 nm reported so far (Table 1, entry 6). The chain ends of the living polymer brushes with lithium counterion were successfully functionalized with hydroxyl group by adding ethylene oxide and further used for the polymerization of ethylene oxide in the presence of potassium counterion.

In a very recent study, Kim and coworkers applied a similar strategy to functionalize silica nanoparticles using (3-chloropropyl)triethoxysilane [32]. They used metal-halogen exchange reaction to graft PS via anionic polymerization in toluene. The efficiency of alkyl halide-metal exchange reaction with *n*-BuLi in nonpolar solvent is, in general, very low. Nevertheless, they conducted the polymerization of styrene in the presence of free *n*-BuLi and obtained two distinct components of the cleaved PS prepared by silica gel SIP (Fig. 6). The high molecular weight PS similar to the PS generated from the free initiator was attributed to grafting-to reaction of the living PS anion.

The PS brushes grown from the silica particles are distinctly different in topography as shown in the TEM images (Fig. 7). Based on the dynamic light and small angle neutron scattering studies on these silica particles, they concluded that the conformation of the grafted PS chains is "coil-like" instead of stretched or extended as expected for surface-initiated polymerization. They attributed "coil-like" brush conformation to poor grafting density (Table 1, entry 8).
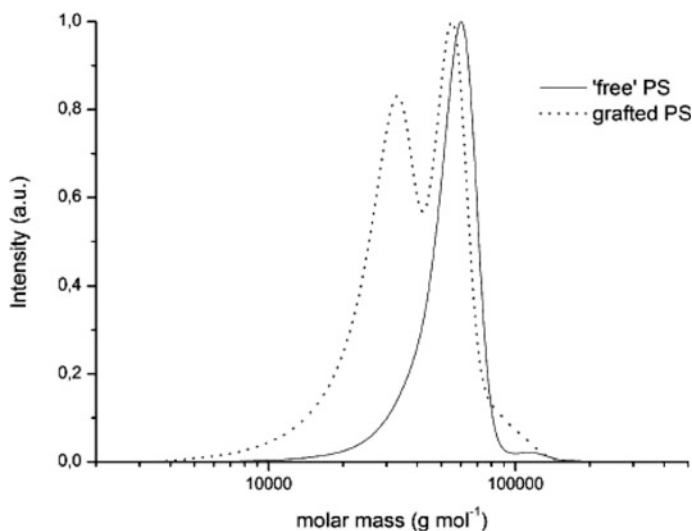
Fig. 6 GPC traces of grafted PS brushes separated from the surface and the solution. The broader bimodally distributed curves (*dotted*) correspond to the surface attached PS, which have been detached by etching. The narrow monomodal distributions (*lined*) correspond to free PS, which was initiated by sacrificial initiator in solution (Reproduced with permission from Ref. [32], Copyright 2013 Springer)
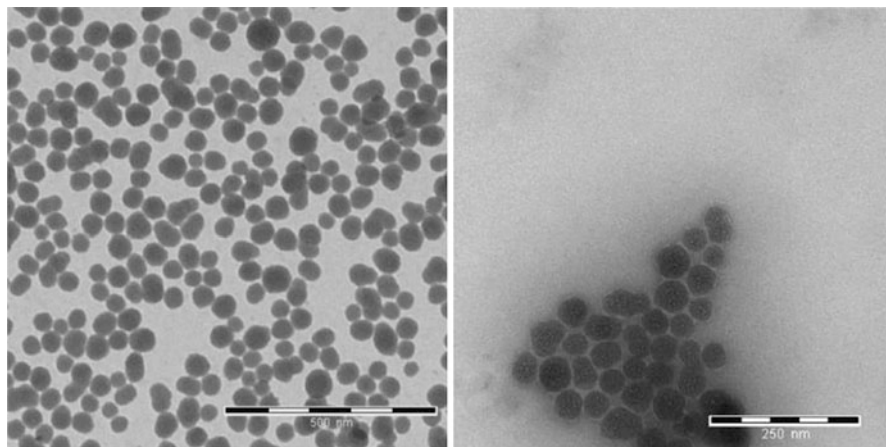
Fig. 7 TEM images of bare silica nanoparticles (*left*) and the PS-grafted silica nanoparticles (*right*) prepared by using the drop-cast method of their dispersions on carbon-coated copper grid (Reproduced with permission from Ref. [32], Copyright 2013 Springer)
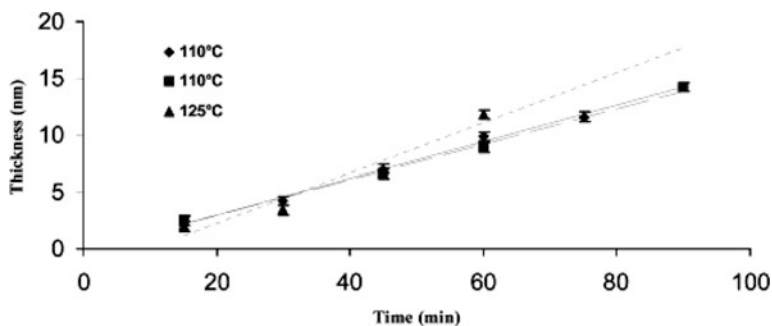
Fig. 8 Increase in polyglycidol brush thickness (measured by ellipsometry) vs polymerization time on Si wafer using various temperatures (Reproduced with permission from Ref. [33], Copyright 2003 ACS)

Other than the most studied PS grafting systems, Huck and coworkers studied the grafting of hyperbranched polyglycidol [33]. In this case, a simple deprotonation of the OH groups on the activated SiO_2 surfaces, in either Si wafer or silica gel, using sodium methoxide was shown to efficiently initiate the anionic ring-opening polymerization of glycidol. The progress of the surface-initiated polymerization was monitored, which showed clearly an increase in polyglycidol brush thickness with time (Fig. 8). Furthermore, the large amount of active OH groups on the grafted hyperbranched polyglycidol enabled them to do post-functionalization, as demonstrated by their reinitiation experiments to increase the polyglycidol brush thickness up to 70 nm (Table 1, entry 9) and the esterification of the hyperbranched polyglycidol-grafted silica gel.

3   Surface-Initiated Anionic Polymerization from Organic Surfaces

Organic substrates are broadly classified into sp^2 carbon-based nanomaterials (Scheme 4) and insoluble polymers (natural or cross-linked synthetic polymers). Depending on the nature of the functional groups present on the organic solids/surfaces, they can be used for covalent or non-covalent modifications. The non-covalent modification replies on adsorption of suitable organic molecules such as pyrenes, poly(*meta*-phenylene vinylene), poly(styrene sulfonate), cyclodextrin, etc., to form weak secondary interactions, including π-π, ionic, and H-bonding [77], and the covalent modification involves direct reactions with either the sp^2 carbons or the preexisting reactive functional groups (COOH, OH, etc.) on the substrate surfaces.

However, the chemical functionalization of organic solids and carbon materials, in particular, is a complex process as the substrates are insoluble; therefore, the reaction must be conducted either in bulk or in a heterogeneous medium. Because of the heterogeneous nature of the reactions, the modification reactions are often incomplete and will form multiple products with variable degrees of functionalization. More importantly, carbon materials, such as carbon black, graphite, graphene, and CNTs, are not monodisperse, particularly in diameter and length. A small difference in the degree of functionalization with organic compounds will introduce solubility variations in the functionalized products during the reaction. As a result, the availability of the carbon nanomaterials that are partially solvated for further reaction will increase, and the reaction will proceed discriminately with respect to the size and the degree of functionalization. Thus, it is difficult to control the efficiency and the specificity of organic reactions with carbon materials, especially with respect to the placement of functional groups and the degree of
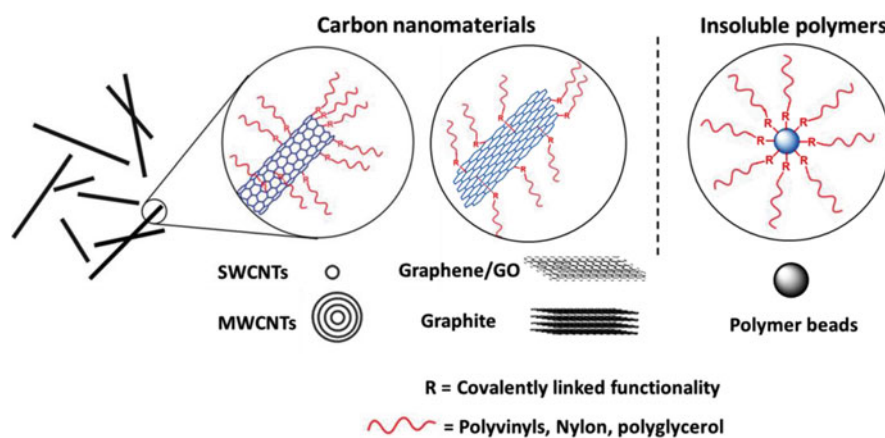
Scheme 4 Organic substrates containing sp^2 carbon back-bone nanomaterials used in surface-initiated anionic polymerization

functionalization on a molecular basis. Nevertheless, the attachment of organic moieties on the sp^2 graphitic carbons introduces an organophilic character and helps dispersing carbon nanomaterials in bulk polymers and in organic solvents. Although the modification affects some inherent properties of carbon nanomaterials, it significantly increases their potential applications.

3.1 Anionic Polymerization from Graphitic Carbon Nanomaterials

In early 1960s, researchers from Japan reported anionic polymerization of styrene from the surface of carbon black-alkali metal complex [67]. This initial result prompted exploration of the possibility to grow polymer chains from the surface of various carbon materials using anionic polymerization for the development of enhanced polymer composites. Ohkita and coworkers [68] attempted the polymerization of styrene from carbon black catalyzed by n-BuLi via grafting-from and grafting-to methods. They found a marked retardation of the polymerization, likely due to the preferential reaction between n-BuLi and the oxygen-containing groups on the carbon black. Tsubokawa et al. demonstrated anionic grafting of poly(β-propiolactone) from carbon black initiated by the surface carboxylate groups [69] and the anionic grafting of PMMA or PS from carbon whisker using n-BuLi/TMEDA complexes as metalating agent (Scheme 5) (Table 1, entry 10) [34].

Graphite is another important substrate that has drawn considerable attention recently [70, 71]. Studies concerning graphite functionalization are occasionally presented in the literature since the early 1960s [72]. Most of the reports describe grafting vinyl polymers from graphite-alkali metal intercalation compounds [73]. Sun and coworkers reported initiation of styrene from the surface and the edges of the K-intercalated graphite [74]. Although this and other publications never caught much attention, the emergence of the graphene research in recent years has attracted significant interest in SIAP. A majority of the publications in this area deals with grafting polymers from surfaces using ATRP, due to its simplicity among other modern controlled radical polymerization processes [75–79]. Nevertheless, anionic polymerization has been used in some cases to take advantages of its process controls (Table 1).

Tour and coworkers reported SIP of styrene via anionic polymerization using anions generated from unzipping of MWNTs in the presence of potassium metal [35]. They claimed that the carbanions are generated via reduction of edge radicals
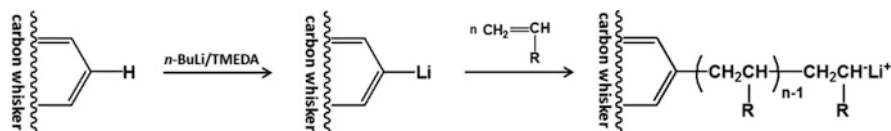
Scheme 5 Anionic polymerization of vinyl monomers from carbon whisker
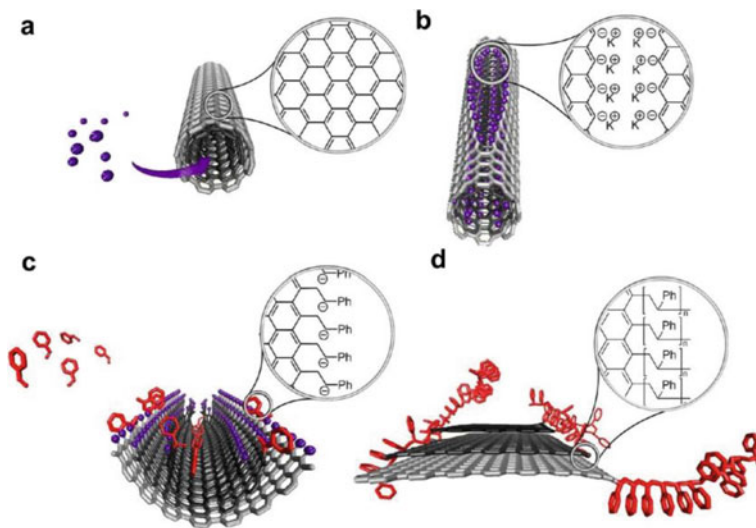
Fig. 9 Reaction scheme for the one-pot synthesis of functionalized GNRs. (**a**) The MWNTs are intercalated with potassium naphthalenide (*blue dots*). (**b**) A longitudinal fissure is formed in the walls of the MWNTs. (**c**) Polymerization of styrene (for instance) assists in exfoliation of MWNTs. (**d**) PF-GNRs are formed upon quenching (Reproduced with permission from Ref. [35], Copyright 2013 ACS)

during the reaction and can be used for the anionic polymerization. As the anions are believed to be generated during unzipping, they are selectively located at the edges of graphene nanoribbons (GNR) (Fig. 9). However, the amount of PS grafted-from such as nanoribbons was reported to be low (~9 wt %, for THF reaction), which may indicate that the formation of anions on the GNR is insufficient for the initiation, or the propagating anions undergo termination, or the sequential reduction of anion radicals is not prevalently occurring. Any of these factors may be responsible for a low graft-density observed by the authors (Table 1, entry 11). It should be mentioned here that the grafting of PS, $M_n = 5,000$ g/mol, for example, on every edge carbon for a theoretical rectangular GNR of 1,000 nm^2 at its length sides would exceed 99 wt % PS. Thus, the grafting efficiency is far less than the reaction scheme proposed in Fig. 9. Although unzipping is clearly evident by TEM images, the dispersion of GNR in any medium without appropriate functionalization would be difficult.

In another study, Zhang et al. used graphene oxide (GO) as a substrate for grafting polymers [36]. By taking advantage of readily accessible oxygen-containing groups on GO, the functional groups are reacted with isocyanate and then used for grafting nylon 6 via anionic ring-opening polymerization (ROP) of ε-caprolactam (Scheme 6, Fig. 10). The authors carefully studied the formation of key intermediates using nuclear magnetic resonance (NMR), FTIR, and XPS
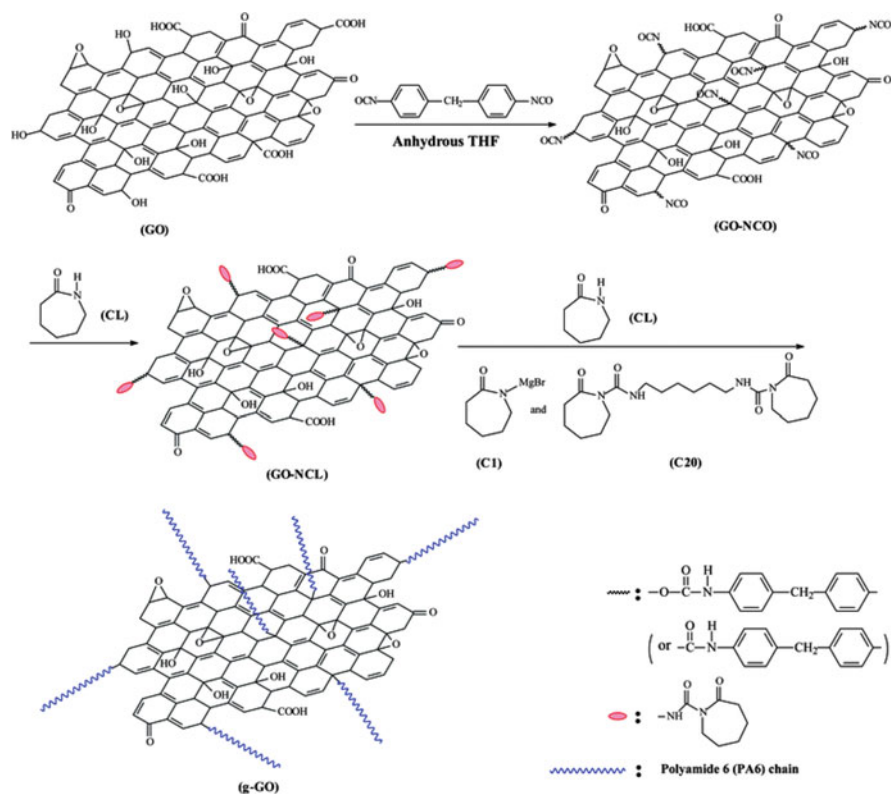
Scheme 6 Synthetic scheme of the modification of graphene oxide (GO) with caprolactam and subsequent grafting of nylon 6 by in situ anionic ring-opening polymerization (Reproduced with permission from Ref. [36], Copyright 2012 RSC)

spectroscopies and provided structural information about the nylon-grafted GO (Table 1, entry 12). The modification of GO was shown to enhance the mechanical and thermal properties of the corresponding nylon composites.

3.2 Anionic Polymerization from Carbon Nanotubes

The living nature of anionic polymerization [80] with its ability to afford polymers of narrow MWD and high molecular weight in a controlled way, even at very low initiator concentration, has made it an attractive choice in grafting polymers from CNTs. Viswanathan et al. [37] were the first to grow polymer from nanotubes via anionic polymerization. They introduced carbanions on the surface of the SWNTs through addition of *sec*-BuLi to the sp^2 carbons. The resulting resonance-stabilized carbanion on the SWNTs was used as initiating site for the polymerization of styrene. It was stated that a mutual electrostatic repulsion between the individual nanotubes could exfoliate the SWNT bundles. The amount of carbanion generated
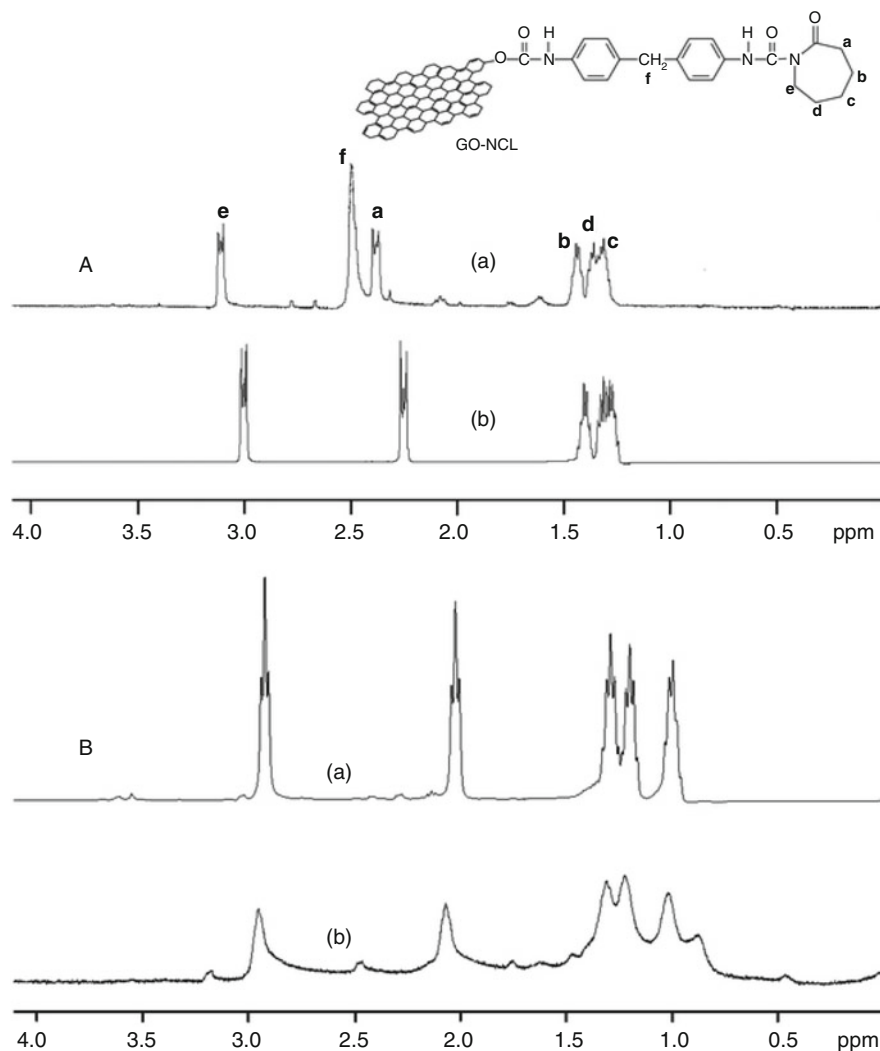
Fig 10 (**a**) ^{1}H NMR spectra of functionalized GO (*a*) and ε-caprolactam (*b*) in deuterated formic acid solution. (**b**) ^{1}H NMR spectra of nylon 6 (*a*) and *g*-GO (*b*) in deuterated formic acid solution (Reproduced with permission from Ref. [36], Copyright 2012 RSC)

on the SWNTs was not determined as the styrene polymerization was conducted in situ in the presence of free *sec*-BuLi. Thus, a concurrent solution polymerization produced PS nanocomposite consisting of MWNTs-*g*-PS. Grafting efficiency was determined after removing the free PS from MWNTs-*g*-PS through a solvent wash by TGA, and it was found to be very low (~10–15 wt %) (Table 1, entry 13). The functionalization with butyl groups and grafted PS was confirmed via Raman spectroscopy, which showed some differences in D/G ratio of the peaks (Fig. 11).
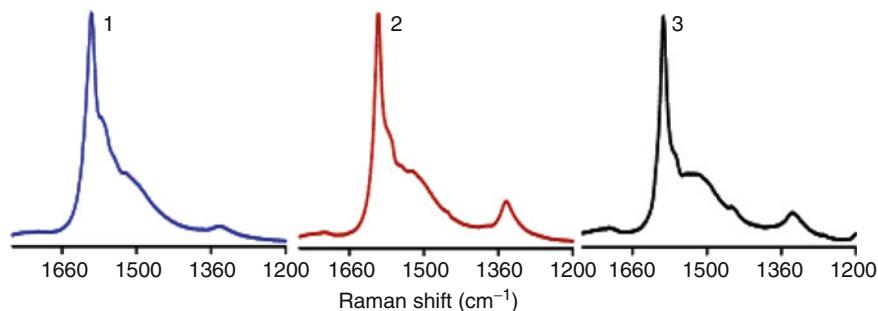
Fig. 11 Raman scattering spectra (514.4 nm) of (*1*) pristine SWNTs, (*2*) butylated SWNTs, and (*3*) PS-grafted SWNTs (Reproduced with permission from Ref. [37], Copyright 2003 ACS)

The observed T_g of the grafted PS in MWNTs-*g*-PS was higher by 15 °C than PS. More importantly, the PS-grafted SWNTs rendered excellent composites that had higher thermal stability even with very low nanotube loading (0.05 wt %), exhibiting good filler dispersion in the polymer matrix.

Using the same approach, Chen et al. [38] showed that the carbanions on the surface of SWNTs can initiate the polymerization of *tert*-butyl acrylate (*t*-BA) but not that of methyl methacrylate (MMA) (Scheme 7). The authors suggested that a possible reason for this behavior was the difference in the reactivity of the two monomers toward the delocalized carbanions on the SWNTs. However, the actual reason for this behavior is not clearly understood as the reactivity of the generated carbanions on the SWNTs was sufficient enough to initiate styrene as shown by Ajayan et al. [37]. Thus, the reactivity differences of the monomers may not be the reason for their observation. Nevertheless, the living nature of the polymerization was confirmed by initiating MMA from the growing P*t*BA enolate anions. The same group also synthesized a diblock copolymer (P*t*BA-*b*-PMMA) from SWNTs with 47 wt % polymer (Scheme 7, Table 1, entry 14).

On the other hand, Liang et al. [39] reduced SWNTs in the presence of Li in ammonia as anionic initiators for the polymerization of MMA.

They showed that an addition of Li/NH₃ to SWNTs leads to SWNT salts that have the ability to exfoliate SWNT bundles and grow PMMA. The CNTs with 45 wt % polymer were synthesized, and the average thickness of an amorphous polymer layer around the SWNTs was 1.0–1.5 nm, as calculated by AFM (Table 1, entry 15). The authors observed a noticeable Raman D-band in the "PMMA-grafted SWNTs" (Fig. 12). However, based on this single piece of evidence alone without a side-by-side comparison with control experiment, they concluded covalent linkage between PMMA chains, and the CNT surface. The enhanced D-band could arise simply from a Birch-like reduction of the preexisting defects in the nanotubes. The radical anion on the SWNTs and the presence of solvated electrons in Li/NH₃ solution can contribute for the formation of PMMA, and hence an inefficient washing of the SWNTs after the reaction may also produce similar results.
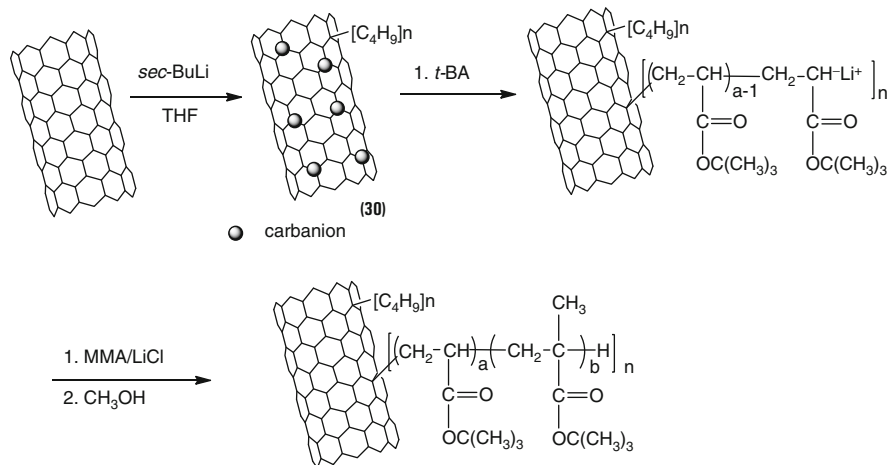
Scheme 7 Anionic polymerizations of methyl acrylate and methyl methacrylate from SWNTs and SWNT-*g*-(P*t*BA), respectively (Reproduced with permission from Ref. [77], Copyright 2013 RSC)
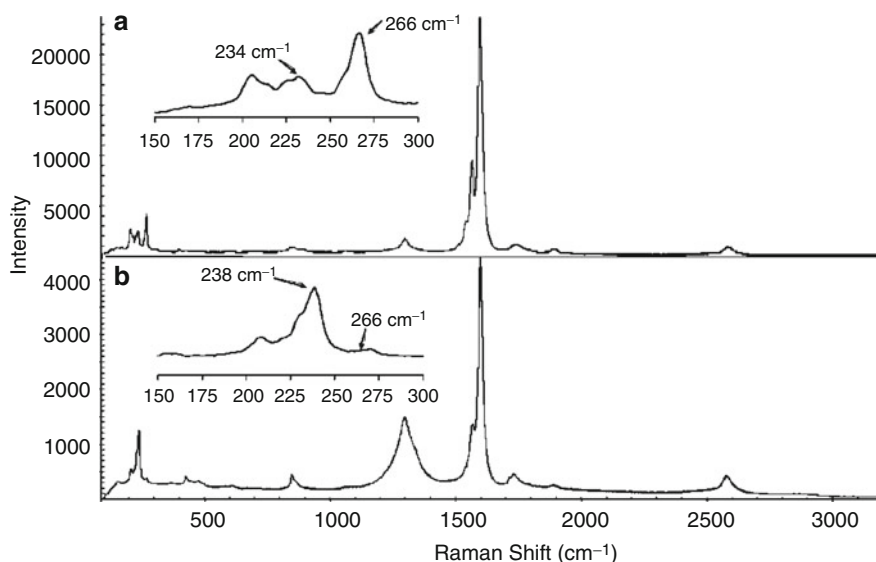
Fig. 12 Raman spectra (780 nm excitation) of pristine SWNTs (**a**) and PMMA-grafted SWNTs (**b**) (Reproduced with permission from Ref. [39], Copyright 2006 ACS)

In order to achieve a higher grafting efficiency with high molecular weight polymers, Baskaran and coworkers used a different approach [40] to grow PS from MWNTs via anionic polymerization. As mentioned previously, the direct reaction of *sec*-BuLi with the sp^2 carbon of MWNTs was inefficient [81, 37].
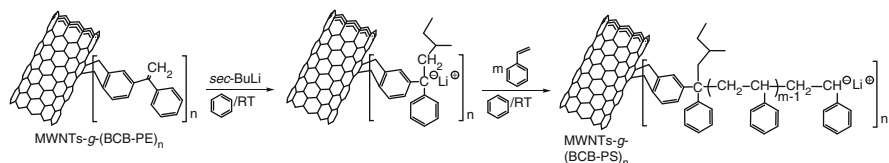
Scheme 8 Anionic polymerization of styrene from MWNTs-*g*-(BCB-PE)-grafted tubes in benzene at RT (Reproduced with permission from Ref. [40], Copyright 2008 ACS)

Therefore, they generated carbanion sites away from the CNT surface. Accordingly, the MWNTs were covalently functionalized with 1-benzocylcobutene-1-′-phenylethylene (BCB-PE) through a [4 + 2] Diels-Alder cycloaddition [82]. A statistical distribution of covalent attachment of the substituted diphenylethylene, a precursor initiator, was introduced throughout the surface of MWNTs. The presence of the olefin was confirmed by FTIR, Raman spectroscopy, and TGA. Reactive carbanions were generated from MWNTs-*g*-(BCB-PE)$_n$, by addition of *sec*-BuLi. The polymerization of styrene was initiated in benzene at room temperature under high-vacuum condition (Scheme 8). Although the typical red color of the phenylhexyllithium anion on the MWNTs was not seen, probably due to an intense black color of the solution, resulting from the gradual dispersion of PS-grafted MWNTs, the initiation of styrene from the surface-grafted phenylhexyllithium anions was found to be slow. This was attributed to the heterogeneous nature of the reaction. A small amount of MWNTs-*g*-initiator was insoluble in the reactor during the polymerization for about an hour. On the other hand, the polymerizations carried out for more than 90 min showed a complete dispersion of MWNTs during the polymerization. The surface-grown polymers were obtained in high conversion, forming MWNTs-*g*-PS containing only a small fraction of MWNTs (<1 wt %). A control polymerization of styrene was carried out using *sec*-BuLi in the presence of pristine MWNTs. Upon addition of styrene, an orange color appeared immediately indicating the initiation of styrene from the free initiator present in the solution. After the termination of the polymerization, the MWNTs were recovered by a thorough solvent wash in THF to remove the free PS. The recovered MWNTs did not have grafted PS as confirmed by TGA and transmission electron microscopy (TEM) analysis in the control experiment.

The MWNTs-*g*-PS were characterized by FTIR, ¹H-NMR, Raman spectroscopy, differential scanning calorimetry (DSC), TGA, and TEM. The TEM images showed the presence of a thick layer of polymer (~30 nm) around the surface of MWNTs (Fig. 13, Table 1, entry 16). The formation of diblock copolymer, MWNTs-*g*-PS-*b*-PI, confirmed the living nature of the polymerization from the surface.
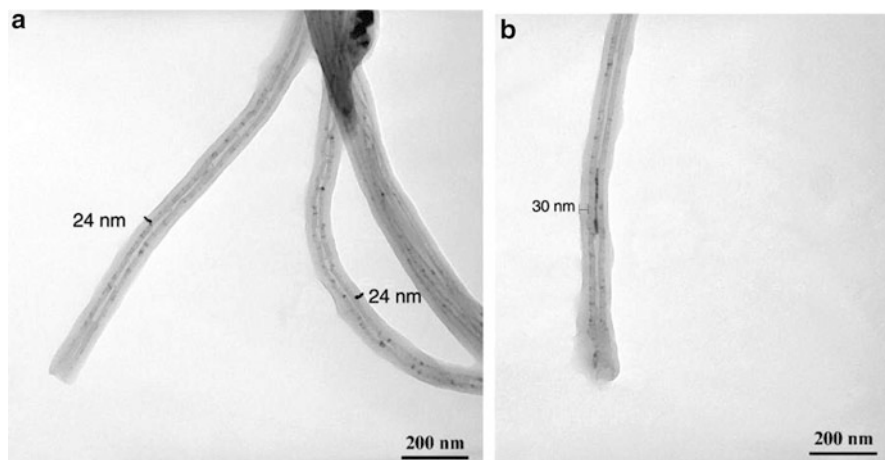
Fig. 13 TEM images of surface-grown PS exhibiting 24 nm (**a**) and 30 nm (**b**) PS layer on the surface of MWNTs (Reproduced with permission from Ref. [40], Copyright 2008 ACS)

3.3 Anionic Ring-Opening Polymerizations from Carbon Nanotubes

Aliphatic polyesters, such as poly(p-dioxanone), poly(ε-caprolactone), poly(L-lactide), polyethers (e.g., PEO), and polypeptides, are biocompatible and in most cases biodegradable polymers. These materials have been proven to be useful as scaffold in implantable medical devices, as surgical sutures and in drug delivery systems, since they eliminate the need for removal of the device after being used. Their synthesis involves ROP techniques [83]. Grafting polyether, polyamide, and polyester from CNTs is very important as these materials can be used as fillers in developing nanocomposites in commodity plastics to enhance mechanical property. The ROP can be performed by several initiating systems such as anionic, cationic, coordination, and metathesis.

3.3.1 Polyesters

Yoon et al. [41] used ROP to graft poly(p-dioxanone) (PPDX) from SWNTs via the grafting-from method. The surface of SWNTs was covalently attached with 6-amino-1-hexanol by reacting with the acid chloride-functionalized SWNTs in dimethylformamide (DMF). The produced hydroxy-functionalized SWNTs-(OH)$_n$ were then used for the initiation of p-dioxanone, in the presence of tin(II) 2--ethylhexanoate (Sn(Oct)$_2$). They found that the thermal stability of the grafted PPDX increased after the covalent attachment onto the SWNTs. The SWNTs-g-PPDX had no noticeable transition corresponding to T_g and T_m up to 125 °C,

although the pure PPDX showed these transitions at -13.4 and 103 °C, respectively. The changes in the grafted PPDX properties were attributed to a strong interaction between SWNTs and PPDX and a decreased mobility of the PPDX chains.

Several methods have been reported to introduce hydroxyl groups on CNTs for the polymerization of ε-caprolactone and other monomers using ROP [84–86]. The reaction of pristine MWNTs with various azide compounds via 1,3-cycloaddition [84], the use of diradicals via Bergman cyclization [85], and the conversion of acid groups of MWNTs to azide for copper-catalyzed Huisgen's 1,3-dipolar cycloaddition [86] with various functional alkynes are a few of these methods.

Buffa et al. [44] functionalized SWNTs produced by the CoMoCAT process, with 4-hydroxymethylaniline (HMA) via the diazonium salt method. The SWNTs-$(OH)_n$, generated by the functionalization, were then used to polymerize ε-caprolactone, in the presence of stannous octanoate as a catalyst. The dispersion of SWNTs grafted with poly(ε-caprolactone) (PCL) was tested in chloroform. A dramatic increase compared to that of neat SWNTs was observed due to the high solubility of PCL in chloroform. TGA of the samples indicated that the amount of PCL grafted was 63 wt % (Table 1, entry 20), while a combined TPD (temperature-programmed desorption)/TPO (temperature-programmed oxidation) technique revealed that the average polymer length was only 5 monomeric units. According to the authors, the two main factors for the limited growth of the grafted chains were the presence of nanotubes in the polymerization medium and the presence of adsorbed water on the CNT surface. The former acts as terminators while the latter as initiator generating a large amount of "free" PCL. Accordingly, it was suggested that an increase in the length of the PCL attached to the nanotubes can only be achieved when the adsorbed water from the nanotubes is eliminated.

In a similar work [45], the hydroxyl groups were introduced on the MWNT surfaces by reacting oxidized MWNTs with excess thionyl chloride and then with glycol. The -OH-functionalized MWNTs were used for the surface-initiated ROP of ε-caprolactone, in butanol at 120 °C in the presence of stannous octanoate. The content of the grafted polymer and the molecular weight of the free polymer initiated by the butanol were increased with increasing the feed ratio of monomer to initiating sites. The polydispersity indices of the free polymer were very broad reaching even 13.0, which was ascribed to the increased possibility of chain termination due to the presence of the CNTs. However, the actual mechanism of the propagating PCL anion undergoing termination with the sp^2 carbon network was not discussed. Biodegradation of the recovered MWNT-g-PCL was tested by using pseudomonas lipase as a bioactive enzyme catalyst. It was revealed that the grafted PCL chains retained their biodegradability and were completely degraded within 4 days.

The influence of MWNT-g-PCL on vapor sensing properties was investigated, by Castro et al. [46], for a series of conductive polymer composite (CPC) transducers. MWNTs-g-PCL were prepared by first reacting MWNTs-$(OH)_n$ with trimethylaluminum (catalyst) to produce aluminum alkoxide initiator followed by the anionic coordination ROP of ε-caprolactone (Scheme 9). AFM observations
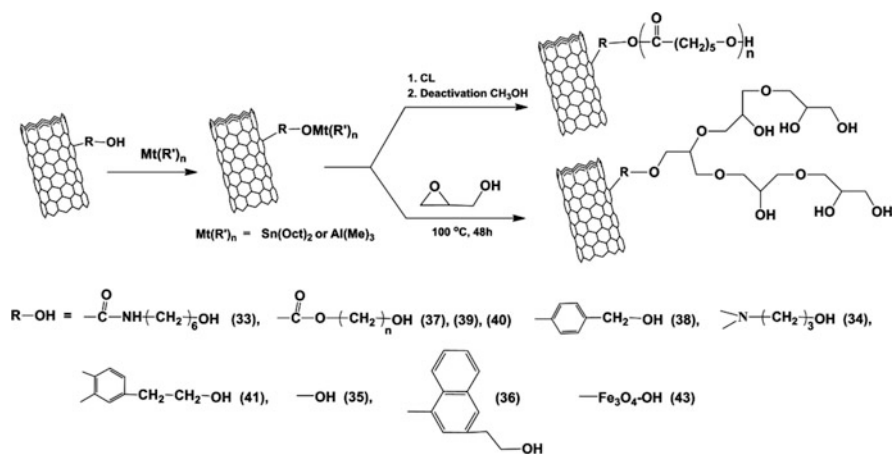
Scheme 9 Synthesis of MWNT-g-PCL and MWNTs-g-HPG using different types of initiators via anionic coordinative ring-opening polymerization (Reproduced with permission from Ref. [77], Copyright 2013 RSC)

allowed an evaluation of the MWNT coating and dispersion levels. Sensors were prepared by spray coating layer-by-layer MWNT-g-PCL solutions onto the inter-digitated copper electrodes that had been etched by photolithography onto an epoxy substrate. Chemo-electrical properties of CPC sensors exposed to different vapors (water, methanol, toluene, tetrahydrofuran, and chloroform) were analyzed in terms of signal sensitivity, selectivity, reproducibility, and stability. The MWNT-g-PCL sensors displayed a very good discrimination capability for all the vapors above (polar and nonpolar), which allowed for the preparation of sensors with a large detection spectrum. The chemo-electrical properties of the sensors exposed to different vapors were found to be reproducible, and the electrical signals displayed reversibility with a fast recovery.

A different synthetic approach for the grafting of ε-caprolactone on MWNTs was presented by Ruelle et al. [47]. MWNTs were placed under an atomic nitrogen flow formed by the dissociation of molecular nitrogen in $Ar + N_2$ mixed microwave plasma in order to covalently functionalize with primary and secondary amines. The amino-MWNTs were activated by triethylaluminum and then used as an initiator for ROP of ε-caprolactone. As revealed by TEM, functionalization was inhomogeneous, and the MWNTs had a high (10 atomic % N) of amine functionalization on the plasma exposed surface of the sample.

Biodegradable supramolecular hybrids of MWNT-g-PCL and α-cyclodextrins (α-CDs) (inclusion complexes), with potential applications in medicine and biology, were prepared by Yang et al. [48]. First, MWNTs were functionalized with hydroxyl groups (MWNTs-(OH)$_n$) via a nitrene cycloaddition with appropriate reagent. The reaction was followed by the surface-initiated ROP of ε-caprolactone in the presence of a metal catalyst to afford MWNTs-g-PCL. The TGA showed about 58 wt % of PCL was grafted onto the MWNTs and TEM images revealed the
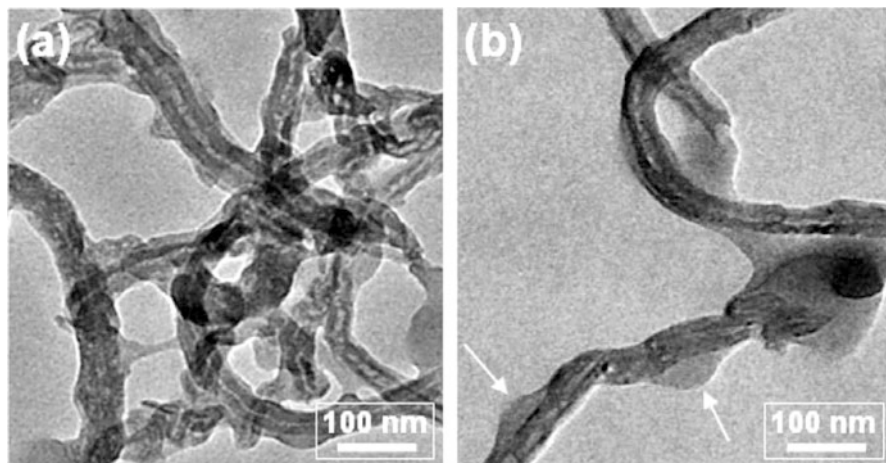
Fig. 14 TEM images of MWNTs-*g*-PCL complexed with α-CDs (**a** and **b**) (Reproduced with permission from Ref. [48], Copyright 2010 Elsevier)

presence of polymer layers with thicknesses in the range of 5–7 nm on the surface of the MWNTs (Table 1, entry 24). Inclusion complexes were formed by hydrogen bonds between the hydroxyl groups of α-CDs and the carbonyl groups of PCL, indicating that supramolecular polypseudorotaxanes were formed through α-CD channel threading onto the PCL chains of MWNT-*g*-PCL (Fig. 14). However, the size of uneven pimples shown in Fig. 14 was very large that it couldn't be interpreted only for supramolecular polypseudorotaxane formation. It is important to mention that the α-CD is also known to get adsorbed onto the CNTs [87]. Therefore, the contribution of adsorption and its influence on the reported results are not known.

Poly(L-lactide) (PLLA) is widely used in tissue engineering, drug delivery systems, and implant materials due to its excellent biocompatibility and biodegradability. However, the mechanical properties of PLLA for high load-bearing biomedical applications are insufficient. The PLLA nanocomposite containing CNTs has been implied to enhance the mechanical properties for various applications. The first attempt to polymerize L-LA from the surface of MWNTs was reported by Chen et al. [51]. Carboxylic acid-functionalized MWNTs were treated with SOCl$_2$, and the acyl chloride-containing CNTs were further reacted with butanediol in order to introduce hydroxyl groups on the surface. The polymerization of L-LA was performed in the presence of stannous octanote. The amount of grafted PLLA increased with time depending on the polarity of the reaction medium. When the polymerization was carried out in DMF, the amount of grafted PLLA on the MWNTs was higher than that obtained in toluene.

Nanocomposites of PLLA with MWNTs-*g*-PLLA were prepared and tested for mechanical property enhancement. The authors claimed that the incorporation of 1 wt % of MWNT-*g*-PLLA in PLLA matrix didn't show any indication of
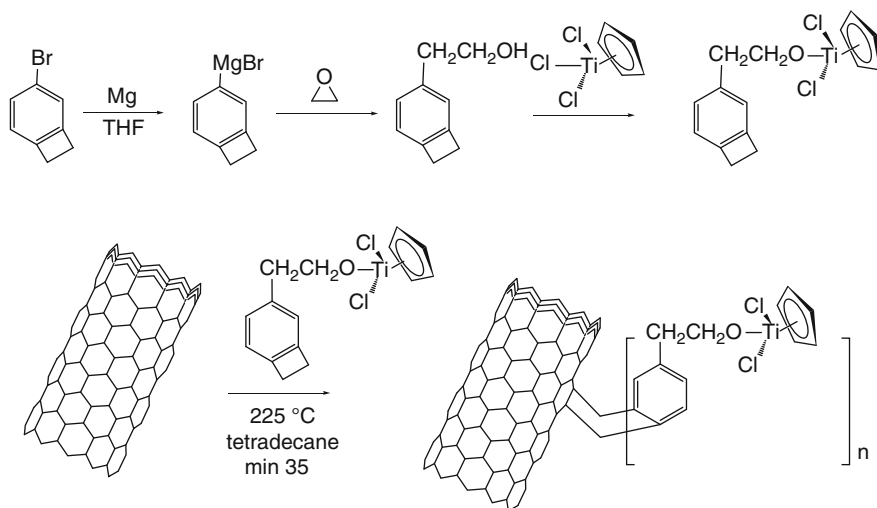
Scheme 10 Grignard synthesis of (1-benzocyclobutene ethoxy) dichlorocyclopentadienyl-titanium (BCB-EOTiCpCl$_2$) and covalent functionalization of MWNTs using a [4 + 2] Diels-Alder cycloaddition reaction (Reproduced with permission from Ref. [54], Copyright 2009 ACS)

aggregation based on SEM, and the nanocomposites exhibited high tensile strength and modulus rendering PLLA more resistant to deformation. Thermal stability, electrical conductivity, as well as mechanical properties of PLLA nanocomposites containing MWNT-g-PLLA were also studied [53, 52]. Good interfacial adhesion between MWNTs and the polymer matrix in PLLA/MWNT-g-PLLA composites also increased the activation energy compared to PLLA/MWNT, indicating that the former was thermally more stable.

Recently, Priftis and coworkers [54] used a titanium alkoxide catalyst (TiCpCl$_2$) to polymerize $_L$-LA, ε-CL, and n-hexyl isocyanate from SWNTs and MWNTs. A Diels-Alder cycloaddition was used to covalently attach benzocyclobutene functionalized with titanium alkoxide, to the sidewalls of CNTs (Scheme 10). The grafted CNTs were used for the titanium-mediated SIP of different monomers. Kinetic study of the $_L$-LA polymerization indicated that the initiation was very slow and characterized by an induction period of about 4 h. After this period, the polymerization medium became homogeneous; the polymerization proceeded fast giving enhanced efficiency for grafting polymers on the CNTs, and the viscosity of the reaction medium was substantially increased in less than 5 h. The long induction period could be attributed to a steric hindrance of MWNT-titanium complex for the initiation. Titanium-mediated coordination polymerization of $_L$-LA, using the same solvent and catalyst, in the absence of CNTs had also an induction period of an hour. The grafted polymer content could be adjusted using the reaction time, when the mole feed ratio of monomer to the grafted initiator was kept constant. A control experiment was performed in which a known amount of the precursor catalyst CpTiCl$_2$(OCH$_2$CH$_3$) was mixed with pristine CNTs in order to study the influence

of Cp ring adsorption onto the CNTs through π-π stacking. A similar procedure as for the MWNTs-*g*-BCB-EOTiCpCl$_2$ was used for the polymerization and found that the MWNTs could be recovered after the polymerization without any polymer grafted on it. This confirmed the absence of polymer adsorption. The polymerization of ε-CL showed a similar trend as the $_L$-LA, while in the case of *n*-hexyl isocyanate the monomer conversion was very low (10 %) even after 20 h of the polymerization.

Cai and coworkers [55] used MWNT-(OH)$_n$ for the copolymerization of L-lactide and ε-caprolactone in the presence of stannous octanoate as the catalyst. The copolymer poly(L-lactide-*co*-caprolactone) nanocomposites with MWNT-*g*-poly(L-lactide-*co*-caprolactone) showed an increase in tensile strength and a decrease in elastic modulus compared to the neat copolymer. The same group used MWNTs that were first functionalized with FeO$_4$-OH for the polymerization of L-LA. The PLLA nanocomposite materials prepared with MWNTs-*g*-PLLA exhibited superparamagnetic performance, and it was possible to align under low magnetic field [56].

3.3.2 Polyethers

Grafting polyethylene oxide (PEO) from CNTs will enable dissolution of CNTs in water and can be used for medical applications. Baskaran and coworkers polymerized ethylene oxide (EO) via anionic ROP from MWNTs functionalized with hydroxyl groups (Scheme 11) [40]. The MWNTs were first covalently functionalized with 4-hydroxyethyl benzocyclobutene (BCB-EO) through [4 + 2] Diels-Alder cycloaddition. The attachment of the BCB-EO, a hydroxyl precursor, was confirmed by FTIR, Raman spectroscopy, and TGA. Polymerization of ethylene oxide was performed under high vacuum using break-seal technique (Fig. 15a). Triphenylmethyl potassium was used to convert the hydroxyl groups on the surface of MWNTs into alkoxide anions. As alkoxide anions exist in rapid equilibrium with the remaining hydroxyl groups in the presence of potassium counterion, a minimum of 30 mol %, hydroxyls was converted into alkoxide anions. The initiation of ethylene oxide from the surface alkoxy anions was very slow. The heterogeneous nature of the reaction and the aggregation of alkoxide anions in the presence of MWNTs could be attributed to a slow propagation. However, at a constant mole
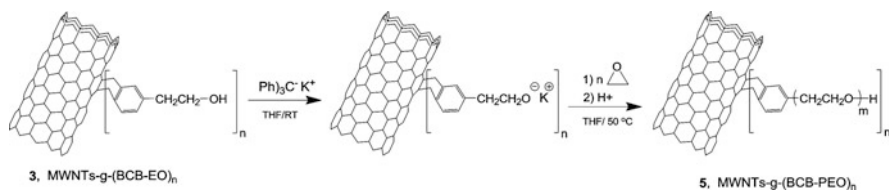
Scheme 11 Surface-initiated anionic polymerization of ethylene oxide from MWNTs-*g*-(BCB-EO)$_n$ surface (Reproduced with permission from Ref. [40], Copyright 2008 ACS)
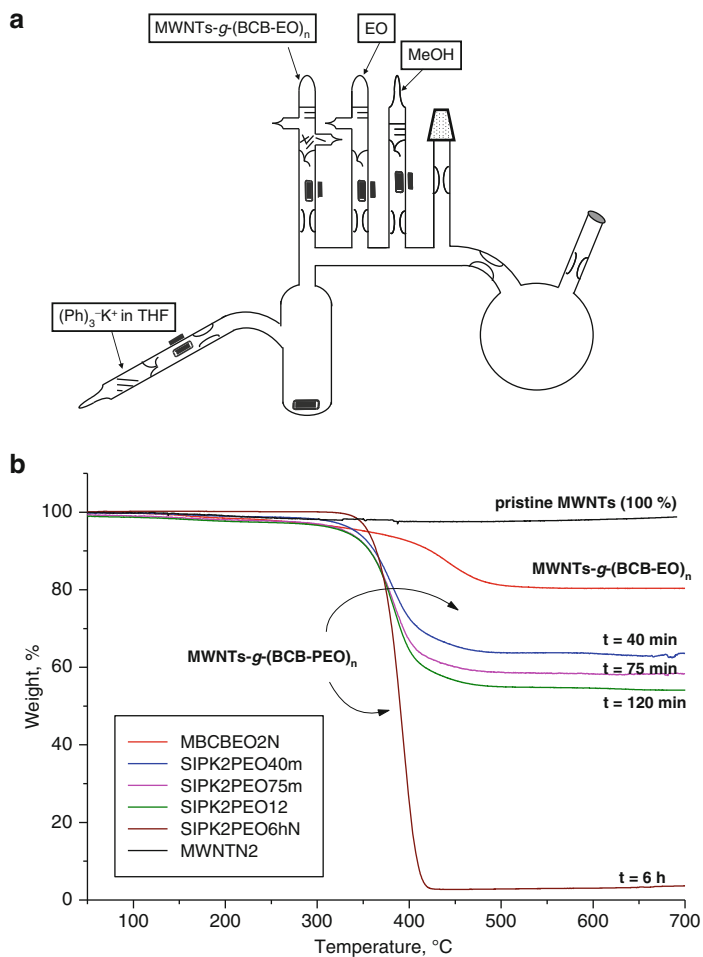
Fig. 15 (**a**) All-glass reactor used for the surface-initiated anionic polymerization of ethylene oxide from MWNTs and (**b**) TGA of MWNTs-*g*-(BCB-PEO)$_n$ at various reaction times in the surface-initiated anionic polymerization of ethylene oxide from MWNTs-*g*-(BCB-EO)$_n$ in THF at 40 °C (Reproduced with permission from Ref. [40], Copyright 2008 ACS)

ratio of monomer to the grafted initiator, the amount of grafted polyethylene oxide (PEO) increased gradually with increasing the polymerization time. The monomer conversion also increased gradually with polymerization time reaching a maximum of 57 % after 48 h, indicating a slow propagation of the surface polymerization (Fig. 15b). The surface-grown polymers were obtained in high wt fraction, forming MWNTs-*g*-PEO containing only a small fraction of MWNTs <4 wt % (Table 1, entry 16).

For samples obtained after a long polymerization time, it was not possible to filter the reaction solution through a Teflon membrane, and the samples were

recovered by precipitation in non-solvent. Size exclusion chromatography (SEC) analysis, using light scattering detector, of these samples showed the presence of multiple peaks. This was attributed to the fact that MWNTs are broadly distributed in terms of length, diameter, and also chemical functionality. Although these samples could be analyzed using SEC, with a styrene-divinylbenzene cross-linked gel column, an efficient resolution of different molecules based on their size is not possible. The hydrodynamic volume of MWNTs-g-PEO is expected to be very high as the tubes are long, and most of them will pass through interparticle gaps rather than getting into the pores. Therefore, such an analysis would only give an apparent molecular weight that can be used for a relative comparison within a set of experiments. One must be careful in treating the $M_{n,(app)}$ obtained from SEC due to the reasons mentioned above. Nevertheless, the MWNT-g-PEO samples taken at different polymerization time showed (in SEC) an increase in apparent molecular weight indicating overall control on the molecular weight of the grafts is possible in these reactions. Light scattering detector showed multiple peaks corresponding to a few thousands to few millions in weight average molecular weight, confirming the presence of multiple distributions of high molecular weight species. The TEM images showed the presence of thick layers of grafted PEO, nonuniformly distributed along the whole surface (Fig. 16).

Very recently, Sakellariou et al. [49] studied the kinetics of ROP of ε-CL from MWNTs and the crystallization behavior of the MWNTs-g-PCL together with that of MWNTs-g-PEO. The polymerization could be controlled with time, though the reaction proceeded rapidly. As revealed by TGA, a 98 wt % PCL was grafted after 4 h, and 70 % monomer conversion was achieved (Table 1, entry 25). A remarkable
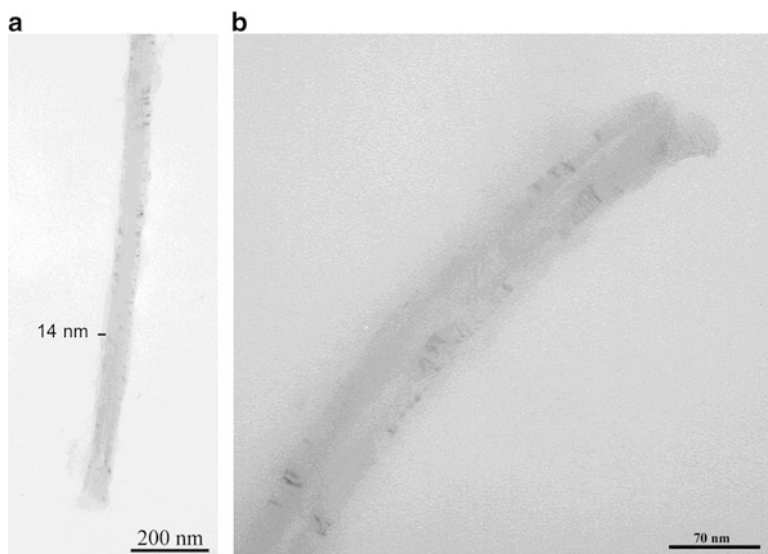
Fig. 16 TEM images of MWNTs-g-(BCB-PEO)$_n$ (**a**, **b**) with nonuniform PEO-grafted chain on the surface of MWNTs (Reproduced with permission from Ref. [40], Copyright 2008 ACS)

nucleation effect was observed by the incorporation of MWNTs that reduced the supercooling needed for crystallization of both PCL and PEO. Furthermore, the isothermal crystallization kinetics of the grafted PCL and PEO were substantially accelerated compared to the neat polymers, which were attributed to the anchoring of the chain ends to the MWNTs via covalent bonding.

In another study by Sakellariou et al. [50], diblock copolymers were grafted onto MWNTs via a combination of polymerization techniques. Using the same method above, a substituted benzocyclobutene containing hydroxyl group was attached on the surface of MWNTs and later used for the polymerization of EO or ε-CL. The hydroxyl groups of the grafted polymer chain ends were used for the initiation of second block. Accordingly, the chain ends of the MWNTs-g-PEO were used as ROP macroinitiator for the polymerization of ε-CL resulting in biocompatible MWNT-g-(PEO-b-PCL). By esterification of the hydroxyl PEO end groups with excess 2-bromoisobutyryl bromide, an ATRP macroinitiator was obtained and used for the polymerization of styrene and 2-(dimethylamino)ethylmethacrylate (DMAEMA) resulting in diblock copolymer grafted MWNTs, which had very high ($>$90 wt %) grafted polymer content (Table 1, entry 25). This strategy, through a combination of two different polymerization techniques, widens the opportunities for the synthesis of even more complex macromolecular structures on the CNT surface.

Gao's group [42] performed anionic ROP of glycidol (2,3-epoxy-1-propanol) in dioxane using potassium methoxide as a catalyst, to grow hyperbranched polyglycerol (HPG) from MWNT-(OH)$_n$ surfaces. The macroinitiator, MWNT-OH, was prepared by reacting with 2-azidoethanol in N-methyl-2-pyrrolidone. The amount of grafted HPG was adjusted, up to 90 wt %, by changing the feed ratio of glycidol to MWNTs-(OH)$_n$ (Table 1, entry 18). When the polymerization was conducted in bulk, the grafted polymer content was never higher than 45 wt %, even at high feed ratios of glycidol to MWNTs-(OH)$_n$. The authors ascribed this phenomenon to the higher viscosity of the reaction mixture in the bulk polymerization. In fact, an extended aggregation of propagating center with potassium counterion and a lack of solvation of counterion could be the other reasons for poor conversion of HPG in the absence of solvent. A concurrent self-condensing ROP of glycidol through counterion exchange to the monomer was monitored. The number average molecular weights of the free HPGs increased linearly with increasing feed ratio of monomer to initiating site, and the polydispersity indices were relatively low ($<$1.8). Although the authors claimed that the polymerization had a living character, such a high MWD confirms that the polymerization proceeded with severe side reactions in the presence of CNTs. The HPG grafted MWNTs (MWNTs-g-HPG) were recovered by dispersion in methanol, followed by centrifugation and washing several times with excess methanol. The remaining solid, MWNTs-g-HPG, was dried overnight. By reacting to the hydroxy groups of the grafted HPG with palmitoyl chloride, they produced MWNT-g-amphiphilic hyperbranched polymers. The resulting product showed good solubility in weak polar or nonpolar solvents in contrast to MWNTs-g-HPG, which were soluble only in strong polar solvents. Fluorescent MWNTs were also prepared by attaching rhodamine 6B molecules to the surface of MWNT-g-(HPG). The abundance of

functional groups on the surface of CNT hybrids can be used as a nanoplatform to conjugate functional molecules for further application in drug delivery, cell imaging, and bioprobing.

Another route for the synthesis of biocompatible and biodegradable CNT hybrids was reported by Adeli et al. [43]. Hyperbranched molecular trees were grown from the surface of MWNTs via in situ anionic ROP of glycidol as described in Scheme 9. Short-term in vitro cytotoxicity and hemocompatibility tests were conducted on HT 1,080 cell line (human fibrosarcoma) for MWNTs-g-HPG. The results showed no sign of toxicity for concentrations up to 1 mg/mL after 24 h of the incubation.

3.3.3 Poly(peptides) and Polyamides

Primary amine acts as an initiator for the polymerization of cyclic amino acids via N-carboxyanhydride (NCA) method to produce polypeptides with controlled molecular weight [88]. The ROP was used to graft a polypeptide from the surface of MWNTs [57]. Oxidized MWNTs were converted into an amine-functionalized MWNTs by amidation of the carboxylic groups with excess of 1,6-diaminohexane. The MWNTs-$(NH_2)_n$ were then used for ROP of γ-benzyl-L-glutamate N-carboxyanhydride (BLG-NCA) (Scheme 12). The resulting hybrid material exhibited core-shell morphology with thickness of the polypeptide layer ranging from 4 to 22 nm. The thickness of the polypeptide could not be controlled by the feed ratio of NCA monomer to MWNTs-$(NH_2)_n$. The MWNT-g-$(PBLG)_n$ was soluble in strong polar solvents, such as DMF and dimethyl sulfoxide, and insoluble in weak polar solvents, such as acetone and esters.

Poly(L-lysine) is a biocompatible and biodegradable polymer, and its structure facilitates various modifications, including conjugation with transferrin, epidermal growth factor, and fusogenic peptides, and thus has been widely used in the field of gene and drug delivery. Surface-initiated ROP of ε-(benzyloxycarbonyl)-L-lysine N-carboxyanhydride used the amine groups of the functionalized MWNTs and resulted in MWNT-g-PLys(Z) [58]. Acidolysis of the benzyl carbamate groups afforded water-soluble MWNT-g-PLL. Core-shell structures were determined by high-resolution TEM with the polymer shell thickness varying between 4 and 18 nm. The heterogeneous coverage of the polymer is resulting from the random distribution of amine groups on the MWNT walls. A thicker polymer layer was observed at the bends and tips than at the straight sections.
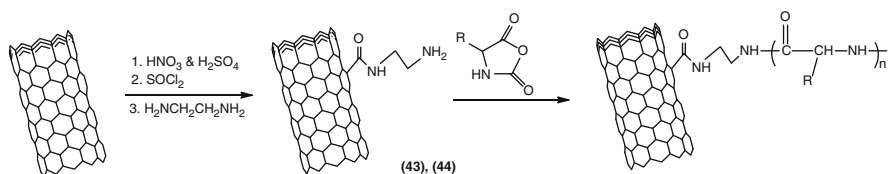
Scheme 12 Surface-initiated ROP of γ-benzyl-L-glutamate from MWNTs (Reproduced with permission from Ref. [77], Copyright 2013 RSC)

A more detailed work involving the surface-initiated ROP of BLG-NCA from amine-functionalized SWNTs revealed that chemically grafted PBLG adopted a random-coil conformation in contrast to the physically adsorbed PBLG, which exhibits an α-helical conformation [59]. It appears that intermolecular interactions of the grafted chains anchored at the one end are not favoring the helical conformation. Microfibers of PBLG nanocomposite containing SWNT-g-PBLG were prepared by electrospinning. Wide-angle X-ray scattering diffractograms suggested the SWNTs-g-PBLG were evenly distributed among PBLG rods in the solution and in the solid state, where PBLGs formed a short-range nematic phase inter-dispersed with amorphous domain.

Anionic ROP was used by Qu et al. [60] to functionalize SWNTs with nylon 6. Nylon 6 is an important commodity polymer used in a wide variety of applications. Thus, the synthesis of nylon-functionalized carbon nanotubes is expected to improve mechanical properties. ε-Caprolactam was covalently attached to the surface of the SWNTs. The monomer-grafted SWNTs were used for the polymerization of the same monomer in bulk to grow nylon 6. The nylon 6-grafted SWNTs, SWNTs-g-nylon 6, contained approximately 30 wt % polymer and were soluble in some organic solvents, such as formic acid and m-cresol (Table 1, entry 35).

The covalent functionalization of MWNTs with nylon 6 was also reported by Adronov et al. [61]. Isocyanate-functionalized CNTs, prepared by reacting MWNTs-(OH)$_n$ with excess of toluene 2,4-diisocyanate, were used as an initiator in anionic ROP of ε-caprolactam, in the presence of a sodium caprolactamate catalyst. A series of polymerizations was performed in order to investigate the effect of the reaction time and of the feed ratio (monomer/MWNT initiator) on the grafting efficiency (f_{wt} %). The results indicated an increase of the f_{wt} % with polymerization time, reaching a limiting value after 6 h and only roughly controlled by adjusting the monomer to the initiator feed ratio within the range between 150 and 800.

Polyamide 6 (PA6) was grafted from MWNTs by Yan et al. [62] in a two-step process. Initially, MWNTs were covalently functionalized with copolymer (styrene-maleic anhydride) (SMA). In the second step, in situ anionic ROP was used for the polymerization of ε-caprolactam activated by the maleic anhydride groups from the grafted polymer on the MWNTs. The MWNT-g-PA6 was homogeneously dispersible in organic solvents such as formic acid and could melt when mixed with ε-caprolactam. In a related study, by the same group, a similar grafting was performed using toluene 2,4-diisocyanate (TDI)-functionalized MWNTs [63].

3.4 Anionic Polymerization from Cross-Linked PS

Other than carbon materials, insoluble plastics, such as cross-linked PS beads, also represent a main category of organic support. Anionic SIP on this platform has been studied mainly by Endo and co-workers from Japan. Specifically, the authors first attached 2-bromoisobutyrate moiety by the condensation of 2-bromoisobutyric acid
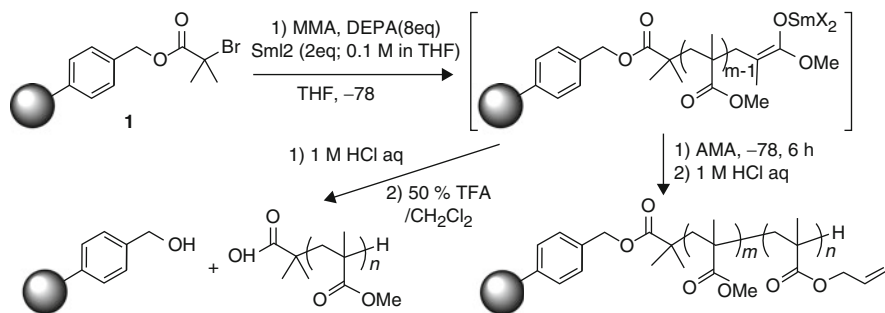
Scheme 13 Samarium (III) enolate formation and living anionic polymerization of methacrylate monomers (Reproduced with permission from Ref. [64], Copyright 2000 RSC)

with cross-linked polystyrene containing hydroxymethyl groups. Afterward, MMA anionic polymerization was initiated by samarium(III) enolate, which was generated in situ by the reduction of the corresponding bromoisobutyrate moiety using divalent samarium iodide (SmI_2). It was also demonstrated that the SIP is living, as shown by the successful block copolymerization of a second type of methacrylate (Scheme 13) [64]. Later, the same technique was extended to allyl methacrylate [65] and hydroxyethyl methacrylate [66].

4 Conclusion

Surface modification of organic and inorganic substrates using polymer grafting is critical for the development of the interface-integrated devices (sensors and actuators), self-assembly patterning, and nanocomposites in various technologies. Among several controlled polymerization techniques used for the surface-initiated polymerization from nanomaterials, living anionic polymerization has great advantages over the control of the molecular weight, the distribution, and the conformation of the polymer brushes. Although results reported so far, in several publications, indicate that obtaining predetermined graft-length and graft-density via surface-initiated anionic polymerization is very complex, it is possible to have a correction of experimental condition and these parameters for a particular system. The complexity arises from factors such as surface impurities, variations in initiator/co-initiator attachment and activation efficiencies, and the heterogeneous reaction with a wide distribution of nanomaterial's shapes and sizes.

   More importantly, the efficiency of formation and the reactivity of ion-pairs in closely packed self-assembled monolayer anions on a flat substrate appear to be low as indicated by the grafting of one PS chain in 18 molecules of SAM initiator. Research in this area so far indicates a significant progress toward understanding of surface grafting and exhibits a feasibility of surface modification of nanomaterials using living anionic polymerization. However, it requires further fundamental

understanding of the efficacy and the properties of quasi-two-dimensional ionic interface-mediated polymerization for constructing precisely controlled surfaces.

Abbreviations

2VP	2-Vinylpyridine
AFM	Atomic force microscopy
AMA	Allyl methacrylate
APA	3-Azidopropan-1-amine
ATRP	Atom transfer radical polymerization
BCB-EO	4-Hydroxyethyl benzocyclobutene
BCB-PE	1-Benzocylcobutene-1′-phenylethylene
BD	Butadiene
BIBA	2-Bromoisobutyric acid
BMBP	4′-Bromo-4-mercaptobiphenyl
BuLi	*sec*-Butyl lithium
BuOLi	Lithium *tert*-butoxide
CMS	Chloromethylstyrene
CNTs	Carbon nanotubes
CoMoCAT	Co-Mo catalyst
CPC	Conductive polymer composite
CP-TES	(3-Chloropropyl)triethoxysilane
$CpTiCl_3$	Cyclopentadienyltitanium(IV) trichloride
d	Density
DAH	1,6-Diaminohexane
DCB	Dichlorobenzene
DEPA	*N*,*N*-diethylphenylacetamide
DMAEMA	2-(Dimethylamino)ethylmethacrylate
DMF	Dimethoxyethylene
DPE	1,1′-Diphenylethylene
DSC	Differential scanning calorimetry
ε-Boc-$_L$-Lys-NCA	ε-(Benzyloxycarbonyl)-$_L$-lysine *N*-carboxyanhydride
ε-CL	ε-Caprolactam
EDA	Ethylene diamine
EG	Ethylene glycol
EO	Ethylene oxide
FT	Film thicknesses
FTIR	Fourier transform infrared
GNRs	Graphene nanoribbons
GO	Graphene oxide
HEMA	Hydroxyethyl methacrylate
HPG	Hyperbranched polyglycerol
I	Isoprene

ᴌ-LA	ᴌ-Lactide
MA	Maleic anhydride
MDI	4,4′-Methylenebis(phenyl isocyanate)
MeOH	Methanol
MeOK	Potassium methoxide
MeONa	Sodium methoxide
MMA	Methyl methacrylate
MWD	Molecular weight distribution
MWNT	Multiwalled carbon nanotubes
NaCL	ε-Caprolactam sodium salt
NCA	N-carboxyanhydride
NMR	Nuclear magnetic resonance
NMR	Nuclear magnetic resonance
NMRP	Nitroxide-mediated radical polymerization
PA6	Polyamide 6
PBLG	Poly(γ-benzyl-ᴌ-glutamate)
PCL	Poly(ε-caprolactam)
PEO	Poly(ethylene oxide)
PI	Polyisoprene
PLLA	Poly(ᴌ-lactide)
PMMA	Poly(methyl methacrylate)
PPDX	Poly(p-dioxanone)
PS	Polystyrene
PVP	Poly(2-vinyl pyridine)
RAFT	Reversible addition fragmentation chain transfer polymerization
ROP	Ring-opening polymerization
RT	Room temperature
S	Styrene
SAM	Self-assembled monolayer
SEC	Size exclusion chromatography
SIAP	Surface-initiated anionic polymerization
SIP	Surface-initiated polymerization
SmI$_2$	Samarium(II) iodide
Sn(Oct)$_2$	Tin(II) 2-ethylhexanoate
SWNT	Single-walled carbon nanotubes
t-BA	$tert$-Butyl acrylate
TEM	Transmission electron microscopy
TGA	Thermal gravimetric analysis
THF	Tetrahydrofuran
TMEDA	Tetramethylethylenediamine
XPS	X-ray photoelectron spectroscopy
α-CDs	α-Cyclodextrins
γ-BLG-NCA	γ-Benzyl-ᴌ-glutamate N-carboxyanhydride

References

1. (a) Staudinger H (1920) Über polymerisation. Ber Deut Chem Ges 53(6):1073. doi:10.1002/cber.19200530627; (b) Paul JF (1953) Principles of polymer chemistry. Cornell University Press, USA; (c) Ajayan PM, Schadler LS, Braun PV (2003) Nanocomposite science and technology, Wiley, Weinheim

2. Hussain F, Hojjati M, Okamoto M, Gorga RE (2006) Review article: polymer-matrix nanocomposites, processing, manufacturing, and application: an overview. J Compos Mater 40(17):1511–1575. doi:10.1177/0021998306067321

3. Paul DR, Robeson LM (2008) Polymer nanotechnology: nanocomposites. Polymer 49(15): 3187–3204. doi:10.1016/j.polymer.2008.04.017

4. Munch E, Launey ME, Alsem DH, Saiz E, Tomsia AP, Ritchie RO (2008) Tough, bio-inspired hybrid materials. Science 322(5907):1516–1520. doi:10.1126/science.1164865

5. Tang ZY, Kotov NA, Magonov S, Ozturk B (2003) Nanostructured artificial nacre. Nat Mater 2(6):413–U418. doi:10.1038/nmat906

6. Kuilla T, Bhadra S, Yao DH, Kim NH, Bose S, Lee JH (2010) Recent advances in graphene based polymer composites. Prog Polym Sci 35(11):1350–1375. doi:10.1016/j.progpolymsci.2010.07.005

7. Moniruzzaman M, Winey KI (2006) Polymer nanocomposites containing carbon nanotubes. Macromolecules 39(16):5194–5205. doi:10.1021/ma060733p

8. Thostenson ET, Ren ZF, Chou TW (2001) Advances in the science and technology of carbon nanotubes and their composites: a review. Compos Sci Technol 61(13):1899–1912. doi:10.1016/s0266-3538(01)00094-x

9. Giannelis EP (1996) Polymer layered silicate nanocomposites. Adv Mater 8(1):29–35. doi:10.1002/adma.19960080104

10. Ajayan PM, Schadler LS, Giannaris C, Rubio A (2000) Single-walled carbon nanotube-polymer composites: strength and weakness. Adv Mater 12(10):750–753. doi:10.1002/(sici)1521-4095(200005)12:10<750::aid-adma750>3.0.co;2-6

11. Wittmer JP, Cates ME, Johner A, Turner MS (1996) Diffusive growth of a polymer layer by in situ polymerization. Europhys Lett 33(5):397–402. doi:10.1209/epl/i1996-00347-0

12. Advincula R (2006) Polymer brushes by anionic and cationic Surface-Initiated Polymerization (SIP). In: Jordan R (ed) Surface-initiated polymerization I, vol 197, Advances in polymer science. Springer, Berlin, pp 107–136. doi:10.1007/12_066

13. Zhou Q, Nakamura Y, Inaoka S, Park M, Wang Y, Mays J (2002) In: Krishnamoorti R, Vaia R A (eds) Polymer nanocomposites. ACS symposium series No 804. American Chemical Society, Washington, DC

14. Zhou QY, Fan XW, Xia CJ, Mays J, Advincula R (2001) Living anionic surface initiated polymerization (SIP) of styrene from clay surfaces. Chem Mater 13(8):2465–2467. doi:10.1021/cm0101780

15. Quirk RP, Mathers RT (2001) Surface-initiated living anionic polymerization of isoprene using a 1,1-diphenylethylene derivative and functionalization with ethylene oxide. Polym Bull (Berlin) 45:471–477. doi:10.1007/s002890170100

16. Advincula R, Zhou Q, Mays J (2001) Nanocomposite materials by surface initiated polymerization on silicate, clay, and Si-gel surfaces: Preparation of high performance barrier materials. Polym Mater Sci Eng 84:875

17. Quirk RP, Mathers RT (2001) Surface grafting to and from 1,1-diphenylethylene using a surface-bound monolayer and functionalization of the living chain ends with ethylene oxide. Polym Mater Sci Eng 84:873

18. Quirk RP, Mathers RT (2001) Surface grafted poly(isoprene-block-ethylene oxide) diblock copolymer brushes from a 1,1-diphenylethylene surface-bound monolayer. Polym Mater Sci Eng 85:198

19. Zhou Q, Fan X, Xia C, Mays J, Advincula R (2001) Anionic polymerization initiated from Si-gel and clay nanoparticle surfaces. Polym Mater Sci Eng 84:835

20. Zhou Q, Nakamura Y, Inaoka S, Park M, Wang Y, Mays J, Advincula R (2000) Surface initiated anionic polymerization on silica and silicate surfaces. Polym Mater Sci Eng 82:290

21. Zhou Q, Wang S, Fan X, Mays J, Advincula R, Sakellariou G, Pispas S, Hadjichristides N (2001) Nanocomposite materials prepared by surface initiated anionic polymerization from Si-gel and clay nanoparticle surfaces: homopolymers and block-copolymers. Polym Prepr (Am Chem Soc Div Polym Chem) 42:59

22. Quirk RP, Mathers RT, Cregger T, Foster MD (2002) Anionic synthesis of block copolymer brushes grafted from a 1,1-diphenylethylene monolayer. Macromolecules 35(27):9964–9974. doi:10.1021/ma011536n

23. Baskaran D, Sivaram S (1997) Specific salt effect of lithium perchlorate in living anionic polymerization of methyl methacrylate and *tert*-butyl acrylate. Macromolecules 30(6): 1550–1555. doi:10.1021/ma961118w

24. Wiles DM, Bywater S (1965) Polymerization of methyl methacrylate initiated by 1,1-diphenylhexyl lithium. Trans Faraday Soc 61(505P):150–158. doi:10.1039/tf9656100150

25. Jordan R, Ulman A, Kang JF, Rafailovich MH, Sokolov J (1999) Surface-initiated anionic polymerization of styrene by means of self-assembled monolayers. J Am Chem Soc 121(5):1016–1022. doi:10.1021/ja981348l

26. Milner ST, Witten TA, Cates ME (1988) Theory of the grafted polymer brush. Macromolecules 21(8):2610–2619. doi:10.1021/ma00186a051

27. Sakellariou G, Park M, Advincula R, Mays JW, Hadjichristidis N (2006) Homopolymer and block copolymer brushes on gold by living anionic surface-initiated polymerization in a polar solvent. J Polym Sci Polym Chem 44(2):769–782. doi:10.1002/pola.21195

28. Fan XW, Zhou QY, Xia CJ, Cristofoli W, Mays J, Advincula R (2002) Living anionic surface-initiated polymerization (LASIP) of styrene from clay nanoparticles using surface bound 1,1-diphenylethylene (DPE) initiators. Langmuir 18(11):4511–4518. doi:10.1021/la025556+

29. Oosterling M, Sein A, Schouten AJ (1992) Anionic grafting of polystyrene and poly(styrene-block-isoprene) onto microparticulate silica and glass slides. Polymer 33(20):4394–4400. doi:10.1016/0032-3861(92)90286-6

30. Zhou QY, Wang SX, Fan XW, Advincula R, Mays J (2002) Living anionic surface-initiated polymerization (LASIP) of a polymer on silica nanoparticles. Langmuir 18(8):3324–3331. doi:10.1021/la015670c

31. Advincula R, Zhou QG, Park M, Wang SG, Mays J, Sakellariou G, Pispas S, Hadjichristidis N (2002) Polymer brushes by living anionic surface initiated polymerization on flat silicon (SiO (x)) and gold surfaces: homopolymers and block copolymers. Langmuir 18(22):8672–8684. doi:10.1021/la025962t

32. Kim CJ, Sondergeld K, Mazurowski M, Gallei M, Rehahn M, Spehr T, Frielinghaus H, Stuhn B (2013) Synthesis and characterization of polystyrene chains on the surface of silica nanoparticles: comparison of SANS, SAXS, and DLS results. Colloid Polym Sci 291(9): 2087–2099. doi:10.1007/s00396-013-2923-z

33. Khan M, Huck WTS (2003) Hyperbranched polyglycidol on Si/SiO2 surfaces via surface-initiated polymerization. Macromolecules 36(14):5088–5093. doi:10.1021/ma0340762

34. Tsubokawa N, Yoshihara T, Sone Y (1992) Grafting of polymers onto carbon whisker by anionic graft-polymerization of vinyl monomers using metallized aromatic rings and or phenoxy lithium groups on the surface as initiator. J Polym Sci A Polym Chem 30(4): 561–567. doi:10.1002/pola.1992.080300406

35. Lu W, Ruan GD, Genorio B, Zhu Y, Novosel B, Peng ZW, Tour JM (2013) Functionalized graphene nanoribbons via anionic polymerization initiated by alkali metal-intercalated carbon nanotubes. ACS Nano 7(3):2669–2675. doi:10.1021/nn400054t

36. Zhang XQ, Fan XY, Li HZ, Yan C (2012) Facile preparation route for graphene oxide reinforced polyamide 6 composites via in situ anionic ring-opening polymerization. J Mater Chem 22(45):24081–24091. doi:10.1039/c2jm34243j

37. Viswanathan G, Chakrapani N, Yang HC, Wei BQ, Chung HS, Cho KW, Ryu CY, Ajayan PM (2003) Single-step in situ synthesis of polymer-grafted single-wall nanotube composites. J Am Chem Soc 125(31):9258–9259. doi:10.1021/ja0354418

38. Chen SM, Chen DY, Wu GZ (2006) Grafting of poly(*t*BA) and P*t*BA-b-PMMA onto the surface of SWNTs using carbanions as the initiator. Macromol Rapid Commun 27(11): 882–887. doi:10.1002/marc.200600049

39. Liang F, Beach JM, Kobashi K, Sadana AK, Vega-Cantu YI, Tour JM, Billups WE (2006) In situ polymerization initiated by single-walled carbon nanotube salts. Chem Mater 18(20): 4764–4767. doi:10.1021/cm0607536

40. Sakellariou G, Ji HN, Mays JW, Baskaran D (2008) Enhanced polymer grafting from multiwalled carbon nanotubes through living anionic surface-initiated polymerization. Chem Mater 20(19):6217–6230. doi:10.1021/cm801449t

41. Yoon KR, Kim WJ, Choi IS (2004) Functionalization of shortened single-walled carbon nanotubes with poly (p-dioxanone) by 'Grafting-From' approach. Macromol Chem Phys 205(9):1218–1221. doi:10.1002/macp.200400077

42. Zhou L, Gao C, Xu WJ (2009) Efficient grafting of hyperbranched polyglycerol from hydroxyl-functionalized multiwalled carbon nanotubes by surface-initiated anionic ring-opening polymerization. Macromol Chem Phys 210(12):1011–1018. doi:10.1002/macp.200900134

43. Adeli M, Mirab N, Alavidjeh MS, Sobhani Z, Atyabi F (2009) Carbon nanotubes-graft-polyglycerol: biocompatible hybrid materials for nanomedicine. Polymer 50(15):3528–3536. doi:10.1016/j.polymer.2009.05.052

44. Buffa F, Hu H, Resasco DE (2005) Side-wall functionalization of single-walled carbon nanotubes with 4-hydroxymethylaniline followed by polymerization of epsilon-caprolactone. Macromolecules 38(20):8258–8263. doi:10.1021/ma050876w

45. Zeng HL, Gao C, Yan DY (2006) Poly(epsilon-caprolactone)-functionalized carbon nanotubes and their biodegradation properties. Adv Funct Mater 16(6):812–818. doi:10.1002/adfm.200500607

46. Castro M, Lu J, Bruzaud S, Kumar B, Feller J-F (2009) Carbon nanotubes/poly(epsilon-caprolactone) composite vapour sensors. Carbon 47(8):1930–1942. doi:10.1016/j.carbon.2009.03.037

47. Ruelle B, Peeterbroeck S, Gouttebaron R, Godfroid T, Monteverde F, Dauchot J-P, Alexandre M, Hecq M, Dubois P (2007) Functionalization of carbon nanotubes by atomic nitrogen formed in a microwave plasma Ar + N-2 and subsequent poly(epsilon-caprolactone) grafting. J Mater Chem 17(2):157–159. doi:10.1039/b613581c

48. Yang Y, Tsui CP, Tang CY, Qiu S, Zhao Q, Cheng X, Sun Z, Li RKY, Xie X (2010) Functionalization of carbon nanotubes with biodegradable supramolecular polypseudorotaxanes from grafted-poly(epsilon-caprolactone) and alpha-cyclodextrins. Eur Polym J 46(2):145–155. doi:10.1016/j.eurpolymj.2009.10.020

49. Priftis D, Sakellariou G, Hadjichristidis N, Penott EK, Lorenzo AT, Muller AJ (2009) Surface modification of multiwalled carbon nanotubes with biocompatible polymers via ring opening and living anionic surface initiated polymerization. Kinetics and crystallization behavior. J Polym Sci Polym Chem 47(17):4379–4390. doi:10.1002/pola.23491

50. Priftis D, Sakellariou G, Mays JW, Hadjichristidis N (2010) Novel diblock copolymer-grafted multiwalled carbon nanotubes via a combination of living and controlled/living surface polymerizations. J Polym Sci Polym Chem 48(5):1104–1112. doi:10.1002/pola.23865

51. Chen G-X, Kim H-S, Park B-H, Yoon J-S (2007) Synthesis of poly(L-lactide)-functionalized multiwalled carbon nanotubes by ring-opening polymerization. Macromol Chem Phys 208 (4):389–398. doi:10.1002/macp.200600411

52. Kim H-S, Park B-H, Yoon J-S, Jin H-J (2007) Thermal and electrical properties of poly (L-lactide)-graft-multiwalled carbon nanotube composites. Eur Polym J 43(5):1729–1735. doi:10.1016/j.eurpolymj.2007.02.025

53. Kim H-S, Chae Y-S, Park B-H, Yoon J-S, Kang M-S, Jin H-J (2008) Thermal and electrical conductivity of poly(L-lactide)/multiwalled carbon nanotube nanocomposites. Curr Appl Phys 8(6):803–806. doi:10.1016/j.cap.2007.04.032

54. Priftis D, Petzetakis N, Sakellariou G, Pitsikalis M, Baskaran D, Mays JW, Hadjichristidis N (2009) Surface-initiated titanium-mediated coordination polymerization from catalyst-functionalized single and multiwalled carbon nanotubes. Macromolecules 42(9):3340–3346. doi:10.1021/ma8027479

55. Chakoli AN, Wan J, Feng J, Amirian M, Sui J, Cai W (2009) Functionalization of multiwalled carbon nanotubes for reinforcing of poly(L-lactide-co-epsilon-caprolactone) biodegradable copolymers. Appl Surf Sci 256(1):170–177. doi:10.1016/j.apsusc.2009.07.103

56. Feng J, Cai W, Sui J, Li Z, Wan J, Chakoli AN (2008) Poly(L-lactide) brushes on magnetic multiwalled carbon nanotubes by in-situ ring-opening polymerization. Polymer 49(23): 4989–4994. doi:10.1016/j.polymer.2008.09.022

57. Yao Y, Li W, Wang S, Yan D, Chen X (2006) Polypeptide modification of multiwalled carbon nanotubes by a graft-from approach. Macromol Rapid Commun 27(23):2019–2025. doi:10.1002/marc.200600447

58. Li J, He W, Yang L, Sun X, Hua Q (2007) Preparation of multi-walled carbon nanotubes grafted with synthetic poly(L-lysine) through surface-initiated ring-opening polymerization. Polymer 48(15):4352–4360. doi:10.1016/j.polymer.2007.05.076

59. Tang H, Zhang D (2010) Poly(gamma-benzyl-l-glutamate)-functionalized single-walled carbon nanotubes from surface-initiated ring-opening polymerizations of N-carboxylanhydride. J Polym Sci Pol Chem 48(11):2340–2350. doi:10.1002/pola.24001

60. Qu LW, Veca LM, Lin Y, Kitaygorodskiy A, Chen BL, McCall AM, Connell JW, Sun YP (2005) Soluble nylon-functionalized carbon nanotubes from anionic ring-opening polymerization from nanotube surface. Macromolecules 38(24):10328–10331. doi:10.1021/ma051762n

61. Yang M, Gao Y, Li H, Adronov A (2007) Functionalization of multiwalled carbon nanotubes with polyamide 6 by anionic ring-opening polymerization. Carbon 45(12):2327–2333. doi:10.1016/j.carboji.2007.07.021

62. Yan D, Yang G (2009) A novel approach of in situ grafting polyamide 6 to the surface of multi-walled carbon nanotubes. Mater Lett 63(2):298–300. doi:10.1016/j.matlet.2008.10.013

63. Yan D, Yang G (2009) Synthesis and properties of homogeneously dispersed polyamide 6/mwnts nanocomposites via simultaneous in situ anionic ring-opening polymerization and compatibilization. J Appl Polym Sci 112(6):3620–3626. doi:10.1002/app.29783

64. Tanaka M, Sudo A, Sanda F, Endo T (2000) Samarium enolate on crosslinked polystyrene beads: anionic initiator for well defined synthesis of polymethacrylate on a solid support. Chem Commun 24:2503–2504. doi:10.1039/b007259l

65. Tanaka M, Sudo A, Sanda F, Endo T (2003) Samarium enolate on crosslinked polystyrene beads. II. An anionic initiator for the well-defined synthesis of poly(allyl methacrylate) on a solid support. J Polym Sci Polym Chem 41(6):853–860. doi:10.1002/pola.10626

66. Tanaka M, Sudo A, Endo T (2004) Samarium enolate on crosslinked polystyrene beads. III. Anionic initiator for well-defined synthesis of poly(hydroxyethyl methacrylate) on solid support. J Polym Sci Polym Chem 42(17):4417–4423. doi:10.1002/pola.20210

67. Minoura Y, Katano M (1969) Graft copolymerization of styrene with carbon black-alkali metal complex. J Appl Polym Sci 13 (10):2057–2068. doi:10.1002/app.1969.070131003

68. Ohkita K, Nakayama N, Shimomura M (1980) The polymerization of styrene catalyzed by normal-butyllithium in the presence of carbon-black. Carbon 18(4):277–280. doi:10.1016/0008-6223(80)90051-2

69. Tsubokawa N, Funaki A, Hada Y, Sone Y (1982) Grafting polyesters onto carbon-black. I. Polymerization of beta-propiolactone initiated by alkali-metal carboxylate group on the surface of carbon-black. J Polym Sci Polym Chem 20(12):3297–3304. doi:10.1002/pol.1982.170201204

70. Dresselhaus MS, Dresselhaus G (2002) Intercalation compounds of graphite. Adv Phys 51(1):1–186. doi:10.1080/00018730110113644
71. Geim AK, Novoselov KS (2007) The rise of graphene. Nat Mater 6(3):183–191. doi:10.1038/nmat1849
72. Stein C, Gole J (1966) Anionic polymerization of dienes under the effect of insertion products of alkaline metals into graphite. Bull Soc Chim Fr 10:3175–3181
73. Leroux F, Besse JP (2001) Polymer interleaved layered double hydroxide: a new emerging class of nanocomposites. Chem Mater 13(10):3507–3515. doi:10.1021/cm0110268
74. Sun LY, Xiao M, Liu JJ, Gong K (2006) A study of the polymerization of styrene initiated by K-THF-GIC system. Eur Polym J 42(2):259–264. doi:10.1016/j.eurpolymj.2005.07.014
75. Barbey R, Lavanant L, Paripovic D, Schuwer N, Sugnaux C, Tugulu S, Klok HA (2009) Polymer brushes via surface-initiated controlled radical polymerization: synthesis, characterization, properties, and applications. Chem Rev 109(11):5437–5527. doi:10.1021/cr900045a
76. Pyun J, Kowalewski T, Matyjaszewski K (2003) Synthesis of polymer brushes using atom transfer radical polymerization. Macromol Rapid Commun 24(18):1043–1059. doi:10.1002/marc.200300078
77. Sakellariou G, Priftis D, Baskaran D (2013) Surface-initiated polymerization from carbon nanotubes: strategies and perspectives. Chem Soc Rev 42(2):677–704. doi:10.1039/c2cs35226e
78. Baskaran D, Mays JW, Bratcher MS (2004) Polymer-grafted multiwalled carbon nanotubes through surface-initiated polymerization. Angew Chem Int Edit 43(16):2138–2142. doi:10.1002/anie.200353329
79. Edmondson S, Osborne VL, Huck WTS (2004) Polymer brushes via surface-initiated polymerizations. Chem Soc Rev 33(1):14–22. doi:10.1039/b210143m
80. Hadjichristidis N, Pitsikalis M, Pispas S, Iatrou H (2001) Polymers with complex architecture by living anionic polymerization. Chem Rev 101(12):3747–3792. doi:10.1021/cr9901337
81. Baskaran D, Sakellariou G, Mays JW, Bratcher MS (2007) Grafting reactions of living macroanions with multi-walled carbon nanotubes. J Nanosci Nanotechnol 7(4–5):1560–1567. doi:10.1166/jnn.2007.459
82. Sakellariou G, Ji H, Mays JW, Hadjichristidis N, Baskaran D (2007) Controlled covalent functionalization of multiwalled carbon nanotubes using 4 + 2 cycloaddition of benzocyclobutenes. Chem Mater 19(26):6370–6372. doi:10.1021/cm702470x
83. Kamber NE, Jeong W, Waymouth RM, Pratt RC, Lohmeijer BGG, Hedrick JL (2007) Organocatalytic ring-opening polymerization. Chem Rev 107(12):5813–5840. doi:10.1021/cr068415b
84. Gao C, He H, Zhou L, Zheng X, Zhang Y (2009) Scalable functional group engineering of carbon nanotubes by improved one-step nitrene chemistry. Chem Mater 21(2):360–370. doi:10.1021/cm802704c
85. Ma J, Cheng X, Ma X, Deng S, Hu A (2010) Functionalization of multiwalled carbon nanotubes with polyesters via bergman cyclization and 'Grafting from' strategy. J Polym Sci Polym Chem 48(23):5541–5548. doi:10.1002/pola.24365
86. Lee R-S, Chen W-H, Lin J-H (2011) Polymer-grafted multi-walled carbon nanotubes through surface-initiated ring-opening polymerization and click reaction. Polymer 52(10):2180–2188. doi:10.1016/j.polymer.2011.03.020
87. Chen J, Dyer MJ, Yu MF (2001) Cyclodextrin-mediated soft cutting of single-walled carbon nanotubes. J Am Chem Soc 123(25):6201–6202. doi:10.1021/ja015766t
88. Hadjichristidis N, Iatrou H, Pitsikalis M, Sakellariou G (2009) Synthesis of well-defined polypeptide-based materials via the ring-opening polymerization of alpha-amino acid N-carboxyanhydrides. Chem Rev 109(11):5528–5578. doi:10.1021/cr900049t

Part II
Strength: Precise Synthesis of Well-Defined Architectural Polymers

Block Copolymers by Anionic Polymerization: Recent Synthetic Routes and Developments

Georgios Theodosopoulos and Marinos Pitsikalis

Abstract Anionic polymerization is the method of choice for the synthesis of well-defined block copolymers characterized by molecular and chemical homogeneity. The applicability of the method has been expanded from the classical monomers, such as styrenes, dienes, methacrylates, acrylates, ethylene oxide, and vinyl pyridines, to a broader range of monomers, such as methacrylates with bulky or functional ester groups, lactones, hexamethylcyclotrisiloxane, 1,3-cyclohexadiene, isocyanates, metal-containing monomers, etc. Recent advances regarding the synthesis of linear block copolymers (e.g., AB diblocks, ABA and ABC triblocks, ABCD tetrablocks, $(AB)_n$ multiblocks) will be presented in this chapter.

1 Introduction

Block copolymers are macromolecules composed of linear arrangements of chemically different polymeric chains (blocks) [1]. In most cases, the different blocks are incompatible, giving rise to a rich variety of well-defined self-assembled structures both in bulk [2] and selective solvents [3]. These self-assembled structures are the basis for applications ranging from thermoplastic elastomers to information storage, drug delivery, and photonic materials [4]. As a result, there is a continuous investigation of the self-assembly processes, as well as, of the response of these materials to external stimuli. Therefore, it is not surprising that these materials play a central role in contemporary macromolecular science covering the full spectrum of polymer chemistry, polymer physics, and applications.

G. Theodosopoulos • M. Pitsikalis (✉)

Department of Chemistry, University of Athens, Panepistimiopolis Zografou, 15771 Athens, Greece

e-mail: pitsikalis@chem.uoa.gr

541

Since the discovery of living anionic polymerization and the first synthesis of diblock copolymers, this technique has emerged as the most reliable and versatile tool for the synthesis of model polymers having controlled architectures, microstructure and molecular weights, narrow molecular weight distributions, and chemical and compositional homogeneity [5]. Under the appropriate experimental conditions, anionic polymerization is associated with the absence of any spontaneous termination or chain transfer reaction, leading to the preparation of well-defined structures. Several initiators, e.g., monofunctional, difunctional, or multifunctional, along with different series of suitable linking agents bearing various functionalities are available for the synthesis of complex macromolecular architectures [6]. An important limitation of anionic polymerization is the demanding experimental conditions, required to achieve a living polymerization system [7], and its applicability to a rather narrow spectrum of monomers (styrenes, dienes, methacrylates, acrylates, ethylene oxide, vinyl pyridines). However, recent developments have allowed for the expansion of the utility of the method to a broad range of monomers such as methacrylates with bulky or functional ester groups, lactones, hexamethylcyclotrisiloxane, 1,3-cyclohexadiene, isocyanates, metal-containing monomers, etc.

Several excellent books and review articles have been published covering this particular area of polymer science [8]. Nevertheless, this chapter will highlight recent (2000–) advances and developments regarding the synthesis of linear block copolymers [AB diblocks, ABA and ABC triblocks, ABCD tetrablocks, (AB)$_n$ multiblocks, etc.].

2 General Synthetic Strategies for the Synthesis of Linear Block Copolymers

An indispensable requirement for the preparation of well-defined block copolymer structures is the utilization of a living or at least a controlled chain-growth polymerization method, in connection with suitable purification methods for all reagents employed (monomers, solvents, linking agents, additives, etc.) and techniques for excluding the introduction of any impurity in the polymerization system. Under such conditions, undesired termination or transfer reactions are absent, or at least minimized, allowing for the synthesis of chemically and molecularly homogeneous structures.

2.1 AB Diblock Copolymers

Two methods have been developed for the synthesis of AB diblock copolymers [8]: (a) sequential addition of monomers and (b) coupling of two appropriately end-functionalized chains. The first method is the most widely used for the

synthesis of block copolymers. An essential consideration for the successful employment of the technique is the order of monomer addition. The living chain from the polymerization of the first monomer must be able to efficiently initiate the polymerization of the second monomer. In other words, the polymerization starts from the monomer that will form the most reactive propagating center followed by the addition of the less reactive monomer. In general, sequential anionic polymerization requires the following order of addition: styrene > dienes > vinyl pyridines > (meth)acrylates > oxiranes > siloxanes. In addition, the rate of the crossover reaction, i.e., the initiation rate of the polymerization of the second monomer by the macroanion of the living first block, must be higher than the propagation rate of the second monomer. Another important requirement is that the conversion of the first monomer must be quantitative. Under these conditions, products with controlled molecular weights and narrow molecular weight distribution having chemical and structural homogeneity can be prepared.

The purity of all reagents used in anionic polymerization should be very high in order to control the molecular weights of the produced polymers. Special care should be taken with the purity of the second monomer. The presence of impurities will cause partial termination of the living chains of the first block, leading finally to a mixture of the homopolymer A with the desired diblock copolymer AB. Moreover, loss of molecular weight control of the second block and the composition of the final copolymer will occur.

2.2 ABA Triblock Copolymers

The synthesis of ABA triblock copolymers can be accomplished using one of the following methods: (a) three-step sequential addition of monomers, (b) two-step sequential addition of monomers followed by a coupling reaction with a suitable difunctional linking agent, and (c) use of a difunctional initiator and a two-step sequential addition of monomers.

The purification requirements mentioned above are also valid for the successful use of the three-step sequential addition. This method has the advantage that asymmetric triblock copolymers ABA', with the two A blocks having different molecular weights, can be prepared. For the synthesis of symmetric ABA triblock copolymers, equal amounts of the A monomer should be used both in the first and the third monomer addition steps in order to avoid differences in the molecular weights of the two A end blocks. The restrictive factor for the successful employment of this methodology is the efficient initiation of the second A block from the living AB diblock copolymer. If the crossover reaction is not efficient, a mixture of AB diblock and ABA triblock copolymers will be obtained. Furthermore, the molecular and compositional control of the desired product will be lost. This problem can be overcome in some cases. For example, the synthesis of the PS-*b*-PI-*b*-PS (polystyrene-*b*-polyisoprene-*b*-polystyrene) triblock copolymer cannot be accomplished in hydrocarbon solvents, since the initiation reaction of the

polymerization of styrene from the living PS-*b*-PI⁻Li⁺ diblock copolymer is not efficient. To solve the problem, the addition of a small amount of a polar compound (tetrahydrofuran, THF, or an amine such as *N,N,N',N'*-tetramethylene ethylenediamine, TMEDA) is needed in order to disrupt the association of the living diblock copolymer chains and thus create the most reactive-free or solvent-separated anions, which are able to accelerate the crossover reaction leading finally to well-defined products. However, this approach cannot be applied in all cases. For example, the synthesis of the PI-*b*-PS-*b*-PI triblock copolymer with the commonly desired 1,4 microstructure of the polydiene cannot be accomplished with this methodology. The living PI⁻Li⁺ chains can efficiently initiate the polymerization of styrene only in the presence of a polar additive, as discussed above. However, this additive will affect the microstructure of the second PI block upon addition of a new quantity of isoprene monomer.

The second method involves the synthesis of the living diblock AB, where the B block has only half the molecular weight compared to the desired one, followed by reaction with a suitable difunctional linking agent (chlorosilanes, dihalomethylene benzene derivatives, terephthaloyl chloride, etc.) [9]. The linking reaction must be efficient and fast, although there are examples where this reaction is a time-consuming process [10]. Moreover, the stoichiometry of the reaction is difficult to control. Consequently, a small excess of the living diblock copolymer is used to ensure complete linking. The excess diblock copolymer has to be removed by fractionation in a later step. This technique can be only used for the synthesis of symmetric ABA triblock copolymers.

The third method is also limited to the synthesis of symmetric triblock copolymers but is versatile, since it only involves a two-step reaction without fractionation or other purification steps. The main limitation, however, of this method is the choice of the difunctional initiator, which must be able to initiate the polymerization of the desired monomer with the same rate from both directions [11]. In this case, the B block is formed first followed by the simultaneous formation of the A end blocks. The purity of all reagents is of crucial importance for the efficient employment of this approach.

2.3   ABC Triblock Terpolymers

A great effort has been recently given on the synthesis of ABC triblock terpolymers, mainly due to their extraordinary bulk morphologies, which differ from those obtained with linear diblock copolymers and their unique self-assembly behavior in selective solvents [12]. The method of choice for the synthesis of these materials is the sequential addition of monomers. The monomer reactivity sequence, along with the purity of all the reagents, plays the most crucial role for the synthesis of well-defined products.

2.4   Multiblock Copolymers

Other more complex linear block co-, ter-, and quaterpolymers, such as ABC, ABCD, and ABABA, can be prepared using the previously mentioned methods. An important tool in the synthesis of block copolymers involves the use of post-polymerization chemical modification reactions. These reactions must be performed under mild conditions to avoid chain scission, cross-linking, or degradation but facile enough to give quantitative conversions. Hydrogenation, hydrolysis, hydrosilylation, and quaternization reactions are among the most important post-polymerization reactions used for the preparation of block copolymers [13].

2.5   Block Copolymers by the Post-polymerization Formation of Metal Complexes

The ability of a broad range of *N*-heterocycles to act as effective complexation agents for several transition metal ions has been known for many years. Such behavior was later used in supramolecular chemistry for the construction of complex architectures [14]. This knowledge has been transferred to polymer chemistry with the development of metal-complexing and metal-containing polymers. The main objective is to combine the polymer properties of the architecture formed with the reversible binding from the supramolecular entities connected to the polymer backbone. In supramolecular chemistry, the linkages can be formed or broken by tuning the external stimuli. 2,2'-Bipyridines were efficiently used in supramolecular chemistry [15]. Since the molecule is symmetric, no directed coupling procedure is possible. In addition, 2,2':6',2"-terpyridine ligands can lead to several metal complexes, usually bis-complexes having octahedral coordination geometries [16]. The metal-polymeric ligand lifetimes depend to a great extent on the metal ion used. Highly labile complexes as well as inert metal complexes have been reported. The latter case is very important since the complexes can be treated as conventional polymers, while the supramolecular interaction remains present as a dormant switch.

A general strategy developed for the synthesis of supramolecular block copolymers involves the preparation of macromolecular chains end capped with 2,2':6',2"-terpyridine ligand which can be selectively complexed with RuCl$_3$. Under these conditions, only the monocomplex between the terpyridine group and Ru(III) is formed. Subsequent reaction with another 2,2':6',2"-terpyridine-terminated polymer under reductive conditions for the transformation of Ru(III) to Ru(II) leads to the formation of supramolecular block copolymers. Using this methodology, the copolymer with PEO (poly(ethylene oxide)) and PS blocks was prepared (Scheme 1) [17].

The synthesis of the supramolecular block copolymer PEO-[Ru]-poly(ethylene-*co*-butylene) was described employing the same procedure [18].
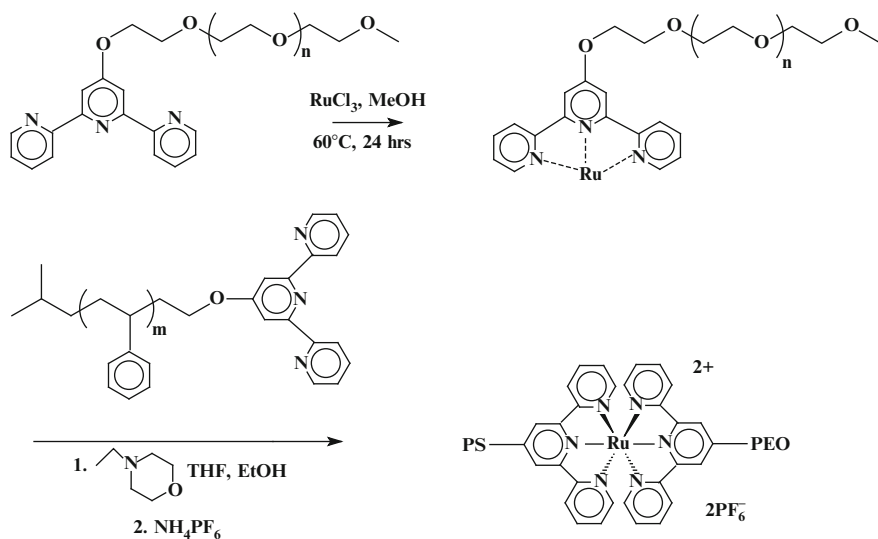
Scheme 1 Synthesis of the supramolecular block copolymer PEO-[Ru]-PS

Using a diblock copolymer PS-*b*-P2VP (poly(2-vinylpyridine)), instead of PS, the supramolecular triblock terpolymer PEO-[Ru]-P2VP-*b*-PS was prepared, as reported in Scheme 2 [19]. The α-methoxy-ω-(2,2':6',2''-terpyridinyl)oxy-PEO was obtained as previously reported. Living anionic polymerization was utilized for the synthesis of hydroxy-terminated PS-*b*-P2VP chains. *t*-BuOK was used to give the corresponding alkoxy end group followed by reaction with 4'--chloroterpyridine to yield the terpyridine-terminated diblock. Combination of the two end-functionalized polymers under reductive conditions provided the desired supramolecular structure PEO-[Ru]-P2VP-*b*-PS.

3   Block Copolymers from Nonpolar Monomers

Most of the published work regarding the synthesis of block copolymers by anionic polymerization refers to the use of nonpolar monomers, mainly styrene, S, and dienic monomers (isoprene, I, and 1,3-butadiene, Bd, are the most common examples). All possible combinations of these monomers have been reported in the literature for the synthesis of well-defined diblock and triblock copolymers and terpolymers. These combinations include polydiene blocks of different microstructure (e.g., PI-1,4, PI-1,2, PI-3,4, PBd-1,4, and PBd-1,2) [20]. In this chapter, emphasis will be given to less common nonpolar monomers, such as 1,3-cyclohexadiene, vinyltrimethylsilane, and trimethylsilylstyrene.

1,3-Cyclohexadiene, CHD, is a monomer which presents a challenge for anionic polymerization due to the obstacles encountered for its controlled polymerization
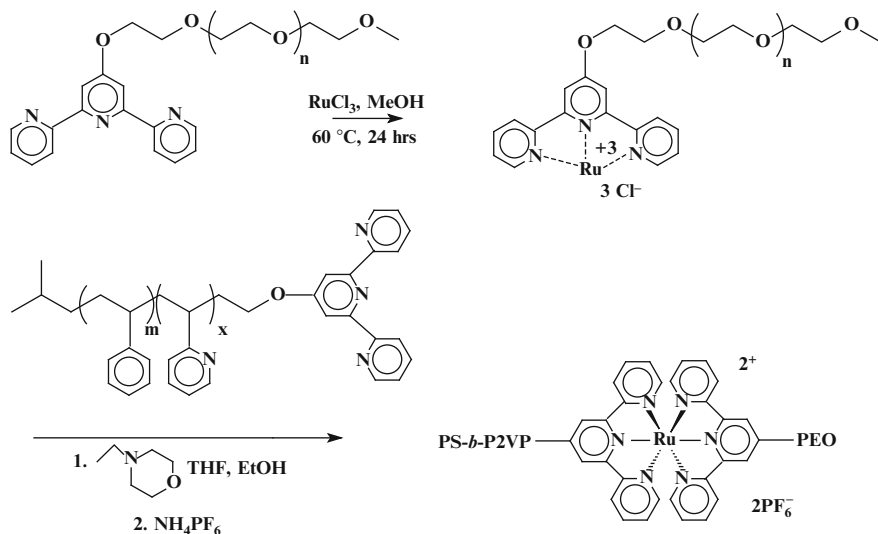
Scheme 2 Synthesis of the supermolecular triblock terpolymer PEO-[Ru]-P2VP-*b*-PS

and its interesting properties both in solution and in bulk. Classic alkyllithium initiation leads to chain transfer reactions, as well as to the lithiated monomer, which is able to reinitiate polymerization. As a result, livingness of PCHD is difficult to achieve. It has been reported that living anionic polymerization of CHD can be achieved using *n*-BuLi and N,N,N',N'-tetramethylethylenediamine, TMEDA, as the initiation system [21]. PCHD was found to have high thermal stability, low specific gravity, and good mechanical properties. Furthermore, the polymer can be transformed to polyphenylene (PPP, conductive polymer) by dehydrogenation and to polycyclohexylene (high Tg polymer) by hydrogenation.

Various effective controlled methods have been reported, and the microstructure of the polymer chain can be tailored. PCHD may consist of two different microstructures 1,2 cyclohexadiene and 1,4 cyclohexadiene (Scheme 3). The desired microstructure is 1,4 CHD and efforts have been made to increase that microstructure. The effect of the microstructure on the physical and chemical properties has been studied [22]. It has been shown that by adjusting the amount and type of multidentate chelating amines (such as TMEDA and DABCO) in combination with the use of alkyllithium initiators, the ratio of 1,2CHD to 1,4CHD can be fixed [22], [23].

Triblock copolymers PCHD-*b*-PBd-*b*-PCHD were also prepared by polymerizing Bd with a difunctional initiator, prepared by the reaction of 1,3-di(1-propene-2-yl)benzene with *sec*-BuLi in the presence of TMEDA, followed by the addition of CHD [24]. The reaction took place in cyclohexane at 40 °C, leading to well-defined products. The PBd block was subsequently hydrogenized selectively using the titanocene complex Cp$_2$TiCl$_2$ and diisobutylaluminum hydride in a molar ratio
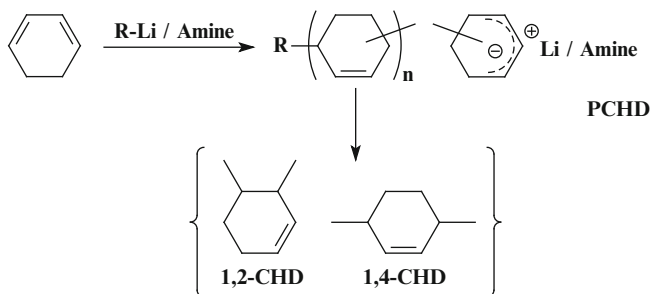
Scheme 3 The two consisting microstructures of PCHD

1/6. Quantitative hydrogenation was conducted by heterogeneous catalysis using palladium supported on aluminum oxide.

It was found that PS-*b*-PCHD block copolymers, where PS is polystyrene, can be prepared in hydrocarbon solvents using *sec*-BuLi as initiator without the presence of any additive [25]. Efficient crossover reactions were obtained from either PSLi (Scheme 4 route A) or PCHDLi (Scheme 4 route B). Using potassium/naphthalene as a difunctional initiator, PS-*b*-PCHD-*b*-PS and PCHD-*b*-PS-*b*-PCHD were prepared. However, the molecular weight distributions were rather broad, and side reactions were observed when copolymers with high CHD contents were required. To avoid this problem, several additives were tested to improve the copolymerization characteristics. The best results were obtained with dimethoxyethane, DME, or 1,4-diazabicyclo[2, 2, 2]octane, DABCO, leading to narrow molecular weight distribution products. However, tailing effects or shoulders were observed in SEC chromatograms when the copolymers had CHD contents higher than 30 %, meaning that the copolymer had to be purified by solvent/non-solvent fractionation.

Multiblock copolymeric structures containing PCHD blocks were also synthesized using *sec*-BuLi as initiator and either TMEDA or DABCO as additive. Sequential monomer addition was performed with CHD being the last monomer added in all cases [26]. The structures prepared include PS-*b*-PCHD, PI-*b*-PCHD, and PBd-*b*-PCHD block copolymers; PS-*b*-PBd-*b*-PCHD, PBd-*b*-PS-*b*-PCHD, and PBd-*b*-PI-*b*-PCHD triblock terpolymers; and PS-*b*-PBd-*b*-PI-*b*-PCHD tetrablock quaterpolymers. In a few cases, chain transfer or termination reactions led to the presence of a small amount of PCHD homopolymer. In general, detailed characterization revealed that narrow molecular weight distribution products with high chemical and compositional homogeneity were obtained.

(PS-*alt*-PCHD)-*b*-PS block copolymers were prepared in a one-pot procedure [27]. It was shown that the anionic statistical copolymerization of CHD and S in cyclohexane at 25 °C, using *sec*-BuLi as initiator, leads to an alternating copolymeric structure, since the reactivity ratios for the two monomers were found to be 0.022 and 0.024 for CHD and S, respectively. When the molar ratio of S over CHD is greater than one, the desired (PS-*alt*-PCHD)-*b*-PS block copolymer is afforded. The molecular weights of the copolymers were rather low (around 10,000), and the molecular weight distributions narrow only when the S content was high. A gradual

Route A

Route B
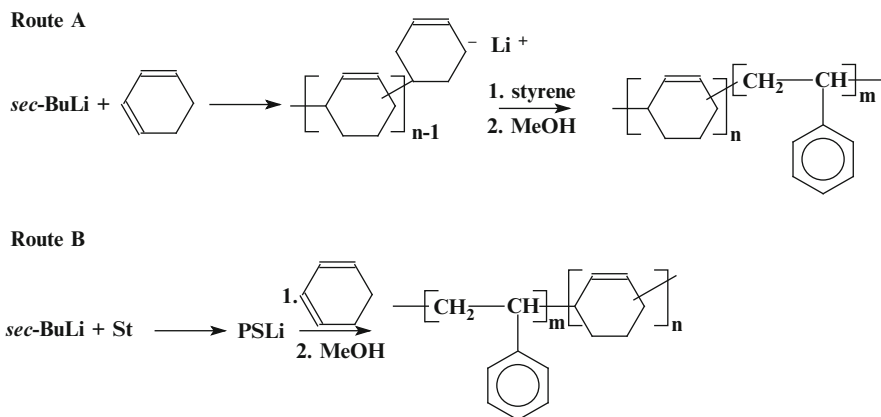
Scheme 4 Preparation of PS-*b*-PCHD block copolymers, possible from both crossover reactions

broadening of the distributions, by increasing the CHD content of the copolymers, was observed. Subsequent selective hydrogenation of the CHD units using a nickel octoate catalyst and triethylaluminum cocatalyst yielded (PS-*alt*-polycyclohexane)-*b*-PS block copolymers. Aromatization of the CHD units using 2,3-dichloro-5,6-dicyano-1,4-benzoquinone under very mild conditions afforded (PS-*alt*-polyphenylene)-*b*-PS block copolymers.

The incorporation of hole transport and electron transport polymer structures in one polymer chain has been attempted through various polymerization methods. The well-defined synthesis, though, of bipolar semiconducting polymers has been achieved through living anionic polymerization, by copolymerizing CHD (PPP is regarded as an electron transfer semiconducting polymer [28]) and 4-diphenylaminostyrene, DAS, which is considered to be a hole transfer semiconducting material [29]. The block copolymers were prepared in a one-pot reaction starting with the polymerization of CHD followed by the sequential addition of DAS. CHD was initially polymerized using *tert*-BuLi [30], at room temperature, in the absence of TMEDA or any other additive. TMEDA was later added, after the polymerization of the first block had been completed, to enhance reactivity followed by the polymerization of DAS (Scheme 5). The homopolymerization of CHD provided polymers with relatively broad molecular weight distribution (~1.2); however, 100 % 1,4-CHD can be produced through the employment of *tert*-BuLi in cyclohexane as the initiating system [31]. It was also revealed that (RLi)/TMEDAs in toluene are the preferable conditions for the polymerization of DAS [32].

Hence, overall, the polymerization of the two monomers resulted in the preparation of well-defined diblocks with narrow molecular weight distribution (~1.1). Dehydrogenation of the CHD units was achieved through the use of a quinone, tetrachloro-1,2-(o)-benzoquinone (TOQ). Judicious planning of dehydrogenation reagent and temperature was essential, because of the sensitive nature of the DAS group. TOQ was the reagent of choice since it does not affect the PDAS block and successfully dehydrogenates at room temperature. High temperatures and long
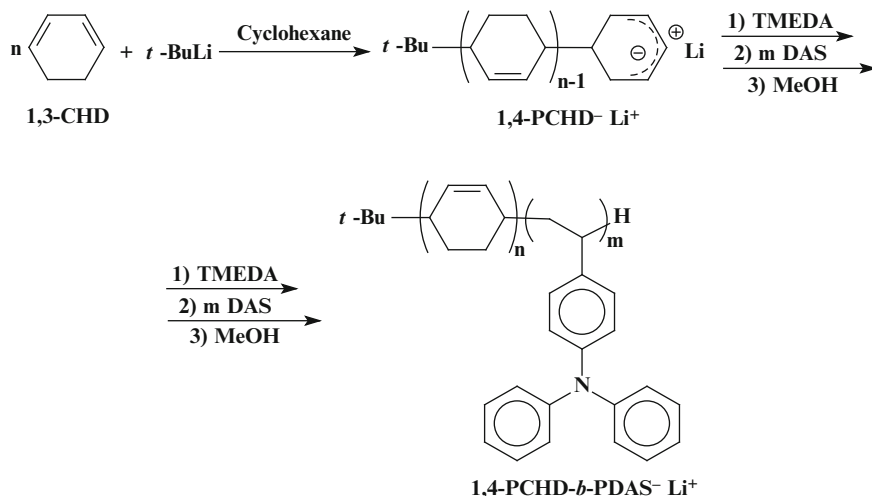
Scheme 5 Copolymerization of CHD and DAS towards 1,4-PCHD-*b*-PDAS

reaction times must be avoided since the exposure of DAS to such conditions causes its decomposition. The dehydrogenation rate and percentage were also shown to be conveniently affected by the molar ratio of 1,4-CHD units to TOQ and by ultrasonic irradiation during dehydrogenation [33].

Trimethylsilane-based monomers such as vinyltrimethylsilane (VTMS) and trimethylsilylstyrene (TMSS) are very attractive since they provide polymers showing lower critical solution temperature (LCST) behavior in their immiscible block copolymer blends.

PTMSS-*b*-PI is an example of such type of block copolymer [34], which can be prepared by sequential addition of monomers. TMSS was initially polymerized in THF at $-78\,^{\circ}$C using cumyl potassium as initiator, followed by the subsequent addition of I. This procedure led to well-defined block copolymers with very narrow molecular weight distributions.

PVTMS has very interesting physical properties such as permeability to O_2 and good O_2/N_2 selectivity. Therefore, it has been copolymerized in block formations in order to fabricate membranes for air component separation. PVTMS-*b*-PDMS [PDMS is poly(dimethyl siloxane)] copolymers have been synthesized through anionic polymerization in THF using *sec*-BuLi as initiator [35]. PDMS-*b*-PVTMS-*b*-PDMS triblock copolymers have been synthesized as well, by using lithium naphthalene [36] in THF at $-78\,^{\circ}$C, as a difunctional initiator starting with the polymerization of PVTMS. PS-*b*-PVTMS block copolymers have also been prepared. The synthesis took place in heptane using *n*-BuLi as initiator [37]. PI-*b*-PVTMS block copolymers have also been prepared in cyclohexane at 35 $^{\circ}$C, using *n*-BuLi as initiator. Block synthesis yields polymers of rather broad molecular weight distributions [38].

4 Block Copolymers from Polar Monomers

4.1 (Meth)acrylates

(Meth)acrylates constitute the most important family of monomers, since a wide variety of polymers with disperse properties can be produced [39]. The anionic polymerization of these monomers is challenging, since it requires polar solvents (usually THF), low reaction temperatures (-78 °C), less active and sterically hindered initiators, to avoid side reactions with the monomer's carbonyl group, and careful purification of the monomers [40]. The most commonly employed initiator is formed in situ from the reaction of *n*-BuLi or *sec*-BuLi with 1,1-diphenylethylene, DPE. The use of LiCl as additive leads to more controlled polymerization reactions [41]. Other stabilizing ligands have been used as well, to restrict the extent of side reactions, such as metal *tert*-alkoxides [42], bidentate lithium alkoxides [43], alkylaluminums lithium perchlorate [44], lithium silanolates [45], etc. These ligands interact with the growing anionic centers forming cross-complexes, thus modifying the immediate environment of the living macroanions. Therefore, the ability of the living chain ends to react with the carbonyl groups of the methacrylate monomeric units is drastically reduced. Numerous block copolymers of different (meth)acrylates but also with styrenic, dienic monomers, etc. have been reported in the literature.

ABA triblock copolymers, where A is poly(methyl methacrylate), PMMA, and B is poly(tert-butyl acrylate), P*t*BuA, have been prepared by anionic polymerization and through the sequential addition of monomers [46]. Polymerization was conducted in THF at -78 °C using 1,1-diphenyl-3-methylpentyllithium as initiator, prepared in situ by the reaction of *sec*-BuLi and DPE. LiCl was used as additive to promote the living polymerization of the (meth)acrylates and led to well-defined products having narrow molecular weight distributions. Selective acid-catalyzed transalcoholysis at 150 °C of the *tert*-butyl ester groups by either *n*-butanol or isooctanol transformed the initial triblock copolymers PMMA-*b*-P*t*BuA-*b*-PMMA to PMMA-*b*-poly(*n*-butyl acrylate)-*b*-PMMA, PMMA-*b*-PnBuA-*b*-PMMA, and PMMA-*b*-poly(isooctyl acrylate)-*b*-PMMA, PMMA-*b*-PIsOA-*b*-PMMA triblocks, respectively. NMR analysis revealed that the transalcoholysis reaction was selective and almost quantitative (95–98 %). With this procedure, thermoplastic elastomers can be prepared with PMMA as the high Tg end blocks and either PnBuA or PIsOA as the soft and low Tg middle block. These materials are expected to provide oxidative stability superior to the classic thermoplastic elastomers PS-*b*-PD-*b*-PS where PD is a polydiene. However, the greater miscibility of the methacrylate blocks with the acrylic blocks compared to the PS and PD blocks leads to inferior mechanical properties.

Block copolymers comprised of PS and polymethacrylate blocks with aliphatic stearyl or decyl side groups were prepared by sequential addition of monomers, as shown in Scheme 6. Styrene was polymerized in THF at -78 °C using *sec*-BuLi as initiator [47]. The nucleophilicity of the living polystyryllithium was reduced by
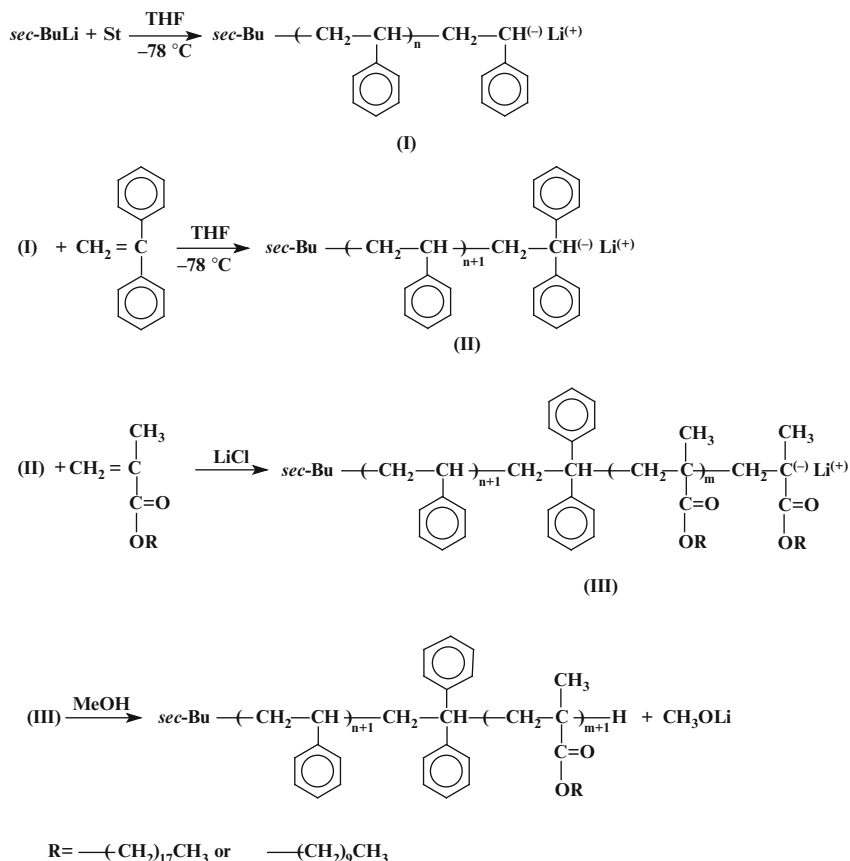
Scheme 6 Synthesis of block copolymers comprising of PS and Polymethacrylate blocks with aliphatic, stearyl or decyl side groups

reaction with DPE (in order to avoid reactions with the carbonyl groups), followed by the polymerization of the methacrylate monomer. Stearyl methacrylate, SMA, is associated with two major limitations, the insolubility of the monomer in THF at $-78\,^\circ$C and its very high boiling point, which prevents purification using standard methods developed for methacrylates [48]. To overcome these drawbacks, the monomer was purified by recrystallization in *n*-hexane at $-30\,^\circ$C, and the polymerization was conducted at $-10\,^\circ$C, where SMA is soluble. Under these conditions, living polymerization was promoted and led to well-defined block copolymers. This was confirmed by the efficient synthesis of a high molecular weight diblock copolymer and a triblock copolymer PS-*b*-PSMA-*b*-PS by coupling the living PS-*b*-PSMA diblocks with 1,4-dibromomethylbenzene as linking agent. A combination of several characterization techniques revealed that model copolymers with high molecular and compositional homogeneity were prepared. The micellization properties of these samples were studied in solvents selective either for the PS or the polymethacrylate blocks.

Scheme 7 Portrayal of PMMA-*b*-Poly(2-perfluorooctyl-ethylmethacrylate) block copolymer
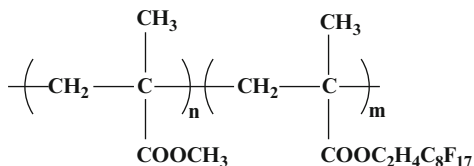
Block copolymers composed of other combinations of styrenic derivatives and methacrylates have also been obtained, such as poly(4-octylstyrene)-*b*-PBuMA, poly(4-fluorostyrene)-*b*-PBuMA, poly(4-octylstyrene)-*b*-PMMA [49], and poly(*tert*-butyl styrene)-*b*-PMMA [50].

Narrow molecular weight distribution PMMA-*b*-poly(2-perfluorooctylethyl methacrylate) block copolymers (Scheme 7) were synthesized in THF at −78 °C in the presence of LiCl [51]. Their self-assembly behavior was studied in selective solvents. Diblock copolymers of t-butyl methacrylate, *t*BuMA, and 2-(*N*-methylperfluorobutanesulfonamido)ethyl methacrylate, FMA, have been prepared by sequential addition of the monomers starting from *t*BuMA using 1,1-diphenyl-3-methylpentyllithium as initiator [52]. Symmetric triblock copolymers PFMA-*b*-*t*BuMA-*b*-PFMA were synthesized using potassium naphthalene as a difunctional initiator to polymerize t-BuMA, followed by the addition of FMA. The polymers were characterized by SEC and NMR spectroscopy, and their microphase separation behavior was studied by atomic force microscopy, AFM, and small angle X-ray scattering, SAXS. Thermal treatment of the copolymers at 200 °C yielded inter- and intramolecular anhydrides due to the splitting of the *tert*-butyl ester groups associated with the formation of isobutene. Reflux in 1 N NaOH resulted in the formation of the sodium salts of the methacrylic acid and consequently in the synthesis of amphiphilic copolymers (Scheme 8). Under these conditions, the FMA units were not cleaved.

Super amphiphobic diblock copolymers poly[3-(triisopropoxysilyl)propyl methacrylate]-*b*-poly[2-(2-perfluorooctylethylmethacrylate)], (PIPSMA-*b*-PFOEMA), were prepared by sequential addition of monomers (Scheme 9). The polymerization was conducted in THF at −78 °C using 1,1-diphenyl-3-methylpentyllithium as initiator, prepared in situ by the reaction of *sec*-BuLi and DPE in the presence of LiCl. 3-(Triisopropoxysilyl)propyl methacrylate was polymerized first followed by the polymerization of 2-(perfluorooctyl)ethyl methacrylate [53].

Similar approaches were developed for the synthesis of PS-*b*-poly(2,2,2-trifluorethyl methacrylate), PS-*b*-PTFEMA, and PS-*b*-P(MMA-*co*-TFEMA) block copolymers or terpolymers, as shown in Scheme 10. The products have also been employed as positive tone resists for lithography [54].

Poly(ethylene glycol)-*b*-PDMAEMA-*b*-poly(2,2,3,3,4,4,5,5-octafluoropentyl-methacrylate), PEG-*b*-PDMAEMA-*b*-POFPMA, triblock terpolymers of low molecular weights have been prepared. The end-hydroxyl group of monomethyl ether PEG was transformed to potassium alcoholate after reaction with potassium
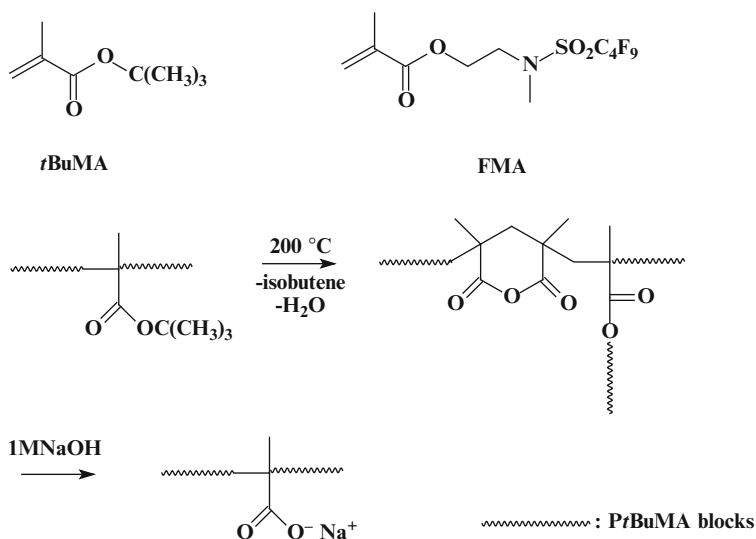
Scheme 8 Chemical structure of *t*BuMA and FMA and modification reactions of the tert-butylester group towards anhydrates and sodium salts of MA
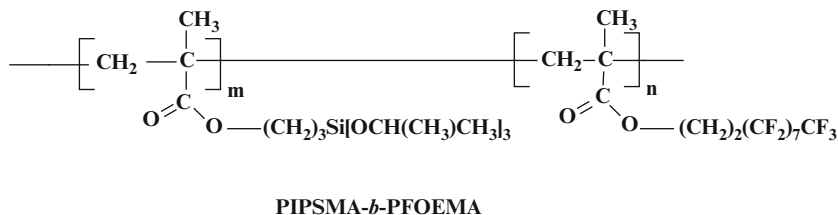
PIPSMA-*b*-PFOEMA

Scheme 9 Portrayal of super amphiphilic diblock copolymer PIPSMA-*b*-PFOEMA

methylsulfinyl carbanion. From these living chain ends, the polymerization of DMAEMA was conducted followed by the polymerization of OFPMA. The reactions took place at 30 °C for 1 h each (Scheme 11) [55].

Oxyanionic polymerization was also adopted for the synthesis of PEG-*b*-poly (ethyl cyanoacrylate)-*b*-poly[2-(*N*-carbazoyl) ethyl methacrylate], PEG-*b*-PECA-*b*-PCzEMA, triblock terpolymers. The end-hydroxyl group of monomethyl ether PEG was reacted with NaH to afford the corresponding sodium alcoholate. Subsequent addition of ECA and CzEMA led to the synthesis of the desired product in THF solutions at 25 °C (Scheme 12) [56].

3-Methacryloyloxy-1,1'-biadamantane, MBA, (Scheme 13) was efficiently polymerized anionically using [1,1-bis(4'-trimethylsilylphenyl)-3-methylpentyl] lithium as initiator, prepared in situ by the reaction of *sec*-BuLi with 1,1-bis (4-trimethylsilylphenyl)ethylene [57]. The polymerization took place at −50 °C in order to avoid the solubility problems of the monomer, observed at −78 °C.
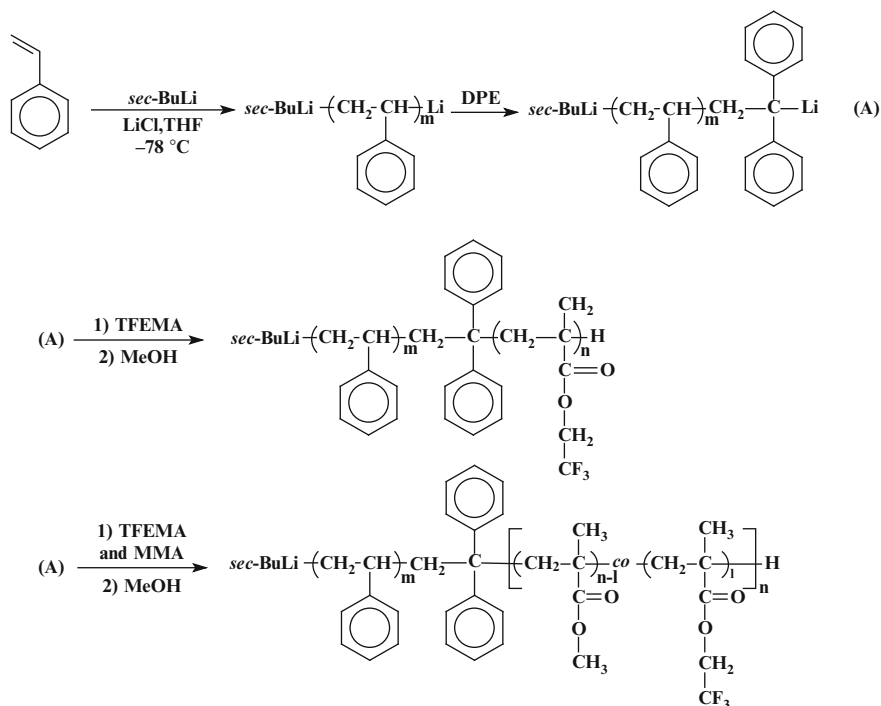
Scheme 10 Synthesis of PS-*b*-PTFEMA block copolymer and PS-*b*-P(MMA-*co*-TFEMA) terpolymer

Narrow molecular weight distribution block copolymers of rather low molecular weights of PMBA with *t*BuMA and (2,2-dimethyl-1,3-dioxolan-4-yl)methyl methacrylate were prepared. Using the difunctional potassium/naphthalene initiator triblock copolymers with polyisoprene middle blocks, PMBA-*b*-PI-*b*-PMBA were also synthesized.

Poly(*N,N*-dimethylaminoethyl methacrylate), PDMAEMA, is a well-known pH and temperature-responsive polymer. Block copolymers with PMMA, P*t*BuMA, PS, poly(α-methyl styrene), PαMeS, and poly(2-vinyl pyridine), P2VP, have been prepared by sequential addition of monomers [58]. In a more recent work, PS-*b*-PDMAEMA, (PBd-1,2)-*b*-PDMAEMA, and P*t*BS-*b*-PDMAEMA were synthesized in THF using *sec*-BuLi as initiator [59]. The first monomer was polymerized at −70 °C for 30 min (styrene), −10 °C for 10 h (butadiene), or −70 °C for 1 h (*tert*-butoxystyrene). The living chains were then end capped with DPE at −70 °C for 1 h followed by the addition of DMAEMA. The temperature was raised up to −50 °C and the polymerization was allowed to take place for 1 h. Well-defined products of low polydispersities and rather high molecular weight PDMAEMA blocks were obtained.

The P*t*BOS-*b*-PDMAEMA block copolymers were also prepared by sequential living anionic polymerization at −78 °C in THF using *sec*-BuLi as initiator. The
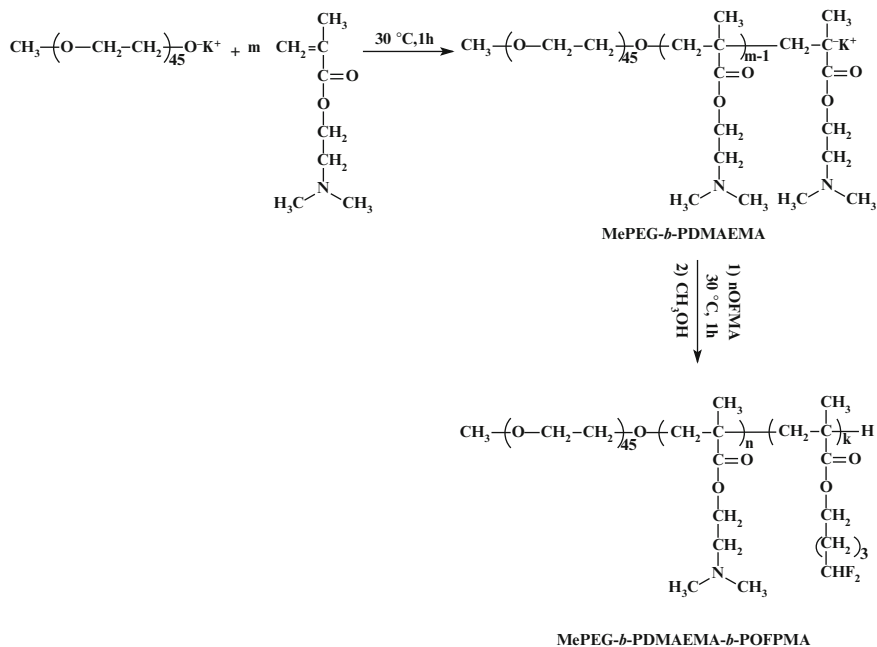
Scheme 11 Synthesis of MePEG-*b*-PDMAEMA-*b*-POFPMA triblock terpolymer
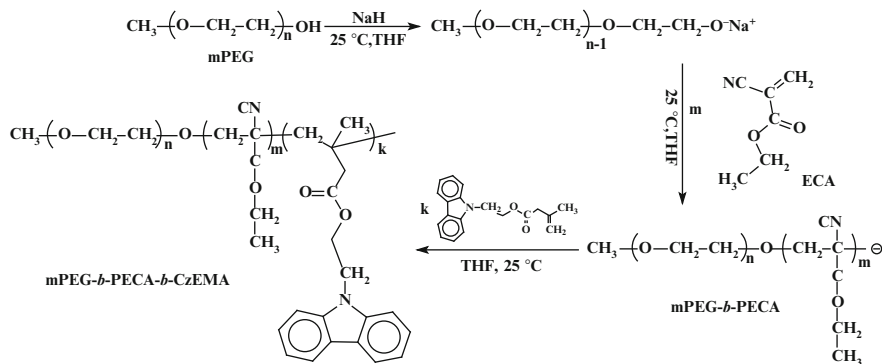
Scheme 12 Synthesis of mPEG-*b*-PECA block copolymer

Scheme 13 Chemical structure of 3-Methacryloyloxy-1,1'-biadamantane

MBA
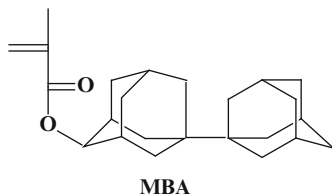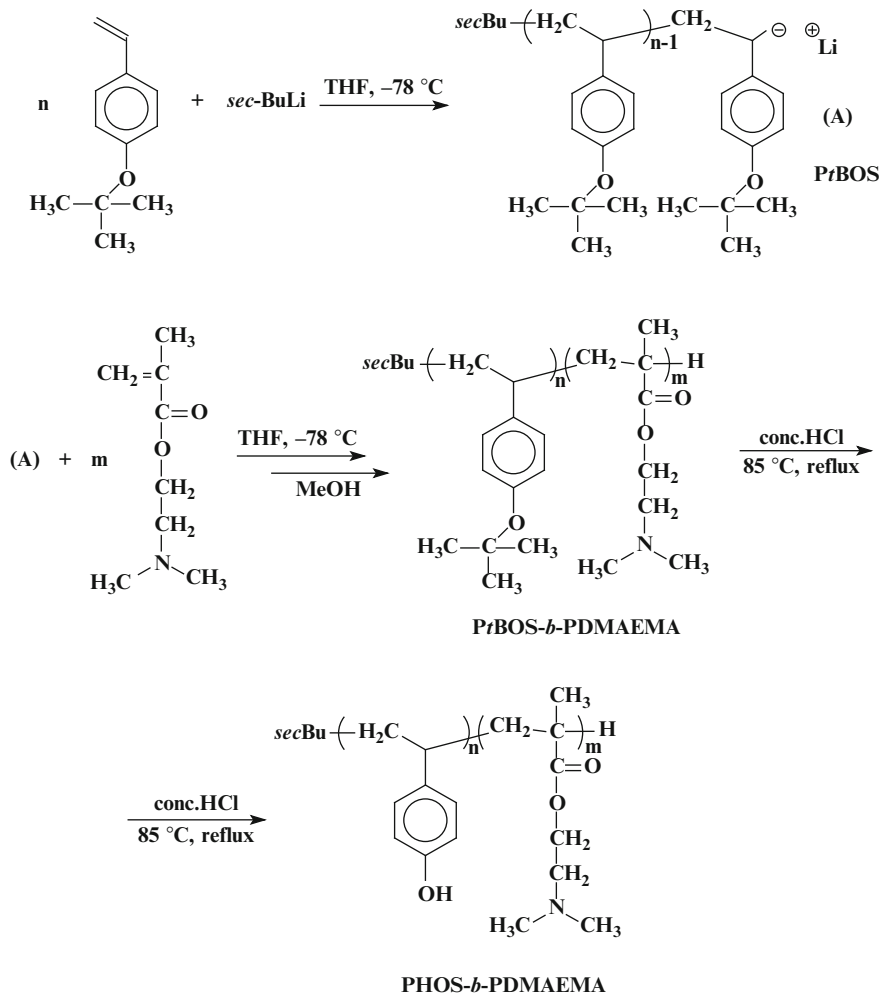
Scheme 14 Synthesis of P*t*BOS-*b*-PDMAEMA block copolymer and chemical modification towards PHOS-*b*-PDMAEMA

living P*t*BOS chains were not capped with DPE prior the addition of DMAEMA, but LiCl was added to prevent side reactions. Subsequent hydrolysis in dioxane solutions using HCl at 85 °C for 2 days afforded the corresponding poly(vinyl phenol)-*b*-PDMAEMA block copolymers (Scheme 14) [60]. The micellization properties of these copolymers were studied in detail in aqueous solutions. A similar synthetic approach was adopted for the synthesis of P*t*BS-*b*-PtBuMA block copolymers which were transformed after acid hydrolysis to poly(vinyl phenol)-*b*-poly(methacrylic acid) double hydrophilic copolymers (Scheme 15) [61].
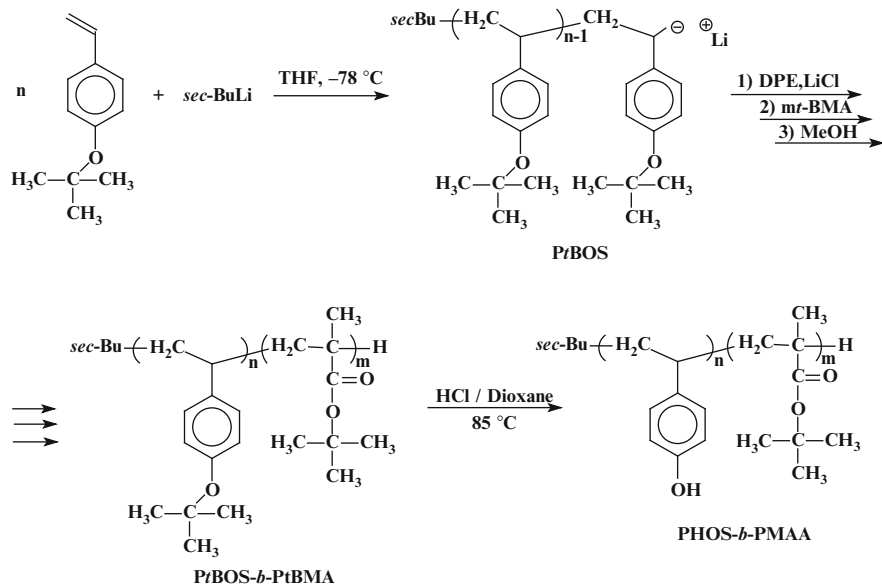
Scheme 15 Synthesis of P*t*BOS-*b*-P*t*BMA block copolymer and chemical modification of both blocks towards PHOS-*b*-PMAA
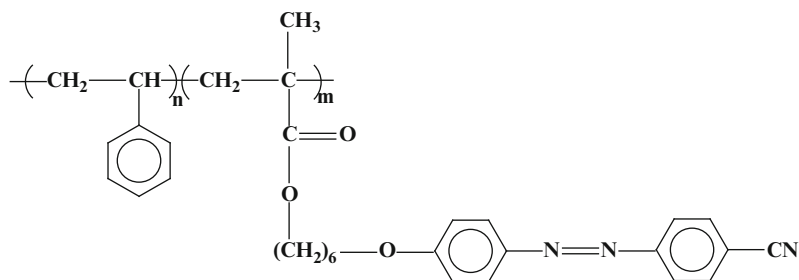
Scheme 16 Portrayal of PS-*b*-Poly{6-[4-(cyanophenylazo)phenoxy]hexylmethacrylate} block copolymer

Block copolymers with PS and a polymethacrylate block carrying a liquid crystalline group, PS-*b*-poly{6-[4-(cyanophenylazo)phenoxy]hexyl methacrylate} (Scheme 16), were successfully prepared in quantitative yields and with relatively narrow molecular weight distributions (Scheme 16) [62]. The thermotropic liquid crystalline behavior of the copolymers was studied by differential scanning calorimetry.

A bifunctional methacrylate monomer, trans, trans-1-methacryloyloxy-2,4-hexadiene, MAHE, was efficiently polymerized anionically [63]. It was found experimentally that the 2,4-hexadienyl side group was not affected during the polymerization. Block copolymers of MAHE with MMA can be prepared by

CH₃

$\left(CH_2-CH\right)_n\left(CH_2-\underset{\underset{\underset{CH_2CH=CH-CH=CHCH_3}{O}}{\overset{C=O}{|}}}{\overset{CH_3}{\underset{|}{C}}}\right)_m$

bromination | osmylation

CH₃

$\left(CH_2-CH\right)_n\left(CH_2-\underset{\underset{\underset{CH_2CHCHCHCHCH_3}{O}}{\overset{C=O}{|}}}{\overset{CH_3}{\underset{|}{C}}}\right)_m$

Br Br Br Br

CH₃

$\left(CH_2-CH\right)_n\left(CH_2-\underset{\underset{\underset{CH_2CHCHCHCHCH_3}{O}}{\overset{C=O}{|}}}{\overset{CH_3}{\underset{|}{C}}}\right)_m$

OHOHOHOH
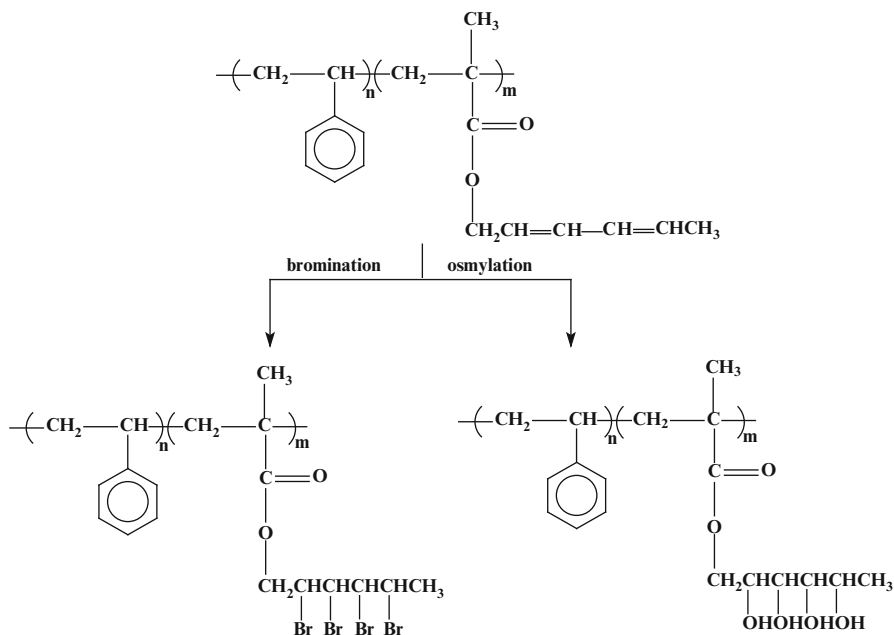
Scheme 17 Bromination and osmylation reactions applied on PS-*b*-PMAHE block copolymers

starting with the polymerization of either monomer. Styrene was polymerized first to result in PS-*b*-PMAHE block copolymers. In all cases, well-defined products were obtained. The pendant dienyl groups were further reacted with bromine or osmium tetroxide to generate amphiphilic functional block copolymers with bromide or hydroxyl side groups (Scheme 17).

Trialkylsilyl-protected oligo(ethylene glycol)methacrylates, 2-{2-[(*tert*-butyldimethylsilyl)oxy]ethoxy}ethyl methacrylate (1) and 2-{2-[2-[(*tert*-butyldimethylsilyl)oxy]ethoxy]ethoxy}ethyl methacrylate (2) (Scheme 18), were used for the synthesis of amphiphilic block copolymers by anionic polymerization [64]. The following structures were prepared: poly(1)-*b*-P*t*BuMA, poly(2)-*b*-P*t*BuMA, poly(1)-*b*-poly(2), PS-*b*-poly(1), and PS-*b*-poly(2). Deprotection of the trialkylsilyl groups was performed with 2 N HCl in aqueous THF at 0 °C for 2 h yielding block copolymers containing the water-soluble poly[di(ethylene glycol) methacrylate] and poly[tri(ethylene glycol) methacrylate].

The monomer 3-(3,5,7,9,11,13,15-heptaisobutyl-pentacyclo[9.5.1³,⁹.1⁵,¹⁵,1⁷,¹³] octasiloxan −1-yl) propyl methacrylate, MAPOSS, has also been efficiently polymerized anionically. Therefore, PMMA-*b*-PMAPOSS and PS-*b*-PMAPOSS block copolymers were prepared in THF at −78 °C using LiCl to prevent side reactions (Scheme 19) [65]. The self-assembly behavior in bulk was studied by TEM and WAXS. In addition, block copolymers consisting of a PMMA block and a thermotropic POSS-containing methacrylate block were also prepared under similar experimental conditions, as shown in Scheme 20.

Scheme 18 Chemical structure of trialkylsilyl-protected oligo(ethylene glycol)methacrylates

1: m=2
2: m=3
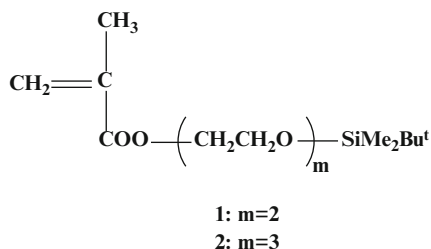
Multiblock copolymers of the type (PS-*b*-PMMA)$_n$ were prepared by the procedure shown in Scheme 21 [66]. The specific methodology combines an α-terminal functionalized living PS-*b*-PMMA as the building block with a specially designed linking reaction. Initially, an α-terminal 3-*tert*-butyldimethylsilyloxypropyl (SiOP)-functionalized living anionic PS-*b*-PMMA diblock was prepared by sequential addition of monomers employing 3-*tert*-butyldimethylsilyloxy-1-propyllithium (SiOPLi) as initiator. In a subsequent step, the α-SiOP end group was converted to an α-phenylacrylate (PA) terminus. The PA end-functionalized PS-*b*-PMMA was then reacted with the SiOP-functionalized living PS-*b*-PMMA chains, previously prepared, as described above, leading to the synthesis of an α-terminal SiOP-functionalized (PS-*b*-PMMA)$_2$ tetrablock copolymer. This procedure can be repeated resulting in the synthesis of multiblock copolymers of controlled molecular weights and narrow molecular weight distribution.

The aforementioned methodology that was adopted for the synthesis of multiblock copolymers of the type (PS-*b*-PMMA)$_n$ was further developed for the synthesis of triblock terpolymers, which cannot be prepared by sequential addition of monomers [67]. The synthesis of the PS-*b*-PMMA-*b*-P2VP triblock terpolymers was reported as depicted in Scheme 22. The approach involves the linking reaction of the living anionic PS-*b*-PMMA diblock with the α-terminal PA-functionalized P2VP. 2VP was polymerized in THF at $-78\,^\circ$C in the presence of LiCl using as initiator the product formed by the reaction of *sec*-BuLi and 1-(3-*tert*-butyldimethylsilyloxy-methylphenyl)-1-phenylethylene. The 3-(*tert*-butyldimethyl-silyloxy methyl) phenyl α-terminus was converted to an α-PA-functional group by treatment with Bu$_4$NF and then with α-phenylacrylic acid. The α-terminal PA-functionalized P2VP was then reacted with a fourfold excess of living PS-*b*-PMMA chains. Initially, the linking reaction took place at $-78\,^\circ$C, but the temperature was subsequently raised to $-40\,^\circ$C and allowed to react for 17 h. After careful fractionation, the pure product was acquired. The same triblock terpolymer can be obtained through the reaction sequence illustrated in Scheme 23. S was polymerized by SiOPLi as initiator followed by conversion of the end SiOP group to the corresponding PA. A living P2VP-*b*-PMMA block copolymer was prepared by sequential addition of the monomers. The in situ-formed (by reacting *sec*-BuLi with DPE) initiator polymerized 2VP at $-78\,^\circ$C in THF in the presence of LiCl. The living P2VP chains were subsequently end capped with a few units of tert-BuMA prior the addition of MMA to avoid the ester carbonyl attack side reaction. A 3.2-fold excess of the living
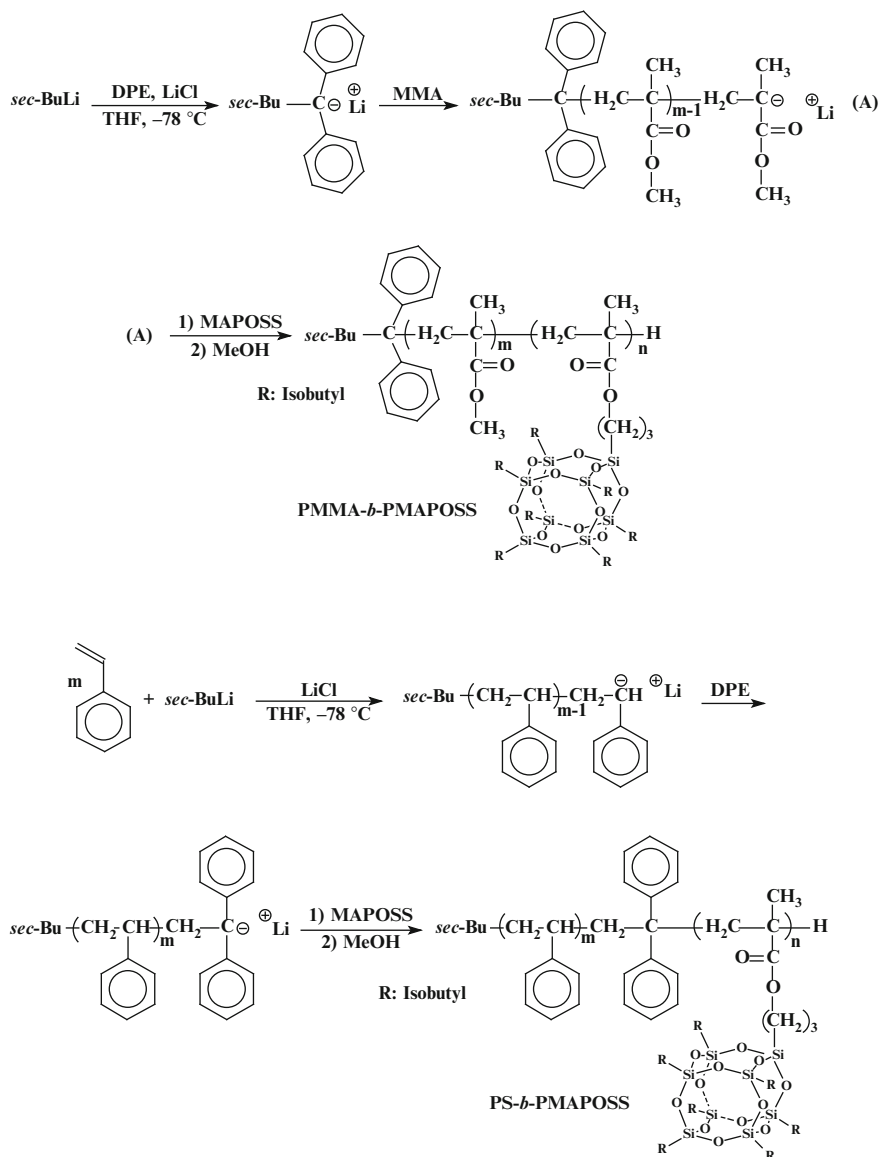
Scheme 19 Synthesis of PMMA-*b*-PMAPOSS and PS-*b*-PMAPOSS block copolymers

P2VP-*b*-PMMA chains was finally reacted with the α-terminal PA-functionalized PS in THF at -40 °C for 24 h to afford the desired terpolymer. Following similar methodologies, P2VP-*b*-PS-*b*-PMMA and PMMA-*b*-PS-*b*-P2VP triblocks along with other more elaborate structures were synthesized [68].

The effective anionic polymerization of acrylates is even more challenging than methacrylates, due to the presence of self-termination backbiting reactions, thus
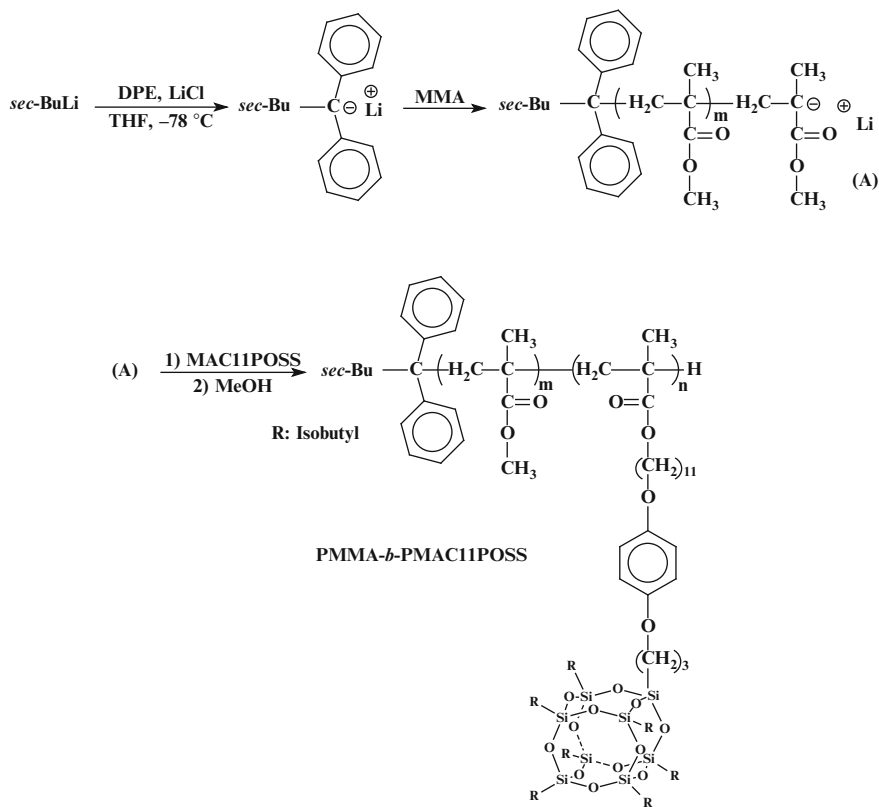
Scheme 20 Synthesis of thermotropic PMMA-*b*-PMAC11POSS block copolymer

requiring the use of ligands with high stabilizing efficiency [69]. One of the most effective systems involves the use of (diphenylmethyl)lithium in the presence of a tenfold excess 2-(2-methoxyethoxy)ethoxide, MEEOLi, at −78 °C in toluene/THF 9/1 or 75/25 (v/v) mixtures [70]. Using this methodology, well-defined block copolymers of MMA with 2-ethyhexyl acrylate, EtHA, BuA, and nonyl acrylate, NoA, have been synthesized starting from the polymerization of MMA. Alternatively, P*t*BuA-*b*-PEtHA and P*t*BuA-*b*-PBuA block copolymers have been successfully prepared employing *tert*-butyl 2-lithioisobutyrate as initiator in the presence of *tert*-BuOLi in toluene/THF mixture [71]. Block copolymers of MMA with EtHMA, BuA, EtA, and *t*BuA were prepared using methyl 2-lithioisobutyrate in the presence of a tenfold excess *tert*-BuOLi at −78 °C in a toluene/THF mixture. Under these conditions, only a very low amount of terminated PMMA block was detected by SEC analysis [72].

The anionic polymerization of dialkyl-substituted acrylamides has been also explored. It was found that polymerizations using initiators having cesium counterions proceeded without chain transfer and termination reactions [73]. More recently, well-controlled polymerization conditions were obtained employing
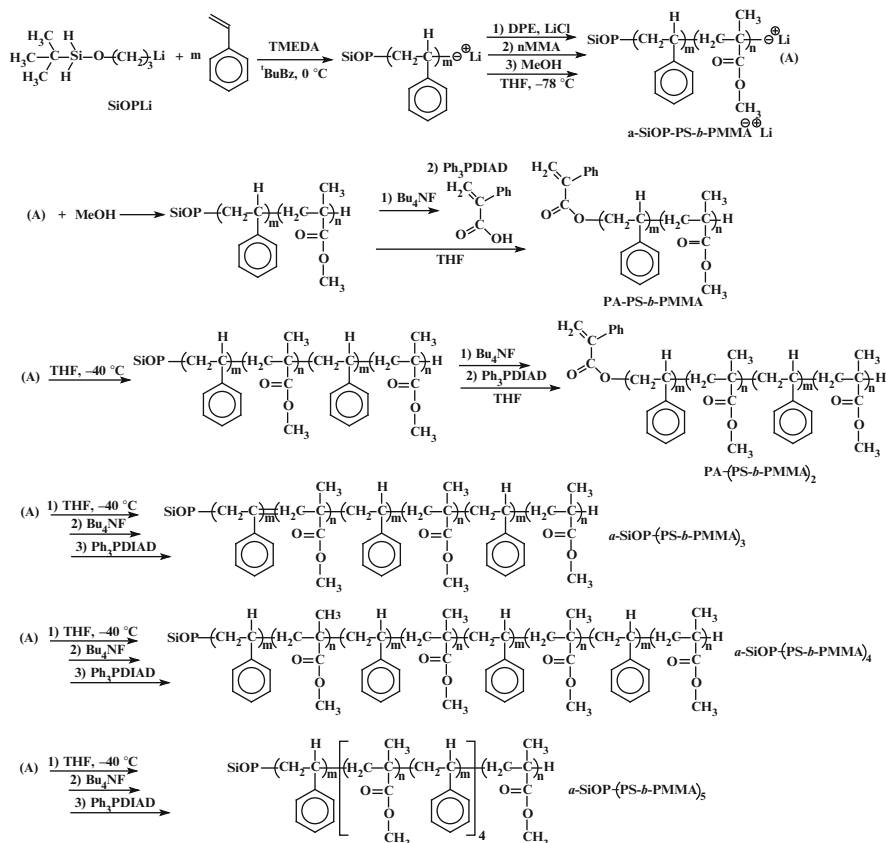
Scheme 21 Synthesis of various types of (PS-*b*-PMMA)$_n$ multiblock copolymers

organolithium or organopotassium initiators in the presence of Lewis acid additives, such as ZnEt$_2$ or Et$_3$B [74]. These additives affect the polymerization kinetics and the stereochemistry of the produced polymers. Using these methodologies, a series of block copolymers were obtained.

P*t*BuA-*b*-poly(*N,N*-diethylacrylamide), P*t*BuA-*b*-PDEAAm, block copolymers were synthesized starting from the polymerization of *t*BuA using 1,1-diphenylhexyllithium as initiator in the presence of LiCl ([LiCl]/[initiator] = 10/1) in THF at −78 °C [75]. A sevenfold excess Et$_3$Al was then added followed by the introduction of DEAAm for the synthesis of the desired product. The SEC trace of the crude polymer showed that a small part of the living first block was deactivated after the addition of the aluminum additive and the DEAAm monomer. Subsequent hydrolysis of the *tert*-butyl groups under acidic conditions resulted in the synthesis of poly(acrylic acid)-*b*-PDEAAm block copolymers.

A series of block copolymers with PS, P2VP, PEO, or P*t*BuA as first block and *N,N*-dimethylacrylamide, PDMAAm, or PDEAAm as the second block were
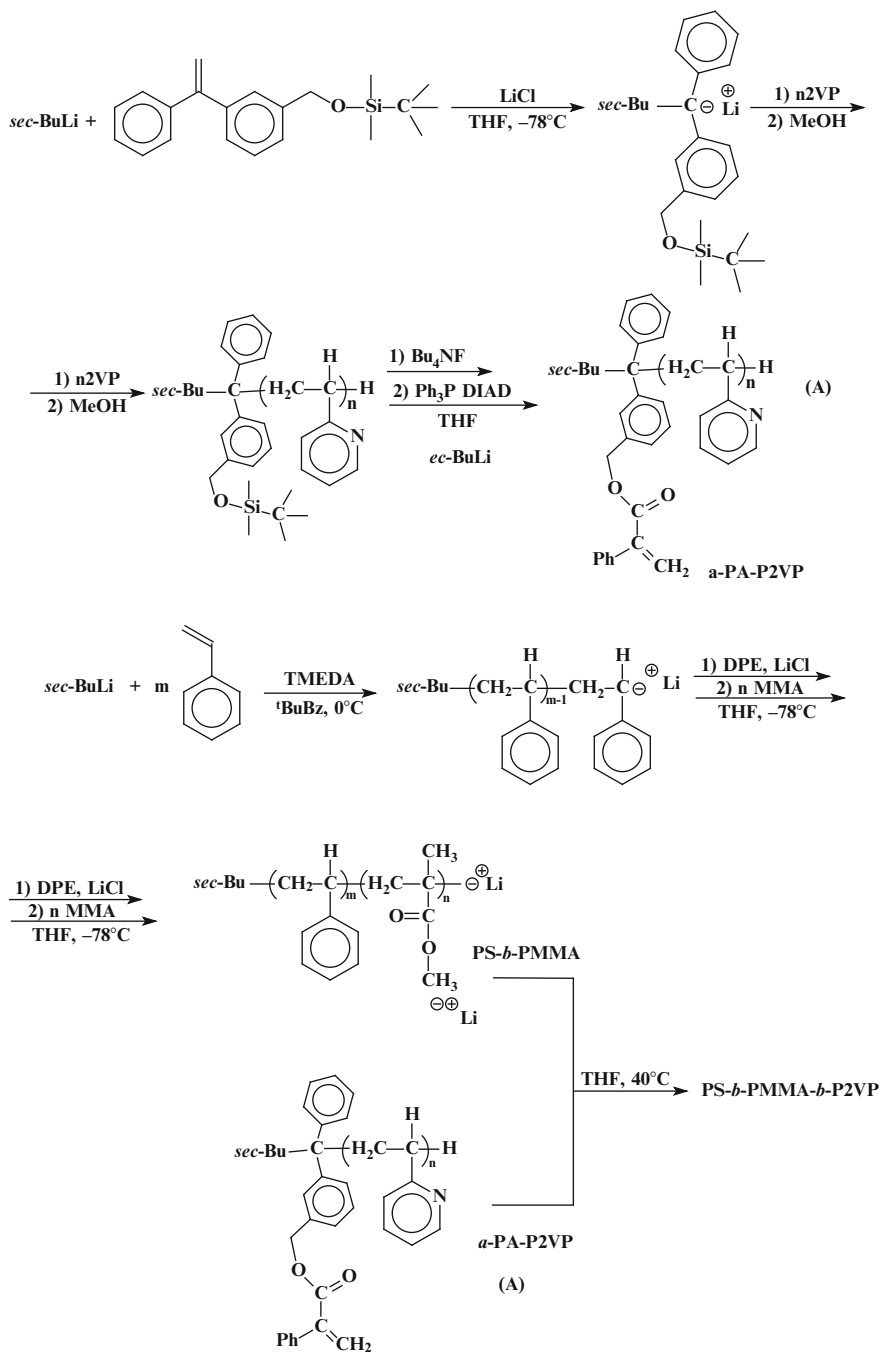
Scheme 22 Synthetic route for the preparation of PS-*b*-PMMA-*b*-P2VP triblock terpolymers
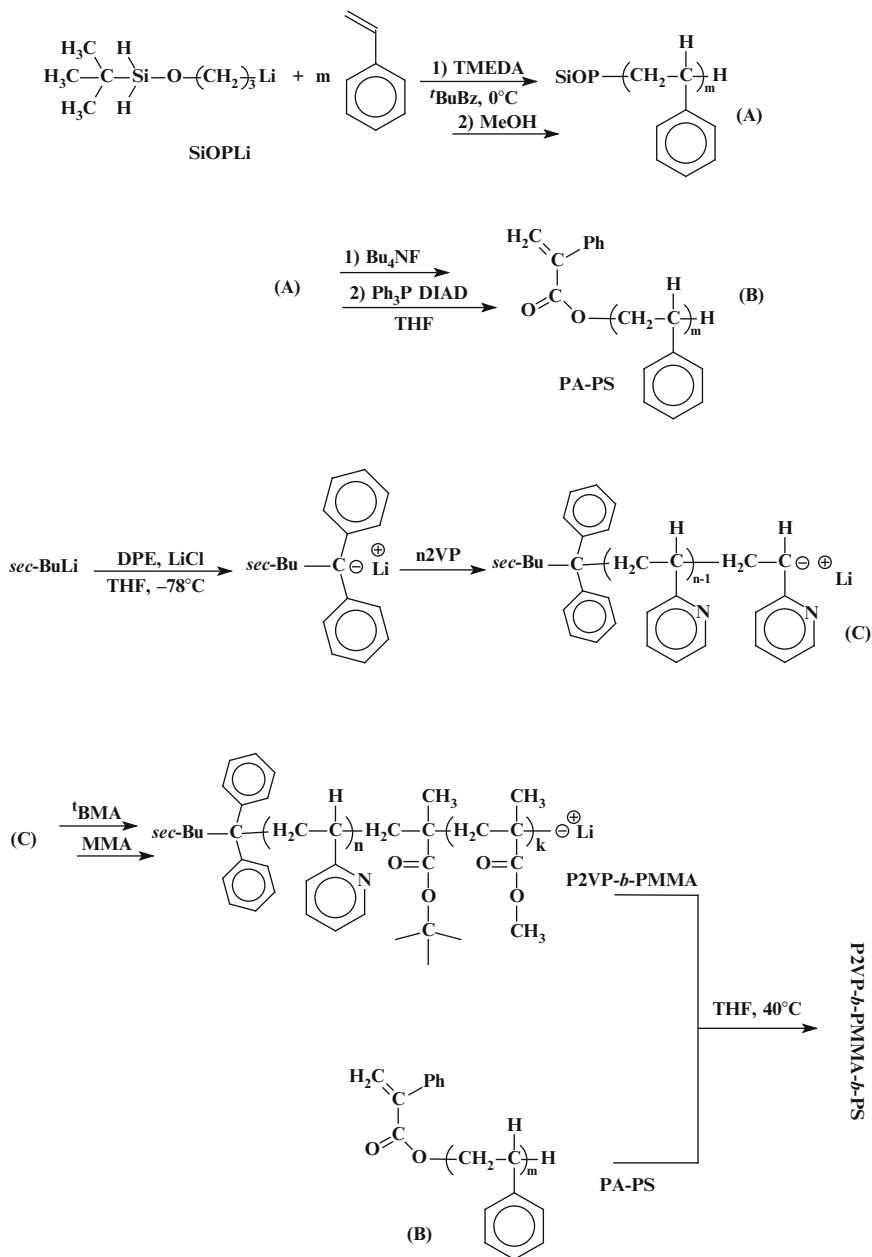
Scheme 23 Synthesis of P2VP-*b*-PMMA-*b*-PS triblock terpolymer by employing a SiOPLi initiator

synthesized by sequential addition of monomers. The first blocks were obtained under typical anionic polymerization conditions. Especially, tBuA and 2VP were polymerized in the presence of LiCl. The acrylamide monomers were polymerized in the presence of ZnEt$_2$. SEC analysis revealed that in most cases, bimodal traces were observed meaning that termination reactions take place during the crossover reactions. Subsequent fractionation afforded the pure copolymers [76].

N-propyl-*N*-(3-triisopropoxysilylpropyl)acrylamide was efficiently polymerized at 0 °C in THF using benzyl potassium as initiator in the presence of ZnEt$_2$. From these living polymer chains, the polymerization of *N,N*-diethylacrylamide was conducted leading to the synthesis of well-defined block copolymers. A similar procedure was adopted for the synthesis of block copolymers with *N,N*-dimethylacrylamide [77].

Well-defined PDEAAm-*b*-P*t*BuA-*b*-PDEAAm triblock copolymers were synthesized by sequential addition of monomers using a difunctional initiator. tBuA was initially polymerized in THF at −70 °C using sodium tetraphenyl di-isobutane as initiator in the presence of a tenfold excess of LiCl. DEAAm was then added at −70 °C to afford the desired products. Subsequent acid hydrolysis led to the synthesis of PDEAAm-*b*-PAA-*b*-PDEAAm triblock copolymers [78].

4.2 Vinyl Pyridines

The living anionic block copolymerization of 2- or 4-vinylpyridine, 2VP or 4VP, respectively, with styrene and dienes can be achieved at low temperatures in polar solvents through sequential monomer addition. The presence of the nitrogen atom reduces the reactivity of the vinyl pyridine anion; therefore 2VP and 4VP are always polymerized as the second monomer. During the anionic polymerization of 2VP or 4VP initiated by organolithium initiators side reactions may occur, forming either branched or cross-linked materials via the nucleophilic attack of another carbanion on the pyridine moiety [79]. In order to prevent these side reactions, the polymerizations are conducted at low temperatures (e.g., −78 °C) in the presence of additives such as LiCl [80], dibutylmagnesium [81], or DPE [82] and by using diphenylmethyl potassium as a weak initiator [83]. Block copolymers containing P2VP or P4VP blocks have been extensively studied [84] because they can be useful to prepare nanoparticles [85], nanofibers [86], or photonic band-gap [87] materials.

PI-*b*-P2VP block copolymers have been synthesized by a two-step sequential addition procedure [88]. The polymerization of I was conducted in benzene at room temperature leading to living polydienes having predominantly 1,4 microstructure. The living PI$^-$Li$^+$ benzene solution was added in an excess of THF (THF: benzene = 3:1), and the temperature was lowered to −78 °C followed by the addition of 2VP. Well-defined block copolymers were obtained. Subsequent reaction of the PI blocks with chlorosulfonyl isocyanate and treatment with NaOH resulted in the formation of block polyampholytes carrying sulfonate and
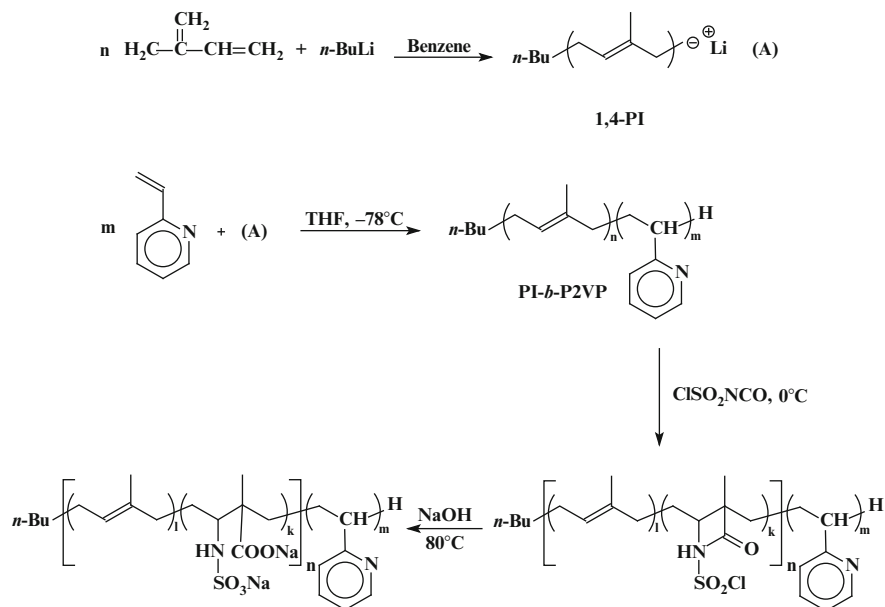
Scheme 24 Synthesis of PI-*b*-P2VP block copolymer and subsequent modification of the PI block to form polyampholytes carrying sulfonate and carboxylate groups

carboxylate groups along the PI block (Scheme 24). The self-assembly behavior of these materials has been studied in aqueous solutions at different pH values.

Block copolymers of poly(4-*tert*-butoxystyrene), P*t*BOS, and P4VP were prepared by sequential addition of monomers in THF at −78 °C using *sec*-BuLi as initiator [89]. For the polymerization of the 4VP, LiCl was added, since it associates with the living chain ends, helping to reduce the cross-linking side reactions realized after nucleophilic addition of organolithium compounds to the pyridine ring [90]. Subsequent hydrolysis of the *tert*-butoxy side groups by treatment with HCl in DMF at 85 °C leads to the synthesis of poly(hydroxystyrene)-*b*-P4VP, PHOS-*b*-P4VP, copolymers (Scheme 25). The intra- and intermolecular interactions through hydrogen bonding of the side pyridine and phenol groups were also studied.

The most efficient linking agents for the linking of living P2VP⁻Li⁺ chains are the bromomethyl benzene derivatives [10]. PS-*b*-P2VP-*b*-PS triblock copolymers were synthesized by linking living PS-*b*-P2VP⁻Li⁺ diblocks with 1,4-bis (bromomethyl)benzene (Scheme 26) [91]. Thick films of these materials were cast from solution and their structures were analyzed by SAXS. Using the same methodology, P2VP-*b*-PEO-*b*-P2VP triblock copolymers were prepared [92]. The linking reaction took place in the presence of a catalytic amount of CsI, which was used to transform the –CH₂Br groups to the more reactive –CH₂I groups in situ (Scheme 27).

P2VP-*b*-P4VP block copolymers were synthesized starting from the polymerization of 2VP in THF at −78 °C using *sec*-BuLi as initiator [93]. Prior to the
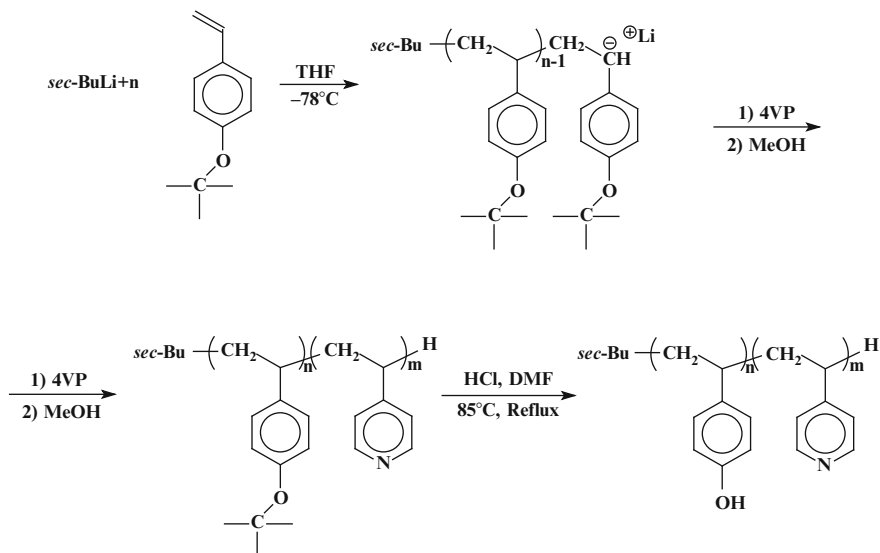
Scheme 25 Synthesis of P*t*BOS-*b*-P4VP and subsequent modification to PHOS-*b*-P4VP

addition of 4VP, the living P2VP⁻Li⁺ chains were end capped with one DPE unit. The phase behavior of these copolymers has been studied.

Triblock terpolymers PS-*b*-PBd-*b*-P2VP and PBd-*b*-PS-*b*-P2VP, where PBd is polybutadiene (mostly 1,2-PBd), have been prepared in order to study the microphase separation by transmission electron microscopy, TEM, and SAXS. In the first case, the triblocks were synthesized by sequential addition of monomers in THF using *sec*-BuLi as initiator [94]. For the second type of copolymers, living PBd-*b*-PS diblocks were prepared in benzene at 40 °C in the presence of a small quantity of THF in order to obtain the desired 1,2-content and to accelerate the crossover reaction as well. DPE was then added to decrease the nucleophilicity of the active centers to avoid side reactions with the THF, which in combination with benzene was the solvent of the final step.

Triblock terpolymers P*t*BOS-*b*-PS-*b*-P4VP were also prepared by sequential addition of monomers, conducting the polymerization in THF at −78 °C using *sec*-BuLi as initiator [95]. The self-assembly behavior has been studied by TEM and SAXS along with the effect induced by the complexation of high molecular weight phenols through hydrogen bonding with the 4VP groups.

Symmetric triblock copolymers P4VP-*b*-PBd-*b*-P4VP were prepared using a difunctional initiator derived from the reaction of *m*-diisopropenylbenzene with *tert*-butyllithium at −20 °C (Scheme 28) [96]. The synthesis was conducted in a mixture of toluene and THF, at temperature higher than room temperature for the polymerization of Bd; the temperature was reduced to −78 °C, prior to the addition of 4VP. The 4VP monomer was added along with an extra quantity of THF and the content of the monomer was kept lower than 30 % to avoid problems arising from the poor solubility of the P4VP blocks in THF. Under these conditions, chain branching side reactions were avoided.
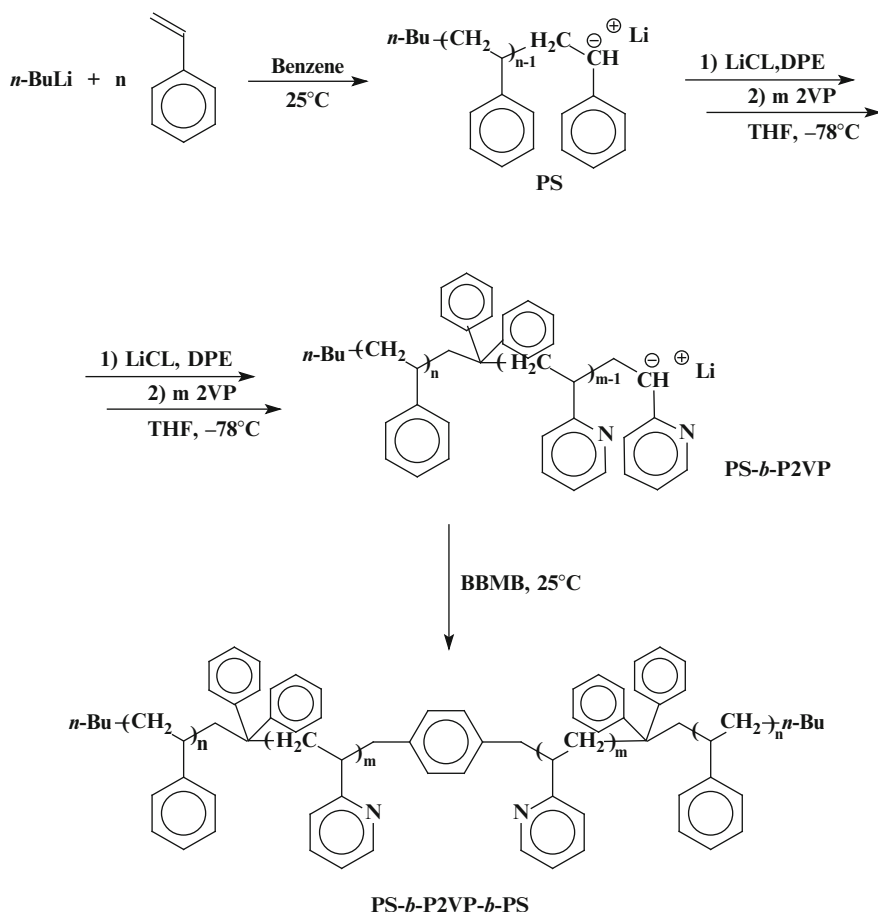
Scheme 26 Synthesis of symmetric PS-*b*-P2VP-*b*-PS triblock copolymer

Block copolymers of poly(1,3-cyclohexadiene), PCHD, and P2VP were efficiently synthesized [97]. CHD was polymerized first in THF at $-78\ ^{\circ}$C using *sec*-BuLi as initiator in the presence of the lithium enolate of acetaldehyde, LiEA (molar ratio of LiEA over *sec*-BuLi equal to 10:1) followed by the addition of 2VP. Subsequent dehydrogenation by reacting with *p*-chloranil afforded the corresponding poly(1,4-phenylene)-*b*-P2VP block copolymers (Scheme 29). The self-assembly behavior of these materials was thoroughly studied in selective solvents, and the micellar structures were used for the synthesis of CdS nanoparticles.

The anionic polymerization of 2-(4-vinylphenyl)pyridine, VPPy, was reported [98] under various experimental conditions (Scheme 30). Coordination of VPPy with LiCl for 72 h at $-45\ ^{\circ}$C followed by polymerization with *sec*-BuLi allowed for the quantitative polymerization of the monomer but only after 3 days. Better results were obtained when employing DPM-K as initiator. In this case, the polymerization proceeds to a 100 % yield, at $-78\ ^{\circ}$C, within 150 min and leading to products of
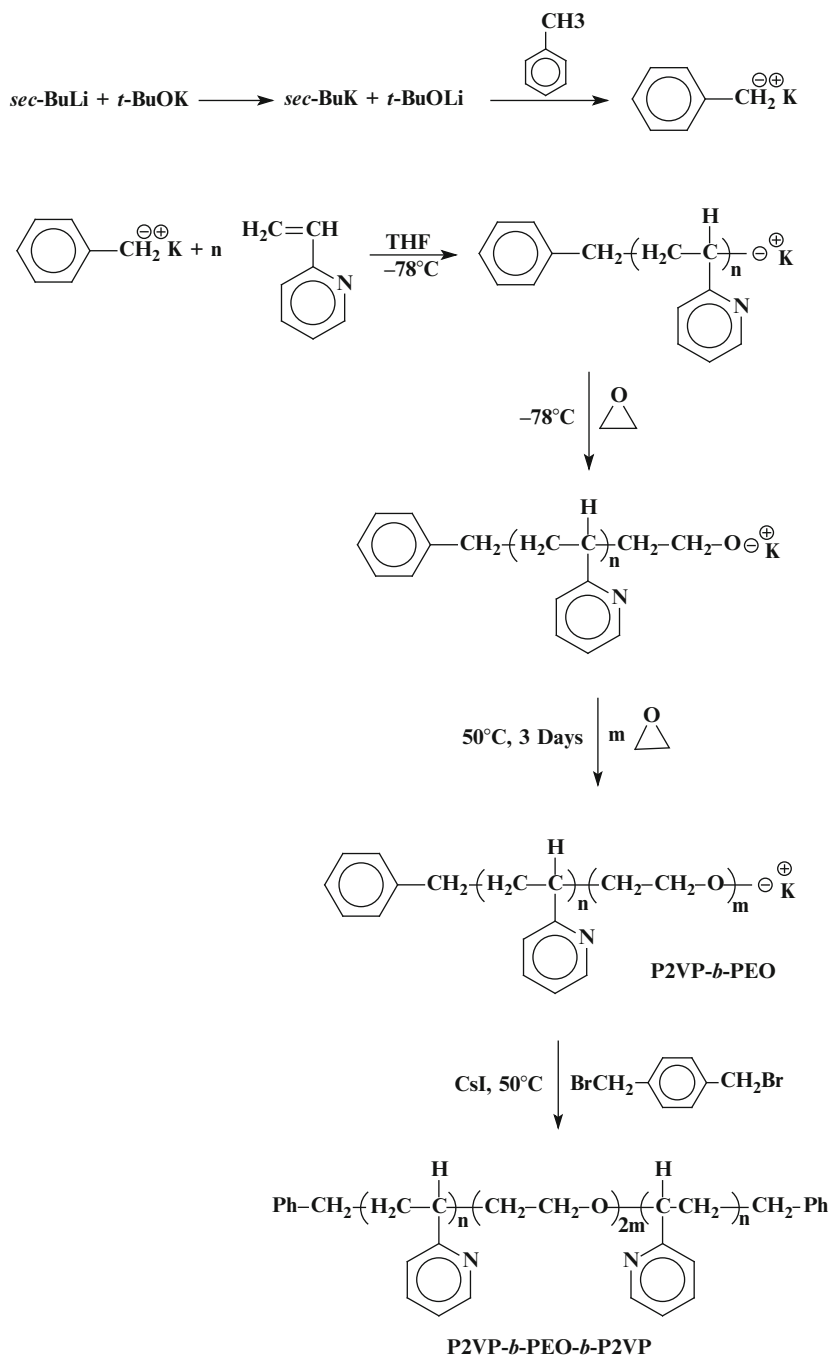
Scheme 27 Synthesis of P2VP-*b*-PEO-*b*-P2VP symmetric triblock copolymer
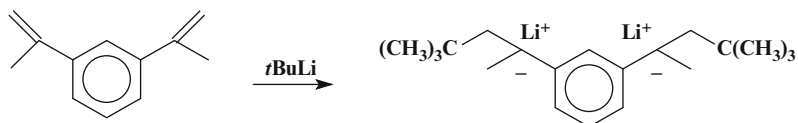
Scheme 28 Bifunctional initiator used in symmetric triblock copolymer synthesis
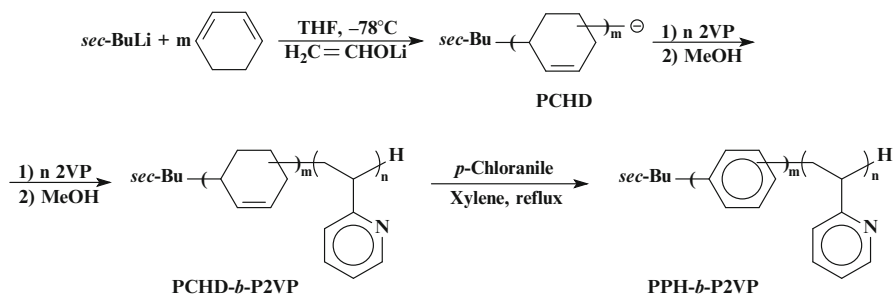
Scheme 29 Synthesis of PCHD-*b*-P2VP block copolymer and subsequent dehydrogenation, to provide PPH-*b*-P2VP block copolymers
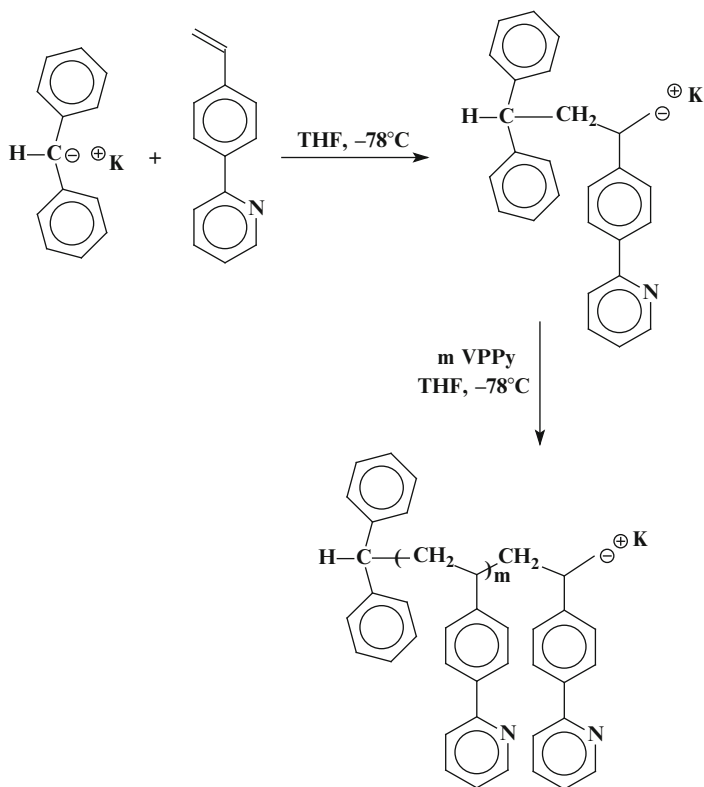
Scheme 30 Anionic Polymerization of VPPy

very narrow molecular weight distribution. Efforts to prepare block copolymers with S and I starting from the polymerization of VPPy were not successful, obviously because the nucleophilicity of the living PVPPy$^-$Li$^+$ is not strong enough to initiate the polymerization of S or I. The synthesis of P2VP-*b*-PVPPy copolymers was successful when starting the polymerization from either monomer. The block copolymerization of VPPy and MMA was also successfully carried out leading to well-defined products.
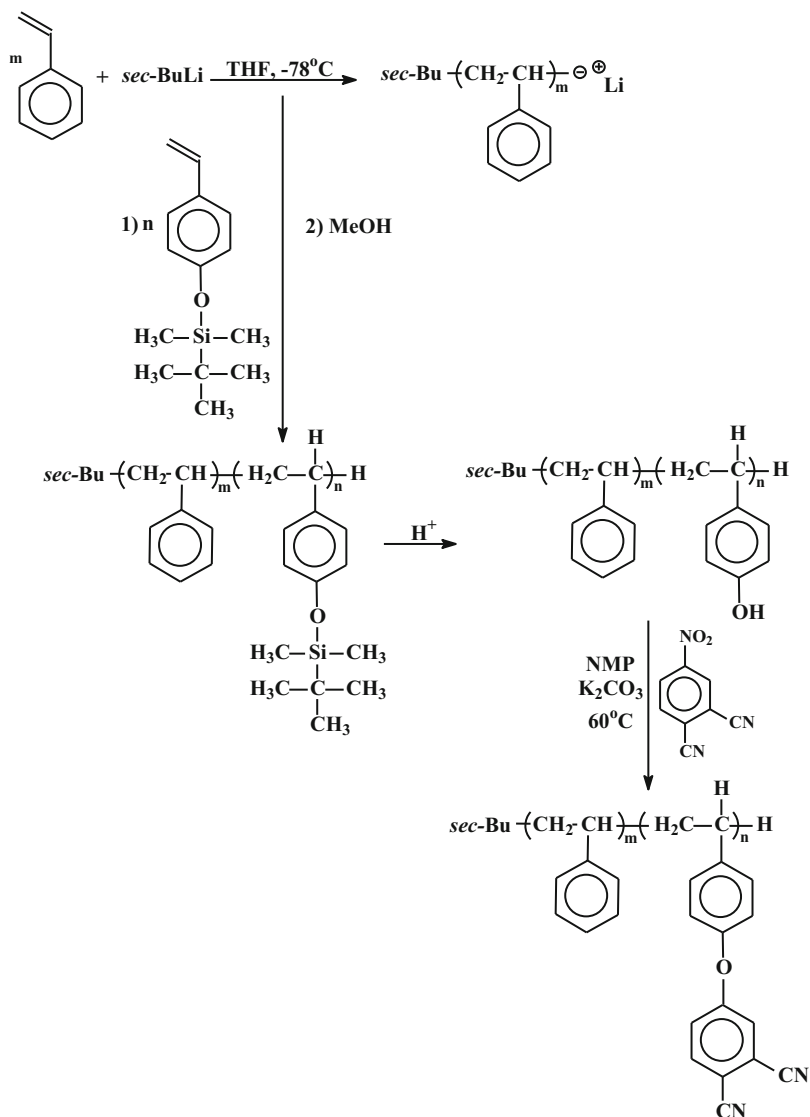
Scheme 31 Synthesis of PS-*b*-PHOS block copolymers, and further modified towards functionalized copolymers
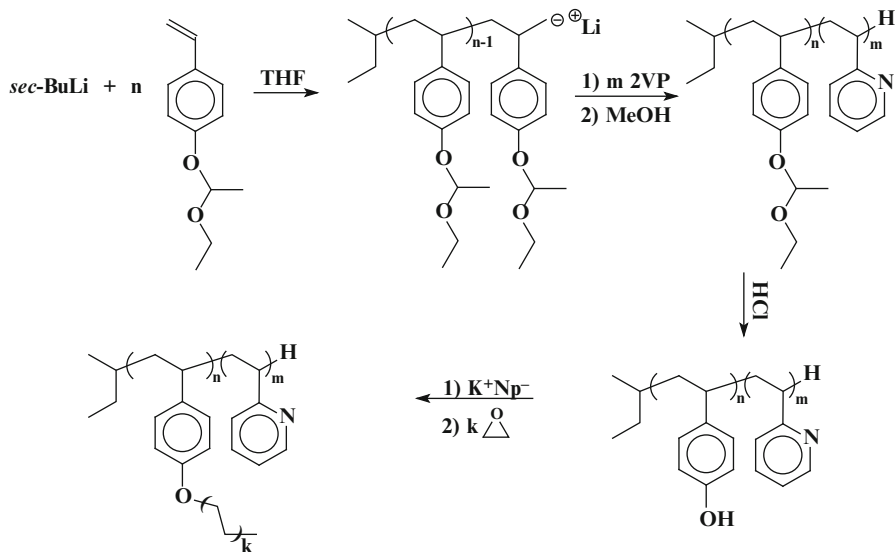
Scheme 32 Synthesis of PHOS-*b*-P2VP block copolymer from a PpEES-*b*-P2VP precursor copolymer

4.3 Other Polar Monomers

Recent achievements in anionic polymerization have expanded the use of this technique to other less conventional monomers. The combination of these monomers with other more common ones has allowed for the synthesis of novel copolymeric materials with very interesting properties.

The living anionic polymerization of *tert*-butyldimethylsilyloxystyrene has been reported [99]. PS-*b*-poly(*tert*-butyldimethylsilyloxystyrene) block copolymers were then synthesized by sequential addition of monomers employing n-BuLi as initiator [100]. The polymerization was conducted in THF at −78 °C in order to avoid the cleavage of the silyl ether bond of *tert*-butyldimethylsilyloxystyrene. Well-defined products of narrow molecular weight distribution were obtained. The silyl ether bonds were subsequently cleaved by HCl in THF solution leading to the synthesis of PS-*b*-PHOS diblocks. These materials were further modified after reaction with 4-nitrophthalonitrile via nucleophilic aromatic substitution reaction leading to the synthesis of PS-*b*-poly(4-vinylphenoxyphthalonitrile) block copolymers (Scheme 31). The copolymers were further employed for the preparation of magnetic cobalt nanoparticles.

Poly[p(1-ethoxy ethoxy) styrene], PpEES, was also employed as precursor for the synthesis of PHOS after deprotection of the protective group in the presence of HCl at room temperature. PpEES-*b*-P2VP block copolymers were prepared in THF at −90 °C by sequential addition of monomers and without the use of any additive during the polymerization of 2VP. These copolymers were transformed to PHOS-*b*-P2VP diblocks after hydrolysis under mild conditions (Scheme 32) [101].
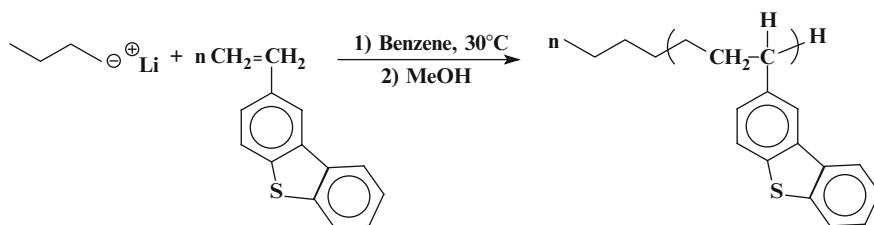
Scheme 33 Anionic polymerization of 2VDBT
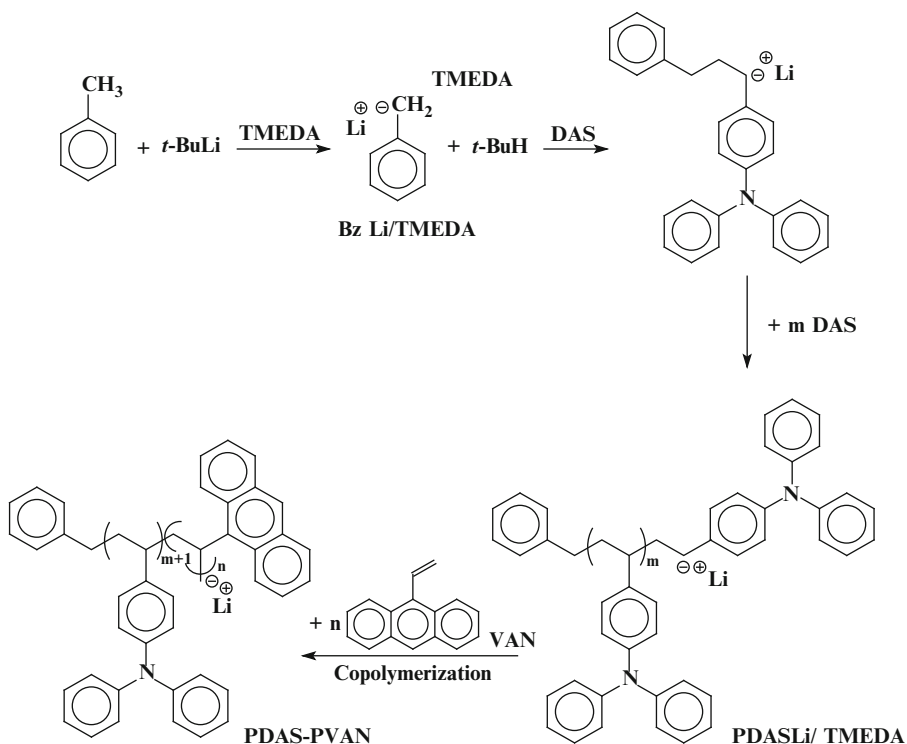
Scheme 34 Synthesis of PDAS-*b*-PVAN block copolymers

2-Vinyldibenzothiophene, 2VDBT, was successfully polymerized anionically at 30 °C in benzene using n-BuLi as initiator, leading to products of predicted molecular weights and low polydispersity (Scheme 33). Block copolymers with styrene were efficiently synthesized starting either from the polymerization of styrene or 2VDBT as well [102].

4-Diphenylaminostyrene, DAS, was anionically polymerized in toluene at room temperature using *tert*-BuLi in the presence of N,N,N',N'-tetramethylethylenediamine, TMEDA. The actual initiator was benzyllithium, in situ generated by the proton

abstraction reaction of toluene with *tert*-BuLi [103]. Using this system, block copolymers of DAS and 9-vinylanthracene, VAN, PDAS-*b*-PVAN, were synthesized (Scheme 34). Although the polymerization of DAS was quantitative, the polymerization yield for VAN was 75 %. Products of rather low molecular weights and moderate polydispersities were prepared. The optical and electrical properties of these copolymers were studied [104].
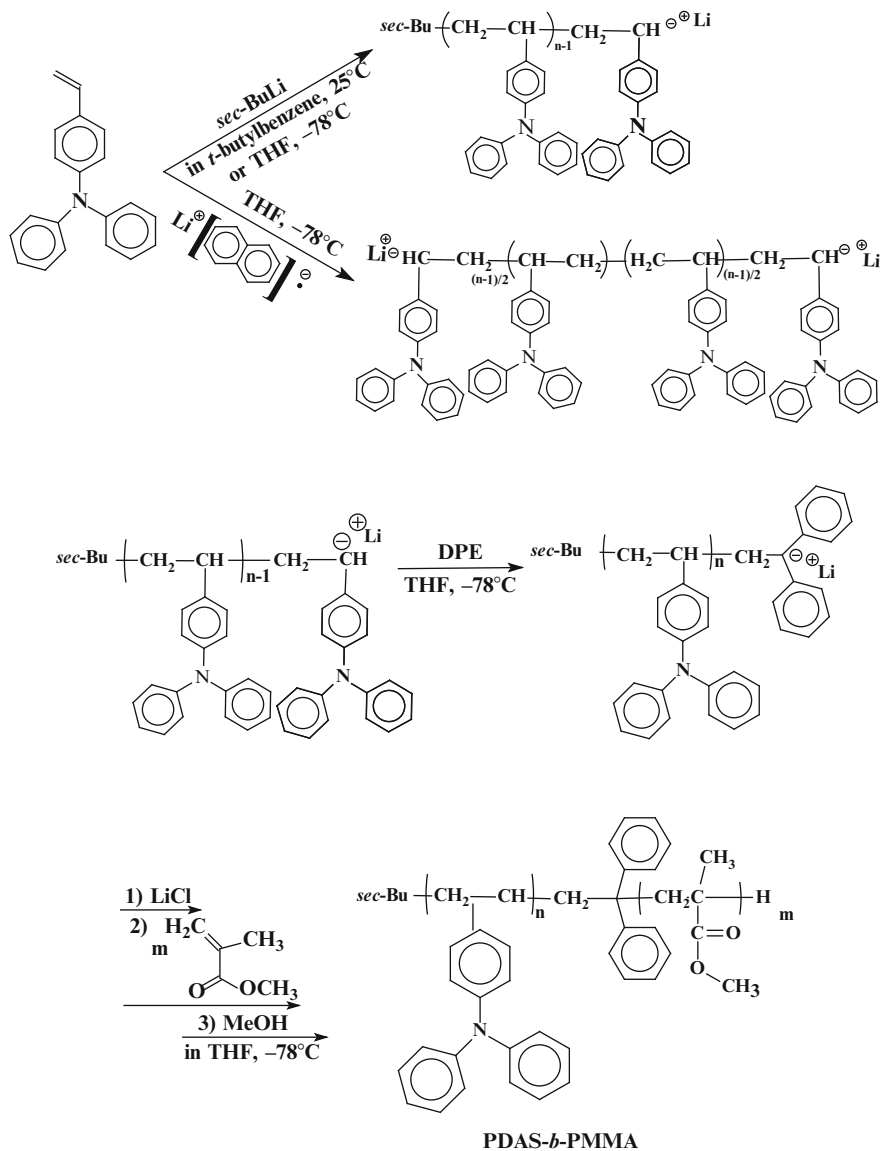
Scheme 35 Polymerization of DAS using a monofunctional and bifunctional initiator; and block copolymer synthesis after addition of MMA. Synthesis of PS-*b*-PDAS-*b*-PS triblock copolymer, using a bifunctional initiator
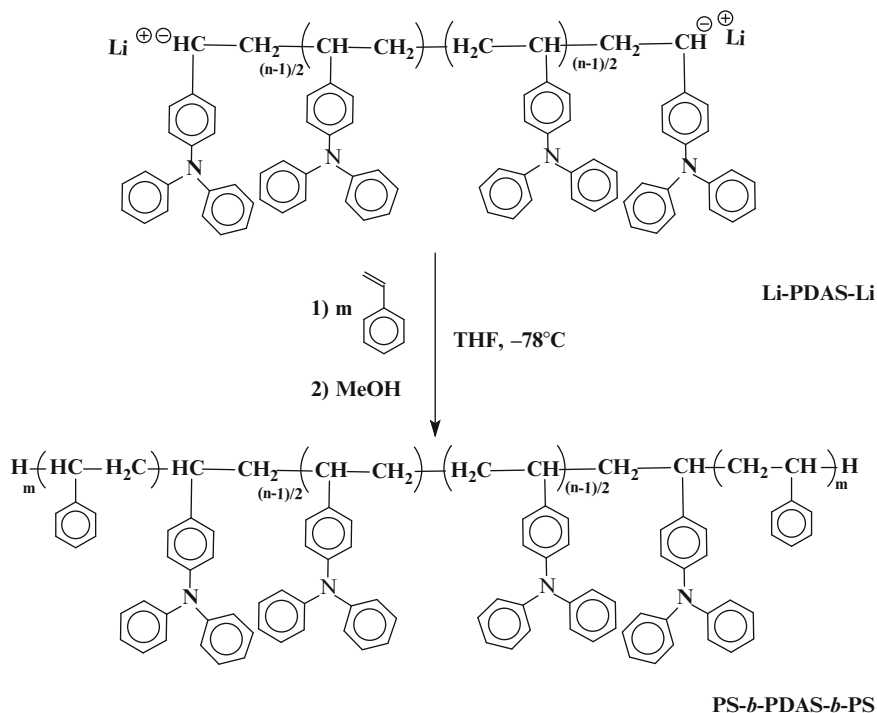
Scheme 35 (continued)

DAS was also polymerized in *tert*-butylbenzene at 25 °C or THF at −78 °C using *sec*-BuLi as initiator. The living polymers in THF solutions were end capped with DPE, followed by the addition of a fivefold excess of LiCl and MMA. Well-defined PDAS-*b*-PMMA block copolymers were obtained. Lithium naphthalenide was also employed as a difunctional initiator for DAS, thus allowing for the synthesis of PS-*b*-PDAS-*b*-PS triblock copolymers (Scheme 35) [105].

The anionic polymerization of dialkylvinyl phosphonates has been reported in the literature [106]. Well-defined polymers were obtained by conducting the polymerization in THF at −78 °C using n-BuLi as initiator. PS-*b*-poly(diethylvinyl phosphonate), PS-*b*-PDEVP, block copolymers were subsequently synthesized. Prior the addition of DEVP, the living polystyryl anions were end capped with DPE to avoid the nucleophilic attack of these highly reactive anions on the phosphorous atoms of the DEVP monomers. Under these conditions, well-defined products were synthesized (Scheme 36) [107].

PS-*b*-poly(diisopropylvinyl phosphonate), PS-*b*-PVPE, block copolymers were also synthesized following similar approaches. However, in this case, styrene was polymerized in cyclohexane at room temperature, using n-BuLi as initiator. The solvent was changed to THF, the temperature was lowered to −78 °C, and PVPE was added, leading to the synthesis of the desired block copolymers. Subsequent hydrolysis with trimethylsilylbromide afforded the corresponding PS-*b*-poly(vinyl phosphonic acid) copolymers (Scheme 37) [108].
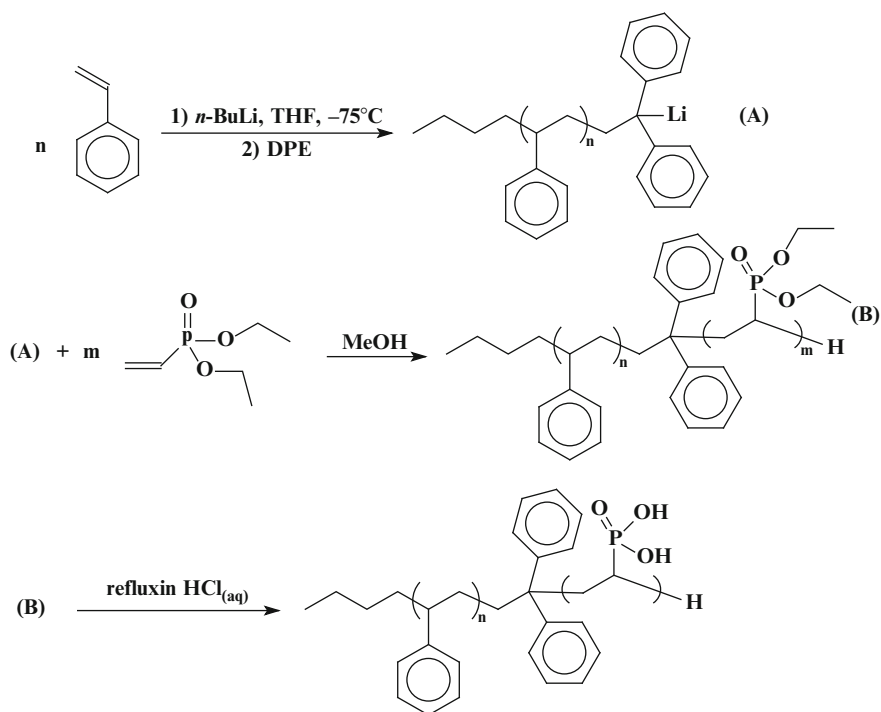
Scheme 36 Synthesis of PS-*b*-PDEVP
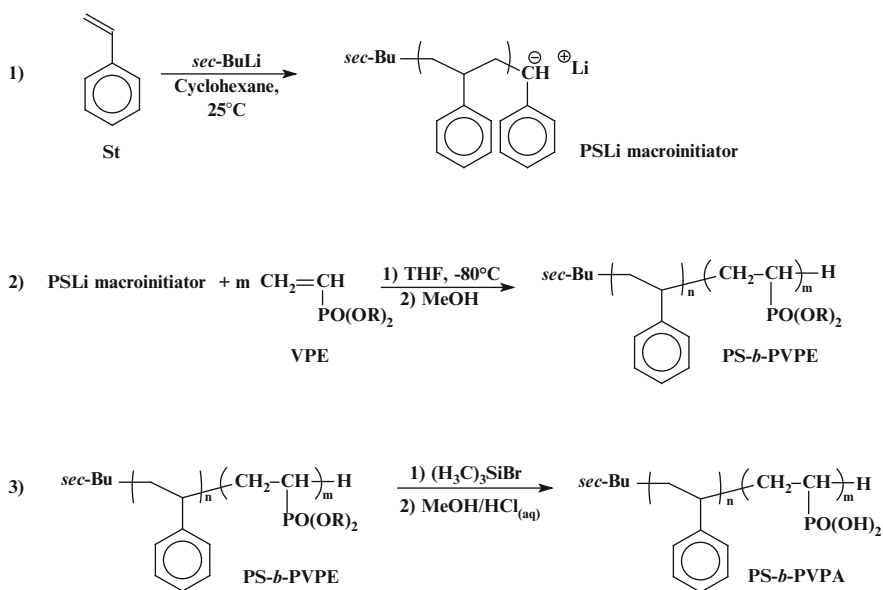
Scheme 37 Synthesis of PS-*b*-PVPA
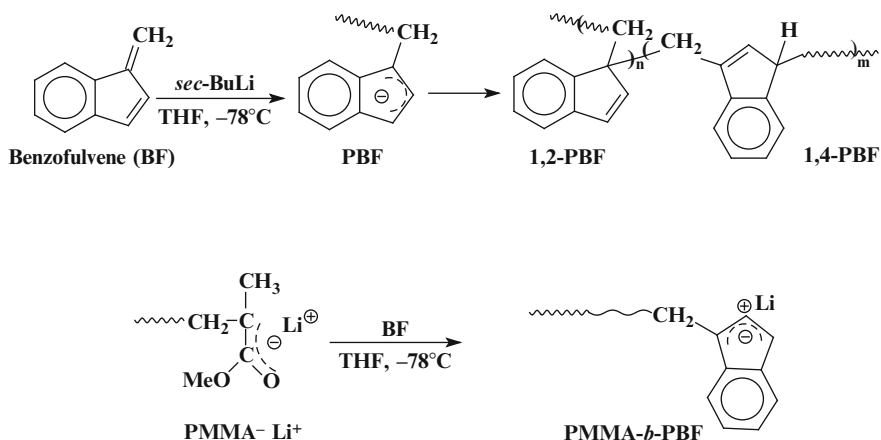
Scheme 38 Synthesis of PMMA-*b*-PBF block copolymer

Benzofulvene, BF, was anionically polymerized with *sec*-BuLi or diphenyl-methylpotassium in THF at −78 °C for 1 h leading to predicted molecular weights and narrow molecular weight distributions. The low nucleophilicity enolate anion of living PMMA was able to initiate the efficient polymerization of BF leading to well-defined PMMA-*b*-PBF block copolymers (Scheme 38) [109].

5 Block Copolymers from Cyclic Monomers

5.1 *Hexamethylcyclotrisiloxane*

Monofunctional and bifunctional low molecular weight poly(dimethylsiloxane), PDMS, carrying one or two end-hydroxyl groups were used as macroinitiators for the synthesis of diblock and triblock copolymers, respectively, with 2-(dimethylamino)ethyl methacrylate, DMAEMA, PDMS-*b*-PDMAEMA, and PDMAEMA-*b*-PDMS-*b*-PDMAEMA [110]. The potassium salt of dimethyl sulfox-ide, DMSO⁻K⁺, was used to convert the terminal hydroxyl groups of the PDMS chains to potassium alcoholates. Subsequent addition of DMAEMA led to the forma-tion of the desired diblock or triblock copolymers. Extreme care should be given in the activation of the macroinitiator, especially regarding control of the stoichiometry of the reaction. Excess DMSO⁻K⁺ will act as an initiator to lead to the formation of PDMAEMA homopolymer along with the diblock or triblock copolymers. Smaller quantities of DMSO⁻K⁺ will lead to residual inactivated PDMS chains. Particularly, in the case of the bifunctional macroinitiator, deficient quantities of DMSO⁻K⁺ will provide a mixture of diblock, triblock, and PDMS homopolymer. Moderately broad molecular weight distributions ($M_w/M_n \sim 1.40$) were obtained. The micellar properties of these products were studied in selective solvents.
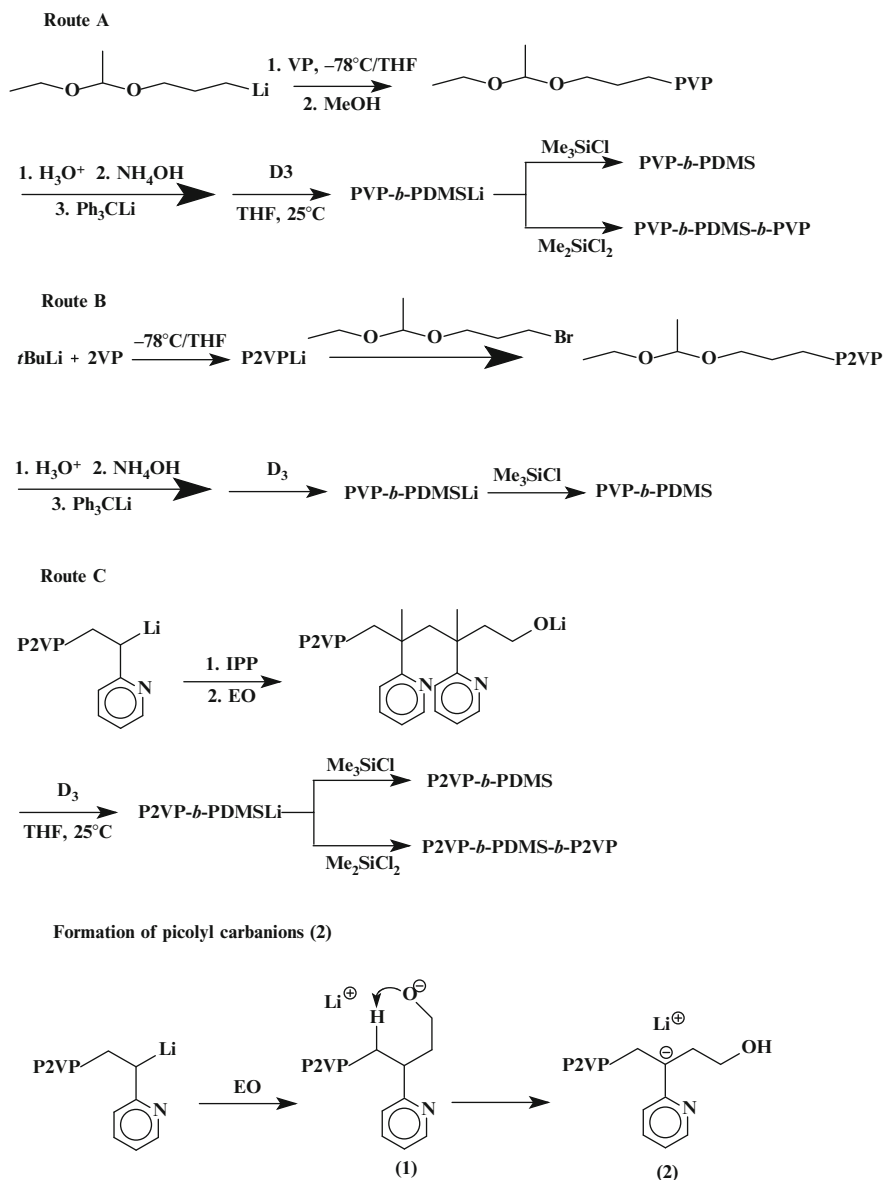
Scheme 39 Synthesis of PVP-*b*-PDMS block copolymers and PVP-*b*-PDMS-*b*-PVP triblock copolymers through different synthetic methods

A series of diblock AB and triblock ABA copolymers, where A is either P2VP or P4VP and B is poly(dimethylsiloxane), PDMS, were prepared by anionic polymerization [111] (Scheme 39). Three different approaches were employed for this purpose. According to the first strategy (route A), an acetal-functionalized alkyllithium initiator

was employed for the polymerization of 2VP or 4VP in THF at $-78\,^{\circ}$C. Acid hydrolysis of the acetal group and titration of the hydroxyl groups with triphenyllithium gave a lithium alkoxide end group. These P2VP- and P4VP-lithium alkoxides can effectively initiate the polymerization of hexamethylcyclotrisiloxane, D_3, to produce the desired diblock copolymers. For extended polymerization times, bimodal distributions were obtained, attributed to lithium silanolate aggregation. However, when high monomer concentrations (between 1.0 and 2.0 M) and relatively low monomer conversions ($<40\,\%$) were used, narrow molecular weight distribution products were obtained. Coupling of the lithium silanolate copolymers with dimethyldichlorosilane was effective in producing the ABA copolymers. According to the alternative route B, instead of using a functional initiator, a functional electrophilic termination reagent was employed. 2VP was polymerized with *tert*-BuLi in THF at $-78\,^{\circ}$C. The living P2VP chains were terminated by the reaction with the suitable bromoacetal. The corresponding termination reaction of P4VP with the same bromoacetal was not effective, probably due to the lower reactivity of the P4VP anion that may be further complicated by the alkylation of the pyridine nitrogen with the bromoacetal. Following procedures similar to those in the previous method, the lithium alkoxide was prepared to afford either the diblock copolymer P2VP-*b*-PDMS or the triblock copolymer P2VP-*b*-PDMS-*b*-P2VP after coupling of the living diblock with dimethyldichlorosilane. In this case, the conversion of the D_3 monomer was also remained low in order to avoid side reactions. The third method (route C) involves the end capping of living P2VPLi with 2-isopropenylpyridine, IPP, followed by the addition of one equivalent of ethylene oxide. The lithium alkoxide, thus produced, efficiently promoted the polymerization of D_3 leading to the formation of the diblock and triblock copolymers. Effort to form the lithium alkoxide by the direct capping of P2VPLi with ethylene oxide finally afforded bimodal distributions. It was proposed that a picolyl carbanion (Scheme 39 (2)) is formed from the lithium alcoholate (Scheme 39 (1)). This anionic site is not able to initiate the polymerization of D_3, thus leading to bimodal distributions. The intramolecular rearrangement reaction was avoided by end capping the living chains with 2-isopropenylpyridine lacking an α-hydrogen, responsible for the side reactions. Under these conditions, well-defined copolymers were prepared. However, this end-capping reaction was not successful for P4VPLi chains.

The problems encountered for the polymerization of D_3 were successfully resolved by performing the polymerization in two steps [112]. In the first step, the polymerization took place in benzene at room temperature with *n*-BuLi as initiator. In the second step, the temperature was lowered to $-20\,^{\circ}$C, and the polymerization was allowed to proceed until completion after several days. With this methodology, the PDMS was obtained in quantitative conversions, controlled molecular weights, and narrow molecular weight distributions. Taking advantage of the living character of the polymerization, model triblock copolymers PS-*b*-PDMS-*b*-PS were prepared by linking the living PS-*b*-PDMSLi with bis(dimethylchlorosilyl)ethane (Scheme 40). This specific linking agent was chosen to accelerate the coupling procedure and to avoid the side reactions at room temperature, where the linking reaction takes place.

In another report, the copolymerization of Bd and hexamethylcyclotrisiloxane (D_3), resulting in the well-defined synthesis of PBd-*b*-PDMS through sequential

sec-BuLi + St $\xrightarrow{\text{benzene}}$ PSLi

PSLi + [cyclic structure: Si-O-Si-O-Si-O ring with methyl substituents] $\xrightarrow[\substack{\text{r.t.} \\ \text{18 hrs}}]{\text{benzene}}$ PS$-\left(\underset{CH_3}{\overset{CH_3}{Si}}-O\right)_{0\text{-}2}\underset{CH_3}{\overset{CH_3}{Si}}-OLi$

$\xrightarrow[\substack{\text{2 hrs at } 25°C \\ \text{7 days at } -20°C}]{\substack{D_3 \\ \text{benzene/THF:1/1}}}$ PS-PDMSOLi $\xrightarrow[\text{24 hrs at } 25°C]{(CH_3)_2(Cl)SiCH_2CH_2Si(Cl)(CH_3)_2}$ PS-b-PDMS-b-PS

Scheme 40 Synthesis of symmetric PS-b-PDMS-b-PS triblock copolymers, with complete polymerization of D_3

monomer addition was presented. First, the polymerization of Bd, using *sec*-BuLi, in cyclohexane took place, followed by the addition of the D_3 monomer along with a volume-equivalent amount of THF. The copolymerization was completed in a two-step reaction process. The first involved the initiation of D_3 with PB^-Li^+ for 20 h at room temperature followed by the propagation after the addition of THF, again in room temperature. The next step involved the complete conversion of the monomer at $-20\,°C$ [113].

PDMS has also been copolymerized with tetramethyltetravinylcyclotetrasiloxane ($D4^v$). Block copolymerization of PDMS-b-PMVS started with the polymerization of D_3 in hexane using *n*-BuLi as initiator for 2 h, followed by the sequential addition of the second monomer. The reaction was quenched through the addition of trimethylsilyl chloride as terminating agent (Scheme 41). Copolymerization resulted in relatively broad molecular weight distributions. In contrast to the very fast polymerization of D_3, the polymerization of D_4^v was much slower, and complete conversion was impossible [114].

5.2 Ethylene Oxide

The biocompatible and physical properties of PEO have rendered it as the monomer of choice for drug delivery, amphiphilic, and water-soluble systems. The lack of immunogenicity is one of its most interesting and unique properties making it a suitable vessel material for outer corona structures that prevents protein adsorption and cell adhesion [115].

It is well known that the classic organolithium initiators fail to polymerize EO in weak or medium polarity solvents in the absence of suitable additives, due to the very strong lithium-oxygen bond produced during the initiation of EO, which is unable to

Scheme 41 Synthesis of PDMS-*b*-PMVS block copolymers

promote the propagation reaction [116]. In contrast, benzyl potassium was success-
fully employed as initiator for the synthesis of block copolymers containing ethylene
oxide, EO. PS-*b*-PEO block copolymer, PI-*b*-P2VP-*b*-PEO triblock terpolymer, PS-
b-PI-*b*-P2VP-*b*-PEO tetrablock quaterpolymer, and PS-*b*-PI-*b*-P2VP-*b*-PtBuMA-*b*-
PEO pentablock quintopolymer were prepared by sequential addition of monomers
[117]. The monomer sequence was based on the relative nucleophilicity of the active
centers. Detailed characterization data revealed that structures with predictable
molecular weights, narrow molecular weight distribution, and chemical and compo-
sitional homogeneity were obtained in all cases.

An alternative initiator, proven to give successful results with PS-*b*-PEO copoly-
mers, is cumylpotassium. PS-PEO block copolymers have been synthesized through
sequential anionic polymerization and have also been terminated with various
end-functional groups such as lipophilic 2,2,3,3-tetrahydroperfluoroundecanoyl
chloride [118]. In general, PS-*b*-PEO-based copolymers offer lipophilic-hydrophilic
amphiphilic systems. In addition, PS-*b*-PEO-based copolymers on a conductivity
point of view, in combination with ionic salts of alkali metals (e.g., lithium perchlo-
rate LiClO$_4$), present highly conductive features and pose the possibility of being
used as solid polymer electrolytes in batteries or as fuel cell membranes. An example
of such a material is PS-*b*-PEO-*b*-PS triblock copolymers, which have been fabri-
cated via anionic polymerization, followed by a coupling reaction. PS was first
polymerized in benzene using *sec*-BuLi and end capped (carbanion terminated)
with a hydroxyl group and later reinitiated with potassium naphthalenide, in THF,
to polymerize EO. The living diblock PS-*b*-PEO was then slowly coupled with a
stoichiometric amount of 1,4-bis(bromomethyl)benzene in dry THF, to finally give
(diblock coupling) the desired PS-*b*-PEO-*b*-PS triblock with low polydispersities
[119]. In another study, PI-*b*-PS-*b*-PEO triblock terpolymers have also been synthe-
sized in order to understand the effect of polydispersity in the middle PS block in PI-
b-PS-*b*-PEO triblock terpolymers. The triblocks were synthesized through sequential

anionic polymerization, starting with the polymerization of I, in cyclohexane at 40 °C, followed by the addition of S, to form the PI-*b*-PS living diblock and then end capped with ethylene oxide creating an oxyanion [120]. Methanol was then added to terminate the living chain and create the terminal hydroxyl groups. These hydroxyl end groups were activated by reaction with potassium naphthalenide followed by the polymerization of EO in THF at 40 °C to afford the desired triblock [121].

In another concept, the introduction of an amine group in the junction point of a PS-*b*-PEO is realized through the controlled living end termination by an epoxy-containing group, in this case, *N,N*-dibenzyl amino glycidol (DBAG), thus gaining functionalization in the junction point of the amphiphilic block copolymer. To specify, initially, PS is polymerized using an alkyllithium initiator, followed by the end capping by the DBAG oxirane. Epoxy monomer monoaddition is ensured due to the strong lithium-oxygen association. The copolymerization of the ethylene oxide was realized in THF using potassium naphthalenide. The deprotection of the DBAG can be processed through the contribution of Pd(OH)$_2$/C, subsequently revealing a functional amine group in the junction point (Scheme 42).

Preparation of multiblock copolymers and terpolymers can also be realized through the synthesis of initial block copolymers with controlled chain-end functionalization, followed by polymer-polymer reactions. This method is useful, especially when the sequence of the building blocks is synthetically impossible through sequential addition of monomers. However, the method is impractical due to the copolymer contamination with building block homopolymers, its nonstoichiometric reaction, and secondary products which require complicated and arduous purification procedures. A more practical route is the use of a protected functional initiator that under specific circumstances (mainly regarding the chemical environment), becomes active. Recruiting the protective hydroxyl-functionalized initiator 3-triisopropylsilyloxy-1-propyllithium (TIPSOPrLi) has led to the successful synthesis of symmetric and asymmetric PEO-*b*-PI-*b*-PEO and PEO-*b*-PS-*b*-PB-*b*-PEO, triblock and tetrablock copolymers, and terpolymers. Symmetric PEO-*b*-PI-*b*-PEO copolymers were synthesized through the initial polymerization of Is, followed by hydroxyl chain-end functionalization (EO oxyanion terminated with MeOH). The resulting polymer (TIPS-O-PI-OH) was treated with tetrabutylammonium fluoride (TBAF), thus revealing the α-hydroxyl group on the homopolymer chain followed by the simultaneous growth of the PEO from both ends [122]. To produce asymmetric PEO-*b*-PI-*b*-PEO triblock terpolymers, EO is first polymerized from the ω-hydroxyl-functional end, and the diblock is then treated with TBAF to create a new diblock macroinitiator. Diligent addition of titration "initiating" reagents is mandatory in order to avoid broad molecular weight distributions. Titration of the α-hydroxyl-functionalized macroinitiator is conducted using either NaphK or DPM-K. PEO-*b*-PS-*b*-PB-*b*-PEO tetrablocks were prepared following the same synthetic procedure with the only difference that TIPS-O-PS-*b*-PB was synthesized first [123] (Scheme 43).

The use of a protected initiator has also been applied for the block copolymerization of ethylene oxide with methacrylates. This route is necessary since the direct
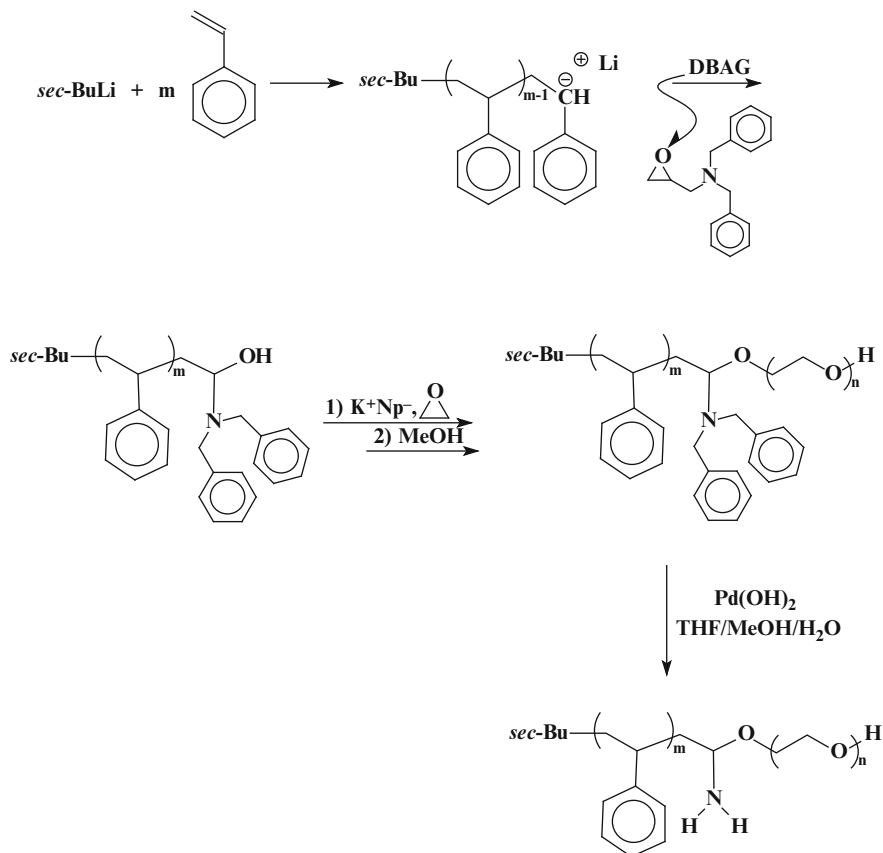
Scheme 42 Synthesis of junction-point amino functionalized PS-*b*-PEO block copolymers

initiation of EO from living PMMA macroanions proceeds with side reactions, mainly attributed to the attack of a propagating alkoxide anion to the ester group of PMMA [124]. However, the direct copolymerization of MMA has been reported through the use of a disodium salt of PEO, yielding a block copolymer, which was contaminated with a by-product coming from the intramolecular grafting of living chains onto carbonyl groups [125], and through the direct initiation of MMA using PEO macroanions resulting in PEO-*b*-PMMA copolymers [126]. In contrast to normal methacrylate living polymers, poly(*tert*-butylmethacrylate) (P*t*BMA) is capable of efficient crossover reactions with EO, due to the fact that the propagating P*t*BMA is stable at ambient temperatures, allowing the successful synthesis of diblock and triblocks [127]. Monohydroxy telechelic PMMAs (PMMA-OH) have led to the successful preparation of well-defined PMMA-*b*-PEO copolymers. Protected hydroxyl-functional initiators such as 1-[*p*-(*tert*-butyldimethylsilyloxy)] phenyl-1'-phenylhexyllithium, 6-(*tert*-butyldimethylsilyloxy) hexyllithium, and 3-(*tert*-butyldimethylsilyloxy) propyllithium have been used (Scheme 44).
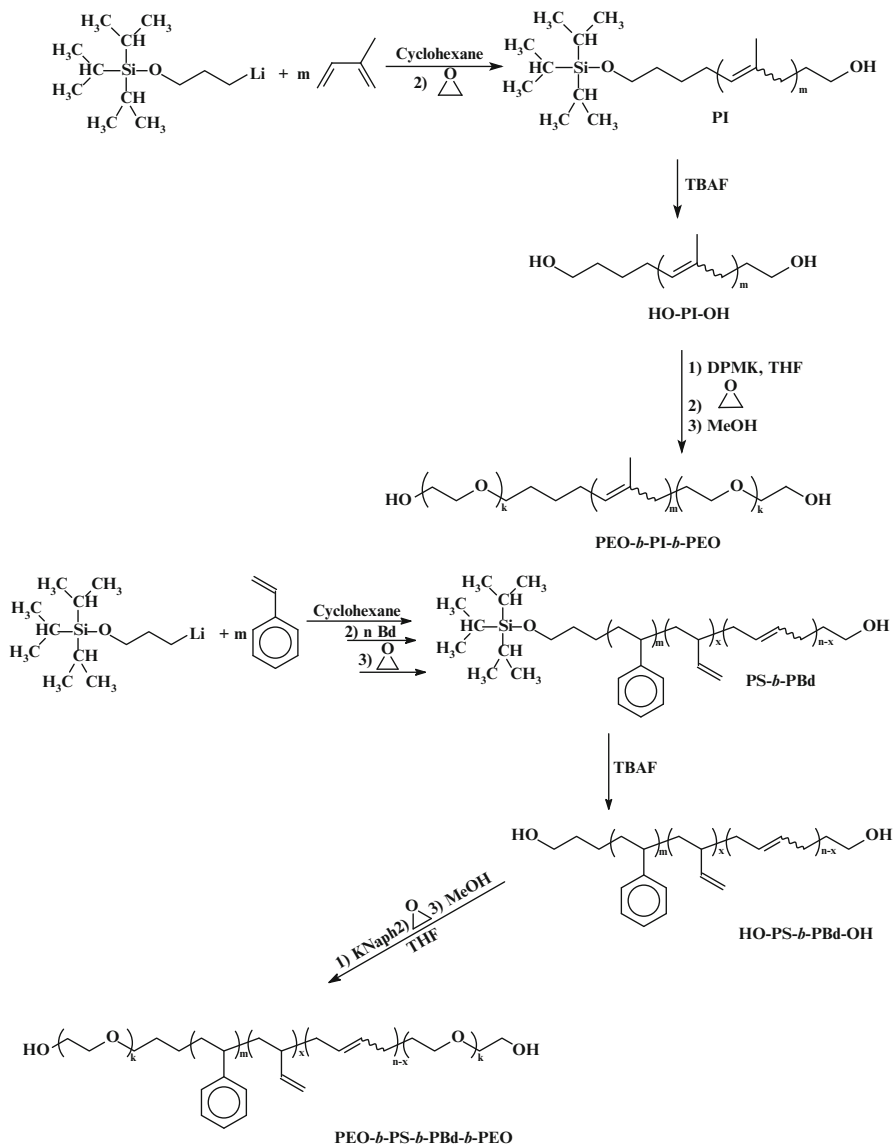
Scheme 43 Synthesis of PEO-*b*-PI-*b*-PEO and PEO-*b*-PS-*b*-PBd-*b*-PEO triblock copolymer and tetrablock terpolymer, respectively, using the protected initiator, TIPS

The polymerization of MMA took place in THF at −78 °C, in the presence of LiClO$_4$ (10:1 as to initiator). Deprotection of the hydroxyl-functional initiator was completed in THF after treatment with a 4 M excess of TBAF. Hydroxy-PMMA was slowly added to *tri*-phenylmethylpotassium, converting the hydroxyl groups
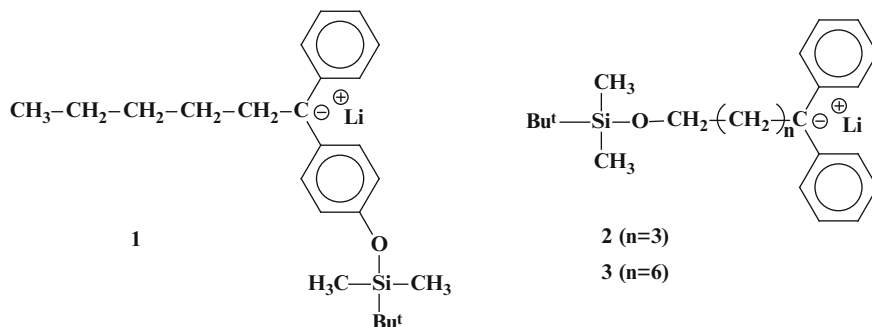
Scheme 44 Protected hydroxy functional initiators for PMMA-*b*-PEO copolymer synthesis
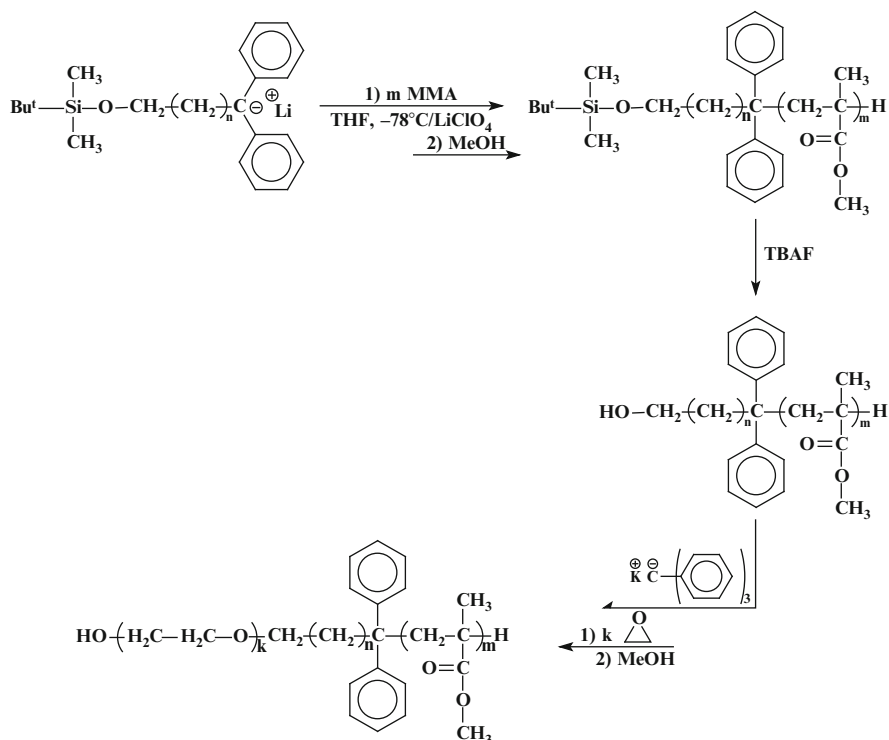
Scheme 45 Synthetic route for PMMA-*b*-PEO block copolymer synthesis, using a protected initiator

into potassium alkoxide groups, active for EO copolymerization (Scheme 45). The method yielded well-defined, controlled polymers of low PDI ($<$1.1) [128].

There have been cases were PEO has been copolymerized with styrene-based functional protected monomers such as *tert*-butoxystyrene (*t*BOS), which can create double hydrophilic copolymers, after the acidic hydrolysis of P*t*BOS,

n · (vinyl monomer with) H$_3$C—C—CH$_3$ / CH$_3$ with O + n-BuLi →(THF, –78°C)→ n-Bu—(H$_2$C)$_{n-1}$ ... H$_2$C—⊖Li⊕

PtBOS

1) O (epoxide), BuP4 / THF, 40°C 2) MeOH → n-Bu—(H$_2$C)$_n$(H$_2$C—CH$_2$—O)$_m$H

→(HCl / Aceton, 60°C)→ n-Bu—(H$_2$C)$_n$(H$_2$C—CH$_2$—O)$_m$H with OH

HCHO / Me$_2$NH → n-Bu—(H$_2$C)$_n$(H$_2$C—CH$_2$—O)$_m$H with H$_2$N / OH / NH$_2$

→(CH$_3$I)→ n-Bu—(H$_2$C)$_n$(H$_2$C—CH$_2$—O)$_m$H with H$_3$N⊕ I⊖ / OH / I⊖ ⊕NH$_3$
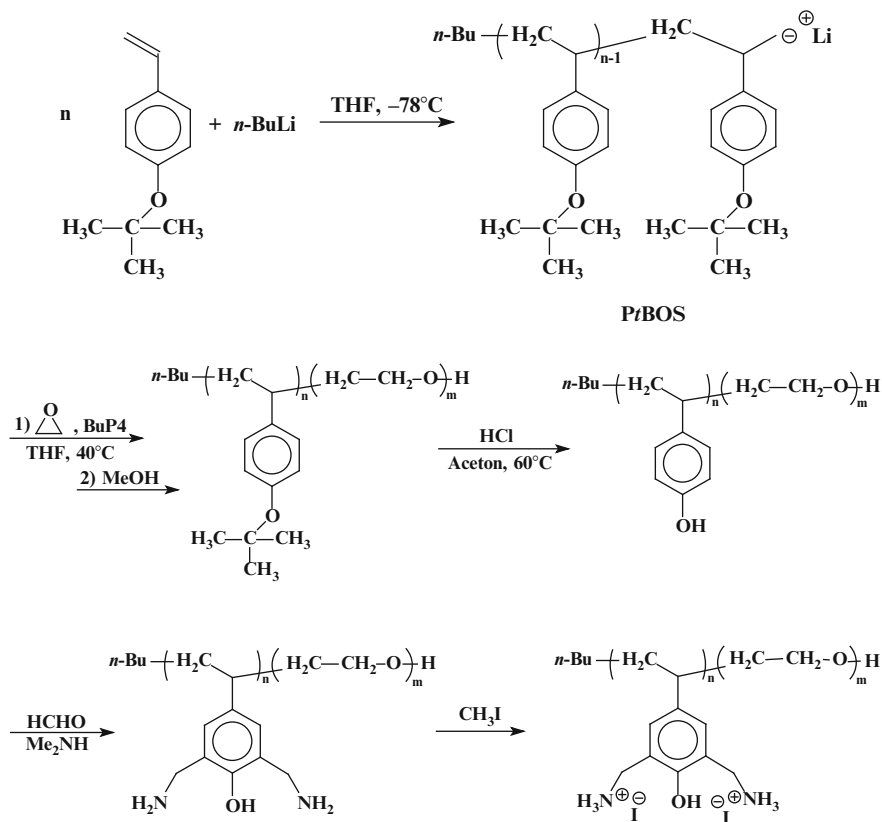
Scheme 46 Synthesis of PtBOS-b-PEO block copolymer, later modified to the double amphiphilic PHOS-b-PEO and finally to the N-PHOS-b-PEO block copolymer

resulting in polyhydroxystyrene PHOS [129]. tBOS was initially polymerized in THF at −78 °C, using n-BuLi as initiator. Phosphazene base (half of the amount of n-BuLi) was then added to enhance reactivity of the active anions, and finally, EO was added. The polymerization was left for 2 days at 40 °C. Diblock PtBOS-b-PEO synthesis resulted to narrow PDI (>1.1) copolymers, with the advantage of hydroxyl functionalization PHOS-PEO (Scheme 46). Hydroxystyrene monomeric units can undergo further tailoring, leading to the synthesis of a high charged density, annealed cationic polyelectrolyte NPHSO [3,5-bis(dimethylamino-methylene)hydroxystyrene], through a Mannich-type reaction [130] consequently obtaining N-PHOS-b-PEO copolymers.

The synthesis of P2VP-b-PEO diblock copolymers and P2VP-b-PEO-b-P2VP symmetric triblock copolymers, Scheme 47, was reported [92]. The last structure was prepared by the reaction of the living P2VP-b-PEO diblock with 1,4-bis (bromomethyl)benzene, as a linking agent. The linking reaction was performed in the presence of a catalytic amount of CsI, which transforms the –CH$_2$Br groups to the more reactive –CH$_2$I groups. Under these conditions, linking was completed
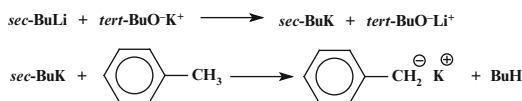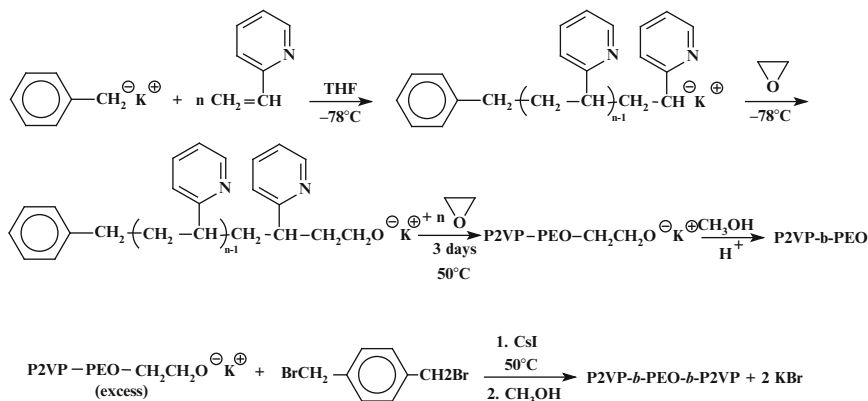
Scheme 47 Synthesis of P2VP-*b*-PEO block copolymer and P2VP-*b*-PEO-*b*-P2VP symmetric triblock copolymer

within 3 h instead of the 3 days without CsI. A small amount (~10 %) of high molecular weight byproduct was observed in most cases. This by-product was attributed to the reaction of the living ends with the pyridine ring to form the high molecular weight graft copolymer.

Further work related to the synthesis of copolymers with either P2VP or P4VP blocks has been reported in the literature. Triblock terpolymers PS-*b*-P2VP-*b*-PEO were synthesized in THF at −78 °C by sequential polymerization of styrene and 2VP, initiated by *sec*-BuLi in the presence of LiCl [131]. The living polymer was terminated with EO. The end-hydroxyl group was treated with potassium naphthalene, and ethylene oxide was added and polymerized at 0 °C leading to narrow molecular weight distribution product. The micellar properties of the terpolymers were studied in water.

PBd-*b*-PI-*b*-PEO triblock terpolymers were prepared by sequential addition of monomers using *sec*-BuLi as initiator [132]. The strong phosphazene base t-BuP$_4$ was employed to promote the polymerization of ethylene oxide in the presence of a lithium counterion. Subsequent hydrogenation in toluene with the Wilkinson catalyst afforded the PE-*b*-PEP-*b*-PEO [PE = polyethylene, PEP = poly(ethylene-*alt*-propylene)] triblock terpolymers. Using *p*-toluenesulfonyl hydrazide as an alternative hydrogenation means, it was found that the PBd block was quantitatively hydrogenized, whereas the degree of hydrogenation was only 70 % for the PI block, due to the steric hindrance involved in the reaction. PBd-*b*-PEO-*b*-PBd
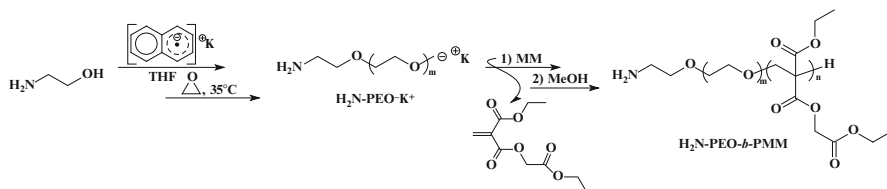
Scheme 48 Synthesis of PEO-*b*-PMM block copolymer

triblock copolymers have also been prepared through the slow addition of 1,4-bis (bromomethyl)benzene and the subsequent linking of the PBd-*b*-PEO living chains [133].

In another study, PEO-*b*-poly(methylidene malonate) block copolymers (PEO-*b*-PMM) have been synthesized [134]. In this classic preparation method, sequential monomer addition was exercised through the sequential addition of the monomers starting with the polymerization of EO using diphenylmethylpotassium as initiator. α'-Amino functionalized PEO-*b*-PMM has been synthesized using potassium 2-aminoethanolate as initiator, generated from the reaction of potassium naphthalide and 2-aminoethanol. Copolymerizations took place in THF at 35 °C for 48 h for the first monomer (EO) and for 1 h at 25 °C after the subsequent addition of the second monomer [135] (Scheme 48).

Following the same approach, biocompatible and biodegradable PEO-*b*-P(ε-CL) [P(ε-CL) = poly(ε-caprolactone)] and PEO-*b*-PLA [PLA = poly(lactic acid)] have been synthesized as drug delivery systems [136]. In order to obtain more selective targeting properties, P2VP has been introduced in a triblock terpolymer system. P2VP presents pH-sensitive (hydrophobic in neutral pH and hydrophilic in lower pH) properties and allows ligand attachment. The terpolymer was synthesized starting with 2VP polymerization, in THF at −78 °C in the presence of LiCl, in order to decrease reactivity and prevent any side reactions on the pyridine ring, followed by the hydroxyl end capping of the living monomer with EO at 25 °C. The ω-hydroxy-P2VP was metallated into ω-potassium alkoxide P2VP and used as macroinitiator for the polymerization of PEO and ε-caprolactone in the presence of tin alkoxide as catalyst [137] (Scheme 49).

PEO-*b*-PDMAEMA has also been synthesized through sequential anionic polymerization; however, EO, being a more selective monomer, requires more attention and additional initiator features. Due to the strong association of Li$^+$ with the oxyanion, a strong base is required; in reported polymerizations, where *sec*-BuLi was used as initiator, *t*-BuP$_4$ phosphazene is employed. For the successful polymerization of EO, higher temperatures are desired, to prevent initiator termination reactions as a result of occurring side reactions of *sec*-BuLi with THF (*sec*-BuLi reacts with THF forming a molecule of ethylene and the lithium enolate of acetaldehyde) [138]. *sec*-BuLi was first coupled with 1,1 diphenylethylene, at −70 °C, creating 1,1 diphenylhexyllithium, which is less reactive with THF. EO was subsequently added to the solution, and after 1 h, the temperature was raised slowly to 10 °C followed by the addition of *t*-BuP$_4$, after which the temperature was
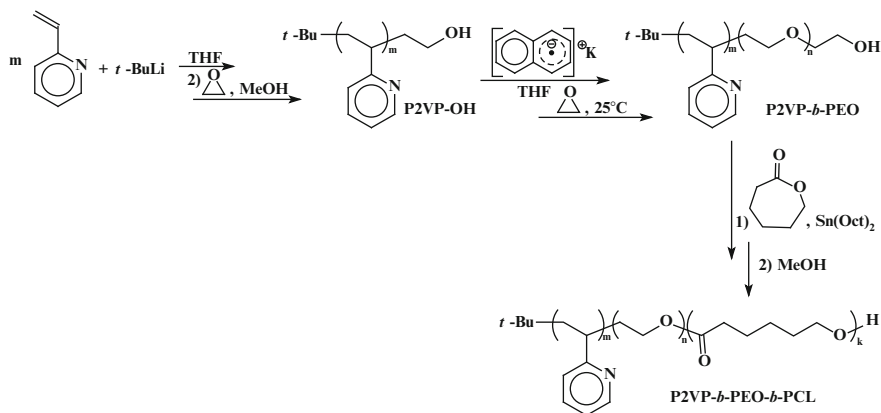
Scheme 49 Synthesis of P2VP-*b*-PEO-*b*-PCl triblock terpolymer

finally elevated to 50 °C. Before the addition of DMAEMA, the temperature was lowered to 10 °C, and after complete addition, the polymerization took place for 30 min and was then terminated with degassed MeOH [59]. PDMAEMA-*b*-PEO-*b*-PDMAEMA triblock terpolymers have also been synthesized through anionic polymerization, using a potassium *tert*-butanoxide initiator (*t*-BuO⁻K⁺). HO-PEO-OH α',ω'-hydroxyl homopolymers have been previously synthesized according to methods already described. HO-PEO-OH was added in THF followed by the addition of *t*-BuO⁻K⁺, and ½ h later, DMAEMA was added, and the reaction was left for polymerization for 2 h at 10 °C. Polymerization is terminated before complete monomer consumption by the addition of acetic acid in the mixture. Moderately broad molecular weight distributions ($M_w/M_n \sim 1.40$) were obtained.

5.3 Other Epoxy Monomers

In other reports, PEO has also been copolymerized with glycerol group containing polymers such as polyglycidol (PG), a polyoxirane carrying one hydroxyl-functional group per polymer monomeric unit, and poly(allyl glycidyl ether) (PAGE), a hydrophobic (PG is hydrophilic) polymer carrying one double bond per polymer monomeric unit.

Mainly due to their biocompatible nature, various other monomers have been copolymerized to create stimuli-responsive (pH and thermally) amphiphilic systems, used in drug encapsulation and delivery processes. Allyl glycidyl ether (AGE) has been copolymerized with EO to create amphiphilic diblock copolymers. PAGE, bearing a double bond on each monomer, can be hydrolyzed with a variety of functional groups, applying pH or thermal sensitivity and drug-engaging abilities. PEO-*b*-PAGE copolymers have been prepared through anionic polymerization. α'-Methoxy PEO was mixed with NaH and heated at 100 °C until the hydride was dissolved, followed by the copolymerization of AGE. After polymerization
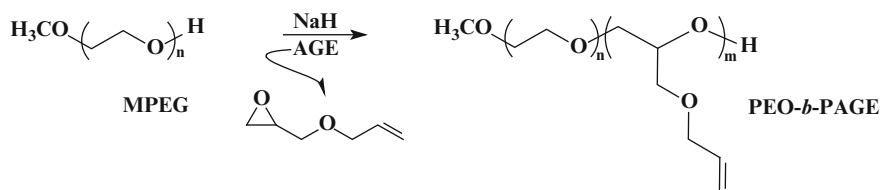
Scheme 50 Synthesis of PEO-*b*-PAGE block copolymers

completion, acetic acid was inserted as terminating agent, and narrow molecular weight distributions were obtained (Scheme 50).

In another monomer variation, ethoxyethyl glycidyl ether (EEGE) has also been copolymerized with PEO. Most frequently used initiators for the polymerization of EEGE are either potassium based or cesium alkoxides [139]; however, in the case of diene copolymerization, these types of initiators are not applicable, since they cannot start polymerization or since they result in polymers of broad molecular weight distribution. On the other hand, organolithium initiators cannot be used for epoxide polymerization because of the strong O-Li association [140]. Alkyllithium initiators can be applied, combining the good properties of organolithium-initiated, diene, and epoxy polymerizations, only when accompanied by a strong base such as phosphazene (*t*-BuP$_4$).

Diblock PEEGE-*b*-PEO and triblock PEO-*b*-PEEGE-*b*-PEO and PEEGE-*b*-PEO-*b*-PEEGE copolymers have been synthesized. For PEEGE-*b*-PEO and PEEGE-*b*-PEO-*b*-PEEGE copolymers, cesium alkoxides of poly(ethylene glycol) (PEG) and poly(ethylene glycol) monomethyl ether (MPEG), generated in benzene after heating under stir at 60 °C (~1 h), were used as macroinitiators for the synthesis of the triblocks and diblocks, respectively (Scheme 51a). In both cases, the use of the Cs alkoxide initiator resulted in the synthesis of well-defined low PDI (<1.1) polymers. For the synthesis of PEO-*b*-PEEGE-*b*-PEO triblock copolymer, a potassium alkoxide of diethylene glycol (*t*-BuOK) was employed. To achieve difunctionality, *t*-BuOK was reacted with diethylene glycol in DMSO. The mixture was slightly heated in order to remove the released *t*-BuOH and EEGE monomer was added. Copolymerization took place for 48 h at 60 °C [141] (Scheme 51b). The synthesis of PEO-*b*-PEEGE diblock, through sequential anionic polymerization, using a [*sec*-BuLi]/[*t*-BuP$_4$] ~ 1/1 initiating system and starting with the polymerization of PEO, has also been described [142].

PS-*b*-PEO-*b*-PEEGE triblock terpolymers have also been prepared using organolithium initiators. First, styrene was polymerized in THF at −70 °C using *sec*-BuLi, subsequently EO was added, and after 1 h the temperature is gradually elevated to 50 °C, followed by the addition of *t*-BuP$_4$ ([*sec*-BuLi]/[*t*-BuP$_4$] ~ 1/1) to promote EO polymerization. Judicious use of the *t*-BuP$_4$ amount added must be applied, since an excess amount might result in side reactions with EEGE. After 2 days, EEGE was added, at room temperature, to the living diblock, and copolymerization continued at 50 °C for 3 days, completed by the addition of a mixture of acetic acid/methanol (3/5 v/v), acting as terminating agent [142] (Scheme 52). In addition to the previously described triblock terpolymers, a new triblock consisting

Scheme 51 Synthesis of PEEGE-*b*-PEO-*b*-PEEGE and PEO-*b*-PEEGE-*b*-PEO triblock terpolymers

of P2VP-*b*-PEO-*b*-PEEGE has been described following the previous copolymerization method, with the only difference that *sec*-BuLi was first reacted with DPE. All triblocks presented low polydispersity indices ($M_w/M_n < 1.1$).
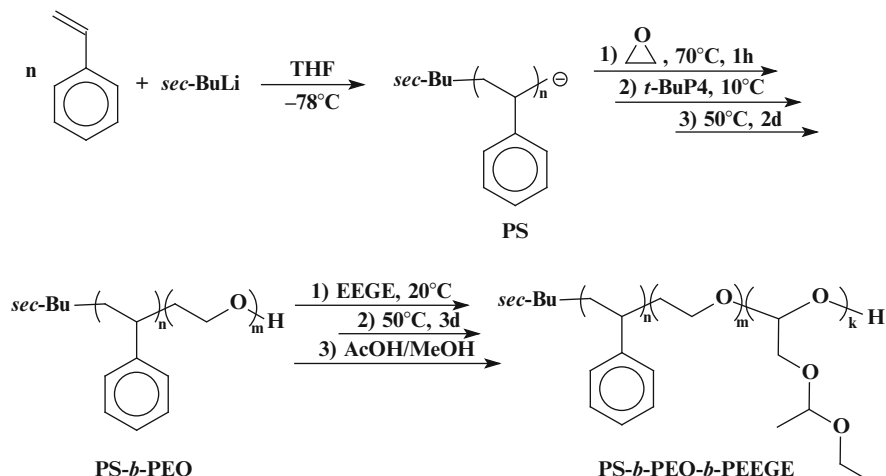
Scheme 52 Synthesis of PS-*b*-PEO-*b*-PEEGE triblock terpolymer
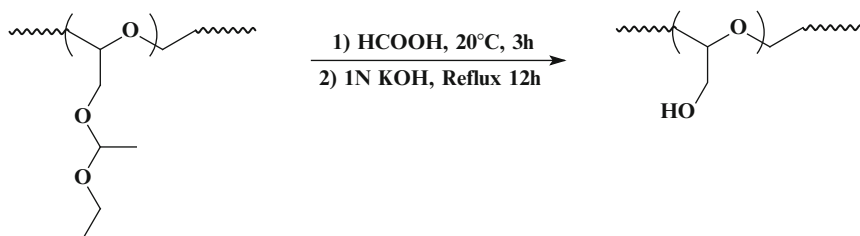
Scheme 53 Deprotection reaction of PEEGEs ethoxyethyl group

Polymerization of PEEGE offers the advantage of hydroxyl functionalization through the deprotection of the ethoxyethyl group, thus leading to the transformation to poly(glycerol). Deprotection was achieved by a two-step reaction with formic acid and subsequent hydrolysis in alkaline media [143] (Scheme 53).

Another epoxy variation, ethyl glycidyl ether (EGE), with thermoresponsive abilities, has also been polymerized using the same preparation techniques. Potassium phenoxy ethoxide was used as initiator offering the formation of α'-phenyl PEGEs. Polymerization took place at 110 °C for ~20 h, and the polymer was quenched with sulfuric acid. In the same way, diblock copolymers PEGE-*b*-PEO have also been synthesized through the sequential addition of PEO after the polymerization (under the same conditions) of PEGE. During EO monomer addition, the temperature was reduced to 60 °C and subsequently raised to 110 °C.

6 Block Copolymers from Alkyl Isocyanates

Polyisocyanates represent a valuable class of polymeric materials since they adopt a rodlike helical conformation in solution and in bulk and since they possess extraordinary liquid crystalline and optical properties [144]. The combination of these rigid chains with flexible blocks leads to novel materials characterized by the microphase separation between the different blocks along with the orientational ordering inside the rodlike phase. The synthesis of polyisocyanates by living anionic polymerization was hindered mainly by the existence of backbiting side reactions of the amidate anions leading to the formation of stable cyclic trimers [145]. The trimerization yield may reach 100 % at temperatures higher than $-40\,°C$. Consequently, severe problems concerning the control over the molecular weight and the molecular weight distribution, the polymerization yield, and the ability to prepare block copolymers or more complex architectures were exhibited. However, it was reported that the living anionic polymerization of isocyanates can be promoted when the polymerization is conducted at $-98\,°C$ in THF with sodium naphthalene as initiator in the presence of the crown ether 15-crown-5 or the sodium salt tetraphenylborate, $NaBPh_4$ [146]. The crown ether entraps the sodium counter cations, thus depleting the anionic active center and greatly accelerating the propagation reaction. If the living polymer is terminated soon after the polymerization reaction is completed, the backbiting process is drastically reduced. On the other hand, $NaBPh_4$ stabilizes the amidate anion of the growing chain as a result of the common ion effect and the steric hindrance of the bulky tetraphenylborate group (Scheme 54). $NaBPh_4$ was proven to be more efficient in promoting the living anionic polymerization of alkyl isocyanates. Using this methodology, triblock copolymers composed of poly(hexyl isocyanate), PHIC, end blocks, and either PS, PI, or poly[3-(triethylsilyl)propyl isocyanate], PTESPI, middle blocks were prepared, using sodium/naphthalene as a difunctional initiator and $NaBPh_4$ as additive [147]. Furthermore, the synthesis of pentablock terpolymers PHIC-*b*-PS-*b*-PI-*b*-PS-*b*-PHIC and PHIC-*b*-PI-*b*-PS-*b*-PI-*b*-PHIC was reported (Scheme 54) [148]. Initial results concerning the microphase separation and the thermal properties of these materials were reported in these studies.

A series of efficient monofunctional anionic initiators were employed for the controlled polymerization of isocyanates, as well. Benzyl sodium, in the presence of a tenfold excess of $NaBPh_4$, was employed as initiator for the synthesis of PS-*b*-PHIC and PI-*b*-PHIC by sequential addition of monomers. The polymerization of the first block was conducted at $-78\,°C$, whereas HIC was polymerized by lowering the temperature to $-98\,°C$ [149].

Potassium diphenyl methane, DPM-K, was also successfully employed as monofunctional initiator for the synthesis of P2VP-*b*-PHIC block copolymers [150]. The polymerization of 2VP was conducted in THF at $-78\,°C$, whereas HIC was polymerized in the presence of a five- to tenfold excess of $NaBPh_4$ by
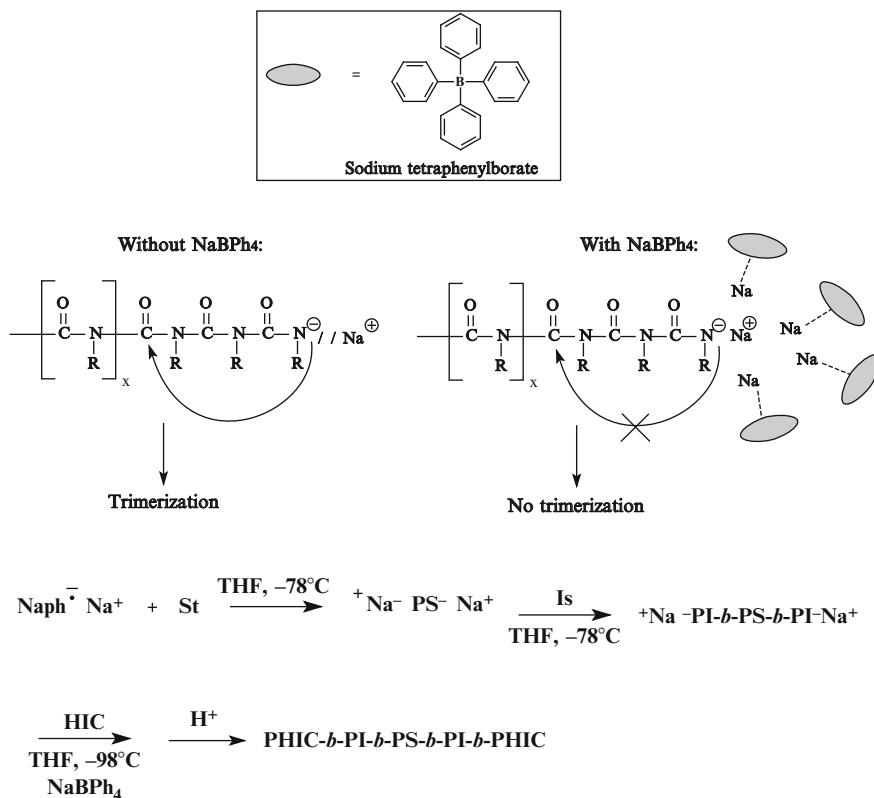
Scheme 54 Synthesis of PHIC-*b*-PI-*b*-PS-*b*-PI-*b*-PHIC pentablock copolymer, in the presence of NaBPh$_4$

lowering the temperature to −98 °C, leading to well-defined products. It was found that aliphatic acid chlorides can be employed as linking agents for living polyisocyanates. The living P2VP-*b*-PHIC⁻Li⁺ diblocks were efficiently linked with malonyl chloride or suberoyl chloride in the presence of pyridine providing P2VP-*b*-PHIC-*b*-P2VP triblock copolymers (Scheme 55). The coupling reaction was conducted at −98 °C for 10–20 min. Careful control of the stoichiometry led to quantitative coupling reactions without any need for fractionation [151].

Sodium benzanilide, Na-BPM, has a dual function, since it serves both as an initiator and as an additive for the protection of the anionic chain ends during the polymerization of isocyanates (Scheme 56). Therefore, Na-BPM was used for the block copolymerization of HIC and (3-triethoxysilyl)propyl isocyanate [152]. Sodium benzydroxide, BH-Na, acts in a similar manner promoting the living polymerization of isocyanates. It was employed for the synthesis of block copolymers of poly(furfuryl isocyanate), PFIC, and PHIC, PFIC-*b*-PHIC. Furthermore,
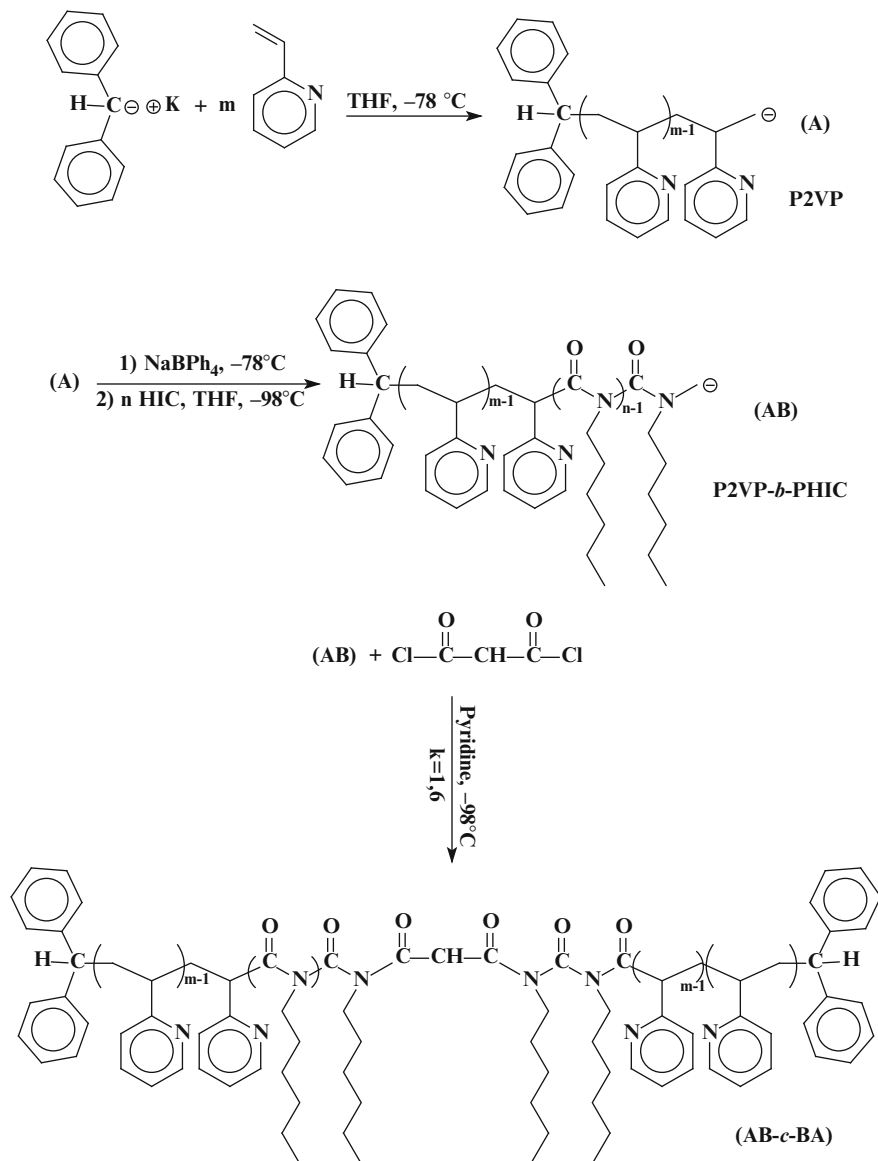
Scheme 55 Synthesis of symmetric P2VP-*b*-PHIC-*b*-P2VP triblock copolymer

sodium deoxybenzoin, DB-Na, was found to be an efficient dual function enolate anionic initiator and additive leading to model polyisocyanates. Using this initiator, block copolymers of HIC and (3-triethoxysilyl)propyl isocyanate were obtained (Scheme 57) [153].
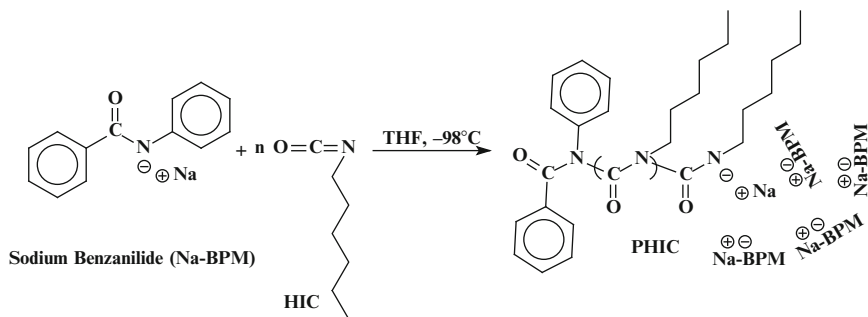
Scheme 56 Dual function of Na-BPM as a initiator and as a anion protection unit
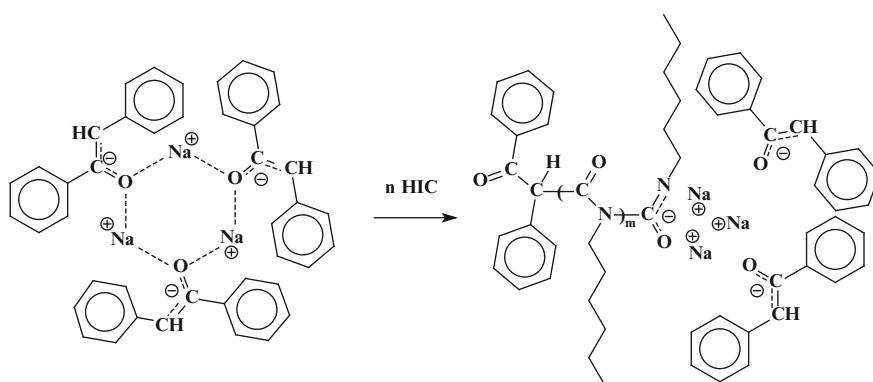
Scheme 57 The dual functional enolate DB-Na for HIC

7 Block Copolymers from Metal-Containing Monomers

Organic polymer substances, combined with metals, depict enhanced mechanical properties and enriched with magnetic, conductive, redox active, catalytic, and many other qualities. The incorporation of organic materials with inorganic solids is not a new concept. As early as 1955, DuPont company synthesized Poly (vinylferrocene) (PVF) to combine the properties of the two different elements foreseeing many possibilities for new applications and the opportunity to combine different polymerization techniques. However, metals, due to their low solubility, also due to stability issues and side reactions during polymerization procedures, overburden the preparation of well-defined polymers having high molecular weights. Thus, various techniques are required for the polymerization of metal-containing monomers.

Metal-containing block copolymers can form ordered arrays, derived from the microphase separation during the self-assembly of two immiscible segments, creating three-dimensional nanostructures of periodical domains. These structures can be utilized to create porous membranes, nanolithographic templates, photonic band-gap materials, and catalyst precursors for the controlled structural synthesis
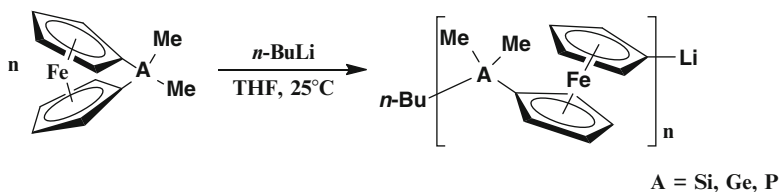
Scheme 58 The first type of Fc monomers (bridged with an element), undergo ROP in the presence of alkyllithium
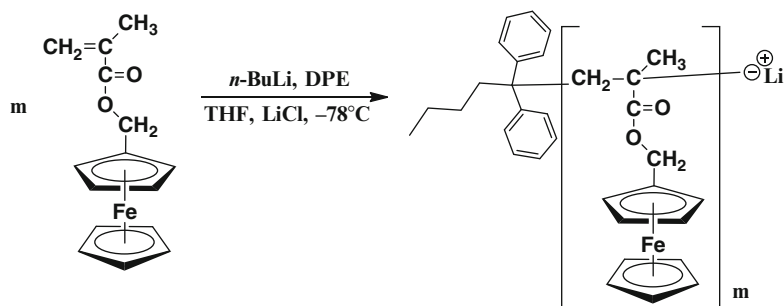
Scheme 59 Second type of Fc monomer (containing a side functional group) undergo vinyl polymerization

of carbon nanotubes [154]. Of special interest are ferrocene, Fc, containing monomers because they can be polymerized in a living/controlled fashion, are free from side reactions, have special electrochemical polymer properties, and have the ability to control aggregation phenomena [155].

Ferrocene-containing monomers can be categorized into two types. The first type includes bridged monomers (ferrocenes bridged with an element), which undergo anionic ring opening polymerization (ROP). A large variety of monomers containing a silicone bridge have been synthesized (polyferrocenosilanes PFSs), but also other elements have been used to create an Fc bridge such as germanium [156] and phosphorus [157] (Scheme 58). The second type includes side-functional monomers consisted of spacer-linked (or non-spacer) functional groups such as methacrylic or vinyl (e.g., methacrylichexylferrocenes MAHFC, PVFs) [158], which undergo anionic vinyl polymerization (Scheme 59).

Block copolymers are prepared either by sequential monomer addition or in cases of chemical incompatibility other techniques can be employed such as the use of chemoselective stepwise coupling reactions [159], protected functional initiators [160] [such as (*tert*-butyldimethylsilyloxy)-1-propyl lithium BDMSPrLi], and macroinitiators [161], or through the coupling of various cycloaddition reactions [162]. The same principles for diblock copolymer synthesis, through sequential addition, also apply for this type of monomer. Copolymerization will only occur if the second monomer carbanion is of higher or similar stability than the carbanion of the first block.
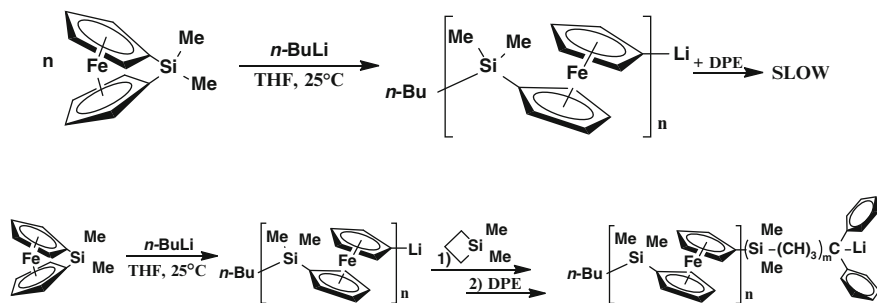
Scheme 60 Carbanion pump, 1,1 dimethyl silacyclobutane, accelerates the addition of DPE on living Fc chains
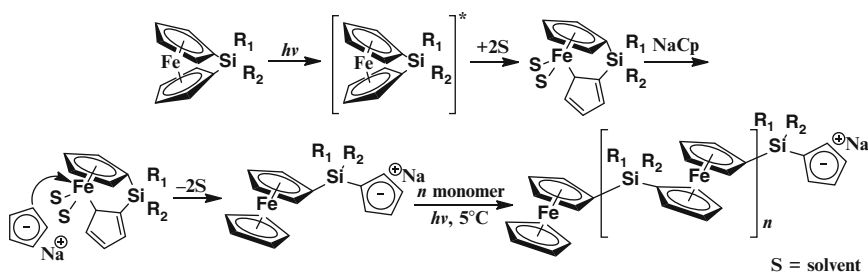
Scheme 61 UV light can initiate photocontrolled ROP of bridged Fc monomers

In special cases, reactivity tailoring is mandatory. Various techniques can be employed for this purpose, for example, reactivity can be moderated with 1,1 diphenylethylene (DPE) (Scheme 60). This widely used linking agent offers the necessary steric hindrance for a one-target reaction and is also a non-homopolymerizable moiety. However, the capping/linking of living Fc polymers with DPE is slow at room temperature; the capping efficiency has been shown to increase upon increasing the reaction temperature. In particular, the percentage of living chains that were capped increased from 28 % after 4.5 h at room temperature to 62 % after the same time at 50 °C. Unfortunately, the termination of living PFS chains could not be avoided (yield less than 100 %); however, the most useful strategy, in order to avoid unwanted side reactions, is to involve a "carbanion pump" as well (with 1,1 dimethylsilacyclobutane as acting material) or by quenching with a proton source followed by deprotonation of the DPE-capped material [163–166]. Usually, a 4/2 M mixture of DPE and 1,1 dimethylsilacyclobutane is used for this purpose.

Silicon and phosphorus-bridged ferrocenes provide the ability for alternative reactivity tailoring. These bridged monomers may also undergo a photocontrolled anionic ROP, in the presence of UV light and through the participation of a mild nucleophiles acting as the initiator, usually Na[C$_5$H$_5$] (NaCp) [157, 167, 168]

(Scheme 61). Polymers of high molecular weights and narrow molecular weight distribution may be obtained through this method. The main advantage of this approach is the mildly basic polymerization environment that overcomes the incompatibilities that follow the use of organolithium initiators with most functional groups and thus allows the living polymerization of more sensitive functionalities [169]. Polymers acquired through this method have been named as "soft living" and the methods itself as "switch on-switch off" [167] since it can be controlled by simply switching on or switching off the light, making possible the sequential addition of different monomers, including even sensitive monomers, providing a facile route for the synthesis of well-defined block copolymers.

7.1 Polyferrocenosilanes (PFSs) and Their Block Copolymers

Out of all ferrocene-containing monomers, the most studied are the ferrocenosilanes. PFSs attract large scientific interest due to the many interesting properties they exhibit. Presenting etch resistance to plasma deems them as possible candidates in nanolithography, as templates [170]. Other properties are high refractive indices [171], controlled response to redox stimulus [172], the ability to form crystalline self-assembled materials, [170] and thus can be used as precursors for the synthesis of nanostructured magnetic ceramics, [173] and have been used for the controlled synthesis, both in size and geometry, of single wall nanotubes [174].

The silicon substituents have been tailored to enhance the thermophysical properties of the silanoferrrocene polymer. When symmetrically substituted by short n-alkyl groups, PFSs embrace semicrystalline formations but remain amorphous when monomers are asymmetrically substituted [175]. Although, poly (ferrocenyldimethylsilane) (PFDMS) has been used in the synthesis of the majority of the ferrocene-containing block copolymers, the use of such semicrystalline blocks might induce complications during microphase separation, in thin films and in bulk, since crystallinity competes the driving force for regular self-assembly, via the random association of the immiscible substances [176]. Thus, the use of asymmetrically substituted PFSs eliminates the problem, providing amorphous products, and allows the synthesis of high quality porous membranes and the applications in fields where distinct microphase separation is necessary [177]. The most commonly used asymmetric PFS is polyferrocenylethyl-methylsilane (PFEMS); however, the disadvantage of PFEMS is its low Tg [177 (a, b)] (25 °C room temp), not allowing the use in nanolithographic techniques and magnetic applications. Higher Tg, combined with amorphous domain, can be acquired with the introduction of bulky moieties on one of the silicon-substituted domains [178].

Ferrocenosilanes are polymerized through anionic ring opening polymerization (ROP). Polymer propagation proceeds through cleavage of the silicon-cyclopentadienyl bond giving well-defined, controlled, living polymers. As

previously noted, ROP can also be realized through photocontrolled anionic ring opening polymerization. This new "soft-living" photopolymerization method [157] yields well-defined high molecular weight polymers. Requirements imposed by this method are the use of a mild nucleophile as initiator, UV irradiation, and a polar environment in order to achieve initiator electron transfer (which leads to delocalization of the Cp anion); most commonly used solvents are THF and CH_3CN. The polymerization temperature may vary depending on the monomer functionality and sensitivity but, in general, approaches relatively low temperatures (~0–5 °C). Preferred initiator is *n*-BuLi, due to its stability and lower reactivity compared to other organolithium initiators.

PFDMS-*b*-PEO block copolymers have been prepared through the introduction of an Si-H end-functionalized methoxy-PEO, as a macroinitiator for the Pt(0)-catalyzed (Karstedt's catalyst) ROP of dimethylsila (1) ferrocenophane [179]. They have also been prepared through the coupling reaction of end-functionalized PEO and PFDMS. Coupling reactions, depending on the functional group, can proceed through "click chemistry" [180] or through the use of ruthenium complexes [181]. In another concept, PFDMS-*b*-PEO copolymers are realized through sequential monomer addition, by end capping the living PFDMS chain with an epoxy group and reinitiating the hydroxyl-terminal group for EO polymerization. This epoxy group can bare more than one functional centers (e.g., allyl glycidyl ether, AGE), thus allowing further polymer manipulation and complex macromolecular structure synthesis (Scheme 62). Copolymer preparation of this type starts with the polymerization of PFDMS in THF at room temperature, using *n*-BuLi as initiator and followed by the end capping with the epoxide. However, before end capping, the living PFDMS end must be modified through the introduction of a "carbanion pump" system (thoroughly presented previously); this action is mandatory since, if not modified, the living PFDMS end is incapable of inducing the ring opening reaction of the epoxide. The resulting hydroxyl group, of the epoxide terminating agent, can be the target point of a cesium hydroxide (CsOH) initiator for the sequential EO polymerization [163]. This strategy offers high yields of controlled molecular weights and narrow monomodal distributions.

In a similar way, 2VP was copolymerized with PFDMS (Scheme 63), through prior living end modification [182]. The polymerization of PFDMS took place at room temperature, however, to prevent potential side reactions during the polymerization of 2VP [183] the reaction mixture was cooled down to −78 °C before the insertion of the also cooled monomer (−78 °C). To avoid side reactions with the pyridine ring, LiCl was also added with the second monomer mixture. The polymerization of the second monomer was allowed to proceed for 40 min giving high yields (97 %) and PDI values <1.1 [165].

PFDMS-*b*-PDMAEMA was synthesized following a similar approach (Scheme 64). PFDMS was initially prepared at room temperature, followed by a suitable end-capping reaction to introduce a hydroxyl end group. In order to achieve ω-functionalization in a one-pot reaction, protected functional initiators such as (*tert*-butyldimethylsilyloxy)-1-propyl lithium (*t*-BDMSPrLi) can be employed. *t*-BDMSPrLi offers the advantage of hydroxyl end functionalization, resulting in
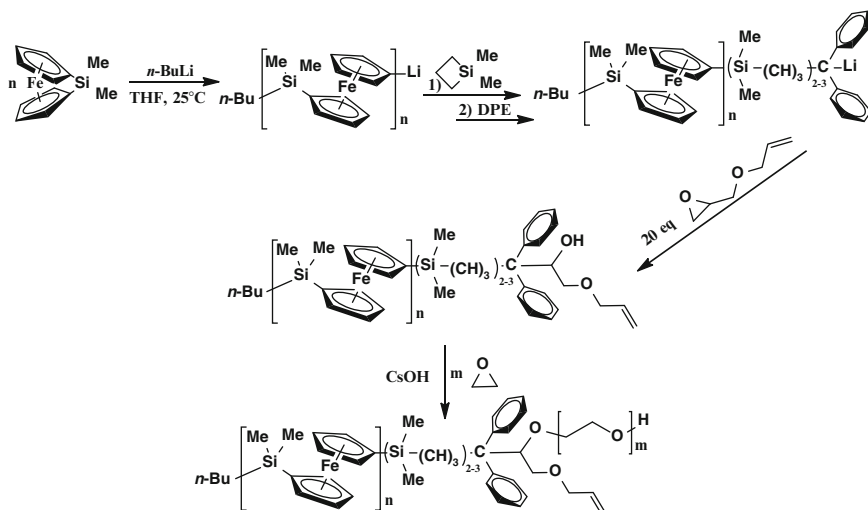
Scheme 62 End capping living ferrocenosilanes with an epoxy group allows further chemical modification, such as the synthesis of PFDMS-*b*-PEO block copolymers
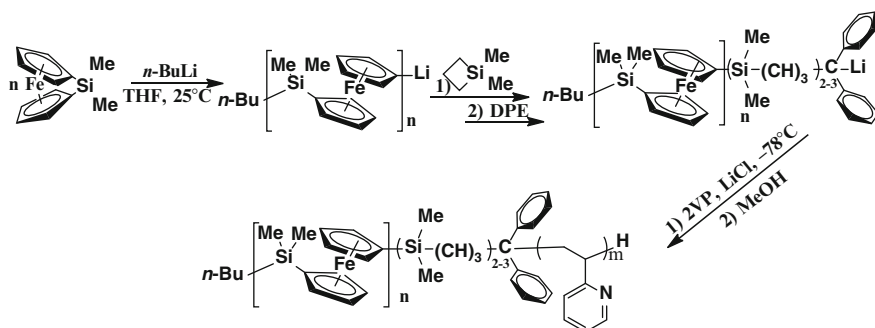
Scheme 63 Synthesis of PFDMS-*b*-P2VP block copolymers

a 100 % yield of hydroxyl-functionalized PFDMS homopolymers since impurity-cased terminations are absent. In this method, first block polymerization takes place at room temperature, in THF solvent. After polymerization completion, the siloxy-end homopolymer is treated for 24 h at room temperature with [Bu₄N]F in THF, thus providing the desired hydroxyl group. The hydroxyl end group of PFS can be activated by KH in order to polymerize DMAEMA (*N,N*-dimethylamino ethyl methacrylate). The resulting block copolymers had relatively broad molecular weight distributions of 1.2 and 1.3 ($M_w/M_n = 1.2$–1.3) [184].

The preparation of styrene-ferrocene block copolymers requires the initial poly-merization of styrene, since styryllithium compared to ferrocenolithium is a weaker electrophile, or in other words, styrene provides a less stable carbanion than bridged ferrocenosilanes.
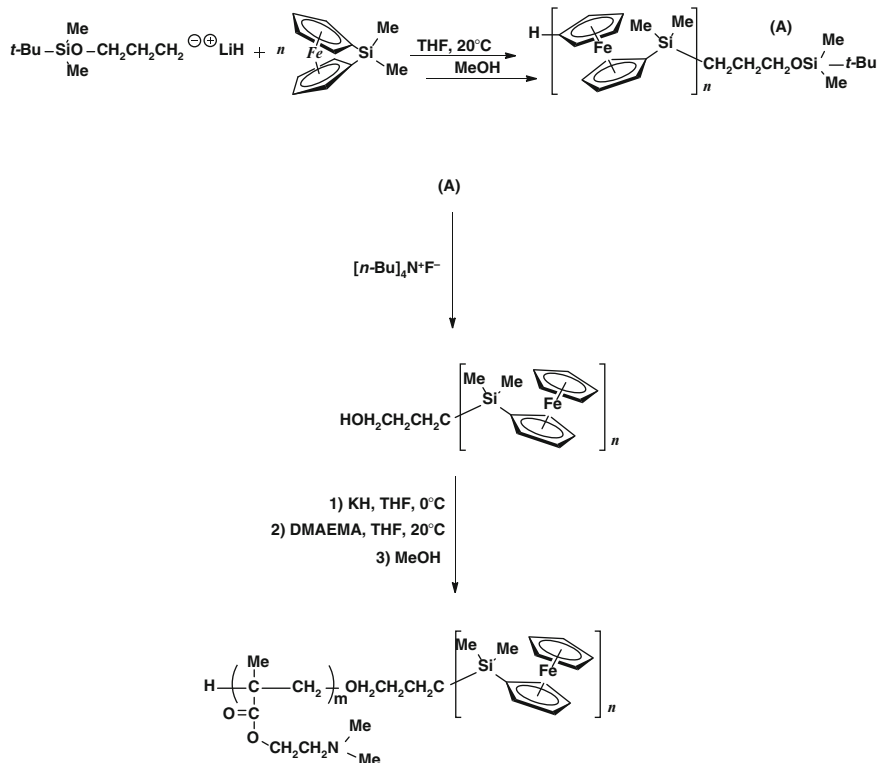
Scheme 64 Synthesis of PFDMS-*b*-PDMAEMA block copolymers

Styrene was first polymerized, in cyclohexane, at room temperature, using *n*-BuLi as initiator. The polymerization took place for 1 h and then ferrocenylethylmethylsilane, dissolved in THF at a volume ratio of 1:1, compared to cyclohexane was added. The copolymerization was left to take place for 30 min, and living diblocks were terminated with degassed and distilled water. Polymers of narrow molecular weight distribution were obtained [185].

Polyferrocenylisopropylmethylsilane (PFiPMS), also an amorphous polymer because of its asymmetric substituents, provides an additional favored property. Because of the bulky isopropyl group, PFiPMS offers a high Tg (45 °C for low molecular weights and 60 °C for higher molecular weights) [178]. PS-*b*-PFiPMS is prepared in the same way as the aforementioned PS block copolymers (Scheme 65). The produced polymers displayed low PDI (~1.1), with well-controlled molecular weights and volume fractions. However, PFiPMS homopolymers for molecular weights from 25,000 to 35,000 presented PDI values from 1.26 to 1.40. This is probably due to a lower propagation rate (compared to PFEMS) probably ascribable to the steric isopropyl group, hence the polymerization time is significantly longer than that required for the polymerization of PFEMS [186].
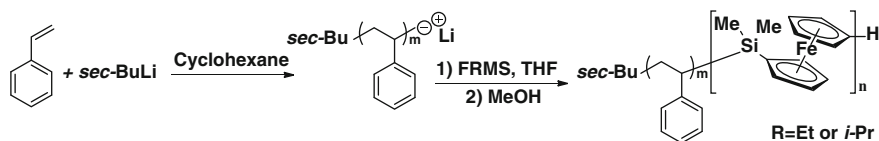
Scheme 65 Synthesis of PS-*b*-PFiPMS and PS-*b*-PFEMS block copolymers

7.2 Phosphorus-Bridged Ferrocenes

Phosphorus-containing polymers have gained significant attention mainly due to their potential application as biomaterials and as catalyst supports in organic transformations [187]. Phosphorus-bridged ferrocenes can also undergo photocontrolled ROP, the advantages of which have been previously mentioned. This "soft-living" polymerization yields well-defined polymers, with narrow molecular weight distributions up to molecular weight values of 30,000; for molecular weights higher than 30,000, broader PDIs are obtained reaching 1.2 for 45,000 and 1.4 for 60,000. Photocontrolled polymerization can take place in the presence of NaCp as initiator, in THF at 5 °C, under UV radiation for 2 h. Polymer molecular weight can be controlled according to monomer-initiator ratio as applied in living polymerization. Block copolymers PFP-*b*-PFS$_F$ with low PDIs (1.05, 1.10) and high yields (~90 %) were acquired employing this method, starting with the polymerization of the phosphorus-bridged ferrocenophanes and followed by the sequential addition of [Fe{(η-C$_5$H$_4$)$_2$SiMe(CH$_2$CH$_2$CF$_3$)}]. After the second monomer addition, the solution was left to photopolymerize for 3 h at 5 °C. The reaction was quenched with a few drops of degassed methanol (Scheme 66). However, since copolymerization yields do not reach 100 %, the block required purification from the homopolymer impurities.

7.3 Germanium-Bridged Ferrocenes

Germanium-bridged ferrocenes were first reported by Osborne in 1980 [188], followed by other reports [189]. The synthesis of a germanium-bridged polymer analogous to PFS was first illustrated in 1993, through the synthesis of polyferrocenyldimethylgermane (PFDMG) by thermal ROP. However, the resulting polymers possessed broad molecular weight distributions with little to no molecular weight control. The synthesis of well-defined PFDMG homopolymers and diblock copolymers through anionic polymerization has been exhibited [156]. Compared to its silicon, analogous PFDMG provides very low yields of pure monomer after purification. PFDMG can be polymerized through anionic ROP following the usual ferrocenophane polymerization technique (*n*-Buli, THF, 25 °C). The polymers were terminated by degassed methanol. Samples of narrow PDI were observed for low molecular weights. Copolymers were also prepared (Scheme 67) [156]; PI-*b*-
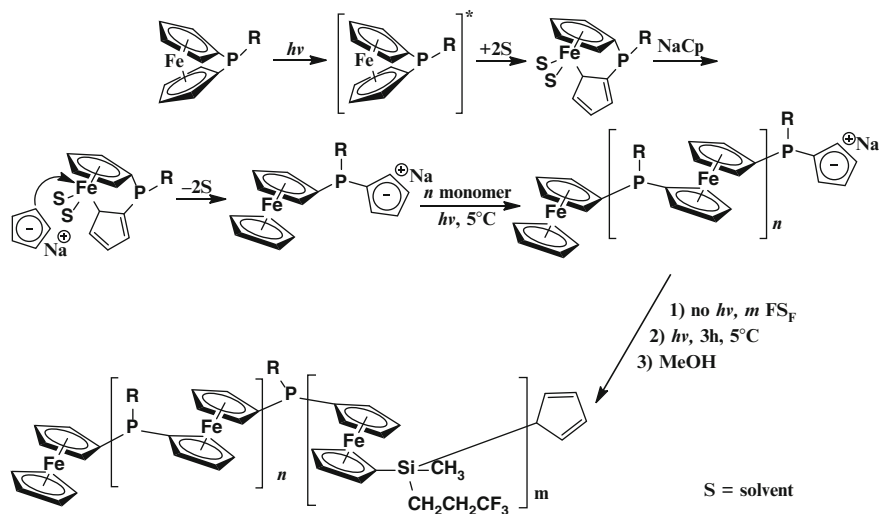
Scheme 66 Photocontrolled polymerization of phosphorus-bridged ferrocenes and block copolymerization with FS_F

PFDMG was synthesized through sequential addition giving also polymers of narrow PDI, starting with PI, initiated with *sec*-Buli, followed by the dilution of living PI in THF-containing FDMG.

7.4 Side-Functional Ferrocene Monomers

Polyvinylferrocene (PVF) is the simplest type of side-functional Fc monomer; it is polymerized through usual vinyl polymerization methods using organometallic initiators (*n*-BuLi, in THF at room temperature). In the case of more sensitive monomers with two possible reaction centers, such as methacrylates, organolithium reactivity adjustments are mandatory. As aforementioned, the insertion of a DPE moiety agent offers the necessary steric hindrance for unique stereoeclectic targeting, eliminating or terminating side reactions. The polymerization and copolymerization of polyferrocenylmethylmethacrylate PFMMA has been described [190]. The homopolymerization of PFMMA is completed like usual methacrylate monomers (*n*-BuLi, in THF at −78 °C, *n*-Buli reactivity reduction through DPE linking and presence of LiCl for higher control). PS-*b*-PFMMA diblocks were also synthesized (Scheme 68) applying the well-established conditions of methacrylate polymerization. Starting with the polymerization of styrene in cyclohexane at 25 °C, and followed by the end capping of PSLi chains with DPE, the solution was then dissolved in THF at −78 °C in the presence of LiCl, completed with the addition of the FMMA monomer. The PFMMA polymers were terminated with degassed methanol.
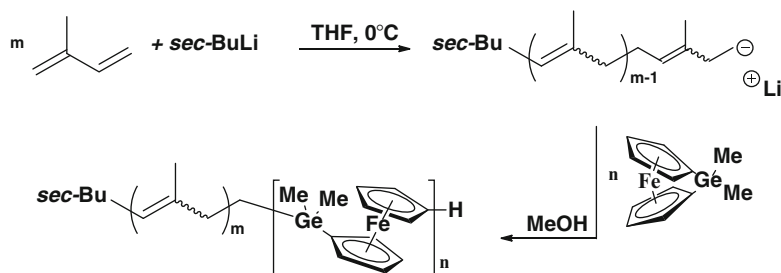
Scheme 67 Synthesis of PI-*b*-PFDMG block copolymers
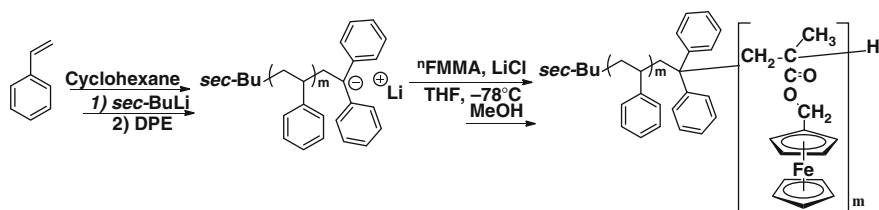
Scheme 68 Synthesis of PS-*b*-PFMMA block copolymers

Abbreviations

2VDBT	2-Vinyldibenzenthiophene
4VP	4-Vinyl pyridine
AFM	Atomic force microscopy
AGE	Allyl glycidyl ether
a-PA	*a*-Phenyl acrylate
Bd	Butadiene
BDMrSPrLi	*(tert*-Butyldimethylsilyloxy)-1-propyl lithium
BF	Benzofulvene
CHD	1,3-Cyclohexadiene
Cp	Cyclopentadienyl
CzEMA	2-(N-carbazoyl)ethyl methacrylate
D_3	Hexamethylcyclotrisiloxane
$D4^v$	Tetramethyltetravinylcyclotetrasiloxane
DABCO	1,4-Diazabicyclo[2,2,2]octane
DAS	4-Diphenylaminostyrene
DBAG	*N,N*-Dibenzyl amino glycidol
DEAAm	*N,N*-Diethylacrylamide
DEVP	Diethylvinyl phosphonate
DIVP	Diisopropylvinyl phosphonate

DMAEMA	Dimethylaminoethylmethacrylate
DMAEMA	2-(Dimethylamino)ethyl methacrylate
DME	Dimethoxyethane
DPE	Diphenylethylene
ECA	Ethylcyanoacrylate
EEGE	Ethoxyethyl glycidyl ether
EO	Ethylene oxide
EtHA	2-Ethyhexyl acrylate
Fc	Ferrocene
FDMG	Ferrocenyldimethylgermane
FMA	2-(N-Methylperfluorbutanesulfonamido)ethyl methacrylate
HIC	Hexyl isocyanate
I	Isoprene
IPP	2-Isopropenylpyridine
LCST	Lower critical solution temperature
LiEA	Lithium enolate of acetaldehyde
MAHE	*trans*-1-Methacryloyloxy-2,4-hexadiene
MAHFC	Methacrylichexylferrocenes
MAPOSS	3-(3,5,7,9,11,13,15-Heptaisobutyl-pentacyclo[$9.5.1^{3,9}.1^{5,15},1^{7,13}$] octasiloxan −1-yl) propyl methacrylate
MBA	3-Methacryloyloxy-1,1'-biadamantane
MEEOLi	2-(2-Methoxyethoxy)ethoxide lithium
MMA	Methyl methacrylate
MPEG	Poly(ethylene glycol)monomethyl ether
n-BuLi	*n*-Butyllithium
NMR	Nuclear magnetic resonance
NPHSO	3,5-Bis(dimethylaminomethylene)hydroxystyrene
OFPMA	2,2,3,3,4,4,5,5-Octafluoropentylmethacrylate
P(ε-CL)	Poly(ε-caprolactone)
P2VP	Poly(2-vinyl pyridine)
P4VP	Poly(4-vinyl pyridine)
PAGE	Poly(allyl glycidyl ether)
PaMeS	Poly(*a*-methylstyrene)
PCHD	Polycyclohexadiene
PCHD	Poly(1,3-cyclohexadiene)
PCzEMA	Poly[2-(N-carbazoyl)ethyl methacrylate]
PDAS	Poly(diphenylaminostyrene)
PDEAAm	Poly(*N,N*-diethylacrylamide)
PDEVP	Poly(diethylvinyl phosphonate)
PDEVP	Poly(diethylvinyl phosphonate)
PDIVP	Poly(diisopropylvinyl phosphonate)
PDMAAm	Poly(*N,N*-dimethylacrylamide)
PDMAEMA	Poly[(dimethylamino)ethyl methacrylate]
PDMS	Poly(dimethylsiloxane)

PE	Polyethylene
PECA	Poly(ethylcyanoacrylate)
PEG	Poly(ethylene glycol)
PEO	Poly(ethylene oxide)
PEP	Poly(ethylene-alt-propylene)
PFDMG	Polyferrocenyldimethylgermane
PFDMS	Poly(ferrocenyldimethylsilane)
PFIC	Poly(furfuryl isocyanate)
PFiPMS	Polyferrocenylisopropylmethylsilane
PFMMA	Polyferrocenylmethylmethacrylate
PFPs	Phosphorus-bridged polyferrocenes
PFS	Poly(ferrocenosilanes)
PG	Polyglycidol
PHIC	Poly(hexyl isocyanate)
PI	Polyisoprene
PIsOA	Poly(isooctyl acrylate)
PLA	Poly(lactic acid)
PMBA	Poly(3-Methacryloyloxy-1,1'-biadamantane)
PMM	Poly(methylidene malonate)
PMMA	Poly(methyl methacrylate)
PMVS	Poly(methylvinyl siloxane)
PnBuA	Poly(n-butyl acrylate)
PNHSO	Poly[3,5-bis(dimethylaminomethylene)hydroxystyrene]
POFPMA	Poly(2,2,3,3,4,4,5,5-octafluoropentylmethacrylate)
PpEES	Poly[p(1-ethoxy ethoxy)styrene]
PPP	Polyphenylene
PS	Polystyrene
P*t*BOS	Poly(4-*tert*-butoxystyrene)
P*t*BS	Poly(*tert*-butoxystyrene)
P*t*BuA	Poly(*tert*-butylacrylate)
PTESPI	Poly[3-(triethylsilyl)propyl isocyanate]
PTFEMA	Poly(2,2,2-trifluorethylmethacrylate)
PTMSS	Poly(trimethylsilylstyrene)
PVAN	Poly(vinylanthracene)
PVF	Poly(vinylferrocene)
PVPh	Poly(vinylphenol)
PVPPy	Poly[2-(4-vinylphenyl)pyridine]
S	Styrene
SAXS	Small angle X-ray scattering
SEC	Size exclusion chromatography
sec-BuLi	*sec*-Butyllithium
SiOPLi	3-tert-Butyldimethylsilyloxy-1-propyllithium
SMA	Stearyl methacrylate
TBAF	Tetrabutylammonium fluoride

*t*BuA	*tert*-Butylacrylate
t-BuOK	Potassium t*ert*-butoxide
TEM	Transmission Electron Microscopy
tert-BuLi	*tert*-Butyllithium
Tg	Glass transition temperature
THF	Tetrahydrofuran
TIPSOPrLi	3-Triisopropylsilyloxy-1-propyllithium
TMEDA	Tetramethylethylenediamine
TMSS	Trimethylsilylstyrene
TOQ	Tertrachloror-1,2-(*o*)-benzoquinone
VAN	Vinylanthracene
VPPy	2-(4-Vinylphenyl)pyridine
VTMS	Vinyltrimethylsilane
WAXS	Wide-angle X-ray scattering

References

1. Riess G, Hurtrez G, Bahadur P (1985) Block copolymers. In: Mark HF, Bikales NM, Overberger CG, Menges G, Kroschwitz JI (eds) Encyclopedia of polymer science and engineering, vol 2, 2nd edn. Wiley, New York, pp 324–434
2. (a) Hamley IW (1998) The physics of block copolymers. Oxford University Press, Oxford; (b) Abetz V, Simon PFW (2005) Phase behavior and morphologies of block copolymers. Adv Polym Sci 189:125–212; (c) Hamley IW (ed) (2004) Developments in block copolymer science and technology. John Wiley & Sons, Chichester; (d) Bates FM, Fredrickson GH (1990) Block copolymer thermodynamics: theory and experiment. Ann Rev Phys Chem 41:525–557
3. (a) Gohy JF (2005) Block copolymer micelles. Adv Polym Sci 190:65–136; (b) Riess G (2003) Micellization of block copolymers. Prog Polym Sci 28:1107–1170
4. (a) Torchilin VP (2001) Structure and design of polymeric surfactant-based drug delivery systems. J Control Release 73:137–172; (b) Kataoka K, Harada A, Nagasaki Y (2001) Block copolymer micelles for drug delivery: design, characterization and biological significance. Adv Drug Deliv Rev 47:113–131; (c) Kabanov AV, Batrakova EV, Alakhov VY (2002) Pluronic® block copolymers as novel polymer therapeutics for drug and gene delivery. J Control Release 82:189–212; (d) Kakizawa Y, Kataoka K (2002) Block copolymer micelles for delivery of gene and related compounds. Adv Drug Deliv Rev 54:203–222; (e) Munch MR, Gast AP (1990) Kinetics of block copolymer adsorption on dielectric surfaces from a selective solvent. Macromolecules 23:2313–2320; (f) Xu R, d' Oliveira JMR, Winnik MA, Riess G, Croucher MD (1992) Characterization of block copolymer micelles and their adsorption onto latex particles. Appl Polym Symp Ser 51:135–149; (g) Breulman M, Förster S, Antonietti M (2000) Mesoscopic surface patterns formed by block copolymer micelles. Macromol Chem Phys 201:204–211; (h) Cao T, Yin W, Armstrong JL, Webber SE (1994) Adsorption of photoactive amphiphilic polymers onto hydrophobic polymer films: polystyrene-block-poly(2-vinylnaphthalene)-block-poly(methacrylic acid). Langmuir 10:1841–1847; (i) Spatz JP, Sheiko S, Möller M (1996) Ion-stabilized block copolymer micelles: film formation and intermicellar interaction. Macromolecules 29:3220–3226

5. (a) Hsieh HL, Quirk RP (1996) Anionic polymerization. Principles and practical applications. Marcel Dekker, New York; (b) Hong K, Urhig D, Mays JW (1999) Living anionic polymerization. Curr Opin Solid State Mater Sci 4:531–538

6. (a) Hadjichristidis N, Pitsikalis M, Pispas S, Iatrou H (2001) Polymers with complex architecture by living anionic polymerization. Chem Rev 101:3747–3792. doi:10.1021/cr9901337; (b) Hadjichristidis N, Pitsikalis M, Pispas S, Iatrou H (2001) Polymers with complex architectures by living anionic polymerization. Chem Rev 101:3747–3792

7. (a) Hadjichristidis N, Iatrou H, Pispas S, Pitsikalis M (2000) Anionic polymerization: high vacuum techniques. J Polym Sci Polym Chem Ed 38:3211–3234; (b) Uhrig D, Mays JW (2005) Experimental techniques in high-vacuum anionic polymerization. J Polym Sci Polym Chem Ed 43:6179–6222

8. (a) Hadjichristidis N, Pispas S, Floudas GA (2003) Block copolymers. Synthetic strategies, physical properties and applications. Wiley, Hoboken; (b) Pitsikalis M, Pispas S, Mays JW, Hadjichristidis N (1998) Nonlinear block copolymer architectures. Adv Polym Sci 135:1; (c) Lodge TP (2003) Block copolymers: past successes and future challenges. Macromol Chem Phys 204:265–273

9. Hadjichristidis N, Pispas S, Iatrou H, Pitsikalis M (2002) Linking chemistry and anionic polymerization. Curr Org Chem 6:155–176

10. Pitsikalis M, Sioula S, Pispas S, Hadjichristidis N, Cook DC, Li J, Mays JW (1999) Linking reactions of living polymers with bromomethylbenzene derivatives: synthesis and characterization of star homopolymers and graft copolymers with polyelectrolyte branches. J Polym Sci Polym Chem Ed 37:4337–4350

11. (a) Guyot P, Favier JC, Fontanille M, Sigwalt P (1982) New perfectly difunctional organolithium initiators for block copolymer synthesis: 2. Difunctional polymers of dienes and of their triblocks copolymers with styrene. Polymer 23:73–76; (b) Tung LH, Lo GYS (1994) Hydrocarbon-soluble di- and multifunctional organolithium initiators. Macromolecules 27:1680–1684; (c) Tung LH, Lo GYS (1994) Studies on dilithium initiators. 1. -Hydrocarbon-soluble initiators 1,3-phenylenebis(3-methyl-1-phenylpentylidene)dilithium and 1,3-phenylenebis[3-methyl-1-(methylphenyl) pentylidene]dilithium. Macromolecules 27:2219–2224; (d) Bandemann F, Speikamp HD, Weigel L (1985) Bifunctional anionic initiators: a critical study and overview. Makromol Chem 186:2017–2024; (e) Vasilakopoulos T, Hadjichristidis N (2013) Influence of (1,3-phenylene)bis(3-methyl-1-phenyl pentylidene)dilithium initiator concentration on the modality of polybutadiene. J Polym Sci Part A Polym Chem 51:824–835

12. (a) Bates FM, Fredrickson GH (1990) Block copolymer thermodynamics: theory and experiment. Ann Rev Phys Chem 41:525–557; (b) Hadjichristidis N, Iatrou H, Pitsikalis M, Pispas S, Avgeropoulos A (2005) Linear and non-linear multiblock terpolymers. Synthesis, self-assembly in selective solvents and in bulk. Prog Polym Sci 30:725–782

13. McGrath MP, Sall ED, Tremont SJ (1995) Functionalization of polymers by metal-mediated processes. Chem Rev 95:381–398

14. Lehn J-M (1995) Supramolecular chemistry, concepts and perspectives. VCH, Weinheim

15. Schubert US, Eschbaumer C (2002) Macromolecules containing bipyridine and terpyridine metal complexes: towards metallosupramolecular polymers. Angew Chem Int Ed 41:2892–2926

16. (a) Lohmeijer BGG, Schubert US (2003) Playing LEGO with macromolecules: design, synthesis, and self-organization with metal complexes. J Polym Sci Polym Chem Ed 41:1413–1427; (b) Andres PR, Schubert US (2004) New functional polymers and materials based on 2,2':6',2''-terpyridine metal complexes. Adv Mater 16:1043–1068

17. Gohy J-F, Lohmeijer BGG, Schubert US (2002) Metallo-supramolecular block copolymer micelles. Macromolecules 35:4560–4563

18. Gohy J-F, Lohmeijer BGG, Schubert US (2002) Reversible metallo-supramolecular block copolymer micelles containing a soft core. Macromol Rapid Commun 23:555–560

19. Gohy J-F, Lohmeijer BGG, Varshney SK, Décamps B, Leroy E, Boileau S, Schubert US (2002) Stimuli-responsive aqueous micelles from an ABC metallo-supramolecular triblock copolymer. Macromolecules 35:9748–9755

20. (a) Morton M (1983) Anionic polymerization: principles and practise. Academic Press, New York; (b) Fetters LJ, Morton M (1969) Synthesis and properties of block copolymers. I. Poly α-methylstyrene-polyisoprene-poly-α-methyl styrene. Macromolecules 2:453–458; (c) Fetters LJ, Firer EM, Dafauti EM (1977) Macromolecules 10:1200–1207; (d) Corbin N (1976) Prud'homme J. J Polym Sci Part A Polym Chem 14:1645–1659; (e) Quirk RP, Lee R (1992) Experimental criteria for living polymerizations. Polym Int 27:359–367

21. (a) Natori I (1997) Synthesis of polymers with an alicyclic structure in the main chain. Living anionic polymerization of 1,3-cyclohexadiene with the n-butyllithium/N,N,N',N'--tetramethyl- ethylenediamine system. Macromolecules 30:3696–3697; (b) Natori I, Inoue S (1998) Living anionic polymerization of 1,3-cyclohexadiene with the n-butyllithium/N,N,N',N'-tetramethylethylenediamine system. Copolymerization and block copolymerization with styrene, butadiene, and isoprene. Macromolecules 31:982–987; (c) Natori I, Inoue S (1998) Anionic polymerization of 1,3-cyclohexadiene with alkyllithium/amine systems. Characteristics of n-butyllithium/N,N,N',N'-tetramethylethylenediamine system for living anionic polymerization. Macromolecules 31:4687–4694

22. (a) Natori I, Imaizumi K, Yamagishi H, Kazunori M (1998) Hydrocarbon polymers containing six-membered rings in the main chain. Microstructure and properties of poly (1,3-cyclohexadiene). J Polym Sci Part B Polym Phys 36:1657–1668; (b) Natori I, Imaizumi K (2000) Synthesis of novel hydrocarbon polymers containing 6-membered rings in the main chain: living anionic polymerization of 1,3-cyclohexadiene. Macromol Symp 157:143–150

23. Natori I, Inoue S (1998) Anionic polymerization of 1,3-cyclohexadiene with alkyllithium/ amine systems. Characteristics of n-butyllithium/N, N, N', N'-tetramethylethylenediamine system for living anionic polymerization. Macromolecules 31:4687–4694

24. Imaizumi K, Ono T, Natori I, Sakurai S, Takeda K (2000) Microphase-separated structure of 1,3-cyclohexadiene/butadiene triblock copolymers and its effect on mechanical and thermal properties. J Polym Sci Polym Phys Ed 39:13–22

25. Hong K, Mays JW (2001) 1,3-cyclohexadiene polymers. 3. Synthesis and characterization of poly(1,3-cyclohexadiene-block-styrene). Macromolecules 34:3540–3547

26. Tsoukatos T, Avgeropoulos A, Hadjichristidis N, Hong K, Mays JW (2002) Model linear block co-, ter-, and quaterpolymers of 1,3-cyclohexadiene with styrene, isoprene, and butadiene. Macromolecules 35:7928–7935

27. Williamson DT, Buchanan TD, Elkins CL, Long TE (2004) Synthesis of block copolymers based on the alternating anionic copolymerization of styrene and 1,3-cyclohexadiene. Macromolecules 37:4505–4511

28. Natori I, Natori S, Sato H (2006) Soluble polyphenylene homopolymers with controllable microstructure and properties: optical and electrical characteristics of completely dehydrogenated poly(1,3-cyclohexadiene) as a π-conjugated polymer semiconductor. Polymer 47:7123–7130

29. Natori I, Natori S, Sekikawa H, Takahashi T, Ogino K, Tsuchiya K, Sato H (2010) Poly (4-diphenylaminostyrene) with a well-defined polymer chain structure: controllable optical and electrical properties. Polymer 51:1501–1506

30. Natori I, Natori S, Sekikawa H, Tsuchiya K, Ogino K (2011) Synthesis of poly(p-phenylene)-poly(4-diphenylaminostyrene) bipolar block copolymers with a well-controlled and defined polymer chain structure. J Polym Sci Part A Polym Chem 49:1655–1663

31. Natori I, Natori S, Sekikawa H, Sato H (2008) Synthesis of soluble poly(para-phenylene) with a long polymer chain: characteristics of regioregular poly(1,4-phenylene). J Polym Sci Part A Polym Chem 46:5223–5231

32. Natori I, Natori S, Usui H, Sato H (2008) Anionic polymerization of 4-diphenylaminostyrene: characteristics of the alkyllithium/N, N, N', N'-tetramethylethylenediamine system for living anionic polymerization. Macromolecules 41:3852–3858

33. Natori I, Natori S (2011) Ultrasound-accelerated dehydrogenation of poly (1,3-cyclohexadiene): efficient synthesis of poly(para-phenylene). Polym Int 60:543–548

34. Harada M, Suzuki T, Ohya M, Kawaguchi D, Takano A, Matsushita Y (2005) Novel miscible polymer blend of poly(4-trimethylsilylstyrene) and polyisoprene. Macromolecules 38:1868–1873

35. Gladkova N, Durgar'yan S (1984) Synthesis of the AB type block copolymers (polyvinyltrimethylsilane-polydimethylsiloxane). Polym Sci USSR 26(7):1642–1648

36. Durgar'yan S, Filippova V (1986) Synthesis and properties of three-block copolymers poly (dimethylsiloxane)-poly(vinyltrimethylsilane)-poly(dimethyl-siloxane). Polym Sci USSR 28(2):364–370

37. Filippova V, Nametkin N, Durgar'yan S (1966) Copolymerization of vinyltrimethylsilane with styrene in the presence of butyllithium. Russ Chem Bull 15(10):1670–1673

38. Rangou S, Shishatskiy S, Filiz V, Abetz V (2011) Poly(vinyl trimethylsilane) and block copolymers of vinyl trimethylsilane with isoprene: anionic polymerization, morphology and gas transport properties. Eur Polym J 47:723–729

39. Mays J, Hadjichristidis N (1988) Characteristic ratios of polymethacrylates. J Macromol Sci C 28:371

40. (a) Baskaran D, Müller AHE (2006) Anionic vinyl polymerization – 50 years after Michael Szwarc. Progr Polym Sci 31:173–219; (b) Mori H, Müller AHE (2008) New polymeric architectures with (meth)acrylic segments. Prog Polym Sci 10:1403–1439

41. Varshney SK, Hautekeer JP, Fayt R, Jérôme P, Teyssié P (1990) Anionic polymerization of (meth)acrylic monomers. 4. Effect of lithium salts as ligands on the "living" polymerization of methyl methacrylate using monofunctional initiators. Macromolecules 23:2618–2622

42. (a) Vlček P, Lochmann L (1999) Anionic polymerization of (meth)acrylate esters in the presence of stabilizers of active centres. Prog Polym Sci 24:793–873; (b) Lochmann L, Kolařík J, Doskočilová D, Vozka S, Trekoval J (1979) Metallo esters. VII. Stabilizing effect of sodium tert-butoxide on the growth center in the anionic polymerization of methacrylic esters. J Polym Sci Polym Chem Ed 17:1727–1737; (c) Vlček P, Lochmann L, Otoupalová J (1992) The anionic polymerization of acrylates, 4 the polymerization of 2-ethylhexyl acrylate initiated with a mixed initiator lithium ester-enolate/lithium tert-butoxide. Makromol Chem Rapid Commun 13:163–167

43. (a) Bayard P, Jérôme R, Teyssié RPh, Varshney SK, Wang JS (1994) A new family of "ligated" anionic initiators for the "living" polymerization of (meth)acrylic esters. Polym Bull 32:381–385; (b) Nugay N, Nugay T, Jérôme R, Teyssié Ph (1997) Anionic polymerization of primary acrylates as promoted by lithium 2-(2-methoxyethoxy) ethoxide. J Polym Sci Part A Polym Chem 35:361–369; (c) Baskaran D (2000) Living anionic polymerization of methyl methacrylate in the presence of polydentate dilithium alkoxides. Macromol Chem Phys 201:890–895

44. Baskaran D, Sivaram S (1997) Specific salt effect of lithium perchlorate in living anionic polymerization of methyl methacrylate and *tert*-butyl acrylate. Macromolecules 30:1550–1555

45. Zundel T, Teyssié P, Jérôme R (1998) New ligands for the living isotactic anionic polymerization of methyl methacrylate in toluene at 0 °C. 1. Ligation of butyllithium by lithium silanolates. Macromolecules 31:2433–2439

46. (a) Tong JD, Jérôme R (2000) Synthesis of poly(methyl methacrylate)-*b*-poly(*n*-butyl acrylate)-*b*-poly(methyl methacrylate) triblocks and their potential as thermoplastic elastomers. Polymer 41:2499–2510; (b) Tong JD, Leclére P, Doneux C, Brédas JL, Lazzaroni R, Jérôme R (2000) Synthesis and bulk properties of poly(methyl methacrylate)-*b*-poly(isooctyl acrylate)-*b*-poly(methyl methacrylate). Polymer 41:4617–4624

47. (a) Pitsikalis M, Siakali-Kioulafa E, Hadjichristidis N (2000) Block copolymers of styrene and stearyl methacrylate. Synthesis and micellization properties in selective solvents. Macromolecules 33:5460–5469; (b) Pitsikalis M, Siakali-Kioulafa E, Hadjichristidis N (2004)

Block copolymers of styrene and n-alkyl methacrylates with long alkyl groups. Micellization behavior in selective solvents. J Polym Sci Polym Chem Ed 42:4177–4188

48. Allen RD, Long TE, McGrath JE (1986) Preparation of high purity, anionic polymerization grade alkyl methacrylate monomers. Polym Bull 15:127–134

49. Černoch P, Štěpánek P, Pleštil P, Šlouf M, Sidorenko A, Stamm M (2007) Surface patterns of block copolymers in thin layers after vapor treatment. Eur Polym J 43:1144–1153

50. Kennemur J, Hillmyer M, Bates F (2012) Synthesis, thermodynamics, and dynamics of poly (4-tertbutylstyrene-b-methylmethacrylate). Macromolecules 45:7228–7236

51. Imae T, Tabuchi H, Funayama K, Sato A, Nakamura T, Amaya N (2000) Self-assemblies of block copolymer of 2-perfluorooctylethyl methacrylate and methyl methacrylate. Colloids Surf A 167:73–81

52. Busse K, Kressler J, van Eck D, Höring S (2002) Synthesis of amphiphilic block copolymers based on *tert*-butyl methacrylate and 2-(*N*-methylperfluorobutane sulfonamido) ethyl methacrylate and its behavior in water. Macromolecules 35:178–184

53. Xiong D, Liu G, Hong L, Duncan S (2011) Superamphiphobic diblock copolymer coatings. Chem Mater 23:4357–4366

54. Maeda R, Hayakawa T, Ober CK (2012) Dual mode patterning of fluorine-containing block copolymers through combined top-down and bottom-up lithography. Chem Mater 24:1454–1461

55. Jie X, Peihong N, Jiang M (2006) Synthesis and characterization of a novel triblock copolymer containing double-hydrophilic blocks and poly(fluoroalkyl methacrylate) block via oxyanioninitiated polymerization. e-Polymers no. 015. ISSN 1618–7229

56. Lin X, Deng L, Dong A (2012) Synthesis of fluorescent methoxy poly(ethylene glycol)-*b*-poly(ethyl cyanoacrylate)–2–(*N*-carbazolyl)ethyl methacrylate copolymer via living oxyanion-initiated polymerization. J Appl Polym Sci 123:3575–3579

57. Ishizone T, Tajima H, Torimae H, Nakahama S (2002) Anionic polymerizations of 1-adamantyl methacrylate and 3-methacryloyloxy-1,1'-biadamantane. Macromol Chem Phys 203:2375–2384

58. (a) De Paz Bàñez M, Robinson K, Armes S (2001) Use of oxyanion-initiated polymerization for the synthesis of amine methacrylate-based homopolymers and block copolymers. Polymer. 42:29–37;(b) Ni P, Zhang M, Ma L, Fu S (2006) Poly(dimethylamino)ethyl methacrylate for use as a surfactant in the miniemulsion polymerization of styrene. Langmuir 22:6016–6023

59. Schacher F, Müllner M, Schmalz H, Müller A (2009) New block copolymers with poly(N,N-dimethylaminoethyl methacrylate) as a double stimuli-responsive block. Macromol Chem Phys 210:256–262

60. Chen S, Kuo S, Liao S, Chang F (2008) Syntheses, specific interactions, and pH-sensitive micellization behavior of poly[vinylphenol-b-2-(dimethylamino)ethyl methacrylate] diblock copolymers. Macromolecules 41:8865–8876

61. Mountrichas G, Pispas S (2006) Synthesis and pH responsive self-assembly of new double hydrophilic block copolymers. Macromolecules 39:4767–4774

62. Lehmann O, Förster S, Springer J (2000) Synthesis of new side-group liquid crystalline block copolymers by living anionic polymerization. Macromol Rapid Commun 21:133–135

63. Zhang H, Ruckestein E (2001) Novel monodisperse functional (co)polymers based on the selective living anionic polymerization of a new bifunctional monomer, trans, trans-1-methacryloyloxy-2,4-hexadiene. Macromolecules 34:3587–3593

64. Ishizone T, Han S, Okuyama S, Nakahama S (2003) Synthesis of water-soluble polymethacrylates by living anionic polymerization of trialkylsilyl-protected oligo(ethylene glycol) methacrylates. Macromolecules 36:42–49

65. (a) Hirai T, Leolukman M, Hayakawa T, Kakimoto M, Gopalan P (2008) Hierarchical nanostructures of organosilicate nanosheets within self-organized block copolymer films. Macromolecules 41:4558–4560; (b) Hirai T, Leolukman M, Jin S, Goseki R, Ishida Y, Kakimoto M, Hayakawa T, Ree M, Gopalan P (2009) Hierarchical self-assembled structures

from POSS-containing block copolymers synthesized by living anionic polymerization. Macromolecules 42(22):8835–8843

66. Sugiyama K, Oie T, El-Magd A, Hirao A (2010) Synthesis of well-defined (AB)n multiblock copolymers composed of polystyrene and poly(methyl methacrylate) segments using specially designed living AB diblock copolymer anion. Macromolecules 43:1403–1410

67. Hirao A, Matsuo Y, Oie T, Goseki R, Ishizone T (2011) Facile synthesis of triblock co- and terpolymers of styrene, 2-vinylpyridine, and methyl methacrylate by a new methodology combining living anionic diblock copolymers with a specially designed linking reaction. Macromolecules 44:6345–6355

68. Matsuo Y, Oie T, Goseki R, Ishizone T, Sugiyama K, Hirao A (2013) Precise synthesis of new triblock co- and terpolymers by a methodology combining living anionic polymers with a specially designed linking reaction. Macromol Symp 323:26–36

69. (a) Busfield W, Mathwen J (1973) Anionic polymerization of methyl acrylate. Polymer 14:137–144; (b) Kitano T, Fujimoto T, Nagasawa M (1997) Anionic polymerization of tert-butyl. Acrylate Polym J 9:153–159

70. (a) Wang J, Jérôme R, Bayard P, Teyssié Ph (1995) Anionic polymerization of acrylic monomers. 21. Anionic sequential polymerization of 2-ethylhexyl acrylate and methyl methacrylate. Macromolecules 27:4908–4913; (b) Nugay N, Nugay T, Jérôme R, Teyssié Ph (1997) Ligated anionic block copolymerization of methyl methacrylate with n-butyl acrylate and n-nonyl acrylate as promoted by lithium 2-(2-methoxyethoxy) ethoxide/diphenylmethyllithium. J Polym Sci Part A Polym Chem 35:1543–1548

71. Vlček P, Otoupalová J, Sikora A, Kříž J (1995) Anionic polymerization of acrylates. 10. Synthesis and characterization of block copolymers with acrylate blocks. Macromolecules 28:7262–7265

72. Vlček P, Čadová E, Kříž J, Látalová P, Janata M, Toman L, Masař B (2005) Anionic polymerization of acrylates. XIV. Synthesis of MMA/acrylate block copolymers initiated with ester-enolate/tert-alkoxide complex. Polymer 46:4991–5000

73. Xie X, Hogen-Esch T (1996) Anionic synthesis of narrow molecular weight distribution water-soluble poly(N, N-dimethylacrylamide) and poly(N-acryloyl-N '-methylpiperazine). Macromolecules 29:1746–1752

74. (a) Kobayashi M, Okuyama S, Ishizone T, Nakahama S (1999) Stereospecific anionic polymerization of N,N-dialkylacrylamides. Macromolecules 32:6466–6477; (b) Kobayashi M, Ishizone T, Nakahama S (2000) Synthesis of highly isotactic poly(N, N-diethylacrylamide) by anionic polymerization with grignard reagents and diethylzinc. J Polym Sci Part A Polym Chem 38:4677–4685

75. André X, Zhang M, Müller A (2005) Thermo- and pH-responsive micelles of poly(acrylic acid)-block-poly(N, N-diethylacrylamide). Macromol Rapid Commun 26:558–563

76. Vinogradova L, Fedorova L, Adler H-J, Kuckling D, Seifert D, Tsvetanov C (2005) Controlled anionic block copolymerization with N, N-dialkylacrylamide as a second block. Macromol Chem Phys 206:1126–1133

77. Kobayachi M, Chiba T, Tsuda K, Takeishi M (2005) Anionic polymerization of N, N-dialkylacrylamides containing alkoxysilyl groups in the presence of Lewis acids. J Polym Sci Part A Polym Chem 43:2754–2764

78. Angelopoulos S, Tsitsilianis C (2006) Thermo-reversible hydrogels based on poly(N, N-diethylacrylamide)-block-poly(acrylic acid)-block-poly(N, N-diethylacrylamide) double hydrophilic triblock copolymer. Macromol Chem Phys 207:2188–2194

79. (a) Tardi M, Sigwalt P (1972) Etude spectrophotometrique de la reaction d'amorcage de la polymerisation anionique de la vinyl-2 pyridine. Eur Polym J 8:137–149; (b) Tardi M, Sigwalt P (1972) Etude de la conductivite des solutions carbanioniques de poly(vinyl-2, pyridine) dans le tetrahydrofuranne. Eur Polym J 8:151–162; (c) Tardi M, Sigwalt P (1973) Etude de la nature des especes ioniques intervenant au cours de la polymerisation anionique de la vinyl-4 pyridine. Eur Polym J 9:1369–1379; (d) Chang C, Hogen-Esch T (1975) Anionic polymerization of polar monomers. I. Ultraviolet–visible spectroscopic and

conductometric studies of ion pairs of alkali salts of vinyl 2-, 3-, and 4-pyridine-type carbanions and their crown ether complexes in aprotic media. J Am Chem Soc 97:2805–2810; (e) Meverden C, Hogen-Esch T (1984) Oligomerization of vinyl monomers, 19. Studies of side reactions occurring in oligomeric models of "living" poly (2-vinylpyridine). Makromol Chem Rapid Commun 5:749–757; (f) Krasnoselskaya I, Erussalimsky B (1985) Non-trivial auto-modification of the active centres in the poly (2-vinylpyridyl)lithium/toluene system. Makromol Chem Rapid Commun 6:191–195; (g) Krasnoselskaya I, Erussalimsky B (1986) Automodification of poly(2-vinylpyridyl) lithium and its consequences for the block copolymerization processes. Acta Polym 37:72–75; (h) Luxton A, Quig A, Delvaux MJ, Fetters L (1978) Star-branched polymers: 2. Linking reaction involving 2- and 4-vinyl pyridine and dienyland styryllithium chain ends. Polymer 19:1320–1324; (i) Varshney S, Zhong X, Eisenberg A (1993) Anionic homopoly-merization and block copolymerization of 4-vinylpyridine and its investigation by high-temperature size-exclusion chromatography in N-methyl-2-pyrrolidinone. Macromolecules 26:701–706; (j) Watanabe H, Shimura T, Kotaka T, Tirrell M (1993) Synthesis, character-ization, and surface structures of styrene-2-vinylpyridine-butadiene three-block polymers. Macromolecules 26:6338–6345

80. (a) Quirk RP, Galvan-Corona S (2001) Controlled anionic synthesis of polyisoprene−poly (2-vinylpyridine) diblock copolymers in hydrocarbon solution. Macromolecules 34:1192–1197; (b) Tsitsilianis C, Sfika V (2001) Heteroarm star-like micelles formed from polystyrene-block-poly(2-vinyl pyridine)-block-poly(methyl methacrylate) ABC triblock copolymers in toluene. Macromol Rapid Commun 22:647–651

81. Möller M, Lenz R (1989) Poly(2-vinylpyridine) block copolymers. Phase separation and electric conductivity of iodine complexes. Makromol Chem 190:1153–1163

82. (a) Ludwigs S, Böker A, Abetz V, Müller A, Krausch G (2003) Phase behavior of linear polystyrene-block-poly(2-vinylpyridine)-block-poly(*tert*-butyl methacrylate) triblock ter-polymers. Polymer 44:6815–6823; (b) Giebeler E, Stadler R (1997) ABC triblock polyampholytes containing a neutral hydrophobic block, a polyacid and a polybase. Macromol Chem Phys 198:381–38255; (c) Watanabe H, Amemiya T, Shimura T, Kotaka T (1994) Anionic synthesis of graft block copolymers with poly(2-vinylpyridine) trunks: effects of trunk and branch molecular weights. Macromolecules 27:2336–2338; (d) Watanabe H, Shimura T, Kotaka T, Tirrell M (1993) Synthesis, characterization, and surface structures of styrene-2-vinylpyridine-butadiene three-block polymers. Macromolecules 26:6338–6345

83. (a) Shin YD, Han SH, Samal S, Lee JS (2005) Synthesis of poly(2-vinyl pyridine)-*b*-poly (*n*-hexyl isocyanate) amphiphilic coil-rod block copolymer by anionic polymerization. J Polym Sci Part A Polym Chem 43:607–615; (b) Isaacs N (1987) Physical organic chemistry. Longman House, Essex, p 136

84. (a) Schultz M, Khandpur A, Bates F, Almdal K, Mortensen K, Hajduk D, Gruner S (1966) Phase behavior of polystyrene−poly(2-vinylpyridine) diblock copolymers. Macromolecules 29:2857–2867; (b) Schultz M, Bates F, Almdal K, Mortensen K (1994) Epitaxial relationship for hexagonal-to-cubic phase transition in a book copolymer mixture. Phys Rev Lett 73:86–89; (c) Shull K, Kramer E, Hadziioannou G, Tang W (1990) Segregation of block copolymers to interfaces between immiscible homopolymers. Macromolecules 23:4780–4787; (d) Ruokolainen J, Makinen R, Torkkeli M, Makela T, Serimaa R, ten Brinke G, Ikkala O (1998) Switching supramolecular polymeric materials with multiple length scales. Science 280:557–560; (e) Rukolainen J, Torkkeli M, Serimaa R, Komanschek E, ten Brinke G, Ikkala O (1997) Order–disorder transition in comblike block copolymers obtained by hydrogen bonding between homopolymers and end-functionalized oligomers: poly(4-vinylpyridine)−pentadecylphenol. Macromolecules 30:2002–2007

85. (a) Sohn B, Seo B (2001) Fabrication of the multilayered nanostructure of alternating poly-mers and gold nanoparticles with thin films of self-assembling diblock copolymers. Chem Mater 13:1752–1757; (b) Yun S, Yoo S, Jung C, Zin W, Sohn B (2006) Highly ordered arrays

of nanoparticles in large areas from diblock copolymer micelles in hexagonal self-assembly. Chem Mater 18:5646–5648

86. de Moel K, Alberda van Ekenstein G, Nijland H, Polushkin E, ten Brinke G (2001) Polymeric nanofibers prepared from self-organized supramolecules. Chem Mater 13:4580

87. Valkama S, Kosonen H, Ruokolainen J, Haatainen T, Torkkeli M, Serimaa R, ten Brinke G, Ikkala O (2004) Self-assembled polymeric solid films with temperature-induced large and reversible photonic-bandgap switching. Nat Mater 3:872–876

88. Mantzaridis C, Pispas S (2011) Poly[(sodium sulfamate/carboxylate)isoprene-*b*-2-vinyl pyridine] block polyampholytes: synthesis and self-assembly in aqueous media. J Polym Sci Part A Polym Chem 49:3090–3098

89. Kuo S-W, Tung P-H, Chang F-C (2006) Synthesis and the study of strongly hydrogen-bonded poly(vinylphenol-*b*-vinylpyridine) diblock copolymer through anionic polymerization. Macromolecules 39:9388–9395

90. (a) Varshney S, Zhong X, Eisenberg A (1993) Anionic homopolymerization and block copolymerization of 4-vinylpyridine and its investigation by high-temperature size-exclusion chromatography in N-methyl-2-pyrrolidinone. Macromolecules 26:701–706; (b) Quirk R, Corona-Galvan S (2001) Controlled anionic synthesis of polyisoprene- poly(2-vinylpyridine) diblock copolymers in hydrocarbon solution. Macromolecules 34:1192–1197; (c) Biggs S, Vincent B (1992) Poly(styrene-b-2-vinylpyridine-1-oxide) and poly(dimethylsiloxane-b-2 vinylpyridine-1-oxide) diblock copolymers. 1. Preparation and characterization. Colloid Polym Sci 270:505–510; (d) Hubert P, Soum A, Fontanille M (1995) Structure and reactivity of propagating species in anionic polymerization of 2-vinylpyridine initiated by lithium derivatives in toluene. Macromol Chem Phys 196:1023–1030; (e) Quirk RP, Lee Y (2000) Oligomerization of 1,3-diolefines with ziegler-type catalysts. J Polym Sci Part A Polym Chem 38:45–50

91. Topham P, Howse J, Fernyhough C, Ryan A (2007) The performance of poly(styrene)-block-poly(2-vinyl pyridine)-blockpoly(styrene) triblock copolymers as pH-driven actuators. Soft Matter 3:1506–1512

92. Fragouli P, Iatrou H, Hadjichristidis N (2002) Synthesis and characterization of linear diblock and triblock copolymers of 2-vinyl pyridine and ethylene oxide. Polymer 43:7141–7144

93. Han S, Lee D, Kim J (2007) Phase behavior of poly(2-vinylpyridine)-block-poly(4-vinylpyridine) copolymers. Macromolecules 40:7416–7419

94. Hückstädt H, Göpfert A, Abetz V (2000) Influence of the block sequence on the morphological behavior of ABC triblock copolymers. Polymer 41:9089–9094

95. du Sart G, Vukovic I, van Ekenstein G, Polushkin E, Loos K, ten Brinke G (2010) Self-assembly of supramolecular triblock copolymer complexes. Macromolecules 43:2970–2980

96. Li H-J, Tsiang C-C R (2000) Preparation and characterization of a linear poly(4-vinyl pyridine)-*b*-polybutadiene-*b*-poly(4-vinylpyridine) using a t-butyllithium/m-diisopropenylbenzene diadduct as a dicarbanion initiator. Polymer 41:5601–5610

97. Lee Y-H, Chang C-J, Kao C-J, Dai C-A (2010) In-situ template synthesis of a polymer/semiconductor nanohybrid using amphiphilic conducting block copolymers. Langmuir 26:4196–4206

98. Kang N-G, Changez M, Lee J-S (2007) Living anionic polymerization of the amphiphilic monomer2-(4-vinylphenyl)pyridine. Macromolecules 40:8553–8559

99. Hirao A, Kitamura K, Takenaka K, Nakahama S (1993) Protection and polymerization of functional monomers. 18. Syntheses of well-defined poly(vinylphenol), poly[(vinylphenyl) methanol], and poly[2-vinylphenyl)ethanol] by means of anionic living polymerization of styrene derivatives containing *tert*-butyldimethylsilyl ethers. Macromolecules 26:4995–5003

100. Baranauskas V III, Zalich M, Saunders M, St. Pierre T, Riffle J (2005) Poly(styrene-b-4-vinylphenoxyphthalonitrile)-cobalt complexes and their conversion to oxidatively stable cobalt nanoparticles. Chem Mater 17:5246–5254

101. Natalello A, Tonhauser C, Frey H (2013) Anionic polymerization of para-(1-ethoxy ethoxy) styrene: rapid access to poly(p-hydroxystyrene) copolymer architectures. ACS Macro Lett 2:409–413

102. Vila-Ortega A, Vázquez-Torres H (2007) Living anionic polymerization of 2-vinyldibenzothiophene: homopolymer and block copolymers with styrene. J Polym Sci Part A Polym Chem 45:1993–2003

103. (a) Natori I, Natori S, Usui H, Sato H (2008) Anionic polymerization of 4-diphenylaminostyrene: characteristics of the alkyllithium/N,N,N',N'- -tetramethylethylenediamine system for living anionic polymerization. Macromolecules 41:3852–3858; (b) Natori I, Natori S, Sekikawa H, Takahashi T, Ogino K, Tsuchiya K, Sato H (2010) Poly(4-diphenylaminostyrene) with a well-defined polymer chain structure: controllable optical and electrical properties. Polymer 51:1501–1506

104. Natori I, Natori S, Sekikawa H, Takahashi T, Sato H (2010) Synthesis and characterization of poly(4-diphenylaminostyrene)-poly(9-vinylanthracene) binary block copolymer. J App Polym Sci 118:69–73

105. Higashihara T, Ueda M (2009) Living anionic polymerization of 4-vinyltriphenylamine for synthesis of novel block copolymers containing low-polydisperse poly(4-vinyltriphe-nylamine) and regioregular poly(3-hexylthiophene) segments. Macromolecules 42:8794–8800

106. (a) Lafitte B, Jannasch P (2007) Chapter three on the prospects for phosphonated polymers as proton-exchange fuel cell membranes. Adv Fuel Cells 1:119–185; (b) Rusanov A, Kostoglodov P, Abadie M, Voytekunas V, Likhachev D (2008) Proton-conducting polymers at membranes carrying phosphonic acid groups. Adv Polym Sci 216:125–155

107. Perrin R, Elomaa M, Jannasch P (2009) Nanostructured proton conducting polystyrene-poly (vinylphosphonic acid) block copolymers prepared via sequential anionic polymerizations. Macromolecules 42:5146–5154

108. Wagner T, Manhart A, Deniz N, Kaltbeitzel A, Wagner M, Brunklaus G, Meyer W (2009) Vinylphosphonic acid homo- and block copolymers. Macromol Chem Phys 210:1903–1914

109. Kosaka Y, Kitazawa K, Inomata S, Ishizone T (2013) Living anionic polymerization of benzofulvene: highly reactive fixed transoid 1,3-diene. ACS Macro Lett 2:164–167

110. de Paz Báñez MV, Robinson KL, Armes SP (2000) Synthesis and solution properties of dimethylsiloxane−2-(dimethylamino)ethyl methacrylate block copolymers. Macromolecules 33:451–456

111. Lee J, Hogen-Esch TE (2001) Synthesis and characterization of narrow molecular weight distribution AB and ABA poly(vinylpyridine)−poly(dimethylsiloxane) block copolymers via anionic polymerization. Macromolecules 34:2805–2811

112. Bellas V, Iatrou H, Hadjichristidis N (2000) Controlled anionic polymerization of hexamethylcyclotrisiloxane. Model linear and miktoarm star co- and terpolymers of dimethylsiloxane with styrene and isoprene. Macromolecules 33:6993–6997

113. Cai GP, Weber WP (2004) Synthesis of terminal Si–H irregular tetra-branched star polysiloxanes. Pt-catalyzed hydrosilylation with unsaturated epoxides. Polysiloxane films by photo-acid catalyzed crosslinking. Polymer 45:2941–2948

114. Boehm P, Mondeshki M, Frey H (2012) Polysiloxane-backbone block copolymers in a one-pot synthesis: a silicone platform for facile functionalization. Macromol Rapid Commun 33:1861–1867

115. Davis S (1997) Biomedical applications of nanotechnology – implications for drug targeting and gene therapy. Trends Biotechnol 15:217–224

116. Quirk RP, Ma J-J (1988) Characterization of the functionalization reaction product of poly (styryl)lithium with ethylene oxide. J Polym Sci Polym Chem Ed 26:2031–2037

117. (a) Ekizoglou N, Hadjichristidis N (2001) Benzyl potassium: an efficient one-pot initiator for the synthesis of block co- and terpolymers of ethylenoxide. J Polym Sci Polym Chem Ed 39:1198–1201; (b) Ekizoglou N, Hadjichristidis N (2002) Synthesis of model linear

tetrablock quaterpolymers and pentablock quintopolymers of ethylene oxide. J Polym Sci Polym Chem Ed 40:2166–2170

118. Boschet F, Branger C, Margaillan A, Hogen-Esch T (2005) Associative properties of perfluorooctyl end-functionalized polystyrene–poly(ethyleneoxide) diblock copolymers. Polym Int 54:90–95

119. Chen J, Frisbie D, Bates F (2009) Lithium perchlorate-doped poly(styrene-*b*-ethylene oxide-*b*-styrene) lamellae-forming triblock copolymer as high capacitance, smooth, thin film dielectric. J Phys Chem C 113:3903–3908

120. Bailey T, Pham H, Bates F (2001) Morphological behavior bridging the symmetric AB and ABC states in the poly(styrene-*b*-isoprene-*b*-ethylene oxide) triblock copolymer system. Macromolecules 34:6994–7008

121. Meuler A, Ellison C, Qin J, Evans C, Hillmyer M, Bates F (2009) Polydispersity effects in poly(isoprene-*b*-styrene-*b*-ethylene oxide) triblock terpolymers. J Chem Phys 130:234903

122. (a) Brannan A, Bates F (2004) ABCA tetrablock copolymer vesicles. Macromolecules 37:8816–8819; (b) Hillmyer M, Bates F (1996) Synthesis and characterization of model polyalkane−poly(ethylene oxide) block copolymers. Macromolecules 29:6994–7002

123. Touris A, Lee S, Hillmyer M, Bates F (2012) Synthesis of tri- and multiblock polymers with asymmetric poly(ethylene oxide) end blocks. ACS Macro Lett 1:768–771

124. Seow PK, Gallot Y, Skoulios A (1975) Synthèse et caractérisation de copolymères séquencés poly(méthacrylate d'alkyle)/poly(oxyéthylène). Makromol Chem 176:3153–3166

125. Suzuki T, Murakami Y, Takegami Y (1980) Synthesis and characterization of block copolymers of poly(ethylene oxide) and poly(methyl methacrylate). Polym J 12:183–192

126. Garg D, Horing S, Ulbricht J (1984) Initiation of anionic polymerization of methyl methacrylate by living poly(ethylene oxide) anions, a new way for the synthesis of poly(ethylene oxide)-*b*-poly(methyl methacrylate). Macromol Chem Rapid Commun 5:615–618

127. Reuter H, Berlinova I, Höring S, Ulbricht J (1991) The anionic block copolymerization of ethylene oxide with *tert*-butyl methacrylate. Diblock and multiblock copolymers. Eur Polym J 27:673–680

128. Dhara M, Baskaran D, Sivram S (2008) Synthesis of amphiphilic poly(methyl methacrylate-ethylene oxide) copolymers from monohydroxy telechelic poly(methyl methacrylate) as macroinitiator. J Polym Sci Part A Polym Chem 46:2132–2144

129. Mountrichas G, Pispas S (2007) Novel double hydrophilic block copolymers based on poly (*p*-hydroxystyrene) derivatives and poly(ethylene oxide). J Polym Sci Part A Polym Chem 45:5790–5799

130. Mountrichas G, Mantzaridis C, Pispas S (2006) Well-defined flexible polyelectrolytes with two cationic sites per monomeric unit. Macromol Rapid Commun 27:289–294

131. Gohy J-F, Willet N, Varshney S, Zhang J-X, Jerôme R (2001) Core–shell–corona micelles with a responsive shell. Angew Chem Int Ed 40:3214–3216

132. Schmalz H, Knoll A, Müller AJ, Abetz V (2002) Synthesis and characterization of ABC triblock copolymers with two different crystalline end blocks: influence of confinement on crystallization behavior and morphology. Macromolecules 35:10004–10013

133. (a) Taribagil R, Hillmyer M, Lodge T (2010) Hydrogels from ABA and ABC triblock polymers. Macromolecules 43:5396–5404; (b) Hillmyer M, Bates F (1996) Synthesis and characterization of model polyalkane−poly(ethylene oxide) block copolymers. Macromolecules 29:6994–7002

134. (a) Larras V, Bru N, Breton P, Riess G (2000) Synthesis and micellization of amphiphilic poly(ethylene oxide)-block-poly(methylidene malonate 2.1.2) diblock copolymers. Macromol Rapid Commun 21:1089–1092; (b) Bru-Magniez N, Larras V, Riess G, Breton P, Couvreur P, Roques Carmes C (1998) Novel surfactant copolymers based on methylidene malonate. WO 99/38898 (1999)/FR19980001001(1998)

135. Studer P, Larras V, Riess G (2008) Amino end-functionalized poly(ethylene oxide)-block-poly(methylidene malonate 2.1.2) block copolymers: synthesis, characterization, and chemical modification for targeting purposes. Eur Polym J 44:1714–1721

136. Jerome C, Lecomte P (2008) Recent advances in the synthesis of aliphatic polyesters by ring-opening polymerization. Adv Drug Deliv Rev 60:1056–1076

137. Van Butsele K, Cajot S, Van Vlierberghe S, Dubruel P, Passirani C, Benoit J-P, Jérôme R, Jérôme C (2009) pH-responsive flower-type micelles formed by a biotinylated poly (2-vinylpyridine)-block-poly(ethylene oxide)-block-poly(e-caprolactone) triblock copolymer. Adv Funct Mater 19:1416–1425

138. Ogle C, Strickler F, Gordon G (1993) Reaction of polystyryllithium with tetrahydrofuran. Macromolecules 26:5803–5805

139. (a) Dimitrov P, Rangelov S, Dworak A, Haraguchi N, Hirao A, Tsvetanov C (2004) Triblock and radial star-block copolymers comprised of poly(ethoxyethyl glycidyl ether), polyglycidol, poly(propylene oxide) and polystyrene obtained by anionic polymerization initiated by Cs initiators. Macromol Symp 215:127–139; (b) Dworak A, Baran G, Trzebicka B, Walach W (1999) Polyglycidol-block-poly(ethylene oxide)-block-polyglycidol: synthesis and swelling properties. React Funct Polym 42:31–36; (c) Lapienis G, Penczek S (2005) One-pot synthesis of star-shaped macromolecules containing polyglycidol and poly(ethylene oxide) arms. Biomacromolecules 6:752–762; (d) Kaluzynski K, Pretula J, Lapienis G, Basko M, Bartczak Z, Dworak A, Penczek S (2001) Dihydrophilic block copolymers with ionic and nonionic blocks. I. Poly(ethylene oxide)-b-polyglycidol with OP(O)(OH)$_2$, COOH, or SO$_3$H functions: synthesis and influence for CaCO3 crystallization. J Polym Sci Part A Polym Chem 39:955–963; (e) Mendrek A, Mendrek S, Trzebicka B, Kuckling D, Walach W, Adler HJ, Dworak A (2005) Polyether core-shell cylinder–polymerization of polyglycidol macromonomers. Macromol Chem Phys 206:2018–2026; (f) Walach W, Kowalczuk A, Trzebicka B, Dworak A (2001) Synthesis of high-molar mass arborescent-branched polyglycidol via sequential grafting. Macromol Rapid Commun 22:1272–1277

140. (a) Hsieh H, Quirk RP (1996) Anionic polymerizations principles and practical applications. Marcel Dekker, New York, p 688; (b) Wesdemiotis C, Arnould MA, Lee Y, Quirk RP (2000) MALDI TOF mass spectrometry of the products from novel anionic polymerizations. Polym Prepr 41(1):629–630

141. Dimitrov P, Utrata-Wesołek A, Rangelov S, Wałach W, Trzebicka B, Dworak A (2006) Synthesis and self-association in aqueous media of poly(ethylene oxide)/poly(ethyl glycidyl carbamate) amphiphilic block copolymers. Polymer 47:4905–4915

142. Ah Toy A, Reinicke S, Müller A, Schmalz H (2007) One-pot synthesis of polyglycidol-containing block copolymers with alkyllithium initiators using the phosphazene base t-BuP$_4$. Macromolecules 40:5241–5244

143. Taton D, Le Borgne A, Sepulchre M, Spassky N (1994) Synthesis of chiral and racemic functional polymers from glycidol and thioglycidol. Macromol Chem Phys 195:139–148

144. (a) Muller M, Zentel R (1994) Photochemical amplification of chiral induction in polyisocyanates. Macromolecules 27:4404–4406; (b) Shibaev PV, Tang K, Genack AZ, Kopp V, Green MM (2002) Lasing from a stiff chain polymeric lyotropic cholesteric liquid crystal. Macromolecules 35:3022–3025; (c) Maeda K, Okamoto Y (1998) Synthesis and conformation of optically active poly(phenyl isocyanate)s bearing an ((S)-(α-methylbenzyl) carbamoyl) group. Macromolecules 31:1046–1052

145. Bur AJ, Fetters LJ (1976) The chain structure, polymerization, and conformation of polyisocyanates. Chem Rev 76:727–746

146. (a) Lee JS, Ryu SW (1999) Anionic living polymerization of 3-(triethoxysilyl)propyl isocyanate. Macromolecules 32:2085–2087; (b) Shin YD, Kim SY, Ahn JH, Lee JS (2001) Synthesis of poly(n-hexyl isocyanate) by controlled anionic polymerization in the presence of NaBPh4. Macromolecules 34:2408–2410

147. (a) Ahn JH, Shin YD, Kim SY, Lee JS (2003) Synthesis of well-defined block copolymers of n-hexyl isocyanate with isoprene by living anionic polymerization. Polymer 44:3847–3854; (b) Ahn JH, Lee CH, Shin YD, Lee JS (2004) Generation of highly stable amidate anion in anionic polymerization of 3-(triethylsilyl)propyl isocyanate. J Polym Sci Part A Polym Chem 42:933–940

148. Vazaios A, Pitsikalis M, Hadjichristidis N (2003) Triblock copolymers and pentablock terpolymers of *n*-hexyl isocyanate with styrene and isoprene: synthesis, characterization and thermal properties. J Polym Sci Polym Chem Ed 41:3094–3102

149. Zorba G, Vazaios A, Pitsikalis M, Hadjichristidis N (2005) Anionic polymerization of *n*-hexyl isocyanate with monofunctional initiators. Application in the synthesis of diblock copolymers with styrene and isoprene. J Polym Sci Polym Chem Ed 43:3533–3542

150. Shin Y-D, Han S-H, Samal S, Lee J-S (2005) Synthesis of poly(2-vinyl pyridine)-*b*-poly (*n*-hexylisocyanate) amphiphilic coil-rod block copolymer by anionic polymerization. J Polym Sci Part A Polym Chem 43:607–615

151. Rahman M, Samal S, Lee J-S (2007) Quantitative in situ coupling of living diblock copolymers for the preparation of amphiphilic coil-rod-coil triblock copolymer poly (2-vinylpyridine)-*b*-poly(*n*-hexylisocyanate)-*b*-poly(2-vinylpyridine). Macromolecules 40:9279–9283

152. Ahn J-H, Shin Y-D, Nath G, Park S-Y, Rahman M, Samal S, Lee J-S (2005) Unprecedented control over polymerization of *n*-hexyl isocyanate using an anionic initiator having synchronized function of chain-end protection. J Am Chem Soc 127:4132–4133

153. Min J, Yoo H-S, Shah P, Chae C-G, Lee J-S (2013) Enolate anionic initiator, sodium deoxybenzoin, for leading living natures by formation of aggregators at the growth chain ends. J Polym Sci Part A Polym Chem 51:1742–1748

154. Wurm F, Hilf S, Frey H (2009) Electroactive linear–hyperbranched block copolymers based on linear poly(ferrocenylsilane)s and hyperbranched poly(carbosilane)s. Chem Eur J 15:09068–09077

155. Ma Y, Dong W-F, Hempenius MA, Möhwald H, JuliusVancso G (2006) Redox-controlled molecular permeability of composite-wall microcapsules. Nat Mater 5:724–729

156. Ieong NS, Manners I (2009) Anionic ring-opening polymerization of a germanium-bridged [1]ferrocenophane: synthesis and morphology of well-defined polyferrocenylgermane homopolymers and block copolymers. Macromol Chem Phys 210:1080–1086

157. Patra SK, Whittell GR, Nagiah S, Ho C-L, Wong W-Y, Manners I (2010) Photocontrolled living anionic polymerization of phosphorus-bridged [1]ferrocenophanes: a route to well-defined polyferrocenylphosphine (PFP) homopolymers and block copolymers. Chem Eur J 16:3240–3250

158. Goseki R, Hirai T, Kakimoto M, Hayakawa T (2012) Iron oxide arrays prepared from ferrocene- and silsesquioxane-containing block copolymers. Int J Polym Sci 2012:1–10

159. Bellas V, Rehahn M (2009) Block copolymer synthesis via chemoselective stepwise coupling reactions. Macromol Chem Phys 210:320–330

160. (a) Wang XS, Winnik MA, Manners I (2002) Synthesis and aqueous self-assembly of a polyferrocenylsilane-block-poly(aminoalkyl methacrylate) diblock copolymer. Macromol Rapid Commun 23:210–213; (b) Lee J, Hogen-Esch TE (2001) Synthesis and characterization of narrow molecular weight distribution AB and ABA poly(vinylpyridine)−poly (dimethylsiloxane) block copolymers via anionic polymerization. Macromolecules 34:2805–2811

161. (a) Mahajan S, Cho B, Allgaiger J, Fetters LJ, Coates GW, Wiesner U (2004) Synthesis of amphiphilic ABC triblock copolymers with PEO as the middle block. Macromol Rapid Commun 25:1889–1894; (b) Zhang K, Ye Z, Subramanian R (2008) Synthesis of block copolymers of ethylene with styrene and *n*-butyl acrylate via a tandem strategy combining ethylene "living" polymerization catalyzed by a functionalized Pd−diimine catalyst with atom transfer radical polymerization. Macromolecules 41:640–649

162. (a) Quémener D, Davis TP, Barner-Kowollik C, Stenzel MH (2006) RAFT and click chemistry: a versatile approach to well-defined block copolymers. Chem Commun 5051–5053; (b) Durmaz H, Dag A, Altintas O, Erdogan T, Hizal G, Tunca U (2007) One-pot synthesis of ABC type triblock copolymers via in situ click [3 + 2] and Diels−Alder [4 + 2] reactions. Macromolecules 40:191–198; (c) Opsteen JA, van Hest JCM (2007) Modular synthesis of ABC type block copolymers by "click" chemistry. J Polym Sci Part

A Polym Chem 45:2913–2924; (d) Sinnwell S, Inglis AJ, Davis TP, Barner-Kowollik C, Stenzel MH (2008) An atom-efficient conjugation approach to well-defined block copolymers using RAFT chemistry and hetero Diels–Alder cycloaddition. Chem Commun 17:2052–2054

163. Natalello A, Alkan A, Friedel A, Lieberwirth I, Frey H, Wurm FR (2013) Enlarging the toolbox: epoxide termination of polyferrocenylsilane (PFS) as a key step for the synthesis of amphiphilic PFS−polyether block copolymers. ACS Macro Lett 2:313–316

164. Vanderark L, Januszewski E, Gwyther J, Manners I (2011) Studies of the end-capping of living anionic poly(ferrocenyldimethylsilane) with 1,1-diphenylethylene. Eur Polym J 47:823–826

165. Wang H, Winnik MA, Manners I (2007) Synthesis and self-assembly of poly(ferrocenyldimethylsilane-b-2-vinylpyridine) diblock copolymers. Macromolecules 40:3784–3789

166. (a) Kloninger C, Rehahn M (2004) 1,1-dimethylsilacyclobutane-mediated living anionic block copolymerization of [1]dimethylsilaferrocenophane and methyl methacrylate. Macromolecules 37:1720–1727; (b) Kloninger C, Rehahn M (2007) Styrene–ferrocenyldimethylsilane–methyl methacrylate triblock copolymers: synthesis and phase morphology. Macromol Chem Phys 208:833–4

167. Smith GS, Patra SK, Vanderark L, Saithong S, Charmant JPH, Manners I (2010) Photocontrolled living anionic polymerization of silicon-bridged [1]ferrocenophanes with fluorinated substituents: synthesis and characterization of fluorinated polyferrocenylsilane (PFS) homopolymers and block copolymers. Macromol Chem Phys 211:303–312

168. Mizuta T, Onishi M, Miyoshi K (2000) Photolytic ring-opening polymerization of phosphorus-bridged [1]ferrocenophane coordinating to an organometallic fragment. Organometallics 19:5005–5009

169. (a) Tanabe M, Manners I (2004) Photolytic living anionic ring-opening polymerization (ROP) of silicon-bridged [1]ferrocenophanes via an iron-cyclopentadienyl bond cleavage mechanism. J Am Chem Soc 126:11434–11435; (b) Tanabe M, Vandermeulen GWM, Chan WY, Cyr PW, Vanderark L, Rider DA, Manners I (2006) Photocontrolled living polymerizations. Nat Mater 5:467–470

170. (a) Cheng JY, Ross CA, Chan VZH, Thomas EL, Lammertink RGH, Vancso GJ (2001) Formation of a cobalt magnetic dot array via block copolymer lithography. Adv Mater 13:1174–1178; (b) Lu J, Chamberlin D, Rider DA, Liu MJ, Manners I, Russell TP (2006) Using a ferrocenylsilane-based block copolymer as a template to produce nanotextured Ag surfaces: uniformly enhanced surface enhanced Raman scattering active substrates. Nanotechnology 17:5792–5797; (c) Lammertink RGH, Hempenius MA, Chan VZH, Thomas EL, Vancso GJ (2001) Poly(ferrocenyldimethylsilanes) for reactive ion etch barrier applications. Chem Mater 13:429–434; (e) Chuang VP, Ross CA, Gwyther J, Manners I (2009) Self-assembled nanoscale ring arrays from a polystyrene-b-polyferrocenylsilane-b-poly (2-vinylpyridine)triblock terpolymer thin film. Adv Mater 21:3789–3793; (f) Chuang VP, Gwyther J, Mickiewicz RA, Manners I, Ross CA (2009) Templated self-assembly of square symmetry arrays from an ABC triblock terpolymer. Nano Lett 9:4364–4369

171. (a) Espada L, Robillard J, Shadaram M, Pannell KH (2000) Ferrocenylenesilylene polymers as coatings for tapered optical-fiber gas sensors. J Inorg Organomet Polym 10:169–176; (b) Paquet C, Cyr PW, Kumacheva E, Manners I (2004) Rationalized approach to molecular tailoring of polymetallocenes with predictable optical properties. Chem Mater 16:5205–5211

172. (a) Eitouni HB, Balsara NP (2004) Effect of chemical oxidation on the self-assembly of organometallic block copolymers. J Am Chem Soc 126:7446–7447; (b) Arsenault AC, Puzzo DP, Manners I, Ozin GA (2007) Photonic-crystal full-colour displays. Nature Photonics 1:468–472

173. Sun Q, Lam JWY, Xu K, Xu H, Cha JAP, Wong PCL, Wen G, Zhang X, Jing X, Wang F, Tang BZ (2000) Nanocluster-containing mesoporous magnetoceramics from hyperbranched organometallic polymer precursors. Chem Mater 12:2617–2624

174. Hinderling C, Keles Y, Stoeckli T, Knapp HF, De Los Arcos T, Oelhafen P, Korezagin I, Hempenius MA, Vancso GJ, Pugin R, Heinzelmann H (2004) Organometallic block copolymers as catalyst precursors for templated carbon nanotube growth. Adv Mater 16:876–879

175. (a) Rider DA, Manners I (2007) Synthesis, self-assembly, and applications of polyferrocenylsilane block copolymers. Polymer Rev 47:165–195; (b) Manners I (1999) Poly (ferrocenylsilanes): novel organometallic plastics. Chem Commun 10:857–865

176. (a) Loo YL, Register RA, Ryan AJ (2002) Modes of crystallization in block copolymer microdomains: breakout, templated, and confined. Macromolecules 35:2365–2374; (b) Zhu L, Cheng SZD, Calhoun BH, Ge Q, Quirk RP, Thomas EL (2000) Crystallization temperature-dependent crystal orientations within nanoscale confined lamellae of a self-assembled crystalline−amorphous diblock copolymer. J Am Chem Soc 122:5957–5967; (c) Li LB, Serero Y, Koch MHJ, de Jeu WH (2003) Microphase separation and crystallization in an asymmetric diblock copolymer: Coupling and competition. Macromolecules 36:529–532; (d) Huang P, Zhu L, Cheng SZD, Ge Q, Quirk RP, Thomas EL (2001) Crystal orientation changes in two-dimensionally confined nanocylinders in a poly(ethylene oxide)-b-polystyrene/polystyrene blend macromolecules 34:6649–6657; (e) Chen HL, Hsiao SC, Lin TL, Yamauchi K, Hasegawa H, Hashimoto T (2001) Microdomain-tailored crystallization kinetics of block copolymers. Macromolecules 34:671–674

177. (a) Rider DA, Cavicchi KA, Power-Billard KN, Russell TP, Manners I (2005) Diblock copolymers with amorphous atactic polyferrocenylsilane blocks: synthesis, characterization, and self-assembly of polystyrene-block-poly(ferrocenylethylmethyl silane) in the bulk state. Macromolecules 38:6931–6938; (b) Eloi JC, Rider DA, Wang JY, Russell TP, Manners I (2008) Amorphous diblock copolymers with a high organometallic block volume fraction: synthesis, characterization and self-assembly of polystyrene-block-poly(ferrocenylethylmethylsilane) in the bulk state. Macromolecules 41:9474–9479; (c) Roerdink M, Hempenius MA, Vancso GJ (2005) Large area ordering at room temperature in thin films of poly (isoprene-block-ferrocenylsilane)s for nanofabrication. Chem Mater 17:1275–1278

178. Gwyther J, Ian Manners I (2009) Diblock copolymers with an amorphous, high glass transition temperature, organometallic block: synthesis, characterisation and self-assembly of polystyrene-b-poly(ferrocenylisopropylmethylsilane) in the bulk state. Polymer 50:5384–5389

179. Resendes R, Massey J, Dorn H, Winnik MA, Manners I (2000) A convenient, transition metal-catalyzed route to water-soluble amphiphilic organometallic block copolymers: synthesis and aqueous self-assembly of poly(ethylene oxide)-block-poly(ferrocenylsilane). Macromolecules 33:8–10

180. Zhang M, Rupar PA, Feng C, Lin K, Lunn DJ, Oliver A, Nunns A, Whittell GR, Manners I, Winnik MA (2013) Modular synthesis of polyferrocenylsilane block copolymers by Cu-catalyzed alkyne/azide "click" reactions. Macromolecules 46:1296–1304

181. Gohy J-F, Lohmeijer BGG, Alexeev A, Wang X-S, Manners I, Winnik MA, Schubert US (2004) Cylindrical micelles from the aqueous self-assembly of an amphiphilic poly(ethylene oxide)–b–poly(ferrocenylsilane) (PEO-b-PFS) block copolymer with a metallo-supramolecular linker at the block junction. Chem Eur J 10:4315–4323

182. (a) Kloninger C, Rehahn M (2004) 1,1-dimethylsilacyclobutane-mediated living anionic block copolymerization of [1]dimethylsilaferrocenophane and methyl methacrylate. Macromolecules 37:1720–1727; (b) Kloninger C, Knecht D, Rehahn M (2004) Microphase behaviour of ferrocenyldimethylsilane-b-methylmethacrylate diblock copolymers. Polymer 45:8323–8332

183. (a) Quirk RP, Corona-Galvan S (2001) Controlled anionic synthesis of polyisoprene−poly (2-vinylpyridine) diblock copolymers in hydrocarbon solution. Macromolecules 34:1192–1197; (b) Clegg W, Dunbar L, Horsburgh L, Mulvey RE (1996) Stoichiometric dependence of the long-established reaction of butyllithium with pyridine: a hidden secondary reaction that produces a pyridine adduct of a lithiodihydropyridine. Angew Chem Int Ed 35:753–755

184. Wang X, Winnik MA, Manners I (2005) Synthesis and self-assembly of poly(ferrocenyldimethylsilane-*b*-dimethylaminoethyl methacrylate): toward water-soluble cylinders with an organometallic core. Macromolecules 38:1928–1935

185. Eloi J-C, Rider DA, Wang J-Y, Russell TP, Manners I (2008) Amorphous diblock copolymers with a high organometallic block volume fraction: synthesis, characterization and self-assembly of polystyrene-block-poly(ferrocenylethylmethylsilane) in the bulk state. Macromolecules 41:9474–9479

186. Rider DA, Cavicchi KA, Power-Billard KN, Russell TP, Manners I (2005) Diblock copolymers with amorphous atactic polyferrocenylsilane blocks: synthesis, characterization, and self-assembly of polystyrene-block-poly(ferrocenylethylmethyl silane) in the bulk state. Macromolecules 38:6931–6938

187. (a) Mark JE, Allcock HR, West R (2005) Inorganic polymers, 2nd edn. Oxford University Press, New York; (b) Baumgartner T, Reau R (2006) Organophosphorus π-conjugated materials. Chem Rev 106:4681–4727; (c) Noonan KJT, Gates DP (2007) Inorganic and organometallic polymers. Annu Rep Prog Chem 103:407–427; (d) Tsang CW, Baharloo B, Riendel D, Yam M, Gates DP (2004) Radical copolymerization of a phosphaalkene with styrene: new phosphine-containing macromolecules and their use in polymer-supported catalysis. Angew Chem Int Ed 43:5682–5685; (e) Huynh K, Lough AJ, Manners I (2006) Reactions of P-donor ligands with N-silyl(halogeno)organophosphoranimines: formation of cations with P−P coordination bonds and poly(alkyl/aryl)phosphazenes at ambient temperature. J Am Chem Soc 128:14002–14003; (f) Raab M, Schick G, Fondermann R, Dolg M, Henze W, Weynand U, Gschwind RM, Fischer K, Schimdt M, Niecke E (2006) A pH-functionalized polyphosphazene: a macromolecule with a highly flexible backbone. Angew Chem Int Ed 45:3083–3086; (g) Su HC, Fadhel O, Yang CJ, Cho TY, Fave C, Hissler M, Wu CC, Réau R (2006) Toward functional π-conjugated organophosphorus materials: design of phosphole-based oligomers for electroluminescent devices. J Am Chem Soc 128:983–995; (h) Vanderark LA, Clark TJ, Rivard E, Manners I, Slootweg JC, Lammertsma K (2006) Anionic ring-opening polymerization of a strained phosphirene: a route to polyvinylenephosphines. Chem Commun 31:3332–3333; (i) Naka K, Umeyama T, Nakahashi A, Chujo Y (2007) Synthesis of poly(vinylene−phosphine)s: ring-collapsed radical alternating copolymerization of methyl-substituted cyclooligophosphine with acetylenic compounds. Macromolecules 40:4854–4858; (j) Noonan KJT, Gillon BH, Cappello V, Gates DP (2008) Phosphorus-containing block copolymer templates can control the size and shape of gold nanostructures. J Am Chem Soc 130:12876–12877; (k) Gillon BH, Patrick BO, Gates DP (2008) Macromolecular complexation of poly(methylenephosphine) to gold(I): a facile route to highly metallated polymers. Chem Commun 18:2161–2163

188. Stoeckli-Evans H, Osborne AG, Whiteley RH (1980) Ring-tilted ferrocenophanes. the crystal and molecular structures of (1,1'-ferrocenediyl)diphenylgermane and (1,1'-ferrocenediyl) phenylphosphine. J Organomet Chem 194:91–101

189. (a) Foucher DA, Edwards M, Burrow RA, Lough AJ, Manners I (1994) Ring-opening polymerization of strained, ring-tilted [1]ferrocenophanes with germanium in the bridge: structures of the [1]germaferrocenophane Fe(η^5-C$_5$H$_4$)$_2$GeMe$_2$ and the ferrocenylgermane Fe (η^5-C$_5$H$_4$GeEt$_2$Cl) (η^5-C$_5$H$_5$) organometallics 13:4959–4966; (b) Zürcher S, Gramlich V, Togni A (1999) Germanium-containing ferrocenes and ferrocenophanes. Potential precursors for ring-opening polymerizations and 'germaferrocenes'. Inorg Chim Acta 291:355–364; (c) MacLachlan MJ, Lough AJ, Geiger WE, Manners I (1998) Synthesis, structures, and properties of strained spirocyclic [1]sila- and [1]germaferrocenophanes and tetraferrocenylsilane. Organometallics 17:1873–1883

190. Gallei M, Schmidt BVKJ, Klein R, Rehahn M (2009) Defined poly[styrene-block-(ferrocenylmethylmethacrylate)] diblock copolymers via living anionic polymerization. Macromol Rapid Commun 30:1463–1469

Graft and Comblike Polymers

Andrew Goodwin, Nam-Goo Kang, and Jimmy W. Mays

Abstract The molecular design and construction of comb polymers and graft copolymers through anionic polymerization have made significant strides over the last quarter century. Grafting methods that utilize anionic polymerization techniques, which are reviewed in this chapter, provide strict control over backbone and side chain molecular weights, branch spacing, number of branch points, and branch point functionality in order to synthesize well-defined grafted materials. These carefully controlled synthetic strategies, and recent progress in macromolecular characterization, allow for synthesis of more complex tailored copolymer materials for a variety of applications, including thermoplastic elastomers, high-impact plastics, pressure-sensitive adhesives, additives, and foams. We predict that future work in this area will focus on better understanding the correlation between macromolecular architecture and properties, as well as the synthesis of even more complex architectures incorporating additional (three or more) chemical building blocks into branched copolymer materials.

Keywords Anionic polymerization • Graft copolymers • Molecular architecture • Multigraft copolymers • Thermoplastic elastomer

1 Introduction

Living anionic polymerization provides a versatile method for the synthesis of macromolecules having a low degree of compositional heterogeneity [1, 2]. The term *living* refers to the ability of the growing polymer anions to propagate without termination or chain transfer reactions, which was elegantly demonstrated by Michael Szwarc in 1956 [3–5]. Since Szwarc's discovery, anionic polymerization

A. Goodwin • N.-G. Kang
Department of Chemistry, University of Tennessee, Knoxville, TN 37996, USA
e-mail: agoodwi2@utk.edu; nkang1@utk.edu

J.W. Mays (✉)
Department of Chemistry, University of Tennessee, Knoxville, TN 37996, USA

Chemical Sciences Division, Oak Ridge National Laboratory, Oak Ridge, TN 37831, USA
e-mail: jimmymays@utk.edu

has been exploited to achieve the controlled polymerization of numerous suitable monomers, as well as the synthesis of linear block copolymers (diblock, triblock, etc.) and various types of branched polymers (stars, combs, and dendrimers) [1, 2, 5–10]. Incorporation of two or more monomers to produce linear block and branched copolymer systems, such as miktoarm stars and graft copolymers, has resulted in a broad range of elegant multiphase tailored materials based on self-assembly of incompatible segments [11]. Polymers exhibiting these complicated structures have sparked the interest of theoreticians, physicists, and synthetic chemists alike, not only because of their exploitation for new applications but for being both processable and recyclable [12].

Well-defined branched structures have steadily gained attention because of their unique properties which can be tuned through chemical design; therefore, these materials can address numerous applications ranging from thermoplastic elastomers and high-impact plastics to pressure-sensitive adhesives, additives, and foams [6]. In particular, graft copolymers with desired functional groups, chemical compositions, and a large grafting density have been of interest for numerous biological and nanoscience applications [13–18]. Over the past quarter century, the synthesis of model branched structures has expanded to include not just anionic polymerization but a variety of living/controlled polymerizations, as well as approaches incorporating a combination of techniques. These developments have been promoted by advancements in anionic, cationic, and radical polymerization methods including: ring-opening polymerization (ROP), ring-opening metathesis polymerization (ROMP), atom transfer radical polymerization (ATRP), single electron transfer living radical polymerization (SET-LRP), reversible addition-fragmentation chain transfer (RAFT) polymerization, and nitroxide-mediated polymerization (NMP) [7, 8, 13]. Although anionic polymerization techniques are limited to a rather small range of monomers, this method offers the maximum control over the polymerization with the absence of chain transfer or other termination reactions, whereas controlled radical methods do suffer from termination events resulting in broader polydispersity indices (PDI – the ratio of weight-average to number-average molecular weights), incomplete monomer conversions ($p < 0.8$), and decreased grafting efficiencies ($f < 0.75$) [8, 19–22]. Strong synthetic control is not only significant to synthetic polymer chemists, but the availability of well-defined precisely tailored polymers is critical to polymer physicists and engineers for use in gaining a fundamental understanding of the correlation between polymer architecture, molecular composition, and physical properties in order to tailor polymers for specific applications [13].

2   General Aspects of Graft Copolymer Synthesis

Comb and graft copolymer architectures consist of a linear polymeric backbone having one or more polymer side chains attached by covalent bonds [1, 6]. Comb structures are the simplest form of these branched architectures, where both the
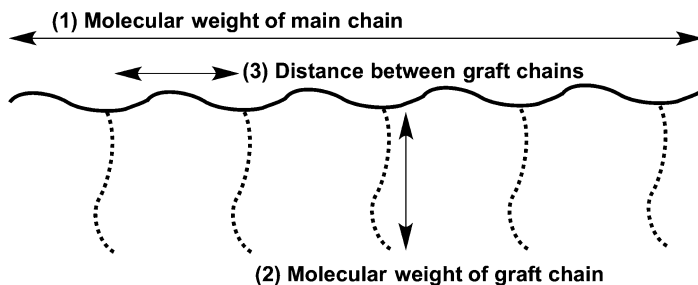
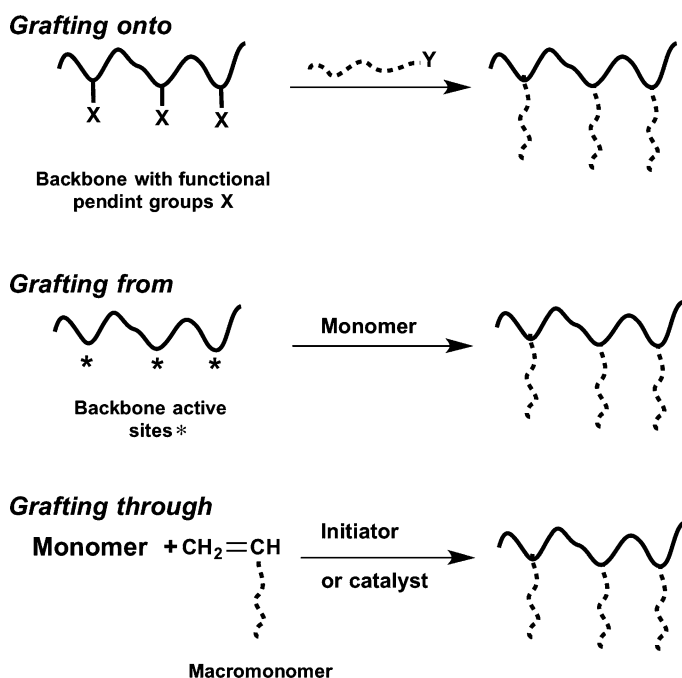**Scheme 1** Three structural factors of graft copolymers [24]

main chain and branches have the same chemical composition. In contrast, graft copolymers are comprised of a backbone and side chains that differ in chemical composition [9, 23]. The structures of both comb and graft copolymers are defined by (1) the molecular weight of the main chain, (2) the molecular weight of the graft chain, and (3) the distance between the graft chains [24] (Scheme 1).

Optimum control of the polymerization provides a basis for the precision synthesis of well-defined graft copolymers. Ideally, these comb and graft copolymer materials would consist of monodisperse side chains bound to a monodisperse main chain, with the number of branches, branch spacing, and branch point functionality all being precisely controlled [25]. This has been most nearly achieved through anionic polymerization, providing an array of branched structures, comprised of a variety of monomers, and exhibiting narrow PDIs with tight control over branch junction functionality and placement, as discussed below. However, most anionic graft copolymer syntheses reported to date, because of their mechanisms, yield a controlled average number of graft branches per molecule and random spacing distribution of graft branches along the backbone [1].

Anionic polymerization is well suited for the synthesis of controlled comb and grafted architectures due to the absence of termination and other transfer reactions that results in an increase of heterogeneity within the polymerization [2, 26–33]. Various other polymerization methods including conventional free radical, living free radical, and cationic polymerizations have been used to synthesize comb and graft polymers, as discussed in detail in prior works [8, 33–35]. It is important to note that the primary advantages of using anionic polymerization approach for the construction of comb and other branched structures include, but not limited to, high grafting efficiency, control of the backbone and side chain molecular weights and polydispersities, and in some cases control of branch point functionality and spacing. However, this methodology is often restricted because of enduring experimental techniques and characterization shortcomings. The following sections provide a general overview of anionic polymerization methods for the synthesis of graft copolymers. It is important to note that the number of branch sites can be

controlled through stoichiometric measures and is randomly distributed along the backbone unless specified.

There are three general methods for the synthesis of grafted polymers (Scheme 2): (a) "grafting onto," where the backbone polymer chain contains heterogeneously placed functional groups, X, that will react with another macromolecule with a chain end antagonistic reactive functional group, Y, a living anion in the case of anionic polymerization; (b) "grafting from," where the active sites are generated along the polymeric backbone, giving way to a pseudo-multifunctional macroinitiator, to be used in the initiation of the second monomer; and (c) "grafting through," in which a living polymer chain is end capped with an unsaturated monomeric head unit, forming a macromonomer that will undergo further homo- or copolymerization during the backbone construction [1]. We will review these three methods for comb polymer and graft copolymer synthesis, citing classic early work and also highlighting recent examples over the past decade. This will be followed by a discussion of the most recent specialized methods for synthesis of combs and graft copolymers, which offer superior control over macromolecular architecture. There is no effort made here to cite all examples, especially those from older literature. Readers are referred to earlier reviews on the subject [1, 2, 8, 10, 24, 36, 37].

Grafting onto

X   X   X

Backbone with functional pendint groups X

Grafting from

*   *   *

Backbone active sites ∗

Monomer

Grafting through

Monomer + CH_2=CH

Initiator

or catalyst

Macromonomer

Scheme 2 Three basic strategies for synthesis of comb polymers and graft copolymers [29]

2.1 Grafting Onto

The grafting onto method involves the nucleophilic attack of the living polymer side chains along the main chain at suitable electrophilic sites, with anhydrides, esters, pyridine, or benzylic halide groups among the most commonly utilized [8, 10, 25]. Branching sites along the backbone can be generated by post-polymerization modification or by copolymerization with monomer(s) bearing the desired functional group. Under appropriate reaction conditions, the backbone and side chains undergo a coupling reaction, covalently bonding the two, resulting in the final comb or graft copolymer architecture. A key advantage to this method is that before the coupling reaction, both the living anionic side chains and polymerized backbone may be isolated, allowing for independent characterization. Measuring the molecular weights of the grafted product and the homo- or copolymer backbone and side chain precursors allows the number of branches and the grafting efficiency to be more accurately determined. Additionally, in cases where both the backbone and side chains are polymerized by anionic methods, the molecular weight, polydispersity, and the chemical composition of each can be controlled, yielding near homogeneous comb- and graft-type products [10].

The most common procedure to synthesize comb or graft structures by a grafting onto approach utilizes chloromethylation of polystyrene (PS) (Scheme 3) [38]. Using this method and living poly(ethylene oxide) (PEO) oxyanions made by anionic polymerization, Rempp and coworkers synthesized PS-g-PEO graft copolymers [39]. However, reaction of many polymeric carbanions with chloromethyl groups results in undesirable metal-halogen exchange, altering the functionality of the branched polymer [40–42]. Conversion of chloromethyl groups of the modified PS into chlorosilyl moieties, established by Rahlwes and coworkers, results in quantitative reaction with poly(isoprenyllithium) to make PS-g-PI, where PI is polyisoprene [43]. Additional PS graft copolymers containing poly (2-vinylpyridine) (P2VP), poly(4-vinylpyridine) (P4VP), poly(methyl methacrylate) (PMMA), and poly(tert-butylmethacrylate) (PtBuMA) side chains were synthesized by partial chloromethylation or bromomethylation of the anionically prepared PS main chain followed by reaction with the living anions of the side chains [39, 44–47]. Hydrolysis of the tert-butyl group of PtBuMA leads to PS-g-PMA, where PMA is poly(methacrylic acid) [48].

**Scheme 3** Chloromethylation of PS [38]
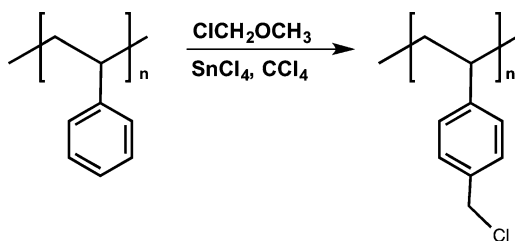
All these linking reactions occur through nucleophilic attack of the living polyanion upon the backbone. A successful reaction often requires reducing the reactivity of the anions to avoid side reactions. Living polycarbanions may be end capped with 1,1-diphenylethylene (DPE) [49] or ethylene oxide for this purpose. DPE end capping of PS anions was employed by Fernyhough et al. [50], followed by reaction with a chloromethylated PS backbone and sulfonation to produce comb-branched sodium poly(styrenesulfonate)s (NaPSS).

Using a modification of this strategy, Wilhelm and coworkers recently reported the synthesis and characterization of well-defined model comb polymers of poly (4-methylstyrene) (P4MS) having very low, but well-controlled, degrees of branching [51]. The backbone and side chains of P4MS were made by living anionic polymerization. The backbone was then treated with N-bromosuccinimide (NBS) to partially brominate the methyl groups of the back-bone polymer, and the living P4MS side chains were end capped with DPE prior to linking. For a degree of bromination, >2 mol% side reactions leading to cross-linking occurred, likely a result of metal-halogen exchange reactions.

Kawahawa et al. reacted a partially brominated polypropylene (PP) backbone, made by a metallocene-catalyzed copolymerization of propylene with 11-bromo-1-undecene, with PSLi to create PP-g-PS [52]. The obtained graft copolymers have potential as compatibilizers for blends of PP and PS. Lin and coworkers prepared an iodinated PBd backbone and demonstrated the synthesis of comb PBd and various graft copolymers by reaction with DPE end-capped living polyanions of various types, including various block copolymers to create complex copolymer architectures including more than one type of grafted side chain [53]. Tang et al. synthesized various comb and graft structures with PI as the backbone by epoxidation of anionically synthesized PI using H_2O_2/HCOOH, followed by reaction with PI, PS, PS-b-PI, and PI-b-PS [54].

More complex architectures have been synthesized by modification of this grafting onto strategy. Graft copolymers with "V-shaped" and "Y-shaped" side chains were synthesized by a combination of controlled radical polymerization and living anionic polymerization (Scheme 4) [55]. The backbone was prepared by TEMPO-mediated copolymerization of styrene and vinylbenzyl chloride. The V-shaped branches were made by reaction of a PS macromonomer, having a DPE end group, with PSLi or PILi, followed by reaction with the benzyl chloride-functionalized PS backbone. The Y-shaped branches were incorporated in a similar manner after further polymerization initiated by the "V-shaped" polyanions.

Borsali and Deffieux and coworkers synthesized PS-b-PI comb copolymers by the selective coupling of PS anions with a poly(chloroethylvinylether) backbone block, followed by reaction of PI anions with chlorobutyl functionality introduced into the second backbone block [56]. The same group synthesized comblike copolymers having randomly distributed PS and PI grafts attached to a poly (chloroethylvinylether) backbone by a grafting onto strategy [57].
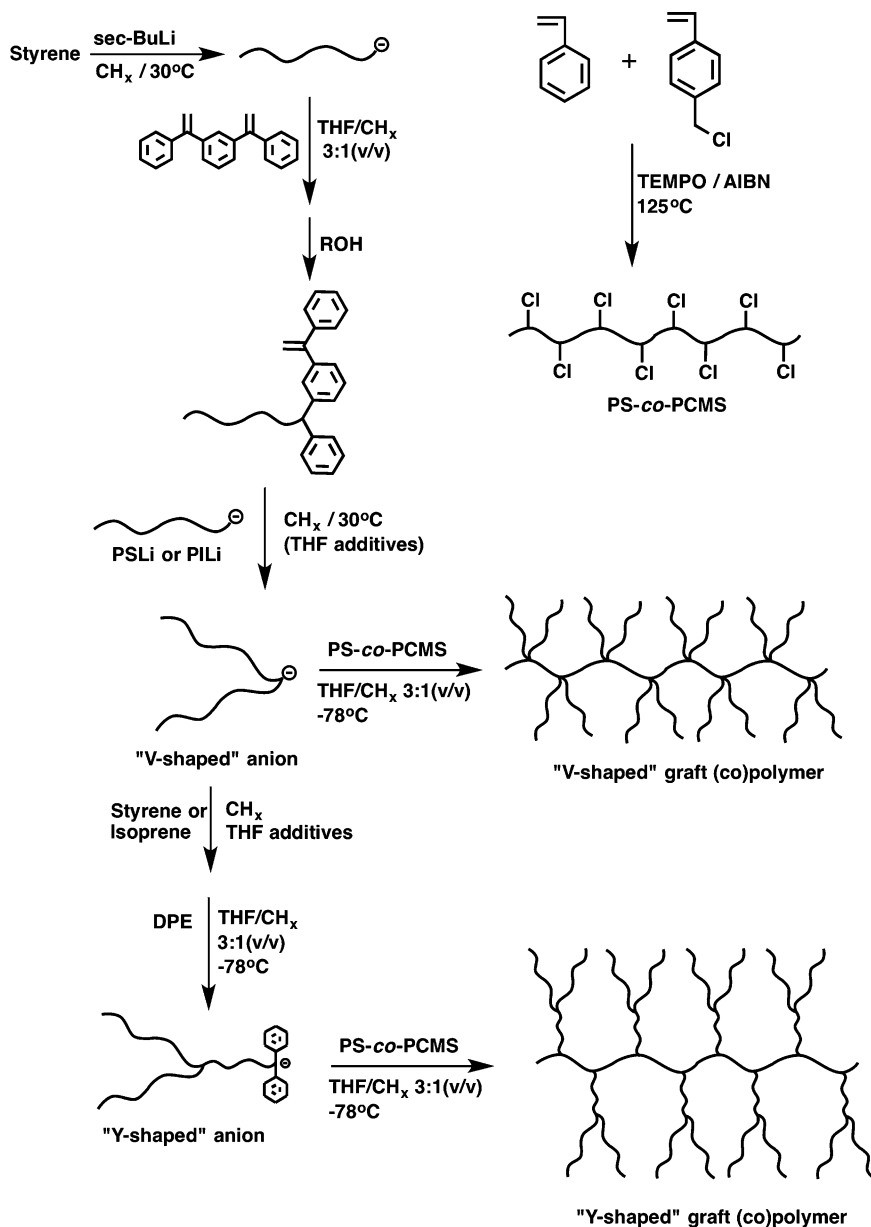
Scheme 4 Synthesis of graft (co)polymers with V- and Y-shaped branches [55]

Hirao et al. prepared poly(m-tert-butyldimethylsiloxymethylstyrene)s with narrow PDIs by living anionic polymerization, transformed them into poly(m-chloromethylstyrene)s by reaction with BCl$_3$, and reacted this functionalized

backbone with living anionic polymers of styrene, isoprene, and 2-vinylpyridine to synthesize comb polymers and graft copolymers having one branch on each repeating unit (macromolecular bottlebrush) [58, 59]. Attempts to produce polymers carrying two branches per repeat unit were carried out using modifications of this approach [59].

Polybutadiene (or alternatively polyisoprene) can be chlorosilylated for preparation of PBd-g-PS graft copolymers and PBd-g-PBd combs, where PBd is polybutadiene [60–62]. The synthesis of PBd-g-PS begins with the anionic polymerization of butadiene in benzene, resulting in a linear PBd backbone with >90 % 1,4-addition. Post-polymerization hydrosilylation using $(CH_3)_2SiHCl$ creates chlorosilane groups at pendant double bonds of the 1,2-polybutadiene units. The reaction with living PS anions or PBd anions gave PBd-g-PS or PBd-g-PBd, respectively, with random branch placement (Scheme 5). Increased functionality of the branching sites can be introduced through the use of multifunctional Si-Cl coupling agents during the hydrosilylation step [10, 63, 64]. The same synthetic scheme produces comb-branched polyethylenes when catalytic hydrogenation is carried out on PBd comb homopolymers [61, 62].

The anionic copolymerization of the difunctional monomer 4-(vinylphenyl)-1-butene with styrene at −40 °C in toluene/THF to yield PS-g-PS, PS-g-PI, and PS-g-PMMA has also been demonstrated [65]. The experimental conditions permit the styrenic double bond to be more reactive, giving a linear backbone with randomly spaced alkene pendant groups. The alkene functionality allows the introduction of Si-Cl groups via hydrosilylation at the olefinic double bonds and when introduced to suitable living polyanions (PS, PI, PMMA) produces well-defined comb polymers or graft copolymers.

This same group described the synthesis of amphiphilic graft copolymers composed of hydrophilic backbones and hydrophobic PS side chains with various acrylic monomers [66, 67]. The synthesis begins with the anionic copolymerization of the desired methacrylic backbone monomer and glycidyl methacrylate (GMA). Living polystyryllithium (PSLi) is then added, which undergoes a rapid reaction between the active PS chain ends and pendant epoxy groups of GMA, forming the desired final graft copolymer composition. The amount of GMA in the copolymer backbone controls the number of available grafting sites along the backbone. After
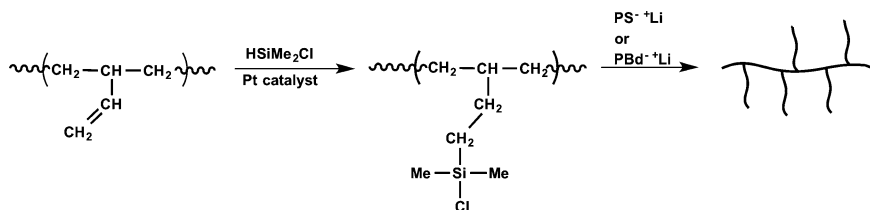
Scheme 5 Hydrosilylation of PBd backbone as a route to grafted polymers and copolymers [60]

reaction with living side chains, all unreacted epoxy groups are neutralized with 1,1-diphenylhexyllithium [66, 67].

A variety of other grafted homopolymers and copolymers have been prepared by reacting living polyanions with suitable functionalized polymer backbones including poly(N-vinylcarbazole) [68], cellulose [69, 70], and maleic anhydride copolymers [71].

Block-graft copolymers are block copolymers having one or more linear block and one or more blocks which are graft copolymers [72]. Poly[styrene-b-(4-vinylphenyl)dimethylvinylsilane)-g-polyisoprene]-b-polystyrene block-graft copolymers were synthesized by Se et al. [73]. (4-Vinylphenyl)dimethylvinylsilane was anionically polymerized using cumylcesium in THF at -78 °C, followed by addition of styrene to create a PVS-b-PS diblock copolymer backbone. Living PI anions were reacted with the PVS functional groups to create the block-graft architecture. Block-graft copolymers having a PS backbone with PI side chains attached to only a portion of the backbone were made by a grafting onto strategy [74]. The backbone block copolymer was made by using TEMPO-mediated radical copolymerization of styrene and vinylbenzyl chloride to grow the first block, followed by addition of styrene to grow the second block. Living PI anions were reacted with benzyl chloride groups in the first block in order to attach the side chains.

2.2   Grafting From

The grafting from method employs creation of active sites along the polymer backbone, which serve to initiate the polymerization of the monomer that will create the side chains. A disadvantage of this approach, as compared to the grafting onto method, is that the side chains cannot usually be isolated and characterized independently, making it more difficult to ascertain side chain length and grafting density. As with the grafting onto strategy, if the backbone and side chains are both made via a controlled/living polymerization process, they can be of narrow PDI. Branch placement is generally random.

Grafting from by anionic polymerization is most often accomplished through acid-base chemistry [25]. Acidic hydrogens on amide, alcohol, or phenol groups can be removed by treatment with tert-BuOK; subsequently, the anionic polymerization of ethylene oxide may then proceed [75]. Acidic hydrogens, adjacent to a carbonyl group, can be removed with lithium diisopropylamide (LDA) and have been shown to be well suited for the polymerization of methacrylate monomers [76].

Metallation by organometallic compounds such as s-BuLi, in the presence of a strong chelating agent, i.e., N,N,N'N'-tetramethylethylenediamine (TMEDA), has been shown to create main chain active sites of allylic, benzylic, and aromatic C-H bonds (Scheme 6). Several groups demonstrated this technique by producing various poly(diene-g-styrene)s [77–82]. Hadjichristidis and Roovers synthesized
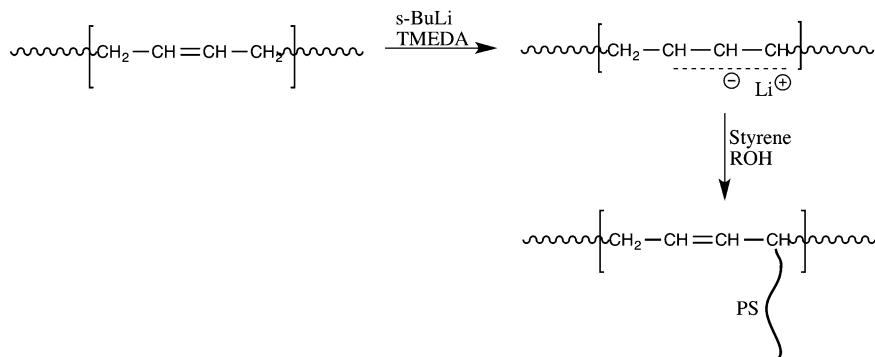
Scheme 6 Metallation of a polydiene backbone, followed by monomer addition to create a graft copolymer by the "grafting from" mechanism [1]
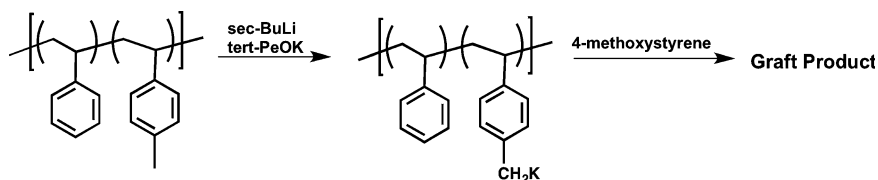
Scheme 7 Synthesis of graft copolymers through metallation of poly(styrene-co-methylstyrene) [85]

model poly(isoprene-g-styrene) via lithiation of PI in the presence of TMEDA and improved this grafting chemistry by performing all manipulations under high vacuum in sealed vessels followed by fractionation to isolate the desired products [78].

An important advancement in the metallation technique by the grafting from approach was the introduction of metallation via a superbase. Lochmann et al. reported the one-pot metallation of a parent PS backbone by a superbase, prepared from 3-lithiomethylheptane and excess potassium alkoxide, followed by the reaction with an electrophile to produce randomly substituted polystyrene containing a variety of side chain pendant groups [83]. Using a less electronegative potassium counterion enhances the reactivity by promoting the favorable association of Li and O, generating potassium-contained substituents along the PS backbone. The superbase reagent provides for rapid deprotonation, at room temperature in cyclohexane, of modestly acidic substances, and the high reactivity of the organopotassium sites is capable of reacting with a large spectrum of electrophiles [83–85]. Therefore, graft copolymers may be synthesized by polymerization or copolymerization of a suitable monomer (e.g., 4-methylstyrene), metallation, and addition of an anionically polymerizable monomer (Scheme 7) [84, 85].

Employing this general strategy, PP-g-PS was recently synthesized by Li et al. [86]. They used Ziegler-Natta copolymerization of propylene and p-allyltoluene to prepare the backbone, followed by metallation of the benzylic

sites using n-BuLi/tert-BuOK and addition of styrene monomer. Polypropylene-g-poly(ethylene-co-1-butene) with a well-defined long-chain branched structure was prepared by a similar strategy (metallocene-initiated copolymerization of propylene and 4-(3-butenyl)toluene, followed by metallation of benzylic sites using sec-BuLi/TMEDA, addition of butadiene monomer to grow PBd side chain, and hydrogenation) (Scheme 8) [87].

Se et al. [88, 89] prepared di- and triblock copolymers of styrene and p-tert-butoxystyrene to prepare a polymer backbone, followed by acid hydrolysis to convert the butoxy groups to hydroxyl groups and activation using cumyl potassium or DPE potassium, and the subsequent addition of ethylene oxide yields the block-graft copolymers. Pispas and coworkers used anionic copolymerization of styrene and p-tert-butoxystyrene, which when deprotected was used to polymerize ethylene oxide in a ring-opening anionic polymerization using phosphazene base (t-BuP$_4$) (Scheme 9) [90]. The same team synthesized thermo-responsive brush copolymers with poly(propylene oxide-r-ethylene oxide) side chains via the same strategy employing a metal-free anionic polymerization grafting from strategy [91].

In another approach, PMMA-g-poly(β-butyrolactone) copolymers have been synthesized [92]. This method involves treating the PMMA backbone with 18-crown-6 and potassium hydroxide to create the macroinitiator. This reaction was determined to have a high grafting efficiency with facile control of the density of grafting sites. Graft copolymers of PMMA-g-polyamide 6 were synthesized by using N-carbamated caprolactam pendants as macroactivators and sodium caprolactamate as a catalyst for the anionic polymerization of caprolactam [93]. This group used a similar approach for synthesis of various graft copolymers with "rigid" backbones via anionic ring-opening polymerization of caprolactam (Scheme 10) [94, 95].
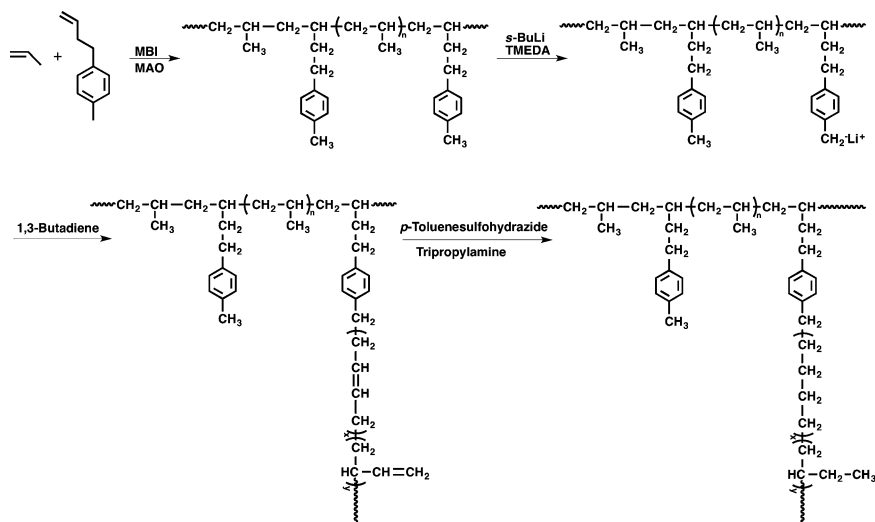
Scheme 8 Synthesis of PP-g-EBR copolymers [87]
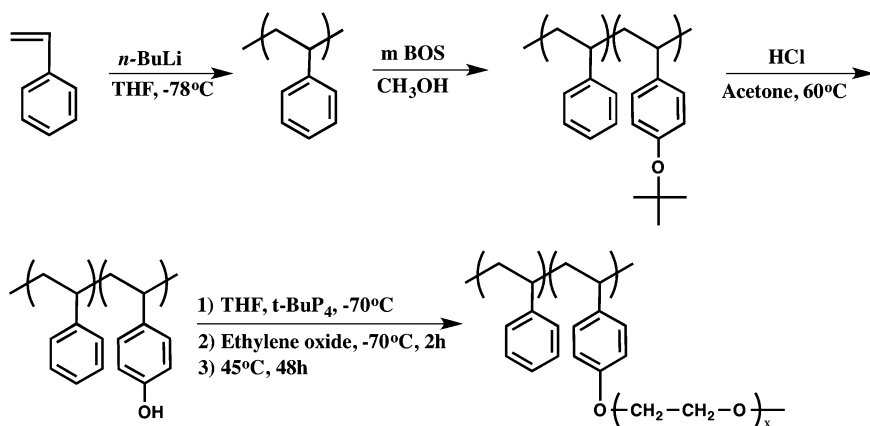
Scheme 9 Synthetic scheme for the preparation of polystyrene-b-poly(p-hydroxystyrene-g-ethylene oxide) [90]
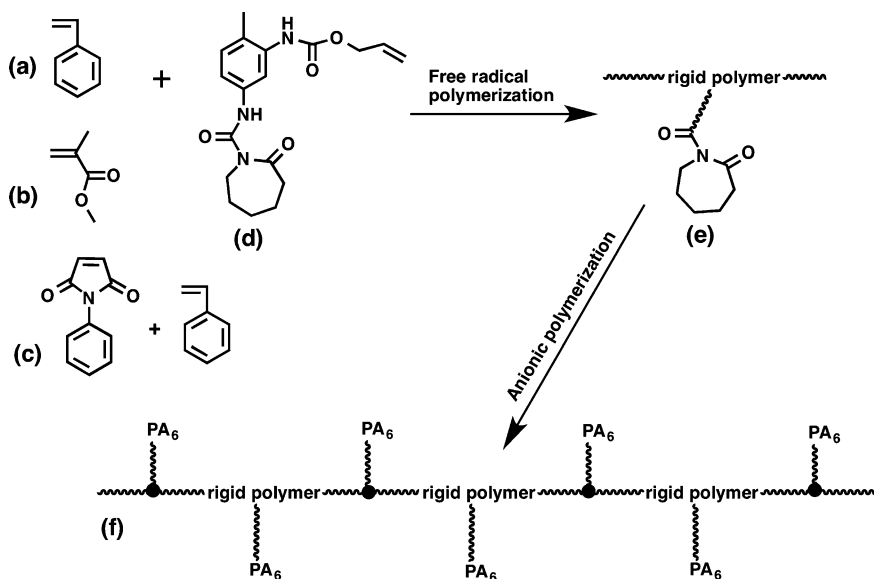
Scheme 10 Mechanism of graft copolymers of (**a**) St, (**b**) MMA, (**c**) NPMI, (**d**) ACCL, (**e**) macroactivator, and (**f**) graft copolymer [94]

Graft copolymers having aromatic polyimide backbones and caprolactam side chains were synthesized by anionic polymerization of caprolactam initiated by imide rings bearing several suitable functional groups [96]. PS-g-polyamide 6 has been synthesized by anionic polymerization of caprolactam from an isocyanate-

bearing PS backbone [97]. Amphiphilic polycaprolactam-g-PMMA and polycaprolactam-g-poly(L-lysine) copolymers have been synthesized by metallation of a PCL backbone using LDA/THF, followed by addition of suitable monomers [98, 99]. These degradable copolymers are of interest in biomedical and pharmaceutical applications. Degradable amphiphilic polycaprolactam-g-P4VP and polycaprolactam-g-poly(dimethylaminoethyl methacrylate) copolymers have been reported by the same group [100]. More recently, Schlaad reported the anionic graft copolymerization of ethylene oxide directly from poly(N-isopropyl acrylamide) via activation of the PNIPAM using phosphazene base [101].

The grafting from strategy via living anionic synthetic procedures has two major disadvantages: (1) knowledge of the precursor polymer chain is generally limited, as noted above, to the backbone, with the isolation and characterization of the branches generally involving selective chemical decomposition, and (2) ionic copolymerization can lead to poor solubility, which results in poor control of the polymerization [9, 10, 25, 65]. However, this methodology is considered particularly attractive for use in controlled radical polymerization techniques since there is a low concentration of instantaneous propagating species present, limiting coupling and other termination events, and the continuous growth of side chains effectively relieves steric effects [13].

2.3 Grafting Through (The Conventional Macromonomer Approach)

The grafting through method relies on the formation and polymerization of macromonomers, which are oligo- or polymeric chains characterized by a polymerizable head group. Following this methodology, the side chains are first covalently bonded to a polymerizable moiety, forming the macromonomer. When homopolymerized, the macromonomer results in molecular brushes, but it is more commonly copolymerized to produce comb polymers and graft copolymers. The macromonomer approach requires consideration of important synthetic factors but offers access to reasonably well-defined grafted architectures, having well-defined side chains and backbones, more easily than other grafting methods based upon anionic polymerization. The most important consideration is the reactivity disparity of the macromonomer (M_1) and comonomer (M_2), typically expressed by reactivity ratios r_1 and r_2, described by the Mayo-Lewis copolymerization equation [102]:

$$\mathrm{d}[M_2]/\mathrm{d}[M_1] \; = \; (1 + r_2[M_2]/[M_1]) \, / \, (1 + r_1[M_1]/[M_2]). \tag{1}$$

Generally, ionic mechanisms exhibit a greater discrepancy between r_1 and r_2, as compared to free radical copolymerization, resulting in limited control of branch

placement along the backbone. Additional factors of inherent incompatibility between the macromonomer and growing polymer chains, fluctuations in concentrations of the two compounds, and phase separation due to the formation of the copolymer can lead to greater compositional and molecular weight heterogeneity of the product [9, 10, 25].

The formation of PS and PMMA macromonomers has been described in numerous publications [103–108]. An example of the PS macromonomer synthesis begins with the homopolymerization of styrene initiated by sec-BuLi. The living polymer is then end capped with ethylene oxide to increase chain end flexibility and reactivity before reacting with methacryloyl chloride to yield a methacrylate polymerizable end group or benzyl bromide (or chloride) for a styrenic polymerizable end group. Living PS has also been end capped with 1,1-dipheylethylene and subsequently reacted with vinyl benzyl bromide (or chloride). Similarly, PMMA macromonomers were synthesized, end capped, and copolymerized with MMA or styrene to yield PMMA-g-PMMA or PS-g-PMMA, respectively.

More recently, an in situ approach has been used to synthesize comb and grafted copolymers and does not require the isolation of the macromonomer as a purification step. The synthesis of the macromonomer involves the slow addition of living polymer to 4-(chlorodimethylsilyl)styrene (CDMSS) (Scheme 11) [109, 110]. This
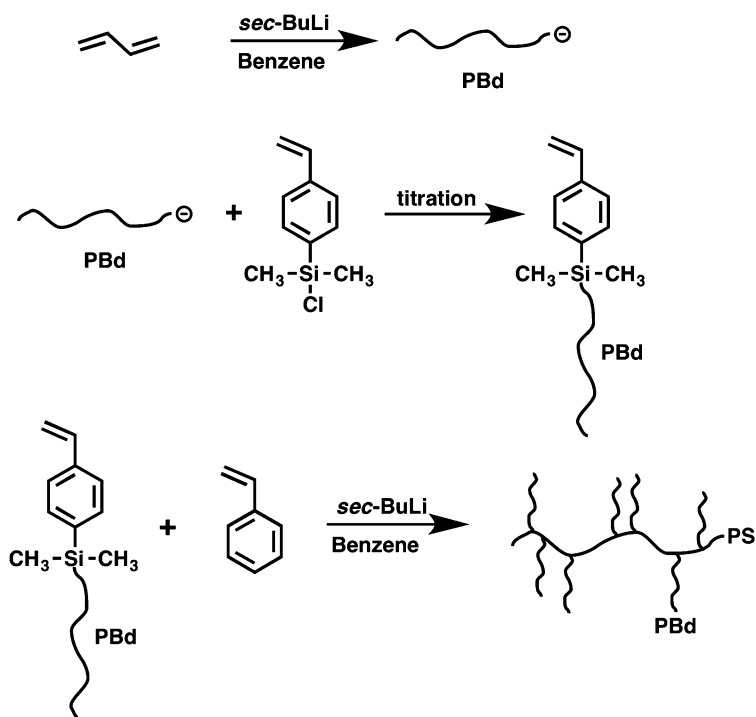
Scheme 11 In situ preparation and copolymerization of macromonomer [110]

is made possible because of the selectivity of the substitution reaction between the organolithium and the silyl chloride rather than with the styrenic double bond. End capping the living polymer with a few butadiene units before introduction of CDMSS provides greater control as a result of the selectivity for the Si-Cl over the double bond being PBdLi > PILi > PSLi [108]. This method also allows for the incorporation of multifunctional branch points via the copolymerization of "double-tailed" and "triple-tailed" macromonomers, as shown by Hadjichristidis and coworkers [111, 112].

The use of this in situ macromonomer approach has been extended by Hadjichristidis and coworkers to the synthesis of a host of complex architecture grafted polymer and copolymers (Scheme 12), including comb, star-comb, comb-on-comb, and double-graft architectures (diblock copolymers where each block is a graft copolymer) [113–115].

Foster and coworkers have very recently introduced a new method combining the macromonomer approach and click chemistry for the synthesis of functionalized comb polystyrenes (Scheme 13) [116]. ω-(p-Vinylbenzyl)PS macromere was synthesized by anionic polymerization of styrene, followed by termination with 4-vinylbenzyl chloride. An unsaturated anionic initiator, 4-pentenyllithium, was used to make α-4-pentenyl-ω-(p-vinylbenzyl)PS macromonomer. These two macromonomers were then anionically copolymerized, with the titration of excess sec-BuLi initiator to remove impurities just prior to polymerization, to afford a polymer backbone where the pendant vinyl end groups could be functionalized in a variety of ways using "click chemistry."
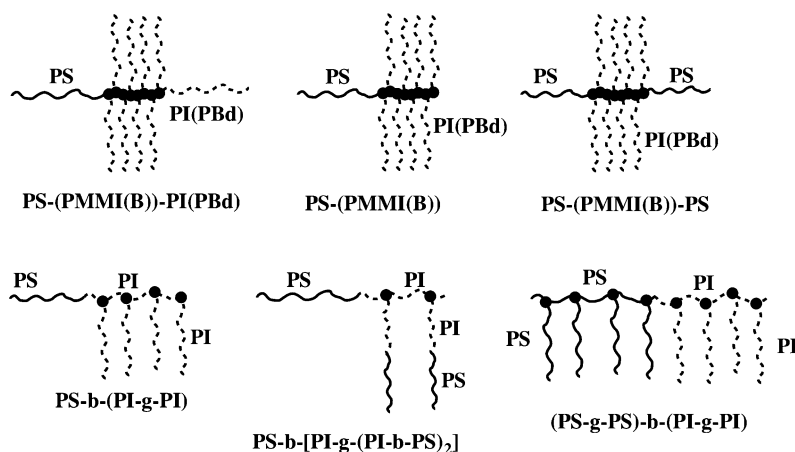
Scheme 12 Complex comblike block copolymer architectures [115]
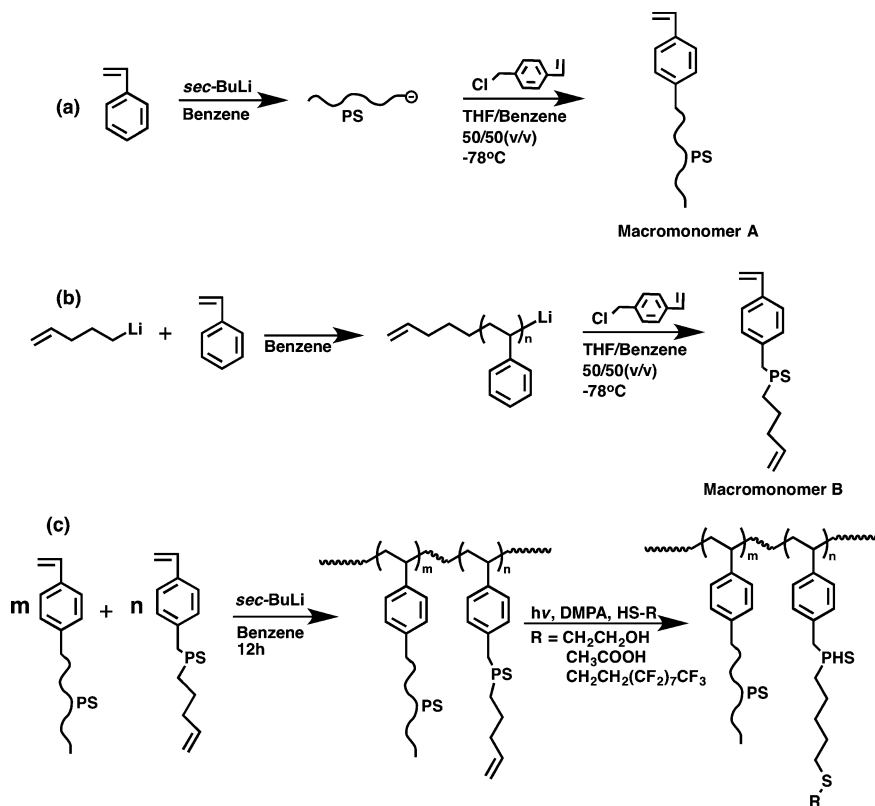
Scheme 13 Mechanism for the synthesis of functionalized comb polystyrenes: (**a**) macromonomer A, (**b**) macromonomer B, and (**c**) synthesis of comb-vinyl copolymer by thiol-ene "click" chemistry [116]

3 More Advanced Methods to Achieve Graft Copolymers with Superior Control of Macromolecular Architecture

The methods previously discussed can, under appropriate conditions, allow for control of side chain length and backbone length. However, they provide only statistical control over the number of branch points per molecule and the spacing of the branch points. Thus, much research has been conducted over the past two decades in order to better control these parameters.

Progress in living anionic polymer synthetic techniques has prompted the creation of many novel branched architectures including bottlebrush, π-shaped, H-shaped, super-H-shaped, and pom-pom-shaped polymers and structures incorporating dendritic motifs [20, 117–125]. The synthesis of graft copolymer systems containing regular branch point spacing has also been achieved primarily through the use of chlorosilane-coupling chemistry, originally demonstrated in the synthesis

Scheme 14 Regular
multigraft poly(isoprene-g-
styrene) architectures: (**a**) A
(BA)$_N$ "comb," (**b**) A
(B$_2$A)$_N$ "centipede," and (**c**)
A(B$_4$A)$_N$ "barbwire" [127]
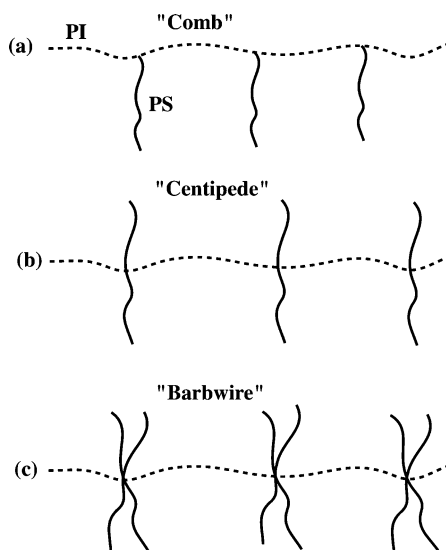
of a simple graft PI-g-PS in 1990 [126]. This material was composed of a polyiso-
prene (PI) backbone with a single centrally located polystyrene (PS) side chain; the
simple graft is equivalent to an A2B miktoarm star. This chemistry has evolved to
allow the synthesis of multigraft copolymers having both regular branch point
spacing and tunable branch point functionality including tri-, tetra-, and
hexafunctional branch points, termed regular comb, centipede, and barbwire archi-
tectures, respectively (Scheme 14), as discussed in the next section [127].

In each case, high molecular weights and a large number of branch points (>10)
have been obtained. PI-g-PS materials have been extensively studied and have
shown noteworthy superelastic characteristics of extremely high elongation at
break and very low hysteresis, with both tensile strength and strain at break
increasing with the number of branch points and branch point functionality
[128]. More recently, a new class of regularly branched and low polydispersity
comb and graft copolymers has been demonstrated and termed "exact" graft
copolymers [129]. This novel technique introduces new and unprecedented control
of branch point placement, but for practical reasons may be limited to low numbers
of branch points (≤5) and moderate molecular weights [9, 130, 131].

3.1 The Chlorosilane Macromonomer Polycondensation Approach

An alternative macromonomer strategy based on step-growth polymerization has
been used to make multigraft copolymers with regularly spaced tri-, tetra-, and
hexafunctional branch points. As noted above, these materials have been termed

"regular combs," "centipedes," and "barbwire" polymers, respectively, and have been studied in detail for graft copolymers containing styrene and isoprene [127, 132]. The construction of each multibranched architecture incorporates the same general methodology of combining living anionic and condensation polymerizations, with appropriate choice of the chlorosilane linking agent. In the case of the tetrafunctional branch points (centipedes), living PSLi is slowly added to SiCl$_4$ ("vacuum titration") to obtain a coupled PS product with two terminal Si-Cl bonds in the middle of the chain. This is then reacted with a small excess of difunctional PI, initiated with a difunctional lithium initiator (DLI) derived from sec-BuLi and (1,3-phenylene)bis(3-methyl-1-phenylpentylidene)dilithium, giving well-defined graft copolymers with a PI backbone and PS branches (Scheme 15). Notice that the last step in the synthesis is a polycondensation reaction yielding a PDI of 2 and allowing the number of branch points to be controlled through stoichiometry.

Correspondingly, tri- or hexa-chlorosilanes are used for the synthesis of comb and barbwire architectures. The hexafunctional multigraft (barbwire) synthesis also requires the strategy of titrating in living PS arms in order to have stoichiometric equivalents of silane and titrant to avoid the substitution of the third Cl at either end of the hexafunctional chlorosilane. In contrast, the synthesis of trifunctional multigrafts requires no titration and is achieved by reacting living PS with an excess of methyltrichlorosilane, followed by removal of excess chlorosilane and addition of living PI having anions at both ends. This method, although painstaking due to the titration step and removal of the excess MeSiCl$_3$ on the high-vacuum line, yields regular branch point spacing, controlled branch point functionality, and is capable of extremely high molecular weights for both homopolymer and copolymer versions [127, 132]. Additionally, narrow molecular weight distribution fractions having high levels of architectural homogeneity were obtained via solvent/nonsolvent fractionation [127, 132].
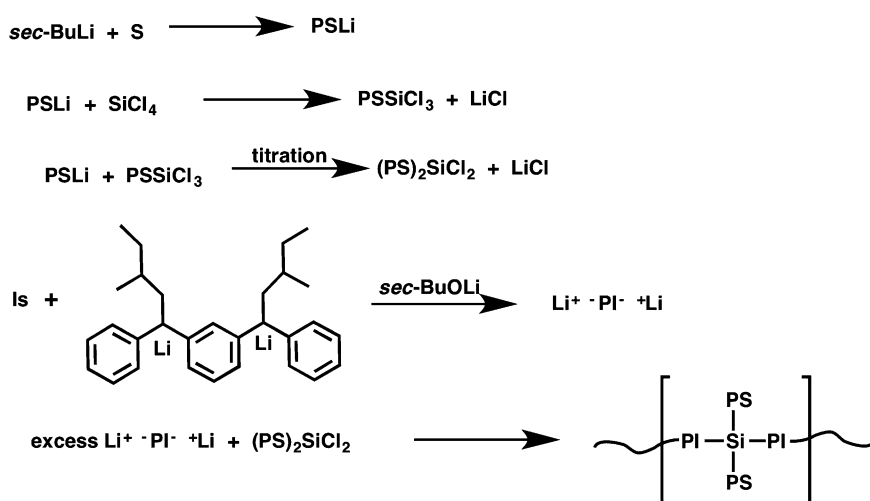
Scheme 15 Synthesis of PI-g-PS centipedes [132]

Plamper et al. recently reported alternate synthetic strategies leading to similar macromolecular architectures, which they called the "pearl necklace architecture" or "threaded star-shaped copolymers" [133]. A polycondensation reaction of PEO macromonomers with partially protected dipentaerythritol leads to a multiblock of PEO. Then the protected hydroxyl groups of dipentaerythritol were removed, allowing attachment of poly(dimethylaminoethyl methacrylate) chains.

3.2 Exact Graft Copolymers

The synthesis of "exact" graft copolymers has been achieved utilizing the macromonomer approach by incorporating moieties based on 1,1-diphenylethylene (DPE). Since DPE shows no self-addition behavior, the dependence on reactivity ratios of the macromonomer and comonomer can be avoided. This technique was first used to synthesize miktoarm stars [134, 135], but its use has now expanded to more complex branched architectures.

Comb, two and three branch symmetric, and asymmetric structures were first shown by Hadjichristidis and coworkers, incorporating 1,4-bis(phenylethenyl) benzene as a macromonomer [136]. This chemistry evolved to produce more elaborate branched structures through the use of 4-(dichloromethylsilyl) diphenylethylene (DCMSPDE). Exact graft copolymer synthesis is highlighted by incorporating two chlorosilane linking molecules, promoting an exchange reaction with living anionic chain ends on a non-homopolymerizable double bond of DPE (Scheme 16). Again, since the substitution reaction is much faster, this allows for
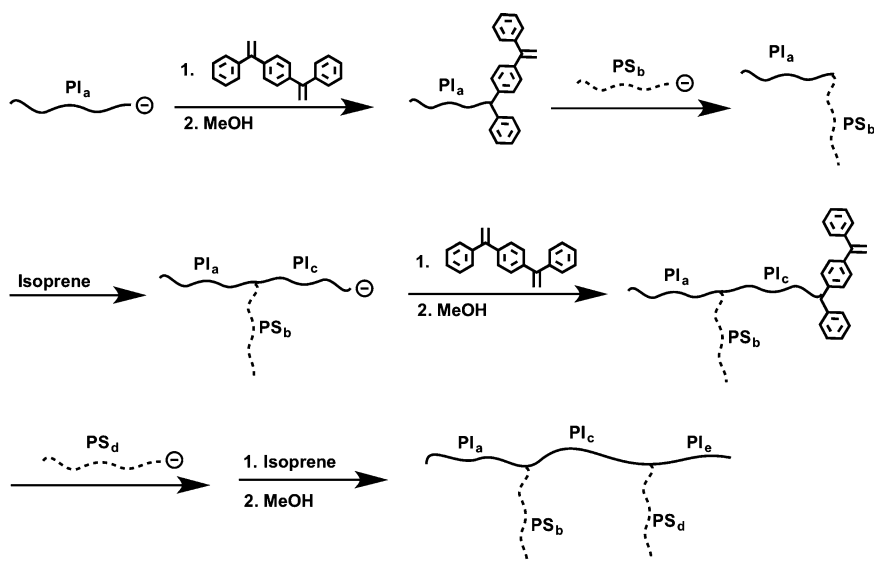
Scheme 16 Synthesis of exact graft copolymer composed of polystyrene and polyisoprene [130]

complete addition of the living polymer chains without initiation and propagation of the sterically hindered vinyl group. Stoichiometry is crucial in order to obtain complete initiation of the DCMSPDE double bond, without leading to linear side products because of excess sec-BuLi [109, 129, 137].

A second exact grafting strategy demonstrated by Hirao and coworkers involves three reaction steps using a double-DPE macromolecule: (1) a transformation reaction of the α-terminal *tert*-butyldimethylsilyloxypropyl (SiOP) group into bromopropyl function via deprotection of the SiOP group followed by bromination, (2) a linking reaction of α-SiOP-ω-DPE-functionalized living PS with α-terminal bromopropyl-functionalized PS to prepare an α-SiOP-in-chain-DPE-functionalized PS backbone chain with the introduction of a DPE moiety between the two PS chains, and (3) an addition reaction of PSLi with the DPE moiety to introduce a PS graft chain (Scheme 17) [130].
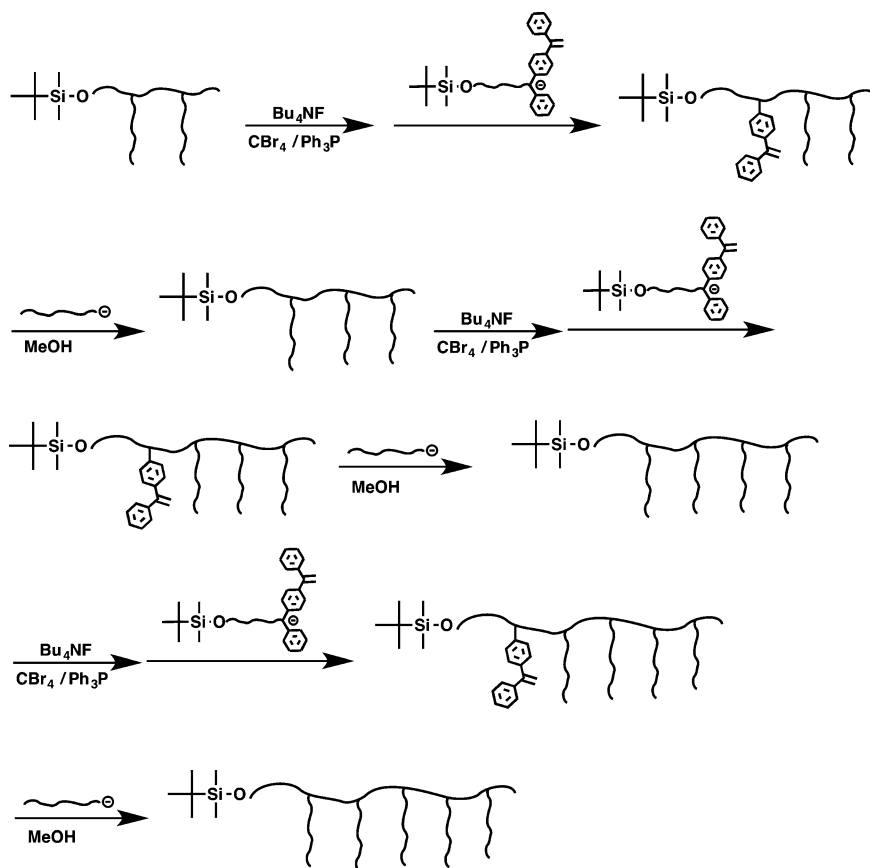
Scheme 17 Successive synthesis of exact graft PS with three, four, and five PS branches [130]
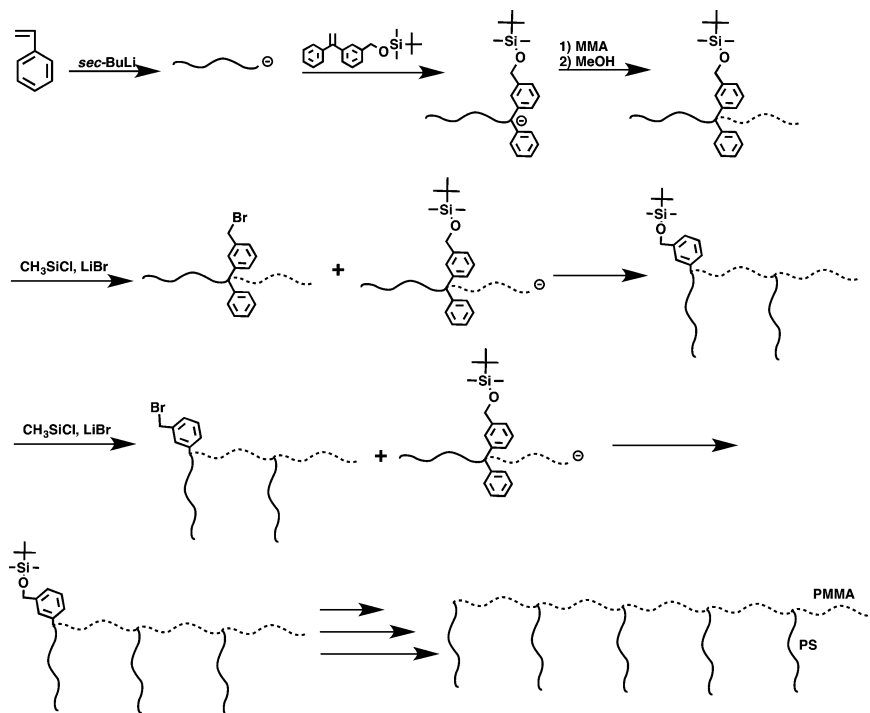
Scheme 18 Synthesis of a series of exact graft copolymers containing PMMA and PS [131]

This general strategy was also used in the synthesis of exact graft copolymers having a PMMA backbone and precisely located PS branches (Scheme 18) [131]. This approach was extended to other polymer combinations including P2VP-g-PS, PtBMA-g-PS, and poly(ferrocenylmethyl methacrylate)-g-PS [138]. In these cases, the maximum number of branches attached was five, although in principle more can be achieved if adequate care is taken.

Most recently, Hirao and coworkers have reported the synthesis of exact (co) polymers having six PS, PI, or PMMA grafts attached to a PS backbone [139]. The PS backbone, precisely controlled in terms of DPE placement, number of DPE groups, and molecular weight, was prepared by combining the iterative synthetic sequence with the subsequent coupling reaction and then reacted with the living anions (Scheme 19). In addition, a new double-tailed exact graft PS having 12 PS side chains (two per branch point) was synthesized by repeating the addition reaction of living PS to the backbone PS [139].
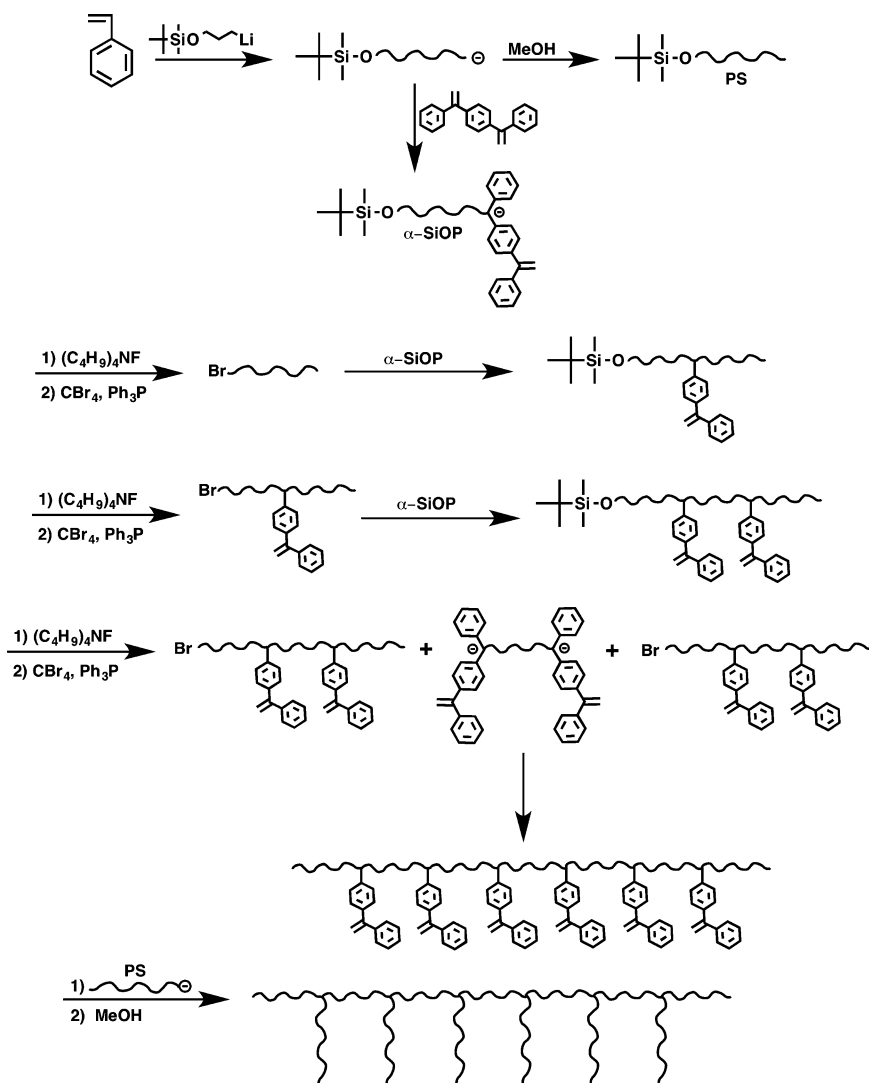
Scheme 19 Iterative method allowing exact graft copolymer synthesis up to six branch points [139]

4 Characterization

4.1 Molecular Weight Determination of Graft Copolymers

It was previously noted that the rigorous molecular characterization of comb, grafts, and other branched polymers and copolymers can be as arduous as their synthesis.

When possible, it is highly desirable to obtain molecular weight (MW) and PDI data on the side chains and backbone prior to linking. Both the "grafting to" and "grafting through" methods allow the backbone and side chains to be characterized independently, as linear constituents. Characterization of the final products (branched polymers and copolymers) is more complicated due to the increase in heterogeneity and their more complex architectures. A prime example of instrument limitations is demonstrated by size exclusion chromatography (SEC). Characterization via SEC is the most commonly utilized approach for MW and PDI determination, but this method is incapable of separating polymers with nearly identical hydrodynamic volumes [140]. Such a restriction is particularly crippling in characterization of model complex branched polymers and copolymers where components of different branching levels, molecular weights, and compositions may all co-elute. Furthermore, SEC suffers from large band broadening effects, which make it even more difficult to resolve the various species present in complex branched polymers and copolymers.

While synthetic polymer chemists continue to develop better synthetic methodologies that reduce structural heterogeneity, finding alternatives to SEC for the rigorous molecular weight characterization of highly branched and other nonlinear structures is a necessity. Where structural perfection is currently not possible, characterization of imperfect structures can be just as beneficial [141]. In the last 15 years, this has been made feasible with the introduction of temperature gradient interaction chromatography (TGIC) and first demonstrated by Chang et al. [142]. TGIC relies on the enthalpic interactions between the solute molecules and the stationary phase; these interactions can allow separation based on molecular weight and not hydrodynamic volume. Strict control of the solvent and temperature leads to superior resolution of branched polymers when compared to SEC with far reduced band broadening [141, 143, 144].

A recent review by Hutchings has extensively discussed the advantages and limitations of TGIC as it pertains to numerous complex branched architectures including comb, H-shaped, and particular emphasis on dendritically branched polymers [141]. In all cases, the use of TGIC was able to show that impurities were present after fractionation, whereas traditional SEC analysis showed only a narrow, single peak. More specifically, in the case of H-shaped polymers, it has been shown that TGIC is capable of removing uncertainty and allowing for validation of current rheological models for branched polymers [145–147]. TGIC will continue its advancement and become a more universal characterization technique as a result of its superior resolution and ability to identify low levels of heterogeneity.

4.2 Morphology and Mechanical Properties of Graft Copolymers

Block copolymers undergo phase separation and self-organization on different length scales, ranging from nanometers to hundreds of nanometers as a result of

molecular weight, block composition, the solvent for film casting, annealing, etc. [6]. For linear diblock and triblock copolymers, the morphology (spheres, cylinders, bicontinuous gyroid, and lamellae) is directly linked to component volume fractions. However, until about 20 years ago, very little was known about how long-chain branching impacts morphology and mechanical properties of block copolymers.

Milner developed a self-consistent mean field model for effects of architectural and conformational asymmetry on "opposing polymer brushes," which approximate miktoarm star copolymers [148]. Milner predicted that changing architecture from an AB diblock to A_2B, A_3B, and A_4B miktoarm stars, while keeping composition constant, would systematically alter the morphology of these materials. Thus, Milner predicted that macromolecular architecture could be used to decouple morphology of copolymers from the hitherto observed strict dependence on composition [148]. This prediction was subsequently verified [149–151].

In order to apply Milner's theory to more complex multigraft copolymers, the constituting block copolymer hypothesis (Scheme 20) is employed. This concept is based on the idea that the overall phase behavior of a grafted copolymer is governed by the behavior of smaller copolymer units associated at each junction point [123, 152–154]. Existing theories of miktoarm star and asymmetric linear diblocks can thus be used to predict the behavior of the overall graft copolymers based upon the local resemblance of multigraft copolymers to miktoarm star copolymers [148, 155–157].

Multigraft systems containing increased branch points per molecule have been shown to suppress long-range ordering (Fig. 1) [128, 159]. Transmission electron microscopy (TEM) images can only provide hints to the microphase-separated
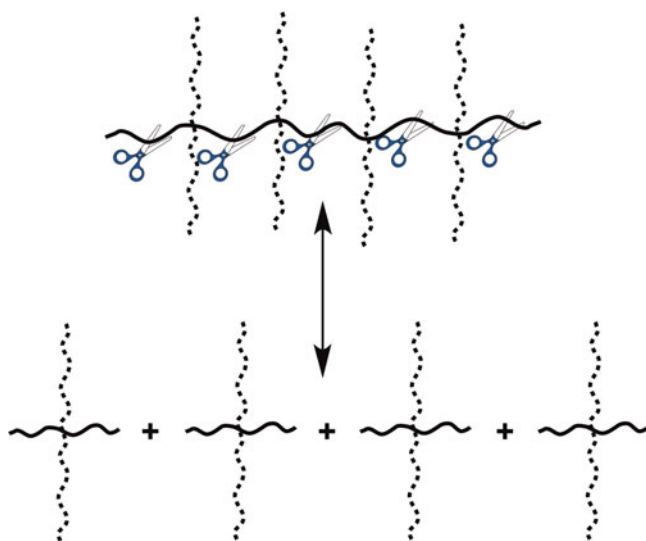
Scheme 20 Constituting miktoarm star concept [159]
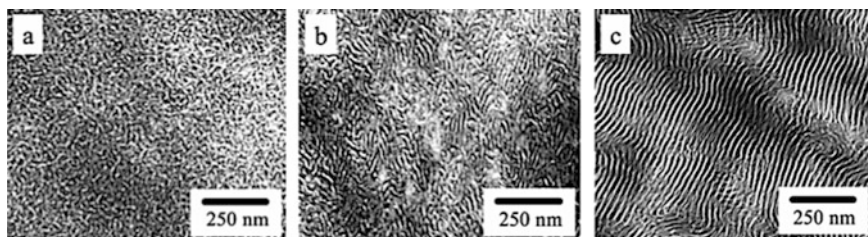
Fig. 1 TEM images of hexafunctional multigraft copolymers containing 21 % PS with (**a**) 5.3, (**b**) 3.6, and (**c**) 2.7 junctions per molecule. Additionally, SAXS confirmed (**a**) microphase-separated and (**b, c**) lamellae morphologies [128] (Reprinted with permission from Macromolecules (2006) American Chemical Society)

domains for these materials [127]. Small-angle X-ray scattering (SAXS) data supply confirmation of morphology and allow for the calculation of periodicity of microphase separation from peak position (q) by application of the Bragg equation [158]. Thus, when TEM observations are inconclusive because the material is disrupted by branching or by alternative chemical/architectural means, SAXS can yield well-reasoned morphological interpretations.

Uniformity of branch placement has been demonstrated to control the morphology of the molecule at large through the preferred behavior at the smaller subunits of the junction points. Beyer et al. showed that the domain shape of PI-*g*-PS with tri- and tetrafunctional branch points can be correctly predicted, with the lamellar morphology being the only to give long-range ordering [159]. A second finding demonstrated in this work was that branch point placement was more significant than the polydispersities of each sample [159]. Supporting these results, graft copolymers with random tri- and tetrafunctional branch junction placement displayed characteristic microphase separation but no long-range ordering as a consequence of different morphologies being preferred throughout the polymer chain [154].

Multigraft copolymers also exhibit unique mechanical properties emphasizing the influence of molecular architecture. Again, well-controlled PI-*g*-PS composed of regularly spaced grafted structure varying in the number of branch junctions per molecule and branch point functionality (synthesized anionically under high-vacuum conditions) was investigated for their stress-strain behavior (Fig. 2) [128, 160]. Analysis showed that the strain at break far exceeded that of their linear counterparts (Styroflex and Kraton) [161]. Both strain at break and tensile strength showed a linear dependence on the number of branch points. Hysteresis upon stretching was extremely small, and the modulus could be tuned at a given composition by varying branch point functionality [162]. PI-*g*-PS structures composed of random branch points yielded similar results, demonstrating the superior properties of multigraft copolymers as a result of their molecular architecture [128, 162, 163]. As the synthesis and characterization of graft copolymer and other complex architectures continue to progress, these materials can continue to be tailored to
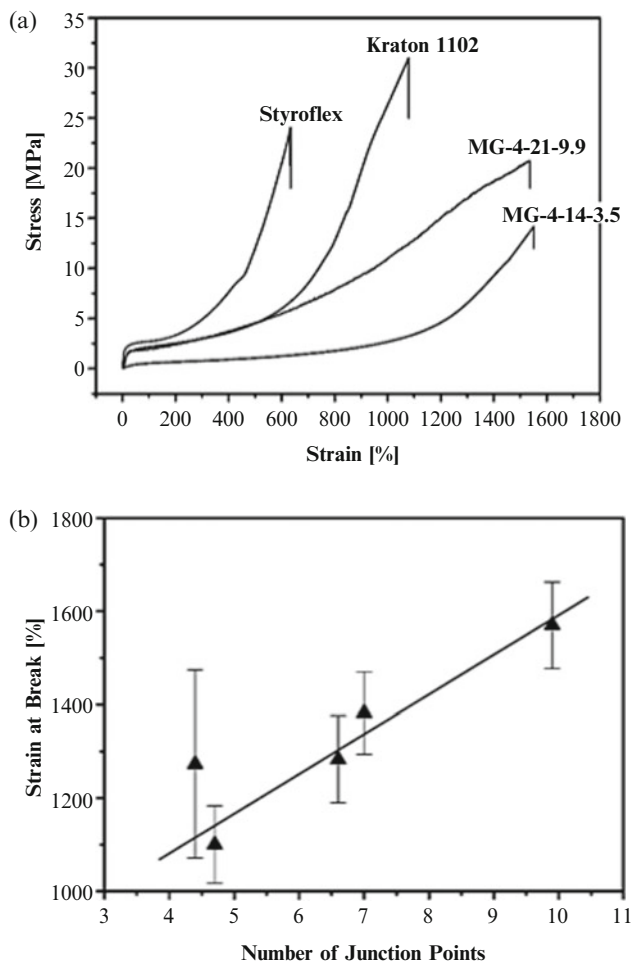
Fig. 2 (**a**) Stress-strain behavior for Styroflex, Kraton, and two tetrafunctional multigraft copolymers (PI-g-PS). (**b**) Influence of junction point functionality on strain at break [128] (Reprinted with permission from Macromolecules (2006) American Chemical Society)

optimize physical properties and exploit control of macromolecular architecture for new and existing applications.

5   Conclusions and Future Prospects

Living anionic polymerization is an extremely valuable and versatile technique for the synthesis of well-defined comb polymers and graft copolymers, both alone and in combination with other living polymerization techniques. Over the past two

decades, enormous advances in polymerization methodologies have led to comb and graft materials having a broad range of chemical compositions and applications ranging from elastomers and tough plastics to biomaterials and pharmaceutical applications. New synthetic strategies allow control, not only of backbone and side chain MW and PDI but also of the exact number of branch points, their placement along the backbone, and the number of branches per branch point.

TGIC is emerging as a key analytical technique for the rigorous molecular characterization of complex branched polymers and copolymers. Superior mechanical properties have been demonstrated for multigraft copolymer-based thermoplastic elastomers.

In the future and following a general trend in block copolymer research, we anticipate additional work in the synthesis of more complex multicomponent graft copolymers, incorporating three or more monomers. We also anticipate the use of self-assembly in creating reversible multigraft copolymers that respond to external stimuli. Polypeptide components may play a key role here.

References

1. Hsieh HL, Quirk RP (1996) Anionic polymerization: principles and practical applications. Marcel Dekker, New York
2. Morton M (1983) Anionic polymerization: principles and practice. Academic, New York
3. Szwarc M, Levy M, Milkovich R (1956) Polymerization initiated by electron transfer to monomer - a New method of formation of block polymers. J Am Chem Soc 78:2656–2657
4. Szwarc M (1956) Living polymers. Nature 178:1168–1169
5. Baskaran D, Muller AHE (2007) Anionic vinyl polymerization – 50 years after Michael Szwarc. Prog Polym Sci 32:173–219
6. Hadjichristidis N, Pispas S, Floudas G (2003) Block copolymers: synthetic strategies, physical properties, and applications. John Wiley & Sons, Hoboken
7. Hadjichristidis N, Pitsikalis M, Iatrou H (2005) Synthesis of block copolymers. Adv Polym Sci 189:1–124
8. Pitsikalis M, Pispas S, Mays JW, Hadjichristidis N (1998) Nonlinear block copolymer architectures. Adv Polym Sci 135:1–137
9. Hadjichristidis N, Iatrou H, Pitsikalis M, Mays J (2006) Macromolecular architectures by living and controlled/living polymerizations. Prog Polym Sci 31:1068–1132
10. Hadjichristidis N, Pitsikalis M, Pispas S, Iatrou H (2001) Polymers with complex architecture by living anionic polymerization. Chem Rev 101:3747–3792
11. Bates FS, Hillmyer MA, Lodge TP, Bates CN, Delaney KT, Fredrickson GH (2012) Multiblock polymers: Panacea or Pandora's Box? Science 336:434–440
12. Matyjaszewski K, Müller AHE (2009) Controlled and living polymerizations: from mechanisms to applications. Wiley, New York
13. Feng C, Li YJ, Yang D, Hu JH, Zhang XH, Huang XY (2011) Well-defined graft copolymers: from controlled synthesis to multipurpose applications. Chem Soc Rev 40:1282–1295
14. Sheiko SS, Sun FC, Randall A, Shirvanyants D, Rubinstein M, Lee H, Matyjaszewski K (2006) Adsorption-induced scission of carbon-carbon bonds. Nature 440:191–194
15. Park I, Sheiko SS, Nese A, Matyjaszewski K (2009) Molecular tensile testing machines: breaking a specific covalent bond by adsorption-induced tension in brushlike macromolecules. Macromolecules 42:1805–1807

16. Runge MB, Bowden NB (2007) Synthesis of high molecular weight comb block copolymers and their assembly into ordered morphologies in the solid state. J Am Chem Soc 129:10551–10560

17. Yuan JY, Xu YY, Walther A, Bolisetty S, Schumacher M, Schmalz H, Ballauff M, Muller AHE (2008) Water-soluble organo-silica hybrid nanowires. Nat Mater 7:718–722

18. Wu LL, Shimada N, Kano A, Maruyama A (2008) Poly(L-lysine)-graft-dextran copolymer accelerates DNA hybridization by two orders. Soft Matter 4:744–747

19. Liu SS, Sen A (2001) Synthesis of novel linear polyethene-based graft copolymers by atom transfer radical polymerization. Macromolecules 34:1529–1532

20. Tsoukatos T, Pispas S, Hajichristidis N (2000) Complex macromolecular architectures by combining TEMPO living free radical and anionic polymerization. Macromolecules 33:9504–9511

21. Stehling UM, Malmstrom EE, Waymouth RM, Hawker CJ (1998) Synthesis of poly(olefin) graft copolymers by a combination of metallocene and "living" free radical polymerization techniques. Macromolecules 31:4396–4398

22. Beers KL, Gaynor SG, Matyjaszewski K, Sheiko SS, Moller M (1998) The synthesis of densely grafted copolymers by atom transfer radical polymerization. Macromolecules 31:9413–9415

23. Jenkins AD, Kratochvil P, Stepto RFT, Suter UW (1996) Glossary of basic terms in polymer science. Pure Appl Chem 68:2287–2311

24. Hirao A, Goseki R, Ishizone T (2014) Advances in living anionic polymerization: from functional monomers, polymerization systems, to macromolecular architectures. Macromolecules 47(6):1883–1905

25. Uhrig D, Mays J (2011) Synthesis of well-defined multigraft copolymers. Polym Chem 2:69–76

26. Rempp P, Franta E, Herz JE (1988) Macromolecular engineering by anionic methods. Adv Polym Sci 86:145–173

27. Young RN, Quirk RP, Fetters LJ (1984) Anionic polymerizations of non-polar monomers involving lithium. Adv Polym Sci 56:1–90

28. Szwarc M, Van Beylen M (1993) Ionic polymerizations and living polymers. Chapman & Hall, New York

29. Rempp PF, Lutz PJ (1989) Synthesis of graft copolymers. In: Allen G et al (eds) Comprehensive polymer science and supplements, vol 6. Pergamon, Oxford, pp 403–421

30. Dreyfuss P, Quirk RP (1987) Graft copolymers. In: Kroschwitz J (ed) Encyclopedia of polymer science and engineering, vol 7. Wiley, New York, p 551

31. Quirk RP (1984) Recent advances in controlled grafting of elastomers. Rubber Chem Technol 57(3):557

32. Morton M, Fetters LJ (1975) Anionic polymerization of vinyl monomers. Rubber Chem Technol 48(3):359

33. Bywater S (1974) Anionic polymerization. Prog Polym Sci 4:27–69

34. Matyjaszewski K (1996) Cationic polymerization mechanisms; synthesis and applications. Marcel Dekker, New York

35. Moad G, Solomon D (2006) The chemistry of radical polymerization. Elsevier, The Netherlands

36. Cowie JMG (1989) Block and graft copolymers. In: Allen G, Bevington JC (eds) Comprehensive polymer science, vol 3. Pergamon, Oxford, p 33

37. Allport DC, Janes WH (1973) Block copolymers. Wiley, New York

38. Pepper KW, Paisley HM (1953) Properties of ion-exchange resins in relation to their structure. Part VI. Anion-exchange resins derived from styrene-divinyl-benzene copolymers. J Chem Soc 4097–4105

39. Candau F, Afchar-Taromi F, Rempp P (1977) Synthesis and characterization of polystyrene-poly(ethylene oxide) graft copolymers. Polymer 18:1253–1257

40. Altares T, Wyman DP, Allen VR, Meyersen K (1965) Preparation and characterization of some star- and comb-type branched polystyrenes. J Polym Sci Part A Gen Pap A3:4131–4151

41. Itsuno S, Uchikoshi K, Ito K (1990) Novel method for halomethylation of cross-linked polystyrenes. J Am Chem Soc 112:8187–8188
42. Candau F, Rempp P (1969) Réctions de greffage sur des dérivés halogénés du polystyreègne. Préparation de polystyrènes en peigne. Makromol Chem 122:15–29
43. Rahlwes D, Roovers JEL, Bywater S (1977) Synthesis and characterization of poly(styrene-g-isoprene) copolymers. Macromolecules 10:604–609
44. George MH, Majid MA, Barrie JA, Rezaian I (1987) The anionic synthesis and characterization of poly(styrene-g-ethylene oxide) copolymers. Polymer 28:1217–1220
45. Pitsikalis M, Sioula S, Pispas S, Hadjichristidis N, Cook DC, Li JB, Mays JW (1999) Linking reactions of living polymers with bromomethylbenzene derivatives: synthesis and characterization of star homopolymers and graft copolymers with polyelectrolyte branches. J Polym Sci A 37:4337–4350
46. Selb J, Gallot Y (1979) Graft-copolymers. 1. Synthesis and characterization of poly(styrene-g-2-vinylpyridine). Polymer 20:1259–1267
47. Selb J, Gallot Y (1979) Graft-copolymers.3. Synthesis and characterization of poly (styrene-g-4 vinylpyridine). Polymer 20:1273–1280
48. Pitsikalis M, Woodward J, Mays JW, Hadjichristidis N (1997) Micellization of model graft copolymers in dilute solution. Macromolecules 30:5384–5389
49. Gautier M, Moeller M (1991) Uniform highly branched polymers by anionic grafting: arborescent graft polymers. Macromolecules 24:4548–4553
50. Fernyhough CM, Young RN, Ryan AJ, Hutchings LR (2006) Synthesis and characterisation of poly(sodium 4-styrenesulfonate) combs. Polymer 47:3455–3463
51. Kempf M, Barroso VC, Wilhelm M (2010) Anionic synthesis and rheological characterization of poly(p-methylstyrene) model comb architectures with a defined and very low degree of long chain branching. Macromol Rapid Commun 31:2140–2145
52. Kawahara N, Saito J, Matsuo S, Kaneko H, Matsugi T, Kojoh S, Kashiwa N (2007) New methodology for synthesizing polypropylene-graft-polystyrene (PP-g-PS) by coupling reaction with brominated polypropylene. Polym Bull 59:177–183
53. Lin Y, Zheng J, Liu F, Tang T (2013) Synthesis of well-defined comb-like graft (co)polymers by nucleophilic substitution reaction between living polymers and polyhalohydrocarbon. J Polym Sci Part A Polym Chem 51:1664–1671
54. Tang T, Huang J, Huang B, Huang J, Wang G (2012) Synthesis of graft polymers with poly (isoprene) as main chain by living anionic polymerization mechanism. J Polym Sci Part A Polym Chem 50:5144–5150
55. Yu F, He J, Wang X, Gao G, Yang Y (2007) Synthesis of graft copolymers with "V-shaped" and "Y-shaped" side chains via controlled radical and anionic polymerizations. J Polym Sci Part A Polym Chem 45:4013–4025
56. Lanson D, Schappacher M, Borsali R, Deffieux A (2007) Synthesis of (poly(chloroethyl vinyl ether)-g-polystyrene)comb-b-(poly(chloropyran ethoxy vinyl ether)-g-polyisoprene)comb copolymers and study of hyper-branched micelle formation in dilute solutions. Macromolecules 40:5559–5565
57. Lanson D, Ariura F, Schappacher M, Borsali R, Deffieux A (2009) Comb copolymers with polystyrene and polyisoprene branches: effect of block topology on film morphology. Macromolecules 42:3942–3950
58. Ryu SW, Hirao A (2000) Anionic synthesis of well-defined poly(m-halomethylstyrene)s and branched polymers via graft-onto methodology. Macromolecules 33:4765–4771
59. Hirao A, Kawano H, Ryu SW (2002) Synthesis of branched polymers by means of living anionic polymerization — Part 6. Synthesis of well-defined comb-like branched polystyrenes and graft copolymers with highly branched architecture. Polym Adv Technol 13:275–284
60. Cameron GG, Qureshi MY (1981) Grafting of polybutadiene functionalized with chlorosilane groups. Makromol Chem Rapid Commun 2:287–291
61. Hadjichristidis N, Xenidou M, Iatrou H, Pitsikalis M, Poulos Y, Avgeropoulos A, Sioula S, Paraskeva S, Velis G, Lohse DJ, Schulz DN, Fetters LJ, Wright PJ, Mendelson RA, Garcia-Franco CA, Sun T, Ruff CJ (2000) Well-defined, model long chain branched polyethylene. 1. Synthesis and characterization. Macromolecules 33:2424–2436

62. Fernyhough CM, Young RN, Poche D, DeGroot AW, Bosscher F (2001) Synthesis and characterization of polybutadiene and poly(ethylene − 1-butene) combs. Macromolecules 34:7034–7041

63. Roovers J, Toporowski P, Martin J (1989) Synthesis and characterization of multiarm star polybutadienes. Macromolecules 22:1897–1903

64. Xenidou M, Hadjichristidis N (1998) Synthesis of model multigraft copolymers of butadiene with randomly placed single and double polystyrene branches. Macromolecules 31:5690–5694

65. Ruckenstein E, Zhang HM (1999) Well-defined graft copolymers based on the selective living anionic polymerization of the bifunctional monomer 4-(vinylphenyl)-1-butene. Macromolecules 32:6082–6087

66. Ruckenstein E, Zhang HM (2000) A successive route to amphiphilic graft copolymers with a hydrophilic poly(3-hydroxypropyl methacrylate) backbone and hydrophobic polystyrene side chains. J Polym Sci Part A Polym Chem 38:1195–1202

67. Zhang HM, Ruckenstein E (2000) One-pot, three-step synthesis of amphiphilic comblike copolymers with hydrophilic backbone and hydrophobic side chains. Macromolecules 33:814–819

68. Ishikawa S (1995) Synthesis of poly(N-vinylcarbazole)-graft-polyisoprene. Macromol Chem Phys 196:485–489

69. Narayan R, Shay M (1986) Synthesis of cellulose-g-polystyrene using anionic polymerization. Abstr Pap Am Chem Soc 191:223

70. Narayan R, Shay M (1987) In: Hogen-Esch TE, Smid J (eds) Recent advances in anionic polymerization. Elsevier, New York, p 441

71. Derand H, Wesslen B (1995) Synthesis and characterization of anionic graft copolymers containing poly(ethylene oxide) grafts. J Polym Sci Part A Polym Chem 33:571–579

72. Deng Y, Zhang S, Lu G, Huang X (2013) Constructing well-defined star graft copolymers. Polym Chem 4:1289–1299

73. Se K, Yamazaki H, Shibamoto T, Takano A, Fujimoto T (1997) Model block-graft copolymer via anionic living polymerization: preparation and characterization of [poly((4-vinylphenyl) dimethylvinylsilane)-graft-polyisoprene]-block-polystyrene. Macromolecules 30:1570–1576

74. Xu F, Li T, Xia J, Qiu F, Yang Y (2007) (Polystyrene-g-polyisoprene)-b-polystyrene comb-coil block copolymer in selective solvent. Polymer 48:1428–1434

75. Jannasch P, Wesslen B (1995) Preparation and properties of alkylated poly(styrene-graft-ethylene oxide). J Polym Sci Part A Polym Chem 33:1465–1474

76. Inoki M, Akutsu F, Yamaguchi H, Naruchi K, Miura M (1994) Graft-copolymerization of methyl-methacrylate by lithium diisopropylamide-treated poly(vinyl propionate). Macromol Chem Phys 195:2799–2804

77. Al-Jarrah MMF, Alkafaji JKH, Apikian RL (1986) Anionic graft-polymerization of styrene from polyisoprene - dependence of grafting efficiency on polyisoprene structure. Br Polym J 18:256–258

78. Hadjichristidis N, Roovers J (1978) Conformation of poly(isoprene-G-styrene) in dilute-solution. J Polym Sci B 16:851–858

79. Falk JC, Schlott RJ (1973) Anionic graft copolymers.2. Styrene grafts on ept rubbers. J Macromol Sci Part A Chem 7:1663–1668

80. Falk JC, Schlott RJ, Hoeg DF (1973) Anionic graft copolymers.1. Vinylaromatic grafts on polydienes. J Macromol Sci Part A Chem 7:1647–1662

81. Falk JC, Schlott RJ, Hoeg DF, Pendleton JF (1973) New thermoplastic elastomers - styrene grafts on lithiated polydienes and their hydrogenated counterparts. Rubber Age 105(3):52

82. Falk JC, Hoeg DF, Schlott RJ, Pendleton JF (1973) Anionic graft copolymers. 3. Hydrogenation of polydienes grafted with vinylaromatics. J Macromol Sci Part A Chem 7:1669–1676

83. Lochmann L, Frechet JMJ (1996) Controlled functionalization of polystyrene: introduction of reactive groups by multisite metalation with superbase and reaction with electrophiles. Macromolecules 29:1767–1771

84. Janata M, Lochmann L, Brus J, Holler P, Tuzar Z, Kratochvil P, Schmitt B, Radke W, Muller AHE (1997) Selective grafting of block copolymers. Macromolecules 30:7370–7374

85. Edgecombe BD, Stein JA, Frechet JMJ, Xu ZH, Kramer EJ (1998) The role of polymer architecture in strengthening polymer-polymer interfaces: a comparison of graft, block, and random copolymers containing hydrogen-bonding moieties. Macromolecules 31:1292–1304

86. Li J, Li H, Wu C, Ke Y, Wang D, Li Q, Zhang L, Hu Y (2009) Morphologies, crystallinity and dynamic mechanical characterizations of polypropylene/polystyrene blends compatibilized with PP-g-PS copolymer: effect of the side chain length. Eur Polym J 45:2619–2628

87. Wang L, Wan D, Zhang Z, Liu F, Xing H, Wang Y, Tang T (2011) Synthesis and structure–property relationships of polypropylene-g-poly(ethylene-co-1-butene) graft copolymers with well-defined long chain branched molecular structures. Macromolecules 44:4167–4179

88. Se K, Watanabe O, Isono Y, Fujimoto T (1989) Synthesis and characterization of model block-graft copolymers via anionic polymerization: introduction of poly(isoprene) and poly (ethylene oxide) as graft chains. Macromol Symp 25:249–261

89. Se K, Miyawaki K, Hirahara K, Takano A, Fujimoto T (1998) Model block–graft copolymer via anionic living polymerization: preparation and characterization of polystyrene-block-[poly(p-hydroxystyrene)-graft-poly(ethyleneoxide)]-block-polystyrene. J Polym Sci Part A Polym Chem 36:3021–3034

90. Zhao J, Mountrichas G, Zhang G, Pispas S (2009) Amphiphilic polystyrene-b-poly (p-hydroxystyrene-g-ethylene oxide) block − graft copolymers via a combination of conventional and metal-free anionic polymerization. Macromolecules 42:8661–8668

91. Zhao J, Zhang G, Pispas S (2010) Thermoresponsive brush copolymers with poly(propylene oxide-ran-ethylene oxide) side chains via metal-free anionic polymerization "grafting from" technique. J Polym Sci Part A Polym Chem 48:2320–2328

92. Kowalczuk M, Adamus G, Jedlinski Z (1994) Synthesis of new graft polymers Via anionic grafting of beta-butyrolactone on poly(methyl methacrylate). Macromolecules 27:572–575

93. Liu Y-C, Wang J-S, Huang K-L, Xu W (2010) Graft copolymers of poly(methyl methacrylate) and polyamide-6 via in situ anionic polymerization of ε-caprolactam and their properties. Polym Bull 64:159–169

94. Liu Y-C, Xu X, Xiong Y-Q, Zhang F, Xu W-J (2008) An efficient route for the synthesis of graft copolymers with rigid backbones via anionic ring-opening polymerization of caprolactam. Mater Lett 62:1849–1852

95. Liu Y-C, Xu W, Xiong Y-Q, Xu W-J (2008) Preparation of PS-g-PA6 copolymers by anionic polymerization of ε-caprolactam using PS precursors with N-carbamated caprolactam pendants as macroactivators. J Appl Polym Sci 108:3177–3184

96. Volkova TV, Vygodskii YS et al (2009) Synthesis and characterization of grafted copolymers of aromatic polyimides and ε-caprolactam. J Appl Polym Sci 114:577–586

97. Zhang C-L, Feng L-F, Hoppe S, Hu G-H (2008) Grafting of polyamide 6 by the anionic polymerization of ε-caprolactam from an isocyanate bearing polystyrene backbone. J Polym Sci Part A Polym Chem 46:4766–4776

98. Ponsart S, Coudane J, Vert M (2000) A novel route to poly(ε-caprolactone)-based copolymers via anionic derivatization. Biomacromolecules 1:275–281

99. Nottelet B, El Ghzaoui A, Coudane J, Vert M (2007) Novel amphiphilic poly(-ε-caprolactone)-g-poly(l-lysine) degradable copolymers. Biomacromolecules 8:2594–2601

100. Nottelet B, Vert M, Coudane J (2008) Novel amphiphilic degradable poly(ε- caprolactone)-graft-poly(4-vinyl pyridine), poly(ε-caprolactone)-graft-poly(dimethylaminoethyl methacrylate) and water-soluble derivatives. Macromol Rapid Commun 29:743–750

101. Zhao J, Schlaad H (2011) Controlled anionic graft polymerization of ethylene oxide directly from poly(N-isopropylacrylamide). Macromolecules 44:5861–5864

102. Mayo FR, Walling C (1950) Copolymerization. Chem Rev 46:191–287

103. Schulz GO, Milkovich R (1982) Graft polymers with macromonomers.1. Synthesis from methacrylate-terminated polystyrene. J Appl Polym Sci 27:4773–4786

104. Feast WJ, Gibson VC, Johnson AF, Khosravi E, Mohsin MA (1994) Tailored copolymers Via coupled anionic and ring-opening metathesis polymerization - synthesis and polymerization of bicyclo 2.2.1 hept-5-ene-2,3-trans-bis(polystyrylcarboxylate)S. Polymer 35:3542–3548

105. Tanaka S, Uno M, Teramachi S, Tsukahara Y (1995) Determination of chemical-composition distribution of poly(methyl methacrylate)-graft-polystyrene prepared from omega-p-

vinylbenzyl polystyrene macromonomer by adsorption high-performance liquid-chromatography. Polymer 36:2219–2225

106. Ederle Y, Isel F, Grutke S, Lutz PJ (1998) Anionic polymerization and copolymerization of macromonomers: kinetics, structure control. Macromol Symp 132:197–206

107. Rempp P, Franta E (1987) Synthesis and applications of macromonomer. Recent advances in anionic polymerization. Springer, The Netherlands

108. Norton R, McCarthy T (1989) ω-Norbornely Polystyrene: an olefin metathesis polymerizable macromonomer. Macromolecules 22(3):1022–1025

109. Vazaios A, Hadjichristidis N (2005) Anionic polymerization of styrenic macromonomers of polyisoprene, polybutadiene, and polystyrene. J Polym Sci Part A Polym Chem 43:1038–1048

110. Pantazis D, Chalari I, Hadjichristidis N (2003) Anionic polymerization of styrenic macromonomers. Macromolecules 36:3783–3785

111. Driva P, Iatrou H, Lohse DJ, Hadjichristidis N (2005) Anionic homo- and copolymerization of double-tailed macromonomers: a route to novel macromolecular architectures. J Polym Sci Part A Polym Chem 43:4070–4078

112. Nikopoulou A, Iatrou H, Lohse DJ, Hadjichristidis N (2007) Anionic homo- and copolymerization of styrenic triple-tailed polybutadiene macromonomers. J Polym Sci Part A Polym Chem 45:3513–3523

113. Koutalas G, Iatrou H, Lohse DJ, Hadjichristidis N (2005) Well-defined comb, star – comb, and comb-on-comb polybutadienes by anionic polymerization and the macromonomer strategy. Macromolecules 38:4996–5001

114. Koutalas G, Lohse DJ, Hadjichristidis N (2005) Novel block–comb/graft copolymers with the macromonomer strategy and anionic polymerization. J Polym Sci Part A Polym Chem 43:4040–4049

115. Zamurovic M, Christodoulou S, Vazaios A, Iatrou E, Pitsikalis M, Hadjichristidis N (2007) Micellization behavior of complex comblike block copolymer architectures. Macromolecules 40:5835–5849

116. Liu B, Quirk RP, Wesdememiotis C, Yol AM, Foster MD (2012) Precision synthesis of ω-branch, End-functionalized comb polystyrenes using living anionic polymerization and thiol–Ene "click" chemistry. Macromolecules 45:9233–9242

117. Velis G, Hadjichristidis N (1999) Synthesis of model PS(PI)(5) and (PI)(5)PS(PI) (5) nonlinear block copolymers of styrene (S) and isoprene (I). Macromolecules 32:534–536

118. Iatrou H, Avgeropoulos A, Hadjichristidis N (1994) Synthesis of model super H-shaped block-copolymers. Macromolecules 27:6232–6233

119. Avgeropoulos A, Hadjichristidis N (1997) Synthesis of model nonlinear block copolymers of A(BA)(2), A(BA)(3), and (AB)(3)A(BA)(3) type. J Polym Sci Part A Polym Chem 35:813–816

120. Roovers J, Toporowski PM (1981) Preparation and characterization of H-shaped polystyrenes. Macromolecules 14:1174–1178

121. Rahman MS, Lee H, Chen X, Chang T, Larson R, Mays J (2012) Model branched polymers: synthesis and characterization of asymmetric H-shaped polybutadienes. Macro Lett 1:537–540

122. Pispas S, Hadjichristidis N, Mays JW (1996) Micellization of model graft copolymers of the H and Pi type in dilute solution. Macromolecules 29:7378–7385

123. Gido SP, Lee C, Pochan DJ, Pispas S, Mays JW, Hadjichristidis N (1996) Synthesis, characterization, and morphology of model graft copolymers with trifunctional branch points. Macromolecules 29:7022–7028

124. Schull C, Frey H (2012) Controlled synthesis of linear polymers with highly branched side chains by "hypergrafting": poly(4-hydroxy styrene)-graft-hyperbranched polyglycerol. Macro Lett 1:461–464

125. Xie C, Ju Z, Zhang C, Yang Y, He J (2013) Dendritic block and dendritic brush copolymers through anionic macroinimer approach. Macromolecules 46:1437–1446

126. Mays JW (1990) Synthesis of simple graft poly(isoprene-G-styrene) by anionic-polymerization. Poly Bull 23:247–250

127. Uhrig D, Mays JW (2002) Synthesis of combs, centipedes, and barbwires: poly(isoprene-graft-styrene) regular multigraft copolymers with trifunctional, tetrafunctional, and hexafunctional branch points. Macromolecules 35:7182–7190

128. Zhu YQ, Burgaz E, Gido SP, Staudinger U, Weidisch R, Uhrig D, Mays JW (2006) Morphology and tensile properties of multigraft copolymers with regularly spaced tri-, tetra-, and hexafunctional junction points. Macromolecules 39:4428–4436

129. Nikopoulou A, Iatrou H, Lohse DJ, Hadjichristidis N (2009) Synthesis of exact comb polybutadienes with two and three branches. J Polym Sci Part A Polym Chem 47:2597–2607

130. Hirao A, Watanabe T, Kurokawa R (2009) Precise synthesis of exact graft polystyrenes with branches from two to five in number by iterative methodology based on living anionic polymerization. Macromolecules 42:3973–3981

131. Hirao A, Murano K, Kurokawa R, Watanabe T, Sugiyama K (2009) Precise synthesis of exact graft copolymers, poly(methyl methacrylate)-exact graft-polystyrene, by iterative methodology using a specially designed in-chain-functionalized AB diblock copolymer anion. Macromolecules 42:7820–7827

132. Iatrou H, Mays JW, Hadjichristidis N (1998) Regular comb polystyrenes and graft polyisoprene/polystyrene copolymers with double branches ("centipedes"). quality of (1,3-phenylene)bis(3-methyl-1-phenylpentylidene)dilithium initiator in the presence of polar additives. Macromolecules 31:6697–6701

133. Plamper FA, Reinicke S, Elomaa M, Schmalz H, Heikki T (2010) Pearl necklace architecture: new threaded star-shaped copolymers. Macromolecules 43:2190–2203

134. Fujimoto T, Zhang HM, Kazama T, Isono Y, Hasegawa H, Hashimoto T (1992) Preparation and characterization of novel star-shaped copolymers having 3 different branches. Polymer 33:2208–2213

135. Uhrig D, Hong K, Mays JW, Kilbey SM II, Britt PF (2008) Synthesis and characterization of an ABC miktoarm star terpolymer of cyclohexadiene, styrene, and 2-vinylpyridine. Macromolecules 41:9480–9482

136. Paraskeva S, Hadjichristidis N (2000) Synthesis of an exact graft copolymer of isoprene and styrene with two branches. J Polym Sci Part A Polym Chem 38:931–935

137. Al-Muallem HA, Knauss DM (2001) Graft copolymers from star-shaped and hyperbranched polystyrene macromonomers. J Polym Sci Part A Polym Chem 39:3547–3555

138. Hirao A, Murao K, Abouelmagd A, Uematsu M, Ito S, Goseki R, Ishizone T (2011) General and facile approach to exact graft copolymers by iterative methodology using living anionic in-chain-functionalized AB diblock copolymers as key building blocks. Macromolecules 44:3302–3311

139. Hirao A, Uematsu M, Kurokawa R, Ishizone T (2011) Facile synthetic approach to exact graft (Co)polymers and double-tailed polystyrene: linking reaction of living anionic polymers with specially designed in-chain-multifunctionalized polystyrenes. Macromolecules 44:5638–5649

140. Chang T, Lee HC, Lee W, Park S, Ko C (1999) Polymer characterization by temperature gradient interaction chromatography. Macromol Chem Phys 200:2188–2204

141. Hutchings LR (2012) Complex branched polymers for structure-property correlation studies: the case for temperature gradient interaction chromatography analysis. Macromolecules 45:5621–5639

142. Lee HC, Chang T (1996) Polymer molecular weight characterization by temperature gradient high performance liquid chromatography. Polymer 37:5747–5749

143. Ryu J, Chang T (2005) Thermodynamic prediction of polymer retention in temperature- 979 programmed HPLC. Anal Chem 77:6347–6352 29

144. Chang T (2005) Polymer characterization by interaction chromatography. J Polym Sci B 43:1591–1607

145. Chen X, Rahman MS, Lee H, Mays J, Chang T, Larson R (2011) Combined synthesis, TGIC characterization, and rheological measurement and prediction of symmetric H polybutadienes and their blends with linear and star-shaped polybutadienes. Macromolecules 44:7799–7809

146. Rahman MS, Aggarwal R, Larson RG, Dealy JM, Mays J (2008) Synthesis and dilute solution properties of well-defined H-shaped polybutadienes. Macromolecules 41:8225–8230
147. Perny S, Allgaier J, Cho DY, Lee W, Chang TY (2001) Synthesis and structural analysis of an H-shaped polybutadiene. Macromolecules 34:5408–5415
148. Milner ST (1994) Chain architecture and asymmetry in copolymer microphases. Macromolecules 27:2333–2335
149. Hadjichristidid N, Iatrou H, Behal SK, Chludzinski JJ, Disko MM, Garner RT, Liang KS, Lohse DJ, Milner ST (2003) Morphology and miscibility of miktoarm styrene-diene copolymers and terpolymers. Macromolecules 26:5812–5815
150. Pochan DJ, Gido SP, Pispas S, Mays JW, Ryan AJ, Fairclough P, Terrill N, Hamley IW (1996) Morphologies of microphase-separated A2B simple graft copolymers. Macromolecules 29:5091–5098
151. Dyer C, Driva P, Sides SW, Sumpter BG, Mays JW, Chen J, Kumar R, Goswami M, Dadmun MD (2013) Effect of macromolecular architecture on the morphology of polystyrene–polyisoprene block copolymers. Macromolecules 46:2023–2031
152. Lee C, Gido SP, Poulos Y, Hadjichristidis N, Tan NB, Trevino SF, Mays JW (1998) Pi-shaped double-graft copolymers: effect of molecular architecture on morphology. Polymer 39:4631–4638
153. Lee C, Gido SP, Poulos Y, Hadjichristidis N, Tan NB, Trevino SF, Mays JW (1997) H-shaped double graft copolymers: effect of molecular architecture on morphology. J Chem Phys 107:6460–6469
154. Xenidou M, Beyer FL, Hadjichristidis N, Gido SP, Tan NB (1998) Morphology of model graft copolymers with randomly placed trifunctional and tetrafunctional branch points. Macromolecules 31:7659–7667
155. Olmsted PD, Milner ST (1998) Strong segregation theory of bicontinuous phases in block copolymers. Macromolecules 31:4011–4022
156. Whitmore MD, Vavasour JD (1995) Self-consistent-field theory of block-copolymers and block-copolymer blends. Acta Polym 46:341–360
157. Vavasour JD, Whitmore MD (1993) Self-consistent-field theory of block-copolymers with conformational asymmetry. Macromolecules 26:7070–7075
158. Laity PR, Taylor JE, Wong SS, Khunkamchoo P, Norris K, Cable M, Andrews GT, Johnson AF, Cameron RE (2004) A review of small-angle scattering models for random segmented poly(ether-urethane) copolymers. Polymer 45:7273–7291
159. Beyer FL, Gido SP, Buschl C, Iatrou H, Uhrig D, Mays JW, Chang MY, Garetz BA, Balsara NP, Tan NB, Hadjichristidis N (2000) Graft copolymers with regularly spaced, tetrafunctional branch points: morphology and grain structure. Macromolecules 33:2039–2048
160. Staudinger U, Schlegel R, Weidisch R, Fritzsche J, Kluppel M, Heinrich G, Mays JW, Uhrig D, Hadjichristidis N (2008) Interpretation of hysteresis behaviour of PI-PS multigraft copolymers by adapting to the dynamic flocculation model. Eur Polym J 44:3790–3796
161. Schlegel R, Wilkin D, Duan Y, Weidisch R, Heinrich G, Uhrig D, Mays JW, Iatrou H, Hadjichristidis N (2009) Stress softening of multigraft copolymers. Polymer 50:6297–6304
162. Duan YX, Thunga M, Schlegel R, Sehneider K, Rettler E, Weidisch R, Siesler HW, Stamm M, Mays JW, Hadjichristidis N (2009) Morphology and deformation mechanisms and tensile properties of tetrafunctional multigraft copolymers. Macromolecules 42:4155–4164
163. Schlegel R, Staudinger U, Thunga M, Weidisch R, Heinrich G, Uhrig D, Mays JW, Iatrou H, Hadjichristidis N (2009) Investigations on mechanical properties of PI-PS multigraft copolymers. Eur Polym J 45:2902–2912

Star-Branched Polymers (Star Polymers)

Akira Hirao, Mayumi Hayashi, Shotaro Ito, Raita Goseki, Tomoya Higashihara, and Nikos Hadjichristidis

Abstract The synthesis of well-defined regular and asymmetric mixed arm (hereinafter miktoarm) star-branched polymers by the living anionic polymerization is reviewed in this chapter. In particular, much attention is being devoted to the synthetic development of miktoarm star polymers since 2000. At the present time, the almost all types of multiarmed and multicomponent miktoarm star polymers have become feasible by using recently developed iterative strategy. For example, the following well-defined stars have been successfully synthesized: 3-arm ABC, 4-arm ABCD, 5-arm ABCDE, 6-arm ABCDEF, 7-arm ABCDEFG, 6-arm $A_2B_2C_2$, 9-arm $A_3B_3C_3$, 12-arm $A_4B_4C_4$, 13-arm $A_4B_4C_4D$, 9-arm AB_8, 17-arm AB_{16}, 33-arm AB_{32}, 7-arm AB_2C_4, 15-arm $AB_2C_4D_8$, and 31-arm $AB_2C_4D_8E_{16}$ miktoarm star polymers, most of which are quite new and difficult

A. Hirao
Polymeric and Organic Materials Department, Graduate School of Science and Engineering, Tokyo Institute of Technology, 2-12-1, Ohokayama, Meguro-ku, Tokyo 152-8552, Japan

Institute of Polymer Science and Engineering, National Taiwan University, No.1, Sec.4, Roosevelt Road, Taipei 10617, Taiwan

College of Chemistry, Chemical Engineering and Materials Science, Soochow University, 199 Ren Ai Road, Suzhou Industrial Park, Suzhou 215123, China
e-mail: ahirao@email.plala.or.jp

M. Hayashi (✉) • S. Ito • R. Goseki
Polymeric and Organic Materials Department, Graduate School of Science and Engineering, Tokyo Institute of Technology, 2-12-1, Ohokayama, Meguro-ku, Tokyo 152-8552, Japan
e-mail: hayashim6@sc.sumitomo-chem.co.jp; sito@polymer.titech.ac.jp; rgoseki@polymer.titech.ac.jp

T. Higashihara
Department of Polymer Science and Engineering, iFront Leading Doctoral Graduate School Program, Yamagata University, 4-3-16, Jonan, Yonezawa, Yamagata 992-8510, Japan

Japan Science and Technology Agency (JST), 4-1-8, Honcho, Kawaguchi, Saitama 332-0012, Japan
e-mail: thigashihara@yz.yamagata-u.ac.jp

N. Hadjichristidis
Division of Physical Sciences and Engineering, KAUST Catalysis Center (KCC), Polymer Synthesis Laboratory, King Abdullah University of Science and Technology (KAUST), Thuwal, Saudi Arabia
e-mail: Nikolaous.Hadjichristidis@kaust.edu.sa

to synthesize by the end of the 1990s. Several new specialty functional star polymers composed of vinyl polymer segments and rigid rodlike poly(acetylene) arms, helical polypeptide, or helical poly(hexyl isocyanate) arms are introduced.

Keywords Living anionic polymerization • Star polymer • Regular star polymer • Asymmetric star polymer • Miktoarm star polymer • μ-Star polymer • Iterative strategy • Multicomponent and multiarmed star polymer

1 Introduction

The availability of star-branched polymers (hereinafter star polymers) with well-defined architectures and low degrees of molecular weight and compositional heterogeneity is essential for fundamental understanding regarding the relationships among the star-branched structure and their basic properties as well as morphologies. If such relationships can be understood and predetermined, new specialty polymers based on star-branched structures are created, because it has long been known that the branched structure significantly influences various physical properties and morphologies.

A star polymer, recognized as the simplest branched polymer among the various branched polymers so far synthesized, consists of three or more linear polymer chains linked together at one end of each chain by a single or junction point. In general, star polymers are categorized into two types, that is, regular and asymmetric star polymers. Regular star polymers are composed of all the same arm segments in molecular weight and chemical structure. Because of several arm segments connected at the single point and the same number of chain ends, these polymers have characteristic features, such as lower viscosities in the bulk and solution, better solubility, smaller hydrodynamic volumes, lower crystallinities, and lower glass transition temperatures (T_g) and melting points (T_m), in comparison to linear polymers with the same molecular weights.

Asymmetric star polymers, whose arms differ in chemical structure, are generally called mixed-arm or miktoarm (coming from the Greek word μικτός meaning mixed) star polymers, abbreviated as μ-star polymers. This type of polymer belongs to a star with a composition asymmetry. Furthermore, there are two additional different asymmetric star polymers as follows: the first example is a star polymer with molecular weight asymmetry, whose arms are identical in chemical structure, but differ in molecular weight. The other one is a star polymer with topological asymmetry, in which the arms are block copolymers, but differ with respect to the block sequence connected to the branch point. Such three asymmetric star polymers are illustrated in Fig. 1 to clearly understand their structures.

Among such asymmetric star polymers, μ-star polymers have received much attention in recent years because they exhibit unique and unusual morphologies in bulk and selected solvents, either by moving the borders of the classical morphology map of linear block polymers or by tremendously increasing the variety of new morphological structures [1–3]. Thus, μ-star polymers are expected as promising

composition asymmetry   *molecular weight asymmetry*   *topological asymmetry*
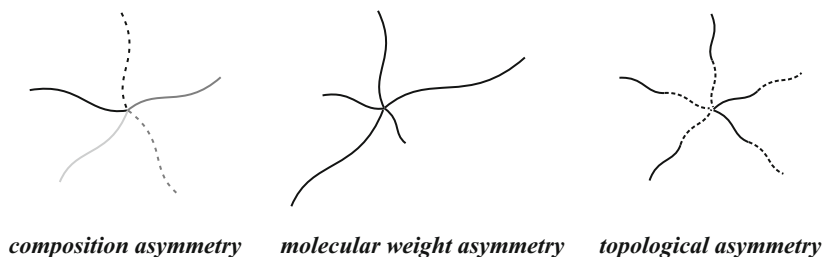
Fig. 1 Three asymmetric star polymers

nonlinear multiphase polymers next to linear block polymers with many potential applications in the fields of nanoscience and nanotechnology such as electronic and optical nanodevices, nanomaterials for lithography, nanoreactors carrying metal catalysts and enzymes, nanoscale microfilters, self-assembled materials for drug and genetic materials delivery, etc.

In this chapter, we will briefly describe the general and basic synthesis of star polymers established until the 1990s to avoid the duplication of previous reviews and books [4–13]. Our attention will focus on the recent developments of multiarmed and multicomponent μ-star polymers synthesized by the living anionic polymerization *"with emphasis on the precise control of synthetic factors involving the molecular weight, molecular weight distribution, arm number, and composition."* The rapid progress in living/controlled radical polymerization systems as well as several living polymerization systems via cationic, transition-metal-mediated, and other mechanisms also enables the synthesis of various different μ-star polymers, which cannot be obtained by anionic polymerization. However, such star polymers, although interesting, are beyond the scope of this chapter and may be covered elsewhere.

2 Regular Star Polymers

2.1 Regular Star Polymers Synthesized Until the 1990s

In order to synthesize regular as well as asymmetric star polymers with well-defined structures, the use of living polymerization systems is essential. Although several living polymerization systems via different active species and reaction mechanisms have been significantly developed, particularly in the last 25 years, the living anionic polymerization of styrene, 1,3-butadiene, isoprene, 2-vinylpyridine, alkyl methacrylates, and their derivatives with certain functional groups [14–18] is still the best system based on the following viewpoints: first, the molecular weight can be precisely controlled in a wide range from 10^3 to even 10^6 mol/l. Second, an extremely narrow molecular weight distribution can be realized, M_w/M_n values being 1.05 or even lower. Finally, the resulting living anionic polymers have chain-

Scheme 1 Synthesis of regular star polymer by "core-first" initiation method
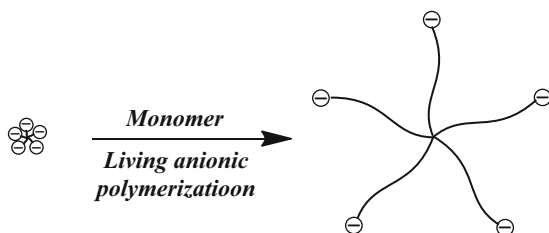

end anions, which are highly reactive, but stable under appropriate conditions. Such characteristics are ideally suited for the synthesis of star polymers with well-defined structures.

Two strategies were proposed for the synthesis of regular star polymers as early as the 1960s soon after the discovery of the living anionic polymerization in 1956. They were strategies based on the "core-first" initiation and "arm-first" termination methodologies. Scheme 1 shows the synthesis of star polymers by the core-first initiation method. A multifunctional anionic initiator having three or more anionic sites exactly defined in number is prepared in advance and used as the initiator for the living anionic polymerization of an appropriate monomer to grow the arm segments. The number of arms in the resulting star corresponds to the number of anionic sites if all of the sites efficiently work. There are advantageous points where steric hindrance is reduced as the polymerization proceeds and fractionation is basically not needed. The most successful examples by this method were the synthesis of polystyrene (PS), poly(ethylene oxide) (PEO), and poly(dimethylsiloxane) (PDMS) star polymers having 4–16 arms by the polymerization of the corresponding monomers with the multifunctional anionic initiators based on carbosilane dendrimers of several generations [19, 20]. A hydrocarbon-soluble trifunctional anionic initiator was prepared from 1,3,5-tris(1-phenylethenyl)benzene and sec-BuLi and found to be an effective initiator for the synthesis of 3-arm PS and poly(1,3-butadiene) (PB) star polymers [21, 22].

A serious problem, however, exists regarding the uniformity of the arm segments in molecular weight. Due to the ionic repulsion among several anionic sites that influences the degree of ion dissociation, it is highly probable that the propagation reaction heterogeneously proceeds, resulting in a large molecular weight distribution of the arm segments. Furthermore, it is difficult or nearly impossible to know how many reaction sites participate in the polymerization. Thus, star architectures including arm the lengths and numbers cannot be always unambiguously defined. For these reasons, the agreement between the calculated and observed molecular weights is not a guarantee to demonstrate the well-defined structures of the resulting polymers. In addition, the insolubility and synthetic difficulty of highly purified multifunctional anionic initiators often prevents the practical synthesis of star polymers.

The second strategy based on the arm-first termination methodology utilizes a multifunctional terminator having the exact number of reaction sites in the linking reaction with living anionic polymers for the star polymer synthesis, as shown in
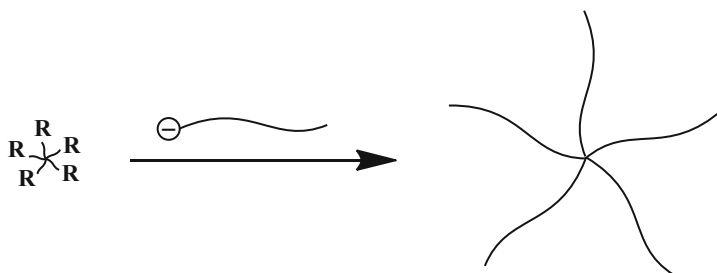
Scheme 2 Synthesis of regular star polymer by "arm-first" termination method
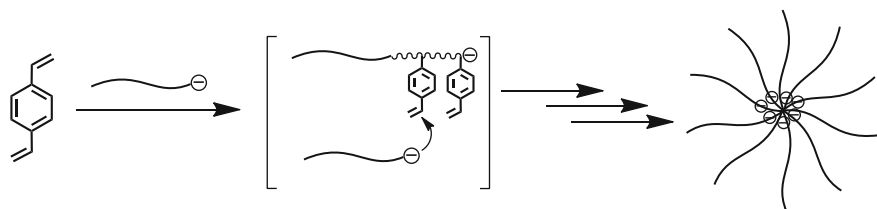
Scheme 2. The premade living anionic polymer with a known molecular weight and a narrow molecular weight distribution is employed in the linking reaction. The number of arms in the resulting star polymer is readily determined by comparing the molecular weight of the final polymer to that of the premade living polymer. Agreement between the molecular weight of the final polymer and the molecular weight calculated by multiplying the M_n value of the premade living polymer by the arm number is direct evidence for the well-defined and expected structure. The uniformity and molecular weight of the arm segment are always guaranteed by the use of the premade living polymer. Thus, the arm-first termination methodology is quite superior to the core-first initiation one with respect to the well-defined star polymer synthesis.

During the early stage of the star polymer synthesis, the use of a wide variety of multifunctional terminators was attempted in the linking reaction with living anionic polymers [23]. These terminators involved 1,3,5-trichloromethylbenzene, 1,3,5-tribromomethylbenzene, 1,2,4,5-tetrabromobenzene, hexa(4-chloromethylphenyl)-benzene, MeSiCl$_3$, SiCl$_4$, SnCl$_4$, PCl$_3$, hexachlorocyclic triphosphazene, 2,4,6-triallyloxytriazine, dimethyl terephthalate, tetrekis((phenyl-1-vinyl)-4-phenyl) plumbane, 1,1,4,4-tetraphenyl-1,4-bis(allyloxytriazine)butane, 1,3,5-tris (phenylethenyl)benzene [22], and even C$_{60}$ [24, 25]. Unfortunately, insufficient linking and undesired side reactions often occurred in the linking reactions of most of these terminators with the living anionic polymers to afford mixtures of target stars, less or extra-armed stars, and other by-products. Moreover, the number of arms was generally limited in range from 3 to 6. Such difficulties and limitations were overcome by developing several functional dendrimer-based multifunctional terminators. The arm-first termination methodology using such multifunctional terminators is currently the most promising procedure for the synthesis of well-defined multiarmed star polymers and will be introduced in the next sections "Arm-first termination methodology using multifunctional chlorosilane reaction site," "Arm-first termination methodology using BnBr reaction site," and "Arm-first termination methodology using DPE reaction site."

The third strategy initially reported by Burchard et al. [26, 27] since the 1970s and later developed by Rempp et al. [28, 29] utilizes certain divinyl monomers either with anionic initiators, followed by polymerization, or with living anionic
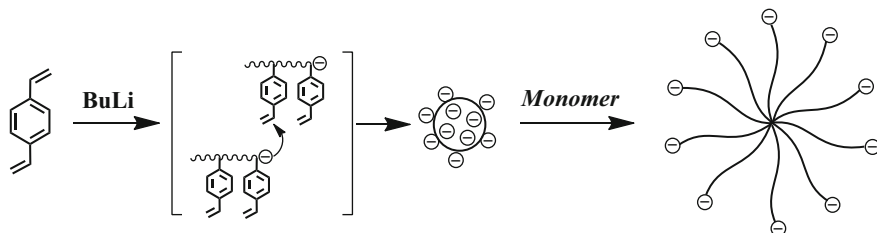
Scheme 3 Synthesis of star polymer by the polymerization with multifunctional initiator prepared from BuLi with 4-DVB


Scheme 4 Synthesis of star polymer by reacting living anionic polymer with 4-DVB

polymers. The typical divinyl monomers used are 4-divinylbenzene (4-DVB), a commercially available mixture of 3- and 4-DVBs, and several bis(methacrylate) monomers. In the former case as shown in Scheme 3, an anionic initiator like BuLi reacts with 4-DVB to polymerize and subsequently undergoes the addition reaction between the chain-end anion and the pendant vinyl group, resulting in the production of a soluble microgel-like multifunctional compound with many anionic reaction sites. This multifunctional compound is used as the anionic initiator in the polymerization of the appropriate monomer. Thus, a variety of PS, PB, poly-isoprene (PI), poly(*tert*-butyl acrylate) (P^{t}BA), and PEO star polymers were synthesized [29–34]. The number of arms can be controlled by the ratio of [4-DVB]/[BuLi] in the range from 5 to even the high number of 1,300. Moreover, the reaction of the growing chain-end anions with either suitable electrophiles or the addition of other monomers allows access to a variety of end-functionalized stars or star block copolymers.

A star polymer can also be synthesized by directly reacting a living anionic polymer with 4-DVB, as illustrated in Scheme 4. Similar to the reaction of BuLi with 4-DVB mentioned above, the living anionic polymer polymerizes a few 4-DVB molecules, followed by the addition reaction of the chain-end anion with the pendant vinyl group, forming a 4-DVB micro gel nodule that serves as the branch point for the produced star polymer. PS, PB, and PI star polymers are typical examples synthesized by this methodology [35–39]. The number of arm segments can also be changed from 5 to 56 by the ratio of [4-DVB] to [chain-end anion].

Since a number of anionic sites are produced by the above reaction, subsequent addition of the same monomer or another monomer yields regular star polymers

14-arm A₁₄ star   **7-arm A₇ star**   **14-arm A₇B₇ star**
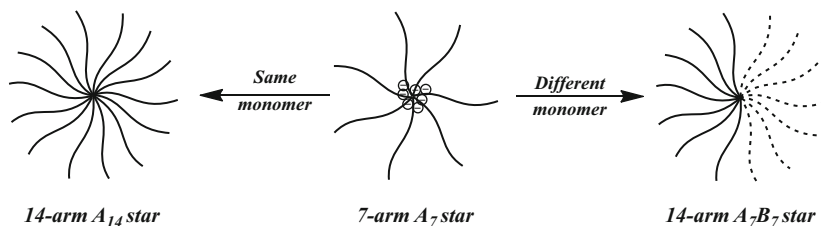
Scheme 5 Synthesis of more armed regular star and AₙBₙ μ-star by the polymerization of the same or different monomer with the polymer anion

having more number of arms or μ-star polymers (see Scheme 5). For example, a variety of AₙBₙ μ-star polymers composed of PS (A) and poly(*tert*-butyl (meth) acrylate) (PᵗB(M)A) (B), PEO (B), or poly(2-vinylpyridine) (P2VP) (B) were successfully synthesized by this methodology [29, 39–42]. The number of arm segments in the star polymers thus synthesized is always widely distributed and even the molecular weight of the arms cannot be controlled. Thus, the third strategy is not suitable to synthesize well-defined star polymers, although it is synthetically straightforward and, therefore, technologically important.

2.2 Arm-First Termination Methodology Using Multifunctional Chlorosilane Reaction Site

In contrast to the above-mentioned terminating agents, chlorosilane compounds quantitatively react with highly reactive living anionic polymers, such as poly (styryl)lithium (PSLi), poly(1,3-butadienyl)lithium (PBLi), and poly(isoprenyl) lithium (PILi), without any side reactions. On the other hand, the incomplete reaction of PSLi with SiCl₄ was observed to occur, resulting in a mixture of star PSs having less than three arms, thus the target 4-arm star PS could not be obtained. This lack of reactivity is attributed to the steric hindrance between the core Si atom and the chain-end PS anion. In contrast, the reaction between a less bulky PBLi and SiCl₄ was found to be complete to afford the expected 4-arm star PB. It was feasible to synthesize the 4-arm star PS by converting the chain-end anion of PSLi to the butadienyl anion by end-capping a few 1,3-butadiene units and subsequently reacting with SiCl₄. Since PILi is situated between PSLi and PBLi in steric bulkiness, the careful choice of chlorosilane compounds and longer reaction times are usually required to complete the linking reaction. Thus, well-defined PSs, PBs, and PIs with arms ranging from 3 to even up to 18 were successfully synthesized [9]. However, the synthesis of multiarmed star polymers was still difficult due to the synthetic difficulty of multifunctional chlorosilane compounds.

Since the 1980s, there appeared a large breakthrough in the development of multiarmed star polymer synthesis. Roovers, Hadjichristidis, and their coworkers
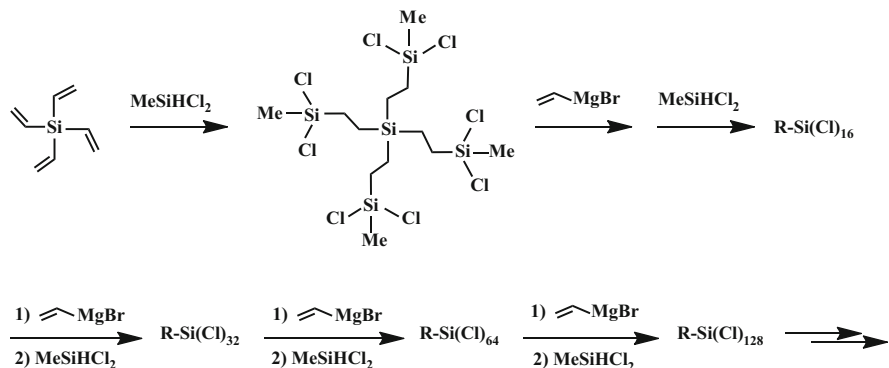
Scheme 6 Synthesis of carbosilane-based multifunctional chlorosilane compounds by iterative methodology

were the first to successfully synthesize a series of carbosilane-based multifunctional chlorosilane compounds having many Si-Cl reaction sites by employing a new iterative approach, as shown in Scheme 6 [43]. The carbosilane dendrimers were prepared starting with tetravinylsilane and using two reaction steps, that is, the hydrosilylation of the vinylsilane moieties with $MeSi(H)Cl_2$ and the reaction of the chlorosilane function with vinylmagnesium bromide to introduce a vinyl group to the silicon atom. The number of chlorosilane reaction sites were dramatically increased from 8 (4×2), 16 (4×2^2), 32 (4×2^3), 64 (4×2^4), even 128 (4×2^5) by repeating the two reaction steps. Thus, a series of multifunctional chlorosilane compounds having 8, 16, 32, 64, and even 128 chlorosilane reaction sites were successively prepared. Similarly, they also prepared another series of multifunctional chlorosilanes, in which 6, 12, and 18 chlorosilane reaction sites were introduced. These carbosilane-based multifunctional chlorosilane compounds are designed so as to separate the chlorosilane reaction site by the methylene chain and to possess only two chlorides on one silicon atom in order to facilitate the next linking reaction stage with living anionic polymers.

With the use of such multifunctional chlorosilane compounds in the linking reactions with living anionic polymers, the following multiarmed star polymers with well-defined structures were successfully synthesized for the first time: typically 6-, 12-, and 18-arm star PSs; 6-, 8-, 12-, and 18-arm star PIs; 8-, 16-, 32-, 64-; and 128-arm star PBs. Most of these star polymers were quite new and possessed remarkably high molecular weights up to 10^8 g/mol in some cases [44–48].

Later, reevaluation of the 32- and 64-arm star PBs by ^{1}H NMR and MALDI-TOF MASS analyses showed that the average number of introduced arms were 29 and 54, respectively, indicating the strict steric requirements in the synthesis of multiarmed star polymers [49, 50]. Nevertheless, the arm-first termination methodology using multifunctional chlorosilane compounds is still one of the most reliable and promising methodologies for the synthesis of well-defined multiarmed star polymers. The chlorosilane compounds also readily react with the living poly

(methyl methacrylate) PMMA and PEO. Unfortunately, the resulting star polymers are not stable due to the formation of hydrolysable Si-O-C linkages between the PMMA or PEO segments and their cores.

2.3 Arm-First Termination Methodology Using BnBr Reaction Site

It has long been believed that the linking reaction of highly reactive living anionic polymers, such as PSLi, PBLi, and PILi, with benzyl chloride (BnCl) or benzyl bromide (BnBr) proceeds along with several undesired side reactions such as the metal–halogen exchange, benzyl proton abstraction, and single-electron transfer reactions. Accordingly, fewer or extra-armed star polymers were by-produced in addition to target stars in the reaction of the living anionic polymer with multifunctional benzyl halides. However, it became feasible to dramatically reduce or almost eliminate such side reactions by end-capping the living anionic polymers with 1,1-diphenylethylene (DPE) prior to the reaction. Moreover, the choice of the reaction conditions is very important. The reaction efficiency could be further improved by carrying out the reaction under the conditions in THF at $-40\ °$C or lower temperature. It is also important to design in such a way that one halomethyl group is substituted on the phenyl ring to minimize the steric hindering and electronic effects. Among the benzyl halides, BnBr is superior to BnCl in the linking reaction, while benzyl iodide is too unstable for the practical use in the star polymer synthesis. Thus, the linking reaction between the BnBr reaction site and the DPE-end-capped living anionic polymer was observed to almost quantitatively proceed [51]. It should be noted that less reactive living polymers of 2VP, MMA, and ^{t}BMA cleanly and quantitatively linked with 1,2,4,5-tetrabromomethylbenzene in THF at $-78\ °$C to afford the corresponding 4-arm star polymers [52, 53].

Similar to the above-mentioned synthesis of multifunctional chlorosilanes by the iterative approach, Hirao et al. successfully synthesized a series of chain-end-(BnBr)$_n$-multifunctionalized polymers with different generations by employing a new iterative approach, which involves two reaction steps in each reaction sequence, that is, the iterative process as follows [51]: first, the reaction of the terminal BnBr reaction sites with a DPE anion prepared from sec-BuLi and 1,1-bis (3-tert-butyldimethylsilyloxymethylphenyl)ethylene (1); second, a transformation reaction of the introduced 3-tert-butyldimethylsilyloxymethylphenyl (TBDMSiOMP) groups into BnBr functions used as the reaction sites by treatment with a 1:1 mixture of Me$_3$SiCl and LiBr.

As shown in Scheme 7, a chain-end-(BnBr)$_2$-functionalized PS was initially prepared by reacting PSLi with 1 to introduce two TBDMSiOMP termini, followed by transformation into two BnBr reaction sites with Me$_3$SiCl/LiBr. In the first process, the DPE anion was prepared from sec-BuLi and 1 and reacted in situ
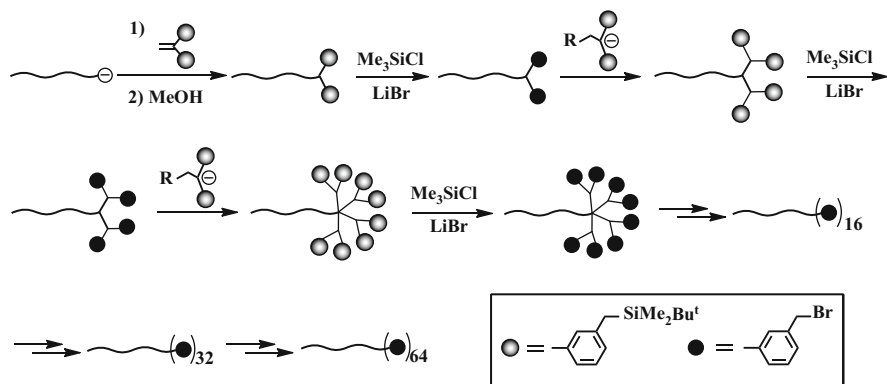
Scheme 7 Synthesis of chain-end-(BnBr)$_n$-multifunctionalized PSs by iterative methodology

with the resulting chain-end-(BnBr)$_2$-functionalized PS to introduce four TBDMOSiMP groups at the chain end. They were transformed into four BnBr reaction sites by the same treatment as that used above. These two reactions exactly correspond to the above-mentioned two reaction steps, respectively. Since the two reactions were observed to quantitatively proceed, the same process could be repeated. In fact, the number of BnBr reaction sites exponentially increased from 8 (2^3) to 16(2^4), 32(2^5), and 64 (2^6). The results are summarized in Table 1.

A star PS was synthesized by the linking reaction of PSLi (M_n = ca. 5,000 g/mol) with each of the chain-end-(BnBr)$_n$-multifunctionalized PSs (M_n values of PSs = ca. 5,000 g/mol) in THF at -78 °C. Prior to the linking reaction, PSLi was end-capped with DPE to avoid any side reaction. The reaction was very fast and actually completed within 1 h under such conditions to result in 3-, 5-, 9-, 17-, and 33-arm star PSs. Their structures were all well defined, as confirmed by the SEC and SLS analyses listed in Table 2.

Since living PMMA cannot react with *1* of the DPE derivative, the DPE anion is used as an initiator in the living anionic polymerization of MMA to introduce two TBDMOSiMP groups at the initiating chain end. As shown in Scheme 8, the same iterative reaction process was performed to increase the number of the BnBr reaction sites by repeating the process [54]. The reaction of the living PMMA (M_n = ca. 10,000 g/mol) with the chain-end-(BnBr)$_n$-multifunctionalized PMMAs (M_n values of PMMAs = ca. 10,000 g/mol) in THF at -78 °C quantitatively yielded well-defined 3-, 5-, 9-, and 17-arm star PMMAs (see also Table 3).

Next, several living anionic polymers with different reactivities were reacted with the chain-end-(BnBr)$_8$-multifunctionalized PS in order to investigate the reactivity of the BnBr reaction site. These polymer segments were all adjusted to be ca. 10,000 g/mol in M_n value. Both PBLi and PILi were end-capped with DPE and subsequently reacted in situ with the BnBr-functionalized PS in THF at -78 °C for 1 h. Under such conditions, 8 PB or 8 PI segments were readily and quantitatively coupled to afford well-defined 9-arm AB$_8$ μ-star polymers composed of PS (A) and PB (B) or PI(B) arms in virtually quantitative yields (see Scheme 9).

Table 1 Characterization results of chain-end-$(BnBr)_n$-multifunctionalized PSs

| Polymer | M_n (g/mol) | | M_w/M_n | BnBr functionality | |
	calcd	VPO	SEC	calcd	^{1}H NMR
PS(BnBr)$_2$	4,790	4,800	1.04	2	2.0$_0$
PS(BnBr)$_4$	5,470	5,420	1.04	4	3.9$_2$
PS(BnBr)$_8$	6,850	6,780	1.03	8	8.0$_8$
PS(BnBr)$_{16}$	9,590	9,640	1.04	16	15.9
PS(BnBr)$_{32}$	15,000	14,800	1.03	32	32.0
PS(BnBr)$_{64}$	25,600	24,700	1.03	64	64.2

Table 2 Synthesis of PS star polymers with 3, 5, 9, 17, and 33 arms by the linking reaction of PSLis with chain-end-$(BnBr)_n$-multifunctionalized PSs

| Star polymer number of arms | M_n (g/mol) | | M_w/M_n |
	calcd	SLS	SEC
3	17,900	17,800	1.03
5	26,800	26,600	1.04
9	44,000	44,700	1.03
17	88,100	87,600	1.05
33	190,000	196,000	1.02
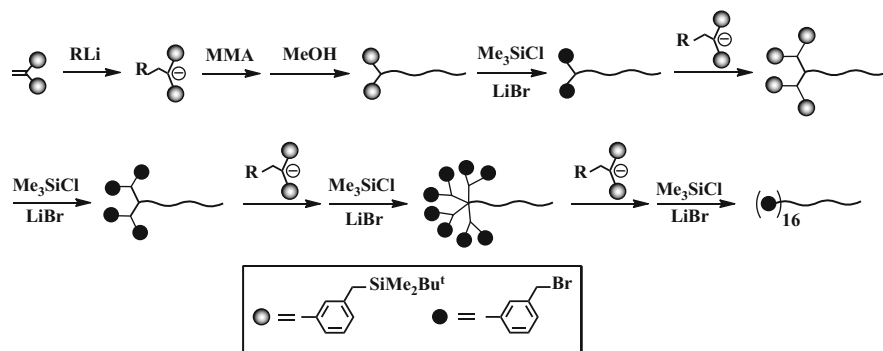
Scheme 8 Synthesis of chain-end-$(BnBr)_n$-multifunctionalized PMMAs by iterative methodology

Table 3 Synthesis of PMMA star polymers with 3, 5, 9, and 17 arms by the reaction of chain-end-$(BnBr)_n$-multifunctionalized PMMAs with living PMMAs

| Star polymer number of arms | M_n (g/mol) | | M_w/M_n |
	calcd	SLS	SEC
3	39,900	40,500	1.02
5	59,600	61,500	1.02
9	99,600	105,000	1.02
17	208,000	205,000	1.04
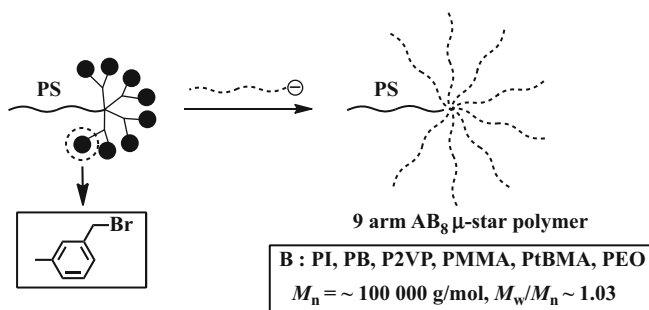
Scheme 9 Synthesis of 9-arm AB_8 μ-stars by the reaction of chain-end-$(BnBr)_8$-functionalized PS with various living anionic polymers

Similarly, the quantitative synthesis of a 9-arm AB_8 star polymer, whose B arm was P2VP or P^tBMA, was also achieved by reacting either the living P2VP or P^tBMA with the same BnBr-functionalized PS under identical conditions. The reaction of living PEO bearing K^+ with the BnBr-functionalized PS resulted in a 100 % linking of the eight PEO chains by adding DMF (ca. 20 vol %) as a cosolvent and gradually raising the temperature to 40 °C for 24 h. Thus, the eight BnBr reaction sites all were satisfactorily reacted with a variety of living anionic polymers to afford the corresponding star polymers. Based on these results, the methodology using the BnBr reaction sites demonstrated the possible synthesis of the multiarmed regular PS, PB, PI, P2VP, PMMA, P^tBMA, and PEO stars [55]. The latter three star polymers were observed to be practically stable, since PMMA, P^tBMA, or PEO arms were linked at the cores via stable C-C or C-O bonds.

It should be noted that the insufficient coupling reactions of chain-end-$(BnBr)_8$-multifunctionalized PSs ($M_n = 100$ kg/mol) were observed with very high-molecular-weight living anionic polymers having M_n values of more than 100 kg/mol even for longer reaction times of 48–168 h. This is at least partly due to the steric hindrance around the reaction sites at the core.

2.4 Arm-First Termination Methodology Using DPE Reaction Site

The final methodology is also based on the arm-first termination methodology involving the DPE reaction sites in conjunction with iterative approach. However, the iterative approach employed in this methodology is different in mechanism from those described in sections "Arm-first termination methodology using multifunctional chlorosilane reaction site" and "Arm-first termination methodology using BnBr reaction site." In the first two iterative approaches used above, the number of the reaction sites increased by repeating the iterative process and the arm segments were then introduced via the prepared reaction sites, resulting in
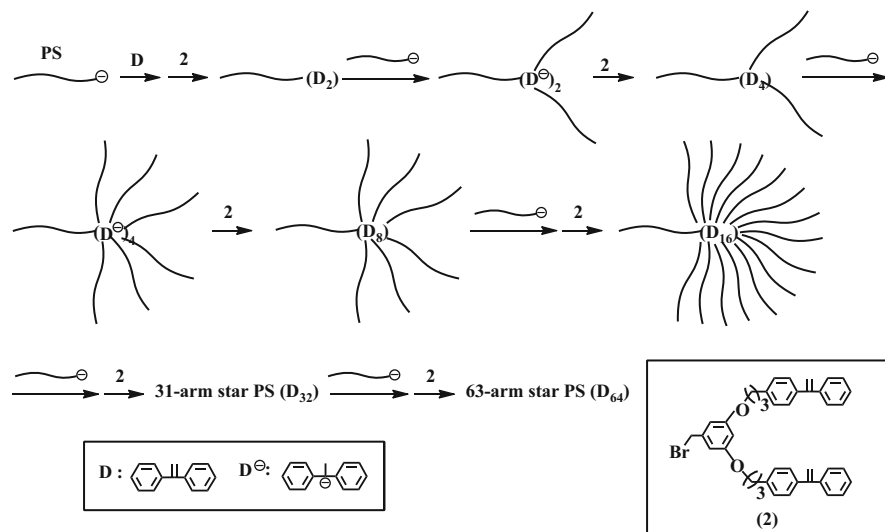
Scheme 10 Synthesis of multiarmed PS stars by iterative methodology using DPE reaction sites

multiarmed star polymers. On the other hand, the iterative approach herein proposed is designed so as to introduce both the reaction sites and arm segments at the same time in each iterative process. Accordingly, each process yields a star polymer and the resulting star polymer is always employed as the starting polymer in the next process. Since the synthetic significance of this methodology will be emphasized in the next section, a possible application to the synthesis of multiarmed star polymer is now described.

As shown in Scheme 10, a new DPE-functionalized agent, 3,5-bis (3-(4-(1-phenylethenyl)phenyl)propoxy)benzyl bromide (2), is used as the key compound in each iterative process [56]. All the polymer segments were fixed at ca. 10,000 g/mol in M_n value throughout the synthesis. PSLi was initially end-capped with DPE and subsequently reacts with 2 to introduce two DPE reaction sites at the chain end. The addition reaction of two equivalents of PSLi to the two DPE reaction sites at the PS chain end was essentially quantitative, resulting in a 3-arm star PS having two DPE anions generated at the linking points. The four DPE reaction sites were introduced by in situ reacting 2 with the generated two DPE anions. Thus, the introduction of two PS arms and four DPE reaction sites was achieved in this process. Since the star PS had the same DPE reaction sites at the core and the two reaction steps were virtually quantitative, the same reaction process could be repeated four more times to successively afford the 7-, 15-, 31-, and 63-arm star PSs.

The yield of the 7-arm star PS was quantitative in THF at $-78\,^\circ$C within 1 h. However, the reaction was not complete in the next process under the same conditions. Accordingly, the reaction conditions were altered as follows: in *tert*-butylbenzene at 30 $^\circ$C for 168 h (the second process) and in *tert*-butylbenzene with

Table 4 Synthesis of multiarmed star PSs by iterative methodology using DPE reaction sites via 2

Star PS arm number	M_n (g/mol)		M_w/M_n
	calcd	SLS	SEC
3	32,200	33,700	1.03
7	79,400	79,000	1.04
15	163,000	166,000	1.05
31	330,000	330,000	1.05
63	625,000	623,000	1.03
127(113)	1,290,000	1,113,000	1.05

two equivalents of TMEDA at 40 °C for 72 h (the third and fourth processes). A further attempt for the synthesis of a 127-arm star PS by reacting PSLi with the core-(DPE)$_{64}$-functionalized 63-arm star PS was not successful even under the same conditions. The resulting polymer was found to possess on average 113 arms. The insufficient linking reaction may be attributed to the steric hindrance around the reaction sites as well as the ionic repulsions among the unreacted anionic sites and (PSLi)s.

As summarized in Table 4, a series of star PSs thus synthesized, except for the 113-arm star PS, was confirmed by ^{1}H NMR, SEC, and SLS to be well defined in star architecture and precisely controlled in arm segment. Even the 113-arm star PS possessed a narrow molecular weight distribution. Thus, this methodology demonstrates the high synthetic potential of the multiarmed star PSs. However, it should be mentioned that only highly reactive living anionic polymers capable of reacting with the DPE function, such as PSLi, PBLi, and PILi, are able to be used at the moment.

This iterative methodology can readily be changed to the original ones shown in sections "Arm-first termination methodology using multifunctional chlorosilane reaction site" and "Arm-first termination methodology using BnBr reaction site" as follows: The reaction of the chain-end-(DPE)$_2$-functionalized PS with two equivalents of sec-BuLi instead of PSLi, followed by in situ reacting the generated DPE anion with 2, yielded a chain-end-(DPE)$_4$-functionalized PS. By repeating the same reaction sequence, the DPE reaction sites increased 8, 16, followed by 32 in number. This indicates that the two original methodologies can also possibly be changed to the second alternative iterative one, with which arms as well as reaction sites are introduced at the same time.

In conclusion, the synthesis of regular star polymers has almost been established in cases using the arm-first termination methodologies with a variety of living anionic polymers with different reactivities. Indeed, regular star PS, PB, PI, P2VP, PMMA, P^{t}BMA, and PEO were successfully synthesized by carefully choosing the reaction site. The resulting stars all have well-defined architectures with controllable molecular weights, narrow molecular weight distributions, and many arms ranging from 6 to 63. A variety of functional star polymers can now be synthesized by applying the living anionic polymerization of new functional styrene derivatives to the above methodologies (see chapter Non-polar monomers:

styrene and 1,3-butadiene derivatives). Furthermore, a variety of recently developed living anionic polymers derived from cyclic monomers may also be usable in these methodologies, resulting in new well-defined multiarmed star polymers.

3 Asymmetric Star Polymers

As mentioned in the introduction, star polymers are usually categorized into regular and asymmetric star polymers. The asymmetric star polymer further subdivides into the following three types according to their architectures: (1) chemical structure asymmetry, (2) molecular-weight asymmetry, and (3) topological asymmetry, as illustrated in Fig. 1. Among them, we now focus on the chemical structure asymmetry-based miktoarm star polymers. These miktoarm arm star (abbreviated μ-star) polymers are classified as nonlinear branched block polymers and have recently attracted much attention because their morphological nanoscale suprastructures and supramolecular assemblies formed in bulk as well as selected solvents are new, characteristic, and, more importantly, quite different from those produced by linear block polymers. These structures and assemblies are expected to play important roles in the fields of nanoscience and nanotechnology with many potential applications. Accordingly, the μ-star polymers are currently recognized as a promising next-generation multiphase polymeric material.

In order to elucidate the formation of such structures and assemblies in detail, well-defined architectures and precisely controlled arm segments in μ-star polymers are strongly demanded. In general, such μ-star polymers are much more difficult in synthesis than regular star polymers due to the following requirements and still a challenging subject even now: (1) multistep reactions to introduce a number of different arms, (2) isolation of the intermediate polymers to obtain pure products, and, most importantly, (3) several different reaction sites selectively worked for the introduction of each arm. These requirements make the molecular design and practical synthesis of multiarmed and multicomponent μ-star polymers extremely difficult. Accordingly, the methodologies currently developed can mainly cover two-component A_xB_y types and several examples of three-component ABC type μ-star polymers. Only a few synthetic examples of the four-component ABCD μ-stars have been reported. Moreover, structural variation is considerably limited in the three- and four-component star polymer syntheses. There is no report about the synthesis of the five-component ABCDE or more-component μ-star polymers except for those to be introduced later. As emphasized in the introduction part, the living anionic polymerization is the most suitable system for the synthesis of well-defined μ-star polymers because of the excellent abilities to precisely control many structural variables.

In the first half of this section, the methodologies established so far for the synthesis of three- and/or four-component μ-star polymers will be introduced. The recently developed methodologies based on iterative strategy possible for the synthesis of multiarmed and multicomponent μ-star polymers will then be described in the latter half.
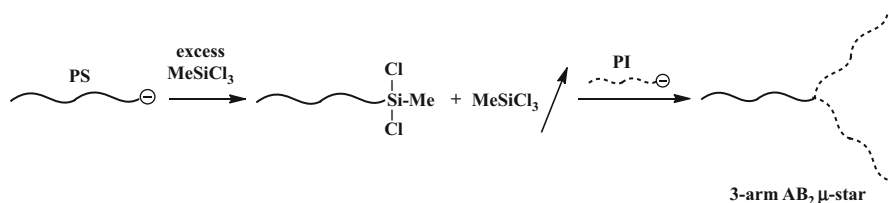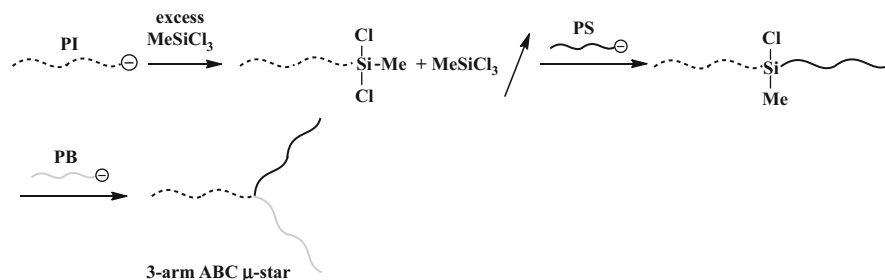
Scheme 11 Synthesis of 3-arm AB$_2$ μ-star polymer by the chlorosilane methodology

3.1 Methodology Using Chlorosilane Reaction Site

As mentioned in section "Arm-first termination methodology using multifunctional chlorosilane reaction site," multifunctional chlorosilane compounds are some of the most effective reaction sites to synthesize multiarmed regular star polymers as these compounds readily and quantitatively react with the living anionic polymers. In the synthesis of regular stars using multifunctional chlorosilane compounds, the reactivity of the living anionic polymer toward the Si-Cl bond was found to follow the sequence of PBLi > PILi > PSLi mainly due to the steric bulkiness of the chain-end anion. It was also found that the reactivity of the Si-Cl bond for the chain-end anion decreased as replacing the chlorine atom by the polymer chain by both the electron donating effect and steric hindrance. By utilizing such different reactivities, the methodology using multifunctional chlorosilane compounds was significantly developed to be an effective procedure for the synthesis of a variety of μ-star polymers.

Mays was the first to successfully synthesize a well-defined μ-star polymer of the 3-arm AB$_2$ type composed of PS (A) and PI (B) by the chlorosilane methodology, as illustrated in Scheme 11 [57]. The most sterically bulky and thereby less reactive PSLi first reacted with a large excess of MeSiCl$_3$ to prepare a chain-end-(SiCl$_2$)-functionalized PS and, after removal of the excess unreacted MeSiCl$_3$ in situ under high vacuum conditions, the more reactive PILi was reacted with the SiCl$_2$ terminus of PS, resulting in a 3-arm AB$_2$ μ-star polymer. The addition order of the living polymer is important in this case. For example, the reverse addition order makes it difficult to synthesize an in-chain-(SiCl)-functionalized (PI)$_2$ and finally introduce a PS chain into the core, due to the combination between the less reactive Si-Cl reaction site and sterically hindered PSLi. This methodology was developed by Hadjichristidis et al. to synthesize all possible combinations of the AB$_2$ star polymers, in which the A and B arms were PS, PB, or PI [58, 59]. Furthermore, an AB$_3$ μ-star polymer was synthesized in a similar manner using SiCl$_4$ instead of MeSiCl$_3$ [60–62].

The same group also successfully synthesized a 3-arm ABC μ-star composed of PS, PI, and PB arms for the first time by utilizing such different reactivities, as shown in Scheme 12 [63]. In the synthesis, PILi first reacted with a large excess of MeSiCl$_3$ to replace the chlorine atom by the PI chain to prepare a chain-end-(SiCl$_2$)-functionalized PI and the excess unreacted MeSiCl$_3$ was removed under

Scheme 12 Synthesis of 3-arm ABC μ-star by the chlorosilane methodology
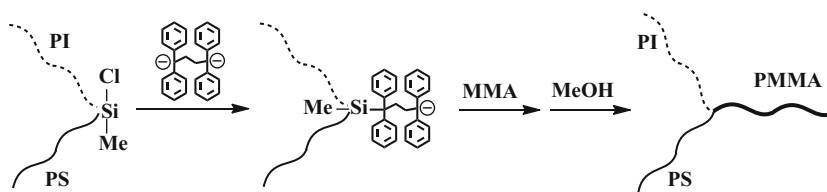
Scheme 13 Synthesis of 3-arm ABC μ-star polymer composed of PS, PI, and PMMA

high vacuum. The most bulky and least reactive PSLi was stoichiometrically reacted in situ with the Si-Cl terminus by a colorimetric titration changing from an orange-red to colorless. No more linking of the PSLi occurred by employing this technique in addition to the steric hindrance of PSLi. Finally, the most reactive PBLi was reacted with the least reactive in-chain-(SiCl)-functionalized PI-*b*-PS to afford a target 3-arm ABC μ-star with well-defined structures ($M_n = 45.4$ kg/mol, $M_w/M_n = 1.03$). Furthermore, a 4-arm ABCD μ-star polymer was synthesized by a similar procedure, in which PSLi, poly(4-methylstyryl)lithium (PMSLi), PILi, followed by PBLi, were sequentially added to SiCl$_4$ [64]. This polymer was the first successful four-component μ-star polymer ($M_n = 62.5$ kg/mol, $M_w/M_n = 1.05$). A very interesting ABC μ-star containing PDMS ($M_n = 58.9$ kg/mol, $M_w/M_n = 1.04$) could also be synthesized by reacting the above-prepared in-chain-(SiCl)-functionalized PS-*b*-PI with the living PDMS [65]. The methodology further demonstrated the effective synthesis of a variety of μ-star polymers, such as the AB$_3$, A$_2$B$_2$, AB$_5$, and A$_8$B$_8$ types, where A and B arms are PS, PI, PB, 2-methyl-1,3-pentadiene, 1,3-cyclohexadiene, and their block copolymer segments. The resulting polymers were all well defined in structure with narrow molecular weight distributions ($M_w/M_n \sim 1.05$) [66–73].

Unfortunately, the living PMMA and other related living polymers derived from alkyl methacrylate monomers cannot be directly applied in this effective methodology, because the silyl enol ether linkage formed between the PMMA arm and the core is readily hydrolyzed even with moisture in the air. In order to introduce the PMMA segment into the μ-star polymer, the reaction site was converted from the Si-Cl reaction site to a DPE anion, as illustrated in Scheme 13. After the in-chain-

(SiCl)-functionalized PS-*b*-PI was prepared in the same manner as that mentioned above, the Si-Cl reaction site was reacted with a dilithium compound, Li (CPh$_2$CH$_2$CH$_2$CPh$_2$)Li, to convert it to the DPE anion. This new anionic reaction site was used as an initiator for the polymerization of MMA, resulting in a 3-arm ABC µ-star polymer composed of PS, PI, and PMMA arms ($M_n = 77.0$ kg/mol, $M_w/M_n = 1.06$) [74]. This modification of the reaction site is advantageous in this respect that any monomer besides MMA that undergoes the living anionic polymerization with the DPE anion can be used.

Thus, a variety of well-defined three- and four-component µ-star polymers can be synthesized by utilizing the different reactivity of the living anionic polymer toward the Si-Cl reaction site as well as the reactivity difference of the Si-Cl bond by the number of chlorine atoms on the Si atom. On the other hand, the reaction order of the living polymers is very critical and limited by the above-mentioned reactivity differences. Moreover, the final linking reaction steps often take longer times even for a few months. Although the living polymers of MMA, other alkyl methacrylates, and ethylene oxide cannot be used in the original methodology, the development of the modified methodology with the anionic reaction site enables the introduction of these polymer segments into the stars.

3.2 Methodology Using Dual-Functionalized Reaction Sites

In 1992, Fujimoto et al. reported a general and versatile methodology for the synthesis of 3-arm ABC µ-star polymers by utilizing the dual-functionalized character of the DPE derivatives [75]. As illustrated in Scheme 14, a chain-end-DPE-functionalized PDMS was first prepared by the polymerization of hexamethylcyclotrisiloxane (D$_3$) with lithium alkoxide of the DPE derivative (see Scheme 14) and then reacted with PSLi to link the PDMS with the PS segment. Since a DPE anion was newly generated by this addition reaction, ^{t}BMA was subsequently added in situ to polymerize with the generated DPE anion, resulting in a 3-arm ABC µ-star polymer composed of PDMS, PS, and P^{t}BMA arms ($M_n = 59.0$ kg/mol and $M_w/M_n = 1.06$). The DPE function works as a dual-functionalized agent, which provides a linking site at first, followed by an initiation site. Consequently, the two different arm segments could be separately introduced. This means that the 3-arm ABC µ-star polymers can always be synthesized with the use of a chain-end-DPE-functionalized polymer as the starting material. Thus, this methodology combines the "arm-first" termination method to link two polymer chains with the "core-first" initiation method to grow the third arm segment. In the final step, any monomer undergoing the living anionic polymerization with the DPE anion can be used. Because of fewer operation steps and more choices of possible monomers including several cyclic monomers, the methodology has been further developed for the synthesis of various 3-arm µ-star polymers by Abetz et al. [1, 76] and recently Matsushita et al. [2, 77–81]. They used 1-(4-bromomethylphenyl)-1-phenylethylene or 1-(3-(3-chloropropyldimethylsilyl)phenyl)-1-phenylethylene in
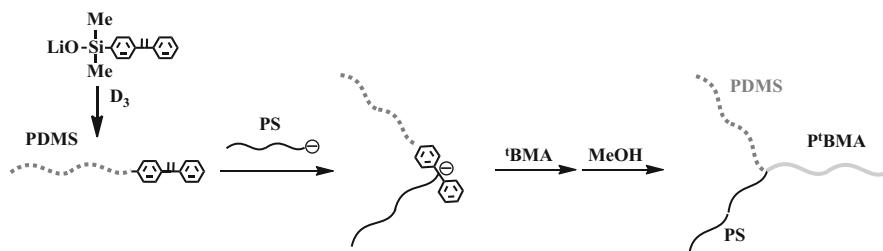
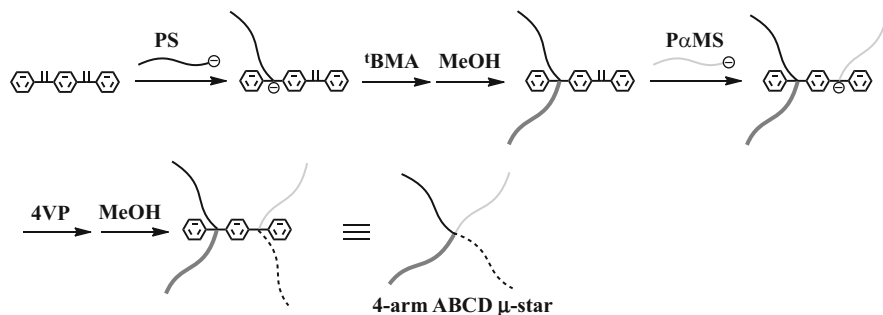**Scheme 14** Synthesis of 3-arm ABC μ-star polymer by the methodology using DPE dual-functionalized reaction site
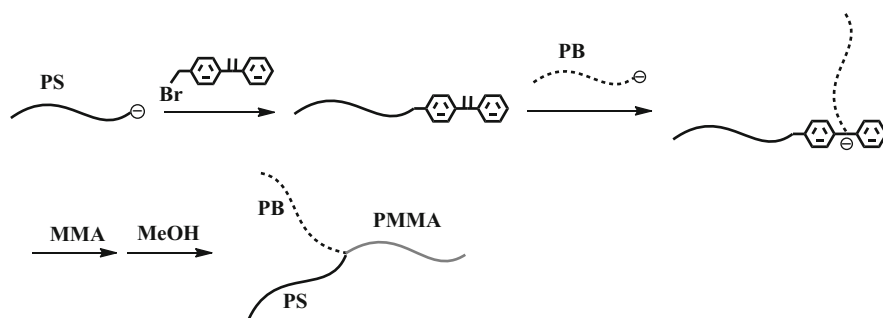
Scheme 15 Synthesis of 3-arm ABC μ-star polymer by the methodology using DPE reaction site

Table 5 Synthesis of 3-arm ABC μ-star polymers by the methodology using DPE reaction site

3-arm ABC μ-star					
A	B	C	M_n (g/mol)	M_w/M_n	lit.
PS	PB	PMMA	250,000	1.13	76
PS	PB	P2VP	96,000	1.01	1
PS	PB	P2VP	288,000	1.04	1
PS	PB	P2VP	134,000	1.04	77
PS	PB	P2VP	199,000	1.04	77
PS	PI	P2VP	154,700	1.02	2
PS	PI	P2VP	192,100	1.02	2
PS	PI	P2VP	241,000	1.03	79
PS	PI	P2VP	401,000	1.04	79

order to introduce the DPE functionality in the starting polymer. Scheme 15 shows the synthesis of the 3-arm ABC μ-star polymer composed of PS, PB, and PMMA arms. Representative μ-star polymers synthesized by this methodology are summarized in Table 5.

It was further reported that several functional DPE derivatives effectively work as the suitable nodules for the synthesis of the μ-star polymers. Quirk et al. synthesized a 4-arm A_2B_2 μ-star polymer by the addition reaction of two
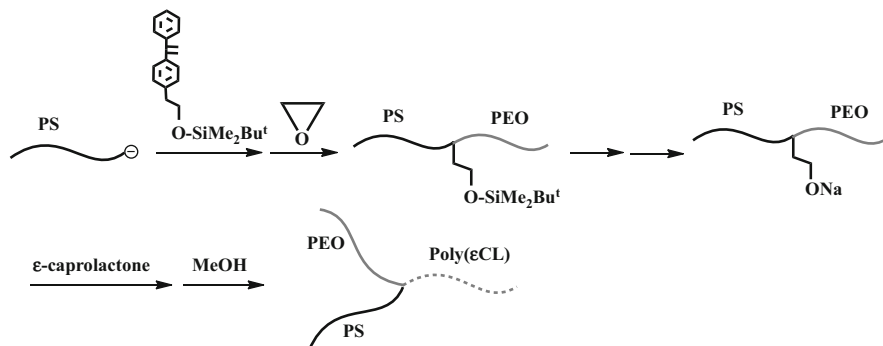
Scheme 16 Synthesis of 4-arm ABCD μ-star polymer by the methodology using two DPE reaction sites

equivalents of PSLi with 1,3-bis(1-phenylethenyl)benzene, which is regarded as a DPE derivative substituted with the DPE function, followed by the polymerization of 1,3-butadiene with the two generated DPE anions ($M_n = 23.4$ kg/mol and $M_w/M_n = 1.05$) [82]. Similarly, another 4-arm A_2B_2 star composed of PS and PMMA arms was synthesized by Young et al. ($M_n = 58.9$ kg/mol and $M_w/M_n = 1.03$) [83]. Quirk et al. also demonstrated the synthesis of a 3-arm AA′A″ star PS composed of three PS arms with different M_n values using 1,4-bis (1-phenylethenyl)benzene [84]. Unlike the reaction of PSLi with the above *meta*-isomer, the PSLi underwent the 1:1 addition reaction with this *para*-isomeric DPE derivative and no more addition occurred due to the delocalization of the generated anion. After quenching with methanol, another PSLi reacted with the resulting chain-end-DPE-functionalized PS, followed by polymerization of the styrene monomer, resulting in the above 3-arm star PS with molecular weight asymmetry. This synthetic success indicates the possible synthesis of 3-arm ABC μ-stars.

He et al. reported that the methodology using the above *para*-isomer allowed access to a 4-arm ABCD μ-star polymer synthesis [85]. The synthesis also takes advantage of the 1:1 addition reaction, as illustrated in Scheme 16. PSLi first reacted with 1,4-bis(1-phenylethenyl)benzene in the 1:1 addition manner, followed by the polymerization of ^{t}BMA with the generated DPE anion. Poly (α-methylstyryl)lithium (PαMSLi) then reacted with the residual DPE moiety to link the PαMS chain, and 4-vinylpyridine (4VP) was subsequently in situ polymerized to grow the fourth arm, resulting in a 4-arm ABCD μ-star composed of PS, P^{t}BMA, PαMS, and P4VP arms ($M_n = 30.0$ kg/mol and $M_w/M_n = 1.05$).

Dumas et al. developed the methodology using 1-(2-*tert*-butyldimethylsilyloxy-yethylplenyl)-1-phenylethylene for the synthesis of different types of 3-arm ABC star polymers [86, 87] (see Scheme 17). PSLi was first reacted with the above DPE derivative, followed by the polymerization of ethylene oxide, to afford the in-chain-functionalized PS-*b*-PEO. The 2-*tert*-butyldimethylsilyloxyethyl group between the two blocks was then deprotected to regenerate the hydroxyl group, which was converted to sodium alkoxide by treatment with Ph$_2$CHNa. The resulting sodium alkoxide function was used as the anionic initiator for the ring-opening
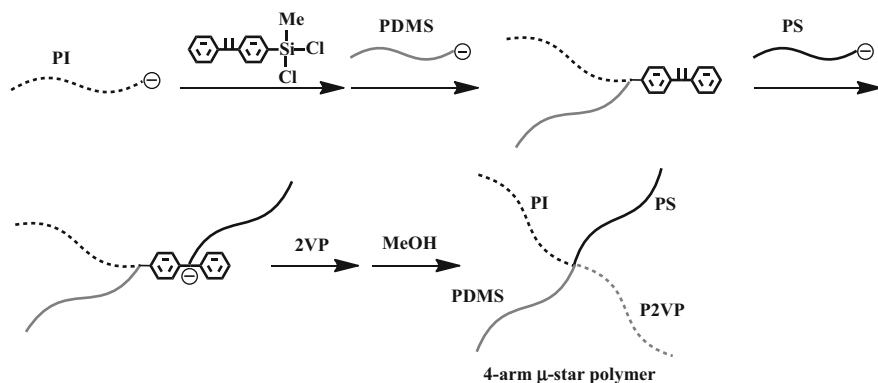
Scheme 17 Synthesis of 3-arm ABC μ-star polymer by the methodology using DPE reaction site
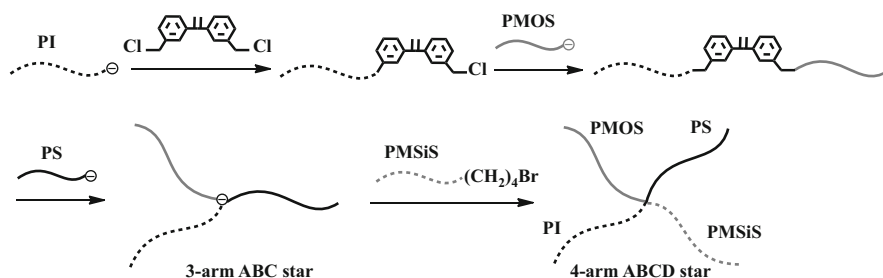
Scheme 18 Synthesis of 3-arm ABC and 4-arm ABCD μ-star polymers by the methodology using DPE reaction site

polymerization of ε-caprolactone, resulting in a 3-arm ABC star composed of PS, PEO, and poly(ε-caprolactone) arms ($M_n = 112$ kg/mol and $M_w/M_n = 1.29$). Similarly, another 3-arm ABC star composed of PS, PEO, and P^{t}BMA arms was synthesized.

Hirao et al. successfully synthesized a 3-arm ABC, followed by a 4-arm ABCD μ-star polymer, by the methodology with 1,1-bis(3-chloromethylphenyl)ethylene, as illustrated in Scheme 18 [88, 89]. A chain-end-(BnCl and DPE)-functionalized PI was first prepared by the reaction of the DPE-end-capped PILi with an excess of the above DPE derivative and subsequently reacted with the DPE-end-capped poly (4-methoxystyryl)lithium (PMOSLi) to prepare an in-chain-DPE-functionalized PI-b-PMOS. A 3-arm ($M_n = 31.8$ kg/mol and $M_w/M_n = 1.03$) was synthesized by reacting PSLi with the resulting DPE-functionalized PI-b-PMOS. The reaction of the intermediate 3-arm ABC star anion formed by the above reaction with a chain-end-(4-bromobutyl)-functionalized poly(4-trimethylsilylstyrene) (PMSiS) yielded a 4-arm ABCD μ-star polymer ($M_n = 43.0$ kg/mol and $M_w/M_n = 1.04$) composed of PI, PMOS, PS, and PMSiS arms. With the use of an in-chain-DPE-functionalized A_2 polymer in place of the in-chain-DPE-functionalized AB diblock copolymer in the above methodology, all possible 3- and 4-arm μ-star polymers including A_2B,
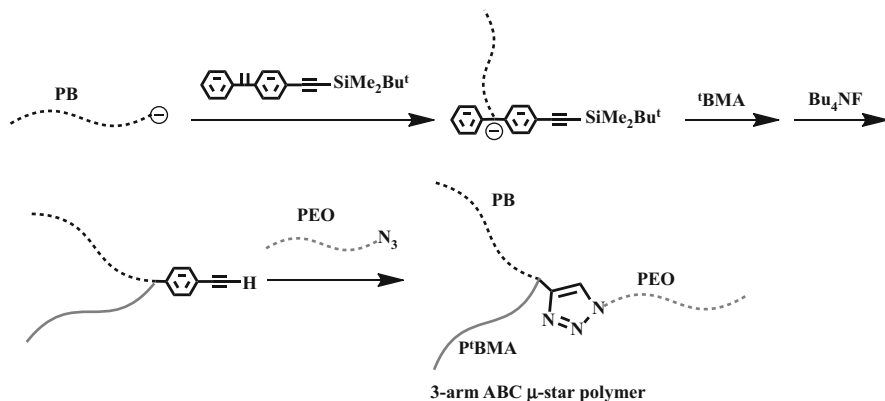
Scheme 19 Synthesis of 4-arm ABCD μ-star polymer by the methodology using chlorosilane and DPE reaction sites

AB$_2$, AB$_3$, A$_2$B$_2$, A$_3$B, A$_2$BC, AB$_2$C, and ABC$_2$ in addition to the ABC and ABCD types were successfully synthesized. The starting in-chain-DPE-functionalized A$_2$ was prepared by reacting two equivalents of a DPE-end-capped living polymer (A) with 1,1-bis(3-chloromethylphenyl)ethylene.

Hadjichristidis et al. successfully synthesized a 4-arm ABCD μ-star polymer by adding the dual functionality of DPE in the methodology with multifunctional chlorosilane compounds [90]. As shown in Scheme 19, 1-(4-dichloromethylsilylphenyl)-1-phenylethylene of a new DPE derivative was used as the key compound and PILi, followed by the living PDMS, was selectively replaced with the two chlorine atoms of this DPE to prepare an in-chain-DPE-functionalized PI-*b*-PDMS. The target 4-arm μ-star polymer was synthesized by the addition reaction of PSLi to the in-chain DPE function and the subsequent polymerization of 2VP with the generated DPE anion ($M_n = 75.9$ kg/mol and $M_w/M_n = 1.06$). A series of 4-arm A$_2$B$_2$, 4-arm A$_2$BC, and 5-arm A$_2$B$_2$C μ-star polymers were also synthesized by the similar methodologies ($M_n = 88.7$, 96.4, 109 kg/mol and $M_w/M_n = 1.05$, 1.02, 1.02). Their A, B, and C arms are PDMS, PS, and PI, respectively.

Recently, Müller et al. reported the methodology by combining a DPE derivative having a protected alkyne functionality with the azide–alkyne Huisgen cycloaddition reaction to synthesize the 3-arm ABC μ-star polymers [91]. As shown in Scheme 20, PBLi reacts with 1-((4-*tert*-butyldimethylsilyl)ethynyl)phenyl-1-phenylethylene, and ^{t}BMA was subsequently polymerized to prepare an in-chain-(ethynyl)-functionalized PB-*b*-P^{t}BMA. A chain-end-N$_3$-functionalized PEO was separately prepared by the anionic ring-opening polymerization, followed by terminating with azido acid chloride, and reacted with the in-chain ethynyl function of PB-*b*-P^{t}BMA to link the PEO chain, resulting in a 3-arm ABC μ-star composed of PB, P^{t}BMA, and PEO arms ($M_n = 32.7$ kg/mol and $M_w/M_n = 1.04$). Other 3-arm star polymers composed of PB, P^{t}BMA, PS and PB, P^{t}BMA, poly(2-*N,N*-dimethylaminoethyl methacrylate) arms were synthesized by the same procedure (M_ns = 20.8–32.5 kg/mol and M_w/M_ns = 1.03–1.11).

Scheme 20 Synthesis of 3-arm ABC μ-star polymer by the methodology using DPE reaction site in conjunction with Click reaction
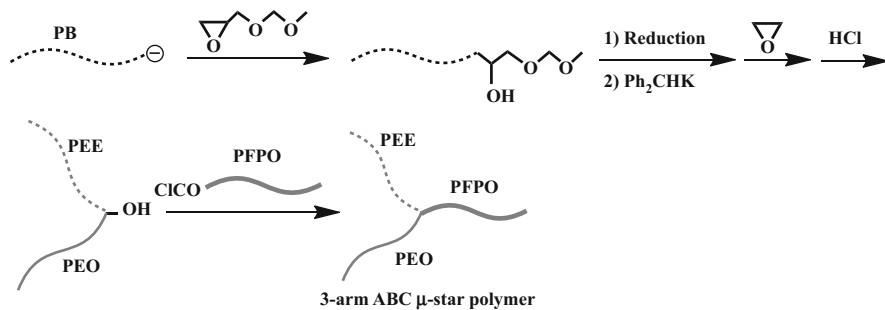
Scheme 21 Synthesis of 3-arm ABC μ-star polymer by the methodology using EO reaction site

Hillmyer et al. developed a new, but basically similar methodology using the dual functionality of the EO derivative in place of the DPE function in order to synthesize two interesting 3-arm ABC star polymers, as illustrated in Scheme 21 [92–94]. The synthesis was started by the reaction of PBLi with methoxymethoxyoxirane to prepare a chain-end-functionalized PB with hydroxyl and acetal-protected hydroxyl functionalities. After catalytic hydrogenation of the PB main chain for conversion to poly(ethylethylene) (PEE), the hydroxyl group was changed to potassium alkoxide, followed by the polymerization of EO to afford an in-chain-OH-functionalized PEE-b-PEO after removal of the acetal protection. Two 3-arm ABC μ-star polymers composed of PEE, PEO, poly(γ-methyl-ε-caprolactone) arms ($M_n = 18.8$ kg/mol and $M_w/M_n = 1.22$) and PEE, PEO, poly(perfluoropropylene oxide) (PFPO) ($M_n = 17.9$ kg/mol and $M_w/M_n = 1.08$) were synthesized by the anionic ring-opening polymerization of γ-methyl-ε-caprolactone and the esterification reaction with a chain-end-(COCl)-functionalized PFPO, respectively.

As often mentioned, the dual-functionalized agent like the DPE and EO derivatives enables the sequential introduction of two of the same or different polymer chains into the core via the linking and initiation sites. Accordingly, if this agent is attached to a

polymer chain in advance, 3-arm ABC μ-star polymers can be synthesized by introducing two different polymer chains via the dual-functionalized reaction sites. If the agent is incorporated between two blocks in the block copolymer, the synthesis of 4-arm ABCD μ-star polymers may be feasible. Furthermore, 3-arm ABC and 4-arm ABCD stars can be synthesized in a similar manner using the DPE derivative having the function(s) capable of linking with other polymer chain(s). The methodologies herein introduced are all based on such mechanisms.

3.3 Methodologies Based on Iterative Strategy

The generality and versatility of the methodologies described above were demonstrated for the effective synthesis of three- and four-component μ-star polymers with well-defined structures. However, these methodologies cannot be used for the synthesis of more component and armed μ-star polymers, since the reaction site (s) always disappears after the introduction of arm(s) in the final stage and thereby the arm can be no longer introduced.

In order to overcome this difficulty, Hirao, Higashihara et al. have proposed a novel methodology, which is based on a new conceptual "*iterative strategy*," since 2001. In this methodology, the reaction system is designed in such a way that the same reaction site is regenerated after the introduction of an arm segment in each reaction sequence and this "arm introduction–regeneration of the same reaction site" sequence is repeatable. Accordingly, the same or different arm segment can be successively and, in principle, limitlessly introduced by repeating the reaction sequence, resulting in the synthesis of a series of many component and armed μ-star polymers. Since a new reaction site is always regenerated for the next reaction stage, several reaction sites selectively worked for the introduction of a number of arms are not needed and the above-mentioned complicated and practically difficult synthetic design can be avoided in this proposed iterative methodology. A variety of iterative methodologies using different reaction sites have been significantly developed based on the same concept and can allow access to a variety of synthetically difficult multiarmed and multicomponent μ-star polymers [10–13, 17, 95, 96].

3.3.1 Iterative Methodologies Using DPE Reaction Site

The first successful iterative methodology, in which a DPE function is used as the reaction site, is illustrated in Scheme 22. At first, a chain-end-DPE-functionalized A was prepared as the starting material by reacting a DPE-end-capped living polymer (A) with 1-(4-(3-bromopropylphenyl))-1-phenylethylene (3) [97]. In the first iterative process, the resulting chain-end-DPE-functionalized A was reacted with another living polymer (B) to link the B chain with the A segment, and a DPE anion was produced at the linking point by the linking reaction. The agent, 3, was then in situ reacted with this DPE anion to reintroduce the DPE function. Thus, the linking
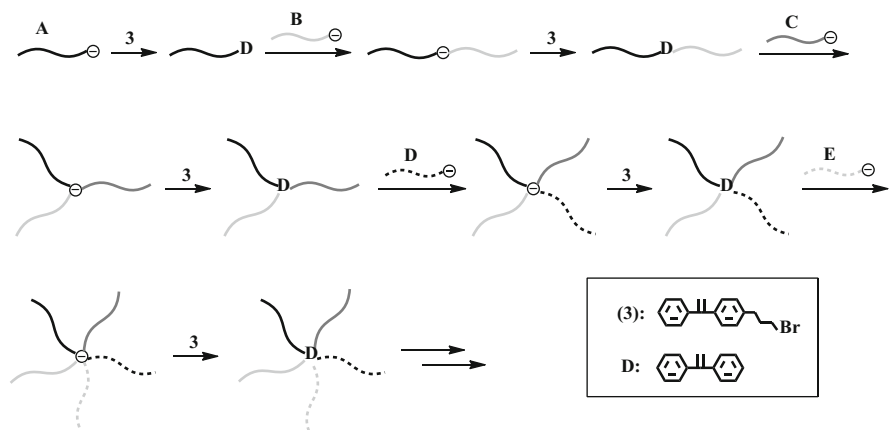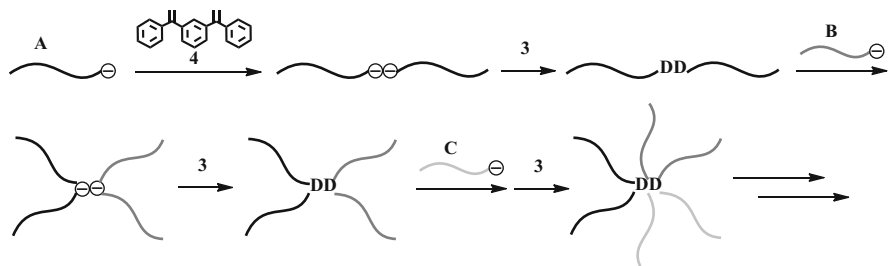
Scheme 22 Iterative methodology using DPE reaction site

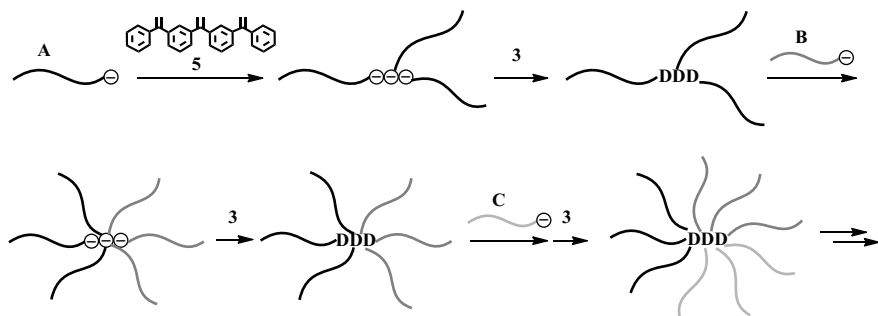**Table 6** Synthesis of μ-star polymers by iterative methodology using DPE reaction site

Polymer	M_n (g/mol)		M_w/M_n
	calcd	SLS	SEC
A	10,500	10,700	1.03
AB diblock	21,300	22,000	1.02
3-arm ABC	32,000	34,400	1.02
4-arm ABCD	42,800	43,000	1.02
5-arm ABCDE	59,300	57,000	1.02

reaction and the reaction of the DPE anion with *3* exactly correspond to "the arm introduction" and "the reaction site regeneration" steps, respectively. Since the resulting A-*b*-B possesses the DPE reaction site introduced between the two blocks, the same reaction process can be repeated. In fact, living polymer (C) reacted with the in-chain-DPE-functionalized A-*b*-B, followed by reacting with *3*, resulting in a 3-arm ABC μ-star polymer core functionalized with the DPE reaction site. By repeating the same process two more times with the sequential uses of living polymers (D) and (E), 4-arm four-component ABCD and 5-arm five-component ABCDE μ-star polymers were successfully synthesized. The DPE reaction site is capable of not only undergoing the linking reaction with a living anionic polymer, but also regenerating the DPE reaction site via the DPE anion produced by the linking reaction. Thus, the dual functionality of the DPE derivative is also utilized in each process of this methodology. Typically, the A, B, C, D, and E arms were the PMSiS, PMOS, PMS, PS, and poly(4-*tert*-butyldimethylsilyloxystyrene) (PTBDMSiOS) segments.

In each process, the two reactions were observed to virtually quantitatively proceed. The resulting μ-star polymers were confirmed by SEC, RALLS, and ^{1}H NMR analyses to be well defined and expected in structure, as listed in Table 6. The final 5-arm ABCDE μ-star polymer is the first successful example composed of five different arms. Hydrolysis of the E arm by treatment with $(C_4H_9)_4NF$ yielded a new 5-arm ABCDE μ-star including an acidic and ionic poly(4-vinylphenol) arm

Scheme 23 Synthesis of μ-star polymers by the iterative methodology with *3* and *4* using DPE reaction site

Scheme 24 Synthesis of μ-star polymers by the iterative methodology with *3* and *5* using DPE reaction site

segment. Since the final polymer possesses the DPE reaction site at the core, the synthesis of μ-stars with more arms and components is expected by further repeating the same process.

With the use of 1,3-bis(1-phenylethenyl)benzene (*4*) in place of DPE in the same iterative methodology, the arm number may increase by two in each iterative process, as illustrated in Scheme 23 [98, 99]. In the first process, two equivalents of a living polymer (A) reacted with *4* to link two A segments (the arm introduction step) and *3* was in situ reacted with the two produced DPE anions to reintroduce two DPE functions (the reaction site regeneration step). Next, the resulting in-chain-(DPE)$_2$-functionalized A$_2$ was reacted with a living polymer (B), followed by the in situ reaction with *3*, and produced a 4-arm A$_2$B$_2$ μ-star polymer core functionalized with two DPE reaction sites. One more repetition of the process using a living polymer (C) gave a 6-arm A$_2$B$_2$C$_2$ μ-star polymer. The A, B, and C arms used were PS, PαMS, PMOS and PS, PαMS, PI.

In the same sense, with the use of 1,1-bis(3-(1-phenylethenyl)phenyl)ethylene (*5*), composed of three DPE skeletons in the same methodology, the number of arms could increase by three in each process, resulting in the 3-arm A$_3$, 6-arm A$_3$B$_3$, and 9-arm A$_3$B$_3$C$_3$ μ-star polymers (see Scheme 24) [100]. Three 9-arm stars composed of PS, PMOS, PI arms, PS, PMOS, PMSiS arms, and PS, PMOS, PTBDMSiOS arms convertible to poly(4-vinylphenyl) segment. Each of these processes in both

Table 7 Synthesis of μ-star polymers by iterative methodology with 3 and 4 or 5 using DPE reaction sites

Polymer	M_n (g/mol)		M_w/M_n
	calcd	SLS	SEC
4-arm A_2B_2	41,100	41,800	1.02
6-arm $A_2B_2C_2$[a]	61,700	62,400	1.02
6-arm $A_2B_2C_2$[b]	34,800	31,800	1.06
6-arm A_3B_3	67,800	66,700	1.03
9-arm $A_3B_3C_3$[c]	97,000	97,100	1.02
9-arm $A_3B_3C_3$[d]	101,000	103,000	1.04
9-arm $A_3B_3C_3$[e]	98,300	97,200	1.03

[a]PS/PαMS/PMOS
[b]PS/PαMS/PI
[c]PS/PMOS/PMSiS
[d]PS/PMOS/PI
[e]PS/PMOS/PTBDMSiOS
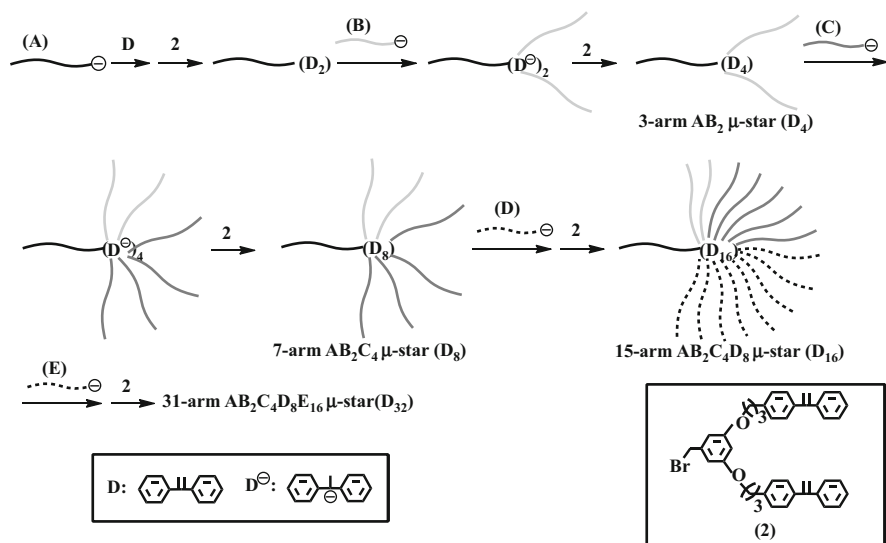
Scheme 25 Synthesis of multiarmed μ-star polymers with up to five components by the iterative methodology with *2* using DPE reaction sites

methodologies efficiently proceeded to afford well-defined μ-star polymers in almost 100 % yields. Their characterization results are listed in Table 7.

As mentioned in section "Arm-first termination methodology using DPE reaction site," it was possible to significantly increase the number of arm segments in each process using 3,5-bis(3-(4-(1-phenylethenyl)phenyl)propoxy)benzyl bromide (*2*) having two DPE and one BnBr functions [56]. This agent, *2*, is designed so as to regenerate the two DPE reaction sites via one DPE anion produced by the arm introduction step. As illustrated in Scheme 25 similar to Scheme 10, a DPE-end-capped living polymer (A) reacts with *2* to prepare a chain-end-(DPE)$_2$-functionalized A as the starting polymer. In the first process, two equivalents of a

Table 8 Synthesis of μ-star polymers by the iterative methodology with 2 using DPE reaction sites

| Polymer	M_n (g/mol)		M_w/M_n
	calcd	SLS	SEC
3-arm AB_2	32,100	35,700	1.02
7-arm AB_2C_4	77,000	79,200	1.02
15-arm $AB_2C_4D_8$	162,000	172,000	1.02
31-arm $AB_2C_4D_8E_{16}$[a]	339,000	363,000	1.02

[a]PS/PαMS/PMS/MOS/PMSiS

living polymer (B) reacted with the two DPE reaction sites of the starting polymer to link two B segments with the A chain and *2* was in situ reacted with two DPE anions produced by the linking reaction. As a consequence, a 3-arm AB_2 star was obtained and, importantly, four DPE reaction sites were regenerated at the core. Similarly, repetition of the same process three more times with the sequential uses of living polymers (C), (D), and (E) quantitatively yielded the 7-arm AB_2C_4, 15-arm $AB_2C_4D_8$, and even 31-arm $AB_2C_4D_8E_{16}$ μ-star polymers. The resulting polymers were all confirmed to be well-defined and expected structures, as listed in Table 8. The regeneration of 8, 16, and 32 DPE reaction sites was confirmed by ^{1}H NMR. Thus, the number of arms significantly increases by repeating the process according to the equation, $f = 2^{(n+1)} - 1$ (f and n are the arm and iterative process numbers, respectively).

Thus, the methodology using *2* allows readily, access to multiarmed μ-star polymers with up to 31 arms and possibly more arms. However, the synthetic variation of the μ-star polymers with more than 10 arms is limited only to 15 and 31 arms due to the rapid divergence of the number of arms. Recently, Higashihara et al. proposed to alternatively use *2* and *3* in each of the reaction site regeneration steps, with which the number of synthetically possible μ-star polymers can exponentially increase to 2, 4 (2^2), 8 (2^3), and 16 (2^4) by repeating the process four times, as illustrated in Scheme 26 [101]. After the completion of the fourth iterative process, a total of 30 ($2 + 4 + 8 + 16$) μ-star polymers can be synthesized, while the methodology using *2* yields only five polymers even after the fifth process.

The synthesis was initiated in order to prepare a chain-end-$(DPE)_2$-fuctionalized A by reacting the living polymer (A) with *2*. During the first iteration, a linking reaction of the $(DPE)_2$-functionalized A with a living polymer (B) was followed by reacting either *3* or *2*, affording two kinds of 3-arm AB_2 star polymers core functionalized two and four DPE reaction sites, which were abbreviated as 3-arm $AB_2(DPE)_2$ and 3-arm $AB_2(DPE)_4$, respectively. During the second iteration, a living polymer (C) reacted with either the 3-arm $AB_2(DPE)_2$ or 3-arm $AB_2(DPE)_4$ and *3* or *2* was in situ reacted to either of the resulting two polymer anions. The following four μ-star polymers were produced: 5-arm $AB_2C_2(DPE)_2$, 5-arm $AB_2C_2(DPE)_4$, 7-arm $AB_2C_4(DPE)_4$, and 7-arm $AB_2C_4(DPE)_8$. During the third iteration, the same process using a living polymer (D) was repeated to synthesize the eight stars as follows: 7-arm $AB_2C_2D_2(DPE)_2$, 7-arm $AB_2C_2D_2(DPE)_4$, 9-arm $AB_2C_2D_4(DPE)_4$, 9-arm $AB_2C_2D_4(DPE)_8$, 11-arm $AB_2C_4D_4(DPE)_4$, 11-arm $AB_2C_4D_4(DPE)_8$, 15-arm $AB_2C_4D_8(DPE)_8$, and 15-arm $AB_2C_4D_8(DPE)_{16}$. Furthermore, 16 five-component μ-stars could be synthesized by repeating the same
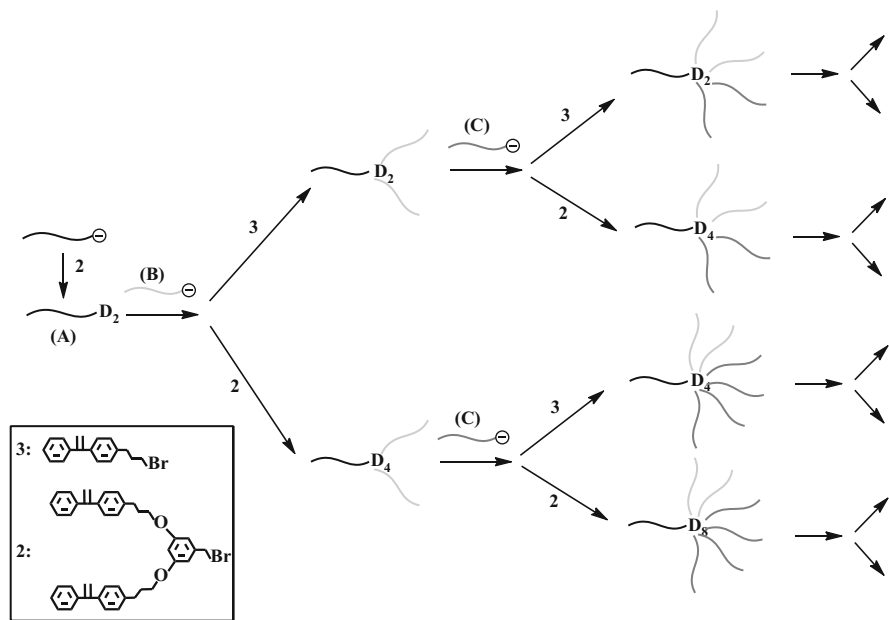
Scheme 26 Synthesis of μ-star polymers by the iterative methodology with an alternative choice of *2* and *3* using DPE reaction sites

process using a living polymer (E) as follows: 9-arm $AB_2C_2D_2E_2(DPE)_2$, 9-arm $AB_2C_2D_2E_2(DPE)_4$, 11-arm $AB_2C_2D_2E_4(DPE)_4$, 11-arm $AB_2C_2D_2E_4(DPE)_8$, 13-arm $AB_2C_2D_4E_4(DPE)_4$, 13-arm $AB_2C_2D_4E_4(DPE)_8$, 15-arm $AB_2C_4D_4E_4(DPE)_4$, 15-arm $AB_2C_4D_4E_4(DPE)_8$, 17-arm $AB_2C_2D_4E_8(DPE)_8$, 17-arm $AB_2C_2D_4E_8(DPE)_{16}$, 19-arm $AB_2C_4D_4E_8(DPE)_8$, 19-arm $AB_2C_4D_4E_8(DPE)_{16}$, 23-arm $AB_2C_4D_8E_8(DPE)_8$, 23-arm $AB_2C_4D_8E_8(DPE)_{16}$, 31-arm $AB_2C_4D_8E_{16}(DPE)_{16}$, and 31-arm $AB_2C_4D_8E_{16}(DPE)_{32}$.

Among them, 22 μ-star polymers were actually synthesized. The polymers obtained by this methodology were all well defined in structure and narrowly distributed in molecular weight distribution. The representative results of μ-star polymers with more than 9 arms are listed in Table 9. Thus, it is quite surprising that the alternative use of *3* and *2* in the reaction site regeneration step enables the synthetic range of μ-star polymers to be significantly broadened.

In all of the iterative methodologies herein developed, the living anionic polymers of styrene and its derivatives are used in order to react with the DPE reaction site(s) to continue the next process. The living anionic polymers of 1,3-butadiene, isoprene, and certain functional 1,3-diene monomers can also be used in these methodologies. Thus, almost all possible multiarmed and multicomponent μ-star polymers composed of such polymer segments are now available.

It is also possible to use 2- and 4-vinylpyridines, alkyl methacrylate monomers, and other vinyl and cyclic monomers that undergo the living anionic polymerization with the DPE anion(s) in the final step of each process. However, once these

Table 9 Synthesis of μ-star polymers by the iterative methodology with 2 and 3 using DPE reaction sites

| Polymer (DPE number)	M_n (g/mol)		M_w/M_n
	calcd	SLS	SEC
9-arm $AB_2C_2D_4(4)$	98,400	100,000	1.05
9-arm $AB_2C_2D_4(8)$	98,200	106,000	1.02
9-arm $AB_2C_2D_2E_4(2)$	87,500	92,900	1.05
11-arm $AB_2C_4D_4(4)$	116,000	119,000	1.05
11-arm $AB_2C_4D_4(8)$	118,000	121,000	1.02
11-arm $AB_2C_2D_2E_4(4)$	116,000	109,000	1.04
13-arm $AB_2C_2D_2E_4(4)$	136,000	150,000	1.04
15-arm $AB_2C_4D_8(8)$	159,000	163,000	1.05
15-arm $AB_2C_4D_8(16)$	159,000	168,000	1.04
15-arm $AB_2C_4D_4E_4(4)$	158,000	154,000	1.02
17-arm $AB_2C_2D_4E_8(8)$	171,000	178,000	1.04
19-arm $AB_2C_4D_4E_8(8)$	188,000	181,000	1.04
23-arm $AB_2C_4D_8E_8(8)$	243,000	260,000	1.04
31-arm $AB_2C_4D_8E_{16}(32)^a$	332,000	356,000	1.02

[a]PS/PαMS/PMS/PMOS/PMSiS

monomers are used, the iterative process can no longer be continued due to loss of the reaction site(s). Unfortunately, their living anionic polymers are not employed in each process due to the lack of reactivity toward the DPE reaction site(s).

3.3.2 Iterative Methodology Using 2-Alkyl-1,3-Butadiene Reaction Site

As mentioned in section "Iterative methodologies using DPE reaction site," the key in the iterative methodology is the dual-functional ability of the DPE reaction site which provides a linking site with a living anionic polymer as well as the same DPE reaction site via the DPE anion produced by the linking reaction. This ability of DPE reaction site makes it possible to carry out both steps (arm introduction and regeneration of reaction site) essential for the iterative methodology. Hirao et al. have found that a 1,3-butadiene (Bd) function attached to the PS chain-end via the 2-position shows the same dual-functionalized ability [102]. For example, PSLi reacted with the Bd terminus in PS in a 1:1 addition manner to link the two PS chains (the arm introduction step) and the PS chain-end anion was converted to a 1,3-butadienyl anion (Bd anion). The same Bd function was reintroduced by reacting in situ the produced Bd anion with 6-bromo-3-methylene-1-hexene (*6*) (the reaction site regeneration step). Somewhat surprisingly, neither polymerization nor even oligomerization of the Bd terminus occurred using a 1.5-fold excess of PSLi toward the Bd function in THF at −78 °C for 24 h. These experimental proofs strongly indicate the possible use of the Bd function in the iterative methodology.

As shown in Scheme 27, the methodology with the Bd reaction site is basically the same as that using the DPE reaction site [103]. The synthesis was started from the preparation of a chain-end-Bd-functionalized PS by reacting a DPE-end-capped
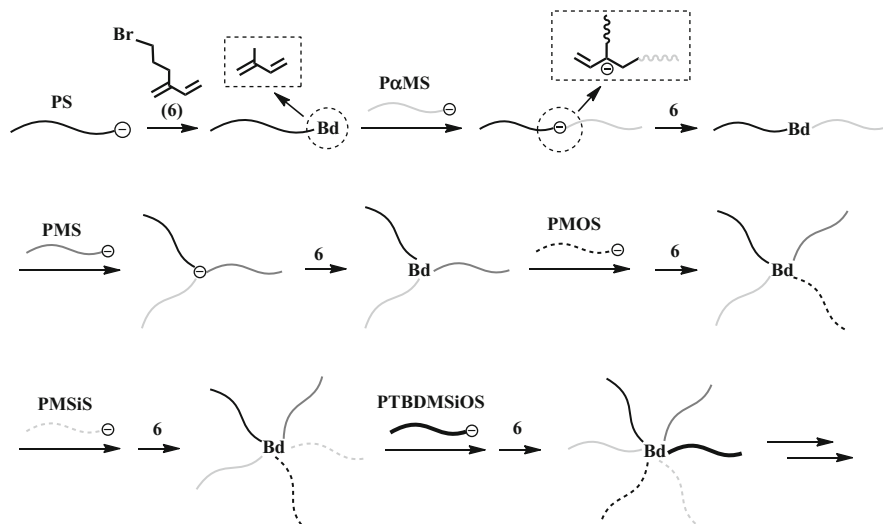
Scheme 27 Synthesis of μ-star polymers up to 6-arm ABCDEF type by the iterative methodology using Bd reaction site

PSLi with *6*. In the first iterative process, PαMSLi reacted with the Bd-functionalized PS, followed by reacting with *6*, to yield an in-chain-Bd-functionalized PS-*b*-PαMS. By conducting the next process using PMSLi, a 3-arm ABC μ-star polymer core functionalized with the Bd reaction site was synthesized. Since the Bd-functionalized AB diblock copolymer and the core-Bd-functionalized 3-arm ABC star were obtained in almost 100 % yields, it is obvious that both the arm introduction and reaction site regeneration steps satisfactorily work via the Bd reaction site. Furthermore, 4-arm ABCD, 5-arm ABCDE, and even 6-arm ABCDEF μ-star polymers were successively synthesized by repetition of the same process three more times. The A, B, C, D, E, and F arms correspond to the PS, PαMS, PMS, PMOS, PMSiS, and PTBDMSiOS (convertible to poly (4-vinylphenol)) segments. As evidenced in Table 10, all of the resulting polymers were confirmed by SEC, RALLS, and ^{1}H NMR analyses to be well defined and expected in structure. The successful use of Bd reaction site is thus obvious in the iterative methodology.

An additional advantage of the Bd reaction site is the quantitative conversion to highly reactive and synthetically useful anhydride and two epoxide functions by the Diels-Alder and oxidation reactions, as shown in Scheme 28 [102, 104].

3.3.3 Iterative Methodologies Using α-Phenylacrylate Reaction Site

The two iterative methodologies using the DPE and Bd reaction sites demonstrate the successful synthesis of a variety of new μ-star polymers. This is undoubtedly attributed to the quantitative linking reactions of such reaction sites with highly

Table 10 Synthesis of μ-star polymers by the iterative methodology using Bd reaction site

Polymer	M_n (g/mol)		M_w/M_n
	calcd	SLS	SEC
A homopolymer	11,200	11,500	1.03
AB diblock copolymer	24,200	25,300	1.04
3-arm ABC	34,800	35,900	1.01
4-arm ABCD	47,100	47,200	1.01
5-arm ABCDE	58,800	58,500	1.02
6-arm ABCDEF[a]	71,800	71,500	1.03

[a]PS/PαMS/PMS/PMOS/PMSiS/PTBDMSiOS

Scheme 28 Preparation of chain-end-anhydride-functionalized or chain-end-two epoxides-functionalized PS by the Diels-Alder or oxidation reaction of chain-end-Bd-functionalized PS
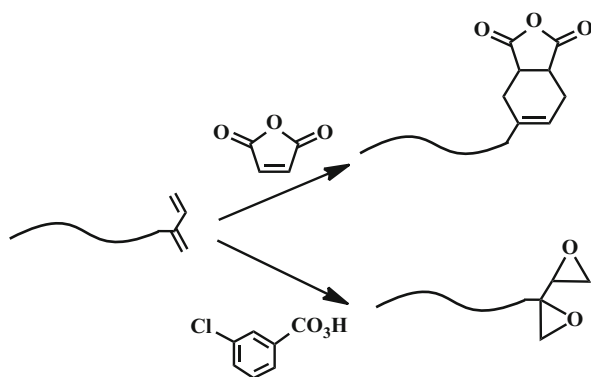
reactive living anionic polymers of styrene, 1,3-butadiene, isoprene, and their derivatives. On the other hand, the living anionic polymers of 2VP and alkyl methacrylates (RMAs) cannot be applied to these iterative methodologies because their chain-end anions are too low in nucleophilicity to react with the DPE and Bd reaction sites.

In order to overcome this difficulty, we have newly developed an α-phenylacrylate (PA) function as the reaction site in the iterative methodology [13, 17, 95, 96, 105]. Since the C=C bond of PA is activated by the ester carbonyl electron-withdrawing character, the PA function is considered to show a higher reactivity toward anionic species than the DPE and Bd functions. Furthermore, a sterically bulky α-phenyl substituent may prevent further addition reactions of the PA function leading to oligomerization and polymerization. In practice, it was observed that the PA reaction site at the polymer chain-end undergoes a 1:1 addition reaction with either the living P2VP or PRMA to link the two polymer chains in THF at low temperatures in the range from −20 to −78 °C. No more addition reactions occurred at all under such conditions. Unfortunately, however, several attempts were unsuccessful to find a suitable reaction to regenerate the PA function, because the enolate anion produced from the PA function was neither stable nor reactive. Accordingly, another route via a hydroxyl group for the regeneration of the PA reaction site is proposed, as illustrated in Scheme 29 [106].

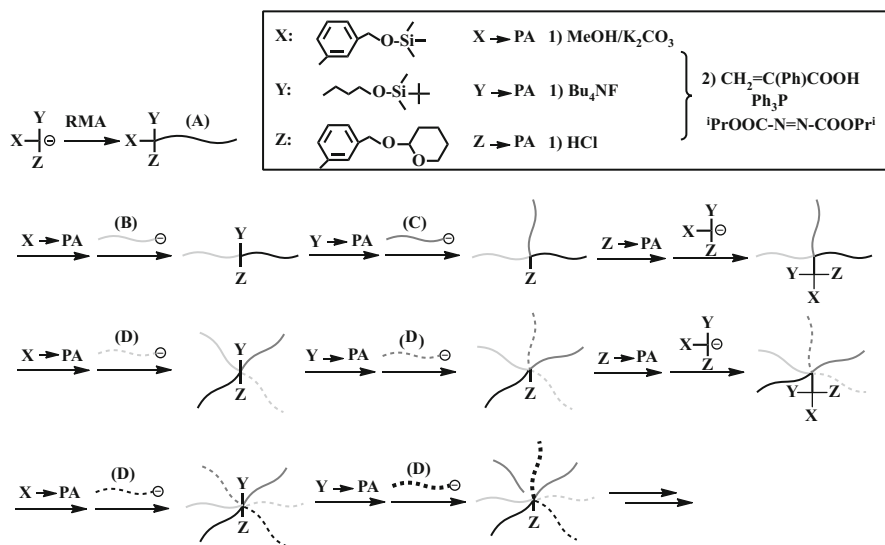**Scheme 29** Synthesis of μ-star polymers by the iterative methodology using PA reaction site

In the proposed methodology, a new DPE derivative substituted with trimethylsilyl (TMS), and *tert*-butyldimethylsilyl (TBDMS) ethers, *7*, is used as the key agent. The two silyl ethers are converted to the PA reaction sites in turn for the arm introduction and reaction site regeneration in each process. A chain-end-(TMS and TBDMS ethers)-functionalized polymer (A) was first prepared as the starting polymer by the polymerization of a certain methacrylate monomer with a DPE anion having TMS and TBDMS ethers prepared from *7* and *sec*-BuLi. The TMS ether was then converted to the first PA reaction site by treatment with methanol containing K_2CO_3 and the subsequent Mitsunobu esterification reaction with α-phenylacrylic acid. Under such conditions, the TBDMS ether remained completely intact. The PA reaction site was reacted with the living polymer (B) to link the B chain to the A segment, resulting in an in-chain-(TBDMS ether)-functionalized A-*b*-B. Next, the TBDMS ether was deprotected with $(C_4H_9)_4NF$, followed by the same esterification with α-phenylacrylic acid to convert to the second PA reaction site. The PA reaction site was then reacted with the DPE anion having TMS and TBDMS ethers to reintroduce both the TMS and TBDMS ethers.

Since the two silyl ethers are the same as those introduced in the starting polymer (A), the above process can be repeated. In fact, it could be repeated three more times by progressively reacting living polymers (C), (D), and (E) to successively synthesize the μ-star polymers with up to five arms. Thus, the TMS ether was converted to the first PA reaction site, which was used for the arm introduction, while the second PA was prepared from TBDMS ether in the same manner for the reintroduction of both the TMS and TBDMS ethers to repeat the same process. Typically, the A, B, C, D, and E arms are PMMA, poly(ethyl methacrylate) (PEMA), P^{t}BMA, poly(benzyl methacrylate) (PBnMA), and poly(2-methoxyethyl methacrylate) (PMOEMA), respectively. The results are summarized in Table 11.

Table 11 Synthesis of μ-star polymers by the iterative methodology using PA reaction site

Polymer	M_n (g/mol)		M_w/M_n
	calcd	SLS	SEC
3-arm ABC	32,200	33,800	1.03
4-arm ABCD	43,400	43,000	1.03
5-arm ABCDE[a]	52,000	51,500	1.03
5-arm ABCDE[b]	52,700	50,200	1.04

[a]PMMA/PEMA/P^{t}BMA/PBnMA/PMOEMA
[b]PS/PMMA/P^{t}BMA/PMS/PBnMA

2-*tert*-Butyldimethylsilyloxyethyl methacrylate (Si-HEMA), (2,2-dimethyl-1,3-dioxolan-4-yl)methyl methacrylate (acetal-DHPMA), and ferrocenylmethyl methacrylate (PFMMA) were also introduced as the arm segments. The first two polymers are readily converted to hydrophilic poly(2-hydroxyethyl methacrylate) (PHEMA) and water-soluble poly(2,3-dihydroxypropyl methacrylate) (PDHPMA) segments by deprotection of the silyl and acetal groups. The resulting 3-arm ABC, 4-arm ABCD, and 5-arm ABCDE stars were the first successful μ-star polymers composed of all different poly(methacrylate)-based arm segments. The living anionic polymers of styrene, 1,3-butadiene, isoprene, and 2VP can also be used in this methodology because the PA reaction site could be quantitatively reacted with these more reactive living anionic polymers. Thus, a wide variety of living anionic polymers with different reactivities can advantageously be employed for the PA reaction site during the iterative methodology, which makes it more general and versatile.

A more efficient iterative methodology using a new trifunctional DPE anion as the key agent was also proposed, as illustrated in Scheme 30 [107]. The trifunctional DPE anion having TMS, TBDMS, and THP ethers is prepared by reacting 3-(*tert*-butyldimethylsilyloxy)-1-propyllithium (TBDMS-PLi) with a DPE derivative substituted with TMS and THP ethers. These three ethers are designed so as to be selectively deprotected in turn to regenerate hydroxyl groups under carefully selected conditions. The hydroxyl groups are then converted step by step to three PA reaction sites by different reaction stages. The two PA reaction sites among them were used for the introduction of two different arms, while the third one was used to reintroduce the three different ethers by reacting the trifunctional DPE anion to continue the methodology.

The trifunctional DPE anion was prepared by reacting TBDMS-PLi with the DPE derivative substituted with TMS and THP ethers and used as an initiator in the polymerization of a certain methacrylate monomer to introduce the three ethers at the initiating chain end of polymer (A). The TMS ether was selectively removed, followed by conversion to the first PA reaction site. The living polymer (B) reacted with the PA reaction site to link the B chain to the A segment, resulting in an in-chain-(TBDMS and THP ethers)-functionalized A-*b*-B. The TBDMS ether was then selectively deprotected and converted to the second PA reaction site. A 3-arm ABC μ-star was obtained by reacting living polymer (C) with the PA reaction site. The THP ether that remained at the core was then converted to the third PA reaction site, followed by reacting the trifunctional DPE anion with the PA reaction site. Thus, the three different ethers were reintroduced into the core.

Scheme 30 Synthesis of μ-star polymers by the iterative methodology with trifunctional Li reagent using PA reaction site

Since the three ether functions were exactly the same as those in the starting polymer (A), the same process using two living polymers, (D) and (E), could be repeated. As a consequence, a core-(TMS, TBDMS, and THP ethers)-functionalized 5-arm ABCDE μ-star polymer could be synthesized. One more repetition yielded a 7-arm ABCDEFG μ-star polymer. Since the three ether functions are reintroduced at the core, μ-stars with more arms and components may possibly be synthesized by repeating the process.

The synthetic key in this methodology is the selective and progressive deprotection of TMS, TBDMS, and THP ethers at each reaction stage. The TMS ether was removed in methanol containing a small amount of K_2CO_3. Both the TBDMS and THP ethers were completely stable under such conditions. The TBDMS ether was selectively deprotected by $(C_4H_9)_4NF$ in the presence of the THP ether. In the μ-star polymer consisting of the PBnMA arm, the addition of phenol equal to $(C_4H_9)_4NF$ in amount is needed to prevent the hydrolysis of the benzyl ester function. Finally, the THP ether was readily and quantitatively cleaved by treatment with 0.2 N HCl. Thus, the selective deprotection of TMS, TBDMS, and THP ethers in this order was successfully carried out in each of all three processes by the above careful treatments. The resulting polymers are all observed to be well defined in structure and architecture, as summarized in Table 12. In addition to the less reactive living PRMAs and P2VP, highly reactive living polymers of styrene, 1,3-diene monomers, and their derivatives are usable in this methodology using the PA reaction site similar to the first methodology shown in Scheme 29.

Table 12 Synthesis of μ-star polymers having up to 7-arm ABCDEFG type by the iterative methodology with a trifunctional reagent using PA reaction site

Polymer	M_n (g/mol)		M_w/M_n
	calcd	SLS	SEC
4-arm ABCD[a]	43,200	43,200	1.03
4-arm ABCD[b]	80,900	80,000	1.04
3-arm ABC	35,000	34,900	1.03
4-arm ABCD	45,900	47,100	1.03
5-arm ABCDE	56,600	53,500	1.04
6-arm ABCDEF	62,800	64,900	1.05
7-arm ABCDEFG[c]	73,800	74,200	1.04

[a]Poly(cyclohexyl methacrylate)/PMMA/PBnMA/PMOEMA
[b]Poly(allyl methacrylate)/PS/PMOEMA/P2VP
[c]Poly(cyclohexyll   methacrylate)/PS/PMOS/PMS/PMMA/
PEMA/PMOEMA
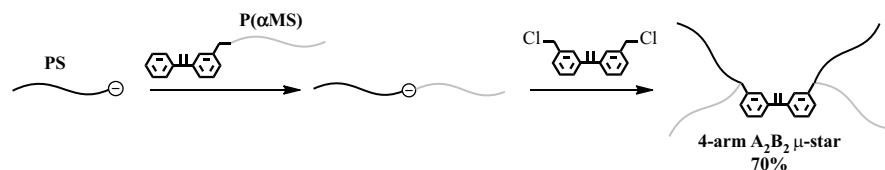
Scheme 31 Synthesis of 4-arm A_2B_2 μ-star polymer by the reaction of in-chain-(DPE anion)-functionalized AB diblock copolymer with *8*

A series of μ-star polymers with up to 7 arms and 7 components were successfully synthesized by repeating the process three times. On the other hand, the six iterative processes are required to synthesize the same 7-arm μ-star polymer by the first methodology. Accordingly, the success of the proposed second methodology makes it possible to synthesize multiarmed and multicomponent μ-star polymers by fewer processes. The universality of the PA reaction site is thus obvious as compared to the DPE reaction site.

3.3.4 Iterative Methodologies Using Intermediate Polymer Anions

In this section, a new iterative methodology based on a different molecular design illustrated in Scheme 31 is proposed [108]. In the methodology, the star polymer synthesis was started from an in-chain-(DPE anion)-functionalized AB diblock copolymer, which was prepared by the reaction of PSLi with a chain-end-DPE-functionalized PαMS. The in situ reaction of the diblock copolymer anion thus prepared with 1,1-bis(3-chloromethylphenyl)ethylene (*8*) yielded a 4-arm A_2B_2 μ-star polymer ($M_n = 45,000$ g/mol) in one pot in THF at $-78\ °C$ for 1 h. Since the resulting star possessed a DPE reaction site convertible to the DPE anion, both the arm introduction and the reaction site regeneration steps essential in the iterative methodology were achieved at the same time in this first iterative process. However, the polymer yield was 70 % and could not be improved by taking a longer
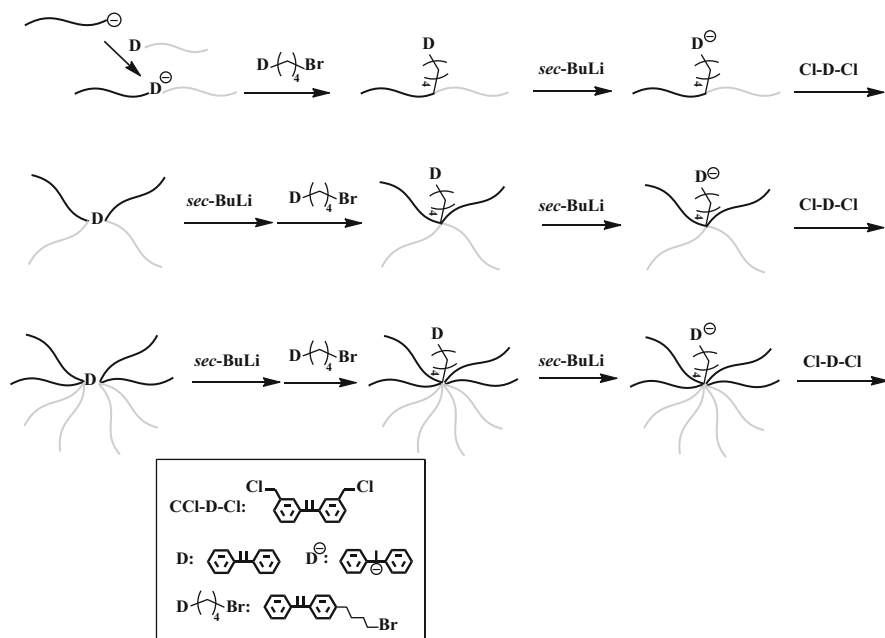
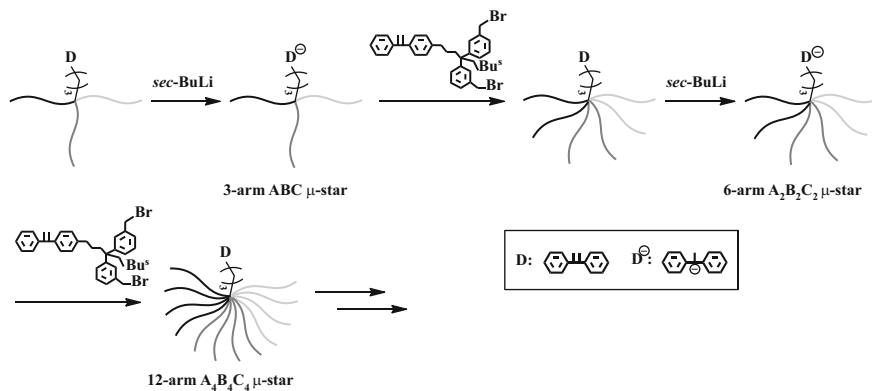**Scheme 32** Synthesis of μ-star polymers by the improved iterative methodology

Table 13 Synthesis of μ-star polymers by the improved iterative methodology using intermediate polymer anion

Polymer	M_n (g/mol)		M_w/M_n
	calcd	SLS	SEC
AB diblock copolymer	22,100	23,200	1.03
4-arm A_2B_2	46,600	48,300	1.03
8-arm A_4B_4	99,000	108,000	1.04
16-arm A_8B_8[a]	208,000	199,000	1.02

[a]PS/PαMS

reaction time of 24 h. The insufficient coupling efficiency is undoubtedly attributed to the steric hindrance around the DPE anions.

In order to reduce the steric hindering effect and improve the polymer yield, one more reaction step was added in each process as shown in Scheme 32. The DPE anion once produced was in situ reacted with 1-(4-(4-bromobutylphenyl))-1-phenylethylene (*9*) to reintroduce the DPE reaction site, which was separated by four methylene chains from the core. The reintroduced DPE was again converted to the DPE anion by treatment with *sec*-BuLi and in situ used in the coupling reaction with *8*. This treatment was effective in improving the polymer yield. Almost quantitative yields of the 4-arm A_2B_2 and 8-arm A_4B_4 stars were realized in THF at $-78\ °C$ within 1 h. A 16-arm A_8B_8 μ-star polymer could also be efficiently synthesized, but the yield was 70 % even after 24 h (Table 13). As expected, the coupling reaction during the fourth iterative process was difficult, resulting in a 32-arm $A_{16}B_{16}$ μ-star polymer in less than 5 % yield.

Scheme 33 Synthesis of μ-star polymers by the iterative methodology using intermediate μ-star polymer anion and *10*

The similar iterative methodology was next carried out using a core-DPE-functionalized 3-arm ABC μ-star polymer in order to synthesize multiarmed three-component μ-star polymers [109]. As illustrated in Scheme 33, the DPE reaction site was always separated by three methylene chains from the core to reduce the steric hindrance similar to the case using in-chain-DPE-functionalized AB diblock copolymer mentioned above. Furthermore, a new agent, 1-(4-(5,5-bis (3-bromomethylphenyl)-7-methylnonyl)phenyl-1-phenylethylene (*10*) having two more reactive BnBr functions, was used as the coupling agent in place of *8*. The starting core-DPE-functionalized 3-arm ABC μ-star polymer was prepared by the reaction of an in-chain-DPE-functionalized PS-*b*-PαMS with PMSLi, followed by in situ reacting with *3*. A target 6-arm $A_2B_2C_2$ μ-star polymer was successfully obtained in 100 % yield in the first process. By repeating the reaction sequence in the second process, a 12-arm $A_4B_4C_4$ μ-star polymer could also be obtained. However, the yield was reduced to 70 %. As expected, the coupling reaction for the synthesis of the 24-arm $A_8B_8C_8$ star in the next process was observed to take place only to a very small extent. By changing the component from PS, PαMS, and PMS to PS, PαMS, and PI in the μ-star polymer, the same iterative methodology was performed under the same conditions. Again, a 6-arm $A_2B_2C_2$ star was quantitatively synthesized, but a 12-arm $A_4B_4C_4$ was obtained in 65 % yield. With the use of a 3-arm A_2B μ-star polymer, a 6-arm A_4B_2 m-star (100 %) and a 12-arm A_8B_4 m-star (75 %) were synthesized by the same methodology. The results are listed in Table 14.

The iterative methodology herein shown is of great value to obtain the synthetically difficult μ-star polymers, such as 6-arm A_4B_2, 6-arm $A_2B_2C_2$, 12-arm A_8B_4, and 12-arm $A_4B_4C_4$ types. The occurrence of the coupling reaction between high-molecular-weight polymers ($M_n \sim 70,000$ g/mol) at a very low temperature of -78 °C is somewhat surprising. However, the increase in both the steric hindrance and molecular weight by repeating the process renders the coupling reactions yielding more armed stars significantly difficult.
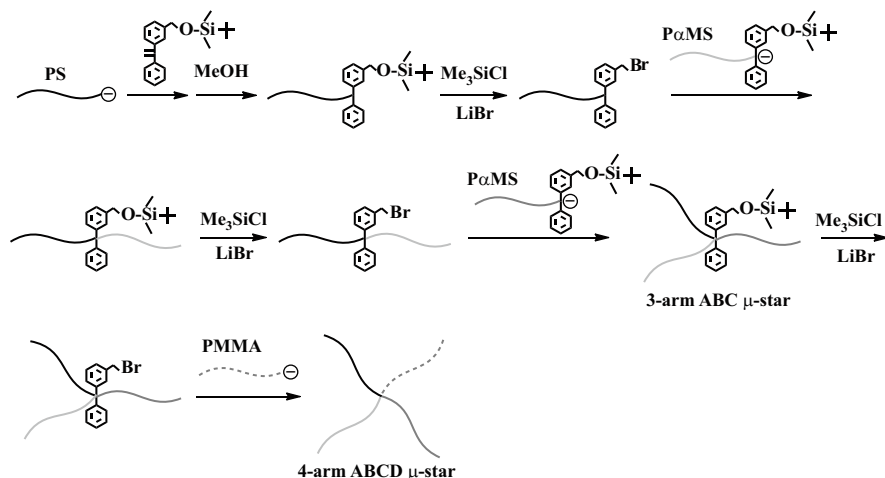
Table 14 Synthesis of μ-star polymers by the iterative methodology using intermediate 3-arm μ-star polymer anion and 10

Polymer	M_n (g/mol)		M_w/M_n
	calcd	SLS	SEC
3-arm ABC	32,000	33,400	1.02
6-arm $A_2B_2C_2$	67,100	66,600	1.02
12-arm $A_4B_4C_4$[a]	134,000	134,000	1.02
3-arm A_2B	36,300	35,300	1.03
6-arm A_4B_2	72,600	73,500	1.03
12-arm A_8B_4[b]	145,000	148,000	1.03

[a]PS/PαMS/PMS
[b]PS/PI

3.3.5 Iterative Methodologies Using BnBr Reaction Site

As already mentioned, the BnBr function was observed to quantitatively react with a variety of living anionic polymers with different reactivities under carefully selected conditions. For example, a highly reactive living polymer of styrene, 1,3-butadiene or isoprene is first end-capped with DPE, followed by a coupling reaction with the BnBr function in THF at −78 °C. Under the same conditions, less reactive living polymers of 2VP and RMA are able to directly react with the BnBr function. The use of a 1.2-fold excess of these living polymers for the BnBr function was sufficient to go to completion in the reaction. An iterative methodology using the BnBr function as a reaction site was also developed, as illustrated in Scheme 34 [110]. The reaction design is somewhat different from those of the methodologies using the DPE, Bd, and PA reaction sites, since the transformation reaction of the 3-*tert*-butyldimethylsilyloxymethylphenyl (TBDMSOMP) group into the BnBr function is employed as the reaction site regeneration step. At first PSLi reacted with 1-(3-*tert*-butyldimethylsilyloxymethylphenyl)-1-phenylethylene (*11*) to introduce the TBDMSOMP group at the chain end, which was quantitatively transformed into the BnBr reaction site by treatment with a 1:1 mixture of Me_3SiCl and LiBr. Next, PαMSLi reacted with *11* to introduce the TBDMSOMP group at the chain end and the resulting polymer anion was coupled in situ with the above chain-end-BnBr-functionalized PS to afford an in-chain-TBDMSOMP-functionalized PS-*b*-PαMS. Again, the TBDMSOMP group introduced between the two blocks was transformed into the BnBr reaction site. Thus, the coupling and transformation reactions exactly correspond to the arm introduction and the BnBr reaction site regeneration steps, respectively. The same reaction process involving the two steps were repeated with the use of PMSLi and *11*, resulting in a 3-arm ABC μ-star polymer consisting of the PS, PαMS, and PMS arms. The TBDMSOMP group introduced at the core was transformed into the BnBr reaction site in the same manner with $Me_3SiCl/LiBr$. In the next process, a less reactive living PMMA was coupled with the 3-arm ABC μ-star core-functionalized with the BnBr reaction site. The coupling reaction was quantitative to afford a 4-arm ABCD star polymer composed of the PS, PαMS, PMS, and PMMA arms. Thus, both steps in each process satisfactorily work to successively synthesize the AB diblock, 3-arm ABC,

Scheme 34 Synthesis of μ-star polymers by the iterative methodology with *11* using BnBr reaction site

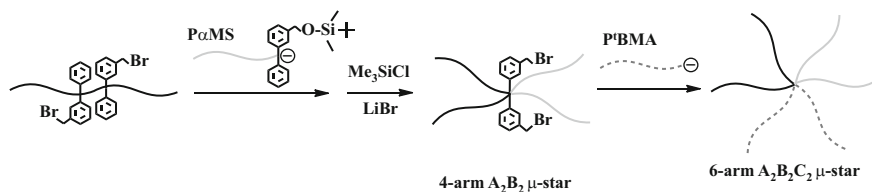**Table 15** Synthesis of μ-star polymers by iterative methodology with 11 using BnBr reaction site

Polymer	M_n (g/mol)		M_w/M_n
	calcd	SLS	SEC
A polymer	10,600	11,200	1.02
AB diblock copolymer	20,200	21,200	1.02
3-arm ABC	32,300	35,700	1.02
4-arm ABCD[a]	46,700	48,800	1.02
A₂ polymer	24,100	25,200	1.02
4-arm A₂B₂	44,300	43,700	1.03
6-arm A₂B₂C₂[b]	65,700	67,000	1.02

[a]PS/PαMS/PMS/PMMA. [b]PS/PαMS/P^{t}BMA

and 4-arm ABCDμ-star polymers (Table 15). In the final reaction stage for the introduction of the PMMA arm, the TBDMSOMP group was not introduced into the 4-arm ABC D μ-star polymer, because the living PMMA could not react with *11*.

Therefore, the same reaction sequence was no longer repeated. On the other hand, since PBLi, PILi, PSLi, or other living polystyrene derivatives react with *11*, the reaction process can be further continued by using such living polymers, leading to the synthesis of more armed and component μ-star polymers.

With the use of an in-chain-(BnBr)₂-functionalized A₂ as the starting polymer in the same methodology, a 4-arm A₂B₂, followed by a 6-arm A₂B₂C₂ μ-star polymer, were synthesized. Thus, the number of arms can increase by two in each process, as shown in Scheme 35. The resulting polymers were all well defined in structure as listed also in Table 15. In order to continue the process in this methodology, a living anionic polymer is always required to react with *11* of the DPE derivative in each process for the regeneration of the reaction site(s). Accordingly, the use of highly reactive living polymers of styrene, 1,3-butadiene, isoprene, and their derivatives

Scheme 35 Synthesis of 4-arm A_2B_2 and 6-arm $A_2B_2C_2$ μ-star polymers by the iterative methodology using two BnBr reaction sites

are required, while the less reactive living P2VP and PRMAs cannot be used except for the final linking step, as mentioned above.

As also shown in Scheme 7, the number of BnBr functions can be exponentially increased by developing an iterative methodology. By repeating the same reaction sequence from chain-end-$(BnBr)_2$-functionalized PS, the number of BnBr reaction sites could indeed increase from 2 to 4 (2^2), 8 (2^3), 16 (2^4), 32 (2^5), and even 64 (2^6). By reacting another living polymer (B) with the chain-end-$(BnBr)_n$-functionalized polymers (A)s at each reaction stage, it was possible to synthesize a series of $(n + 1)$ arm AB_n μ-star polymers, in which the A and B arms were PS (A) and PI (B), PB (B), P2VP (B), PMMA (B), or PEO (B) segments as mentioned in section "Arm-first termination methodology using BnBr reaction site."

Although the living PMMA cannot directly react with *1*, the DPE anion prepared from *1* and *sec*-BuLi initiates the polymerization of MMA to introduce two TBDMSOMP groups at the initiating chain end. The same iterative treatment enabled a series of chain-end-$(BnBr)_n$-functionalized PMMAs, in which the "n" number readily increased from 2 (2^1) to 4 (2^2), 8 (2^3), and 16 (2^4) in the same manner as that described above. The coupling reaction of the chain-end-$(BnBr)_n$-functionalized PMMA with other living anionic polymers also gave various $(n + 1)$ arm AB_n μ-star polymers. Typically, the A and B arms were PMMA and P^tBMA, PS, PI, or P2VP segments. In practice, a variety of 3-arm AB_2, 5-arm AB_4, 9-arm AB_8 μ-star polymers, etc., were successfully synthesized, also as described in section "Arm-first termination methodology using BnBr reaction site" [54, 55].

In the iterative methodologies described in the preceding sections and the methodology using BnBr reaction site(s) described in the first part of this section, the μ-star polymer synthesized in each process always became the starting polymer in the next process. On the other hand, although the number of BnBr reaction sites increased by basically the same iterative approach in the above-mentioned methodology, the μ-star polymer synthesized in each process did not correspond to the next starting material. Accordingly, the above-mentioned methodology deviated from the definition of an iterative methodology introduced in the beginning of this section "Methodologies based on iterative strategy," but considered to be one of the iterative methodologies.

In addition to the chain-end-$(BnBr)_n$-functionalized polymers, in-chain-$(BnBr)_2$-functionalized A_2 as well as A-*b*-B could also be used. These polymers were prepared as shown in Scheme 36. The living chain-end-$(TBDMSOMP)_2$-
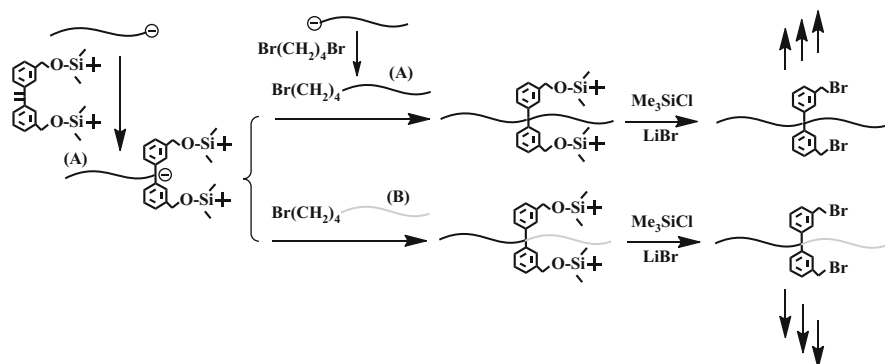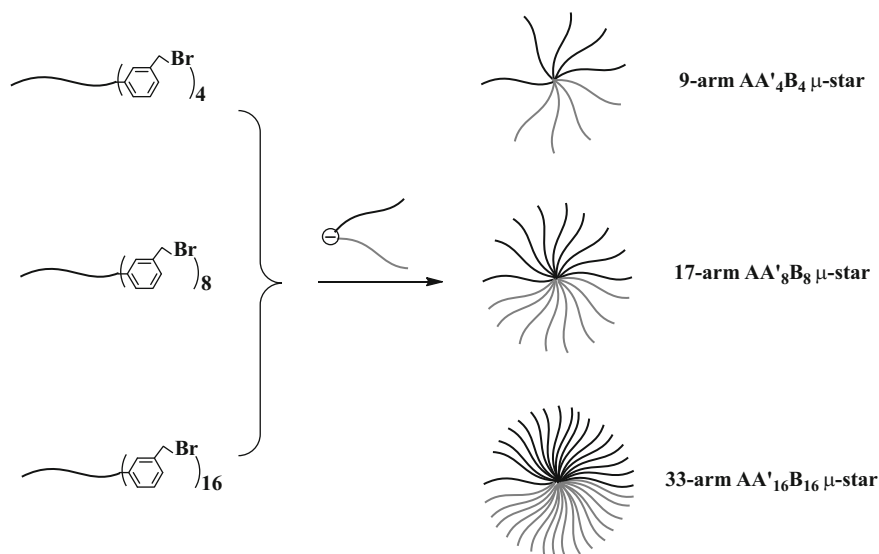
Scheme 36 Synthesis of in-chain-functionalized A_2 or A-*b*-B

functionalized polymer (A) was first prepared by reacting living polymer (A) with *1* and subsequently in situ reacted with a chain-end-(4-bromobutyl)-functionalized polymer (A) or (B). The two introduced TBDMSOMP groups were transformed into two BnBr functions. In these polymers, the number of BnBr functions can readily increase to 4 (2^2), 8 (2^3), 16 (2^4), etc., by the same iterative methodology as that used above. With these in-chain-$(BnBr)_n$-functionalized polymers, the synthesis of two series of (2 + n) arm A_2B_n and (2 + n) arm ABC_n μ-star polymers were possible by the coupling reaction of either the living polymer (B) or living polymer (C). Furthermore, the synthesis of the (2 + n) arm $A_{1+n}B$ as well as (2 + n) arm AB_{1+n} μ-star polymers was also possible using either the living polymer (A) or living polymer (B) in the reaction with the in-chain-$(BnBr)_2$-functionalized A-*b*-B [111, 112].

The methodology was extended to the synthesis of multiarmed μ-star polymers by reacting an off-centered A-*b*-B anion with either of a series of the chain-end-$(BnBr)_n$-As, in which the A and B arms were the PS and PMSiS segments, as shown in Scheme 37 [113–115]. The term "off-centered A-*b*-B anion" is defined as a polymer consisting of A and B blocks having an anionic site present at the junction of such blocks. This polymer anion was prepared by reacting PMSiSLi with the chain-end-DPE-functionalized PS and used in situ in the coupling reaction with the chain-end-$(BnBr)_n$-functionalized PS. In order to examine the possibility of the coupling reaction, the off-centered A-*b*-B anions and BnBr-functionalized PSs were adjusted to be ca. 10,000 g/mol (5,000 g/mol/5,000 g/mol) and ca. 10,000 g/mol in M_n value.

Surprisingly, the coupling reaction was complete in THF within 10 min even at −78 °C. 9-Arm AA'_4B_4, 17-arm AA'_8B_8, and even 33-arm $AA'_{16}B_{16}$ μ-star polymers were successfully synthesized (A, A', and B are PS (M_n = 10,000 g/mol), PS (M_n = 5,000 g/mol), and PMSiS (M_n = 5,000 g/mol)). However, the quantitative coupling reaction between the chain-end-$(BnBr)_{32}$-functionalized PS and the polymer anion was not achieved. The coupling efficiency was observed to be 75 %, but not improved by allowing the reaction mixture to react for the longer reaction time of 168 h. A 49-arm (on average) $AA'_{24}B_{24}$ star polymer was obtained. Thus, the steric hindrance appeared at this stage using the $(BnBr)_{32}$-functionalized PS (Table 16).

Scheme 37 Synthesis of μ-star polymers by the reaction of chain-end-(BnBr)$_n$-multifunctionalized PSs with the off-centered PS-*b*-PMSiM anions
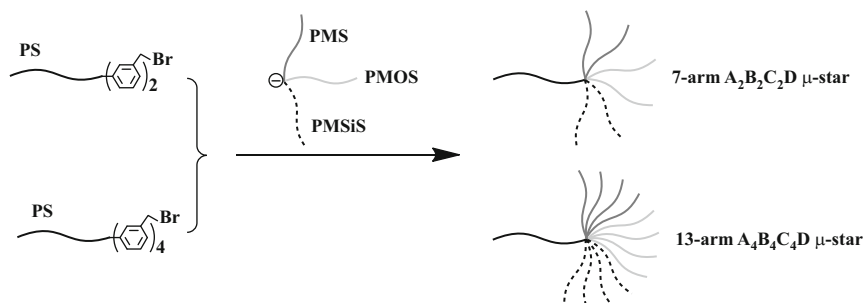
Table 16 Synthesis of μ-star polymers by the reaction of chain-end-(BnBr)$_n$-multifunctionalized PSs with the off-centered PS-*b*-PMSiS anions

Polymer	M_n (g/mol)		M_w/M_n
	calcd	SLS	SEC
9-arm AA$'_4$B$_4$	50,500	51,200	1.03
17-arm AA$'_8$B$_8$	93,900	96,800	1.03
33-arm AA$'_{16}$B$_{16}$	188,000	190,000	1.02
65-arm AA$'_{33}$B$_{33}$	358,000	270,000[a]	1.02

[a]48 arms were introduced based on the observed molecular weight. Efficiency = 75 %

The above success of the coupling reactions using the off-centered AB diblock anion motivated us to use a bulkier 3-arm ABC μ-star polymer having an anionic site at the core in the same reaction. According to the procedure shown in Scheme 38, a 3-arm ABC μ-star polymer anion (M_n = 30,000 (10,000/10,000/10,000) g/mol) composed of P(MSiS), P(MOS), and P(MS) arms was prepared by the procedure shown in Scheme 22 and in situ reacted with either the chain-end-(BnBr)$_2$-, or (BnBr)$_4$-functionalized PS (M_n = 10,000 g/mol) in THF at −78 °C for 24 h [116, 117]. The coupling reaction smoothly proceeded to afford the 7-arm A$_2$B$_2$C$_2$D and 17-arm A$_4$B$_4$C$_4$D μ-star polymers in virtually a 100 % yield. The results are listed in Table 17.

All of the μ-star polymers were observed to possess predictable M_n values and narrow molecular weight distributions. Their compositions were very close to the

Scheme 38 Synthesis of μ-star polymers by the reaction of chain-end-(BnBr)$_n$-multifunctionalized PSs with 3-arm ABC μ-star polymer anions

Table 17 Synthesis of μ-star polymers by the reaction of chain-end-(BnBr)$_n$-multifunctionalized PSs with 3-arm ABC μ-star polymer anions
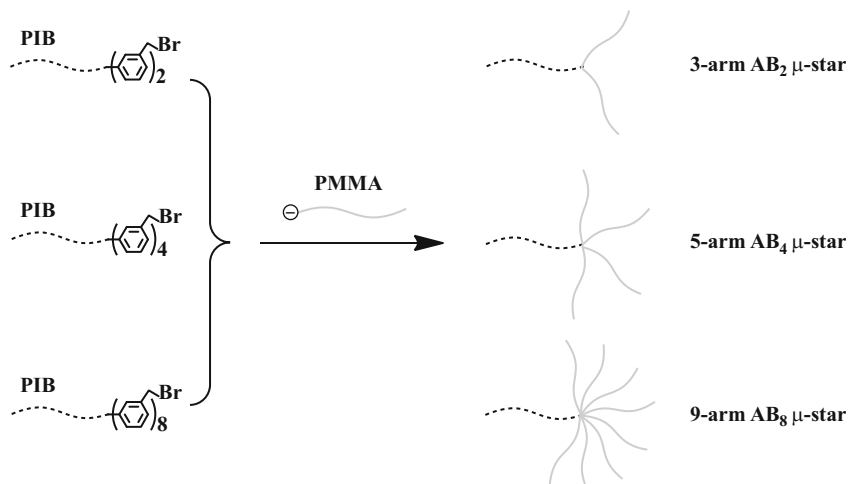
Polymer	M_n (g/mol)			M_w/M_n
	calcd	SLS		SEC
7-arm $A_2B_2C_2D$[a]	73,600	77,900		1.03
13-arm $A_4B_4C_4D$	134,000	133,000		1.02

[a]PMSiS/PMS/PMOS/PS

theoretical values. Thus, it was demonstrated that the iterative methodology based on the coupling reaction of the chain-end-(BnBr)$_n$-functionalized polymers with off-centered block copolymer anions or 3-arm μ-star terpolymer anions well worked for synthetic access to a series of characteristic multiarmed μ-star polymers, which are synthetically difficult by any other methods.

As mentioned above, the synthesis of a 65-arm $AA'_{32}B_{32}$ μ-star polymer was not successful possibly due to the steric hindrance around the core by reacting the chain-end-(BnBr)$_{32}$-multifunctionalized A with an off-centered A'-*b*-B. Similarly, several attempts failed to synthesize a 49-arm $A_{16}B_{16}C_{16}D$ μ-star polymer composed of the PMSiS (A), PMOS (B), PMS (C), and PS(D) arms by coupling of the 3-arm ABC star polymer anion with the chain-end-(BnBr)$_{16}$-multifunctionalized PS. Insufficient coupling efficiencies are also possibly due to the steric hindering effect. However, high efficiencies of 80–90 % could be achieved by changing the reaction time (168 h) and temperature (−40 °C).

Faust and Higashihara et al. synthesized a series of multiarmed AB_n μ-star polymers composed of poly(isobutylene) (PIB) (A) and PMMA (B) arms by developing a similar iterative approach [118]. As shown in Scheme 39, a PIB having an allyl chloride terminus was first prepared by the living cationic polymerization of IB, followed by terminating with 1,3-butadiene. The resulting chain-end-(allyl chloride)-functionalized PIB was reacted with the DPE anion prepared from *1* and *sec*-BuLi to introduce two TBDMSOMP groups at the chain end. The two TBDMSOMP groups were then transformed into BnBr reaction sites by the

Scheme 39 Synthesis of μ-star polymers composed of PIB and PMMA by the reaction of chain-end-(BnBr)$_n$-multifunctionalized PIBs with living PMMAs

Table 18 Synthesis of μ-star and pom-pom polymers composed of PIB and PMMA

| Polymer	M_n (g/mol)		M_w/M_n
	calcd	SLS	SEC
3-arm AB$_2$[a]	26,600	27,200	1.06
5-arm AB$_4$	47,600	45,800	1.03
9-arm AB$_8$	119,000	124,000	1.02
pom-pom B$_2$AB$_2$	50,100	51,000	1.02
pom-pom B$_4$AB$_4$	56,600	55,600	1.02
pom-pom B$_8$AB$_8$	52,200	54,500	1.03

[a]PIB/PMMA

treatment with Me$_3$SiCl/LiBr in the same manner as that already described. By repeating the reaction sequence involving the reaction of the BnBr reaction sites with the DPE anion and the transformation reaction to the BnBr reaction site, the number of terminal BnBr functions increased to $2(2^1)$, $4(2^2)$, and $8(2^3)$. The living PMMA reacted with each of the prepared chain-end-(BnBr)$_n$-multifunctionalized PIBs, resulting in the successful formation of well-defined 3-arm AB$_2$, 5-arm AB$_4$, and 9-arm AB$_8$ μ-star polymers. A new B$_2$AB$_2$, B$_4$AB$_4$, or B$_8$AB$_8$ pom-pom polymer was also synthesized in a similar manner by reacting the living PMMA with an end-functionalized PIB with BnBr functions at both chain ends. The results are summarized in Table 18. Thus, in this procedure for the synthesis of μ-star polymers, the chain-end-functionalized polymers obtained by the living cationic polymerization could also be employed.

4 μ-Star Polymers Composed of Random Coil and Rigid Segments

Block polymers composed of random coil and rigid segments have recently received much attention because such molecular conjugates combine the characteristics of random coils such as flexibility, elasticity, solubility, and processability with mechanically tough rigid segments. It is now recognized that very unique and unconventional morphologies at the molecular level, previously unknown for fully amorphous block polymers, are often produced. Furthermore, the individual characteristic features of the rigid segments are also advantageous to provide additional functionalities to the polymers. For these reasons, a variety of such block polymers have been already synthesized and their potential applications have been widely investigated especially in the fields of nanomaterial and nanoscience. In contrast, only a few μ-star polymers including rigid segments have been synthesized, although such polymers could also be of significant interest for the same reasons. In this section, three recently synthesized μ-star polymers composed of vinyl polymers and rigid segments will be introduced.

The first example is the μ-star polymers including rigid rodlike π-conjugated poly(acetylene) (PA) segments, which show high conductivities and nonlinear optical activities. However, the PA generally prepared by the transition-metal-mediated polymerization of acetylene is not suitable for the star polymer synthesis because the polymerization is not well controlled. In 1990, Hogen-Esch et al. developed an efficient two-step methodology for the synthesis of a well-defined PA via the living anionic polymerization of phenyl vinyl sulfoxide (PVS), followed by thermal elimination of the resulting polymer, converting to the PA segment, as shown in Scheme 40 [119, 120]. With this methodology, linear PAs with known molecular weights and relatively narrow molecular weight distributions ($M_w/M_n = 1.2$–1.5) were first synthesized. Later, the polymerization was improved with respect to the control using 4-methylphenyl vinyl sulfoxide (4MPVS) and by adding a tenfold or more excess of LiCl to the initiator [121, 122]. The molecular weight distributions of the resulting polymers became narrower ($M_w/M_n < 1.2$).

By applying this improved polymerization system to the iterative methodology (see Scheme 22) described in section "Iterative methodologies using DPE reaction site," a series of μ-star polymers containing the PA segments were synthesized as illustrated in Scheme 41 [123, 124].
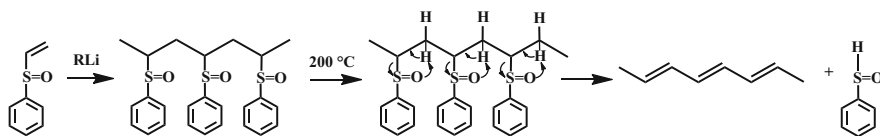
Scheme 40 Preparation of well-defined PA by the anionic polymerization of phenyl vinyl sulfoxide, followed by thermal elimination of the resulting polymer
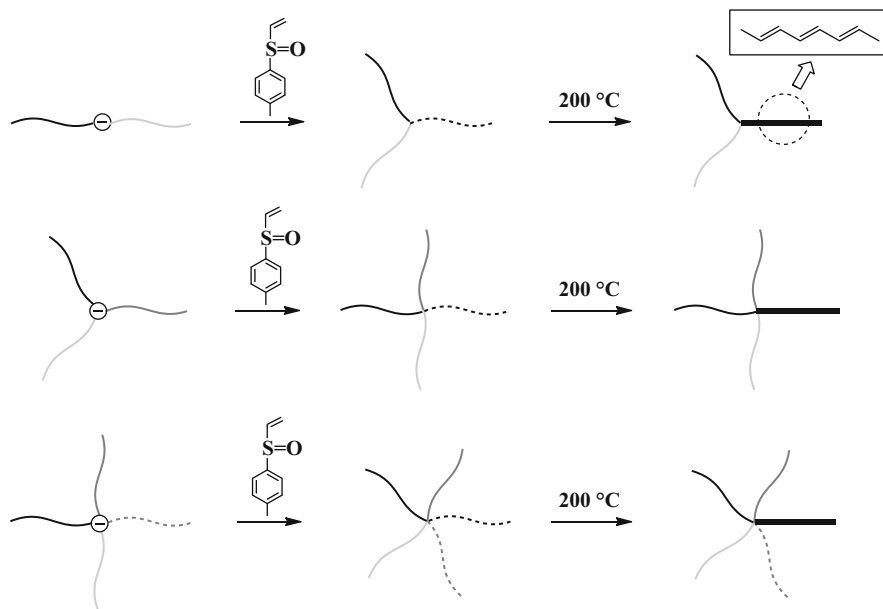
**Scheme 41** Synthesis of coil-rod μ-star polymers using iterative methodology

Table 19 Characterization results of μ-star polymers including (P4MPVS)s convertible to PA segments

Polymer	M_n (g/mol)		M_w/M_n
	calcd	SLS	SEC
3-arm ABE	31,800	32,700	1.02
3-arm ACE	31,800	34,600	1.03
4-arm ABCE	42,700	44,600	1.02
4-arm ABDE	43,300	43,600	1.03
5-arm ABCDE[c]	51,600	53,600	1.03

[a]PS/PaMS/PMOS/PMSiS/poly(4MVS)

In the synthesis, the intermediate polymer anion was used as a macroinitiator in the living anionic polymerization of 4MPVS, and the resulting P4MPVS was converted to the PA segment by thermal treatment. In practice, 4MPVS was quantitatively polymerized with either an AB diblock copolymer anion, a 3-arm ABC μ-star polymer anion, or a 4-arm ABCD μ-star polymer anion, yielding the corresponding 3-arm ABE, 4-arm ABCE, or 5-arm ABCDE μ-star polymer with well-defined and expected structures (Table 19). The A, B, C, D, and E segments were PS, PaMS, PMOS, PMSiS, and P4MPVS segments, respectively.

Similarly, two 3-arm AB₂ μ-star polymers ($M_n = 22,000–54,000$ g/mol and $M_w/M_n < 1.1$) were synthesized via the ion-bond by the stoichiometric reaction either between chain-end-(NMe₂)₂-functionalized PPVS and chain-end-(COOH)-functionalized PS or chain-end-(NMe₂)-functionalized PPVS and in-chain-(COOH)-functionalized PS, followed by thermal treatment, as shown in Scheme 42
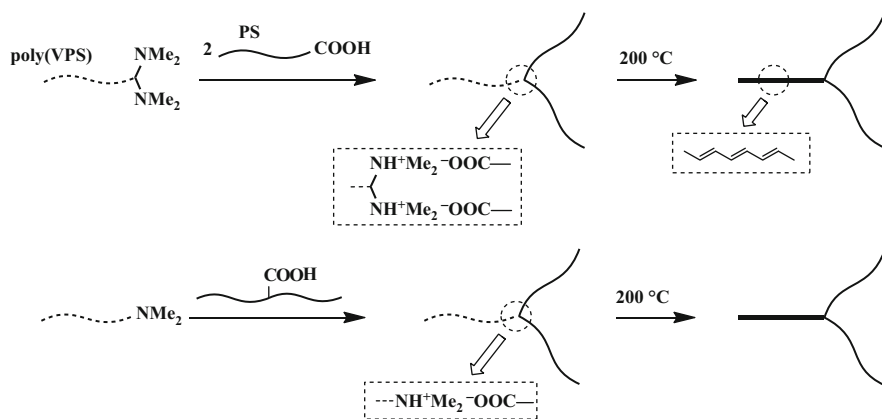
Scheme 42 Synthesis of ion-bonded 3-arm AB$_2$ μ-star polymers having one PA segment

[122]. Periodic lamellar morphologies were observed in the cast films of such polymers by TEM measurement.

The resulting polymers are of special interest in that the PA arms are phase-separated, followed by self-organizing to arrange the conductive PA segments inside the microdomains or self-assemblies in selected solvents. In addition, their mechanical properties and behavior are also of interest because of rigid rodlike characters of the PA segment. Thus, various μ-star polymers having the PA segment (s) are now available by developing the methodology via the living anionic polymerization, followed by thermal treatment.

The second example is the μ-star polymers having poly(alkyl isocyanate) segment(s), which adopt an extended helical conformation with unique optical activities and liquid crystallinities. Lee et al. were the first to succeed in achieving the living anionic polymerization of hexyl isocyanate (HIC) and the related isocyanate monomers under rather specific conditions in THF at -98 °C with the use of initiators bearing Na$^+$ [125–127]. Certain suitable additives, such as NaBPh$_4$ and 15-crown-5, were needed to prevent the unwanted trimer formation by the back-biting that occurred after the polymerization. Under such conditions, PHICs with controlled molecular weights ($M_n \sim 50,000$ g/mol) and narrow molecular weight distributions ($M_w/M_n < 1.1$) were quantitatively obtained. Well-defined block copolymers of PHIC-b-PS-b-PHIC, PHIC-b-PI-b-PHIC, and PHIC-b-P2VP-b-PHIC could also be synthesized by the sequential polymerization of styrene, isoprene, or 2VP, followed by HIC, to sodium naphthalene [128].

The synthesis of μ-star polymers with PHIC arms by Lee et al. are shown in Scheme 43 [129]. A PHIC-COCH$_2$CO-PHIC with an active methylene reaction site between the two blocks was first prepared by coupling of the living PHIC with malonyl chloride.

Subsequently, the Michael reaction of the PHIC-COCH$_2$CO-PHIC with the α-methacryloyl-functionalized polyethylene glycol (PEG) macromonomer in the
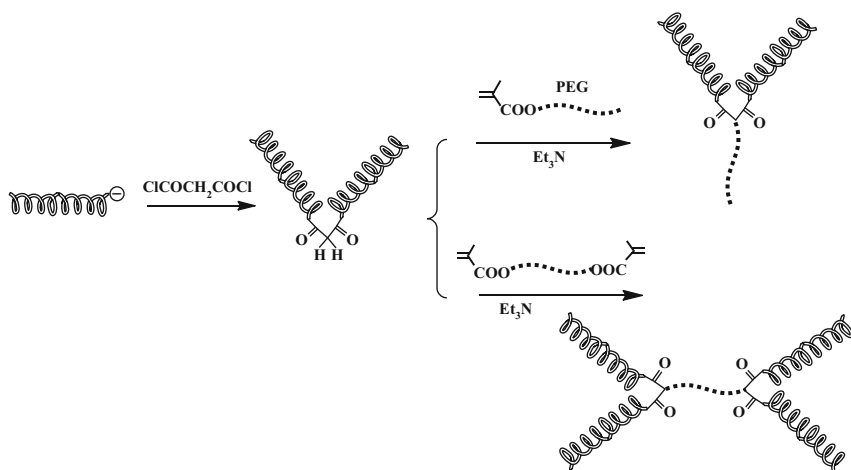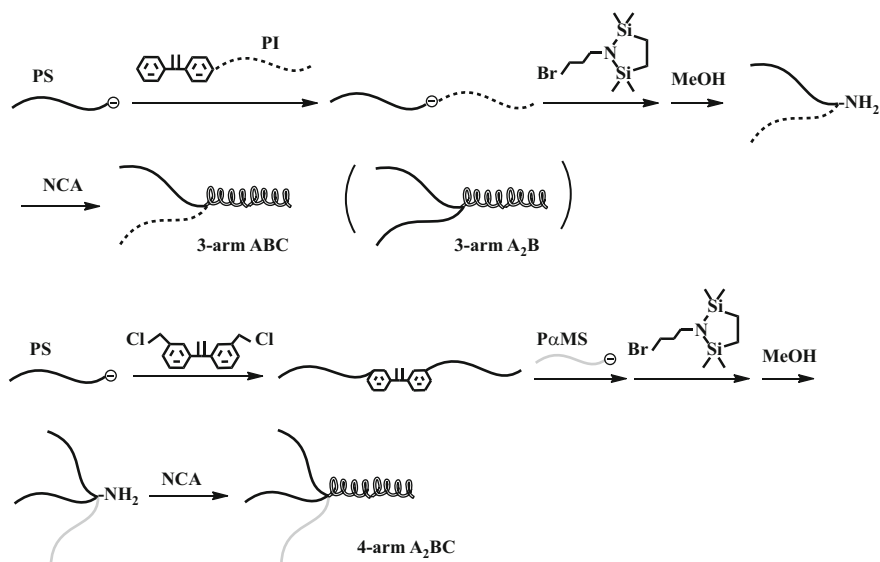
Scheme 43 Synthesis of coil–helix 3-arm AB$_2$ μ-star and B$_2$AB$_2$ pom-pom polymer

presence of triethylamine yielded a 3-arm AB$_2$ μ-star polymer composed of PEG (A) and PHIC (B). Two polymer chains of PHIC-COCH$_2$CO-PHIC could be linked with an α,ω-dimethacryloyl-functionalized PEG macromonomer leading to an B$_2$AB$_2$ pom-pom type of (PHIC)$_2$(PEG)(PHIC)$_2$. The resulting μ-star polymers were composed of helical PHIC and biocompatible PEG arms and possessed controlled M_n values ($M_n = 9{,}600$–$12{,}400$ g/mol) and narrow molecular weight distributions ($M_w/M_n = 1.08$–1.14). It was observed that the 3-arm AB$_2$ μ-star polymers form solid core-shell or hollow spherical micelles simply by changing the solvent from THF to a mixed solvent of THF and ethanol (1/9, v/v).

A variety of block polymers combining polypeptide sequences with synthetic polymers have already been synthesized, since rigid ordered conformations, such as α-helices or β-strands, can be incorporated, with which unusual nanostructures are produced and control over the nanoscale structures is significantly enhanced through intramolecular hydrogen bonding. It is also interesting that the resulting polypeptide–vinyl polymer conjugates behave as potentially biocompatible and new smart materials, whose conformation and association properties can reversibly respond by changing the pH and temperature [130–132]. These polymers were generally prepared by the anionic ring-opening polymerization of α-amino acid N-carboxyanhydrides (NCAs) with chain-end-amine-functionalized vinyl polymers, but the polymerization control was somewhat difficult until recently. This difficulty has been overcome by the use of an organonickel complex, ammonium chloride, hexamethyldisilazane, and several primary amines as the initiators. Thus, the molecular weights could be controlled up to a 10^5 g/mol order with narrow molecular weight distributions ($M_w/M_n = 1.04$–1.18) [133–140].

With these improved polymerization systems, Hadjichristidis et al. first synthesized new μ-star polymers including polypeptide segments by anionic polymerization [141]. These polymers involved 3-arm A$_2$B, 3-arm ABC, and 4-arm A$_2$BC

Scheme 44 Synthesis of coil–helix μ-star polymers

Table 20 Synthesis of coil–helix μ-star polymers with polypeptide arms

Polymer	M_n (g/mol)		M_w/M_n
	calcd	SEC-TALLS	SEC
3-arm (PS)(PI)(PBLG)	35,000	33,300	1.09
3-arm (PS)(PI)(PBocLL)	35,000	34,200	1.07
3-arm (PS)$_2$(PBLG)	32,000	32,600	1.05
3-arm (PS)$_2$(PBocLL)	32,000	31,500	1.02
4-arm (PS)$_2$(PαMS)(PBLG)	40,000	38,900	1.08
4-arm (PS)$_2$(PαMS)(PBocLL)	40,000	38,500	1.07

PBLG poly(γ-benzyl-L-glutamate), *PBocLL* poly(ε-*tert*-butoxycarbonyl-L-lysine)

μ-stars, where the A, B, and C arms are polypeptide, PI, PS, or PαMS, respectively. The reaction sequences for the synthesis of such μ-star polymers are given in Scheme 44. In-chain-NH$_2$-functionalized (PS)$_2$, PS-*b*-PI diblock copolymer, or 3-arm core-NH$_2$-functionalized (PS)$_2$(PαMS) μ-star are first synthesized by reacting 1-(3-bromopropyl)-2,2,5,5-tetramethyl-aza-2,5-disilacyclopentane with the corresponding polymer anions, followed by deprotection. These amine-functionalized polymers were used as the macroinitiators in the living anionic polymerization of the NCAs.

All the macroinitiators were completely consumed, as evidenced by the absence of the corresponding peaks in the SEC charts of the final products. From the characterization results in Table 20, it can be seen that the final μ-star polymers have low polydispersities and their stoichiometric molecular weights are in good

agreement with those determined by SEC-TALLS. Consequently, the resulting μ-star polymers having polypeptide arms are well defined in structure. Among these synthesized μ-star polymers, 3-arm (PS)$_2$PBocLL and 4-arm (PS)$_2$(PBocLL)$_2$ stars (PBocLL: poly(ε-*tert*-butoxycarbonyl-L-lysine)) were first deprotected and then complexed with sodium dodecyl sulfonate of an anionic surfactant to give the supramolecular complexes [142]. They are lamellar polypeptide–surfactant self-assemblies with a β-sheet conformation. The ionic complexation leads to a particularly pronounced small-scale ordering of the polypeptide–surfactant complex arms that dominate over the formation of block copolymer scale structures.

5 Conclusions

At the present time, well-defined regular star polymers having multiarms can be synthesized by the linking reaction using multifunctional chlorosilane compounds, followed by the development of the linking reaction using BnBr reaction sites. Both the methodologies are based on "arm-first termination" procedure. The usable arms of such star polymers are PS, PαMS, PI, PB, P2VP, PMMA, P^{t}BMA, and PEO. Any monomer including cyclic monomers that undergoes living anionic polymerization can be used to result in the synthesis of the corresponding multiarmed regular star polymers. It should be emphasized that the chlorosilane methodology is excellent with respect to the synthesis of very high-molecular-weight star polymers with M_n values of over 10^7 g/mol.

Regarding the μ-star polymer synthesis, only one example concerning the synthesis of a four-component 4-arm ABCD μ-star polymer appeared before 2000. Even in the 3-arm ABC stars, a few examples were synthesized by the methodologies using multifunctional chlorosilanes or dual-functionalized DPE reaction sites. Since 2001, Hirao, Higashihara et al. have proposed the iterative strategy using repeatable reaction sequences capable of simultaneous introduction of arm(s) and reaction site(s). With the use of the methodologies based on this iterative strategy, the limit for the synthesis of μ-star polymers is readily surpassed and the almost all types of multiarmed and multicomponent μ-star polymers have been successfully synthesized, as introduced in section "Methodologies based on iterative strategy." With the development of various reaction sites, any monomer that undergoes living anionic polymerization can be used. Furthermore, since the iterative strategy may possibly be applied to other living polymerization systems in conjunction with several click reactions, the range of available star polymers will be greatly expanded in the near future. The development of living anionic polymerization of phenyl vinyl sulfoxide, alkyl isocyanate monomers, and NCAs has allowed access to various well-defined coil–rod and coil–helix μ-star polymers with interesting functionalities. Thus, a wide variety of multiphase polymers with star-branched architectures having more structural variables than linear block polymers are now available. Their applications to both material science and nanoscience will be expected.

Abbreviations

4-DVB	4-Divinylbenzene
4MPVS	4-Methylphenyl vinyl sulfoxide
acetal-DHPMA	(2,2-Dimethyl-1,3-dioxolan-4-yl)methyl methacrylate
Bd	1,3-Butadiene
BnBr	Benzyl bromide
BnCl	Benzyl chloride (BnCl)
DPE	1,1-Diphenylethylene
HIC	Hexyl isocyanate
NCAs	*N*-carboxyanhydrides
P2VP	Poly(2-vinylpyridine)
P4VP	Poly(4-vinylpyridine)
PA	Poly(acetylene)
PA	α-Phenylacrylate
PB	Poly(1,3-butadiene)
PBLG	Poly(γ-benzyl-L-glutamate)
PBLi	Poly(1,3-butadienyl)lithium
PBnMA	Poly(benzyl methacrylate)
PBocLL	Poly(ε-*tert*-butoxycarbonyl-L-lysine)
PDHPMA	Poly(2,3-dihydroxypropyl methacrylate)
PDMS	Poly(dimethylsiloxane)
PEE	Poly(ethylethylene)
PEG	Polyethylene glycol
PEMA	Poly(ethyl methacrylate)
PEO	Poly(ethylene oxide)
PFMMA	Poly(ferrocenylmethyl methacrylate)
PFPO	Poly(perfluoropropylene oxide)
PHEMA	Poly(2-hydroxyethyl methacrylate)
PHIC	Poly(hexyl isocyanate)
PI	Polyisoprene
PILi	Poly(isoprenyl)lithium)
PMMA	Poly(methyl methacrylate)
PMOEMA	Poly(2-methoxyethyl methacrylate)
PMOSLi	Poly(4-methoxystyryl)lithium
PMSiS	Poly(4-trimethylsilylstyrene)
PS	Polystyrene
PSLi	Poly(styryl)lithium
P^{t}BA	Poly(*tert*-butyl acrylate)
PTBDMSiOS	Poly(4-*tert*-butyldimethylsilyloxystyrene)
P^{t}BMA	Poly(*tert*-butyl methacrylate)
PVS	Phenyl vinyl sulfoxide
PαMSLi	Poly(α-methylstyryl)lithium
RMAs	Alkyl methacrylates

sec-BuLi	*sec*-Butyllithium
Si-HEMA	2-*tert*-Butyldimethylsilyloxyethyl methacrylate
TBDMS	*tert*-Butyldimethylsilyl
TBDMSiOMP	3-*tert*-Butyldimethylsilyloxymethylphenyl
TBDMSOMP	3-*tert*-Butyldimethylsilyloxymethylphenyl
TBDMS-PLi	3-(*tert*-butyldimethylsilyloxy)-1-Propyllithium
TMS	Trimethylsilyl

References

1. Hückstädt H, Göpfert A, Abetz V (2000) Synthesis and morphology of ABC heterarm star terpolymers of polystyrene, polybutadiene, and poly(2-vinylpyridine). Macromol Chem Phys 201:296–307
2. Hayashida K, Arai S, Shinohara Y, Amemiya Y, Matsushita Y (2006) Systematic transitions of tiling patterns formed by ABC star shaped terpolymers. Macromolecules 39:9402–9408
3. Li Z, Hillmyer MC, Lodge TP (2006) Morphologies of multicompartment micelles formed by ABC miktoarm star terpolymers. Langmuir 22:9409–9417
4. Quirk RP (1996) IV Anionic synthesis of polymers with well-defined structures. 13 Star polymers. In: Hsieh HL, Quirk RP (eds) Anionic polymerization: principles and applications. Marcel Dekker, New York, pp 333–368
5. Grest GS, Fetters LJ, Huang JS, Richter D (1996) Star polymers: experiment, theory, and simulation. Adv Chem Phys 94:67–163
6. Meneghetti SP, Lutz PJ, Rein D (1999) Star-shaped polymers via anionic polymerization methods. In: Mishra MK, Kobayashi S (eds) Star and hyperbranched polymers. Marcel Dekker, New York, pp 27–57
7. Hadjichristidis N (1999) Synthesis of miktoarm star (μ-star) polymers. J Polym Sci Part A Polym Chem 37:857–871
8. Hadjichristidis N, Pispas S, Pitsikalis M, Iatrou H, Vlahos C (1999) Asymmetric star polymers: synthesis and properties. Adv Polym Sci 142:71–127
9. Hadjichristidis N, Pitsikalis M, Pispas S, Iatrou H (2001) Polymers with complex architectures by living anionic polymerization. Chem Rev 101:3747–3792
10. Hadjichristidis N, Pitsikalis M, Iatrou H, Driva P, Sakellariou G, Chatzichristidi M (2012) Polymers with star-related structure: synthesis, properties, and applications. In: Matyjaszewski K, Möller M (eds) Polymer science: a comprehensive reference, vol 6. Elsevier BV, Amsterdam, pp 29–111
11. Hirao A, Hayashi M, Loykulnant S, Ryu SW, Haraguchi N, Matsuo A, Higashihara T (2005) Precise synthesis of chain-multi-functionalized polymers, star-branched polymers, star-linear block polymers, densely branched polymers, and dendritic branched polymers based on iterative approach using functionalized 1,1-diphenylethylene derivatives. Prog Polym Sci 30:111–182
12. Higashihara T, Hayashi M, Hirao A (2011) Synthesis of well-defined star-branched polymers by stepwise iterative methodology using living anionic polymerization. Prog Polym Sci 36:323–375
13. Ito S, Goseki R, Ishizone T, Hirao A (2013) Successive synthesis of well-defined multiarmed miktoarm star polymers by iterative methodology using living anionic polymerization. Eur Polym J 49:2545–2566

14. Nakahama S, Hirao A (1990) Protection and polymerization of functional monomers: anionic living polymerization of protected monomers. Prog Polym Sci 15:299–335

15. Hirao A, Nakahama S (1992) Anionic living polymerization of monomers with functional silyl groups. Prog Polym Sci 17:283–317

16. Hirao A, Roykulnant S, Ishizone T (2002) Recent advance in living anionic polymerization of functionalized styrene derivatives. Prog Polym Sci 27:1399–1471

17. Ishizone T, Hirao A (2012) Anionic polymerization: recent advances. In: Schlüter AD, Hawker CJ, Sakamoto J (eds) Synthesis of polymers: new structures and methods, vol 1. Willey-VCH, Weinheim, pp 81–133

18. Ishizone T, Sugiyama K, Hirao A (2012) Anionic polymerization of protected functional monomers. In: Matyjaszewski MM (ed) Polymer science: comprehensive reference, vol 3. Elsevier BV, Amsterdam, pp 591–621

19. Comanita B, Noren B, Roovers J (1999) Star poly(ethylene oxide)s from carbosilane dendrimers. Macromolecules 32:1069–1072

20. Vasilenko NG, Rebrov EA, Muzafarov AM, Edwein B, Striegel B, Möller M (1998) Preparation of multi-arm star polymers with polylithiated carbosilane dendrimers. Macromol Chem Phys 199:889–895

21. Quirk RP, Tsai Y (1998) Trifunctional organolithium initiator based on 1,3,5-tris (1-phenylethenyl)benzene. Synthesis of functionalized, three-armed, star-branched polystyrenes. Macromolecules 31:8016–8025

22. Quirk RP, Yoo T, Lee Y, Kim J, Lee B (2000) Applications of 1,1-diphenylethylene chemistry in anionic synthesis of polymers with controlled structures. Adv Polym Sci 153:67–162

23. Quirk RP (1996) IV Anionic synthesis of polymers with well-defined structures. 13 Star polymers. In: Hsieh HL, Quirk RP (eds) Anionic polymerization: principles and applications. Marcel Dekker, New York, pp 334–335

24. Samulski ET, Desimone JM, Hunt MO, Menceloglu Y, Jarnagin RC, York GA, Wang H (1992) Flagellenes: nanophase-separated, polymer-substituted fullerenes. Chem Mater 4:1153–1157

25. Ederle Y, Mathis C (1997) Grafting on anionic polymers onto C_{60} in polar and nonpolar solvents. Macromolecules 30:2546–2555

26. Eschwey H, Hallensleben ML, Burchard W (1973) Preparation and some properties of star-shaped polymers with more than hundred side chains. Makromol Chem 173:235–239

27. Burchard W, Eschwey H (1975) Star polymers from styrene and divinylbenzene. Polymer 16:180–184

28. Lutz P, Rempp P (1988) New developments in star polymer synthesis. Star-shaped polystyrenes and star-block copolymers. Makromol Chem 189:1051–1060

29. Tsitsilianis C, Lutz P, Graff S, Lamps JP, Rempp P (1991) Core-first synthesis of star polymers with potentially ionogenic branches. Macromolecules 24:5897–5902

30. Okay O, Funke W (1990) Steric stabilization of reactive microgels from 1,4-divinylbenzene. Makromol Chem Rapid Commun 11:583–587

31. Funke W, Okay O (1991) Anionic dispersion polymerization of 1,4-divinylbenzene. Macromolecules 2423:2623–2628

32. Gnanou Y, Lutz P, Rempp P (1988) Synthesis of star-shaped poly(ethylene oxide). Makromol Chem 189:2885–2892

33. Fayt R, Forte R, Jacobs C, Jerome R, Ouhadi T, Teyssie P, Varshney SK (1987) New initiator system for the living anionic polymerization of tert-alkyl acrylates. Macromolecules 20:1442–1444

34. Varshney SK, Jacobs C, Hautekeer JP, Bayard P, Jerome R, Fayt R, Teyssie P (1991) Anionic polymerization of acrylic monomers. 6. Synthesis, characterization, and modification of poly (methyl methacrylate)-poly(tert-butyl acrylate) di- and triblock copolymers. Macromolecules 24:4997–5000

35. Masuda T, Ohota Y, Yamauchi T, Onogi S (1984) Characterization and rheological properties of multi-branched star polystyrenes. Polymer J 16:273–291
36. Bi LK, Fetters LJ (1976) Synthesis and properties of block copolymers. 3. Polystyrene-polydiene star block copolymers. Macromolecules 9:732–742
37. Mays JW, Hadjichristidis N, Fetters LJ (1988) Star branched polystyrenes: an evaluation of solvent and temperature influences on unperturbed chain dimensions. Polymer 29:680–685
38. Tsitsilianis C, Chaumont P, Rempp P (1990) Synthesis and characterization of hetero-arm star copolymers. Makromol Chem 191:2319–2328
39. Tsitsilianis C, Graff S, Rempp P (1991) Hetero-arm star copolymers with potentially ionogenic branches. Eur Polym J 27:243–246
40. Rein D, Lutz P, Rempp P (1993) Recent developments in the field of star-shaped polymers. Macromol Symp 67:237–249
41. Tsitsilianis Panagopoulos D, Lutz P (1995) Amphiphilic heteroarm star copolymers of polystyrene and poly(ethylene oxide). Polymer 36:3745–3752
42. Tsitsilianis C, Voulgaris D (1997) Poly(2-vinylpyridine)-based star-shaped polymers. Synthesis of heteroarm star (A_nB_n) and star-block (AB)$_n$ copolymers. Macromol Chem Phys 198:997–1007
43. Zhou LL, Roovers J (1993) Synthesis of novel carbosilane dendritic macromolecules. Macromolecules 26:963–968
44. Roovers J, Hadjichristidis N, Fetters LJ (1983) Analysis and dilute solution properties of 12- and 18-arm star polystyrene. Macromolecules 16:214–220
45. Hadjichristidis N, Guyot A, Fetters LJ (1978) The synthesis of star polyisoprenes using octa- and dodecachlorosilanes as linking agent. Macromolecules 11:668–672
46. Hadjichristidis N, Fetters LJ (1980) Synthesis of 18-arm polyisoprenes. Macromolecules 13:191–193
47. Zhou LL, Hadjichristidis N, Toporowski PM, Roovers J (1992) Synthesis and properties of regular star polybutadienes with 32 arms. Rubber Chem Technol 65:303–314
48. Roovers J, Zhou LL, Toporowski PM, van der Zwan M, Iatrou H, Hadjichristidis N (1993) Regular star polymers with 64 and 128 arms. Macromolecules 26:4324–4331
49. Pitsikalis M, Hadjichristidis N, Silvestro GD, Sozzani P (1995) Direct evidence of star structure from nuclear magnetic resonance spectroscopy. Macromol Chem Phys 196:2767–2774
50. Allgaier J, Martin K, Räder HJ, Müllen K (1999) Many-arm star polymers synthesized using chlorosilane linking agents. Macromolecules 32:3190–3194
51. Hirao A, Haraguchi N (2002) Anionic synthesis of well-defined star-branched polymers by using chain-end-functionalized PSs with dendritic BnBr moieties. Macromolecules 35:7224–7231
52. Hogen-Esch TE, Toreki W (1989) Synthesis of macrocyclic- and star-vinyl polymers ACS Polym. Preprints 30:129–130
53. Pitsikalis M, Sioula S, Pispas S, Hadjichristidis N, Cook DC, Li J, Mays JW (1999) Linking reactions of living polymers with bromomethylbenzene derivatives: synthesis and characterization of star homopolymers and graft copolymers with polyelectrolyte branches. J Polym Sci Part A Polym Chem 37:4337–4350
54. Hirao A, Matsuo A (2003) Synthesis of chain-end-functionalized PMMAs with a definite number of BnBr moieties and their application to star-branched polymers. Macromolecules 36:9742–9751
55. Hirao A, Hayashi M, Haraguchi N, Matsuo A, Higashihara T (2004) Synthesis of chain-end-functionalized PSs with a definite number of BnBr moieties by a novel iterative divergent approach and their synthetic application to well-defined star-branched polymers. Macromol Synth 13:69–80
56. Hirao A, Higashihara T, Nagura M, Sakurai T (2006) Successive synthesis of well-defined many arm star-branched polymers by an iterative methodology using a specially designed DPE derivatives. Macromolecules 39:6081–6091

57. Mays JW (1990) Synthesis of "simple graft" poly(isoprene-*g*-styrene) by anionic polymerization. Polym Bull 23:247–250
58. Iatrou H, Siakali-Kioulafa E, Hadjichristidis N, Roovers J, Mays JW (1995) Hydrodynamic properties of model 3-miktoarm star copolymers. J Polym Sci Polym Phys Ed 33:1925–1932
59. Pochan DJ, Gido SP, Pispas S, Mays JW, Ryan AJ, Fairclough JPA, Hamly IW, Terrill NJ (1996) Morphologies of microphase-separated A_2B simple graft copolymers. Macromolecules 29:5091–5098
60. Tselikas Y, Hadjichristidis N, Iatrou H, Liang KS, Lohse DJ (1996) Morphology of miktoarm star block copolymers of styrene and isoprene. J Chem Phys 105:2456–2462
61. Avgeropoulos A, Hadjichristidis N (1997) Synthesis of model nonlinear block copolymers of $A(BA)_2$, $A(BA)_3$, and $(AB)_3A(BA)_3$ type. J Polym Sci Polym Chem Ed 35:813–816
62. Tsiang RCC (1994) GPC Analysis of an alternative multistep linking process for making asymmetric star polymers from living polymeric arms. Macromolecules 27:4399–4403
63. Iatrou H, Hadjichristidis N (1992) Synthesis of a model 3-miktoarm star terpolymer. Macromolecules 25:4649–4651
64. Iatrou H, Hadjichristidis N (1993) Synthesis and characterization of model 4-miktoarm star co- and quaterpolymer. Macromolecules 26:2479–2484
65. Bellas V, Iatrou H, Hadjichristidis N (2000) Controlled anionic polymerization of hexamethylcyclotrisiloxane. Model linear and miktoarm star co- and terpolymers of PDMS with styrene and isoprene. Macromolecules 33:6993–6997
66. Tsoukatos T, Hadjichristidis N (2002) Synthesis of model polycyclohexadiene/polyethylene miktoarm star copolymers with three and four arms. J Polym Sci Part A Polym Chem 40:2575–2582
67. Mavroudis A, Avgeropoulos A, Hadjichristidis N, Thomas EL, Lohse DJ (2003) Synthesis and morphological behavior of model linear and miktoarm star copolymers of 2-methyl-1,3-pentadiene and styrene. Chem Mater 15:1976–1983
68. Zioga A, Siloula S, Hadjichristidis N (2000) Synthesis and morphology of model 3-miktoarm star terpolymers of styrene, isoprene, and 2VP. Macromol Symp 157:239–249
69. Cho D, Park S, Chang T, Avgeropoulos A, Hadjichristidis N (2003) Characterization of a 4-miktoarm star copolymer of the (PS-*b*-PI)$_3$PS type by temperature gradient interaction chromatography. Eur Polym J 39:2155–2160
70. Allgaier J, Young RN, Efstratiadis V, Hadjichristidis N (1996) Synthesis and characterization of PI/PB A_2B_2 star copolymers. Macromolecules 29:1794–1797
71. Bellas V, Hadjichristidis N (1999) Synthesis of model PS(PI)$_5$ and (PI)$_5$PS(PI)$_5$ non-linear block copolymers of styrene and isoprene. Macromolecules 32:534–536
72. Mavroudis A, Avgeropoulos A, Hadjichristidis N, Thomas EL, Lohse DJ (2006) Synthesis and morphological behavior of model 6-miktoarm star copolymers, PS(P2MP)$_5$, of styrene and 2-methyl-1,3-pentadiene (2MP). Chem Mater 18:2164–2168
73. Avgeropoulos A, Poulos Y, Hadjichristidis N, Roovers J (1996) Synthesis of model 16-miktoarm (vergina) star copolymers of the A_8B_8 type. Macromolecules 29:6076–6078
74. Siloula S, Hadjichristidis N, Thomas EL (1998) Novel dimensionally periodic non-constant mean curvature morphologies of 3-miktoarm star terpolymers of styrene, isoprene, and MMA. Macromolecules 31:5272–5277
75. Fujimoto T, Zhang H, Kazama T, Isono Y, Hasegawa H, Hashimoto T (1992) Preparation and characterization of novel star-shaped copolymers having three different branches. Polymer 33:2208–2213
76. Hückstädt H, Abetz V, Stadler R (1996) Synthesis of a PS arm-PB arm-PMMA triarm star copolymer. Macromol Rapid Commun 17:599–606
77. Takano A, Wada S, Sato S, Araki T, Hirayama K, Kazama T, Kawahara S, Isono Y, Ohono A, Tanaka N, Matsushita Y (2004) Observation of cylinder based microphase-separated structures from ABC star-shaped terpolymers investigated by computerized tomography. Macromolecules 37:9941–9946

78. Hayashida K, Kawashima W, Shinohara Y, Amemiya Y, Nozue Y, Matsushita Y (2006) Arcimedean tiling patterns of ABC star-shaped terpolymers studied by microbeam SAXS. Macromolecules 39:4869–4872

79. Hayashida K, Saito N, Arai S, Tanaka N, Matsushita Y (2007) Hierarchical morphologies formed by ABC star-shaped terpolymers. Macromolecules 40:3695–3699

80. Hayashida K, Takano A, Dotera T, Matsushita Y (2008) Giant zincblende structures formed by an ABC star-shaped terpolymers/ homopolymer blend system. Macromolecules 41:6269–6271

81. Matsushita Y (2008) Precise molecular design of complex polymers and morphology control of their hierarchical multiphase structures. Polymer J 40:177–183

82. Quirk RP, Lee B, Schock LE (1992) Anionic synthesis of PS and PB heteroarm star polymers. Macromol Symp 53:201–210

83. Fernyhough CM, Young RN, Tack RD (1999) Synthesis and characterization of PI-PMMA AB diblock and A_2B_2 hereroarm star copolymers. Macromolecules 32:5760–5764

84. Quirk RP, Yoo T, Lee B (1994) Anionic synthesis of heteroarm star-branched polymers. J Macromol Sci Pure Appl Chem A 31:911–926

85. Wang X, He J, Yang Y (2007) Synthesis of ABCD-type miktoarm star copolymers. J Polym Sci Part A Polym Chem 45:4818–4828

86. Lambert O, Dumas P, Hurtrez G, Riess G (1997) Synthesis of amphiphilic triarm star copolymer based on PS, PEO, and poly(ε-caprotactone). Macromol Rapid Commun 18:343–351

87. Nasser-Eddine M, Reutenauer S, Delaite C, Hurtrez G, Dumas P (2004) Synthesis of PS-P (^{t}BMA)-PEO triarm star block copolymers. J Polym Sci Part A Polym Chem 42:1745–1751

88. Hirao A, Higashihara T (2004) Precise synthesis of star-branched polymers by means of living anionic polymerization using 1,1-bis(3-chloromethylphenyl)ethylene. Macromol Symp 215:57–65

89. Higashihara T, Hirao A (2004) Synthesis of asymmetric star-branched polymers consisting of 3 or 4 different segments in composition by means of living anionic polymerization with a dual-functionalized 1,1-bis(3-chloromethylphenyl)ethylene. J Polym Sci Part A Polym Chem 42:4535–4547

90. Mavroudis A, Hadjichristidis N (2006) Synthesis of well-defined 4-miktoarm star quaterpolymers (4m-SIDV) with incompatible arms. Macromolecules 39:535–540

91. Hanisch A, Schmalz H, Müller AHE (2012) A modular route for the synthesis of ABC miktoarm star terpolymer via a new alkyne-substituted DPE derivative. Macromolecules 45:8300–8309

92. Li Z, Hillmyer MA, Lodge TP (2004) Synthesis and characterization of triptych μ-ABC star triblock copolymers. Macromolecules 37:8933–8940

93. Saito N, Liu C, Lodge TP, Hillmyer MA (2008) Multicompartment micelles from polyester-containing ABC miktoarm star terpolymers. Macromolecules 41:8815–8822

94. Liu C, Hillmyer MA, Lodge TP (2009) Multicompartment micelles from pH-responsible miktoarm star block terpolymers. Langmuir 25:13718–13725

95. Higashihara T, Yoo HS, Hayashi M, Hirao A (2010) Combining living anionic polymerization with branching reactions in an iterative fashion to design branched polymers. Macromol Rapid Commun 31:1031–1059

96. Hirao A, Goseki R, Ishizone T (2014) Advance in living anionic polymerization. Macromolecules 47:1883–1905

97. Higashihara T, Inoue K, Nagura M, Hirao A (2006) Successive synthesis of well-defined star-branched polymers by an iterative approach based on living anionic polymerization. Macromol Res 14:287–299

98. Hirao A, Hayashi M, Higashihara T (2001) Synthesis of well-defined star-branched polymers by an iterative approach based on living anionic polymerization using DPE derivatives. Macromol Chem Phys 202:3165–3173

99. Higashihara T, Hayashi M, Hirao A (2002) Radical coupling reaction of DPE-functionalized polymers with potassium naphthalenide and its application to syntheses of in-chain-functionalized polymers and star-branched polymers. Macromol Chem Phys 203:166–175

100. Hirao A, Higashihara T (2002) Synthesis of well-defined star-branched polymers via an iterative approach using living anionic polymers. Macromolecules 35:7238–7245

101. Higashihara T, Sakura T, Hirao A (2009) Successive synthesis of asymmetric star-branched polymers based on iterative methodology using DPE derivatives of alternative choice at each iteration. Macromolecules 42:6006–6014

102. Sugiyama K, Inoue K, Higashihara T, Hayashi H, Hirao A (2009) Synthesis of well-defined block copolymers and star-branched polymers by using terminal 1,3-butadiene functionalized polymers as reactive building blocks. React Funct Polym 69:480–492

103. Hirao A, Higashihara T, Inoue K (2008) Successive synthesis of well-defined asymmetric star-branched polymers up to seven-arm, seven-component ABCDEFG type by an iterative methodology base on living anionic polymerization. Macromolecules 41:3579–3587

104. Higashihara T, Kitamura M, Haraguchi N, Sugiyama K, Hirao Ahn JH, Lee JS (2003) Synthesis of well-defined star-branched polymers by using chain-end-functionalized PSs with a definite number of 1,3-butadienyl groups and its derivatized functions. Macromolecules 36:6730–6738

105. Hirao A, Murano K, Oie T, Uematsu M, Goseki R, Matsuo Y (2011) Chain-end- and in-chain-functionalized AB diblock copolymers as key building blocks in the synthesis of well-defined architectural polymers. Polym Chem 2:1219–1233

106. Ito S, Senda S, Goseki R, Hirao A (2012) Precise synthesis of miktoarm star polymers by using a new dual-functionalized 1,1-diphenylethylene derivative in conjunction with living anionic polymerization system. Macromolecules 45:4997–5011

107. Ito S, Goseki R, Ishizone T, Senda S, Hirao A (2013) Successive synthesis of miktoarm star polymers having up to seven arms by a new iterative methodology based on living anionic polymerization using a trifunctional lithium reagent. Macromolecules 46:819–827

108. Hirao A, Inoue K, Higashihara T (2006) Successive synthesis of regular and asymmetric star-branched polymers by iterative methodology based on living anionic polymerization using functionalized DPE derivatives. Macromol Symp 240:31–40

109. Higashihara T, Inoue K, Hirao A (2010) Successive synthesis of well-defined star-branched polymers by "convergent" iterative methodology using core-functionalized 3-arm star-branched polymer and a specially designed functionalized DPE derivatives. Macromol Symp 296:53–62

110. Higashihara T, Nagura M, Inoue K, Haraguchi N, Hirao A (2005) Successive synthesis of well-defined star-branched polymers by a new iterative approach involving coupling and transformation reactions. Macromolecules 38:4577–4587

111. Hayashi M, Negishi Y, Hirao A (1999) Synthesis of heteroarm star-branched polymers by means of living anionic polymerization in conjunction with functional group transformation. Proc Jpn Acad Ser B Phys Biol Sci 75:93–96

112. Hirao A, Hayashi M, Matsuo A (2002) Synthesis of well-defined heteroarm star-branched polymers by coupling reaction of chain-functionalized PSs with BnX moieties with living anionic polymers of *tert*-butyl methacrylate. Polymer 43:7125–7131

113. Hirao A, Tokuda Y, Morifuji K, Hayashi M (2001) Synthesis of star polymers by reactions of end-functionalized PSs with chloromethylphenyl groups with polymer anions consisting of two polymer chains. Macromol Chem Phys 202:1606–1613

114. Hirao A, Matsuo A, Morifuji K, Tokuda Y, Hayashi M (2001) Synthesis of heteroarm star polymers by means of living anionic polymerization. Polym Adv Tech 12:680–686

115. Hirao A, Tokuda Y (2003) Synthesis of well-defined star polymers by coupling reactions of polymer anions consisting of two polymer chains with chain-end-multifunctionalized PSs with BnBr moieties. Macromolecules 36:6081–6086

116. Hirao A, Kawasaki K, Higashihara T (2004) Precise synthesis of asymmetric star shaped polymers by coupling reactions of new specially designed polymer anions with chain-end-functionalized PSs with BnBr moieties. Sci Tech Adv Mater 5:469–477

117. Hirao A, Kawasaki K, Higashihara T (2004) Synthesis of well-defined star-branched polymers by coupling reaction of star-branched polymer anions comprising three polymer segments with chain-end-functionalized PSs with a definite number of BnBr moieties. Macromolecules 37:5179–5189

118. Higashihara T, Faust R, Inoue K, Hirao A (2008) Synthesis of novel multi-functional polyisobutylenes at chain end(s) and their application to A_nB asymmetric star and A_nBA_n pompom polymers by combination of living cationic and anionic polymerizations. Macromolecules 41:5616–5625

119. Kanga RS, Hogen-Esch TE, Randrianalimanana E, Soum A, Fontanille M (1990) Studies of anionic polymerization of phenyl vinyl sulfoxide and its copolymer with styrene. Macromolecules 23:4235–4240

120. Kanga RS, Hogen-Esch TE, Randrianalimanana E, Soum A, Fontanille M (1990) Thermal elimination of poly(phenyl vinyl sulfoxide) and its polystyrene block copolymers. Macromolecules 23:4241–4246

121. Hirao A, Karasawa Y, Higashihara T, Zhao Y, Sugiyama K (2004) Synthesis of block copolymers and star-branched polymers consisting of conducting poly(acetylene) segments via ionic interaction to form ionic bond. Des Monomers Polym 7:647–660

122. Sugiyama K, Karasawa Y, Higashihara T, Zhao Y, Hirao A (2006) Synthesis of block copolymers and asymmetric star-branched polymers comprised of PA and PS segments via ionic bond formation. Chemical Monthly 137:869–880

123. Zhao Y, Higashihara T, Sugiyama K, Hirao A (2005) Synthesis of functionalized asymmetric star-branched polymers containing conductive PA segments by living anionic polymerization. J Am Chem Soc 127:14158–14159

124. Zhao Y, Higashihara T, Sugiyama K, Hirao A (2007) Synthesis of asymmetric star-branched polymers having two PA arms by means of living anionic polymerization using DPE derivatives. Macromolecules 40:228–238

125. Lee JS, Ryu SW (1999) Anionic living polymerization of 3-(triethoxysilyl)propyl isocyanate. Macromolecules 32:2085–2087

126. Shin YD, Kim SY, Ahn JH, Lee JS (2001) Synthesis of poly(n-hexyl isocyanate) by controlled anionic polymerization in the presence of $NaBPh_4$. Macromolecules 34:2408–2410

127. Ahn JH, Shin YD, Nath GY, Park SY, Rahman MS, Samal S (2005) Unprecedented control over polymerization of n-hexyl isocyanate using an anionic initiator having synchronized function of chain-end protection. J Am Chem Soc 127:4132–4133

128. Rahman MS, Samal S, Lee JS (2007) Quantitative in situ coupling of living diblock copolymers for the preparation of amphiphilic coil-rod-coil triblock copolymer, P2VP-*b*-poly(n-hexyl isocyanate)-*b*-P2VP. Macromolecules 41:7029–7032

129. Rahman MS, Changez M, Yoo JW, Lee CH, Samal S, Lee JS (2008) Synthesis of amphiphilic miktoarm star copolymers of poly(n-hexyl Isocyanate) and poly(ethylene glycol) through reaction with the active methylene group. Macromolecules 41:7029–7032

130. Rodriguez-Hernandes J, Checot F, Gnanou Y, Lecommandoux S (2005) Toward 'smart' nano-object by self-assembly of block copolymers in solution. Prog Polym Sci 30:691–724

131. Klok H, Lecommandoux S (2006) Solid-state structure, organization, and properties of peptide-synthetic hybrid block copolymers. Adv Polym Sci 202:75–111

132. Lecommandoux S (2011) Bulk self-assembly of linear hybrid polypeptide-based diblock and triblock copolymers. In: Hadjichristidis N, Hirao A, Tezuka Y, Du Prez F (eds) Complex macromolecular architectures: synthesis, characterization, and self-assembly. John-Wiley & Sons (Asia), Singapore, pp 623–645

133. Deming TJ (2006) Polypeptide and polypeptide hybrid copolymer synthesis via NCA polymerization. Adv Polym Sci 202:1–18

134. Aliferis T, Iatrou H, Hadjichristidis N (2004) Living polypeptides. Biomacromolecules 5:1653–1656
135. Aliferis T, Iatrou H, Hadjichristidis N (2005) Well-defined linear multiblock and branched polypeptides by linking chemistry. J Polym Sci Part A Polym Chem 43:4670–4673
136. Hanski S, Houbenov N, Ruokolainen J (2006) Hierarchical ionic self-assembly of rod-comb block copolypeptide-surfactant complexes. Biomacromolecules 7:3379–3384
137. Lu H, Cheng J (2007) Hexamethyldisilazane-mediated controlled polymerization of NCAs. J Am Chem Soc 129:14114–14115
138. Schlaad H, Antonietti M (2003) Block copolymer amino acid sequences: molecular chimeras of polypeptides and synthetic polymers. Eur Phys J E Soft Matter 10:17–23
139. Hadjichristidis N, Iatrou H, Pitsikalis M, Sakellariou G (2009) Synthesis of well-defined polypeptide-based materials via the ring-opening polymerization of NCAs. Chem Rev 109:5528–5578
140. Iatrou H, Pitsikalis M, Sakellariou G, Hadjichristidis N (2011) Complex macromolecular chimeras. In: Hadjichristidis N, Hirao A, Tezuka Y, Du Prez F (eds) Complex macromolecular architectures: synthesis, characterization, and self-assembly. John-Wiley & Sons (Asia), Singapore, pp 461–490
141. Karatzas A, Iatrou H, Hadjichristidis N, Inoue K, Sugiyama K, Hirao A (2008) Complex macromolecular chimeras. Biomacromolecules 9:2072–2080
142. Junnila S, Houbenov N, Karatzas A, Hadjichristidis N, Hirao A, Iatrou H, Ikkala O (2012) Side-chain-controlled self-assembly of polystyrene-polypeptide miktoarm star copolymer. Macromolecules 45:2850–2856

Synthesis of Dendrimer-Like Polymers

Junpo He, Jia Li, and Shaohui Yang

Abstract This chapter reviews the synthesis of dendrimer-like polymers based on controlled or living polymerization techniques. Dendrimer-like polymers possess multiple chains interconnected in a dendritic way. The synthetic strategies include divergent and convergent methods, as those for regular dendrimers, in combination with the preparation of the polymer chains either in situ or in separate batches. The divergent approach usually starts from a core with multifunctional initiation or coupling reaction sites, followed by iterative polymerization/chain-end functionalization, or grafting-to reaction/end-group transformation of the upcoming polymer chains, respectively, to form dendrimer-like polymers of up to seventh generation. The convergent approach involves efficient coupling reactions, such as reaction between chlorosilane and living polymeric anion, and the reactivation of the joint point into living anion in an alternating way. The latter suffers from more serious steric hindrance than the former. A variety of dendrimer-like polymers, such as poly (ethylene oxide) (PEO), polystyrene (PS), poly(meth)acrylates, polycaprolactone (PCL), and their related copolymers, have been reported in the literature. The control of molecular parameters of dendrimer-like products will be discussed in the synthetic point of view.

Keywords Dendrimer-like polymers • Anionic polymerization • Divergent method • Convergent method • Polymer architecture

1 Introduction

Dendrimer-like star-branched polymers are a kind of dendritic architectures in which successive generations are interlinked by polymer chains emanating radially from a central core [1]. The presence of polymer chain spacers between consecutive generations may render the dendrimer-like polymers new properties associated with the dendritic effect as well as the chemical structure of the repeating and branching

---

J. He (✉) • J. Li • S. Yang
Department of Macromolecular Science, The State Key Laboratory of Molecular Engineering of Polymers, Collaborative Innovation Center of Polymers and Polymer Composite Materials, Fudan University, Shanghai 200433, China
e-mail: jphe@fudan.edu.cn

units. Therefore, the molecular parameters that need to be controlled in the synthesis may include: (1) the chemical structure that builds the backbone of the dendritic molecule; (2) the molecular weights of the polymer chains as the spacers; (3) the number of functionalities of the branch units; (4) the generation number; and (5) the number and chemical structure of the peripheral functionalities. These factors determine, independently or concurrently, the size, shape, compactness of molecular conformation, solubility, viscosity, rheology, surface properties, etc., of the resulting dendrimer-like star-branched polymers [2–6].

In comparison with the synthesis of regular dendrimers, the synthesis of dendrimer-like star polymers is complicated by the incorporation of polymer chains into dendritically branched structures. In order to control the length and the end functionality of the spacers, controlled/"living" polymerization techniques are usually employed for the formation of corresponding polymer chains either in situ or prior to the construction of dendritic structure. These polymerizations techniques, such as anionic polymerization, ring-opening polymerization (ROP), and atom transfer radical polymerizations (ATRP) afford branches with well-controlled length, narrow length distribution, and precision number and location of the functional groups.

This chapter reviews the synthesis of dendrimer-like star polymers with different structural designation, arm number, and composition by stepwise iterative methodologies. We will focus on the synthetic strategies based on the divergent or convergent approaches in combination with the principle of polymer chain formation. Star-like polymers prepared using dendritic initiators will not be included in this chapter.

2 Synthetic Methodology

In a similar way to the synthesis of conventional dendrimers [7, 8], dendrimer-like star polymers are prepared through either divergent or convergent approaches (Scheme 1) [9, 10]. In both approaches, the polymer segments are formed either by in situ polymerization starting from a core ("core first") or by presynthesized polymer precursors with terminal functionalities ("arm first").
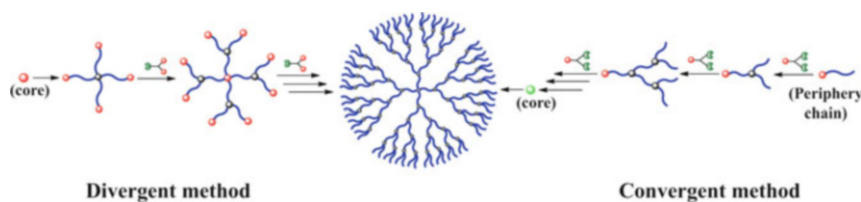
Scheme 1 Synthesis of dendrimer-like polymers through divergent and convergent methodologies (Redrawn from Ref. [9])

Five structural parameters must be considered in the synthesis, that is, the core, the polymer chain, the branch point, the surface functionality, as well as the overall structure of the dendrimer-like polymers (e.g., homopolymer or block copolymer). In general, the selection of a synthetic route is a result of comprehensive consideration of these parameters.

2.1 Divergent Chain Growing/Branching Approach

The synthesis of dendrimer-like star polymers was first reported by Gnanou and coworkers [11]. They developed a divergent chain growing/branching approach in the synthesis of dendritic star-branched poly(ethylene oxide) (PEO) up to the second generation [11]. The work set up a general principle for the synthesis of dendrimer-like star polymers, in which iterative polymerization and chain branching led to the "growing up" of the dendritic molecules. The synthesis usually starts from a multifunctional core with certain number of functionalities (Table 1). The choice of the polymerization type is associated with the chemical nature of the target molecules. Thus, the core initiates the polymerization of a monomer, yielding a star-like polymer with same number of end groups as the core. Fidelity of the end group is very important for the subsequent branching reaction, and therefore to the perfection of the final product. Then, the end groups of the star-like polymer are converted into double or multiple numbers of functionalities that are able to initiate further polymerization. Dendrimer-like polymers can be prepared after performing polymerization and end-group transformation several times in an alternating way.
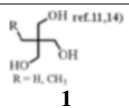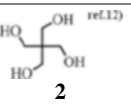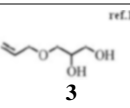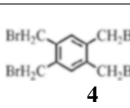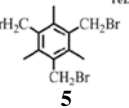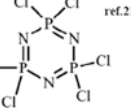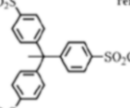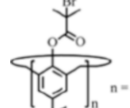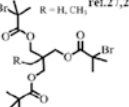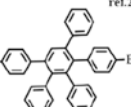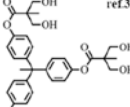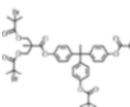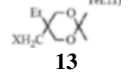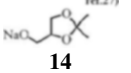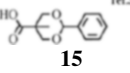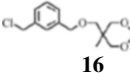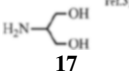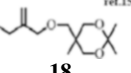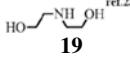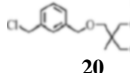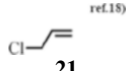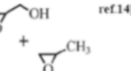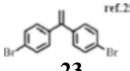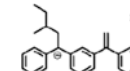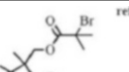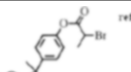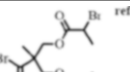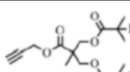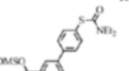
The compounds of core precursors are usually multifunctional initiators possessing initiating sites such as hydroxyl groups for ROP of ethylene oxide (EO) or ε-caprolactone (ε-CL) or lactide, alkyl halides for ATRP or living radical polymerization of vinyl monomers, as well as living anionic polymerization. The branching agents are AB_n-type compounds bearing one A group for coupling and n (protected) B group for branching. Representative core precursors and branching agents are listed in Table 1.

2.1.1 PEO-Based Dendrimer-Like Polymers

PEO-based dendrimer-like polymers exhibit three kinds of featured structures, that is, dendrimer-like PEO homopolymers, dendrimer-like PEO with various functionalities, and dendrimer-like PEO containing block copolymers.

Dendrimer-like PEOs and PEO-containing copolymers were synthesized by using commercially available or readily accessible multihydroxyl compounds, such as **1** and **2**, as the starting core precursors [11, 12]. The hydroxyl groups were partially activated through deprotonation by diphenylmethyl potassium (DPMK) for subsequent initiating ROP of EO. The polymerization was mediated by the dynamic equilibrium between the activated and dormant species, resulting in

Table 1 Multifunctional core molecules and branching agents in the synthesis of dendrimer-like polymers

Multifunctional core molecules			
1	**2**	**3**	**4**
5	**6**	**7**	**8**
9	**10**	**11**	**12**
Branching agents			
13	**14**	**15**	**16**
17	**18**	**19**	**20**
21	**22**	**23**	**24**
25	**26**	**27**	**28**
29	**30**		

star-like PEO possessing same number of hydroxyl end groups as that in the precursor. The branching reaction was achieved using various branching agent or reactions, usually in two or more steps, to afford double or multiple number of hydroxyls for the initiation/polymerization of the next generation. For instance, 2,2-dimethyl-5-ethyl-5- chloromethyl-1,3-dioxane (**13**), a compound bearing one
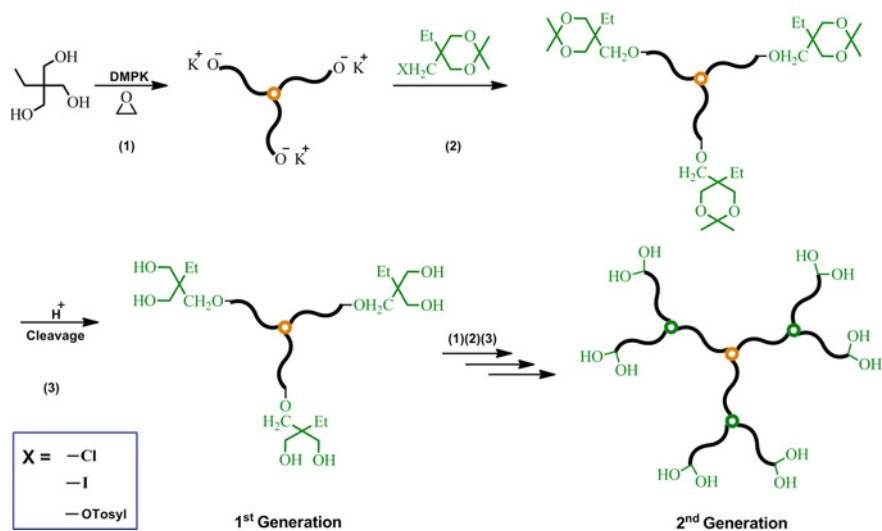
Scheme 2 Synthesis of dendrimer-like PEO reported by Gnanou. Adapted from Ref. [11] with permission from Wiley

chloromethyl and two hydroxyl groups protected in acetal form, was used as branching agent in the synthesis of dendrimer-like PEO. The branching reaction was accomplished through formation of ether linkage between chloromethyl and hydroxyl end groups in the core or preceding generation, followed by recovery of dihydroxyl groups via acidic hydrolysis of the protecting ketal function (Scheme 2) [11]. In this synthesis, the molecular weight of the PEO chain was determined by the feed ratio of EO to hydroxyl groups, whereas the number of branch points and peripheral groups were controlled by stepwise branching reactions.

An alternative way of branching was a two-step process using allyl chloride as the branching agent. The hydroxyl groups of the core or dendritic PEO were vinylated through nucleophilic attack towards allyl chloride, followed by dihydroxylation using OsO_4 and N-methylmorpholine-N-oxide (NMO). Dendrimer-like PEOs of up to eight generations was synthesized with the molecular weight of 900,000 g/mol and ~384 external hydroxyl functions [13].

The above-mentioned branching reactions were two- or multistep processes. Later on, Gnanou and coworkers developed a one-pot procedure for faster formation of branching sites using glycidol as the branching agent [14]. After completion of EO polymerization initiated by **1**, glycidol and propylene oxide (PO) were introduced sequentially or as a mixture. Copolymerization occurred to produce polyether chains with multiple alkoxides. The role of PO was to minimize the aggregation of the generated alkoxides. The resulting multiple alkoxides were able to initiate the polymerization of EO and subsequently glycidol and PO in a cascade manner. The process did not require separation of the intermediates. Although the number of branches was not precisely controllable for each branching segment

(copolymer of glycidol and PO), the average number of hydroxyl groups depended on the feed ratio of glycidol to PO. The overall synthesis was performed in a semicontinuous way in one pot, affording third-generation dendrimer-like PEO with an average molecular weight of up to 55,000 g/mol [14].

Functional dendrimer-like PEOs bearing vinylic groups at the branch points were synthesized. For this purpose, a specific AB$_2$C type branching agent, 2,2-dimethyl-5-(2'-chloromethyl-propenyloxymethyl)-5-methyl-1,3-dioxane (**18** in Table 1), was designed and utilized to introduce vinylic group during chain branching process (the vinylic group can also be introduced by copolymerization of allyl glycidyl ether with glycidol and PO [14]). The vinyl group was subsequently transformed into ATRP initiating sites via a two-step process: hydroboration–oxidation reaction to yield two hydroxyl groups from one allylic group and then esterification of the hydroxyl groups with 2-bromopropionyl bromide; finally, the bromopropionate initiate ATRP of *tert*-butyl acrylate, yielding pH sensitive dendrimer-like PEO carrying interior poly(acrylic acid) (PAA) after hydrolysis [15].

Propionyl halide derivatives **26** and **27** possessing two bromopropionates were used as branching agents capable of switching ROP to ATRP. The peripheral groups of star-like or dendrimer-like PEO were converted from hydroxyl into 2-bromopropionate moieties through esterification with **26** or **27**. Styrene and *tert*-butyl acrylate were polymerized with the initiation of 2-bromopropionate groups, leading to the formation of amphiphilic dendrimer-like block copolymer, PEO-*b*-P*t*BA [16] or PEO-*b*-PS [12, 17], respectively.

A number of dendrimer-like PEO-based polymers with various structures, compositions, and functionalities were reported employing core-first divergent growing/branching strategy. In addition to PEO homopolymers, dendrimer-like copolymers with layered-type, Janus-type, and bouquet-type chain arrangements were synthesized. For instance, amphiphilic layered-type PEO$_n$-*b*-PS$_{2n}$ [12, 17] and PEO$_n$-*b*-P*t*BA$_{2n}$ (precursor of water-soluble PEO$_n$-*b*-PAA$_{2n}$) [16] were obtained by combining AROP of EO and ATRP of styrene or *t*-BA, as mentioned above. Janus-type dendrimer-like PEOs consist of two dendrons of different branching units and surface functionalities were prepared starting from an asymmetric core, 3-allyloxy-1,2-propanediol (**3**), in which one dendron grew from diol with the branching agent **20** and the other dendron was formed from allyl moiety, after hydroxylation, with the branching agent **21** [18, 19]. The growth of the two dendrons was performed in an alternate way under different reaction conditions, resulting in Janus-type dendrimer-like PEO bearing orthogonal functionalizations on the surface. Bouquet-type dendrimer-like PEOs with an aldehyde focus and 16 peripheral hydroxyls were prepared using a protected acetal compound, 3,3-diethoxyl-1,2-propanediol, through a two-step branching reaction involving hydroxyl allylation and then vinyl osmylation [20]. The two hydroxyl groups were initiating sites for ROP of EO, while the protected acetal was converted into aldehyde after the synthesis of the target products.

Combination of core-first and arm-first methods, using hexachlorocyclophosphazene as the core, resulted in the synthesis of dendrimer-like PEO with a phosphazene core [21]. After the peripheral hydroxyl moieties were functionalized

with sulfated β-lactose, the dendrimer-like product exhibited anti-inflammatory activity [22].

2.1.2 PS-Based Dendrimer-Like Polymers

Gnanou and coworkers also prepared dendrimer-like polystyrene (PS) and copolymers in a similar way by combination of atom transfer radical polymerization (ATRP) and chain-end transformation [3]. In these studies, calixarene derivatives bearing 4, 6, or 8 bromoisobutyl groups, prepared from esterification with 2-bromo-isobutyryl bromide, were used as cores to initiate ATRP of styrene to generate PS stars as the first generation containing same number of terminal bromo functionalities. The bromo end groups were transformed into twofold terminal 2-bromo-isobutyrate groups through a two-step process, for example, reaction with 2-amino-1,3-propanediol and subsequent with 2-bromo-isobutyryl bromide. The resulting products served as multifunctional macroinitiators for the formation of the second generation. Repeating ATRP and end-group modification yielded dendrimer-like PSs of third generation comprising of 16, 24, or 32 arms in the outmost layer, respectively [3].

The method can be readily applied to other vinyl monomers that are polymerizable through ATRP. Dendrimer-like block copolymers of styrene and *t*-butyl acrylate were prepared by direct sequential polymerization [23]. Dendrimer-like block copolymers PS-*b*-PEOs with layered structure were synthesized by combination of ATRP of styrene and ROP of EO. The ATRP steps resulted in multiple bromo termini, which were transformed into hydroxyl groups and used to initiate ROP of EO [24].
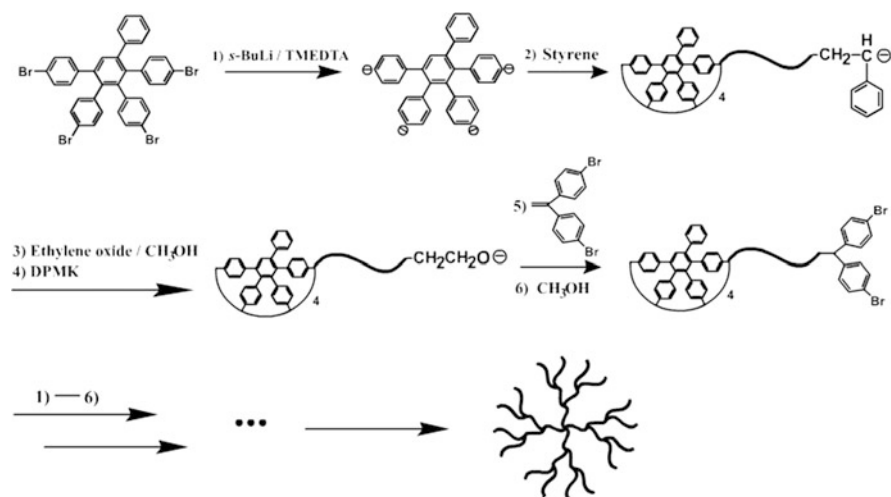
Scheme 3 Synthesis of dendrimer-like polymers by anionic polymerization using TERMINI strategy reported by Gnanou. Adapted from Ref. [25] with permission from ACS

Anionic polymerization was applied in the synthesis of dendrimer-like polystyrene through TERMINI technique (TERminating agent and Multifunctional INItiator, a concept proposed by Percec, *vide infra*) [25]. As shown in Scheme 3, the synthesis started from a multianion core prepared by bromine–lithium exchange between *sec*-butyllithium (*sec*-BuLi) and multibromoaryl compound. The multianion core initiated the polymerization styrene. After the polymerization the living chain ends were transformed into oxygen anion through ring-opening reaction of EO, followed by addition to 4,4'-dibromodiphenylethylene, the TERMINI agent. The resulting multibromoaryl compound was activated again by bromine–lithium exchange with *sec*-BuLi, followed by the initiation of styrene anionic polymerization. Dendrimer-like PS and PB up to seventh and third generations, respectively, were obtained in such a divergent way [25].

A notable double way of polymerization transformation, for example, from ATRP to ROP and to ATRP again, was developed by Pan and coworkers in the synthesis of dendrimer-like star copolymers of styrene and $_L$-lactide or carprolactone [26–28]. ATRP of styrene initiated by a tri(alkyl bromide) compound **9** resulted in the first-generation star-like polystyrene. The bromo end groups were converted into six hydroxyl groups through reaction with a branching agent, 2,2-dimethyl-1,3-dioxolane-4-methanol (**14**), followed by ROP of $_L$-lactide. The hydroxyl end groups were then transformed into 12 alkylbromide groups via reaction with 2,2-bis(methylene-α-bromoisobutyryl)propionyl chloride (**25**), followed by ATRP of styrene to form the third generation. Dendrimer-like star copolymer, PS_3-b-$PLLA_6$-b-PS_{12}, was obtained as the final product. Similarly, starting from pentaerythritol, dendrimer-like star block copolymer of styrene and ε-CL was synthesized and labelled with fluorescent pyrene as the peripheral functionality.

Copper catalyzed azide–alkyne cycloaddition is an efficient cross-coupling reaction (the "click" reaction). The bromo terminal of ATRP products can be readily transformed into azido group by the reaction with NaN_3. Thus, a star-like PS, made from ATRP of styrene initiated by a tri(alkyl bromide) core (**9**), was functionalized with three azido groups and then underwent "click" reaction with propargyl 2,2-bis(2'-bromo-2'methylpropinoyloxy)methyl propionate (**28**). The resulting star polymer had six terminal bromides and was used to initiate ATRP of styrene. Repeating the above process afforded dendrimer-like star polystyrene or PS-b-PtBA up to third generation [29].

2.1.3 PCL-Based Dendrimer-Like Polymers

Hedrick is the first to give the name "dendrimer-like star polymers" to a series of dendritic poly(ε-caprolactone)s (PCL)s and poly(L-lactide)s synthesized by a divergent approach using repetitive living ROP and end-group functionalization [6, 30–36]. As shown in Scheme 4, the synthesis started from a trimeric 2,2-bis (hydroxymethyl)propionate (**11**) bearing six hydroxyl groups as the core initiator. ROP of ε-CL or lactide in the presence of stannous-2-ethylhexanoate ($Sn(Oct)_2$)
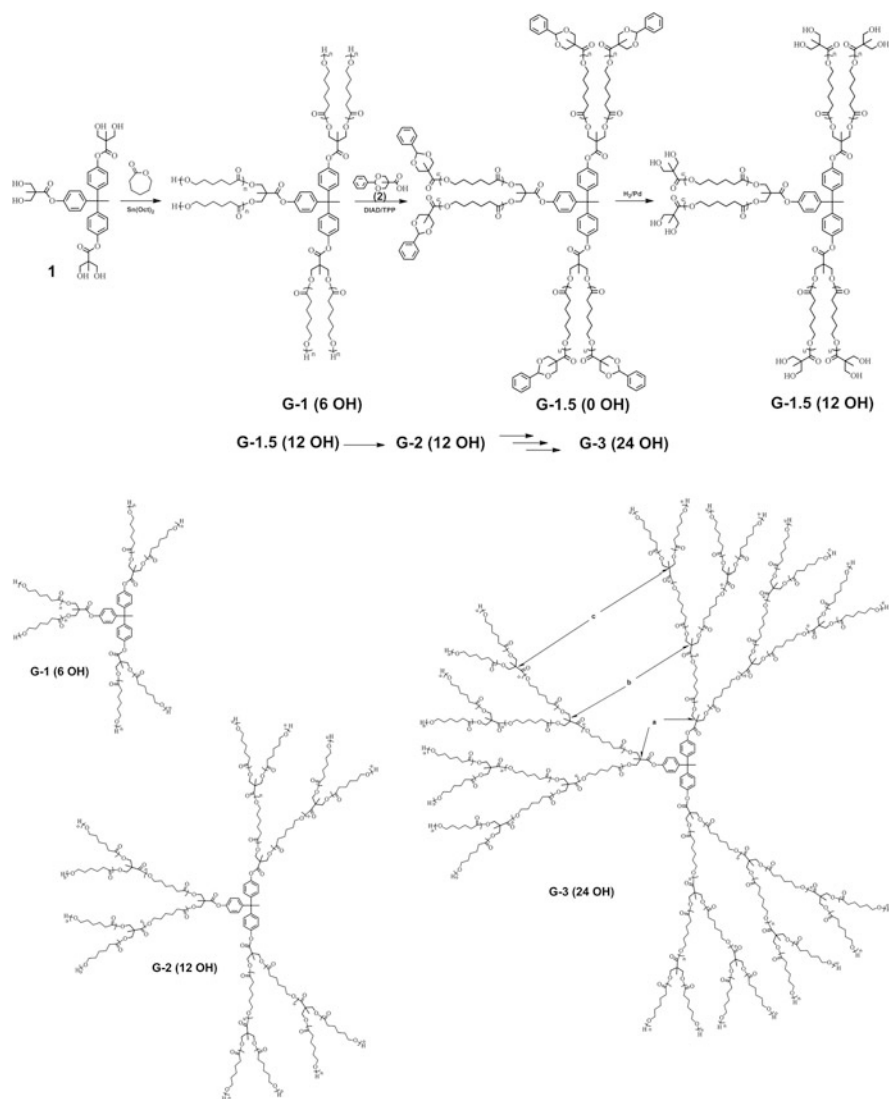
Scheme 4 Synthesis of dendrimer-like PCL via ring-opening polymerization reported by Hedrick et al. Reproduced from Ref. [30] with permission from ACS

proceeded in a living fashion and resulted in six-arm products (G-1) with six hydroxyl termini. The branching reaction was achieved via esterification of hydroxyls with 2,2-bis(hydroxymethyl)propionic acid in which the two hydroxyl groups were protected by benzylidene in an acetal form(15). After hydrolysis under appropriate conditions 12 hydroxyl groups were recovered and used to initiate the polymerization of ε-CL to yield the second-generation dendrimer-like PCL (G-2).

Repeating the above steps resulted in the third-generation (G-3) product possessing 24 arms at the periphery, with $M_n = 96,000$ g/mol and $M_w/M_n = 1.14$.

The above process involved the living ROP and quantitative organic transformation of branching groups, therefore allowing precise control on molecular weight and the number of functional chain ends. The method was then extended to the preparation of layered dendrimer-like star copolymers consisted of chain polymers and dendrons for different generations. Thus, the hexahydroxyl compound **11** was used to initiate the ROP of ε-CL to prepare a six-arm star PCL bearing six hydroxyl end groups as the first generation, G1(6OH). The hydroxyl termini were then coupled, via esterification, with *Bis-HMPA*-derived dendrons (1–3 generations, Scheme 5) to build the second generation. The dendrons carried a benzylidene protected carboxylic group and different number of potential hydroxyl groups protected in the form of *tert*-butyldimethylsiloxy (*t*-BuMe$_2$SiO-) groups. The carboxylic and hydroxyl groups could be selectively recovered by hydrogenolysis and BF$_3$-Et$_2$O treatment, respectively, in different steps. The obtained two-layered dendrimer-like star copolymers contained a central six-arm star PCL (as the first generation) and 12, 24, or 48 hydroxyl groups in the second generation. Further initiation of ROP of ε-CL resulted in the formation of three-layered dendrimer-like products [6].

The combination of ROP and coupling with dendron facilitated the synthesis of constitutional isomers of PCL-based dendrimer-like star polymers [31]. In these isomers, the molecular weights were very close and the molecular weight distributions were narrow. The number of branching points (45) and surface hydroxyl groups (48) were identical among various isomers. The difference among these isomers was the radial location of branch points tuned by controlling the molecular weights in ROP and coupling with different generations of dendrons. In addition, amphiphilic linear-dendritic block copolymers with orthogonal number of head (dendron) and tail (PCL chain) were synthesized through ROP initiated by rationally designed functionalized dendrons with various functionalities based on the protection and deprotection of *Bis-HMPA* derivatives [33].

The hydroxyl peripheral groups can be directly used to initiate the polymerization of lactide, or easily transformed into alkyl bromide, the initiator for ATRP, through esterification with 2-bromo-isobutyryl bromide. The former allowed the synthesis of dendrimer-like star block copolymers containing a star-like core made from polymerization of various substituted lactone (substitution in order to prevent crystallization) and an outer layer of poly(lactide) [36], whereas the latter facilitated the synthesis of dendrimer-like star block copolymers containing PCL, PMMA, and poly(hydroxyethyl methacrylate) segments [37, 38].

2.1.4 PMMA-Based Dendrimer-Like Polymers

Percec and coworkers developed a new synthetic approach named TERMINI, in which the chain branching was fulfilled by using irreversible TERminator Multifunctional INItiator (TERMINI). TERMINI is a masked multifunctional
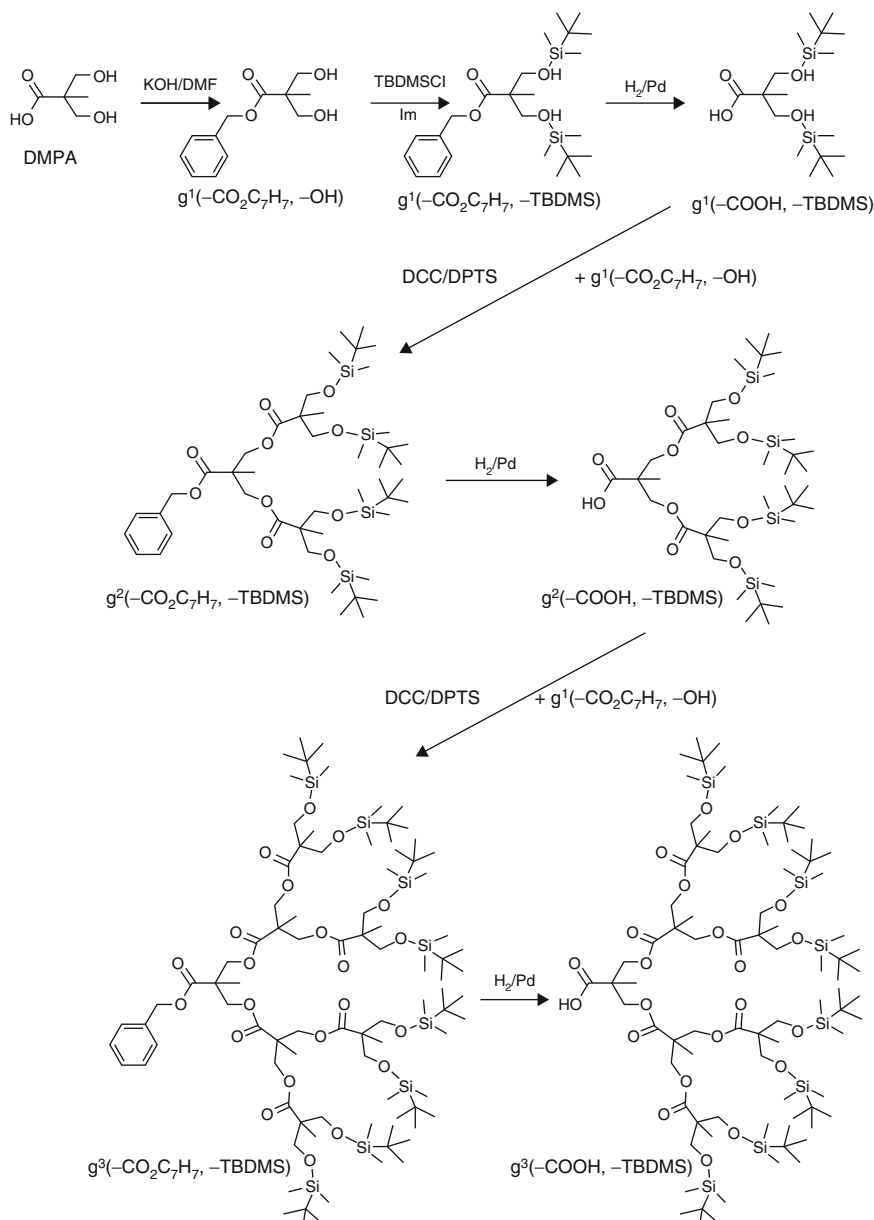
Scheme 5 Synthesis of *Bis*-HMPA-derived dendrons as the branching agent. Reproduced from Ref. [6] with permission from Wiley

compound possessing terminating moiety to living chain polymerization and initiating moieties, after deprotection, for further polymerizations in two or more directions [39–41]. Thus, TERMINI played the role of a branching agent. The termination, deprotection reaction, and reinitiation were quantitative. A series of
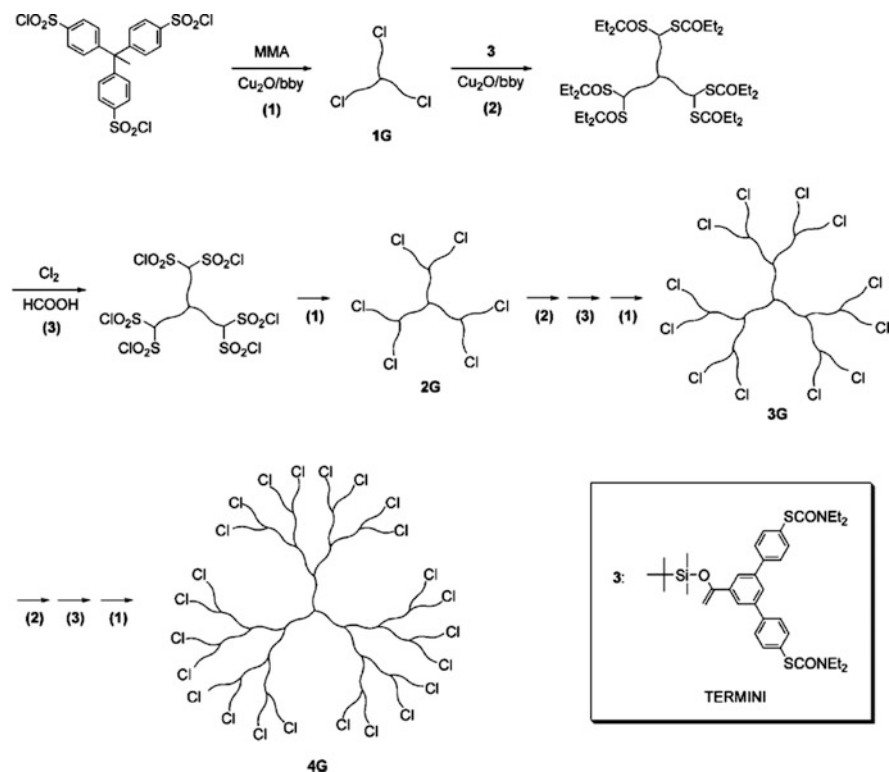
Scheme 6 Synthesis of 4G dendrimer-like PMMA via TERMINI strategy by Percec et al. Adapted from Ref. [39] with permission from ACS

dendrimer-like PMMAs with structural perfections were synthesized by suitable combinations of living free radical polymerization and TERMINI technique. For example, Cu_2O catalyzed living radical polymerization of MMA, initiated with a tri (sulfonyl chloride) core **7**, was interrupted by (1,1-dimethylethyl)[[1-[3,5-bis(S-phenyl 4-N,N'-diethylthio-carbamate) phenyl]ethenyl]oxy] dimethylsilane as the TERMINI agent. After deprotection, two sulfonyl chloride groups were regenerated and initiated the living radical polymerization of MMA. After four times of iterative reactions, dendrimer-like PMMA of fourth generation was successfully synthesized with $M_n = 4.56 \times 10^5$ g/mol and $M_w/M_n = 1.23$ (Scheme 6) [39].

2.1.5 Living Dendrimer-Like Polymers Made from a Continuous Method

Synthesis of dendrimer-like polymers is intensively time-consuming due to a number of polymerization, protection/deprotection, and purification steps. To overcome this shortcoming, a continuous anionic living process for fast synthesis was
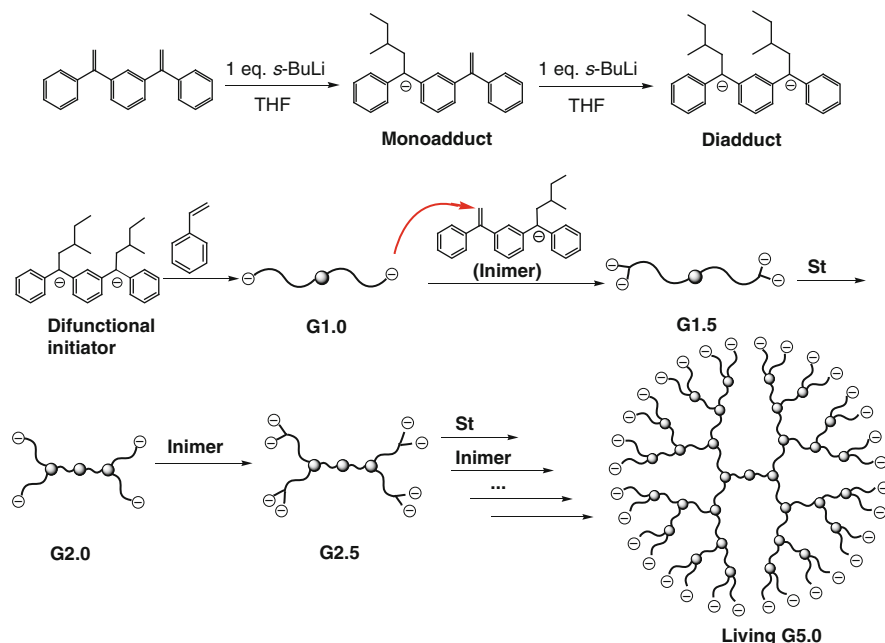
Scheme 7 Continuous synthesis of dendrimer-like star living polystyrene in a divergent process. Reproduced from Ref. [42] with permission from ACS

developed (Scheme 7) [42]. The process used an anionic species, for example, the monoadduct of *sec*-butyllithium (*s*-BuLi) and 1,3-bis(1-phenylethenyl)benzene (MDDPE) as the branching agent. The monoadduct was prepared via a stoichiometric reaction of *s*-BuLi and MDDPE in THF and then stored in cyclohexane solution. Thus, α,ω-bifunctional polystyryllithium (*G1.0*), initiated by a difunctional anionic initiator, underwent addition reaction with the monoadduct to form a tetra anionic species. Anionic polymerization of styrene initiated by the tetra anionic species formed a four-arm star with four terminal anions (*G2.0*). Repeating addition/polymerization in an alternating way led to the formation of a dendrimer-like star polystyrene up to the fifth generation, *G5.0*. The process was performed continuously without separation of the intermediate species. The synthesis of dendritic polystyrene was greatly accelerated, for example, *G5.0*, with 32 terminal groups being obtained within 12 h. Owing to the living property, the product was used as a dendritic precursor to prepare dendrimer-like star block copolymers such as PS-*b*-polyisoprene, PS-*b*-PMMA, and dendrimer-like star polymer with a graft-on-graft periphery.

   In general, the divergent growing/branching approach for the synthesis of dendrimer-like star polymers involves two main reaction steps in the formation of each generation: (a) the controlled/living polymerization of an appropriate monomer initiated from either a multifunctional core or the peripheral moieties of the preceding generation; (b) chain-end modification reaction to introduce two or more initiation sites. Reiteration of these reaction steps results in the synthesis of the

high-generation and high-molecular-weight dendrimer-like star polymer and block copolymers. However, concerns have been paid to the imperfections caused in the methodology. It was pointed out that the uniformity of chain growth and the number of initiating sites that actually take part in the initiation are not exactly determined, especially at higher generations [43]. Therefore, defects may exist in the final product despite that the measured molecular weight distribution was narrow. This is because the defects are random and can be averaged among molecules. Indeed, it was found in the continuous process that the efficiency of chain initiation become low along with the generation growth, partly due to the aggregation of anions in nonpolar solvent that causes heterogeneity to the polymerization system [42].

2.2 Divergent Coupling/Branching Approach

The divergent polymerization/branching approach is a "core first" method in which polymer chains originate from the initiating sites of the preceding generation. This method allows efficient transformation of the branching functionality and well-controlled polymerization due to the lack of steric hindrance, but suffers from the unavailability of analytic information of well-defined arm structure. Another way of making dendrimer-like star polymers, mainly developed by Hirao and coworkers, is the divergent coupling/chain branching approach. This "arm first" approach combines the precise control on molecular weight by anionic polymerization and the quantitative deprotection and transformation of the end groups for chain branching reactions. The precursor of the arm is a polymer chain bearing a living anion and two protected functional groups at the α- and ω-end, respectively. In the synthesis, the living anionic end is attached to the core or preceding generation, whereas the protected groups are positioned at the peripheral part in the topological structure. Then the protecting groups are removed and active sites for further linking reactions are released. Repeating the above two reactions leads to the formation of dendrimer-like star-branched polymers with growing generations. Notably, the chemistry used for linking and transformation must match the applied monomers, such as MMA, styrene, and *tert*-butyl methacrylate, in anionic polymerizations [43–47].

2.2.1 Dendrimer-Like Star Polymethacrylates

The preparation of dendrimer-like PMMA was fulfilled by a typical iterative "arm first" process. As shown in Scheme 8, living PMMA chains were prepared via anionic polymerization of MMA initiated by the adduct of *sec*-BuLi and 1,1-bis (3-*tert*-butyl- dimethylsilyloxymethylphenyl)ethylene (DPE-diSMP) in the presence of LiCl, thus affording two SMPs and an anion at the α- and ω-end, respectively, hereafter coded diSMP-PMMA$^\ominus$. The living PMMA chains were linked to benzyl bromide of *para*-dibromomethyl benzene. After the linking reaction, the
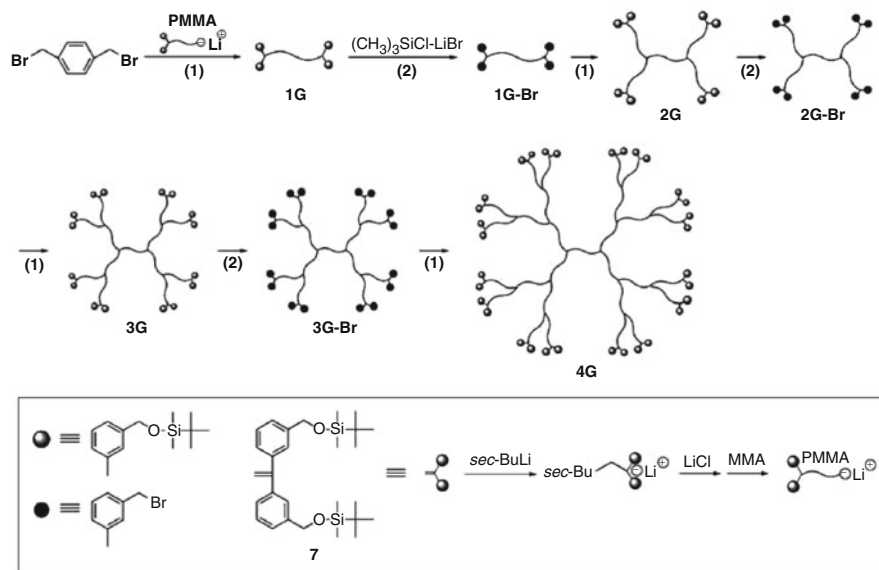
Scheme 8 Synthesis of dendrimer-like star PMMAs with two branches reported by Hirao. Adapted from Ref. [48] with permission from ACS

SMP groups were subsequently transformed into benzyl bromide (BnBr) by treatment with 1:1 mixture of LiBr and $(CH_3)_3SiCl$. The resulting star-branched PMMA with peripheral BnBr moieties underwent further linking reaction with diSMP-$PMMA^\ominus$ [43–49]. Both the linking and the end-group modification reactions were quantitative, resulting in dendrimer-like PMMA with high structural perfection [48]. In each step of the linking reaction, an excess amount of living PMMA was used. Thus, the reaction mixture needed to be fractionated to get the pure dendrimer-like product. After the purification, dendrimer-like products with M_w/M_n values less than 1.1 were obtained. The calculated molecular weights were in good agreement with those determined by ^{1}H NMR and SLS. Moreover, dendrimer-like block copolymer was prepared in a similar manner by the use of the living anionic polymer of the protected 2-hydroxyethyl methacrylate (HEMA) instead of living anionic PMMA at the final reaction stage. After hydrolysis, an amphiphilic dendrimer-like star block copolymer PMMA-*b*-PHEMA was obtained.

Using a similar strategy, dendrimer-like star PMMA of up to seven generations was synthesized starting from a core with tetra BnBr moieties (Scheme 9) [50]. The SEC peak of each generation was monomodal after removal of the "arm" species, and moved to the higher molecular weight region as the generation growth (Fig. 1). The observed and calculated molecular weight were in good agreement with each other. A seventh-generation product was obtained with large molecular weight $(1.94 \times 10^6$ g/mol) and narrow molecular weight distribution $(M_w/M_n = 1.02)$, comprised of 508 PMMA segments and 512 BnBr functionalities at the periphery.
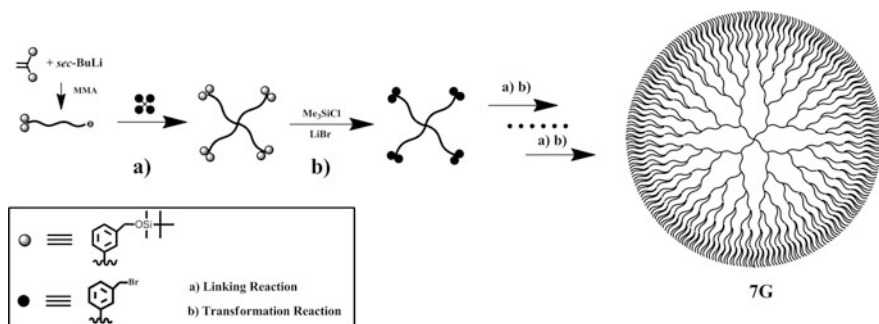
Scheme 9 Synthesis of 7G dendrimer-like star PMMA starting from a tetrafunctional core by Hirao. Adapted from Ref. [50] with permission from ACS
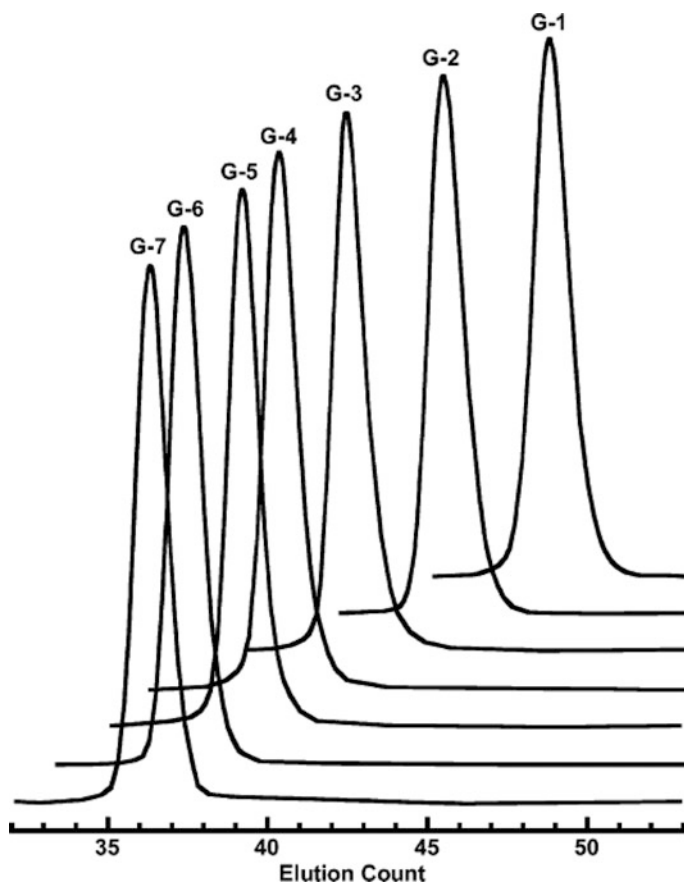
Fig. 1 SEC profiles of dendrimer-like PMMAs from first to seventh generation. Reproduced from Ref. [50] with permission from ACS
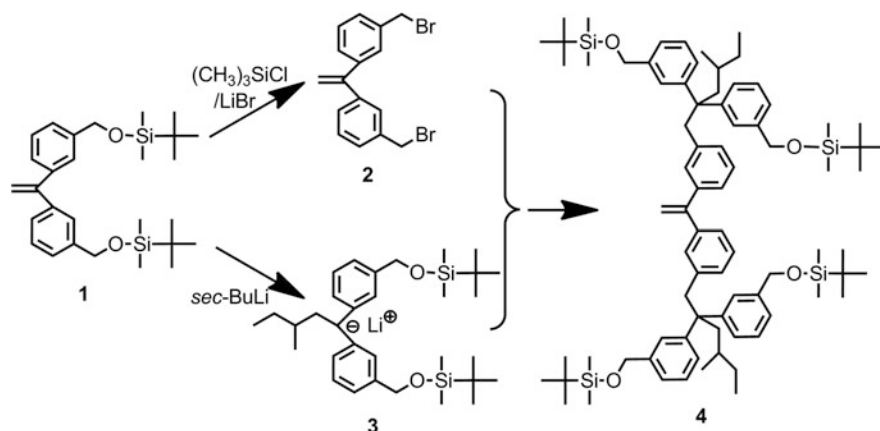
Scheme 10 Synthesis of DPE derivative with four SMP groups. Adapted from Ref. [52] with permission from Wiley

In the divergent coupling/branching process, the branching functionality of the dendrimer-like product can be controlled by changing the number of functionalities in the branching agent or at the ω-end of the arm precursor. For example, using difunctional DPE-diSMP or tetrafunctional DPE-tetraSMP (Scheme 10), branching functionality of $1 \rightarrow 2$ or $1 \rightarrow 4$ was obtained, respectively, after the attachment of the subsequent generation [51]. The tetrafunctional molecule was prepared by coupling of 1,1-bis(3-bromomethylphenyl)ethylene and DPE$^{\ominus}$-diSMP anion, both derived from DPE-diSMP. The use of tetrafunctional branching agent resulted in a much faster increase in molecular weight of the dendrimer-like products (Scheme 11).

Branching agents with different number of functionalities can also be fixed simultaneously within the same dendrimer-like star molecule, therefore providing a way of tuning the branching density along the radial direction. DPE-derived branching agents with four SMP groups were synthesized using DPE-diSMP as the starting material (Scheme 10). The application of these branching agents with different number of SMPs resulted in the synthesis of a series of dendrimer-like polymers with various constitutional branching junctures at different generations (Fig. 2) [52, 53].

Other monomers, such as *tert*-butyl methacrylate, (2,2-dimethyl-1,3-dioxolan-4-yl)methyl methacrylate, and 2-vinylpyridine, showed similar reactivity in the iterative process. Therefore, it is easy to prepare dendrimer-like block copolymers containing segments from these monomers (Scheme 12) [53]. The block copolymers were further treated with $(CH_3)_3SiCl/LiBr$ or 2 N HCl to convert the functional segments into polar and water-soluble poly(methacrylic, acid), poly (2,3-dihydroxypropyl methacrylate), or poly(2-vinylpyridinium hydrochloride), respectively, therefore producing amphiphilic dendrimer-like star copolymers.
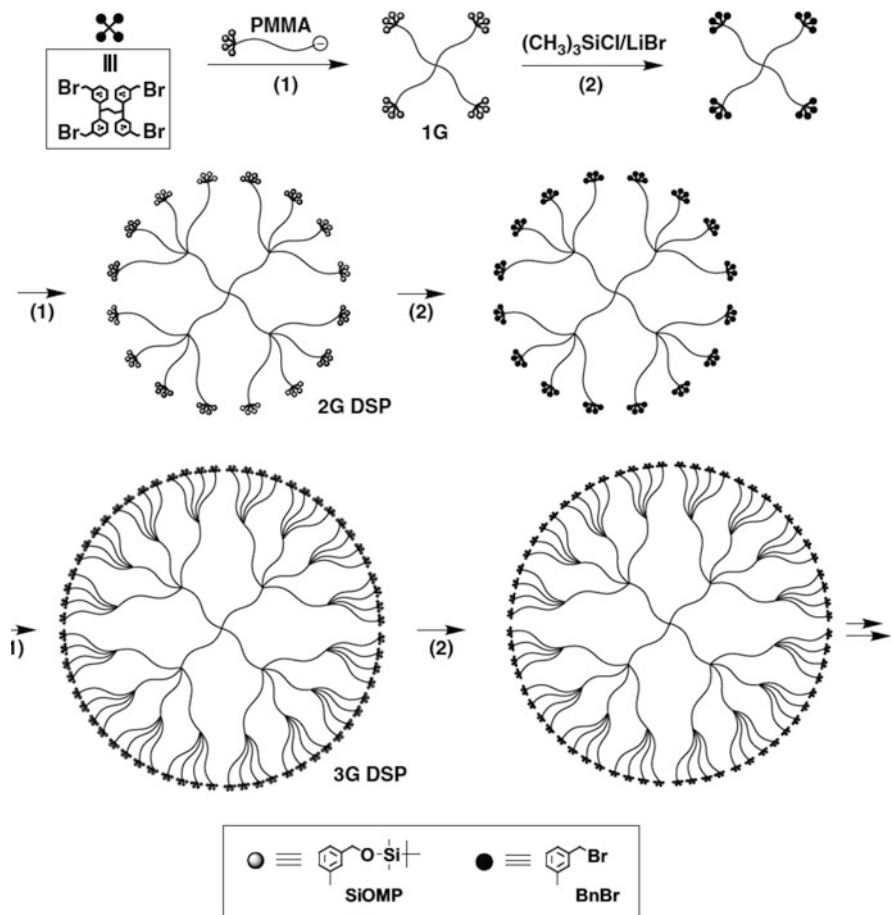
Scheme 11 Synthesis of 3G dendrimer-like PMMA with four branches at each generation reported by Hirao. Reproduced from Ref. [51] with permission from Wiley

2.2.2 Dendrimer-Like Star Polystyrenes

In the preparation of dendrimer-like polymethacrylates, the polymer arm precursor was living PMMA chain anion bearing bifunctional SMPs at the ω-end. The precursor was synthesized by anionic polymerization of MMA initiated by the adduct of *sec*-BuLi and DPE-diSMP. In the synthesis of the adduct, the feed amount of DPE-diSMP was in excess, usually 1.5-fold of the lithium, in order to convert *sec*-BuLi into DPE-derived organolithium in high yield. The residual DPE-diSMP would not take part in the following-up anionic polymerization of MMA, since PMMA enolate is not capable of adding to the double bond of DPE moiety. This method is, however, not applicable for the preparation of styrenic dendrimer-like polymers because of similar reactivity of styrene and DPE double bond. Otherwise,
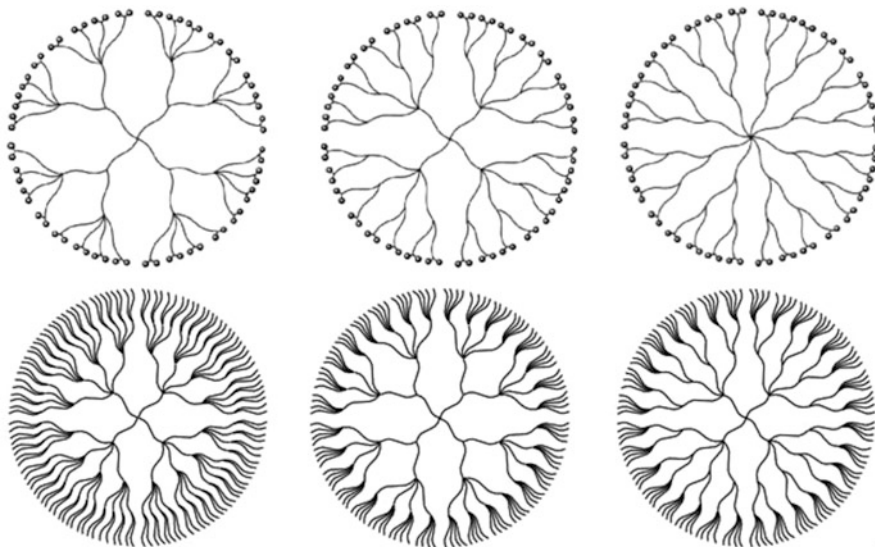
Fig. 2 A series of 3G, 4G dendrimer-like star PMMAs with different branched architectures reported by Hirao. Adapted from Ref. [51, 53] with permission from Wiley and ACS
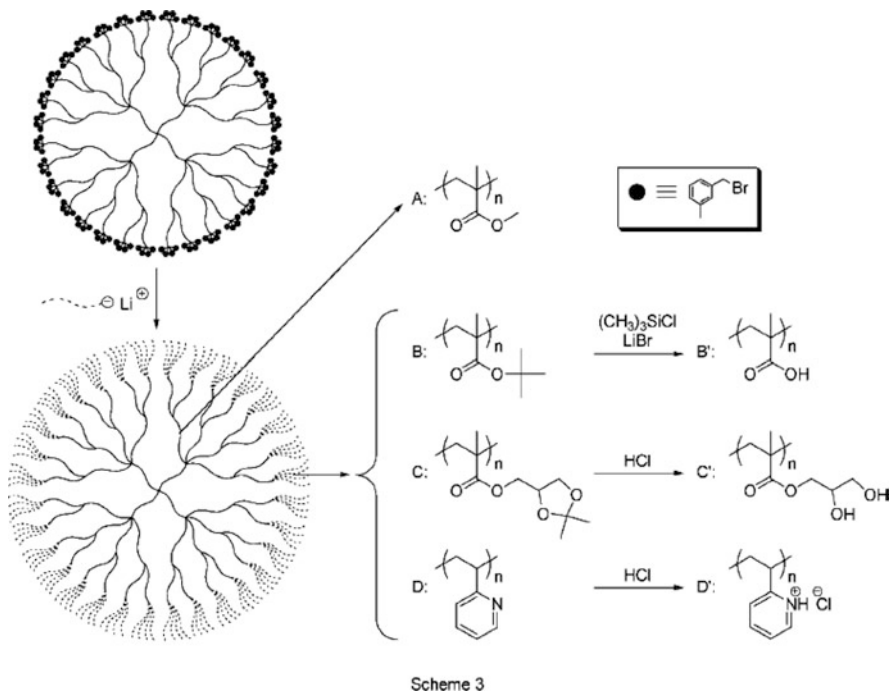
Scheme 3

Scheme 12 Synthesis of amphiphilic dendrimer-like block copolymers reported by Hirao. Reproduced from Ref. [53] with permission from ACS

the random incorporation of residual DPE-diSMP into the polymer chain would result in uncontrolled functionalization reaction. Therefore, an alternative strategy was developed for the synthesis of the well-defined dendrimer-like star PS based on the divergent coupling/branching approach [54].

In this new strategy, the chain precursor was a living polystyrene chain bearing monofunctionality (instead of bifunctionality), 3-*tert*-butyldimethyl-silyloxy-1-propyl (BudiMeSiOPr), at the ω-end. The precursor was synthesized from the styrene polymerization initiated by a commercially available anionic initiator, 3-*tert*-butyldimethyl- silyloxy-1-propyllithium (BMSiOPrLi). The resulting precursor, BMSiOPr-PS$^\ominus$, was end-capped with DPE and then coupled with either a core or preceding generation possessing multi alkyl–bromide moieties. The branching reaction was accomplished by two steps: first transformation of the terminal BMSiOPr group into 3-bromopropyl; then nucleophilic attack of the adduct of *sec*-BuLi and DPE-diSMP towards 3-bromopropyl. In this way, the monofunctional end group became a bifunctional one. Repeating the reaction sequence four times led to the formation of dendrimer-like polystyrene of fifth generation with $M_n = 1.8 \times 10^6$ g/mol, 124 PS segments and 128 alkylbromide terminal groups (Scheme 13).
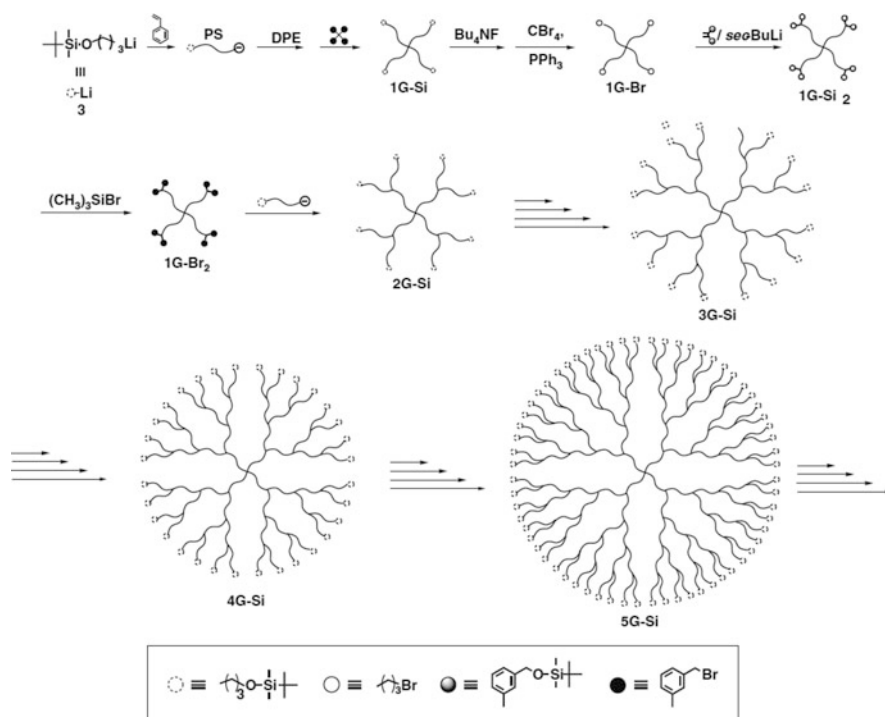
Scheme 13 Synthesis of dendrimer-like star PSs reported by Hirao et al. Adapted from Ref. [54] with permission from ACS

Orthogonal linking reactions were performed using two different living chains, BMSiOPr-PS$^\ominus$ and diSMP-PMMA$^\ominus$, as the building blocks. Therefore, dendrimer-like star block copolymers composed of PS and PMMA segments at different generations were synthesized [54]. In principle, these segments can be introduced at any generation in a dendrimer-like structure.

The iterative divergent/branching approach was also used in the synthesis of dendrimer-like polymers with extremely high branch densities [4]. In this particular process, chain branching took place on a short segment of poly (4-bromomethylstyrene) as multifunctional BnBr branching site, instead of two or xfour BnBr moieties at the chain end in previous studies. Poly (4-bromomethylstyrene) segment was derived from poly(3-SMP styrene) block (by treatment with $(CH_3)_3SiCl/LiBr$) incorporated through copolymerization shown in Scheme 14. Thus, anionic sequential copolymerization of SMP-substituted styrene and styrene produced a living block copolymer, P (SMP-St)-*b*-PS$^\ominus$, which was linked to BnBr moieties of the core or poly (4-bromomethylstyrene) segments of the preceding generations. The degree of
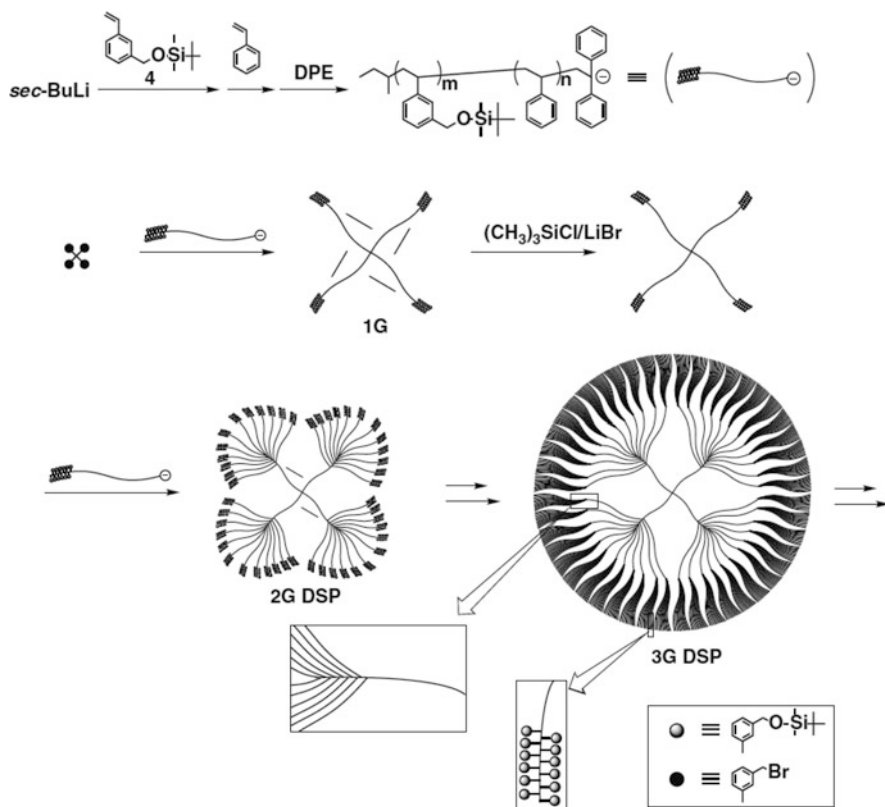
Scheme 14 Synthesis of densely branched dendrimer-like star PS of third generation reported by Hirao. Adapted from Ref. [4] with permission from ACS

polymerization of poly(4-bromomethylstyrene) was controlled to an average value of 12, affording a branching functionality of $1 \rightarrow 12$. After the linking reaction, SMP moieties were converted into BnBrs which would subject to further linking reaction. Repeating these steps yielded dendrimer-like PS of third generation with very high M_n (1.43×10^7 g/mol) and narrow molecular weight distribution ($M_w/M_n = 1.05$). Although the number of branches could not be exactly controlled, the calculated value was up to 608 bearing 7,600 BnBr termini at the periphery. The high density of the branches was proved by AFM observation.

A more convenient strategy was developed using only one kind of block copolymer as both the arm precursor and branching agent [55]. As shown in Scheme 15, a block copolymer of isoprene and styrene, PI-*b*-PS$^\ominus$, consisting of a short segment of PI with average degree of polymerization 8, was end-linked by a multifunctional core to form a star-like copolymer (G1-star). The PI segment was then epoxidized using HCOOOH, and attached by the same block copolymer PI-*b*-PS$^\ominus$ to form the second generation (G2-star). Iterative epoxidation and attachment multiple times resulted in dendrimer-like polymers of up to generation 5, with $M_w = 4.0 \times 10^7$ g/mol and about 7,000 branches. A feature of the process was the easy accessible high chain density and high molecular weight of the final product, although imperfections existed due to steric hindrance in the reactions of high generations.

2.2.3 Dendrimer-Like Star Poly(tert-butyl methacrylates)s (PtBMAs)

The above-mentioned method for the syntheses of dendrimer-like star PMMAs and polystyrene required the transformation of SMP to BnBr functions be performed in highly acidic conditions. This method could not be applied to a variety of polymers bearing either acid-labile or base groups. An alternative method was developed in which diSMPs were transformed into bifunctional α-phenylacrylate (diPhA) in neutral media. The resulting multiple diPhAs served as linking sites for the living anionic polymer chains such as poly(*tert*-butyl acrylate), polymethacrylates with protected hydroxyl groups or oligomeric ethylene oxide side groups, and poly (2-vinylpyridine), etc. Thus, living polymer chains such as diSMP-P*t*BMA$^\ominus$ were prepared and linked to a core with four BnBr moieties. The conversion of diSMP
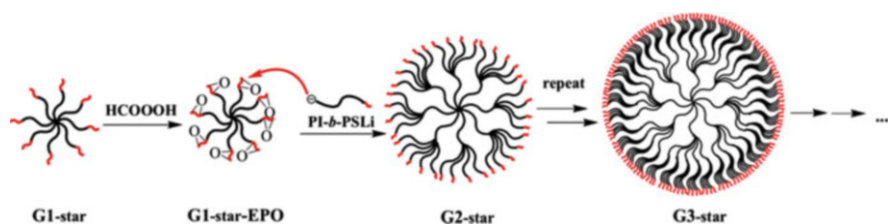
Scheme 15 Synthesis of dendrimer-like PS from star-like core using PI-*b*-PSLi as the building block. Adapted from Ref. [55] with permission from RSC

into diPhA esters was accomplished by sequential hydrolysis of SMP into hydroxyl (using Bu$_4$NF) and then esterification with α-phenylacrylic acid. The resulting diPhA moieties undergo further addition reaction by diSMP-PtBMA$^\ominus$. Well-defined fifth-generation with high molecular weight (~10^7 g/mol) dendrimer-like PtBMA was synthesized (Scheme 16) [56]. Furthermore, dendrimer-like block
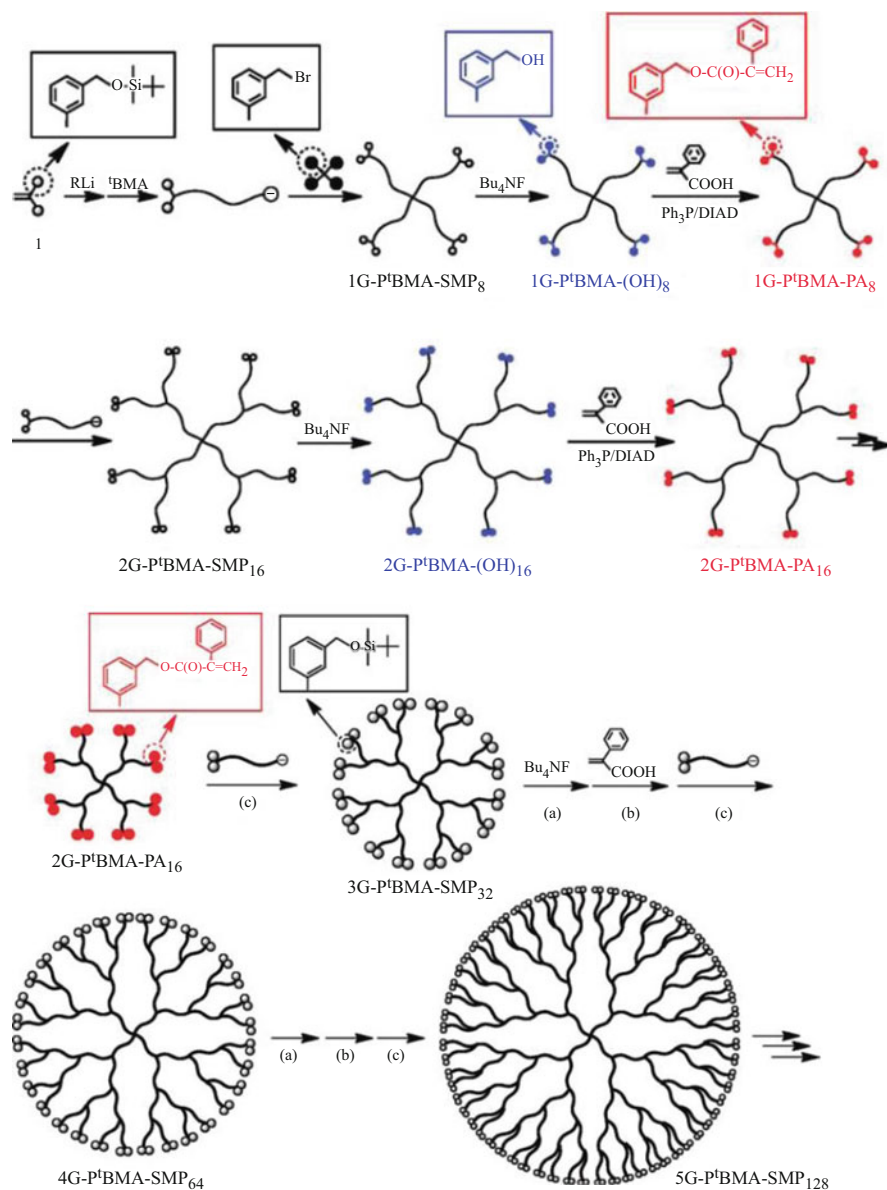
Scheme 16 Synthesis of the fifth-generation dendrimer-like star PtBMA reported by Hirao. Reproduced from Ref. [56] with permission from ACS

copolymers composed of P*t*BMA and PS segments were also reported [23, 29, 57]. These block copolymers could be converted to amphiphilic block copolymers by the selective hydrolysis of P*t*BMA to poly(methacrylic acid) (PAA) (Fig. 3).

2.3 Convergent Approach

The synthesis of dendrimer-like star polymers through convergent approach involves coupling of polymer chains and in situ polymerization in some cases. This was accomplished through two strategies, for example, alternate coupling of polymer chains by an asymmetric coupling agent and further in situ polymerization, and alternate coupling by symmetric coupling agent and chain-end transformation.

The first strategy was developed by Hadjichristidis using anionic living polymers as the arm precursor [58]. As shown in Scheme 17, polyisoprenyllithium (PILi) was coupled via two steps by 4-(chlorodimethylsilyl)styrene (CDMSS), an asymmetric coupling agent in which the chlorosilane group was much more reactive than the vinyl group towards anionic species. The second step of the reaction was the addition of PILi to the double bond, forming a styrenic anion that in situ initiated polymerization of isoprene. The resulting PI "living star"

$(P^tBMA-(P^tBMA)_2-(P^tBMA)_4-(PS)_8)_4$ $(PS-(PS)_2-(PS)_4-(P^tBMA)_8)_4$
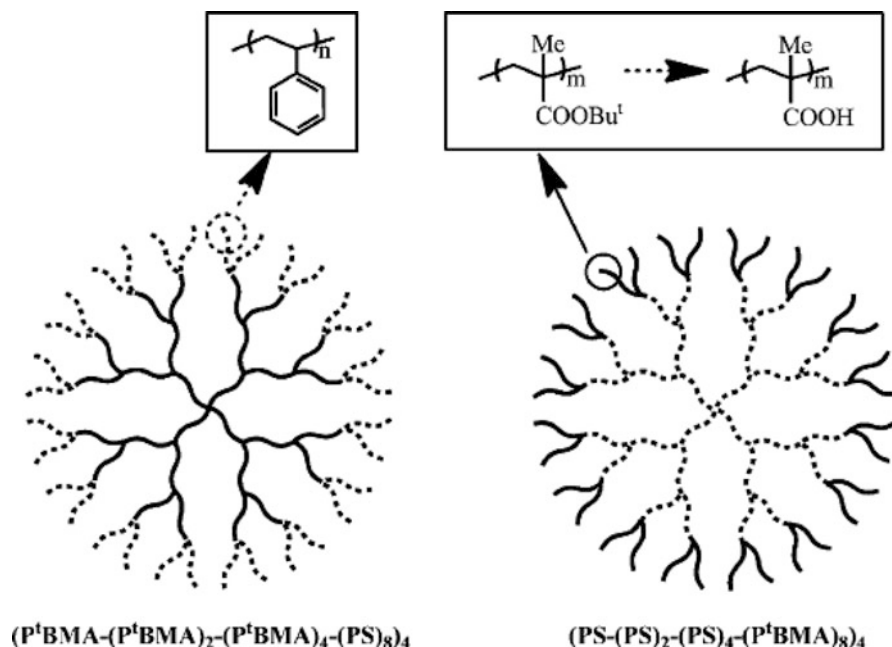
Fig. 3 Dendrimer-like star copolymers consisting of P*t*BMA and PS segments at different radical locations, in which P*t*BMA can be hydrolyzed into segment bearing carboxylic groups. Reproduced from Ref. [56] with permission from ACS

possessing an off-center anion was coupled with either $MeSiCl_3$ or $SiCl_4$ to obtain second generation of dendrimer-like PIs with 6 or 8 chain ends, respectively. In addition, dendrimer-like block copolymers composed of PS and PI segments were also synthesized through a similar sequential polymerization and coupling process [58].

The styrenic unit in CDMSS may undergo polymerization in the second step of coupling and therefore cause complexity in the structural control. To overcome this disadvantage, a novel coupling agent, 1-(4-dichloromethylsilylphenyl)-1-phenylethylene (DCMSDPE), was designed for the synthesis of dendrimer-like star polybutadienes (PBs) (Scheme 18) [59]. DCMSDPE interlinked two living PB chains by its $-MeSiCl_2$ group, and then was activated at its vinyl group by sec-BuLi addition. The resulting in-chain anion was used to initiate the polymerization of butadiene to generate a "living star" of PB. The "living star" was either end-linked with $MeSiCl_3$ to form second-generation dendrimer-like star PB, or coupled by DCMSDPE again followed by activation, polymerization of butadiene, and end-linked with $MeSiCl_3$, finally affording third generation of dendrimer-like star PB.

A faster and continuously performable one-pot process was developed by Knauss and coworkers using CDMSS as the coupling agent (Scheme 19) [60–63]. In this process, CDMSS was slowly added to a solution of anionic living PS chains (PSLi). The amount of CDMSS was kept slightly below the stoichiometric
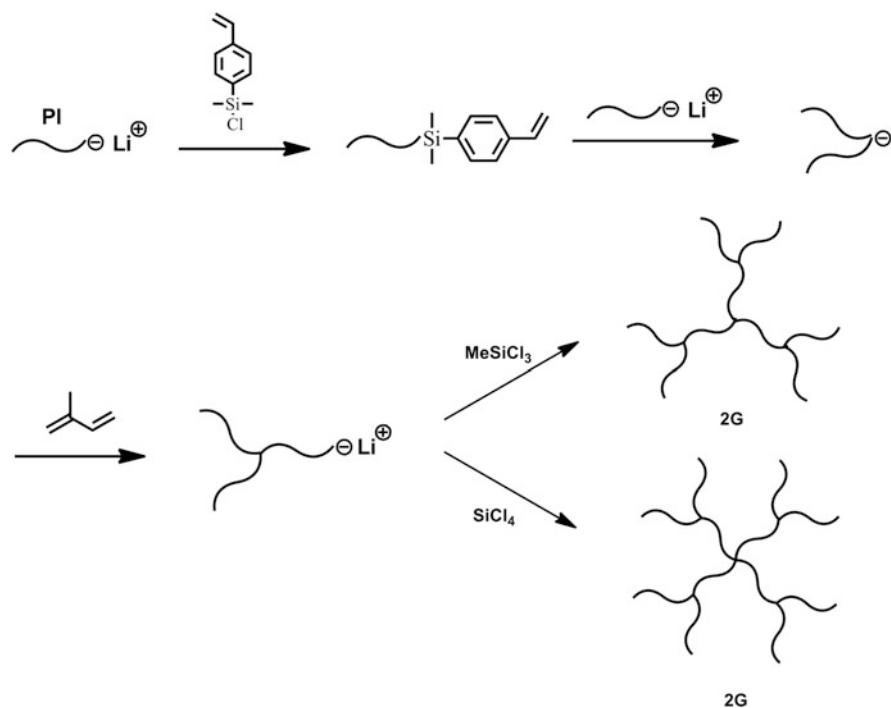
Scheme 17 Synthesis of 2G dendrimer-like star PIs reported by Hadjichristidis. Adapted from Ref. [58] with permission from Wiley
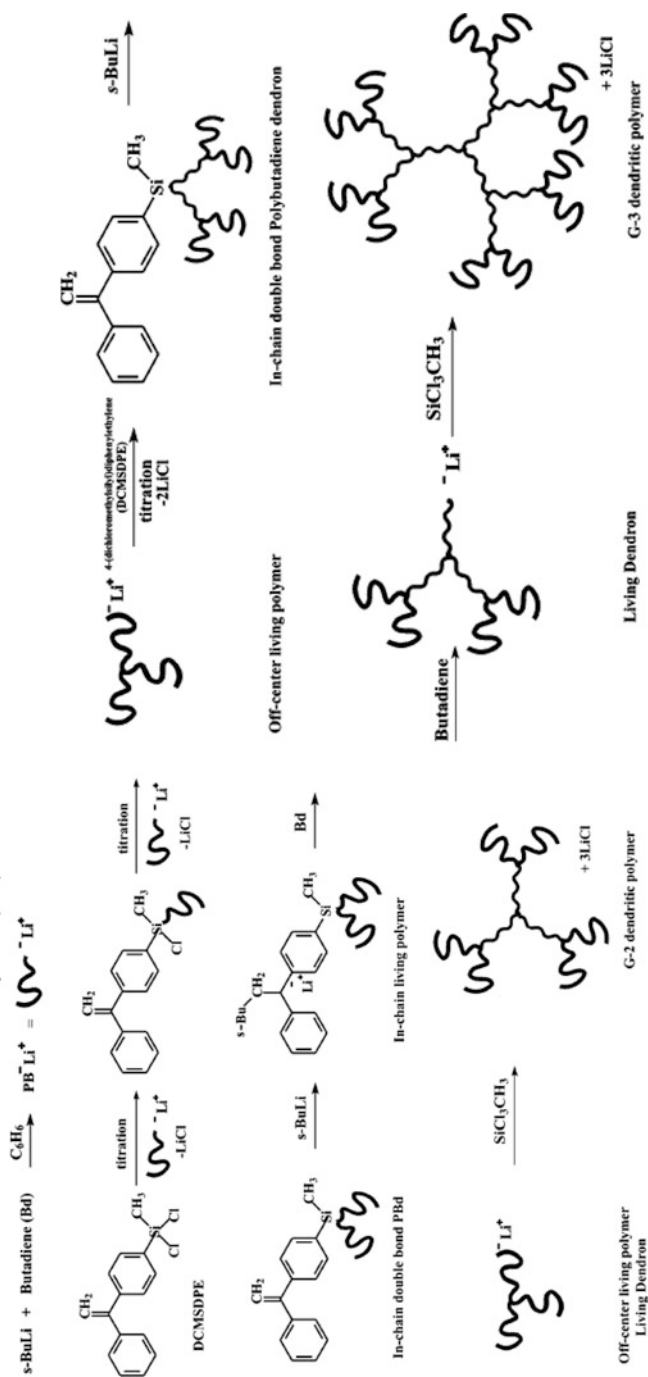
Scheme 18 Synthesis of second- (*left*) and third (*right*)-generation dendrimer-like PBs reported by Hadjichristidis. Reproduced from Ref. [59] with permission from ACS
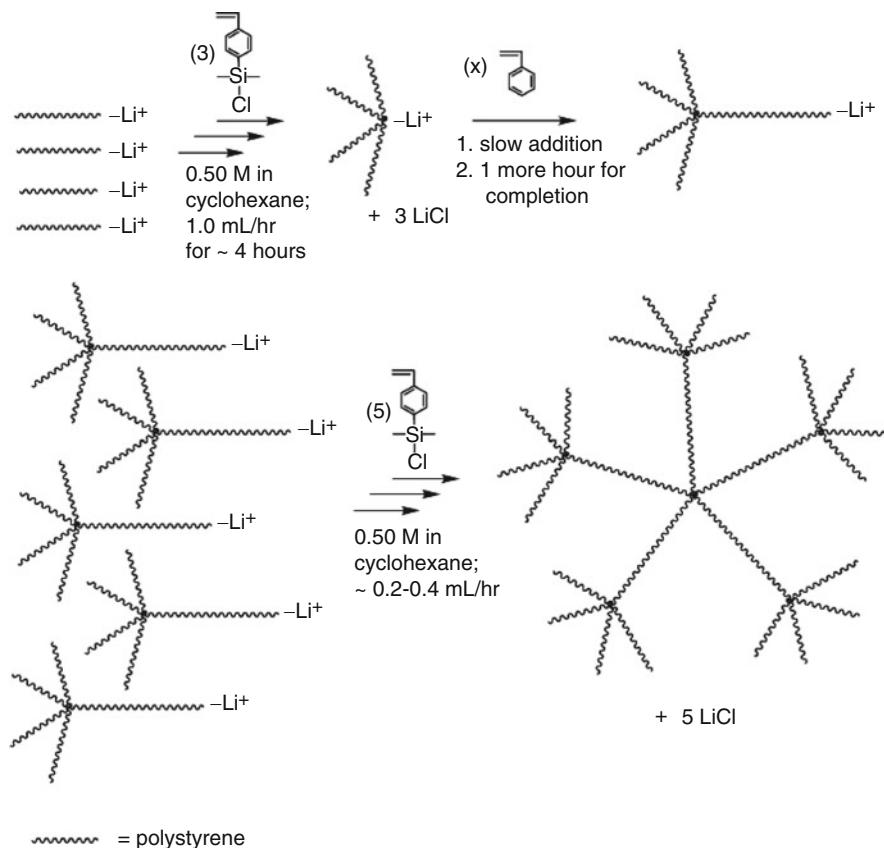
Scheme 19 Synthesis of second-generation dendrimer-like star PS in one-pot approach reported by Knauss. Reproduced from Ref. [60] with permission from ACS

amount relative to the initial PSLi in order to maintain a living site at the focal point. The central living anion was used to initiate the polymerization of styrene to form a multiarm "living star," which was coupled by slow addition of CDMSS up to a stoichiometric amount. After termination, second-generation dendrimer-like star polymer was obtained. This straightforward process was very efficient yet the number of arms was variable.

The second strategy was developed by Hutchings and coworkers in the synthesis of DendriMarcs, for example, dendrimer-like polymers formed by convergent coupling of end-functionalized chain precursors using symmetric linking agent. For example, a living polystyrene initiated with 3-*tert*-butyldimethylsiloxy-1-propyllithium (BudiMeSiOPrLi) was transformed separately into both polystyrene with alkylchloride terminus (PS-Cl) and polystyrene with α-hydroxyl and ω-biphenol termini, an AB$_2$-type macromonomer (HO-PS-PhOH$_2$) (Scheme 20) [64]. Then, PS-Cl was coupled with the phenol moieties of HO-PS-PhOH$_2$ through
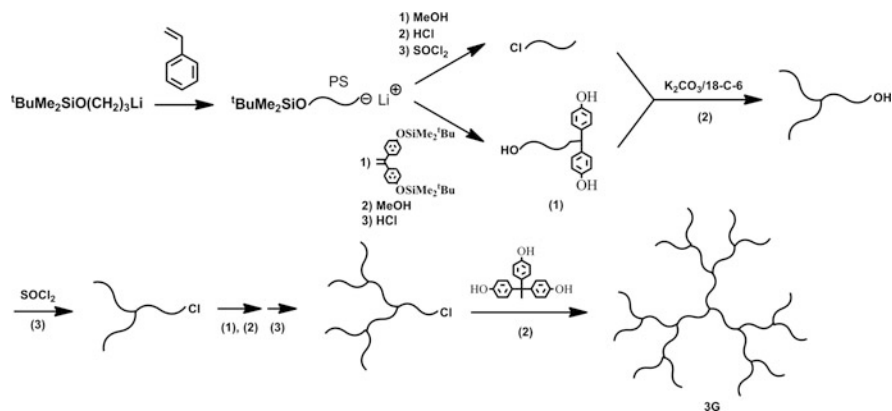
Scheme 20 Synthesis of 3G dendrimer-like PS reported by Hutchings and Roberts-Bleming. Adapted from Ref. [64] with permission from ACS

Williamson reaction, forming a star-like PS with one terminal hydroxyl group which was subsequently converted into alkylchloride in reaction with $SOCl_2$. The resulting star-like PS with chloro end groups was coupled by $HO-PS-PhOH_2$ again, and the remaining hydroxyl was subsequently converted into terminal chloride, affording a second-generation PS dendron. Finally, dendrimer-like star PS of third generation was obtained by coupling PS dendron to a triphenyl core, 1,1,1-tris (4-hydroxyphenyl) ethane. The characterization results of all purified polymers showed that the observed molecular weights were in good agreement with theoretical values and narrow molecular-weight distributions were obtained ($M_w/M_n \leq 1.06$).

The convergent method obviously suffered from steric hindrance in the coupling reactions and thus was limited to the synthesis of relatively low generation dendritic products. Finding high efficient reaction is a long-standing goal for this strategy. Along this line, the "click" chemistry between alkyne and azide groups was applied as a coupling reaction in the synthesis of dendrimer-like star polymers. As shown in Scheme 21, combination of copper wire catalyzed "click" chemistry, ATRP of styrene or acrylates, and the transformation of alkylbromide terminus into azido end group led to the formation of miktoarm dendrimer-like star polymers [65–67]. Three-arm star polymer bearing three azido termini derived from alkylbromides was coupled with AB-type diblock copolymers with alkyne groups at the junction to yield dendrimer-like miktoarm star terpolymers [68]. In the latter, the diblock copolymer was prepared through simultaneous controlled radical polymerization of styrene and ring-opening polymerization of ε-CL with a dual head initiator possessing an alkoxyamine and a hydroxyl moieties as well as an alkyne group. In addition, ABC-type miktoarm star copolymer of styrene, EO and ethoxyethyl glycidyl ether (EEGE) bearing one alkyne group at the end of PEEGE segment was coupled to diazidobutane or a tetra azido core to form amphiphilic dendrimer-like miktoarm star polymers [69].
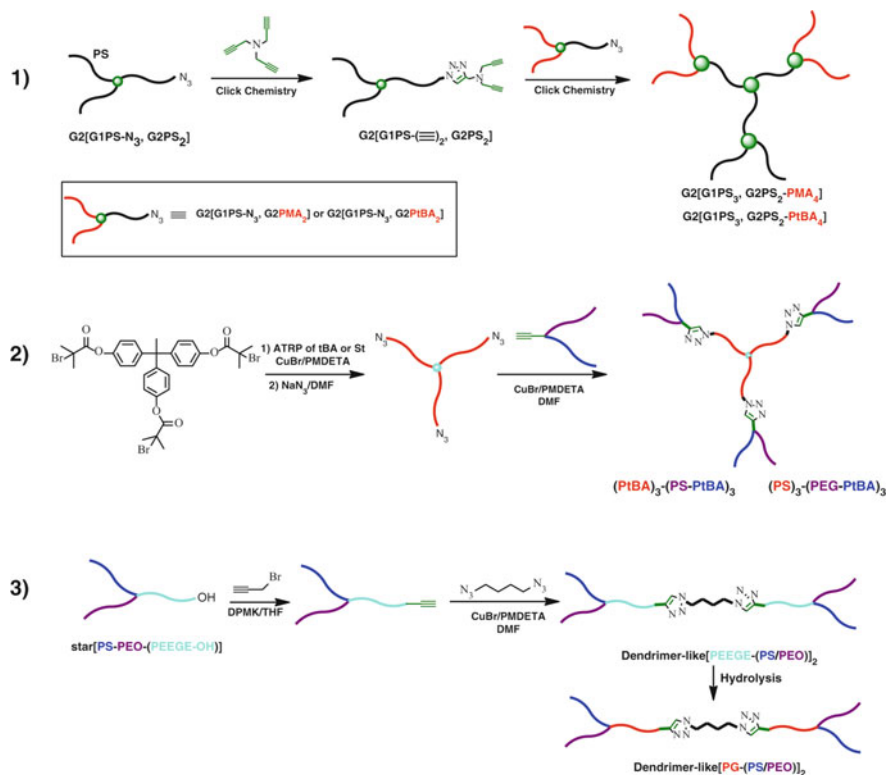
Scheme 21 Synthesis of dendrimer-like miktoarm star copolymer via adizo-alkyne click reaction. Adapted from Ref. [65–69] with permission from ACS and Wiley

3 Concluding Remarks

This chapter highlights the synthesis of dendrimer-like star polymers based on iterative methodologies of either divergent or convergent approach in combination with living or controlled polymerizations. The divergent approach can be performed either through in situ initiation/polymerization and chain branching process or through coupling and chain branching process, whereas the convergent approach can be performed either through in situ coupling and polymerization or through coupling of AB$_2$-type macromonomers. The molecular parameters, such as chemical structure, branching density in one branch point or along the radial direction, layered structure through block copolymerization, molecular weight, and polydispersity, were able to be controlled at different levels through the design of branching agents and the synthetic route. Although for a specific dendrimer-like polymer there is a most suitable approach: it seems that the divergent coupling and chain branching approach combines the advantages of less steric hindrance and availability of well-defined polymer precursor.

Molecular engineering of dendrimer-like star polymers was achieved in the past decade. This includes the synthesis of dendrimer-like star polymers with specific functionalities on the surface, at the core, and at the branch points, dendrimer-like star polymers with layered chemical or architectural heterogeneity, and the synthesis of linear-dendritic block copolymers with various arrangements of linear and dendritic segments. For example, Janus-type dendrimer-like PEOs served as scaffolds for bioconjugation with multiple folic acid and camptothecin moieties in the same molecule. The resulting prodrugs combined the biocompatibility of PEO, the targeting ability of folic acid, as well as the therapy of the camptothecin, and was expected to exhibit better therapeutic effects than the linear PEO counterparts [19].

One unique feature of dendrimer-like star polymers is the accessibility to extremely high molecular weight. This means that the size of dendrimer-like star polymers can range from nanometer to hundreds of nanometers. These nano- or mesosized molecules can be used as sacrificial macromolecular template to make nanoporous or mesoporous silicate materials that are useful in microelectronics and nanotechnology [19, 70, 71].

References

1. Taton D, Feng X, Gnanou Y (2007) Dendrimer-like polymers: a new class of structurally precise dendrimers with macromolecular generations. New J Chem 31:1097–1110
2. Van Renterghem LM, Feng X, Taton D, Gnanou Y, Du Prez FE (2005) MALDI-TOF analysis of dendrimer-like poly(ethylene oxide)s. Macromolecules 38:10609–10613
3. Lepoittevin B, Matmour R, Francis R, Taton D, Gnanou Y (2005) Synthesis of dendrimer-like polystyrene by atom transfer padical polymerization and investigation of their viscosity behavior. Macromolecules 38:3120–3128
4. Deffieux A, Schappacher M, Hirao A, Watanabe T (2008) Synthesis and AFM structural imaging of dendrimer-like star-branched polystyrenes. J Am Chem Soc 130:5670–5672
5. Hirao A, Matsuo A (2003) Synthesis of chain-end-functionalized poly(methyl methacrylate)s with a definite number of benzyl bromide moieties and their application to star-branched polymers. Macromolecules 36:9742–9751
6. Trollsås M, Claesson H, Atthof B, Hedrick JL (1998) Layered dendritic block copolymers. Angew Chem Int Ed 37:3132–3136
7. Fréchet JM, Tomalia DA (2001) Dendrimers and other dendritic polymers. Wiley, West Sussex
8. Newkome GR, Moorefield CN, Vögtle F (2001) Dendrimers and dendrons: concepts, syntheses, and applications. Wiley-VCH, Weinheim
9. Konkolewicz D, Monteiro MJ, Perrier S (2011) Dendritic and hyperbranched polymers from macromolecular units: elegant approaches to the synthesis of functional polymers. Macromolecules 44:7067–7087
10. Vögtle F, Rackstraw AJ, Werner N (2009) Dendrimer chemistry: concepts, syntheses, properties and applications. Wiley-VCH, Weinheim

11. Six JL, Gnanou Y (1995) From star-shaped to dendritic poly(ethylene oxide)s toward increasingly branched architectures by anionic polymerization. Macromol Symp 95:137–150

12. Angot S, Taton D, Gnanou Y (2000) Amphiphilic stars and dendrimer-like architectures based on poly(ethylene oxide) and polystyrene. Macromolecules 33:5418–5426

13. Feng X, Taton D, Chaikof EL, Gnanou Y (2005) Toward an easy access to dendrimer-like poly (ethylene oxide)s. J Am Chem Soc 127:10956–10966

14. Feng X, Taton D, Chaikof EL, Gnanou Y (2009) Fast access to dendrimer-like poly(ethylene oxide)s through anionic ring-opening polymerization of ethylene oxide and use of nonprotected glycidol as branching Agent. Macromolecules 42:7292–7298

15. Feng X, Taton D, Borsali R, Chaikof EL, Gnanou Y (2006) pH responsiveness of dendrimer-like poly(ethylene oxide)s. J Am Chem Soc 128:11551–11562

16. Hou SJ, Chaikof EL, Taton D, Gnanou Y (2003) Synthesis of water-soluble star-block and dendrimer-like copolymers based on poly(ethylene oxide) and poly(acrylic acid). Macromolecules 36:3874–3881

17. Gnanou Y, Taton D (2001) Star and dendrimer-like architectures by the divergent method using controlled radical polymerization. Macromol Symp 174:333–341

18. Feng X, Taton D, Ibarboure E, Chaikof EL, Gnanou Y (2008) Janus-type dendrimer-like poly (ethylene oxide)s. J Am Chem Soc 130:11662–11676

19. Feng X, Pinaud J, Chaikof EL, Taton D, Gnanou Y (2011) Sequential functionalization of janus-type dendrimer-like poly(ethylene oxide)s with camptothecin and folic acid. J Polym Sci Part A Polym Chem 49:2839–2849

20. Feng X, Taton D, Chaikof EL, Gnanou Y (2007) Bouquet-type dendrimerlike poly(ethylene oxide)s with a focal aldehyde and peripheral hydroxyls. Biomacromolecules 8:2374–2378

21. Hou S, Taton D, Saule M, Logan J, Chaikof EL, Gnanou Y (2003) Synthesis of functionalized multiarm poly(ethylene oxide) stars. Polymer 44:5067–5074

22. Rele SM, Cui W, Wang L, Hou S, Barr-Zarse G, Taton D, Gnanou Y, Esko JD, Chaikof EL (2005) Dendrimer-like PEO glycopolymers exhibit anti-inflammatory properties. J Am Chem Soc 127:10132–10133

23. Matmour R, Lepoittevin B, Joncheray TJ, El-khouri RJ, Taton D, Duran RS, Gnanou Y (2005) Synthesis and investigation of surface properties of dendrimer-like copolymers based on polystyrene and poly(tert-butylacrylate). Macromolecules 38:5459–5467

24. Francis R, Taton D, Logan JL, Masse P, Gnanou Y, Duran RS (2003) Synthesis and surface properties of amphiphilic star-shaped and dendrimer-like Copolymers based on polystyrene core and poly(ethylene oxide) corona. Macromolecules 36:8253–8259

25. Matmour R, Gnanou Y (2008) Combination of an anionic terminator multifunctional initiator and divergent carbanionic polymerization: application to the synthesis of dendrimer-like polymers and of asymmetric and miktoarm stars. J Am Chem Soc 130:1350–1361

26. Luan B, Pan C (2006) Synthesis and characterizations of well-defined dendrimer-like copolymers with the second and third generation based on polystyrene and poly(L-lactide). Eur Polym J 42:1467–1478

27. Yuan W, Yuan J, Zhou M, Pan C (2008) Synthesis, characterization, and fluorescence of pyrene-containing eight-arm star-shaped dendrimer-like copolymer with pentaerythritol core. J Polym Sci Part A Polym Chem 46:2788–2798

28. Kong L, Pan C (2008) Preparation of dendrimer-like copolymers based on polystyrene and poly(L-lactide) and formation of hollow microspheres. Polymer 49:200–210

29. Liu Q, Zhao P, Chen Y (2007) Divergent synthesis of dendrimer-like macromolecules through a combination of atom transfer radical polymerization and click reaction. J Polym Sci Part A Polym Chem 45:3330–3341

30. Trollsås M, Hedrick JL (1998) Dendrimer-like star polymers. J Am Chem Soc 120:4644–4651

31. Trollsås M, Atthof B, Würsch A, Hedrick JL (2000) Constitutional isomers of dendrimer-like star polymers: design, synthesis, and conformational and sructural properties. Macromolecules 33:6423–6438

32. Hedenqvist MS, Yousefi H, Malmström E, Johansson M, Hult A, Gedde UW, Trollsås M, Hedrick JL (2000) Transport properties of hyperbranched and dendrimer-like star polymers. Polymer 41:1827–1840

33. Würsch A, Möller M, Glauser T, Lim LS, Voytek SB, Hedrick JL (2001) Dendritic-linear AxBx block copolymers prepared via controlled ring-opening polymerization of lactones from orthogonally protected multifunctional initiators. Macromolecules 34:6601–6615

34. Trollsås M, Atthof B, Claesson H, Hedrick JL (2004) Dendritic homopolymers and block copolymers: tuning the morphology and properties. J Polym Sci Part A Polym Chem 42:1174–1188

35. Trollsås M, Claesson H, Atthof B, Hedrick JL (2000) Conformational and structure properties of high functionality dendrimer-like star polymers synthesized from living polymerization techniques. Macromol Symp 153:87–108

36. Trollsås M, Kelly MA, Claesson H, Siemens R, Hedrick JL (1999) Highly branched block copolymers: design, synthesis, and morphology. Macromolecules 32:4917–4924

37. Hedrick JL, Trollsås M, Hawker CJ, Atthof B, Claesson H, Heise A, Miller RD (1998) Dendrimer-like star block and amphiphilic copolymers by combination of ring opening and atom transfer radical polymerization. Macromolecules 31:8691–8705

38. Stancik CM, Pople JA, Trollsås M, Lindner P, Hedrick JL, Gast AP (2003) Impact of core architecture on solution properties of dendrimer-like star copolymers. Macromolecules 36:5765–5775

39. Percec V, Barboiu B, Grigoras C, Bera TK (2003) Universal iterative strategy for the divergent synthesis of dendritic macromolecules from conventional monomers by a combination of living radical polymerization and irreversible TERminator multifunctional initiator (TERMINI). J Am Chem Soc 125:6503–6516

40. Percec V, Grigoras C, Bera TK, Barboiu B, Bissel P (2005) Accelerated iterative strategy for the divergent synthesis of dendritic macromolecules using a combination of livingradical polymerization and an irreversible terminator multifunctional initiator. J Polym Sci Part A Polym Chem 43:4894–4906

41. Percec V, Grigoras C, Kim HJ (2004) Toward self-assembling dendritic macromolecules from conventional monomers by a combination of living radical polymerization and irreversible terminator multifunctional initiator. J Polym Sci Part A Polym Chem 42:505–513

42. Zhang H, He J, Zhang C, Ju Z, Li J, Yang Y (2012) Continuous process for the synthesis of dendrimer-like star polymers by anionic polymerization. Macromolecules 45:828–841

43. Hirao A, Sugiyama K, Tsunoda Y, Matsuo A, Watanabe T (2006) Precise synthesis of well-defined dendrimer-like star-branched polymers by iterative methodology based on living anionic polymerization. J Polym Sci Part A Polym Chem 44:6659–6687

44. Hirao A, Yoo HS (2011) Dendrimer-like star-branched polymers: novel structurally well-defined hyperbranched polymers. Polym J 43:2–17

45. Higashihara T, Sugiyama K, Yoo HS, Hayashi M, Hirao A (2010) Combining living anionic polymerization with branching reactions in an iterative fashion to design branched polymers. Macromol Rapid Commun 31:1031–1059

46. Hirao A, Hayashi M, Loykulnant S, Sugiyama K, Ryu SW, Haraguchi N, Matsuo A, Higashihara T (2005) Precise syntheses of chain-multi-functionalized polymers, star-branched polymers, star-linear block polymers, densely branched polymers, and dendritic branched polymers based on iterative approach using functionalized 1,1-diphenylethylene derivatives. Prog Polym Sci 30:111–182

47. Hirao A, Sugiyama K, Matsuo A, Tsunoda Y, Watanabe T (2008) Synthesis of well-defined dendritic hyperbranched polymers by iterative methodologies using living/controlled polymerizations. Polym Int 57(4):554–570

48. Matsuo A, Watanabe T, Hirao A (2004) Synthesis of well-defined dendrimer-like branched polymers and block copolymer by the iterative approach involving coupling reaction of living anionic polymer and functionalization. Macromolecules 37:6283–6290

49. Jin S, Jin KS, Yoon J, Heo K, Kim J, Kim KW, Ree M, Higashihara T, Watanabe T, Hirao A (2008) X-ray scattering studies on molecular structures of star and fendritic polymers. Macromol Res 16:686–694

50. Hirao A, Matsuo A, Watanabe T (2005) Precise synthesis of dendrimer-like star-branched poly (methyl methacrylate)s up to seventh generation by an iterative divergent approach involving coupling and transformation reactions. Macromolecules 38:8701–8711

51. Watanabe T, Tsunoda Y, Matsuo A, Sugiyama K, Hirao A (2006) Synthesis of dendrimer-like star-branched poly(methyl methacrylate)s of generations consisting of four branched polymer chains at each junction by iterative methodology involving coupling and transformation reactions. Macromol Symp 240:23–30

52. Watanabe T, Hirao A (2006) Precise synthesis of dendrimer-like star-branched poly(methyl methacrylate)s with different branched architectures up to third-generation by iterative methodology. Macromol Symp 245(246):5–13

53. Hirao A, Watanabe T, Ishizu K, Ree M, Jin S, Jin KS, Deffieux A, Schappacher M, Carlotti S (2009) Precise synthesis and characterization of fourth-generation dendrimer-like star-branched poly(methyl methacrylate)s and block copolymers by iterative methodology based on living anionic polymerization. Macromolecules 42:682–693

54. Yoo HS, Watanabe T, Hirao A (2009) Precise synthesis and characterization of fourth-generation dendrimer-like star-branched poly(methyl methacrylate)s and block copolymers by iterative methodology based on living anionic polymerization. Macromolecules 42:4558–4570

55. Zhang H, Zhu J, He J, Qiu F, Zhang H, Yang Y, Lee H, Chang T (2013) Easy synthesis of dendrimer-like polymers through a divergent iterative "end-grafting" method. Polym Chem 4:830–839

56. Yoo HS, Watanabe T, Matsunaga Y, Hirao A (2012) Precise synthesis of dendrimer-like star-branched poly(tert-butyl methacrylate)s and their block copolymers by a methodology combining α-terminal-functionalized living anionic polymers with a specially designed linking reaction in an iterative fashion. Macromolecules 45:100–112

57. Joncheray TJ, Bernard SA, Matmour R, Lepoittevin B, EI-Khouri RJ, Taton D, Gnanou Y, Duran RS (2007) Polystyrene-b-poly(tert-butyl acrylate) and polystyrene-b-poly(acrylic acid) dendrimer-like copolymers: two-dimensional self-assembly at the air-water interface. Langmuir 23:2531–2538

58. Chalari I, Hadjichristidis N (2002) Synthesis of well-defined second-generation dendritic polymers of isoprene (I) and styrene (S): (S₂I)₃, (SI' I)₃, (I'I'I)₃, and (I'₂I)₄. J Polym Sci Part A Polym Chem 40:1519–1526

59. Orfanou K, Iatrou H, Lohse DJ, Hadjichristidis N (2006) Synthesis of well-defined second (G-2) and third (G-3) generation dendritic polybutadienes. Macromolecules 39:4361–4365

60. Knauss DM, Huang T (2003) ((PS)nPS)m star-shaped polystyrene with star-shaped branches at the terminal chain ends byconvergent living anionic polymerization. Macromolecules 36:6036–6042

61. Bender JT, Knauss DM (2009) Dendritic polystyrene with hydroxyl-functionalized branch points by convergent living anionic polymerization. Macromolecules 42:2411–2418

62. Knauss DM, Al-Muallem HA, Huang T, Wu DT (2000) Polystyrene with dendritic branching by convergent living anionic polymerization. Macromolecules 33:3557–3568

63. Knauss DM, Huang T (2002) Star-block-linear-block-star triblock (pom-pom) polystyrene by convergent living anionic polymerization. Macromolecules 35:2055–2062

64. Hutchings LR, Roberts-Bleming SJ (2006) DendriMacs. Well-defined dendritically branched polymers synthesized by an iterative convergent strategy involving the coupling reaction of AB₂ macromonomers. Macromolecules 39:2144–2152

65. Urbani CN, Bell CA, Whittaker MR, Monteiro MJ (2008) Convergent synthesis of second generation AB-type Miktoarm dendrimers using "Click" chemistry catalyzed by copper wire. Macromolecules 41:1057–1060

66. Whittaker MR, Urbani CN, Monteiro MJ (2006) Synthesis of 3-miktoarm stars and 1st generation mikto dendritic copolymers by "living" radical polymerization and "click" chemistry. J Am Chem Soc 128:11360–11361

67. Lonsdale D, Whittaker MR, Monteiro MJ (2009) Self-assembly of well-defined amphiphilic polymeric miktoarm stars, dendrons, and dendrimers in water: the effect of architecture. J Polym Sci Part A Polym Chem 47:6292–6303

68. Altintas O, Demirel AL, Hizal G, Tunca U (2008) Dendrimer-like miktoarm star terpolymers: A3-(B-C)3 via click reaction strategy. J Polym Sci Part A Polym Chem 46:5916–5928

69. Wang G, Luo X, Zhang Y, Huang J (2009) Synthesis of dendrimer-like copolymers based on the star [polystyrene-poly(ethylene oxide)-poly(ethoxyethyl glycidyl ether)] terpolymers by click chemistry. J Polym Sci Part A Polym Chem 47:4800–4810
70. Feng X, Chaikof EL, Absalon C, Drummond C, Taton D, Gnanou Y (2011) Dendritic carrier based on PEG: design and degradation of acid-sensitive dendrimer-like poly(ethylene oxide)s. Macromol Rapid Commun 32:1722–1728
71. Hedrick JL, Magbitang T, Connor EF, Glauser T, Volksen W, Hawker CJ, Lee VY, Miller RD (2002) Application of complex macromolecular architectures for advanced microelectronic materials. Chem Eur J 8:3308–3319

Complex Branched Polymers

Georgios Theodosopoulos and Marinos Pitsikalis

Abstract The synthesis of complex macromolecular architectures, such as ω-, α,ω-branched, block-graft, complex comb-like and dendritic-like polymers can be achieved either by a divergent or by a convergent method. The synthesis of new anionic initiators, the use of linking agents and transformation reactions along the polymer chain are some of the means to achieve these complex architectures. Linear chains with a number of polymer chains covalently attached at one of their ends, also referred to as ω-branched polymers, depict a variety of products such as palm-tree and umbrella type polymers. α,ω-Branched polymers consist of linear macromolecules with a number of covalently attached chains at both chain ends. Super-H and pom-pom like polymers are an example of this type of formation. The former are possible through the employment of a variety of linking, terminating or multifunctional-initiating agents. Block-grafted copolymers are prepared via backbone modification reactions (e.g., hydrosilylation, epoxidation) and post-polymerization reactions. Well-defined comb-like polymers are obtained through the use of macromonomers selectively bonded to complex linking agents. Dendritic-like and dendritic-graft architectures are possible through the convergent as well as the divergent approach; with main methods of preparation being the use of linking agents, multifunctional initiators, epoxidation reactions and self-condensing vinyl polymerization.

Keywords ω-Branched polymers • α,ω-Branched polymers • Block-graft copolymers • Complex comb-like polymers • Dendritic-like polymers

1 Complex Macromolecular Architectures

Recent developments in anionic polymerization have allowed the synthesis of novel macromolecular structures with excellent control over the topology, microstructure and composition [1]. The application of organic chemistry reactions for the transformation of the macromolecular chains along with the synthesis of new anionic

G. Theodosopoulos • M. Pitsikalis (✉)
Department of Chemistry, University of Athens, Panepistimiopolis Zografou,
15771 Athens, Greece
e-mail: pitsikalis@chem.uoa.gr

initiators and linking agents are the main tools for the synthesis of complex macromolecular architectures. Since there are specific chapters of this book covering the synthesis of star, graft, dendritic and hyperbranched polymers by anionic polymerization, the synthesis of more complex macromolecular architectures, such as the ω-, the α,ω-branched, the block-graft, the complex comb-like and dendritic-like polymers, will be the subject of this chapter.

2   ω-Branched Polymers

These polymers can be considered as linear chains having a number of covalently attached chains at one of their ends. Such products are called palm-tree or even umbrella polymers, and their synthesis can be achieved either by a divergent or a convergent method. According to the divergent method, the linear polymer has a number of anionic initiating sites located at the chain end. Through these sites new polymer chains can grow, leading to the formation of a ω-branched structure.

The convergent method involves the linking of preformed chains to suitable linking sites located at the main chain end. This approach was applied for the synthesis of the umbrella-type copolymers. PS-*b*-PBd block copolymers with a short PBd block of the 1,2 microstructure were prepared by anionic polymerization. The polydiene block was hydrosilylated for the introduction of Si–Cl groups. Subsequent linking of these groups with living PBd chains afforded the desired $PS(PBd)_x$ structures [2] (Scheme 1).

Living polymer chains may react with the double bonds of fullerene C_{60}, and a maximum of six chains may be grafted onto the C_{60} molecules, leading to the formation of well-defined stars with a C_{60} core bearing up to six arms and an equal number of negative charges. It was found that only one of these six carbanions of the living six-arm stars was able to initiate the polymerization of another monomer, thus allowing for the synthesis of a ω-branched structure (Scheme 2) [3]. Size exclusion chromatography (SEC) analysis revealed that the products had moderate molecular weight distributions ($I = 1.2$–1.3), indicating a slow initiation process for the growth of the PS arm from the living star. Moreover, unreacted stars were always detected showing that actually less than one sixth of the theoretically available anions are able to lead to efficient polymerization. Preparative SEC was employed to obtain the pure palm-tree structure. Using this methodology $(PS)_6PI$ and $(PI)_6PS$ structures were synthesized.

$(PS_A)_nPS_B$ homopolymers and $(PS)_nPI$ copolymers were prepared by a synthetic scheme involving anionic polymerization of styrene followed by slow addition of a dual functional coupling agent 4-(chlorodimethylsilyl)styrene (CDMSS) in the first step [4]. CDMSS is functionalized with one group that can quantitatively couple with the living chain end and a vinyl functionality that allows quantitative addition and the preservation of the living chain end. The slow addition of the coupling agent leads to the formation of a star polymer bearing a hyperbranched core. By controlling the amount of CDMSS added to the solution of the living PS^-Li^+, relative to

Scheme 1 Synthesis of umbrella copolymers

butadiene + s-BuLi $\xrightarrow{\text{dipip}}$

Bu$-$[CH$_2$$-$CH]$_9CH_2$$-CH-CH-CH_2$
    | ⊖
    CH$_2$$=$CH
                              Li ⊕

$\xrightarrow[\text{2. } t\text{-BuOH}]{\text{1. styrene}}$ Bu$-$[CH$_2$$-$CH]$_{10}$[CH$_2$$-$CH]$_{260}$H $\xrightarrow[\text{Pt}]{\text{HSi(CH}_3\text{)Cl}_2}$
    |
    CH$_2$$=$CH
(phenyl)

Bu$-$[CH$_2$$-$CH]$_{10}$[CH$_2$$-$CH]$_{260}$H   (I)
        |
        CH$_2$
        |
        CH$_2$
        |
        Si(CH$_3$)Cl$_2$
(phenyl)

butadiene + s-BuLi $\longrightarrow$ PBd $^\ominus$ Li $^\oplus$ (II)

(I) + (II) $\longrightarrow$

umbrella copolymer
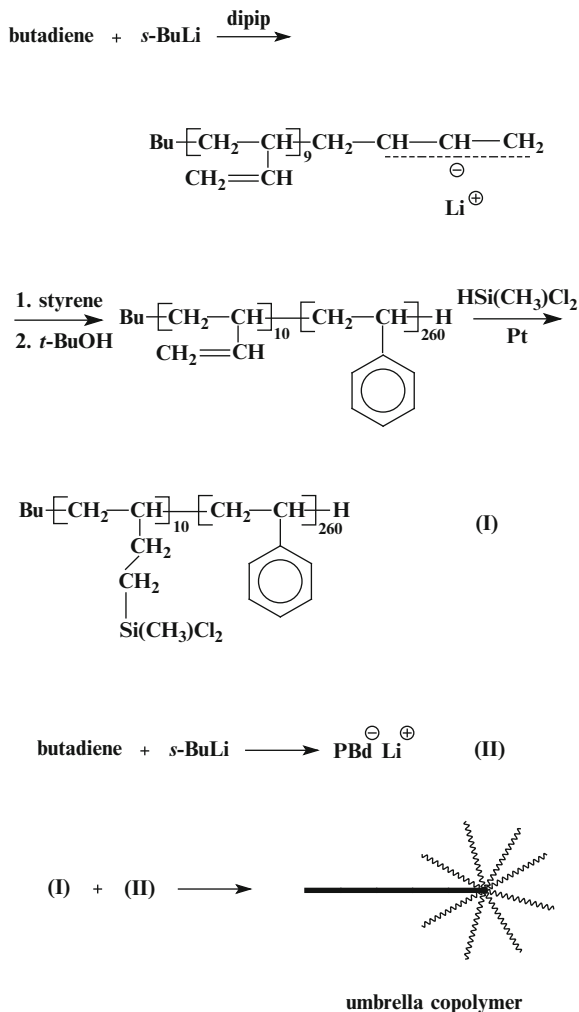
the amount of the initial chain ends, the extent of coupling (number of arms, n) can be controlled. When less than the stoichiometric quantity of the CDMSS over the living PS$^-$Li$^+$ chains is added, the star polymer contains a single living chain end at the core. This living chain end can be used for the polymerization of additional styrene or isoprene in the second step, leading to the formation of the desired palm-tree polymers (Scheme 3) [5].

The same convergent approach was adopted for the synthesis of (PCHD)$_n$PS copolymers, where CHD is 1,3-cyclohexadiene. Slow addition of CDMSS into living PCHD$^-$Li$^+$ chains afforded the living PCHD star polymer with a hyperbranched core bearing a living chain end, which was subsequently used for the polymerization of styrene. It was found that the average number of PCHD arms was equal to four [6].

$$6 \text{ PS-Li} + C_{60} \xrightarrow[\text{25 °C}]{\text{Toluene}} (PS)_6 C_{60}{}^{6-}(Li^+)_6 \quad (A):$$

$$(A) + \text{Monomer} \xrightarrow[\text{25 °C}]{\text{Toluene}} (PS)_6\, C_{60}{}^{5-}(Li^+)_5(PM^-)(Li^+)$$
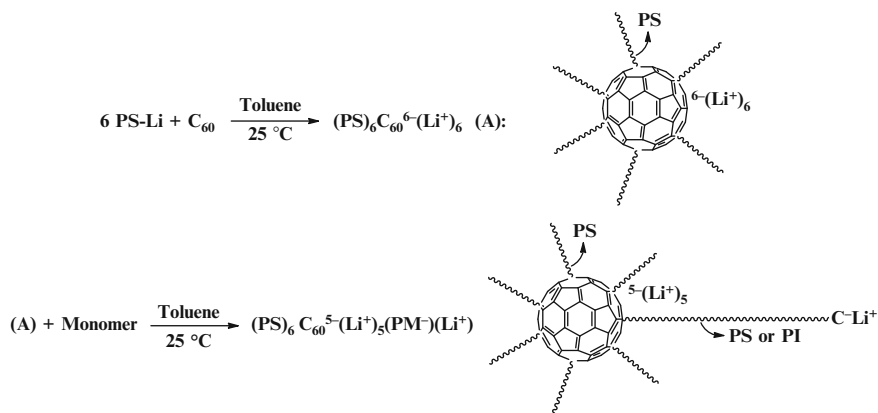
Scheme 2 Synthesis of 6-arm star PS polymers and $(PS)_6PI$ palm-tree type copolymers bearing C_{60} cores

3 α,ω-Branched Polymers

These polymers can be considered linear macromolecules having a number of covalently attached chains at both chain ends. Their synthesis can be achieved employing similar methods used for the ω-branched polymers, except that the reactions are performed at both chain ends. Copolymers of the type B_3AB_3 are termed super-H-shaped copolymers and, more generally, copolymers of the type B_nAB_n are characterized in the literature as pom-pom or dumbbell copolymers.

By the use of anionic polymerization and controlled chlorosilane chemistry, the exact placement of the side chains along the backbone is possible.

Using this combination, H- and super-H-shaped copolymers were synthesized. In the case of H-shaped copolymers [7], living PS^-Li^+ and $MeSiCl_3$ were reacted in a ratio $SiCl:Li = 3:2.1$. Due to the sterically hindered PSLi anion only two Cl atoms were substituted, resulting in a PS dimer with an active Si–Cl bond at the center. The macromolecular linking agent was reacted with a difunctional PI chain (the connector), synthesized using the difunctional initiator derived from 1,3-bis (1-phenylethenyl)benzene (MDDPE) and *sec*-BuLi in benzene solution and in the presence of lithium-*tert*-butoxide, giving the H-copolymer as shown in Scheme 4. This synthetic scheme is an extension of the one used for the preparation of H-shaped polystyrene homopolymers [8].

Using a convergent approach and anionic polymerization techniques associated with suitable chlorosilane chemistry, $(PI)_3PS(PI)_3$ super-H-shaped copolymers were prepared [9]. A difunctional PS chain, derived from the polymerization of styrene in THF using sodium naphthalene as initiator, was reacted with a large excess of $SiCl_4$, leading to the synthesis of a PS chain, end-functionalized at both ends with $-SiCl_3$ groups. After elimination of the excess $SiCl_4$ and addition of living PI arms, the desired super-H structure was achieved (Scheme 5).
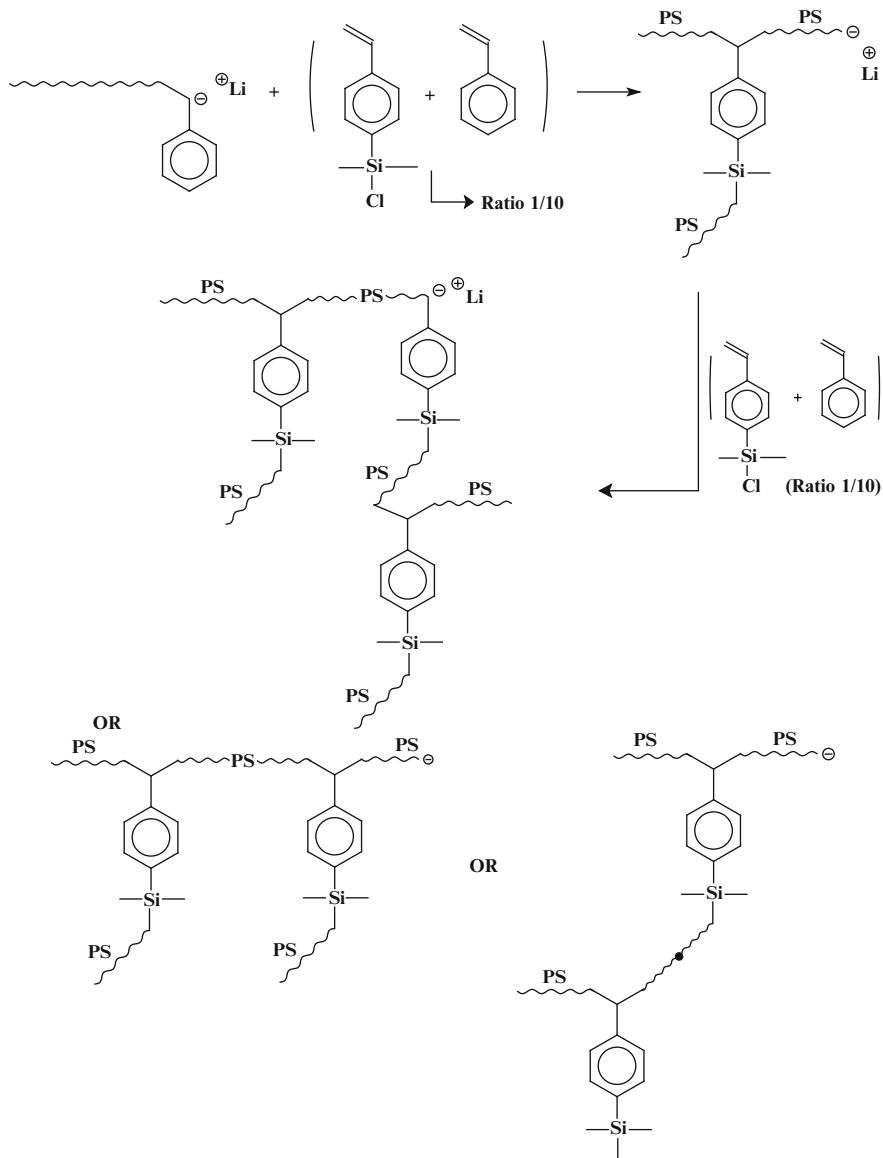
Scheme 3 The use of CDMSS in the preparation of palm-tree architectures

Scheme 3 (continued)

$$PS^{\ominus} Li^{\oplus} \quad + \quad MeSiCl_3 \quad \longrightarrow \quad PS_2MeSiCl \quad I$$

$$I \text{ (excess)} \quad + \quad II \quad \longrightarrow \quad PS_2PIPS_2$$
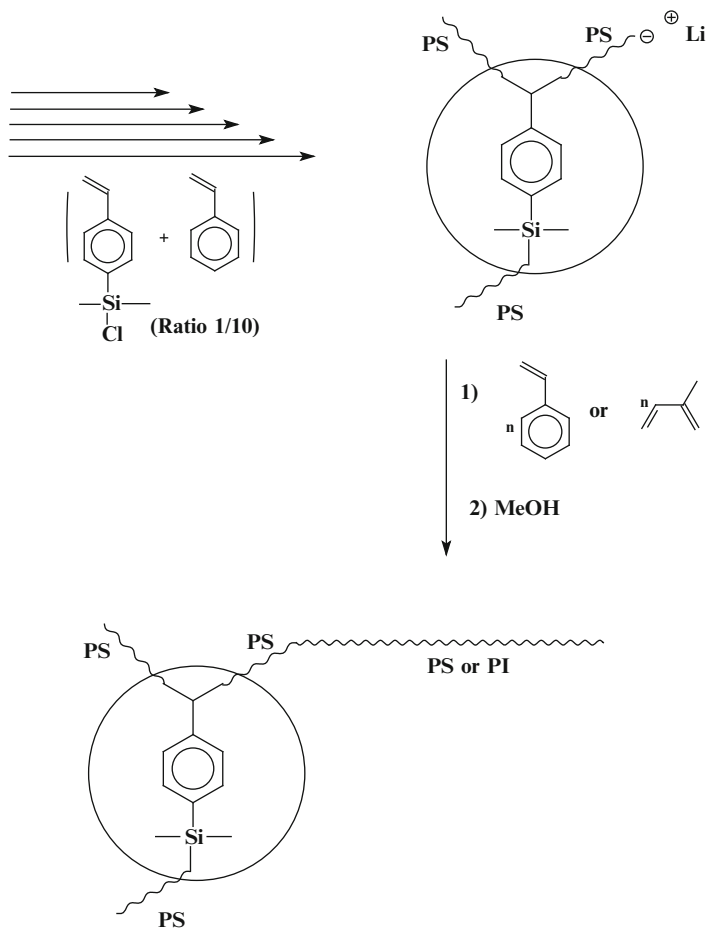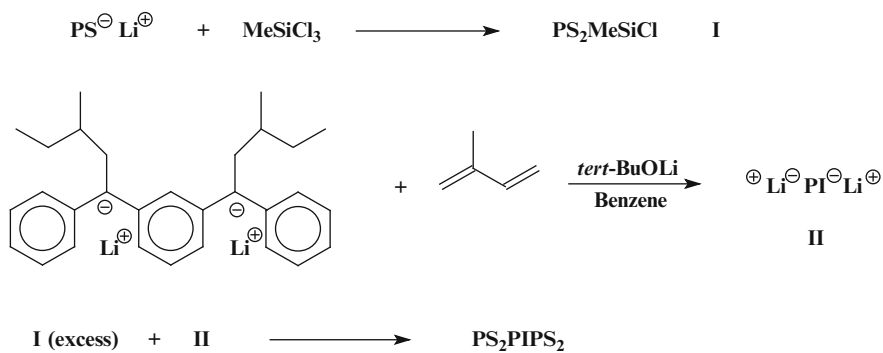
Scheme 4 Synthesis of H-shaped copolymers with the chlorosilane methodology

$$^{\oplus}Na \; ^{\ominus}PS^{\ominus} \, Na^{\oplus} \; + \; SiCl_4 \; (excess) \longrightarrow Cl_3SiPSSiCl_3 \; + \; SiCl_4$$

$$Cl_3SiPSSiCl_3 \; + \; PI^{\ominus} \, Li^{\oplus} (excess) \longrightarrow (PI)_3PS(PI)_3$$
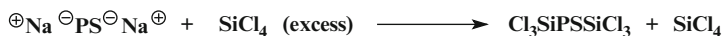
Scheme 5 Synthesis of super H-shaped copolymers with the chlorosilane methodology

$$PI^{\ominus}Li^{\oplus} \; (\sim 20\% \; excess) \; + \; Cl_3Si \diagup \diagdown SiCl_3 \longrightarrow (PI)_5\_SiCl$$

$$^{\oplus}Li \; ^{\ominus}PS^{\ominus} \, Li^{\oplus} \; + \; (PI)_5\_SiCl \; (excess) \xrightarrow{\text{THF 3\%}} (PI)_5PS(PI)_5$$
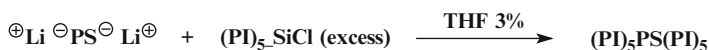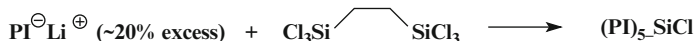
Scheme 6 Chlorosilane chemistry for the synthesis of pom-pom structures

Employing a similar method, $(PI)_5PS(PI)_5$ copolymers (pom-pom shaped) were synthesized [10]. Living PI^-Li^+ chains were reacted with the hexafunctional chlorosilane $Cl_3SiCH_2CH_2SiCl_3$ in a SiCl:Li ratio $= 6:5$, giving the five-arm star with a remaining SiCl group at the central point. Subsequent reaction with a difunctional PS led to the synthesis of the pom-pom copolymer (Scheme 6).

The aforementioned divergent and convergent approaches based on chlorosilane chemistry were utilized for the synthesis of well-defined H-, super-H- and pom-pom-shaped PBds, as shown in the general synthetic Scheme 7 [11]. The samples were subsequently subjected to catalytic hydrogenation, using either Pd supported onto $CaCO_3$ or Wilkinson's catalyst, to obtain the corresponding polyethylene structures.

α,ω-Branched polymers were prepared through the linking of the corresponding living ω-branched structures using a suitable linking agent. According to this methodology, living $(PS)_6PS^-Li^+$ or $(PS)_6PI^-Li^+$ stars bearing a C_{60} core were efficiently linked employing dibromo-p-xylene as linking agent leading to the synthesis of pom-pom structures, as shown in Scheme 8 [3].

$(PS_A)_nPS_B(PS_A)_n$ homopolymers and $(PS_A)_nPI(PS_A)_n$ copolymers were prepared by a synthetic scheme involving anionic polymerization of styrene followed by the addition of 4-(chlorodimethylsilyl)styrene (CDMSS) in the first step [12]. The star PS thus formed contained one living chain end which was further used for the polymerization of additional styrene or isoprene in the second step. Coupling of the living stars with $(CH_3)_2SiCl_2$ in the third step resulted in the formation of the pom-pom polymers (Scheme 9) [4, 5, 13]. Due to the statistical nature of the first step, there is a distribution in the number of arms connected to the ends of the main PS or PI chain. The average number of arms, n, was kept low, varying between three and nine.
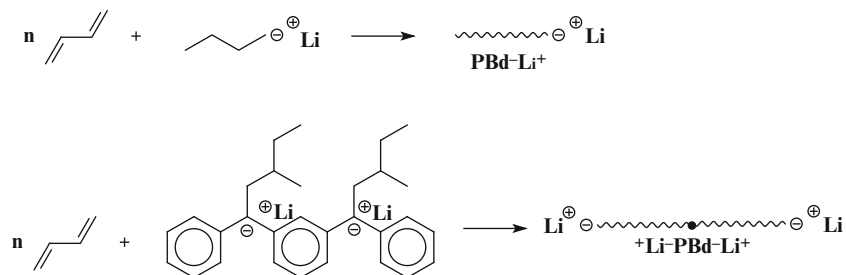
$$n \diagup\!\!\!\!\diagdown + \diagdown\!\!\diagup \ominus \; {}^{\oplus}Li \longrightarrow \text{wwww} \ominus \; {}^{\oplus}Li$$
$$\text{PBd}^-\text{Li}^+$$

$$n \diagup\!\!\!\!\diagdown + \quad \longrightarrow \quad Li^{\oplus}\ominus \text{wwww}\bullet\text{wwww}\ominus{}^{\oplus}Li$$
$$\text{}^+\text{Li}^-\text{PBd}^-\text{Li}^+$$

Divergent Method

$$Li^{\oplus}\ominus \text{wwww}\bullet\text{wwww}\ominus{}^{\oplus}Li + \textbf{excess SiCl}_{x+1} \longrightarrow ClxSi \text{ wwww}\bullet\text{wwww} SiClx + 2LiCl$$
$$\text{}^+\text{Li}^-\text{PBd}^-\text{Li}^+ \qquad\qquad\qquad\qquad\qquad \textbf{ClxSiPBdClxSi}$$

$$ClxSi \text{ wwww}\bullet\text{wwww} SiClx + \textbf{excess PBd}^-\textbf{Li}^+ \longrightarrow \textbf{(PBd)}_x\textbf{-SiPBdSi-(PBd)}_x + \textbf{2xLiCl}$$
$$\textbf{ClxSiPBdClxSi}$$

Convergent Method

$$x \quad \text{wwww}\ominus{}^{\oplus}Li + SiCl_{x+1} \longrightarrow \textbf{Si-(PBd)xCl} + \textbf{xLiCl}$$
$$\textbf{PBd}^-\textbf{Li}^+$$

$$\textbf{excess Si-(PBd)x Cl} + Li^{\oplus}\ominus\text{wwww}\bullet\text{wwww}\ominus{}^{\oplus}Li \longrightarrow \textbf{(PBd)}_x\textbf{-SiPBdSi-(PBd)}_x + \textbf{2LiCl}$$
$$\text{}^+\textbf{Li}^-\textbf{PBd}^-\textbf{Li}^+$$
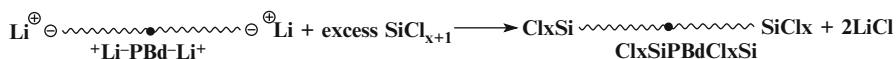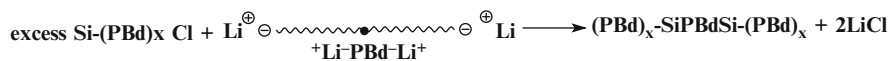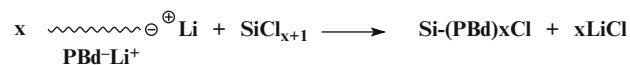
Scheme 7 Synthesis of well-defined H-, super H- and pom-pom PBd structures through the divergent and convergent manipulations of chlorosilane chemistry
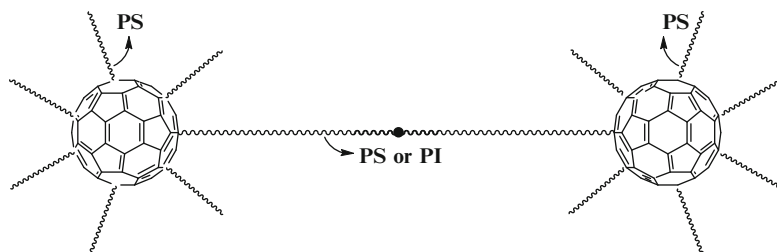
Scheme 8 Fullerenes employed for the synthesis of pom-pom structures
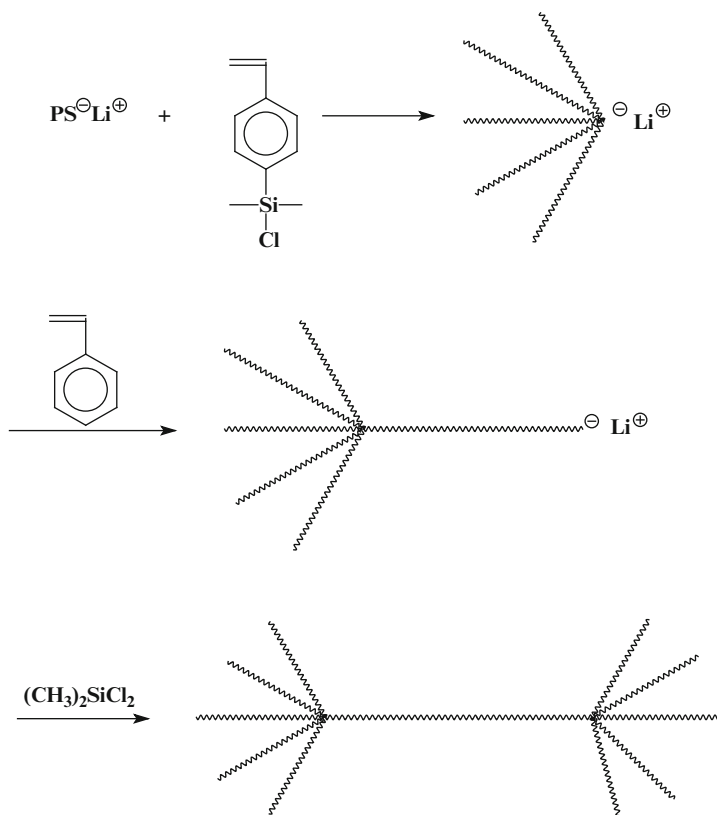
Scheme 9 Synthesis of PS pom-pom homopolymers

A similar macromonomer-based methodology was adopted for the synthesis of $(PS)_nPI(PS)_n$ α,ω-branched copolymers. Living PS^-Li^+ chains were reacted with p-chloromethylene styrene to afford the corresponding vinyl-terminated macromonomer. These macromonomers were then polymerized with *n*-BuLi, leading to the formation of a living star bearing an active anionic center, which was able to subsequently polymerize isoprene to result in $(PS)_nPI^-Li^+$ living structures. Coupling with 1,2-dibromoethane resulted in the synthesis of the desired branched copolymer (Scheme 10) [14]. Molecular characterization studies revealed that products with *n* values equal to 4 and 6 were obtained.

Pom-pom or dumbbell copolymers with a high functionality of the end-grafted chains were synthesized according to the divergent methodology by first preparing a PBd-1,2-PS-PBd-1,2 triblock copolymer having short PBd blocks by anionic polymerization, using naphthalene potassium as difunctional initiator [15]. The pendant double bonds in the PBd blocks were subjected to hydroboration–oxidation, producing OH groups. These groups were transformed to alkoxides, by
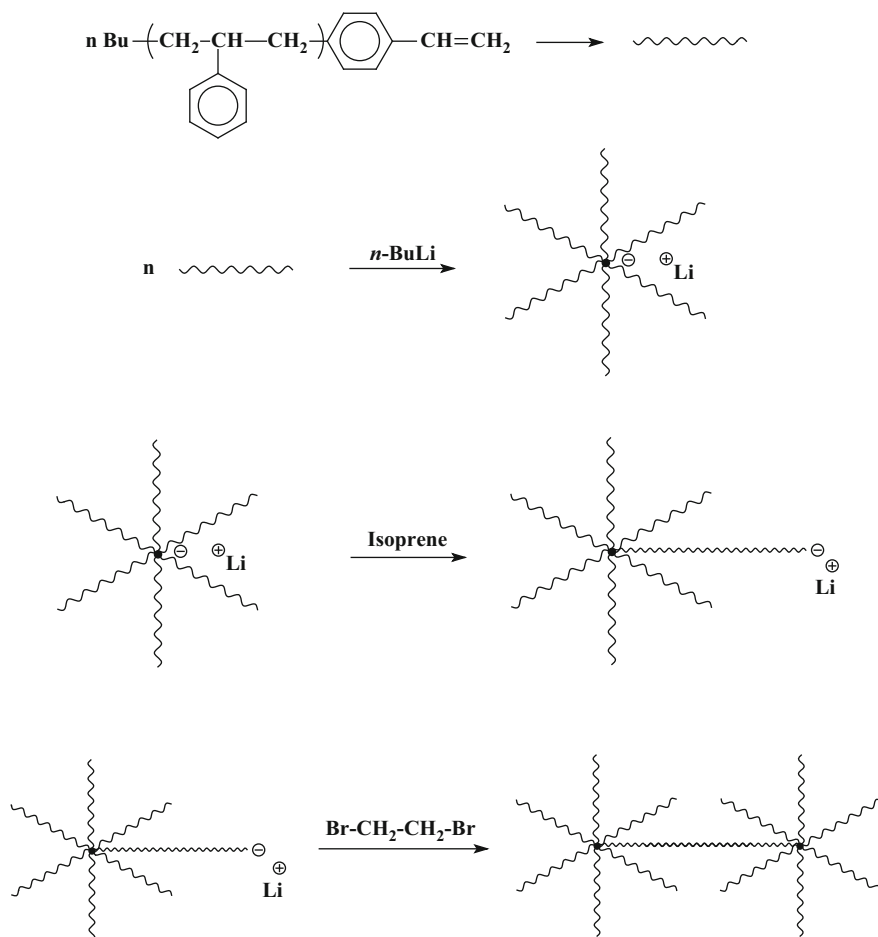
Scheme 10 α,ω-branched copolymers through the coupling of living miktoarm stars

reacting with cumylpotassium in the presence of cryptand (Kryptofix [2.2.2]). This way, precipitation of the polyfunctional initiator was avoided. The alkoxide groups were subsequently used as initiating sites for the polymerization of ethylene oxide. The dumbbell-shaped $(PEO)_nPS(PEO)_n$ copolymer was prepared this way (Scheme 11). Characterization of the obtained polymers indicated low degree of polymerization and compositional heterogeneity.

The convergent approaches offer a better structural control, provided that the linking reactions are efficient and free of steric hindrance effects. On the other hand, the divergent methods usually lack the precise control over the structure, since they require the generation of initiation centers at both ends of a polymer chain. The growth of polymer chains through these initiation sites may not be uniform, due to steric hindrance, association phenomena, kinetic differentiations, etc., leading to products with structural defects and chemical inhomogeneities.
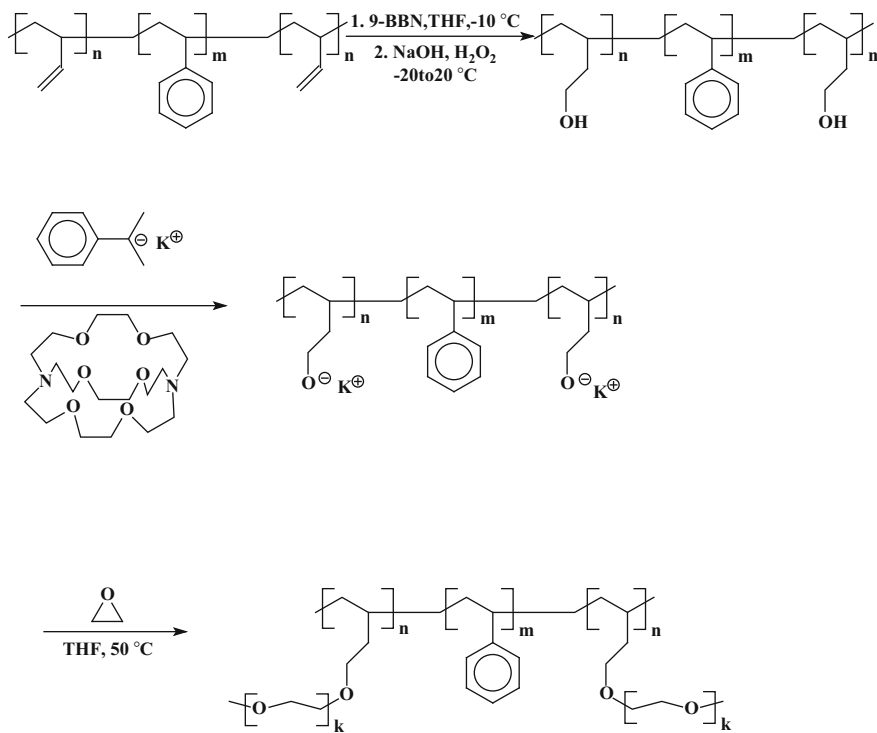
9-BBN=9-boracyclo[3.3.1]nonane

Scheme 11 Synthetic route for (PEO)ₙPS(PEO)ₙ dumbbell-shaped copolymers

Scheme 12 Schematic representation of pom-pom structures

pom-pom

Macromonomers can also be used for the synthesis of α,ω-branched polymers. A bifunctional living polymer chain, acting as a macroinitiator, can polymerize macromonomers thus producing a pom-pom (or dumbbell) copolymer, under the condition that a small number (Scheme 12) [16].

In an extension of the methodology involving diphenylethylenes, DPEs, the preparation of chain-end-functionalized polymers with a definite number of bromomethylphenyl (BnBr) end groups and their utilization in the synthesis of dumbbell polymers has been reported [17]. The synthesis of linear PS chain capped at each end with 2, 4, 8 or 16 bromomethylphenyl (BnBr) groups is illustrated in Scheme 13. A living difunctional PS chain was reacted with a DPE derivative
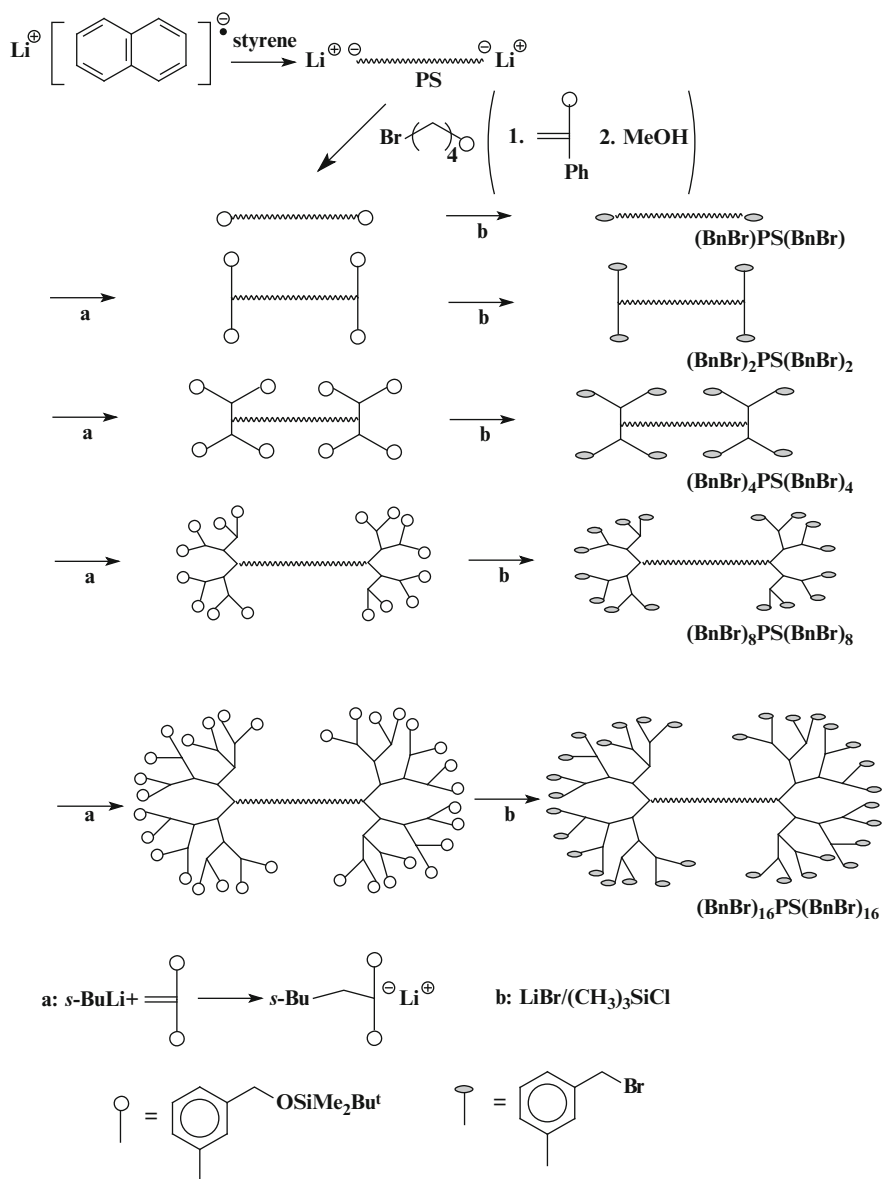
Scheme 13 Dumbbell formations through the introduction of a definite number of bromomethyl-phenyl groups

bearing one *tert*-butyldimethylsilyloxymethylene group. Subsequent reaction with $LiBr/(CH_3)_3SiCl$ transformed the end groups to bromomethylphenyl moieties. DPE carrying two *tert*-butyldimethylsilyloxymethylene groups was activated with *sec*-BuLi and reacted with the bromomethyl units of the telechelic PS chains. Subsequent transformation to bromomethylphenyl functions afforded a linear PS

macromolecule with two end groups at each chain end. The procedure can be repeated for the incorporation of up to 16 BnBr groups at each chain end. Linking of living PS polymers end-capped with a DPE unit has resulted in the formation of well-defined dumbbell polymers with a predetermined number of branches.

4 Block-Graft Copolymers

Block-graft copolymers, having a PS-PBd diblock as a backbone and PS, PI, PBd and PS-*b*-PI branches were prepared by anionic polymerization and hydrosilylation reactions [18]. The diblock copolymer backbone was prepared by sequential addition of styrene and butadiene. The polymerization of butadiene took place in the presence of dipiperidinoethane resulting in high 1,2 content. The backbone was then subjected to hydrosilylation in order to incorporate the desired amount of SiCl groups on the PBd block. These groups were then used as branching sites where
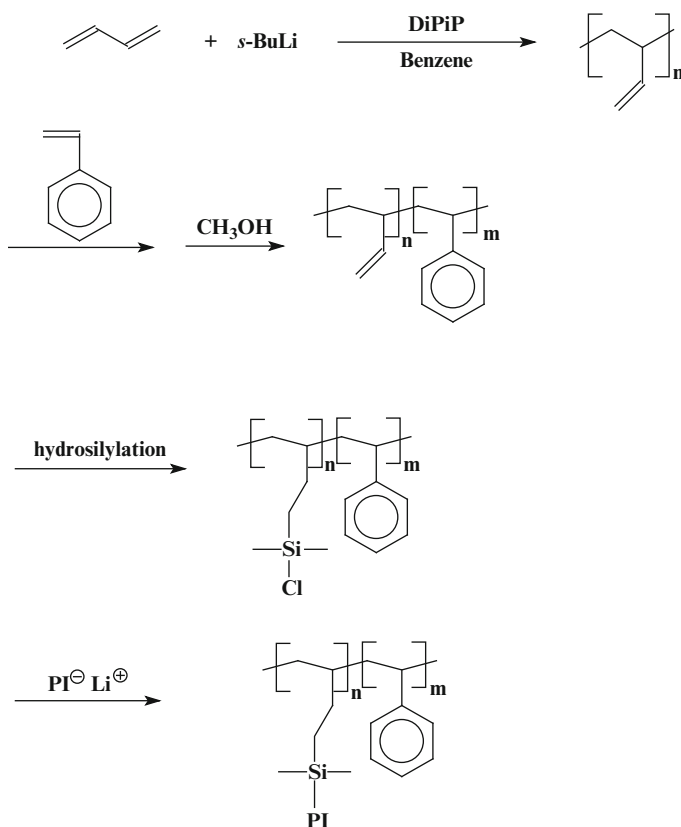
Scheme 14 Block-graft copolymers through the hydrosilytation of PS-*b*-PI copolymers
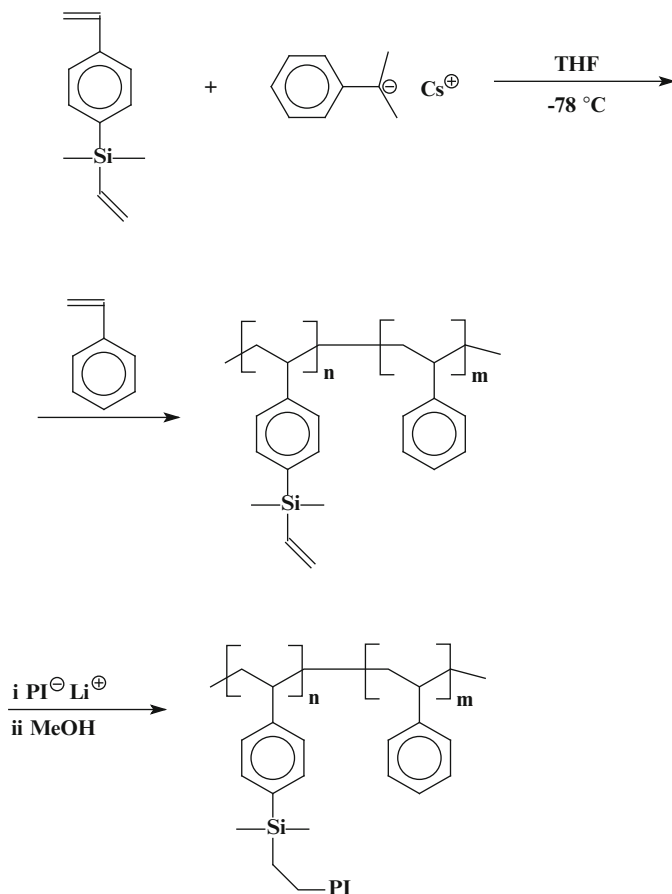
Scheme 15 Synthesis of P[(VS-*g*-I)-*b*-S] block graft copolymers

PS⁻Li⁺, PI⁻Li⁺, PBd⁻Li⁺, and PSPI⁻Li⁺ living chains were linked (Scheme 14). The use of MeSiHCl₂ instead of Me₂SiHCl in the hydrosilylation step produced difunctional branching sites along the PBd part of the backbone, leading to the formation of block-graft copolymers with two chains grafted on each branching point.

The synthesis of poly[(VS-*g*-I)-*b*-S] block-graft copolymers, where VS is 4-(vinyldimethylsilyl)styrene, has been presented [19]. The backbone, a diblock copolymer of VS and styrene, was prepared first by anionic polymerization. The VS monomer was selectively polymerized through the styryl double bond at low temperature in THF using cumylcesium as initiator followed by the addition of styrene. Living PI⁻Li⁺ was then allowed to react with the vinylsilyl groups of the VS block giving the final graft copolymer (Scheme 15). Detailed characterization of the polymers obtained by SEC, membrane osmometry and ultracentrifugation

techniques proved their high molecular weight and compositional homogeneity and also confirmed the desired architecture.

The synthesis of block-graft copolymer containing styrene, hydroxystyrene and ethylene oxide of the types PS-*b*-(PHS-*g*-PEO) and PS-*b*-(PHS-*g*-PEO)-*b*-PS, where PHS is poly(*p*-hydroxystyrene), has been reported [20]. The ABA triblock copolymer comprising the backbone was synthesized through a three-step sequential addition of monomers, which are styrene and *p-tert*-butoxystyrene, BS, (the precursor to hydroxystyrene). The PBS blocks were converted to poly(*p*-hydroxystyrene) by reaction with hydrogen bromide. The OH groups, thus formed, were transformed to potassium alkoxide groups by reaction with cumyl potassium or 1,1-diphenylethylene potassium. The resulting macromolecular initiators were used for the polymerization of EO, forming the branches of the block-graft-block copolymers (Scheme 16). Molecular characterization of the products by SEC and osmometry indicated that they possessed narrow molecular weight distributions and predictable molecular weights and compositions. Alternatively, the PEO side chains were synthesized by metal-free anionic ring opening polymerization of EO using the phenolic hydroxyl groups of the backbone and the phosphazene base *t*-BuP$_4$ as the complex multifunctional-initiating system [21]. It is well known [22] that the phosphazene base *t*-BuP$_4$ generates effective counterions with protons (*t*-BuP$_4$H)$^+$, which are suitable for the anionic polymerization of EO. In this case, the crude block-graft copolymers were contaminated with linear PEO homopolymer. Most probably, part of the phosphazene base was not protonated by the phenolic groups of the backbone but generated initiating sites after reaction with low molecular weight impurities, which are present in the system. Fractionation was necessary to obtain the pure block-graft amphiphilic copolymers.

The preparation of PMMA-*b*-(PGMA-*g*-PS) and PMMA-*b*-(PGMA-*g*-PI) block-graft copolymers, where PMMA is poly(methyl methacrylate) and PGMA is poly (glycidyl methacrylate), has been reported [23]. The PMMA-*b*-PGMA diblock was obtained first by anionic polymerization through sequential addition of monomers. Then living PS$^-$Li$^+$ and PI$^-$Li$^+$ chains were linked to the diblock backbone by reaction with the glycidyl groups of the GMA block. Molecular characterization of the final products confirmed the formation of the intended architecture having relatively narrow molecular weight distributions.

5 Comb-Like Complex Macromolecular Architectures

Macromonomers have been widely and successfully used as building blocks for the synthesis of an enormous number of branched macromolecular architectures [24]. This is a consequence of (a) the vast range of macromonomers that have been prepared and (b) the different processes employed for their homo- and copolymerization (conventional free radical, group transfer, anionic, cationic, controlled free radical, ring opening metathesis, metallocene and late transition metal catalyzed polymerizations) with either low molecular weight monomers or other
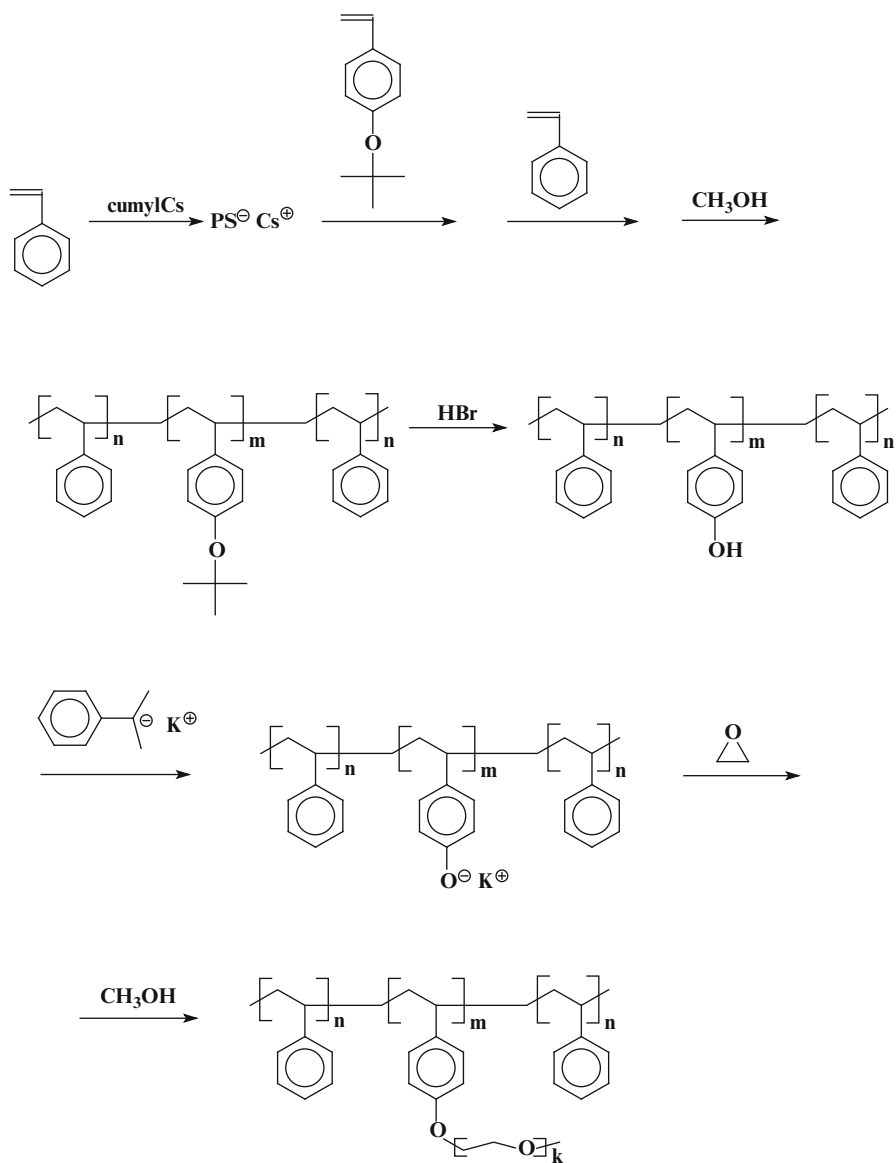
Scheme 16 Synthesis of PS-*b*-(PHS-*g*-PEO)-*b*-PS block-graft copolymers

macromonomers. These branched structures are well-defined, since (a) the length of the branches is fixed by the molecular weight of the macromonomer, which is known and can be predetermined using a living polymerization method for the synthesis of the macromonomer; (b) the size of the main chain of the branched structure can be controlled using a living polymerization method; and (c) the

Scheme 17 Employment
of single- and double-tailed
macromonomers in the
synthesis of model branched
copolymers
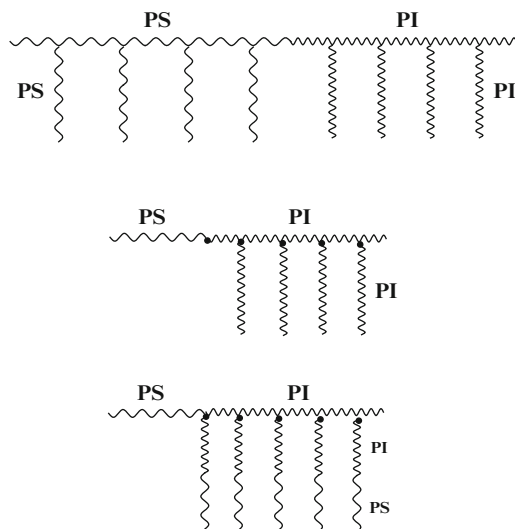
distribution of the branches can be controlled by the composition of the copoly-
merization mixture and the reactivity ratio of the macromonomers.

Using 4-(chlorodimethylsilyl)styrene, CDMSS, and 4-(dichloromethylsilyl)
styrene, DCMSS, a rich variety of single- and double-tailed macromonomers
were prepared by anionic polymerization procedures and were further employed,
in situ, for the synthesis of a wide range of polymer brushes, block-graft and star-
graft copolymers [25], as shown in Scheme 17.

Styrenic-tipped macromonomers of PI were obtained from the reaction of living
PI^-Li^+ with CDMSS. The reaction of the living chain ends with the chlorosilane
group is much faster than with the styrenic double bond. The appearance of the
orange color of the styrenic anion, obtained from the reaction of the slight excess of
the PI^-Li^+ chains with the double bond of CDMSS, allows the visual monitoring of
the end point of the linking reaction. These PI macromonomers were then
copolymerized with isoprene using living PS^-Li^+ chains as initiators leading to
the synthesis of PS-*b*-(PI-*g*-PI) diblock-comb copolymers (Scheme 18). In order to
achieve the random placement of the PI branches along the backbone, the copoly-
merization was performed in the presence of potassium alkoxide of 2,3-dimethyl-3-
pentanol, DMPOK, which equalizes the reactivity ratios of the styrenic
macromonomers and isoprene. The linking reaction of the living PS-*b*-(PI-*g*-
PI)$^-Li^+$ diblock-comb copolymers with $(CH_3)_2SiCl_2$ afforded the symmetric
PS-*b*-(PI-*g*-PI)-*b*-PS triblock-comb copolymers (Scheme 19). This methodology
was also adopted for the synthesis of PS-*b*-[PI-*g*-(PI-*b*-PS)] and PS-*b*-[PI-*g*-(PI-*b*-
PS)]-*b*-PS copolymers. In this case, styrenic-tipped macromonomers of PS-*b*-PI
were obtained by the reaction of living PS-*b*-PI$^-Li^+$ with CDMSS (Scheme 20).
This approach was further developed for the synthesis of diblock and triblock
copolymers where each block is a comb polymer (Scheme 21). In this case, a living
PS comb was employed as macroinitiator instead of linear PS^-Li^+ chains. For the

Scheme 18 Styrenic-tipped PS and PI macromonomers for the synthesis of model branched copolymers

synthesis of these living combs, styrenic-tipped macromonomers of PS were copolymerized with styrene using *sec*-BuLi as initiator. For the successful synthesis of the PS macromonomers, the living $PS^{-}Li^{+}$ chains were end-capped with a few isoprene units to avoid the steric hindrance of the linking reaction between the styryl lithium end group and CDMSS [26].

Living $PBd^{-}Li^{+}$ chains were added dropwise to a dilute solution of CDMSS, to afford the styrenic PB macromonomer. The efficiency of this approach relies on the much higher reactivity of the living polymer toward the chlorosilane group compared to the styrenic double bond. Subsequent copolymerization of the macromonomers with butadiene led to the synthesis of living PBd combs, $PBC^{-}Li^{+}$. The copolymerization was performed in the presence of DMPOK for

Scheme 19 Synthesis of symmetric PS-*b*-(PI-*g*-PI)-*b*-PS triblock comb copolymer

the random placement of the branches along the backbone, as previously mentioned (Scheme 22). PBC⁻Li⁺ was employed as initiator for the polymerization of 2VP at −78 °C in THF solution, leading to the formation of P2VP-*b*-(PBd-*g*-PBd) block-graft copolymers (Scheme 23). Living PS⁻Li⁺ was added to a solution of the PBd macromonomer, butadiene and DMPOK to give a living block-graft copolymer. Subsequent reaction with dichlorodimethylsilane afforded the PS-*b*-(PBd-*g*-PBd)-*b*-PS block-graft copolymer (Scheme 24). In addition, living PS⁻Li⁺ was reacted with CH₃SiCl₃ in a molar ratio 2.5/1 to give the macromolecular linking agent CH₃Si(PS)₂Cl. The third PS arm cannot be incorporated into the star structure due to the increased steric hindrance of the living polymer chain end. Reaction of CH₃Si (PS)₂Cl with the living PBd comb, PBC⁻Li⁺, led to the preparation of a miktoarm star-comb copolymer (Scheme 25). More complex structures were also synthesized using this methodology. Specifically, diblock, triblock and pentablock terpolymers, where each block was a graft copolymer, were obtained in a multistep reaction series. The PBd macromonomer was copolymerized with styrene to give the living graft copolymer (PS-*g*-PBd)⁻Li⁺. This living structure was employed as initiator for the copolymerization of isoprene and PS macromonomer in the presence of the randomizer DMPOK and thus forming the diblock terpolymer (PS-*g*-PBd)-*b*-(PI-*g*-PS)⁻Li⁺. Subsequent addition of Bd and PI macromonomer resulted in the synthesis of the triblock terpolymer (PS-*g*-PBd)-*b*-(PI-*g*-PS)-*b*-(PBd-*g*-PI)⁻Li⁺. Finally, linking of these living branched structures with (CH₃)₂SiCl₂ led to the formation of the corresponding pentablock terpolymer (PS-*g*-PBd)-*b*-(PI-*g*-PS)-*b*-(PBd-*g*-PI)-*b*-(PI-*g*-PS)-*b*-(PS-*g*-PBd) (Scheme 26). The synthesis of all these complex structures

Scheme 20 Synthesis of PS-*b*-[PI-*g*-(PI-*b*-PS)]-*b*-PS

was monitored by SEC and, when necessary, the crude products were purified by fractionation, resulting to well-defined branched polymers [27].

The living PBd combs, PBC$^-$Li$^+$, were further reacted with CH$_3$SiCl$_3$ and SiCl$_4$ to afford the corresponding three- and four-arm stars bearing PBd comb branches (Scheme 27). In addition, reaction of the living PBd combs, PBC$^-$Li$^+$, with CDMSS resulted in the formation of the corresponding comb-like styrenic

Scheme 21 Synthesis of triblock copolymers, where each block is a comb polymer

Scheme 21 (continued)

macromonomer. Copolymerization of these macromonomers with Bd using *sec*-BuLi as initiator led to the synthesis of comb-on-comb PBds, as revealed in Scheme 28 [28].

4-(Dichloromethylsilyl)styrene, DCMSS, was also employed for the synthesis of double-tailed styrenic-tipped macromonomers of PBd (Scheme 29). The macromonomers were either homopolymerized employing *sec*-BuLi as initiator, to afford double macromolecular brushes or copolymerized with Bd, in the presence of the randomizer DMPOK to provide double-comb PBds. The single- or double-tailed macromonomers were prepared and polymerized in situ, without isolation and purification, thus avoiding the introduction of impurities and leading to well-defined products. The living double-comb PBds were further reacted with CH_3SiCl_3 to provide the corresponding three-arm star double-comb PBd (Scheme 30) [29].

Further implementation of the macromonomer methodology as a tool for the synthesis of complex branched structures was reported with the use of 2-(dichloromethylsilyl)ethylchloro methylsilyl-4-styrene, TCDSS, for the preparation of styrenic triple-tailed PBd macromonomers. Living PB^-Li^+ chains were selectively reacted (titration) with the Si–Cl groups of TCDSS and were polymerized in situ, without isolation to avoid the introduction of impurities. Homopolymerization of these macromonomers led to the synthesis of triple molecular brushes of PBd or triple PBd polymacromonomers (Scheme 31). Copolymerization of the macromonomers with Bd in the presence of the randomizer DMPOK yielded triple-comb PBds, whereas copolymerization with styrene afforded triple-graft PS-*g*-(PBd)$_3$. Reaction of the living triple-tailed PBd combs with CH_3SiCl_3 gave the three-arm triple-comb PBd stars (Scheme 32). Extensive molecular
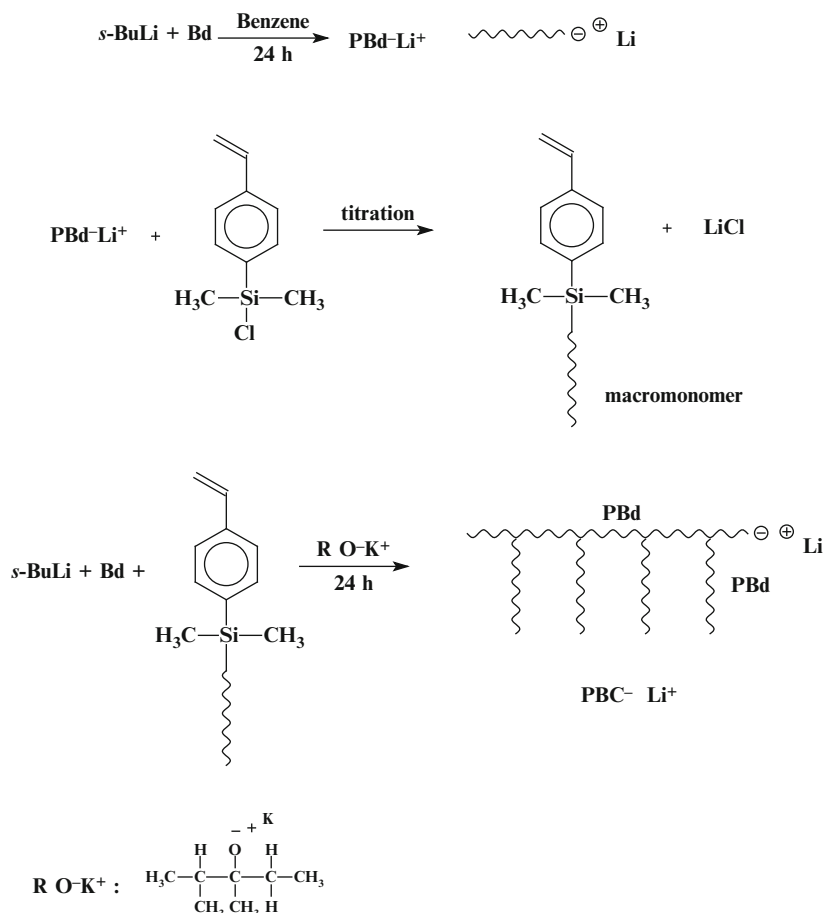
Scheme 22 Synthesis of PBd comb polymers through the use of CDMSS
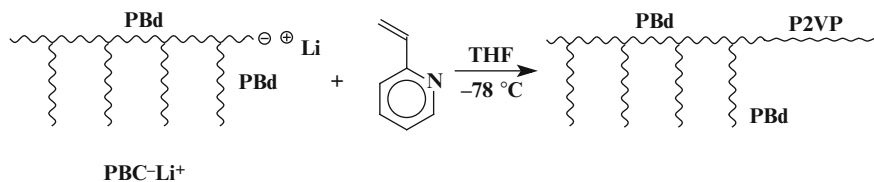
Scheme 23 Synthesis of P2VP-*b*-(PBd-*g*-PBd) block-graft copolymers

characterization by a wide variety of techniques revealed that well-defined structures were obtained [30].

An even better control for the synthesis of dendritic PBd polymers was adopted using the non-homopolymerizable dual functional linking agent, 4-(dichloromethylsilyl) diphenylethylene (DCMSDPE). Living PBd⁻Li⁺ chains
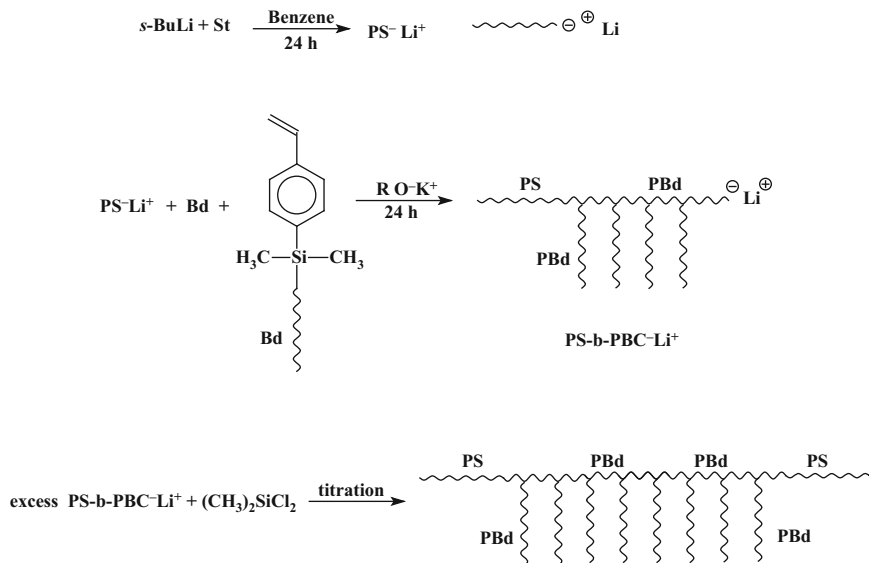
Scheme 24 Synthesis of PS-*b*-(PBd-*g*-PBd)-*b*-PS block-graft copolymers
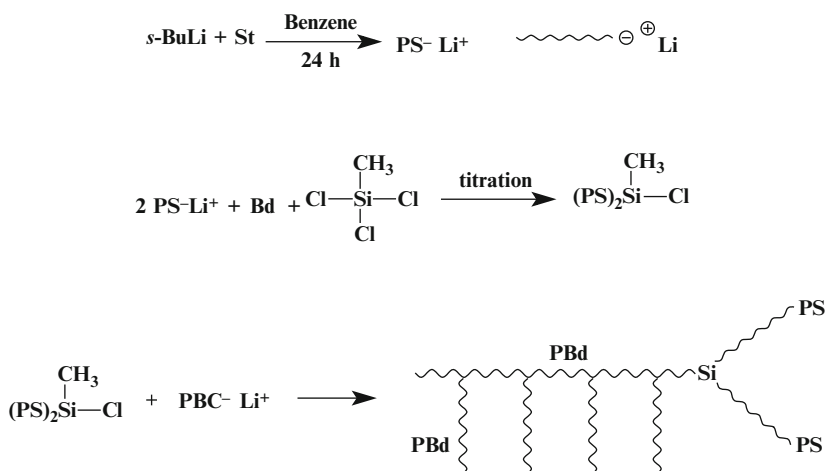
Scheme 25 Synthesis of miktoarm star-comb polymer

were linked selectively with the two chlorosilyl groups, leading to the synthesis of PBds bearing in-chain double bonds. The steric hindrance of the two phenyl groups of DCMSDPE prevented the reaction of the double bond with the living polymers. The remaining double bond was subsequently activated by *sec*-BuLi to afford the in-chain living polymer. Addition of a new quantity of Bd resulted in the formation of a living three-arm star polymer (Scheme 33) [31]. These living stars were subsequently linked with CDMSS and DCMSS for the synthesis of single and
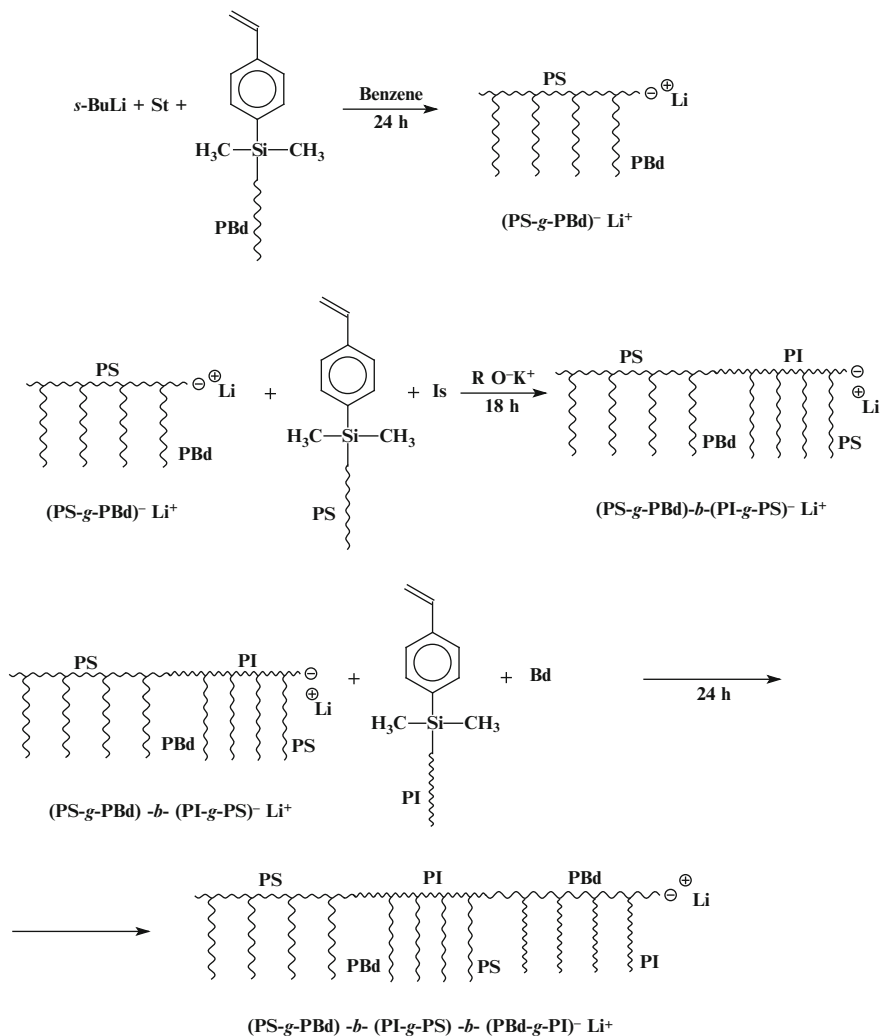
Scheme 26 Synthesis of (PS-*g*-PBd)-*b*-(PI-*g*-PS-*b*-(PBd-*g*-PI) pentablock terpolymer

double star-tailed macromonomers (Scheme 34). These macromonomers were in situ homopolymerized yielding PBd single and double homostar-tailed brushes (Scheme 35). Copolymerization with Bd in the presence of the randomizer DMPOK gave the PBd single and double homostar-tailed combs (Scheme 36). DCMSDPE was also employed for the synthesis of living miktoarm star polymers (PS)$_2$PBd$^-$Li$^+$. Living PS$^-$Li$^+$ chains were linked selectively with the two chlorosilyl groups, leading to the synthesis of PS bearing in-chain double bond. This double bond was subsequently activated by *sec*-BuLi to afford the in-chain living polymer. Addition of Bd resulted in the formation of the desired living three-
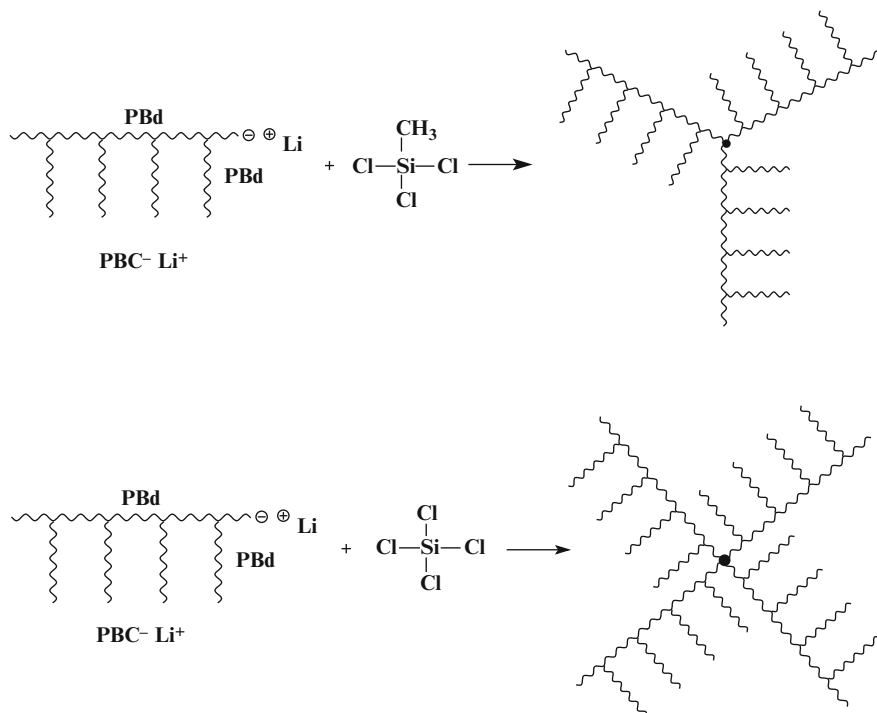
Scheme 27 Synthesis of three- and four-arm stars bearing PBd comb branches

miktoarm star polymer. These living stars were then reacted with DCMSS for the synthesis of double miktoarm star-tailed macromonomers. Copolymerization of these macromonomers with S gave the miktoarm star-tailed graft copolymers (Scheme 37). Finally, living PS⁻Li⁺ chains were employed as macroinitiators for the polymerization of the double miktoarm star-tailed macromonomers, leading to the synthesis of structures having a PS block and a PBd-PS polymacromonomer block (Scheme 38). Well-defined architectures of controlled molecular characteristics were obtained through this approach [32].

6 Dendritic-Like Complex Macromolecular Architectures

Macromonomers have also been used as intermediate structures for the synthesis of highly branched or dentritic macromolecules by means of the convergent approach. When a bifunctional compound carrying a polymerizable vinyl group and a group capable of linking a living polymer chain is slowly added into a living polymer solution, consecutive macromonomer formation and macromonomer addition reactions can take place. Bifunctional compounds that have been used are CDMSS and
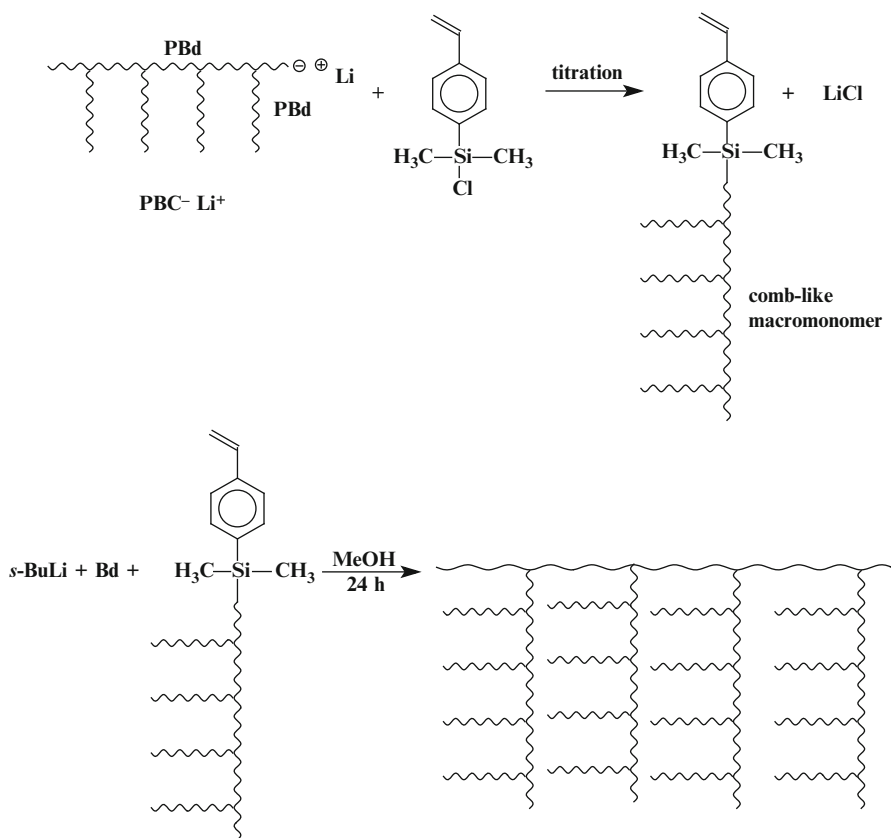
Scheme 28 Synthesis of comb-on-comb PBds
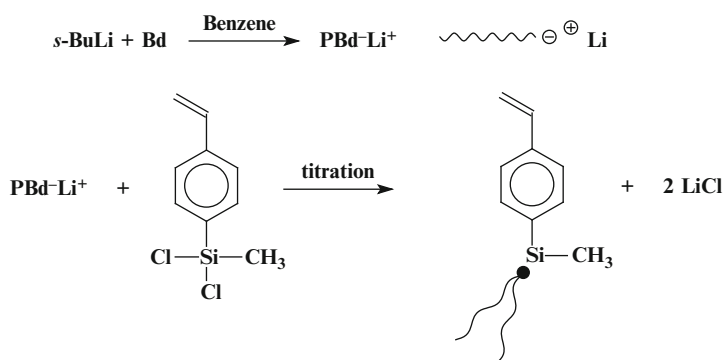
Scheme 29 Synthesis of double-tailed styrenic-tipped macromonomers of PBd

Scheme 30 Schematic representation of PBd double-combs, 3-arm-double-comb star and double molecular brushes

Double-Combs (dcPBd)

3-Arm-Double-Comb Star (3-Arm Star dc PBd)

Double Molecular Brushes (dmbPBd)

tmbPBd
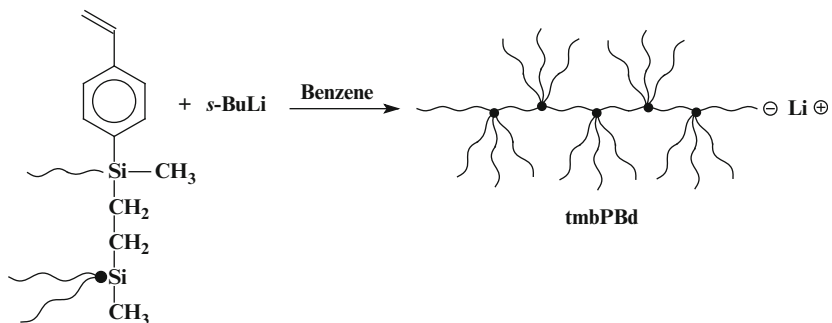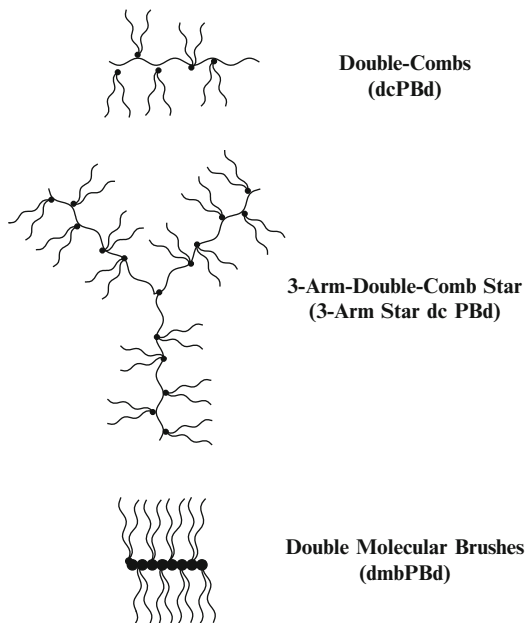
Scheme 31 Synthesis of triple molecular brushes of PBd

vinylbenzyl chloride (VBC) [33]. Depending on the degree of branching and the molecular weight of the living polymers, the final product may be a dendrigraft structure. Possible reactions, involving the reaction of polystyryllithium with VBC, are given in Scheme 39.

The characteristic of this procedure is that the complex architectures are formed in a one-pot reaction. However, there is no absolute control during the progress of the synthesis and the products are rather polydisperse with high molecular weight heterogeneity. Especially in the case of VBC, several side reactions may take place imposing extra difficulties in obtaining well-defined polymers. Monomeric or dimeric terminations of the living PS^-Li^+ chains, α-proton abstraction from VBC
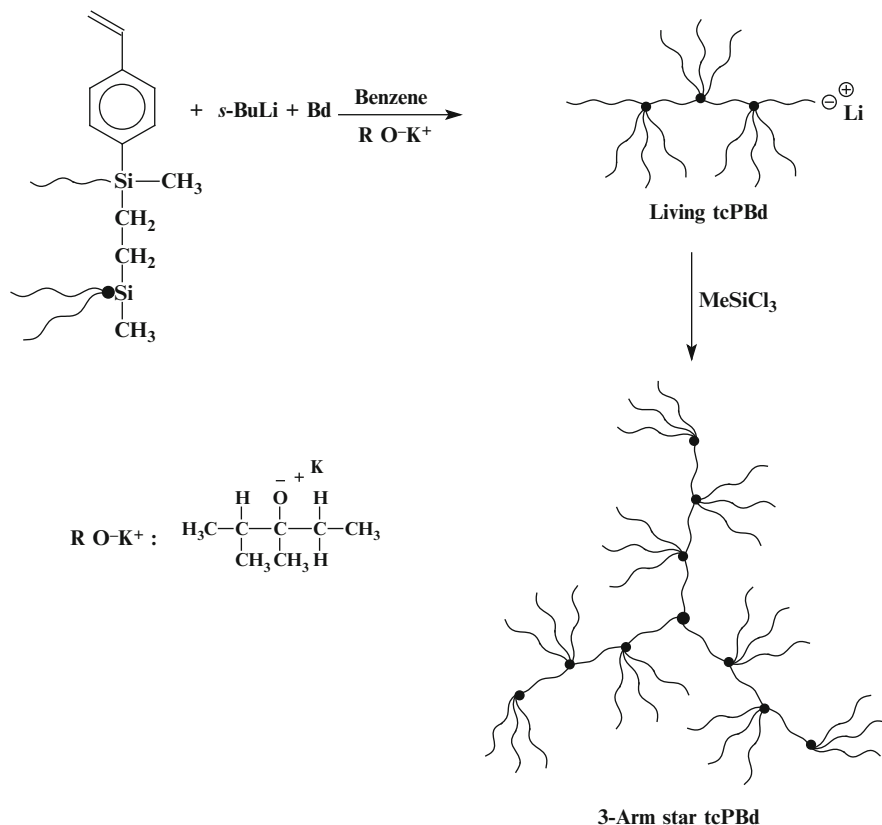
Scheme 32 Synthesis of three-arm triple comb PBd stars

and lithium-halogen exchange are possible side reactions. By choosing the suitable reaction conditions (solvent, temperature, reaction time, etc.) these side reactions can be minimized but not eliminated. The dendritic structures prepared were characterized from the existence of a functional styryl group at the focal point or the core, respectively. It was therefore possible to copolymerize these complex macromonomers with styrene or MMA for the synthesis of graft copolymers imposing star polymers or dendrimers as side chains [34]. The products, shown in Scheme 40, had very broad molecular weight distributions and were characterized by increased compositional and molecular heterogeneity.

The DPE methodology and anionic polymerization techniques were adopted for the synthesis of linear-star-linear polystyrenes of the types PS-(PS)$_n$-PS ($n = 2,4,8,16$) and PS-(PS)$_n$-PS-(PS)$_n$-PS ($n = 2,4,8$) [17]. The synthesis involved the preparation of the corresponding in-chain functionalized polymers with a definite number of BnBr groups, as shown in Schemes 41 and 42.

Living PS$^-$Li$^+$ macroanion was reacted with a PS chain end-functionalized with a DPE unit resulting in the synthesis of a linear PS macromolecule with an in-chain
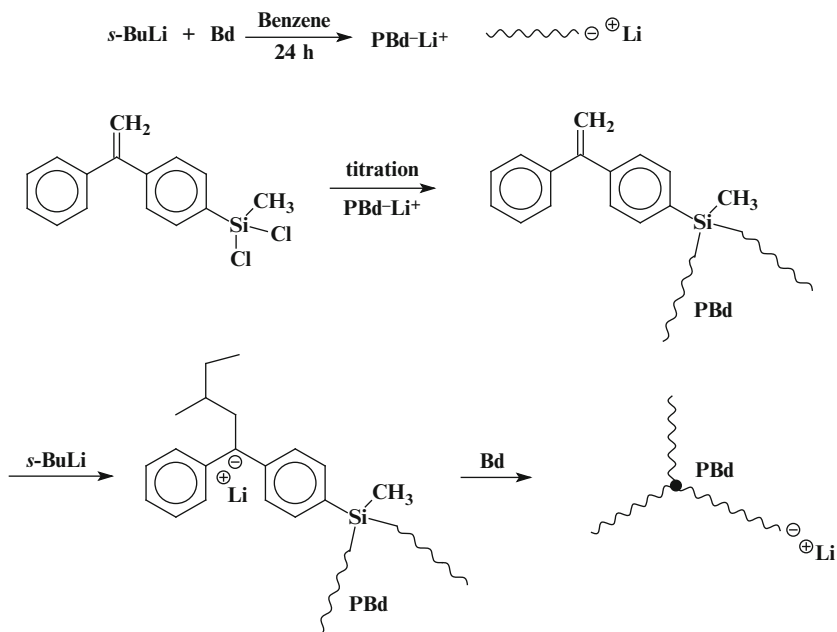
Scheme 33 DCMSDPE in the formation of living three-arm star PBd polymer
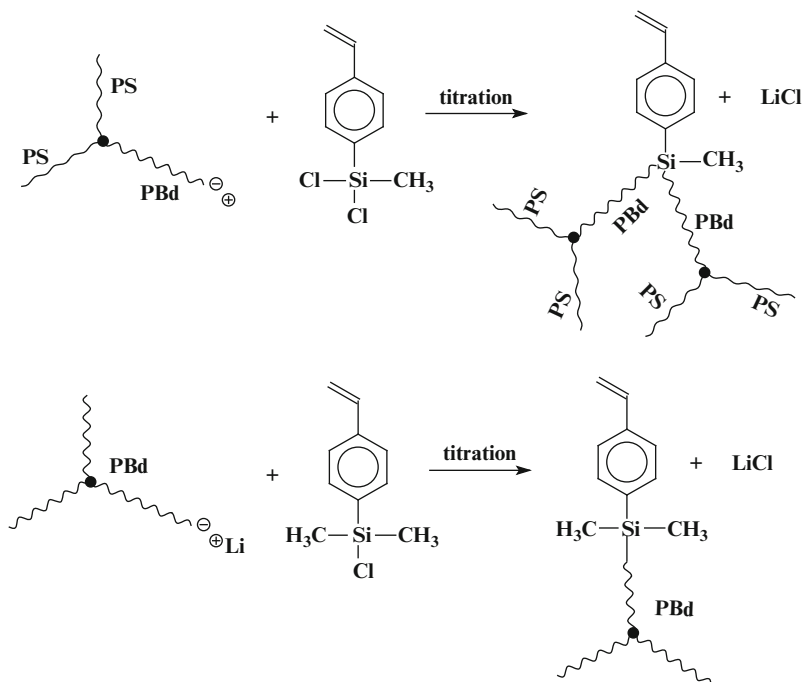
Scheme 34 Synthesis of double and single star-tailed macromonomers
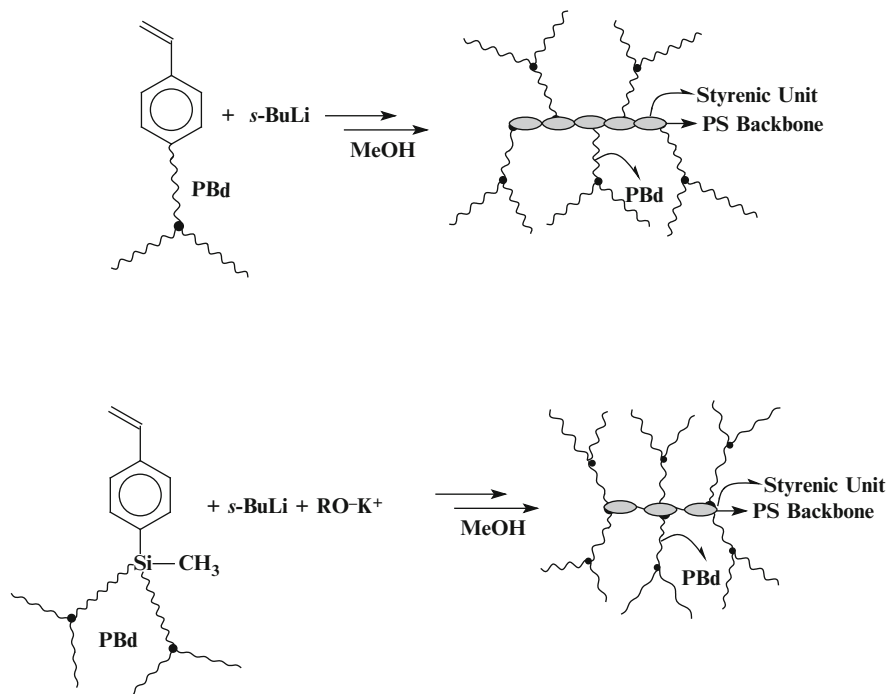
Scheme 35 Synthesis of single and double homostar-tailed brushes

anionic center, which was deactivated in situ with 1-(4-bromobutyl)-4-(*tert*-butyldimethylsilyloxymethyl)benzene. The silyl ether groups were further transformed to BnBr moieties by treatment with LiBr/(CH₃)₃SiCl. Using the PS-(BnBr)-PS intermediate, the coupling and transformation reactions in the iterative reaction sequence were repeated four more times to synthesize the PS-(BnBr)$_n$-PS ($n = 2,4,8,16$) in-chain functionalized polymers. Subsequent coupling with living PS chains end-capped with a DPE unit produced the desired PS-(PS)$_n$-PS ($n = 2,4,8,16$) structures.

A similar method was adopted for the synthesis of the PS-(PS)$_n$-PS-(PS)$_n$-PS ($n = 2,4,8$) polymers. Living PS$^-$Li$^+$ was reacted with an α,ω-chain end-functionalized PS with DPE moieties followed by reaction with 1-(4-bromobutyl)-4-(*tert*-butyldimethylsilyloxymethyl)benzene to deactivate the generated two anionic sites. The same procedure, as previously reported, was employed for the introduction of BnBr functions and by employing the iterative reaction sequence, the synthesis of the PS-(BnBr)$_n$-PS-(BnBr)$_n$-PS ($n = 2,4,8$) functionalized polymers was achieved. Coupling with PS$^-$Li$^+$ end-capped with DPE afforded the PS-(PS)$_n$-PS-(PS)$_n$-PS ($n = 2,4,8$) structures.

Four-arm star-block copolymers, where each arm had a dendritic structure, were prepared by sequential anionic ring opening polymerization of ethylene oxide and
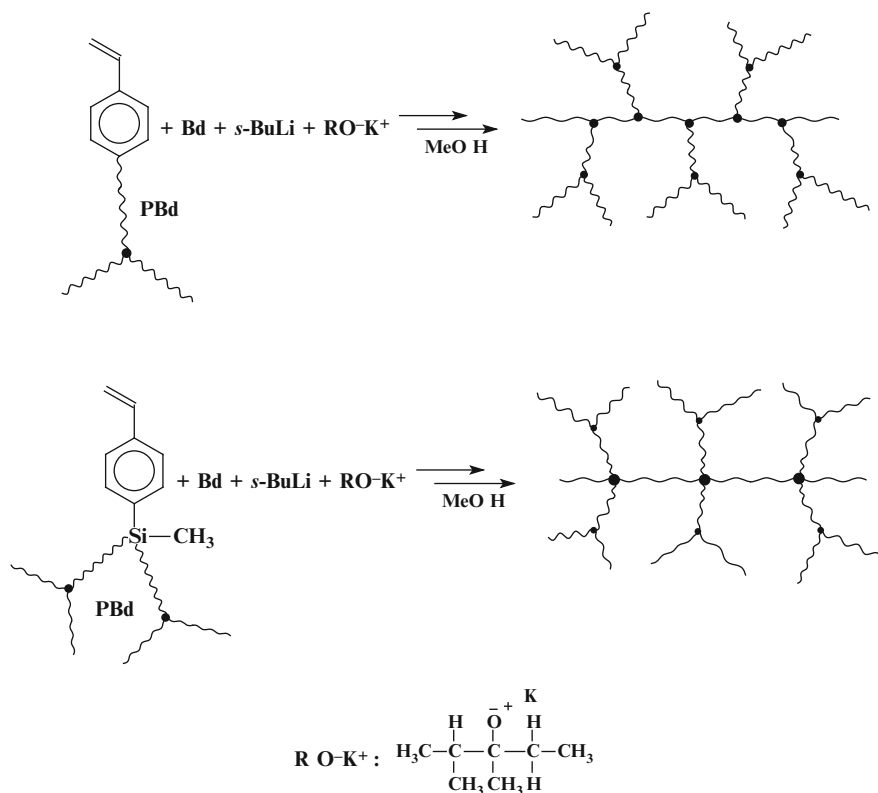
Scheme 36 Synthesis of single and double homostar-tailed combs
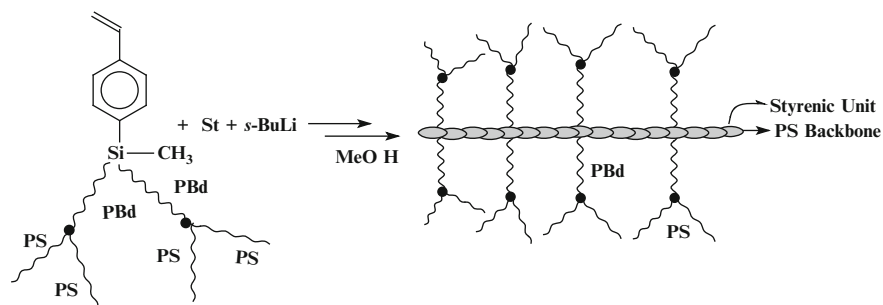
Scheme 37 Synthesis of miktoarm star-tailed graft copolymers

glycidol. Pentaerythritol was employed as multifunctional initiator after conversion of the hydroxyl groups to alcoholates using potassium *tert*-butoxide. Only 20 % of the hydroxyl groups were ionized to avoid the precipitation of the alcoholates. The produced *tert*-butyl alcohol was removed by distillation followed by the polymerization of ethylene oxide at 45 °C for 24 h leading to the formation of the four-arm
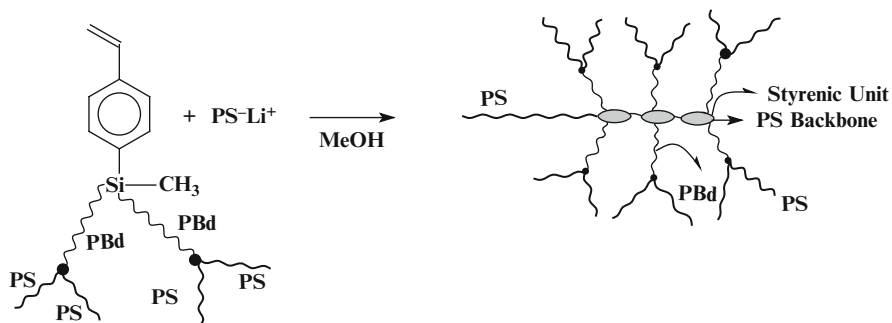
Scheme 38 Synthesis of miktoarm star-tailed graft copolymers bearing a PS block
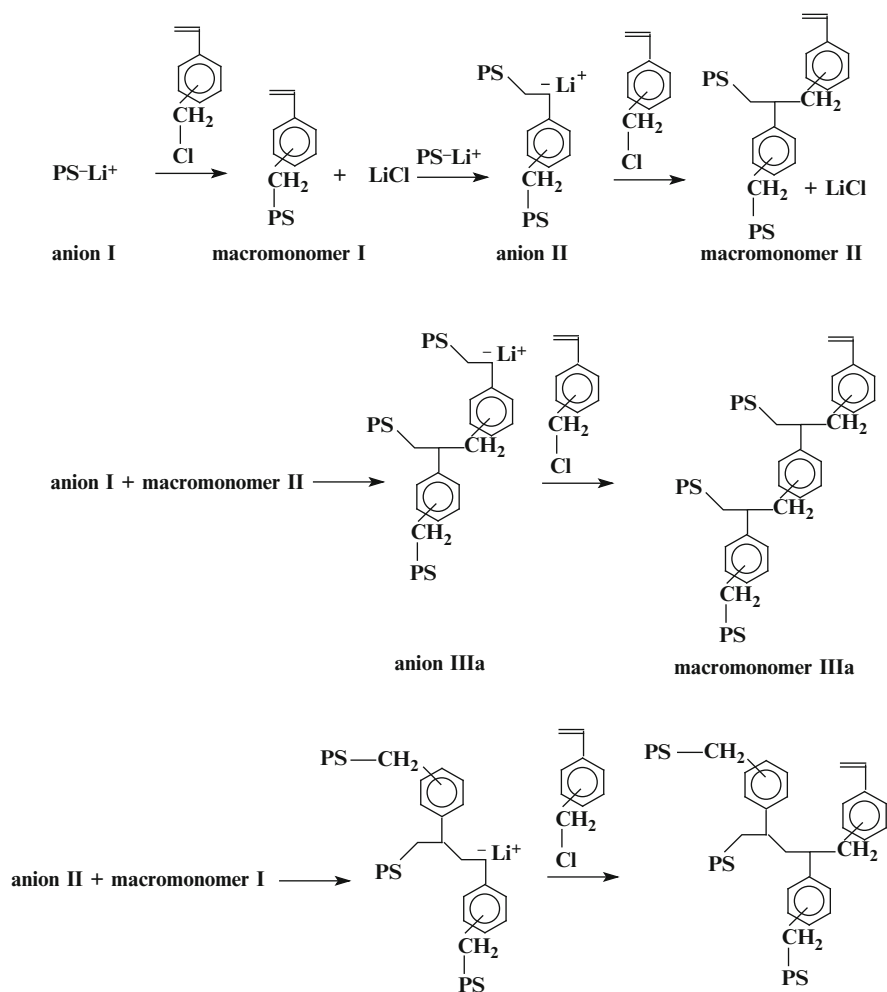
Scheme 39 Possible reactions involving PS⁻Li⁺ and VBC

Scheme 40 Graft copolymers with star polymers or dendrimers as side chains

a: *s*-BuLi + ⟍ ⟶ *s*-Bu⟍⊖ Li⊕   b: LiBr/(CH₃)₃SiCl

○ = benzyl-OSiMe₂Buᵗ   ▮ = benzyl-Br
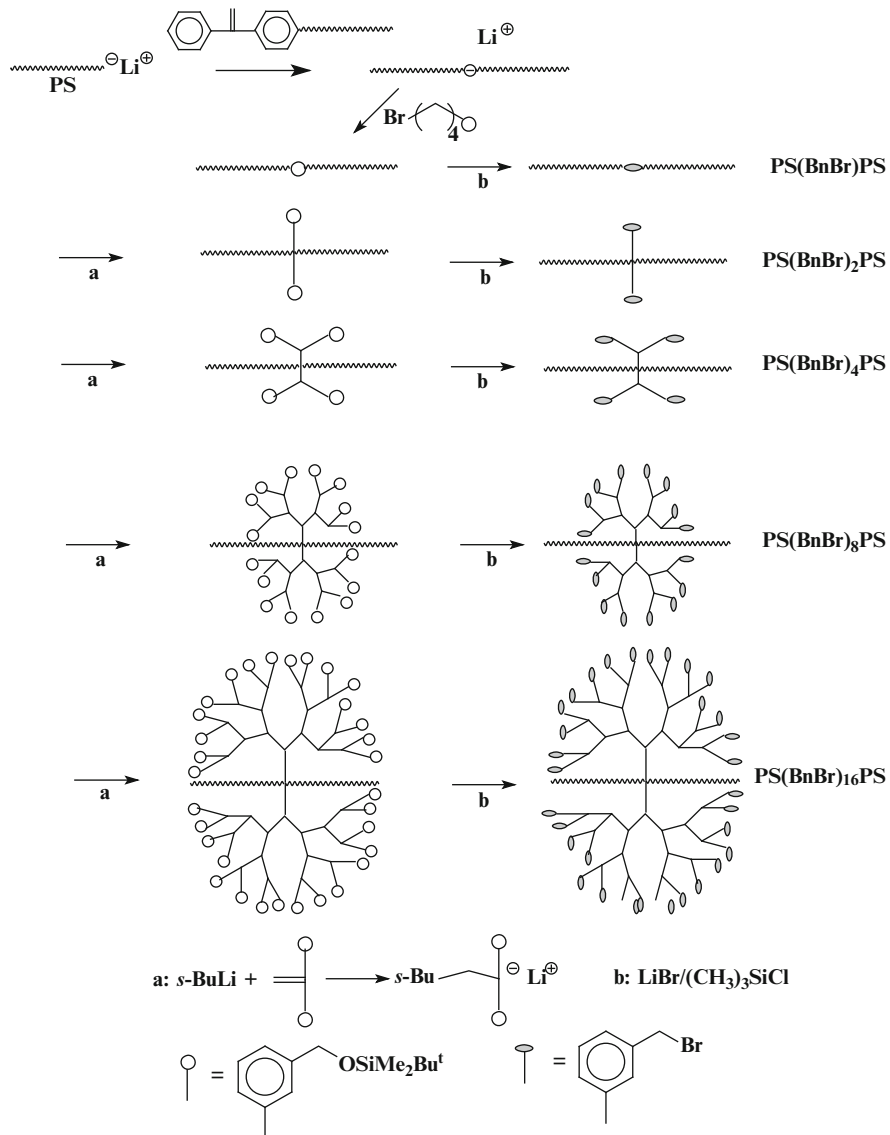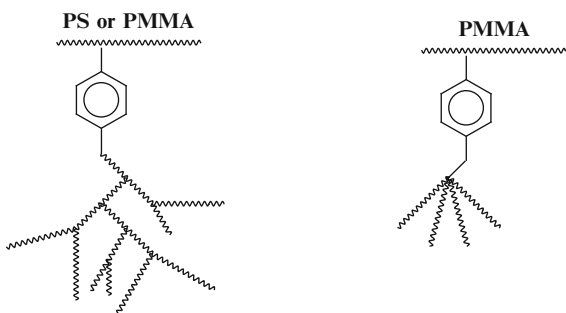
Scheme 41 Synthesis of PS(BnBr)ₓPS structures (x = 1, 2, 4, 8, 16)
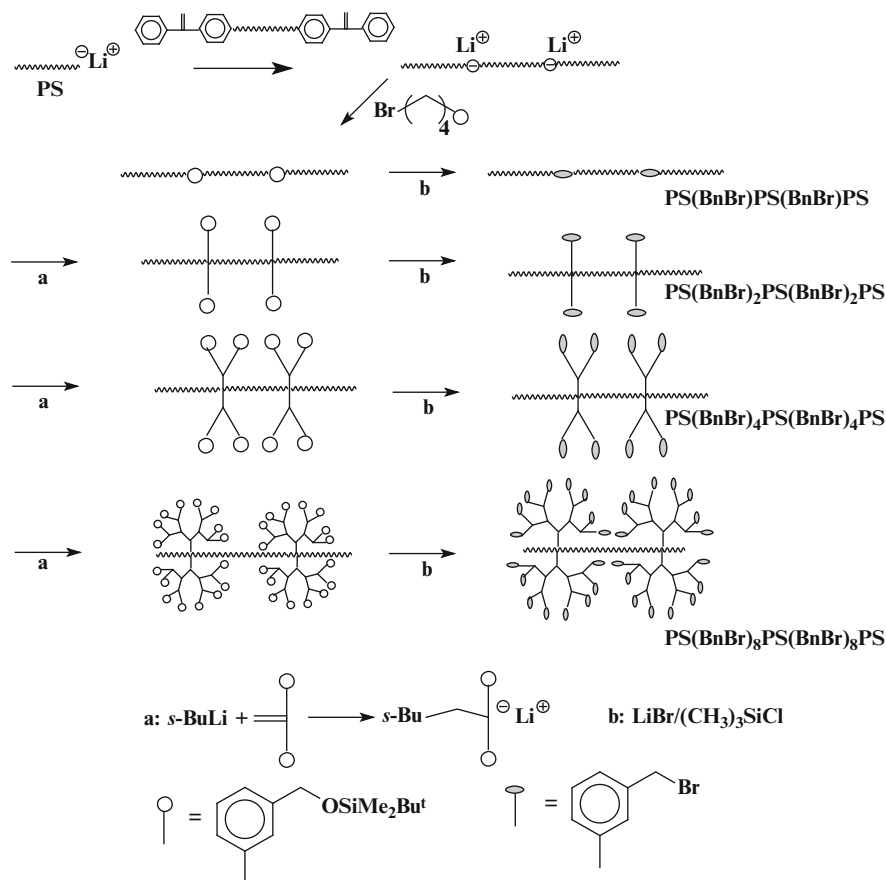
Scheme 42 Synthesis of PS(BnBr)$_x$PS(BnBr)xPS structures (x = 1, 2, 4, 8)

PEO stars. Protected glycidol was subsequently added and polymerization was allowed at 45 °C for 24 h. The four-arm star-block copolymer was treated with oxalic acid to recover the hydroxyl groups of the polyglycidol blocks. Careful characterization revealed that 22–28 hydroxyl groups per molecule were available in the products. These hydroxyl groups served as multifunctional macroinitiators for the polymerization of ethylene oxide and glycidol leading to the synthesis of dendritic, highly functional copolymers (Scheme 43) [35].

A series of well-defined star-branched polystyrenes of different architectures were synthesized by anionic polymerization. Three-arm PS stars end-branched with 6, 9 and 13 PS branches were obtained using a trifunctional initiator. This initiator was prepared by the gradual addition of *sec*-BuLi to 1,3,5-tris(1-phenylethenyl) benzene in a molar ratio 3:1 in benzene solution and was further employed for the polymerization of styrene at 0 °C in the presence of a small amount of THF, to eliminate chain association effects and increase the initiation rate. The produced

Scheme 43 Synthesis of dendritic, highly functional PEO copolymers

$$\text{1) } \textit{t-} \textbf{BuOK / DMSO}$$
$$\textbf{-t-BuOH}$$

2) (epoxide)

3) (glycidyl ethoxyethyl ether structure)

4) **deprotection**

$$\text{HO}\!\left(\text{CH}-\text{CH}_2-\text{O}\right)_{\!n}\!\text{CH}_2-\text{CH}_2-\text{O}-\!\!\!\longleftarrow$$
$$\qquad\quad\;\text{CH}_2$$
$$\qquad\quad\;\text{OH}$$
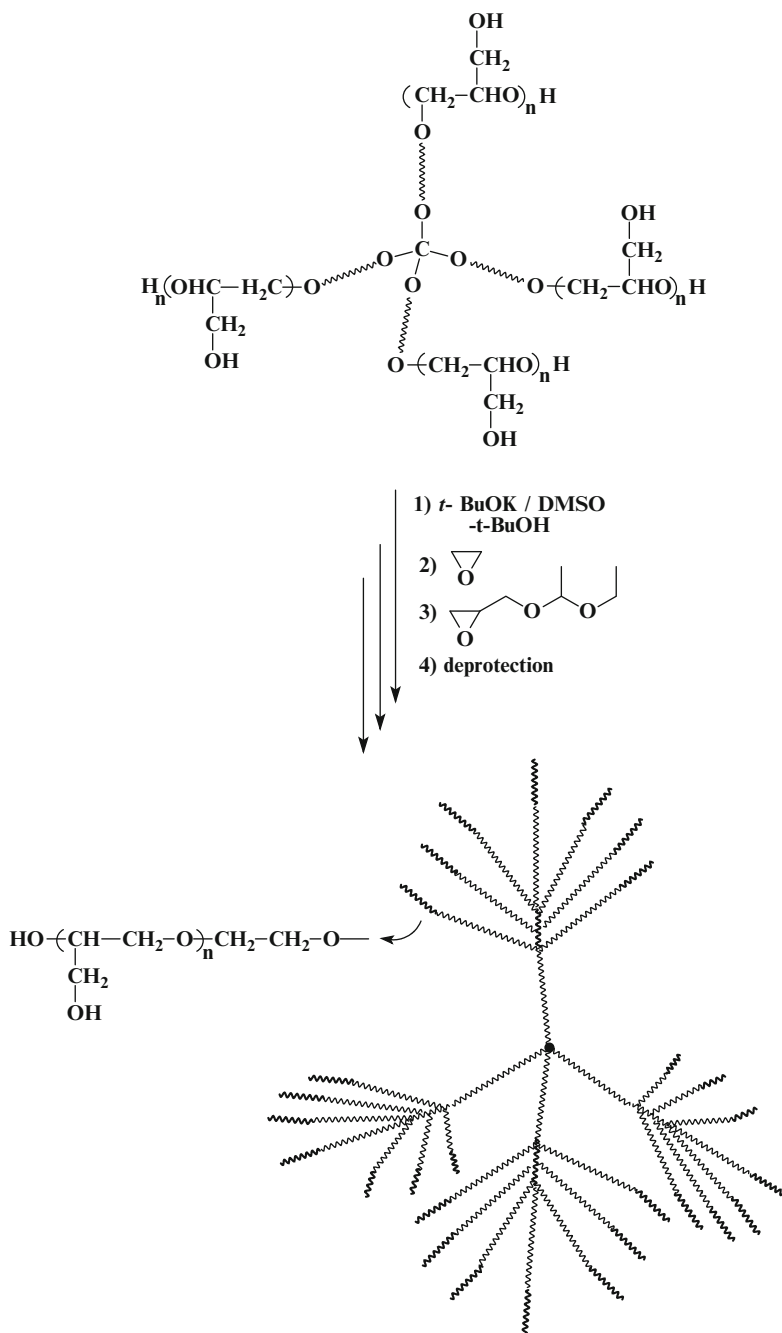
Scheme 43 (continued)

living three-arm PS star was subsequently reacted with an excess of different chlorosilane linking agents: CH_3SiCl_3, $SiCl_4$ and $Cl_3SiCH_2CH_2SiCl_3$, in order to provide three-arm PS stars bearing 6, 9 and 15 Si–Cl groups at the end of each arm. The excess of CH_3SiCl_3 and $SiCl_4$ was removed by evaporation on the vacuum line. However, $Cl_3SiCH_2CH_2SiCl_3$ is not volatile and therefore the excess of this silane cannot be removed effectively by distillation. In this case, the excess silane was removed by a different methodology. The chlorosilyl-functionalized three-arm star along with the excess silane was treated with anhydrous methanol. The reaction took place in the presence of triethylamine to scavenge the produced hydrochloric acid. In another reactor, linear low molecular weight living PS^-Li^+ chains were synthesized and end-capped with a few units of Bd to reduce the steric hindrance of the chain ends. These living polymers were finally linked to the end-functionalized three-arm PS stars leading to the desired structures (Scheme 44). The linking reactions were conducted for 1 week at 40 °C in the presence of triethylamine. The methoxysilyl end-functionalized star was allowed to react for 3 weeks, since the methoxy groups are not as reactive as the chlorosilyl groups. Characterization results revealed that in this case the steric hindrance limited the arm functionality to 13, instead of the targeted 15, during the synthesis [36].
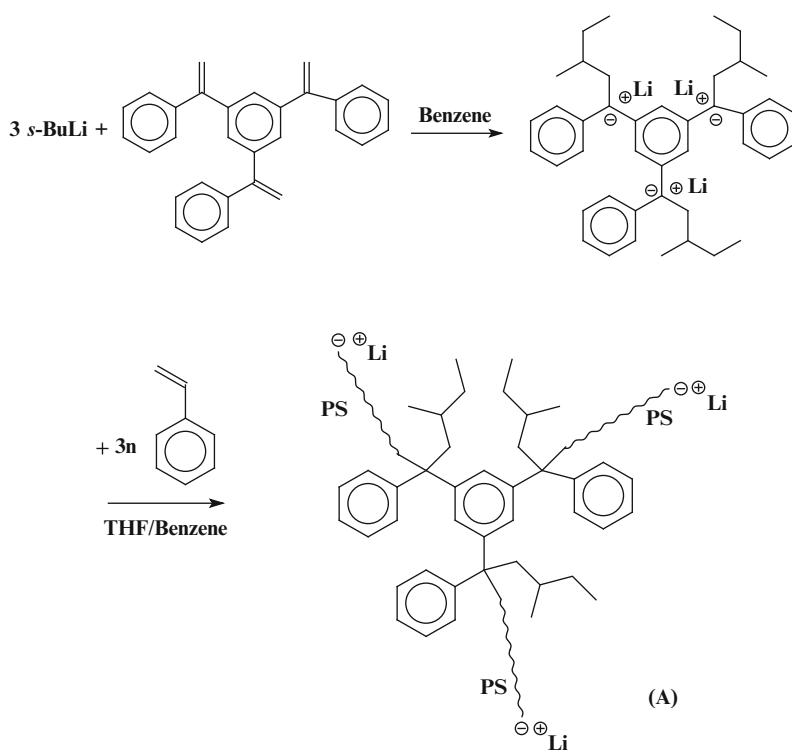
Scheme 44 Synthesis of PS dendritic-like structures through the use of a trifunctional organolithium initiator
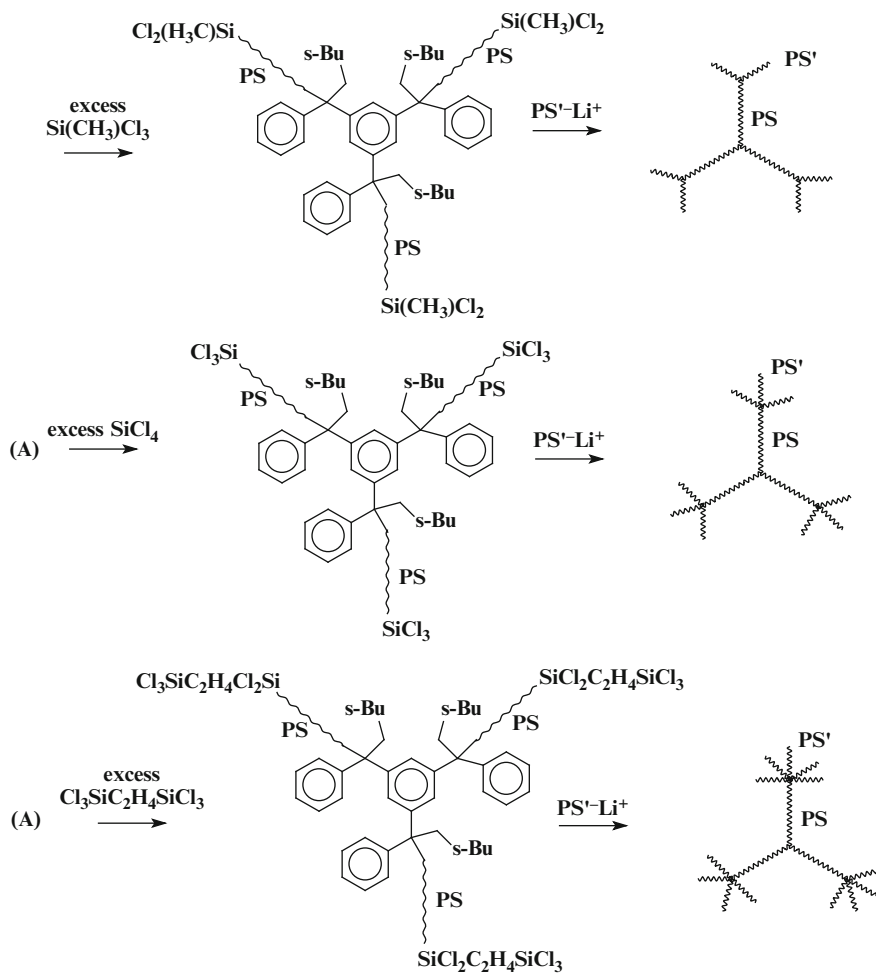
Scheme 44 (continued)

Umbrella star copolymers of PS and PBd or P2VP were prepared as well. The structure of these copolymers can be described as a multiarm star in which each arm, instead of a free end, is linked to another star molecule. The core of the umbrella polymers was PS chains while the shell was either PBd or P2VP. The synthesis of these copolymers involved the preparation of 1,2-PBd-*b*-PS polymeric chains in which the 1,2-PBd block is short, followed by coupling with an appropriate chlorosilane linking agent, depending on the desired number of arms. After isolation of the star by fractional precipitation, the double bonds of the 1,2-PBd were hydrosilylated in order to incorporate $-Si(CH_3)Cl_2$ or $-Si(CH_3)Cl$, and finally reacted with living PBd or P2VP chains (Scheme 45).
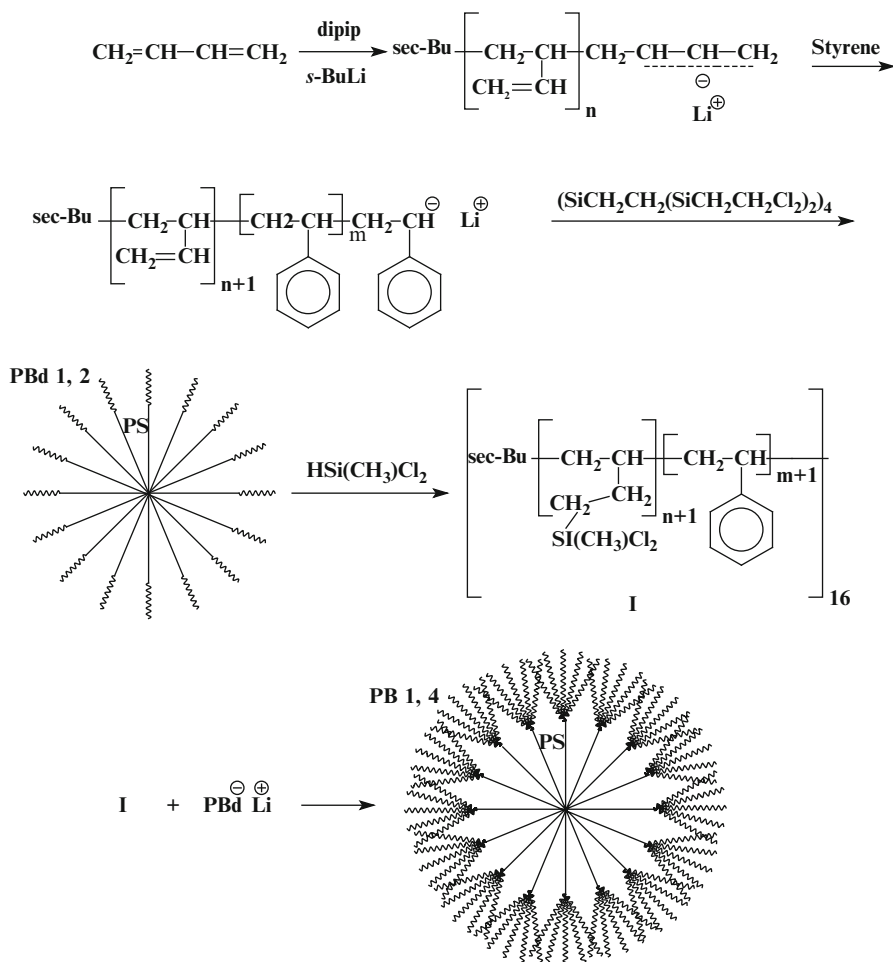
Scheme 45 Synthesis of umbrella star copolymers

Using a monoadduct (inimer), as core material, the synthesis of dendritic and dendrimer-like star polymers has been achieved [37, 38]. This monoadduct was a monoactivated 1,3- *bis* (1-phenyl vinyl) benzene (MDDPE) compound; monoactivation is possible, in nearly quantitative yields, in THF solvent through the stoichiometric addition of *sec*-BuLi to MDDPE at low temperature. The success of the reaction was based on the polarity of the solvent, since THF creates an environment in which the ion pairs of the MDDPE anion and the approaching *sec*-BuLi pose a repulsion strong enough so as to prevent the addition of a second one. The inimer was consequently polymerized with styrene; as the PS^-Li^+ chain grew, SCVP was possible (Scheme 46). The product of this step exhibited a broad, however, monomondal distribution and was proved to be linear. Better results
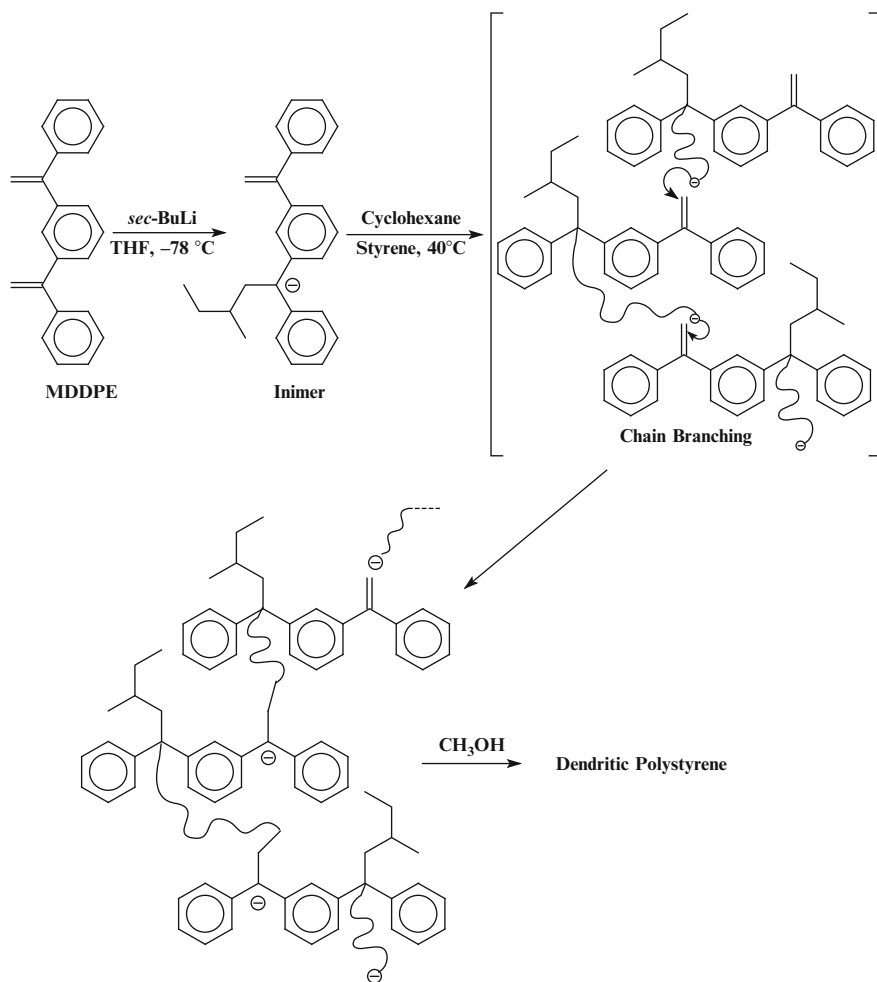
Scheme 46 Synthesis of dendritic-like PS via the employment of an anionic inimer

were obtained when SCVP was conducted in cyclohexane. For solvent alteration, from THF to cyclohexane, THF was removed by distillation at low temperature (<5 °C), in order to avoid the decomposition of the anionic species [39].

In another report [40], dendritic block and dendritic brush copolymers were prepared through equimolar selective monoaddition of polyisoprenyllithium (PI⁻Li⁺) to MDDPE (Scheme 47). The addition was performed in a THF/cyclohexane solvent mixture (3/1 v/v) at −80 °C for 5 h. This solvent mixture provides an environment in which carbanions are generally more [41].

After preparation, the monoadduct was copolymerized with styrene and underwent SCVCP [42] resulting in the synthesis of dendritic block copolymers
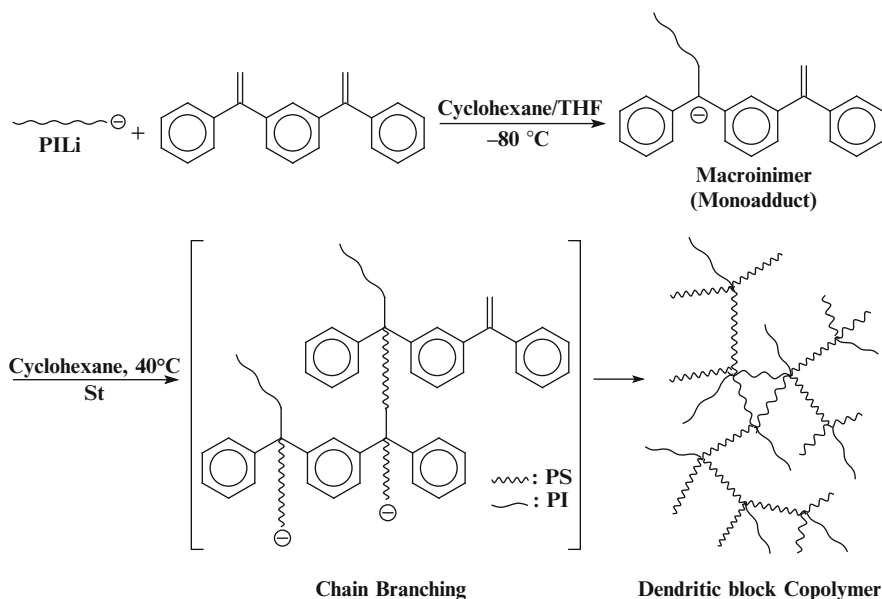
Scheme 47 Synthesis of dendritic-like block copolymer via the employment of an inimer undergoing SCVCP

of styrene and isoprene. Before copolymerization, the solvent mixture was altered (from THF/cyclohexane) to cyclohexane. The resulting polymer presented a multimodal distribution, due to intermolar coupling reactions. It was also shown [40] that higher ratios of monomer to living monoadduct (macroinimer) led to much larger molecular weights due to the more effective branching that occurs, as a result of less steric hindrance present (larger spacer between branches).

The previous dendritic block copolymer was also employed in the synthesis of dendritic polymer brushes (Scheme 48). This was realized through the epoxidation of the PI chains and the sequential ring opening addition of living polymer chains (PI$^-$Li$^+$ or PS$^-$Li$^+$). The PI segments, located at each branch, acted as backbones of the later-developed polymer brushes. The epoxidized PI chains were subjected to nucleophilic attack by an excess of living PS$^-$Li$^+$ or PI$^-$ Li$^+$, in the presence of LiCl. The branching efficiency was calculated to be ~45 %, which was attributed to the incomplete epoxidation of the PI chain [43] and to steric hindrance.

In a similar way, ABC-type dendritic terpolymers were also synthesized [44], containing PI, PS and poly(*tert*-butylmethacrylate) (P*t*BMA) segments (Scheme 49). The macroinimer, being a MDDPE PI monoadduct, has been copolymerized with styrene in cyclohexane, allowing it to undergo SCVCP, thus forming a dendritic copolymer. Since this technique follows the core-first method, the dendritic copolymer was living, and therefore could act as a precursor reinitiating a new monomer, thus forming a dendritic terpolymer a dendritic terpolymer. To avoid side reactions during the addition of tBuMA, the living
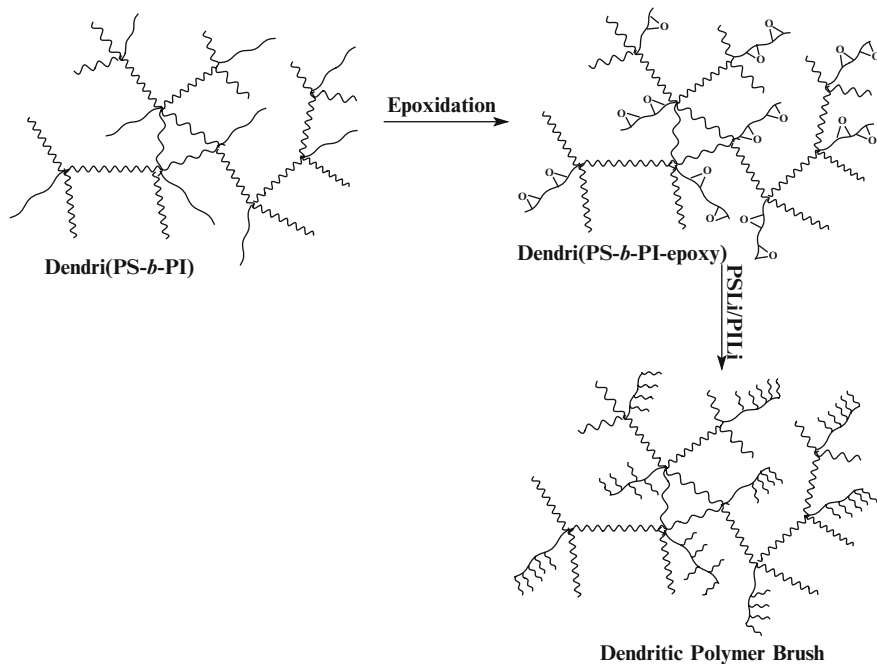
Scheme 48 Synthesis of dendritic polymer brushes from dendritic block copolymers

PS^-Li^+ chains were first end-capped with DPE, and for better polymerization results, tBMA was polymerized in the presence of LiCl salt.

More controlled dendrimer-like star polymers structures have also been synthesized, however, using a different approach. The reaction philosophy of the approach was based on the combined use of an inimer and α,ω-bifunctional polystyryllithium. The product of the reaction formed the dendrimer-like star core. In particular, MDDPE was activated with sec-BuLi, creating both a monoadduct (inimer) and a diadduct (bifunctional initiator). The selective synthesis of either was ensured by controlling the stoichiometry of the addition reaction [38]. Afterward the inimer (MDDPE monoadduct) was introduced to the diadduct, yielding a $\alpha,\alpha',\omega,\omega'$-tetrafunctional polystyryllithiium. Further polymerization with styrene resulted in an H-shaped star polymer (Scheme 50). The sequential and repeated addition of stoichiometric amounts of inimer and monomer lead to the growth of further generations on the dendrimer-like structure, up to five generations.

Due to the aggregation of the polymeric anions, the formation of a pseudogel was observed. This resulted in an increase of the system's heterogeneity, thus hindering or even halting further reaction. A dependence of the gel formation on the arm length (M_n) and the structure of the periphery anions was observed. Longer arm lengths lead to earlier gelation. Also, pseudogel formed with peripheral polystyryl anions presented a decrease in viscosity upon addition of the inimer. This was attributed to the different aggregation numbers of the terminal groups.
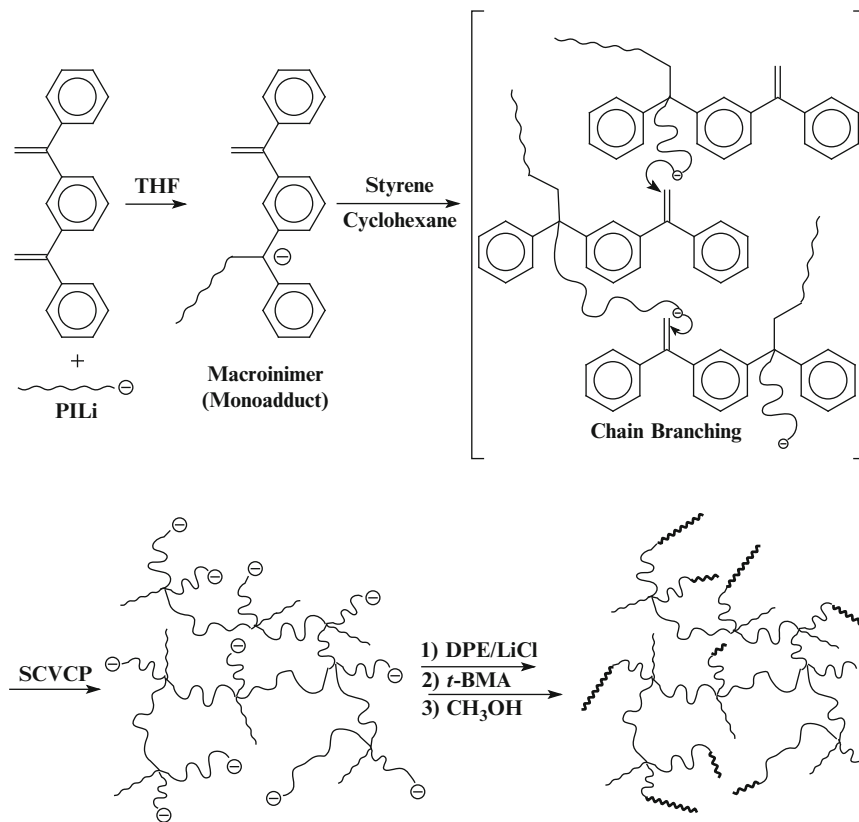
Scheme 49 Synthesis of dendritic block terpolymer through SCVCP

Polystyryl anions aggregate into dimers [45], whereas MDDPE derived dianions exhibit an aggregation number less than two. Pseudogelation was prevented upon the addition of a polar additive such as THF or TMEDA. The ability of the additives to dissociate has been shown to increase with the following line of order TMEDA > THF > ethyl ethere. In the presence of ethyl ether gelation was formed in the second generation, THF was able to break aggregation up to the fourth generation, and TMEDA proved to be the most effective, keeping the solution homogeneous throughout the whole reaction (five generations). However, THF was preferred for the synthesis of lower generations and TMEDA for higher generations, since the latter when used as an additive tends to give broader molecular weight distributions. In general, the increase of generations was followed by an increase in PDIs of the resulting polymers, possibly due to the increase of heterogeneity in the system.

A great advantage of these dendrimer-like stars is the living end; a living dendritic polystyrene, end-capped with the inimer (to avoid cross-linking), can either be further functionalized with an electrophilic linking agent or
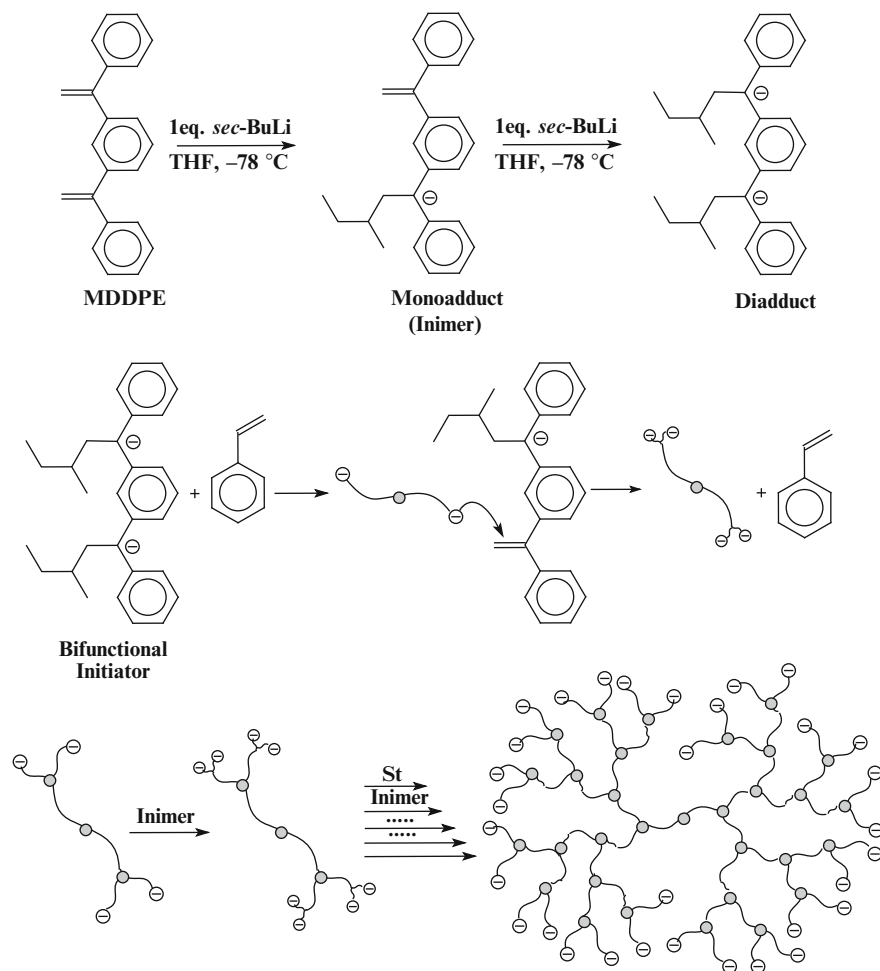
Scheme 50 Synthesis of dendritic-like living PS star through a divergent process

copolymerized with other monomer compounds like isoprene or methyl methacrylate (Scheme 52). The multiple hydroxyl end-functionalization of these species was achieved [46] through allyl bromide termination followed by a thiol-ene reaction with 1-thioglycerol (Scheme 51).

Copolymerization of dendritic polystyrenes (end-capped with the inimer) with isoprene has been realized in cyclohexane, in the presence of THF and TMEDA polar additives. Applying the same formula copolymerization with MMA was performed in a mixture of THF/cyclohexane (3/1) at low temperature (Scheme 52). The PI copolymerized PS dendrimer stars were further modified, through epoxidation treated with H_2O_2/formic acid in toluene, to create grafted-dendrimer stars. By grafting the epoxidized PI segments with a PI-*b*-PS$^-$Li$^+$ living diblock copolymers, graft-on-graft dendrimer-like star polymers were prepared, by further epoxidation
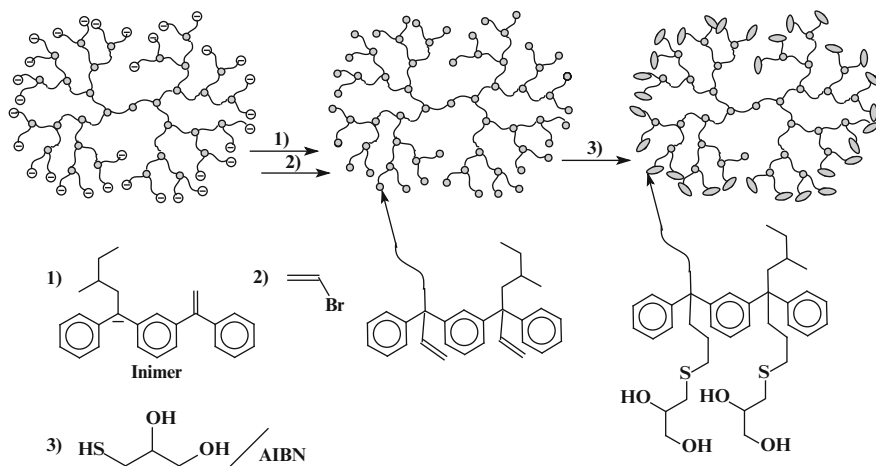
Scheme 51 Functionalization of living PS dendritic-like star with allyl and hydroxyl peripheral groups
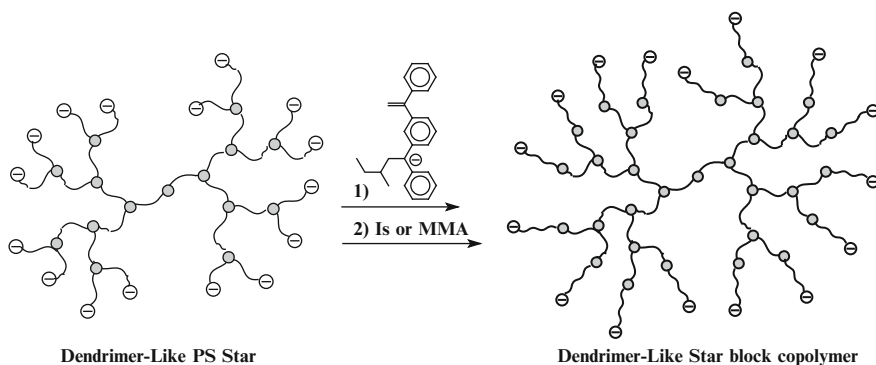
Scheme 52 Synthesis of dendritic-like star-block copolymers

of the newly added PI chains followed by grafting with living polystyrene (Scheme 53).

Following a similar synthetic pattern, a different approach for the synthesis of dendrimer-like polymers was accomplished [47], by grafting reactions of living PI-b-PS$^-$Li$^+$ copolymers on multiple oxirane groups. Through this method two types of dendrimer-like polymers were synthesized using two different types of cores. The first being a star-like core, resulting from the epoxidation of a linear PI cain and the consequential grafting of a diblock PI-b-PS$^-$Li$^+$ copolymer, forming a total grafting of eight or nine arms. The second core derived from a linear ABA triblock copolymer, consisting of PI-b-PS-b-PI, like the previous type, was created through epoxidation of the PI side chains and the consequential grafting of a diblock PI-b-PS$^-$Li$^+$ copolymer. All the diblocks and triblocks used in this procedure contained

Dendrimer-Like Star PS-*b*-PI block copolymer

Dendrimer-Like Star graft copolymer

1) H$_2$O$_2$/HCOOH
2) PI-*b*-PS$^-$ $^+$Li ⌇
3) PS$^-$ $^+$Li ⌒

Dendrimer-Like Star graft-on-garft copolymer
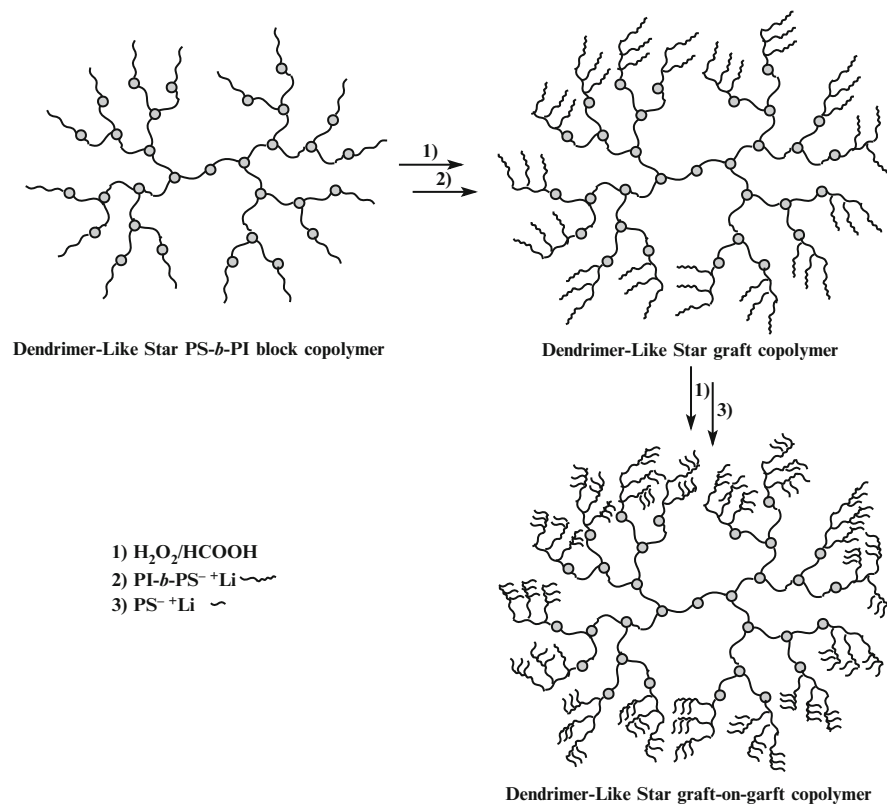
Scheme 53 Synthesis of dendritic-like star polymer with a graft-on-graft periphery

no more than 8 mer units on each PI block. However, the PS chain was different; the core ABA center consisted of a much larger PS chain than the one used for grafting additions. All epoxidations of the double bonds were conducted using HCOOH/ H$_2$O$_2$. This reaction was only efficient for double bonds in the 1,4 structure. The epoxidation reaction and the sequential ring opening addition of the living PI-*b*-PS$^-$Li$^+$ copolymer was repeated, resulting each time to the growth of a new generation. However, the grafting reaction was only highly efficient at lower generations, and grafting reactions were found to be inefficient at higher generations due to steric hindrance.

Abbreviations

BnBr	Bromomethylphenyl
BS	*p-tert*-Butoxystyrene
CDMSS	4-(Chlorodimethylsilyl)styrene

DCMSDPE	4-(Dichloromethylsilyl)diphenylethylene
DCMSS	4-(Dichloromethylsilyl)styrene
DMPOK	Potassium salt of 2,3-dimethyl-3-pentanol
DPE	Diphenylethylene
EO	Ethylene oxide
GMA	Glycidyl methacrylate
MDDPE	1,3-Bis(1-phenylethenyl)benzene
MMA	Methyl methacrylate
n-BuLi	*n*-Butyllithium
P2VP	Poly(2-vinyl pyridine)
PBd	Polybutadiene
PBS	Poly(*p-tert*-butoxy)styrene
Pd	Palladium
PEO	poly(ethylene oxide)
PGMA	Poly(glycidyl methacrylate)
PHS	Poly(*p*-hydroxystyrene)
PI	polyisoprene
PMMA	Poly(methyl methacrylate)
PS	Polystyrene
P*t*BMA	Poly(*tert*-butyl methacrylate)
SCVCP	Self-condensing vinyl copolymerization
SCVP	Self-condensing vinyl polymerization
SEC	Size exclusion chromatography
sec-BuLi	*sec*-Butyllithium
*t*BMA	*tert*-Butyl methacrylate
t-BuP$_4$	Phosphazene base
TCDSS	2-(Dichloromethylsilyl)ethylchloromethylsilyl-4-styrene
THF	Tetrahydrofurane
TMEDA	Tetramethylethylenediamine
VBC	Vinylbenzyl chloride
VS	4-(Vinyldimethylsilyl)styrene

References

1. (a) Szwarc M (1998) Living polymers. Their discovery, characterization, and properties. J Polym Sci Part A Polym Chem 36:ix–xv; (b) Szwarc M (1970) Living polymers: a tool in studies of ions and ion-pairs. Science 170:23–31; (c) Lee L, Adams R, Jagur-Grodzinski J, Szwarc M (1971) Thermodynamic and electron spin resonance studies of ion pairs in mixed solvents. J Am Chem Soc 93:4149–4154; (d) Szwarc M (1973) Block and graft polymers their synthesis, especially by living polymer technique, and their properties. Polym Eng Sci 13:1–9; (e) Szwarc M (1972) Radical anions and carbanions as donors in electron-transfer processes. Acc Chem Res 5:169–176
2. (a) Wang F, Roovers J, Toporowski PM (1995) Synthesis and characterization of "umbrella" shaped polymers. Macromol Symp 95:255–263; (b) Wang F, Roovers J, Toporowski PM

(1995) Umbrella-star block copolymers. J Macromol Sci Part A Pure Appl Chem A32(Suppls 5 and 6):951–958

3. Ederlé Y, Mathis C (1999) Palm tree- and dumbbell-like polymer architectures based on C60. Macromolecules 32:554–558

4. (a) Al-Muallem HA, Knauss DM (2001) Synthesis of hybrid dendritic-linear block copolymers with dendritic initiators prepared by convergent living anionic polymerization. J Polym Sci Part A Polym Chem 39:152–161; (b) Knauss DM, Huang T (2002) Star-block-linear-block-star triblock (pom-pom) polystyrene by convergent living anionic polymerization. Macromolecules 35:2055–2062

5. (a) Al-Muallem HA, Knauss DM (1997) Development of a living polymerization approach towards dendritic polymers. Polym Prep Am Chem Soc Div Polym Chem 38(1):68–69; (b) Knauss DM, Al-Muallem HA, Huang T, Wu DT (2000) Polystyrene with dendritic branching by convergent living anionic polymerization. Macromolecules 33:3557–3568; (c) - Al-Muallem HA, Knauss DM (2001) Graft copolymers from star-shaped and hyperbranched polystyrene macromonomers. J Polym Sci Part A Polym Chem 39:3547–3555; (d) Al-Muallem HA, Knauss DM (2001) Synthesis of hybrid dendritic-linear block copolymers with dendritic initiators prepared by convergent living anionic polymerization. J Polym Sci Part A Polym Chem 39:152–161; (e) Huang T (2000) Synthesis of pom-star polystyrene. Polym Prep Am Chem Soc Div Polym Chem 41:1397–1398; (f) Knauss DM, Huang T (2002) Star-block-linear-block-star triblock (pom-pom) polystyrene by convergent living anionic polymerization. Macromolecules 35:2055–2062; (g) Knauss DM, Huang T (2003) ((PS)nPS)m star-shaped polystyrene with star-shaped branches at the terminal chain ends by convergent living anionic polymerization. Macromolecules 36:6036–6042

6. Huang T, Zhou H, Hong K, Simonson JM, Mays JW (2008) Architecturally and chemically modified poly(1,3-cyclohexadiene). Macromol Chem Phys 209:308–314

7. Gido SP, Lee C, Pochan DJ, Pispas S, Mays JW, Hadjichristidis N (1996) Synthesis, characterization, and morphology of model graft copolymers with trifunctional branch points. Macromolecules 29:7022–7028

8. Roovers J, Toporowski PM (1981) Preparation and characterization of H-shaped polystyrene. Macromolecules 14:1174–1178

9. (a) Iatrou H, Avgeropoulos A, Hadjichristidis N (1994) Synthesis of model super H-shaped block copolymers. Macromolecules 27:6232–6233; (b) Avgeropoulos A, Hadjichristidis N (1997) Synthesis of model nonlinear block copolymers of A(BA)2, A(BA)3, and (AB)3A(BA) 3 type. J Polym Sci Part A Polym Chem 35:813–816

10. Velis G, Hadjichristidis N (1999) Synthesis of model PS(PI)$_5$ and (PI)$_5$PS(PI)$_5$ nonlinear block copolymers of styrene (S) and isoprene (I). Macromolecules 32:534–536

11. Hadjichristidis N, Xenidou M, Iatrou H, Pitsikalis M, Poulos Y, Avgeropoulos A, Sioula S, Paraskeva S, Velis G (2000) Well-defined, model long chain branched polyethylene. 1. Synthesis and characterization. Macromolecules 33:2424–2436

12. Knauss DM, Huang T (2000) Pom-pom polystyrene by convergent living anionic polymerization. Polym Prepr 41(2):1332–1333

13. Knauss DM, Huang T (2002) Star-block-linear-block-star triblock (pom-pom) polystyrene by convergent living anionic polymerization. Macromolecules 35:2055–2062

14. Lai M-K, Wang J-Y, Tsiang RC-C (2005) Synthesis and characterization of (star polystyrene)-block-(polyisoprene)-block-(star polystyrene) copolymers. Polymer 46:2558–2566

15. Bayer U, Stadler R (1994) Synthesis and properties of amphiphilic "dumbbell"-shaped grafted block copolymers, 1. Anionic synthesis via a polyfunctional initiator. Macromol Chem Phys 195:2709–2722

16. Hadjichristidis N, Pitsikalis M, Iatrou H, Pispas S (2003) The strength of the macromonomer strategy for complex macromolecular architecture: molecular characterization. Properties and applications of polymacromonomers. Macromol Rapid Commun 24:979–1013

17. Haraguchi N, Hirao A (2003) Synthesis of well-defined star − linear block polystyrenes by coupling reaction of chain-functionalized polystyrenes with a definite number of benzyl bromide moieties with polystyryllithiums. Macromolecules 36:9364–9372

18. Velis G, Hadjichristidis N (2000) Synthesis of model block–double-graft copolymers and terpolymers of styrene (S), butadiene (Bd), and isoprene (I): Poly[S-b-(1,2 Bd-g-X2)] (X: S, Bd, I, S-b-I). J Polym Sci Part A Polym Chem 38:1136–1138

19. Se K, Yamazaki H, Shibamoto T, Takano A, Fujimoto T (1997) Model block − graft copolymer via anionic living polymerization: preparation and characterization of [poly ((4-vinylphenyl)dimethylvinylsilane)-graft-polyisoprene]-block-polystyrene. Macromolecules 30:1570–1576

20. Se K, Miyawaki K, Hirahara K, Takano A, Fujimoto T (1998) Model block–graft copolymer via anionic living polymerization: preparation and characterization of polystyrene-block-[poly (p-hydroxystyrene)-graft-poly(ethyleneoxide)]-block-polystyrene. J Polym Sci Part A Polym Chem 36:3021–3034

21. Zhao J, Mountrichas G, Zhang G, Pispas S (2009) Amphiphilic polystyrene-b-poly (p-hydroxystyrene-g-ethylene oxide)block-graft copolymers via a combination of conventional and metal-free anionic polymerization. Macromolecules 42:8661–8668

22. (a) Esswein B, Steidl NM, Möller M (1996) Anionic polymerization of oxirane in the presence of the polyiminophosphazene base t-Bu-P4. Macromol Rapid Commun 17:143–148; (b) Schlaad H, Kukula H, Rudloff J, Below I (2001) Synthesis of α,ω-heterobifunctional poly(ethylene glycol)s by metal-free anionic ring-opening polymerization. Macromolecules 34:4302–4304; (c) Groenewolt M, Brezesinski T, Schlaad H, Antonietti M, Groh PW, Iván B (2005) Polyisobutylene-block-poly(ethylene oxide) for robust templating of highly ordered mesoporous materials. Adv Mater 17:1158–1162

23. Zhang H, Ruckenstein E (1998) Graft, block − graft and star-shaped copolymers by an in situ coupling reaction. Macromolecules 31:4753–4759

24. Ito K (1998) Polymeric design by macromonomer technique. Progr Polym Sci 23:581–620

25. Vazaios A, Lohse DJ, Hadjichristidis N (2005) Linear and star block copolymers of styrenic macromonomers by anionic polymerization. Macromolecules 38:5468–5474

26. Christodoulou S, Iatrou H, Lohse DJ, Hadjichristidis N (2005) Anionic copolymerization of styrenic-tipped macromonomers: a route to novel triblock-comb copolymers of styrene and isoprene. J Polym Sci Part A Polym Chem 43:4030–4039

27. Koutalas G, Lohse DJ, Hadjichristidis N (2005) Novel block-comb/graft copolymers with the macromonomer strategy and anionic polymerization. J Polym Sci Part A Polym Chem 43:4040–4049

28. Koutalas G, Iatrou H, Lohse DJ, Hadjichristidis N (2005) Well-defined comb, star −comb, and comb-on-comb polybutadienes by anionic polymerization and the macromonomer strategy. Macromolecules 38:4996–5001

29. Driva P, Iatrou H, Lohse DJ, Hadjichristidis N (2005) Anionic homo- and copolymerization of double-tailed macromonomers: a route to novel macromolecular architectures. J Polym Sci Part A Polym Chem 43:4070–4078

30. Nikopoulou A, Iatrou H, Lohse DJ, Hadjichristidis N (2007) Anionic homo- and copolymerization of styrenic triple-tailed polybutadiene macromonomers. J Polym Sci Part A Polym Chem 45:3513–3523

31. Orfanou K, Iatrou H, Lohse DJ, Hadjichristidis N (2006) Synthesis of well-defined second (G-2) and third (G-3) generation dendritic polybutadienes. Macromolecules 39:4361–4365

32. Driva P, Lohse DJ, Hadjichristidis N (2008) Well-defined complex macromolecular architectures by anionic polymerization of styrenic single and double homo/miktoarm star-tailed macromonomers. J Polym Sci Part A Polym Chem 46:1826–1842

33. (a) Knauss DM, Al-Muallem HA, Huang T, Wu DT (2000) Polystyrene with dendritic branching by convergent living anionic polymerization. Macromolecules 33:3557–3568; (b) Knauss D M, Al-Muallem HA (2000) Polystyrene with dendritic branching by convergent

living anionic polymerization. II. Approach using vinylbenzyl chloride. J Polym Sci Part A Polym Chem 38:4289–4298

34. Al-Muallem HA, Knauss DM (2001) Graft copolymers from star-shaped and hyperbranched polystyrene macromonomers. J Polym Sci Part A Polym Chem 39:3547–3555

35. Dworak A, Walach W (2009) Synthesis, characterization and properties of functional star and dendritic blockcopolymers of ethylene oxide and glycidol with oligoglycidol branching units. Polymer 50:3440–3447

36. Lee JS, Quirk RP, Foster MD (2005) Synthesis and characterization of well-defined, regularly branched polystyrenes utilizing multifunctional initiators. Macromolecules 38:5381–5392

37. Sun W, He J, Wang X, Zhang C, Zhang H, Yang Y (2009) Synthesis of dandritic polystyrenes from an anionic inimer. Macromolecules 42:7309–7317

38. (a)Tung LH, Lo GYS (1994) Hydrocarbon-Soluble Di- and multifunctional organolithium Initiators. Macromolecules 27:1680–1684; (b) Lo GYS, Otterbacher EW, Gatzke AL, Tung LH (1994) Studies on dilithium initiators. 3. Effect of additives and seeding. Macromolecules 27:2233–2240; (c) Higashihara T, Nagura M, Inoue K, Haraguchi N, Hirao A (2005) Successive synthesis of well-defined star-branched polymers by a new iterative approach involving coupling and transformation reactions. Macromolecules 38:4577–4587; (d) Pispas S, Hadjichristidis N (1996) Micellization of model graft copolymers of the H and π type in dilute solution. Macromolecules 29:7378–7385

39. Stanetty P, Mihovilovic MD (1997) Half-lives of organolithium reagents in common ethereal solvents. J Org Chem 62:1514–1515

40. Xie C, Ju Z, Zhang C, Yang Y, He J (2013) Dendritic block and dendritic brush copolymers through anionic macroinimer approach. Macromolecules 46:1437–1446

41. (a) Quirk RP, Yoo T, Lee Y, Kim J, Lee B (2000) Applications of 1,1-diphenylethylene chemistry in anionic synthesis of polymers with controlled structures. Adv Polym Sci 153:67–162; (b) Schulz G, Höcker H (1980) 1,3-bis(1-lithio-3-methyl-1-phenylpentyl)benzene, an organodilithium compound soluble in aromatic hydrocarbons. Angew Chem Int Ed Engl 19:219–220; (c) Leitz E, Höcker H (1983) Kinetics of the addition reaction of sec-butyllithium onto bis(1-phenylvinyl)benzenes. Makromol Chem 184:1893–1899

42. Fréchet JMJ, Henmi M, Gitsov I, Aoshima S, Leduc MR, Bernard Grubbs BR (1995) Self-condensing vinyl polymerization: an approach to dendritic materials. Science 269:1080–1083

43. Yuan Z, Gauthier M (2005) Synthesis of arborescent isoprene homopolymers. Macromolecules 38:4124–4132

44. Ju Z, He J (2014) Organic nanospheres with an internal bicontinuous structure and their responsive phase inversion. Chem Commun (Camb) 50:8480–8483

45. Worsfold DJ, Bywater SM (1972) Degree of association of polystyryl-polyisoprenyl-, and polybutadienyllithium in hydrocarbon solvents. Macromolecules 5:393–397

46. Zhang H, He J, Zhang C, Ju Z, Li J, Yang Y (2012) Continuous process for the synthesis of dendrimer-like star polymers by anionic polymerization. Macromolecules 45:828–841

47. Zhang H, Zhu J, He J, Qiu F, Zhang H, Yang Y, Lee H, Chang T (2013) Easy synthesis of dendrimer-like polymers through a divergent iterative "end grafting" method. Polym Chem 4:830–839

Block Copolymers Containing Polythiophene Segments

Tomoya Higashihara, Eisuke Goto, and Mitsuru Ueda

Abstract Much attention has recently been paid to block copolymers (BCPs) containing π-conjugated stiff-rod segments, because of their many potential optical and electronic applications, including batteries, capacitors, light-emitting diodes, transistors, photovoltaics, and so on, by exploiting their semiconductivity. Based on the discoveries of living/controlled polymerization systems, including anionic, cationic, radical, and, recently, condensative chain-growth polymerization, a huge number of BCPs and related heterophase copolymers have been synthesized and well characterized so far. The chemically bonded structure between dissimilar polymer segments in BCPs induces self-organization, resulting in the formation of microphase separated domains at the molecular level. Recently, a wide variety of novel BCPs containing stiff rod polythiophene segments have been competitively synthesized by many researchers and their unique self-assembly behavior has been studied in detail. Due to the rigidity/crystallinity of polythiophene segments in addition to the heterophase structure, the self-assembly behavior of such BCPs becomes rather more complicated than that of conventional coil-based BCPs. Nevertheless, there are numerous merits for developing these BCPs, taking into consideration that the functions of rod and opto/electronically active segments would be useful resources for high-performance materials in actual device application. Therefore, this area is still attractive at the present time. In this chapter, recent progresses in the synthesis of well-defined BCPs containing polythiophenes, their morphology, and representative application to organic solar cells are reviewed.

T. Higashihara (✉) • E. Goto
Department of Polymer Science and Engineering, iFront Leading Doctoral Graduate School Program, Yamagata University, 4-3-16, Jonan, Yonezawa, Yamagata 992-8510, Japan

Japan Science and Technology Agency (JST), 4-1-8, Honcho, Kawaguchi, Saitama 332-0012, Japan
e-mail: thigashihara@yz.yamagata-u.ac.jp; eisukegoto115@gmail.com

M. Ueda
Department of Polymer Science and Engineering, iFront Leading Doctoral Graduate School Program, Yamagata University, 4-3-16, Jonan, Yonezawa, Yamagata 992-8510, Japan
e-mail: ueda.m.ad@m.titech.ac.jp

1 Introduction

Block copolymers (BCPs) have been of great interest for more than 40 years in
many areas, including morphological studies, micelles, processing, material sci-
ences, and functional device applications [1–9]. Many researchers have pursued
well-defined shapes and useful functions derived from such BCPs, making fasci-
nating supramolecular architectures accessible in advanced nanotechnology.
Indeed, well-defined BCPs with predictable molecular weights and low dispersities
(Đs) have been synthesized based on the feasibility of the established living/
controlled polymerization systems such as living anionic [10–12], living cationic
[13–19], and living radical polymerization [20–27]. Other new living/controlled
systems have recently been developed, including ring-opening polymerization
(ROP) [28], coordination polymerization [29], metathesis polymerization [30–
33], group transfer polymerization [34, 35], and condensative chain-growth poly-
merization [36–42], all of which allow for the creation of novel types of BCPs. To
typically synthesize well-defined BCPs, the second monomer is in situ charged after
the polymerization of the first monomer, leading an efficient crossover reaction,
followed by the polymerization of the second monomer in a living manner. Under
the current situation whereby the requirements for polymer properties and perfor-
mances have become stricter and more versatile, not only monomer varieties but
also combinations of polymer segments must be broadened.

BCPs containing π-conjugated polymers have emerged as intriguing and unique
materials due to their stiff rod-like structure in solution, melt, and/or solid states,
heterophase structures, as well as optoelectronic performance. Typical
π-conjugated polymers include polyacetylenes, polyphenylenes, polyfluorenes,
poly(phenylene vinylene)s, and polythiophenes. The breakthrough for condensative
chain-growth polymerization technique permits synthesizing well-defined
π-conjugated polymers and BCPs containing low polydisperse π-conjugated poly-
mer segments via living/controlled systems [37–42]. These efforts may contribute
to the accelerated evolution of potential application areas such as polymer photon-
ics materials, optoelectronic devices, and so on.

Herein, recent progresses in the synthesis of well-defined BCPs containing
polythiophene segments, especially those based on living/controlled polymeriza-
tion systems are reviewed. Especially, the recent advances have been focused on in
the synthesis of not only polythiophene-based BCPs but also homo polythiophene
with low Đ, chain-end-functionalized polythiophenes, and nanoporous membranes.
In the final section, recent contributions of polythiophene-based BCPs and related
materials to organic solar cell application are also introduced.

2   Precise Synthesis of Polythiophenes

Regioregular P3HT is a capable candidate in the field of polymer electronic devices, such as organic field-effect transistors [43] and organic photovoltaic cells [44–49], because of the balanced high-performance materials as *p*-type semi-conductors in terms of solubility, chemical stability, charge mobility, and commercial availability. The synthetic method for regioregular P3HT, first discovered by McCullough et al. [50, 51], followed by Rieke [52], affords the formation of head-to-tail P3HT with >98 % regioregularity, based on the nickel-catalyzed cross-coupling reactions using Grignard thiophene monomers or Rieke zinc, respectively (Scheme 1a, b). The development of Kumada Catalyst-Transfer Polymerization (KCTP) system starting from 2,5-dihalo-substituted thiophene monomers then allowed the media to be at room or reflux temperature, which was preferable for the low-cost and large scale synthesis of P3HT (Scheme 1c) [53, 54]. Alternatively, the more simple and straightforward dehydrogenative polycondensation afforded P3HT with a 92 % regioregularity by carefully controlling the monomer concentration and polymerization temperature (Scheme 1d) [55].

A further breakthrough of KCTP system came from its living nature, as independently reported by Yokozawa et al. [56, 57] and McCullough et al. [58, 59]. The mechanism proposed by Yokozawa [57] is as follows (see Scheme 2): two equivalents of the thiophene monomer, 2-bromo-5-chloromagnesio-3-hexylthiophene (**1**), are coupled by adding the catalytic Ni(dppp)Cl$_2$ (dppp = 1,3-diphenylphosphinopropane) to afford the tail-to-tail dimer. The Ni species then transfers to the next C-Br bonding walking through the π-conjugation without diffusion of the Ni(0) species to afford the dimer (**2**). **2** acts as the virtual initiator to start the polymerization of **1** by transmetalation. The polymerization proceeds in a chain-growth manner without diffusion of the Ni(0) species, in which only the transmetallation reaction takes place between the activated polymer chain end and the incoming monomer of **1**. When the initiation rate is faster or similar to the propagation rate, the resulting P3HT possesses a controlled molecular weight with the feed ratio of **1** to Ni(dppp) Cl$_2$ as well as the low Đ < 1.2. McCullough et al. proposed in a different way that the associate pair between generating polymer and Ni(0) species prevents the diffusion of Ni(0) species into the polymerization media to achieve the chain-growth mechanism [59].

However, thorough purification steps of the monomers and solvents are often necessary for KCTP system, because highly reactive and moisture-sensitive Grignard agents are employed. In addition, many functional groups, such as hydroxy, aldehyde, ketone, ester, amide, etc., cannot generally be tolerated in the presence of the Grignard reagents. Uchiyama et al. reported the anionic polymerization of *N*-isopropylacrylamide in aqueous media using the newly designed bulky zincate complex of ^{t}Bu$_4$ZnLi$_2$ with a low basicity as a highly selective anionic initiator [60]. These results indicated that ^{t}Bu$_4$ZnLi$_2$ is tolerable toward hydroxyl functional
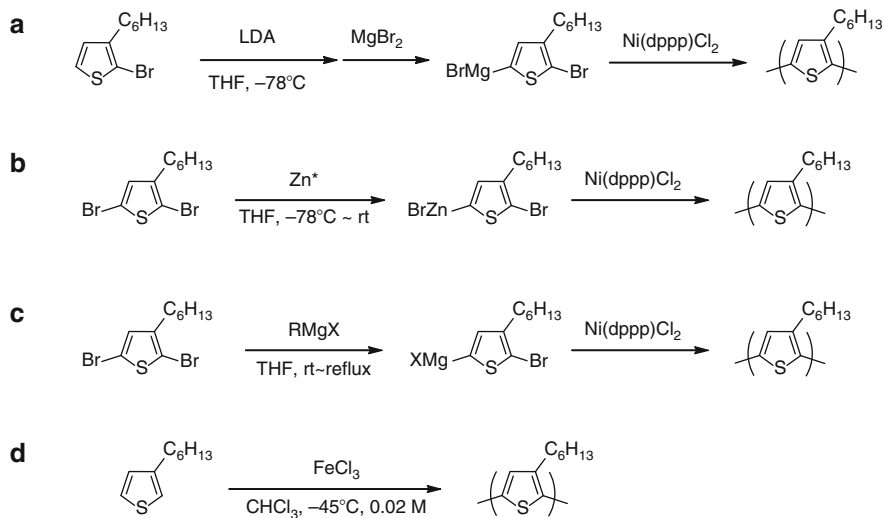
Scheme 1 Conventional synthesis of regioregular P3HT
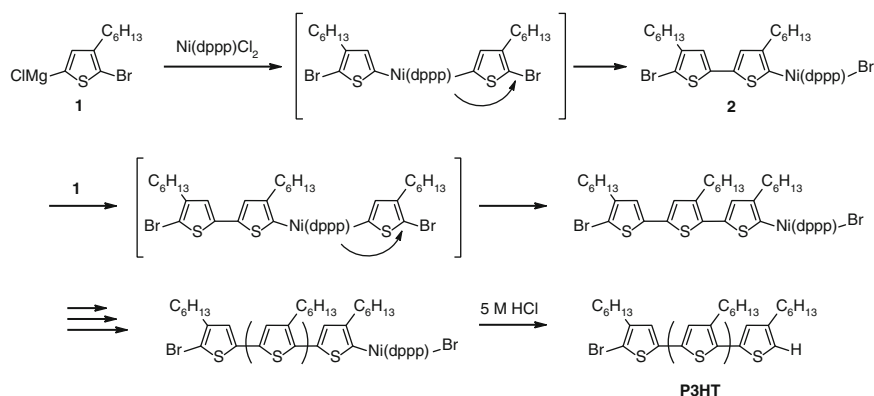
Scheme 2 Proposed mechanism for catalyst-transfer polycondensation to synthesize regioregular P3HT

groups. Indeed, regioregular P3HT could be synthesized based on Negishi-type catalyst-transfer polymerization (NCTP) by replacing the Grignard type monomer **1** with the zincate complex, as shown in Scheme 3a [61].

The average number molecular weight (M_n) value proportionally increased from 2,500 to 30,700 by increasing the feed ratio of the monomer to Ni catalyst, while maintaining the relatively low Đ < 1.2. The quasi-livingness of NCTP has been

a

b
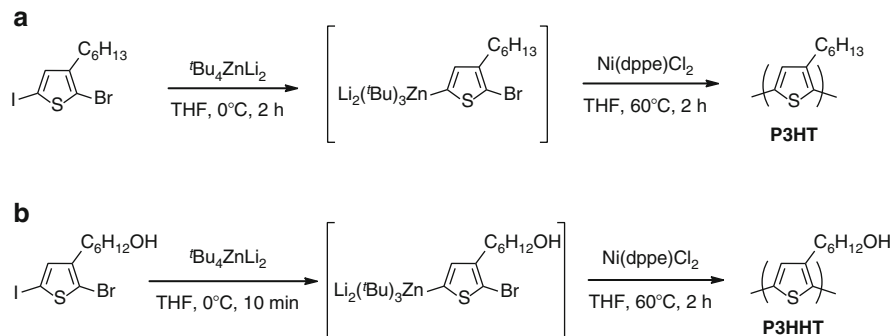
Scheme 3 Synthesis of regioregular P3HT and P3HHT using a zincate complex, $^tBu_4ZnLi_2$

Table 1 Conditions and results for synthesis of regioregular P3HT

Reagent	Catalyst	Temperature	M_n	Đ	RR	Reference
LDA/MgBr$_2$	Ni(dppp)Cl$_2$	−40 °C	10,000	1.6	98	[50]
Rieke Zinc	Ni(dppe)Cl$_2$	−78 °C	5,500	1.48	>98.5	[51]
RMgX	Ni(dppp)Cl$_2$	rt ~ reflux	12,000	1.2	98	[59]
FeCl$_3$		−45 °C, 0.02 M	68,000	1.9	91	[55]
$^tBu_4ZnLi_2$	Ni(dppe)Cl$_2$	0 °C	30,700	1.19	99	[61]
Cs$_2$CO$_3$	Pd cat.	120–125 °C	30,600	2.42	98	[64]
TMPMgCl-LiCl	Ni(dppe)Cl$_2$	rt	44,900	1.32	98	[65]

shown by a monomer addition experiment in which the molecular weight increased after the second addition of the same monomer as the first. The regioregularity of P3HT was over 97 % when the M_n exceeds 10,000. In addition, this new system could be used in as-received THF as well as in THF containing artificially added protic impurities, such as isopropanol, methanol, and even 1,000 ppm water (equal molar ratio to the monomer). Based on these successful results, the direct synthesis of poly[3-(6-hydroxyhexyl)thiophene] (P3HHT) could also be performed without protection (Scheme 3b). Very recently, the Ni catalyst with the optimized phosphine ligand of 1,2-bis(cyclohexyl)ethane successfully provided P3HTs with extremely low Đ values (1.03–1.17) [62]. The controlled synthesis of P3HT based on NCTP was well reviewed elsewhere [63].

Quite recently, the "atom-economical" methods involving the dehydrogenative polycondensation of 2-bromo-3-hexylthiophene [64, 65] or 2-chloro-3-hexylthiophene [66] were reported to synthesize regioregular P3HT (r.r. >98 %). All the conditions and results for the synthesis of regioregular P3HT introduced in this chapter are briefly summarized in Table 1 with corresponding references.

3 Rod-Rod Type Block Copolymer

Based on the quasi-living catalyst-transfer chain-growth polycondensation, an array of block copolythiophenes has been synthesized by the simple sequential monomer addition technique. All-conjugated block copolythiophenes, in which the π-conjugated structures are totally constructed along the main chains, are categorized as rod-rod type BCPs. McCullough and coworkers first reported the sequential polymerization of 2-bromo-5-chloromagnesio-3-dodecylthiophene (**3**) just after the completion of the first block obtained by the polymerization of **1** to afford P3HT-*block*-poly(3-dodecylthiophene) (**4**) (Scheme 4) [59]. Yokozawa and coworkers reported the synthesis of P3HT-*block*-poly(3-(2-(2-methoxyethoxy)ethoxy)thiophene) (**5**) based on a similar approach [67]. Ueda and Tajima groups independently synthesized crystalline-amorphous block copolythiophenes, that is, P3HT-*block*-poly(3-phenoxymethylthiophene) (**6**) [68] and P3HT-*block*-poly(3-(2-ethylhexyl) thiophene) (**7**) [69], respectively. Many other all-conjugated block copolythiophenes have also been reported, including P3HT-*block*-poly(2,5-dihexyloxy-1,4-phenylene) (**8**) [70], poly(3-butylthiophene)-*block*-poly(3-octylthiophene) (**9**) [71], P3HT-*block*-poly(3-hexylselenophene) (**10**) [72], P3HT-*block*-poly(3-(2-(2-(2-methoxyethoxy) ethoxy)ethoxy)thiophene)(P3TEGT) (**11**) [73], P3HT-*block*-poly(3-(3-aminopropyloxy)methylthiophene) (**12**) [74], P3HT-*block*-poly(3-thiophene hexylacetate) (**13**) [75]. Higashihara and coworkers also reported the synthesis of P3HT-*block*-poly(3-(4-(3,7-dimethyloctyloxy)-3-pyridyl)thiophene) (**14**) [76] and a soluble BCP having P3HT and a graphene-like nanoribbon (**15**) [77].

Interestingly, Scherf, Greenham, and coworkers reported the synthesis of donor-acceptor fully conjugated diblock copolymer (**16**), by the polycondensation of AB type monomer together with Br-terminated P3HT based on the Stille coupling reaction as illustrated in Scheme 5a [78]. Hawker and coworkers reported a donor-acceptor BCP (**17**) comprising P3HT and a diketopyrrolopyrrole (DPP)-based narrow bandgap block segments (Scheme 5b) [79].

Nakabayashi et al. reported a donor-acceptor BCP (**18**) having P3HT and n-type π-conjugated polymer based on naphthalene diimide (NDI)-based block segments (Scheme 6a) by Yamamoto Coupling between dibrominated NDI monomer and Br-terminated P3HT [80]. Soon after, Wang, Higashihara, and coworkers synthesized the similar BCP (**19**) (Scheme 6b) [81]. Br-terminated NDI-based polymer was first prepared by the Stille coupling polymerization of bis(trimethylstannyl) thiophene and a small excess of dibrominated NDI monomer. It was then utilized as a macroinitiator for KCTP of the thiophene monomer **1** after insertion of Ni catalyst with $Ni(COD)_2/PPh_3$, followed by the ligand exchange with dppp. The BCP **19** showed the phase separation of two distinct crystalline domains corresponding to P3HT (edge-on rich) and NDI-based polymer segments (face-on rich) by glazing incidence small angle X-ray scattering (GIWAXS) [82]. Bielawski and coworkers reported the successful one-pot synthesis of donor-acceptor BCP (**20**) by sequential monomer addition of **1** and a perylene diimide-functionalized arylisocyanide monomer (Scheme 7) [83].
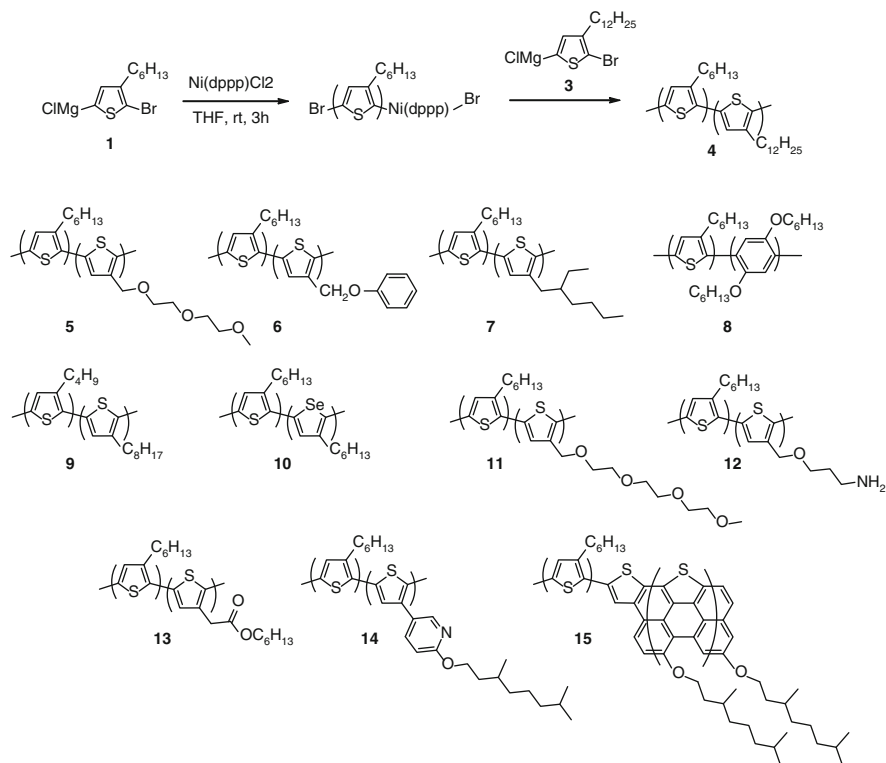
Scheme 4 Synthesis of rod-rod block copolythiophenes

During the course of our morphological studies on block copolythiophenes, it was found that the thin film of BCP **11**, carrying an amphiphilic structure, displayed a periodic perpendicular lamellar morphology at the nano level, as observed by atomic force microscopy (AFM) and transition electron microscopy (TEM) [73]. These results suggested that a microphase separation took place between hydrophobic P3HT and hydrophilic P3TEGT domains. A further detailed investigation has been done by Ree and coworkers by GIWAXS and glazing incidence small angle X-ray scattering (GISAXS) experiments [73]. As a result, the thin film BCP **11** consists of a hierarchical morphology of perpendicularly aligned lamellae with the *d*-spacing of 25.9 nm, in which crystalline P3HT domains construct the edge-on structure to the substrate excluded by amorphous P3TEGT domains. Such a perpendicularly oriented morphology should be very important in the field of organic photovoltaic (OPV) application due to the high speed charge transportation before the recombination of the separated charges occurs. However, a detailed relationship between the morphology and OPV performance has never been reported; therefore, it should be one of the top priority issues to be addressed in the OPV field.
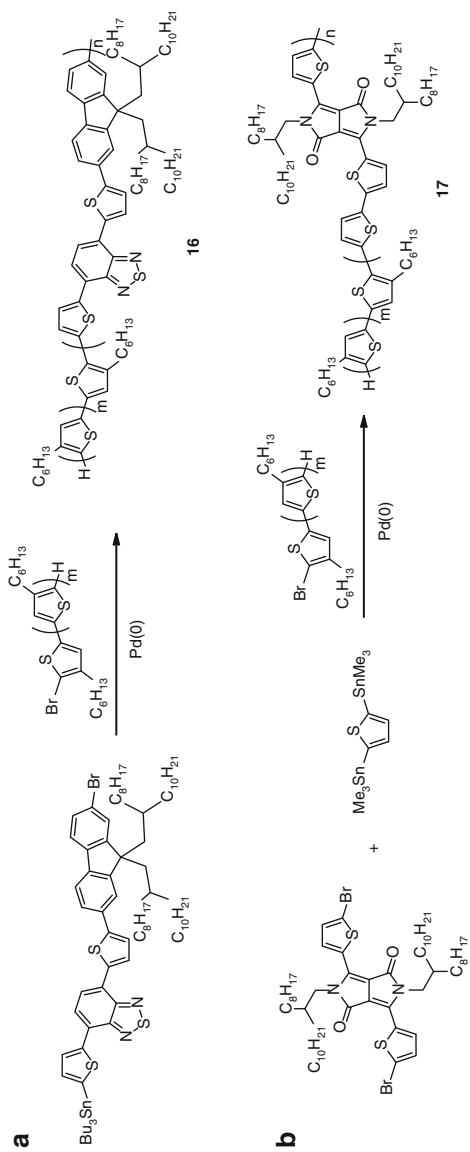
Scheme 5 Synthesis of donor-acceptor fully conjugated BCPs based on Stille coupling polymerization with Br-terminated P3HT
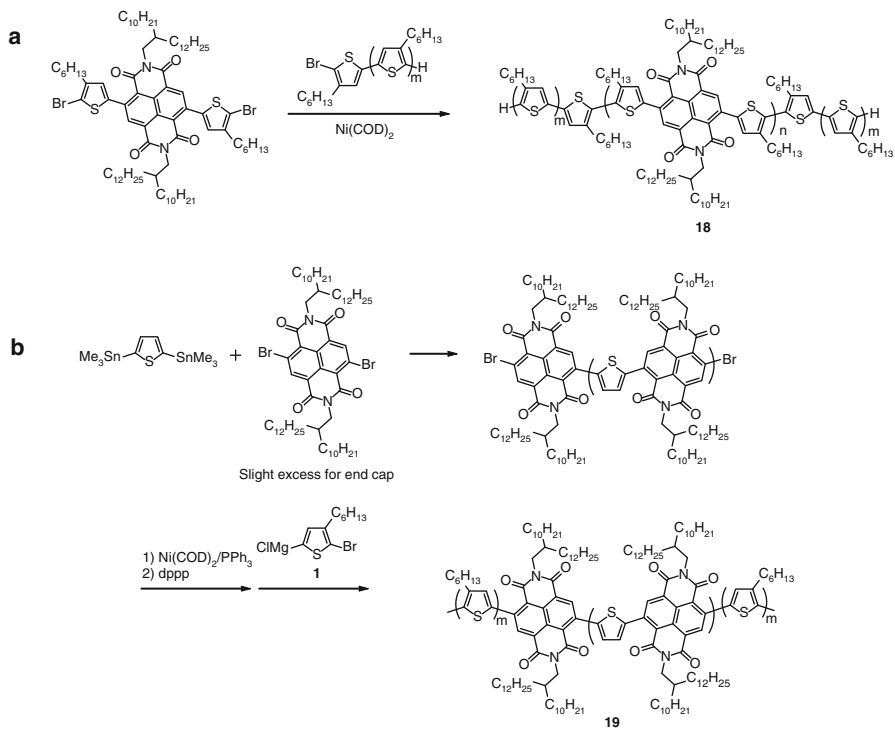
Scheme 6 Synthesis of donor-acceptor fully conjugated BCPs with NDI-based polymers
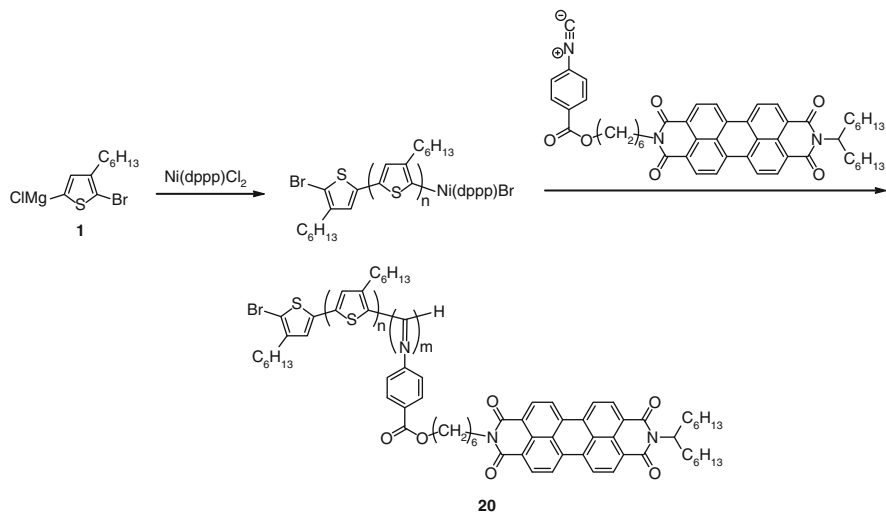
Scheme 7 One-pot synthesis of donor-acceptor fully conjugated BCPs by sequential polymerization

4 Precise Synthesis of Chain-End-Functionalized Polythiophenes

The chain-end functionalization of polythiophenes is a very important step for obtaining BCPs, because the terminal functional groups are responsible for the introduction of the second block in the subsequent reactions or polymerizations. McCullough reported the chain-end functionalization of P3HT by terminating the quasi-living P3HT-Ni(dppp)Br with the Grignard reagent (R-MgX) (see Scheme 8) [84, 85]. The functionality widely includes vinyl, allyl, acetyl, phenyl, tolyl, formyl (protected by acetal), phenol (protected by tetrahydropyran), and *p*-aminophenyl (protected by trimethylsilane).

However, the type of R-MgX significantly affected the final product structures as to whether the monofunctionalization at the ω-terminal or difunctionalization at the α,ω-termini takes place. In Scheme 8, the difunctionalized P3HT can possibly be obtained by the following mechanisms: (1) reductive elimination of Ni catalyst after the monofunctionalization, (2) the generated Ni(0) oxidatively inserts into α-terminal, and (3) the transmetalation reaction with excess R-MgX, eliminating again Ni(0). This mechanism suggested the difficulty in selectively synthesizing either mono- or difunctionalized P3HT derivatives.

Luscombe and coworkers reported the efficient initiation from an *o*-halotoluene based on a ligand exchange approach, aimed at the synthesis of a defect-free regioregular P3HT [86]. On the other hand, Higashihara et al. succeeded in synthesizing the α,ω-chain-end-functionalized P3HTs with tolyl and bromobutyl groups by the combination of initiation and termination methods in a one-pot process (see Scheme 9) [87]. Fortunately, when using Ni(dppp)Cl$_2$ as an initiator, difunctionalized P3HTs with 4-bromobutyl groups at both ends could be formed. In Fig. 1, mono-series of peaks were obtained from MALDI-TOF mass spectra for monobromo- and dibromo-functionalized P3HTs, indicating nearly quantitative end functionality.

The selective synthesis of monobromo- and dibromo-functionalized P3HTs is for the first time. It should be mentioned that bromoalkyl group can be transformed
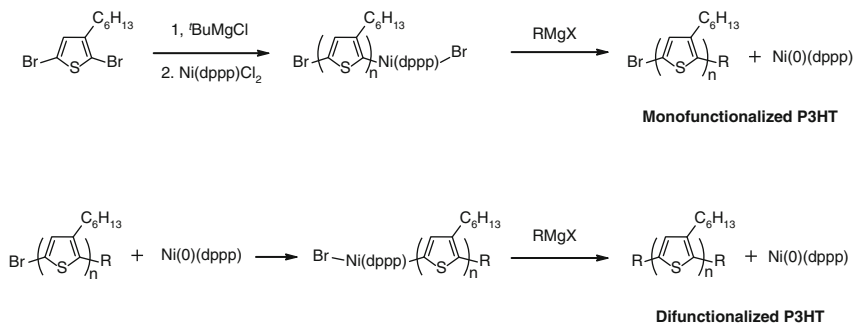
Scheme 8 Synthesis of chain-end-functionalized P3HTs
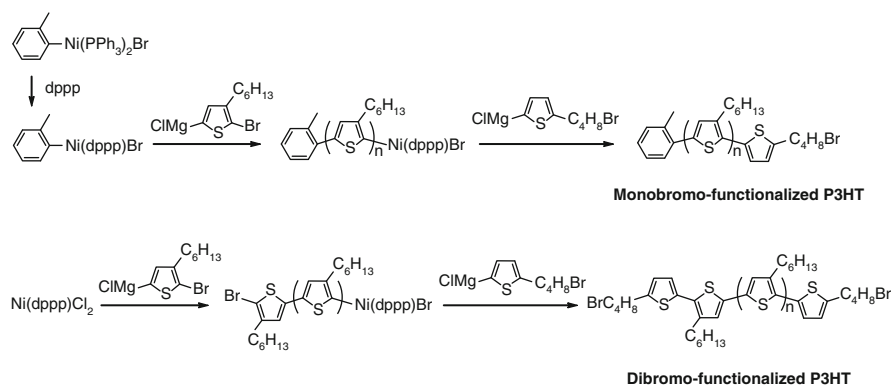
Scheme 9 Synthesis of bromobutyl-chain-end-functionalized P3HTs

Fig. 1 MALDI-TOF mass spectra of (**a**) monobromo-functionalized P3HT and (**b**) dibromo-functionalized P3HT. *Inset*: enlarged spectra of the most intense peaks
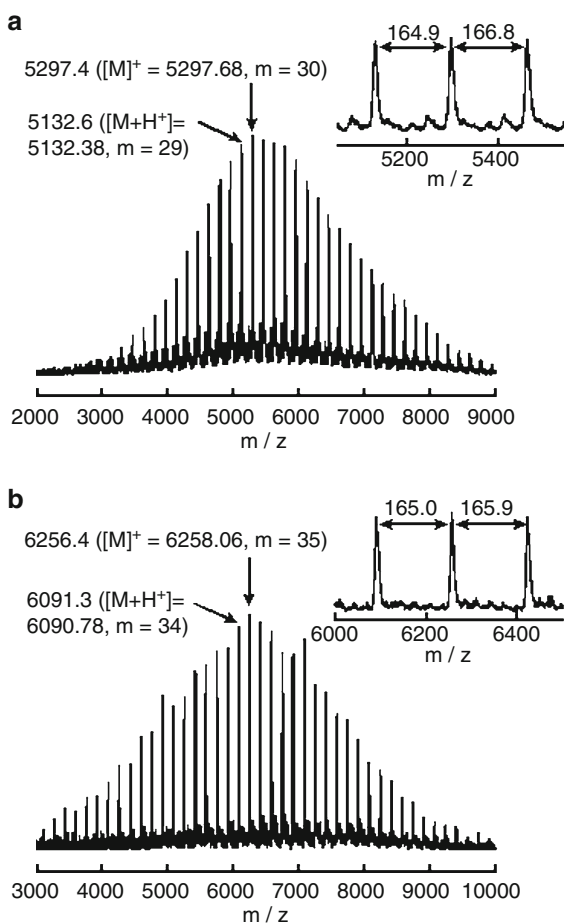
into a wide variety of other useful functionalities, such as amine, cyano, ether, alcohol, aldehyde, etc. This system is also quite important for BCP synthesis using chain-end-functionalized P3HT as a precursor, because the end functionality of P3HT is predominant for the sequence control of AB diblock or ABA triblock copolymers.

5 Precise Synthesis of Rod-Coil and Coil-Rod-Coil Block Copolymers Containing Polythiophene Segments

5.1 Combination of KCTP and Living/Controlled Radical Polymerization

To synthesize rod-coil BCPs containing P3HT and poly(acrylate) (PMA) segments, McCullough combined KCTP with an ATRP system involving several site-transformation steps, as shown in Scheme 10 [88]. First, ω-chain-end-vinyl-functionalized P3HT was synthesized by terminating quasi-living P3HT having an ω-Ni-Br chain end with an excess of vinylmagnesium bromide. Then, the introduced vinyl group was transformed into a hydroxyl one by a hydroboration/oxidation process. After transforming the hydroxyl group into a 2-bromopropionate one by an esterfication reaction, ATRP of the acrylates was performed to afford P3HT-*b*-poly(methyl acrylate)(PMA) and P3HT-*b*-poly(*t*butyl acrylate)(P*t*BMA). They also succeeded in synthesizing P3HT-*b*-polyisoprene(PI) (**21**) and P3HT-*b*-polystyrene(PS) (**22**) (see Fig. 2) using NMP and reversible addition fragmentation chain-transfer (RAFT) polymerization, respectively, and found that the nanofibril surface structures of those polymer films could be observed by atomic force microscopy (AFM) [89]. Furthermore, new conducting amphiphilic BCPs of P3HT-*b*-poly(acrylic acid) (PAA) (**23**) were synthesized by hydrolysis of P3HT-*b*-P*t*BMA, which was prepared by a similar method [90]. Zou et al. synthesized a
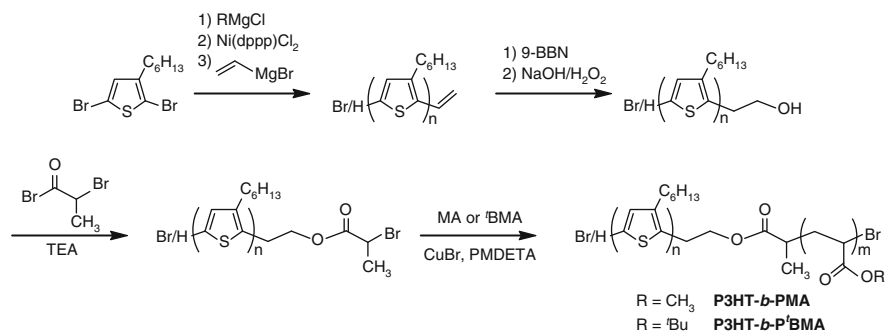
Scheme 10 Synthesis of P3HT-*b*-PMA and P3HT-*b*-P*t*BMA by the combination of KCTP and ATRP
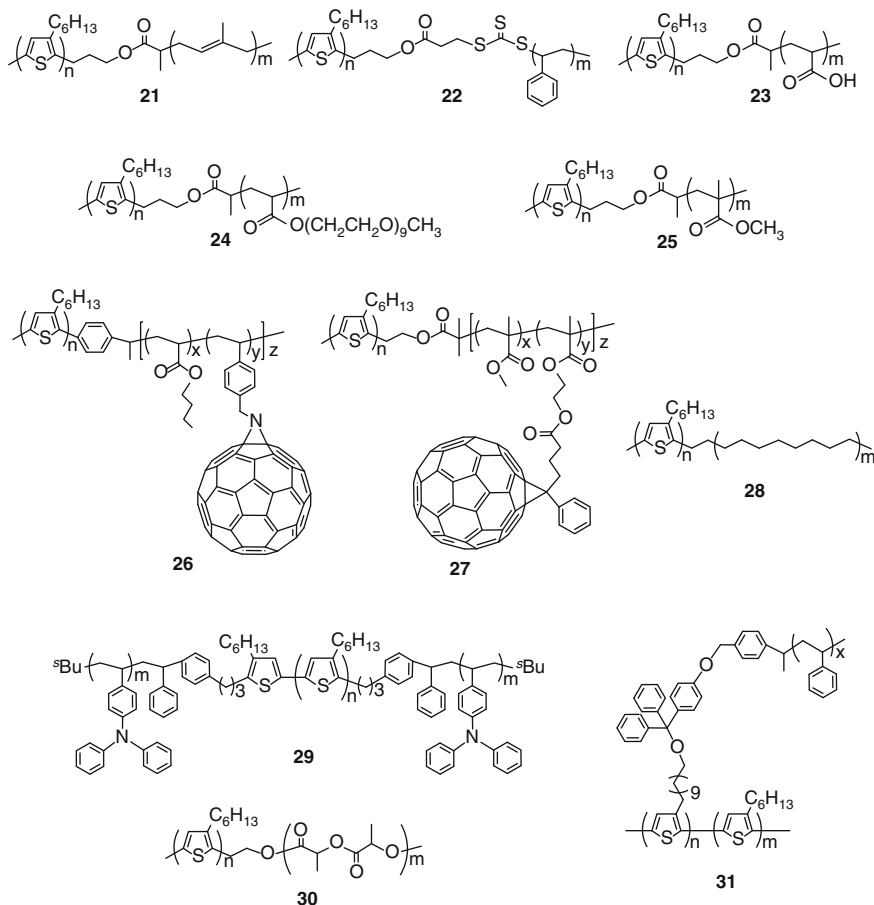
Fig. 2 Chemical structures of P3HT-based BCPs

series of P3HT containing BCPs with PAA, poly(PEG acrylate) (**24**), and PMMA (**25**) and used it as an efficient dispersant for carbon nanotubes [91]. Urien and coworkers reported an alternative synthetic approach via a copper (I)-catalyzed Huisgen [3 + 2] dipolar cycloaddition reaction based on "Click" chemistry, combined with KCTP and ATRP, to afford AB and ABA BCPs containing P3HT and PS segments [92]. Very recently, a series of interesting donor-acceptor BCPs was synthesized based on living/controlled radical polymerization co-systems. Richard et al. synthesized P3HT-based rod-coil BCPs with fullerene-grafted PS segments (**26**) using the NMP system [93]. Soon thereafter, Lee et al. synthesized P3HT-based rod-coil BCPs with fullerene-grafted PMMA segments (**27**) [94]. Although many examples have been developed based on KCTP in conjunction with the living/controlled radical polymerization system, tedious site-transformation reactions as well as the limited control nature of radical polymerization frequently cause
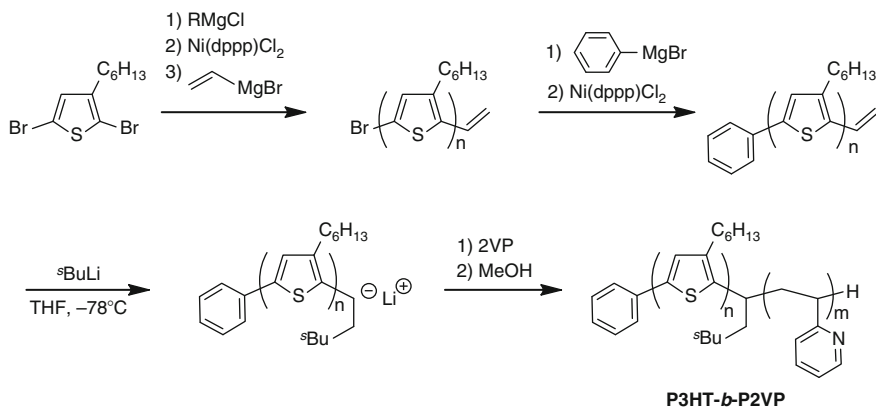
Scheme 11 Synthesis of P3HT-*b*-P2VP by the combination of KCTP and living anionic polymerization

a large Đ value (>1.3). Furthermore, a thorough purification process to remove the residual copper catalyst from the products is sometimes essential for optoelectronic application.

5.2   Combination of KCTP and Living Anionic Polymerization

Besides radical polymerization co-systems, Jannssen and coworkers reported the synthesis of crystalline-crystalline BCPs comprised of P3HT and polyethylene segments (**28**) by a combination of KCTP and ROP [95]. Chi-An Dai synthesized new P3HT-*b*-P2VP by a combination of KCTP and living anionic polymerization [96]. As shown in Scheme 11, ω-chain-end-vinyl-functionalized P3HT was synthesized by the established method. Then, the α-Br chain end was converted into a phenyl group so that the unwanted side reactions such as Li-Br exchange or single-electron transfer reactions could be eliminated. After lithiation of the terminal vinyl groups with ^{s}BuLi, living anionic polymerization of 2VP was carried out to synthesize the desired BCPs. Simply by changing the block compositional ratio, spherical, cylindrical, lamellar, and nanofibril structures could clearly be observed by TEM and SAXS. The molecular weight distributions of all BCP samples were relatively narrow due to the use of the living anionic polymerization system (Đ = 1.18 − 1.28). However, there are still multistep reactions, especially for the modification reaction of the α-Br chain end of P3HT. Furthermore, in the lithiation reaction, a possible homopolymerization of the terminal thiophenylvinyl units might generate higher coupling by-products.
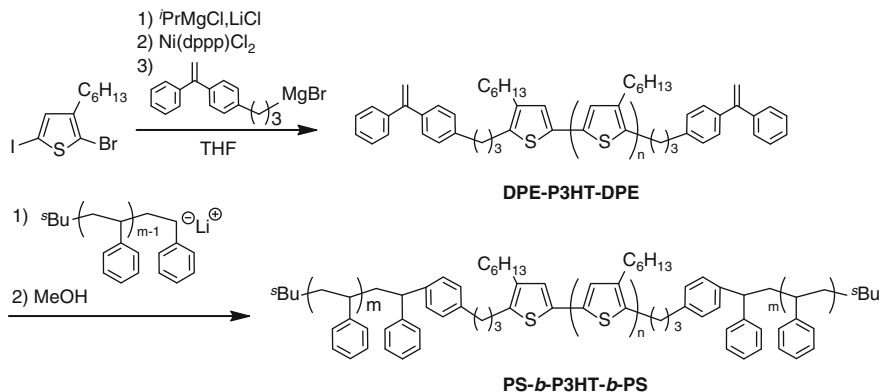
Scheme 12 Synthesis of PS-*b*-P3HT-*b*-PS by the combination of KCTP and living anionic polymerization

A facile synthesis of PS-*b*-P3HT-*b*-PS has been reported by Higashihara et al. based on a novel approach involving only two steps, an in situ introduction of non-homopolymerizable 1,1-diphenylethylene (DPE) moieties at the α,ω-ends of P3HT, and a linking reaction with a living anionic polymer of styrene [97]. The synthetic routes are shown in Scheme 12. The key step is an in situ introduction of DPE moieties simultaneously at the α,ω-ends of P3HT, which readily and quantitatively link with living PS without homopolymerization of the DPE units due to its steric hindrance and resonance effect. The di-substitution feature was experimentally supported by MALDI-TOF mass spectroscopy (>90 %) and a previous paper describing the end functionalization of P3HT with an alkyl-type terminating Grignard reagent [84, 85]. This spontaneous di-substitution permits skipping the extra steps of the transformation reactions at the chain end. In addition, the developed polymer-polymer linking method provides more reliable molecular weights and compositions of BCPs than by conventional macroinitiator methods because both segments can be pre-made and separately characterized. The purified PS-*b*-P3HT-*b*-PS possesses a molecular weight of 18,900 and a Đ value of 1.15, as determined by GPC. The surface morphology of the BCP thin films was observed by AFM and continuous nanofibril and nanowire structures were observed. The formation of the nanowire structures may be dictated by the immiscibility of PS and P3HT segments, as reported in the literature describing the nanowire structures of the P3HT-*b*-PS diblock copolymer [89]. The precursor α,ω-end-DPE-functionalized P3HT was also used for synthesizing well-defined PMMA-*b*-P3HT-*b*-PMMA with low Đ value (1.10) according to Scheme 13 [98]. J. K. Kim et al. synthesized well-defined P3HT-*b*-PMMA based on the polymer-polymer linking approach which involves the utility of chain-end-phenylacrylate-functionalized P3HT [99] (Scheme 14). The advantage of using phenylacrylate unit is the quantitative linking efficiency with living anionic PMMA without homopolymerization as first demonstrated by A. Hirao's group [100].
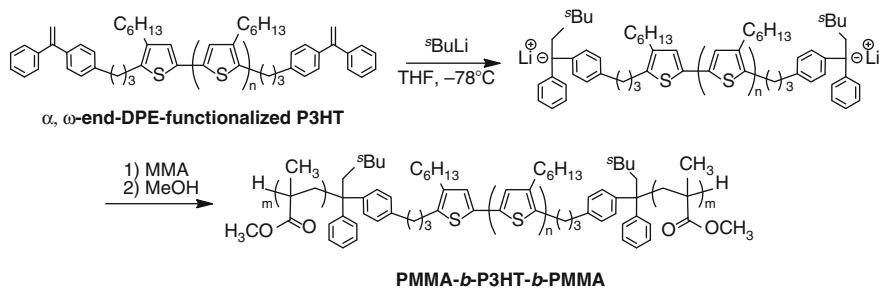
Scheme 13 Synthesis of PMMA-*b*-P3HT-*b*-PMMA by the combination of KCTP and living anionic polymerization
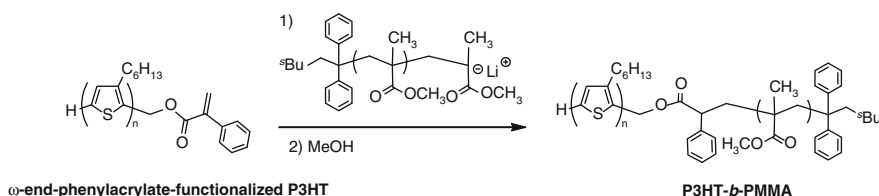
Scheme 14 Synthesis of P3HT-*b*-PMMA by polymer-polymer linking approach

Unfortunately these BCPs contain insulating segments, so their electronic performance is probably limited. Therefore, the introduction of optoelectronically active coil segments into P3HT-based BCPs is highly desired. We further synthesized novel BCPs containing P3HT and optoelectronically active poly (4-vinyltriphenylamine) (PVTPA) by the similar approach [101]. PVTPA-*b*-P3HT-*b*-PVTPA (**29**) may be one of the candidates for better hole-transporting material than PS-*b*-P3HT-*b*-PS or PMMA-*b*-P3HT-*b*-PMMA. The surface morphology of cast film **29** was observed by AFM. When the cast film was treated by solvent annealing under exposure of a toluene vapor, a neat, uniform, and periodic morphology emerged over a large area, in which each phase-separated domain with 12–15-nm widths was well connected with some micrometer length (see Fig. 3). These periodic self-assemble structures may possibly be derived from the well-defined structure of PVTPA-*b*-P3HT-*b*-PVTPA with low Đ value (1.15). A TEM image of the sample film also supported such microphase separation.

A rod-rod-rod triblock copolymer comprised of outer PA block and inner P3HT block by the combination of KCTP and living anionic polymerization through a precursory block for thermal conversion by Higashihara et al. [102]. As shown in Scheme 15, the exactly same macroinitiator was utilized derived from α,-ω-end-DPE-functionalized P3HT for the synthesis of PMMA-*b*-P3HT-*b*-PMMA. 4-methylphenyl vinyl sulfoxide was then anionically polymerized with the macroinitiator in a living manner to prepare poly(4-methylphenyl vinyl sulfoxide) (PMPVS)-*b*-P3HT-*b*-PMPVS. Finally, the outer PMPVS segments could
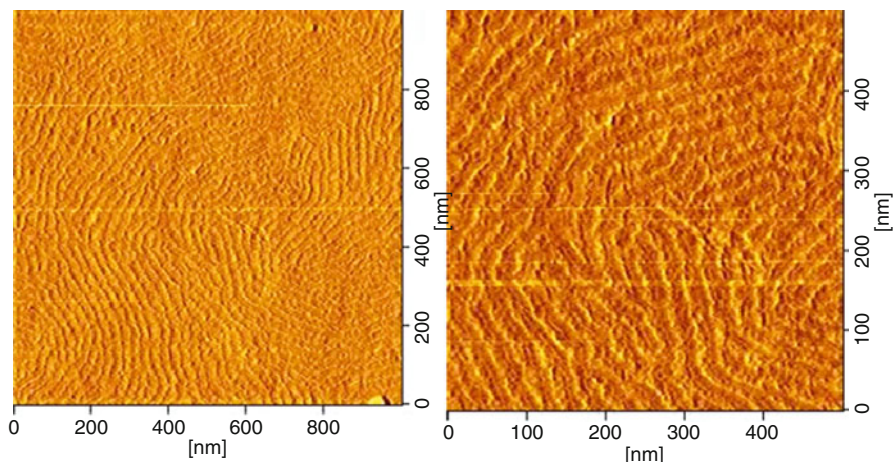
Fig. 3 Tapping mode AFM phase images of PVTPA-*b*-P3HT-*b*-PVTPA after solvent annealing
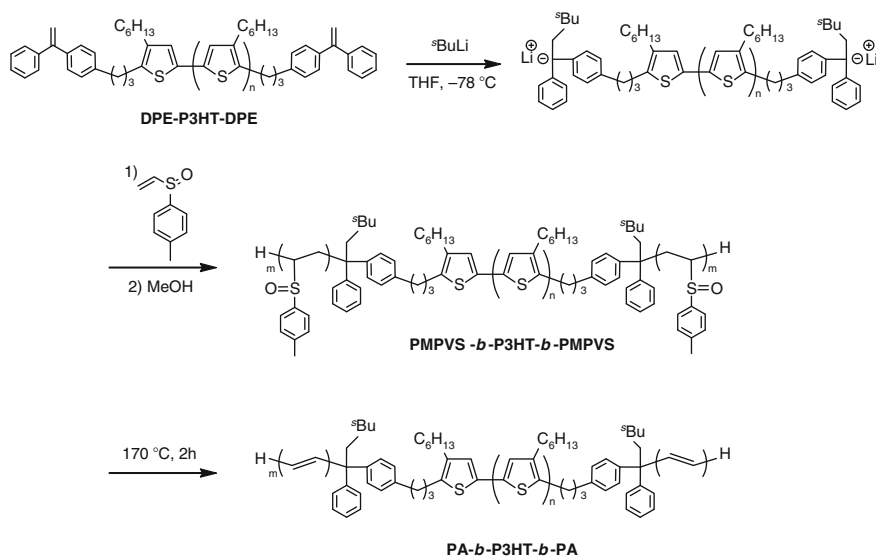
Scheme 15 Synthesis of PA-*b*-P3HT-*b*-PA

completely be transformed into PA segments to afford the objective rod-rod-rod BCP, PA-*b*-P3HT-*b*-PA.

As already mentioned in Sect. 4, KCTP allowed for the synthesis of monobromo- and dibromo-functionalized P3HTs, respectively, by selecting the appropriate initiators as reported by T. Higashihara and T. Michinobu [87]. On the other hand, the living anionic polymerization of 4-(4'-*N,N*-dihexylaminophenylethynyl)styrene
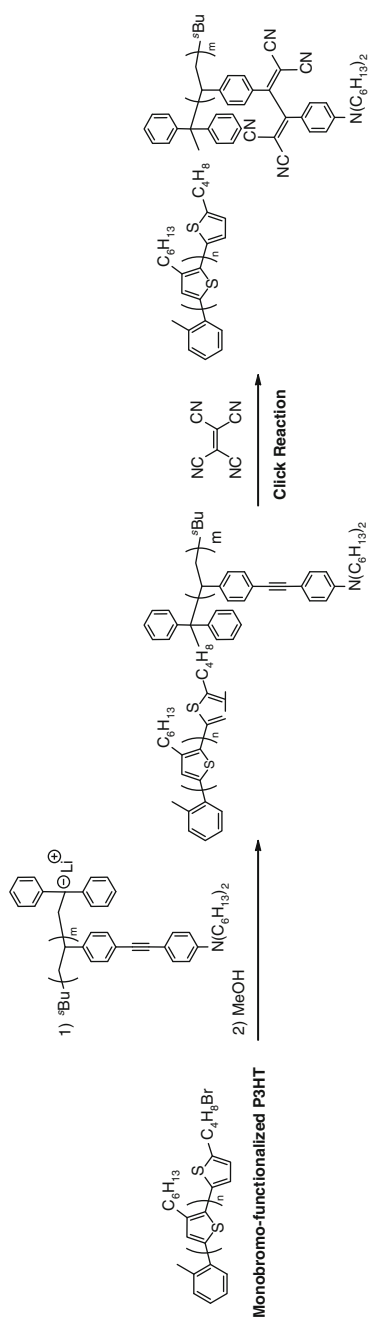
Scheme 16 Synthesis of donor-acceptor type rod-coil BCP based on the combination of KCTP, living anionic polymerization, and click postfunctionalization

(DHPS) with the initiator of ^{s}BuLi was demonstrated. By the coupling reaction of PDHPS-Li with monobromo- and dibromo-functionalized P3HTs, novel rod-coil diblock and coil-rod-coil triblock copolymers composed of the P3HT and PDHPS segments were synthesized. The obtained BCPs were then quantitatively functionalized by the click chemistry-type tetracyanoethylene (TCNE) addition, producing the corresponding BCPs with donor-acceptor moieties in the flexible polystyrene segments. The representative synthetic scheme for AB diblock copolymer is shown in Scheme 16. This click postfunctionalization approach could become a general route to the P3HT-based rod-coil BCPs with electron-accepting units in the coil segments. The TCNE addition significantly affected both the absorption spectra and redox activities. Moreover, the AFM images demonstrated the microphase separation of these BCPs. All these results reasonably suggest that they are an interesting class of new P3HT-based BCPs for advanced studies of various organic devices. In particular, the application to organic solar cells is promising because of the expanded absorption, tunable energy levels for fast energy transfer between both segments, and well-defined microphase separation.

6 Preparation of Nanoporous P3HT Films

The thin films of BCPs can self-assemble into many types of highly ordered nanostructures on a wide variety of substrates after being cast from a number of solvents. Selective etching of one of the domains can lead to nanoporous materials that are useful for separations and templates of nanotechnology [5, 6, 103, 104]. Nanoporous P3HT films derived from BCP templates are quite interesting and are expected to be used for such applications as voltaic chemical sensors and, especially, BHJ organic photovoltaic cells, after a back-fill of *n*-type semiconductors into the porous films. Due to the large interface areas and well-connected charge transporting channels having widths comparable to exciton diffusion lengths (~10 nm), it is expected that efficient charge separation with less recombination and fast charge transport will be realized, resulting in improved PCE.

Hillmyer and coworkers reported nanoporous P3HT films for the first time by using a template of P3HT-*b*-poly(${}_{D,L}$-lactide) (**30**) [105]. Starting from ω-chain-end-vinyl-functionalized P3HT, the chain end is transformed into a hydroxy group, followed by controlled ROP of ${}_{D,L}$-lactide from an aluminum alkoxide macroinitiator to synthesize **30**. The back-fill of water-soluble fullerene derivatives into a similar nanoporous P3HT, derived from **30**, was recently performed to create an ideal *p/n* BHJ active layer, however, the characterization of photovoltaic cells was not shown [106]. Hawker and coworkers recently reported the creation of nanoporous P3HT films by the selective solvent etching of PS segments after being cleaved off from the template of P3HT grafted with PS segments via the trityl ether linkage (**31**) [107].

Higashihara et al. developed an alternative approach for nanoporous P3HT by employing P3HT-based BCPs with ionic interaction [108, 109]. Although
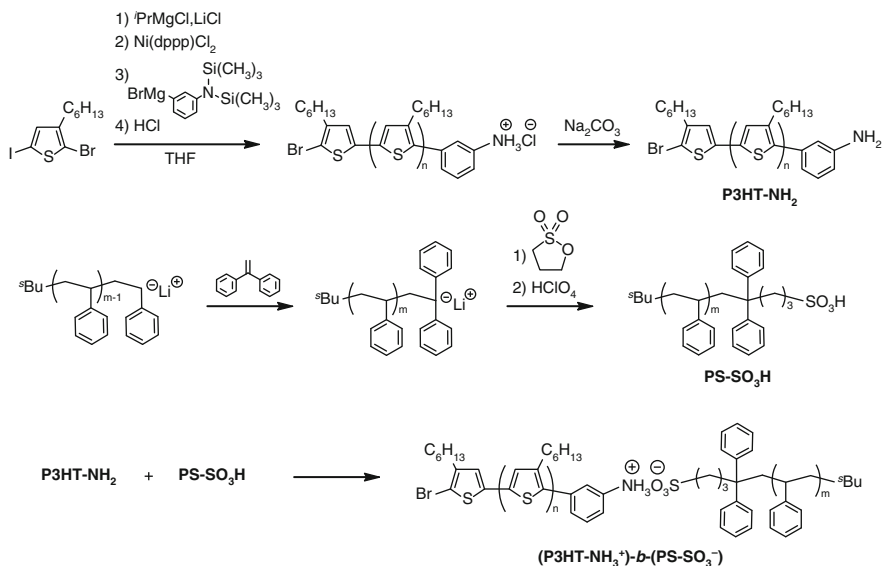
Scheme 17 Synthesis of (P3HT-NH$_3^+$)-b-(PS-SO$_3^-$)

covalently bonded P3HT-based BCPs are presently very competitive, a blend system of well-defined chain-end-functionalized polymers to achieve similar nanostructures has scarcely been focused on yet. The advantageous points of using such a blend system are as follows: (1) more facile synthetic approaches are available for chain-end-functionalized polymers than for BCPs, thereby being preferred for industry, (2) the combination of block segments is versatile, (3) the facile preparation of nanoporous films by the removal of one of the segments with a selective solvent after cleaving the ionic bonds under acidic or alkaline conditions. The first example of P3HT-based BCPs via ionic interaction was prepared by blending ω-chain-end-aniline-functionalized P3HT (P3HT-NH$_2$) and ω-chain-end-carboxy-functionalized PS (PS-COOH) [108] or sulfonic-acid-chain-end-functionalized PS (PS-SO$_3$H) [109]. The representative synthetic routes for the BCPs of (P3HT-NH$_3^+$)-b-(PS-SO$_3^-$) are depicted in Scheme 17.

The termination of P3HT with an ω-Ni-Br chain end with an excess of a Grignard reagent carrying a protected aniline moiety, followed by quenching the system with 5 N-HCl aq. afforded an HCl salt of P3HT-NH$_2$. After washing with an alkaline solution, P3HT-NH$_2$ could be regenerated. The Đ values were very low, in the range of from 1.08 to 1.12, and NH$_2$-end functionalities were in the range of 85–92 %. On the other hand, PS-SO$_3$H with 100 % end functionality was synthesized based on living anionic polymerization according to Scheme 17.

AFM images of the surface morphology of a (P3HT-NH$_3^+$)-b-(PS-SO$_3^-$) thin film showed nanofibril structures having 15 to 20-nm widths and a few hundred nanometer lengths are observed (see Fig. 4a). In order to create the desired nanoporous P3HT films, selective etching of PS domains with ethyl acetate/
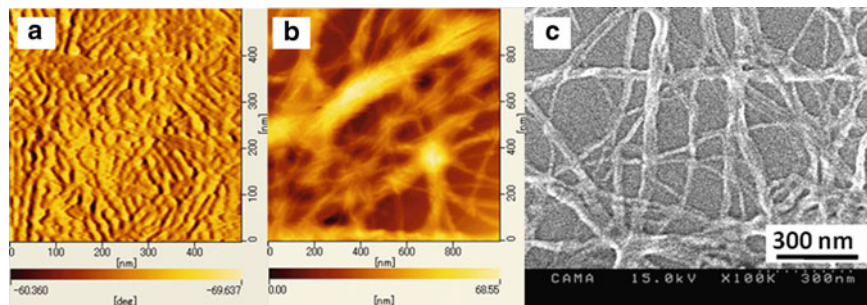
Fig. 4 (**a**) Tapping mode AFM phase image of (P3HT-NH$_3^+$)-*b*-(PS-SO$_3^-$) thin film, (**b**) tapping mode AFM height image of nanoporous P3HT thin film, and (**c**) SEM image of nanoporous P3HT thin film

triethylamine (100/1, v/v) was performed by exploiting the pH stimulating ionic interaction between the P3HT and PS segments. Ethyl acetate and triethylamine play important roles in the selective solvent for PS and the cleavage of aniline-sulfonic acid interaction, respectively. Nanoporous textures are indeed observed in some areas in AFM (Fig. 4b) and SEM images (Fig. 4c), but P3HT domains tend to collapse, probably due to the wet process and high aspect ratio of more than 5.

7 Polymer Solar Cell Application

Since the Japanese government has decided to enforce buying electricity produced by solar cells on electric power companies at 42 JPY/kWh in 2012, which is about four times than the conventional price, many companies related to solar cells, their modules and panels, have been encouraged to participate in this society. New low-cost solar cells produced by a facile process have been highly demanded in order to replace with current silicon-based solar cells, taking into consideration the strict competition of production costs in the world. OPVs have recently received much attention due to their lightweight, flexible, and low-cost large area productivity based on a roll-to-roll printing process [110]. However, the low power conversion efficiencies (PCEs < 10 %) of OPVs are serious problems, being inferior to silicon-based solar cells (PCEs > 20 %) and preventing commercialization. In addition, the long-term stability of the OPVs has to be improved. The mechanism of solar cell involves four steps: (1) light absorption within the active layers to generate an exiton, (2) exiton diffusion to the interface between the donor and acceptor domains, (3) charge separation at the interface, and (4) charge transportation to both the cathode and anode. The PCE value is determined by the following equation:

$$PCE \, (\eta_{\mathrm{eff}}) \; = \; V_{\mathrm{oc}} \times J_{\mathrm{sc}} \times \mathrm{FF}$$

where V_{oc} is the open circuit voltage, J_{sc} is the short circuit current density, and FF is the fill factor. In order to improve the PCE, each factor must be improved by careful design of the active layers as well as the optimization of the device fabrication process. V_{oc} is generally related to the difference between the highest occupied molecular orbital (HOMO) energy level of a donor and lowest unoccupied molecular orbital (LUMO) energy level of an acceptor, so that the donor molecules, especially, a donor polymer with a low HOMO energy level and/or an acceptor molecule with a high LUMO energy level, are required for achieving high V_{oc} values. J_{sc} is related to the light harvesting, charge separation, and recombination of the separated charges; therefore, a low bandgap polymer harvesting light over wide wavelengths covering the visible to near-infrared (IR) regions should be a strong candidate for improving the J_{sc} values. In addition, the morphological control in the donor and acceptor domains is quite important for efficient charge separation and reduced recombination of the separated charges also improve the J_{sc} values. A well-connected morphology with a 10–20 nm mean distance between the donor and acceptor is ideal, because the exciton diffusion length is normally 10–20 nm for organic molecules. *FF* is concerned with the output resistance and shunt resistance, which are generally improved by a high charge mobility and ultrahigh purity of the semiconductors. The connectivity and arrangement of the donor-acceptor morphology is also important for efficient charge transportation to both electrodes, thus resulting in high *FF* values.

7.1 Use of Block Copolymers

A BHJ-type OPV device using regioregular P3HT and [6,6]-phenyl-C_{61}-butyric acid methyl ester (PCBM) is one of the most basic and successful systems as well as a platform for other efficient BHJ OPVs until now, normally giving power conversion efficiencies (PCEs) in the range of 4–5 % after optimization [48, 111, 112]. Much attention has been paid to the influence of P3HT:PCBM binary phase morphology on device performance. A serious problem in the morphological control involves the reduction of the interface area between the P3HT and PCBM domains by large aggregation causes an inefficient charge separation, especially after long-term operation. The morphology can temporally be optimized by a thermal and/or solvent annealing treatment, but it is thermodynamically unstable and changeable due to significant difference in the surface energies of P3HT and PCBM in the absence of anchoring structures between them. To remedy this problem, the ideal morphology has to be pursued by increasing the donor/acceptor interface on a 10–20 nm scale and be fixed even after a long operating time. The arrangement and direction of the morphology is also very important for the smooth and fast charge transportation to reduce recombination of the separated charges. In

order to meet the above requirements, the self-assemble behavior of BCPs may be utilized; however, the relationship between the polymer structure, morphology, and OPV performance of the BCP containing crystalline segments, such as P3HT, is not fully understood.

Recently, a series of interesting donor-acceptor BCPs was synthesized based on the living/controlled radical polymerization co-systems as already mentioned in Sect. 5.1. Yang et al. reported a photovoltaic device application using similar donor-acceptor BCPs as the processing surfactant in the BHJ system (P3HT/ PCBM) [113]. They achieved a higher PCE = 3.5 % than that in the BHJ system of P3HT/PCBM without the surfactant (PCE = 2.6 %), probably due to the construction of stable p/n phase domains. Thelakkat and coworkers synthesized another type of donor-acceptor BCP containing P3HT and perylene-bisimide-grafted polyacrylate segments based on NMP [114]. Subsequently, Ruseell, Emrick, and coworkers synthesized similar BCPs and used them in photovoltaic cells and achieved a PCE = 0.49 % which was higher than the blend system of P3HT and a perylene-bisimide-based compound (PCE = 0.4 %) [115]. Segalman et al. also reported the synthesis of similar BCPs by the combination of KCTP and ATRP polymerization together with click chemistry. Unfortunately, their photovoltaic cell performance was not high (PCE < 0.1 %) [116].

During the course of the study using BCPs in OPV applications, none of the devices have exceeded 4 % PCE by the time of our report in 2010 [117], probably due to the incorporation of unwanted insulating chains such as non-conjugated polymer segments or a long alkyl spacer for improved solubility. In addition, the synthetic strategies for rod-coil BCP s were quite complex, sometimes affording the sample with a high Ð value (>1.3). As introduced in the preceding section, the BCP containing P3HT and PVTPA segments (**29**) could be easily synthesized by the combination of the quasi-living KCTP and living anionic polymerization [101]. **29** was first investigated as surfactants for the P3HT:PCBM based BHJ OPVs, in which amorphous PVTPA segments can interact with PCBM domains to fix the P3HT:PCBM phase segregated structures without losing the charge mobility due to the triphenylamine electronically active moieties [117]. Indeed, the OPV device was fabricated with a sandwich structure of ITO/PEDOT:PSS/P3HT:PCBM:**29**/Ca/ Al. The weight ratio of P3HT:PCBM was 1:1 with a variable wt% of **29**. The OPV characteristics during the illumination of AM1.5 results are summarized in Table 2.

The PCE increased from 3.9 to 4.4 % by increasing the wt% (0–1.5 %) of **29**, whereas it decreased to 3.0 % after adding 20 wt% of **29**. The V_{oc} and FF values are almost unchanged, instead the J_{sc} values were improved from 9.7 to 11.2 (mA/cm^2) for the highest PCE. The PCE = 4.4 % based on a device using a BCP is the highest of those already reported.

The long-term stability of the devices was then elucidated by the PCE decay compared to the initial device performance after a specific time, because it is well known that the P3HT:PCBM BHJ OPV devices generally lose their performance after aging due to large aggregation of PCBM crystallites. Without **29**, the PCE decay was 28 % after 70 days of storage at room temperature and 80 % relative humidity in air. On the other hand, the PCE decay was only 11 % after 70 days of

Table 2 OPV characteristics of ITO/PEDOT:PSS/P3HT:PCBM:**29**/Ca/Al devices

wt% of **29**	J_{sc} (mA/m^2)	V_{oc} (V)	FF	PCE (%)
0	9.7	0.62	0.65	3.9
0.5	10.4	0.62	0.62	4.0
1.0	10.8	0.61	0.63	4.2
1.5	11.2	0.62	0.63	4.4
2.5	10.6	0.63	0.64	4.2
5	10.9	0.62	0.62	4.2
10	10.0	0.61	0.60	3.6
20	8.4	0.63	0.60	3.0
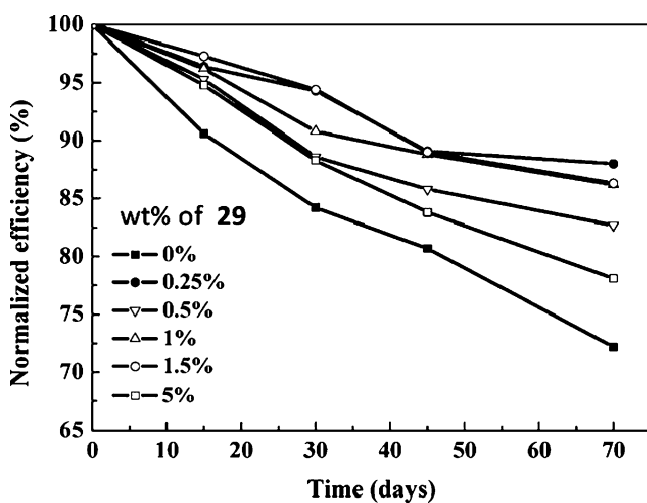
Fig. 5 Long-term stability test of ITO/PEDOT:PSS/P3HT:PCBM:**29**/Ca/Al devices

storage under the same conditions when 0.25 wt% of **29** was added to the P3HT:PCBM system (Fig. 5).

In addition, thermal stability was also tested by the PCE decay of the devices after long annealing time of 10 h at 140 °C, compared to the ones treated under normal annealing condition at 140 °C for 20 min. The similar results were obtained as long-term stability, showing that the PCE decay is only 10 % in the case of adding 10 wt% with **29**, whereas it was 41 % without **29** (Table 3).

Figure 6 shows the optical microscope images of devices with and without **29**. After the long annealing time of 10 h at 140 °C, large aggregated domains of PCBM, corresponding to a few hundred micrometers, can be seen over the whole regions. In contrast, the aggregation can significantly be suppressed by adding **29**, indicating the efficient surfactant performance of **29** in P3HT:PCBM BHJ OPV devices. This observation plus differential scanning calorimetry results [117] support the fact that the triphenylamine segments of **29** are selectively miscible in the PCBM domains to fix the phase segregated P3HT:PCBM nanostructures. Similar surfactant effects have been seen using the all-conjugated BCP, **14** [76], as well as

Table 3 Thermal stability test of ITO/PEDOT:PSS/P3HT:PCBM:**29**/Ca/Al devices

wt% of **29**	J_{sc} (mA/m^2)	V_{oc} (V)	FF	PCE (%)	PCE decay (%)
0	6.4	0.65	0.55	2.3	41
5	8.1	0.62	0.62	3.1	25
10	7.5	0.63	0.60	2.8	10
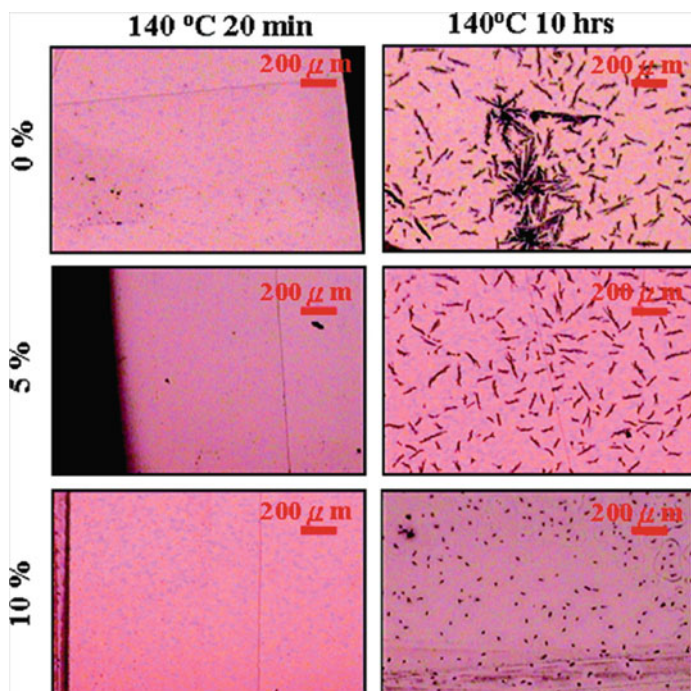
Fig. 6 Optical microscope images of ITO/PEDOT:PSS/P3HT:PCBM:**29**/Ca/Al devices

binary low molecular weight fullerene derivatives having oligothiophene units [118]. In 2012, Hadziioannou and coworkers also reported the surfactant effects of P3HT-*b*-poly(4-vinylpyridine) in the P3HT:PCBM OPV system, showing a high PCE of 4.3 % in case of 8 wt% addition. They investigated the detailed morphological properties using GIXRD experiments and concluded that the enhancement of PCE was related to the formation of a well-optimized nanoscale structure after adding the surfactant that allows for a more efficient exciton dissociation and charge transport, by lowering the charge recombination and/or trapping [119].

7.2 New Polythiophene Derivatives

In order to improve the PCE of OPV devices, the V_{oc} values should also be increased as mentioned in the preceding section. However, the HOMO energy level of P3HT is relatively high (ca −4.76 eV [120]) that limits the V_{oc} values of the OPVs to ca 0.6 V. It is well known that the modulation of the HOMO/LUMO energy levels for the polymers is essential to realize a high V_{oc} value without sacrificing the broad light harvesting and efficient charge separation, which correspond to a J_{sc} value [121]. Donor-acceptor alternating copolymers are attractive as p-type materials for OPVs due to the facile tunability of the HOMO/LUMO energy levels by properly choosing the donor and acceptor moieties. Indeed, much effort has been made to achieve very high PCEs over 7 % for the OPV devices [122–127]. 1,3,4-Oxadiazole (OXD) and 1,3,4-thiadiazole (TD) are electron-deficient units containing two electron-withdrawing imine groups (C = N) and can be used as A units. For instance, a structure similar to the benzothiadiazole units has frequently been utilized as an acceptor unit in donor-acceptor alternating copolymers to achieve high PCEs [128–133]. However, a few reports have described the OPVs using donor-acceptor alternating copolymers bearing OXD and TD units [134, 135], regardless of their electron-withdrawing nature as well as more compact structures compared to the benzothiadiazole units, which would be preferable for more densely packed structures for the polymer films to induce a high charge mobility.

Therefore, the synthesis of new donor-acceptor alternating copolymers carrying OXD or TD units, that is, **32** and **33** (see Scheme 18), was first demonstrated based on the Stille coupling reaction of 2,5-bis(trimethylstannyl)thiophene and the corresponding monomers of 2,5-bis(5'-bromo-3',4'-dihexylthien-2'-yl)-1,3,4-oxadiazole or 2,5-bis(5'-bromo-3',4'-dihexylthien-2'-yl)-1,3,4-thiadiazole, respectively [136]. Indeed, the OPV devices of **32** and **33** showed high V_{oc} values in the range of 0.80–0.90 V. The highest field-effect (FET) mobilities of **32** and **33** with the OXD and TD moieties were 1.41×10^{-3} and 8.81×10^{-2} cm^2V^{-1} s^{-1}, respectively. The higher mobility of **33** was related to its orderly nanofibrillar structure as evidenced from the TEM images. Moreover, the higher absorption coefficient and smaller band gap of **33** provided more efficient light harvest ability. The PCE of the OPV based on **33**:PCBM = 1:1 (w/w) reached 3.04 % with the J_{sc} value of 6.60 mA/cm^2, the V_{oc} value of 0.80 V, and the FF value of 0.576 under illumination of AM 1.5 (100 mW/cm^2). In comparison, the parent PDHBT (Scheme 18) [137] without the electron-accepting moiety exhibited an inferior device performance (FET mobility = 2.10×10^{-4} cm^2V^{-1} s^{-1} and PCE = 1.91 %). The experimental results demonstrated that incorporating the small electron-acceptor moiety, such as the TD unit, into the polythiophene backbone could enhance the device performance due to the low-lying HOMO levels, compact packing structure, and high charge carrier mobility. This is the first report for the achievement of a PCE > 3 % using OPVs based on polythiophenes having TD units in the main chain.
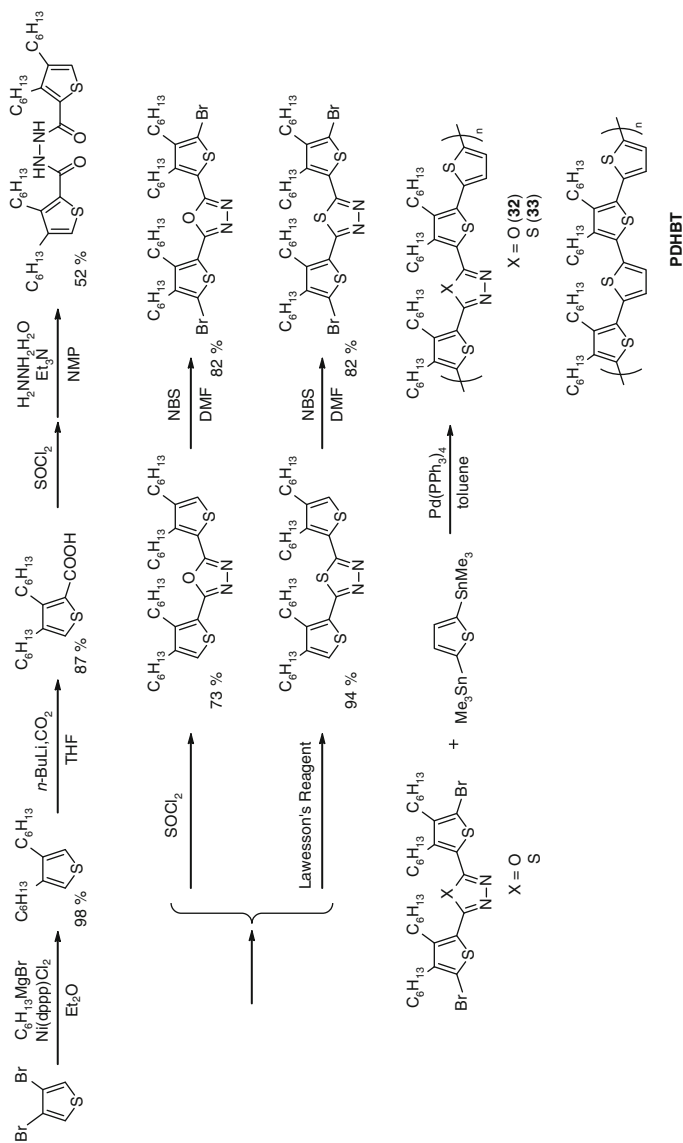
Scheme 18 Synthetic routes for **32** and **33** and the chemical structure of *PDHBT*

8   Concluding Remarks

In this chapter, recent progresses in the synthesis of BCPs containing polythiophene segments, their morphology, and representative application to organic solar cells are reviewed. In order to design and synthesize such BCPs with predictable molecular weights and low Đ values, the controlled synthesis of P3HT segment itself and the related materials (e.g., well-defined chain-end functionalized P3HT), as well as the combination with well established methodology of living anionic polymerization. Based on many efforts on controlled polymerization systems, a wide variety of BCPs containing P3HT segments have emerged. Their highly ordered nanostructures related to the primary chemical structures have become major subjects in these areas. However, the relationship between the morphology and optoelectronic properties is still not fully understood and it should be systematically clarified using a library of "well-defined" polymer samples for providing reliable and reproducible conclusions. As introduced in the latter sections, one of the most significant advantages of using a BCP in the OPV systems is its surfactant effect, in which the nano-scaled morphology of the P3HT and PCBM domains could be fixed even after long-term operation to maintain the device performance. Besides, in order to achieve a high PCE of approx. 15 % in OPV in the next 3–5 years, a breakthrough in material science and device fabrication technology must be realized. It is undoubtedly important to keep finding new materials with an efficient light harvesting property, high charge mobility, low HOMO energy level (for donors) and high LUMO level (for acceptors), and well-defined *p*-type/*n*-type morphology. In addition, tandem or more multilayer solar cells should be the candidates for achieving the very high PCE > 10 %, taking into consideration that Heeger and coworkers estimated the maximum PCE of 10 % from a single-component solar cell [138].

Abbreviations

AFM	Atomic force microscopy
BCP	Block copolymer
Đ	Dispersity
DHPS	4-(4'-*N*,*N*-dihexylaminophenylethynyl)styrene
DPE	1,1-Diphenylethylene
DPP	Diketopyrrolopyrrole
dppp	1,3-Diphenylphosphinopropane

FET	Field-effect transistor
GISAXS	Glazing incidence small angle X-ray scattering
GIWAXS	Glazing incidence wide angle X-ray scattering
HOMO	Highest occupied molecular orbital
KCTP	Kumada catalyst-transfer polymerization
LUMO	Lowest unoccupied molecular orbital
M_n	Number average molecular weight
NCTP	Negishi catalyst-transfer polymerization
NDI	Naphthalene diimide
NIR	Near-infrared
NMP	Nitroxy-mediated radical polymerization
OPV	Organic photovoltaics
OXD	1,3,4-Oxadiazole
P3HHT	Poly[3-(6-hydroxyhexyl)thiophene]
P3HT	Poly(3-hexylthiphene)
P3HT-NH$_2$	ω-Chain-end-aniline-functionalized poly(3-hexylthiphene)
P3TEGT	Poly(3-(2-(2-(2-methoxyethoxy)ethoxy)ethoxy)thiophene)
PAA	Poly(acrylic acid)
PCBM	[6,6]-Phenyl-C$_{61}$-butyric acid methyl ester
PCE	Power conversion efficiency
PEG	Poly(ethylene glycol)
PI	Polyisoprene
PMA	Poly(methyl acrylate)
PMMA	Poly(methyl methacrylate)
PMPVS	Poly(4-methylphenyl vinyl sulfoxide)
PS	Polystyrene
PS-COOH	ω-Chain-end-carboxy-functionalized polystyrene
PS-SO$_3$H	Sulfonic-acid-chain-end-functionalized polystyrene
P^{t}BMA	Poly(*tert*-butyl acrylate)
PVTPA	Poly(4-vinyltriphenylamine)
r.r.	Regioregularity
RAFT	Addition fragmentation chain-transfer polymerization
ROP	Ring-opening polymerization
TCNE	Tetracyanoethylene
TD	1,3,4-Thiadiazole
TEM	Transition electron microscopy

References

1. Krausch G, Magerle R (2002) Nanostructured thin films via self-assembly of block copolymers. Adv Mater 14:1579–1583
2. Ishizu K, Tsubaki K, Mori A, Uchida S (2002) Architecture of nanostructured polymers. Prog Polym Sci 28:27–54

3. Mori H, Mueller AHE (2003) New polymeric architectures with (meth)acrylic acid segments. Prog Polym Sci 28:1403–1439
4. Park C, Yoonand J, Thomas EL (2003) Enabling nanotechnology with self assembled block copolymer patterns. Polymer 44:6725–6760
5. Hillmyer MA (2005) Nanoporous materials from block copolymer precursors. Adv Polym Sci 190:137–181
6. Olson DA, Chen L, Hillmyer MA (2008) Templating nanoporous polymers with ordered block copolymers. Chem Mater 20:869–890
7. Hoeben FJM, Jonkheijm P, Meijer EW, Schenning APHJ (2005) About supramolecular assemblies of π-conjugated systems. Chem Rev 105:1491–1546
8. Tseng WH, Chen CK, Chiang YW, Ho RM, Akasaka S, Hasegawa H (2009) Helical nanocomposites from chiral block copolymer templates. J Am Chem Soc 131:1356–1357
9. Ho RM, Chen CK, Chiang YW (2009) Novel nanostructures from self-assembly of chiral block copolymers. Macromol Rapid Commun 30:1439–1456
10. Hsieh HL, Quirk RP (1996) Anionic polymerization: principles and applications. Marcel Dekker, New York/Basel/Hong Kong
11. Hadjichristidis N, Pitsikalis M, Pispas S, Iatrou H (2001) Polymers with complex architecture by living anionic polymerization. Chem Rev 101:3747–3792
12. Hirao A, Nakahama S (1992) Anionic living polymerization of monomers with functional silyl groups. Prog Polym Sci 17:283–317
13. Sawamoto M, Higashimura T (1990) Living polymer systems, living cationic polymerization, alkenyl. Encycl Polym Sci Eng Suppl 399–412
14. Sawamoto M (1993) The synthesis of well-defined polymers by living cationic polymerization of vinyl monomers. Trend Polym Sci 1:111–115
15. Percec V, Tomazos D (1992) Molecular engineering of side-chain liquid-crystalline polymers by living cationic polymerization. Adv Mater 4:548–561
16. Kennedy JP (1999) Living cationic polymerization of olefins. How did the discovery come about? J Polym Sci Part A Polym Chem 37:2285–2293
17. Kwon Y, Faust R (2004) Synthesis of polyisobutylene-based block copolymers with precisely controlled architecture by living cationic polymerization. Adv Polym Sci 167:107–135
18. Aoshima S, Yoshida T, Kanazawa A, Kanaoka S (2007) New stage in living cationic polymerization: an array of effective lewis acid catalysts and fast living polymerization in seconds. J Polym Sci Part A Polym Chem 45:1801–1813
19. Aoshima S, Kanaoka S (2009) A renaissance in living cationic polymerization. Chem Rev 109:5245–5287
20. Matyjaszewski K, Miller PJ, Pyun J, Kickelbick G, Diamanti S (1999) Synthesis and characterization of star polymers with varying arm number, length, and composition from organic and hybrid inorganic/organic multifunctional initiators. Macromolecules 32:6526–6535
21. Matyjaszewski K, Xia J (2001) Atom transfer radical polymerization. Chem Rev 101:2921–2990
22. Heise A, Hedrick JL, Frank CW, Miller RD (1999) Starlike block copolymers with amphiphilic arms as models for unimolecular micelles. J Am Chem Soc 121:8647–8648
23. Heise A, Hedrick JL, Trollss M, Miller RD, Frank CW (1999) Novel starlike poly(methyl methacrylate)s by controlled dendritic free radical initiation. Macromolecules 32:231–235
24. Cloutet E, Fillaut JL, Astruc D, Gnanou Y (1999) Star block copolymers and hexafullerene stars via derivatization of star-shaped polystyrenes. Macromolecules 32:1043–1054
25. Angot S, Murthy KS, Taton D, Gnanou Y (2000) Scope of the copper halide/bipyridyl system associated with calixarene-based multihalides for the synthesis of well-defined polystyrene and poly(meth)acrylate stars. Macromolecules 33:7261–7274
26. Stenzel-Rosenbaum M, Davis TP, Chen V, Fane AG (2001) Star-polymer synthesis via radical reversible addition-fragmentation chain-transfer polymerization. J Polym Sci Part A Polym Chem 39:2777–2783

27. Barner-Kowollik C, Davis TP, Heuts JPA, Stenzel MH, Vana P, Whittaker M (2003) RAFTing down under: tales of missing radicals, fancy architectures, and mysterious holes. J Polym Sci Part A Polym Chem 41:365–375
28. Bazan GC, Schrock RR (1991) Synthesis of star block copolymers by controlled ring-opening metathesis polymerization. Macromolecules 24:817–823
29. Mason AF, Coates GW (2007) Coordination polymerization: synthesis of new homo- and copolymer architectures from ethylene and propylene using homogeneous ziegler-natta polymerization catalysts. Macromol Eng 1:217–249
30. Bielawski CW, Grubbs RH (2007) Living ring-opening metathesis polymerization. Prog Polym Sci 32:1–29
31. Frenzel U, Nuyken O (2002) Ruthenium-based metathesis initiators: development and use in ring-opening metathesis polymerization. J Polym Sci Part A Polym Chem 40:2895–2916
32. Baughman TW, Wagener KB (2005) Recent advances in ADMET polymerization. Adv Polym Sci 176:1–42
33. Berda EB, Baughman TW, Wagener KB (2006) Precision branching in ethylene copolymers: synthesis and thermal behavior. J Polym Sci Part A Polym Chem 44:4981–4989
34. Webster OW (2000) The discovery and commercialization of group transfer polymerization. J Polym Sci Part A Polym Chem 38:2855–2860
35. Webster OW (2004) Group transfer polymerization: mechanism and comparison with other methods for controlled polymerization of acrylic monomers. Adv Polym Sci 167:1–34
36. Yokozawa T, Yokoyama A (2004) Chain-growth polycondensation: living polymerization nature in polycondensation and approach to condensation polymer architecture. Polym J 36:65–83
37. Yokozawa T, Yokoyama A (2007) Chain-growth polycondensation: the living polymerization process in polycondensation. Prog Polym Sci 32:147–172
38. Yokoyama A, Yokozawa T (2007) Converting step-growth to chain-growth condensation polymerization. Macromolecules 40:4093–4101
39. Miyakoshi R, Yokoyama A, Yokozawa T (2008) Development of catalyst-transfer condensation polymerization. Synthesis of π-conjugated polymers with controlled molecular weight and low polydispersity. J Polym Sci Part A Polym Chem 46:753–765
40. Yokozawa T, Ajioka N, Yokoyama A (2008) Reaction control in condensation polymerization. Adv Polym Sci 217:1–77
41. Yokozawa T, Yokoyama A (2009) Chain-growth condensation polymerization for the synthesis of well-defined condensation polymers and π-conjugated polymers. Chem Rev 109:5595–5619
42. Shibasaki Y, Ueda M (2003) Precise control of molecular weight and its distribution in polycondensation. Kino Zairyo 23:22–29
43. Di CA, Yu C, Liu YQ, Zhu DB (2007) High-performance organic field-effect transistors: molecular design, device fabrication, and physical properties. J Phys Chem B 111:14083–14096
44. Kim JY, Lee K, Coates NE, Moses D, Nguyen TQ, Dante M, Heeger AJ (2007) Efficient tandem polymer solar cells fabricated by all-solution processing. Science 317:222–225
45. Thompson BC, Fréchet JMJ (2008) Polymer-fullerene composite solar cells. Angew Chem Int Ed 47:58–77
46. Wei Q, Nishizawa T, Tajima K, Hashimoto K (2008) Self-organized buffer layers in organic solar cells. Adv Mater 20:2211–2216
47. Chen J, Cao Y (2009) Development of novel conjugated donor polymers for high-efficiency bulk-heterojunction photovoltaic devices. Acc Chem Res 42:1709–1718
48. Cheng YJ, Yang SH, Hsu CS (2009) Synthesis of conjugated polymers for organic solar cell applications. Chem Rev 109:5868–5923
49. Green MA, Emery K, Hishikawa Y, Warta W (2010) Solar cell efficiency tables. Prog Photovolt Res Appl 18:144–150

50. McCullough RD, Lowe RD (1992) Enhanced electrical conductivity in regioselectively synthesized poly(3-alkylthiophenes). J Chem Soc Chem Commun 1:70–72

51. McCullough RD, Lowe RD, Jayaraman M, Ewbank PC, Anderson DL (1993) Design, synthesis, and control of conducting polymer architectures: structurally homogeneous poly (3-alkylthiophenes). J Org Chem 58:904–912

52. Chen TA, Wu X, Rieke RD (1995) Regiocontrolled synthesis of poly(3-alkylthiophenes) mediated by Rieke zinc: their characterization and solid-state properties. J Am Chem Soc 117:233–244

53. Loewe RS, Khersonsky SM, McCullough RD (1999) A simple method to prepare head-to-tail coupled, regioregular poly(3-alkylthiophenes) using Grignard metathesis. Adv Mater 11:250–253

54. Loewe RS, Ewbank PC, Liu J, Zhai L, McCullough RD (2001) Regioregular, head-to-tail coupled poly(3-alkylthiophenes) made easy by the GRIM method: investigation of the reaction and the origin of regioselectivity. Macromolecules 34:4324–4333

55. Amou S, Haba O, Shirota K, Hayakawa T, Ueda M, Takeuchi K, Asai M (1999) Head-to-tail regioregularity of poly(3-hexylthiophene) in oxidative coupling polymerization with $FeCl_3$. J Polym Sci Part A Polym Chem 37:1943–1948

56. Yokoyama A, Miyakoshi R, Yokozawa T (2004) Chain-growth polymerization for poly (3-hexylthiophene) with a defined molecular weight and a low polydispersity. Macromolecules 37:1169–1171

57. Miyakoshi R, Yokoyama A, Yokozawa T (2005) Catalyst-transfer plycondensation. Mechanism of Ni-catalyzed chain-growth polymerization leading to well-defined poly (3-hexylthiophene). J Am Chem Soc 127:17542–17547

58. Sheina EE, Liu J, Iovu MC, Laird DW, McCullough R (2004) Chain growth mechanism for regioregular nickel-initiated cross-coupling polymerizations. Macromolecules 37:3526–3528

59. Iovu MC, Sheina EE, Gil RR, McCullough RD (2005) Experimental evidence for the quasi-"living" nature of the Grignard metathesis method for the synthesis of regioregular poly (3-alkylthiophenes). Macromolecules 38:8649–8656

60. Kobayashi M, Matsumoto Y, Uchiyama M, Ohwada T (2004) A new chemoselective anionic polymerization method for poly(N-isopropylacrylamide) (PNIPAm) in aqueous media: design and application of bulky zincate possessing little basicity. Macromolecules 37:4339–4341

61. Higashihara T, Goto E, Ueda M (2012) Purification-free and protection-free synthesis of regioregular poly(3-hexylthiophene) and poly(3-(6-hydroxyhexyl)thiophene) using a zincate complex of $^tBu_4ZnLi_2$. ACS Macro Lett 1:167–170

62. Goto E, Nakamura S, Kawauchi S, Mori H, Ueda M, Higashihara T (2014) Precision synthesis of regioregular poly(3-hexylthiophene) with low dispersity using zincate complex catalyzed by nickel with ligand of 1,2-bis(dicyclohexylphosphino)ethane. J Polym Sci Part A Polym Chem 52(16):2287–2296

63. Higashihara T, Goto E (2014) Controlled synthesis of low-polydisperse regioregular poly (3-hexylthiophene) and related materials by zincate-complex metathesis polymerization. Polym J 46:381–390

64. Wang Q, Takita R, Kikuzaki Y, Ozawa F (2010) Palladium-catalyzed dehydrohalogenative polycondensation of 2-bromo-3-hexylthiophene: An efficient approach to head-to-tail poly (3-hexylthiophene). J Am Chem Soc 132:11420–11421

65. Tamba S, Tanaka S, Okubo Y, Okamoto S, Meguro H, Mori A (2011) Nickel-catalyzed dehydrobrominative polycondensation for the practical preparation of regioregular poly (3-substituted thiophene)s. Chem Lett 40:398–399

66. Tamba S, Shono K, Sugie A, Mori A (2011) C–H functionalization polycondensation of chlorothiophenes in the presence of nickel catalyst with stoichiometric or catalytically generated magnesium amide. J Am Chem Soc 133:9700–9703

67. Yokozawa T, Adachi I, Miyakoshi R, Yokoyama A (2007) Catalyst-transfer condensation polymerization for the synthesis of well-defined polythiophene with hydrophilic side chain

and of diblock copolythiophene with hydrophilic and hydrophobic side chains. High Perform Polym 19:684–699

68. Ohshimizu K, Ueda M (2008) Well-controlled synthesis of block copolythiophenes. Macromolecules 41:5289–5294

69. Zhang Y, Tajima K, Hirota K, Hashimoto K (2008) Synthesis of all-conjugated diblock copolymers by quasi-living polymerization and observation of their microphase separation. J Am Chem Soc 130:7812–7813

70. Miyakoshi R, Yokoyama A, Yokozawa T (2008) Importance of the order of successive catalyst-transfer condensation polymerization in the synthesis of block copolymers of polythiophene and poly(p-phenylene). Chem Lett 37:1022–1023

71. Wu PT, Ren G, Li C, Mezzenga R, Jenekhe SA (2009) Crystalline diblock conjugated copolymers: synthesis, self-assembly, and microphase separation of poly (3-butylthiophene)-b-poly(3-octylthiophene). Macromolecules 42:2317–2320

72. Hollinger J, Jahnke AA, Coombs N, Seferos DS (2010) Controlling phase separation and optical properties in conjugated polymers through selenophene – thiophene copolymerization. J Am Chem Soc 132:8546–8547

73. Higashihara T, Ohshimizu K, Ryo Y, Sakurai T, Takahashi A, Nojima S, Ree M, Ueda M (2009) Synthesis and characterization of block copolythiophene with hexyl and triethylene glycol side chains. Polymer 52:3687–3695

74. Hammer BAG, Bokel FA, Hayward RC, Emrick T (2011) Cross-linked conjugated polymer fibrils: robust nanowires from functional polythiophene diblock copolymers. Chem Mater 23:4250–4256

75. Ho CC, Liu YC, Lin SH, Su WF (2012) Synthesis, morphology, and optical and electrochemical properties of poly(3-hexylthiophene)-b-poly(3-thiophene hexylacetate). Macromolecules 45:813–820

76. Lai YC, Ohshimizu K, Takahashi A, Hsu JC, Higashihara T, Ueda M, Chen WC (2011) Synthesis of all-conjugated poly(3-hexylthiophene)-block-poly(3-(4'-(3",7"-dimethyloctyloxy)-3'-pyridinyl)thiophene) and its blend for photovoltaic applications. J Polym Sci Part A Polym Chem 49:2577–2587

77. Takahashi A, Lin CJ, Ohshimizu K, Higashihara T, Chen WC, Ueda M (2012) Synthesis and characterization of novel polythiophenes with graphene-like structures via intramolecular oxidative coupling. Polym Chem 3:479–485

78. Mulherin RC, Jung S, Huetter S, Johnson K, Kohn P, Sommer M, Allard S, Scherf U, Greenham NC (2011) Ternary photovoltaic blends incorporating an all-conjugated donor–acceptor diblock copolymer. Nano Lett 11:4846–4851

79. Ku SY, Brady MA, Treat ND, Cochran JE, Robb MJ, Kramer EJ, Chabinyc ML, Hawker CJ (2012) A modular strategy for fully conjugated donor–acceptor block copolymers. J Am Chem Soc 134:16040–16046

80. Nakabayashi K, Mori H (2012) All-polymer solar cells based on fully conjugated block copolymers composed of poly(3-hexylthiophene) and poly(naphthalene bisimide) segments. Macromolecules 45:9618–9625

81. Wang J, Ueda M, Higashihara T (2013) Synthesis of all-conjugated donor-acceptor-donor ABA-type triblock copolymers via Kumada catalyst-transfer polycondensation. ACS Macro Lett 2:506–510

82. Wang J, Ueda M, Higashihara T (2014) Synthesis and morphology of all-conjugated donor-acceptor block copolymers based on poly(3-hexylthiophene) and poly(naphthalene diimide). J Polym Sci Part A Polym Chem 52:1139–1148

83. Ono RJ, Todd AD, Hu Z, Vanden BDA, Bielawski CW (2014) Synthesis of a donor–acceptor diblock copolymer via two mechanistically distinct, sequential polymerizations using a single catalyst. Macromol Rapid Commun 35:204–209

84. Jeffries-EL M, Sauvé G, McCullough RD (2004) In-situ end-group functionalization of regioregular poly(3-alkylthiophene) using the Grignard metathesis polymerization method. Adv Mater 16:1017–1019

85. Jeffries-EL M, Sauvé G, McCullough RD (2005) Facile synthesis of end-functionalized regioregular poly(3-alkylthiophene)s via modified Grignard metathesis reaction. Macromolecules 38:10346–10352

86. Bronstein HA, Luscombe CK (2009) Externally initiated regioregular P3HT with controlled molecular weight and narrow polydispersity. J Am Chem Soc 131:12894–12895

87. Fujita H, Michinobu T, Tokita M, Ueda M, Higashihara T (2012) Synthesis and postfunctionalization of rod-coil diblock and coil-rod-coil triblock copolymers composed of poly(3-hexylthiophene) and poly(4-(4'-N, N-dihexylaminophenylethynyl)styrene) segments. Macromolecules 45:9643–9656

88. Iovu MC, Jeffries-EL M, Sheina EE, Cooper JR, McCullough RD (2005) Regioregular poly(3-alkylthiophene) conducting block copolymers. Polymer 46:8582–8586

89. Iovu MC, Craley CR, Jeffries-EL M, Krankowski AB, Zhang R, Kowalewski T, McCullough RD (2007) Conducting regioregular polythiophene block copolymer nanofibrils synthesized by reversible addition fragmentation chain transfer polymerization (RAFT) and nitroxide mediated polymerization (NMP). Macromolecules 40:4733–4735

90. Craley CR, Zhang R, Kowalewski T, McCullough RD, Stefan M (2009) Regioregular poly(3-hexylthiophene) in a novel conducting amphiphilic block copolymer. Macromol Rapid Commun 30:11–16

91. Zou J, Khondaker SI, Huo Q, Zhai L (2009) A general strategy to disperse and functionalize carbon nanotubes using conjugated block copolymers. Adv Funct Mater 19:479–483

92. Urien M, Erothu H, Cloutet E, Hiorns RC, Vignau L, Cramail H (2008) Poly(3-hexylthiophene) based block copolymers prepared by Click chemistry. Macromolecules 41:7033–7040

93. Richard F, Brochon C, Leclerc N, Eckhardt D, Heiser T, Hadziioannou G (2008) Design of a linear poly(3-hexylthiophene)/fullerene-based donor-acceptor rod-coil block copolymer. Macromol Rapid Commun 29:885–891

94. Lee JU, Cirpan A, Emrick T, Russell TP, Jo WH (2009) Synthesis and photophysical property of well-defined donor-acceptor diblock copolymer based on regioregular poly(3-hexylthiophene) and fullerene. J Mater Chem 19:1483–1489

95. Radano CP, Scherman OA, Stingelin-Stutzmann N, Mueller C, Breiby DW, Smith P, Janssen RAJ, Meijer EW (2005) Crystalline-crystalline block copolymers of regioregular poly(3-hexylthiophene) and polyethylene by ring-opening metathesis polymerization. J Am Chem Soc 127:12502–12503

96. Dai CA, Yen WC, Lee YH, Ho CC, Su WF (2007) Facile synthesis of well-defined block copolymers containing regioregular poly(3-hexylthiophene) via anionic macroinitiation method and their self-assembly behavior. J Am Chem Soc 129:11036–11038

97. Higashihara T, Ohshimizu K, Hirao A, Ueda M (2008) Facile synthesis of ABA triblock copolymer containing regioregular poly(3-hexylthiophene) and polystyrene segments via linking reaction of poly(styryl)lithium. Macromolecules 41:9505–9507

98. Higashihara T, Ueda M (2009) Synthesis and characterization of a novel coil-rod-coil triblock copolymers comprised of regioregular poly(3-hexylthiophene) and poly(methyl methacrylate) segments. React Funct Polym 69:457–462

99. Moon HC, Anthonysamy A, Kim JK, Hirao A (2011) Facile synthetic route for well-defined poly(3-hexylthiophene)-*block*-poly(methyl methacrylate) copolymer by anionic coupling reaction. Macromolecules 44:1894–1899

100. Sugiyama K, Oie T, El-Magd AA, Hirao A (2010) Synthesis of well-defined $(AB)_n$ multiblock copolymers composed of polystyrene and poly(methyl methacrylate) segments using specially designed living AB diblock copolymer anion. Macromolecules 43:1403–1410

101. Higashihara T, Ueda M (2009) Living anionic polymerization of 4-vinyltriphenylamine for synthesis of novel block copolymers containing low-polydisperse poly(4-vinyltriphenylamine) and regioregular poly(3-hexylthiophene) segments. Macromolecules 42:8794–8800

102. Higashihara T, Liu CL, Chen WC, Ueda M (2011) Synthesis of novel π-conjugated rod-rod-rod triblock copolymers containing poly(3-hexylthiophene) and polyacetylene segments by combination of quasi-living GRIM and living anionic polymerization. Polymers 3:236–251

103. Lee JS, Hirao A, Nakahama S (1988) Polymerization of monomers containing functional silyl groups. 5. Synthesis of new porous membranes with functional groups. Macromolecules 21:274–276
104. Lee JS, Hirao A, Nakahama S (1989) Polymerization of monomers containing functional silyl groups. 7. Porous membranes with controlled microstructures. Macromolecules 22:2602–2606
105. Boudouris BW, Frisbie CD, Hillmyer MA (2008) Nanoporous poly(3-alkylthiophene) thin films generated from block copolymer templates. Macromolecules 41:67–75
106. Botiz I, Darling SB (2009) Self-assembly of poly(3-hexylthiophene)-*block*-polylactide block copolymer and subsequent incorporation of electron acceptor material. Macromolecules 42:8211–8217
107. Sivanandan K, Chatterjee T, Treat N, Kramer EJ, Hawker CJ (2009) High surface area poly (3-hexylthiophenes) thin films from cleavable graft copolymers. Macromolecules 43:233–241
108. Higashihara T, Takahashi A, Tajima S, Jin S, Rho Y, Ree M, Ueda M (2010) Synthesis of block copolymers consisting of poly(3-hexylthiophene) and polystyrene segments via ionic interaction and their self-assembly behavior. Polym J 42:43–50
109. Takahashi A, Rho Y, Higashihara T, Ahn B, Ree M, Ueda M (2010) Preparation of nanoporous poly(3-hexylthiophene) films based on a template system of block copolymers via ionic interaction. Macromolecules 43:4843–4852
110. Krebs FC (2010) Polymeric solar cells. DEStech Publication, Inc., Lancaster
111. Li G, Shrotriya V, Huang JS, Yao Y, Moriarty T, Emery K, Yang Y (2005) High-efficiency solution processable polymer photovoltaic cells by self-organization of polymer blends. Nat Mater 4:864–868
112. Yang XN, Loos J, Veenstra SC, Verhees WJH, Wienk MM, Kroon JM, Michels MAJ, Janssen RAJ (2005) Nanoscale morphology of high-performance polymer solar cells. Nano Lett 5:579–583
113. Yang C, Lee JK, Heeger AJ, Wudl F (2009) Well-defined donor–acceptor rod–coil diblock copolymers based on P3HT containing C60: the morphology and role as a surfactant in bulk-heterojunction solar cells. J Mater Chem 19:5416–5423
114. Sommer M, Lang AS, Thelakkat M (2008) Crystalline–crystalline donor–acceptor block copolymers. Angew Chem Int Ed 47:7901–7904
115. Zhang Q, Cirpan A, Russell TP, Emrick T (2009) Donor – acceptor poly(thiophene-block-perylene diimide) copolymers: synthesis and solar cell fabrication. Macromolecules 42:1079–1082
116. Tao Y, McCulloch B, Kim S, Segalman RA (2009) The relationship between morphology and performance of donor–acceptor rod–coil block copolymer solar cells. Soft Matter 5:4219–4230
117. Tsai JH, Lai YC, Higashihara T, Lin CJ, Ueda M, Chen WC (2010) Enhancement of P3HT/PCBM photovoltaic efficiency using the surfactant of triblock copolymer containing poly (3-hexylthiophene) and poly(4-vinyltriphenylamine) segments. Macromolecules 43:6085–6091
118. Lai YC, Higahsihara T, Hsu JC, Ueda M, Chen WC (2012) Enhancement of power conversion efficiency and long-term stability of P3HT/PCBM solar cells using C_{60} derivatives with thiophene units as surfactants. Sol Energy Mater Sol Cells 97:164–170
119. Renaud C, Mougnier SJ, Pavlopoulou E, Brochon C, Fleury G, Deribew D, Portale G, Cloutet E, Chambon S, Vignau L, Hadziioannou G (2012) Block copolymer as a nanostructuring agent for high-efficiency and annealing-free bulk heterojunction organic solar cells. Adv Mater 24:2196–2201
120. Hou JH, Tan ZA, Yan Y, He YJ, Yang CH, Li YF (2006) Synthesis and photovoltaic properties of two-dimensional conjugated polythiophenes with bi(thienylenevinylene) side chains. J Am Chem Soc 128:4911–4916

121. Scharber MC, Mühlbacher D, Koppe M, Denk P, Waldauf C, Heeger AJ, Brabec CJ (2006) Design rules for donors in bulk-heterojunction solar cells—towards 10 % energy-conversion efficiency. Adv Mater 18:789–794

122. Liang Y, Xu Z, Xia J, Tsai ST, Wu Y, Li G, Ray C, Yu L (2010) For the bright future-bulk heterojunction polymer solar cells with power conversion efficiency of 7.4 %. Adv Mater 22: E135–E138

123. Chu TY, Lu J, Beaupré S, Zhang Y, Pouliot JR, Wakim S, Zhou J, Leclerc M, Li Z, Ding J, Tao Y (2011) Bulk heterojunction solar cells using thieno[3,4-c]pyrrole-4,6-dione and Dithieno[3,2-b: 2',3'-d]silole copolymer with a power conversion efficiency of 7.3 %. J Am Chem Soc 133:4250–4253

124. Zhou H, Yang L, Stuart AC, Price SC, Liu S, You W (2011) Development of fluorinated benzothiadiazole as a structural unit for a polymer solar cell of 7 % efficiency. Angew Chem Int Ed 50:2995–2997

125. Amb CM, Chen S, Graham KR, Subbiah J, Small CE, So F, Reynolds JR (2011) Dithienogermole as a fused electron donor in bulk heterojunction solar cells. J Am Chem Soc 133:10062–10065

126. He Z, Zhong C, Huang X, Wong WY, Wu H, Chen L, Su S, Cao Y (2011) Simultaneous enhancement of open-circuit voltage, short-circuit current density, and fill factor in polymer solar cells. Adv Mater 23:4636–4643

127. Service RF (2011) Outlook brightens for plastic solar cells. Science 332:293

128. Mühlbacher D, Scharber M, Morana M, Zhu Z, Waller D, Gaudiana R, Brabec C (2006) High photovoltaic performance of a low-bandgap polymer. Adv Mater 18:2884–2889

129. Coffin RC, Peet J, Rogers J, Bazan GC (2009) Streamlined microwave-assisted preparation of narrow-bandgap conjugated polymers for high-performance bulk heterojunction solar cells. Nat Chem 1:57–661

130. Park SH, Roy A, Beaupré S, Cho S, Coates N, Moon JS, Moses D, Leclerc M, Lee K, Heeger AJ (2009) Bulk heterojunction solar cells with internal quantum efficiency approaching 100 %. Nat Photonics 3:297–302

131. Ong KH, Lim SL, Tan HS, Wong HK, Li J, Ma Z, Moh LCH, Lim SH, de Mello JC, Chen ZK (2011) A versatile low bandgap polymer for air-stable, high-mobility field-effect transistors and efficient polymer solar cells. Adv Mater 23:1409–1413

132. Zhang M, Guo X, Wang X, Wang H, Li Y (2011) Synthesis and photovoltaic properties of D–A copolymers based on alkyl-substituted indacenodithiophene donor unit. Chem Mater 23:4264–4270

133. Du C, Li C, Li W, Chen X, Bo Z, Veit C, Ma Z, Wuerfel U, Zhu H, Hu W, Zhang F (2011) 9-Alkylidene-9H-fluorene-containing polymer for high-efficiency polymer solar cells. Macromolecules 44:7617–7624

134. Umeyama T, Douvogianni E, Imahori H (2012) Synthesis and photovoltaic properties of conjugated polymer based on 1,3,4-thiadiazole unit. Chem Lett 41:354–356

135. Patil PS, Haram NS, Pal RR, Periasamy N, Wadgaonkar PP, Salunkhe MM (2012) Synthesis, spectroscopy, and electrochemical investigation of new conjugated polymers containing thiophene and 1,3,4-thiadiazole in the main chain. J Appl Polym Sci 125:1882–1889

136. Higashihara T, Wu HC, Mizobe T, Lu C, Ueda M, Chen WC (2012) Synthesis of thiophene-based π-conjugated polymers containing oxadiazole or thiadiazole moieties and their application to organic photovoltaics. Macromolecules 45:9046–9055

137. Ko S, Hoke ET, Pandey L, Hong S, Mondal R, Risko C, Yi Y, Noriega R, McGehee MD, Bredas JL, Salleo A, Bao Z (2012) Controlled conjugated backbone twisting for an increased open-circuit voltage while having a high short-circuit current in poly(hexylthiophene) derivatives. J Am Chem Soc 134:5222–5232

138. Peet J, Heeger AJ, Bazan GC (2009) "Plastic" solar cells: self-assembly of bulk heterojunction nanomaterials by spontaneous phase separation. Acc Chem Res 42:1700–1708

Part III
Consequences: Morphologies and Self-Assembled Hierarchical Structures

Block Copolymers and Miktoarm Star-Branched Polymers

Hirokazu Hasegawa

Abstract Block copolymers self-assemble to form extremely regular nanoscale microdomain structures with a variety of morphologies. The microdomain morphology depends on the chain architectures, number of components, copolymer compositions, segregation power between the components as well as the ordering processes. In this chapter how these factors affect the microdomain morphology is mentioned.

Keywords Microdomain morphology • Self-assembly • Phase diagram • Strong segregation • Diblock copolymer • Triblock terpolymer • Miktoarm star-branched polymer

Block copolymers and miktoarm star-branched polymers are composed of more than two kinds of polymer chains connected by covalent bonds linearly and radially, respectively. For example, if A and B polymer chains are linked together, AB diblock copolymer is formed. Further addition of A polymer chain at the end of B block chain results in ABA triblock copolymer. Or addition of C polymer chain at the end of B block chain results in ABC linear triblock terpolymer and further addition of D polymer chain in ABCD linear tetrablock quaterpolymer and so on (Fig. 1a). On the other hand, a variety of polymer architectures can be produced by connecting the chain ends of three or more polymer chains for miktoarm star-branched polymers (Fig. 1b).

When the segregation power between the block chains of different kinds is strong enough for block copolymers and miktoarm star-branched polymers, they segregate from each other to form a phase-separated structure. However, because of the connectivity between the block chains, large domain structures typically of the order of micron sizes observed in polymer blends cannot grow into block copolymers and miktoarm star-branched polymers. Instead, they form regular periodic domain structures of 10–100 nm size with various morphologies via self-assembly. The morphologies depend on the connectivity and relative volume of the

---

H. Hasegawa (✉)
Graduate School of Engineering, Kyoto University, 1-30 Goryo-ohara, Nishikyo-ku, Kyoto 615-8245, Japan
e-mail: hasegawa.hirokazu.3v@kyoto-u.ac.jp
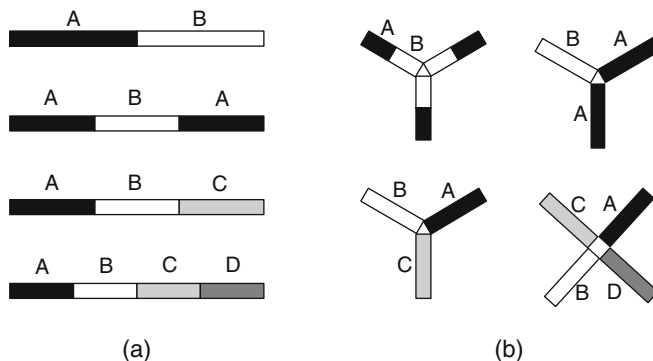
Fig. 1 Molecular architectures: (**a**) from the *top*, *AB* diblock copolymer, *ABA* linear triblock copolymer, *ABC* linear triblock terpolymer, and *ABCD* linear tetrablock quaterpolymer and (**b**) clockwise from the *top left*, (*AB*)$_3$ miktoarm star copolymer, A_2B miktoarm star copolymer, *ABCD* miktoarm star quaterpolymer, and *ABC* miktoarm star terpolymer

constituent block chains as well as the strength of the repulsive interactions between the block chains. On the other hand, the sizes of the self-assembled structures depend on the degree of polymerizations of the constituent block chains. This chapter gives the overview of the phase behavior of block copolymers and the morphologies of block copolymers and miktoarm star-branched polymers.

1 Phase Behavior of Diblock Copolymers

Block copolymers and miktoarm star-branched polymers consisting of immiscible combination of polymers self-assemble to form periodic ordered structures with sub-micron-scale (typically 10–100 nm) phases referred to as "microdomains." Let us consider the most simple case, AB diblock copolymer, where A and B block chains are linked together by a covalent bond, and overlook their phase behavior. As the segregation power between the two components of the diblock copolymer decreases, segmental mixing of them occurs and the phase transition from the ordered phase to the disordered phase (DIS) takes place as schematically illustrated in Fig. 2. This is known as "order-disorder transition (ODT)" and is observed by temperature change (usually by heating) for relatively low molecular weight block copolymer or by adding common solvent for the two components. In the disordered state (Fig. 2b), only the thermally induced concentration fluctuation exists. The segregation power can be scaled by the product of two parameters, χN, where χ is the Flory-Huggins segmental interaction parameter between the two components and N is the total degree of polymerization of the diblock copolymer. In the case of AB diblock copolymer consisting of A and B block chains having the degrees of polymerization, N_A and N_B, respectively, $N = N_A + N_B$. The reason why the segregation power is proportional to N is that an increase in entropy caused by mixing is
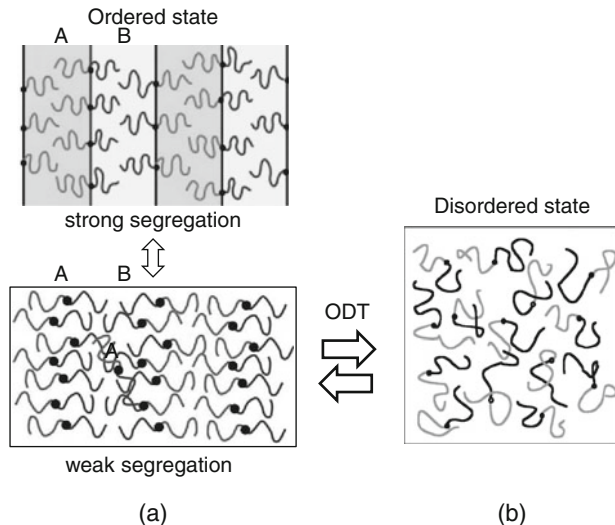
Fig. 2 Molecular packing models for (**a**) ordered state and (**b**) disordered state for diblock copolymer. Order-disorder transition (*ODT*) occurs between the disordered state and the ordered state at $\chi N = (\chi N)_c$

proportional to $1/N$ as can be seen in the Flory-Huggins theory. Usually, χ is proportional to the inverse temperature and obeys the relationship $\chi = A + BT^{-1}$, where T is absolute temperature and A and B are constants. ODT takes place when χN reaches its critical value, $(\chi N)_c$. Using random phase approximation based on the mean-field model, Leibler [1] has shown that the diblock copolymer with a symmetric composition $f = 0.5$ has the critical point at $(\chi N)_c = 10.5$ and first-order phase transition takes place for other compositions.

When $\chi N > (\chi N)_c$, A and B block chains segregate into A and B rich phases, respectively. However, due to the connectivity between A and B block chains, they cannot separate from each other to accomplish macroscopic phase separation unlike the case of the blends of A and B homopolymers. Instead, the block copolymer forms a periodic alternating A and B microdomains with a long-range order as shown for strong segregation of the ordered state in Fig. 2a. The domain size is limited by the coil size of the block chains and the domain spacing, D, is of the order of the radius of gyration of the block copolymer, which is 10–100 nm depending primarily on N or the molecular weight. The equilibrium domain spacing is attained when the enthalpic and entropic effects are balanced. The enthalpic effect originated by the repulsive interaction between A and B block chains drives D to expand by reducing the interfacial area or the area per junction between A and B block chains. Stronger the repulsive interaction, less interfacial area per block chain, resulting in stretching the block chains in the direction normal to the interface. On the other hand, the stretching of the block chains decreases the conformational entropy of the block chains. Therefore, the entropic force tends to shrink and relax

the block chains by decreasing D. Thus, the equilibrium domain spacing depends on χ and N. When the thermal noise becomes significant, especially for a block copolymer of small molecular weight at high temperatures, the ODT occurs at a stronger segregation power than the critical point predicted by the mean field theory, that is, $(\chi N)_c = 10.495 + 41.022\,N^{-1/3}$ [2]. Also, this effect has been found even at the critical point and the phase transition becomes first-order. Since the ODT temperature is very high for a block copolymer of relatively high molecular weight, it is not possible to observe the ODT by heating. However, we can reduce the segregation power by adding common good solvent for A and B components to observe the ODT in the solution system.

In the strong segregation limit of $\chi N > 100$, the fraction of each component in A and B microdomains is very close to either 1 or 0 as illustrated in the upper part of Fig. 2a. The thickness of the microdomain interface, the region where A and B block chains are partially mixed, is as small as $a\chi^{1/2}$ (a: statistical segment length) and much smaller than the domain spacing D. Theoretical predictions [3–5] of the phase diagrams for the strong segregation limit of AB diblock copolymer based on the three classical microdomain morphologies, alternating layers of A and B microdomains (lamellae, LAM), hexagonally packed cylinders (HEX), and spheres packed in body-centered cubic (BCC) lattice (schematically illustrated in Fig. 3a, d and e, respectively), showed that the morphology depends only on the copolymer composition and changes in this order as the composition deviates from the symmetrical composition (50/50) but does not depend on temperature (or χ). Hasegawa et al. [6] reported the experimental phase diagram for polystyrene-*block*-polyisoprene (SI) diblock copolymers with various compositions and molecular weights. They found that the morphology did not depend on molecular weight (or N) but changed in this order with composition and showed the composition window for each microdomain structure. In addition, they first reported the existence of composition window (the volume fraction of polystyrene component between 63 and 67 %) for the regular network morphology between the windows for lamellae and cylinders. The network morphology was first assigned to ordered bicontinuous double diamond (OBDD) but later corrected to double gyroid (or Ia$\bar{3}$d) (Fig. 3c).
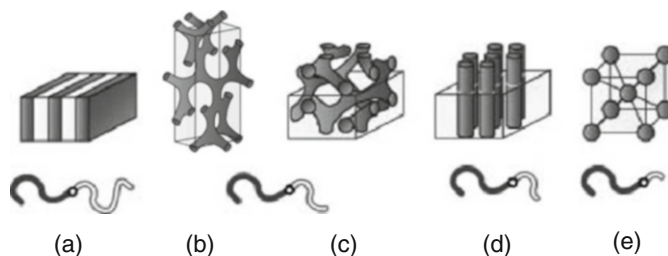
Fig. 3 Models of five equilibrium microdomain morphologies for diblock copolymers. (**a**) Lamellae (LAM), (**b**) Fddd network, (**c**) double gyroid network (Ia$\bar{3}$d), (**d**) hexagonally packed cylinders (HEX), (**e**) body-centered cubic (BCC) spheres

Fig. 4 Packing of block chains with asymmetric composition along (**a**) a flat interface and (**b**) curved interface
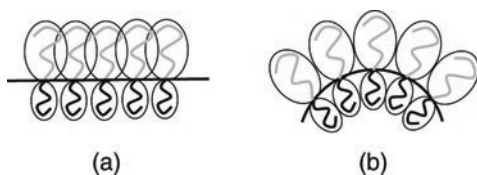
The equilibrium domain spacing D in the strong segregation limit of AB diblock copolymer is determined to balance the two conflicting effects, enthalpic and entropic, under the condition of incompressibility. By minimizing the total free energy, one can get the scaling law for the equilibrium domain spacing: $D \sim aN^{2/3}\chi^{1/6}$. The exponent 2/3 of N dependence was experimentally confirmed by the small-angle X-ray scattering (SAXS) studies of SI diblock copolymers [6–8]. There is no experimental study on the dependence of D on χ in the strong segregation limit in bulk, but there are some studies of the dependence of D on the polymer concentration ϕ_P of SI diblock copolymer solutions in neutral solvents. Hashimoto et al. [9] obtained $D \sim (\phi_P/T)^{1/3}$ for SI diblock copolymers in toluene, while Hanley and Lodge [10] reported $D \sim \phi_P^{0.32}\chi^{0.25\sim0.33}$ for SI diblock copolymer in dioctyl phthalate (DOP).

The microdomain morphology illustrated in Fig. 3a for the ordered state in the strong segregation limit is known as lamellae (LAM), where the volumes of A and B block chains are nearly symmetric. As the asymmetry in copolymer composition f (ex. $f_A = N_A/N$) is introduced and increased, the flat interfaces of lamellae become unstable because the homogeneous packing of the chain segments is no longer possible (Fig. 4a). Thus, curvature is introduced into the interfaces to fulfill the requirements of the uniform segmental distribution while keeping the balance of enthalpic and entropic effects (Fig. 4b). Consequently, the morphology changes from LAM to Fddd, Ia$\overline{3}$d, HEX and BCC with increasing the asymmetry in composition as illustrated in Fig. 3. The mean curvature of the interface increases from 0 for LAM to the maximum at BCC in this order.

In the ordered state near $\chi N = 10$, which is called the weak segregation limit, the segregation power is weak resulting in the broad concentration gradient across the microdomain interfaces due to the partial mixing of the block chains as illustrated in the lower part of Fig. 2a. It should be noted that the thermal motion of the polymer chains in the weak segregation limit is very active and the interfaces fluctuate dynamically in contrast to the strong segregation limit where the junctions of the block chains are fixed on the narrow interfaces. Therefore, the local concentration in the weak segregation limit changes from time to time. Pulling out a block chain from the related microdomain, as denoted by A in the center of the lower part of Fig. 2a, may also happen, which is not possible in the strong segregation limit. Leibler [1] predicted the microdomain morphology and the phase diagram in f vs. χN space in the weak segregation limit by comparing the free energy of Landau-Ginzburg type for the three possible morphologies: LAM, HEX, and BCC. The phase diagram first suggested the possibility of morphological transition (or order-
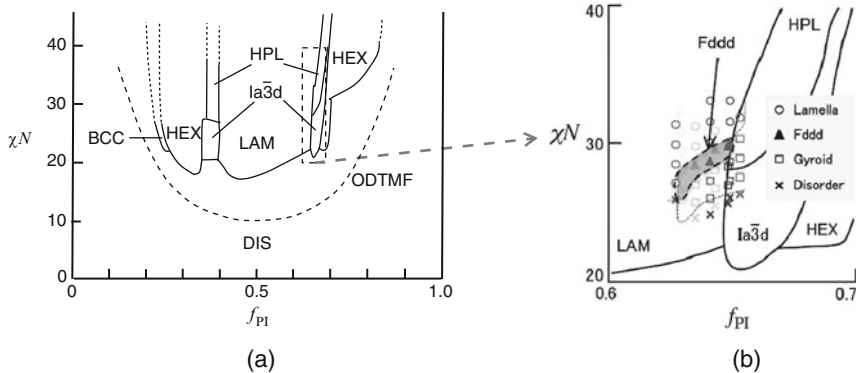
Fig. 5 Experimental phase diagrams of SI diblock copolymers in the weak segregation limit after Khandpur et al. (**a**) and Kim et al. (**b**). Phases are labeled by LAM (lamellae), HEX (hexagonally packed cylinders), HPL (hexagonally perforated layer), Ia$\bar{3}$d (double gyroid network), BCC (bcc spheres), Fddd (Fddd network), DIS (disordered state). f_{PI} is the volume fraction of polyisoprene component. Phase diagram (**b**) was obtained by minute examination of the enclosed rectangular area in phase diagram (**a**)

order transition, OOT) from LAM to HEX and then to BCC before reaching ODT with decreasing χN.

Matsen et al. [11, 12] employed self-consistent field theory (SCFT) with a mean-field model to obtain the phase diagram of diblock copolymer covering the space from weak to strong segregation limits. SCFT calculates the behavior of polymer chains assuming a single chain in the mean field obtained as the self-consisting field of many chains interacting with each other. It can predict the phase diagram, spatial concentration distribution as well as the chain conformation. A phase diagram similar to that reported by Leibler [1] was obtained. In addition, they found Ia$\bar{3}$d phase on both sides of LAM in the composition ranges between LAM and HEX for weak to medium segregation ($\chi N < 40$), but not for strong segregation. They also found close-packed spheres (CPS) phase, spherical microdomains forming a face-centered cubic lattice, in a very narrow region outside of BCC. In the strong segregation limit, the microdomain morphology depends only on composition.

Khandpur et al. [13] experimentally determined a phase diagram (Fig. 5a) of relatively low molecular weight SI diblock copolymers ($\chi N < 40$). Their result qualitatively agreed with the SCFT prediction except for some discrepancies between the theory and the experiment. SCFT predicts the morphological change from DIS to BCC, HEX, Ia$\bar{3}$d, and LAM with increasing χN for the slightly asymmetric composition near $f = 0.5$. On the other hand, the experiment showed the ODT at ca. $\chi N \sim 20$ and the transition occurred directly from the disordered state to Ia$\bar{3}$d or HEX. Moreover, CPS phase was not observed. This discrepancy was due to the fact that the SCFT calculation was performed with a mean-field model and did not take the effect of thermal noise into consideration. The asymmetry of the experimental phase diagram with respect to $f = 0.5$ is due to the difference in shape

and size of the two monomer units used for the experiment. Nevertheless, SCFT is a useful tool to predict the phase diagrams of various architectures of block copolymer, as shown in Fig. 1, for wide span of χN after the improvements such as the correction for the asymmetry of the statistical segment length and the calculations of the phase diagrams for ABA triblock copolymer and miktarm star polymer have been reported [14–16]. Besides, the experimental phase diagram introduced a new morphology, hexagonally perforated layer (HPL) phase, which has the structure of stacked layers with hexagonally located holes, as well as the OOT between $Ia\bar{3}d$ and HPL or HPL and LAM. However, later on the experiment was repeated and it was found that HPL was the metastable phase [17].

Fddd (schematically illustrated in Fig. 3b) [18–20] is another equilibrium morphology discovered recently in SI diblock copolymers with the polyisoprene-rich composition around $f_{PI} = 0.65$, where f_{PI} is the volume fraction of polyisoprene component. Fddd phase was found in the weak segregation region in the f_{PI} range between LAM and $Ia\bar{3}d$. The thermoreversible OOTs between LAM and Fddd and between Fddd and $Ia\bar{3}d$ were observed indicating Fddd is an equilibrium morphology. The Fddd window is presented by superposing on a part of the experimental phase diagram of Khandpur et al. [13] as shown in Fig. 5b. This composition window qualitatively agrees with the SCFT prediction [21]. It should be noted that the Fddd microdomain structure is stable only at elevated temperatures and cannot be observed at room temperature unless it is quenched below the glass transition temperature of the polystyrene component.

2 Analysis of Microdomain Structures

Transmission electron microscopy (TEM) has been regularly used to determine the microdomain structures of 10–100 nm domain spacing of block copolymers because the wavelength of accelerated electrons is much smaller than the wavelength of light used in optical microscopy. Since electron beam is easily absorbed by polymers even at the acceleration voltage of 100–200 kV used for commercial TEM instruments, it is necessary to prepare ultrathin sections of 100 nm thick or less, which are usually cut from bulk samples using an ultramicrotome. To obtain the contrast against electrons between two different microdomains, it is usually necessary to stain one component with a staining agent containing heavy elements such as osmium tetraoxide (OsO_4) and ruthenium tetraoxide (RuO_4) or iodine. Analyzing TEM images of microdomain structures and determining the morphology were very simple when only three classical morphologies, that is, LAM, HEX, and BCC, were known. Figure 6 shows typical TEM images for the three morphologies of SI diblock copolymers. Since polyisoprene (PI) microdomains are stained with OsO_4, which is covalently attached to the C=C double bonds of PI, they appear dark in the TEM images by absorbing electrons more than the polystyrene (PS) microdomains. TEM images in a, b, and c of Fig. 6 exhibit dark dots only, a mix of dots and lines and lines only, respectively. A simple consideration of the
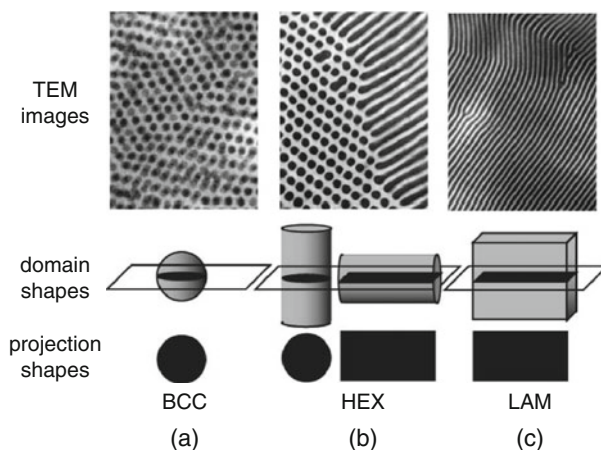
Fig. 6 From the *top*, TEM images of SI diblock copolymers, shapes of the microdomain units, and shapes of the projection of the units for the classical microdomain morphologies: (**a**) BCC, (**b**) HEX, and (**c**) LAM

projections from single microdomain model units, such as a dot for a sphere, a dot or line for a perpendicular or parallel cylinder, and a line for a perpendicular plate (lamella), provides the guess of the morphology as BCC, HEX, and LAM, respectively. However, if more than two morphologies coexist, the analysis is not so simple and additional information such as the observation by tilting the specimens is necessary. Discovery of network structures such as $Ia\overline{3}d$ [22] and Fddd [18] made the TEM analysis more difficult due to their complexity of the TEM images. Some examples of the network morphologies are shown in Fig. 7.

Small-angle X-ray scattering (SAXS) is a useful technique to investigate the structures of 1 nm or larger sizes. Hashimoto et al. [23] first demonstrated how useful SAXS technique is to analyze the microdomain structure of block copolymer in detail. Not only the domain spacing and the symmetry (or morphology), but also the volume fraction of each domain, size distribution, and interface thickness can be estimated as the fitting parameters of the scattering models. Since X-ray beam used in SAXS measurements observes much larger area of the sample than TEM, quantitative and statistical information on the microdomain structure can be obtained. In the analysis of the microdomain morphology by SAXS, scattering intensity distribution curves plotted against the magnitude of scattering vector q are useful. Here, q is defined as $q = 4\pi\sin\theta/\lambda$ where 2θ is the scattering angle and λ is the wavelength of the incident X-ray beam. Due to the crystallographic nature of the microdomain structures, Bragg reflections can be observed as the scattering intensity peaks in the SAXS intensity distribution curves. By applying Bragg's law to the q values at the scattering peaks q_m, one can evaluate the spacing d of the microdomain arrays as the crystallographic lattice spacing of the (hkl) mirror plane: $d_{hkl} = 2\pi/q_m$. If multiple peaks are obtained in a scattering curve, the relative q values of the peaks provide the key to estimate the microdomain morphologies in block copolymer because different morphologies have different crystallographic

Double Gyroid (a)   Ia$\bar{3}$d (b)   Fddd (c)
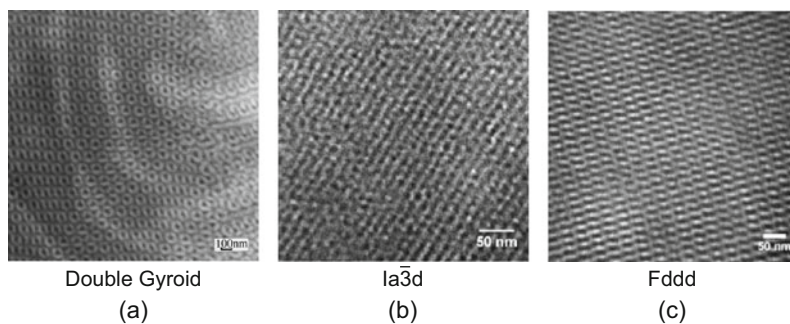
Fig. 7 TEM images of SI diblock copolymers for the network microdomain morphologies: (**a**) double gyroid network observed in a high molecular weight sample (Mn = 146 kD), (**b**) Ia$\bar{3}$d in low molecular weight sample (Mn = 24.6 kD) quenched from 170 °C, and (**c**) Fddd in the same sample as (**b**) quenched from 150 °C

Table 1 Allowed SAXS peaks for various morphologies

Morphology	Abbreviation	Peak position ratios q_1:q_2:q_3:q_4:q_5:...
Lamellae	LAM	$1:2:3:4:5:6:7\ldots$
Fddd	Fddd	$\sqrt{4}:\sqrt{6}:\sqrt{10}:\sqrt{12}:\sqrt{13}:\sqrt{15}\ldots$
Double gyroid, Ia$\bar{3}$d	Ia$\bar{3}$d	$\sqrt{3}:\sqrt{4}:\sqrt{7}:\sqrt{8}:\sqrt{10}:\sqrt{11}\ldots$
Hexagonally packed cylinders	HEX	$1:\sqrt{3}:\sqrt{4}:\sqrt{7}:\sqrt{9}:\sqrt{12}\ldots$
Spheres on the body-centered cubic lattice	BCC	$1:\sqrt{2}:\sqrt{3}:\sqrt{4}:\sqrt{5}:\sqrt{6}:\sqrt{7}\ldots$
Spheres on the face-centered cubic lattice	CPS	$\sqrt{3}:\sqrt{4}:\sqrt{8}:\sqrt{11}:\sqrt{12}:\sqrt{16}\ldots$

symmetry and, therefore, different ratios of q values at the peak positions. The ratios of q values at the peak positions for the morphologies discussed above are listed in Table 1.

The advantage of SAXS study is that one can use melt or solution samples if an appropriate sample holder is used. Therefore, Ia$\bar{3}$d and Fddd in the weak segregation regime as well as the OOT between them can be studied [18–20]. Here, it should be noted that SAXS observes the structures averaged in space and time, although the microdomain structures in the weak segregation regime are dynamic. The SAXS curves for the Ia$\bar{3}$d and Fddd exhibit many scattering peaks enough to identify the morphologies. Large numbers of the scattering peaks usually suggest highly regular structures. However, the specimens quenched from the equilibrium melt at high temperatures for TEM observation exhibit poor short-range order (poor regularity of local structures) although the long-range order is high (high symmetry in large area) as shown in the TEM images in Fig. 7b, c. This is because the TEM images represent the instantaneous shots of the dynamic structures. If the images were averaged in time, much more regular images in short-range order also should

be obtained. Therefore, it is reasonable that the structure in the weak segregation limit is called Ia$\bar{3}$d instead of double gyroid because two networks are connected dynamically. On the other hand, the double gyroid structure in the strong segregation limit obtained from the cast film of a high molecular weight SI diblock copolymer shows clear interfaces and good short-range order as shown in Fig. 7a. The feature of the two interwoven networks of double gyroid is clear. It is suggested that the factor controlling the morphology in the weak segregation limit is the wavelengths of the concentration fluctuations [18] while that in the strong segregation limit is the spontaneous interfacial curvatures [24].

The narrow composition region in the phase diagram in Fig. 5, where Ia$\bar{3}$d, Fddd, and HPL are observed, is called "complex phase window" [10] because of the geometrical complexity of the structures located between LAM and HEX. These complex structures are difficult to analyze by the conventional TEM techniques due to the overlapping of the structures through the thicknesses of the ultrathin specimens. Recently, electron tomography [25], which combines the computed tomography (CT) and TEM, has been developed to observe the 3D images of nano structures. Three-dimensional observation of the microdomain structures is a powerful tool for the analysis of not only the network structures [26] but also the miktoarm star polymers [27].

Double gyroid network structure consists of two interwoven networks as illustrated in Fig. 3c. Each network is characterized by threefold connectors. The primary element of the network is a planer tripod with three arms each forming 120° angle. Two tripods are jointed together by twisting. The network consists of 10-nord rings, that is, ten tripod elements form a ring. Each network has right- and left-handed helices in itself, but since their size and number are different, the network is chiral. However, the two networks have the shape of mirror images, and hence double gyroid structure is achiral. Double gyroid has a cubic unit cell with Ia$\bar{3}$d space group. Usually, the minor component of double gyroid forms the double network and the major component forms the matrix, which is also a network. On the other hand, Fddd is a single-network structure, though it also consists of tripod elements. The network consists of 6-nord rings. Fddd is named after its crystallographic symmetry. It has a face-centered orthorhombic unit cell with Fddd space group. The Fddd found in SI diblock copolymer [18] has the lattice constants a:b:c $= 2(3)^{1/2}$:1:2, which allows the superposition of (111), (220), and (004) reflections at the first peak position stabilizing the concentration fluctuation of the particular wavelength.

3   Linear ABC Triblock Terpolymers

Adding just one component C to the end of AB diblock copolymer gives tremendous variety and complexity to the microdomain morphologies and the phase behavior. For ABC triblock terpolymer, three different states can be possible:

Fig. 8 Microdomain structure models of linear ABC triblock terpolymers by combination of two different shapes with lamellae, cylinders, and spheres. Three morphologies with asterisks are possible for a frustrated system
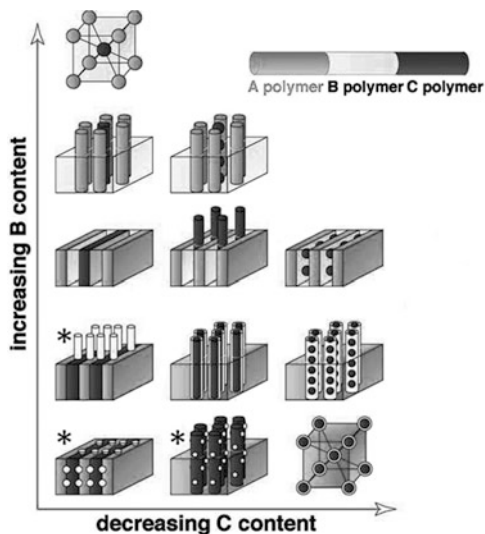
one-phase state (disordered state of mixed ABC), two-phase state (A/mixed BC, B/mixed AC, and C/mixed AB) and three-phase state (A/B/C). Here, we deal with only the three-phase state as the consequences of the phase behavior because the microdomain morphologies of the two-phase state may be similar to those of diblock copolymers. How many kinds of microdomain morphologies are possible when A, B, and C components segregate to form independent microdomains? Simple combination of three basic geometrical shapes such as planes (lamellae), cylinders, and spheres comprising LAM, HEX, and BCC morphology of diblock copolymers, respectively, can generate 12 different morphologies as illustrated in Fig. 8. The morphological variation expands further when we take into account combination with the network morphology such as Fddd and Ia$\overline{3}$d. In reality, extremely complex morphologies such as "knitting pattern" morphology [28] and "barber pattern" morphology [29], which are hard to imagine from our knowledge on the microdomain morphology of AB diblock copolymers, have been observed. Because of such wide variety of morphologies, ABC triblock terpolymers should have much better capability for applications than AB diblock copolymers if their microdomain structures can be appropriately controlled and useful functions are given to each microdomain. There are so many parameters to manipulate in case of ABC triblock terpolymers compared to AB diblock copolymers. While AB diblock copolymer is defined by three parameters, f_A, χ and N, ABC triblock terpolymer requires six parameters, f_A, f_B ($f_C = 1 - f_A - f_B$), χ_{AB}, χ_{BC}, χ_{AC}, and N in addition to the variation in block sequence (ABC, BAC, and ACB). Therefore, it is extremely difficult to complete a systematic study by changing f_A, f_B and N even for a given ABC triblock terpolymer system. Nevertheless, there are some excellent works which have been reviewed [30–34].

Fig. 9 Molecular packing and microdomain interfaces in linear *ABC* triblock terpolymers for (**a**) nonfrustrated system and (**b**) frustrated system
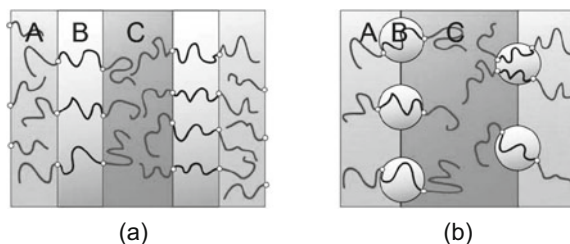
Linear ABC triblock terpolymers are classified into two groups depending on the relative strength of pair interaction parameters, χ_{AB}, χ_{BC}, and χ_{AC}. When $\chi_{AC} > \chi_{AB} \approx \chi_{BC}$, the system is "nonfrustrated" and AB and BC interfaces are formed as illustrated in Fig. 9a. On the other hand, when $\chi_{AC} < \chi_{AB} \approx \chi_{BC}$, the system is "frustrated" and AC contact is preferred to BC contact possibly resulting in coexistence of AB, BC, and AC interfaces depending on the composition as illustrated in Fig. 9b despite the fact that there are no chemical junctions on the AC interfaces. Three examples of frustrated morphologies are highlighted by asterisks in Fig. 8. Obviously, the change of the sequence order switches the frustrated system to the nonfrustrated system.

Network morphologies in linear ABC triblock terpolymers are also richer than in AB diblock copolymers [33]. Three types of equilibrium network morphologies have been known for linear ABC triblock terpolymers. They are double gyroid (Ia$\overline{3}$d), single gyroid (I4$_1$32) and Fddd. The I4$_1$32 morphology was first observed by Mogi et al. [35, 36] in polyisoprene-*block*- polystyrene-*block*-poly(2-vinylpyridine) triblock terpolymer, a nonfrustrated system, but they misinterpreted the structure as OTDD, ordered tricontinuous double diamond as in the case of OBDD. The networks in Ia$\overline{3}$d and I4$_1$32 both consist of two interwoven gyroid networks embedded in the matrix phase of the major component. The difference is that the two end blocks, A and C, form individual networks separately in the matrix phase of the middle (B) block in I4$_1$32 but two core-shell networks composed of A/B (cores of A encased in shells of B) or B/C blocks are embedded in the matrix phase of C or A component, respectively, in Ia$\overline{3}$d. Because of the spatial connectivity of each phase, the former is called "tricontinuous gyroid" or "alternating gyroid" and the latter "pentacontinuous gyroid" or "core-shell gyroid," On the other hand, Fddd has only one core-shell network embedded in the matrix phase of the major terminal block [37].

4　ABC Miktoarm Star Terpolymers

In ABC miktoarm star terpolymers as shown in Fig. 1b, three kinds of block chains share a single junction that generate a quite unique microdomain morphology completely different from that of linear ABC triblock terpolymer. In case of

Fig. 10 Molecular packing of an ABC miktoarm star terpolymer with the junctions (*circles*) on linear lines forming cylindrical microdomains of a particular type (6,6,6)
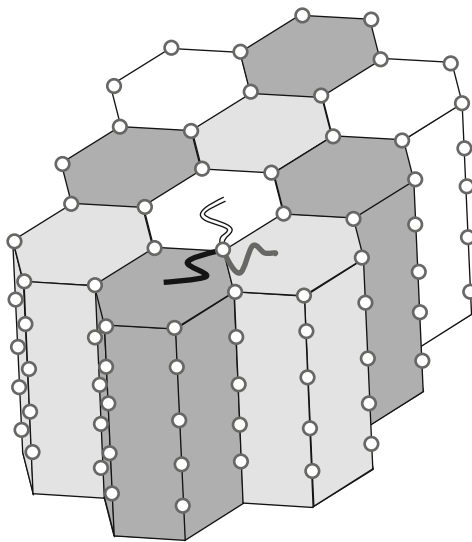
microphase separation into three phases, three different microphases of ABC miktoarm star terpolymers must meet in space to share a single line as their common intersection, as illustrated in Fig. 10, for a particular case of equal volume fraction for the three components. Thus, each microdomain has the shape similar to that of a hexagonal cylinder. The junctions are all confined on the lines where AB, BC, and AC interfaces meet. Consequently, there will be no junctions on the interfaces except for those lines at their intersections. This circumstance will not change for the asymmetric compositions with different volume fractions for A, B, and C components if the segregation power is strong enough to maintain microphase separation into three phases. For the case of asymmetric compositions, it is required for the parallel cylindrical microdomains with different volumes for A, B, and C components must fill the space in a different but regular manner. In this case, the vertical cross sections to the cylindrical axes must have the regular geometrical patterns called Archimedean tiling patterns consisting of regular polygons and there exist only eleven types as illustrated in Fig. 11 [38]. Every vertex in one type of the tilings is under the same environment and a tiling type is denoted by a set of integers standing for polygons, which meet consecutively on each vertex. For example, the tiling type of the microdomain structure as shown in Fig. 10 is (6, 6, 6) because there are three hexagons around each vertex.

Figure 12 shows the examples of the TEM images and the model patterns for two types of Archimedean tilings, (4, 8, 8) and (6, 6, 6), observed for polystyrene-polyisoprene-polydimethylsiloxane miktoarm star terpolymer. It should be noted that the sides of the polygons of the Archimedean tiling patterns would not necessarily match the microdomain interfaces. If the junctions are allocated on curved or helical lines or branched lines, the expected microdomains are not cylindrical anymore but must form an extremely complex geometry [39]. The

(3,3,3,3,3,3) (4,4,4,4) (6,6,6) (3,3,3,6)

(3,3,3,4,4) (3,4,6,4) (3,6,3,6) (3,12,12)

(4,6,12) (4,8,8) (3,3,4,3,4)
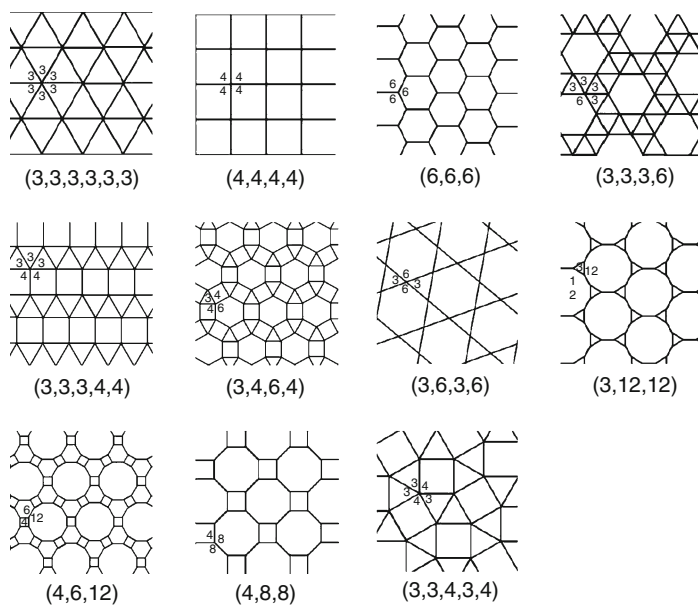
Fig. 11 Known 11 Archimedean tilings having the tessellation of regular polygons with every vertex under the same environment. A tiling type is denoted by a set of integers standing for polygons, which meet consecutively on each vertex. (3,3,4,3,4) is a quasicrystalline tiling

Fig. 12 TEM images and microdomain models of polystyrene-polyisoprene-polydimethylsiloxane miktoarm star terpolymer with Archimedean tilings of (**a**), (**b**) (4,8,8), and (**c**), (**d**) (6,6,6) types

(a) (b)

(c) (d)
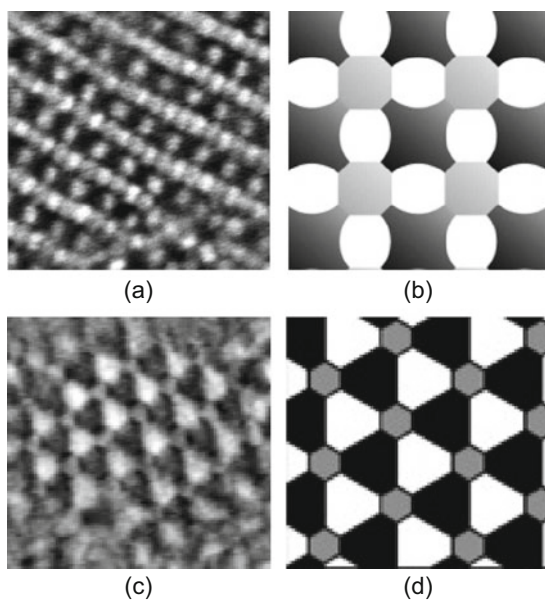
systematic studies on the microdomain morphology of ABC miktoarm star terpolymers were performed experimentally [40–42] and theoretically [43]. A variety of patterns of cylindrical microdomain morphologies have been observed by TEM.

Yamauchi et al. [27] performed 3D observation of a cylindrical morphology using electron tomography technique and pointed out that the cylinders are curved along the cylindrical axes resulting in the small grain size. The tendency of the cylinders to curve was attributed to the frustration of the block chains confined with their junctions on the lines. They thought that the addition of a small amount of homopolymer would release the frustration of the star-shaped molecules by filling the space and reducing the stretching of the block chains. In fact, they found that the grain size dramatically increased just by adding a small amount of low molecular weight homopolymer without alternating the tiling pattern [44]. The asymmetric interactions between three components such as $\chi_{AC} < \chi_{AB} \approx \chi_{BC}$ might cause partial mixing of two components. Sioula et al. [45] investigated such a system and observed core-shell cylinders, which suggests partial mixing of two components across their interfaces.

Abbreviations

BCC	Spheres packed in body-centered cubic lattice
CPS	Close-packed spheres
CT	Computed tomography
DIS	Disordered phase
Fddd	Fddd network
HEX	Hexagonally packed cylinders
HPL	Hexagonally perforated layer
$Ia\overline{3}d$	Double gyroid network
LAM	Lamellae
OBDD	Ordered bicontinuous double diamond network
ODT	Order-disorder transition
OOT	Order-order transition
OsO_4	Osmium tetraoxide
OTDD	Ordered tricontinuous double diamond network
PI	Polyisoprene
PL	Perforated layer
PS	Polystyrene
RuO_4	Ruthenium tetraoxide
SAXS	Small-angle X-ray scattering
SCFT	Self-consistent field theory
SI	Polystyrene-*block*-polyisoprene
TEM	Transmission electron microscopy

References

1. Leibler L (1980) Theory of microphase separation in block copolymers. Macromolecules 13:1602–1617
2. Fredrickson GH, Helfand E (1987) Fluctuation effects in the theory of microphase separation in block copolymers. J Chem Phys 87:697–705
3. Helfand E, Wasserman ZR (1984) Microdomain structure and the interface in block copolymers. In: Goodman I (ed) Developments in block copolymers. Applied Science, Essex
4. Semenov AN (1993) Theory of block-copolymer interfaces in the strong segregation limit. Macromolecules 26:6617–6621
5. Ohta T, Kawasaki K (1986) Equilibrium morphology of block copolymer melts. Macromolecules 19:2621–2632
6. Hasegawa H, Tanaka H, Yamasaki K, Hashimoto T (1987) Bicontinuous microdomain morphology of block copolymers. 1. Tetrapod-network structure of polystyrene-polyisoprene diblock polymers. Macromolecules 20:1651–1662
7. Hashimoto H, Shibayama M, Kawai H (1980) Domain-boundary structure of styrene-isoprene block copolymer films cast from solution. 4. Molecular-weight dependence of lamellar microdomains. Macromolecules 13:1237–1247
8. Hashimoto T, Fujimura M, Kawai H (1980) Domain-boundary structure of styrene-isoprene block copolymer films cast from solutions. 5. Molecular-weight dependence of spherical microdomains. Macromolecules 13:1660–1669
9. Hashimoto T, Shibayama M, Kawai H (1983) Ordered structure in block polymer solutions. 4. Scaling rules on size of fluctuations with block molecular weight, concentration, and temperature in segregation and homogeneous regimes. Macromolecules 16:1093–1101
10. Hanley KJ, Lodge TP (1998) Effect of dilution on a block copolymer in the complex phase window. J Polym Sci Part B Polym Phys 36:3101–3113
11. Matsen MW, Schick M (1994) Stable and unstable phases of a diblock copolymer melt. Phys Rev Lett 72:2660–2663
12. Matsen MW, Bates FS (1996) Unifying weak- and strong-segregation block copolymer theories. Macromolecules 29:1091–1098
13. Khandpur AK, Forster S, Bates FS, Hamley IW, Ryan AJ, Bras W, Almdal K, Mortensen K (1995) Polyisoprene-polystyrene diblock copolymer phase diagram near the order-disorder transition. Macromolecules 28:8796–8806
14. Matsen MW, Thompson RB (1999) Equilibrium behavior of symmetric ABA triblock copolymer melts. J Chem Phys 111:7139–7146
15. Matsen MW, Schick M (1994) Microphase separation in starblock copolymer melt. Macromolecules 27:6761–6767
16. Matsen MW (2012) Effect of architecture on the phase behavior of AB-type block copolymer melts. Macromolecules 45:2161–2165
17. Hajduk DA, Takenouchi H, Hillmyer MA, Bates FS, Vigrid ME, Almdal K (1997) Stability of the perforated layer (PL) phase in diblock copolymer melts. Macromolecules 30:3788–3795
18. Takenaka M, Wakada T, Akasaka S, Nishitsuji S, Saijo K, Shimizu H, Kim MI, Hasegawa H (2007) Orthorhombic *Fddd* network in diblock copolymer melts. Macromolecules 40:4399–4402
19. Kim MI, Wakada T, Akasaka S, Nishitsuji S, Saijo K, Shimizu H, Hasegawa H, Ito K, Takenaka M (2008) Stability of the *Fddd* phase in diblock copolymer melt. Macromolecules 41:7667–7670
20. Kim MI, Wakada T, Akasaka S, Nishitsuji S, Saijo K, Shimizu H, Hasegawa H, Ito K, Takenaka M (2009) Determination of the Fddd phase boundary in polystyrene-block-polyisoprene diblock copolymer melts. Macromolecules 42:5266–5271
21. Tyler CA, Morse DC (2005) Orthorhombic Fddd network in triblock and diblock copolymer melts. Phys Rev Lett 94:208302
22. Hajduk DA, Harper PE, Gruner SM, Honeker CC, Kim G, Thomas EL, Fetters LJ (1994) The gyroid: a new equilibrium morphology in weakly segregated diblock copolymers. Macromolecules 27:4063–4075

23. Hashimoto T, Nagatoshi K, Todo A, Hasegawa H, Kawai H (1974) Domain boundary structure of styrene-isoprene block copolymer films cast from solutions. Macromolecules 7:364–377
24. Hyde ST, Fogden A, Ninham BW (1993) Self-assembly of linear block copolymers. Relative stability of hyperbolic phases. Macromolecules 26:6782–6788
25. Frank J (2005) Electron tomography, 2nd edn. Springer, New York
26. Mareau VH, Akasaka S, Osaka T, Hasegawa H (2007) Direct visualization of the perforated layer/gyroid grain boundary in a PS-*b*-PI/PS blend by electron tomography. Macromolecules 40:9032–9039
27. Yamauchi K, Takahashi K, Hasegawa H, Iatrou H, Hadjichristidis N, Kaneko T, Nishikawa Y, Jinnai H, Matsui T, Nishioka H, Shimizu M, Fukukawa H (2003) Microdomain morphology in an ABC three-arm star-shaped triblock terpolymer: a study by energy filtering TEM and 3D electron tomography. Macromolecules 36:6962–6966
28. Breiner U, Krappe U, Stadler R (1996) Evolution of the "knitting pattern" morphology in ABC triblock copolymers. Macromol Rapid Commun 17:567–575
29. Krappe U, Stadler R, Voigt-Martin I (1995) Chiral assembly in amorphous ABC triblock copolymers. Formation of a helical morphology in polystyrene-*block*-polybutadiene-*block*-poly(methyl methacrylate) block copolymers. Macromolecules 28:4558–4561 (correction in Macromolecules 28:7583)
30. Bates FS, Fredrickson GL (1999) Block copolymer – designer soft materials. Phys Today 52:32–39
31. Abetz V, Simon PFW (2005) Phase behaviour and morphologies of block copolymers. Adv Polym Sci 189:125–212
32. Bates FS (2005) Network phases in block copolymer melts. MRS Bull 30:525–532
33. Meuler AJ, Hillmyer MA, Bates FS (2009) Ordered network mesostructures in block polymer materials. Macromolecules 42:7221–7250
34. Hasegawa H (2011) Morphologies of block and star-branched polymers having three components. In: Hadjichristidis N, Hirao A, Tezuka Y, Du Prez F (eds) Complex macromolecular architectures – synthesis, characterization, and self-assembly. Wiley (Asia), Singapore, pp 569–591
35. Mogi Y, Kotsuji H, Kaneko Y et al (1992) Preparation and morphology of triblock copolymers of the ABC type. Macromolecules 25:5408–5411
36. Mogi Y, Mori K, Matsushita Y, Noda I (1992) Tricontinuous morphology of triblock copolymers of the ABC type. Macromolecules 25:5412–5415
37. Epps TH, Cochran EW, Hardy CM et al (2004) Network phases in ABC triblock copolymers. Macromolecules 37:7085–7088
38. Ueda K, Dotera T, Gemma T (2007) Photonic band structure calculations of two-dimensional Archimedean tiling patterns. Phys Rev B 75:195122
39. Judas J, Kirkensgaard K, Hyde S (2009) Beyond amphiphiles: coarse-grained simulations of star-polyphile liquid crystalline assemblies. Phys Chem Chem Phys 11:2016–2022
40. Matsushita Y (2007) Creation of hierarchically ordered nanophase structures in block polymers having various competing interactions. Macromolecules 40:771–776
41. Matsushuta Y (2008) Precise molecular design of complex polymers and morphology control of their hierarchical multiphase structures. Polym J 40:177–183
42. Matsushita Y, Takano A, Hayashida K et al (2009) Hierarchical nanophase-separated structures created by precisely designed polymers with complexity. Polymer 50:2191–2203
43. Dotera T, Hatano A (1996) The diagonal bond method: a new lattice polymer model for simulation study of block copolymers. J Chem Phys 105:8413–8427
44. Yamauchi K, Akasaka S, Hasegawa H et al (2005) Blends of a 3-Miktoarm star terpolymer (3 μ-ISD) of isoprene (I), styrene (S), and dimethylsiloxane (D) with PS and PDMS. Effect on microdomain morphology and grain size. Macromolecules 38:8022–8027
45. Sioula S, Hadjichristidis N, Thomas EL (1998) Novel 2-dimensionally periodic non-constant mean curvature morphologies of 3-Miktoarm star terpolymers of styrene, isoprene, and methyl methacrylate. Macromolecules 31:5272–5277

Control of Surface Structure and Dynamics of Polymers Based on Precision Synthesis

Tomoyasu Hirai, Yukari Oda, David P. Penaloza Jr., Daisuke Kawaguchi, and Keiji Tanaka

Abstract Aggregation states and dynamics of polymers at the surface are generally different from those in the corresponding bulk state. To what extent they differ from that of the bulk strongly depends on the polymer primary structure. Therefore, fine-tuning the surface properties of polymers can be achieved by exhibiting control over their structure using precision polymer synthesis. We here show how the polymer design effectively impacts the structure and dynamics at the surfaces.

Keywords Surface • Interface • Aggregation states • Molecular motion

1 Enhanced Surface Mobility

1.1 General Remarks

As polymer film gets thinner, its physical properties, especially the dynamics, deviate from the corresponding bulk behaviors [1–10]. This fact is fundamentally linked to the large ratio of the interfaces against the total volume, which becomes larger with decreasing film thickness. In short, the chain mobility at the air

T. Hirai • Y. Oda
Department of Applied Chemistry, Kyushu University, Fukuoka 819-0395, Japan
e-mail: t-hirai@cstf.kyushu-u.ac.jp; y-oda@cstf.kyushu-u.ac.jp

D.P. Penaloza Jr.
Department of Chemical System Engineering, Keimyung University, Daegu 704-701, Republic of Korea
e-mail: dppenaloza@alumni.uconn.edu

D. Kawaguchi
Education Center for Global Leaders in Molecular System for Devices, Kyushu University, Fukuoka 819-0395, Japan
e-mail: d-kawaguchi@cstf.kyushu-u.ac.jp

K. Tanaka (✉)
Department of Applied Chemistry, Kyushu University, Fukuoka 819-0395, Japan

International Institute for Carbon-Neutral Energy Research (WPI-I2CNER), Kyushu University, Fukuoka 819-0395, Japan
e-mail: k-tanaka@cstf.kyushu-u.ac.jp

861

interface, so called surface, is much more enhanced in comparison with that in the bulk [11–22]. This has been confirmed in a wide range of measurements employing different characterization techniques such as angular-dependent X-ray photoelectron spectroscopy XPS [11, 12], various modes of scanning force microscopy (SFM) [13, 14], near-edge X-ray absorption fine structure [15, 16], positron annihilation lifetime spectroscopy [17, 18], optical birefringence measurement [19, 20], melting of topographic structure [21, 22], to name a few. However, in the case of the substrate interface, the chain mobility is confirmed to be opposite, where the chain becomes less active [23–28]. These concepts of the mobility of polymer chains in thin films are important in many technological applications [29–31]. Thus, a thorough understanding of interfacial properties in polymer thin films can lead to the improvement of the performance for these functional polymeric materials.

1.2   Effect of Synthetic Method

Samples of different number-average molecular weights (M_ns) of monodisperse proton-terminated polystyrenes (PSs) were synthesized by a living anionic polymerization using *sec*-butyl lithium and methanol as an initiator and a terminator, respectively [32, 33]. From these various PS samples, films were prepared and the surface mobility was examined by scanning viscoelasticity microscopy in conjunction with lateral force microscopy. The measured surface T_g (T_g^s) of each of the films is generally much lower than the corresponding bulk T_g (T_g^b) evaluated by differential scanning calorimetry (DSC). A possible explanation for the enhanced surface dynamics is that the chain end portions were found to be segregated at the air interface leading to an excess free volume in this region. This will be discussed in the later section accompanied by experimental evidences.

The choice of different polymerization techniques also yielded an interesting finding on the polymer surface properties. We have found that the surface mobility of a PS sample synthesized by free radical polymerization is different compared to a well-defined PS prepared by living anionic polymerization [34]. Figure 1 shows the schematic illustration of the surface aggregation states for PSs by living anionic and
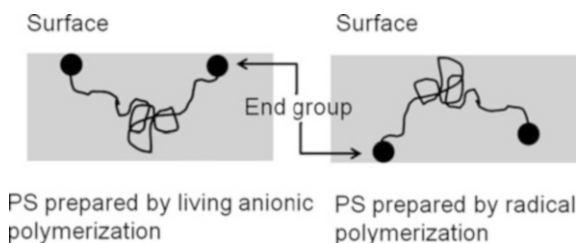
Fig. 1 Schematic illustration of the surface molecular aggregation states for PS prepared by living anionic polymerization and free radical polymerization (Reprinted with permission from (Tanaka K, Takahara A, Kajiyama T (1997) Effect of polydispersity on surface molecular motion of polystyrene films. *Macromolecules* 30:6626–6632. doi:10.1021/ma970057e). Copyright (1997) American Chemical Society)

free radical polymerizations, respectively. In these samples, all parameters were made equal except for the chain end structure and the polydispersity index (PDI) [34]. In the case of the PS mentioned above, both ends contained a *sec*-butyl fragment and a repeating unit terminated with a proton. In this case, since the surface free energy for the chain ends is smaller than that of the main chain, they are preferentially segregated at the film surface. On the other hand, when PS is synthesized by free radical polymerization using azoisobutyronitrile, redox initiator, or any other type of initiators, the hydrophilic fragments of the initiator used are incorporated into the chain ends because most of the radical chain ends are quenched during by recombination [35]. This leads to the surface depletion of the chain ends because of a higher surface free energy due to these kinds of fragments.

In addition, the molecular weight distribution of PS is larger when prepared via free radical polymerization than living anionic polymerization. Since smaller molecular weight components are generally segregated at the film surface [36, 37], this effect should be also taken into account for the observed surface dynamics [34].

1.3 Chain End Chemistry

The enhanced surface mobility can be explained in terms of the surface segregation of chain ends resulting in an excess free volume in the surface region [32, 33, 38]. To give a better understanding of this concept, well-defined polymers with polar chain ends were consequently studied.

Here, α,ω-diamino-terminated PS (α,ω-PS(NH$_2$)$_2$) and α,ω-dicarboxy-terminated PS (α,ω-PS(COOH)$_2$) in addition to proton-terminated PS (PS-H) synthesized by living anionic polymerization were used [33, 39]. Figure 2 shows the chemical structures of PS-H, α,ω-PS(NH$_2$)$_2$, and α,ω-PS(COOH)$_2$.

proton-terminated PS

α,ω-diamino-terminated PS

α,ω-dicarboxy-terminated PS
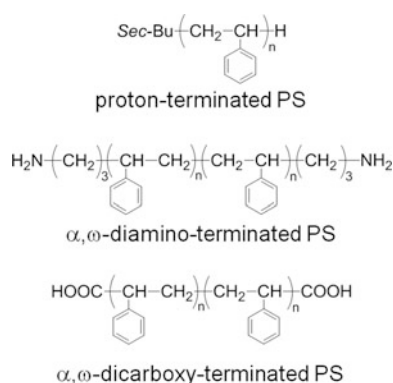
Fig. 2 Chemical structures of PS-H, α,ω-PS(NH$_2$)$_2$, and α,ω-PS(COOH)$_2$, respectively (Reprinted with permission from (Satomi N, Tanaka K, Takahara A, Kajiyama T, Ishizone T, Nakahama S (2001) Surface molecular motion of monodisperse α,ω-diamino-terminated and α,ω-dicarboxy-terminated polystyrenes. *Macromolecules* 34:8761–8767. doi:10.1021/ma010126w). Copyright (2001) American Chemical Society)
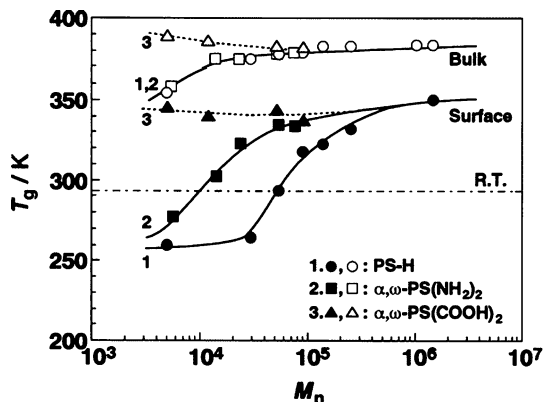
Fig. 3 M_n dependence of T_g^s and T_g^b for the PS with various chain end groups. The *filled* and *open* symbols denote T_g^s and T_g^b, respectively (Reprinted with permission from (Satomi N, Tanaka K, Takahara A, Kajiyama T, Ishizone T, Nakahama S (2001) Surface molecular motion of monodisperse α,ω-diamino-terminated and α,ω-dicarboxy-terminated polystyrenes. *Macromolecules* 34:8761–8767. doi:10.1021/ma010126w). Copyright (2001) American Chemical Society)

Figure 3 shows the effect of M_n and chain end groups on T_g^s. As a general trend, T_g^s is much lower than the corresponding T_g^b at a given molecular weight. Also, T_g^s has a stronger M_n dependence than T_g^b. The T_g^s value depends on the chain end chemistry at a given M_n, as will be later discussed. Further, the extent of the T_g depression at the surface is more striking for PS terminated with hydrophobic groups. Thus, it is no doubt that the chain end segregation is one of the factors for the observed T_g depression at the surface. A possible explanation for the enhanced surface dynamics is that chain end portions are segregated at the air interface leading to an excess free volume. However, even at ultrahigh M_n being larger than 1,000 k, where in this case the chain end effect is deemed negligible, the T_g^s is still lower than the T_g^b. This only means to suggest that the chain end effect alone cannot entirely account for the enhanced mobility at the surface [32]. It is noteworthy that the film surface is already in a glass-rubber transition or rubbery state at room temperature in the case of M_n smaller than approximately 40 k.

The surface free energy of the end-amino groups is larger than that of the main chain part. This implies that the chain ends should be depleted in the surface region. Actually, this was what was observed by XPS, a surface sensitive technique at a depth range of down to 10 nm. If this is the case, the excess free volume induced by chain ends would not contribute significantly to the mobility in the surface region probed by SFM. Thus, the extent of the T_g^s depression is milder for PS with higher surface energy ends than for PS with hydrophobic end groups at a given M_n, as seen in Fig. 3.

In contrast to the PS-H and α,ω-PS(NH$_2$)$_2$, the M_n dependence of T_g^s as well as T_g^b for α,ω-PS(COOH)$_2$ is not so clear. Since the α,ω-PS(COOH)$_2$ chains are intermolecularly associated between carboxyl groups at the chain ends via hydrogen bonding, the apparent M_n of the α,ω-PS(COOH)$_2$ increases in comparison with the original M_n. The intermolecular association between carboxyl groups was confirmed by Fourier-transform infrared spectroscopy. Hence, it is difficult to

discuss about the M_n dependence of T_g^s and T_g^b for the α,ω-PS(COOH)$_2$. In any event, chain end chemistry is one of the responsible factors influencing the magnitude of T_g^s. Thus, it can be concluded that the precision synthesis can control the surface mobility of polymers in films without changing M_n.

2 Surface Segregation in Polymer Blends

2.1 General Remarks

The aggregation states of polymers at the air interface are often different from those in its interior bulk region. For example, in the case of symmetric miscible mixtures of two polymers, studies revealed that the lower surface energy component is enriched at the surface [40–42]. Also, the concentration profile near the surface can be well expressed by mean-field and self-consistent mean-field models [43–45]. This can be simply understood by taking into account the thermodynamics at the air interface; that is, the lower surface energy component energetically prefers to come in contact with the zero surface energy medium such as air. However, depending on the intended technological applications of polymeric materials, sometimes the surface segregation of a higher surface energy component in the blends might be desired [46, 47]. Hence, to design and construct highly functionalized polymer surfaces, it is crucially important to explore how the surface properties can be controlled without changing the bulk structure and properties. This can be also made on the basis of the precision synthesis of polymers, especially chain end chemistry, as will be discussed below.

2.2 Surface Segregation

A pair of PS and poly(vinyl methyl ether) (PVME) has been widely studied as a complete miscible mixture at room temperature [48]. PVME having a much lower surface energy than PS by 7 mJ m^{-2} was preferentially segregated at the surface [40, 42]. Here, we focused our study on the surface region of the PS/PVME blend system [48]. At first, the surface segregation in blend films composed of monodisperse PS and fractionated PVME is shown on the basis of XPS. Then, we present how the chemical composition at the surface in the PS/PVME blend films can be controlled.

Figure 4 shows the average volume fraction of PVME within a given analytical depth, ϕ_{ave}, in symmetric dPS/PVME blend films with various M_n pairs as a function of sin θ. Here, θ is the take-off-angle of photoelectrons for the XPS measurement. Since the analytical depth of XPS is given by $3\lambda/\sin \theta$, where λ is the mean-free path of photoelectrons in the film, the abscissa corresponds to the depth. The term *symmetric* means that the degrees of polymerization, N, for both the components are almost the same. Also, dPS was used instead of PS so that the surface composition in the blend films obtained by XPS can be directly compared
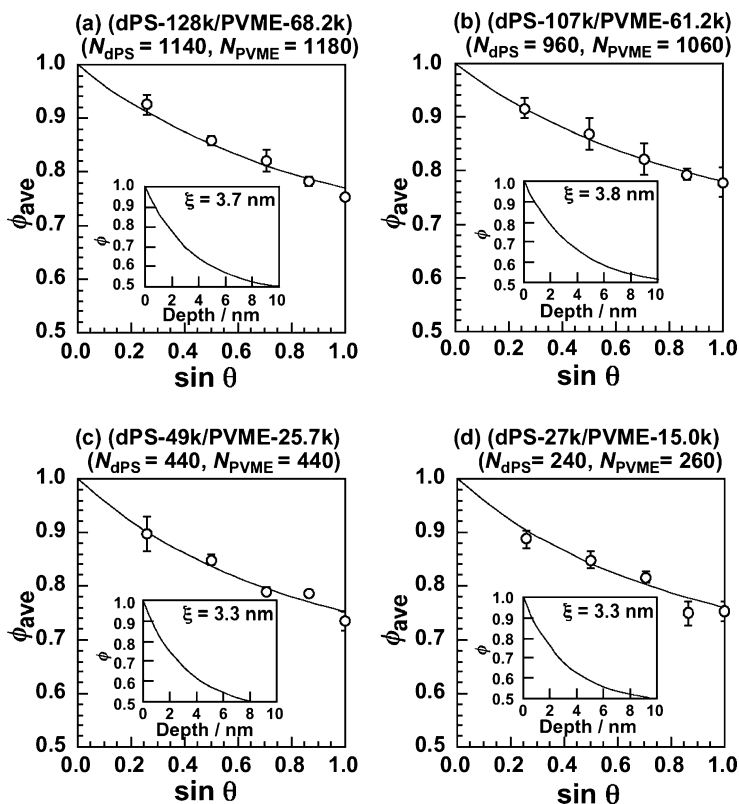
Fig. 4 Sin θ dependence of average PVME volume fraction for symmetric dPS/PVME blend films with different M_n pairs. (**a**) dPS-128k/PVME-58.2k, (**b**) dPS-107k/PVME-61.2k, (**c**) dPS-49k/PVME-25.7k, and (**d**) dPS-27k/PVME-15.0k, respectively. The abscissa of sin θ corresponds to the analytical depth. *Open circles* are the experimental data, and *solid curves* in the main panels denote the best-fit ones. The *insets* show real composition profile in the surface region deduced by a mean-field approximation using the XPS data (Reprinted with permission from (Kawaguchi, Tanaka K, Kajiyama T, Takahara A, Tasaki S (2003) Surface composition control via chain end segregation in blend films of polystyrene and poly(vinyl methyl ether). *Macromolecules* 36:6824–6830. doi:10.1021/ma034117u). Copyright (2003) American Chemical Society)

with the results obtained by other methods such as secondary ion mass spectrometry and neutron reflectivity (not shown in this review). For all films studied, ϕ_{ave} increased with decreasing sin θ, meaning that the PVME component was gradually enriched toward the surface. However, such increase is not sensitive to change in M_n namely, the degree of polymerization, N, as long as symmetric blends (same M_n for the components) were prepared. The ϕ_{ave} vs. sin θ relation can somehow be converted to the composition profile in the real space after some calculations [48]. Each inset depicts the corrected composition profile in the surface region down to 10 nm. Here, the outermost surface of the dPS/PVME blend films is ensured to be completely covered with the lower surface energy component of PVME being independent of N.

2.3 Chain End Chemistry

In studying the effect of chain end chemistry, we introduced lower surface energy fluoroalkyl groups (R_f) into both ends of PS by living anionic polymerization, hereafter, designated as α,ω-PS$(R_f)_2$. The surface properties of the α,ω-PS$(R_f)_2$/PVME blends were then investigated. Figure 5 shows the analytical depth dependence of surface PVME fraction for the symmetric α,ω-PS$(R_f)_2$/PVME blend films as a function of N. The dotted line denotes the PVME volume fraction in the bulk. Two blend systems were considered: α,ω-PS$(R_f)_2$ having an M_n of 157 k/PVME (M_n of 87.7 k); and α,ω-PS$(R_f)_2$ (M_n of 47.8 k)/PVME (M_n of 28.9 k). The surface PVME fraction was higher than the bulk value and was invariant with respect to sin θ, implying that there exists a uniform PVME-rich layer in the measured depth region. Also, the surface composition is almost equivalent to the bulk one for the α,ω-PS$(R_f)_2$ with M_n of 25.2 k/PVME with M_n of 12.5 k film. That is, no surface enrichment took place for this blend film. These results were, however, inconsistent with the prediction of the mean-field theory. Since the surface PVME fraction decreased with decreasing N, or increasing number density of R_f chain ends, it is conceivable that the surface enrichment of PVME was suppressed by the presence of R_f chain end groups.

XPS results revealed that even in the α,ω-PS$(R_f)_2$/PVME blend films, the R_f end groups are almost perfectly localized at the surface due to the lowest surface energy in the system. Since the PS segments are directly connected to the R_f groups, they are inevitably pulled out from the surface. This is as though the chain ends behave like floating buoys for the PS segments [49]. Assuming that this is valid, the extent by which the PVME component is enriched at the surface should be inversely
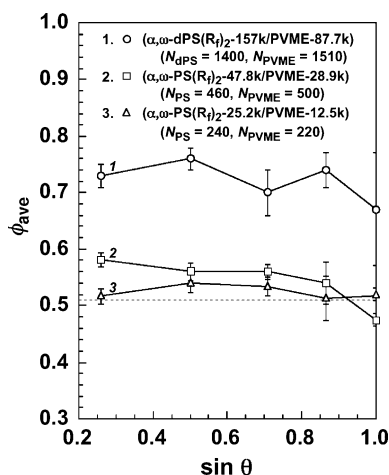
Fig. 5 Sin θ dependence of surface PVME fraction for symmetric α,ω-PS$(R_f)_2$/PVME blend films with different M_n pairs (Reprinted with permission from (Kawaguchi D, Tanaka K, Kajiyama T, Takahara A, Tasaki S (2003) Surface composition control via chain end segregation in blend films of polystyrene and poly(vinyl methyl ether). *Macromolecules* 36:6824–6830. doi:10.1021/ma034117u). Copyright (2003) American Chemical Society)

proportional to the number density of the R_f chains ends, namely N. This is strongly supported by the data in Fig. 5. Hence, it seems reasonable to conclude that the suppression of the PVME fraction at the surface in the α,ω-PS(R_f)$_2$/PVME films is connected to the surface localization of the R_f chain ends. The results presented here satisfactorily support our claim that the surface chemical composition in polymer blends can be somehow controlled by structurally modifying one of the components by chain end chemistry.

Although the chemical modification of the chain ends of PS is quite effective to control the surface composition in the blends, using such approach to achieve the surface segregation of the PS component is not satisfactory enough. Hence, a study of the effect of molecular weight disparity between components combined with chain end chemistry was also conducted. A low molecular weight component is generally enriched at the surface [36, 37], which can be attributed to conformational entropy loss and localization of chain ends at the surface. Figure 6 shows the relation of $\sin \theta$ versus surface composition for asymmetric α,ω-PS(R_f)$_2$ with M_n of 10.2 k/PVME with M_n of 77 k ($N_{PS} = 90$, $N_{PVME} = 1,330$) blend film. Interestingly, the PVME fraction decreased with decreasing $\sin \theta$, meaning that the PS segments were enriched at the surface and that the concentration asymptotically reached the bulk value with increasing depth. On the other hand, in the case of asymmetric PS with M_n of 10.2 k/ PVME with M_n of 77 k film, the surface PVME fraction is still higher than the bulk value, although the extent is also suppressed (not shown). Hence, the surface segregation of the PS component could only be attained through the combination of chain end chemistry and molecular weight disparity. The results clearly support our claim that the surface composition in miscible binary polymer mixtures can be effectively regulated by chain end chemistry.
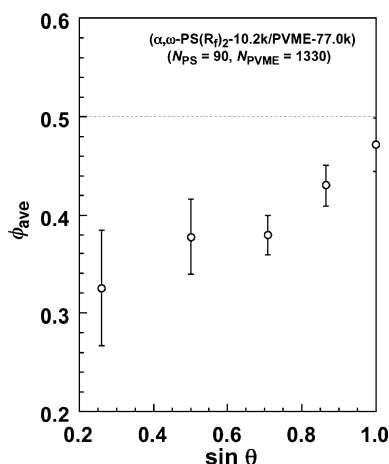
Fig. 6 Sin θ dependence of surface PVME fraction for asymmetric α,ω-PS(R_f)$_2$-10.2 k/ PVME-77.0 k blend film (Reprinted with permission from (Kawaguchi D, Tanaka K, Kajiyama T, Takahara A, Tasaki S (2003) Surface composition control via chain end segregation in blend films of polystyrene and poly(vinyl methyl ether). *Macromolecules* 36:6824–6830. doi:10.1021/ma034117u). Copyright (2003) American Chemical Society)

3   Interfacial Chain Conformation

3.1   General Remarks

Today, there are numerous technological applications where polymers are interfaced with water such as in the case of polymers used in filtration membranes, biomedical devices, fuel cells, implants, etc. [50, 51]. In such applications, the performance of these devices is strongly related to the aggregation states and dynamics of the polymers at the interfaces. Crucially important as well is the structure of water surrounding the polymer chains. Obviously, these interactions between the components, both from the perspective of the polymer and the water environment at the interface are essential in the design and construction of such devices [52, 53]. However, our knowledge of polymer interfaces with liquids, including water, is still lacking in as far as the general level of understanding of the aggregation states and dynamics of polymers.

Poly(methyl methacrylate) (PMMA), a glassy polymer at room temperature, has been widely used in membranes for water filtration and dialysis [54, 55], artificial lenses in ophthalmology [56, 57], biotips in micro-total-analysis (μ-TAS) systems [58, 59]. The stereoregularity of PMMA has been found to significantly affect its physical properties [60–62]. For instance, we have shown that the isotactic-PMMA (i-PMMA) and syndiotactic-PMMA (s-PMMA) despite having the same chemical structure for their repeating units and only differ in the connectivity for the sequential units, exhibited different local conformation at the air and water interfaces, as shown below. Both samples were prepared by anionic polymerization.

3.2   Surface Conformation

To probe the local conformation of these polymers, sum-frequency generation (SFG) vibrational spectroscopy that possesses the best depth resolution among available techniques at the moment and capable of probing structures at depths better than 1 nm [63–65], was applied. Here, three repeating units for each stereoregular isomer were taken into account [66]. Figure 7 shows the schematic representation of possible local conformations for i-PMMA with (a) *trans-trans* and (b) *trans-gauche* backbone conformations at the air interface. Spheres in red, green, and white correspond to oxygen, carbon, and hydrogen atoms, respectively. Also, spheres and bonds in yellow represent the methylene backbone. Based on the SFG spectra, the *trans-gauche* backbone conformation is more likely for i-PMMA.

If the main chain is distorted along the chain axis, the steric repulsion among side chains, especially involving the ester groups, becomes less. While the repulsion becomes less, the results of theoretical calculations show that the steric repulsion among the ester groups of a PMMA chain cannot be simply ignored [67]. Hence, it seems reasonable to assume that i-PMMA does not take the well-defined *trans-trans* backbone conformation, but instead leads to a slight different
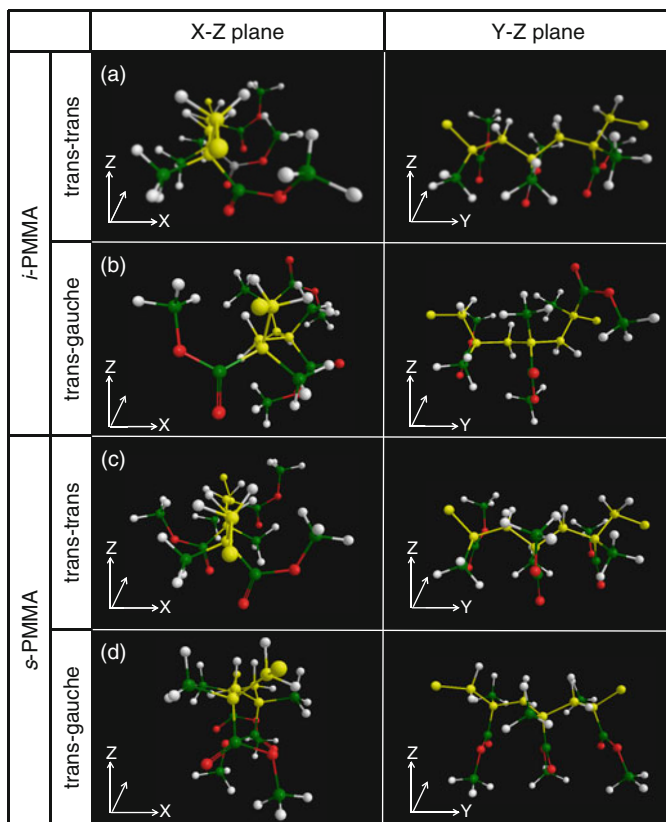
Fig. 7 Schematic illustration of models for *i*-PMMA formed by (**a**) *trans-trans* and (**b**) *trans-gauche* backbone conformation and for *s*-PMMA formed by (**c**) *trans-trans* and (**d**) *trans-gauche* backbone conformation at the air interface. *Left* and *right* columns correspond to the X–Z and Y–Z planes, respectively. The *red*, *green*, and *white spheres* denote oxygen, carbon, and hydrogen atoms, respectively. *Yellow spheres* and *bonds* represent the main chain part (Horinouchi A, Tanaka K (2013) An effect of stereoregularity on the structure of poly(methyl methacrylate) at air and water interfaces. *RSC Adv*. 3:9446-9452. doi:10.1039/c3ra40631h]-Reproduced by permission of The Royal Society of Chemistry)

form with some degree of distortion. In the case of the *trans-gauche* backbone conformation, all of the functional groups are not oriented in one direction, or in the interfacial plane, as shown in panel (b). This suggests that the hydrophilic carbonyl groups can be also oriented to the air phase.

The local conformation of *s*-PMMA at the air interface is also discussed. In the case of the *trans-trans* backbone conformation, the methylene groups of *s*-PMMA orient along the direction normal to the interface, as shown in the panel (c) of Fig. 7. On the other hand, in the case of the *trans-gauche* backbone conformation, the methylene groups orient along the direction almost parallel to the air interface, as shown in panel (d). SFG results suggest that *s*-PMMA chains are in the *trans-trans* as well as the *trans-gauche* backbone conformations at the outermost interface with air. Also, it is noteworthy that both backbone conformations have the hydrophobic

functional groups, methylene, α-methyl, and ester methyl groups, oriented toward the air interface. As a consequence, s-PMMA is more hydrophobic than i-PMMA, as confirmed by the water contact angle measurement.

3.3   Interfacial Conformation at Water Interface

The SFG spectrum for i-PMMA at the water interface is quite similar to the one at the air interface in shape, meaning that the local conformation of i-PMMA at the outermost region may not be much altered under the water phase. That is, similar to the conformation at the air interface, the main chain part of i-PMMA is minimally oriented at the water interface, with ester methyl groups oriented along the direction normal to the water interface and α-methyl groups oriented almost parallel to the interface. As previously stated, the hydrophilic carbonyl groups might be oriented at the air interface. Considering these things, although the outermost region comes in contact with water, the PMMA chains do not have to undergo a significant conformational change to form attractive interactions with water molecules via hydrogen bonds. The air-facing surface of s-PMMA is covered with hydrophobic groups, as already stated. Thus, to form hydrogen bonds between carbonyl groups with water molecules, the side chains have to turn over. This could only be possible if the main chain part is randomized. This scenario is strongly supported by the corresponding SFG spectra.

We here discuss the local conformation of PMMA with three monomer units, this time at the water interface. Figure 8 illustrates a model for i-PMMA and s-PMMA with the *trans-trans* and *trans-gauche* backbone conformations at the water interface. The carbonyl groups of i-PMMA strongly bond to water molecules as well as other carbonyl groups. When the triad of i-PMMA is in the *trans-trans* conformation, carbonyl groups could efficiently orient to the water phase, as shown in panel (a). However, such a conformation is not energetically preferable at the air interface. Thus, if i-PMMA chains were to adopt the *trans-trans* conformation, hydrophilic carbonyl groups should orient to the internal direction at the air interface and then turn around toward the water phase. However, this is not consistent with the experimental result discussed above. Another possibility is for the local conformation of i-PMMA at the water interface assumes a helical structure due to a *trans-gauche* conformation with some degree of backbone distortion and/or of *trans-trans* conformation. In this case, a clear surface reorganization caused by water may not have occurred. This is because the carbonyl groups at the outermost region, which are already oriented toward the interface even without water, could easily bind water molecules once the film surface comes in contact with water. This latter explanation complements our experimental results. Thus, the most plausible conformation of i-PMMA should be the one shown in panel (b) of Fig. 7. On the other hand, s-PMMA is in the *trans-trans* conformation at the air interface. Thus, once the film comes in contact with water, the carbonyl groups turn around to orient toward the water phase so that they form hydrogen bonds with water. To do so, hydrophobic ester methyl groups simultaneously turn toward the internal direction, as shown in panel (c). This results in a more preferable stable form due to a decrease
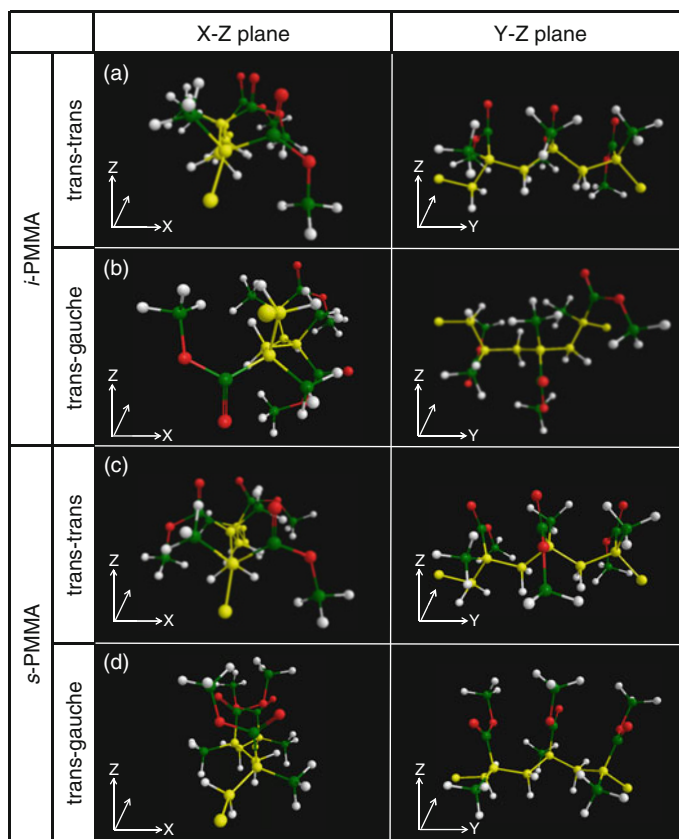
Fig. 8 Schematic illustration of models for *i*-PMMA formed by (**a**) *trans-trans* and (**b**) *trans-gauche* backbone conformation and for *s*-PMMA formed by (**c**) *trans-trans* and (**d**) *trans-gauche* backbone conformation at the water interface. *Left* and *right* columns correspond to the X–Z and Y–Z planes, respectively. The *red*, *green*, and *white spheres* denote oxygen, carbon, and hydrogen atoms, respectively. *Yellow spheres* and *bonds* represent the main chain part (Horinouchi A, Tanaka K (2013) An effect of stereoregularity on the structure of poly(methyl methacrylate) at air and water interfaces. *RSC Adv*. 3:9446-9452. doi:10.1039/c3ra40631h]-Reproduced by permission of The Royal Society of Chemistry)

in interfacial free energy. Thus, it can be claimed that the precision polymerization can control the local conformation of polymers at the interface.

4 Water Structure Induced by Polymer Interface

4.1 General Remarks

The interaction of polymers in aqueous environments plays a crucial role in several important chemical, physical, and biological areas of interest such as coatings, self-assemblies, and biocompatibility of polymeric implants, to name a few. In

bio-related applications, the quantity of polymers used for medical diagnosis continually increases [50, 51]. New tools for tailor-made diagnostics, such as arrays and tips for μ-TAS, are generally made from polymers [58, 59]. In addition, biomedical devices such as catheters and heart-lung machines improve the quality of human life. In these applications, the polymer surface is in contact with the body fluid mainly composed of water. Thus, the fundamental interactions of the polymer with water should be addressed as the first benchmark for the design and construction of highly functionalized μ-TAS tips as well as safe and long term-usable biomedical devices [68–70]. Despite the importance of this issue, little is known about controlling factors of the primary structure of the polymer on the properties of the water interface. We here show how the primary structure of polymers can regulate aggregation states of water molecules at the interface.

4.2 Water Structure at PMMA Interface

So far, we present that the local conformation of PMMA is dependent on its stereoregularity. Given that water molecules interact with the hydrophilic portion of PMMA, the aggregation states of water at the PMMA interface should depend on the polymer tacticity. Figure 9 shows the SFG spectra in the O-H vibration region for water on *i*- and *s*-PMMA with the *ssp* polarization combination, which enables us to gain direct access to the information along the direction normal to the interface. The shape of the SFG spectrum on *i*-PMMA significantly differs from the one on *s*-PMMA. According to published reports, the peaks around 3,150, 3,600 and 3,750 cm^{-1} are assigned to the O-H vibration of ice-like water, of highly ordered water molecules, and of free water, respectively [71–73]. The peak around 3,150 cm^{-1} is clearly observed both on PMMA, and its intensity in the two
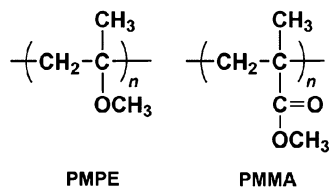
Fig. 10 Chemical structures of PMPE and PMMA, respectively (Reprinted with permission from (Oda Y, Horinouchi A, Kawaguchi D, Matsuno H, Kanaoka S, Aoshima S, Tanaka K (2014) An effect of side-chain carbonyl groups on the interface of vinyl polymers with water. Langmuir 30:1215–1219. doi:10.1021/la404802j). Copyright (2014) American Chemical Society)

conformations differs. Generally, it has been widely accepted that water molecules easily form hydrogen bonds among themselves near the hydrophobic domains, resulting in the formation of an ice-like structure at the interface. In the case of *i*-PMMA, a helical conformation is assumed by the polymer, even in water. Thus, nanoscopic hydrophobic domains could be formed at the water interface. For *s*-PMMA, the α-methyl groups are aligned along the direction parallel to the water interface, leading to the formation of hydrophobic domains at a sub-nanometer scale at the water interface. The size of the hydrophobic domains is a particularly challenging topic that cannot be readily investigated by SFG. However, assuming that the domain size in *i*-PMMA is smaller than that in *s*-PMMA, the difference in the peak intensity between *i*- and *s*-PMMA can be rationalized.

4.3 Effect of Water Structure at PMMA Interface

An effect of side chain carbonyl groups presence on the water structure at the polymer interface is finally discussed [74]. Here, poly(methyl 2-propenyl ether) (PMPE), structurally similar to PMMA except for the absence of a carbonyl group, synthesized by a base-assisting living cationic polymerization is used [75, 76]. Figure 10 shows the chemical structures of PMPE and PMMA. SFG spectroscopy revealed that although the polar methoxy groups of PMPE is favorably toward the D_2O phase, the extent of the side chain ordering for PMPE is not as striking as that for PMMA. Figure 11 shows the SFG spectra in the O-H vibration region for PMPE and PMMA with the *ssp* polarization combination. The peaks around 3,150, 3,450, 3,600 and 3,750 cm^{-1} are assignable to the O-H vibration of ice-like and liquid-like waters, dangling O-H vibration, and free O-H vibration, respectively. On the PMPE film, the peak derived from the ice-like water is clearly observed around 3,150 cm^{-1} as well as on the PMMA film. In general, it is accepted that the ice-like water is induced via hydrogen bonding among water molecules near the hydrophobic domains. If this is the case, PMPE may form hydrophobic domains at the water interfaces.
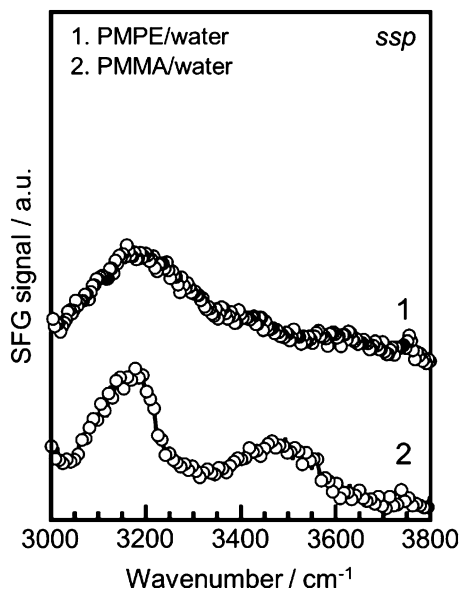
A broad peak around 3,400–3,600 cm^{-1} is observed for PMMA. This is a signature of the presence of highly ordered water structure, probably composed of liquid-like waters and waters with dangling O-H, which may be understood to be caused by hydrogen bonding between the carbonyl groups and water molecules. On the other hand, it is not as clear in the case of PMPE. Taking into account that the side chain carbonyl groups do not exist on PMPE, the result seems to be reasonable. At the same time, looking at the spectrum carefully, it may be possible to claim that there are slight peaks or shoulders around 3,450 and 3,600 cm^{-1}. If that is the case, this could be because of the methoxy groups of PMPE forming a relatively weak interaction with water. However, either way, the highly ordered water structure is not clearly formed on PMPE.

A small peak indicating the presence of free water is observed on PMPE around 3,750 cm^{-1}. This implies that PMPE forms a distinctive water interface; the existence of α-methyl groups forms hydrophobic domains that induce the formation of the ice-like water and the absence of the carbonyl groups discourages water molecules from hydrogen bonding with polymer chains at the interface.

5   Concluding Remarks

Aggregation states and molecular motion of polymers prepared by precision syntheses have been reviewed. As has been discussed, chain end groups of polymers have an impact on the aggregation states at an air interface of the films. In particular, hydrophobic chain end groups relative to the main chain parts of PS

such as *sec*-butyl group are preferentially segregated at surfaces whereas hydrophilic chain end groups such as carboxy and amino groups are biased toward the bulk. Further, the T_g at the surface can be effectively reduced in comparison with the bulk value by surface segregation of the hydrophobic chain end groups. Surface segregation of hydrophobic chain ends takes place even in PS/PVME blend films and can control the surface composition if chain end groups are the most hydrophobic moiety among the components.

The local conformation of polymers at the interfaces can be evaluated by SFG. We have compared the local conformation of *i*-PMMA and *s*-PMMA at air and water interfaces using SFG. In air, the SFG results suggest that the carbonyl groups in *i*-PMMA can be oriented to the air phase, while hydrophobic methylene, α-methyl, and ester methyl groups in *s*-PMMA are oriented toward the air interface. On the other hand, in water, a clear surface reorganization is not occurred in *i*-PMMA, while the carbonyl groups turn around to orient toward the water phase so that they form hydrogen bonds with water in *s*-PMMA.

The structures of water coming in contact with polymers can be also evaluated by SFG. As an example, we have confirmed that the water structure on *i*-PMMA is different from that of *s*-PMMA. The results can be explained in terms of the difference in the size of nanoscopic hydrophobic domains formed by α-methyl groups. An effect of the presence of carbonyl group on water structures was also studied by using PMMA and PMPE as samples. The highly ordered water structures are observed for PMMA but not for PMPE. This suggests that the absence of the carbonyl groups discourages water molecules from hydrogen bonding with polymer chains at the interface.

In conclusion, aggregation states at interfaces can be regulated by the local parts of polymer chains such as chain ends and side chain moieties. Clearly, precision synthesis is an effective methodology in fine-tuning the surface and interfacial properties without varying the bulk properties.

Abbreviations

α,ω-PS(NH$_2$)$_2$	α,ω-Diamino-terminated polystyrene
α,ω-PS(COOH)$_2$	α,ω-Dicarboxy-terminated polystyrene
α,ω-PS(R$_f$)$_2$	Fluoroalkyl into both ends of polystyrene
DSC	Differential scanning calorimetry

i-PMMA	Isotactic-PMMA
PMMA	Poly(methyl methacrylate)
PMPE	Poly(methyl-2-propenyl ether)
PS	Polystyrene
PVME	Poly(vinyl methyl ether)
SFG	Sum-frequency generation
SFM	Scanning force microscopy
s-PMMA	Syndiotactic PMMA
T_g^b	Bulk glass transition temperature
T_g^s	Surface glass transition temperature
XPS	X-ray photoelectron spectroscopy

References

1. Karim A, Kumar S (2000) Polymer surfaces, interfaces and thin films. World Scientific, Singapore
2. Tsui OKC, Russell TP (2008) Polymer thin films, vol 1, Series in soft condensed matter. World Scientific, Singapore
3. Kanaya T (2013) Glass transition, dynamics and heterogeneity of polymer thin films, vol 252, Advances in polymer science. Springer, Heidelberg. doi:10.1007/978-3-642-34339-1
4. Keddie JL, Jones RAL, Cory RA (1994) Size-dependent depression of the glass transition temperature in polymer films. Europhys Lett 27:59–64. doi:10.1209/0295-5075/27/1/011
5. Forrest JA, DalnokiVeress K, Dutcher JR (1997) Interface and chain confinement effects on the glass transition temperature of thin polymer films. Phys Rev E 56:5705–5716. doi:10.1103/PhysRevE.56.5705
6. DeMaggio GB, Frieze WE, Gidley DW, Zhu M, Hristov HA, Yee AF (1997) Interface and surface effects on the glass transition in thin polystyrene films. Phys Rev Lett 78:1524–1527. doi:10.1103/PhysRevLett.78.1524
7. Ellison CJ, Torkelson JM (2003) The distribution of glass-transition temperatures in nanoscopically confined glass formers. Nat Mater 17:461–524. doi:10.1038/nmat980
8. Akabori K, Tanaka K, Nagamura T, Takahara A, Kajiyama T (2005) Molecular motion in ultrathin polystyrene films: dynamic mechanical analysis of surface and interfacial effects. Macromolecules 38:9735–9741. doi:10.1021/ma051143e
9. Alcoutlabi M, McKenna GB (2005) Effects of confinement on material behaviour at the nanometre size scale. J Phys Condens Matter 17:R461–R524. doi:10.1088/0953-8984/17/15/R01
10. Zhang C, Fujii Y, Tanaka K (2012) Effect of long range interactions on the glass transition temperature of thin polystyrene films. ACS Macro Lett 1:1317–1320. doi:10.1021/mz300391g
11. Tanaka K, Takahara A, Kajiyama T (1995) Surface molecular motion in thin films of poly (styrene-*block*-methyl methacrylate) diblock copolymer. Acta Polym 46:476–482. doi:10.1002/actp.1995.010460612
12. Kajiyama T, Tanaka K, Takahara A (1995) Depth dependence of the surface glass transition temperature of a poly(styrene-*block*-methyl methacrylate) diblock copolymer film on the basis of temperature-dependent X-ray photoelectron spectroscopy. Macromolecules 28:3482–3484. doi:10.1021/ma00113a059
13. Tanaka K, Taura A, Shou-Ren G, Takahara A, Kajiyama T (1996) Molecular weight dependence of surface dynamic viscoelastic properties for the monodisperse polystyrene film. Macromolecules 29:3040–3042. doi:10.1021/ma951378y

14. Tanaka K, Hashimoto K, Kajiyama T, Takahara A (2003) Visualization of active surface molecular motion in a polystyrene film by scanning viscoelasticity microscopy. Langmuir 19:6573–6575. doi:10.1021/la034542g

15. Liu Y, Russeell TP, Samant MG, Stohr J, Brown H, Cossy-Favre A, Diaz J (1997) Surface relaxations in polymers. Macromolecules 30:7768–7771. doi:10.1021/ma970869a

16. Wallace WE, Fischer DA, Efimenko K, Wu W-L, Genzer J (2001) Polymer chain relaxation: surface outpaces bulk. Macromolecules 34:5081–5082. doi:10.1021/ma002075t

17. Xie L, DeMaggoio GB, Frieze WE, DeVries J, Gidley DW, Hristov HA, Yee AF (1995) Positronium formation as a probe of polymer surface and thin films. Phys Rev Lett 74:4947–4950. doi:10.1103/PhysRevLett.74.4947

18. Jean YC, Zhang R, Cao H, Yuan J–P, Huang C–M, Nielsen B, Asoka-Kumar P (1997) Glass transition of polystyrene near the surface studied by slow-positron-annihilation spectroscopy. Phys Rev B 56:R8459–R8462. doi:10.1103/PhysRevB.56.R8459

19. Schwab AD, Agra DMG, Kim J–H, Kumar S, Dhinojwala A (2000) Surface dynamics in rubbed polymer thin films probed with optical birefringence measurements. Macromolecules 33:4903–4909. doi:10.1021/ma9919514

20. Tsang OC, Xie FC, Tsui OKC, Yang Z, Zhang JM, Shen DY, Yang XZ (2001) Rubbing-induced molecular alignment and its relaxation in polystyrene thin films. J Polym Sci Part B Polym Phys 39:2906–2914. doi:10.1002/polb.10048

21. Kerle T, Lin Z, Kim H–C, Russell TP (2001) Mobility of polymers at the air/polymer interface. Macromolecules 34:3484–3492. doi:10.1021/ma0020335

22. Hamdorf M, Johannsmann D (2000) Surface-rheological measurements on glass forming polymers based on the surface tension driven decay of imprinted corrugation gratings. J Chem Phys 112:4262–4270. doi:10.1063/1.481002

23. Tanaka K, Tateishi Y, Okada Y, Nagamura T, Doi M, Morita H (2009) Interfacial mobility of polymers on inorganic solids. J Phys Chem B 113:4571–4577. doi:10.1021/jp810370f

24. Fujii Y, Yang Z, Leach J, Atarashi H, Tanaka K, Tsui OKC (2009) Affinity of polystyrene films to hydrogen-passivated silicon and its relevance to the T_g of the films. Macromolecules 42:7418–7422. doi:10.1021/ma901851w

25. Inoue R, Kawashima K, Matsui K, Nakamura M, Nishida K, Kanaya T, Yamada NL (2011) Interfacial properties of polystyrene thin films as revealed by neutron reflectivity. Phys Rev E 84:031802/1–031802/7. doi:10.1103/PhysRevE.84.031802

26. Napolitano S, Wubbenhorst M (2011) The lifetime of the deviations from bulk behaviour in polymers confined at the nanoscale. Nat Commun 2:1259/1–1259/7. doi:10.1038/ncomms1259

27. Tsuruta H, Fujii Y, Kai N, Kataoka H, Ishizone T, Doi M, Morita H, Tanaka K (2012) Local conformation and relaxation of polystyrene at substrate interface. Macromolecules 45:4643–4649. doi:10.1021/ma3007202

28. Gin P, Jiang NS, Liang C, Taniguchi T, Akgun B, Satija SK, Endoh MK, Koga T (2012) Revealed architectures of adsorbed polymer chains at solid-polymer melt interfaces. Phys Rev Lett 109:265501/1–265501/5. doi:10.1103/PhysRevLett.109.265501

29. Paul DR, Yampol'skii YP (1993) Polymeric gas separation membranes. CRC Press, Boca Raton

30. Mittal KL (2001) Adhesion aspects of thin films, vol 1. VSP BV, Utrecht

31. Mittal KL (2013) Advances in contact angle, wettability and adhesion, vol 1. Wiley-Scrivener, Hoboken, New Jersey

32. Tanaka K, Takahara A, Kajiyama T (2000) Rheological analysis of surface relaxation process of monodisperse polystyrene films. Macromolecules 33:7588–7593. doi:10.1021/ma000406w

33. Satomi N, Tanaka K, Takahara A, Kajiyama T, Ishizone T, Nakahama S (2001) Surface molecular motion of monodisperse α, ω-diamino-terminated and α, ω-dicarboxy-terminated polystyrenes. Macromolecules 34:8761–8767. doi:10.1021/ma010126w

34. Tanaka K, Takahara A, Kajiyama T (1997) Effect of polydispersity on surface molecular motion of polystyrene films. Macromolecules 30:6626–6632. doi:10.1021/ma970057e

35. Müller AHE, Matyjaszeuski K (2009) Controlled and living polymerizations. Wiley-VCH, Weinheim

36. Hariharan A, Kumar SK, Russell TP (1993) Reversal of the isotopic effect in the surface behavior of binary polymer blends. J Chem Phys 98:4163–4173. doi:10.1063/1.465024

37. Tanaka K, Kajiyama T, Takahara A, Tasaki S (2002) A novel method to examine surface composition in mixtures of chemically identical two polymers with different molecular weights. Macromolecules 35:4702–4706. doi:10.1021/ma011960o

38. Kajiyama T, Tanaka K, Takahara A (1997) Surface molecular motion of the monodisperse polystyrene films. Macromolecules 30:280–285. doi:10.1021/MA960582Y

39. Tanaka K, Jiang X, Nakamura K, Takahara A, Kajiyama T, Ishizone T, Hirao A, Nakahama A (1998) Effect of chain end chemistry on surface molecular motion of polystyrene films. Macromolecules 31:5148–5149. doi:10.1021/ma9712561

40. Bhatia QS, Pan DH, Koberstein JT (1988) Preferential surface-adsorption in miscible blends of polystyrene and poly(vinyl methyl ether). Macromolecules 21:2166–2175. doi:10.1021/ma00185a049

41. Jones RAL, Norton LJ, Kramer EJ, Composto RJ, Stein RS, Russell TP, Mansour A, Karim A, Felcher GP, Rafailovich MH, Sokolov J, Zhao X, Schwarz SA (1990) The form of the enriched surface layer in polymer blends. Europhys Lett 12:41–46. doi:10.1209/0295-5075/12/1/008

42. Tanaka K, Yoon J-S, Takahara A, Kajiyama T (1995) Ultrathinning-induced surface phase separation of polystyrene/poly(vinyl methyl ether) blend film. Macromolecules 28:934–938. doi:10.1021/ma00108a021

43. Cahn JW (1977) Critical-point wetting. J Chem Phys 66:3667–3672. doi:10.1063/1.434402

44. Schmidt I, Binder K (1985) Model-calculations for wetting transitions in polymer mixtures. J Phys 46:1631–1644. doi:10.1051/jphys:0198500460100163100

45. Jones RAL, Kramer EJ, Rafailovich MH, Sokolov J, Schwarz SA (1989) Surface enrichment in an isotopic polymer blend. Phys Rev Lett 62:280–283. doi:10.1103/PhysRevLett.62.280

46. Nishi T, Wang TT, Kwei TK (1975) Thermally induced phase separation behavior of compatible polymer mixtures. Macromolecules 8:227–234. doi:10.1021/ma60044a025

47. Kumar CSSR (2010) Nanostructured thin films and surfaces. Wiley-VCH, Weinheim

48. Kawaguchi D, Tanaka K, Kajiyama T, Takahara A, Tasaki S (2003) Surface composition control via chain end segregation in blend films of polystyrene and poly(vinyl methyl ether). Macromolecules 36:6824–6830. doi:10.1021/ma034117u

49. Tanaka K, Kawaguchi D, Yokoe Y, Kajiyama T, Takahara A, Tasaki S (2003) Surface segregation of chain ends in α, ω-fluoroalkyl-terminated polystyrenes films. Polymer 44:4171–4177. doi:10.1016/S0032-3861(03)00391-4

50. Scherer GG (2008) Fuel cells I. Springer, Berlin

51. Zaidi J, Matsuura T (2009) Polymer membranes for fuel cells. Springer, New York

52. Tanaka M, Mochizuki A, Ishii N, Motomura T, Hatakeyama T (2000) Study of blood compatibility with poly(2-methoxyethyl acrylate). Relationship between water structure and platelet compatibility in poly(2-methoxyethylacrylate-co-2-hydroxyethylmethacrylate). Biomacromolecules 3:36–41. doi:10.1021/bm010072y

53. Susanto H, Ulbricht M (2008) High-performance thin-layer membranes for ultrafiltration hydrogel composite of natural organic matter. Water Res 42:2827–2835. doi:10.1016/j.watres.2008.02.017

54. Varin KJ, Lin NH, Cohen Y (2013) Biofouling and cleaning effectiveness of surface nanostructured reverse osmosis membranes. J Membr Sci 446:472–481. doi:10.1016/j.memsci.2013.06.064

55. Kizler TA, Flakoll PJ, Parker RA, Hakim RM (1994) Amino-acid and albumin losses during hemodialysis. Kidney Int 46:830–837. doi:10.1038/ki.1994.339

56. Trivedi RH, Werner L, Apple DJ, Pandey SK, Izak AM (2002) Post cataract-intraocular lens (IOL) surgery opacification. Eye (Lond) 16:217–241. doi:10.1038/sj.eye.6700066

57. Oner FH, Gunenc U, Ferliel ST (2000) Posterior capsule opacification after phacoemulsification: foldable acrylic versus poly(methyl methacrylate) intraocular lenses. J Cataract Refract Sug 26:722–726. doi:10.1016/S0886-3350(99)00456-3

58. Yamasaki K, Juodkazis S, Matsuo S, Misawa H (2003) Three-dimensional micro-channels in polymers: one-step fabrication. Appl Phys A 77:371–373. doi:10.1007/s00339-003-2191-8

59. Mahabadi KA, Rodriguez I, Haur SC, van Kan JA, Bettiol AA, Watt F (2006) Fabrication of PMMA micro- and nanofluidic channels by proton beam writing: electrokinetic and morphological characterization. J Micromech Microeng 16:1170–1180. doi:10.1088/0960-1317/16/7/009

60. Ute K, Miyatake N, Hatada K (1995) Glass-transition temperature and melting temperature of uniform isotactic and syndiotactic poly(methyl methacrylate)s from 13mer to 50mer. Polymer 36:1415–1419. doi:10.1016/0032-3861(95)95919-R

61. Grohens Y, Brogly M, Labbe C, David MO, Schultz J (1998) Glass transition of stereoregular poly(methyl methacrylate) at interfaces. Langmuir 14:2929–2932. doi:10.1021/la971397w

62. Fujii Y, Akabori K, Tanaka K, Nagamura T (2007) Chain conformation effects on molecular motions at the surface of poly(methyl methacrylate) films. Polym J 39:928–993. doi:10.1295/polymj.PJ2006270

63. Shen YR (1989) Surface-properties probed by 2nd-harmonic and sum-frequency generation. Nature 337:519–525. doi:10.1038/337519a0

64. Tateishi Y, Kai N, Noguchi H, Uosaki K, Nagamura T, Tanaka K (2010) Local conformation of poly(methyl methacrylate) at nitrogen and water interfaces. Polym Chem 1:303–311. doi:10.1039/B9PY00227H

65. Horinouchi A, Atarashi H, Fujii Y, Tanaka K (2012) Dynamics of water-induced surface reorganization in poly(methyl methacrylate) films. Macromolecules 45:4638–4642. doi:10.1021/ma3002559

66. Horinouchi A, Tanaka K (2013) An effect of stereoregularity on the structure of poly(methyl methacrylate) at air and water interfaces. RSC Adv 3:9446–9452. doi:10.1039/c3ra40631h

67. Sundararajan PR, Flory PJ (1974) Configurational characteristics of poly(methyl methacrylate). J Am Chem Soc 96:5025–5031. doi:10.1021/ja00823a002

68. Klee D, Höcker H (1999) Polymers for biomedical applications: improvement of the interface compatibility. Adv Polym Sci 149:1–57. doi:10.1007/3-540-48838-3_1

69. Lutolf MP, Hubbell JA (2005) Synthetic biomaterials as instructive extracellular microenvironments for morphogenesis in tissue engineering. Nat Biotechnol 23:47–55. doi:10.1038/nbt1055

70. Jagur-Grodzinski J (2006) Polymers for tissue engineering, medical devices, and regenerative medicine. Concise general review of recent studies. Polym Adv Technol 17:395–418. doi:10.1002/pat.729

71. Richmond GL (2002) Molecular bonding and interactions at aqueous surfaces as probed by vibrational sum frequency spectroscopy. Chem Rev 102:2693–2724. doi:10.1021/cr0006876

72. Du Q, Freysz E, Shen YR (1994) Surface vibrational spectroscopic studies of hydrogen bonding and hydrophobicity. Science 264:826–828. doi:10.1126/science.264.5160.826

73. Kim J, Cremer PS (2000) IR − visible SFG investigations of interfacial water structure upon polyelectrolyte adsorption at the solid/liquid interface. J Am Chem Soc 122:12371–12372. doi:10.1021/ja003215h

74. Oda Y, Horinouchi A, Kawaguchi D, Matsuno H, Kanaoka S, Aoshima S, Tanaka K (2014) An effect of side-chain carbonyl groups on the interface of vinyl polymers with water. Langmuir 30:1215–1219. doi:10.1021/la404802j

75. Yonezumi M, Takaku R, Kanaoka S, Aoshima S (2008) Living cationic polymerization of α-methyl vinyl ethers using SnCl$_4$. J Polym Sci Part A Polym Chem 46:2202–2211. doi:10.1002/pola.22555

76. Aoshima S, Kanaoka S (2009) A renaissance in living cationic polymerization. Chem Rev 10:5245–5287. doi:10.1021/cr900225g

Block Copolymers as Antifouling and Fouling Resistant Coatings

David Calabrese, Brandon Wenning, and Christopher K. Ober

Abstract Biofouling is a natural phenomenon in which biomolecules, cells, and more complex organisms attach themselves to surfaces. It is a problem affecting ship surfaces, water filtering systems, and piping systems that diminishes efficiency, possibly rendering a device inoperative and requires routine maintenance and even repair. Previously in marine applications, metal-based coatings have been used for their antifouling properties; however, these coatings are biocides and an increasing number of regulations have been passed to limit their use due to their environmental toxicity. Block copolymer coatings have been shown to have antifouling and fouling release properties and are being pursued as a nontoxic alternative. This chapter will present an in-depth exploration of different polymer architectures, fouling resistance structures, and strategies that have been employed to prevent biofouling including hyperbranched polymers, zwitterionic structures, amphiphilic polymers, and more. We will also discuss different methods used to test a coating's ability for antifouling and fouling release.

Keywords Antifouling • Biofouling • Surface-active block copolymers • Surface structure

1 Introduction

Biofouling occurs when a surface is placed in the environment and especially when it is immersed in a natural water supply and is exposed to the settlement of marine organisms. There are four stages of biofouling (Fig. 1): (1) the conditioning stage: the accumulation of organic matter creating a conditioning film (this layer is usually proteins, polysaccharides, and glycoproteins [2]); (2) the formation of a microbial

D. Calabrese • B. Wenning
Department of Chemistry and Chemical Biology, Cornell University, Ithaca, NY 14853, USA
e-mail: drc228@cornell.edu; bmw97@cornell.edu

C.K. Ober (✉)
Department of Chemistry and Chemical Biology, Cornell University, Ithaca, NY 14853, USA

Department of Materials Science and Engineering, Cornell University, Ithaca, NY 14853, USA
e-mail: cko3@cornell.edu
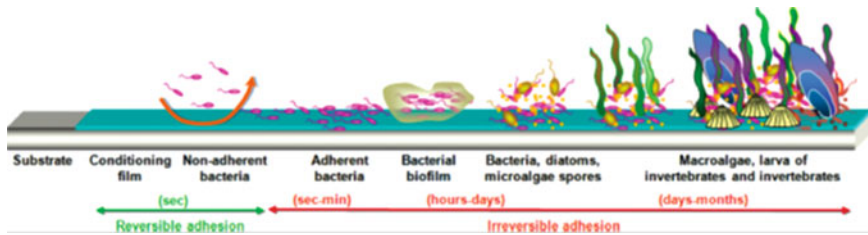
Fig. 1 Development processes of marine fouling (Adapted with permission from [1]. Copyright 2005 EDP Sciences)

film: the first settlement and growth of bacteria creating a biofilm matrix [2]. (Initially, planktonic bacteria reversibly adhere weakly to the surface, usually through electrostatic or van der Waals forces. Eventually the bacteria adhere more strongly to the surface using a cellular appendix and exopolymers.); (3) the maturation of biofilms: microbial colonies grow and mature and pave the way for settlement of algae by providing a sufficient amount of food; and (4) hard fouling: settlement of marine organisms such as barnacles, mussels, bryozoans, tubeworms in conjunction with further algal growth [2]. Settlement and colonization of biofoulers can occur within minutes to hours of immersion in water [3].

The complexity of such systems makes the design of an effective coating that will address all these stages of fouling a daunting task. This chapter will discuss approaches to fouling resistant and antifouling coatings that are based on block copolymers. The use of block copolymers enables the design of surface materials that are both flexible in their application and able to use a variety of strategies to solve this technological challenge. Biofouling, despite its challenges, must be dealt with because it has great economic impact through increased fuel consumption during ship transport, clogging of membranes and heat exchangers, disabled underwater sensors, and growth of biofoulers in aquaculture systems [4].

Settlement of biofoulers leads to significant effects. For ships it increases drag, which reduces the fuel efficiency of the vessel, lowers obtainable speeds, requires a higher frequency of maintenance, and increases the amount of noise. In addition, marine life can be placed in nonnative environments through ship transport, which can then potentially cause problems to the ecosystem if it is an invasive species, for example. These problems cost billions of dollars per year in transportation for the US Navy [5]. A study by the National Oceanic and Atmospheric Administration at the University of Colorado at Boulder reports that the world fleet emits about 3 % of the of all anthropogenic CO_2 and nitrogen oxide gas, which can produce smog. Exhaust from the world fleet produces 30 % of total worldwide emissions [6]. The world fleet consumes 300 million tons of fuel annually, which could double in the case of heavy hull fouling [7].

For piping systems and heat-exchanger tubes, biofouling causes an overall efficiency decline. For membrane filtration systems, it leads to a significant reduction of the permeate flux, a higher energy consumption, and eventually, failure to meet regulatory standards. Membranes, used in desalination plants or in reverse

osmosis for water purification are clogged by biofoulers and need to be replaced often, increasing the price of water [4]. Biofouling can also affect concrete structures on land in humid environments [4]. The absorption of proteins can reduce the sensitivity for in vitro diagnostics and the effectiveness of biological implants, which can result in harmful side effects [8]. In addition the proteins absorbed on the surface provide a conditioning layer for bacteria and other microorganisms to grow. This could potentially lead to infection and other complications.

To prevent biofouling, antifouling coatings have been produced previously. The first known antifouling coatings were based on pitch, wax, lead, or arsenic [9]. In the 1960s, self-polishing antifouling coatings using tributyl tin (TBT) were the first to display long-lasting efficiency at low costs. The TBT in the coatings would leach out into the water and act as an effective biocide. Over a decade later, several studies observed that TBT had strong negative effects on both fouling and non-fouling aquatic life due to its high persistence and toxicity [10, 11].

The most successful coatings were block copolymers with a TBT pendent group and cuprous oxides as an additional biocidal filler and pigment, since both are toxic and self-cleaning. This structure resulted in the hydrolysis of the polymer, releasing the biocides and removing the biofoulers from the side of the ship. The TBT and cuprous oxides leached into the seawater leading to massive pollution and causing damaging effects on non-fouling marine organisms including extinction [12]. The negative effects of TBT caused many governments to restrict its use, eventually leading to its ban from manufacture in new antifouling coatings in January 2003 [13].

The current generation of antifouling coating incorporates high levels of copper. However, while less toxic than TBT and other heavy metals, copper still acts as a biocide and may create environmental problems [14]. Currently, newer copper-based and other heavy metal biocides are being subjected to restrictive legislation, which has been encouraging the development of nontoxic low-energy surfaces for antifouling coatings. The two properties that are being pursued in these new surfaces are antifouling behavior, which is the initial prevention of biofoulants attaching to a surface, and fouling release, which is the detachment of biofoulants from a surface through shear stresses such as those caused by water pressure from a boat moving through water.

2 Classes of Block Copolymer Coatings

Nontoxic, nonbiocidal antifouling coatings, generally, are based on minimizing the intermolecular forces of the interactions between extracellular biomolecules and the synthetic surface causing biofoulers to detach at low shear stresses [15]. Some of the early work on nontoxic coatings has shown two main classes of single component surfaces designed to resist biofoulers. The first class is hydrophobic coatings, such as poly(dimethylsiloxane) (PDMS), which been shown to demonstrate good, intrinsic fouling release properties. The second class consists of
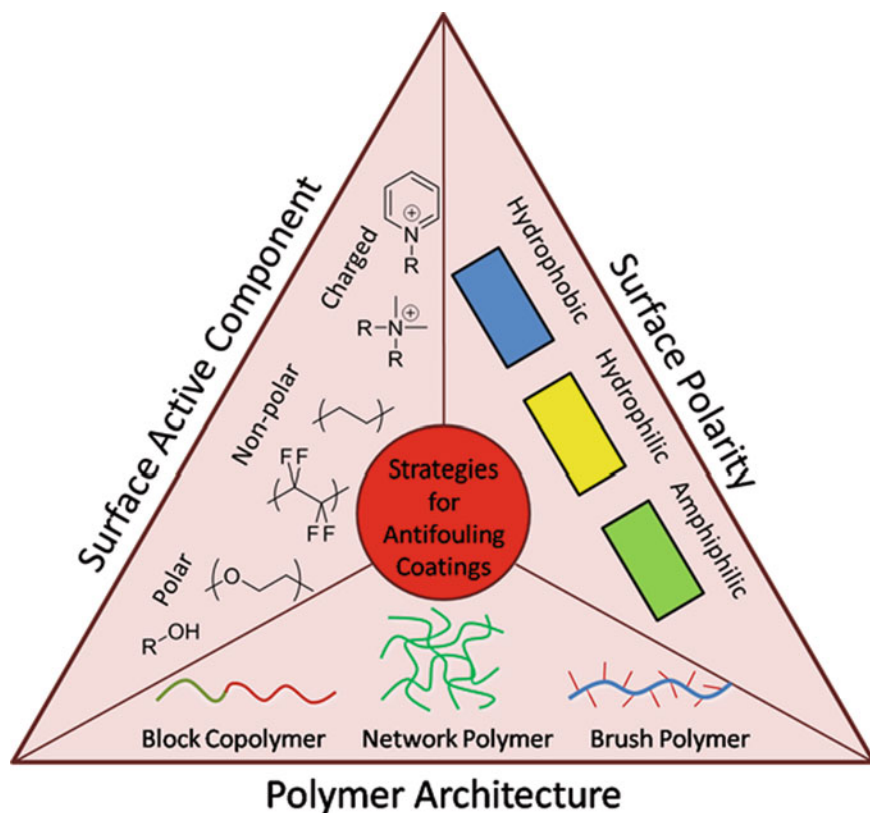
Fig. 2 Strategies for antifouling coatings described in this chapter [15]

hydrophilic coatings, such as poly(ethylene glycol) (PEG), due to its low polymer-water interfacial energy values, and displays the ability to resist protein absorption and cell adhesion [15] (See Fig. 2). Thus, it is anticipated that the interfacial energy between the surface and the water is a significant factor in determining antifouling characteristics. This chapter will discuss these early categories of nontoxic, antifouling coatings.

2.1 Hydrophobic Surfaces

Nonpolar hydrophobic surfaces have high interfacial energy with water. PDMS, for example, has an interfacial energy with water of 52 mJ m^{-2} [15]. Thus, when a hydrophobic surface contacts amphiphilic biomolecules, such as proteins, the biomolecules will adsorb on the surface to reduce the interactions between the water and the surface. As a result, hydrophobic surfaces using elastomeric polymers, like

PDMS, have been strongly investigated as fouling release coatings because of their low surface energy and also their low modulus [16–21]. Low surface energies reduce the adhesion properties of the surface preventing the biofoulers from attaching strongly. The low modulus makes it easy to propagate a crack along the foulant-PDMS interface and thus the foulant may be more easily removed. It has been shown that having a lower modulus, creating a more elastic surface, will prevent biofoulers from strongly attaching to the surface but only to a point. Once the modulus is as low as 4 MPa, there is no additional fouling release benefit from decreasing the modulus [22]. There have been several studies with PDMS-based coatings that were shown to have high fouling release properties against *Ulva*, a marine microalgae [22, 23]. However, hydrophobic surfaces are not as effective at fouling release with all marine species. *Navicula*, a marine diatom, has demonstrated strong adhesion to PDMS [24]. It is suspected that differences in the adhesion between the diatoms and the microalgae are due to the difference in surface interactions of the adhesive extracellular polymeric substances (EPS) secreted by the two organisms [15].

2.2 Hydrophilic Surfaces

Polar hydrophilic surfaces have a lower interfacial energy with water. PEG, for example, has an interfacial energy with water of 5 mJ m^{-2} [25, 26], which is an order of magnitude lower than PDMS. As a result, when a hydrophilic surface is in contact with an amphiphilic molecule, the surface will favor being in contact with the water more than the biomolecule. Thus, amphiphilic molecules tend to exhibit resistance towards protein absorption. Due to their higher surface energy and higher mobility than many of the hydrophobic surfaces, hydrophilic surfaces are not generally as effective at fouling release as hydrophobic surfaces. However, hydrophilic surfaces have been shown to be effective at fouling release for diatoms such as *Navicula* [2, 27–30].

2.3 Amphiphilic and Mixed Surface Block Copolymers

Since there are beneficial antifouling and fouling characteristics from both extremes of wettability, combining hydrophobic and hydrophilic materials to make an amphiphilic surface has been widely investigated. Furthermore, there is a desire to create "ambiguous" surface activated block copolymers (SABC) to aid in antifouling and fouling release. These "ambiguous" surfaces are designed to be dynamic and change in response to settlement on a surface, which hinders biofoulers from attaching as strongly to that surface. This is demonstrated in Fig. 1 where in air the nonpolar, hydrophobic component of the amphiphilic side chain is extended to the surface, but if in contact with water, the same nonpolar

groups in the side chain become buried in the coating and expose the hydrophilic part of the chain [15].

These amphiphilic surfaces have been created using three different methods: (1) a homogeneous material with amphiphilic components, (2) a heterogeneous material with hydrophobic and hydrophilic components randomly mixed on the surface, and (3) a heterogeneous material with hydrophobic and hydrophilic components that is patterned on the surface in an exact order. Similar characteristics have been observed in block copolymers in which mixed polar and nonpolar side groups are included. Both amphiphilic and mixed surfaces are reviewed in this chapter.

2.4   *Quaternary Ammonium Surfaces*

Charged surfaces have also been examined as materials for antifouling and fouling resistant surfaces. Quaternary ammonium salts are well known as antimicrobial materials and have been used effectively to produce surfaces that kill bacteria. Charge can be a fouling deterrent and these surfaces have been combined with other antifouling strategies to explore their effectiveness.

The following sections discuss in detail the various approaches to antifouling/ fouling resistant coatings explored using block copolymers. Each shows promise with the amphiphilic coatings showing the most effective surfaces to date. Most of the work on block copolymers has been built on chemically modified block copolymers of poly(styrene)-block-poly(diene). Routes to chemical modification as well as the effectiveness of the different compositions are described.

3   Algae and Diatom Antifouling and Fouling Release Assays

To study how marine organisms settle and grow on experimental coatings, it is necessary to test coatings against living organisms. These tests need to be standardized and capable of differentiating the performance of multiple coatings in a controlled way on the laboratory scale. Two of the most common standardized tests for antifouling and fouling release performance utilize a marine alga, *Ulva linza* [31] and a diatom species, *Navicula perminuta* [24]. These tests can probe both settlement and attachment characteristics of different marine fouling species with very different settlement characteristics.

Ulva linza is a marine alga harvested from natural marine environments for experimental purposes [31]. After harvesting, zoospores are released from the mature plants for use in the settlement experiments. Surfaces prepared for experiments are immersed in sterile artificial seawater to prepare the surface. The

surfaces are then immersed in a suspension of the freshly released zoospores in darkness, allowing the zoospores to attach to the surfaces. After this time all surfaces are rinsed, and the surface attachment of zoospores is quantified. The zoospores of *Ulva linza* are somewhat selective settlers, meaning that they are able to move across surfaces to settle on the most preferential surfaces.

After initial settlement, attached *Ulva linza* spores are incubated and matured into sporelings, or young plants. At this point, the sporeling biomass is determined by measuring the autofluorescence of chlorophyll. To determine the adhesion strength, the surfaces are placed into a water flow channel and exposed to a turbulent flow of water at a controlled wall shear stress as described by Finlay et al. [32]. This shear stress removes some of the attached sporelings, based on how strongly attached they are to the surface. This flow rate is designed to mimic that of water flowing across the hull of a ship, and modeling has been done to relate flow rate and pressure in laboratory setups to that on vessels moving through water [23]. By doing this release test, the fouling release properties of the coatings can be investigated.

The second major organism studied as a test for antifouling and fouling release performance is a single-celled diatom, *Navicula perminuta* [24]. Diatom slimes are major contributors to persistent marine fouling which can be difficult to prevent. These single-celled organisms are cultured in a laboratory to be used in these standardized assays. Because they are simple single-celled organisms, they approach surfaces simply by settling out of solution by the forces of gravity. This nonselective settlement forces the cells to attach at any location where they are deposited. Once settled onto a surface, the cells secrete adhesive molecules to firmly attach themselves to the surface.

To perform the attachment assay, surfaces are immersed in artificial seawater as with the *Ulva linza* tests, and then exposed to a standardized suspension of diatoms. After this initial settlement time, surfaces are rinsed to remove unattached cells and the density of cells on the surface is quantified by microscopy to determine the antifouling performance of the coatings. Then, the surfaces with attached diatoms are placed into a water flow channel or exposed to a pressurized water jet at a controlled pressure to remove the cells. The proportion of removed cells is indicative of the adhesion strength of the diatoms to the surface and helps to probe the fouling release properties of the coatings studied.

These studies, as well as many others investigating different algae, diatoms, bacteria, barnacles, and other marine fouling organisms are necessary to quickly assess the performance of many experimental coatings. Field trials investigating the performance of experimental coatings when immersed in natural marine environments are also performed. This can be done by immersing test panels in an experimental setup, or by applying coatings to marine vessels in service to observe performance. These experiments, while more representative of actual marine operating conditions, are significantly more time consuming, and difficult to quickly screen many coatings at one time. Additionally, the data can be more difficult to interpret as natural systems are much more complex than those created in a laboratory.

4   General Coating Strategies

The use of block copolymers allows for the control of surface microstructures by tuning the molecular weight of the polymer as well as the ratio of the molecular weight of each of the components (Fig. 3). Due to the very small size of these domains, cellular fouling organisms can interact with them. By tailoring the surface microstructure, control of the settlement of these organisms can be achieved. Grozea et al. [33] compared block copolymers of polystyrene (PS) and poly (2-vinyl pyridine) (P2VP) to study the effect of microstructure on settlement of *Ulva linza* algae (Fig. 4). By comparing a random block copolymer to a block copolymer this work was able to create surfaces with similar chemical compositions at the surface, but which differed by exhibiting ordered microstructure or not. Additionally they compared a block copolymer of polystyrene and poly(methyl methacrylate) (PMMA) to compare chemical differences between two ordered polymeric systems.

To assess the ability of these materials to resist settlement of *Ulva* spores, samples were prepared of PS, P2VP, PS-*r*-P2VP, PS-*b*-P2VP, PS-*b*-P2VP cross-linked with benzophenone and UV irradiation, and PS-*b*-PMMA. Surfaces containing only the homopolymer of either PS or P2VP had the highest settlement of *Ulva* spores on the surface, indicating that it is not exclusively the chemistry of either block which contributes to the overall antifouling performance of the copolymer surfaces. Additionally, the block copolymer showed lower settlement than the random copolymer, in this case indicating that the microstructure of the block copolymer is important to the resistance of settling organisms. The cross-linked
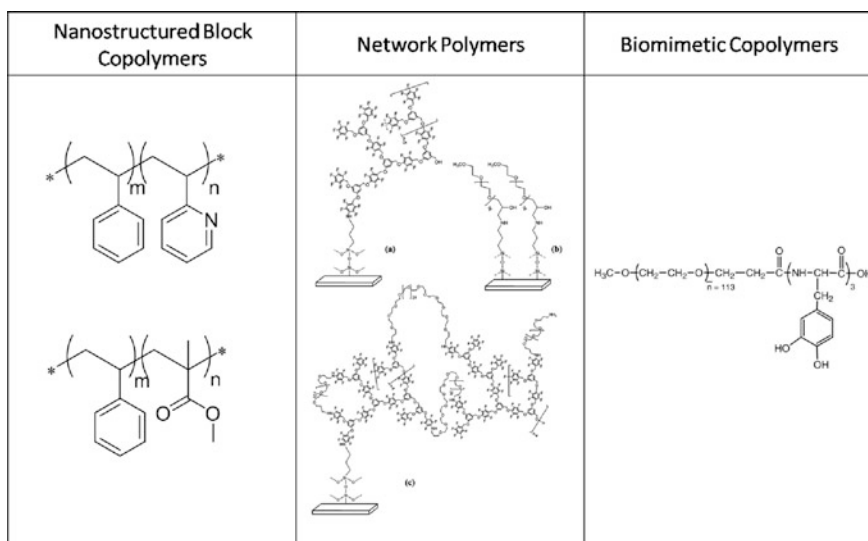
Fig. 3 Polymer structures used for antifouling and fouling release applications [30, 33–36]
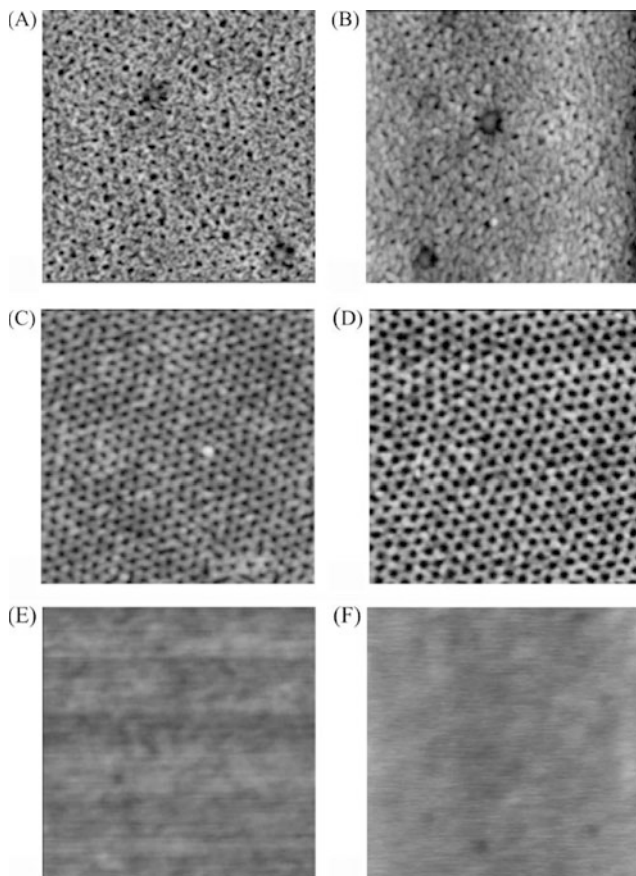
Fig. 4 AFM height images comparing cross-linked PS-*b*-P2VP (**a–d**) to PS-r-P2VP. (**a**) In water after 1 h, (**b**) in water after 48 h, (**c**) in air after 2 h in water, (**d**) in air after 8 days in water, (**e**) in air, (**f**) in water after 1 h [33]

block copolymer and the PS-*b*-PMMA were the best at resisting the settlement of the *Ulva* spores of the set of samples analyzed.

5 Hyperbranched Polymer Structures

Hyperbranched polymeric structures have been shown to perform very well as antifouling and fouling release coatings (Fig. 3). By synthesizing materials which are highly branched or cross-linked, the surface properties are altered significantly. These surfaces exhibit complex nanoscale compositional and topographic structures which aid in inhibiting protein adsorption as well as the adhesion of marine fouling organisms.

By making these materials from both low surface-energy fluorinated components as well as hydrophilic components of PEG, an additional layer of complexity is added to the surfaces. Such amphiphilic surfaces have been shown to be highly effective as antifouling and fouling release coatings. These structures with fluorinated and PEG containing components have been shown to create highly dynamic surfaces which undergo microphase segregation.

Using a hydroxyl terminated hyperbranched fluoropolymer (HBFP), diamine terminated PEG, and an amine functionalized glass surface, Gudipati et al. [37] showed that a cross-linked hyperbranched amphiphilic surface can be created. The condensation reaction between the three components creates a cross-linked network containing both fluorinated and PEG containing groups at the surface.

Surfaces created by this method exhibited complex surface topography and morphology by atomic force microscopy (AFM), indicating phase segregation of the components at the surface as well as a complex structure. Additionally, studies measuring water contact angle over time as well as XPS before and after immersion in water showed a dynamic surface capable of a reversible reorganization. By controlling the relative content of fluoropolymer to PEG groups, the overall hydrophilicity of the surfaces could be controlled. This allows for highly tunable surfaces, capable of being tailored for optimal performance.

Complex hyperbranched surfaces studied by Gudipati et al. [34] are very successful at reducing protein adsorption of several bacterial proteins. This type of protein resistance is important in resisting the settlement of more complex organisms. Additionally, these surfaces were seen to be effective at reducing the settlement of *Ulva linza* spores when compared to glass and PDMS control samples. This was true for compositions containing high and low percentages of PEG material. In addition to being highly effective at reducing settlement of these algae, one composition showed significantly higher removal of juvenile sporelings than either glass or PDMS materials. There was nearly 100 % removal of sporelings from one of the hyperbranched coatings, while PDMS showed only 50 % removal, and glass had less than 5 % removed. This highlights the need to tune delicately the balance of hydrophobic and hydrophilic components when developing an effective coating of this type.

Another method to create cross-linked and highly branched systems is through the use of thiol-ene click chemistry. This technique, studied by Imbesi et al. [38], allows for a highly efficient coupling of an alkene and a thiol via a radical reaction. The method employed by Imbesi et al. involves first synthesizing a copolymer of fluorinated styrene and a PEG functionalized fluorinated styrene. The PEG chain was terminated with an alkene to be used for thiol-ene chemistry. This polymer was then coated onto a surface along with a di- or tetra-thiol and a photoradical generator. After the films were coated, they were exposed to UV light to initiate the cross-linking reaction. This technique allows for better control over film thickness and surface roughness while still allowing for the incorporation of fluorinated and PEG containing structures in a hyperbranched cross-linked film. Surface studies show it is an amphiphilic surface with dynamic response and complex microstructure.
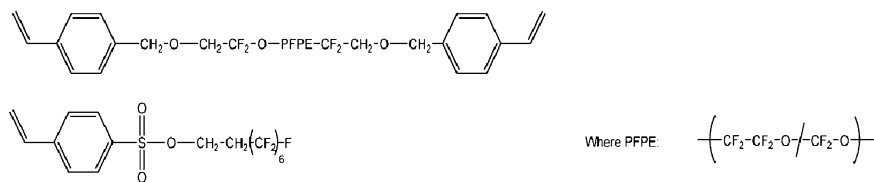
Fig. 5 Macromonomers for perfluoroether-containing network copolymers [35]

Hu et al. [35] also utilized cross-linked networks of perfluorinated ethers to develop antifouling and fouling release coatings. The networks were synthesized from macromonomers containing either one or two styrene groups as seen in Fig. 5. These macromonomers also contain a perfluorinated ether, and in the case of the single styrene monomer also contained a sulfonic ester to link the styrene to the perfluorinated ether, which imparts the antifouling and fouling release properties to the polymers. The network polymers were formed by exposing the macromonomers to UV light with a small amount of photoinitiator over a silicon wafer substrate. Each macromonomer was synthesized into a unique coating for analysis.

Both coatings were then prepared for testing of antifouling and fouling release performance by *Ulva linza* bioassays. These surfaces were exceptionally high performing antifouling coatings, reducing settlement of *Ulva* spores by roughly 80 % when compared to a PDMS standard. Additionally, these surfaces showed a greater percentage of release of *Ulva* sporelings when exposed to wall shear stress in a water flow channel.

Other groups have focused on biomimetic strategies for developing antifouling and fouling release coatings. The strategy used by Dalsin et al. and Statz et al. [30, 36] used a methyl terminated PEG attached to peptides inspired by marine mussels (Fig. 3). These peptides contain a significant amount of L-3,4-dihydroxyphenylalanine (L-DOPA), which is abundant in adhesive proteins used by marine mussels. This segment serves to bind the PEG, a well known antifouling polymer, to the surface to create a water-stable coating. The polymers are then coated onto a titanium surface to be used as functional antifouling coatings.

These coatings were shown to reduce the settlement of *Navicula* by roughly 80 % when compared to glass, PDMS, and titanium control surfaces. Additionally, when exposed to a wall shear stress of 20 Pa using a water flow chamber, these coatings were able to release nearly 100 % of attached cells, again performing significantly better than any of the control surfaces. Studies of the attachment and release of *Ulva* spores showed that these surfaces were able to reduce attachment to very low levels compared to controls. Removal of both spores and sporelings showed removal significantly improved over titanium surfaces, and performing as well as the PDMS control surfaces. Overall, these coatings perform exceptionally well at both resisting the attachment of fouling organisms to the surface as well as releasing them under flow conditions.

6 Single Component Surfaces

An important observation in the design of nontoxic, antifouling surfaces has been a series of observations summarized by the Baier curve [39]. In it, the surface energy of a polymer coating is plotted against the fouling resistance of the polymer. It was shown that there was a minimum in the fouling behavior when the surface energy was that of PDMS and polymers with lower surface energy such as fluoropolymers (e.g. PTFE) or higher such as hydrocarbon polymers (e.g. polyethylene) exhibited much greater fouling properties. This result, while true, seemed to make little sense from a surface energy argument alone and was further complicated by the observation that in the biomedical field, the use of hydrophilic polymers such as polyethylene glycol produces very effective fouling resistant surfaces. These confusing and contradictory observations prompted a study of new antifouling materials based on block copolymers.

One of the key inconsistencies of the Baier study was the use of PDMS, an elastomer, in contrast to the other materials, which were generally rigid thermoplastics. It has now been shown that one aspect of the fouling release mechanism involved the formation of a crack between the substrate and foulant and this behavior is aided by the use of elastomers as the majority of the coating [40]. PDMS has an excellent combination of low surface energy and the right mechanical properties and is thus an excellent material for nontoxic fouling release materials. However, with the right experimental design other systems should be possible and possibly superior.

6.1 Block Copolymers as Versatile Coatings (Fig. 6)

In order to test a number of coatings with differing polarity it was important to develop a strategy that would enable the various coatings to have the same mechanical properties, especially the same Young's modulus. Incorporating these characteristics into a coating was made possible by the use of block copolymers with a common glass forming block, polystyrene. A commercial thermoplastic elastomer was selected for the rubbery phase. This particular polymer, made by Kraton (G-1652), has been shown to be light stable, environmentally safe, to have suitable mechanical properties and to be capable of solution coating. The new surface-active block copolymers were designed to have a variety of surface-modifying segments and still physically lock into the elastomer phase through the common polystyrene segment (Scheme 1). A general strategy for the formation of these coatings is shown in the following schematic.

In order to introduce the surface-active component onto a well-prepared block copolymer backbone, it was elected to carry out polymer modification on a polystyrene-block-polyisoprene, used in common on all test surfaces. A number of
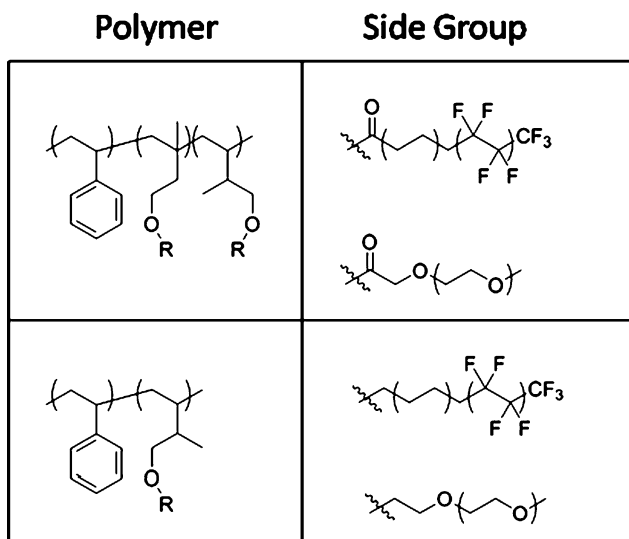
Fig. 6 Compositions of polymers and side groups for single component systems [28, 41–46]
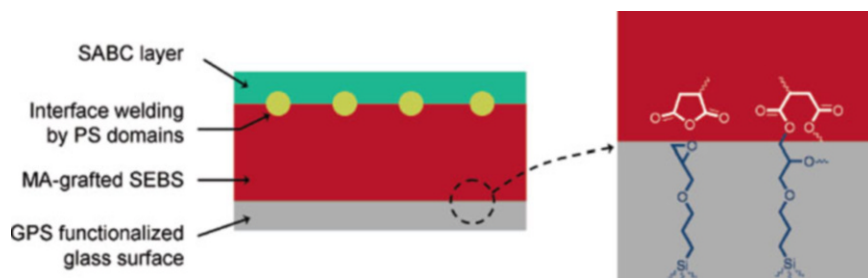
Scheme 1 Schematic of bilayer coatings on 3-(glycidoxypropyl)trimethoxy silane (GPS)-functionalized glass slides (cross-sectional view, not to scale). The PS domains at the interface of the SABC and the SEBS bond the two polymer layers. Adhesion to glass is achieved by reaction between the epoxy groups on the glass surface and maleic anhydride (MA) groups of the MA-grafted SEBS [29]

chemistries were explored but the use of hydroboration chemistry to introduce a hydroxyl group was selected (Fig. 7). This approach enabled the incorporation of functional acids as the surface-modifying component. A series of semifluorinated acids were synthesized and added to the block copolymer backbone. In parallel, PEG side groups were developed for attachment on a modified isoprene block of a polystyrene-block-polyisoprene diblock copolymer. The resulting polymers were then coated on the substrate and the resulting surface properties were analyzed using a variety of methods including contact angle measurements, near edge X-ray absorption fine structure (NEXAFS), XPS, AFM, and related methods.

$$\text{(CH}_2\text{-CH)}_{395}^b \text{(CH}_2\text{-CH)}_{64} \text{(CH}_2\text{-C)}_{43} \tag{1}$$

(i) 9BBN (ii) H_2O_2/NaOH

$$\text{(CH}_2\text{-CH)}_{395}^b \text{(CH}_2\text{-CH)}_{64} \text{(CH}_2\text{-C)}_{43} \tag{2}$$

$$F(CF_2)_q\!-\!I \qquad CH_2\!=\!CH\!-\!(CH_2)_{p-2}\!-\!OH$$

(q=6, 8, 10, p =4, 6, 10)   (i) AIBN (ii)Bu$_3$SnH/AIBN

$$F(CF_2)_q\!-\!(CH_2)_p\!-\!OH \tag{3}$$

N_2O_4

$$F(CF_2)_q\!-\!(CH_2)_{p-1}\!-\!COOH \tag{4}$$

$SOCl_2$

$$F(CF_2)_q\!-\!(CH_2)_{p-1}\!-\!COCl \tag{5}$$

$$(2) + (5) \longrightarrow \text{(CH}_2\text{-CH)}_{395}^b \text{(CH}_2\text{-CH)}_{64} \text{(CH}_2\text{-C)}_{43} \tag{6}$$

6a; q=6, p=10
6b; q=8, p=4
6c; q=8, p=6
6d; q=8, p=10
6e; q=10, p=10

$$R = -\overset{O}{\underset{}{C}}\!-\!(CH_2)_{p-1}\!-\!(CF_2)_qF$$

$$\longrightarrow \text{(CH}_2\text{-CH)}_m^b \text{((CH}_2\text{-CH)}_{0.6} \text{(CH}_2\text{-C)}_{0.4})_n \tag{7}$$

7a; m=0, n=191
7b; m=48, n=162
7c; m=138, n=187
7d; m=635, n=150
7e; m=1692, n=137

$$R = -\overset{O}{\underset{}{C}}\!-\!(CH_2)_3\!-\!(CF_2)_8F$$

Fig. 7 Synthesis of semifluorinated block copolymers using ester group [41]

These analytical techniques were used to determine the structure of the surface-active groups on the SABC. Near edge X-ray absorption fine structure (NEXAFS) is a type of surface sensitive absorption spectroscopy that is able to determine the presence, the relative amount, and orientation of functional groups in the upper 10 nm of a surface. NEXAFS allows the determination of functional group behavior on a surface, and how these groups direct themselves. X-ray photoelectron spectroscopy (XPS) is a surface sensitive absorption technique that is able to determine elemental composition. If XPS is run at different angles relative to the surface it is possible to relate elemental compositions to depth. However, XPS, like NEXAFS, is operated under a high vacuum. While structures can be immersed under water prior to measurement, while under vacuum for performing XPS or NEXAFS experiments, some surface reconstruction will still be possible. Both dynamic contact angle and bubble contact angle measurements are methods for determining the wettability and hydrophilicity of a surface. For bubble contact angle studies the sample remains submerged in water. Air bubbles are added onto the inverted surface, and the angle that the bubble makes with the surface is measured. This allows for the sample to be immersed in water and measured for days or weeks to see how the surface changes over time. Atomic force microscopy (AFM) can be used to determine the microstructure of the surface. Unlike NEXAFS or XPS, AFM and underwater contact angle measurements can be performed for extended periods of time, allowing submerged samples to be studied as a function of exposure. Ultimately the fouling behavior of these coatings was assessed using two marker species, *Ulva linza*, a type of seaweed and *Navicula*, a diatom.

One of the challenges of working with surfaces underwater is that they will reconstruct. It was a hypothesis that a non-reconstructing surface would be ideal for assessing the nature of a truly nonpolar surface in a fouling environment and testing the notion that fluorinated materials, despite their lower surface energy, were not as effective as silicones. In order to make these non-reconstructing surfaces, the semifluorinated groups were designed to form a smectic liquid crystalline phase. This had the effect of directing the CF_3 groups to the surface (Fig. 8) and in stabilizing the surface against reconstruction.

The internal structure of the semifluorinated block copolymer is complex because the microphase separation of the liquid crystal and the block copolymer are in competition. The smectic layers organize with the fluorinated groups lying perpendicular to the plan of the layers. This restricts the kinds of microstructures possible in these LC block copolymers [43]. Either the polymer forms lamellar structures where the smectic layers lie perpendicular to the block copolymer layers, or the smectic phase surrounds cylinders of the amorphous phase where the smectic layers lie perpendicular to the long axis of the cylinders [44]. A spherical phase or more complicated structure such as the gyroid phase with its curvature is disfavored because the curvature of these phases interferes with the smectic ordering at the phase boundary [42]. An X-ray diffraction pattern of a lamellar structure with a smectic layer perpendicular to it is shown in Fig. 8. The high electron density contrast of the fluorinated phase enables many orders of diffraction to show up in the pattern.
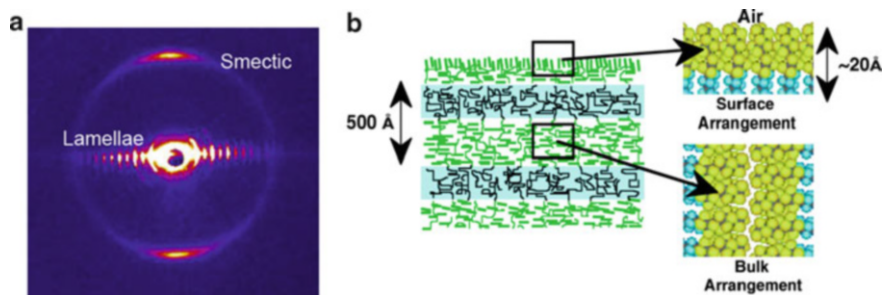
Fig. 8 Order within order. (**a**) The combined wide and small angle X-ray scattering pattern shows both lamellar and smectic organization in the semifluorinated polymers. (**b**) Illustration of the bulk vs. surface organization observed in the semifluorinated surfaces [42]

Interestingly, this arrangement if continued at the surface would place the perfluorinated groups lying parallel to the substrate, a less than desirable situation since not only would the fluorinated segments be present, but also the hydrocarbon and the relatively polar linking groups. However, the surface is populated by CF_3 groups as indicated both by contact angle measurements and by NEXAFS studies. The Zisman plot was made by measuring the contact angle of a series of liquids on the film surface (Fig. 9). In the Zisman plot the contact angles are extrapolated to a value of ~8 mN/m for the semifluorinated surfaces, which suggests that the only possible structure that could lead to this low surface energy would be that produced from $-CF_3$ groups. This possibility is supported by a NEXAFS study which shows that the perfluorinated segment stands up from the surface in the film, consistent with a $-CF_3$ surface (Fig. 10). This arrangement appears to be locked in by the smectic phase and as a result, the contact angles of the surface do not change with time as shown in Fig. 11. Provided that the perfluorinated segment was eight carbon atoms or longer, the film remained stable to extended exposure to water. Thus this material is ideal for testing of low surface energy as a tool for preventing fouling and in aiding fouling release.

In order to compare how the performance of a polar surface would compare to a stable fluorinated material, a polymer surface made with PEG units was produced. The same diblock copolymer backbone was used; however, in the case of both PEG units and semifluorinated groups a new modification strategy was developed. Instead of using hydrolytically unstable ester groups, the side groups were attached to the hydroxylated polyisoprene backbone by an etherification reaction using either a brominated monofunctional PEG unit or a brominated monofunctional semifluorinated group (Fig. 12). In both cases, efficient stable attachment to the backbone hydroxyl group was carried out and the materials could be coated on a substrate and tested.

A study of the fouling behavior of the polar, hydrophilic PEG surface was compared to the nonpolar, hydrophobic semifluorinated surface as shown in Fig. 13 [28]. These materials were also compared to glass and silicone. Glass is known to be polar and silicone is known to be of low surface energy. When *Ulva*
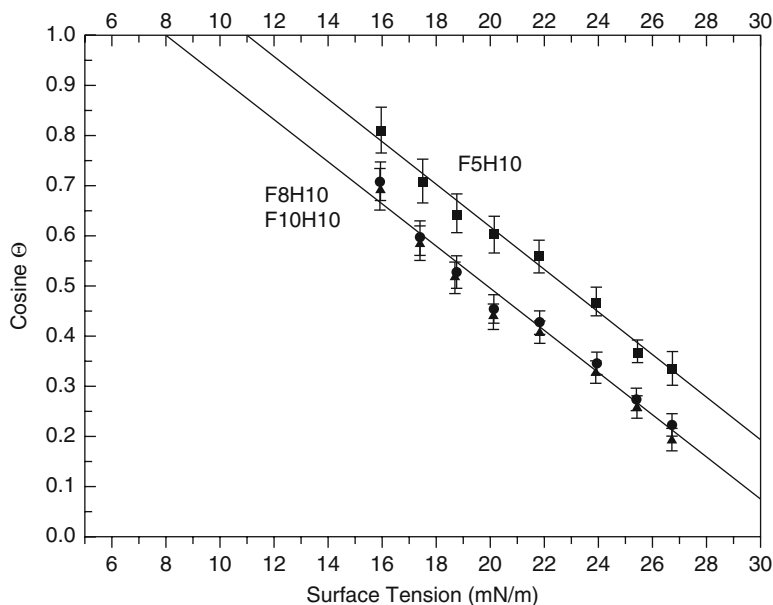
Fig. 9 Zisman plot of block copolymers of poly(styrene)-block-poly(isoprene modified) with semifluorinated side groups [44]

Fig. 10 PEY (*upper part*) and FY (*lower part*) NEXAFS spectra (*solid lines*) from the H-F8H4 sample at EGB = −150 V and θEY 90°. The *dotted lines* in the figure denote the 1 s → σ* transitions for the C-H (E = 287.9 eV), C-F (E = 292.0 eV), and C-C (E = 294.8 eV) bonds [45]
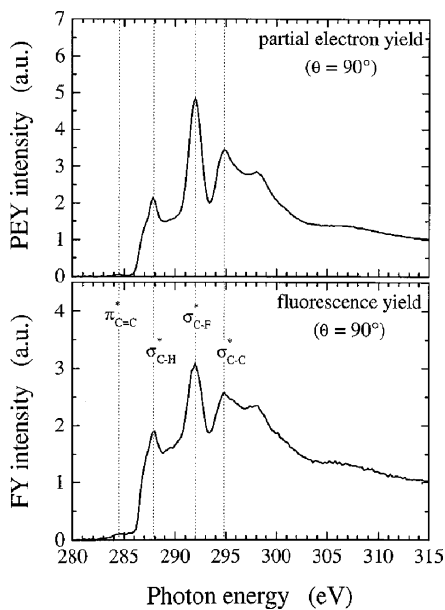
Fig. 11 Time-dependent advancing (*a*) and receding (*r*) water contact angles. TheFxHy notation refers to the size of the semifluorinated side groups, where *x* is the number of CF_2 units and *y* is the number of CH_2 units. F6 units show surface reconstructions while longer CF2 units (eight or more) possess stable surfaces [44]
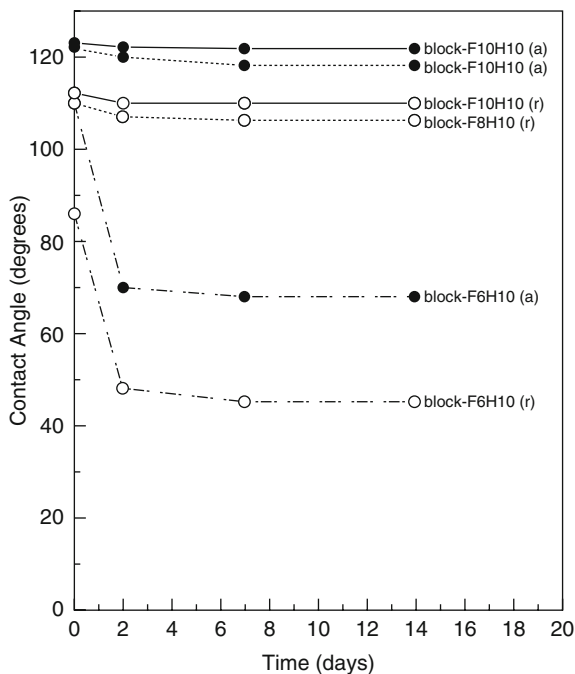
linza was tested as the fouling species, the semifluorinated surface showed extraordinary resistance to fouling. This surface was superior to the silicone and especially the glass and PEG surfaces. However, when *Navicula* was tested on this same group of surfaces a new order emerged. The PEG surfaces easily shed the gravitational settlers, while the semifluorinated surface was readily fouled. In the case of glass *Navicula* was also shed and the silicone showed fouling behavior although not as extreme as the semifluorinated materials. This study highlights the challenge of producing fouling resistant and antifouling surfaces, the need to respond well to many fouling species with a broad range of fouling behaviors.

6.2 Monodendron Nonpolar Side Groups

In another study, 2- and 3-armed monodendrons made from semifluorinated groups were attached to a block copolymer backbone in order to provide even higher loadings of fluorinated groups on the polymer surface [46]. The liquid crystalline organized as before with polymers having single side groups, but the combination of crowding and the LC phase caused the structures to exhibit splay on the surface. With splay there is a gentle curvature to an otherwise flat surface or interface. As
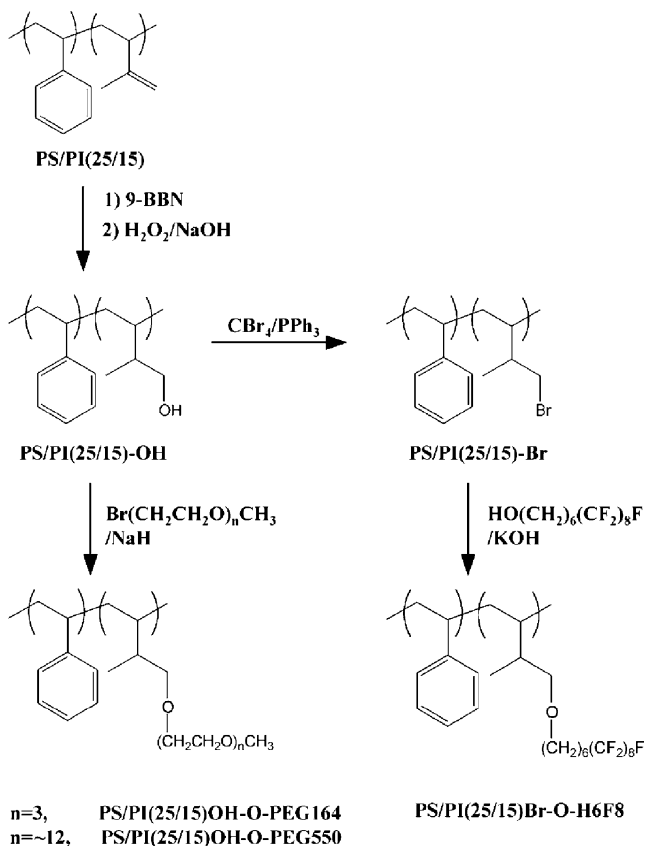
Fig. 12 Reaction scheme for the preparation of PEGylated and semifluorinated side chain block copolymers [28]

seen in Fig. 14, the 3-armed monodendrons led to a curvature that manifested itself in a surface covered with nanobumps that could be detected using AFM height imaging of the surface. The viscoelastic differences between the monodendron surface layer and the elastomer used as a substrate enabled detection of the presence of the coverage of the monodendron. This curvature had a subtle effect on apparent surface orientation and led to a measured value of weaker orientation than the surfaces made from single-armed monodendrons. When fouling behavior was evaluated, there was no detectable difference between the performance of the single side group surfaces or those made from the 2- and 3-armed monodendrons. Evidently the small nanobumps are below the size regime detected by the fouling microorganisms that were evaluated and this observation is consistent with other studies in which patterned surfaces were used to detect the role of dimension on fouling release properties.
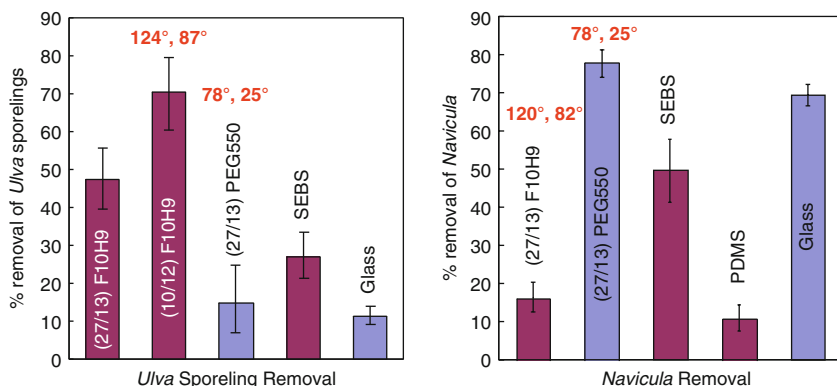
Fig. 13 Results of antifouling tests using *Ulva linza* and *Navicula* on PEG surfaces, semifluorinated surfaces, glass (silica), SEBS (an ABA triblock copolymer thermoplastic elastomer), and silicone. Numbers are advancing and receding contact angles of specific surfaces. FxHy refers to the size of the semifluorinated groups as noted above and the PEG550 is the molecular weight of the PEG side group [28]
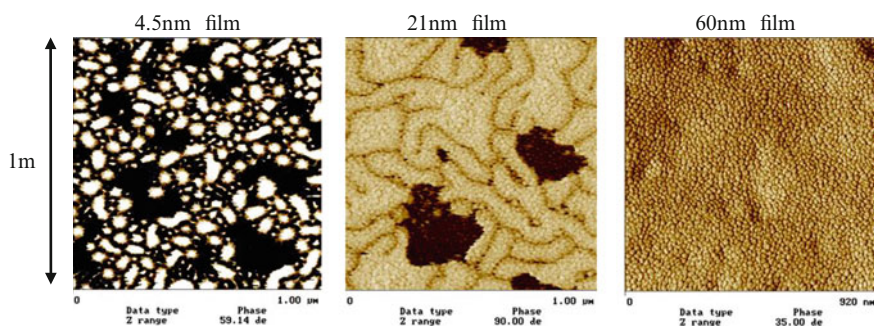
Fig. 14 SFM images of the surface of the 3-armed monodendron bilayer film covering the SEBS surface as a function of SABC thickness [47]

7   Block Copolymers with Amphiphilic Brushes

Given the inability of single component surfaces to act as broad-spectrum antifouling and fouling resistant coatings [29], studies have focused on creating new materials rather than pursuing a rigorously hydrophobic or hydrophilic structure to induce antifouling and fouling release. Block copolymers with either hydrophobic or hydrophilic side chains were tested against two complementary ubiquitous types of marine algae. For example, hydrophilic block copolymers containing PEG side chains exhibited strong fouling release for *Navicula* diatoms. Hydrophobic side
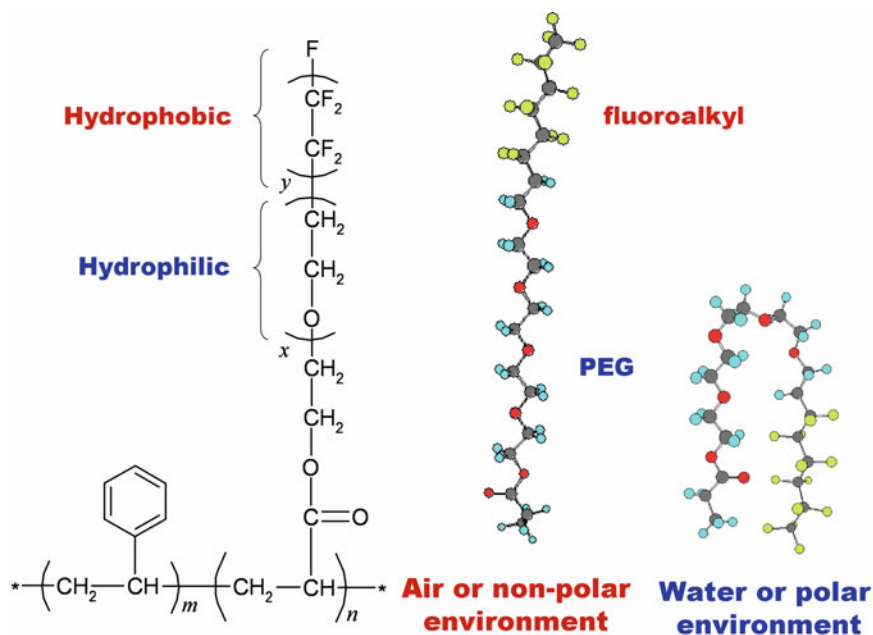
Fig. 15 Different arrangements of a Zonyl™ side group in the presence of a nonpolar and polar environment [48]

chains containing either fluorinated or PDMS-based side groups performed well for fouling release against *Ulva*. However, none of the surfaces performed well against both of the biofoulers. Therefore a significant amount of research has been focused on producing ambiguous amphiphilic coatings containing both hydrophobic and hydrophilic moieties at the surface.

One method to create an amphiphilic surface is to introduce both the hydrophobic and hydrophilic moieties in the same side unit attached to the block copolymer backbone. This allows both moieties access to the surface as shown schematically in Fig. 15. In addition, the side chains can respond to the environment when in contact with the surface to expose either the hydrophobic or hydrophilic segment of the side group. As a result, the surface constantly readjusts to form a responsive surface. The ability to respond creates an ambiguous surface, one in which the foulant has to deal with a changing surface and which inhibits biofoulers from adhering to the surface as strongly as a surface of fixed compositions. Initial studies of amphiphilic block copolymers were produced using a surface-active block copolymer made using ATRP to be combined with block copolymers of an epoxidized polystyrene-block-poly(ethylene-ran-butylene)-block-polyisoprene as shown in Fig. 16.
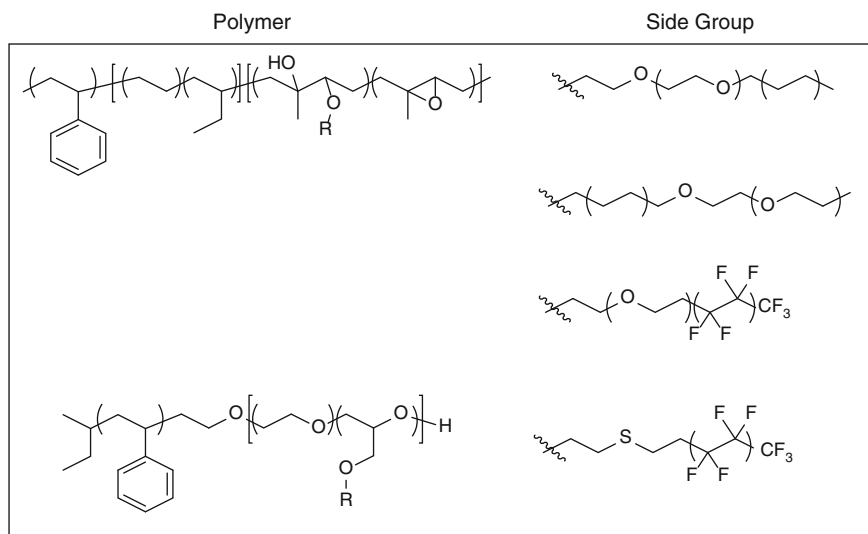
Fig. 16 Table of different block copolymers and different amphiphilic side groups that have been used for antifouling and fouling release applications [48–53]
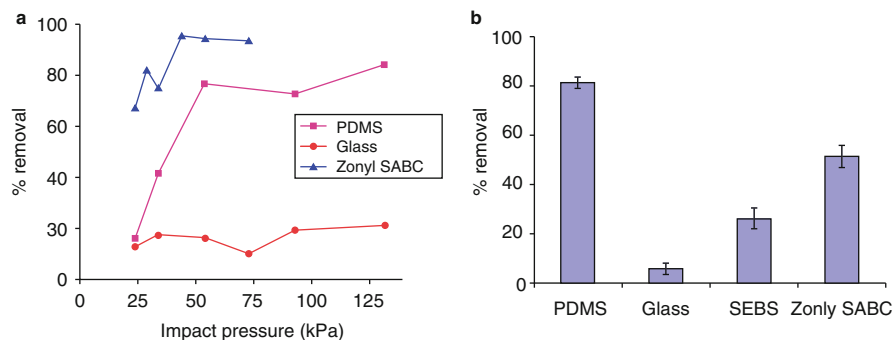
Fig. 17 (**a**) Percent removal of *Ulva* from PS-b-P(E/B)-b-PI triblock copolymer with Zonyl™ side groups at different impact pressures compared to a PDMS sample and the SEBS (polystyrene-block- poly(ethylene-ran-butylene)-block-polystyrene) underlayer; (**b**) percent removal of *Navicula* [48]

Despite the similarity to the single component surfaces described above, these new amphiphilic surfaces proved to be very effective against both test foulers. Tests against *Ulva linza* and *Navicula* showed that the amphiphilic Zonyl™ derived surface was more effective than either a polar glass or a nonpolar silicone surface. This behavior can be seen in Fig. 17 in which fouling release behavior of *Ulva linza* and *Navicula* on a surface subjected to a jet of water is displayed [48]. The amphiphilic surfaces are easily cleaned in this process as shown in the image showing a microscope slide before and after exposure to the water jet.

7.1 Method for Preparing Side Groups for the Polystyrene-Block-Poly(ethylene-ran-butylene)-Block-Polyisoprene (PS-b-P(E/B)-b-PI) Triblock Copolymer

The PS-b-P(E/B)-b-PI triblock copolymer was epoxidized on the isoprene block using m-chloroperoxybenzoic acid (mCBPA) to prepare the block copolymer. Side groups were amphiphilic alcohols that were either prepared commercially or synthesized specifically for this purpose in a two step process. These alcohols were then allowed to react with the epoxy groups on the block copolymer, catalyzed with $BF_3 \cdot Et_2O$. The ring opening step usually produced <50 % attachment of the side groups due to steric hindrance by the already reacted side groups.

Ober et al. grafted a single side chain containing a PEG segment and a fluorinated segment (Zonyl™) to their PS-b-P(E/B)-b-PI triblock copolymer where the PEG segment was directly grafted to the triblock copolymer. XPS was used to determine that both the fluorinated and PEG segments populated the surface [48]. The XPS was taken at 0° and 75° which showed that the PEG and fluorinated segments dominated the top few nanometers of the surface, which suggests the preferential segregation of the side chains on the surface. The samples exhibited strong antifouling and fouling release properties of *Ulva* sporelings. These surfaces were especially effective at fouling release because at low flow pressures, the samples exhibited near quantitative removal of *Ulva* foulant. The surfaces also demonstrated strong fouling release properties against *Navicula* diatoms.

Ober et al. have also grafted a single side chain containing a PEG segment and an alkyl segment to a PS-b-P(E/B)-b-PI triblock precursor copolymer, where the PEG segment was directly grafted to the triblock copolymer. The PEG portion of the side group was determined to be at the surface of the coating using NEXAFS and XPS data analysis, indicating that the PEG segments were present in the top few nanometers of the surface. Samples that had the same length of alkyl segment and progressively larger PEG segments were shown to be more hydrophilic by dynamic contact angle measurements despite that fact that PEG was the interior segment, suggesting that a larger portion of the hydrophilic PEG segment is exposed at the surface. Smaller PEG segments (two and ten repeat units) were more similar in dynamic contact angle studies than when comparing the 10 repeat unit with the 20 repeat unit side groups, suggesting that there is a length where the PEG segment is more easily brought to the surface. These coatings were determined to possess strong properties for fouling release of *Ulva* sporelings (Fig. 18a). Two of the samples, also exhibited strong fouling release properties for *Navicula* diatoms (Fig. 18c). These coatings were the assembled from the lengthier PEG and unsaturated alkyl segments [49].

More recently, Ober et al. reversed the order of the these side groups, thus having the PEG segments further away from the alkyl segments and closer to the backbone (Brij™), grafted to the same (PS-b-P(E/B)-b-PI) triblock copolymer. It was determined by dynamic contact angle that the reversed side group samples were more hydrophilic on the surface, indicating that being placed in the terminal part of the
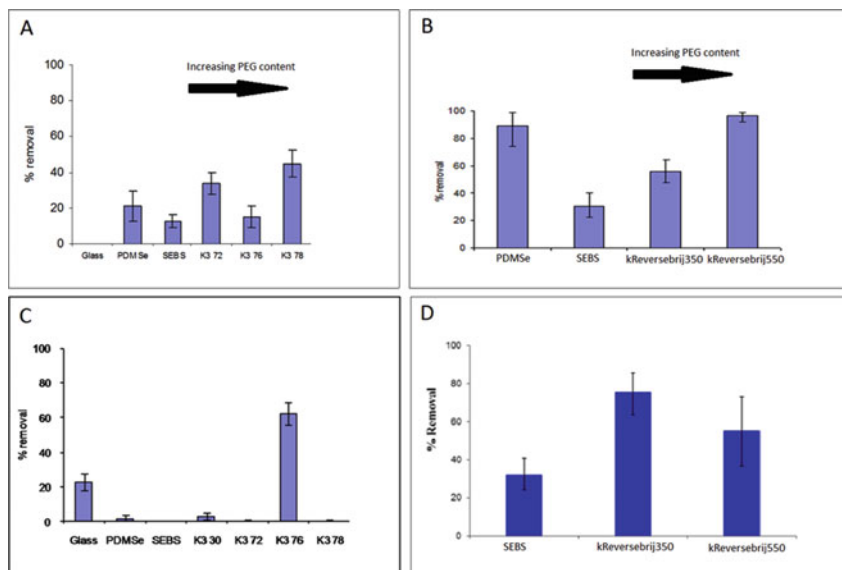
Fig. 18 (**a**) Removal of *Ulva* on Brij™ coatings, (**b**) removal of *Ulva* on reverse-brij coatings, (**c**) removal of *Navicula* on Brij™ coatings, (**d**) removal of *Navicula* on reverse-brij coatings. K3 72, K3 76, and K3 78 all have the same length alkyl segments, with progressively longer PEG chains. Reversebrij350 and Reversebrij550 have the same alkyl chain length and Reversebrij550 has a longer PEG segment [49]

side chain allowed the PEG segments to more densely populate the surface. Bubble contact angle measurements were able to determine that the surfaces rearranged after being submerged in water, and came to equilibrium after 72 h. AFM also demonstrated the same difference in the surface's microstructure after being submerged in water for over 72 h. One of these structures demonstrated near quantitative removal of *Ulva* sporelings (Fig. 18b). The same sample prevented almost any diatoms from adhering to the surface and provided some fouling removal of the same *Navicula* diatoms (Fig. 18d). Similarly the original PEG-hydrocarbon side groups with the longest PEG segments also performed the best.

An alternate version of creating an amphiphilic surface is to create either a hydrophilic or hydrophobic block copolymer backbone, and graft on side groups of the opposite polarity. Kramer et al. were able to produce such an example using fluorinated side groups attached to the PEG segment of a polystyrene-block-poly [(ethylene oxide)-stat-(allyl glycidyl ether)] [PS-b-P(EO-stat-AGE)] [49, 50]. The diblock copolymer backbone contained the PEG-like hydrophilic structures, while the side groups contained the hydrophobic portion. The allyl glycidyl ether unit was used as the point of attachment of the fluorinated side groups using thiol-ene "click" chemistry. Several different polymers were prepared with incorporation of the AGE ranging from 0 to 17 % allowing for the amount of the hydrophobic content to be readily tuned over that range. XPS and NEXAFS were able to determine that the increased amount of AGE monomer in the second block led to an increase in the number of fluorinated groups that were able to come to the surface of the coatings.

NEXAFS also demonstrated that the polystyrene block itself was present at lower concentrations at the surface with increasing fluorine content, indicating that the side groups occupied the surface and thereby inhibited other structures from populating the surface. However, the PEG-like portion of the diblock copolymer stayed relatively constant with its presence on the surface due its direct attachment to the fluorinated side groups. All of the samples showed strong antifouling release properties with *Ulva* sporelings. The samples with the higher fluorinated content showed excellent fouling release properties overall.

Similarly a nonpolar polymer backbone with polar side groups can be used. Webster et al. have synthesized a siloxane-based polymer with a 25 and 50 % incorporation of vinyl groups [52]. Using thiol-ene click chemistry carboxylic acid groups were attached to create an amphiphilic surface. Water contact angles show that the surfaces are still quite hydrophobic, similar to the dry surface, after 1 month of water immersion, but become more hydrophilic after an additional week in artificial seawater. The surface energies of the dry and submerged samples were similar, but the coatings that were submerged in artificial seawater for 1 week had significantly increased surface energy. The acid functionalized coatings showed high removal of *Navicula* diatoms at 138 kPa. However the samples showed a low percent removal of *Ulva* sporelings; lower than the percent removal of the base polymer. These samples also showed near quantitative removal of *A. amphitrite*. *C. lytica* and *H. pacifica* were also tested for removal with results comparable to the standards used in testing [52].

Koh et al. synthesized a poly(vinylidene fluoride-co-chlorotrifluoroethylene)-graft-poly(oxyethylene methacrylate) (P(VDF-*co*-CTFE)g-POEM) polymer via ATRP [51]. The concentration of the CTFE copolymer was varied between 0 and 10 % of the polymer. Dynamic contact angles of the surfaces showed the trend that a higher incorporation of the CTFE copolymer decreased the contact angle. This indicated that the PEG chains on the polymer were able to populate the surface. XPS data indicated that the higher the concentration of the CTFE copolymer, the lower the concentration of fluorine, and a higher concentration of oxygen on the surface. This suggests that PEG was able to populate the surface quite effectively. This surface was evaluated for water filtration systems, so it was tested by the water flux through the membrane over time. There was a trend where the higher fractional CTFE incorporation enabled the membrane to maintain the same amount of water flux [51].

Zonyl™ side groups were further pursued by Galli et al. who attached the Zonyl™ groups to a modified styrene block of a PDMS-b-PS diblock copolymer. The coatings were obtained from blends of the block copolymer (1–10 wt%) in a PDMS matrix. XPS measurements demonstrated that there was a higher amount of fluorine and a lower amount of silicone at the top few nanometers than would be present in the bulk of the coating. This observation suggests that the Zonyl™ side groups of the diblock copolymer were dominating the surface over the PDMS block and the PDMS matrix. This behavior was observed in both dry and wet samples. These surfaces were tested for fouling removal against *Ulva* sporelings and showed superior results. The samples allowed 50–80 % removal of the sporelings at a low shear stress of 13.6 Pa, greatly outperforming the PDMS-based standard. In addition, the best fouling removal samples were then further optimized by the addition

of 0.1 wt% multiwall carbon nanotubes. These coatings also showed excellent fouling release of the *Ulva* sporelings; however, there was not a significant difference from the earlier coatings indicating that the multiwall carbon nanotubes did not have a significant effect on the fouling release properties [53].

8 Block Copolymers with Randomly Mixed Polar and Nonpolar Side Groups

In addition to the homogeneous surfaces that uniformly contain hydrophilic or hydrophobic side groups described above, heterogeneous surfaces containing mixed polar and nonpolar side groups have received some attention, as they have been demonstrated to be effective at antifouling and fouling release behavior. A rationale for the development of such materials was the observation that generally for block copolymers with mixed side groups, there are two types of side groups that are used: polar and nonpolar to create an amphiphilic environment on the surface. Predominately, the hydrophilic surfaces have focused on PEG, due to its high resistance to protein adsorption and cell adhesion [27, 54, 55] while the hydrophobic surfaces come from fluorinated side chains [28, 56] which display strong fouling release properties due to their low Young's modulus and their low surface energy [16, 17] (Fig. 19).

Several examples of heterogeneous surfaces for antifouling and fouling release applications have used combinations of fluorinated and PEGylated side groups. Gudipati et al. reported the development of coatings consisting of an amphiphilic
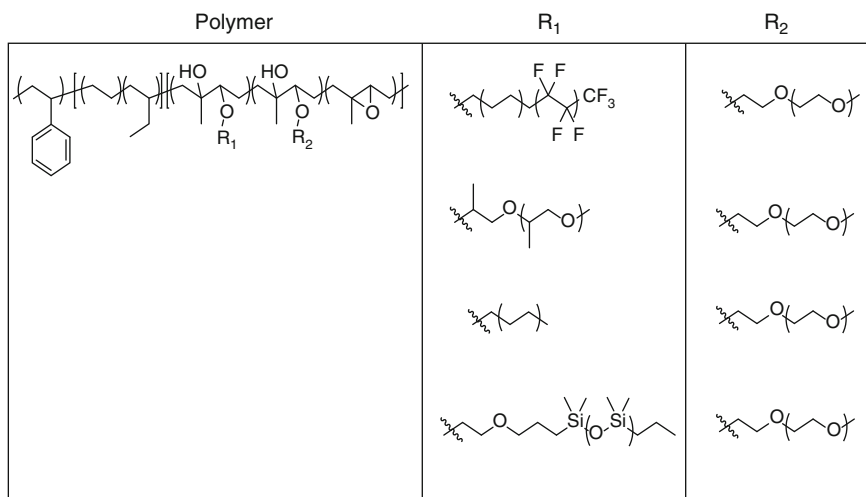
Fig. 19 Chemical structures of the block copolymer and side groups used for mixed side groups [57–61]
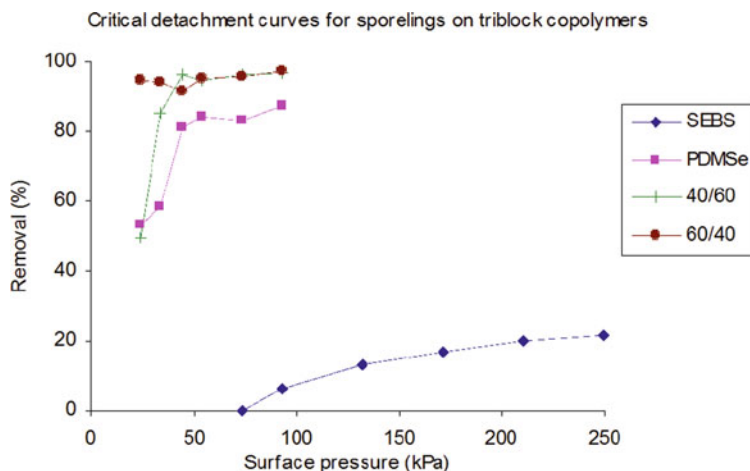
Fig. 20 Percent removal of *Ulva* from a PS-b-P(E/B)-b-PI triblock copolymer with Fluorine/PEG mixed side groups (40:60 and 60:40 refer to the feed ratio of the fluorinated and PEG side groups respectively) at an array of surface pressures [57]

network of hyperbranched fluoropolymer groups combined with linear PEG moieties that shower better release of *Ulva* sporelings than a PDMS coating [34]. In two other studies, both Krishnan et al. and Martinelli et al. report block copolymers with side chains containing grafted ethoxylated perfluoralkyl groups that were able to release both *Ulva* and *Navicula*, even though these test species have different fouling release mechanisms and favor attachment to opposite polarity surfaces [62, 63]. However, these examples are limited by their use of nonionic surfactant moieties as a basis of the amphiphilic structure [57] which limits the range of compositions possible. While covalently attaching the hydrophobic and hydrophilic groups as a single unit guarantees a heterogeneous surface and the ability to rearrange and alter their relative composition is restricted by the polymer modification reactions [57]. If the hydrophobic and hydrophilic units are introduced as individual side chains where the relative ratio can be modified, it allows the surface chemistry to be easily modified to enhance antifouling and fouling release properties.

Ober et al. grafted two different side chains to their PS-b-P(E/B)-b-PI triblock copolymer where one side chain was a PEG segment, and the other side chain was a fluorinated side chain [57]. The side chains were added in 100:0, 80:20, 60:40, 40:60, 20:80, 0:100 feed ratios. XPS was used to determine that the population of the fluorinated segment on the surface increased proportionally to the feed ratio. XPS also determined that the PEG side group was also present on the surface. NEXAFS was able to show the progressively increasing amount of the fluorinated segments at the surface. These surfaces demonstrated excellent antifouling and fouling release behavior against *Ulva* sporelings even at low surface pressures as shown in Fig. 20. The coatings were then tested against *Navicula* diatoms for fouling release and formed a trend where the samples with the most fluorine content demonstrated the strongest fouling release (Fig. 21).

Removal of diatoms from triblock copolymers
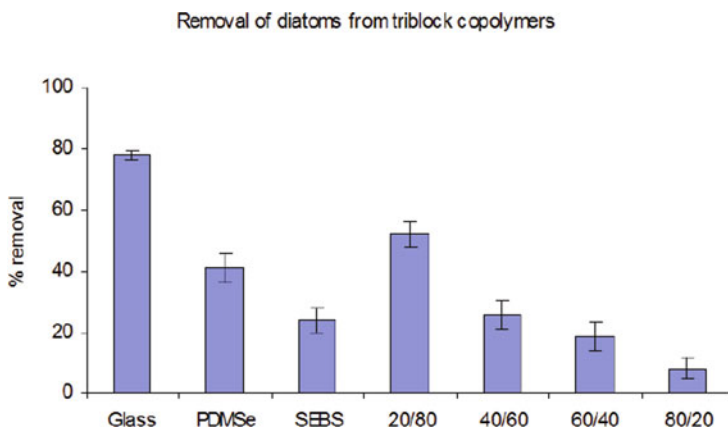
Fig. 21 Percent removal of *Navicula* from a PS-b-P(E/B)-b-PI triblock copolymer with Fluorine/ PEG mixed side groups (20/80, 40/60, 60/40, and 80/20 refer to the feed ratio of the fluorinated and PEG side groups respectively) tested against a PDMS coating and the SEBS underlayer [57]

While the majority of antifouling surfaces have incorporated fluorinated segments as the hydrophobic moiety in amphiphilic systems, it has been shown that fluorinated segments with more than four consecutive CF_2 units can bioaccumulate in mammalian blood, which causes them to be recognized as environmentally hazardous materials [58, 64–66]. For these reasons, several alternative hydrophobic side groups have been developed for block copolymers with mixed side groups.

A wide variety of alkyl groups used in combination with PEG side units have been grafted to the PS-b-P(E/B)-b-PI triblock copolymer backbone for antifouling and fouling release applications. Two types of alkyl side chains that differed in length were used, and four different PEG chains of various lengths were used. After these samples were analyzed the most promising surfaces were then optimized by adjusting the feed ratio of the two side groups. These surfaces were characterized using dynamic water contact angle, captive air-bubble contact angle, AFM, XPS, and NEXAFS, which were able to indicate that the surfaces "reconstruct" when submerged in water [58]. When immersed in water, the PEG side chains rise to the surface [58]. Bubble contact angles showed that all of the samples rearranged at roughly the same rate, reaching equilibrium after 1 day. All of the samples demonstrated excellent antifouling and fouling release properties against *Ulva* sporelings (some shown in Fig. 22). There is a trend where the heterogeneous samples do provide better fouling release than the homogeneous alkyl samples. Against diatoms, there was a trend where higher feed ratios that favored a higher PEG content exhibited stronger antifouling properties.

Polypropylene glycol (PPG) has been used as a hydrophobic moiety as well. PPG and PEG chains have been grafted to PS-b-P(E/B)-b-PI triblock copolymer for antifouling and fouling release applications. The side chains were added in 100:0, 75:25, 50:50, 25:75, 0:100 feed ratios. AFM illustrated that the cylinder microstructure that forms doubles to triples in size, after the coatings have been immersed
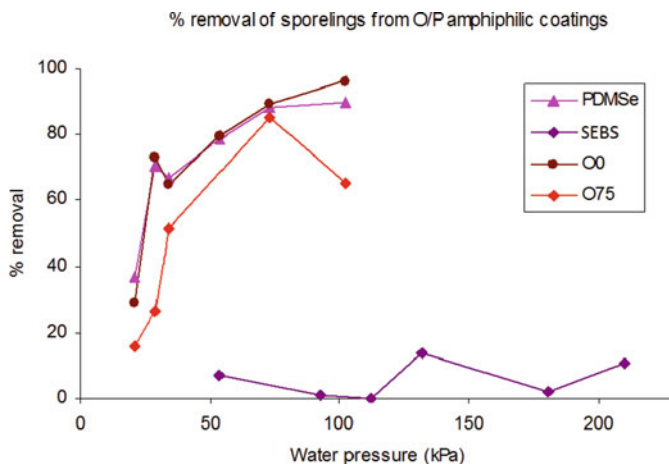
Fig. 22 Percent removal of *Ulva* from a PS-b-P(E/B)-b-PI triblock copolymer with alkyl and PEG mixed side groups (O0 is 100 % PEG side groups, O75 has 75 % alkyl and 25 % PEG) at an array of surface pressures against a PDMS coating and the SEBS underlayer [58]

in water after 7 days. This indicates the reorganization of the P(E/B) block and the side chains on the functionalized end block. All of the heterogeneous coatings show strong affinity for antifouling and fouling release of *Ulva* sporelings, while the homogeneous coatings tended to not perform as well. This result strongly suggests that it is an important aspect of nontoxic antifouling coatings to present both polar and nonpolar units in order to be effective against a broad range of fouling species.

Ober et al. have also investigated other polar: nonpolar combinations by attaching to the PS-b-P(E/B)-b-PI triblock copolymer both a PEG segment, and a PDMS side unit [59]. These side chains were added at 0:100, 25:75, 50:50, 75:25, and 100:0 feed ratios. NEXAFS and XPS were used to show that the varying degree of PEG and PDMS side groups that were at the surface were roughly proportional to the feed ratios of the two side chains. Dynamic contact angles were able to show that the surfaces with the higher PEG content were more hydrophilic. Bubble contact angles were used to demonstrate that the surfaces with a higher PEG content could rearrange their surface structure faster than samples with a higher PDMS content. Only the sample with a PEG:PDMS feed ratio of 75:25 was able to show strong fouling release properties; however it showed a near quantitative release at pressures of 50 Pa. At lower pressures as shown in Fig. 23 the samples with a PEG: PDMS feed ratio of 75:25 still show a moderate amount of fouling release for *Ulva* sporelings. The samples with higher PDMS content showed poorer fouling release, despite the fact that the most successful commercial coatings are built from PDMS. When tested against *Navicula* diatoms at low pressures, the coating showed a modest amount of fouling release (Fig. 24).

Zonyl™ and PDMS side groups were utilized by Galli et al. on a copolymer for antifouling and fouling release applications [60]. The coatings were prepared by

Fig. 23 Percent removal of *Ulva* from a PS-b-P(E/B)-b-PI triblock copolymer with PDMS and PEG mixed side groups (Si0 is 100 % PEG side groups, Si25 has 25 % PDMS and 75 % PEG side groups, Si50 has 50 % PDMS and 50 % PEG side groups, Si75 has 75 % PDMS and 25 % PEG side groups, and Si100 has 100 % PDMS side groups) at an array of surface pressures against a PDMS coating and the SEBS underlayer [59]
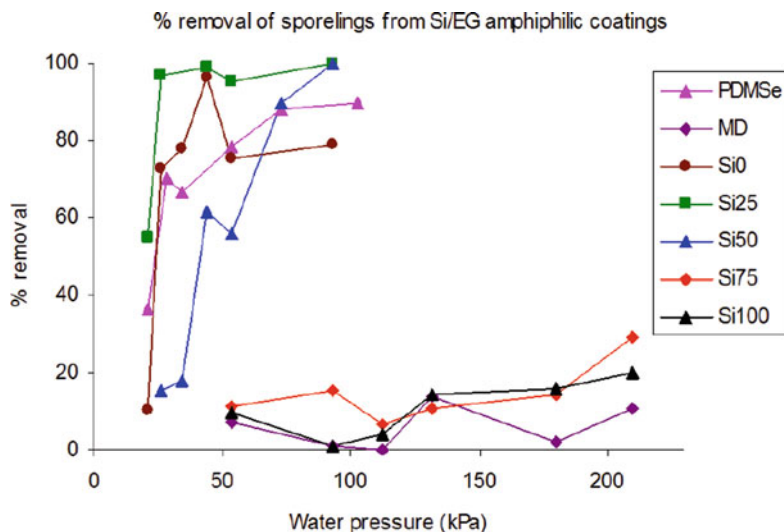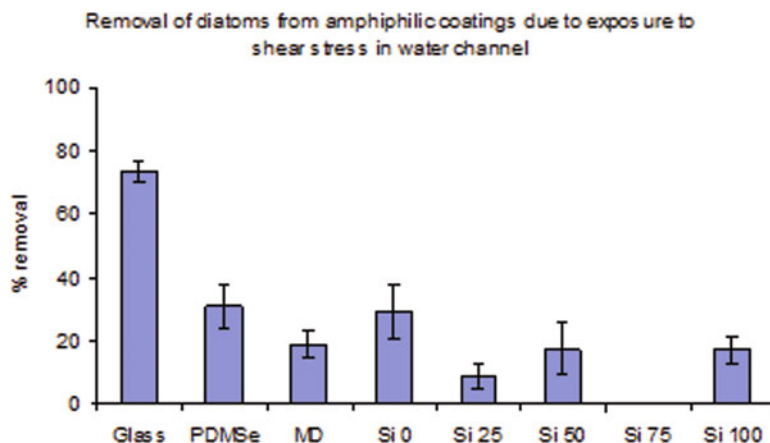

Fig. 24 Percent removal of *Navicula* from a PS-b-P(E/B)-b-PI triblock copolymer with PDMS and PEG mixed side groups (Si0 is 100 % PEG side groups, Si25 has 25 % PDMS and 75 % PEG side groups, Si50 has 50 % PDMS and 50 % PEG side groups, Si75 has 75 % PDMS and 25 % PEG side groups, and Si100 has 100 % PDMS side groups) tested against a PDMS coating and the SEBS underlayer [59]

blending 1 or 4 wt% of the copolymer into the PDMS matrix. Dynamic contact angles were taken of the surfaces over a week of being submerged in water, which indicated that the surface became progressively more hydrophilic after each day. This suggests that the surface was still rearranging for the PEG segments of the Zonyl™ side groups after 7 days under water. Similarly the surface energy was shown to increase over the course of a week, indicating that less of the PDMS side groups and PDMS matrix were populating the surface the longer the samples were submerged [60]. All of the coatings under XPS showed that the upper five nanometers contained a higher amount of fluorine and a lower amount of silicon than would be present in the average composition of the surface. The difference in the experimental and averaged amounts increased with the higher composition of the Zonyl™ side group in the copolymer. This suggests that the Zonyl™ side group is able to populate the surface more effectively than the PDMS from the side groups and the matrix [60]. The samples with the lower percentage of incorporation of the Zonyl™ copolymer demonstrated high fouling removal of *Ulva* sporelings. However, the other coatings with higher Zonyl™ content show poorer results [61]. In addition, the coatings with lower Zonyl™ incorporation show the best results for removal of barnacles displaying good antifouling properties, while the coatings with the higher incorporation of the Zonyl™ side group perform poorly against *B. amphitrite* cyprids. These higher performing coatings were tested in the ocean against Intersleek 700™, a high-performing antifouling industry coating. The Zonyl™ coatings showed significantly improved results over the PDMS-based standards and equivalent results for the Intersleek 700™ coating [61].

Galli et al. then studied fluorinated and PDMS side groups on a random copolymer. Coatings were prepared by blending the copolymers (0.15–10 wt%) in a PDMS matrix. Similar to their previous studies, under XPS all of the samples containing fluorinated side groups showed that the upper five nanometers contained a higher amount of fluorine and a lower amount of silicon than would be present in the average composition of the surface. The difference in the experimental and averaged amounts increased with the higher composition of the fluorinated side group in the copolymer and with higher copolymer loading in the sample [67]. Dynamic contact angles in water indicated that the surfaces were hydrophobic, and much more hydrophobic than the similar random copolymers that Galli et al. used before with the Zonyl™ side groups [60, 68]. Similarly, the surface energies of these coatings were much lower than the surface energies with the Zonyl™ groups [60, 68]. These findings seem to be the results of the absence of a PEG group in these coatings. If there was a PEG segment present, it would likely rise to the surface to interact with the water, making the surface more hydrophilic and increasing the surface energy. When tested against *Ulva* sporelings, these coatings showed good fouling release properties. A trend formed when the coatings were used against cyprid larvae showing that there was less settlement of the larvae with the higher loading of the random copolymer in the PDMS matrix. The samples were also tested against barnacles, and the coatings were able to prevent the barnacles from adhering as strongly to the surface as the PDMS control did [68].

9   Cationically Charged Surfaces

Combining polycations and hydrophobic alkyl groups produces compounds which disrupt lipid bilayer formation in aqueous environments [69]. Cations studied include ammonium [70–80], pyridinium [81–87], phosphonium [88–94], and sulfonium [95] groups (Fig. 25). These groups, however, are toxic to the environment when released [96–98]. By tethering them to a polymeric backbone, the coatings are not able to leach toxic materials into the local environment where these coatings are being used [74, 99–105]. Quaternary ammonium salts specifically have advantages over other antibacterial agents. They penetrate cell membranes very efficiently, have low toxicity to mammalian organisms, are environmentally stable, minimally corrosive, and remain biologically active on surfaces for an extended time [101, 106]. This section will focus on surfaces that incorporate quaternary nitrogen.

Biofouling on marine surfaces occurs in several phases. The early stages of this process include bacterial settlement and colonization of the surfaces. Bacterial biofilms on surfaces then promote the settlement of larger organisms which are part of advanced stage biofouling. Studies have shown that the presence of bacterial biofilms promote more attachment and growth of these fouling organisms than surfaces without bacterial films [107, 108]. Therefore, being able to minimize the growth of bacterial biofilms on marine surfaces through the use of antibacterial surfaces is quite promising for reducing overall growth of marine fouling on a surface.

The antibacterial effect of cationic structures can be capitalized upon to produce surfaces which are highly unfavorable for cellular settlement and as a result may inhibit fouling. The membranes in bacterial cells are made up of a lipid bilayer consisting of molecules such as phosphatidyl ethanolamine and phosphatidyl glycerol. Molecular modeling of the interactions of these polycations with the lipid bilayers show that the negatively charged phosphate strongly associates with the positively charged component of the polycation. Additionally the hydrophobic region of the polycations inserts itself into the bilayer itself resulting in disorganization of the membrane, leakage, and cell death [109].

Although the exact mechanism of disruption has not been determined, the activity of these compounds is believed to be due to the electrostatic interactions between the polycations and the lipid bilayer membranes [69–71, 110, 111]. It has been proposed by Ivanov et al. [109] that the insertion of the hydrophobic groups of these materials is the main cause of the cell membrane disruption. However, Kugler et al. [112] proposed that the insertion of these cations causes a release of cations from the membranes, causing the disruption of membrane functions. By displacing

Fig. 25 Cations studied as a part of antifouling coatings [69–97]

Ammonium   Pyridinium   Phosphonium   Sulfonium
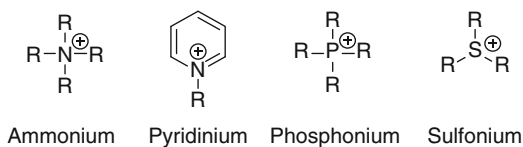
the Mg^{2+} and Ca^{2+} divalent cations which bridge the phosphate groups the bacterial cell membranes are disrupted. In both cases, it is the polycation's ability to destabilize the membranes of the cells which leads to the antibacterial properties.

9.1 Polymer-Bound Quaternary Ammonium Cations as Antibacterial and Antifouling Surfaces

Surface-tethered brushes of N-hexylpyridinium polymer reported by Tiller et al. [84] were shown to be highly effective against even airborne bacteria. These surfaces effectively killed a number of types of airborne bacteria on contact, showing how effective quaternary ammonium salts can be as antibacterial surfaces. The polymers prepared were poly(4-vinylpyridine) (P4VP) which were then quaternized through the N-alkylation of the pyridine rings of the P4VP with n-alkyl bromides of different lengths. It was noted that the n-hexyl ammonium salt was the most effective against S. aureus.

The effect of the molecular weight of the surface-tethered brushes was also studied. Surfaces were prepared from P4VP polymers of 60 and 160 kDa. The surfaces with lower chain length P4VP showed reduced antibacterial activity, likely because the longer polymer chains were more readily able to penetrate into the 30 nm thick cell walls of the bacteria used. This gives further evidence that penetration of the polycations into cell membranes is important to the antibacterial function of these structures.

Similar structures containing alkyl and fluorinated alkyl groups were prepared by Krishnan et al. [102] to study the effect of hydrophobic groups attached to the quaternary ammonium units and their role in antibacterial surfaces. In particular, the fluorinated unit aided surface placement of the quaternary ammonium through surface directed phase separation. In this study, block copolymers of polystyrene (PS) and poly(4-vinylpyridine) (P4VP) were prepared by anionic polymerization in THF at $-78\ ^\circ$C. The polymerization was initiated by sec-butyl lithium in a solution containing lithium chloride. The styrene block was polymerized first followed by the 4-vinyl pyridine. One polymer with PS and P4VP molecular weights of 11 and 21 kDa respectively and another with PS and P4VP molecular weights of 62 and 66 kDa respectively were prepared. The quaternization reaction was performed with 1-bromohexane to produce non-fluorinated quaternary ammonium containing block copolymers. A second quaternization reaction was performed with 6-perfluorooctyl-1-bromohexane and 1-bromohexane to give block copolymers with semifluorinated side groups, where 30 % of the quaternary ammonium groups were fluorinated, and the rest simply had alkyl groups attached.

Surfaces from these materials were then prepared by first coating an elastomeric underlayer of SEBS on glass slides [102]. The ammonium salt containing block copolymers were then spray coated onto this underlayer and annealed. Bacterial bioassays were performed with S. aureus cells to determine the antibacterial
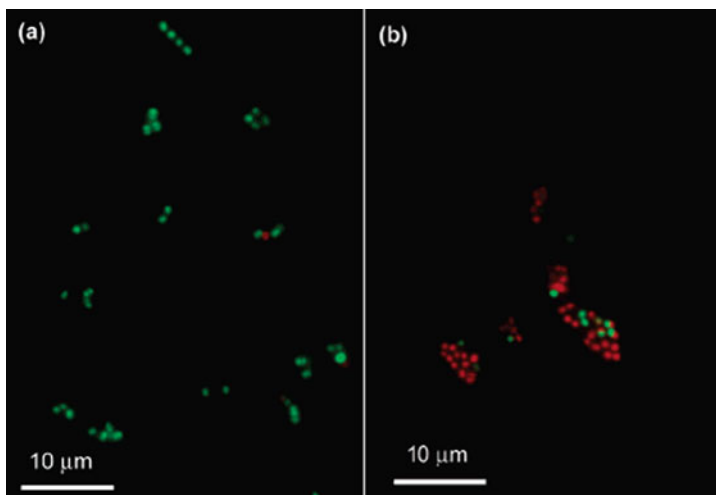
Fig. 26 Fluorescence microscopy of *S. aureus* cells. *Green* cells indicate live cells, and *red* indicated dead cells. Surfaces are (**a**) untreated glass (**b**) coated surface [102]

performance of these surfaces relative to a glass control surface. It was observed that the non-fluorinated ammonium salt structures were able to reduce the viable bacteria by 15–30 % compared to glass. However, the polymers containing semifluorinated ammonium salts showed a nearly 100 % decrease in the viable cell counts at the surface as seen in fluorescence microscopy images in Fig. 26. Surface analysis showed that polymers containing the semifluorinated structures had a higher surface population of the quaternary ammonium structures, which likely increased the activity of the antibacterial surfaces. However, surface population does not entirely describe the change in performance, and it is apparent that the presence of fluorinated groups additionally increases the antibacterial activity of these surfaces.

Similar fluorinated quaternary ammonium groups were utilized by Park et al. [113] for the purpose of creating antimicrobial and antifouling surfaces. This work, however, utilized a polymer backbone of polystyrene-*b*-poly(ethylene-*ran*-butylene)-*b*-polyisoprene (SEBI) as shown in Fig. 25. To functionalize this polymer, the double bonds of the polyisoprene block were epoxidized, and then reacted with 3-(dimethylamino)-1-propylamine (DMAPA) to introduce amines onto the polymer. The amine was then quaternized using a semifluorinated alkyl bromide similar to that used by Krishnan et al. (Fig. 27) [102]. Remaining amine groups were then quaternized using 1-bromohexane. Surfaces were prepared in a similar manner as done by Krishnan et al. [102], utilizing an elastomeric underlayer of SEBS on glass slides. The functionalized SEBI polymer was then spray coated onto the surface and annealed to create the active coating.

Antibacterial activity of these coatings was determined by comparing the number of bacterial colonies of *S. aureus* grown on the coatings when compared to a glass surface. No colonies of bacteria were able to colonize the coated surface when
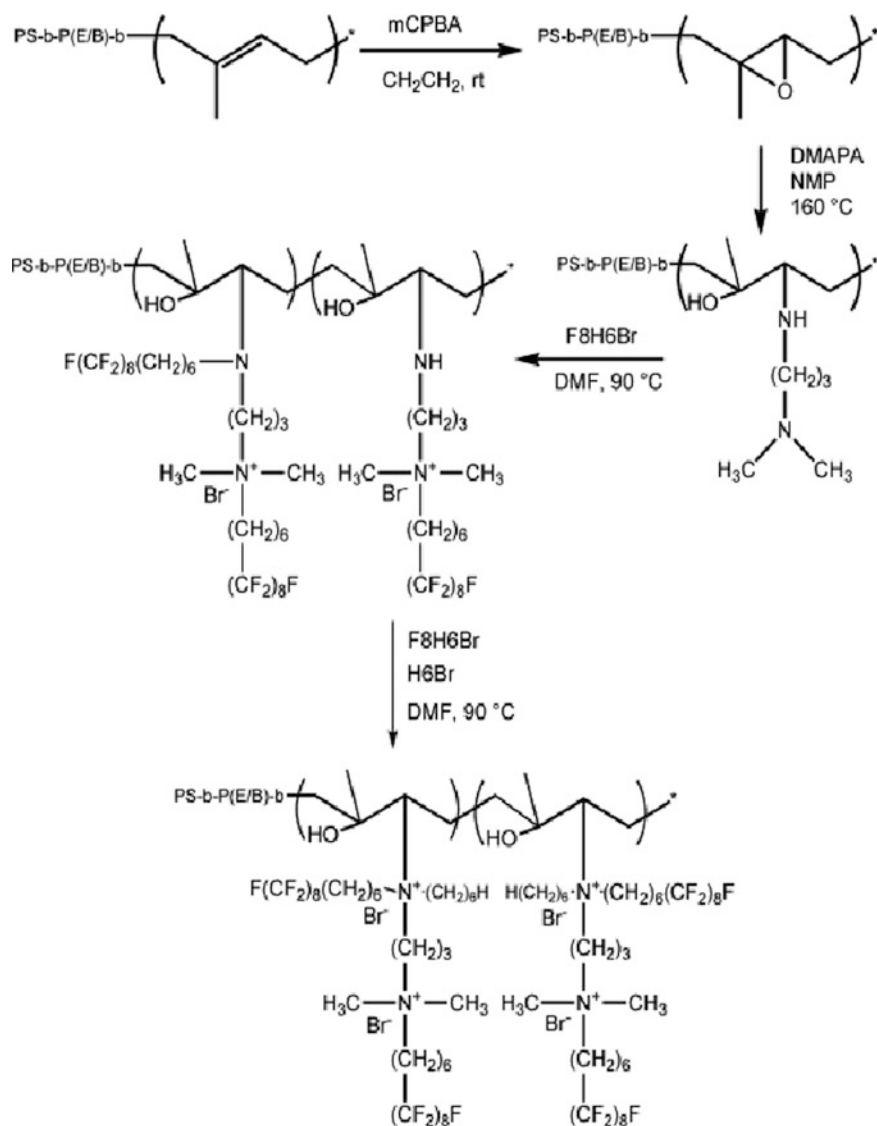
Fig. 27 Synthesis of quaternary ammonium salt functionalized SEBI [102]

incubated overnight, indicating the high antibacterial performance of this polymer. Additionally, a LIVE/DEAD assay was performed to determine how readily bacteria in contact with the surface were killed. These coatings were able to kill roughly 20 % of cells at the surface in 1 h, compared to 5–10 % killed by a glass surface.

Additional work by Zhou [114] shows the antimicrobial effect of combining a quaternary amine with a poly(ethylene glycol) (PEG) side group on a block copolymer. The block copolymer used in this work was SEBI, the same as was used by Park et al. [113]. The alkene groups of the polyisoprene block were epoxidized, and
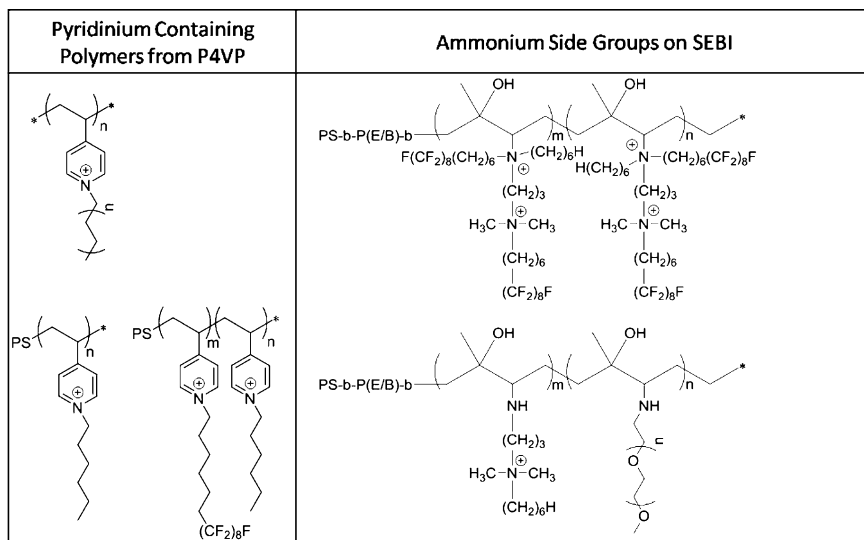
Fig. 28 Quaternary ammonium structures used in block copolymer coatings [102, 113, 114]

then functionalized using both DMAPA as used by Park et al. as well as an amine functionalized PEG. The amine groups were then quaternized using 1-bromohexane. Two polymers were prepared, one containing only quaternary ammonium salt side groups, and one with only 30 % of available sites functionalized with the quaternary ammonium salts and the remaining 70 % being functionalized with the PEG side groups. Functional coatings were prepared in the same manner as by Krishnan et al. [102] and Park et al. [113] by using a SEBS coated glass surface spray coated with the functionalized block copolymer (Fig. 28).

The incorporation of the PEG side groups to the polymer was able to significantly reduce the absorption of bovine serum albium (BSA) to the surfaces relative to both the control as well as to the polymer containing only quaternary ammonium salts with no PEG. To test the antibacterial activity of these surfaces, experiments using *S. aureus*, *E. coli*, and *C. Marina* were performed. These experiments determined how readily surfaces could be colonized as well as the ratio of live cells to dead cells at the surface. All experiments were performed using an unfunctionalized SEBI block copolymer surface as a standard. As was observed by Krishnan et al. [102], the quaternary ammonium salt containing polymers were highly effective at killing cells at the surface for all three bacteria studied. The PEG containing block copolymer was not as effective at killing the cells, likely due to the lower percentage of quaternary ammonium salts. The PEG containing block copolymers, although not as effective at killing bacteria, was able to significantly reduce the number of bacteria able to attach to the surface for both *S. aureus* and *C. Marina*, and performed as well as the block copolymer without PEG for *E. coli*. This overall indicates a better performance antifouling coating, as the surface remains cleaner when PEG is incorporated.

10 Summary

Producing fouling resistant and antifouling coatings that address all the fouling species likely to be encountered remains a daunting challenge. With the current efforts to create coatings that contain no biocidal material, the challenge is even greater. Block copolymers appear to be ideal platforms to test new concepts in antifouling coatings and in developing practical new materials that can be applied to a broad range of surfaces. This chapter describes the design and study of a variety of di- and triblock copolymers which examined a variety of strategies for creating a surface-active block copolymer including the use of single polarity compositions, incorporation of uncharged amphiphilic materials, blocks with mixed polar and nonpolar units and even charged polymers in the form of quaternary ammonium salts.

Using a block copolymer combination, in which a thermoplastic elastomer block provides the basic coating and the appropriate mechanical properties for fouling release, enables the fine-tuning of the surface composition in the surface-active block copolymers. Strategies for making self-healing structures using this strategy have been undertaken, but were not discussed in this chapter. Coating strategies, also not discussed here, are important in creating the final coating material. When done properly, this strategy enables a head-to-head comparison of subtle changes in the structure of the antifouling units.

It is now possible to demonstrate that single polarity coatings are insufficient to prevent fouling by the host of species that can settle on surfaces in the aquatic environment. Amphiphilic materials have broad-spectrum action and can prevent fouling by a broad range of species. The availability of many nonionic surfactants makes amphiphilic materials easily available and at low cost, but the nature of the side group is fixed by the supplier (and subject to the whims of the manufacturer, as we learned in our studies). If tuning of the ratio of polar and nonpolar components is necessary, then amphiphilic units become limiting. For this reason the use of mixed structures shows great promise. Surprisingly, in most compositions, coatings with a molar excess of PEG as the polar unit show better fouling resistance than those with a majority of the nonpolar component. To date there is little known about the combination of charged groups with amphiphilic or combined polar/nonpolar surfaces. In future, this is likely to be a rich area to examine.

Abbreviations

AFM	Atomic force microscopy
AGE	Allyl glycidyl ether
ATRP	Atom-transfer radical-polymerization
BSA	Bovine serum albumin
CTFE	Polychlorotrifluoroethylene
Da	Daltons
DMAPA	3-(Dimethylamino)-1-propylamine
EPS	Extracellular polymeric substances
GPS	3-(Glycidoxypropyl)trimethoxy silane
HBFP	Hyperbranched fluoropolymer
L-DOPA	L-3,4-dihydroxyphenylalanine
MA	Maleic anhydride
mCPBA	m-Chloroperoxybenzoic acid
NEXAFS	Near edge X-ray absorption fine structure
P2VP	Poly(2-vinyl pyridine)
P4VP	Poly(4-vinylpyridine)
Pa	Pascals
PDMS	Poly(dimethylsiloxane)
PEG	Poly(ethylene glycol)
PMMA	Poly(methyl methacrylate)
PS	Polystyrene
PS-b-P(E/B)-b-PI	Polystyrene-*b*-poly(ethylene-*stat*-butylene)-*b*-polyisoprene
PTFE	Polytetrafluoroethylene
SABC	Surface activated block copolymers
SEBS	Polystyrene-*b*-poly(ethylene-*stat*-butylene)-*b*-polystyrene
SFM	Scanning force microscopy
TBT	Tributyl tin
UV	Ultraviolet
XPS	X-ray photoelectron spectroscopy

References

1. Haras D (2006) Biofilms et Altérations des Matériaux: de L'analyse du Phénomène aux Stratégies de Prévention. Mater Tech 93:s.27
2. Lejars M, Margaillan A, Bressy C (2012) Fouling release coatings: a nontoxic alternative to biocidal antifouling coatings. Chem Rev 112:4347–4390
3. Callow JA, Callow ME (2006) Biofilms. In: Fusetani N, Clare AS (eds) Antifouling compounds. Progress in molecular and subcellular biology, sub-series marine molecular biotechnology. Springer, Berlin/Heidelberg/New York, pp 141–169
4. Rosenhahn A, Schilp S, Kreuzer HJ, Grunze M (2010) The role of "inert" surface chemistry in marine biofouling prevention. Phys Chem Chem Phys 12:4275
5. Callow ME, Callow JA (2002) Marine biofouling: a sticky problem. Biologist 49(1):10–14

6. Lack DA, Corbett JJ, Onasch T, Lerner B, Massoli PK, Bates TS, Covert DS, Coffman D, Sierau B, Herndon S, Allan J, Baynard T, Lovejoy E, Ravishankara AR, Williams E (2009) Particulate emissions from commercial shipping: chemical, physical, and optical properties. J Geophys Res 114:D00F04

7. Corbett JJ, Koehler HW (2003) Updated emissions from ocean shipping. J Geophys Res 108:4650

8. Werner C, Maitz CF, Sperling C (2007) Current strategies towards hemocompatible coatings. J Mater Chem 17:3376–3384

9. Woods Hole Oceanographic Institution (1952) Marine fouling and its prevention. U.S. Naval Institute, Annapolis

10. Alzieu CL, Sanjuan J, Deltreil JP, Borel M (1986) Tin contamination in Arcachan Bay effect on oyster shell anomalies. Mar Pollut Bull 17:494–498

11. Alzieu C (2000) Environmental impact of TBT: the French Experience. Sci Total Environ 258:99–102

12. Ruiz JM, Bachelet G, Caumette P, Donard OFX (1996) Three decades of tributyltin in the coastal environment with emphasis on Arcachon Bay, France. Environ Pollut 93:195–203

13. Pereira M, Ankjaergaard C (2009) Advances in marine antifouling coatings and technologies. In: Legislation affecting antifouling products. Woodshead Publishing, Cambridge, UK, p 240

14. Ytreberg E, Karlsson J, Eklund B (2010) Comparison of toxicity and release rates of Cu and Zn from anti-fouling paints leached in natural and artificial brackish seawater. Sci Total Environ 408:2459–2466

15. Krishnan S, Weinman CJ, Ober CK (2008) Advances in polymers for anti-biofouling surface. J Mater Chem 18:3405–3414

16. Beigbeder A, Degee P, Conlan SL, Mutton RJ, Clare AS, Pettitt ME, Callow ME, Callow JA, Dubois P (2008) Preparation and characterisation of silicone-based coatings filled with carbon nanotubes and natural sepiolite and their application as marine fouling-release coatings. Biofouling 24:291–302

17. Wynne KJ, Swain GW, Fox RB, Bullock S, Ulik J (2000) Two silicone nontoxic fouling coating hydrosilation cured PDMS and CaCO$_3$ filled, ethoxysiloxane cured RTV11. Biofouling 16:277–288

18. Brady RF (2000) ABC triblock surface active block copolymer with grafted ethoxylated fluoroalkyl amphiphilic side chains for marine antifouling/fouling-release applications. Polym Paint Colour J 190:18–20

19. Wendt DE, Kowalke GL, Kim J, Singer IL (2006) Factors that influence elastomeric coating performance: the effect of coating thickness on basal plate morphology, growth and critical removal stress of the barnacle balanus amphitrite. Biofouling 22:1–9

20. Kim J, Chisholm BJ, Bahr J (2007) Adhesion study of silicone coatings: the interaction of thickness, modulus and shear rate on adhesion force. Biofouling 23:113–120

21. Kim J, Nyren-Erikson E, Stafslien S, Daniels J, Bahr J, Chisholm BJ (2008) Release characteristics of reattached barnacles to non-toxic silicone coatings. Biofouling 24:313–319

22. Chaudhury MK, Finlay JA, JChung JY, Callow ME, Callow JA (2005) The influence of elastic modulus and thickness on the release of the soft-fouling green alga Ulva Linza (Syn. Enteromorpha Linza) from poly(dimethylsiloxane) (PDMS) model networks. Biofouling 21:41–48

23. Schultz MP, Finlay JA, Callow ME, Callow JA (2003) Three models to relate detachment of low form fouling at laboratory and ship scale. Biofouling 19:17–26

24. Holland R, Dugdale TM, Wetherbee R, Brennan AB, Finlay JA, Callow JA, Callow ME (2004) Adhesion and motility of fouling diatoms on a silicone elastomer. Biofouling 20:323–329

25. Andrade JD, King RN, Gregonis DE, Coleman DL (1979) Surface characterization of poly (hydroxyethyl methacrylate) and related polymers. I. Contact angle methods in water. J Polym Sci Polym Symp 66:313–336

26. Ikada Y (2001) Water, ch. 11. In: Morra M (ed) Biomaterials surface science, 1st edn. Wiley, New York, pp 291–306

27. Schilp S, Kueller A, Rosenhahn A, Grunze M, Pettitt ME, Callow ME, Callow JA (2007) Settlement and adhesion of algal cells to hexa(ethylene glycol)-containing self-assembled monolayers with systematically changed wetting properties. Biointerphases 2:143–150

28. Youngblood JP, Andruzzi L, Ober CK, Hexemer A, Kramer EJ, Callow JA, Finlay JA, Callow ME (2003) Coatings based on side-chain ether-linked poly (ethylene glycol) and fluorocarbon polymers for the control of marine biofouling. Biofouling 19:91–98

29. Krishnan S, Wang N, Ober CK, Finlay JA, Callow ME, Callow JA, Hexemer A, Sohn KE, Kramer EJ, Fischer DA (2006) Comparison of the fouling release properties of hydrophobic fluorinated and hydrophilic PEGylated block copolymer surfaces: attachment strength of the diatom Navicula and the green alga Ulva. Biomacromolecules 7:1449–1462

30. Statz A, Finlay JA, Dalsin J, Callow ME, Callow JA, Messersmith PB (2006) Algal antifouling and fouling-release properties of metal surfaces coated with a polymer inspired by marine mussels. Biofouling 22:391–399

31. Callow ME, Callow JA, Pickett-Heaps JD, Wetherbee R (1997) Primary adhesion of enteromorpha (chlorophyta, Ulvales) propagules: quantitative settlement studies and video microscopy. J Phycol 33:938–947

32. Schultz MP, Finlay JA, Callow ME, Callow JA (2000) A turbulent channel flow apparatus for the determination of the adhesion strength of microfouling organisms. Biofouling 15:243–251

33. Grozea CM, Gunari N, Finlay JA, Grozea D, Callow ME, Callow JA, Lu ZH, Walker GC (2009) Water-stable diblock polystyrene-block-poly(2-vinyl pyridine) and diblock polystyrene-block-poly(methyl methacrylate) cylindrical patterned surfaces inhibit settlement of Zoospores of the green alga Ulva. Biomacromolecules 10:1004–1012

34. Gudipati CS, Finlay JA, Callow JA, Callow ME, Wooley KL (2005) The antifouling and fouling-release performance of hyperbranched fluoropolymer (HBFP) – poly(ethylene glycol) (PEG) composite coatings evaluated by adsorption of biomacromolecules and the green fouling alga Ulva. Langmuir 21:3044–3053

35. Hu Z, Finlay JA, Chen L, Betts DE, Hillmyer MA, Callow ME, Callow JA, DeSimone JM (2009) Photochemically cross-linked perfluoropolyether-based elastomers: synthesis, physical characterization, and biofouling evaluation. Macromolecules 42:6999–7007

36. Dalsin JL, Hu BH, Lee BP, Messersmith PB (2003) Mussel adhesive protein mimetic polymers for the preparation of nonfouling surfaces. J Am Chem Soc 125:4253–4258

37. Gudipati CS, Greenlief CM, Johnson JA, Prayongpan P, Wooley KL (2004) Hyperbranched fluoropolymer and linear poly(ethylene glycol) based amphiphilic crosslinked networks as efficient antifouling coatings: an insight into the surface compositions, topographies, and morphologies. J Poly Sci Part A Polym Chem 42:6193–6208

38. Imbesi PM, Raymond JE, Tucker BS, Wooley KL (2012) Thiol-ene 'click' networks from amphiphilic fluoropolymers: full synthesis and characterization of a benchmark antibiofouling surface. J Mater Chem 22:19462

39. Brady RF Jr, Singer IL (2000) Mechanical factors favoring release from fouling release coatings. Biofouling 15:73–81

40. Brady RF, Aronson CL (2003) Elastomeric fluorinated polyurethane coatings for nontoxic fouling control. Biofouling 19:59–62

41. Wang J, Mao G, Ober CK, Kramer EJ (1997) Liquid crystalline, semifluorinated side group block copolymers with stable low energy surfaces: synthesis, liquid crystalline structure, and critical surface tension. Macromolecules 30:1906–1914

42. Ober CK, Wang JG, Mao GP (1997) Order within order: studies of semifluorinated block copolymers. Macromol Symp 18:701–706

43. Osuji CO, Chen JT, Mao G, Ober CK, Thomas EL (2000) Understanding and controlling the morphology of styrene–isoprene side-group liquid crystalline diblock copolymers. Polymer 41:8897–8907

44. Mao G, Wang J, Clingman SR, Ober CK, Thomas EL, Chen JT (1997) Molecular design, synthesis, and characterization of liquid crystal – coil diblock copolymers with azobenzene side groups. Macromolecules 30:2556–2567

45. Genzer J, Sivaniah E, Kramer EJ, Wang J, Korner H, Xiang M, Char K, Ober CK, DeKoven BM, Bubeck RA, Chaudhury MK, Sambasivan S, Fischer DA (2000) The orientation of semifluorinated alkanes attached to polymers at the surface of polymer films. Macromolecules 33:1882–1887

46. Xiang M, Li X, Ober CK, Char K, Genzer J, Sivaniah E, Kramer EJ, Fischer DA (2000) Surface stability in liquid-crystalline block copolymers with semifluorinated monodendron side groups. Macromolecules 33:6106–6119

47. Hexemer A, Sivaniah E, Kramer EJ, Xiang M, Li X, Ober CK (2004) Managing polymer surface structure using surface active block copolymers in block copolymer mixtures. J Poly Sci Part B Polym Phys 42:411–420

48. Weinman CJ, Finlay JA, Park D, Paik MY, Krishnan S, Sundaram HS, Dimitriou M, Sohn KE, Callow ME, Callow JA, Handlin DL, Willis CL, Kramer EJ, Ober CK (2009) ABC triblock surface active block copolymer with grafted ethoxylated fluoroalkyl amphiphilic side chains for marine antifouling/fouling-release applications. Langmuir 25:12266–12274

49. Cho Y, Sundaram HS, Weinman CJ, Paik MY, Dimitriou MD, Finlay JA, Callow ME, Callow JA, Kramer EJ, Ober CK (2011) Triblock copolymers with grafted fluorine-free, amphiphilic, non-ionic side chains for antifouling and fouling-release applications. Macromolecules 44:4783–4792

50. Dimitriou MD, Zhou Z, Yoo H-S, Killops KL, Finlay JA, Cone G, Sundaram HS, Lynd NA, Barteau KP, Campos LM, Fischer DA, Callow ME, Callow JA, Ober CK, Hawker CJ, Kramer EJ (2011) A general approach to controlling the surface composition of poly(ethylene oxide)-based block copolymers for antifouling coatings. Langmuir 27:13762–13772

51. Koh JK, Kim YW, Ahn SH, Min BR, Kim JH (2010) Antifouling poly(vinylidene fluoride) ultrafiltration membranes containing amphiphilic comb polymer additive. J Poly Sci Part B Polym Phys 48:183–189

52. Bodkhea RB, Stafslien SJ, Cilz N, Daniels J, Thompson SEM, Callow ME, Callow JA, Webster DC (2012) Polyurethanes with amphiphilic surfaces made using telechelic functional PDMS having orthogonal acid functional groups. Prog Org Coat 75:38–48

53. Martinelli E, Suffredini M, Galli G, Glisenti A, Pettitt ME, Callow ME, Callow JA, Williams D, Lyall G (2011) Amphiphilic block copolymer/poly(dimethylsiloxane) (PDMS) blends and nanocomposites for improved fouling-release. Biofouling 27:529–541

54. Prime KL, Whitesides GM (1993) Adsorption of proteins onto surfaces containing end-attached oligo(ethylene oxide): a model system using self-assembled monolayers. J Am Chem Soc 1993(115):10714–10721

55. Ma H, Hyun J, Stiller P, Chilkoti A (2004) "Non-fouling" oligo(ethylene glycol)-functionalized polymer brushes synthesized by surface-initiated atom transfer radical polymerization. Adv Mater 16:338–341

56. Yarbrough JC, Rolland JP, DeSimone JM, Callow ME, Finlay JA, Callow JA (2006) Contact angle analysis, surface dynamics, and biofouling characteristics of cross-linkable, random perfluoropolyether-based graft terpolymers. Macromolecules 39:2521–2528

57. Park D, Weinman CJ, Finlay JA, Fletcher BA, Paik MY, Sundaram HS, Dimitriou MD, Sohn KE, Callow ME, Callow JA, Handlin DL, Willis CL, Fischer DA, Kramer EJ, Ober CK (2010) Amphiphilic surface active triblock copolymers with mixed hydrophobic and hydrophilic side chains for tuned marine fouling-release properties. Langmuir 26:9772–9781

58. Cho Y, Sundaram HS, Finlay JA, Dimitriou MD, Callow ME, Callow JA, Kramer EJ, Ober CK (2012) Reconstruction of surfaces from mixed hydrocarbon and PEG components in water: responsive surfaces aid fouling release. Biomacromolecules 13:1864–1874

59. Sundaram HS, Cho YJ, Dimitriou MD, Weinman CJ, Finlay JA, Cone G, Callow ME, Callow JA, Kramer EJ, Ober CK (2011) Fluorine-free mixed amphiphilic polymers based on PDMS and PEG side chains for fouling release applications. Biofouling 27:589–601

60. Martinelli E, Sarvothaman MK, Alderighi M, Galli G, Mielczarski E, Mielczarski JA (2012) PDMS network blends of amphiphilic acrylic copolymers with poly(ethylene glycol)-fluoroalkyl side chains for fouling-release coatings. I. Chemistry and stability of the film surface. J Poly Sci Part A Polym Chem 50:2677–2686

61. Martinelli E, Sarvothaman MK, Galli G, Pettitt ME, Callow ME, Callow JA, Conlan SL, Clare AS, Sugiharto AB, Davies C, Williams D (2012) Poly(dimethyl siloxane) (PDMS) network blends of amphiphilic acrylic copolymers with poly(ethylene glycol)-fluoroalkyl side chains for fouling-release coatings. II. Laboratory assays and field immersion trials. Biofouling 28:571–582

62. Krishnan S, Ayothi R, Hexemer A, Finlay JA, Sohn KE, Perry R, Ober CK, Kramer EJ, Callow ME, Callow JA, Fischer DA (2006) Anti-biofouling properties of comblike block copolymers with amphiphilic side chains. Langmuir 22:5075–5086

63. Martinelli E, Agostini S, Galli G, Chiellini E, Glisenti A, Pettiitt ME, Callow ME, Callow JA, Graf K, Bartels FW (2008) Nanostructured films of amphiphilic fluorinated block copolymers for fouling release application. Langmuir 24:13138–13147

64. Kannan K, Koistinen J, Beckmen K, Evans T, Gorzelany JF, Hansen KJ, Jones OPD, Helle E, Nyman M, Giesy JP (2001) Accumulation of perfluorooctane sulfonate in marine mammals. Environ Sci Technol 35:1593–1598

65. Martin JW, Mabury SA, Solomon KR, Muir DCG (2003) Bioconcentration and tissue distribution of perfluorinated acids in rainbow trout (oncorhynchus mykiss). Environ Toxicol Chem 22:196–204

66. Olsen GW, Huang HY, Helzlsouer KJ, Hansen KJ, Butenhoff JL, Mandel JH (2005) Historical comparison of perfluorooctanesulfonate, perfluorooctanoate, and other fluorochemicals in human blood. Environ Health Perspect 113:539–545

67. Mielczarski JA, Mielczarski E, Galli G, Morelli A, Martinelli E, Chiellini E (2010) The surface-segregated nanostructure of fluorinated copolymer – poly(dimethylsiloxane) blend films. Langmuir 26:2871–2876

68. Marabotti I, Morelli A, Orsini LM, Martinelli E, Galli G, Chiellini E, Lien EM, Pettitt ME, Callow ME, Callow JA, Conlan SL, Mutton RL, Clare AS, Kocijan A, Donik C, Jenko M (2009) Fluorinated/siloxane copolymer blends for fouling release: chemical characterisation and biological evaluation with algae and barnacles. Biofouling 25:481–493

69. Ikeda T, Lee B, Yamaguchi H, Tazuke S (1990) Time-resolved fluorescence anisotropy studies on the interaction of biologically active polycations with phospholipid membranes. Biochem Biophys Acta Biomembr 1021:56–62

70. Ikeda T, Hirayama H, Yamaguchi H, Tazuke S, Watanabe M (1986) Polycationic biocides with pendant active groups: molecular weight dependence of antibacterial activity. Anitmicrob Agents Chemother 30:132–136

71. Ikeda T, Tazuke S, Suzuki Y (1984) Biologically active polycations, 4. Synthesis and antimicrobial activity of poly(trialkylvinylbenzylammonium chloride)s. Makromol Chem 185:869–876

72. Ikeda T, Yamaguchi H, Tazuke S (1990) Phase separation in phospholipid bilayers induced by biologically active polycations. Biochim Biophys Acta Biomembr 1026:105–112

73. Ikeda T, Yamaguchi H, Tazuke S (1990) Molecular weight dependence of antibacterial activity in cationic disinfectants. J Bioactive Compatible Polym 5:31–41

74. Chen CZ, Beck-Tan NC, Dhurjati P, van Dyk TK, LaRossa RA, Cooper SL (2000) Quaternary ammonium functionalized poly(propylene imine) dendrimers as effective antimicrobials: structure − activity studies. Biomacromolecules 1:473–480

75. Sauvet G, Fortuniak W, Kazmierski K, Chojnowski J (2003) Amphiphilic block and statistical siloxane copolymers with antimicrobial activity. J Polym Sci Part A Polym Chem 41:2939–2948

76. Thome J, Hollander A, Jaeger W, Trick I, Oehr C (2003) Ultrathin antibacterial polyammonium coatings on polymer surfaces. Surf Coat Technol 174–175:584–587

77. Gelman MA, Weisblum B, Lynn DM, Gellman SH (2004) Biocidal activity of polystyrenes that are cationic by virtue of protonation. Org Lett 6:557–560

78. Ilker MF, Nusslein K, Tew GN, Coughlin EB (2004) Tuning the hemolytic and antibacterial activities of amphiphilic polynorbornene derivatives. J Am Chem Soc 126:15870–15875

79. Lee SB, Koepsel RR, Morley SW, Matyjaszewski K, Sun Y, Russell AJ (2004) Permanent, nonleaching antibacterial surfaces. 1. Synthesis by atom transfer radical polymerization. Biomacromolecules 5:877–882

80. Waschinski CJ, Tiller JC (2005) Poly(oxazoline)s with telechelic antimicrobial functions. Biomacromolecules 6:235–243
81. Kawabata N, Nishiguchi M (1988) Antibacterial activity of soluble pyridinium-type polymers. Appl Environ Microbiol 54:2532–2535
82. Li G, Shen J, Zhu Y (1998) Study of pyridinium-type functional polymers. II. Antibacterial activity of soluble pyridinium-type polymers. J Appl Polym Sci 67:1761–1768
83. Li G, Shen J (2000) A study of pyridinium-type functional polymers. IV. Behavioral features of the antibacterial activity of insoluble pyridinium-type polymers. J Appl Polym Sci 78:676–684
84. Tiller JC, Liao C-J, Lewis K, Klibanov AM (2001) Designing surfaces that kill bacteria on contact. Proc Natl Acad Sci U S A 98:5981–5985
85. Grapski JA, Cooper SL (2001) Synthesis and characterization of non-leaching biocidal polyurethanes. Biomaterials 22:2239–2246
86. Cen L, Neoh KG, Kang ET (2003) Surface functionalization technique for conferring antibacterial properties to polymeric and cellulosic surfaces. Langmuir 19:10295–10303
87. Park ES, Kim HS, Kim MN, Yoon JS (2004) Antibacterial activities of polystyrene-block-poly(4-vinyl pyridine) and poly(styrene-random-4-vinyl pyridine). Eur Polym J 40:2819–2822
88. Kanazawa A, Ikeda T, Endo T (1993) Novel polycationic biocides: synthesis and antibacterial activity of polymeric phosphonium salts. J Polym Sci Part A Polym Chem 31:335–343
89. Kanazawa A, Ikeda T, Endo T (1993) Polymeric phosphonium salts as a novel class of cationic biocides. III. Immobilization of phosphonium salts by surface photografting and antibacterial activity of the surface-treated polymer films. J Polym Sci Part A Polym Chem 31:1467–1472
90. Kanazawa A, Ikeda T, Endo T (1993) Polymeric phosphonium salts as a novel class of cationic biocides. IV. Synthesis and antibacterial activity of polymers with phosphonium salts in the main chain. J Polym Sci Part A Polym Chem 31:3031–3038
91. Kanazawa A, Ikeda T, Endo T (1994) Polymeric phosphonium salts as a novel class of cationic biocides. VII. Synthesis and antibacterial activity of polymeric phosphonium salts and their model compounds containing long alkyl chains. J Appl Polym Sci 53:1237–1244
92. Kanazawa A, Ikeda T, Endo T (1994) Polymeric phosphonium salts as a novel class of cationic biocides. VIII. Synergistic effect on antibacterial activity of polymeric phosphonium and ammonium salts. J Appl Polym Sci 53:1245–1249
93. Kenawy E-R, Abdel-Hay FI, El-Shanshoury AE-RR, El-Newehy M (2002) Biologically active polymers. V. Synthesis and antimicrobial activity of modified poly(glycidyl methacrylate-co-2-hydroxyethyl methacrylate) derivatives with quaternary ammonium and phosphonium salts H. J Polym Sci Part A Polym Chem 40:2384–2393
94. Popa A, Davidescu CM, Trif R, Ilia Gh, Iliescu S, Dehelean Gh (2003) Study of quaternary 'onium' salts grafted on polymers: antibacterial activity of quaternary phosphonium salts grafted on 'gel-type' styene-divinylbenzene copolymers. React Funct Polym 55:151–158
95. Kanazawa A, Ikeda T, Endo T (1993) Antibacterial activity of polymeric sulfonium salts. J Polym Sci Part A Polym Chem 31:2873–2876
96. Nonaka T, Noda E, Kurihara S (2000) Graft copolymerization of vinyl monomers bearing positive charges or episulfide groups onto Loofah fibers and their antibacterial activity. J Appl Polym Sci 77:1077–1086
97. Li GJ, Shen JR, Zhu YL (2000) A study of pyridinium-type functional polymers. III. Preparation and characterization of insoluble pyridinium-type polymers. J Appl Polym Sci 78:668–675
98. Tashiro T (2001) Antibacterial and bacterium adsorbing macromolecules. Macromol Mater Eng 286:63–87
99. Dizman B, Elasri MO, Mathias LJ (2006) Synthesis and characterization of antibacterial and temperature responsive methacrylamide polymers. Macromolecules 39:5738–5746

100. Huang JY, Murata H, Koepsel RR, Russell AJ, Matyjaszewski K (2007) Antibacterial polypropylene via surface-initiated atom transfer radical polymerization. Biomacromolecules 8:1396–1399
101. Kenawy ERJ (2001) Biologically active polymers. IV. Synthesis and antimicrobial activity of polymers containing 8-hydroxyquinoline moiety. J Appl Polym Sci 82:1364–1374
102. Krishnan S, Ward RJ, Hexemer A, Sohn KE, Lee KL, Angert ER, Fischer DA, Kramer EJ, Ober CK (2006) Surfaces of fluorinated pyridinium block copolymers with enhanced antibacterial activity. Langmuir 22:11255–11266
103. Kurt P, Wood L, Ohman DE, Wynne KJ (2007) Highly effective contact antimicrobial surfaces via polymer surface modifiers. Langmuir 23:4719–4723
104. Cheng ZP, Zhu XL, Shi ZL, Neoh KG, Kang ET (2005) Polymer microspheres with permanent antibacterial surface from surface-initiated atom transfer radical polymerization. Ind Eng Chem Res 44:7098–7104
105. Park D, Wang J, Klibanov AM (2006) One-step, painting-like coating procedures to make surfaces highly and permanently bactericidal. Biotechnol Prog 22:584–589
106. Kawabata N, Fujita I, Inoue T (1996) Removal of virus from water by filtration using microporous membranes made of poly(N-benzyl-4-vinylpyridinium chloride). J Appl Polym Sci 60:911–917
107. Mieszkin S, Martin-Tanchereau P, Callow ME, Callow JA (2012) Effect of bacterial biofilms formed on fouling-release coatings from natural seawater and cobetia marina, on the adhesion of two marine algae. Biofouling 28:953–968
108. Mieszkin S, Callow ME, Callow JA (2013) Interactions between microbial biofilms and marine fouling algae: a mini review. Biofouling 29:1097–1113
109. Ivanov I, Vemparala S, Pophristic V, Kuroda K, DeGrado WF, McCammon JA, Klein ML (2006) Characterization of nonbiological antimicrobial polymers in aqueous solution and at water−lipid interfaces from all-atom molecular dynamics. J Am Chem Soc 128:1778–1779
110. Lin J, Qiu S, Lewis K, Klibanov AM (2003) Mechanism of bactericidal and fungicidal activities of textiles covalently modified with alkylated polyethylenimine. Biotechnol Bioeng 83:168–172
111. Milovic NM, Wang J, Lewis K, Klibanov AM (2005) Immobilized N-alkylated polyethylenimine avidly kills bacteria by rupturing cell membranes with no resistance developed. Biotechnol Bioeng 90:715–722
112. Kugler R, Bouloussa O, Rondelez F (2005) Evidence of a charge-density threshold for optimum efficiency of biocidal cationic surfaces. Microbiology 151:1341–1348
113. Park D, Finlay JA, Ward RJ, Weinman DJ, Krishnan S, Paik M, Sohn KE, Callow ME, Callow JA, Handlin DL, Willis CL, Fischer DA, Angert ER, Kramer EJ, Ober CK (2010) Antimicrobial behavior of semifluorinated-quaternized triblock copolymers against airborne and marine microorganisms. Appl Mater Interfaces 2:703–711
114. Zhou Z (2013) Adjustment of surface chemical and physical properties with functionalized polymers to control cell adhesion. PhD dissertation, Cornell University, Ithaca

Micellar Structures from Anionically Synthesized Block Copolymers

Jean-François Gohy

Abstract This chapter summarizes progresses achieved to date in the formation of micellar structures prepared from anionically synthesized block copolymers. Generalities about the preparation, the characterization, and the dynamics of such block copolymer micelles are first outlined. Selected examples of micelle formation in aqueous and organic media are shown for anionically synthesized block copolymers with various architectures. The different types of micellar morphologies and the strategies devised to control them are discussed.

1   Introduction

Block copolymers have been widely investigated during the last four decades due to the immiscibility generally encountered by their constituent blocks, leading to microphase separation. Because the different blocks are linked together by covalent bonds, this microphase separation is spatially limited and results in self-assembled structures with characteristic sizes of the order of a few times the radius of gyration, R_g, of the constituent blocks and thus ranging from ca 10 to 100 nm [1].

Moreover, these self-assembled structures are generally regularly distributed throughout the bulk material, giving rise to long-range ordering and the formation of a variety of structures such as cubic array of spheres or hexagonally packed cylinders. However, the long-range order in these polymeric materials is not perfect and the size of the ordered domains or is generally limited to a few μm or less. Several annealing methodologies in which block copolymer materials have been exposed to solvents, temperature, or electric field have been therefore developed to improve the ordering.

The prediction of the characteristic sizes and morphologies of these nanostructured materials has been an intense topic of investigations from both the theoretical

J.-F. Gohy (✉)

Bio and Soft Matter (BSMA), Institute of Condensed Matter and Nanosciences (IMCN), Université catholique de Louvain, Place Louis Pasteur 1, Louvain-la-Neuve B-1348, Belgium
e-mail: jean-francois.gohy@uclouvain.be

and experimental points of views. Critical parameters such as the degree of polymerization and the volume fraction of the constituent blocks, as well as the Flory-Huggins parameter between them have been widely investigated [2].

Whenever, block copolymers are dissolved in a selective solvent, that is, a good solvent for one block and a precipitant for the other blocks, the copolymer chains associate to form micellar aggregates in deep analogy with the situation observed for classical low molar mass surfactants. A CMC can be thus defined and experimentally measured for block copolymer micelles. In comparison to low molar mass surfactants, the values of the CMC are much lower in case of block copolymers. This allows, for example, the use of block copolymer micelles as nanocontainers for drug delivery. Indeed, block copolymer nanocontainers do not usually reach their CMC and thus do not dissociate into unimers whenever they are diluted in the blood stream and can therefore transport the drugs to a specifically targeted area [3]. Nevertheless, macromolecular chains can meet some dissolution problems during the preparation of micelles. This problem is especially emphasized for block copolymers containing a high T_g or a large insoluble block. A strategy to improve solubility is based on the temporary use of an organic solvent which then allows the formation of micelles. Moreover, it should be pointed out that block copolymer micelles are generally not at the thermodynamic equilibrium.

Block copolymer micelles can be considered as a multicompartmentalized polymeric system in which a minimum of two compartments are brought together. Those two compartments are, on one hand, a more or less swollen core resulting from the aggregation of the insoluble blocks surrounded and, on the other hand, a corona formed by the soluble blocks. Micelles with more than two compartments have been also designed. Such micelles are generally obtained from triblock terpolymers and may either contain two separated compartments in the core or in the corona of the accordingly obtained micelles.

The development of block copolymer micelles is strongly linked to the progresses encountered in the fields of living and controlled polymerization techniques. Indeed such techniques are a prerequisite to obtain well-defined block copolymers with narrow polydispersity indices and controlled molar masses for each constituent block. Moreover, those techniques also allow to precisely control the architecture of the block copolymer, for example, linear, star-like, grafted, hyperbranched. Although controlled radical polymerization techniques are nowadays used as main synthetic tools to produce well-defined block copolymers for micellization studies, the initial investigations on block copolymer micelles have been realized on anionically synthesized block copolymers. This is the reason why the first part of this chapter will be dedicated to the presentation of general concepts related to the micellization process (Sect. 2) and to the control of micellar sizes and morphologies (Sect. 3). Selected examples of block copolymer micelles from anionically synthesized block copolymers in both aqueous and organic media will be then presented in Sects. 4 and 5.

More recently, unique structures with complex morphologies have been obtained from anionically synthesized triblock terpolymers. This is the reason

why Sect. 6 will focus on these complex morphologies that are paving the way toward new types of applications for block copolymer micelles.

Micellar structures can be generated by mixing mutually interacting anionically synthesized block copolymers. This can lead to micellar structure whose characteristic features can be easily modulated by adjusting the relative amounts of the mixed polymers and the interaction strength between the interacting blocks in the mixture (Sect. 7).

Due to the huge number of publications on block copolymer micelles prepared from anionically synthesized block copolymers, an exhaustive description of all these previous works would not be possible in the frame of this chapter. In term of polymers, we will restrict our discussions to olefinic, styrenic, (meth)acrylates and ethylene oxide-based systems. This chapter has rather the purpose to give a general overview about block copolymer micelles for the nonspecialist and will therefore try to answer practical questions about the preparation of block copolymer micelles, their characterization, the different types of morphologies, and their prediction. These basic questions and the related answers will be illustrated by selected examples. Then, we will focus on the recent directions that are currently under development.

2 Generalities About Block Copolymer Micelles

Generalities about block copolymer micelles have been previously reviewed by Hamley [2], Riess [4], and Gohy [5] based on previous works from the 1980s and 1990s. This topic will not be covered in details but the basic principle will be recalled as well as some important practical issues. The essential experimental techniques used for block copolymer micelle characterization will be also briefly outlined.

2.1 The Critical Micelle Concentration

Whenever amphiphilic block copolymer chains are dissolved, at a fixed temperature, in a selective solvent for one of the blocks, they self-associate through a closed association process to form micelles.

The critical concentration at which the first micelle forms is called the critical micelle concentration or CMC. As the concentration of block copolymer chains increases in the solution, more micelles are formed while the concentration of nonassociated chains, called unimers, remains constant and is equal to the value of the CMC. This ideal situation corresponds to a system at the thermodynamic equilibrium. However, experimental investigations on the CMC have revealed that its value depends on the method used for its determination. Therefore, it seems more reasonable to define phenomenologically the CMC as the concentration at

which a sufficient number of micelles is formed to be detected by a given method [6].

Information about the process associated with the CMC has been provided by Tsunashima et al. [7], who investigated the micellization of a PS-*b*-PB diblock in various solvents. In these studies, DLS was used to measure R_h. Measurements were performed in solvents having the same refractive index of either the PS or PB chains, allowing the determination of the characteristic sizes of the individual blocks. In nonselective solvents, it was confirmed that the PS-*b*-PB chains were molecularly dissolved and that both blocks adopted a stretched conformation due to intersegmental repulsive interactions. In *n*-decane, a selective solvent for the PB block, PS-*b*-PB unimers with collapsed PS segments were observed at low concentration while aggregated PS-*b*-PB chains forming spherical micelles were observed at higher concentrations.

The variation of the CMC with the composition of the copolymer has been extensively studied for PEO-*b*-PPO-*b*-PEO triblock copolymers, often referred as their commercial name Pluronics[TM], in aqueous solution. Pluronics are one of the only examples of commercially available anionically synthesized block copolymer which is used for relatively large-scale applications. It was found that copolymers with a larger hydrophobic PPO block had a lower CMC. The CMC was indeed found to decrease exponentially with the PPO block length [8–10] while an increase in the number of PEO units only resulted in a small increase of the CMC [9]. At a constant PPO/PEO ratio, the CMC was found to decrease with increasing total *MW* of the copolymer [9].

A critical micelle temperature or CMT is a very useful value for PEO-*b*-PPO-*b*-PEO copolymers because such copolymers are themoresponsive exhibiting a LCST behavior. This arises from the fact that micellization in these copolymers is due to the dehydration of the PPO block with increasing temperature. The value of the CMT ranges from 20 to 50 °C in commercially available PEO-*b*-PPO-*b*-PEO copolymers [9].

The influence of the copolymer chain architecture on the CMC has been investigated in PEO- and PBO-containing bock copolymers. From an entropic point of view, the formation of micelles should be favored for diblock architectures compared to triblock and cyclic ones, the reason being that two block junctions should reside at the core-corona interface for triblock and cyclic copolymers while unfavorable loop formation will not be observed for the diblock copolymer. Finally, the less entropically favored situation will be observed for the cyclic copolymers since both of their blocks should form a loop. Experimental investigations by Booth et al. on PEO_{2m}-*b*-PBO_{2n} and PBO_n-*b*-PEO_{2m}-*b*-PBO_n [11] revealed that the CMC is two orders of magnitude lower for the diblocks at a constant n value. The CMC for PEO_m-*b*-PBO_{2n}-*b*-PEO_m was found to be intermediate between the two latter architectures [11]. Surprisingly, micellization was favored for the cyclic copolymer compared to the triblock [11]. This can be understood by considering that the conformation of the cyclic copolymer is restricted in both the unassociated and associated states, and has therefore no impact on the Gibbs free energy of micellization. In addition to the abovementioned considerations, bridging of chains

between micelles could occur in the particular case of PBO-*b*-PEO-*b*-PBO copolymers, as confirmed by DLS measurements [12]. In very dilute solutions, flower-like micelles with all the triblock chains making loops are likely formed while bridging and formation of larger structures were already detected for a concentration of 1 wt% as evidenced by a markedly increased viscosity of the solution [12].

Previous work of Pispas et al. on PI-*b*-PS miktoarm copolymers dissolved in *n*-decane revealed that the micellar characteristic features such as Z and R_h were strongly dependent on the architecture, but the corresponding CMCs could not be determined [13]. For highly asymmetric block copolymers with a large insoluble block, the copolymer chains cannot be directly solubilized in the selective solvent. However, micelles can be obtained from these copolymers by the temporary use of a nonselective solvent which is further eliminated. In principle, all the copolymer chains are aggregated for these systems and the CMC is therefore estimated to be infinitely low, as discussed by Eisenberg et al. [14].

2.2   Preparation of Block Copolymer Micelles

The most direct way to prepare a block copolymer micellar solution consists in the direct dissolution of the bulk sample in a selective solvent for one of the blocks. However, this method generally only works if the total molar mass of the copolymer is low and the length of the insoluble block is short enough. A way to improve solubility then consists in "annealing" the solution by prolonged stirring, thermal, or ultrasound treatments. According to the literature, these techniques have the disadvantage to lead, depending on the block copolymer, to nonequilibrium micelles, especially when the core-forming chains of the block copolymer are below T_g [15]. The characteristic features of the resulting micelles will then depend on the bulk morphology of the starting bulk sample. It can be assumed that the annealing treatment will result rather in the dispersion of bulk particles into the selective solvent than in the formation of micelles based on a unimer-aggregate equilibrium. These particles will be protected against flocculation by the solvated chains at their outer surface but their morphology will be essentially dictated by the annealing conditions [15]. It should however be mentioned that the transfer of a bulk-organized system into solution can lead to very interesting structures as it will be demonstrated in the case of Janus micelles [16]. In this case, a micellar structure is preformed in the bulk, its core is stabilized by cross-linking and the whole material is finally dissolved in a very good solvent for the coronal chains.

Another method is based on the dissolution of the block copolymer in a nonselective solvent resulting in the formation of molecularly dissolved chains. The properties of this solvent are further changed in order to trigger aggregation of the dissolved chains and hence micelle formation. A selective solvent for one of the blocks and precipitant for the others is generally added to the molecularly dissolved chains, although other ways such as temperature or pH changes can be used for micellization as well. In this case, the unimer-micelle equilibrium can be generally

reversibly tuned by pH or temperature changes. These systems are then rather considered as stimuli-responsive micelles which can be disassembled or assembled depending on the applied stimulus.

Addition of a selective solvent to the molecularly dissolved chains has been used by many research teams to prepare block copolymer micelles. The initial nonselective solvent can be further eliminated by evaporation or can be gradually replaced by the selective solvent via a dialysis process. The step-wise dialysis initially introduced by Tuzar and Kratochvil is now widely used for micelle preparation [17], especially for the formation of aqueous micelles [18]. This technique does not, however, overcome the formation of "frozen" micelles due to the formation of glassy cores at a specific nonselective solvent/selective solvent composition. This method offers nevertheless several advantages. Firstly, the formation of large aggregates can be suppressed for block copolymers that were previously solubilized directly in the selective solvent. Secondly, it allows the formation of micelles for highly asymmetric copolymers with a large insoluble block, as illustrated by the works of Eisenberg et al. on the so-called "crew-cut" micelles [16, 19]. "Crew-cut" micelles have been prepared from highly asymmetric diblock copolymers containing very short water-soluble blocks that were initially dissolved in a nonselective solvent. Water has been then slowly added to these solutions. After addition of a critical amount of water defined as the CWC, aggregation has been observed. An additional amount of water has been added in order to freeze-in the morphology of the accordingly formed aggregates that were generally characterized by a high T_g PS core. Observations on the CWC have been realized by turbidimetry and rationalized by Eisenberg et al. [20]. These authors have shown that the CWC depends on both the copolymer concentration in the nonselective solvent and the molar mass of the insoluble block. The higher the copolymer concentration and the MW of the insoluble block, the lower the CWC [20].

2.3 Micellar Structure

It is important to define clearly the characteristic features of block copolymer micelles. In the former subsections, we already mentioned that the insoluble blocks were forming a micellar core surrounded by a corona. Depending on the composition of the starting block copolymer, two limiting structures can be drawn: (1) "star-like" micelles with a small core compared to the corona and (2) "crew-cut" micelles with a large core and highly stretched coronal chains. The process of micellization is thus characterized by the aggregation of a given number of block copolymer chains, defined as the aggregation number or Z. The core is characterized by its radius R_c while the overall radius of the micelle is defined as R_m. Other ways for defining the overall dimension of a micelle are the radius of gyration R_g and the hydrodynamic radius R_h, both are defined elsewhere [21]. The distance between neighboring blocks at the core/corona interface is called the grafting distance b. Therefore, b^2 is the area occupied by one chain at the core/corona interface and can be compared to the area by head group as defined for low MW surfactant micelles [22].

Key parameters that control R_c, R_m, b, and Z are the degree of polymerization of the polymer blocks, N_A and N_B, and the Flory-Huggins interaction parameter χ. The free energy of a micelle is mainly determined by (1) the interfacial energy of the core/shell interface, (2) the stretching energy of the block copolymer chains, (3) the repulsion among coronal chains. The minimum of the free energy corresponds to an equilibrium grafting distance b which depends on block lengths and salt concentration in the case of charged coronal blocks.

2.4 Characterization of Block Copolymer Micelles: Experimental Techniques

Extensive reviews on experimental techniques suitable for block copolymer micelle characterization have been provided [18]. Moreover, Hamley has systematically listed the different techniques specifically used for different types of block copolymer micelles [2].

TEM techniques have been widely used over the last 40 years for the direct visualization of block copolymer micelles. Different methods for sample preparation have been tested. Most of the preparation techniques have been devoted to enhance both the electronic contrast and the stability of the micellar objects for TEM observations. Contrasting techniques with heavy metals have been widely used to reach these two goals. In these experiments, the micelles are usually initially deposited on a TEM grid covered with an amorphous film and further observed in the dried state. Heavy metals can interact with block copolymers micelles bearing suitable functional moieties. Typical examples are the reactions of RuO_4 to aromatic double bonds and OsO_4 to aliphatic double bonds. These staining techniques can also allow the direct visualization of a specific compartment of the micelles, for example, the core. This is illustrated in Fig. 1 for aqueous micelles from a PS-b-P2VP-b-PEO triblock copolymer and contrasted with RuO_4 [23, 24]. At basic pH, both the PS core and hydrophobic P2VP shell are equally stained and could not be distinguished while, at acidic pH, the protonated and water-soluble P2VP shell is less contrasted and could be discriminated from the PS core. The PEO corona is never visualized in these experiments.

Negative contrasting techniques are based on the use of a contrasting agent which is not interacting with the micelles and which therefore spreads onto the substrate. Micelles then appear as bright spots on a dark background. Phosphotungstic acid is a typical negative staining agent. The dimension of the core plus dried corona is measured from this experiment. Metal can be sputtered on block copolymer micelles by exposing the TEM grid to metal vapor under a certain angle. Each micelle will generate a shadow whose size and shape depend on the metal deposition angle and on the morphological characteristic features of the micelles [5]. Metallic replica of freeze-fractured micellar solution can be also examined.
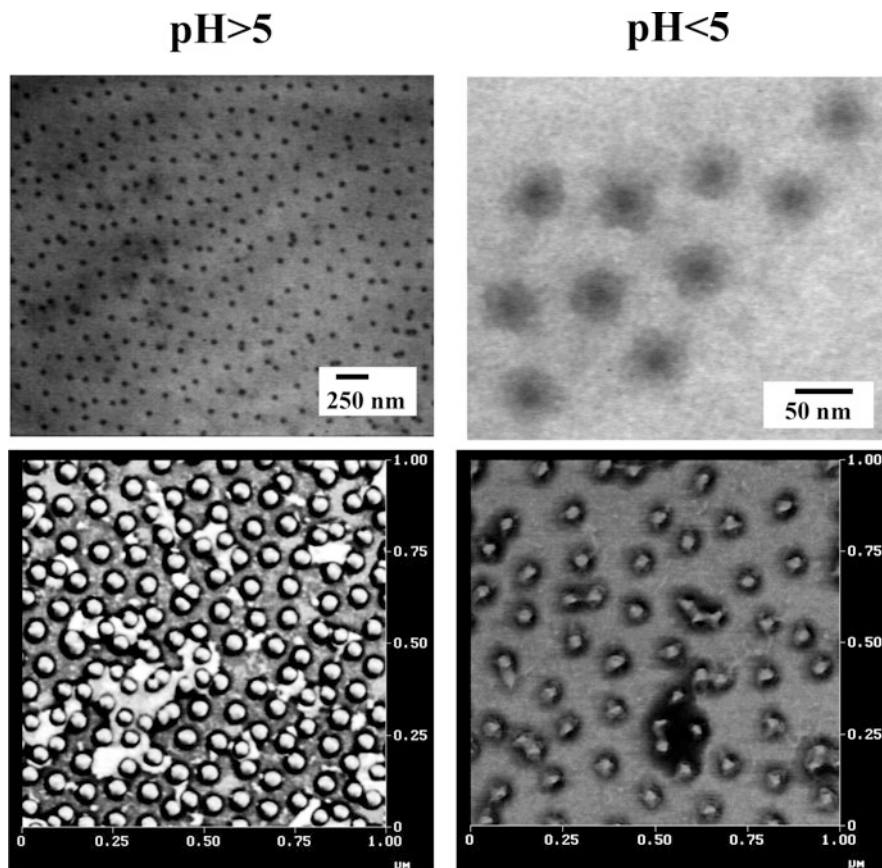
Fig. 1 TEM (*up*) and AFM phase contrast images (*down*) of aqueous micelles formed by the PS_{200}-*b*-$P2VP_{140}$-*b*-PEO_{590} ABC triblock copolymer at pH >5 (*left*) and pH <5 (*right*). For TEM pictures, the PS and P2VP blocks have been stained by RuO_4. The AFM image has been recorded with the tapping mode (contrast scale: *black*: $0°$, *white*: $45°$) (Adapted from Ref. [23])

The more recently developed cryo-TEM technique is nowadays more and more frequently used for block copolymer micelle characterization in aqueous solution [25]. Cryo-TEM has the advantage to allow a direct observation of the micelles in a glassy water phase and to accordingly determine the characteristic dimensions of both the core and swollen corona provided that a sufficient electronic contrast is observed between these two domains. Typical studies on core-shell structure in block copolymer micelles as visualized by the cryo-TEM techniques have been reported by Talmon et al. [26] and Förster and coworkers [27].

SEM techniques have been proven to be suitable for the visualization of block copolymer micelles, as illustrated in, for example, the work of Erhardt et al. on "Janus" micelles (see Sect. 6.2) [28].

Direct visualization of block copolymer micelles can also be achieved by AFM. AFM measurements can be performed either in the dried state or directly "in situ" within a liquid cell. Measurements in the dried state are realized on micelles adsorbed or deposited on a flat solid substrate (silicon wafer, mica, etc.). The shape and size of the micelles can however be affected by tip-convolution effects, by specific interactions between the substrate and some moieties of the block copolymer or by relaxation of a low T_g micellar core resulting in the flattening of the micelles on the substrate. Typical AFM pictures from dried PS-*b*-P2VP-*b*-PEO aqueous micelles at basic or acidic pH are shown in Fig. 1 and can be directly compared with the corresponding TEM pictures [23, 24]. At a first glance, AFM measurements in a liquid cell seem to be more appropriate to get pertinent morphological information on micelles in their original swollen state. In these AFM experiments, the micelles have a more or less developed tendency to adsorb at the substrate/liquid interface which is the locus where the measurements are performed. Nevertheless, several artifacts such as sticking of the micelles on the AFM tips can perturb the observation.

Information on micellar morphology can also be obtained by scattering techniques with the advantage of giving a mean value calculated over a large number of micelles, but with the drawback being that they are model-dependent. A recent review on SAXS on block copolymer micelles has recently been published by Mortensen [29]. SANS has been also widely used to elucidate micellar structures. In order to generate a sufficient scattering contrast, SANS experiments are generally conducted in deuterated solvents and/or with partially deuterated copolymers. Under such labeling conditions, the core and corona of the micelles can be selectively studied. Light scattering is a very common technique used for block copolymer micelle characterization. SLS allows the determination of the absolute weight-averaged MW and thus Z of the micelles, as well as R_g. Information about the quality of the selective solvent for the coronal chains through the second virial coefficient can also be obtained [21]. R_h can be measured by DLS [21].

AUC has been rarely used to characterize block copolymer micelles although it allows the determination of the weight fraction of micelles, unimers, and eventually other species such as superaggregates of micelles. The sedimentation coefficient of the different species in solution depends on their MW, buoyancy, and friction coefficient, and on the centrifugal force applied. Although it can be argued that the unimer-micelle-aggregate equilibrium is continuously disturbed and re-established during the AUC experiment, it has been successfully applied to block copolymer micelles as demonstrated by the early works of Selb and Gallot [30].

SEC has been used to characterize the unimer-micelle distribution. However, SEC is not an absolute method and thus requires calibration. Since it is practically not possible to calibrate a SEC apparatus for the unimers and micelles formed by a block copolymer, only indicative MW values will be obtained. Moreover, several authors have noted a strong perturbation of the unimer-micelle equilibrium during SEC experiments even when interaction of the material with the SEC column was minimized [31, 32].

Other characterization techniques are devoted to the determination of the CMC. They have been previously reviewed [2] and will not be discussed here. Various NMR, fluorescence and stop-flow techniques have been also used to characterize different aspects related to the dynamics of block copolymer micelles, as it will be discussed in the next section.

2.5   Dynamics of Block Copolymer Micelles

The dynamics of micellar systems is a very important concern that is relevant at several levels. In this respect, the dynamics required for the establishment of the unimer-micelle equilibrium is one aspect. The so-called problem of micelle hybridization that deals with the exchange rate of unimers between different micelles is closely related. Finally, the chain dynamics of polymer blocks in either the core or the corona is another concern that can, however, be linked to some extent to the two first mentioned concepts. These different aspects have been scarcely studied and reviewed by Hamley [2] and by Riess [4]. However, we feel that these important problems should be briefly discussed in this chapter.

Stop-flow experiments have been performed in order to study the kinetics of micellization, as illustrated by the work of Tuzar and coworkers on PS-*b*-PB diblocks and the parent PS-*b*-PB-*b*-PS triblocks [33]. In these experiments, the block copolymers are initially dissolved as unimers in a nonselective mixed solvent. The composition of the mixed solvent is then changed in order to trigger micellization and the scattered light intensity is recorded as a function of time. The experiment is repeated in the reverse order, that is, starting from the block copolymer micelles which are then disassembled by a change in the mixed solvent composition. The analysis of the experimental results revealed two distinct processes assigned to as unimer-micelle equilibration at constant micelle concentration (fast process) and association-dissociation equilibration, accompanied by changes in micellar concentration (slow process).

The differences observed between AB di- and ABA triblock copolymers could be explained because two A blocks have to escape from the micellar core in case of ABA triblock chains.

The exchange of block copolymer chains between micelles is also a problem of high interest. The unimer-micelle exchange rate has been studied by Creutz et al. using steady-state fluorescence [34, 35]. In such experiments, micelles from PDMAEMA-*b*-PMANa copolymers labeled with a covalently bound donor, naphthalene, were mixed with micelles formed from the same copolymers in which the donor has been replaced by an acceptor, pyrene (pyrene was not bound to the copolymer but simply mixed). Upon mixing the two solutions, exchange of PDMAEMA-*b*-PMANa chains occurred and donor-tagged chains entered micelles containing the acceptor. Specifically exciting the donor and monitoring the emission of the acceptor has been simultaneously performed in order to measure the energy transfer between the two molecules. The increasing emission intensity of the

acceptor with time has been then considered as a measure of the exchange rate of unimers between micelles. The rate constants for the PDMAEMA-b-PMANa copolymers were found to be of the order of 10^{-3} s^{-1}. Moreover, the influence of the molecular architecture and the composition of the copolymers were also studied. The exchange rate was slower whenever the length of the insoluble block was increased and a triblock architecture with the outer insoluble blocks was considered. The influence of temperature was studied by the same authors on aqueous micelles formed by PS–b-PMANa and PtBS–b-PMANa copolymers. No exchange rate could be detected at room temperature, while the exchange rate was measurable at 60 °C. The influence of the addition of a small amount of a good solvent for the micellar core was also studied as a way to increase the exchange rate in frozen micelles. In a similar way, the addition of a plasticizer such as dimethyladipate has been successfully used to increase the micelle-unimer exchange rate in frozen PMMA-b-PMANa micelles [36].

Similar fluorescence techniques were used by other authors on micelles containing PS cores such as PS-b-PEO micelles for which no chains were exchanged even for rather low PS *MW* [37].

SANS has been recently used to study problems related to micelle preparation and kinetics, as reported by Bates and coworkers who have used time-resolved SANS to study molecular exchange and micelle equilibration for PEO-b-PB diblocks in water [38]. The authors have shown that the micellar structures initially formed upon dissolution were completely locked in up to 8 days after preparation. Fluorometry and DLS have been also used to monitor micelle equilibration [39].

Exchange of unimers between two different types of block copolymer micelles has been often referred to as hybridization. This situation is more complex than for the case described earlier because thermodynamic parameters come now in addition to the kinetic ones. A typical example of such hybridization is related to the mixing of micelles formed by two different copolymers of the same chemical nature but with different composition and/or length for the constituent blocks. Tuzar et al. [40, 41] studied the mixing of PS–b-PMAA micelles with different sizes in water–dioxane mixtures by sedimentation velocity measurements. These authors concluded that the different chains were mixing with time, the driving force being to reach the maximum entropy.

The last feature about micellar dynamics is related to the local mobility of chain segments in the core or in the corona of the micelles. SAXS, SANS, and fluorescence techniques have proven to be effective techniques to gain information about chain conformation and dynamics in the different micellar domains, as reviewed by Zana [42]. Neutron spin echo has been used to measure the dynamic structure factor from intensity fluctuations as a function of time. Farago et al. have used this technique to probe the dynamics of the coronal PI chains for PS-b-PI micelles in decane [43]. The results were found in agreement with the model of de Gennes for "breathing" coronal chains. A recent investigation of Castelletto et al. by neutron spin echo dynamics on PBO-b-PEO micelles in D_2O revealed the presence of two dynamic modes, that is, fast and slow modes, whatever the concentration of the solution [44]. The slow mode that dominates at low scattering angles was shown to

correspond to the translational diffusion of micelles while the additional fast mode was attributed to internal "blob scattering" in the micellar corona.

Direct information on the chain mobility can be easily obtained by NMR while considering that a decreased mobility of protons in polymer chains with hindered motion results in broadening of the respective NMR lines and even disappearance of the corresponding signal when the polymer is in the glassy state. This last feature has been widely used to prove micelle formation as illustrated by Spevacek [45] on PS-*b*-PB micelles with a PS core. At room temperature, the aromatic signals associated to PS chains could not be detected while they were visible at 87 °C.

^{2}H NMR measurements on partially deuterated PS-*b*-PMANa copolymers have been performed by Gao et al. [46] Deuterated segments were introduced in several locations of the core-forming chains and their mobility was measured. For segments buried into the PS micellar core, the mobility was found to be essentially the same as in a bulk PS sample while the segments located near the PS/PMANa interface were characterized by a restricted mobility due to the neighboring ionic groups that were thought to experience ionic association as in ionomers.

3   Control of Morphology and Micellar Sizes

Spherical micelles are observed for the vast majority of self-associating block copolymers in solution. One of the major concern is to determine how the characteristic dimensions of these micelles, that is, R_c, R_m, b, and Z (see Sect. 2.3), are changing with the composition of the starting copolymer, that is, N_A and N_B in case of an AB diblock copolymer with A being the core-forming insoluble block and B being the corona-forming soluble block. This key problem has been investigated from a long time from both the theoretical and experimental points of view. In this section, we will first briefly summarize the main results obtained from the theoretical investigations on block copolymer micelles. Those theories are based on one side on the scaling concepts derived from the Alexander–de Gennes theories, and on the other side on the mean-field theories developed by Noolandi and Hong [47], Leibler et al. [48], Nagarajan and Ganesh [49], and by Hurter et al. [50]. In addition to theory, computer simulations have been also carried out on block copolymer micellar systems, as illustrated by the works of, for example, Binder and Müller [51, 52] and by Mattice and Haliloğlu [53]. For micelles containing polyelectrolyte coronal blocks, specific theories have been developed [54–56]. They predict a strong influence of the polyelectrolyte blocks on the micellization behavior. In scaling theories, R_c, R_m, and Z are directly correlated to N_A and N_B for the investigated micelles. Two limiting cases have to be distinguished, the star-like or hairy micelles with $N_A < N_B$, and the crew-cut micelles with $N_A > N_B$. Daoud and Cotton have developed a scaling model for hairy micelles and have found that the micelle total radius, R_m, scales as $N_B^{3/5} Z^{1/5}$ [57]. Since $Z \sim N_A^{4/5}$, $R_m \sim N_A^{4/25} N_B^{3/5}$. A similar scaling law was obtained by Halperin for a star-like micellar model [58],

which demonstrates the predominant contribution of the coronal chains to the total micelle size.

For crew-cut micelles, Zhulina and Birshtein demonstrated that the dependence of the micellar parameters on N_B disappears and R_c scales as $\gamma^{1/3} N_A^{2/3} a$ and $Z \sim \gamma N_A$, where γ is the interfacial tension between the A and B block and a is the segment length [59].

Scaling theories are restricted to long polymer chains in good solvents and do not include finite chain effects and polymer-solvent interactions. These models should be complemented by more detailed mean-field calculations and molecular simulations.

Semi-analytical mean-field theories of block copolymer micellization were formulated by Noolandi et al. [47] and by Leibler et al. [48]. In the approach of Noolandi et al., the micellar characteristics were obtained through a minimization of the Gibbs free energy for an isolated micelle. This was applied on PS-*b*-PB micelles and the obtained theoretical values were in good agreement with the experimental ones.

A further development in mean-field theories was achieved by Nagarajan and Ganesh [49]. These authors have shown that $R_c \sim N_A^{0.73} N_B^{-0.17}$ and $Z \sim N_A^{1.19} N_B^{-0.51}$ for PPO-*b*-PEO micelles in water. In contrast to previous results, Nagarajan and Ganesh demonstrated that the coronal B block can have a strong influence on the micellar characteristic features such as R_c, especially whenever the solvent is very good for the B block. By extending this concept, Nagarajan and Ganesh could obtain "universal" correlations for R_c, R_m, and Z as a function of N_A, N_B, the interaction parameter between the B block and the solvent χ_{BS}, the interfacial tension between the A block and the solvent γ_{AS} and the molar volume of the solvent v_s [49]. Monte Carlo simulations are additional methods for the study of block copolymer micelles as reviewed by Binder and Müller [52] and by Shelley and Shelley [60].

Extensive experimental characterization has been carried out by many groups in order to determine how the characteristic dimensions of block copolymer micelles were depending on the composition of the starting copolymers. TEM and SAXS were two of the mainly used methods for the determination of R_c and R_m. These results have been rationalized by Förster et al. who found that, in the case of uncharged block copolymers, the grafting distance was depending on the soluble block length as $b_0 N_B^{\beta/6}$ with $b_0 \sim 1$ nm and $\beta \sim 0.8$ while Z was scaling as $Z_0 N_a^2 N_B^{-\beta}$ with $Z_0 \sim 1$ and $\beta \sim 0.8$ [61]. As shown in Fig. 2, this equation successfully describes the micelles formed by uncharged diblock, triblock, graft, and heteroarm-star copolymers in organic and aqueous solvents as well as for low *MW* cationic, anionic, and nonionic surfactants [61].

Nevertheless, this equation failed to describe micelles containing highly charged polyelectrolyte coronal blocks [62]. Indeed, the grafting distance was observed to scale as $b = b_0 N_A^{1/2}$ while the addition of salt decreases the value of R_m without affecting the 1/2-slope [62].

Salt-effects in polyelectrolyte block copolymer micelles are particularly pronounced because the polyelectrolyte chains are closely assembled in the micellar
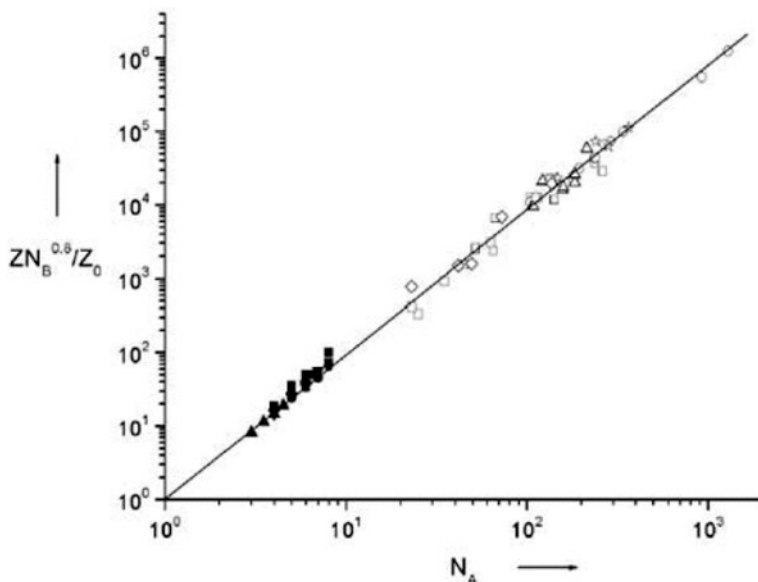
Fig. 2 Aggregation numbers Z as a function of the degree of polymerization of the insoluble block for uncharged block copolymers. *Open symbols* stand for different diblock-, triblock-, graft-, and star polymers. *Filled symbols* are low *MW* surfactants (Reprinted with permission from Ref. [61])

shell [63]. The situation is quite reminiscent of tethered polymer brushes to which polyelectrolyte block copolymer micelles have been compared, as summarized in the review of Förster et al. [62].

All the previously discussed features in this section are related to spherical micelles. However, other morphologies can be formed for block copolymer micelles including rod-like micelles, vesicles, and more intricate morphologies. In principle, one can draw a phase diagram for block copolymer micelles emphasizing the different micellar reachable morphologies as a function of the block copolymer composition in a similar way as the phase diagram determined for the bulk phase morphologies [2]. However, drawing such a diagram will imply that the different kinds of micellar morphologies represent a thermodynamical equilibrium state, a situation which is rarely reached for block copolymer micelles. Thus, different strategies have been implemented to trap out-of-equilibrium morphologies as it will be illustrated in the following.

Eisenberg and coworkers have pioneered the field of micellar morphology control with the so-called "crew-cut" micelles. They initially examined a series of anionically synthesized PS-*b*-PAA copolymers with a PS block of constant length ($N = 200$) while N of the short PAA block was varied from 4 to 21. Transitions from spheres-to-rods-to-vesicles were observed as the length of the PAA block was decreased (see Fig. 3). According to these authors, the morphology of a micelle basically depends on three factors: (1) the stretching of the core-forming chains, (2) the core-corona interfacial energy, and (3) the repulsion
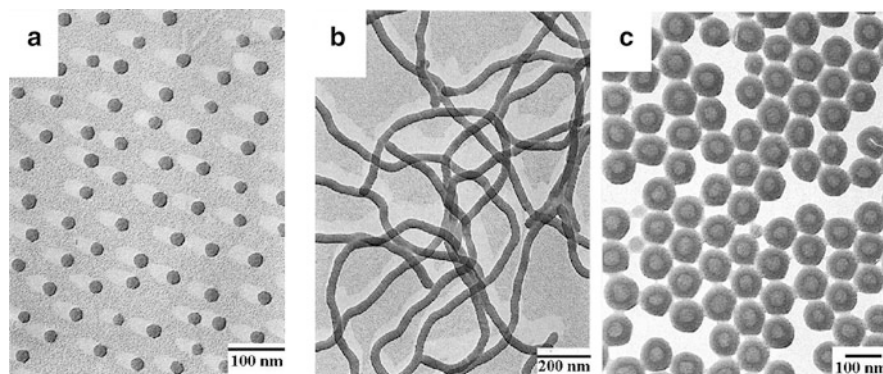
Fig. 3 Spherical (**a**), rod-like (**b**), and vesicular (**c**) morphologies for crew-cut micelles (Adapted from Ref. [14])

among coronal chains. These three factors are directly related to the Gibbs free energy of the micelles, would it be the enthalpic or entropic term. A change in one of these three parameters directly affects the free energy of the micelles. In other words, the micelles could become thermodynamically unstable and will modify their morphology in order to reach another stable state.

On this basis, Eisenberg and coworkers were able to rationalize morphological transitions occurring in series of PS-*b*-PAA [14, 64] and PS-*b*-PEO copolymers [65]. The effect of the starting nonselective solvent [66] and added salts [67, 68] during the micellization process on the finally observed morphologies was also rationalized by using this simple approach. In addition to spheres, rods, and vesicles, other morphologies were observed by Eisenberg et al. for crew-cut micelles, including tubules, interconnected tubules called plumber nightmare, single- or multi-walled vesicles, hexagonally packed hollow hoops, large compound micelles with cores containing inverse micelles, etc. [69]. Some of these morphologies are shown in Fig. 4.

Besides the effects of copolymer composition and preparation conditions on the observed morphologies, copolymer polydispersity can also play an important role for the formation and stabilization of some morphologies. This effect is illustrated for crew-cut vesicles formed by PS-*b*-PAA copolymers [70, 71]. In addition to the curvature energy, vesicles are characterized by a lateral strain that arises from a mismatched number of molecules in one side of the vesicular layer relative to the other. Actually, there are less molecules in the inner side than for the outer side of the vesicular layer. For low molar mass amphiphiles, the stress resulting from this mismatch is relaxed by a "flip-flop" mechanism of the amphiphiles from one side of the vesicular layer to the other [72]. In case of PS-*b*-PAA with a glassy wall, such a flip-flop mechanism is only possible for a fluidized PS wall (e.g., by a selective solvent). For a glassy PS wall, the stress can be minimized by segregating the long
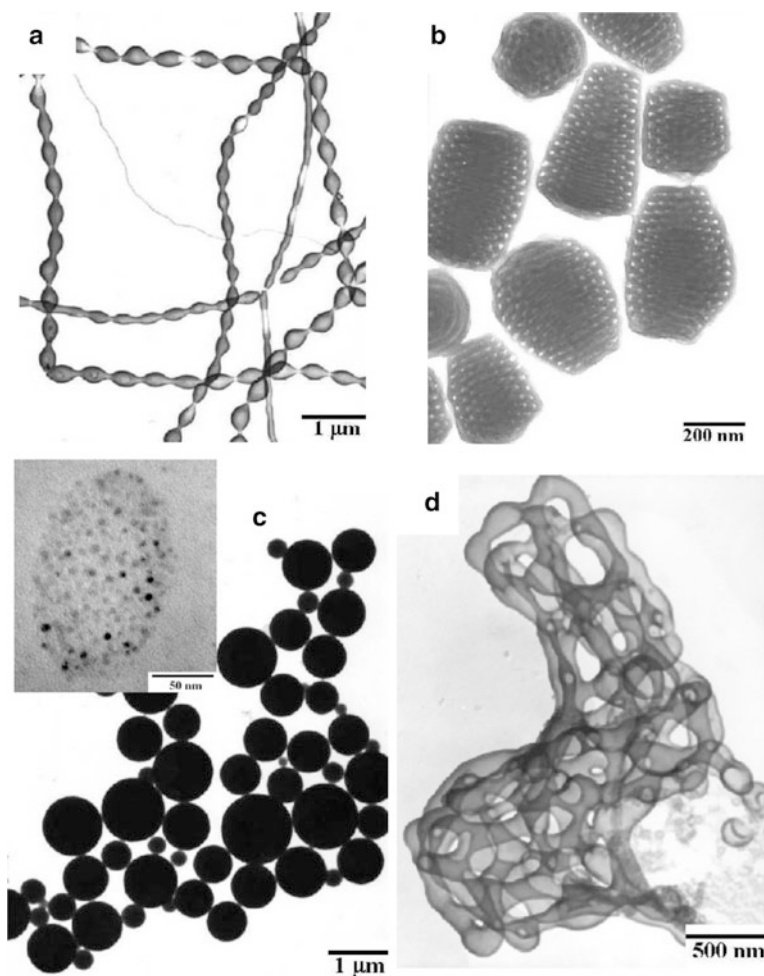
Fig. 4 Some peculiar morphologies observed for "crew-cut" micelles. Baroclinic tubes (**a**); tube-walled vesicles (**b**); large compound micelles, the insert showing their internal structure (**c**); and interconnected tubules or "plumber nightmare" (**d**) (Adapted from Ref. [65])

chains to the outer side of the vesicular layer while the shorter chains will preferentially localize to the inside of the vesicles [70, 71, 73].

One of the drawbacks of crew-cut micelles is that they systematically require the use of a nonselective solvent for their preparation and that they definitely represent out-of-equilibrium micelles once they have been transferred in pure water. Micelles with rod-like or vesicular morphologies can however be obtained by direct dissolution of a block copolymer in a selective solvent for one of the block [74]. Discher and coworkers have investigated the formation of micelles with various

morphologies by directly dissolving PEO-*b*-PB and PEO-*b*-PEB copolymers in water [75–77]. These authors especially focused on the formation of large unilamellar vesicles which were referred to as "polymersomes" [75]. Giant vesicles were prepared from these copolymers by extrusion techniques, and were further characterized by single vesicle micromanipulation. This has allowed to get a deep insight into the typical physical properties of these vesicles including membrane viscosity, area elasticity measurements of the interfacial tension as well as electro-mechanical stability [76]. Permeation of water through the polymersome membranes has been measured to be considerably reduced compared to phospholipid membranes [75]. Spontaneous self-organization of block copolymers into vesicles has been also reported for PEO-*b*-PPO-*b*-PEO copolymers with a large PPO midblock [78].

One unifying rule accounting for block copolymer micelle morphology has been proposed by Discher and Eisenberg [79]. This rule should be considered for coil-coil block copolymer readily soluble in the selective solvent and is expressed as a function of the mass fraction of the hydrophilic block to total mass of the copolymer ($f_{hydrophilic}$): Spherical micelles are observed for $f_{hydrophilic}$ >45 %; rod-like micelles are observed for $f_{hydrophilic}$ <50 %; vesicles are observed for $f_{hydrophilic}$ ~35 %; and inverted microstructures such as large compounds micelles are observed for $f_{hydrophilic}$ <25 %. The sensitivity of these rules to the chemical composition and to the *MW* of the copolymer chains has not yet been fully probed. According to previous experimental results, it seems that they can be applied for *MW*s ranging from 2,700 to 20,000 g/mol.

Another possibility to trigger the formation of nonspherical micelles is to use rod-coil copolymers [80, 81]. The interest on rod-coil copolymers stems from the fact that the aggregation of the rigid segments into liquid-crystalline domains competes with the phase separation between the blocks during the phase separation process. Moreover, the introduction of stiff segments results in an increase of the Flory-Huggins parameters in comparison with coil-coil copolymer [81]. As a result, phase-separated structures can be observed at lower total *MW* for rod-coil copolymers than for coil-coil ones.

Block copolymer micelles in which the core-forming polymer blocks are able to crystallize are relatively similar to rod-coil copolymers. A significant part of these crystalline-core micelles is actually resulting from the self-assembly of rod-coil block copolymers. PEO blocks are good candidates for the formation of micelles with crystallized cores, as demonstrated by Kovacs and Manson [82] and then by Gast et al. [83]. These authors demonstrated that lamellar microcrystals or shish-kebab structures were formed by chain-folding crystallization of the PEO blocks in the absence of water. These lamellar microcrystals, called "platelets" by Gast et al., are typically formed by a central part of PEO, with a lamellar thickness depending on the crystallization conditions, having on its surface a fringe of PS blocks solubilized in the organic solvent. A typical TEM picture of these "platelets" is shown in Fig. 5.
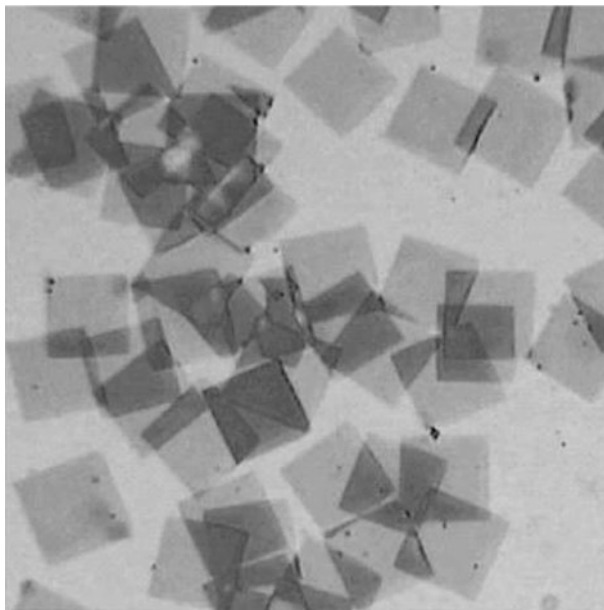
Fig. 5 TEM micrograph of "platelets" micelles from a PS$_{100}$-*b*-PEO$_{2500}$ diblock copolymer dissolved in methylcyclohexane. Total size of the picture 200×200 μm^2 (Reprinted with permission from Ref. [4])

4 Micelles from Anionically Synthesized Diblock Copolymers in Organic Solvents

A wide range of anionically synthesized styrene-, (meth)acrylates-, dienes-based block copolymers were investigated for the formation of micelles in organic solvents. Excellent reviews on micelles formed in organic solvents have been published by Hamley [2] and Riess [5]. We will thus briefly outline some selected examples in the following.

As far as micelles in organic media are concerned, two types of block copolymers can be considered, that is, those with two hydrophobic blocks and those with one hydrophilic and one hydrophobic block. The latter form the so-called reverse micelles that contain a hydrophilic core surrounded by a soluble hydrophobic corona.

The micellization behavior of copolymers containing two hydrophobic blocks, or double-hydrophobic block copolymers, has been shown to be mainly controlled by the solvent and its interaction with the copolymer blocks. The micellization of these copolymers can thus be tuned by changing the organic solvent. In this respect, large differences in Z, R_h, R_c, etc., are expected whenever the interaction parameter between the polymer and the solvent is varied. This is illustrated by, for example, the work of Pitsikalis et al. [84] for PS-*b*-PSMA diblock copolymers dissolved in

either ethyl- or methylacetate. The effect of temperature has been studied by Quintana et al. [85, 86] who have clearly shown the decrease of CMC with increasing temperature for PS–b-PEB copolymers in alkanes.

Reverse micelles from amphiphilic block copolymers have been widely investigated. In such micelles, the core is typically formed from PEO, PMAA, PAA, or P2VPQ hydrophilic blocks while the corona consists of hydrophobic chains. PEO-based copolymers have received much attention. In this respect, PEO-b-PPO and PEO-b-PPO-b-PEO copolymers were investigated in organic solvents such as formamides [87–89]. However, the formation of reverse micelles in organic solvents from PEO-based block copolymers has been shown to be a complex phenomenon due to the ability of PEO to crystallize. The crystallization of PEO has been studied in PS–b-PEO and PB–b-PEO micelles by several groups including Gallot and Gervais [90] and Gast et al. [83, 91, 92], as previously discussed in this chapter. Wu and Chu [93] and Guo et al. [94] demonstrated that a key parameter in the crystallization of PEO was the amount of residual water. PS-b-PEO reverse spherical micelles have been used as nanoreactors for the synthesis of metallic nanoparticles as shown by the works of Spatz et al. [95] and Bronstein et al. [96].

Reverse micelles from PMAA and PAA-containing copolymers have been extensively studied by Eisenberg and coworkers [67]. These authors considered the micellization of the so-called block ionomers formed of a major PS block linked to ionized PAA and PMAA segments. Stable spherical micelles were formed by these copolymers in organic solvents such as toluene. Their characteristic size was systematically investigated by a combination of experimental techniques including TEM, SAXS, DLS, and SLS. The micelles were shown to consist of an ionic core and a PS corona.

P2VP- and P4VP-containing reverse micelles have been also widely investigated. Förster et al. reported a very detailed investigation on PS-b-P4VP copolymers dissolved in toluene, a selective solvent for the PS block [97]. PS-b-P4VP and PS-b-P2VP block copolymer micelles have been often used as templates for the synthesis of metallic nanoparticles as illustrated by the works of Möller et al. [98–100] and Antonietti and coworkers [101]. Bronstein et al. reported on the synthesis of bimetallic colloids formed in PS-b-P4VP micelles and their catalytic behavior for the selective hydrogenation of dehydrolinalool [102]. Besides metallic nanoparticle synthesis, interaction of metal salts with P2VP or P4VP blocks has a deep effect on the micellization behavior of the corresponding PS-b-P2VP and PS-b-P4VP copolymers. Indeed, the incompatibility between the core and the shell in the micelles can be enhanced by reacting the 2VP or 4VP units of the core-forming block with $HAuCl_4$. To minimize the unfavorable contacts, the core chains stretch and Z is increased. This is illustrated by the work of Möller and coworkers who studied the association behavior of PS-b-P2VP copolymers in the presence of $HAuCl_4$ [103]. In the case of short PS coronal blocks, that is, "crew-cut" micelles, spherical micelles were formed at dilute concentration. However, upon evaporation of the solvent, cylindrical micelles were observed. PS-b-P2VP copolymers with a miktoarm star-like architecture deposited onto mica or Si wafers have been investigated by Kiryi et al. [104]. They studied by AFM with molecular resolution single

molecule conformations formed in controlled environment. In toluene, unimolecular micelles were formed with the P2VP arms in the micellar core and the swollen PS arms as the micellar shell. The reverse situation was observed in acidic water. The transition between those two inverse types of micelles was strongly modified by interaction with the mica substrate. Indeed, the micelles deposited onto mica from acidic water were trapped via P2VP extended arms. Upon treatment of the trapped micelles with toluene the PS core was swollen and PS arms gradually adapted an extended conformation, whereas P2VP trapped arms retained their extended conformation due to the strong interaction with the mica substrate. The obtained structures exhibited a unique conformation that does not exist in any solvent and could not be obtained upon a simple adsorption procedure.

5 Micelles from Anionically Synthesized Diblock Copolymers in Aqueous Solution

5.1 Nonionic Amphiphilic Diblock Copolymers in Aqueous Solution

Nonionic amphiphilic block copolymers in aqueous solution are typically formed of a water-soluble hydrophilic block, for example, PEO linked to a hydrophilic block, for example PEO, linked to a hydrophobic block, such as PPO, PBO, PS, and PMMA.

The commercially available PEO-*b*-PPO and PEO-*b*-PBO amphiphilic di- and triblock copolymers have been widely investigated in aqueous medium. Depending on temperature and concentration, different structures have been reported for the corresponding micellar solutions, including micelles of various morphologies and physical gels. Their micellization behavior has been studied quite extensively and summarized in several review articles [2, 105–108], Bahadur et al. have examined the role of various additives on the micellization behavior of PEO–*b*-PPO and PEO–*b*-PBO copolymers [109]. Guo et al. have used FT-Raman spectroscopy to study the hydration and conformation as a function of temperature [110]. Booth and coworkers have investigated PEO-*b*-PBO block copolymers with long PEO sequences [111]. Hamley et al. have used in situ AFM measurements in water to characterize the morphology of PEO-*b*-PPO micelles [112, 113].

PS-*b*-PEO diblock copolymers have been the subject of many investigations. Those micelles are characterized by two typical characteristic features: nonequilibrium "frozen" micelles were formed due to the high T_g PS core and these micelles were prone to secondary aggregation. Aggregation of PS-*b*-PEO micelles has been reported by, for example, Khan et al. who observed two populations of objects by TEM [114]. Two populations, with D_h at 40 and 150 nm, respectively, were also detected by Xu et al. by light scattering in similar samples [115]. The smaller population was attributed to regular micelles while the

larger one was believed to consist of loose micellar clusters. Mortensen et al. have studied a PS-*b*-PEO copolymer by SANS, DLS, and SLS and have evidenced the formation of anisotropic clusters in water at concentrations up to 10 wt% [116]. These authors considered the clusters as a result of the merging of the initial spherical micelles into larger aggregates. Clustering of PS-*b*-PEO micelles in water was also investigated by SLS and AUC [117]. In this study, it was demonstrated that the micellar clusters could be decomposed by addition of toluene due to an increase of mobility of the PS core-forming chains. It was suggested that forces leading to clustering of PEO chains could involve hydrogen bonding, the structure of water, and the hydrophobic effect. The aggregated PEO chains were then thought to form either spherulites or noncrystalline microgel particles.

Nonionic hydrophilic PEO blocks have also been combined with a variety of other hydrophobic blocks. It is not possible to review all the published works on these copolymers due to space limitations. The reader could get more information on those systems in other reviews [4, 5].

5.2 Amphiphilic Diblock Copolymers with One Ionic Block in Aqueous Solution

Block copolymer micelles with a polyelectrolyte corona are often referred to as polyelectrolyte block copolymer micelles. The micellization behavior of these charged micelles has been reviewed by Riess [4] and Förster et al. [62]. A brief overview of the topic will be therefore presented in the following. Amphiphilic block copolymers consisting of one hydrophobic block linked to one ionic block will only be discussed in this section.

The interest on these block copolymer micelles arises from the polyelectrolyte coronal block which is influenced by many parameters including pH and salt concentration. Typical examples of polyelectrolyte micelles have been reported for quaternized PS-*b*-P4VP block copolymers by Selb and Gallot [118]. Eisenberg et al. [119–122] and Tuzar and coworkers [123] have studied the PS-*b*-PAA and PS-*b*-PMAA systems in their acidic or neutralized "anionic" form. Typical polyelectrolyte behavior was detected for these types of micelles. It should be noted that those block copolymers were not directly prepared by anioning living polymerization, carboxylic acids being not compatible with this polymerization mechanism. Therefore, *tert*-butyl ester precursors were copolymerized and then hydrolyzed under acidic conditions to lead to PAA and PMAA blocks. Eisenberg and coworkers investigated highly asymmetric PS-*b*-PAA copolymers with a long PS block and a very short PAA sequence [68]. These compounds led to the so-called "crew-cut" micelles. The morphology of the "crew-cut" micelles could be changed from spheres to rods to vesicles and other complex micellar structures by decreasing the PAA/PS ratio in the starting copolymer, by adding salt or by changing the initial nonselective solvent, as previously discussed in this chapter.

Most of the works on anionic polyelectrolyte block copolymer micelles has been carried out on P(M)AA-containing copolymers. The ionization degree of these anionic blocks is strongly dependent on the pH: at low pH, the P(M)AA sequence is in the acidic form while at higher pH it is partially or totally ionized. This feature could be a drawback for some applications in which a pH-independent ionization behavior is desirable. This situation could be circumvented by the use of anionic polymers derived from strong acids like PGMAS. PGMAS-containing micelles have been scarcely studied. We have investigated the micellization of PMMA-*b*-PGMAS and PtBMA-*b*-PGMAS copolymers in water [124]. Formation of superaggregates of micelles was evidenced in these samples by a combination of DLS and SEC experiments on the aqueous micellar solutions. PMMA-*b*-PGMAS copolymers with a short PMMA block were also adsorbed on hydrophobized mica surfaces in order to create polyelectrolyte brushes showing remarkable lubrication properties upon shearing in extreme confinement [125].

Some insight about the typical polyelectrolyte behavior of cationic block copolymer micelles was obtained by Förster et al. [62]. In this study, a cryo-TEM study on PB-*b*-P2VP micelles in which the P2VP block was reacted with HCl revealed that the micellar PB core was surrounded by a thin dark layer containing a high density of condensed counterions, since the electronic contrast directly originates from the concentration of chlorine ions in this experiment. Furthermore thin filaments consisting of protonated P2VP chain bundles were observed, that extended from the interior shell into the dilute outer part of the corona (Fig. 6). Micelles were connected by these filaments forming a random filament network. The formation of such structures was attributed to short-range attractive forces arising from transient fluctuations in the periphery of the corona leading at times to attractive interactions between micelles. These aggregated states, that is, strings and networks, were observed whenever the added salt concentration was increased. Further increase of salt concentration eventually led to very large networks and macrophase separation into a dilute micellar phase and a concentrated gel phase [62].
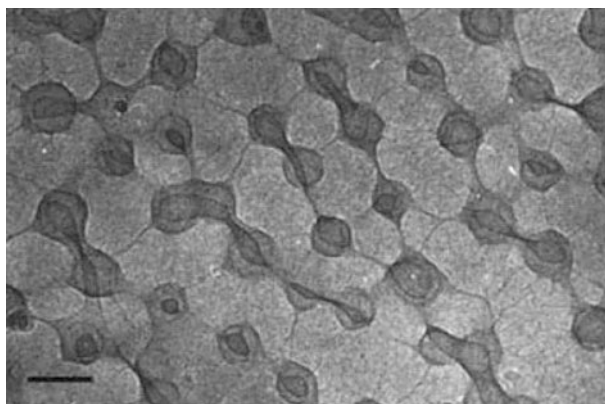
Fig. 6 Cryo-TEM image of aqueous PB-*b*-P2VP micelles showing a filament network of polyelectrolyte chain bundles. The scale bar is 50 nm (Reprinted with permission from Ref. [62])

5.3 Double-Hydrophilic Diblock Copolymers in Aqueous Solution

Diblock copolymer containing two water-soluble blocks are often referred to as "double-hydrophilic" block copolymers. These copolymers have raised much interest during the last few years because they can generally be transformed into amphiphilic copolymers once an adequate stimulus is applied. Since these copolymers may contain one or two polyelectrolytic blocks, the typical features of polyelectrolytes described in Sect. 5.2 should also be considered for some double-hydrophilic block copolymers. Double hydrophilic block copolymers have been reviewed by Cölfen [126]. In the following, we will focus on the stimuli-responsive properties of double-hydrophilic copolymers. Typical examples are copolymers containing weak polyacid or polybasic blocks that can be turned from hydrophilic to hydrophobic depending on their ionization degree.

An early illustration of pH-responsive micellization can be found in P2VP-*b*-PEO copolymers that exist as unimers at pH <5 and form micelles at higher pH values, as demonstrated by Webber et al. [127]. We investigated a P2VP-*b*-PEO copolymer with a larger P2VP block [128]. Although this copolymer precipitated out from the solution when it was totally deprotonated, micellar structures were observed in a limited pH-range located near the pKa of P2VP. Moreover, a transition from spherical to rod-like micelles and finally vesicles was observed for this sample as the deprotonation degree was increasing, in agreement with the resulting changes in the hydrophilic/hydrophobic balance of the copolymer [128]. Giant vesicles with diameters of 5–10 μm were also obtained by Förster et al. from PEO-*b*-P2VP copolymers [62]. These vesicles were stable down to pH 4.5, below which the P2VP-block is protonated and the vesicles dissolved.

Micellization for P2VP-*b*-PEO and P4VP-*b*-PEO copolymers has been induced at low pH by the addition of noble-metal salts [129, 130]. The driving force for such a micellization is the coordination of vinylpyridine units with metal ions. Reduction of the metal ions embedded in the P2VP-*b*-PEO and P4VP-*b*-PEO micelles finally resulted in the formation of well-defined metal nanoparticles.

Another example of pH-driven aggregation is illustrated in double hydrophilic block copolymers based on ethylene oxide, EO, and (meth)acrylic acid, (M)AA. Once again, the (M)AA units were generated after anionic polymerization by hydrolysis of the *tert*-butyl ester precursor. At low pH, hydrogen bonds form between (M)AA and EO, that are further disrupted by an increase in pH due to the ionization of the (M)AA units [131]. Micellization was observed for an asymmetric PMAA-*b*-PEO diblock copolymer containing a major PEO block [132]. Intra- and intermolecular hydrogen bonding between the PMAA blocks and PEO segments was thought to result into micellar core that were stabilized by a corona formed by the excess of PEO segments. These micelles were disintegrated whenever the surrounding pH was raised above 5 as a result of the ionization of PMAA. Furthermore, these micelles showed a thermo-responsive behavior related to the limited thermal stability of the PMAA/PEO hydrogen-bonded complexes.

Double amphiphilic block copolymers have been also obtained from diblock copolymers consisting of two different charged blocks. Diblock copolymers containing positive and negatively charged blocks have been referred to as polyampholytic systems. IPEC between the oppositely charged blocks are observed in these systems, that can lead to insoluble material in aqueous solution. Asymmetric copolymers with an excess of negative or positive charges can however give rise to water-soluble micellar systems, in which the micellar cores are formed by the insoluble interpolyelectrolyte complexes, surrounded by a corona formed by the uncomplexed segments. The first example of polyampholytic block copolymers has been reported for P2VP-*b*-P(M)AA copolymers [133]. The authors showed that the isoelectric point of these copolymers in water was controlled by the block length ratio of the two oppositely charged blocks. PDMAEMA-*b*-PMAA copolymers were also shown to behave as polyampholytic systems [134]. Since the ionization degrees of both the PDMAEMA and PMAA blocks depend on pH, the polyampholytic character is only observed in a restricted pH region in which both the constituent blocks are partially or totally ionized. An analogous behavior has to be pointed out for the P2VP-P(M)AA copolymers. In the case of the PDMAEMA-*b*-PMAA system, vesicular morphologies were observed around pH $= 9$ for copolymers containing a major PMAA block. Cryo-TEM images of these vesicles are shown in Fig. 7. These vesicles are thought to consist of an insoluble layer formed by PDMAEMA/PMAA IPEC stabilized by dangling negatively charged PMAA segments. Another class of charged double-hydrophilic block copolymers is found in diblock copolymers containing two charged blocks, both of them carrying the same type of charge. This situation is exemplified by P2VP-*b*-PDMAEMA diblocks [135]. pH-induced micellization was observed for these block copolymers. However, the relatively large difference between the pKas of the P2VP and PDMAEMA

Fig. 7 Cryo-TEM picture of vesicles formed by a PMAA$_{49}$-*b*-PDMAEMA$_{11}$ ampholytic copolymer in water at pH $= 9$ (Reprinted with permission from Ref. [134])

blocks allowed the formation of three different association states in aqueous solution depending on pH: at low pH, both the P2VP and PDMAEMA blocks were protonated and water-soluble; at intermediate pH, polyelectrolyte block copolymer micelles were formed with an insoluble P2VP core and a positively charged PDMAEMA corona; at high pH, micelles were formed with the same insoluble P2VP core and thermo-responsive uncharged PDMAEMA coronal chains.

# 6 Micelles from Anionically Synthesized Triblock Copolymers

ABC triblock terpolymers have attracted great interest due to the huge number of different morphologies that have been observed so far in the bulk [136]. The main motivation for studying ABC triblock terpolymer micelles is related to the presence of a third nano-sized compartment in the micellar structure. Depending on the investigated systems, this third compartment can either be soluble or insoluble in the considered solvent, leading to different types of micelles that will be discussed in the following. In 2005, we published a review on triblock terpolymer micelles [137]. In the following, we will summarize the main developments that occurred recently. More complete information about previous works on triblock terpolymer micelles can be thus obtained in this previous review [137].

6.1 Micelles with a Compartmentalized Core

These micelles are generally characterized by the so-called "onion," "three-layers," or "core-shell-corona" structures in which the first insoluble A block forms the micellar core, the second insoluble B block is wrapped around the core, and the third soluble C block extents into the solution to form the micellar corona. Most of the reported examples have used water as the selective solvent. Early examples include the works of Kriz et al. [138], Eisenberg et al. on crew-cut systems [139], Ishizone et al. [140], and Dumas et al. [141].

Stimuli-responsive properties were imparted to core-shell-corona micelles. In this case, one of the compartment of the core can become soluble upon application of a stimulus (pH, temperature, etc.). Such systems could be very interesting for the controlled-release of active species encapsulated in the stimuli-responsive compartment. In this respect, we reported on pH-responsive micelles formed by PS-*b*-P2VP-*b*-PEO triblock terpolymers in water and consisting of a PS core, a pH-sensitive P2VP shell, and a PEO corona [23, 24]. At pH values above 5, the P2VP blocks are hydrophobic and collapsed on the PS core, while at pH values below 5, they are protonated and adopt a stretched conformation because of the

mutual electrostatic repulsions. These two micellar states have been characterized by DLS and visualized by TEM and AFM (Fig. 1). Moreover, the transition between the two types of micelles was entirely reversible and could be repeated many times [23]. Similar PS-*b*-P2VP-*b*-PEO micelles were also studied by Prochazka et al. [142, 143]. The pH-responsive P2VP shell was also used as template for the production of gold nanoparticles [23] or of hollow silica nanoparticles [144] and can be complexed with low molecular weight anionic surfactants [145]. Interestingly enough, cylindrical micelles were prepared from the same PS-*b*-P2VP-*b*-PEO copolymers by using a mixture of toluene and DMF as initial solvent before transfer to a pure water phase [146, 147]. Those micelles had a core-shell-corona structure but the P2VP chains in the tubular shell were found to be in a stretched conformation whatever the pH. Further swelling of the PS core of the PS-*b*-P2VP-*b*-PEO micelles resulted in segmented wormlike micelles and ultimately in vesicular structures (Fig. 8) [148]. Giant segmented wormlike micelles were also prepared from PS-*b*-P2VP-*b*-PEO copolymers with larger PS and P2VP blocks. This study showed that those micelles comprised sequences of repeated elemental disks that further became connected through threads to form various giant segmented wormlike micelles [149].
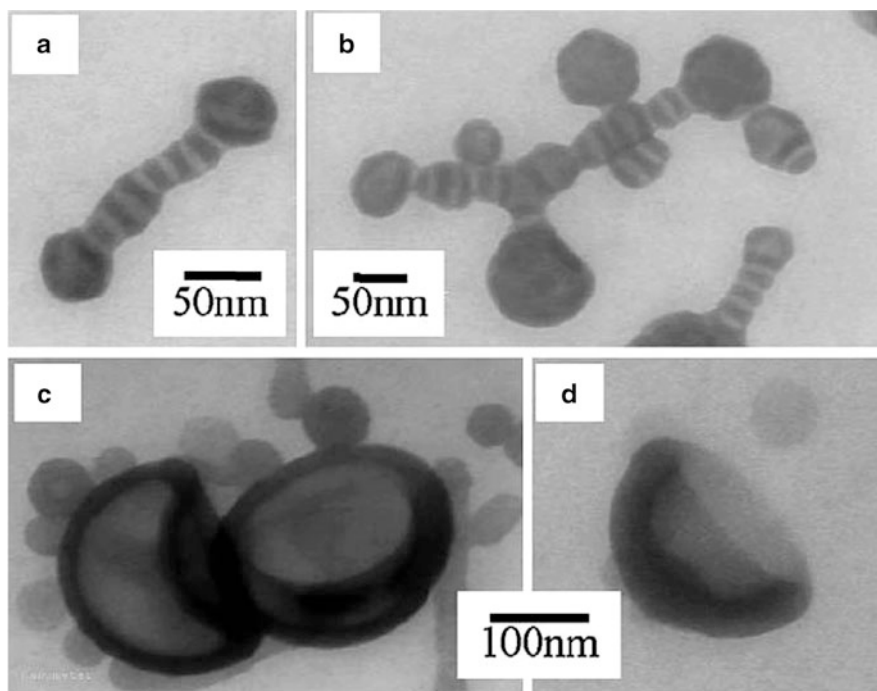
Fig. 8 Segmented worm-like micelles (**a,b**) and vesicles (**c,d**) prepared from a PS-b-P2VP-b-PEO triblock terpolymer in toluene/water mixtures (Adapted with permission from Ref. [148])

pH-responsive micelles from PS-*b*-P2(4)VP-*b*-PMAA triblock terpolymers were prepared by Giebeler and Stadler [150]. These authors investigated the polyelectrolyte complex formation in these micelles by potentiometric, conductimetric, and turbidimetric titrations of acidic THF/water solutions. The formation of an interpolyelectrolyte complex at the isoelectric point was evidenced, in which the hydrophobic PS cores are most likely embedded in a mixed corona of the two polyelectrolyte blocks. pH-sensitive P2VP-*b*-PAA-*b*-PnBMA were investigated in aqueous solution [151]. A unique diversity of structural organizations was observed including thermosensitive centrosymmetric core-shell-corona micelles, compact spheres, polyelectrolyte flowerlike micelles, a charged pH-sensitive 3D network, toroidal nanostructures, and finite size clusters (microgels). The transition between different micelles and the hydrogel was induced via the regulation of electrostatic and hydrophobic interactions in the system [151].

In all these examples, the two compartments found in the micellar core are expected to adopt a sphere-in-sphere morphology (core-shell model). Other morphologies could however be expected for multicompartment cores.

Multicompartment micelles in dilute aqueous solution were reported for miktoarm ABC triblock copolymers containing PEO, PEE, and perfluorinated polyether blocks [152]. Because of the miktoarm architecture of the copolymers, the two incompatible hydrophobic blocks were forced to make contact with the PEO coronal chains. The resulting micellar structures were shown to depend on the relative lengths of the blocks and could be tuned from discrete multicompartment micelles to extended wormlike structures with segmented cores (Fig. 9). The wormlike structures were shown to result from the uniaxial clustering of discrete micelles. In this peculiar morphology, the different cores are able to share their PEO coronas, thus protecting them from the highly unfavorable exposure to water [152]. The addition of THF (60 wt%) into those aqueous solutions induced an evolution from multicompartment micelles to mixed PEE + PEO corona micelles [153]. Cryo-TEM suggested that, as the PEE block transitions from the core to the corona, the micelle morphologies evolve from disks to oblate ellipsoid micelles, with worms and spheres evident at intermediate compositions [153].

The micellization of (ABC)$_n$ multi-arm star triblock terpolymers was also recently studied by Tsitsilianis and coworkers [154]. Four linear and four star equimolar terpolymers based on hydrophilic methoxyhexa(ethyleneglycol) methacrylate, 2-(dimethylamino)ethyl methacrylate, and methylmethacrylate were investigated in aqueous dilute solutions. It was found that the (ABC)$_n$ multi-arm star terpolymers formed unimolecular micelles comprising three centrosymmetric compartments. The position of each compartment could be determined by the block sequence (ABC, ACB, or BAC). The ABC linear counterparts formed loose associates with very low aggregation numbers [154].

For some applications, it is desirable to lock the micellar structure by cross-linking one of the micellar compartments. Cross-linked core-shell-corona micelles have been prepared and investigated by several groups as illustrated by the work of Wooley and coworkers [155] who reported the cross-linking of micelles made from PS–*b*-PMA–*b*-PAA triblocks in aqueous solution by amidation of the PAA shell.
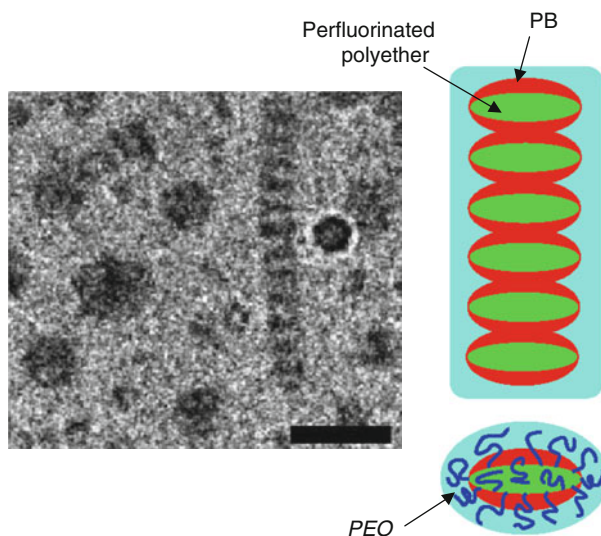
Fig. 9 Cryo-TEM image of isolated micelles and segmented rods made from miktoarm ABC block copolymers containing PEO, PEE, and perfluorinated polyether blocks. A schematic representation of the stacking of block copolymer chains in segmented worms is also shown (Reprinted with permission from Ref. [152])

Wooley and coworkers prepared toroidal block copolymer micelles from similar PS-*b*-PMA-*b*-PAA copolymers dissolved in a mixture of water, THF and 2,2-(ethylenedioxy)diethylamine [156]. Under optimized conditions, the toroidal phase was the predominant structure of the amphiphilic triblock copolymer (Fig. 10).

The collapse of the negatively charged cylindrical micelles into toroids was found to be driven by the divalent 2,2-(ethylenedioxy)diethylamine cation. The same group reported on a various cross-linked micellar aggregates prepared by the same strategy [157, 158]. For example, nanoparticles with different internal structures (lamellar, bicontinuous-like, or porous) were formed by PS–*b*-PMA–*b*-PAA triblock copolymers in THF/water mixed solvents in the presence of multivalent organic counterions [159, 160]. The internal lamellar spacing of the particles could be tuned by using triblock copolymers with different block lengths. In addition, the internal symmetry of the nanoparticles was changed simply by changing the solvent composition (Fig. 10). When spermidine was used as multiamine counterion, nanoparticles with pores or channels were produced by adjusting the water content (Fig. 11). In these systems, the internal nanostructure is due to local phase separation of the block copolymers and can be tuned by varying the solvent composition, the relative block composition, and the valency of the organic counterion [159, 160].

Liu and coworkers have investigated the micellization of PI–*b*-PCEMA–*b*-PtBA triblock terpolymers in mixtures of THF and methanol and have used these micelles
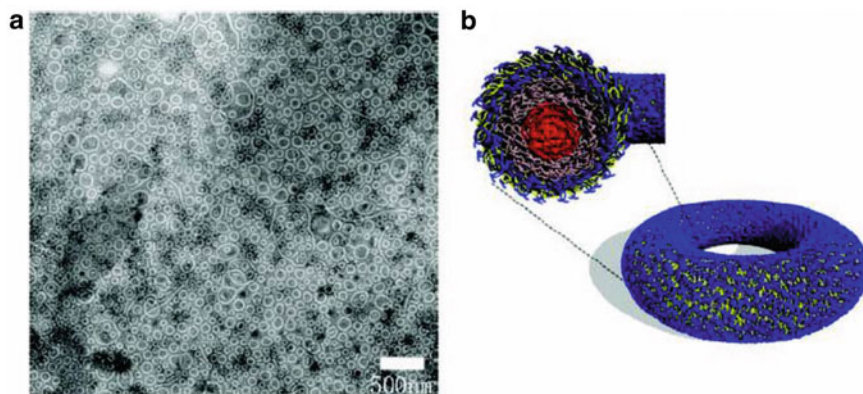
Fig. 10 (**a**) TEM image of toroidal micelles from a PAA-*b*-PMA-*b*-PS triblock copolymer. This sample was cast from a solution with 0.1 wt% PAA$_{99}$-*b*-PMA$_{73}$-*b*-PS$_{66}$ triblock copolymer, a THF: water volume ratio of 1:2, and an amine: acid molar ratio of 0.5:1 by addition of 2,2-(ethylenedioxy)diethylamine. The cast film was negatively stained with uranyl acetate. (**b**) A schematic representation of these micelles is also shown (Reprinted with permission from Ref. [156])
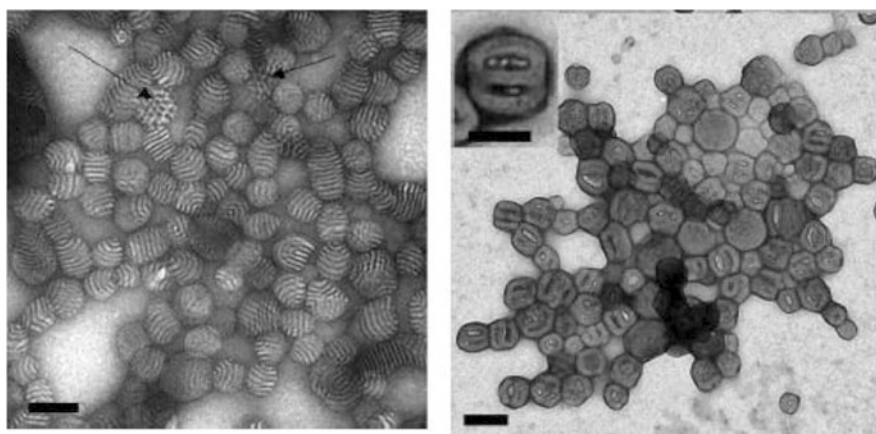
Fig. 11 TEM image (*left*) showing nanoparticles formed via the self-assembly of the PS–*b*-PMA–*b*-PAA triblock copolymer complexed with the 2,2-(ethylenedioxy)diethylamine counterion in 1:0.4 THF:water volume ratio (lamellar phase-separated particles and a few with a hexagonal phase are observed) and TEM image (*right*) porous and channel-like particles formed by PS–*b*-PMA–*b*-PAA triblock copolymer complexed with spermidine. Scale bars are 200 nm (Reprinted with permission from Ref. [159])

to create various nano-objects. The shell-forming PCEMA block was then cross-linked by UV irradiation to lock the structure [161]. In a further step, hollow nanospheres were obtained by ozonolysis of the PI micellar core. If pure methanol

is used as solvent, cylindrical micelles are formed which can also be transformed into nanotubes by the same procedure [162]. The micellization of the same copolymer in mixtures of THF and hexane was also studied [163]. Under these conditions the corona is formed by the PI block, the shell by PCEMA, and the core by PtBA. After cross-linking the shell, the PI corona was hydroxylated to make the micelles dispersible in water, and the PtBA core was made compatible with inorganic species by cleaving the *tert*-butyl groups.

6.2   Micelles with a Compartmentalized Corona

Micelles of this type are formed by ABC triblock terpolymers containing an insoluble A block while the B and C blocks are soluble in the considered solvent. The insoluble block can either be located in between the two soluble blocks (BAC structure) or can be located at one extremity of the triblock (ABC or BCA structures). Different situations have to be considered, depending on the extent of segregation observed between the two solvated coronal blocks. Indeed, the two coronal blocks can give rise to a homogeneously mixed corona or to segregated corona. If there is no segregation between the coronal chains, only two compartments are obtained and micelles similar to usual AB diblock copolymers are formed. The factors controlling the extent of segregation among coronal chains have not yet been clearly established nor experimentally investigated. They will be shortly discussed here in view of the few following examples.

Early examples of micelles containing two types of coronal chains homogeneously mixed were reported by Patrickios and coworkers who studied the formation of micelles from different "isomers" of PDMAEMA–*b*-PMMA–*b*-PMAA triblock terpolymers as a function of pH [164–166]. The isomer having the hydrophobic block in the center yielded micelles characterized by a AB-like structure with a PMMA core and a shell composed of a mixture of the PDMAEMA and PMAA blocks. The other two isomers yielded core-shell-corona micelles twice as big with a PMMA core, and a shell and corona formed by the chains of the two other blocks. Micelles from PS–*b*-P2VP–*b*-PMMA triblock terpolymers dissolved in toluene were reported by Tsitsilianis and Sfika [167]. Spherical micelles with a dense P2VP core, surrounded by mixed PS and PMMA chains in the corona were observed. It was shown that the aggregation number Z and the micellar size were strongly influenced by the length of the P2VP middle block. A similar study was performed on PS-*b*-PI-*b*-PMMA terpolymers in nonsolvents of the PI block. In this case, Z is much larger in DMF than in dimethylacetamide because the latter is a better solvent for the PS and PMMA blocks [168].

In all the examples previously discussed in this section, the coronal chains are expected to be statistically mixed in the corona. It is not clear whether partial or complete phase separation is occurring among coronal chains. A method to produce micelles with completely segregated coronal chains has been reported for the so-called "Janus" micelles. The strategy to create such Janus micelles is based on
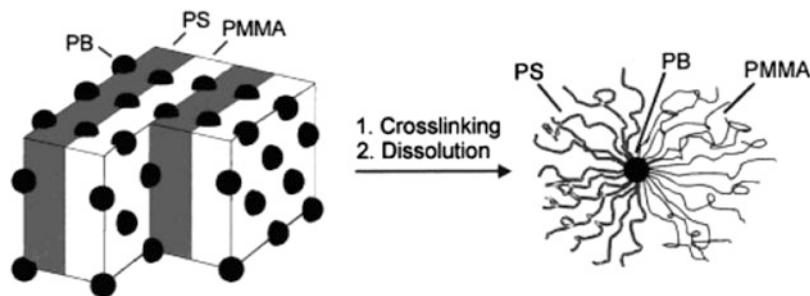
Fig. 12 Schematic representation of the Janus micelle preparation (Reprinted with permission from Ref. [16])

the transfer of a preformed bulk organization in solution directly leading to noncentrosymmetric objects. Janus micelles have been initially obtained by transferring in solution the bulk morphology of a PS-*b*-PB-*b*-PMMA triblock copolymer in which the central PB minor block forms spheres at the interface between PS and PMMA lamellae. In order to preserve the PS and PMMA coronal hemispheres, the PB spheres had to be cross-linked in the bulk structure. Dissolution of the bulk material in THF, a good solvent for both the PS and PMMA chains, yielded Janus micelles with a PB core surrounded by PS and PMMA half coronas (Fig. 12) [16]. These Janus micelles showed a strong tendency to form larger aggregates that can be regarded as supermicelles. Supermicelles coexist with single Janus micelles, as evidenced by various morphological observations realized both in THF solution and on silicon and water surfaces [16, 169].

The hydrophobic/hydrophilic contrast in the Janus micelles can be strongly enhanced by the hydrolysis of the PMMA chains resulting into PMAA hydrophilic blocks [28]. The resulting micelles can then be gradually transferred in pure water starting from a 1,4-dioxane solution. However, the hydrophobic PS hemi-corona collapses on the PB core and the whole insoluble part is then fully or partially surrounded by the PMAA chains. Aggregation into supermicelles and formation of aggregates of supermicelles was also evidenced in this investigation [28]. The influence of pH on PS-*b*-PB-*b*-PMAA Janus micelles was also investigated. At high pH, the hydrodynamic radius of the supermicelles is larger than under acidic conditions as a result of the ionization of the PMAA chains leading to their stretching [28]. Cylindrical micelles with an asymmetric corona, that is, Janus cylinders, were also produced from PS-*b*-PB-*b*-PMMA triblock terpolymer. Those asymmetric nanocylinders were prepared by the same procedure as for spherical Janus micelles but with a polymer composition forming another bulk morphology. In this case, the PS-*b*-PB-*b*-PMMA terpolymer formed PB cylinders embedded at the interface between PS and PMMA lamellae [170]. Preliminary investigations on Janus spherical micelles with a cross-linked P2VP core and PS and PnBMA coronal hemispheres have also been reported by Saito et al. [171].

Segregated coronal chains were also obtained by direct dissolution of triblock terpolymer chains without the need to stabilize a preexisting bulk organization as presented for Janus micelles. Indeed, the self-assembly of PtBA-*b*-PCEMA-*b*-PGMA triblock terpolymers in pyridine/methanol mixtures yielded to (partial) segregation of PtBa and PGMA blocks, as recently demonstrated by Liu and coworkers [172]. While pyridine is a good solvent for all of the three blocks, methanol is selective for PtBA and PGMA. For methanol fractions in the solvent mixture of 80 and 90 vol% and at 50 °C, spherical and cylindrical micelles with PtBA and PGMA coronal chains were observed. At methanol fraction of 95 vol%, vesicles were formed whose outer surface was mostly consisting PGMA chains while some PtBA chains formed circular patches. In pure methanol, tubular micelle-like aggregates coexisted with vesicles [172]. The same group also evidenced the formation of twisted cylinders with segregated A and C coronal chains from an ABC triblock copolymer in a block-selective solvent for the A and C blocks [173]. Such cylinders consisted of left- and right-handed helical sections (3D twisting) connected by wriggling (2D twisting) sections after aspiration on a solid substrate. The copolymer used was again a PtBA-*b*-PCEMA-*b*-PGMA triblock terpolymer but a composition different form the one described in Ref. [172]. Twisted cylinders were prepared from the dialysis of an aqueous solution of the triblock copolymer against methanol (Fig. 13).

In water, the copolymer formed core-shell-corona cylinders with a core of PtBA blocks surrounded by a shell of PCEMA blocks and a corona of PGMA blocks. The
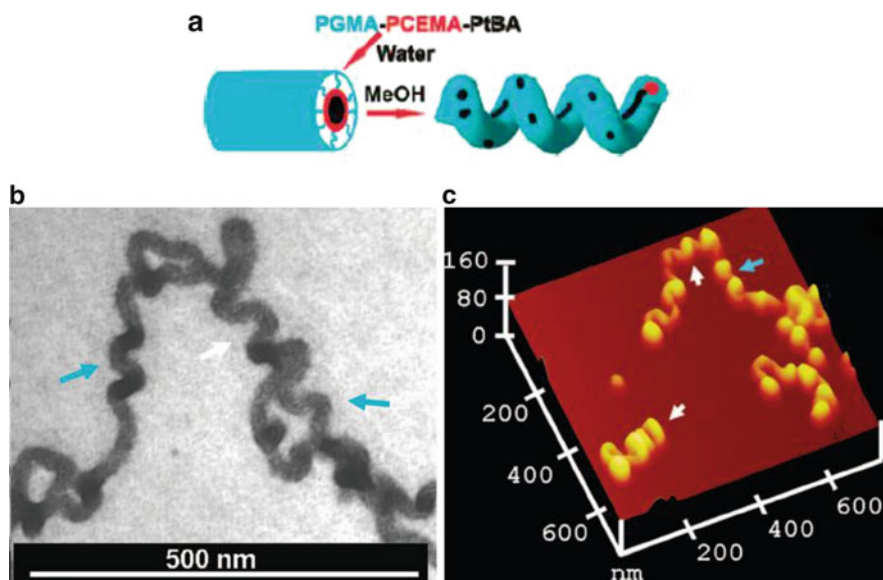
Fig. 13 (**a**) Schematic representation for the formation of twisted cylinders from PtBA-*b*-PCEMA-*b*-PGMA triblock terpolymer micelles in methanol. Typical (**b**) TEM and (**c**) AFM pictures are also shown (Reprinted with permission from Ref. [135])

cylinders with PCEMA cores twisted in water/methanol with high methanol contents, for example, >90 vol%, probably to create more space to accommodate the segregated PGMA chains, which were longer, better solvated, and more crowded than the PtBA chains.

Segregated coronal chains were also recently evidenced in thermo-responsive wormlike micelles from a PS-*b*-PE-*b*-PMMA triblock terpolymer with a crystallizable PE middle block in organic solvent [174]. Those micelles were composed of a core formed by crystalline PE domains and a patched corona formed by microphase-separated PS and PMMA chains. The formation of wormlike micelles is rather unexpected, because PE containing diblock copolymers usually form platelet-like structures.

Very recently, Müller and coworkers demonstrated the precise prediction of substructures, morphologies, size, and superstructures of self-assembled multicompartment micelles based on linear triblock terpolymers [175]. They devised a directed step-wise self-assembly via preassembled subunits. Sequential reductions of the degrees of freedom proved to be the key steps to reliably generate thermodynamically labile patchy morphologies. In particular, for low patch numbers, the multicompartment micelles exhibited precise geometry (with control of the angle and interpatch distance) and sizes (Fig. 14). Furthermore, the switching of the geometries and patchiness of spherical multicompartment micelles, as well as the reversible aggregation of linear multicompartment micelles via a step-growth polymerization-like process was enabled by the straightforward manipulation of the corona volume fraction (Fig. 14). Such a high precision in structure and tunability paves the way toward future bottom-up materials from block copolymer micelles.

7 Micelles Obtained by Mixing Anionically Synthesized Block Copolymers

Up to now, we have considered the micellization behavior of isolated block copolymer chains. It has been, however, demonstrated that micellization can be induced by complexation of one of the constituent block of the copolymer with other macromolecules or low molar mass molecules. Such aqueous micelles can be obtained from the mixing of a double-hydrophilic copolymer AB with a homopolymer C or a diblock copolymer AC or a diblock copolymer DC, provided that IPEC can form between the B and C blocks. This kind of electrostatic complexes has also been referred to as "block ionomer complexes" or BIC.

The AB + C case is illustrated by the works of Kabanov et al. [176] who investigated mixtures of PEO-*b*-PMANa with P4VPQ and of Gohy et al. on the pH-dependent complexation of P2VP-*b*-PEO with PSS [177, 178]. In all these studies, the resulting micelles contained an IPEC core and a PEO corona.
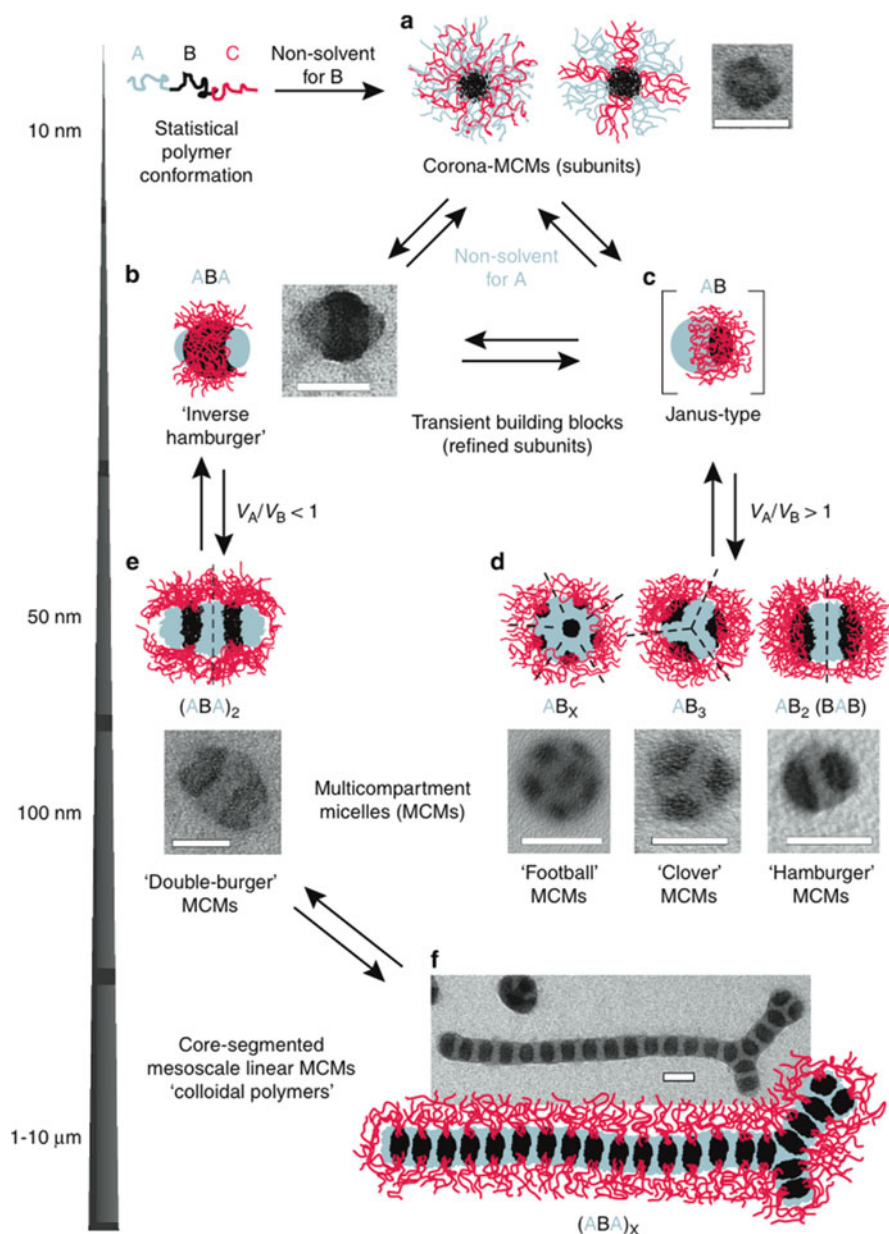
Fig. 14 Mechanism for the preparation and directed hierarchical self-assembly of well-defined multicomparment micelles. First, the ABC triblock terpolymers are forced into (**a**) micelles with a compartmentalized corona via dissolution in a nonsolvent for B (termed subunits). Upon dialysis into a nonsolvent for A and B, these subunits self-assemble via a refinement of the corona (**b**, **c**) into various structures with well-defined number of patches (**d**, **e**). (**f**) A step-growth like colloidal polymerization into segmented worms can be triggered under suitable conditions. (TEM images, OsO$_4$-stained; scale bars are 50 nm; PS gray, PB black, and PMMA not visible due to e-beam degradation) (Reproduced with permission from Ref. [175])

IPEC-based micelles in aqueous solutions have also been reported from AB + AC mixtures, as illustrated by Gohy et al. on mixtures of P2VP-*b*-PEO and PMAA-*b*-PEO copolymers [132]. IPEC formation was observed in a limited range of pH in which both the PMAA and P2VP blocks were ionized. The IPEC cores formed through electrostatic interaction between the ionized PMAA and P2VP blocks were surrounded by PEO corona. When the pH of the aqueous medium was decreased, the PMAA and P2VP blocks were essentially observed in their protonated form. The PMAA/P2VP interaction was therefore suppressed at low pH at the expense of hydrogen bonding in the PMAA/PEO pair. As a result, micelles were formed by the PMAA-*b*-PEO diblock while the protonated P2VP-*b*-PEO chains existed as unimers. In addition, a thermo-responsive behavior was observed for the hydrogen-bonded PMAA-*b*-PEO micelles [132]. Above 45 °C, the hydrogen-bonded PMAA/PEO complexes were disrupted while the cloud point of the PMAA block was reached, resulting in stable colloidal particles. Moreover, the temperature effect was found to be entirely reversible. At higher pH, the P2VP block was deprotonated and hydrophobic while the PMAA blocks were essentially ionized in the form of PMANa salt. As a result, PMANa-*b*-PEO chains were observed as unimers while P2VP-*b*-PEO chains aggregated into micelles.

IPEC complexation between the B and C blocks of AB and CD copolymers is a very promising route for the formation of complex micellar structures with compartmentalized corona. Noncentrosymmetric "Janus"-like micelles could in principle be obtained by using this strategy. Schlaad and coworkers investigated an AB + CD system formed by the PS-*b*-PMACs and PB-*b*-P4VPQ copolymers in THF [179]. However, this resulted in the formation of centrosymmetric vesicles with a vesicular layer formed by the PMACs/P4VPQ IPEC while the incompatibility between the two types of coronal chains resulted in an outer PS corona and an inner PB one (Fig. 15).

It should also be noted that vesicles were prepared from a mixture of PS-*b*-PAA and PS-*b*-P4VP diblock copolymers [73]. In this case, micelle formation was not driven by IPEC formation between the PAA and P4VP blocks because micellization was carried out at low pH where the PAA blocks are protonated and the P4VP chains are positively charged. The vesicular layer was thus formed by PS chains coming from both copolymers while the PAA blocks were segregated into the inside of the vesicles and the outside corona of the vesicles consisted of P4VP chains. This segregation occurred because the PAA chains were much shorter than the P4VP chains and stabilize the curvature. Electrostatic repulsion between charged P4VP blocks were also minimized.

We reported on hydrogen-bonded complexed cores obtained in DMF through the interaction of a PS-*b*-P2VP-*b*-PEO triblock copolymer with a tapered triblock copolymer consisting of a central PAA block and two outer comb-like blocks containing short PEO branches [180]. Hydrogen bonding was observed between the P2VP and PAA blocks resulting into micellar cores while three types of coronal chains were coexisting: linear PS and PEO chains and comb-like PEO. Segregation was observed between the comb-like PEO and the other coronal chains. Whenever
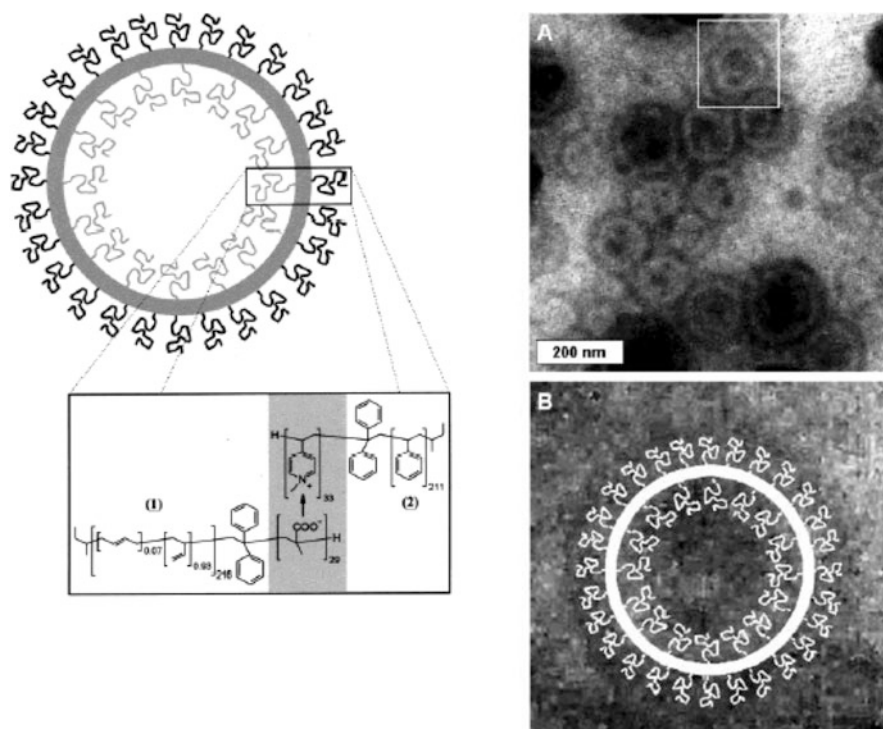
Fig. 15 Formation of vesicles with distinct inner (PB) and outer (PS) coronal blocks from a mixture of PS-*b*-P4VPQ and PB-*b*-PMACs copolymers. Vesicles are stained with CsI in the TEM pictures. TEM picture *B* is a magnification of the framed area in *A* (Reprinted with permission from Ref. [179])

the PS-*b*-P2VP-*b*-PEO triblock was complexed with PAA homopolymer, no segregation in the corona was observed.

IPEC or hydrogen-bonded complexes may form not only between mutually interacting polymer blocks but also between a polymer block and low *MW* molecules. Complexes between surfactants and block copolymers have been investigated for the formation of micelles. As illustrated by the work of Ikkala and coworkers [181], one of the major interest of these systems is that they combine two different length scales of supramolecular organizations, that is, the nanometer scale organization of the (liquid) crystalline surfactant molecules and the 10 nm scale relative to block copolymers. This gives rise to the so-called hierarchical systems. Water-soluble surfactants-block copolymer complexes were reported by Eisenberg et al. for PEO-*b*-PMANa-cationic surfactants mixtures [182, 183]. This resulted in the formation of vesicles in water with PMANa-cationic surfactants insoluble vesicular layers surrounded by PEO coronal chains. The characteristic features of the complexes were found to be strongly dependent on the PMANa-cationic surfactants stoichiometry, the more dense and defined structures being observed whenever all the MANa units were interacting with one surfactant

molecule. We obtained larger vesicles while complexing a PEO-b-P2VPQ copolymer with negatively charged fluorinated surfactants [184].

Block copolymer/low *MW* molecules complexes were also examined in organic solvents, as very recently exemplified by the works of Jiang and coworkers [185, 186]. These authors investigated mixtures of PS-b-P4VP copolymers with various low *MW* molecules including perfluorooctanoic acid and formic acid. Such molecules are expected to form hydrogen-bonded complexes with 4VP units in organic solvents such as chloroform. This further resulted in the formation of vesicles. We also obtained vesicles by mixing PS-b-P4VP copolymers with various low *MW* perfluoroalkyl molecules that exhibited an interesting dilution-induced morphological transition toward spherical micelles [187].

8   Conclusions and Outlook

Block copolymer micelles have been the subject of an enormous body of work during the last 40 years. The interest on block copolymer micelles certainly stems from the numerous practical applications of such systems. including biomedical applications, emulsion stabilization, viscosity regulation, catalyst support, surface modification, etc. Amphiphilic block copolymers with biocompatible and/or biodegradable sequences have potential for applications in the biomedical field, for example, as drug delivery systems and as carriers in gene therapy. The recent developments in nanotechnology have also created an important demand for self-organized materials including block copolymer micelles. In this respect, block copolymer micelles are used as templating reactors for the production of metallic conducting, semiconducting, or magnetic nanoparticles. In addition to the shape and size control due to the micellar templating, such nanoparticles embedded in a polymer matrix exhibit enhanced chemical stability to oxidation, better colloidal stability and could also display an increased catalytic activity. Block copolymer micelles can be also used as resists for lithographic processes.

Although the basic principles of block copolymer micellization have been already discovered and experimentally investigated in the 1980s, intense research on this topic has been performed since the mid-1990s by many research groups. Because it was not possible to include every contribution to that field in the frame of this chapter, only selected examples have been discussed. The well-defined chemical compositions, low polydispersity indices and perfectly controlled architectures of block copolymers synthesized by living anionic polymerization techniques have boosted the field of block copolymer micelles. This chapter focuses on the initial contribution of anionically synthesized block copolymers in the 1980s and 1990s on the understanding of the basic principles related to block copolymer micelles. With the development of the controlled radical polymerization techniques since the mid-1990s and the rather easy experimental conditions required for their implementation, amphiphilic block copolymers became easily accessible for more and more laboratories around the world and a real blossoming in the number of papers

related to block copolymers micelles was observed. More specifically, those developments were mostly triggered by the development of the so-called responsive micellar systems, exhibiting abrupt variations of their properties upon changes in pH, temperature, light illumination, etc. In that respect, polymerization techniques tolerant to many functional groups like the reversible addition − fragmentation chain-transfer (RAFT) polymerization played and are still playing a significant role toward the development of such stimuli-responsive micellar systems.

Nevertheless, living anionic polymerization techniques still allow a control over polymeric architecture which is not reachable with controlled radical polymerization techniques and have recently lead to block copolymer micelles with an unprecedented control over the morphology and properties. This is particularly illustrated in the field of complex micellar structures derived from triblock terpolymer (see Sect. 6) in which very recent examples of such complex micellar structures have been discussed. Those examples certainly demonstrate that anionically synthesized block copolymer still has a bright future for the formation of complex micellar structures.

Abbreviations and Symbols

AFM	Atomic force microscopy
AUC	Analytical ultra-centrifugation
b	Grafting distance
BIC	Block ionomer complex
CMC	Critical micelle concentration
CMT	Critical micelle temperature
CWC	Critical water concentration
DLS	Dynamic light scattering
DMF	N,N-dimethylformamide
IPEC	Interpolyelectrolyte complex
LCST	Lower critical solubility temperature
MW	Molecular weight
N	Degree of polymerization
N_A	Degree of polymerization of the core-forming block
N_B	Degree of polymerization of the corona-forming block
NMR	Nuclear magnetic resonance
P2VP	Poly(2-vinylpyridine)
P2VPQ	Poly(2-vinylpyridine) quaternized
P4VP	Poly(4-vinylpyridine)
PAA	Poly(acrylic acid)
PB	Polybutadiene
PBO	Poly(butylene oxide)
PCEMA	Poly(cinnamoylethyl methacrylate)
PDMAEMA	Poly(N,N-dimethylaminoethyl methacrylate)

PEB	Poly(ethylene-*co*-butylene)
PEE	Hydrogenated polybutadiene
PEO	Poly(ethylene oxide)
PGMA	Poly(glycidylmethacrylate)
PGMAS	Poly(glycidylmethacrylate) sulfonated
PI	Poly(isoprene)
PMA	Poly(methylacrylate)
PMAA	Poly(methacrylic acid)
PMACs	Poly(cesium methacrylate)
PMANa	Poly(sodium methacrylate)
PMMA	Poly(methylmethacrylate)
PnBMA	Poly(n-butylmethacrylate)
PPO	Poly(propylene oxide)
PS	Polystyrene
PtBA	Poly(*tert*-butylacrylate)
PtBMA	Poly(*tert*-butyl methacrylate)
PtBS	Poly(*tert*-butyl styrene)
R_c	Micellar core radius
R_g	Radius of gyration
R_h	Hydrodynamic radius
R_m	Total micellar radius
SANS	Small angle neutron scattering
SAXS	Small angle X-ray scattering
SEC	Size exclusion chromatography
SEM	Scanning electron microscopy
SLS	Static light scattering
TEM	Transmission electron microscopy
T_g	Glass transition temperature
THF	Tetrahydrofuran
Z	Aggregation number

References

1. Bates FM, Fredrickson GH (1990) Block copolymer thermodynamics: theory and experiment. Annu Rev Phys Chem 1990(41):525
2. Hamley IW (ed) (1998) The physics of block copolymers. Oxford Science Publication, Oxford
3. See for examples: (a) Okano T (ed) (1998) Biorelated polymers and gels. Academic Press, San Diego. (b) Jeong B, Gutowska A (2002) Lessons from nature: stimuli-responsive polymers and their biomedical applications. Trends Biotechnol 20:305. (c) Galaev LY, Mattiasson B (1999) 'Smart' polymers and what they could do in biotechnology and medicine. Trends Biotechnol 17:335. (d) Yokoyama M (2002) Gene delivery using temperature-responsive polymeric carriers. Drug Discov Today 7:426. (e) Kataoka K, Harada A, Nagasaki Y (2001) Block copolymer micelles for drug delivery: design, characterization and biological significance. Adv Drug Deliv Rev 47:113

4. Riess G (2003) Micellization of block copolymers. Prog Polym Sci 28:1107
5. Gohy JF (2005) Block copolymer micelles. Adv Polym Sci 190:65
6. Elias HG (1973) Nonionic micelles. J Macromol Sci Chem 7:601
7. Tsunashima Y, Hirata M, Kawamata Y (1990) Diffusion motions and microphase separation of styrene-butadiene diblock copolymer in solution. 1. Extremely dilute solution region. Macromolecules 23:1089
8. Alexandridis P, Holzwarth JF, Hatton TA (1994) Micellization of poly(ethylene oxide)-poly (propylene oxide)-poly(ethylene oxide) triblock copolymers in aqueous solutions: thermodynamics of copolymer association. Macromolecules 27:2414
9. Chu B, Zhou Z (1996) Physical chemistry of polyoxyalkylene block copolymer surfactants. In: Nace VN (ed) Nonionic surfactants: polyoxyalkylene block copolymers, vol 60. Marcel Dekker, New York
10. Wanka G, Hofmann H, Ulbricht W (1994) Phase diagrams and aggregation behavior of poly (oxyethylene)-poly(oxypropylene)-poly(oxyethylene) triblock copolymers in aqueous solutions. Macromolecules 27:4145
11. Nace VM (ed) (1996) Nonionic surfactants: polyoxyalkylene block copolymers, vol 60, Surfactant science series. Marcel Dekker, New York
12. Zhou Z, Yang YW, Booth C, Chu B (1996) Association of a triblock ethylene oxide (E) and butylene oxide (B) copolymer ($B_{12}E_{260}B_{12}$) in aqueous solution. Macromolecules 29:8357
13. Pispas S, Hadjichristidis N, Potemkin I, Khokhlov A (2000) Effect of architecture on the micellization properties of block copolymers: A2B miktoarm stars vs AB diblocks. Macromolecules 33:1741
14. Zhang L, Eisenbergn A (1996) Multiple morphologies and characteristics of "Crew-Cut" micelle-like aggregates of polystyrene-*b*-poly(acrylic acid) diblock copolymers in aqueous solutions. J Am Chem Soc 118:3168
15. Munk P (1996) Equilibrium and nonequilibrium polymer micelles. In: Webber SE, Munk P, Tuzar Z (eds) NATO ASI series, serie E: applied sciences, vol 327. Kluwer Academic Publisher, Dordrecht 327:19–32
16. Erhardt R, Böker A, Zettl H, Kaya H, Pyckhout-Hintzen W, Krausch G, Abetz V, Müller AHE (2001) Janus micelle. Macromolecules 34:1069
17. Tuzar Z, Kratochvil P (1993) Micelles of block and graft copolymers in solution. In: Matijevic E (ed) Surface and colloid science, vol 15. Plenum Press, New York
18. Webber SE, Munk P, Tuzar Z (eds) (1996) Solvents and self-organization of polymer, NATO ASI series, serie E: applied sciences, vol 327. Kluwer Academic Publisher, Dordrecht
19. Zhang L, Eisenberg A (1996) Ion-induced morphological changes in "Crew-Cut" aggregates of amphiphilic block copolymers. Science 272:1777
20. Zhang L, Shen H, Eisenberg A (1997) Phase separation behavior and crew-cut micelle formation of polystyrene-*b*-poly(acrylic acid) copolymers in solutions. Macromolecules 30:1001
21. Brown W (ed) (1972) Dynamic light scattering. Oxford University Press, Oxford
22. Israelachvili JN (ed) (1985) Intermolecular and surface forces. Academic, London
23. Gohy JF, Willet N, Varshney S, Zhang JX, Jérôme R (2001) Core–shell–corona micelles with a responsive shell. Angew Chem Int Ed 40:3214
24. Gohy JF, Willet N, Varshney SK, Zhang JX, Jérôme R (2002) pH-Dependence of the morphology of micelles formed by poly(2-vinylpyridine)-block-poly(ethylene oxide) copolymers in water. E-Polymers paper 35
25. Goldraich M, Talmon Y (2000) Direct-imaging cryo-transmission electron microscopy in the study of colloids and polymer solutions. In: Alexandridis P, Lindman B (eds) Amphiphilic block copolymers: self assembly and applications. Elsevier, Amsterdam
26. Mortensen K, Talmon Y, Gao B, Kops J (1997) Structural properties of bulk and aqueous systems of PEO−PIB−PEO triblock copolymers as studied by small-angle neutron scattering and cryo-transmission electron microscopy. Macromolecules 30:6764
27. Förster S, Hermsdorf N, Böttcher C, Lindner P (2002) Structure of polyelectrolyte block copolymer micelles. Macromolecules 35:4096

28. Erhardt R, Zhang MF, Böker A, Zettl H, Abetz C, Frederik P, Krausch G, Abetz V, Müller AHE (2003) Amphiphilic janus micelles with polystyrene and poly(methacrylic acid) hemispheres. J Am Chem Soc 125:3260

29. Mortensen K (2000) Small angle scattering studies of block copolymer micelles, micellar mesophases and networks. In: Alexandridis P, Lindman B (eds) Amphiphilic block copolymers: self assembly and applications. Elsevier, Amsterdam

30. Selb J, Gallot Y (1981) Micellisation de copolymères séquencés polystyrène-polyvinylpyridinium, 3. Influence de la concentration en sel et de la température. Makromol Chem 182:1513

31. Booth C, Naylor TD, Price C, Rajab NS, Stubbersfield RB (1978) Investigation of the size distribution of non-ionic micelles formed from a polystyrene–polyisoprene block copolymer in N,N-dimethylacetamide. J Chem Soc Faraday Trans I 74:2352

32. Teo HH, Styring MG, Yeates SG, Price C, Booth C (1986) Size-exclusion chromatography of micellar solutions of poly(oxyethylene) n-alkyl ethers. J Coll Interf Sci 114:416

33. Bednar B, Edwards K, Almgren M, Tormod S, Tuzar Z (1998) Rates of association and dissociation of block copolymer micelles: light scattering stopped-flow experiments. Makromol Chem Rapid Commun 9:785

34. Creutz S, van Stam J, Antoun S, De Schryver FC, Jérôme R (1997) Exchange of polymer molecules between block copolymer micelles studied by emission spectroscopy. A method for the quantification of unimer exchange rates. Macromolecules 30:4078

35. Creutz S, van Stam J, De Schryver FC, Jérôme R (1998) Dynamics of poly((dimethylamino) alkyl methacrylate-block-sodium methacrylate) micelles. Influence of hydrophobicity and molecular architecture on the exchange rate of copolymer molecules. Macromolecules 31:681

36. Van Stam J, Creutz S, de Schryver FC, Jérôme R (2000) Tuning of the exchange dynamics of unimers between block copolymer micelles with temperature, cosolvents, and cosurfactants. Macromolecules 33:6388

37. Riess G, Hurtrez G (1996) Block copolymers: synthesis, colloidal properties and application possibilities of micellar systems. In: Webber SE, Munk P, Tuzar Z (eds) NATO ASI series, serie E: applied sciences, vol 327. Kluwer Academic Publisher, Dordrecht

38. Won YY, Davis HT, Bates FS (2003) Molecular exchange in PEO-PB micelles in water. Macromolecules 36:953

39. Stepanek M, Prochazka K (2000) Time-dependent behavior of block polyelectrolyte micelles in aqueous media studied by potentiometric titrations, QELS and fluorometry. Langmuir 16:2502

40. Tuzar Z (1996) Overview of polymer micelles. In: Webber SE, Munk P, Tuzar Z (eds) NATO ASI series, serie E: applied sciences, vol 327. Kluwer Academic Publisher, Dordrecht

41. Munk P (1996) Classical methods for the study of block copolymer micelles. In: Webber SE, Munk P, Tuzar Z (eds) NATO ASI series, serie E: applied sciences, vol 327. Kluwer Academic Publisher, Dordrecht

42. Zana R (2000) Fluorescence studies of amphiphilic block copolymers in solution. In: Alexandridis P, Lindman B (eds) Amphiphilic block copolymers: self assembly and applications. Elsevier, Amsterdam

43. Farago BJ, Monkenbusch M, Richter D, Huang JS, Fetters LJ, Gast AP (1993) Collective dynamics of tethered chains: breathing modes. Phys Rev Lett 71:1015

44. Castelletto V, Hamley IW, Yang Z, Haeussler W (2003) Neutron spin-echo investigation of the dynamics of block copolymer micelles. J Chem Phys 119:8158

45. Spevacek J (1982) ^{1}H NMR study of styrene-butadiene block copolymer micelles in selective solvent. Makromol Chem Rapid Commun 3:697

46. Gao Z, Zhong XF, Eisenberg A (1994) Chain dynamics in coronas of ionomer aggregates. Macromolecules 27:794

47. Noolandi J, Hong KM (1983) Theory of block copolymer micelles in solution. Macromolecules 16:1443

48. Leibler L, Orland H, Wheeler JC (1983) Theory of critical micelle concentration for solutions of block copolymers. J Chem Phys 79:3550
49. Nagarajan R, Ganesh K (1989) Block copolymer self-assembly in selective solvents: theory of solubilization in spherical micelles. Macromolecules 22:4312
50. Hurter PN, Scheutjens JMHM, Hatton TA (1993) Molecular modeling of micelle formation and solubilization in block copolymer micelles. 1. A self-consistent mean-field lattice theory. Macromolecules 26:5592
51. Binder K (ed) (1995) Monte Carlo and molecular dynamics simulations in polymer science. Oxford University Press, New York
52. Binder K, Müller M (2000) Monte Carlo simulation of block copolymers. Curr Opin Colloid Interf Sci 5:314
53. Halilog¢lu T, Mattice WL (1996) Monte Carlo simulations of self-assembly in macromolecular systems. In: Webber SE, Munk P, Tuzar Z (eds) NATO ASI series, serie E: applied sciences, vol 327. Kluwer Academic Publisher, Dordrecht
54. Marko JF, Rabin Y (1992) Microphase separation of charged diblock copolymers: melts and solutions. Macromolecules 25:1503
55. Dan N, Tirrell M (1993) Self-assembly of block copolymers with a strongly charged and a hydrophobic block in a selective, polar solvent. Micelles and adsorbed layers. Macromolecules 26:4310
56. Shusharina NP, Nyrkova IA, Khokhlov AR (1996) Diblock copolymers with a charged block in a selective solvent: micellar structure. Macromolecules 29:3167
57. Daoud M, Cotton JP (1982) Star shaped polymers: a model for the conformation and its concentration dependence. J Phys (Fr) 43:531
58. Halperin A (1987) Polymeric micelles: a star model. Macromolecules 20:2943
59. Zhulina EB, Birshtein TM (1986) Conformations of block-copolymer molecules in selective solvents micellar structures. Polym Sci USSR (Eng) 27:570
60. Shelley JC, Shelley MY (2000) Computer simulation of surfactant solutions. Curr Opin Colloid Interf Sci 5:101
61. Förster S, Plantenberg T (2002) From self-organizing polymers to nanohybrid and biomaterials. Angew Chem Int Ed 41:688
62. Förster S, Abetz V, Müller AHE (2004) Polyelectrolyte block copolymer micelles. Adv Polym Sci 166:173
63. Borisov OV, Zhulina EB (2002) Effect of salt on self-assembly in charged block copolymer micelles. Macromolecules 35:4472
64. Zhang L, Eisenberg A (1995) Multiple morphologies of "crew-cut" aggregates of polystyrene-b-poly(acrylic acid) block copolymers. Science 268:1728
65. Cameron NS, Corbierre MK, Eisenberg A (1999) Asymmetric amphiphilic block copolymers in solution: a morphological wonderland. Can J Chem 77:1311
66. Yu Y, Zhang L, Eisenberg A (1998) Morphogenic effect of solvent on crew-cut aggregates of amphiphilic diblock copolymers. Macromolecules 31:1144
67. Moffitt M, Zhang L, Khougaz K, Eisenberg A (1996) Micellization of ionic block copolymers in three dimensions. In: Webber SE, Munk P, Tuzar Z (eds) NATO ASI series, serie E: applied sciences, vol 327. Kluwer Academic Publisher, Dordrecht
68. Zhang L, Eisenberg A (1996) Morphogenic effect of added ions on crew-cut aggregates of polystyrene-b-poly(acrylic acid) block copolymers in solutions. Macromolecules 29:8805
69. Zhang L, Khougaz K, Moffitt M, Eisenberg A (2000) Self assembly of block polyelectrolytes. In: Alexandridis P, Lindman B (eds) Amphiphilic block copolymers: self-assembly and applications. Elsevier, Amsterdam
70. Luo L, Eisenberg A (2001) Thermodynamic stabilization mechanism of block copolymer vesicles. J Am Chem Soc 123:1012
71. Luo L, Eisenberg A (2001) Thermodynamic size control of block copolymer vesicles in solution. Langmuir 17:6804

72. Dobereiner HG, Evans E, Kraus M, Seifert U, Wortis M (1997) Mapping vesicle shapes into the phase diagram: a comparison of experiment and theory. Phys Rev E 55:4458
73. Luo L, Eisenberg A (2002) One-step preparation of block copolymer vesicles with preferentially segregated acidic and basic corona chains. Angew Chem Int Ed 41:1001
74. Won YY, Davis HT, Bates FS (1999) Giant wormlike rubber micelles. Science 283:960
75. Discher BM, Won YY, Ege DS, Lee JCM, Bates FS, Discher DE, Hammer DA (1999) Polymersomes: tough vesicles made from diblock copolymers. Science 284:1143
76. Aranda-Spinoza H, Bermudez H, Bates FS, Discher DE (2001) Electromechanical limits of polymersomes. Phys Rev Lett 87:208301
77. Lee JCM, Santore M, Bates FS, Discher DE (2002) From membranes to melts, rouse to reptation: diffusion in polymersome versus lipid bilayers. Macromolecules 35:323
78. Schillen K, Bryskhe K, Melnikova YS (1999) Vesicles formed from a poly(ethylene oxide)−poly(propylene oxide)−poly(ethylene oxide) triblock copolymer in dilute aqueous solution. Macromolecules 32:6885
79. Discher DE, Eisenberg A (2002) Polymer vesicles. Science 297:967
80. Lee M, Cho BK, Zin WC (2001) Supramolecular structures from rod−coil block copolymers. Chem Rev 101:3869
81. Klok HA, Lecommandoux S (2001) Supramolecular materials via block copolymer self-assembly. Adv Mater 13:1217
82. Kovacs AJ, Manson JA (1966) Propriétés des copolymères biséquencés polyoxyéthylène-polystyrène. Kolloid Z Z Polym 214:1
83. Gast AP, Vinson PK, Cogan-Farinas KA (1993) An intriguing morphology in crystallizable block copolymers. Macromolecules 26:1774
84. Pitsikalis M, Siakali-Kioulafa E, Hadjichristidis N (2000) Block copolymers of styrene and stearyl methacrylate. Synthesis and micellization properties in selective solvents. Macromolecules 33:5460
85. Quintana JR, Salazar RA, Katime I (1995) Micelle formation and polyisobutylene solubilization by polystyrene-block-poly(ethylene-co-butylene)-block-polystyrene block copolymers. Macromol Chem Phys 196:1625
86. Quintana JR, Janez MD, Katime I (1995) Formation of block copolymer micelles in solutions of a linear homopolymer in a good solvent. Macromol Rapid Commun 16:607
87. Samii AA, Lindman B, Karlstrom G (1990) Phase behavior of some nonionic polymers in nonaqueous solvents. Prog Colloid Polym Sci 82:280
88. Samii AA, Karlstrom G, Lindman B (1991) Phase behavior of poly(ethylene oxide)-poly(propylene oxide) block copolymers in nonaqueous solution. Langmuir 7:1067
89. Alexandridis P, Yang L (2000) Micellization of polyoxyalkylene block copolymers in formamide. Macromolecules 33:3382
90. Gervais M, Gallot B (1977) Influence of the nature of the solvent on the lamellar crystalline structure of block copolymers with an amorphous block and a crystallizable poly(ethylene oxide) block. Makromol Chem 178:2071
91. Lin EK, Gast AP (1996) Semicrystalline diblock copolymer platelets in dilute solution. Macromolecules 29:4432
92. Vagberg LJM, Cogan KA, Gast AP (1991) Light-scattering study of starlike polymeric micelles. Macromolecules 24:1670
93. Wu G, Chu B (1994) Light-scattering studies of a block poly(oxyethylene-oxypropylene-oxyethylene) copolymer in water/o-xylene mixtures. Macromolecules 27:1766
94. Guo C, Liu HZ, Chen JY (2000) A Fourier transform infrared study on water-induced reverse micelle formation of block copoly(oxyethylene–oxypropylene–oxyethylene) in organic solvent. Colloids Surf A Physicochem Eng Asp 175:193
95. Spatz JP, Roescher A, Möller M (1996) Gold nanoparticles in micellar poly(styrene)-b-poly(ethylene oxide) films—size and interparticle distance control in monoparticulate films. Adv Mater 8:337

96. Bronstein LM, Chernyshov DM, Timofeeva GI, Dubrovina LV, Valetsky PM, Obolonkova ES, Khokhlov AR (2000) Interaction of polystyrene-*block*-poly(ethylene oxide) micelles with cationic surfactant in aqueous solutions. Metal colloid formation in hybrid systems. Langmuir 16:3626

97. Förster S, Zisenis M, Wenz E, Antonietti M (1996) Micellization of strongly segregated block copolymers. J Chem Phys 104:9956

98. Spatz JP, Röscher A, Sheiko S, Krausch G, Möller M (1995) Noble metal loaded block lonomers: micelle organization, adsorption of free chains and formation of thin films. Adv Mater 7:731

99. Spatz JP, Sheiko S, Möller M (1996) Ion-stabilized block copolymer micelles: film formation and intermicellar interaction. Macromolecules 29:3220

100. Roescher A, Möller M (1995) Extraction of aqueous gold sols with styrene/2-vinylpyridine block copolymers in toluene. Adv Mater 7:151

101. Antonietti M, Wenz E, Bronstein LM, Seregina MS (1995) Synthesis and characterization of noble metal colloids in block copolymer micelles. Adv Mater 7:1000

102. Sulman E, Bodrova Y, Matveeva V, Semagina N, Cerveny L, Kurtc V, Bronstein L, Platonova O, Valetsky P (1999) Hydrogenation of dehydrolinalool with novel catalyst derived from Pd colloids stabilized in micelle cores of polystyrene-poly-4-vinylpyridine block copolymers. Appl Catal A Gen 176:75

103. Spatz JP, Mössmer S, Möller M (1996) Metastable reverse globular micelles and giant micellar wires from block copolymers. Angew Chem Int Ed 35:1510

104. Kiriy A, Gorodyska G, Minko S, Stamm M, Tsitsilianis C (2003) Single molecules and associates of heteroarm star copolymer visualized by atomic force microscopy. Macromolecules 36:8704

105. Almgren M, Brown W, Hvidt S (1995) Self-aggregation and phase behavior of poly(ethylene oxide)-poly(propylene oxide)-poly(ethylene oxide) block copolymers in aqueous solution. Colloid Polym Sci 273:2

106. Booth C, Attwood D (2000) Effects of block architecture and composition on the association properties of poly(oxyalkylene) copolymers in aqueous solution. Macromol Rapid Commun 21:501

107. Wanka G, Hoffmann H, Ulbricht W (1990) The aggregation behavior of poly-(oxyethylene)-poly-(oxypropylene)-poly-(oxyethylene)-block-copolymers in aqueous solution. Colloid Polym Sci 268:101

108. Nakashima K, Bahadur P (2006) Aggregation of water-soluble block copolymers in aqueous solutions: recent trends. Adv Colloid Interface Sci 123:75

109. Jain NJ, Aswal VK, Goyal PS, Bahadur P (2000) Salt induced micellization and micelle structures of' PEO/PPO/PEO block copolymers in aqueous solution. Colloids Surf A Physicochem Eng Asp 173:85

110. Guo C, Wang J, Liu HZ, Chen JY (1999) Hydration and conformation of temperature-dependent micellization of PEO−PPO−PEO block copolymers in aqueous solutions by FT-raman. Langmuir 15:2703

111. Chaibundit C, Mai SM, Heatley F, Booth C (2000) Association properties of triblock copolymers in aqueous solution: copolymers of ethylene oxide and 1,2-butylene oxide with long E-blocks. Langmuir 16:9645

112. Connell SD, Collins S, Fundin J, Yang Z, Hamley IW (2003) In situ atomic force microscopy imaging of block copolymer micelles adsorbed on a solid substrate. Langmuir 19:10449

113. Hamley IW, Connell SD, Collins S (2004) In situ atomic force microscopy imaging of adsorbed block copolymer micelles. Macromolecules 37:5337

114. Khan TN, Mobbs RH, Price C, Quintana JR, Stubbersfield RB (1987) Synthesis and colloidal behaviour of a polystyrene-b-poly(ethylene oxide) block copolymer. Eur Polym J 23:191

115. Xu R, Winnik MA, Riess G, Chu B, Croucher MD (1992) Micellization of polystyrene-poly (ethylene oxide) block copolymers in water. 5. A test of the star and mean-field models. Macromolecules 25:644

116. Mortensen K, Brown W, Almdal K, Alami E, Jada A (1997) Structure of PS−PEO diblock copolymers in solution and the bulk state probed using dynamic light-scattering and small-angle neutron-scattering and dynamic mechanical measurements. Langmuir 13:3635

117. Bronstein LM, Chernyshov DM, Timofeeva GI, Dubrovina LV, Valetsky PM, Khokhlov AR (1999) Polystyrene-block-poly(ethylene oxide) micelles in aqueous solution. Langmuir 15:6195

118. Selb J, Gallot Y (1980) Distinction entre les phénomènes d'agrégation et de micellisation présentés par des copolymères amphipathiques. Cas des copolymères polystyrène/polyvinyl-pyridinium en milieu aqueux. Makromol Chem 181:809

119. Astafieva I, Zhong XF, Eisenberg A (1993) Critical micellization phenomena in block polyelectrolyte solutions. Macromolecules 26:7339

120. Astafieva I, Khougaz K, Eisenberg A (1995) Micellization in block polyelectrolyte solutions. 2. Fluorescence study of the critical micelle concentration as a function of soluble block length and salt concentration. Macromolecules 28:7127

121. Zhang LF, Barlow RJ, Eisenberg A (1995) Scaling relations and coronal dimensions in aqueous block polyelectrolyte micelles. Macromolecules 28:6055

122. Khougaz K, Astafieva I, Zhong XF, Eisenberg A (1995) Micellization in block polyelectrolyte solutions. 3. Static light scattering characterization. Macromolecules 28:7135

123. Tuzar Z (1996) Copolymer micelles in aqueous media. In: Webber SE, Munk P, Tuzar Z (eds) NATO ASI series, serie E: applied sciences, vol 327. Kluwer Academic Publisher, Dordrecht

124. Gohy JF, Antoun S, Jérôme R (2001) Self-aggregation of poly(methyl methacrylate)-block-poly(sulfonated glycidyl methacrylate) copolymers. Polymer 42:8637

125. Raviv U, Giasson S, Kampf N, Gohy JF, Jérôme R, Klein J (2003) Lubrication by charged polymers. Nature 425:163

126. Cölfen H (2001) Double-hydrophilic block copolymers: synthesis and application as novel surfactants and crystal growth modifiers. Macromol Rapid Commun 22:219

127. Martin TJ, Prochazka K, Munk P, Webber SE (1996) pH-dependent micellization of poly(2-vinylpyridine)-block-poly(ethylene oxide). Macromolecules 29:6071

128. Gohy JF, Mores S, Varshney SK, Zhang JX, Jérôme R (2002) pH-dependence of the morphology of micelles formed by poly(2-vinylpyridine)-block-poly(ethylene oxide) copolymers in water. e-polymers 21:1–8

129. Bronstein LM, Sidorov SN, Valetsky PM, Hartmann J, Cölfen H, Antonietti M (1999) Induced micellization by interaction of poly(2-vinylpyridine)-block-poly(ethylene oxide) with metal compounds. Micelle characteristics and metal nanoparticle formation. Langmuir 15:6256

130. Sidorov SN, Bronstein LM, Kabachii YA, Valetsky PM, Soo PL, Maysinger D, Eisenberg A (2004) Influence of metalation on the morphologies of poly(ethylene oxide)-block-poly(4-vinylpyridine) block copolymer micelles. Langmuir 20:3543

131. Mathur AM, Drescher B, Scranton AB, Klier J (1998) Polymeric emulsifiers based on reversible formation of hydrophobic units. Nature 392:367

132. Gohy JF, Varshney SK, Jérôme R (2001) Water-soluble complexes formed by poly(2-vinylpyridinium)-block-poly(ethylene oxide) and poly(sodium methacrylate)-block-poly(ethylene oxide) copolymers. Macromolecules 34:3361

133. Kamachi M, Kurihara M, Stille JK (1972) Synthesis of block polymers for desalination membranes. Preparation of block copolymers of 2-vinylpyridine and methacrylic acid or acylic acid. Macromolecules 5:161

134. Gohy JF, Creutz S, Garcia M, Mahltig B, Stamm M, Jérôme R (2000) Aggregates formed by amphoteric diblock copolymers in water. Macromolecules 33:6378

135. Gohy JF, Antoun S, Jérôme R (2001) pH-dependent micellization of poly(2-vinylpyridine)-block-poly((dimethylamino)ethyl methacrylate) diblock copolymers. Macromolecules 24:7435

136. Bates FS, Fredrickson GH (1999) Block copolymers—designer soft materials. Phys Today 52:32

137. Fustin C-A, Abetz V, Gohy J-F (2005) Triblock terpolymer micelles: a personal outlook. Eur Phys J E Soft Matter 16:291
138. Kriz J, Masar B, Plestil J, Tuzar Z, Pospisil H, Doskocilova D (1998) Three-layer micelles of an ABC block copolymer: NMR, SANS, and LS study of a poly(2−ethylhexyl acrylate)-block-poly(methyl methacrylate)-block-poly(acrylic acid) copolymer in D2O. Macromolecules 31:41
139. Yu GE, Eisenberg A (1998) Multiple morphologies formed from an amphiphilic ABC triblock copolymer in solution. Macromolecules 31:5546
140. Ishizone T, Sugiyama K, Sakano Y, Mori H, Hirao A, Nakahama S (1999) Anionic polymerizations of perfluoroalkyl methacrylates and synthesis of well-defined ABC triblock copolymers of methacrylates containing hydrophilic, hydrophobic, and perfluoroalkyl groups. Polym J 31:983
141. Lambert O, Reutenauer S, Hurtrez G, Dumas P (2000) Synthesis of three-arm star block copolymers. Macromol Symp 161:97
142. Stepanek M, Matejicek P, Humpolickova J, Prochazka K (2005) Reversible aggregation of polystyrene-*block*-poly(2-vinylpyridine)-*block*-poly(ethylene oxide) block copolymer micelles in acidic aqueous solutions. Langmuir 21:10783
143. Humpolickova J, Stepanek M, Prochazka K, Hof M (2005) Solvent relaxation study of pH-dependent hydration of poly(oxyethylene) shells in polystyrene-*block*-poly(2-vinylpyridine)-*block*-poly(oxyethylene) micelles in aqueous solutions. J Phys Chem A 109:10803
144. Khanal A, Inoue Y, Yada M, Nakashima K (2007) Synthesis of silica hollow nanoparticles templated by polymeric micelle with core−shell−corona structure. J Am Chem Soc 129:1534
145. Khanal A, Li Y, Takisawa N, Kawasaki N, Oishi Y, Nakashima K (2004) Morphological change of the micelle of poly(styrene)-b-poly(2-vinylpyridine)-b-poly(ethylene oxide) induced by binding of sodium dodecyl sulfate. Langmuir 20:4809
146. Lei LC, Gohy JF, Willet N, Zhang JX, Varshney S, Jérôme R (2004) Morphology of core-shell-corona aqueous micelles: II. Addition of core-forming homopolymer. Polymer 45:4375
147. Lei LC, Gohy JF, Willet N, Zhang JX, Varshney S, Jérôme R (2004) Tuning of the morphology of core−shell−corona micelles in water. I. Transition from sphere to cylinder. Macromolecules 37:1089
148. Lei L, Gohy J-F, Willet N, Zhang J-X, Varshney S, Jérôme R (2006) Dependence of the structure of core–shell–corona micelles on the composition of water/toluene mixtures. Polymer 47:2723
149. Zhu J, Jiang W (2005) Self-assembly of ABC triblock copolymer into giant segmented wormlike micelles in dilute solution. Macromolecules 38:9315
150. Giebeler E, Stadler R (1997) ABC triblock polyampholytes containing a neutral hydrophobic block, a polyacid and a polybase. Macromol Chem Phys 198:3815
151. Tsitsilianis C, Roiter Y, Katsampas I, Minko S (2008) Diversity of nanostructured self-assemblies from a pH-responsive ABC terpolymer in aqueous media. Macromolecules 41:925
152. Li Z, Kesselman E, Talmon Y, Hillmyer MA, Lodge TP (2004) Multicompartment micelles from ABC miktoarm stars in water. Science 306:98
153. Liu C, Hillmyer MA, Lodge TP (2008) Evolution of multicompartment micelles to mixed corona micelles using solvent mixtures. Langmuir 24:12001
154. Stavrouli N, Triftaridou AI, Patrickios CS, Tsitsilianis C (2007) Multi-compartment unimolecular micelles from (ABC)*n* multi-Arm star triblock terpolymers. Macromol Rapid Commun 28:560
155. Ma Q, Wooley KL (2000) The preparation of *t*-butyl acrylate, methyl acrylate, and styrene block copolymers by atom transfer radical polymerization: precursors to amphiphilic and hydrophilic block copolymers and conversion to complex nanostructured materials. J Polym Sci Part A Polym Chem 38:4805
156. Pochan DJ, Chen Z, Cui H, Hales K, Qi K, Wooley KL (2004) Toroidal triblock copolymer assemblies. Science 306:94

157. Zhong S, Cui H, Chen Z, Wooley KL, Pochan DJ (2008) Helix self-assembly through the coiling of cylindrical micelles. Soft Matter 4:90
158. Li Z, Chen Z, Cui H, Hales K, Qi K, Wooley KL, Pochan DJ (2005) Disk morphology and disk-to-cylinder tunability of poly(acrylic acid)-*b*-poly(methyl acrylate)-*b*-polystyrene triblock copolymer solution-state assemblies. Langmuir 21:7533
159. Hales K, Chen Z, Wooley KL, Pochan DJ (2008) Nanoparticles with tunable internal structure from triblock copolymers of PAA-*b*-PMA-*b*-PS. Nano Lett 8:2023
160. Cui H, Chen Z, Wooley KL, Pochan DJ (2006) Controlling micellar structure of amphiphilic charged triblock copolymers in dilute solution via coassembly with organic counterions of different spacer lengths. Macromolecules 39:6599
161. Stewart S, Liu GJ (1999) Hollow nanospheres from polyisoprene-*block*-poly(2-cinnamoy-lethylmethacrylate)-*block*-poly(*tert*-butyl acrylate). Chem Mater 11:1048
162. Stewart S, Liu G (2000) Block copolymer nanotubes. Angew Chem Int Ed 39:340
163. Underhill RS, Liu GJ (2000) Triblock nanospheres and their use as templates for inorganic nanoparticle preparation. Chem Mater 12:2082
164. Patrickios CS, Hertler WR, Abbott NL, Hatton TA (1994) Diblock, ABC triblock, and random methacrylic polyampholytes: synthesis by group transfer polymerization and solution behavior. Macromolecules 27:930
165. Chen WY, Alexandridis P, Su CK, Patrickios CS, Hertler WR, Hatton TA (1995) Effect of block size and sequence on the micellization of ABC triblock methacrylic polyampholytes. Macromolecules 28:8604
166. Patrickios CS, Lowe AB, Armes SP, Billingham NC (1998) ABC triblock polymethacrylates: group transfer polymerization synthesis of the ABC, ACB, and BAC topological isomers and solution characterization. J Polym Sci Part A Polym Chem 36:617
167. Tsitsilianis C, Sfika V (2001) Heteroarm star-like micelles formed from polystyrene-block-poly(2-vinyl pyridine)-block-poly(methyl methacrylate) ABC triblock copolymers in toluene. Macromol Rapid Commun 22:647
168. Fernyhough CM, Pantazis D, Pispas S, Hadjichristidis N (2004) The micellar behavior of linear triblock terpolymers of styrene (S), isoprene (I), and methyl methacrylate (MMA) in selective solvents for PS and PMMA. Eur Polym J 40:237
169. Xu H, Erhardt R, Abetz V, Müller AHE, Goedel WA (2001) Janus micelles at the air/water interface. Langmuir 17:6787
170. Liu YF, Abetz V, Müller AHE (2003) Janus cylinders. Macromolecules 36:7894
171. Saito R, Fujita A, Ichimura A, Ishizu K (2000) Synthesis of microspheres with microphase-separated shells. J Polym Sci Part A Polym Chem 38:2091
172. Njikang G, Han D, Wang J, Liu G (2008) ABC triblock copolymer micelle-like aggregates in selective solvents for A and C. Macromolecules 41:9727
173. Hu J, Njikang G, Liu G (2008) Twisted ABC triblock copolymer cylinders with segregated A and C coronal chains. Macromolecules 41:7993
174. Schmalz H, Schmelz J, Drechsler M, Yuan J, Walther A, Schweimer K, Mihut AM (2008) Thermo-reversible formation of wormlike micelles with a microphase-separated corona from a semicrystalline triblock terpolymer. Macromolecules 41:3235
175. Gröschel AH, Schacher FH, Schmalz H, Borisov OV, Zhulina EB, Walther A, Müller AHE (2012) Precise hierarchical self-assembly of multicompartment micelles. Nat Commun 3:710
176. Kabanov AV, Bronich TK, Kabanov VA, Yu K, Eisenberg A (1996) Soluble stoichiometric complexes from poly(N-ethyl-4-vinylpyridinium) cations and poly(ethylene oxide)-block-polymethacrylate anions. Macromolecules 29:6797
177. Gohy JF, Varshney SK, Antoun S, Jérôme R (2000) Water-soluble complexes formed by sodium poly(4-styrenesulfonate) and a poly(2-vinylpyridinium)-block-poly(ethyleneoxide) copolymer. Macromolecules 33:9298
178. Gohy JF, Varshney SK, Jérôme R (2001) Morphology of water-soluble interpolyelectrolyte complexes formed by poly(2-vinylpyridinium)-block-poly(ethylene oxide) diblocks and poly (4-styrenesulfonate) polyanions. Macromolecules 24:2745

179. Schrage S, Sigel R, Schlaad H (2003) Formation of amphiphilic polyion complex vesicles from mixtures of oppositely charged block ionomers. Macromolecules 36:1417

180. Gohy J-F, Khousakhoun E, Willet N, Varshney SK, Jérôme R (2004) Segregation of coronal chains in micelles formed by supramolecular interactions. Macromol Rapid Commun 25:1536

181. Ruokolainen R, Mäkinen R, Torkelli M, Mäkelä T, Serimaa R, ten Brinke G, Ikkala O (1998) Switching supramolecular polymeric materials with multiple length scales. Science 280:557

182. Kabanov AV, Bronich TK, Kabanov VA, Yu K, Eisenberg A (1998) Spontaneous formation of vesicles from complexes of block ionomers and surfactants. J Am Chem Soc 120:9941

183. Bronich TK, Popov AM, Eisenberg A, Kabanov VA, Kabanov AV (2000) Effects of block length and structure of surfactant on self-assembly and solution behavior of block ionomer complexes. Langmuir 16:481

184. Gohy J-F, Mores S, Varshney SK, Jérôme R (2003) Self-organization of water-soluble complexes of a poly(2-vinylpyridinium)-block-poly(ethylene oxide) diblock with fluorinated anionic surfactants. Macromolecules 36:2579

185. Peng H, Chen D, Jiang M (2003) Self-assembly of perfluorooctanoic acid (PFOA) and PS-b-P4VP in chloroform and the encapsulation of PFOA in the formed aggregates as the nanocrystallites. J Phys Chem B 107:12461

186. Peng H, Chen D, Jiang M (2003) Self-assembly of formic acid/polystyrene-block-poly(4-vinylpyridine) complexes into vesicles in a low-polar organic solvent chloroform. Langmuir 19:10989

187. Hu Z, Jonas AM, Varshney SK, Gohy JF (2005) Dilution-induced spheres-to-vesicles morphological transition in micelles from block copolymer/surfactant complexes. J Am Chem Soc 127:6526

Part IV
Applications

Block Polymers for Self-Assembling: Lithographic Materials

Teruaki Hayakawa

Abstract This chapter reviews the recent progress made in the application of block polymers for self-assembling lithographic materials. It specifically focuses on polyhedral oligomeric silsesquioxane (POSS)-containing block copolymers prepared by living anionic polymerization and their self-assembled nanostructures. Special emphasis is laid on our own research with regard to the control of morphologies and directed self-assembly.

Keywords Block copolymers • Polyhedral oligomeric silsesquioxane (POSS) • Lithography • Thin film • Directed self-assembly (DSA)

1 Introduction

The use of block copolymer (BCP) thin films as a mask to create dense periodic arrays of small features is termed as "BCP lithography." It has inspired the synthesis of a rich array of new BCPs [1–3] to address demanding lithography applications such as magnetic storage and semiconductor devices, and has fueled extensive research into the attainment of long-range ordering, good feature registration, and accurate placement while minimizing the number of defects. BCP self-assembly can be directed by grapho-epitaxy (lithographically predefined templates with topographic relief) [4–11] or chemo-epitaxy (chemically prepatterned substrates) [12–19]. Recent studies have demonstrated that directed self-assembly (DSA) can provide long-range ordering with many times the density and improved feature placement in comparison to the original lithographic templates [4, 16–22]. Additionally, recent reports in which chemo-epitaxy is combined with nanofabrication techniques has shown much more complex patterns such as jogs, bends, junctions, chevrons, dashes, rectangular features, and even three-dimensional structures [23–26].

To use BCPs as lithographic materials, it is essential to understand what kinds of BCP structures are most suitable on the basis of the characteristic properties. BCPs

T. Hayakawa (✉)
Department of Organic and Polymeric Materials, Tokyo Institute of Technology,
2-12-1-S8-36 Ookayama, Meguro-ku, Tokyo 152-8552, Japan
e-mail: hayakawa.t.ac@m.titech.ac.jp

self-assemble via microphase separation to form periodic nanometer-scale structures with sizes in the range 5–100 nm [27–30], with the most commonly observed morphologies being spherical domains in a body-centered lattice, hexagonally packed cylinders, or alternating lamellae. The particular morphology of the self-assembled structure is determined by the relative volume fraction of the constituent blocks. The lattice length parameter of the phase-separated structure depends on the degree of polymerization, N. To assemble, the polymer chains must have sufficient mobility, obtained either by heating them above their glass transition temperature, T_g (thermal annealing), or by plasticizing them with a solvent (solvent annealing). However, both thermal and solvent annealing lower the strength of BCP segregation, defined by the Flory−Huggins interaction parameter, χ, meaning conditions must be tuned to allow sufficient mobility for assembly while still falling below conditions that lead to the order-disorder transition (ODT). Further, when annealing between T_g and ODT, the amount of microphase separation is limited by molecular diffusion. The slow mechanism of diffusion causes the self-assembled phase lattices to form with localized order form into numerous polycrystalline structures with grain boundaries.

A vast majority of research work on BCP lithography has been devoted to polystyrene-*block*-poly(methyl methacrylate) (PS-*b*-PMMA) materials, as the PMMA block is a convenient lithographic photoresist [5, 7, 10–19]. PS-*b*-PMMA can be thermally annealed and selectively removed by UV exposure and the patterns can be transferred to the underlying silicon substrate using the remaining PS template. Other examples of BCPs which have been examined as candidates for nanofabrication include polystyrene-*b*-poly(4-vinylpyridine) (PS-*b*-P4VP) [31], polystyrene-*b*-polylactide (PS-*b*-PLA) [32], and polystyrene-*b*-poly(ethylene oxide) (PS-*b*-PEO) [33].

A limitation of PS-*b*-PMMA is its difficulty in forming features with a full pitch below 25 nm due to its small Flory−Huggins interaction parameter. More strongly segregating BCPs have been reported with ≤10 nm scale features [10, 11, 33–37]. In one report, 10 terabit per square inch ordered cylindrical arrays can be fabricated by the self-assembly of a BCP in which an Au salt is complexed selectively to the PEO domain of a PS-*b*-PEO BCP. The incorporation can increase not only the segregation property of polymer chains, but also etch selectively between the blocks Fe-containing blocks, such as polystyrene-*b*-polyferrocenylsilane (PS-*b*-PFS) have been explored extensively as etch masks [38, 39]. -Silicon-containing BCPs have etching behavior similar to transition metal-containing polymers and are compatible with the integrated circuit processes [40]. Polystyrene-*b*-polydimethylsiloxane (PS-*b*-PDMS) BCPs, which form in-plane cylinders, have been adapted as templates [35]. However, the significantly lower surface tension and lower T_g of the PDMS block in comparison to PS poses challenges for film formation and pattern transfer. The PDMS-containing BCPs also tend to easily dewet from the substrate.

It is highly desirable to explore thin-film nanostructures with morphologies such as vertically oriented lamella or cylinders which have direct connectivity to the

underlying substrate while avoiding dewetting and retaining the high etch selectivity between the two blocks yet retaining the ability to access sub 10 nm feature sizes [41]. We have focused our efforts on polyhedral oligomeric silsesquioxane (POSS) containing BCPs [42–54] that can self-assemble into much smaller periodic feature (10 nm scale) due to the strongly segregating blocks. A high etch contrast advantage over PS and PMMA BCPs can be also obtained with POSS-containing polymers in dry etching with an oxygen plasma. This can lead to reliable high-resolution patterns in BCP lithography.

In this chapter, two aspects of POSS containing BCPs will be addressed. First, the synthesis and characterization of higher order nanostructures in bulk and thin films will be discussed for POSS containing BCPs, including a typical PMMA-b-Poly(POSS methacrylate) material, namely PMMA-b-PMAPOSS. This is followed by a review of PMMA-b-PMAPOSS characteristics for self-assembly nanopatterning with the discussion centering on directed self-assembly (DSA) for long-range ordering and pattern transfer of the nanostructures by applying various external fields.

2 Synthesis of POSS-Containing BCPs

2.1 Living Anionic Polymerization

Living anionic polymerization is a popular approach for the formation of BCPs. The technique was utilized here for POSS block copolymers, starting with PMMA-b-PMAPOSS and PS-b-PMAPOSS [43]. The synthesis scheme is illustrated in Fig. 1.

Both reactions were carried out with a five- to tenfold excess of lithium chloride (LiCl) and a fourfold excess of 1,1-diphenylethylene (DPE), as both methyl methacrylate (MMA) and 3-(3,5,7,9,11,13,15-hepta-isobutyl-pentacyclo[9.5.1.1^{3,9}.1^{5,15}1^{7,13}]octasiloxan-1-yl)propyl methacrylate (MAPOSS) have carbonyl groups. Attempts to polymerize MAPOSS using sec-butyl lithium (sec-BuLi) initiator even at low temperature were unsuccessful and the high reactivity of sec-BuLi resulted in significant side reactions by attacking the carbonyl groups in MAPOSS. It is known that the reactivity of initiators such as BuLi in the living anionic polymerization of methacrylates can be inhibited by using an excess of LiCl and 1,1-diphenylethylene (DPE) [21]. In fact, this approach works quite well for MAPOSS as well. PMAPOSS homopolymers were synthesized by living anionic polymerization using sec-BuLi initiator in the presence of excess LiCl and DPE at −78 °C for 6 h. Quantitative conversions were obtained in 6 h as monitored by ^{1}H NMR spectroscopy. The polydispersity index (PDI) of the resulting polymers was less than 1.1. As expected, the M_n (MALS) was two to three times higher than M_n (SEC). The compact cage structure of PMAPOSS in comparison to PS explains the
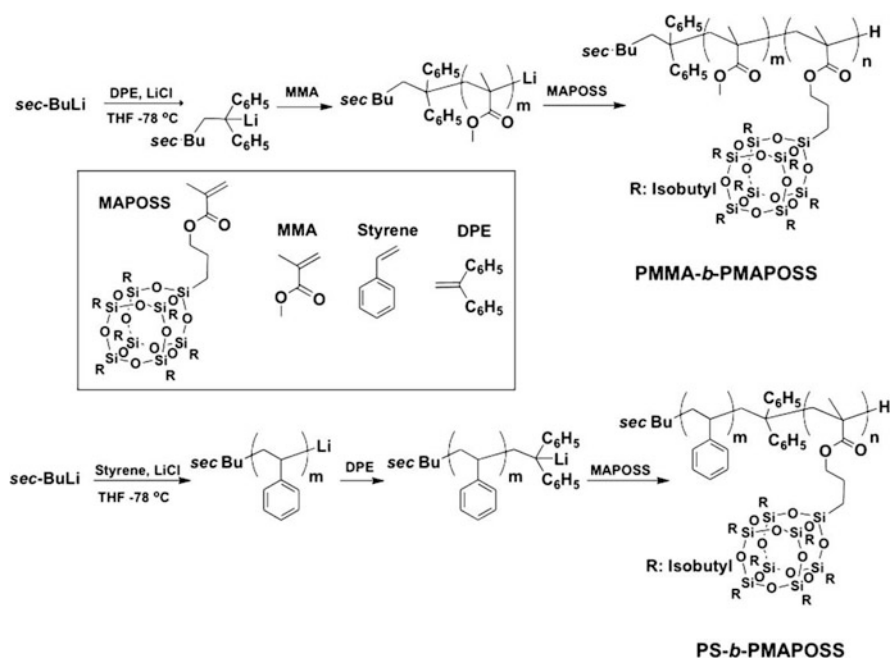
Fig. 1 Synthesis of PMMA-*b*-PMAPOSS and PS-*b*-PMAPOSS block copolymers by living anionic polymerization

higher absolute molecular weights. The degree of polymerization (DP) (determined from M_n (SEC)) for PMAPOSS was as high as 30, which is two times higher than the values reported in the literature for BCPs synthesized by atom transfer radical polymerization (ATRP) [55]. It should be noted that even higher DPs should be possible by the anionic route. The higher DP can be attributed to the very low activation energy for the propagation of the anion, while the activation of the radical can be inhibited by the bulky POSS. Using the optimized conditions, two sets of BCPs, PMMA-*b*-PMAPOSS and PS-*b*-PMAPOSS, were synthesized with varying volume fractions of each block.

The other monomer of the POSS-containing methacrylate can be also polymerized by living anionic polymerization. For the development of POSS-containing thermotropic BCPs, promising materials that effectively form well-ordered nanostructures by thermal annealing, the synthesis of a poly(methacrylate) with a long alkyl chain tethered to the POSS molecule, were desired. PMAC11POSS and PMAC11POSS based BCPs combined with PMMA (PMMA-*b*-PMAC11POSS) were synthesized with almost the same polymerization procedure as used for MAPOSS [49]. The desired PMAC11POSS and its BCPs of PMMA-*b*-PMAC11POSSs were successfully obtained (Fig. 2).
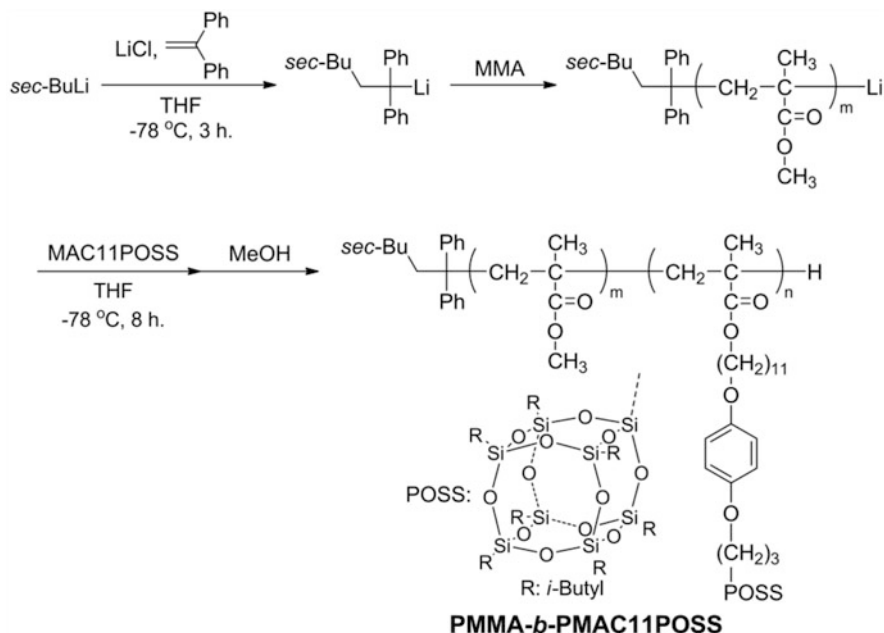
Fig. 2 Synthesis of PMMA-*b*-PMAC11POSSs by living anionic polymerization

2.2 Atom Transfer Radical Polymerization (ATRP)

POSS containing BCPs with a low polydispersity index can also be prepared by ATRP. One example is the synthesis of poly(ethylene oxide)-*b*-PMAPOSS (PEO-*b*-PMAPOSS) [48]. ATRP of POSS methacrylate monomer was carried out in the presence of a PEO macroinitiator ($M_n = 6,300$ g mol^{-1}), copper chloride (I) (Cu^{I}Cl), and *N,N,N',N',N"*-pentamethyldiethylenetriamine (PMDETA) in anhydrous toluene at 50 °C for 24 h (Fig. 3). In this case, the M_n and PDI of PEO-*b*-PMAPOSS against linear PS standards were 18,600 g mol^{-1} and 1.20, with a volume ratio of 11 % of PEO and 89 % of PMAPOSS for each block.

3 Morphologies of BCPs in Bulk and Thin Films

3.1 Bulk Morphology

Bulk morphology characterization is essential to study the formation of nanostructures in thin films. The density of PMAPOSS was measured using a density gradient column [47] and was found to be 1.14 g/cm^3 at 25 °C. Taking the density of polystyrene to be 1.05 g/cm^3 and PMMA to be 1.15 g/cm [3], in
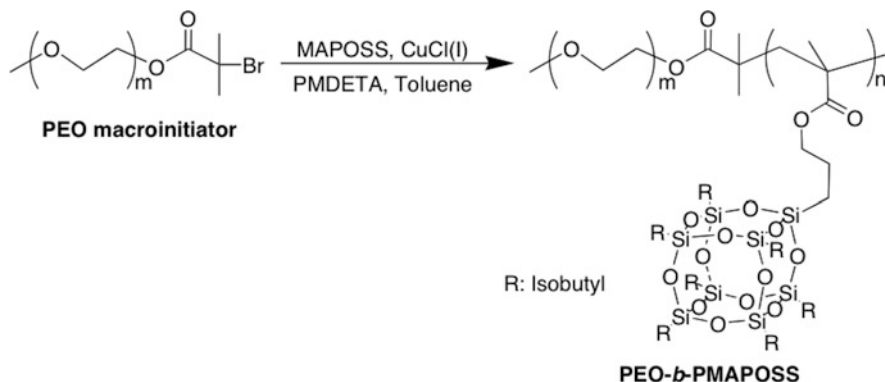
Fig. 3 Scheme for the synthesis of PEO-*b*-PMAPOSS by atom transfer radical polymerization

combination with ^{1}H NMR data, the volume ratios for each block was determined. Bulk samples of the POSS-containing BCPs can be prepared by slow evaporation from solutions in a variety of solvents, such as chloroform, toluene, cyclohexane, and tetrahydrofuran. They can be characterized by transmission electron microscopy (TEM) and transmission small angle X-ray scattering (TSAXS). In the TEM measurements, all the samples are imaged without staining because the high mass contrast of the POSS-containing block compared to PS and PMMA blocks results in PMAPOSS domains appearing as darker regions with either PS or PMMA domains appearing as brighter regions.

Figure 4 shows the TEM images and TSAXS results of some of the PMMA-*b*-PMAPOSS (Fig. 4a–f) and PS-*b*-PMAPOSS (Fig. 4g–l) BCPs [47]. For instance, the TEM images of PMMA$_{450}$-*b*-PMAPOSS$_7$ and PS$_{587}$-*b*-PMAPOSS$_4$ with a PMAPOSS volume fraction of 13 and 4 %, respectively, show spherical PMAPOSS morphologies (Fig. 4a, g). The scattering profile of the PMMA$_{450}$-*b*-PMAPOSS$_7$ sample shows a first-order diffraction peak and a broad second-order diffraction peak (Fig. 4d), while that of the PS$_{587}$-*b*-PMAPOSS$_4$ sample reveals only a broad first-order diffraction peak (Fig. 4j). From the TEM and TSAXS data, the spheres are estimated to have an average diameter of 10 nm and a mean interdistance of 24 nm for the PMMA$_{450}$-*b*-PMAPOSS$_7$ sample, and an average diameter of 6 nm and a mean interdistance of 14 nm for the PS$_{587}$-*b*-PMAPOSS$_4$ sample. These results show that while PMMA$_{450}$-*b*-PMAPOSS$_7$ and PS$_{587}$-*b*-PMAPOSS$_4$ can phase separate into PMAPOSS spheres with a diameter of 6–10 nm, they lack long-range order. In contrast, well-defined lamellar structures were observed in the case of PMMA$_{262}$-*b*-PMAPOSS$_{23}$ and PS$_{266}$-*b*-PMAPOSS$_{20}$ with PMAPOSS volume fractions of 44 and 37 %, respectively (Fig. 4b, h). The scattering profiles show up to fourth-order diffraction peaks with a characteristic ratio of 1:2:3:4, which can be assigned to the (001), (002), (003), and (004) planes, indicating lamellar morphologies (Fig. 4e, k). The lamellar *d*-spacing was 38.7 and 37.3 nm for PMMA$_{262}$-*b*-PMAPOSS$_{23}$ and PS$_{266}$-*b*-PMAPOSS$_{20}$, respectively, which is in a good agreement with the values observed in the TEM. In the case of PMMA$_{52}$-*b*-
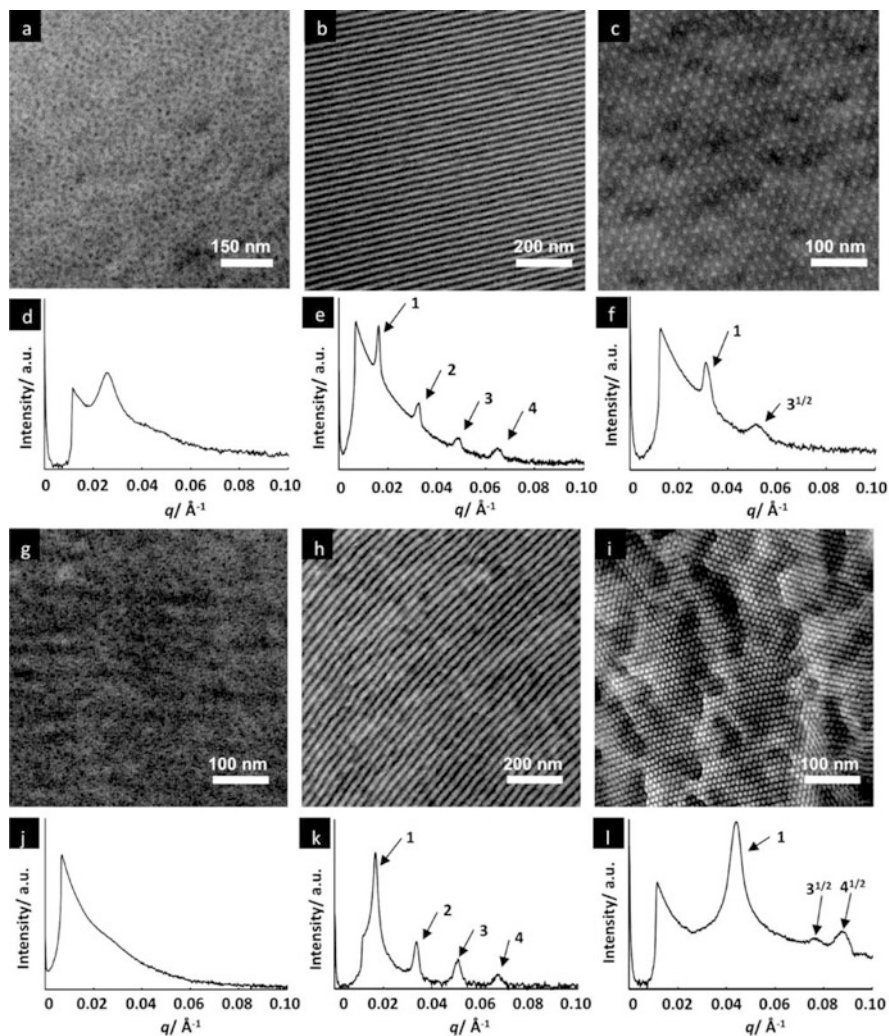
Fig. 4 TEM and TSAXS profiles of (**a, d**) $PMMA_{450}$-b-$PMAPOSS_7$, (**b, e**) $PMMA_{262}$-b-$PMAPOSS_{23}$, (**c, f**) $PMMA_{52}$-b-$PMAPOSS_{18}$, (**g, j**) PS_{587}-b-$PMAPOSS_4$, (**h, k**) PS_{266}-b-$PMAPOSS_{20}$, and (**i, l**) PS_{52}-b-$PMAPOSS_9$

$PMAPOSS_{18}$ and PS_{52}-b-$PMAPOSS_9$ with PMAPOSS volume fractions of 77 and 58 %, respectively (Fig. 4c, i), cylindrical morphology was observed. The TEM images show a hexagonally packed PS or PMMA cylinder structure in a PMAPOSS matrix. These results are supported by X-ray observations, which show diffraction peaks with a ratio of $1:\sqrt{3}$ for $PMMA_{52}$-b-$PMAPOSS_{18}$ and $1:\sqrt{3}$ and $1:2$ for the PS_{52}-b-$PMAPOSS_9$ sample (Fig. 4f, l), which is characteristic of a cylindrical morphology. These peaks are assigned as the diffractions of the (001), (011), and (002) planes, respectively. The distance between the cylinders was found to be 20.4

and 14.3 nm for PMMA$_{52}$-b-PMAPOSS$_{18}$ and PS$_{52}$-b-PMAPOSS$_9$, respectively. The diameter of the cylinders was found to be 9.1 nm for PMMA$_{52}$-b-PMAPOSS$_{18}$ and 9.5 nm for PS$_{52}$-b-PMAPOSS$_9$.

Lamella (PMMA$_{262}$-b-PMAPOSS$_{23}$ and PS$_{266}$-b-PMAPOSS$_{20}$) and cylinder (PMMA$_{52}$-b-PMAPOSS$_{18}$ and PS$_{52}$-b-PMAPOSS$_9$) forming bulk samples were annealed at 190 °C for 24 h to examine any morphological changes [47]. TWAXS studies were carried out to see if the POSS cages were organized within the phase-separated structure. The unannealed PMMA$_{52}$-b-PMAPOSS$_{18}$ sample showed a weak diffraction peak in the high q region, corresponding to a d-spacing of 2.6–2.7 nm, whereas for PS$_{52}$-b-PMAPOSS$_9$, this peak is not visible. Upon annealing the PMMA$_{52}$-b-PMAPOSS$_{18}$ sample, diffraction peaks corresponding to a d-spacing of 5.0, 2.5, and 2.3 nm emerged, indicating the aggregation of POSS units within the majority domain in the cylinder forming BCP. Thermal annealing did not result in additional diffraction peaks in the case of the PS$_{52}$-b-PMAPOSS$_9$ BCP in the scattering profile, suggesting that the short length of the PMAPOSS block was insufficient to drive the formation of hierarchical structures. Similar results indicating aggregation of POSS units within a phase-separated domain were observed upon annealing both PMMA$_{262}$-b-PMAPOSS$_{23}$ and PS$_{267}$-b-PMAPOSS$_{20}$ lamellar morphologies.

3.2   Thin Film Morphology

Based on the knowledge of the bulk morphologies of the PMAPOSS-containing BCPs, thin films of PMMA-b-PMAPOSS were spin cast on Si substrates from dilute solutions of either cyclohexane or chloroform. The film thickness was controlled by the concentration of the solutions and the spinning speed. In order to assemble, the polymer chains must have obtained sufficient mobility, which can be achieved either by heating above their T_g (thermal annealing), or by being plasticizing with a solvent (solvent annealing). Herein, we describe the thermal annealing and solvent annealing of PMMA-b-PMAPOSSs.

3.2.1   Solvent Annealing

In general, achieving long-range order with some highly desirable BCP materials by thermal annealing is not possible because the T_g exceeds the thermal degradation temperature of the BCP. In such cases, solvent annealing offers an attractive alternative to thermal annealing to order the BCP. In this technique, the solvent vapors dissolve in the BCP and acts as a plasticizer. The swollen polymer chains attain sufficient mobility to order at temperatures well below their degradation temperature (commonly at room temperature). Solvent annealing can be applied to most types of self-assembling BCPs, opening many opportunities to extend directed self-assembly feature below 10 nm. Furthermore, by controlling the degree of
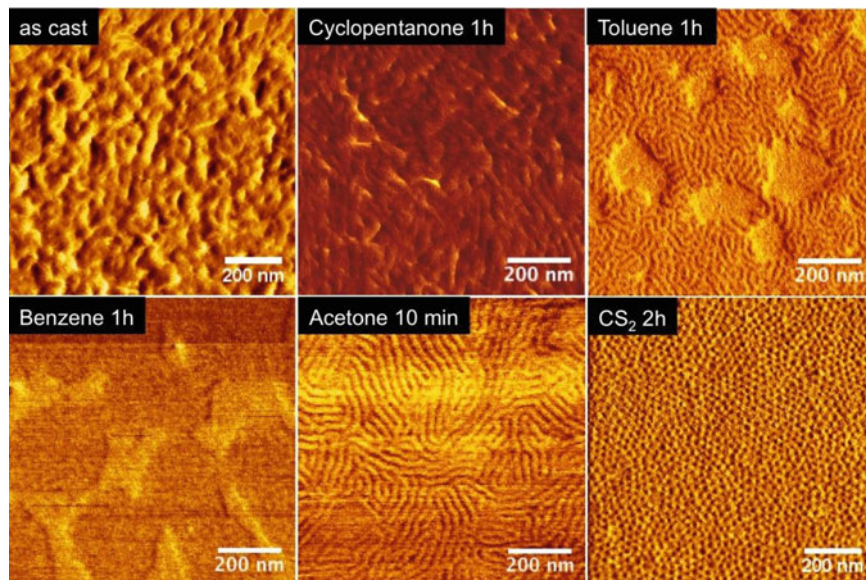
Fig. 5 AFM images of nanostructures in solvent annealed thin films of PMMA$_{52}$-*b*-PMAisobutylPOSS$_{18}$ obtained with different kinds of solvents

swelling of each block, it is possible to reversibly tune the microdomain morphology (i.e., from spherical to cylindrical morphology and vice versa) through order−order transitions [34, 35, 56, 57]. In a solvent annealing process, the following steps occur. First, the as-spun BCP thin film is exposed to solvent vapor. Solvent vapor infiltrates into the BCP and swells the film, creating more free volume in the structure and a different conformational structure for the polymer chains, depending on the solubility. In the swollen state, the BCP molecules have the mobility to form the self-assembled patterns [58, 59]. After the solvent evaporates, the BCP molecules become frozen in the ordered structure. The morphology of the ordered structure depends on the solubility of the solvent vapor in the polymer blocks and on the degree of swelling during annealing. In fact, the morphologies of BCPs, such as polystyrene-*b*-polydimethylsiloxane and poly(α-methylstyrene)-*b*-poly(4-vinylpyridine), have been engineered into a wide range of structures by controlling the amount and mixture of the solvent vapors [34, 56]. Bosworth et al. [60] reported that the self-assembled structure of poly(α-methylstyrene)-*b*-poly(4-vinylpyridine) ordered by solvent annealing can multiply the areal density of the chemically patterned template with a hexagonal array.

For POSS-containing BCPs, we first investigated suitable solvents for PMMA-*b*-PMAPOSSs. We found that carbon disulfide (CS$_2$) and acetone are the most effective solvents to trigger the swelling of PMAPOSS and PMMA, respectively [44] (Fig. 5). Figure 6 illustrates the solvent annealing apparatus to expose the spin-cast films to CS$_2$ vapor [53]. The concentration (or partial pressure) of CS$_2$ vapor can be controlled indirectly with the nitrogen counterflow in a sealed stainless steel
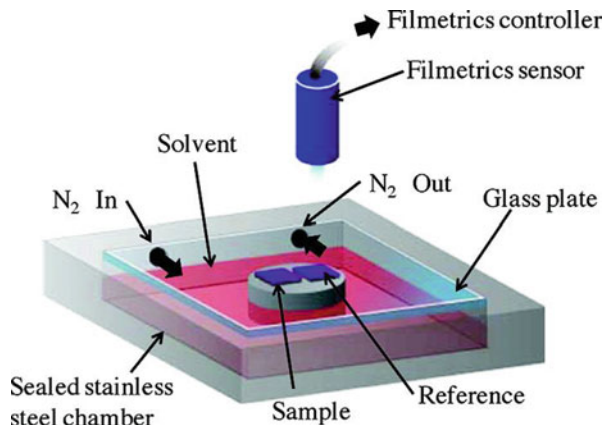
chamber. The degree of swelling (or swelling factor) of the PMMA-*b*-PMAPOSS film, t_{DS}, is defined as the thickness of the reference sample in the swollen state divided by the initial film thickness.

We first focused on the effect of the degree of swelling of the BCP on the self-assembled structures during solvent annealing and observed the microdomain structures of the quenched films [53].

Figure 7 shows the SEM images of the thin films of $PMMA_{41}$-*b*-$PMAPOSS_{29}$ after solvent evaporation. The dark and bright parts of the SEM images correspond to the PMMA and the PMAPOSS domains, respectively. The as-spun film shown in Fig. 7a did not exhibit a regular structure, although we can distinguish the PMMA domains from the PMAPOSS domains. The rapid evaporation of solvent during the spin-coating of the BCP did not allow sufficient molecular mobility for the complete microphase separation of $PMMA_{41}$-*b*-$PMAPOSS_{29}$. In Fig. 7b, line structures of the PMMA domains were observed in the films annealed with $t_{DS} = 125$ %. Figure 7c shows the coexistence of line and dot structures of the PMMA domains after solvent annealing with $t_{DS} = 150$ %. The film annealed with $t_{DS} = 175$ % shown in Fig. 7d exhibited only the dot structures, where the dots formed hexagonal lattices in the polycrystalline structure. Figure 7e illustrates a two-dimensional fast Fourier transform (2D-FFT) [53] image of the hexagonally packed dot structure shown in Fig. 7d. The 2D-FFT image exhibits isotropic halos with some spots. From the radius of the circular average of the intensity profile of the first halo in the 2D-FFT image, the lattice spacing of the self-assembled $PMMA_{41}$-*b*-$PMAPOSS_{29}$ structure, d_0, is calculated to be 23.7 nm. The average radial distribution of the intensity was fitted to a Gaussian function.

A morphology change could be explained by a change in the relative volume fraction of the constituent blocks of the BCP in the swollen state. Since the BCP comprises of two immiscible chains, we would expect the solvent molecules to have different affinities for the microdomains with the different blocks [56]. To investigate the relative solubility of the PMMA and PMAPOSS blocks with CS_2, we evaluated the swelling behaviors of the single component films of hPMMA and
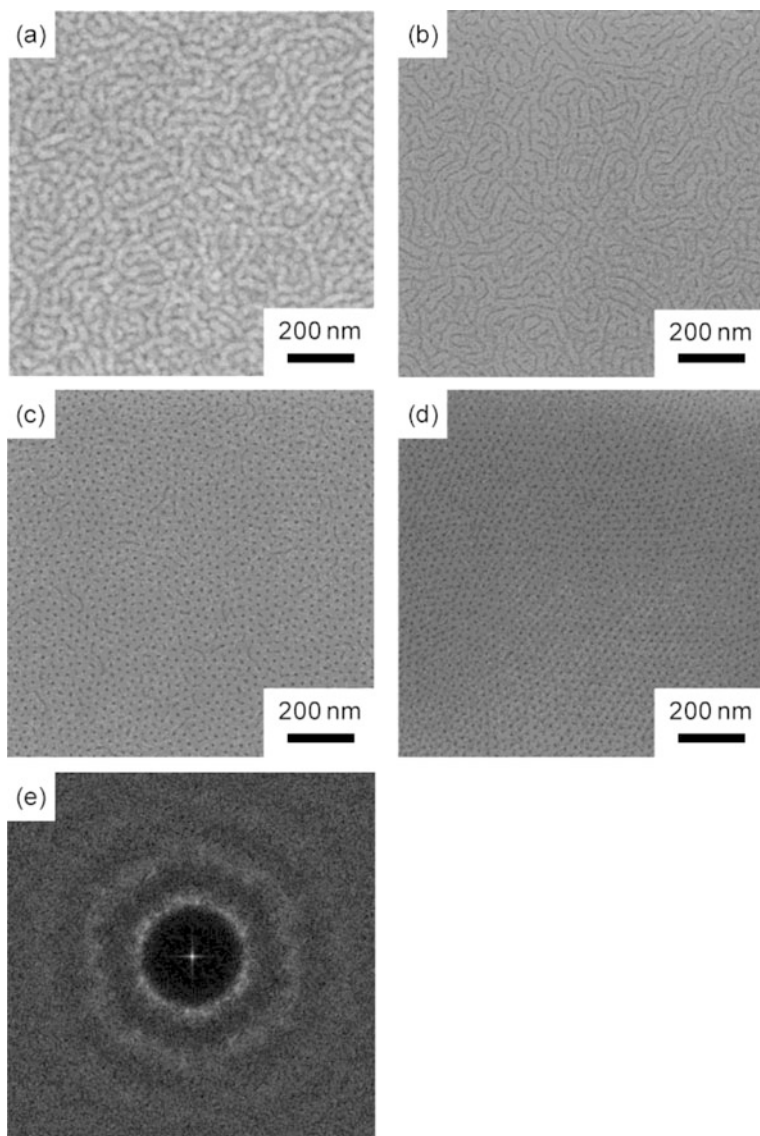
Fig. 7 SEM images of the PMMA$_{41}$-b-PMAPOSS$_{29}$ films on Si substrates. (**a**) As-spun film. (**b**–**d**) Solvent annealed films. The films were solvent annealed under CS$_2$ vapor for 1 h at t$_{DS}$ of (**b**) 125 %, (**c**) 150 %, and (**d**) 175 %. (**e**) The 2D-FFT image of the SEM image (**c**). The dark and bright parts of the SEM images correspond to the PMMA and PMAPOSS domains, respectively

hPMAPOSS (Fig. 8). The hPMMA and hPMAPOSS films spun on the Si substrates was exposed to CS$_2$ vapor with the N$_2$ counter flow adjusted to 20 mL/min and the t$_{DS}$ was measured as a function of time until the value became constant. Under this counter flow, the t$_{DS}$ was 123 % for hPMMA and 139 % for hPMAPOSS. This
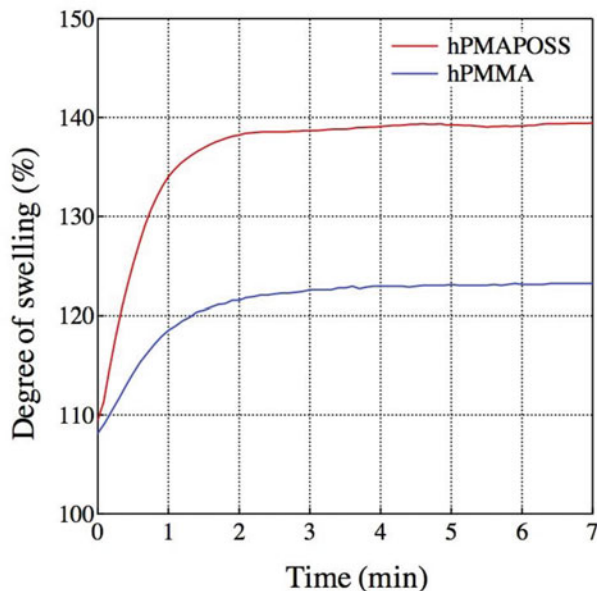
Fig. 8 Comparison of the degree of swelling of homoPMMA (hPMMA) and homoPMAPOSS (hPMAPOSS) films under a constant N_2 counterflow and therefore, under a constant CS_2 vapor pressure

suggests that CS_2 is slightly selective to PMAPOSS. Thus, preferential partitioning of CS_2 into the PMAPOSS domains is expected in the solvent annealing of the PMMA-b-PMAPOSS films. We propose that solvent annealing induces a change in the effective volume fractions of the two constituent blocks and can change the microdomain morphology from cylinders to spheres in this case.

We can further explain the morphologies in terms of the surface energies. Figure 9a shows the schematic of the solvent annealing process and the possible cross-sectional structure of the PMMA-b-PMAPOSS film at each stage. At the as-spun stage, PMMA-b-PMAPOSS is mostly in the disordered state, although there may be slightly phase-separated regions. In the swollen stage, the solvent-swollen PMMA-b-PMAPOSS chains gain the mobility to diffuse and undergo microphase separation to form the self-assembled structure in thermodynamic equilibrium. If t_{DS} is large enough to induce the order−order transition, the morphology of the PMMA domains might change from cylinders to spheres. Since the surface tension of PMMA against the Si surface is smaller than that of PMAPOSS [50], a thin wetting layer of PMMA may be formed next to the Si surface. In contrast, the CS_2 vapor at the surface of the film has preference to PMAPOSS. Upon solvent evaporation after solvent annealing, the PMMA-b-PMAPOSS film may decrease in thickness, while the lateral size of the film remains unchanged. Therefore, the shape of the PMMA domains in the dried film may not be spherical but ellipsoidal. This expectation was confirmed by TEM observations
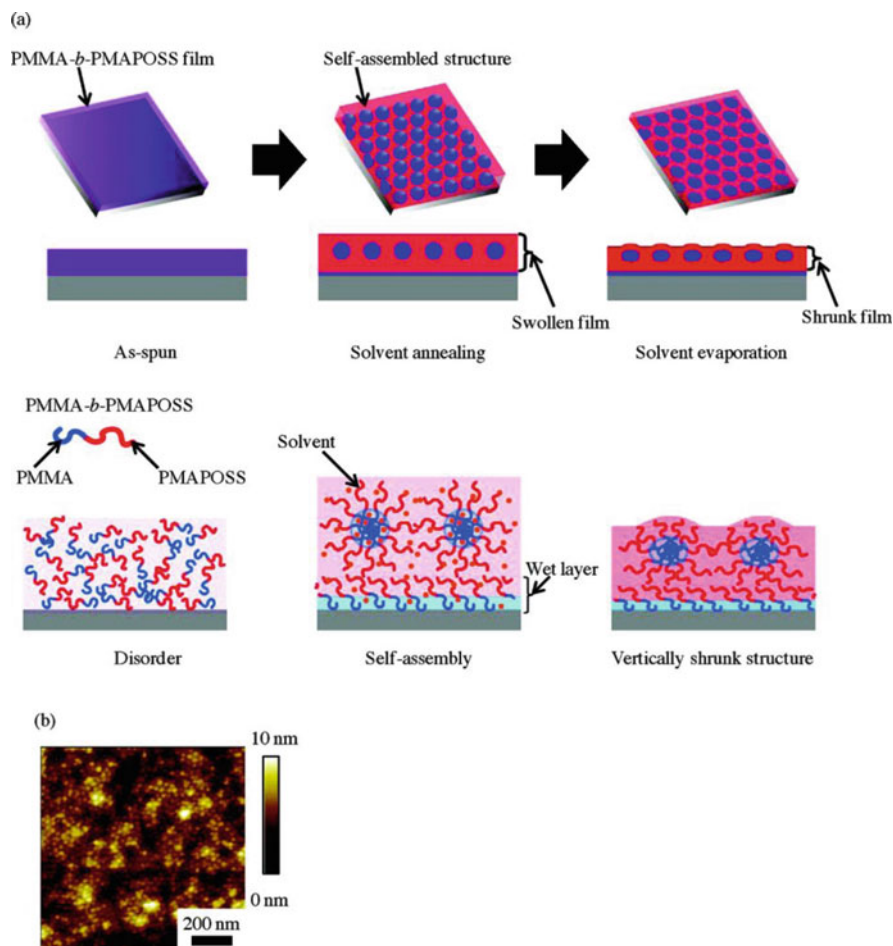
Fig. 9 (**a**) Schematic illustrations of the solvent annealing process and the possible cross-sectional structures obtained at each stage of the process. The *red* and *blue* chains represent the PMAPOSS and PMMA chains, respectively. *Orange dots* represent the CS_2 solvent molecules. (**b**) AFM topographic image of the PMMA$_{41}$-*b*-PMAPOSS$_{29}$ film solvent annealed at $t_{DS} = 185$ % for 1 h on the Si substrate

of the cross-sectional images of the dried film. Figure 9b shows the atomic force microscope (AFM) height image of a thin film of PMMA$_{41}$-*b*-PMAPOSS$_{29}$ solvent annealed at $t_{DS} = 185$ %. The hexagonally packed bright dots of the PMMA domains were observed under topographical contrast and the dots were found to be 2–3 nm thicker than the PMAPOSS matrix. This suggests that the degree of shrinkage of the PMMA domains is less than that of the PMAPOSS matrix, which is consistent with the higher solubility of CS_2 in PMAPOSS.

We further examined the CS_2 solvent annealing behavior of other molecular weight PMMA-*b*-PMAPOSS materials. Figure 10 shows the SEM images of the
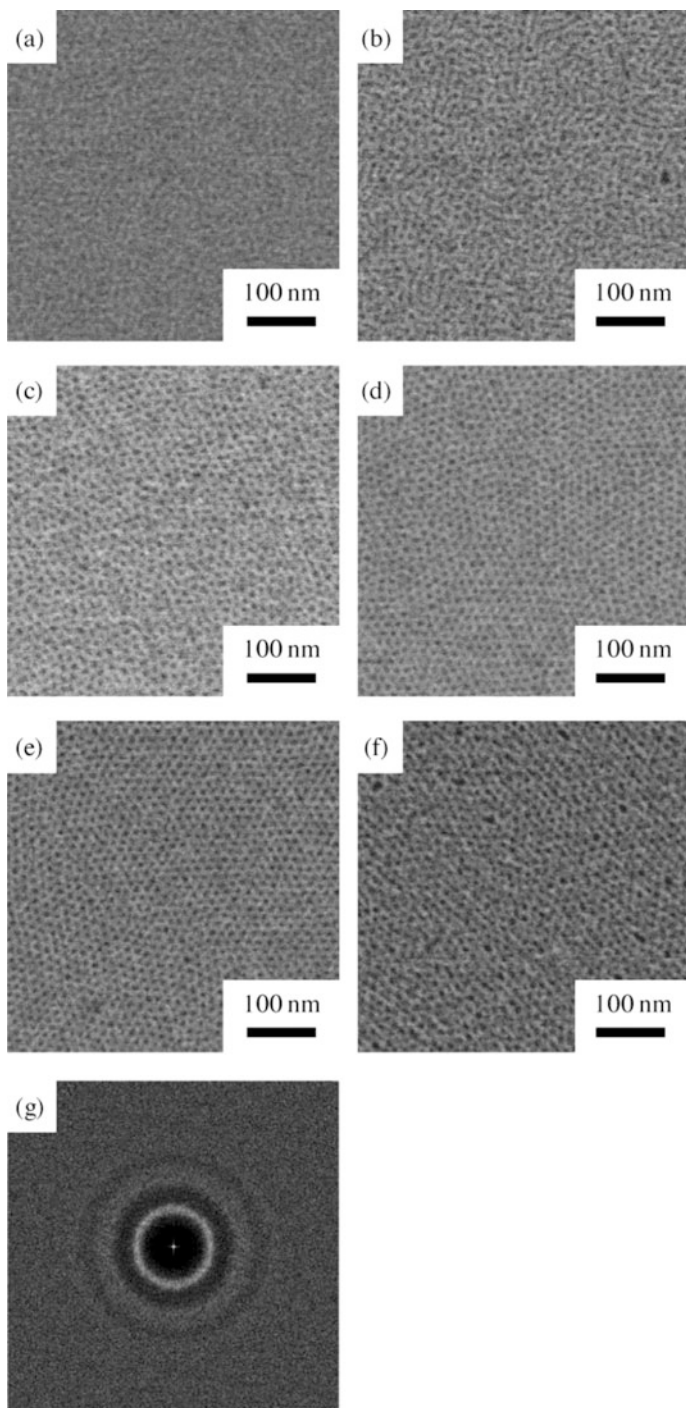
Fig. 10 SEM images of the $PMMA_{25}$-b-$PMAPOSS_{13}$ films. (**a**) As-spun film. (**b**–**f**) Solvent annealed films. The films were solvent annealed on Si substrates at t_{DS} of (**b**) 120 %, (**c**) 130 %, (**d**) 140 %, (**e**) 150 %, and (**f**) 175 %. (**g**) The 2D-FFT image of the SEM image (**d**). The *dark* and *bright* parts of the SEM images correspond to the PMMA and PMAPOSS domains, respectively

15 nm thick as-spun films of PMMA$_{25}$-b-PMAPOSS$_{13}$ solvent annealed for 1 h under different swelling factors. As expected and as shown in Fig. 10a, the as-spun film did not exhibit a periodic structure. Figure 10b shows the coexistence of line and dot structures of the PMMA domains when the swelling factor was $t_{DS} = 120$ % during annealing. The line structures are derived from the cylindrical PMMA microdomains oriented parallel to the Si substrate. The dot structures are probably the spherical PMMA microdomains. When $t_{DS} = 130$ %, the PMMA domains exhibited a disordered dot structure, as shown in Fig. 10c. This suggests that with $t_{DS} = 130$ %, the PMMA-b-PMAPOSS chains do not gain sufficient mobility to form a single hexagonal lattice. However, when $t_{DS} = 140$ and 150 %, a regular hexagonal array of dots formed, as shown in Fig. 10d, e. From the position of the first-order halo observed in the 2D-FFT image of Fig. 10g, obtained from the SEM image shown in Fig. 10d, the d_0 of the self-assembled structure of PMMA$_{25}$-b-PMAPOSS$_{13}$ at $t_{DS} = 140$ % was determined to be 12.4 nm. Similarly, d_0 at $t_{DS} = 150$ % was calculated to be 12.7 nm. Conversely, t_{DS} increased to 175 %, the hexagonally packed dot pattern did not exhibit the extent of order observed in the samples annealed with $t_{DS} = 140$ and 150 %, as shown in Fig. 10f. According to Lodge et al. [61], swelling of cylinder forming BCP systems with a neutral solvent lowers the effective Flory−Huggins interaction parameter of the copolymers. In addition, greater swelling of one component of the BCP with a slightly greater affinity for the solvent can increase the volume fraction of the corresponding microdomains in the swollen state. CS$_2$ is slightly more selective toward PMAPOSS than PMMA and the solvent annealing can increase $\varphi_{PMAPOSS}$ and decrease χ in the swollen state [43].

The effects of solvent annealing can be described with the schematic phase diagram of the microdomain morphology in the $\chi_{eff}N$ vs. $\varphi_{PMAPOSS,eff}$ space, as shown in Fig. 11, where χ_{eff}, N, and $\varphi_{PMAPOSS,eff}$ are the effective Flory−Huggins interaction parameter in the swollen state, the degree of polymerization, and the effective volume fraction of the PMAPOSS blocks in the swollen state, respectively [56, 61, 62]. The morphological change with increasing t_{DS} can be recognized as a diagonal shift in the phase diagram along the solid arrow in Fig. 11. Therefore, the morphology of the PMMA domains changes from cylindrical to spherical with increase in t_{DS}. Furthermore, the phase-separated structure may become unstable and the long-range order may worsen when solvent annealing is carried out at t_{DS} >175 % because of the transition from the spherical microdomain morphology to the disordered state. This case is represented by a further diagonal shift on the dashed line in the phase diagram. Our results show that the optimum t_{DS} required to form a well-defined hexagonally packed dot pattern with PMMA$_{25}$-b-PMAPOSS$_{13}$ ranges of 140 and 150 %.

Similarly, we investigated the effect of t_{DS} on the self-assembled structures of PMMA$_{34}$-b-PMAPOSS$_{18}$ and PMMA$_{27}$-b-PMAPOSS$_{14}$ with $\varphi_{PMAPOSS}$ values 83 and 84 %, respectively, which are similar to the $\varphi_{PMAPOSS}$ values of PMMA$_{41}$-b-PMAPOSS$_{29}$ and PMMA$_{25}$-b-PMAPOSS$_{13}$.

The results are summarized in Fig. 12, which presents the phase diagram of the self-assembled structures of the solvent annealed PMMA-b-PMAPOSS. The open
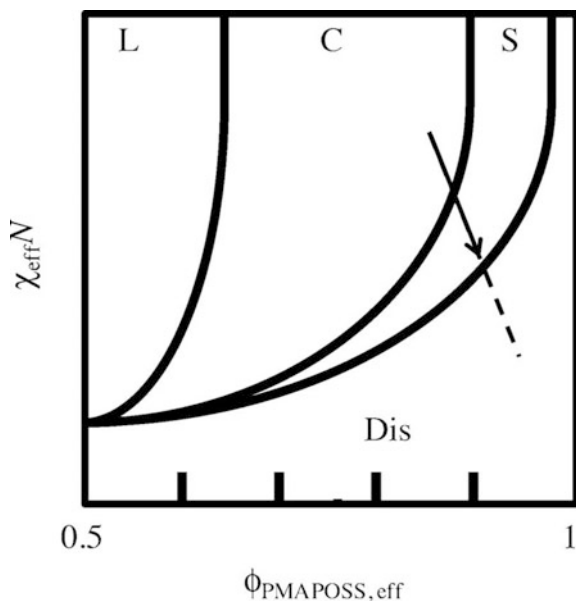
Fig. 11 Right half of the schematic phase diagram of $\chi_{eff}N$ vs. $\varphi_{PMAPOSS,eff}$ for the PMMA-*b*-PMAPOSS/CS$_2$ system. PMMA is the minor component and forms the dispersed domains in the cylindrical (*C*) and spherical (*S*) morphologies. The $\chi_{eff}N$ value of the BCP decreases with the infiltration of the solvent into the film. Since CS$_2$ swells the PMAPOSS matrix more than the PMMA domains, the effective volume fraction of PMAPOSS, $\varphi_{PMAPOSS,eff}$ increases on swelling. The phase behavior of the BCP with increasing t_{DS} on solvent annealing is represented by the *solid arrow*, which predicts the morphological transition from cylinders to spheres upon swelling. The *dashed line* predicts the order-disorder transition at excess t_{DS}. The behavior of the BCP with a higher M_n on solvent annealing is represented by the *dotted arrow*, which is obtained by the vertical shift of the *solid arrow*

circles and diamonds denote the spherical and cylindrical morphologies, respectively, while the open triangles indicate the coexistence of the spheres and cylinders. Figure 12 shows that the phase boundary for the cylinder-to-sphere transition shifts toward the higher values of t_{DS} with increase in the M_n of PMMA-*b*-PMAPOSS. This can be understood qualitatively in terms of $\chi_{eff}N$ and $\varphi_{PMAPOSS,eff}$ in the swollen state using Fig. 11. As t_{DS} increases upon swelling on exposure to CS$_2$, χ_{eff} decreases, while $\varphi_{PMAPOSS,eff}$ increases because of the higher affinity of CS$_2$ for PMAPOSS. This eventually induces the transition of morphology from cylinders to spheres, as represented by the arrow in Fig. 11 for the PMMA-*b*-PMAPOSS with a smaller M_n. On the other hand, an increase in the M_n of PMMA-b-PMAPOSS increases the $\chi_{eff}N$ and prompts the backward shift along the arrow. Thus, a larger t_{DS}, which further reduces the χ_{eff} value, is necessary for the PMMA-*b*-PMAPOSS with a larger M_n, to undergo the morphological transition from cylinders to spheres. Consequently, the phase boundary for the cylinder-to-sphere transition shifts toward higher values of t_{DS} with increase in the M_n of PMMA-b-
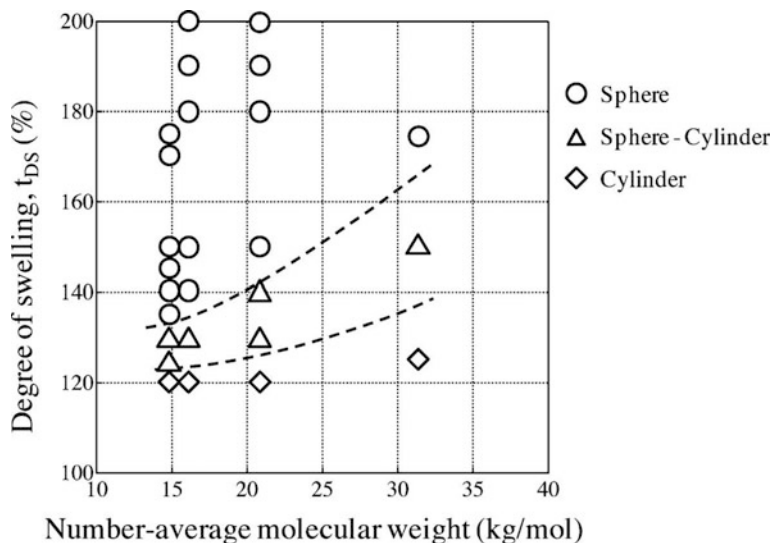
Fig. 12 Phase diagram showing the morphologies of PMMA-*b*-PMAPOSS assembled via solvent annealing with CS$_2$ vapor as a function of t_{DS} and the number average molecular weight of PMMA-*b*-PMAPOSS. The volume fraction of PMAPOSS in the PMMA-*b*-PMAPOSS samples, $\varphi_{PMAPOSS}$, was in the range 83−87 %. *Open circles*, *triangles*, and *diamonds* represent spherical, mixtures of spherical and cylindrical, and cylindrical morphologies of the PMMA domains, respectively

PMAPOSS, as shown in Fig. 12. The discussion given above is qualitative; it suggests that we need to optimize the degree of swelling in solvent annealing to obtain the desired hexagonally packed dot pattern depending on the M_n of the PMMA-*b*-PMAPOSS.

3.2.2 Thermal Annealing

Since thermal annealing leads to a second level of ordering within the PMAPOSS domain, we further examined the self-assembly in thin films by grazing incident wide-angle X-ray scattering (GIWAXS) and AFM [45]. GIWAXS is known to provide a high intensity scattering pattern with high statistical significance even for nanoscale thin films supported on substrates. The thin films were annealed in CS$_2$ for 10 h, followed by thermal annealing at 190 °C for 6 h under vacuum.

The AFM phase images clearly showed hexagonally packed PMMA domains in the thin films in both thermally unannealed (Fig. 13a) and thermally annealed samples (Fig. 13b). The GIWAXS pattern of the unannealed sample (Fig. 13c) showed three amorphous hollow rings at $2\theta_f = 3.20°$ (2.5 nm), 7.88° (1.0 nm), and 16.10° (0.49 nm) which was attributed to an average distance between the main chains of PMAPOSS (Fig. 13f), the average distance between the POSS cages in the PMAPOSS block (Fig. 13e), and the average distance between the -COOCH$_3$
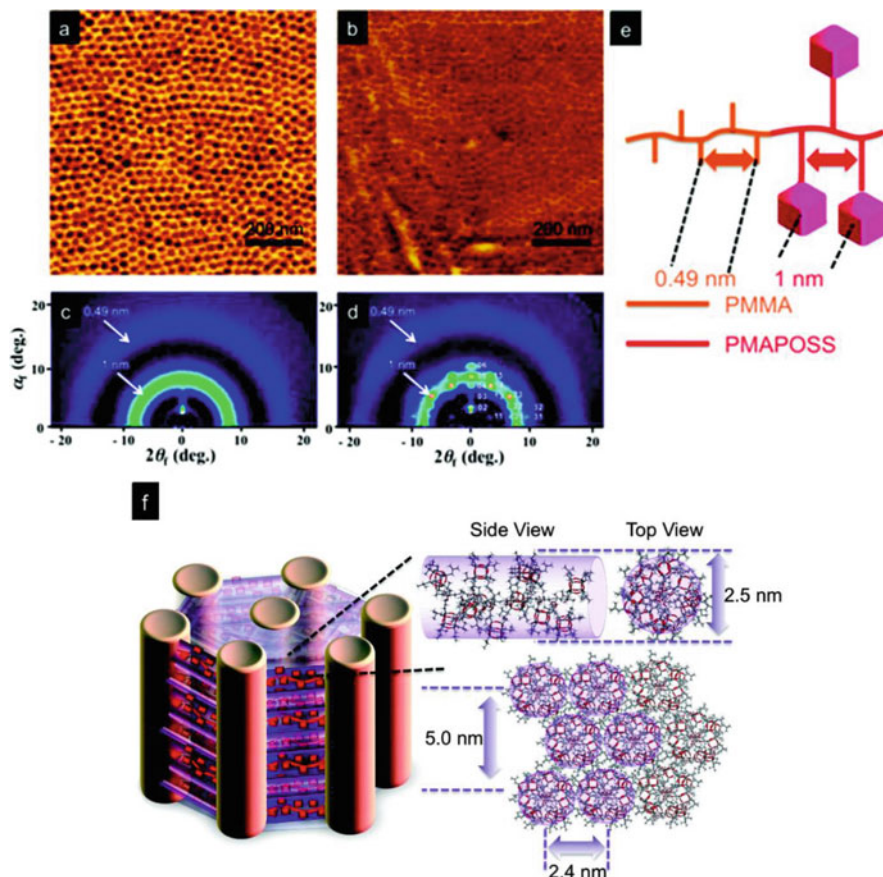
Fig. 13 AFM phase images and 2D GIWAXS patterns of PMMA$_{41}$-*b*-PMAPOSS$_{29}$ subjected to (**a**, **c**) CS$_2$ solvent annealing for 10 h and (**b**, **d**) thermal annealing at 190 °C for 6 h after solvent annealing. (**e**) Schematic illustration of the relevant length scales in PMMA-*b*-PMAPOSS BCP and (**f**) representation of the morphology of thermally annealed PMMA$_{41}$-*b*-PMAPOSS$_{29}$ consisting of PMMA cylinders in a PMAPOSS matrix, where the PMAPOSS segments assume a helix-like structure and the helices are further arranged in an orthorhombic lattice structure

groups of the PMMA segments, respectively (Fig. 13e). Since these are amorphous hollow rings, there is no net orientation within the PMAPOSS segments. However, after thermal annealing, a number of sharp and regular scattering spots (Fig. 13d) appear over a wide range of scattering angles that are characteristic of a lattice structure. By indexing the scattering spots in the 2D GIWAXS pattern (Fig. 13d), the lattice structure was determined to be an orthorhombic unit cell with dimensions of 2.4 and 5.0 nm on the *y*- and *z*-axes directions, respectively. Figure 13f is a cartoon representation of the lattice structure of the PMAPOSS block as simulated by the Cerius [2] software package. In thin films, the PMAPOSS block formed a helix-like structure to relieve the steric crowding of the POSS units. In the thermally

unannealed sample, these helix-like structures were randomly oriented; however, upon thermal annealing, POSS aggregation drove the helical units to pack into an orthorhombic lattice. Upon annealing, the average distance between the PMMA cylinders changed from 32 to 27 nm (measured by AFM) and the size of the PMMA cylinder changes from 15 to 11 nm because of POSS aggregation. These results in thin films were consistent with the observations in the bulk sample where the appearance of diffraction peaks at 5.0 and 2.3 nm upon annealing showed the formation of an orthorhombic unit cell by the aggregation of POSS units. The diffraction peak at 2.5 nm was a higher order peak of the peak at 5.0 nm.

3.2.3 Rapid and Reversible Morphology Changes by Solvent and Thermal Annealing

By a combination of thermal annealing and solvent annealing, the reversible morphology control of the other POSS-containing BCP thin films was demonstrated. This control is enabled by distinctive properties of poly(ethylene oxide)-*b*-PMAPOSS (PEO-*b*-PMAPOSS) [48]. Each PS and PMMA in POSS containing BCPs, which are hydrocarbon polymer segments, exists in the amorphous state over a wide range of temperatures during thermal annealing. In contrast, crystalline PEO usually melts at relatively low temperatures, below ~60 °C. Therefore, when PEO is used, rather than PS and PMMA, in the POSS-containing BCP, the higher mobility of the PEO at isotropic state leads to sufficient diffusing and reassembling of the POSS-containing BCP for the formation of self-assembled nanostructures by thermal annealing.

As example sample was PEO_{143}-*b*-$PMAPOSS_{12}$ [48]. Thin films were prepared by spin casting from a 1 wt% of a PEO_{143}-*b*-$PMAPOSS_{12}$ solution in chloroform onto silicon wafers. The thickness of the film was well controlled and found to be around 40 nm by ellipsometry. As-spun films did not exhibit a regular structure, but coexisting line and dot disordered structures were formed (Fig. 14a). The line structures are derived from the cylindrical PEO microdomains oriented parallel to the substrate. The dot structures were probably the spherical PEO microdomains. Thermal annealing of the as-spun film was carried out at 90 °C for 60 s. Shown in Fig. 14b, only dot structures of the PEO domains within the PMAPOSS matrix were observed in the film, where the dots formed hexagonal lattices in the polycrystalline structure. Next, solvent annealing of the resulting film with dot nanostructures was performed with chloroform vapor for 120 s. As shown in Fig. 14c, line nanostructures were formed. Thermal annealing, once more at 90 °C for 60 s, changed the nanostructures from lines to dots again (Fig. 14d).

A morphology change could be explained by a change in the relative volume fraction of the constituent blocks of the BCP at each annealing state. For the as-spun film, rapid evaporation of the casting solvent during spin casting does not allow sufficient mobility of the polymer chains of PEO_{143}-*b*-$PMAPOSS_{12}$ to lead to microphase separation into well-ordered nanostructures in thermodynamic equilibrium. Thermal annealing at 90 °C, above the melting temperature of the PEO block
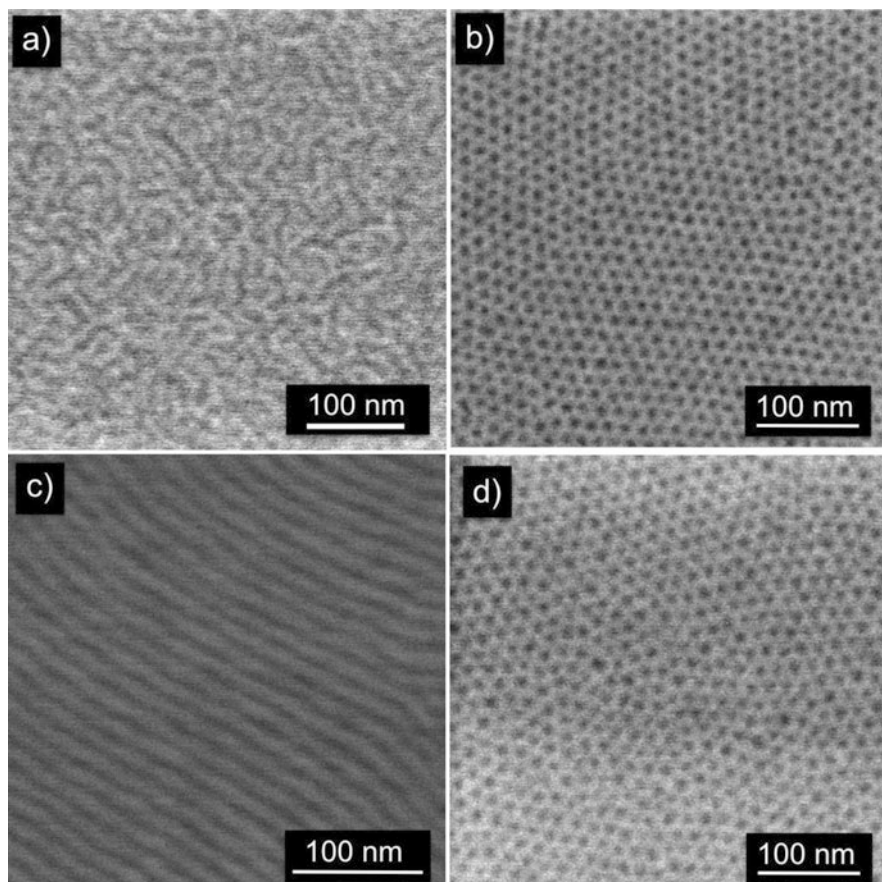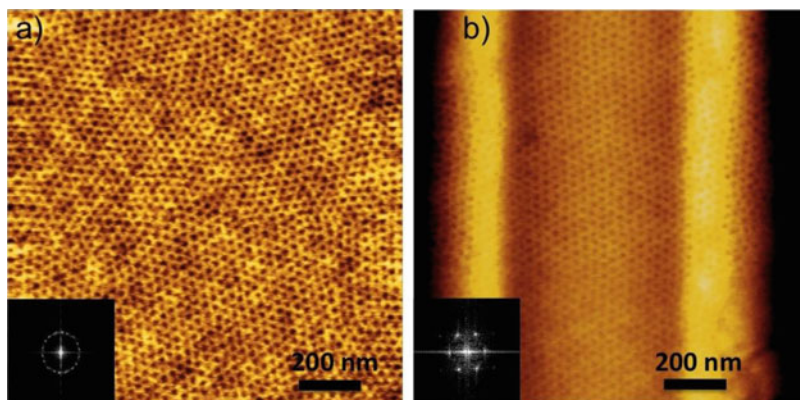
Fig. 14 SEM images of PEO$_{143}$-b-PMAPOSS$_{12}$ thin films. SEM image of the (**a**) as-spun cast film, (**b**) film thermally annealed at 90 °C for 60 s, (**c**) film subjected to solvent annealing with chloroform vapor for 120 s, and (**d**) film obtained after additional thermal annealing of the film shown in (**c**) at 90 °C for 60 s

(50 °C) and the glass transition temperature of the PMAPOSS block (82 °C), induces the formation of hexagonally packed dot nanostructures. The volume fraction of the corresponding PEO microdomains in the as-spun film might decrease with the removal of a very small amount of remaining casting solvent, with reassembly of the polymer chains to metastable structures, which possess relatively larger free volume, by thermal annealing. In the melt state, the isotropic PEO chains play a significant role in reassembly. Neither PS-b-PMAPOSS nor PMMA-b-PMAPOSS allows effective reassembly of morphologies by thermal annealing. This is because the appropriate annealing temperatures exceed the thermal degradation temperature of the BCPs. Thus, at those annealing temperatures, the BCPs are in the amorphous state and the mobility of the polymer chains is insufficient for reassembly in relatively short times. On the other hand, in solvent annealing, the

chloroform vapor dissolves in the PEO_{143}-b-$PMAPOSS_{12}$ and acts as a plasticizer. Since the BCP comprises two immiscible chains, the solvent molecule of chloroform has different affinities in each microdomain. To investigate the relative solubility of chloroform in the PEO and PMAPOSS block chains, we evaluated the swelling behaviors of the homopolymers of PEO and PMAPOSS. A thin film of each homopolymers on a silicon wafer was exposed to chloroform vapor, and the degree of swelling was measured in situ, with the annealing time determined by measuring the film thicknesses. Under this annealing condition, almost no change in the degree of swelling was found for 40 s with both PEO and PMAPOSS films. After 45 s, abrupt swelling in the PEO film was observed, while slight swelling occurred in the PMAPOSS. The degree of swelling for the PEO film to chloroform vapor was ca. 180 % at 55 s. After 120 s, the thickness of PEO film increased from 202 to 522 nm, and the degree of swelling was 258 %. In contrast, the degree of swelling in the PMAPOSS film was 134 %. This result suggests that chloroform was selective to PEO. Thus, preferential partitioning of chloroform into the PEO domains was expected in the solvent annealing of the PEO_{143}-b-$PMAPOSS_{12}$ thin films. We proposed that the solvent annealing induced a change in the effective volume fractions of the two constituent blocks and changed the microdomain morphology from spheres to cylinders in this case. The resulting cylinders in the film changed spherical microdomains again by thermal annealing at 90 s. No change was observed in the sizes of the dots and the interdistance between before and after this annealing cycle. The diameters of dots were the same in 12 nm before and after the annealing. The center-to-center interdistances of dots slightly changed from 18 to 20 nm. The thicknesses of films with microdomains of dots, then lines, and then dots again, were 45 nm, 46 nm, and 45 nm, respectively. These results indicated that the PEO-b-PMAPOSS chains gained the mobility to diffuse and undergo microphase separation to form the self-assembled nanostructure in thermodynamic equilibrium at appropriate annealed stages. The remarkable rapid morphology change in several tens of seconds in this study might have been caused by the high mobility of PEO-b-PMAPOSS chains at the melt state and swollen state and the unique abrupt swelling behavior of PEO at the early stage in the solvent annealing.

Based on the remarkable rapid reassembly of PEO_{143}-b-$PMAPOSS_{12}$, we attempted to prepare well-ordered nanostructures in thin films by only spin casting without further annealing [48]. As PEO was easily swollen by chloroform vapor in less than 60 s, we prepared the PEO_{143}-b-$PMAPOSS_{12}$ thin films by simultaneously spin casting and solvent annealing with chloroform vapor in the spin-coat chamber. First, the PEO_{143}-b-$PMAPOSS_{12}$ solution in chloroform was placed on a silicon wafer and the wafer rotated at 4,000 rpm for 90 s after closing the lid. Before beginning the rotation, a small amount of chloroform, about 30 ml, was spread around the rotating pedestal. Figure 15a shows the AFM phase image of the spin-casted thin film of PEO_{143}-b-$PMAPOSS_{12}$ under these conditions. The as-spun film exhibited only a periodic dot nanostructure, composed of the spherical domains of PEO within the PMAPOSS matrix. In the previous section, the thin film annealed with chloroform vapor showed the formation of line nanostructures. In the solvent

Fig. 15 AFM phase images of PEO$_{143}$-b-PMAPOSS$_{12}$ thin films prepared by spin casting under chloroform vapor for 90 s (**a**) on a flat Si substrate and (**b**) on a trench-patterned Si substrate with a 50-nm-deep and 500-nm-wide groove

vapor conditions employed presently, the slight swelling did not induce a change in the volume fraction required for formation of the PEO cylinders; however, the swollen PEO$_{143}$-b-PMAPOSS$_{12}$ chains were able to gain the mobility necessary to diffuse and undergo microphase separation to form the dot nanostructures. A slight amount of chloroform vapor in the chamber could have prevented the rapid evaporation of solvent during film formation, leading to sufficient time for formation of regular dot nanostructures via microphase separation.

The self-assembly of this block copolymer was also investigated using grapho-epitaxy. A trench-patterned silicon wafer was used with a 50 nm deep groove with a width of 500 nm. As shown in Fig. 15b, a well-defined hexagonally packed dot pattern with PEO$_{143}$-b-PMAPOSS$_{12}$ was obtained under the same film preparation conditions as described previously. Without any further annealing, PEO$_{143}$-b-PMAPOSS$_{12}$ formed a regular array of dots in the thin film. The fast Fourier transformed (FFT) images in Fig. 15 (insets) indicate that a trench-patterned silicon wafer effectively aligned the dot pattern of PEO$_{143}$-b-PMAPOSS$_{12}$ nanostructures.

4   Directed Self-Assembly (DSA)

Advances in directed self-assembly (DSA) of BCP thin films are quickly positioning self-assembly as a next-generation lithographic technique. The self-assembled phase lattices usually form into numerous grain boundary separated polycrystalline type structures with localized order. This is because the amount of microphase separation is limited by molecular diffusion when annealing is carried out between T_g and order-disorder transition (ODT). To overcome this issue, DSA approaches such as grapho-epitaxy and chemo-epitaxy for BCPs have proven to be powerful techniques. It has been reported that DSA can allow the formation of long-range
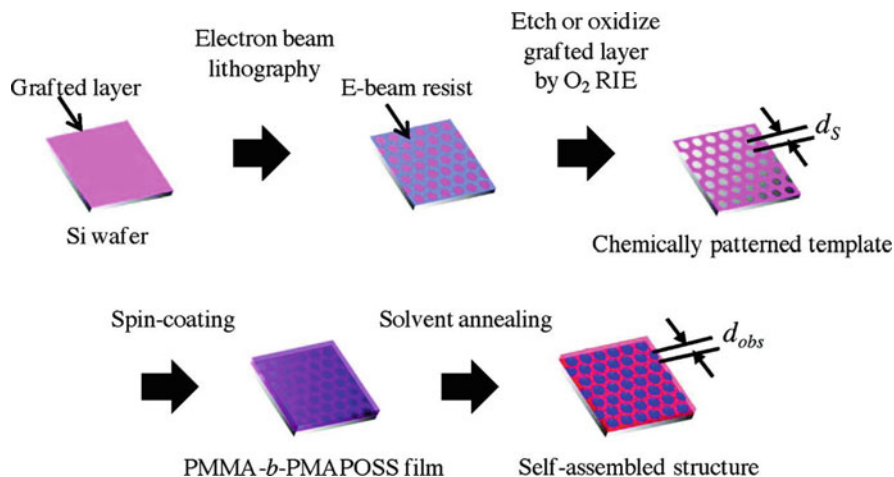
Fig. 16 Schematic illustration of the directed self-assembly process with a chemically patterned template

ordering, with higher densities and improved feature placement compared to the original lithographic templates.

In the previous section, we studied the optimized solvent-annealing conditions to prepare well-defined highly ordered arrays of dots of PMMA-*b*-PMAPOSS BCPs on Si substrates. We now consider directing the self-assembly process during the solvent annealing with chemo-epitaxy. Figure 16 shows a schematic illustration of the DSA process of PMMA-*b*-PMAPOSS, which results in PMMA spheres in PMAPOSS matrix, on a chemically patterned template [53]. The template with a chemical contrast was composed of a hexagonal array of circular dots preferentially wetted by PMMA surrounded by a background matrix with higher affinity for PMAPOSS. The lattice spacing, the distance between adjacent planes, is denoted as d_s, while the lattice constant, the distance between nearest neighbors, is represented as L_s. The patterned template contained an array of etched dots with a surface affinity for the PMMA component of the BCP. The surrounding matrix of the unetched surface favored the PMAPOSS component of the BCP.

The geometric components of the e-beam lithography defined the chemically patterned templates with regard to d_s and L_s. To evaluate the pattern quality of the chemically patterned templates, we evaluated the PMMA e-beam resist patterns on the PS brush after development. The surface of the PMMA e-beam resist was sputter coated with about 1 nm thick layer of Pt prior to SEM observations. Figure 17 shows the SEM images of the resist layer. The dark and bright parts of the SEM images correspond to the patterned holes in the PMMA e-beam resist layer and the remaining PMMA resist layer, respectively. As shown in Fig. 17, there were several defects in the patterns with $d_s = 23$ nm (Fig. 17a), while there were almost no defects in the patterns with $d_s = 24$, 26, and 28 nm (Fig. 17 b–d, respectively). The summary of the characteristics of the observed patterns is shown in Fig. 17. The
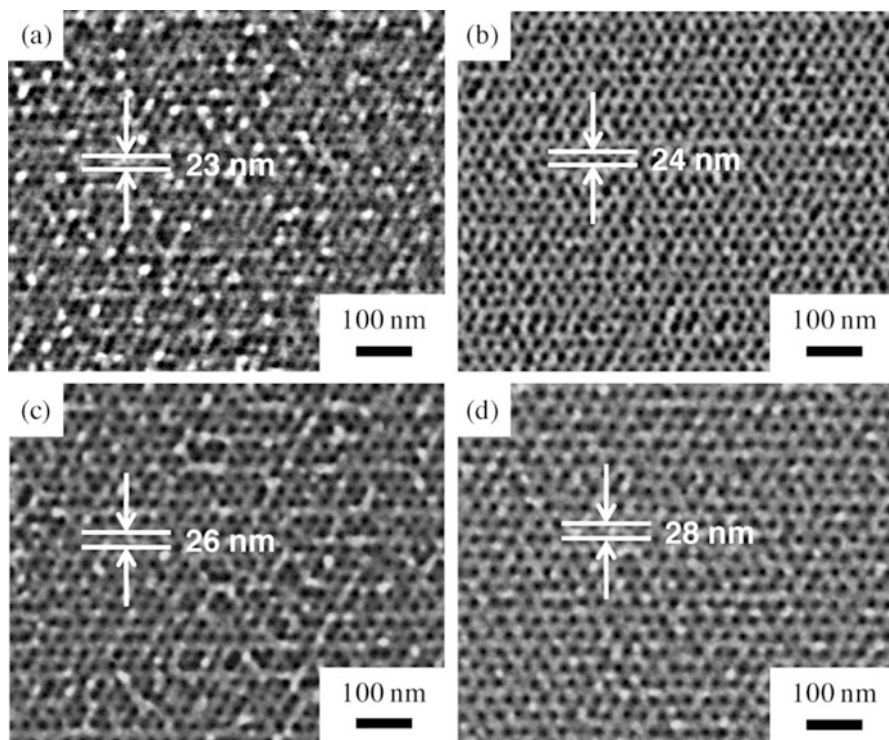
Fig. 17 SEM images of the PMMA e-beam resist layer formed by e-beam lithography, which was employed to prepare the chemically patterned substrates. The resist pattern was etched with oxygen plasma required to change the chemistry of the substrate. (**a**) $ds = 23$ nm, (**b**) $ds = 24$ nm, (**c**) $ds = 26$ nm, and (**d**) $ds = 28$ nm

average lattice spacing of the patterns, as measured by SEM, is denoted as d_{eb} and its standard deviation is denoted as σ_{eb}. The method employed to evaluate d_{eb} and σ_{eb} has been described in a previous study [18]. The d_{eb} values nearly agreed with the designed values, d_s. The pattern with $d_s = 23$ nm showed the largest σ_{eb} value of 3.4 nm, but the σ_{eb} values of the other patterns were less than 3 nm.

We investigated the effect of solvent annealing on the chemo-epitaxy of thin films of PMMA-b-PMAPOSS on chemically patterned templates of grafted PS-OH on Si substrates. For example, thin films of PMMA$_{41}$-b-PMAPOSS$_{29}$ with $d_0 = 23.7$ nm were spin-coated onto chemically patterned substrates and solvent annealed for 3 h. The solvent annealing was performed with $t_{DS} = 185$ % so that PMMA$_{41}$-b-PMAPOSS$_{29}$ self-assembled into a well-defined hexagonal array of dots. The thickness of the PMMA$_{41}$-b-PMAPOSS$_{29}$ film was optimized to 12 nm to prevent the spherical PMMA domains from forming double layers upon swelling. At $t_{DS} = 185$ %, the thickness of the film was expected to increase because of swelling from 12 to 22 nm, which was nearly equal to the d_0 value inherent to PMMA$_{41}$-b-PMAPOSS$_{29}$.
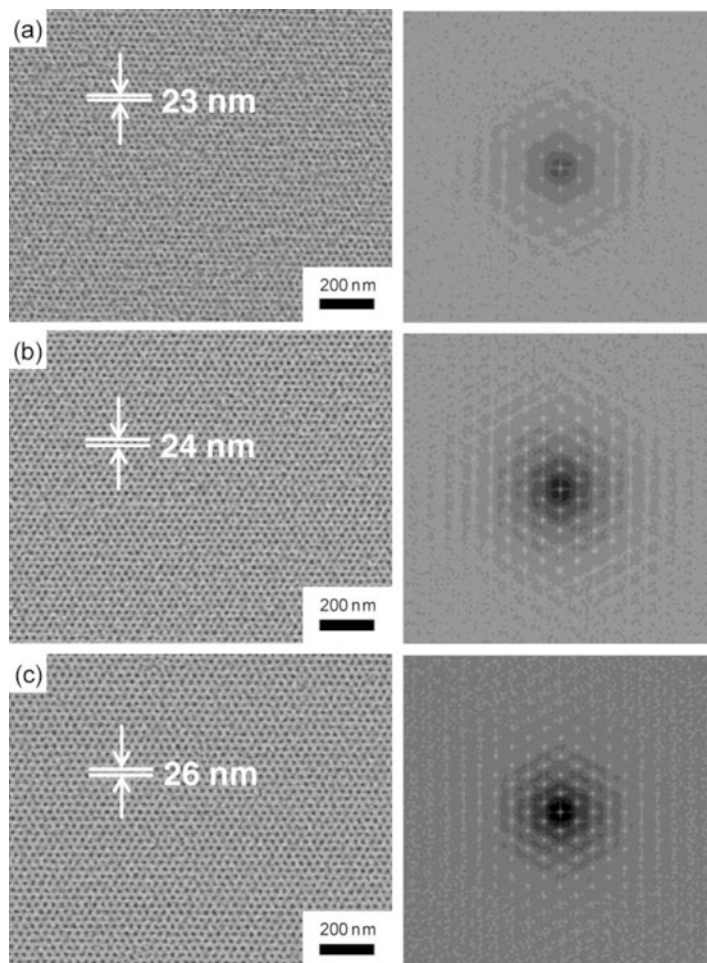
Fig. 18 SEM images and the corresponding 2D-FFT images of the PMMA41-*b*-PMAPOSS29 thin films solvent annealed on the chemically patterned templates composed of the PS-OH grafted layer. (**a**) ds = 23 nm, (**b**) ds = 24 nm, and (**c**) ds = 26 nm. The film thickness is 12 nm

Figure 18 shows that chemical epitaxial direction can be achieved with the sphere forming BCP solvent annealing conditions [53]. The SEM image and the corresponding 2D-FFT image of a thin film of PMMA$_{41}$-*b*-PMAPOSS$_{29}$ self-assembled on the chemically patterned template with $d_s = 23$ nm is shown in Fig. 18a. The self-assembled structure on the template with $d_s = 23$ nm resulted in a single hexagonal lattice with almost no point defects, in contrast to the relatively poor quality of the chemically patterned template shown in Fig. 18a. The 2D-FFT image exhibits only spots, as expected from the single hexagonal lattice, with the peaks to at least the fifth order. The lattice spacing of the self-assembled structure on the template, denoted as d_{obs}, calculated from the 2D-FFT

image was 23.2 nm, the same as that of the underlying template, $d_s = 23$ nm. This result demonstrated that with appropriate solvent annealing conditions, PMMA-*b*-PMAPOSS, like thermally annealed PS-*b*-PMMA [18], can self-assemble to form a well-oriented hexagonal lattice pattern with long-range order along the chemically patterned template and rectify the defects of the chemically patterned template.

In Fig. 18b, c, we examined the effect of lattice mismatch of the chemically patterned template on the quality of the self-assembled structure. Single hexagonal lattices were observed on the templates with $d_s = 24$ and 26 nm, which were both slightly larger than the d_0 (=23.7 nm) of $PMMA_{41}$-*b*-$PMAPOSS_{29}$. The corresponding 2D-FFT images exhibited only spots, with the peaks at least to the sixth order. The d_{obs} values of the self-assembled structures for parts b and c of Fig. 18 were 24.3 and 26.5 nm, respectively, which agreed with the d_s values of the template patterns. This suggested that the lattice spacing d_{obs} of the self-assembled structures can be stretched to match the d_s of the underlying templates by at least up to 12 % ($d_{obs}/d_0 = 26.5/23.7 = 1.12$) larger than d_0. This finding implied some extended flexibility in the chemically patterned template design.

Xiao et al. [20] proposed that the spherical microdomains of a BCP formed on chemically patterned templates could be spherical, hemispherical, or disk-like, depending on the relative size of the patterned features with respect to the inherent size of the BCP spherical domains. We also believe that the morphology of the spherical microdomains on the patterned template might have been deformed by the favorable interaction between the PMMA blocks and the Si substrate of the patterned template. However, confirming such a hypothesis requires a direct observation of the cross sections of the BCP thin films by SEM or TEM, which is beyond the scope of this chapter.

The limit of the commensurability may be determined by two competing thermodynamic factors, (a) the interfacial free energy reduction by lattice matching between the BCP microdomains and the template patterns and (b) the conformational entropy loss accompanying the stretching or shrinking of chains stretch to achieve the template lattice spacing.

Next, we examined the use of a PMAPOSS-OH chemically patterned template for the ordering of a thin film of $PMMA_{41}$-*b*-$PMAPOSS_{29}$ with solvent annealing, again with a chemical pattern pitch of 23, 24, and 26 nm [53]. The samples were solvent annealed under $t_{DS} = 185$ % for 3 h. Figure 19 shows the SEM images and the corresponding 2D-FFT images of the self-assembled structures on the templates prepared with the PMAPOSS-grafted surface. Ordering on the $d_s = 23$ nm template pattern shown in Fig. 19a resulted in mixed results. The lattices of some grains of the BCP self-assembled structure matched with that of the underlying template with $d_s = 23$ nm, while large dark regions were also observed, which differed from the observations made in the case of the PS-grafted template. The 2D-FFT image presented in Fig. 19a exhibited a spot and a halo pattern. Better results were obtained from the chemically patterned template patterns with $d_s = 24$ and 26 nm. Single, well-ordered hexagonal lattices were observed, as shown in Fig. 19b, c. The accompanying 2D-FFT images exhibited only spots with peaks up to fourth order. Thus, well-ordered self-assembled structures formed on chemically patterned
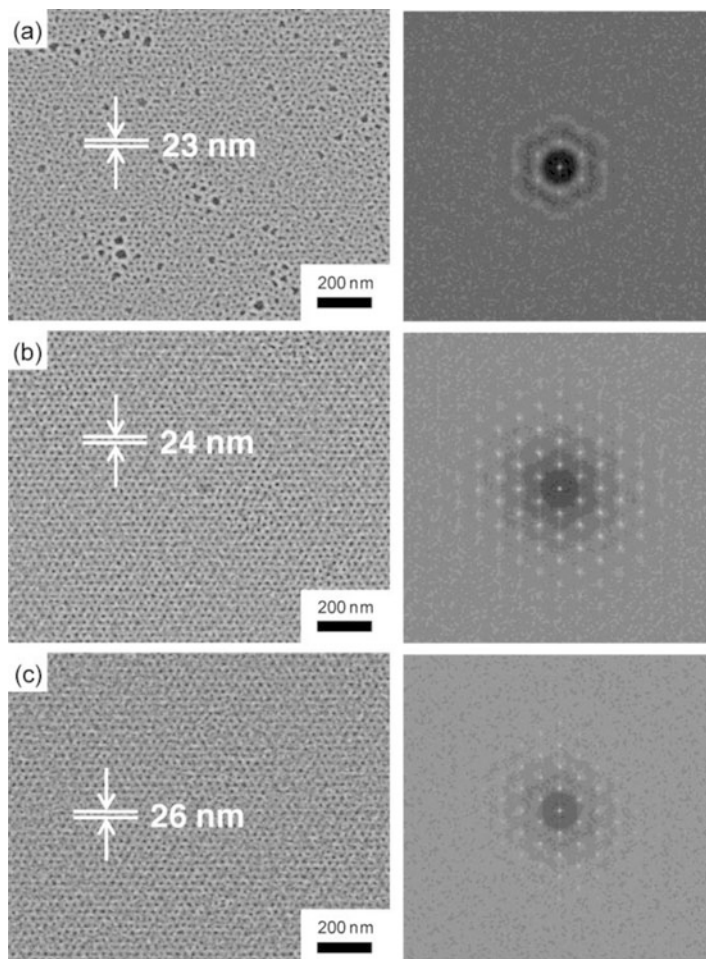
Fig. 19 SEM images and the corresponding 2D-FFT images of the PMMA41-*b*-PMAPOSS29 thin films solvent annealed on the chemically patterned templates composed of the PMAPOSS-OH grafted layer. (**a**) $d_s = 23$ nm, (**b**) $d_s = 24$ nm, and (**c**) $d_s = 26$ nm. The film thickness is 12 nm

templates of PMAPOSS-OH patterned with $d_s = 24$ and 26 nm were observed. However, the $d_s = 23$ nm lattice clearly formed more readily on the chemically patterned PS-OH template than on the chemically patterned PMAPOSS-OH template. The interfacial energy between the PMMA component of the BCP and the PS grafted surface is less than that of the PMAPOSS-grafted surface. The lower chemical contrast of the PS surface could explain the wider latitude in lattice spacing on the PS grafted surface. These results implied that the template prepared by patterning the PS-grafted layer is more suitable for the DSA of PMMA-*b*-PMAPOSS as compared to that fabricated by employing the substrate with the PMAPOSS-grafted layer. However, for a thorough understanding of the effect,

studies on the dependences on M_n and/or grafting density of the grafted polymer are required.

The primary motivation behind the use DSA of BCP is to enhance the achievable lithographic resolution. With the use of lower molecular weight BCPs, we examined the ability to multiply the density of the lithographic chemical pattern arrays. We examined the DSA of PMMA$_{25}$-b-PMAPOSS$_{13}$ with $d_0 = 12.4$ nm on the chemically patterned PS-OH templates with $d_s = 26$ nm by solvent annealing with CS$_2$. PMMA$_{25}$-b-PMAPOSS$_{13}$ films of 9 nm in thickness were annealed under CS$_2$ vapor with $t_{DS} = 130$, 140, and 150 %. In the swollen state, the film thicknesses were expected to be about 12, 13, and 14 nm at $t_{DS} = 130$, 140, and 150 %, respectively, which nearly correspond to the d_0 of the PMMA$_{25}$-b-PMAPOSS$_{13}$ BCP.

Figure 20a–c presents the SEM images and the corresponding 2D-FFT images of the thin films of PMMA$_{25}$-b-PMAPOSS$_{13}$ solvent annealed on chemically patterned TEM plates with $d_s = 26$ nm $\approx 2d_0$ at $t_{DS} = 130$, 140, and 150 %, respectively. Figure 20a shows the film annealed at $t_{DS} = 130$ %. Here, the PMMA$_{25}$-b-PMAPOSS$_{13}$ self-assembled to form a dot structure of PMMA, but the accompanying 2D-FFT image shows only halos, indicating a lack of long-range order in the array. Under solvent annealing, a swell factor of $t_{DS} = 130$ %, components did not have sufficient mobility to fully order. Figure 20b shows the PMMA$_{25}$-b-PMAPOSS$_{13}$ film on the PS chemically patterned substrate with $d_s = 26$ nm annealed at $t_{DS} = 140$ %. Both the SEM image on the left and the 2D-FFT of the image on the right show a long-range ordered hexagonal array of dots with a lattice spacing of 13.4 nm, almost half of the d_s value (=26 nm) of the template. In contrast, the film annealed with $t_{DS} = 150$ % shown in Fig. 20c shows a distorted hexagonal lattice pattern and streaks on the spots in the accompanying 2D-FFT of the image. These results show that solvent annealing with $t_{DS} = 140$ % is optimal for the DSA of PMMA$_{25}$-b-PMAPOSS$_{13}$, which leads to density multiplication by a factor of 4.

To evaluate the orientation distribution of the lattice patterns in Fig. 20, we examined the azimuthal distribution of the first-order peak in the 2D autocorrelation pattern from the 2D-FFT image. The length scale of the lithographically directed patterns lattice spacing was 13.4 nm compared to a length scale of 12.4 nm in the case of the unguided BCP lattice spacing on the substrates. The standard deviation, σ, of the center-to-center distance of the solvent annealed lattices with $t_{DS} = 140$ and 150 % were calculated to be 1.5 and 1.7 nm, respectively. The σ_s values of the self-assembled lattice spacings were 20−30 % smaller than the σ_{eb} values of the chemically patterned template ($d_s = 26$ nm), which was 2.2 nm. As can be expected, σ values at $t_{DS} = 140$ % were found to be small, and significantly smaller than the σ_{eb} value of the underlying chemically patterned template at 1/4th the BCP pattern density. The lower perfection exhibited by the BCP annealed with $t_{DS} = 150$ % compared to that of the BCP annealed with $t_{DS} = 140$ % may be caused by a slight difference in the lattice spacing of the self-assembled structure at the swollen state.

The density multiplication occurred with PMMA dots interpolating between dots in the substrate chemically patterned template pattern and the placement
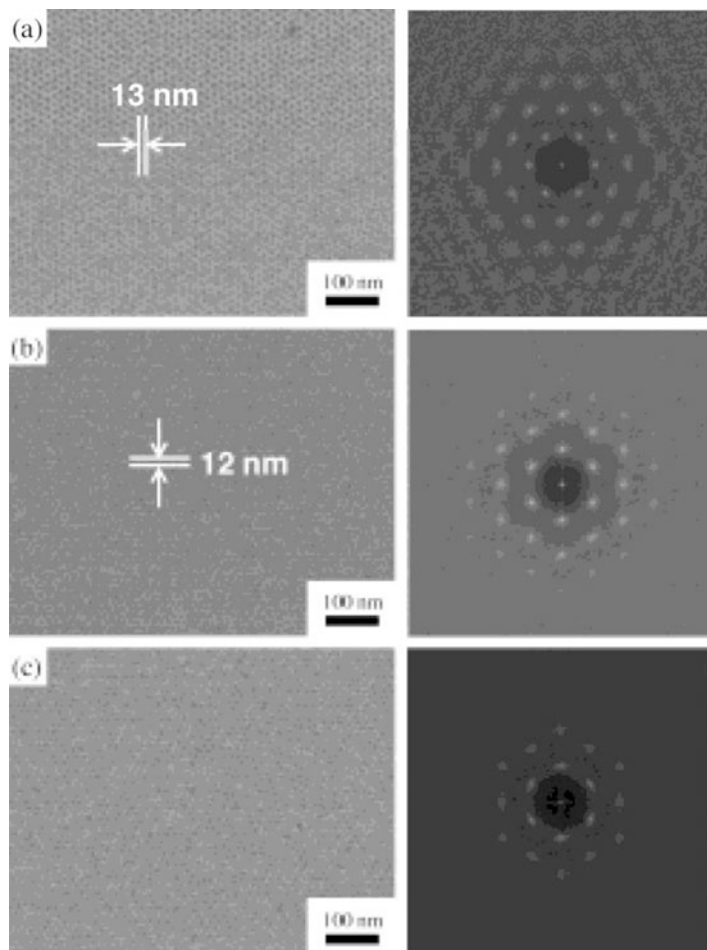
Fig. 20 SEM images and the corresponding 2D-FFT images of the PMMA25-*b*-PMAPOSS13 thin films solvent annealed at $t_{DS} = 140$ % on the chemically patterned template with $ds \approx 2d0$. (**a**) $ds = 23$ nm, (**b**) $ds = 24$ nm, and (**c**) $ds = 28$ nm. The film thickness is 9 nm. The chemically patterned templates were fabricated employing the PS-OH grafted layer

accuracy of the quadruple density pattern was $20-30$ % better than that of the original lithographic pattern on the template. The pattern density multiplication was achieved by careful optimization of the amount of BCP swelling during solvent annealing.

Next, we investigated the effect of lattice mismatch between the $PMMA_{25}$-*b*-$PMAPOSS_{13}$ BCP and that of the original lithographic chemically patterned template pattern [53]. The lattice spacing of $PMMA_{25}$-*b*-$PMAPOSS_{13}$ self-assembled on the Si substrate without a chemically patterned template was found to be $d_0 = 12.4$ nm. We examined the DSA of $PMMA_{25}$-*b*-$PMAPOSS_{13}$ by solvent annealing with CS_2 with chemically patterned template prepatterns slightly above

and below the value of $2d_0$ for $4\times$ density multiplication. The PMMA$_{25}$-b-PMAPOSS$_{13}$ films were spun onto chemically patterned PS-OH layers on Si substrates and annealed in CS$_2$ with a t_{DS} of 140 %. The length scales of the hexagonal lattices on the chemically patterned templates were $d_s = 23$, 24, and 28 nm. The SEM images and the associated 2D-FFT images of the resulting ordered BCP are shown in Fig. 20.

Figure 20a shows resulting DSA BCP lattice on a chemically patterned template with a single hexagonal lattice pattern spacing of $d_s = 23$ nm. From the first-order peak positions in the circular averaged 2D-FFT image, the dot lattice spacing of the self-assembled structures on the template was determined to be $d_{obs} = 13.2$ nm. Also note that the orientation of the BCP self-assembled lattice pattern was rotated by 30° with respect to that of the template pattern, as is schematically illustrated in Fig. 15. Therefore, the interpolation of the dots occurred as illustrated in Fig. 15, resulting in a hexagonal lattice with the orientation rotated by 30° with respect to the chemical pattern, and the density of the self-assembled BCP was three times the density of the underlying chemically patterned template [20].

As shown in Fig. 20b, the interplanar spacing and the dot-to-dot spacing on the axis of the underlying chemically patterned template pattern were 24 and 28 nm, respectively. The DSA BCP consisted of a single hexagonal lattice, as shown Fig. 20b. The corresponding 2D-FFT image exhibits a spot-like pattern with three orders of peaks. Analysis of the first-order peaks gave an average lattice inter-row spacing of $d_{obs} = 12.3$ nm, which was a half of the value of the lithographically defined chemical pattern with $d_s = 24$ nm. As determined above, the lattice spacing of the BCP self-assembled structure on Si, d_0, was 12.4 nm. In this case, the directed BCP lattice had the same spacing as the spacing of the BCP lattice on Si. The areal density of the hexagonal lattice pattern with lattice inter-row spacing of $d_{obs} = 12.3$ nm achieved in this study corresponds to 3.7 Tdot/in.^{2}. Most importantly we demonstrated successful template pattern density multiplication with a PMMA-b-PMAPOSS BCP to an ultrahigh pattern density.

Figure 20c shows the DSA PMMA$_{25}$-b-PMAPOSS$_{13}$ BCP and its 2D-FFT image on a chemically patterned template with $d_s = 28$ nm. The mismatched chemical pattern on the substrate was further from the period of the PMMA$_{25}$-b-PMAPOSS$_{13}$ BCP lattice on Si than the sample in Fig. 20a, b, and the long-range order of the self-assembled structure looked worse. However, a closer observation of the 2D-FFT image in Fig. 20c showed the superposition of two different hexagonal lattices with different lattice spacings, that is, $d_{obs} = 12.3$ and 13.8 nm. The first-order peaks for the lattice spacing $d_{obs} = 12.3$ nm contain streaks, which suggested much a broader orientation distribution of the hexagonal lattice than those shown in Fig. 20a, b. This result suggested that a number of hexagonal lattices of the self-assembled structure with $d_{obs} = 12.3$ nm, each with slightly different orientations, gave rise to the arc-like peaks. It should be noted that $d_{obs} = 12.3$ nm was almost identical to $d_0 = 12.4$ nm of the self-assembled structure on the Si substrate, suggesting that the lattice spacing of the majority of the self-assembled structures was unaffected by the template lattice spacing. The first-order peaks of the lattice pattern with $d_{obs} = 13.8$ nm appeared as sharp points in the 2D-FFT image. In the latter lattice,

the spacing was $\sim 2\times$ the lithographic pattern spacing and the BCP matrix stretched by 11 % ($d_{obs}/d_0 = 13.8/12.4 = 1.11$) relative to the lattice spacing of the self-assembled structure on the Si substrate as a result of the chemically patterned template with $d_s = 28$ nm. Thus, Figs. 12b and 14 show one region where the self-assembled BCP was directed by the template with $d_s = 26$ nm and another that was directed by $d_s = 23$ nm. Both lattices formed a $\sim 4\times$ density multiplication of the original lithographic pattern, although the orientation in the case of $d_{obs} = 13.8$ nm was better controlled. From these results, the reduction of the interface interaction enthalpy between the template surface and the polymer overcame the loss of the conformational entropy of the block chains up to an 8 % ($d_{obs}/d_0 = 13.4/12.4 = 1.11$) stretch in terms of d_{obs}/d_0 induced by the template pattern with d_s.

The key factor for the successful density multiplication with sufficient long-range order was to control the degree of swelling during the solvent annealing process because the lattice spacing of the self-assembled structure of the PMMA-*b*-PMAPOSS film is sensitive to the degree of swelling.

5 Pattern Transfer

We demonstrated pattern transfer from the PMMA-*b*-PMAPOSSs with and without applying the DSA process to a silicon substrate as a template, as shown in Fig. 21 [54]. The effect of applying the DSA processes was evaluated in terms of pattern homogeneity.

Optimized dry development conditions were applied to form holes on a silicon substrate (to depth of 18.2 nm and diameter of 12.3 nm) by pattern transfer from the PMMA-*b*-PMAPOSS film. By applying a DSA process, the defect ratio decreased by about 60 %. An imprint mold pattern of 1.7 Tdpsi with a defect ratio of 2 % was successfully fabricated on a silicon substrate.

6 Summary and Outlook

BCP patterning provides a simple and low-cost route to fabricate arrays of nanostructures for pattern transfer. POSS-containing BCPs prepared by living anionic or controlled radical polymerization represent an unprecedented breakthrough in the synthesis of BCP lithographic resists, allowing access to a wide range of nanofabrication processes.

Self-assembly of POSS-containing BCPs in thin films generated a number of interesting nanostructures with silicon-rich phases, good film formation, and morphological transitions depending on the degree of swelling as well as molecular weight. So far, we have limited the study to applying the technique only to hexagonally packed dot patterns or simple line patterns, although the results
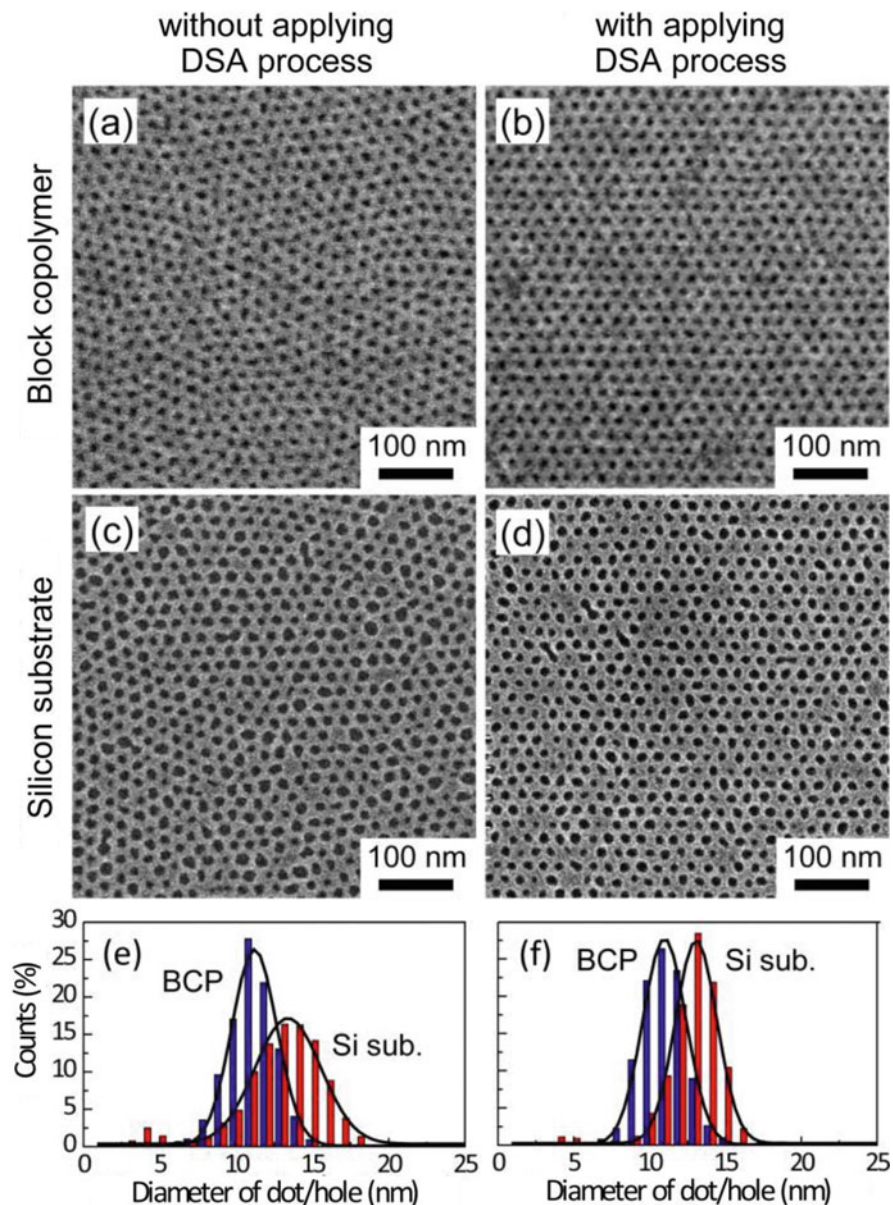
Fig. 21 (**a**–**d**) Top-view SEM images of the PMMA-*b*-PMAPOSS (BCP) film (**a**) without DSA process using a chemically patterned template and (**b**) with the DSA process. Silicon substrate (**c**) processed without DSA and (**d**) with the DSA process. (**e**) and (**f**) Dot-size distribution of the initial BCP and pattern transferred silicon substrate. RSD of dot/hole-diameter of (**a**–**d**) are 15, 15, 24, and 16 %, respectively

strongly support the possibility of adaption to other domain structures as well as to more complex features. A series of POSS-containing BCPs have proven useful as templates for magnetic storage and semiconductor devices and in applications related to nanoceramics and catalysts.

References

1. Park M, Harrison C, Chailin PM, Register RA, Adamson DH (1997) Block copolymer lithography: periodic arrays of ~10^{11} holes in 1 square centimeter. Science 276:1401
2. Kim H-C, Park S-M, Hinsberg WD (2010) Block copolymer based nanostructures: materials, processes, and applications to electronics. Chem Rev 110:146
3. Galatsis K, Wang KL, Ozkan M, Ozkan CS, Huang Y, Chang JP, Monbouquette HG, Chen Y, Nealey PF, Botros Y (2010) Patterning and templating for nanoelectronics. Adv Mater 22:769
4. Bita I, Yang JKW, Jung YS, Ross CA, Thomas EL, Berggren KK (2008) Graphoepitaxy of self-assembled block copolymers on two-dimensional periodic patterned templates. Science 321:939
5. Black CT, Guarini KW, Milkove KR, Baker SM, Russell TP, Tuominen MT (2001) Integration of self-assembled diblock copolymers for semiconductor capacitor fabrication. Appl Phys Lett 79:409
6. Segalman RA, Yokoyama H, Kramer E (2001) Graphoepitaxy of spherical domain block copolymer films. J Adv Mater 13:1152
7. Sundrani D, Sibener SJ (2002) Spontaneous spatial alignment of polymer cylindrical nanodomains on silicon nitride gratings. Macromolecules 35:8531
8. Cheng JY, Ross CA, Thomas EL, Smith HI, Vancso G (2002) Fabrication of nanostructures with long-range order using block copolymer lithography. J Appl Phys Lett 81:3657
9. Cheng JY, Mayes AM, Ross CA (2004) Nanostructure engineering by templated self-assembly of block copolymers. Nat Mater 3:823
10. Xiao SG, Yang XM, Edwards EW, La YH, Nealey PF (2005) Graphoepitaxy of cylinder-forming block copolymers for use as templates to pattern magnetic metal dot arrays. Nanotechnology 16:S324
11. Chen F, Akasaka S, Inoue T, Takenaka M, Hasegawa H, Yoshida H (2007) Ordering cylindrical microdomains for binary blends of block copolymers with graphoepitaxy. Macromol Rapid Commun 28:2137
12. Rockford L, Liu Y, Mansky P, Russell TP, Yoon M, Mochrie SG (1999) Polymers on nanoperiodic, heterogeneous surfaces. J Phys Rev Lett 82:2602
13. Kim SO, Solak HH, Stoykovich MP, Ferrier NJ, de Pablo JJ, Nealey PF (2003) Epitaxial self-assembly of block copolymers on lithographically defined nanopatterned substrates. Nature 424:411

14. Edwards EW, Stoykovich MP, Solak HH, Nealey PF (2006) Long-range order and orientation of cylinder-forming block copolymers on chemically nanopatterned striped surfaces. Macromolecules 39:3598

15. Welander AM, Kang H, Stuen KO, Solak HH, Müller M, de Pablo JJ, Nealey PF (2008) Solubility and diffusion of polybutadiene in polystyrene at elevated temperatures. Macromolecules 41:2759

16. Ruiz R, Kang H, Detcheverry FA, Dobisz E, Kercher DS, Alberecht TR, de Pablo JJ, Nealey PF (2008) Density multiplication and improved lithography by directed block copolymer assembly. Science 321:936

17. Cheng JY, Rettner CT, Snaders DP, Kim HC, Hinsberg WD (2008) Dense self-assembly on sparse chemical patterns: rectifying and multiplying lithographic patterns using block copolymers. Adv Mater 20:3155

18. Tada Y, Akasaka S, Yoshida H, Hasegawa H, Dobisz E, Kercher D, Takenaka M (2008) Directed self-assembly of diblock copolymer thin films on chemically-patterned substrates for defect-free nano-patterning. Macromolecules 41:9267

19. Tada Y, Akasaka S, Takenaka M, Yoshida H, Ruiz R, Dobisz E, Hasegawa H (2009) Nine-fold density multiplication of hcp lattice pattern by directed self-assembly of block copolymer. Polymer 50:4250

20. Xiao S, Yang XM, Park S, Weller D, Russell TP (2009) A novel approach to addressable 4 teradot/in.^{2} patterned media. Adv Mater 21:2516

21. Wan L, Yang XM (2009) Directed self-assembly of cylinder-forming block copolymers: prepatterning effect on pattern quality and density multiplication factor. Langmuir 25:12408

22. Cheng JY, Snaders DP, Truong HD, Harrer S, Friz A, Holmes S, Colburn M, Hinsberg WD (2010) Simple and versatile methods to integrate directed self-assembly with optical lithography using a polarity-switched photoresist. ACS Nano 4:4815

23. Stoykovich MP, Kang H, Daoulas KC, Liu G, Liu C-C, Pablo JJ, Muller M, Nealey PF (2007) Directed self-assembly of block copolymers for nanolithography: fabrication of isolated features and essential integrated circuit geometries. ACS Nano 1:168

24. Ruiz R, Dobisz E, Albrecht TR (2011) Rectangular patterns using block copolymer directed assembly for high bit aspect ratio patterned media. ACS Nano 5:79

25. Kang H, Crag GSW, Nealey PF (2008) Directed assembly of asymmetric ternary block copolymer-homopolymer blends using symmetric block copolymer into checkerboard trimming chemical pattern. J Vac Sci Technol B 26:2495

26. Liu G, Thomas CS, Craig GSW, Nealey PF (2010) Integration of density multiplication in the formation of device-oriented structures by directed assembly of block copolymer–homopolymer blends. Adv Funct Mater 20:1251

27. Khandpur AK, Forster S, Bates FS, Hamely IW, Ryan AJ, Bras W, Almdal K, Mortensen K (1995) Polyisoprene-polystyrene diblock copolymer phase diagram near the order–disorder transition. Macromolecules 28:8796

28. Hashimoto T (1998) Chapter 15: Order–disorder transition in block copolymers. In: Holden G, Legge NR, Quirk RP, Schroeder HE (eds) Thermoplastic elastomers, 2nd edn. Hanser Publishers, Munich, pp 429–463

29. Matsen MW, Schick M (1994) Stable and unstable phases of a diblock copolymer melt. Phys Rev Lett 72:2660

30. Takenaka M, Wakada T, Akasaka S, Nishitsuji S, Saijo K, Shimizu H, Kim MI, Hasegawa H (2007) Orthorhombic *Fddd* network in diblock copolymer melts. Macromolecules 40:4399

31. Park S, Wang J-Y, Kim B, Russell TP (2008) From nanorings to nanodots by patterning with block copolymers. Nano Lett 8:1667

32. Olayo-Valles R, Guo S, Lund MS, Leighton C, Hillmyer MA (2005) Perpendicular domain orientation in thin films of polystyrene−polylactide diblock copolymers. Macromolecules 38:10101

33. Park S, Lee DH, Xu J, Kim B, Hong SW, Jeong U, Xu T, Russell TP (2009) Macroscopic 10-terabit–per–square-inch arrays from block copolymers with lateral order. Science 323:1030

34. Jung YS, Ross CA (2009) Solvent-vapor-induced tunability of self-assembled block copolymer patterns. Adv Mater 21:2540
35. Jung YS, Ross CA (2007) Orientation-controlled self-assembled nanolithography using a polystyrene−polydimethylsiloxane block copolymer. Nano Lett 7:2046
36. Jung YS, Chang JB, Verploegen E, Berggren KK, Ross CA (2010) A path to ultranarrow patterns using self-assembled lithography. Nano Lett 10:1000
37. Takenaka M, Aburaya S, Akasaka S, Hasegawa H, Hadjichristidis N, Sakellariou G, Tada Y, Yoshida H (2010) Formation of long-range stripe patterns with sub-10-nm half-pitch from directed self-assembly of block copolymer. J Polym Sci Part B Polym Phys 48:2297
38. Lammertink RGH, Hempenius MA, van den Enk JE, Chan VZ-H, Thomas EL, Vancso G (2000) Nanostructured thin films of organic–organometallic block copolymers: one-step lithography with poly(ferrocenylsilanes) by reactive Ion etching. J Adv Mater 12:98
39. Lu J, Chamberlin D, Rider DA, Liu M, Manners I, Russell TP (2006) Using a ferrocenylsilane-based block copolymer as a template to produce nanotextured Ag surfaces: uniformly enhanced surface enhanced Raman scattering active substrates. Nanotechnology 17:5792
40. Fukukawa K, Zhu L, Gopalan P, Ueda M, Yang S (2005) Synthesis and characterization of silicon-containing block copolymers from nitroxide-mediated living free radical polymerization. Macromolecules 38:263
41. Stoykovich MP, Nealey PF (2006) Mater Today 9:20. (12) Tegou E, Bellas V, Gogolides E, Argitis P, Eon D, Cartry G, Cardinaud C (2004) Chem Mater 16:2567. (13) Haddad TS, Lichtenhan JD (1996) Hybrid organic–inorganic thermoplastics: styryl-based polyhedral oligomeric silsesquioxane polymers. Macromolecules 29:7302
42. Hayakawa T, Seino M, Goseki R, Hirai T, Kikuchi R, Kakimoto M, Tokita M, Yokoyama H, Horiuchi S (2006) Fabrication of hierarchically ordered hybrid structures over multiple length scales *via* direct etching of self-organized polyhedral oligomeric silsesquioxane (POSS) functionalized block copolymer films. Polym J 38:567
43. Hirai T, Leolukman M, Hayakawa T, Kakimoto M, Gopalan P (2008) Hierarchical nanostructures of organosilicate nanosheets within self-organized block copolymer films. Macromolecules 41:4558
44. Hirai T, Leolukman M, Liu CC, Han E, Kim YJ, Ishida Y, Hayakawa T, Kakimoto M, Nealey PF, Gopalan P (2009) One-step direct-patterning template utilizing self-assembly of POSS-containing block copolymers. Adv Mater 21:4334
45. Hirai T, Leolukman M, Jin S, Goseki R, Ishida Y, Kakimoto M, Hayakawa T, Ree M, Gopalan P (2009) Hierarchical self-assembled structures from POSS-containing block copolymers synthesized by living anionic polymerization. Macromolecules 42:8835
46. Ahn B, Hirai T, Jin S, Ryo Y, Kim K-W, Kakimoto M, Gopalan P, Hayakawa T, Ree M (2010) Hierarchical structure in nanoscale thin films of a poly(styrene-*b*- methacrylate grafted with POSS) (PS$_{214}$-*b*-PMAPOSS$_{27}$). Macromolecules 43:10568
47. Jin S, Hirai T, Ahn B, Ryo Y, Kim K-W, Kakimoto M, Gopalan P, Hayakawa T, Ree M (2010) Synchrotron grazing incidence X-ray scattering study of the morphological structures in thin films of a polymethacrylate diblock copolymer bearing POSS moieties. J Phys Chem B 114:8033
48. Goseki R, Hirai T, Ishida Y, Kakimoto M, Hayakawa T (2012) Rapid and reversible morphology control in thin films of poly(ethylene oxide)-block-POSS-containing poly(methacrylate). Polym J 44:658
49. Ishida Y, Hirai T, Goseki R, Tokita M, Kakimoto M, Hayakawa T (2011) Synthesis and self-assembly of thermotropic block copolymer with long alkyl tethered cage silsesquioxane in the side chain. J Polym Sci Part A Polym Chem 49:2653
50. Ishida Y, Tada Y, Hirai T, Goseki R, Kakimoto M, Yoshida H, Hayakawa T (2010) Directed self-assembly of cage silsesquioxane containing block copolymers via graphoepitaxy techniques. J Photopolym Sci Technol 23(2):155
51. Yoshida H, Tada Y, Ishida Y, Hayakawa T, Takenaka M, Hasegawa H (2011) Synthesis and self-assembly of thermotropic block copolymer with long alkyl tethered cage silsesquioxane in the side chain. J Photopolym Sci Technol 24(5):577

52. Goseki R, Hirao A, Kakimoto M, Hayakawa T (2013) Cylindrical nanostructure of rigid-rod POSS-containing polymethacrylate from a star-branched block copolymer. ACS Macro Lett 2(7):625
53. Tada Y, Yoshida H, Ishida Y, Hirai T, Bosworth JK, Dobisz E, Ruiz R, Takenaka M, Hayakawa T, Hasegawa H (2012) Directed self-assembly of POSS containing block copolymer on lithographically defined chemical template with morphology control by solvent vapor. Macromolecules 45(1):292
54. Iwase T, Kurihara M, Hirayama Y, Negishi N, Hayakawa T, Tada Y, Yoshida H (2013) Reducing hole-size variation and defect ratio after pattern transfer by using self-assembled polymer with spherical structure. J Vac Sci Technol B 31(4):041807/1
55. Pyun J, Matyjaszewski K (2000) The synthesis of hybrid polymers using atom transfer radical polymerization: homopolymers and block copolymers from polyhedral oligomeric silsesquioxane monomers. Macromolecules 33:217
56. Bosworth JK, Paik MY, Ruiz R, Schwartz EL, Huang JQ, Ko AW, Smilgies D-M, Black CT, Ober CK (2008) Control of self-assembly of lithographically patternable block copolymer films. ACS Nano 2:1396
57. Paik MY, Bosworth JK, Smilges D-M, Schwartz EL, Andre X, Ober CK (2010) Reversible morphology control in block copolymer films via solvent vapor processing: an in situ GISAXS study. Macromolecules 43:4253
58. Saraf RF, Niu S, Stumb E (2002) Spontaneous planarization of nanoscale phase separated thin film. Appl Phys Lett 80:4425
59. Niu S, Saraf RF (2003) Stability of order in solvent-annealed block copolymer thin films. Macromolecules 36:2428
60. Bosworth JK, Dobisz E, Ruiz R (2010) 20 nm pitch directed block copolymer assembly using solvent annealing for bit patterned media. J Photopolym Sci Technol 23:145
61. Hanley KJ, Lodge TP, Huang C-I (2000) Phase behavior of a block copolymer in solvents of varying selectivity. Macromolecules 33:5918
62. Tokarev I, Krenek R, Burkov Y, Schmeisser D, Sidorenko A, Minko S, Stamm M (2005) Microphase separation in thin films of poly(styrene-*block*-4-vinylpyridine) copolymer−2-(4'-hydroxybenzeneazo)benzoic acid assembly. Macromolecules 38:507

Methacrylate-Based Polymers for Industrial Uses

Kenichi Hamada, Yoshihiro Morishita, Toyoaki Kurihara, and Kazushige Ishiura

Abstract Controlling anionic polymerization is one of the key technologies in the synthesis of well-defined polymers such as block copolymers. KURARAY Co. Ltd., has developed a new living polymerization system of (meth)acrylates using compounds consisting of a Lewis base and bulky aluminum (LA system). Observations supported by kinetics studies point to a mechanism consisting of stabilization of enolate anion and aluminum-based coordination of monomers. This LA system can be leveraged not only for (meth)acrylate block copolymers, but also for block copolymers of (meth)acrylate and other anionic polymerization monomers. "KURARITY™"—an acrylic triblock copolymer (ABCP) produced by using this LA system—has unique properties suitable for employment in various applications, such as thermoplastic elastomers, flexible and transparent films, modifiers, and adhesives.

Keywords Anionic polymerization • (Meth)acrylate • Acrylic triblock copolymer

1 Introduction

To meet demand for revolutionary polymer products, new polymerization technologies have been developed.

Anionic polymerization is one of the best technologies for living polymerization of vinyl monomers. Products produced by anionic polymerization of nonpolar monomers, such as polybutadiene rubbers (BR), polyisoprene rubbers (IR), styrene/butadiene rubbers (SBR), thermoplastic elastomers of block copolymers (SBS and SIS), already dominate important positions in industries; examples include thermoplastic elastomers, adhesives, impact modifiers, lubricant modifiers, and others [1].

Polymer materials of polar monomers, such as polymethyl methacrylate (PMMA), poly(n-butyl acrylate) (PnBA), and poly(2-ethylhexyl acrylate) (P2EHA), are also widely used in optically transparent, highly weatherable, high heat resistant applications. However, it is difficult to avoid undesirable side

K. Hamada (✉) • Y. Morishita • T. Kurihara • K. Ishiura
Elastomer Division, KURARAY CO., LTD. Isoprene Company,
Ote Center Building,1-1-3, Otemachi, Chiyoda-ku, Tokyo 100-8115, Japan
e-mail: Kenichi_Hamada@kuraray.co.jp

reactions when producing (meth)acrylate monomers with living anionic polymerization (LAP) [2, 3]. KURARAY has succeeded in developing proprietary technologies for living anionic polymerization of (meth)acrylate monomers that eliminate these side reactions, and which enable the manufacture of acrylic block copolymers as industrial products.

2 History

Beginning in the 1950s, after anionic polymerization of nonpolar monomers in hydrocarbon solutions was invented, a wide variety of rubber products have been commercialized; KURARAY, a manufacturer of synthetic isoprene monomers, has focused on developing isoprene-based unique polymers using its high-purity monomer.

Living anionic polymerization technologies can produce various polymers with a narrow molecular weight distribution, a block copolymer structure, and a controlled microstructure suitable for a variety of applications. Leveraging these advantages, KURARAY has produced a number of materials, including a liquid isoprene rubber (L-IR), which has proved useful as a co-crosslink modifier for rubber material; a block copolymer consisting of a hydrogenated polyisoprene copolymer block sandwiched between polystyrene blocks (SEPTON™; S-EP-S, S-EEP-S), which exhibit high oil detainment and high heat resistance properties; a block copolymer consisting of a non-hydrogenated polyisoprene block with a 3,4-microstructure sandwiched between polystyrene blocks (HYBRAR™; S-VI-S), which has superior vibration damping properties; a block copolymer consisting of a hydrogenated polyisoprene copolymer block with a 3,4- microstructure sandwiched between polystyrene blocks (HYBRAR™; S-HVI-S), which has excellent miscibility with polypropylenes (PP), and which elicits transparent materials when combined with PP. SEPTON™ products can also be produced in other variations, such as with a hydroxyl group placed at the end of the polymer chain for polymer-reacting applications [4].

KURARAY has continued developing new high-performance polymer products by advancing technologies such as high scratch resistance elastomers, crosslinkable and curable thermoplastic elastomers, and block copolymers of (meth) acrylate—the last of which are described in detail below.

3 Anionic Polymerization of (Meth)acrylate Monomers

Compared to nonpolar monomers, it is difficult to control living anionic polymerization of (meth)acrylate monomers for industrial applications. A number of studies have been published on various means to avoid side reactions of enolate anion with ester carbonyl groups. Acrylate monomers are a particularly crucial challenge [2, 3].

One approach is living anionic polymerization of methyl methacrylate (MMA) in THF at temperatures below $-60\ ^{\circ}C$, which tends to aggregate enolate anion toward the end of the propagation. Some approaches to improve stabilization have also been researched; for example, adding TMEDA [2] or LiCl [5], have produced good results.

However, using a hydrocarbon solvent such as toluene is more preferable from a manufacturing point of view. In the later part of the 1980s and into the 1990s, examples of living anionic polymerization in toluene were reported. Hatada et al. discovered stereospecific living anionic polymerization of MMA occurring in isotactic PMMA, by using a Grignard reagent as the initiator [6] and a trialkyl aluminum-based syndiotactic PMMA as a ligand [7]. PMMA is well known as an optically transparent, high UV resistance plastic material. Its Tg is depending on tacticity, and syndiotactic PMMA is generally more preferable in terms of heat resistance.

In the later 1990s, Müller et al. reported the effects of using Lewis bases [8]; Ballard et al. [9] and Hatada and Kitayama et al. [10] were able to improve both stability and stereoselectivity by using a bulky phenoxyalkylaluminum ligand.

However, living polymerization of alkyl acrylates, especially acrylate esters with primary alcohols such as n-butyl acrylate (nBA) and 2-ethylhexyl acrylate (2EHA), which are widely used in adhesive, rubber, and modifier industries, still proved impossible to achieve using the systems cited above. Metallocenes systems, such as $[SmMe(C_5Me_5)_2]_2$ at $-78\ ^{\circ}C$ reported by Yasuda et al. [11], was the only example of living polymerization of nBA in toluene.

3.1 KURARAY's Living Anionic Technology (LA System)

KURARAY has succeeded in designing perfect living polymerization of nBA using a Lewis base combined with di-phenoxyalkyl aluminum (LA system) [12, 13]. Figure 1 shows SEC charts of polymers obtained two-step monomer feeding polymerization of nBA at $-30\ ^{\circ}C$ with di-phenoxyalkyl aluminums having different alkyl groups and with or without 1,2-dimethoxyethane. These studies indicate that the steric structure contributes to the stability of the enolate anion [14]. The contribution of the Lewis base is even more significant. There is no precursor poly(nBA) produced in the first step polymerization and the resultant polymer has very narrow molecular weight distribution.

We have concluded that stabilization is achieved because the terrifically high bulky structure of di-phenoxyalkyl aluminum allows insertion of the monomer in only the most suitable conformations. 1,2-dimethoxyethane (DME), a Lewis base, grabs the lithium counter cation and removes it from the center of propagation (Fig. 2).

Et-Al(BHT)₂

Mn=27,300 Mw/Mn=1.96
(2nd-nBA Conv. =42%)

iso-Bu-Al(BHT)₂

Mn=27,800 Mw/Mn=1.60
(2nd-nBA Conv. =45%)

iso-Bu-Al(BHT)₂+ DME

Mn=56,700 Mw/Mn=1.02
(2nd-nBA Conv. =100%)

*Two-stage polymerization (nBA-b-nBA block polymerization)
1. Toluene:64ml, t-BuLi:0.19mmol, RAl(BHT)₂:1.9mmol, DME:6.3mmol
2. Polymerization of 1.9g of nBA(n-butyl acrylate) at –30°C
3. Interval of 1hr at –30°C
4. Polymerization of 5.7g of 2nd-nBA at –30°C

RAl(BHT)₂   DME

Fig. 1 SEC curve of PnBA by two-stage polymerization (60-min interval time at $-30\,°C$) [12, 13]
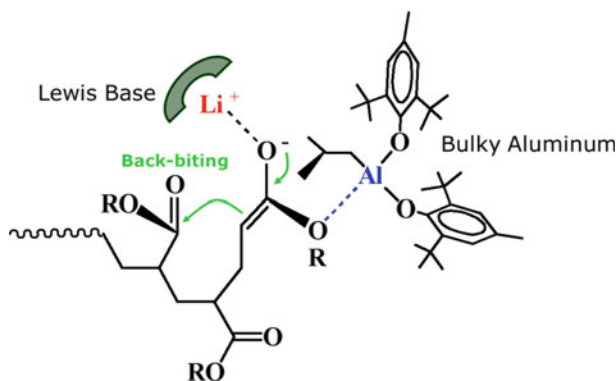
Fig. 2 The stabilization structure of the LA system

3.2 Kinetic Studies of LA System

Kinetic studies of the polymerization of MMA and nBA revealed the mechanism of the LA system more clearly.

Figure 3 shows the results of polymerization of MMA, which obviously suggest that the aluminum acts as an accelerator, although it is considered to act as a stabilizer of the propagation center. As seen above, the time-conversion plot also deviates from the curve of the first-order plot.

Obtaining reliable data on polymerization of nBA sufficient enough for validating the mechanism and designing a manufacturing process is much more difficult, however, because the rate of polymerization is so fast. Flow tube reactor [15, 16],
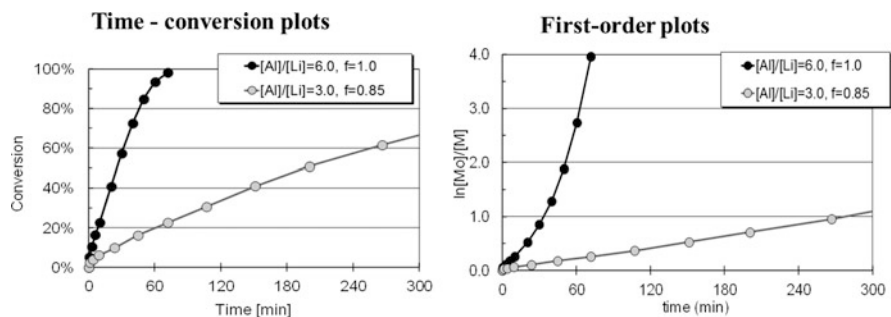
Fig. 3 Anionic polymerization of MMA using iBu(BHT)$_2$Al and DME at 0 °C. Polymerization conditions: Toluene 50 ml, 1,2-dimethoxyethane (DME) 2.5 ml, [sec-BuLi] = 4.8 mmol/L, [MMA]/[Li] = 300. iBu(BHT)$_2$Al : isobutylbis(2, 6- di tert butyl-4-methylphenoxy)aluminum. Results: Initiator efficiency = 1.0 with PMMA M_w/M_n = 1.06 obtained at [Al]/[Li] = 6.0, Initiator efficiency = 0.85 with PMMA M_w/M_n = 1.05 obtained at [Al]/[Li] = 3.0
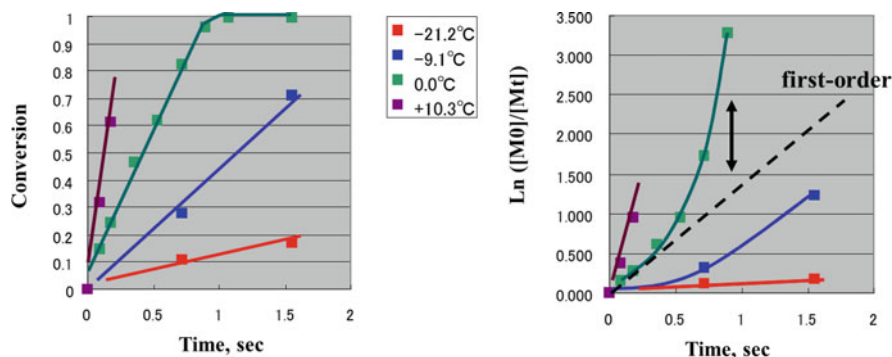
Fig. 4 Anionic polymerization of nBA using iBu(BHT)$_2$Al and a Lewis base, LA system. *Initiator*; PMMA living polymer anion (M_n = 1,980, M_w/M_n = 1.13)

which is extraordinarily fast (<1 ms) in mixing of the reaction components and superior for controlling the reaction temperature, is the best equipment to use for attempting such validation.

Figure 4 shows the time-conversion and first-order plot of the polymerization of nBA at temperatures from −21 °C to +10 °C in the flow tube reactor using PMMA (M_n = 1,980) living polymer anion solution synthesized by LA system as the initiator solution. The polymerization of nBA is completed in less than 1 s at 0 °C. The results of polymerization of nBA suggest that the rate has a proportional relationship with the aluminum concentration and does not have a first-order correlation with time.

The polymerization rate depends on the concentration of the aluminum compound and not on the monomer concentration. These results elicit a potential mechanism, suggesting that the aluminum coordinates the enolate anion and stabilizes the propagation center. At the same time, the aluminum coordinates the

$$-\frac{d[M]}{dt} = k_{p1}[P^-][M\text{-}Al] + k_{p2}[P^-][M]$$

$$\cong k_{p1}[P^-][M\text{-}Al]$$

$$\cong k_{p1}[P^-][Al] \quad \text{(in case of [M]>>[Al])}$$
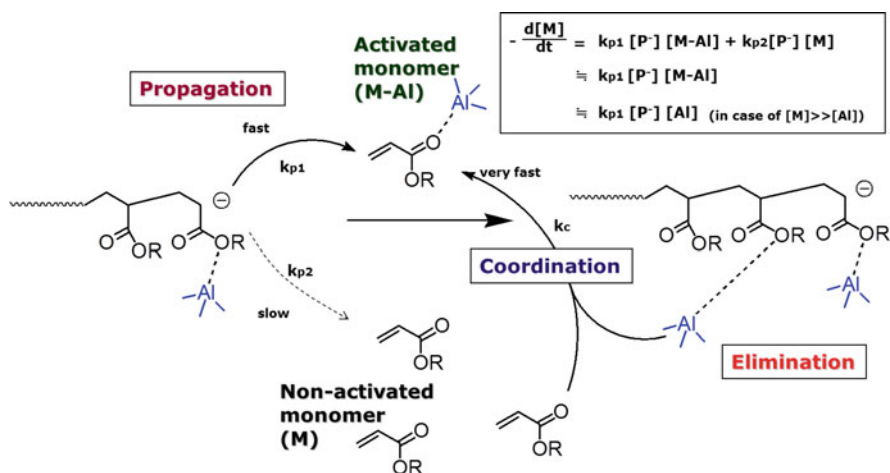
Fig. 5 Mechanism of anionic polymerization of (meth)acrylate of LA system

λmax=305nm λmax=260nm
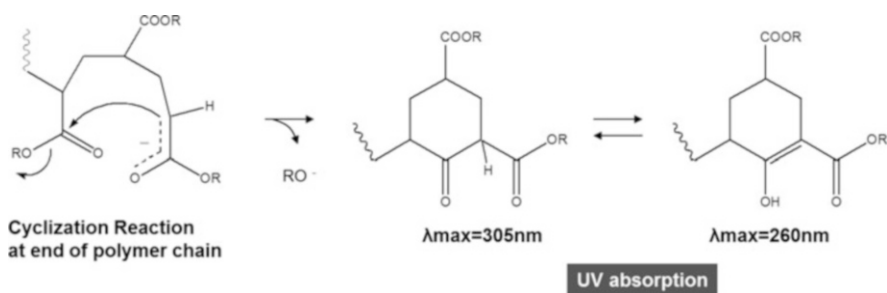
Fig. 6 Cyclization reaction of propagation end units

monomer and works as an accelerator of the addition reaction with increasing the nucleophilicity of the monomer and selectivity of 1,4-addition. The main polymerization takes place due to the monomer coordination by the aluminum, while reaction with the monomer not coordinated by the aluminum causes a side reaction (Fig. 5).

This theory is also supported by the results of termination reaction studies. Reports suggest that the termination reaction mainly takes place by cyclization of carbanion attacking the acrylate ester carbonyl group unit located at the second monomer unit from the end of the polymer chain. This cyclization reaction forms a β-ketoester group, which exhibits UV absorbance (Fig. 6).

The initiator PMMA has no absorbance in the UV spectrum, while the PnBA obtained (more precisely, PMMA-b-PnBA obtained) from the flow tube reactor polymerization exhibits UV absorbance in the portion that has lower molecular weight (Figure 7 table), which indicates more of the cyclization reaction takes place

Fig. 7 SEC chart of poly
(n-butyl acrylate) (PnBA)
initiated by the PMMA
living anion in the flow tube
reactor at 0 °C. (*a*) PMMA
living anion initiator,
$M_w = 1,980$, $M_w/M_n = 1.13$,
(*b*) PnBA, $M_w = 7,240$,
$M_w/M_n = 1.13$
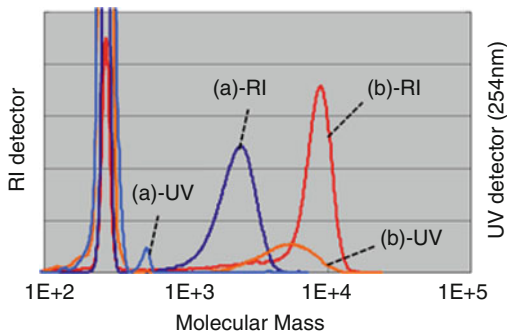
during the earlier part of the polymerization. The UV value plot, which is obtained
by dividing UV area by (RI area/M_n), provides the rate of the cyclization. The rate is
proportional to the initial concentration of nBA.

3.3 Stereoregularity and Crystallization of Poly(n-Butyl Acrylate) (PnBA)

This is a very intelligent system in which polymerization takes place at a much higher
temperature than with other methods. This is significant not only from a manufactur-
ing point of view, but also from a materials standpoint. Anionic polymerization with
an alkyl aluminum compound results in stereoregular poly(meth)acrylates. PnBA
synthesized using the LA system at low temperature was slightly syndiotactic (rr/rm/
mm = 61/36/3), and had a melting point of around 50 °C. This is not preferable for
elastomer applications. Increasing the polymerization temperature through improve-
ment of the polymerization stability resulted in a polymer that was more atactic,
which produced a material that was soft and flexible at room temperature (Fig. 8).

Selection of a polymerization reactor should be determined by considering
factors such as the rate of polymerization, removal of reaction heat, aluminum
concentration, and monomer concentration. By optimizing these parameters, living
polymerization of acrylates can be performed at roughly −10 °C, and at roughly
+50 °C in methacrylate by using the LA system.

3.4 Initiator and Block Copolymerization with 1,3-Diene Monomers

Alkyl lithium compounds can be used as the initiators of LA system polymeriza-
tion. The initiator efficiency depends entirely on the structure of the alkyl group.
For example, branched alkyl lithiums, such as sec-butyl lithium and tert-butyl
lithium, work with high initiator efficiency, while n-butyl lithium does not generate
any polymer. This kind of selectivity is also observed in anionic polymerization of
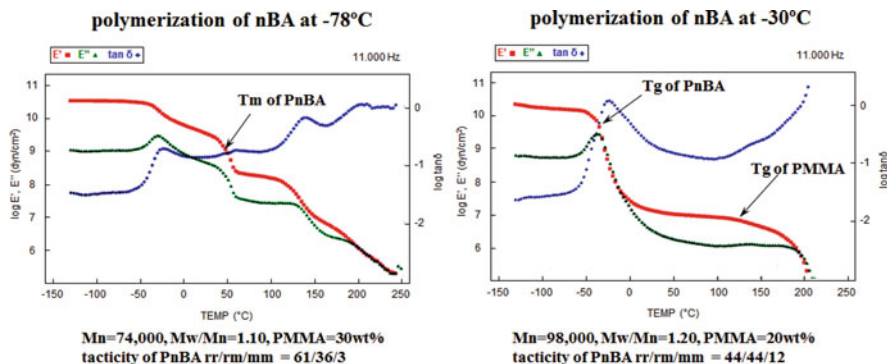
Fig. 8 Stereoregularity of PnBA of PMMA-PnBA-PMMA block copolymer and its crystallinity

methacrylate with trialkyl aluminum. The LA system increases the available range, which is significant from a manufacturing economics standpoint [13].

Block copolymers can be made by using living anions of living polymerization as initiators. Unsurprising, the LA system is applicable to block copolymerization of (meth)acrylates and other kinds of anionic polymer monomers, such as 1,3-diene and styrene monomers. For such cases, the polymer living anion used to initiate living polymerization of the (meth)acrylates must also be carefully selected. When poly(1,3-dienyl)lithiums are used as the carbanion species, the block copolymer ratio is high. On the other hand, use of poly(styrenyl)lithium generates no block copolymers [17].

These kinds of block copolymers are reportedly applicable as compatibilizers of nonpolar and polar materials. For example, the diblock copolymer of polyethylene (PE) and PMMA obtained by hydrogenation of polybutadiene (PBD) block PMMA have outstanding properties for applications of polyvinyl chloride (PVC) and PE alloys [18, 19]. The triblock copolymer of polystyrene (PS), PBD, and PMMA (SBM), works not only as a compatibilizer, but also as an impact modifier of poly(styrene-co-acrylonitrile) (SAN) and polyphenylene ether (PPE) [20]. PE-b-EB-b-PMMA, a hydrogenated block copolymer composed of 1,4-structure PBD, 1,2-structure PBD, and PMMA, has unique properties, such as superior solvent resistance [21].

4 Characteristics of Acrylic Block Copolymers Produced Using the LA System

The acrylic block copolymers (ABCP), "KURARITY™", are synthesized using the LA system, and are well-defined, pure PMMA-b-PnBA-b-PMMA triblock (MnBM) copolymers consisting of sequential polymerization of MMA, nBA, and MMA. (No homo-PMMAs or PMMA-b-PnBA diblock copolymers are ever included) (Fig. 9).
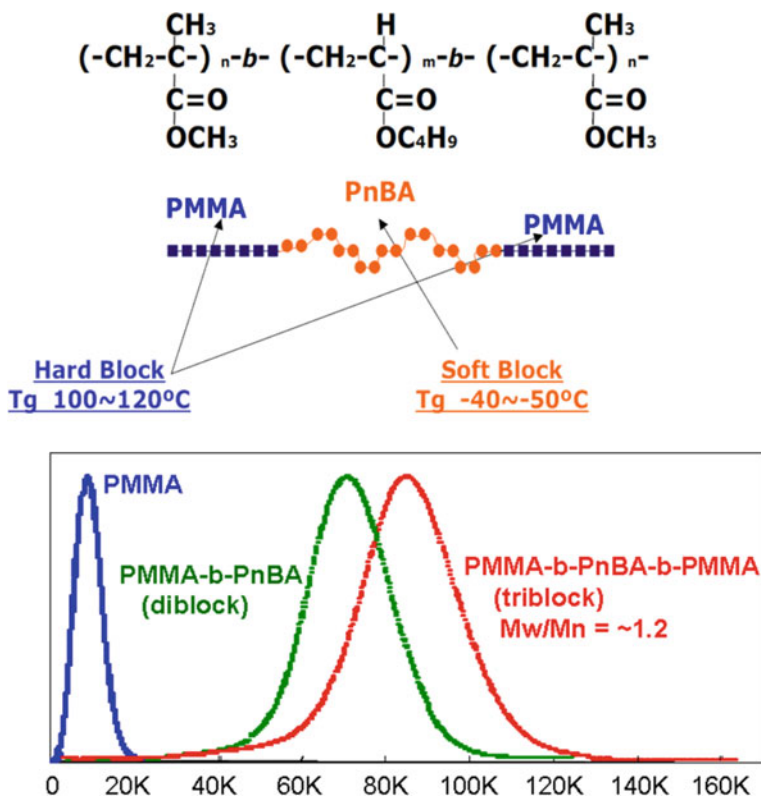
Fig. 9 Structure and SEC curve of "KURARITY™" acrylic triblock copolymer (ABCP)

An ABCP produced using the LA system has a narrow molecular weight distribution not only in the triblock copolymer area, but also in each polymer block segment, which means that the ABCP has a narrow distribution of PMMA/PnBA composition. As a practical matter, these characteristics hold great advantages over living radical polymerization such as ATRP. The triblock copolymers produced using living anionic polymerization (LAP) have better mechanical properties and lower melting viscosities than those produced by ATRP. Jerome et al. reported that the tensile strength and elongation of ABCPs produced by LAP are much larger than those produced by ATRP [22].

4.1 Morphologies

ABCP has micro phase separation morphologies. The particle size of the PMMA domain is less than 50 nm, which is a result of the well-defined structure, and this small particle size elicits a high transparency property, even though the PMMA and PnBA domains have different reflective indexes (Fig. 10).
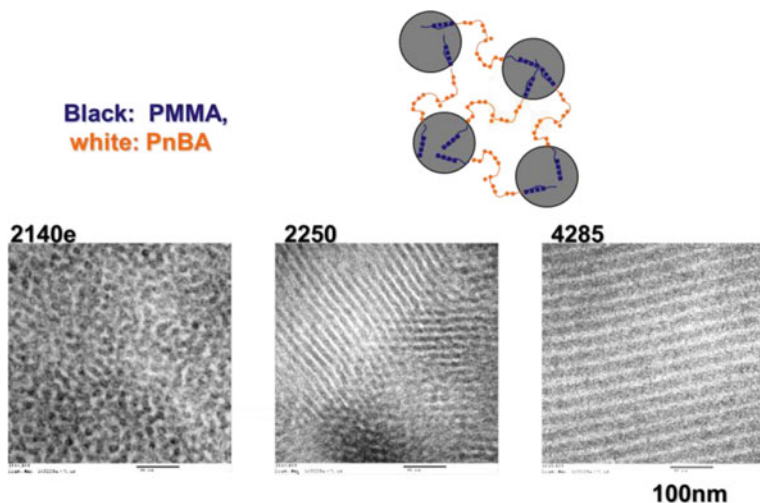
Fig. 10 Grade map and TEM photo of "KURARITY™" acrylic triblock copolymer (ABCP) [23]

Fig. 11 Transparency property of "KURARITY™" ABCP, PMMA PC, PS (140-μm thickness)
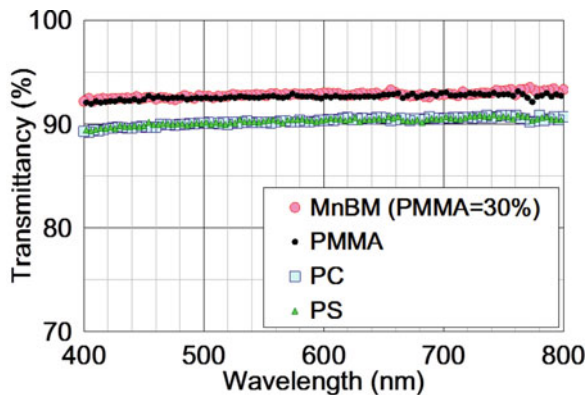
The primary market for PMMA is applications that leverage its optically transparent property. An ABCP produced using the LA system is transparent, and so can be employed in such applications (Fig. 11).

4.2 Flow Properties

Compared with styrenic block copolymers, such as SEBS, ABCP has low viscosity and high fluidity in melting and solution states owing to its high entanglement molecular weight (Fig. 12). Furthermore, the Flory–Huggins interaction parameters

Fig. 12 Angular velocity dependence of the complex viscosity at different temperatures for MnBM, "KURARITY™" acrylic block copolymer (ABCP) and SEBS, and their characterization table
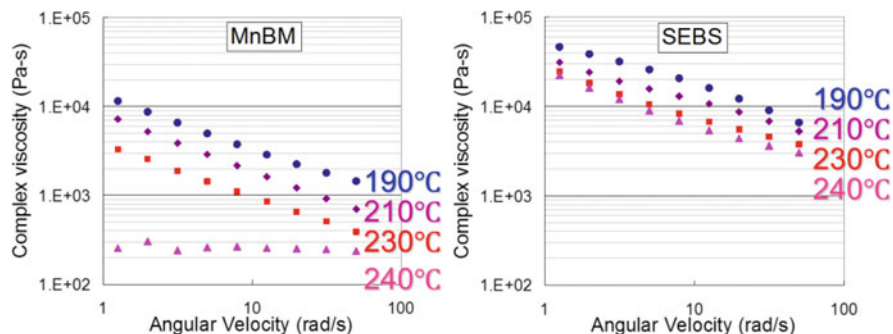
	Mw	Hard block PMMA or PS	Hardness (shore A)	MFR (g/10min) 190°C 2.16kg	MFR (g/10min) 230°C 2.16kg
MnBM	77000	30wt%	60	7	110
SEBS	80000	30wt%	80	0.04	0.46
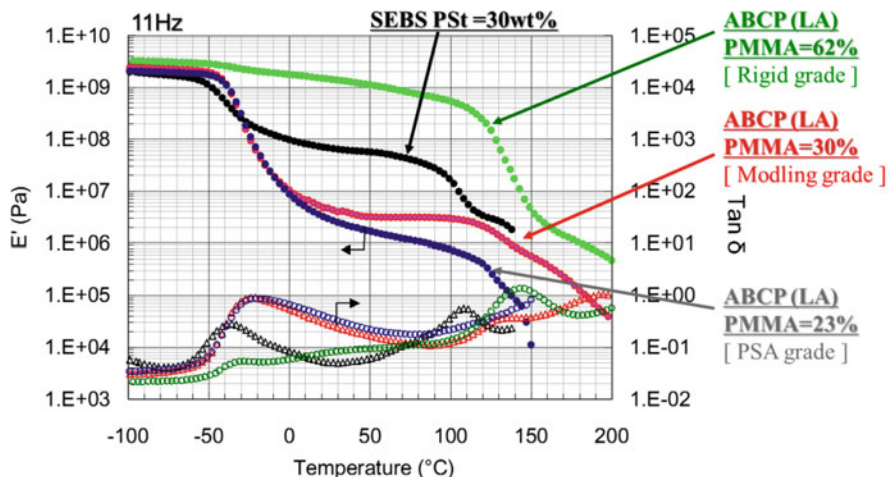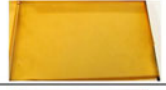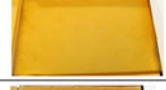
Fig. 13 Dynamic mechanical properties of "KURARITY™" ABCP and SEBS, temperature dependence of E' and tan δ (rate: 3 °C/min, $w = 11$ Hz)

χ of PMMA and PnBA are more similar than those of polystyrene (PS) and hydrogenated polybutadiene (EB), which is significant in phase separation diagrams. As a result, ABCP is softer than PS-b-EB-b-PS (SEBS) at room temperature [24] (Fig. 13).

Fig. 14 Weatherability test of "KURARITY™" ABCP and other selected materials

4.3 Dynamic Mechanical Properties

The PMMA block of ABCP produced using the LA system has 115–120 °C Tg, which is 15–20 °C higher than the PS block of SEBS [24] (Fig. 13).

4.4 Durability

One of the most significant properties of ABCP compared with other elastomer materials is weatherability, especially in terms of UV light resistance (Fig. 14).

5 Industrial Applications of "KURARITY™"

Kuraray supplies ABCP produced using the LA system as "KURARITY™" for a variety of industrial applications. This material features PMMA, optically rigid plastics, PnBA, a flexible, adhesive material, and a triblock copolymer structure (Fig. 15).

What is "KURARITY™"?

The products have high block copolymer purity, which are shown in the following HPLC chart (Fig. 16). KURARAY produces several grades, ranging from low to high PMMA content and molecular weight (Fig. 17). These grades can be employed in a wide variety of applications (Table 1).

Both the PMMA and PnBA polymer blocks of KURARITY[TM] are either compatible or miscible with conventional polar polymer materials. If the blending
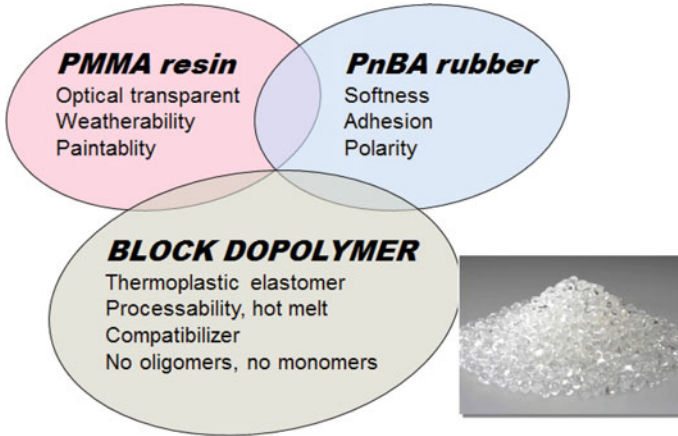
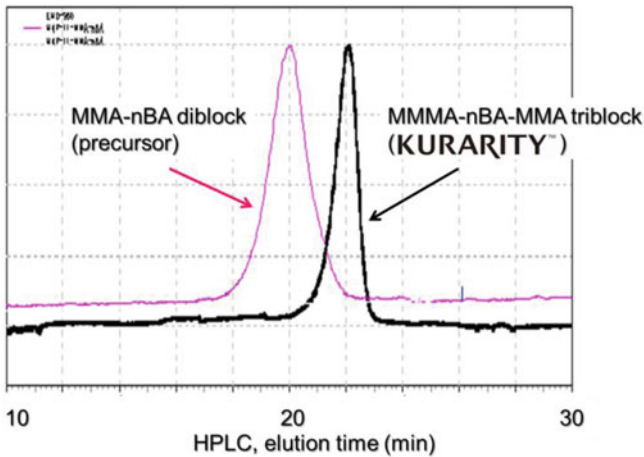**Fig. 15** Concept of "KURARITY™"

Fig. 16 HPLC chart of "KURARITY™" acrylic triblock copolymer and its precursor diblock copolymer

material is rigid, "KURARITY™" works as an impact modifier, softening agent, fluidity modifier, and/or adhesion modifier. KURARITY™ is applicable to PMMA, polybutylene terephthalate (PBT), polylactic acid (PLA), and polyvinyl chloride (PVC). When the blend material is a soft or elastomer material; for example, styrenic thermoplastic elastomer, thermoplastic polyurethane, or soft PVC, mixing with "KURARITY™" can improve the material's paintability and adhesion properties.

Fig. 17 Grade map of "KURARITY™"

*) Di-block copolymer, viscous liquid
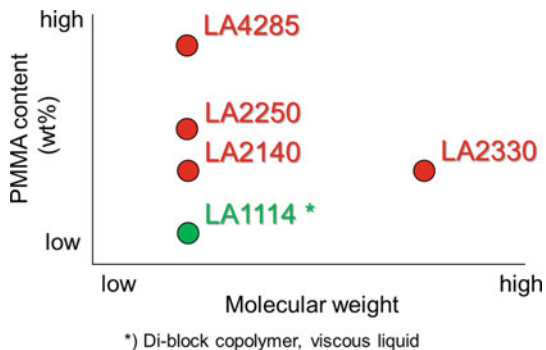
Table 1 Grades and properties of "KURARITY™"

| Property	Units	Test method	LA2140e	LA2330	LA2250	LA4285
			<Kuraray in-house data>			
Hardness [Type A]	(–)	ISO 7619-1	32	32	65	95
Hardness [Type D]		ISO 7619-1	<5	<5	18	46
Specific gravity	(–)	ISO 1183	1.08	1.08	1.08	1.11
Modulus at 100 %	(M Pa)	ISO 37	0.3	0.3	3.7	19
Tensile strength	(M Pa)	ISO 37	8.0	7.2	9.0	19
		ISO 527-2	–	–	–	19
Tensile elongation	(%)	ISO 37	570	490	380	140
		ISO 527-2	–	–	–	90
MFR [190 °C 2.16 kgf/cm^2]	(g/10 min)	ISO 1133	31	3.7	25	1.5
MFR [230 °C 2.16 kgf/cm^2]		ISO 1133	>350	42	330	31
Charpy impact (notched:1eA)	(KJ/m^2)	ISO 179-1	NB	NB	NB	28
Flexural modulus	(M Pa)	ISO 178	–	–	–	650
Transmittance[3mmt]	(%)	ISO 13468-1	91<	91<	91<	91<
Haze[3mmt]	(%)	ISO 14782	2–6[a]	2–6[a]	2–6[a]	<2
Suitable applications	For PSA		+	+	+	
	For molding		-	-	+[b]	+
	For compound, additives		+[b]	+[b]	+[b]	+

a) The HAZE value is normally worse due to the anti-blocking agent dusted onto the material
b) These grades can block or bridge while feeding into the extruder
   Some solutions to break it should be implemented
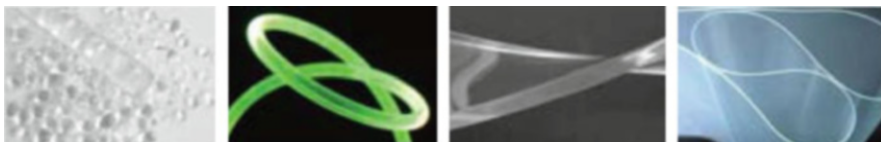
**Fig. 18** Possible combinations of "KURARITY™" with plastic materials
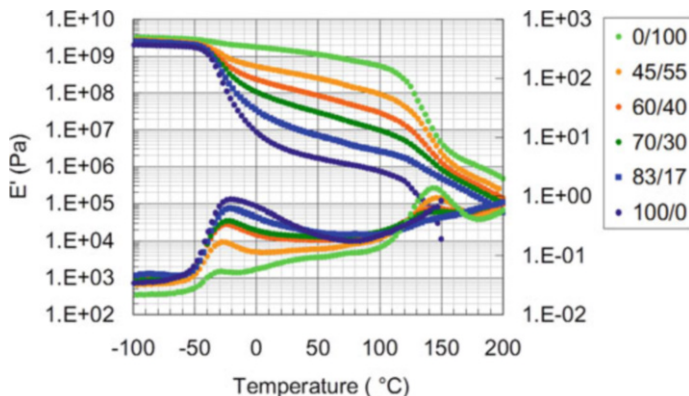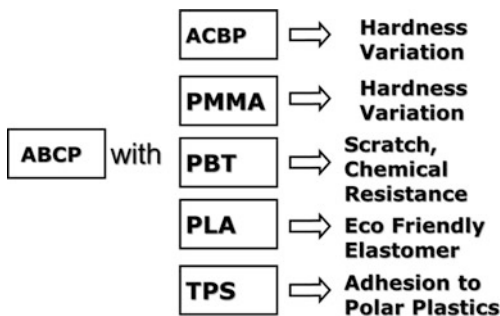
Fig. 19 Dynamic mechanical properties of deferent PMMA/PnBA "KURARITY™" blends; temperature dependence of E' and tan δ at w = 11(Hz) and a heating rate of 3 °C /min

5.1 Controlling the Modulus

One of the advantages of "KURARITY™" is a characteristic where each of PMMA and nBA block of the ABCP is miscible with the others (Fig. 18). This makes it possible to control the modulus or softness by blending two different grades. Figure 19 shows the temperature dependence of E' and tan δ of each Flexible-"KURARITY™"/Rigid-"KURARITY™" blend. It was observed that the modulus of the rubbery plateau changes according to the amount of Rigid-"KURARITY™" content. Additionally, E' values at the end of the glassy plateau and the end of the rubbery plateau are the same for the blends. This indicates that the each blend has the good heat resistance and good low temperature properties. In addition, the transparency of each blend is not lost [24].

**Fig. 20** Phase separation of a "KURARITY™"–PBT compound. (particles: PBT, Matrix: "KURARITY™")
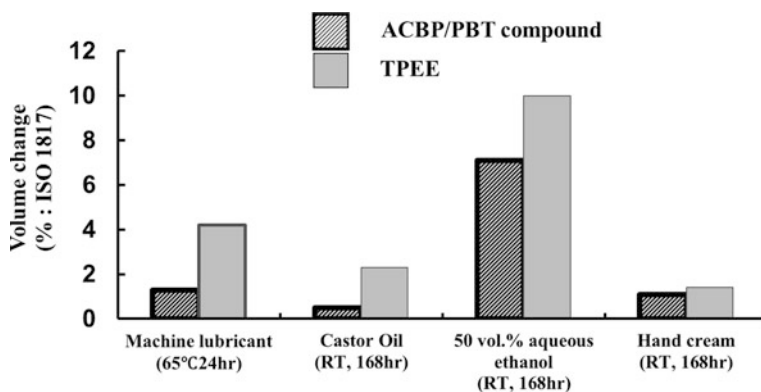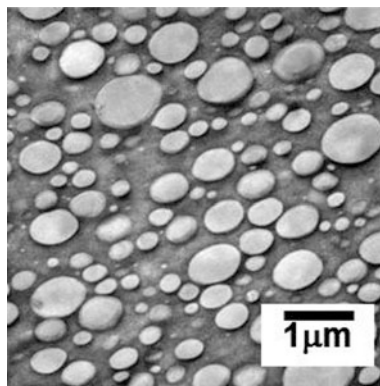
Fig. 21 Oil resistance of a "KURARITY™"–PBT (=50/50) compound according to ISO1817, 200 mm*50 mm*2 mm specimen

5.2 Compounding

"KURARITY™" blends with other materials can be designed to match the requirements of an application. A "KURARITY™"–PBT compound provides a good example of a designed blend that maintains a balance between oil resistance and flexibility [23, 25] (Figs. 20 and 21).

Another outstanding feature of "KURARITY™" is good affinity with inorganic materials. This property allows loading of higher amounts of inorganic filler than other olefinic elastomers. Thanks to the "KURARITY™" property of high fluidity at low temperature, it can be combined with $Al(OH)_3$ (Fig. 22). This compound material exhibits high flame retardancy while retaining its soft and flexible properties [26] (Table 2).

Fig. 22 Thermal degradation properties of "KURARITY™", Al(OH)$_3$, and Mg(OH)$_2$

[5 °C/min heating rate]
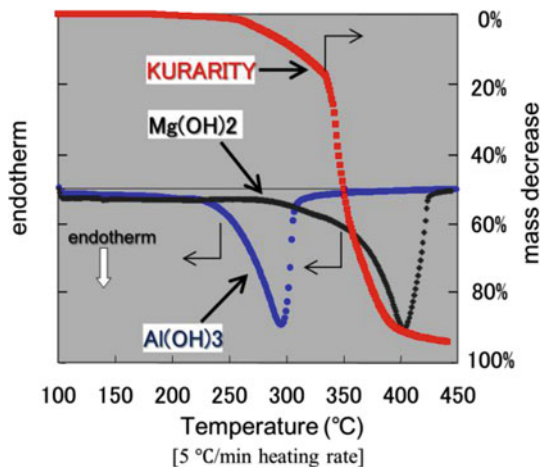
Table 2 Properties of "KURARITY™"–Al(OH)$_3$ flame retardant compound

LA2140/Al(OH)3	100/100	100/200
Specific gravity (g/cm^3)	1.4	1.62
Oxygen index (%)	20.9	51.3
UL-94	V-2	V-0
MFR		
180 °C, 2.16 kg (g/10 min)	7.0	1.0
180 °C, 10 kg (g/10 min)	81	19
TB(MPa)/EB(%)	4.5/290	7.0/90
Hardness (A)	61	78

5.3 Film

Film is another appropriate application of "KURARITY™" (Fig. 23). Through the use of "KURARITY™", it is possible to produce highly transparent film that exhibits high UV resistance. This is achieved with the "KURARITY™" compound mentioned above or with a "KURARITY™"–PMMA compound by controlling the morphology of the alloy [27]. "KURARITY™" film can be used in light guide and outdoor applications as a flexible PMMA.

5.4 Adhesive

As with styrenic block copolymers such as SEBS and SIS, which are widely used in the adhesives industry, "KURARITY™" has great potential in adhesives applications [28]. Acrylic adhesives have good heat resistance and creep properties due to chemical crosslinking. "KURARITY™", on the other hand, has physical crosslinks

Fig. 23 Sample of "KURARITY™" film

Table 3 Hot-melt adhesion properties of "KURARITY™"

	1	CE1	CE2
Formulation			
LA2140	100	Hot melt rubber Adhesive	Double-sided acrylic tape with non-woven fabric base film
Tackifier A (hydrogenated rosin ester)	35		
Coating thickness (μm)	53	35	165
Rolling ball tack test (JIS test method)	7	<4	16
Creep test (holding power at 80 °C)	>1 week	10 min	9.6 h
180° peel adhesion			
To stainless steel (N/25 mm)	16	27	32
To PE (N/25 mm)	8.6	20	14
Viscosity at 180 °C (mPa/s)	30,000	51,000	(Cross-linked)

Test piece: PET(50 μm)/PSA (casted by Toluene solution)
Test condition: Ball tack test: JIS test method (the larger ball number means better tack)
             Creep test: load 1.0 kg, sample size 25 mm × 25 mm, to stainless steel
             180° peel test: 300 mm/min at r.t.
             Viscosity: measured by "Brookfield viscometer"

with high PMMA Tg, making these crosslinks thermally reversible. As previously explained, "KURARITY™" produced using the LA system exhibits a lower viscosity in its melting and solution states, which is enormously beneficial for formulating high-creep, hot-melt type adhesives, extrusion type adhesives, and high solid content solution type adhesives (Table 3).

6 Conclusion

The last three decades have brought forth great challenges in achieving living anionic polymerization and synthesis of block copolymers of (meth)acrylates. The LA system is the solution. The LA system features an intelligent mechanism and is supported from a kinetics standpoint. A new acrylic triblock copolymer (ABCP), product name "KURARITY™", is now commercially available alongside styrenic block copolymers. It holds great promise for a wide variety of applications.

Abbreviations

2EHA	2-Ethylhexyl acrylate
ABCP	Acrylic triblock copolymer
BR	Polybutadiene rubbers
DME	1,2-Dimethoxyethane
EB	Hydrogenated polybutadiene
iBu(BHT) 2Al	Isobutylbis(2,6-di-tert-butyl-4-methylphenoxy)aluminum
IR	Polyisoprene rubbers
LA system	Living polymerization system of (meth)acrylates using compounds consisting of a Lewis base and bulky aluminum
LAP	Living anionic polymerization
MMA	Methyl methacrylate
MnBM	PMMA-b-PnBA-b-PMMA triblock
nBA	*n*-Butyl acrylate
P2EHA	Poly(2-ethylhexyl acrylate)
PBD	Polybutadiene
PBT	Polybutylene terephthalate
PE	Polyethylene
PLA	Polylactic acid
PMMA	Polymethyl methacrylate
PnBA	Poly(n-butyl acrylate)
PP	Polypropylenes
PPE	Polyphenylene ether
PS	Polystyrene
PVC	Polyvinyl chloride
SAN	Poly(styrene-co-acrylonitrile)
SBM	Triblock copolymer of polystyrene (PS), PBD, and PMMA

SBR	Styrene/butadiene rubbers
SBS and SIS	Thermoplastic elastomers of block copolymers
SEBS	PS-b-EB-b-PS

References

1. Hsieh HL (1998) Chapter 2: Applications of anionic polymerization research. In: Quirk RP (ed) Industrial applications of anionic polymerization: an introduction. American Chemical Society, Washington, DC, p 28
2. Baskaran D (2003) Strategic developments in living anionic polymerization of alkyl (meth) acrylates. Prog Polym Sci 28:521
3. Baskaran D, Müller AHE (2010) Chapter 1: Controlled and living polymerizations: from mechanisms to applications. In: Matyjaszewski K, Müller AHE (eds) Anionic vinyl polymerization. Wiley-VCH, Weinheim
4. Nishikawa M (1998) Chapter 14: Applications of anionic polymerization research. In: Quirk RP (ed) New isoprene polymers, vol 696, ACS symposium series. American Chemical Society, Washington, DC, p 186
5. Jérôme R, Teyssié R (1990) Anionic polymerization of (Meth)acrylic monomers. 4. Effect of lithium salts as ligands on the "living" polymerization of methyl methacrylate using monofunctional initiators. Macromolecules 23:2618
6. Hatada K, Ute K, Kitayama T, Okamoto Y (1985) Preparation of highly isotactic poly(methyl methacrylate) of low polydispersity. Polym J 17:977
7. Kitayama T, Masuda T, Hatada K (1988) Highly syndiotactic poly(methyl methacrylate) with narrow molecular weight distribution formed by tert-butyllithium-trialkylaluminium in toluene. Polym Bull 20:505
8. Schlaad H, Schmitt B, Müller B (1998) Mechanism of anionic polymerization of (Meth) acrylates in the presence of aluminum alkyls. 5. Effect of lewis bases on kinetics and molecular weight distributions. Macromolecules 31:573
9. Ballard DGH, Haddleton DM, Twose DL (1992) Controlled polymerization of methyl methacrylate using lithium aluminum alkyls. Macromolecules 25:5907
10. Hatada K, Kitayama T (2000) Structurally controlled polymerizations of methacrylates and acrylates. Polym Int 49:11
11. Ihara E, Yasuda H (1993) Living polymerization of alkyl acrylates catalyzed by organolanthanide complexes. Kidorui 22:128
12. Naohiko U, Kenichi H, MASAJI K, Tomohiro O, Sachie Y, Kazushige I (1999) Preparation process of acrylic acid ester polymer. EP0945470 (A1), 29 Aug 1999
13. Kenichi H, Kazushige I, Masaji K, Sachie Y (2001) Anionic polymerization process, and process for producing a polymer by the anionic polymerization process. EP1078942 (A1), 28 Feb 2001
14. Tabuchi K, Kitayama T, Hatada K (2002) Living polymerization of primary alkyl acrylates with t-butyllithium/bulky aluminum Lewis acids. Polymer 43:7185
15. Janata M, Dybal J, Müller AHE (1992) A new flow tube reactor for kinetic studies of fast chemical reactions. Makromol Chem 193:101
16. Hofe T, Mauer A, Müller AHE (1998) GIT Labor Fachzeitschrift 42:1127
17. Kenichi H, Kazushige I, Toru T, Sachie Y, Makoto A, Tomohiro O, Kenji S (2001) Process for polymerizing a methacrylic ester or an acrylic ester. EP1085029 (A1), 21 Mar 2001

18. Qing-Ye Z, Zhang Bang-Hua, He Bing-Lin (1996) Compatibilizing effect of poly(hydrogenated) butadiene-methyl methacrylate) copolymer for PVC/LLDPE blends. Eur Polym J 32:1145

19. Kenji S, Kenichi H, Susumu T, Kazunari I, Kazuhiko M (2001) 熱可塑性樹脂組成物(Thermoplastic resin composition). JP2001294712 (A), 23 Oct 2001

20. Ruckdäschel H, Altstädt V, Rettig C, Müller AHE (2006) Polymer 47:2772

21. Koji K, Kenichi H, Makoto A, Kazushige I (2000) Block copolymer and polymer composition comprising the same. EP0970979 (A1), 12 Jan 2000

22. Tong JD, Jérôme R (2000) Macromolecules 33:470

23. Kobukata S, Kurihara T (2007) A TEM Study on highly ordered structure of the acrylic thermoplastic elastomer. 16th Polymer material forum. 116 1PD 27

24. Kurihara T, Morishita Y, Hamada K (2005) A novel (meth)acrylic block copolymers, synthesis, characteristics, and applications. International rubber conference. Pacifico Yokohama exhibition center, Yokohama, 26-G1-07

25. Oertel J, Kishii S (2010) TPE Magazine 1:34

26. Toyoaki K, Kenichi H, Kazunari I, Shiro K (2006) Flameretardant acrylic polymer composition. JP2006045418 (A), 16 Feb 2006

27. Oshima H, Kurihara T (2011) Thermoplastic polymer compositions and sheetshaped moldings made therefrom. EP2345698 (A1), 20 July 2011

28. Hamada K, Morishita Y, Ishiura K (2007) Characteristics and application of novel acrylic block copolymers. The annual meeting of the Adhesion Society 30th. The Westin Tampa Harbour Island, Tampa Bay, p 307

The Critical Role of Anionic Polymerization for Advances in the Physics of Polyolefins

David J. Lohse

Abstract This chapter shows how the great power and versatility of anionic polymerization, which has been described in the rest of this book, has been used to develop an improved understanding of the basic physical principles that underlie the performance of polyolefin materials. When these synthetic tools are employed to polymerize dienes and are then combined with controlled saturation methods, a wide panoply of saturated hydrocarbon polymers can be made. These products can serve as models for commercial polyolefins, which is the most widely used class of synthetic polymers and which continues to develop at a strong pace. The ability to make such models with highly controlled chain architectures, plus the ability to label the molecules for use in techniques such as NMR and neutron scattering, has provided polymer physicists with means to understand polyolefin physics at a deep level. This has been used to determine the size of polyolefin chains (both in dilute solution and in melt state), the ways that polyolefins mix, how their rheology depends on the chemical structure of the chains, and how long branches control their performance. This chapter covers not only the scientific results of this research, but also how these can be applied in the development of novel, useful polyolefin products.

Keywords Polyolefins • Chain dimensions • Packing length • Blends • Thermodynamics • Miscibility • Rheology • Entanglements • Long-chain branching • Polyethylene • Polypropylene • Applications

1 Importance of Polyolefins

Polyolefins, such as polyethylene (PE), polyisobutylene (PIB), and polypropylene (PP), are by far the largest class of synthetic polymers. More than 100 million metric tons are produced each year worldwide [1]. These materials have enjoyed such great success because of a fortuitous combination of useful properties, among

D.J. Lohse (✉)
ExxonMobil Research & Engineering Co. (retired), 300 East 71st Street, #7M, New York, NY 10021, USA
e-mail: davidjlohse@gmail.com

which are relatively low density, low cost of production, high strength, high chemical resistance, and low dielectric constant and losses. A wide range of mechanical properties are possible through the use of copolymerization, blending, and additives to make products from elastomers to thermoplastics to high strength fibers. Although they were first produced in the 1930s, important advances are still being made in improving the process and performance of these materials and their use is growing at a rate well above the GDP. Several factors have been principally responsible for the great success that polyolefins have enjoyed: an abundant supply of cheap and simple monomers; advances in reactor engineering and catalysis; and the ability to compound these polymers with fillers and other polymers. The combination of all of these factors has led to the enormous number of ways in which polyolefins are now being used to improve our lives.

In general polyolefins are defined as polymers made from olefins, which are principally ethylene and propylene, but also 1-butene, 1-hexene, 1-octene, isobutylene, and other monomers. These are thus fully saturated hydrocarbon molecules (i.e., much less than one double bond per molecule), which is the fundamental basis of their properties. The density of all amorphous polyolefins (at 25 °C) is about 0.855 g/cc (the exception being polyisobutylene at 0.917 g/cc), and the density of a crystalline phase is never more than 1.00 g/cc. This means that a polyolefin will nearly always be lighter in weight for a given application than any alternative material. Because they are fully saturated, their interactions are dominated by dispersive, van der Waals forces. As a result, they have a high degree of chemical resistance to many of the solvents and liquids encountered in use. The lack of double bonds means that they are low in reactivity, and so are highly stable to oxidation. These general properties explain much of the usefulness of polyolefins.

The great interest in polyolefins has two sources. One is simply the practical importance of these ubiquitous materials, so methods to improve their performance will clearly be highly beneficial to society. The other is scientific, in that polyolefins can serve as models for the polymer systems in general. The wealth of data on properties such as their mutual miscibility provides a test for various theories of polymer physics. Since the interactions between the chains are dispersive, van der Waals forces, the influence of chemical architecture can be seen much more clearly for polyolefins than for other macromolecules. For instance, mutual solubility of polyolefins turns out to be highly dependent on the details of the chemical architecture of the polymer chains, especially the degree, length, and location of side groups. Polyolefins are also the class of polymers that most commonly exhibit long-chain branching, so the understanding achieved for their branching can help develop improved performance in other systems. The strong influence of chain architecture on the characteristics of saturated hydrocarbon polymers gives us not only a way to probe the predictive power of various theories, but also to design new materials from an understanding of the intrinsic properties of these polymers.

There is thus a well-founded interest in developing a deep understanding of the relations between the chemical structures of saturated hydrocarbon chains and the properties of the materials made from them. The quality of these relations and the confidence one can have in them depends strongly on the depth of understanding of

the structure of these polymers, and so synthetic means to control such architecture precisely are very useful to advance these studies. The original polyolefins made in the 1930s were generally broadly distributed in terms of their molecular characteristics, such as molar mass, tacticity, composition, and branching [2]. The development of coordination catalysts in the 1950s by Ziegler [3, 4] increased the control of chain structure, but rarely to the extent that allowed precise control. Single-site catalysts such as metallocenes and constrained geometry compounds [5–8] have given much better control. But these methods still have significant limitations.

Fortunately, the ability to make well-controlled macromolecules by the anionic polymerization schemes outlined throughout this book, combined with methods to saturate such polymers, has provided ways to make polyolefin-like structures with very precise control. These techniques were pioneered by the group of W. W. Graessley, who discovered methods to fully saturate such polydienes without disturbing the well-controlled architectures made by anionic polymerization [9]. For instance, the saturation of polybutadienes with varying levels of vinyl incorporation of the monomer produces structures equivalent to an ethylene-butene copolymer with corresponding levels of butene [10]. When 2-methyl-1,3 pentadiene is polymerized with 100 % 1,4 incorporation and then hydrogenated, the structure equivalent to an atactic, head-to-tail polypropylene is achieved [11]. Many such polyolefinic architectures can be made by the saturation of polydienes. Moreover, the methods described earlier in this book to make block copolymers and branched polymers with control of the location and length of the branches have proven very useful to develop the basic physics of polyolefins. In the following sections of this chapter, this method will be demonstrated for the sizes of polyolefins chains in the melt, the mixing thermodynamics of polyolefins, the rheology of linear polyolefin chains, and the properties of polyolefins with long branches. Finally, some other areas where the use of these model polymers can further enhance our understanding of polyolefin performance are outlined.

2 Chain Dimensions

2.1 Measurement of Chain Dimensions in the Melt

The chief way in which flexible polymers differ from other chemical substances is that they are so long that, in order to fill the available space, the individual molecules overlap with each other – that is, they entangle [12]. So the measurement of melt chain dimensions becomes critical to furthering our understanding of the state of entanglement. The entangled state is fundamentally responsible for the properties that distinguish polymers from other materials: their extremely slow dynamics (as seen in diffusion and viscosity), the fact that they are generally in a nonequilibrium state (e.g., semi-crystallinity), their mechanical performance (e.g., viscoelasticity), and so on. In fact, a common definition of the transition from

"oligomers" to "polymers" is the molecular weight at which the chains begin to entangle. Thus, in order to see how polymer properties are related to their chemical makeup and so control the performance of polymeric materials, one needs to understand how the state of entanglement is determined by the chemical architecture of the chains.

In recent years, it has become apparent that the entangled nature of polymers is due to the fact that there are two measures of how "large" polymer coils are in the liquid or melt state [13–19]. One of these is just the volume "occupied" by each chain, that is, the total volume divided by the number of molecules. The other is some measure of the extent of the space "pervaded" by the polymer chain. This can be related to the radius of the smallest sphere to totally enclose the chain (called the "span" of the chain) [20], the distance between the chain ends, R, or the radius of gyration of the chain, r_g. For small molecules, such as methane or n-hexane, the occupied and pervaded volumes are same. The advent of small angle neutron scattering in the 1970s confirmed Flory's hypothesis that, when the chains are long enough, the pervaded volume is much larger than the occupied one [21]. The part of the pervaded volume that is not occupied by the chain itself is occupied by other molecules, which gives rise to the state of entanglement (due to the fact that covalent chains cannot cross each other). The ability to relate chain dimensions to chemical structure will then allow one to predict how performance can be derived from the chemistry. This provides the roadmap to realizing the vision expressed by Flory in his text: "*Comprehension of the configurational statistics of chain molecules is indispensable for a rational interpretation and understanding of their properties*" [22].

In 1949, Flory [23] reasoned that chains should have their ideal, random walk dimensions in the bulk because the attractive van der Waals forces would be exactly balanced by the repulsive excluded volume forces. Others contended that there was little overlap of neighboring chains. In order to test the Flory hypothesis, a method to measure the dimensions of long polymer chains in the melt state was required. This was the first problem in polymer physics tackled by small angle neutron scattering (SANS) and the one which first showed its power. Until the advent of SANS, however, there was no way to determine the size of polymer chains in the bulk, because there was no way to distinguish an individual chain from the surrounding "sea" of its neighbors. The need was for a way to label a chain, so that it would stand out from the background of the rest of the polymer, without significantly changing its chemistry. Labeling techniques that work with light or x-ray scattering seriously disrupt the chemistry of the system, leading to phase separation. Use of deuterated polymer, however, provided good contrast without affecting the physical chemistry (see above). This was done first for poly(methyl methacrylate) by Kirste, Kruse, and Schelten, and for polystyrene by Ballard, Wignall, and Schelten [24, 25] in 1978. Experiments on several other systems quickly followed [26–31]. This was also done for model polyolefins, using polydienes that had been saturated with both hydrogen and deuterium [32, 33]. In all cases Flory's hypothesis was proven to be correct; polymer chains in the bulk assumed their ideal random walk dimensions. The dimensions of the chains were

the same in the bulk as in a theta solution. The establishment of the Flory hypothesis has served as the basis for important developments in the rheology, miscibility, and performance of polyolefins, as will be seen below.

2.2 Chain Dimensions and the Packing Length

There are several ways to describe the chain dimensions of polymer chains. One that has proven to be very useful for understanding many polymer properties is the so-called packing length. This parameter can be derived from a comparison of the occupied and pervaded volumes of a chain, and arises naturally in theories of polymer blend interfaces [34] and block copolymers [35], as well as entanglements and rheology [17]. As this is crucial for understanding some of the properties considered below, the derivation of the packing length will be described in some detail here.

Consider first the occupied volume, V_{occ}, which is simply the volume per polymer molecule. This can be directly determined from the polymer density, ρ, Avogadro's number, N_A, and the molecular weight of the polymer molecule, M:

$$V_{occ} = \frac{M}{\rho N_A} \tag{1}$$

The volume that is pervaded by a polymer chain is related to a measure of the chain size such as its radius of gyration, r_g, or the distance between the chain ends, R. Due to the Flory hypothesis the average of r_g^2 is proportional to M (in the limit of large M):

$$r_g^2 = KM \tag{2}$$

The value of K depends on temperature and the chemical structure of the polymer, which control factors such as the probability of *trans* and *gauche* rotations of the backbone bonds. Moreover, $R^2 = 6r_g^2$. Since both V_{occ} and r_g^2 are proportional to M, their ratio is a parameter independent of molecular weight and thus is a constant characteristic of the chemical structure of the polymer at a given temperature. This is called the packing length, l_p:

$$l_p = \frac{V_{occ}}{r_g^2} = \frac{M}{r_g^2 \rho N_A} \tag{3}$$

The packing length is directly related to the statistical segment length of a polymer, b, defined by $R = nb^2$ where n is the number of monomer repeat units [22]. This quantity is also related to the size of the chain and is given by

$$b^2 = \frac{R}{n} = 6r_g^2\frac{m_0}{M} = \frac{6r_g^2 N_A \rho v_0}{M} = \frac{6v_0}{l_p} \tag{4}$$

where m_0 is the molecular weight of a monomer repeat unit, and v_0 its volume. Note that the definition of b requires the specification of a repeat unit, which is often problematic, especially for copolymers. Moreover, when comparing a number of different polymers, one needs to define a constant value of v_0 as a reference volume, meaning that it will be arbitrary, and may have no relation to the structure of the polymers. Because of this arbitrariness, the packing length formulation is more straightforward and more closely related to the actually measured parameters than is one using the statistical segment length. Another parameter often used to show how much larger the chain dimensions are than those expected from an unrestricted random walk model ($R_{rw} = [M/m_o]l_o^2$) is the characteristic ratio, C_∞ [22] which is given by

$$C_\infty = \frac{R^2}{R_{rw}^2} = \frac{6r_g^2 m_0}{M l_0^2} = \frac{6m_0}{l_p l_o^2 \rho N_A} \tag{5}$$

Here l_0 is the length of the repeat unit bond (0.154 nm for C-C single bonds). This can be very useful in comparing various polymers, as will be seen in the next section.

2.3 Models of Chain Dimensions

In the following sections it will be shown that several properties of polyolefins correlate strongly with chain dimensions, and a rationale for this will be given. While the melt chain dimensions for many polyolefins have been measured by neutron scattering, the ability to predict performance becomes all the more useful if ways to estimate the sizes of polyolefin molecules can be found, especially for those that have not yet been synthesized. This is especially true since SANS generally requires access to deuterated polymers and a neutron source. Estimates of the bulk melt dimensions are sometimes possible from dilute solution, theta-state values, but this only gives a qualitative idea of chain size, and not a numerical value [17]. One method that often works to calculate polymer dimensions from first principles is the rotational isomeric state model [22], but for many polyolefins this has given results at odds with experiment [17]. A promising new correlation of polyolefin chain dimensions with chemical structure has recently been found [36], and this is described in the rest of this section.

This correlation comes from an observation of how the dimensions of chains depend on a simple feature of the chemical architecture, which is m_b, the molecular weight per backbone bond [37]. In Fig. 1 l_p is plotted *vs.* m_b at 190 °C for a wide range of polyolefins. While there is not yet a clear physical model for these
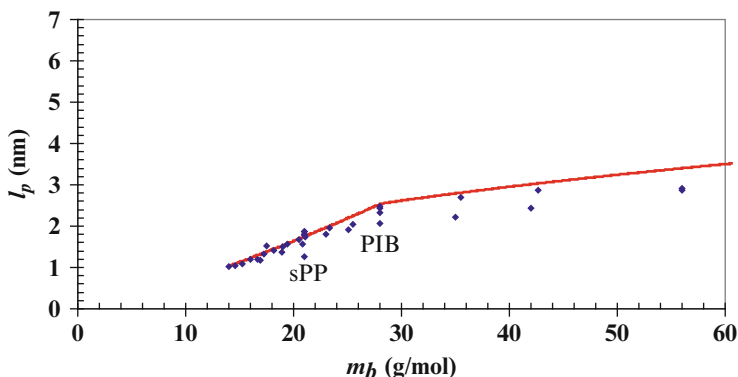
Fig. 1 Dependence of l_p on m_b at 190 °C. Solid line is from Eq. 6

relations, it has been found that the dimensions of most polyolefin chains obey the following relations with m_b at 190 °C (for l_p in units of nm):

$$l_p = 0.0333m_b^{1.30} \quad 14 \text{ g/mol} < m_b < 28 \text{ g/mol} \tag{6a}$$

$$l_p = 0.627m_b^{0.42} \quad m_b > 28 \text{ g/mol} \tag{6b}$$

Of course, the values of l_p depend on temperature, but this dependence is fairly small and of secondary importance to that on m_b. Moreover, the temperature dependence of l_p is quite similar for most polyolefins, so the relative rankings are fairly consistent at all temperatures. Therefore Eq. 6 satisfies the main objective of a reasonable estimate of l_p for most polyolefins in the melt. The clearest outlier is syndiotactic polypropylene (sPP), which is known to have large chain dimensions due to a preponderance of *trans* rotations [37].

The variation of l_p with m_b is mostly due to changes in the "thickness" of the chain (i.e., how much of the chain is in the side branches instead of in the backbone), but also is partly a result of differences in chain stiffness (i.e., the tendency for *trans vs. gauche* rotations). A good way to separate out the effects of stiffness is to look at how C_∞ depends on m_b. This is shown in Fig. 2, and from Eqs. 5 and 6 one can derive, at 190 °C:

$$C_\infty = 16.1m_b^{-0.30} \quad 14 \text{ g/mol} < m_b < 28 \text{ g/mol} \tag{7a}$$

$$C_\infty = 0.859m_b^{0.58} \quad m_b > 28 \text{ g/mol} \tag{7b}$$

Another representation of this is to plot C_∞ *vs. f*, the fraction of carbons that are in the backbone. For polyolefins f is simply given by $14/m_b$. This gives the corresponding dependence of C_∞ depending on f, which is shown in Fig. 3:

$$C_\infty = 7.29 f^{0.30} \quad 0.5 < f < 1.0 \tag{8a}$$

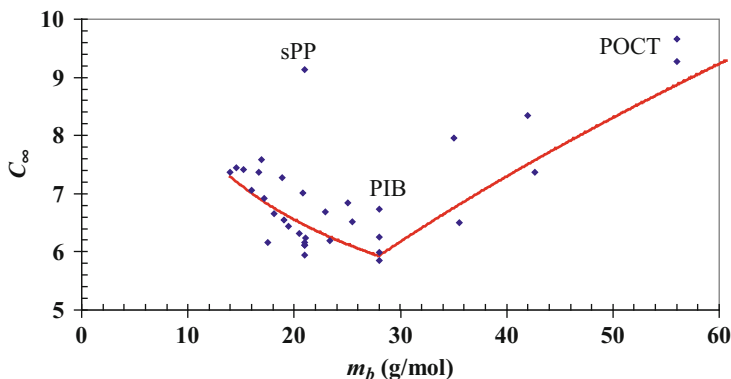$$C_\infty = 4.14 f^{-0.58} \quad f < 0.5 \tag{8b}$$

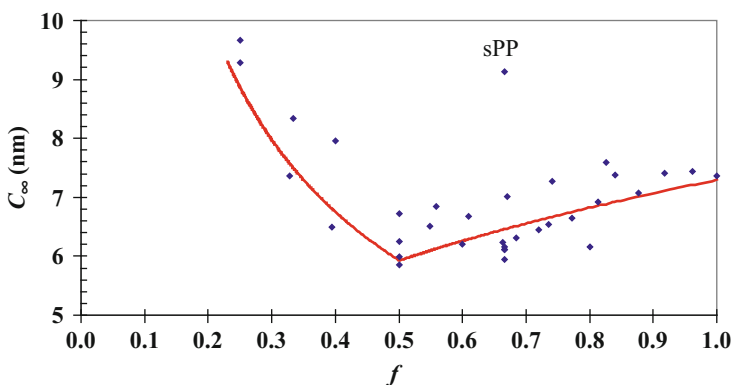**Fig. 2** Dependence of C_∞ on m_b at 190 °C. Solid line is from Eq. 7

Fig. 3 Dependence of C_∞ on f at 190 °C. Solid line is from Eq. 8

In Fig. 3, one can see that C_∞ reaches a minimum of about 5.9 at $f = \frac{1}{2}$, that is, when half of the polymer is in the backbone and half is in the branches. This applies to both atactic polybutene, with an ethyl branch for every two backbone carbons, and an ethylene-octene copolymer with 33 mol% octene, with a hexyl branch for every six backbone carbons. One might speculate that this is the point at which the presence of the branches is most effective at changing the bond rotations of the backbone, that is, at increasing the proportion of *gauche* rotations. For $f > \frac{1}{2}$, there are significant long stretches of methylene segments that will favor *trans* rotations. For $f < \frac{1}{2}$, the branches are longer than the spacing between them, and so the chain cannot twist enough to avoid eclipsing of the branches with each other. However, it would be good to put this empirical observation on a firmer foundation of understanding. Moreover, it is important to point out the exceptions to this rule, such as syndiotactic polypropylene (sPP) and polyisobutylene (PIB), as the utility of such materials depends on their special values of chain dimensions. However, the

relations shown in Eqs. 6, 7, and 8 can be used to give a rough estimate of the dimensions of most polyolefins, and so an estimate of their melt properties.

3 Miscibility

3.1 Polyolefin Blends Thermodynamics

About one third of all polyolefin materials are produced and used as blends of several different polyolefins. In some cases these are blended in the melt, after polymerization, while often the products made in polymerization reactors are blends because of the presence of multiple catalyst species or multiple reactor environments. For all of these blends, the state of miscibility is critically important to their use. The last 30 years have seen a veritable explosion of information about the thermodynamics of polyolefin blends, which has shown that many of those in use today – those with molecular weights and compositions of commercial interest – are near the boundary of miscibility [38]. Blends of polyolefins can have complex phase diagrams, displaying the same gamut of phase behavior as mixtures of monomeric liquids.

An important learning from this work is that the key parameter that differentiates the cohesive and mixing properties of polyolefins is a measure of their chain dimensions in the melt. In the first section below, a summary of the experimental results on polyolefin mixing is provided, and also a description about how these fit into a regular mixing scheme. It will then be shown how polyolefin solubility parameters correlate with chain dimensions, through the packing length. The third section describes why one might expect the cohesive energy of a polymer would depend on the chain size, and how this compares with a prediction of Schweizer and Singh from a PRISM model [39].

3.2 Summary of Polyolefin Miscibility Data

The wealth of data on polyolefin blends that has been generated over the last several years has been compiled in a number of reviews [38, 40]. One of the most interesting features of polyolefin miscibility that has been discovered in this work is the great range of phase behavior shown by these systems. Most polyolefin blends display UCST (upper critical solution temperature) phase diagrams with phase separation occurring upon cooling, but many are characterized by LCST (lower critical solution temperature) behavior by phase separating when heated. Some show both an LCST and a UCST. This great diversity in phase behavior may be regarded as surprising from saturated hydrocarbon polymers that interact only through dispersive, van der Waals forces.

The second interesting feature is that the great majority of these data can be explained by regular solution theory [41]. This is based on the model of Hildebrand that the enthalpic part of the free energy of mixing two substances can be derived in a simple way from the cohesive energies of each substance. The expression for this is shown in Eq. 11, which relates the interaction energy density of the mixture to the solubility parameters of the components. It does not always work – for example, some blends, especially those involving polyisobutylene [42], show negative values of the interaction energy density, which is impossible to rectify with regular solution theory. Nevertheless, regular solution theory does describe the miscibility data of around 90 % of the blends, and for most of the irregular ones the difference of the data from the regular solution predictions can be used to characterize the anomalies [43]. So the understanding of the origins of polyolefin solubility parameters provides a basis for understanding polyolefin miscibility.

The most critical set of information for polyolefin solubility parameters has been the direct measure of miscible blend interaction energies from SANS [44–55]. Important contributions have also come from determinations of phase diagrams by nuclear reaction analysis (NRA) [56, 57], light scattering [58–61], thermal analysis [62], and NMR [63, 64]. Model polyolefins made by saturating anionically polymerized polydienes were crucial for most of this work. SANS, NMR, and NRA are techniques that depend on deuterium labeling; the fact that polydienes can be saturated using either deuterium or hydrogen, giving labeled and unlabeled polymers that are identical (save for the label) makes these techniques work well. The thermal analysis work used block copolymers that also relied on the combination of anionic polymerization and saturation. Measurements of the dependence of specific volume on temperature and pressure (*PVT*) properties of polyolefins [65, 66] have provided data on their internal pressure, which is directly related to cohesive energy.

A large number of polyolefin solubility parameters have now been derived from neutron scattering and compiled [67]. Some of these values are shown in Table 1. These are polyolefins for which there are direct measures of density, melt chain dimensions [68], and solubility parameters derived from interaction energies measured on polyolefin blends by small angle neutron scattering. A significant hurdle in developing the solubility parameter model of polyolefin miscibility is that the cohesive energies of the polymers cannot be directly measured [41]. However, the solubility parameter values in Table 1 have been corroborated by measurements of the internal pressure of pure polyolefin components, which have been determined from *PVT* data. The reader is directed to reference 38 (Chap. 8, Sect. II.D therein) for a fuller discussion of the relation of internal pressure to cohesive energy density, but it is worthwhile to point out that this relation for polyolefins is very similar to that seen for low molecular weight alkanes [69] for which both cohesive energy density and internal pressure can be directly measured. There is thus a great deal of confidence in these numbers, and as will be shown below, they can be used to predict the miscibility of polyolefin blends quite well.

It is well known that a chief distinguishing feature of polymer blends is that the entropy of mixing is very small, due to the large size of macromolecules [70]. This

Table 1 Solubility parameters for selected polyolefin δ, in units of MPa$^{1/2}$

			T (°C)		
Polymer	27	51	83	121	167
HPI-75	18.00	17.59	16.91	16.53	15.70
EB97	18.17	17.76	17.08	16.69	15.86
EB88	18.40	17.98	17.29	16.89	16.04
a-PP	18.39	17.98	17.33	16.95	16.11
EB78	18.66	18.24	17.54	17.13	16.27
HPI-50	18.68	18.26	17.56	17.14	16.29
EB66	18.90	18.48	17.77	17.35	16.48
alt-PEB	18.89	18.48	17.79	17.38	16.52
HHPP	18.99	18.55	17.84	17.41	16.53
EB52	19.18	18.74	18.03	17.60	16.72
alt-PEP	19.09	18.67	17.98	17.58	16.74
EB38		18.96	18.24	17.80	16.91
EB35		18.98	18.25	17.82	16.93
EB32		19.10	18.36	17.91	17.01
EB25			18.45	18.00	17.09
EB17				18.06	17.16
EB08				18.23	17.29

Name	Description
alt-PEB	Essentially alternating poly(ethylene-co-1-butene)
alt-PEP	Essentially alternating poly(ethylene-co-propylene)
a-PP	Atactic polypropylene
EBx	Ethylene-butene random copolymer with x mole percent butene incorporation
HHPP	Head-to-head polypropylene; HPDMBd-100
HPI-x	Hydrogenated polyisoprene, x = 3.4 content of parent polyisoprene

can be seen in the Flory-Huggins-Staverman [71–73] expression for the free energy of mixing ΔG_m:

$$\Delta G_\mathrm{m} = RT\left\{\frac{\phi_1\rho_1}{M_1}\ln\phi_1 + \frac{\phi_2\rho_2}{M_2}\ln\phi_2\right\} + X_{12}\phi_1\phi_2 \tag{9}$$

where R is the gas constant, ρ_i is the density of polymer i, ϕ_i is the volume fraction of component i, and X_{12} is the interaction energy density between the two polymers. The interaction energy density is directly related to the more commonly used Flory interaction parameter, χ_{12}, by the relation:

$$X_{12} = \frac{\chi_{12}}{v_0}RT \tag{10}$$

where v_0 is a reference volume to normalize the value of χ_{12}. When comparing the interactions for many different blends, the choice of v_0 becomes arbitrary. To avoid confusion when comparing so many polymers and blends, herein the interaction energy density formulation of Eq. 9 will be used.

The power of regular solution theory is that it provides a way to predict miscibility in blends from parameters that are determined for the individual components. This basic parameter is the so-called solubility parameter for polymer i, δ_i, which is just the square root of the cohesive energy density of the polymer [41]. The cohesive energy is that which holds the molecules of a substance together in the condensed (liquid) state, and so is given by the heat of vaporization [69]. Obviously, this cannot be directly determined for most polymers, since they degrade at temperatures well below those at which they would boil. However, one can get reasonable estimates of δ_i from PVT measurements and values can also be derived by redundancy from a large set of measured values for X_{12} when the number of blends is significantly greater than the number of component polymers [38]. One caution for the reader is that the values of δ_i from group contribution schemes do not work for polyolefins, as explained in Ref. [38].

Given the values of solubility parameters, it is quite simple to estimate the interaction energy density, since:

$$X_{12} = (\delta_1 - \delta_2)^2 \tag{11}$$

On the other hand, by measuring X_{12} for many pairs of polymers, one can extract values of δ_i for the components, given the value for just one of them. [Herein, the reference value is taken to be that for atactic polybutene, determined from PVT evaluation of internal pressure.] Such an assignment becomes more well founded, the greater the number of blends measured, and the greater the redundancy of assigning solubility parameters. The values for the 17 polymers in Table 1 come from measuring X_{12} for 42 blends over a range of temperatures. These values have been shown to work well in explaining the mixing behavior for a number of polyolefin blend systems [74–77]. Note that the derivation of δ's from X_{12} needs to be performed at each temperature separately. Cohesive energy density, and so δ, generally decreases as T increases, but at different rates for different polymers. This is the reason that, even under regular solution theory, all kinds of phase behavior (LCST and UCST) can be seen.

3.3 Dependence of Polyolefin Solubility Parameters on Packing Length

In Fig. 4, the values of δ are plotted vs. l_p for a number of polyolefins at several temperatures, showing that there is a clear correlation of solubility parameter with chain dimensions. This correlation of polyolefin miscibility with their chain
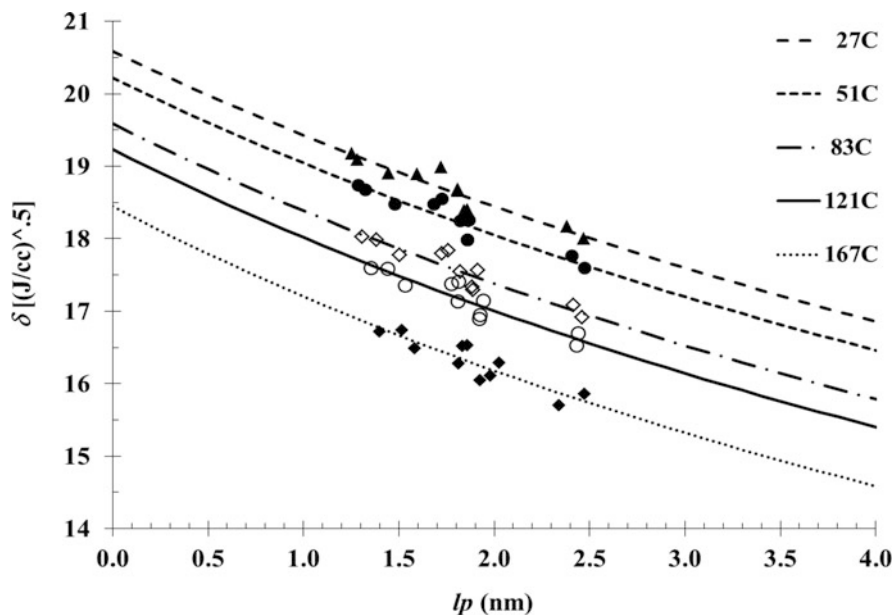
Fig. 4 Solubility parameters of polyolefins versus packing length

dimensions has been noted by several authors [38, 78], but the explanations for this have been quite different. Fredrickson, Liu, and Bates [79] have developed a theory of mixing based on the idea that a mismatch in component values of l_p or b will lead to a loss of configurational entropy upon mixing. This is a different explanation for polyolefin miscibility than the one described herein [38] based on solubility parameters, which emphasizes local enthalpic contributions to the free energy of mixing. How does one distinguish between entropic and enthalpic contributions to the interactions controlling miscibility? Since the solubility parameters for different polyolefins decrease with temperature at different rates (see Table 1), the difference between any two of them and so X can have any sort of dependence on T, simply due to enthalpic interactions. It is thus not possible to separate "enthalpic" and "entropic" contributions to X simply from its temperature dependence.

There are now several pieces of evidence that indicate rather conclusively that the enthalpic contribution dominates in the case of polyolefin blends. First, the dependence of the values of δ derived from SANS on branching structure for high molecular weight polyolefins closely parallels that for the solubility parameters for saturated hydrocarbons of low molecular weight derived from their heats of vaporization [41]. For example, whether considering the cohesive energy data for a series of C_8 alkanes [69] or the SANS-based solubility parameters for the corresponding polymers, it is clear that the normal, linear molecules have the highest values of δ, and that the longer and more frequent the branching, the lower these values become. Even effects associated with details of the branch architecture, such as higher values for molecules with methyls on adjacent carbons rather than on alternating

ones, are reproduced with C_8 analogs. The C_8 alkanes do not have the configurational entropy characteristic of the polymers, so the distinctions within both groups are most likely due to enthalpic effects.

Second, Maranas et al. [80] have simulated the cohesive energy densities of a number of polyolefins with interactions based solely on enthalpic interactions. These results agree very well with the values determined from neutron scattering or *PVT* experiments. Finally, the impact of deuterium labeling on miscibility has also been well explained as due to enthalpy. Bates et al. [81] noted that deuterium substitution changes the polarizability of a molecule or repeat unit, and so affects its cohesive energy. Their enthalpy-based model quantitatively explains the effect of deuteration on interaction strength, so there is no need in that case to invoke configurational entropy arguments. So the circumstantial case for an enthalpic origin of the cohesive energy of polyolefins is strong.

But why should the chain dimensions of polyolefins determine the enthalpy of their interactions? In a qualitative sense, this has to do with the degree to which the nonbonded neighbors of a monomer or repeat unit are from the same or different molecules. The overall number of van der Waals interactions per unit volume in a polyolefin melt does not depend very much on the chemical architecture of that chain, since the densities of nearly every polyolefin is about the same as that of all the others. However, the more tightly the polymer is coiled (at a given molecular weight), the more likely it is that a nearest neighbor is from another monomer on the same chain, and not from another molecule. The van der Waals, nonbonded interactions between such intramolecular monomers will not contribute to cohesive energy. Monomers on more open coils will have larger fraction of close neighbors from other molecules, which increases its cohesive energy density.

This argument has been made quantitative in the PRISM theory of Schwiezer and Singh [39]. This is based on a theory of liquids that has been successfully applied to many polymer problems. The chains are modeled as "threads" with variable thickness that can be related to l_p. A quite simple expression for the dependence of δ on temperature and chain dimensions comes from this model:

$$\delta = \frac{\rho N_A}{m_0} \left[\frac{2\pi\varepsilon a^3}{\left(1 + \frac{l_p}{2\pi a}\right)} \right]^{1/2} \qquad (12)$$

In Eq. 12, a and ε are parameters that represent the length and energy scales, respectively, of the interactions between the polymers. To examine how well Eq. 12 works, the experimental data in Fig. 4 are plotted as (δ/ρ) *vs.* l_p in Fig. 5. The fit to Eq. 12 is excellent and gives $a = 0.80$ nm and $\varepsilon = 6.53 \times 10^{-4}$ eV, or $\varepsilon/k = 7.6$ K (taking $m_0 = 14$ g/mol for a methylene unit), which are reasonable values for the van der Waals potential typical of polyolefin blends. The power of Eq. 12 is that it allows the prediction of polyolefin miscibility from simply knowing chain dimensions. Even when these have not (or cannot) be measured directly by a method such as neutron scattering, a way to estimate the chain dimensions (say, by a simulation or a relation such as Eq. 6) can thus lead to a well-founded prediction of the cohesive energy of that polymer and so its miscibility with other polyolefins.

Fig. 5 Plot of δ vs. l_p for polyolefins. Solid line is the fit from Eq. 12 with $a = 0.80$ nm and $\varepsilon/k = 7.6$ K
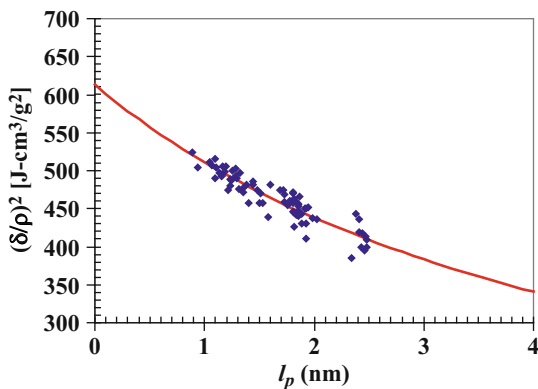
3.4 Applications of Polyolefin Blend Thermodynamics

A broad range of polyolefin blends are used commercially, both in the homogeneous state and as multiphase materials. The ability of a particular blend to perform well in a given application depends on whether the melt is phase separated. It can be shown from the results summarized above that many commercial blend systems are near a phase boundary at the molecular weights and compositions used. In this final section the utility of predictions of miscibility in polyolefin blends is shown by applying the solubility parameter data to two cases taken from the recent literature.

Bensason et al. [74] have studied blends of an ethylene-octene copolymer (EO) containing 14.6 mole % octene with three other EO copolymers of lower octene content. All of the EO copolymers had approximately the same molecular weight. Using the solubility parameters given in Table 1 to estimate the interaction strength for these EO blends, and then using Eq. 9 allows one to estimate which of these will be miscible at the melt temperature. This procedure predicts that only an EO with 8.5 mole % octene would be miscible in the melt with the 14.6 % EO; the blends of the other two with the high octene copolymer are predicted to be phase separated. This is exactly what Bensason et al. observed using thermal and mechanical analysis of the blends. The solubility parameter data also do a good job of describing and predicting phase behavior in many other blends containing ethylene copolymers. Analysis of this type supports the conclusion that many linear ethylene copolymer blend systems, whether they contain many components because of deliberate blending or because of the use of multi-site catalysts, are at or near phase separation.

The second example involves blends of PP with various copolymers of ethylene with either butene (EB) or hexene (EH). Yamaguchi et al. [75, 82–84] have investigated the rheological and mechanical properties of several of these blends, and found remarkable differences based on comonomer content. Using the solubility parameter and regular mixing ideas in the way described above, one can predict that at $M \sim 100$ kg/mol, EB copolymers require at least 58 mol % butene, and EH copolymers require at least 47 mol % hexene, to be miscible with PP. This agrees quite well with the observations made by Yamaguchi, in that a 45 % butene EB was

immiscible with PP, but a 62 % butane EB was miscible. Similar agreement holds for the EH/PP blends.

Many of the PP blends that have been examined showed irregular mixing effects [43], and it may be that irregularity also played a role in this second example. However, both of the examples above clearly show that the regular mixing ideas, combined with reliable data on how these depend on polymer architecture, can provide useful guidance in the development polyolefin blends. The miscibility of saturated hydrocarbon polymers (polyolefins) has been shown to be essentially controlled by the values of their solubility parameters as determined from SANS or *PVT* measurements. Moreover, these solubility parameters can be derived from a knowledge of the chain dimensions of the chains, which is most conveniently expressed through the packing length, l_p. Even when the dimensions are not known directly, they can be estimated for many cases by a correlation of the fraction of carbons that are on side branches *vs*. the backbone. This string of relations thus allows for a very powerful mechanism to predict which polyolefins can mix based simply on their chemical structure.

4 Rheology of Linear Polyolefin Chains

4.1 *Entanglement Density and the Packing Length*

Research on the rheology of linear polymer chains predates the discovery of living anionic polymerization. However, these synthetic techniques have provided the ability to make linear chains with excellent control of molecular weight and its distribution over a very wide range. This facility has been useful in both improving the quality of rheological data and in extending the class of polymers for which such data exist. Once again, this has been particularly important for polyolefins, due to the large number of model polymers that can be made by the saturation of polydienes. In this section the ways that the availability of such models has been useful in understanding the basic melt rheology of linear polymers is outlined, and how this can be applied to develop useful polyolefin materials is shown.

The entanglement molecular weight, M_e, is derived from modeling the entangled state of long, flexible polymers as a physically crosslinked network, on time scales shorter than relaxation time of the entanglements [85]. Experimentally, M_e is found from the measurement of the plateau modulus. The rubbery plateau is much clearer and easier to measure the narrower molecular weight distribution, so the availability of nearly monodisperse polymers from anionic polymerization has been invaluable in extending the range of polymers for which there are good data on the plateau modulus. Several authors [13–19] have developed successful models that relate M_e to chain dimensions. The relevant result is that M_e can be related to the packing length and density, and is in fact proportional to $\rho l_p{}^3$. The coefficient of proportionality is independent of polymer type and temperature. This has now been shown

to hold for a wide range of flexible polymers, including polydienes, polyolefins, styrenic polymers, acrylics, and even polymeric sulfur [67]:

$$M_e = 1.98 N_A \rho l_p^3 \tag{13}$$

If one uses ρ in units of kg/m^3, l_p in nm, and M_e in g/mol, then $M_e = 1.19 \rho l_p^3$. Since the relation between M_e and the plateau modulus is defined [86] as $M_e \equiv \rho RT/G_N^0$, for the packing length model this means that

$$G_N^0 = \frac{kT}{1.98 l_p^3} \tag{14}$$

Here k is Boltzmann's constant with T in units of K, l_p in nm, and G_N^0 in kPa, $G_N^0 = 6.97 T/l_p^3$. The utility of such a simple expression for a fundamental property like plateau modulus is clear, as will be demonstrated below.

There are several other parameters that can be used to describe the state of entanglement for flexible polymers. One of these is the volume per entanglement, V_e, which is the volume occupied by a chain of molecular weight M_e. By Eq. 1 this means

$$V_e = \frac{M_e}{\rho N_A} \tag{15}$$

Combined with Eq. 13 this gives

$$V_e = 1.98 l_p^3 \tag{16}$$

The reptation model of polymer rheology was first discussed by deGennes [87] and fully developed by Doi and Edwards [88]. In this theory the restrictions on the motions of an entangled chain are modeled by confining it to a tube of diameter d_t formed by the surrounding molecules. This is defined by the relation

$$\frac{d_t^2}{M_e} = \frac{R^2}{M} \tag{17}$$

From the packing length model [17] one gets

$$d_t = l_p n_t/6 = n_t^{1/3} V_e^{1/3} \tag{18}$$

The numerical coefficient in Eq. 18, n_t, is the number of chain segments [14] of molecular weight M_e that can be found in a cube of edge length d_t. This is a constant for all flexible polymers; from the extensive data that exist [89] on many polymers, this has a value of $n_t = 20.6 \pm 1.8$.

There are good data on the plateau modulus (and thus, on M_e) for over 50 different polyolefins, mostly at several temperatures [67, 89–91]. The ability to make

Fig. 6 Plot of V_e *vs.* l_p^3 for
polyolefins. Solid line is
from Eq. 16
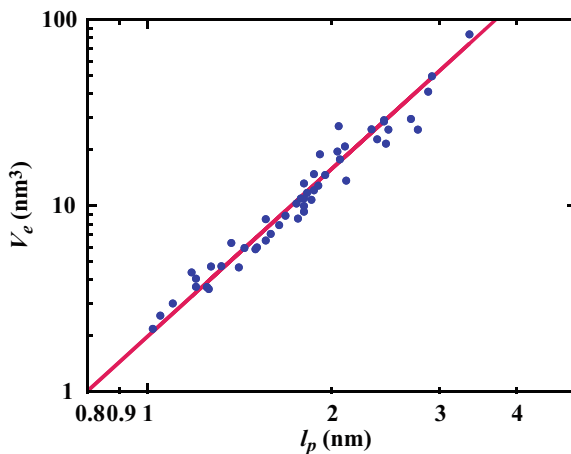
model polyolefins by the saturation of polydienes has greatly increased the amount
of good data for the plateau modulus. This is not only because these polymers are
nearly monodisperse, but also because some of these can only be made by saturat-
ing polydienes. For this reason well-controlled anionic polymerization has been
central to this research. Moreover, as mentioned in the first section, since anionic
polymerization has allowed for labeled versions of these polymers to be made, most
of the data on polyolefin melt dimensions also come from samples made in this
way. It is not an overstatement to say that, without anionic polymerization, there
would not be enough data to derive sound relations entanglement density and chain
dimensions for polyolefins. The data that are available are plotted in Fig. 6 as V_e *vs.*
l_p^3. From the figure, one can see that Eq. 16 (and Eq. 14) works very well to describe
polyolefin rheology over several orders of magnitude in plateau modulus. The
quality of the fit in Fig. 6 is more impressive when one considers that these two
parameters are derived from separate sets of data, l_p from SANS-derived chain
dimensions, and V_e from rheology.

4.2 Other Rheological Properties

Several other rheological properties have also been related to the packing length
[18, 19]. One of these is M_c, the critical molecular weight at which the zero-shear
viscosity of a polymer begins to rapidly increase (generally from a linear depen-
dence on M to a power-law function, usually on the order of $M^{3.4}$) [12]. Here again
anionic polymerization has been very useful. To get a good value for M_c, one needs
not just a single sample of a narrow, entangled polymer, which is all that is needed
for M_e and G_N^0. Rather, what is required is a range of samples covering both the
entangled and unentangled states, on the order of ten (or more) polymers over a
decade or more of molecular weight. So clearly the control of polymerization

provided by anionic techniques is very useful for measuring M_c, and most of these data come from polymers made by such means. An empirical fit to the data that exist on M_c (for about a dozen polymers) gives [18, 19]

$$M_c = M_e \left[l_p^* / l_p \right]^{0.65} \tag{19}$$

In Eq. 19 l_p^* is a constant of value ~ 6 nm. Similarly, Graessley has predicted [92] that at some large value of M, polymer viscosity should show the M^3 dependence expected from the Doi-Edwards model [88]. This phenomenon has been seen for several polymers now [19, 67], and this molecular weight, M_r, is given by

$$M_r = M_e \left[l_p^* / l_p \right]^{3.9} \tag{20}$$

Equations 19 and 20 can be used to estimate these technologically important critical molecular weights to model performance in, for instance, extrusion.

4.3 Applications of Linear Polyolefin Rheology

The success of the packing length model for explaining the degree of entanglement of a polymer can be very useful in the design of new materials. This is because the plateau modulus and M_e are the key to many of the basic performance aspects of polymers, such as processability, adhesive strength, and crystallization kinetics. For instance, this model can be used to explain the effects of tacticity on the plateau modulus of propylene polymers. The observation that syndiotactic polypropylene (sPP) has a much higher value of G_N^0 than isotactic (iPP) or atactic polypropylene (aPP) was first made in the late 1990s [93, 94]. This is due to the significantly larger chain dimensions of sPP [95], which is presumably due to a larger probability of *trans* over *gauche* bond rotations in sPP compared to iPP or aPP. A similar influence of tacticity can also be seen in ethylene-propylene copolymers [96].

It is thus possible to make a good prediction of the plateau modulus for polyolefins even before they have been synthesized, as long as there is a way to make a reasonable estimate of their chain dimensions [22]. This can be a very powerful tool for modeling polymer material performance since the applications where a particular polymer will be useful depend to a large degree on its plateau modulus. For example, the tensile modulus of crosslinked elastomers depends not only on the number of chemical crosslinks (i.e., on the level of curing), but also on the number of entanglements that are trapped by those chemical crosslinks [97]. For this reason, ethylene-propylene elastomers have a higher tensile strength than other rubbers (see Figure 24 and Table VIII in Ref. [97]). On the other hand, for adhesive applications, a low plateau modulus is desired, as captured in the well-known Dahlquist criterion [98]. This states that for a compound to work well as an adhesive, it must have a plateau modulus below 0.3 MPa. Such a low modulus is needed to ensure that the
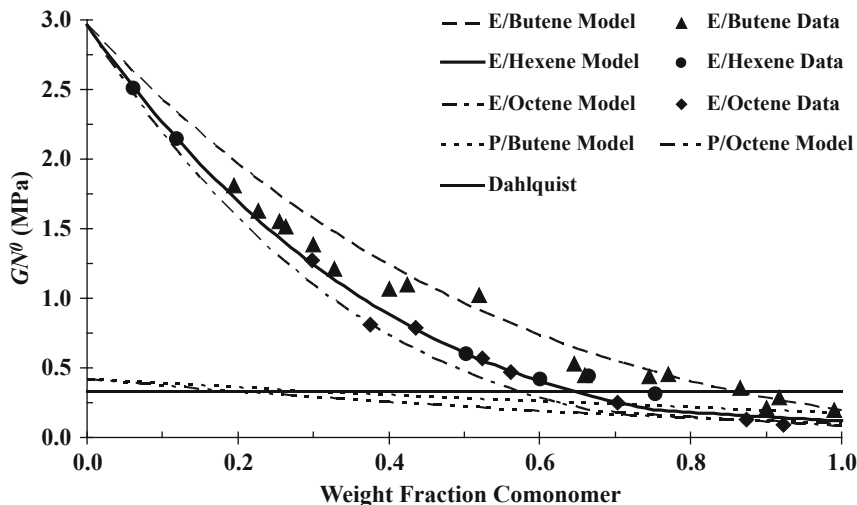
Fig. 7 Plateau moduli of ethylene and propylene copolymers

adhesive will flow over all the asperities on a surface and so provide a large bonding area and good adhesion. These examples show there is a need to provide polyolefins with a wide range of plateau modulus, and the practical benefit of knowing how this is controlled by chemical architecture.

An example is given in Fig. 7 [67], where the predictions of Eqs. 6 and 14 for the plateau moduli of ethylene- and propylene copolymers are shown. For the available data, these descriptions work well (as discussed above). As a class, it is clear that propylene copolymers have a much lower plateau modulus than ethylene copolymers. The influence of the amount and length of the short braches is also apparent. The Dahlquist criterion [98] is also shown in Fig. 7, showing where one might expect good adhesive behavior. It is clear how the kind of information contained in Eqs. 6 and 14, and Fig. 7, can be used to define promising areas in which to explore new product opportunities that depend on rheological performance.

5 Polyolefins and Long-Chain Branching

5.1 LCB in Polyethylene

Even though most polymers are found as linear chains, nonlinear, branched macromolecules are also useful materials. The paramount example of this is polyethylene (PE). The commercial value of long-chain branching (LCB) in polyethylene (PE) has long been known. Even though most of the physical properties (e.g., toughness) of low density PE (LDPE) are generally inferior to those of linear low

density PE (LLDPE), the former still has a large share of the market due to its superior processability. The rheological behavior that leads to this enhanced processability of LDPE is attributed to the presence of long branches [99]. Here "long" means a branch with a molecular weight greater than the entanglement molecular weight, M_e, which is around 1 kg/mol for PE [89]. The demand for improved PE products has driven research on ways to control LCB to optimize both the processability and mechanical performance of these polymers.

Unfortunately, this has proven to be extremely difficult, due to the complex nature of the branching. The effects of LCB depend on many factors: the number of branches per molecule, the lengths of the branches, where the branches are placed along the backbone, and the distribution in each of these parameters. This complexity has required branched model polymers for which the architecture is known from the way they were synthesized. Nearly all of this work has relied upon the anionic polymerization techniques described in this book. The structures have ranged from simple ones, such as three-armed stars, to more sophisticated combs, pom-poms, and dendritic architectures. Methods have also been developed to vary the lengths and placements of the branches with a high degree of control. Much of this work has been on polystyrene [100–104] and polydienes [105–111]. In this section the work that has been done on model polyethylenes made by saturating low-vinyl polybutadienes with many levels and kinds of branching will be described. The application of this to commercial polyethylenes, both in developing novel characterization techniques and in developing new products, is also covered.

LDPE was discovered by Fawcett et al. at ICI in 1933 and became the first form of PE to become commercially viable [2, 112]. Although this was an unintentional consequence of research on general chemical reactions at high pressure, the value of the new material was quickly realized and exploited as, for example, cable insulation for radar in World War II. In the 80 years of its history, its use has grown until its production is now one of the largest of any material in the world.

LDPE is made in a high-pressure free radical process and the polymer molecules are characterized as having a highly branched structure. This branching is believed to come about from two main processes [113, 114]. In the first, a free radical on the growing end of a chain loops back to some other portion of the chain; this loop breaks at the point of reaction, to which the radical is transferred; and the loop then becomes a branch off of the chain, which continues to grow from the reaction point. This backbiting reaction mainly leads to short branches a few repeat units long. Much longer branches are produced from the second mechanism, in which the growing end of a chain terminates on another molecule. Several other mechanisms have also been proposed, and the complete suite of reactions that occur has still not been firmly elucidated. It is clear though, that these result in a very complicated, tree-like architecture with both short-and long-chain branches.

These are called "low-density" polyethylenes in contrast to the higher density, linear versions that were first produced about 20 years later. The reason that the products of the high-pressure process have lower density is that they are lower in crystallinity. Only long methylene sequences can participate in the paraffin-like crystals of PE, so the side branches serve to lower the crystallizability of LDPE.

This effect is mainly due to the short branches (e.g., ethyl, butyl, and hexyl) that arise from the backbiting mechanism, simply because there are many more of these. Since the frequency of such branching can be controlled by various process variables (T, P, initiators), so can the density or crystallinity of the polymers.

LDPE finds application in a wide variety of markets, but its main application is in film. The mechanical properties of the resulting films can be varied by controlling the density and molecular weight of the polymer, but in general they are not as tough as those made from linear polyethylenes without long side branches. On the other hand, these long branches are responsible for the superior ease of processing of LDPE in comparison to its linear counterparts, and this factor has kept it as an important product to this day.

The advent of metallocene and other "single-site" catalysts has renewed interest in LCB for PE and its effects on rheology. There are now many reports of polyethylenes (homopolymers and copolymers) made by such catalysts that clearly exhibit many of the features of long branches [6, 115]. There is evidence for a difference in how the sizes of these polyethylene chains depend on molecular weight compared to linear ones, which can only be due to high levels of branching [116–118]. Spectroscopic data cannot provide direct proof for the presence of branches as long as those of interest here, but do lend indirect support to the formation of long branches [119]. Most importantly, the rheological behavior of these polymers is highly consistent with the presence of LCB, and they do show greater ease of processing than linear PE [99, 120–122]. The mechanisms for the formation of LCB by metallocene and other single-site catalysts are still not completely clear, and probably differ among the various catalysts and polymerization conditions. It is clear, however, that the method of LCB formation is different from that in free radical ethylene polymerization, which means that the nature of the LCB is different as well.

Defining the nature of LCB in a particular polymer sample is both a difficult and complicated task. It is difficult because of the level of branching present in the polymers of most interest is actually quite low. Since the branches (and the spacing between the branch points on the backbone) need to have a molecular weight greater than the entanglement molecular weight of polyethylene, which is about 1 kg/mol, the number of carbons serving as the node of a long branch can be no more than one in a hundred, and is generally much less. Often the signal from such branch points can be masked by a large degree of short branching, such as that due to the incorporation of α-olefins like 1-butene or 1-octene [119]. This makes spectroscopic identification of LCB highly problematic.

The complication in characterization of LCB arises from the fact that many variables are needed to completely specify the nature of LCB in a polymer. The first is the functionality of the branch point – trifunctional, tetrafunctional, or greater. Second, one also has to specify the length of the branch and the separation between branches on the backbone. Then there is the number of branches per backbone. One can also have branches on the branches. Moreover, all of these variables will have some distribution in values, which may or may not be correlated with each other.

Thus, precise description of the LCB in a particular sample is a complicated, daunting task.

It is therefore critical to the development of an understanding of LCB to study polymers with simple, well-characterized structures so that the basic rules of their behavior can be established. This has been done primarily on anionically polymerized materials, both for the ability to make polymers that are nearly monodisperse and also for the availability of various coupling techniques to control the architecture of the polymers made [123]. Model branched PE samples covering a wide range of branching structures have been synthesized using well-defined anionic polymerization methods to make branched polybutadienes of low vinyl content followed by saturation. Much of this sort of work has been done on symmetric stars (i.e., equal arm lengths) [124–126], as well as stars with various arm lengths made by the miktoarm techniques of Hadjichristidis et al. [127–130]. Some model PE polymers with multiple branch points, including some pom-pom structures [131–134], combs [135–139], and dendritic polymers [140–144], have also been studied in this regard. All of them have a local structure identical to an LLDPE with 7 to 10 wt% butene (i.e., 2 to 3 ethyl branches per 100 backbone carbons). So a wide range of structures are now available to help understand branched polyethylenes made by commercial means.

In the rest of this section, the lessons that have been learned from the work on these model polymers are summarized. This falls into two main areas: the development of methods to more accurately characterize the nature of LCB in polyethylenes, with regard to the level, length, and distribution of the branches [130, 145–147], and then showing how these details control the rheological performance of such polymers [148–152]. The latter aspect can be related to the effects of branching on ease of processing them into products such as films or fibers. It is more difficult to understand the impact of the branching on the mechanical performance of such materials, as this relates to the ways that the semi-crystalline morphology develops during formation, and the response of this to the stresses they encounter in use. While there is not yet a full understanding of how LCB impacts the performance and utility of polyethylene products, many advances have been made, some of which are described herein.

5.2 Effects of LCB on Chain Dimensions

One possible way to characterize LCB is to show how chain dimensions vary with the nature of long-chain branching for polyethylene. By taking advantage of the rich ability to make model PE by saturating polybutadienes with low vinyl content, the effects of short-chain branching can be neglected since the frequency of these is the same in all cases. One of the best ways to characterize LCB is to combine size exclusion chromatography (SEC) with multiple angle light scattering [153]. At the same molecular weight, branched chains are more compact than linear ones. This is commonly expressed in terms of the Zimm-Stockmayer model [154–158], which

characterizes the radius of gyration of a branched molecule in terms of that of a linear one of equal total molecular weight:

$$g = \frac{\left\langle r_g^2 \right\rangle_{\text{branched}}}{\left\langle r_g^2 \right\rangle_{\text{linear}}} \tag{21}$$

From the chain dimensions and molecular weight data available for linear hydrogenated polybutadienes [106, 148, 159–161], one can derive an expression for how r_g in the melt depends on $\overline{M}_w$ for linear polyethylene:

$$r_g = 0.0149 \overline{M}_w^{0.612} \tag{22}$$

where r_g is in nm and $\overline{M}_w$ in g/mol. In deriving Eq. 22 only the data for polymers with $\overline{M}_w > 100$ kg/mol were used, so that there is no screening of the excluded volume. This is in very good agreement with other relations for PE in good solvents [99]. Equation 22 allows us to estimate the r_g for a linear polyethylene that can be used to calculate the Zimm-Stockmayer g for a branched polymer using Equation 21.

The basic assumption in the Zimm-Stockmayer calculation is that each linear chain section (i.e., arm, backbone, and connector) has its random walk dimensions. For an A_2B star the predicted value of g is [154, 156]:

$$g^{\text{pred}} = 1 - \frac{6s}{(s+2)^3} \quad [A_2B\text{star}] \tag{23}$$

where $s = M_A/M_B$ is the ratio of molecular weight of the A arm to that of the B arm. The Zimm-Stockmayer prediction for H polymers was first made by Berry and Orofino [156]. The more general expression for pom-pom polymers is [145]:

$$g^{\text{pred}} = \kappa^3 + 3\kappa^2(1-\kappa) + \frac{3}{2}\left(\frac{f+1}{f}\right)\kappa(1-\kappa)^2$$
$$+ \frac{3f-1}{2f^2}(1-\kappa)^3 \quad [\text{pom} - \text{pom}] \tag{24}$$

where κ is the fraction of the polymer in the connector and f is the functionality of the end branch points. The Berry and Orofino expression for combs is [145]:

$$g^{\text{pred}} = \lambda^3 + \frac{(2p+1)}{(p+1)}\lambda^2(1-\lambda) + \frac{p+2}{p}\lambda(1-\lambda)^2$$
$$+ \frac{(3p-2)}{p^2}(1-\lambda)^3 \quad [\text{comb}] \tag{25}$$

where λ is the fraction of the molecule in the backbone and p is the number of arms per comb.
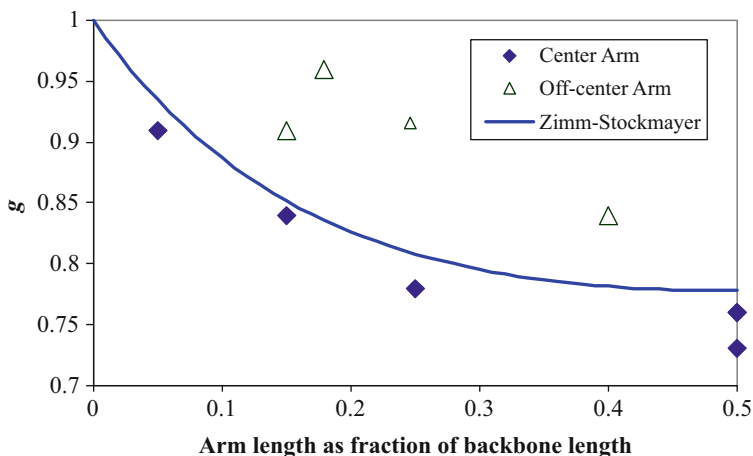
Fig. 8 g vs. ratio of length of arm to that of backbone for three-arm stars

Another common measure of LCB comes from a comparison of the intrinsic viscosity, $[\eta]$, of a polymer with that of a linear chain of the same molecular weight. This ratio is called g':

$$g' = \frac{[\eta]_{\text{branched}}}{[\eta]_{\text{linear}}} \tag{26}$$

From the data on model linear polyethylenes [106, 148, 159–161], one can write an expression for how the intrinsic viscosity varies with molecular weight:

$$[\eta] = 0.000309 M_w^{0.740} \tag{27}$$

where $[\eta]$ is in dl/g and M_w in g/mol. g' can be calculated for a branched PE using Eqs. 23 and 24 and the measured $[\eta]$.

There has been much less theoretical work to predict g' for a given branching architecture than for g. For lightly branched polymers, it is expected that g' will be the square root of g [155]. The relation between these two quantities can be expressed in terms of an exponent, ε:

$$g' = g^{\varepsilon} \tag{28}$$

For stars and some combs, it has been found that $\varepsilon \approx 0.6$. For more complicated structures there is no prediction for ε.

The predictions for stars (Eq. 23) work quite well [145, 148]. This is somewhat surprising, given that the predictions apply to ideal, theta conditions and the experimental results are for polymers in good solvent (trichlorobenzene at 135 °C). The effect of the length of the arm can be seen in Fig. 8, which compares the predicted and measured values for the stars with a centrally located branch $(s \leq 1)$.
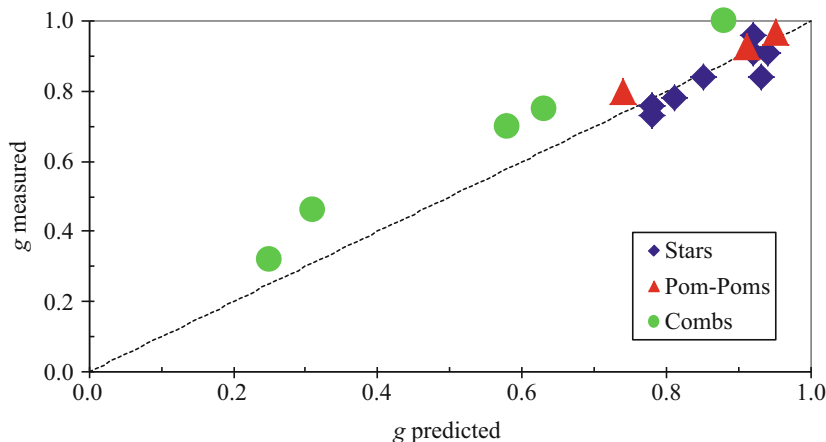
Fig. 9 g^{meas} vs. g^{pred} for branched model polyethylene. The *dotted line* is that for equality of the predicted and measured values

Also plotted on this figure are the values for stars where the branch is not at the center of the backbone ($s > 1$). Although Zimm-Stockmayer still predicts g well for the stars with off-center branches, it is clear from the figure that the greatest effect on chain dimensions occurs when the branch is located near the center of the backbone.

The data on model polymers [145, 148] show that the prediction of Eq. 24 is fairly good for the H ($f = 2$), super-H ($f = 3$), and pom-pom ($f = 5$) polymers, but in each case the value predicted is somewhat too small. This can be understood qualitatively in terms of the crowding of the arms that occurs for such highly branched molecules. This is similar to the result for symmetric stars [162]. The Zimm-Stockmayer prediction works well for three- and four-arm symmetric stars, but is too small when the branch functionality is greater than four.

A similar result holds for combs [145]. The predictions from Eq. 25 underestimate g for all of the combs here and the discrepancy tends to be larger as the number and length of the arms increase. As with the $\alpha - \omega$ polymers, this is likely due to crowding of the arms. Similar behavior has been seen for polystyrene combs by Roovers [163, 164], although the values of ε for the combs are all approximately one.

For all of the branched polymers discussed herein, the degree to which the Zimm-Stockmayer model fails to predict the true chain dimensions can be seen in Fig. 9. Here the measured values of g have been plotted *vs.* its predicted value. In general the predictions work fairly well, but tend to fail by predicting the chain dimensions that are too small. It appears that the greater the amount of polymer that is in the branches, the larger the discrepancy seen from assuming random walk statistics for each chain section. A better theory of the dimensions of such highly branched chains would be useful. It may well be that this would involve a better model for the effect of the size and geometry of the pores in an SEC column on the size of multiple-branched polymers [145], as Casassa has shown worked for symmetric stars [165].

Another way to characterize branching has been proposed by Beaucage based on a general scaling model [166]. The basic idea is to compare measures of the various parts of the molecule over a range of scales, and from this derive a measure of how ramified it is. This has been tested for model star polyethylenes by SANS measurements on dilute solutions of the polymers in deuterated solvent [147]. The model has worked quite well. However, it remains to be seen if it can also be useful for branched polymers with more complicated architectures.

5.3   Effects of LCB on Melt Rheology

In this section the way that our understanding of the melt rheology of branched polyethylene can be applied both to better characterize these materials and also to improve their processability will be covered. As this chapter is about the way that anionic polymerization has been applied to polyolefin physics, for the most part this section will discuss the studies of model saturated polybutadienes [105, 106, 143, 144, 148–152, 159–161]. (For details of the polymers used and the experimental methods, please see the particular references.) The extensive literature on the rheology of branched polyethylene itself will occasionally be referenced, but the focus will be on the learnings from the model polymers.

Much of the interest in LCB rheology revolves around the response of the samples under shear. Not only is this the simplest rheological technique to use for characterization of the nature of the LCB, but it also relates to certain aspects of processability, such as the energy needed to extrude a product such as film or a molded part. Two particular parameters that are derivable from small amplitude oscillatory shear (SAOS) experiments are the zero-shear viscosity, η_0, and the activation energy for flow, E_a [12, 148]. The former is the limiting viscosity at very long times (i.e., longer than any entanglement relaxation time) and so is related to the size of the chain in the melt [85]. The latter is derived from the dependence of the flow on temperature, and reveals more about the dynamics of the chain. The first part of this section will discuss how these parameters can be related to the nature of branching in the model LCB polyethylenes.

The first example shows how much branching architecture can impact a parameter such as η_0. Figure 10 shows the absolute value of the complex viscosity plotted versus frequency for three simple structures – PEL123, a linear chain with $M_w = 123$ kg/mol, PES(50)3, a symmetric star with three equal arms of $M_w = 50$ kg/mol each, and PES50(2)5, an asymmetric star with two arms of $M_w = 50$ kg/mol and one of 5 kg/mol [148]. All of these were essentially monodisperse in molar mass. Effectively, both stars have a backbone of 100 kg/mol (two of the long arms) and an arm branching from the center of that backbone, in one case of length 50 kg/mol (PES(50)3) and in the other of 5 kg/mol (PES50(2)5). Both stars had η_0 orders of magnitude larger than the linear chain, even though PEL123 had a higher molar mass than the smaller star. Clearly the length of the branch had a
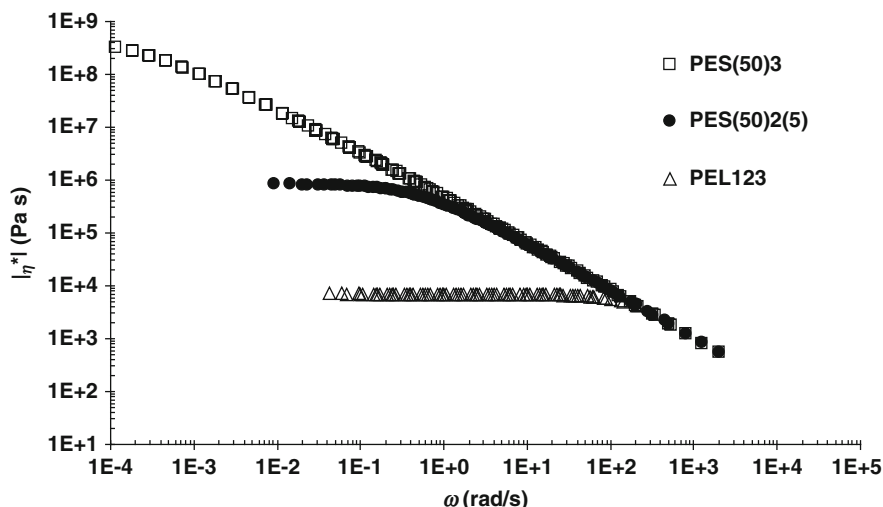
Fig. 10 Complex viscosity |η*| for linear and star model polyethylenes

great effect as well, but even a small branch (slightly larger than M_e) had an enormous effect.

In fact it has long been observed that η_0 for symmetric stars does not depend just on the total molecular weight, or on the functionality of the stars, but rather exponentially on the arm molecular weight, M_{arm} [167, 168]. This is in marked contrast to the power-law dependence on molecular weight seen for linear polymer chains. From the data on linear saturated polybutadienes [12, 99, 160], it is known that the zero-shear viscosity depends on molar mass as:

$$\eta_0(190^{\mathrm{o}}\mathrm{C}) = 6.04 \times 10^{-14} M_w^{3.33} \quad \text{(linears)} \tag{29}$$

This occurs because the stress relaxation of stars is controlled by arm retraction, rather than chain reptation as in the case of linear polymers. One equation which has been put forth for the M_{arm} dependence of η_0 in stars is:

$$\eta_0 = A\exp\left\{\gamma\frac{M_{\mathrm{arm}}}{M_e}\right\} \tag{30}$$

where γ and A are constants independent of M_{arm}. It has generally been found that $\gamma \cong 0.6$. Fitting the data on model PE symmetric stars [148, 159–161, 169] to Eq. 26 yields

$$\eta_0 = 6.96\exp\left\{2.63 \times 10^{-4} M_{\mathrm{arm}}\right\} \quad \text{(symmetric stars)} \tag{31}$$

which, taking $\gamma = 0.6$, gives $M_e = 2.28$ kg/mol. This result is intermediate between the values of M_e and M_c for polyethylene [89], which suggests a deficiency in the
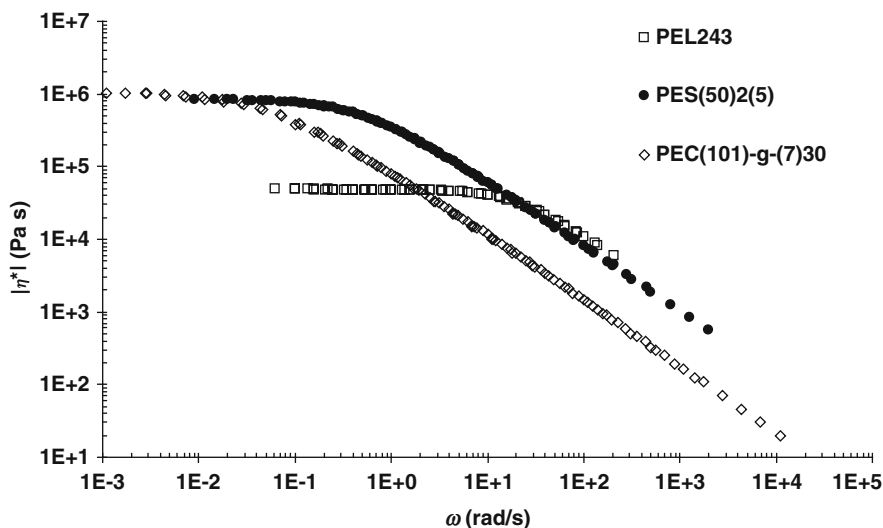
Fig. 11 $|\eta^*|$ for PEL243, PES(50)2(5), and PEC(101)-g-(7)30

current models of arm retraction [170]. Note the marked contrast between the power-law dependence of η_0 on M in Eqs. 29 and 30.

In Fig. 11 the effects of the number of branches on η_0 are shown [148]. Here a comparison is made between a linear chain, PEL243 with $M_w = 243$ kg/mol, the PES50(2)5 star described above, and PEC(101)-g-(7)30, a model comb polymer with a backbone of $M_w = 101$ kg/mol and 30 randomly placed arms of $M_w = 7$ kg/mol. The backbones of the star and the comb had nearly identical molar masses, and the arms lengths were nearly the same as well; the only difference in architecture was that PES50(2)5 had a single arm, and PEC(101)-g-(7)30 had thirty arms. Both of the branched structure again showed η_0 well above that of the linear polymer (even though the molar mass of PEL243 was much larger than that of PES50(2)5, and about the same as that of PEC(101)-g-(7)30), but the η_0 of the comb and the star were about the same. The big difference in the viscosities of the two branched polymers occurred at higher frequencies; the viscosity of the comb dropped from its zero-shear value at much lower frequencies than for the star (reflecting its much longer relaxation times), and so can be said to have had a greater degree of shear thinning. The lower viscosities of both the star and especially the comb at frequencies of 100–1,000 rad/s show the importance of branching for processability, as this range corresponds to the shear rates typical of the extrusion of film, for example.

Given these examples on how η_0 depends on the branch length in symmetric stars (Eq. 26) and the number of branches, one might hope that zero-shear viscosity alone could be used to characterize the architecture of branched polyethylene. Alas, this is not the case as can be seen in Fig. 12 [148]. Here the zero-shear viscosities of many branched polymers are shown along with that of several linear chains. There is no clear correlation of structure with η_0, and in fact there is no correlation with
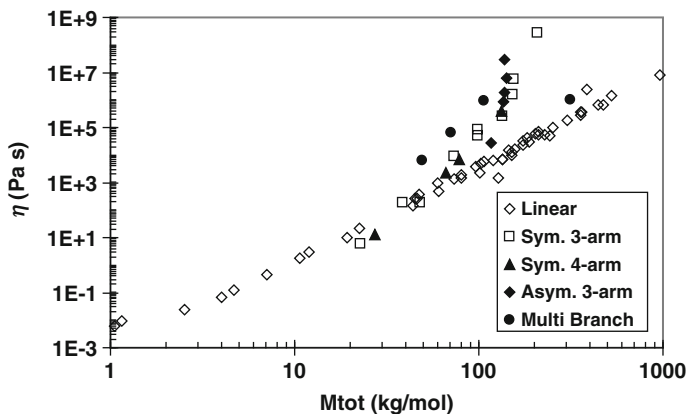
Fig. 12 η_0 *vs.* M_{tot} (i.e., the M_w of the whole molecule) for many model polyethylenes
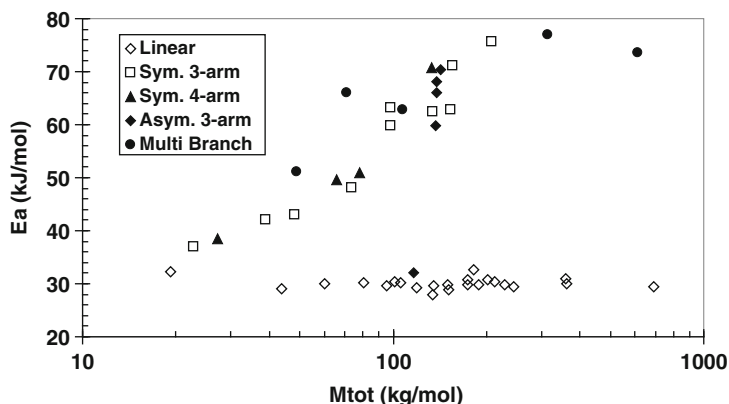
Fig. 13 E_a *vs.* M_{tot} (i.e., the M_w of the whole molecule) for many model polyethylenes

arm molar mass either. This is due to two competing forces as branching becomes more complicated. The longer the branch (and, to a lesser degree, the number of branches), the more difficult it is for an arm to retract from the entangled melt, which drives up relaxation times and so zero-shear viscosity. But the denser the branching becomes, the less the molecule can overlap with neighboring chains, which make it less entangled with the melt. When the branch lengths become much larger than the distance between the branch points on the backbone, the molecules become nearly totally disentangled with their neighbors. These two factors make a characterization of branching based on zero-shear viscosity alone impossible.

Figure 13 shows E_a for the same set of polymers. While E_a is certainly larger for the branched polymers than for the linear chains, there is no obvious pattern that can be used to specify the nature of the LCB from knowledge of E_a alone. The

activation energy clearly rises with the molecular weight of the branched chain, but the architecture seemingly plays little role. So this parameter does not give us a direct means to characterize LCB architecture either.

Shroff and Mavridis [171, 172] have proposed using zero-shear viscosity combined with intrinsic viscosity to characterize the architecture of a branched polyethylene. The basic idea is to first get an idea of the size of the molecule from $[\eta]$; although this is measured in dilute solution, the melt state chain size is likely correlated. This value is then compared to zero-shear viscosity, which as stated above depends on both chain size and how much the chains overlap with one another. Since all these polyethylenes will be essentially identical on the monomer scale, differences in their state of overlap must relate to long-chain branching [17]. Since both $[\eta]$ and η_0 have a power-law dependence on molar mass for linear chains (Eqs. 24 and 29), they also have a power-law dependence on each other:

$$\eta_0{}^\alpha = k[\eta] \tag{32}$$

where k is a constant to be determined (see below). This allows the definition of a long-chain branching index (LCBI) by comparing the measured values of $[\eta]$ and η_0 for a branched polymer with the expectation for a linear chain of the same molar mass:

$$LCBI = \frac{\eta_0^\alpha}{k[\eta]} - 1 \tag{33}$$

Shroff and Mavridis derived such a relation using data on branched polyethylenes, which worked to a certain extent. But this relied on NMR-based measures of the level of branching, which can be problematic as mentioned above. Another version of *LCBI* was determined from the data on hydrogenated polybutadienes [146], giving the following formula:

$$LCBI = \frac{\eta_0^{0.208}}{3.272[\eta]} - 1 \tag{34}$$

(with $[\eta]$ measured in dL/g and η_0 in kPa·s). This gave a much better fit to the data for branched polymers, both those made by saturating polybutadiene and those made from polymerizing olefins by various means. So this technique can be useful to give an idea of the degree of branching in a polyethylene sample with reasonably good accuracy from just rheological data. However, this method clearly does not provide any information on the nature of the branching, and other methods are needed to distinguish, for example, stars from combs from pom-poms.

Another way to look at the data obtained from small amplitude oscillatory shear experiments has been proposed by van Gurp and Palmen [173]. The main idea of the so-called van Gurp-Palmen analysis is to plot δ ($= \tan^{-1}[G''/G']$) *vs.* the magnitude of the complex modulus, $|G^*|$. This form of plotting the data highlights
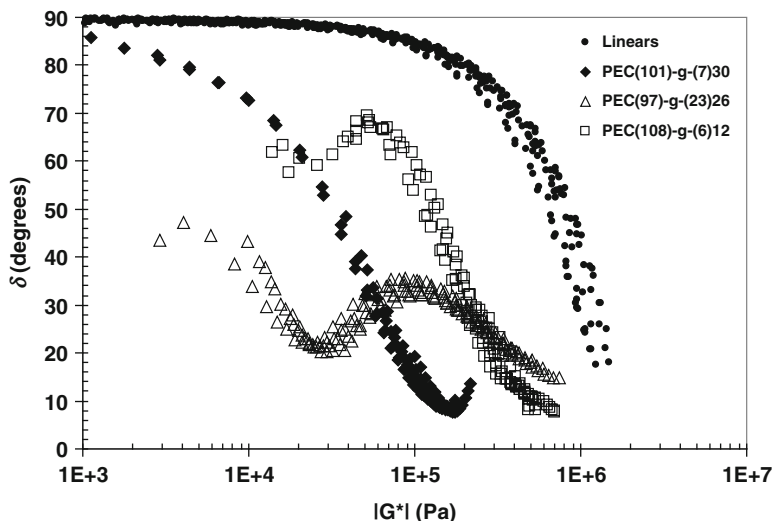
Fig. 14 Van Gurp-Palmen plot for linear and comb model polyethylenes

the effects of branching, since the data from any linear polymer will lie on a common line independent of molecular weight (with slight variations for molecular weight distribution). This method has been shown to illuminate the nature of branching in many polymer systems [174], including polyolefins [175]. Figure 14 shows this sort of plot for linear polyethylene and several combs [148]. All of the data for the linear polymers (which have molecular weights from 19 to 800 kg/mol) fall on one curve, with a very characteristic shape. At low values of |G^*|, δ is nearly 90° (corresponding to purely viscous behavior). The point at which the value drops precipitously to 0° (corresponding to complete elastic behavior) is close to the plateau modulus. The behavior of the branched polymers is quite different from that of the linear polymers, and the difference in the area under the curves can be related to the degree of branching [176]. The comb polymers for which the data are plotted in Fig. 14 had a variety of structures. PEC(108)-g-(6)12 and PEC(101)-g-(7)30 had similar backbones with $M_w = 108$ and 101 kg/mol, respectively, and similar arms with $M_w = 6$ and 7 kg/mol; the major difference was that PEC(108)-g-(6)12 had 12 arms per chain and PEC(101)-g-(7)30 had 30. The backbone for PEC(97)-g-(23) 26 was similar ($M_w = 97$ kg/mol), but with 26 much longer arms ($M_w = 23$ kg/mol). Note that there was a minimum in δ for PEC(101)-g-(7)30 at 0.160 MPa, which is much lower than the plateau modulus of PE. This secondary plateau modulus appeared due to the great separation of relaxation times that arises in comb polymers. In this frequency region, the branches have completely relaxed, but the backbone has not. An expected value for this secondary plateau can be calculated by assuming that the arms act simply as a diluent for the backbones [161, 177]. This was also seen for PEC(108)-g-(6)12. For PEC(97)-g-(23)26, there is a minimum in δ at a much smaller modulus value, 0.029 MPa. This makes sense, in that the longer
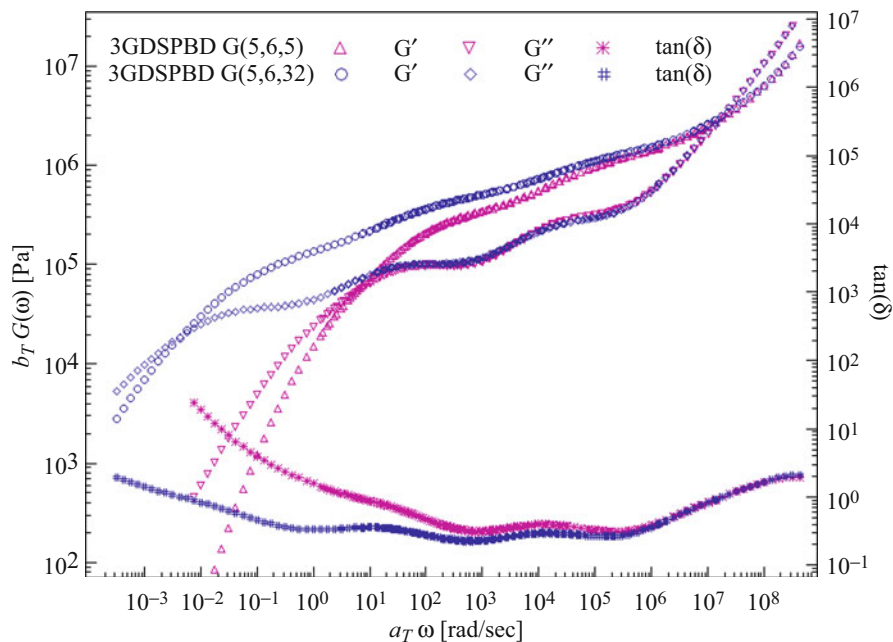
Fig. 15 Experimental storage and loss moduli as well as tanδ of 3GDSPBDG(5,6,5) and 3GDSPBDG(5,6,32) at $T_{\mathrm{ref}} = 28\,°C$

arms of PEC(97)-g-(23)26 increased the degree of dilution. Obviously, there are no new data in the van Gurp-Palmen curve than provided by the usual curves of G' and G'' vs. ω, but this way of presenting that data shows the LCB features more transparently and serves as a useful tool for the rheological characterization of LCB.

Such secondary plateaus have been seen in many kinds of branched polymers [100, 149–152]. Moreover, when the polymers show a third level of hierarchy (i.e., a backbone with branches that themselves have branches long enough to entangle), a tertiary plateau has also been seen. The outer branches relax first, followed by the inner branches, and then the core part of the molecule. The ability to distinguish all three relaxations in SAOS shear data requires a good separation in these relaxation times and data over a wide range of frequency. The data in Fig. 15 for third-generation dendritic star polybutadienes offers a good example. (This is done for polybutadiene to allow for a greater range of temperature and so of frequency, since the crystallization of saturated polybutadiene reduces the temperatures that can be accessed.) For 3GDSPBDG(5,6,5) there was an inner core of a three-arm star, with each arm having $M_w = 5$ kg/mol; at the end of each of these three primary arms there were attached two chains having $M_w = 6$ kg/mol, and then at the ends of each of these six secondary arms were attached two more chains having $M_w = 5$ kg/mol. The only difference for 3GDSPBDG(5,6,32) was that the inner primary arms have $M_w = 32$ kg/mol; the secondary and tertiary arms had the same lengths as for
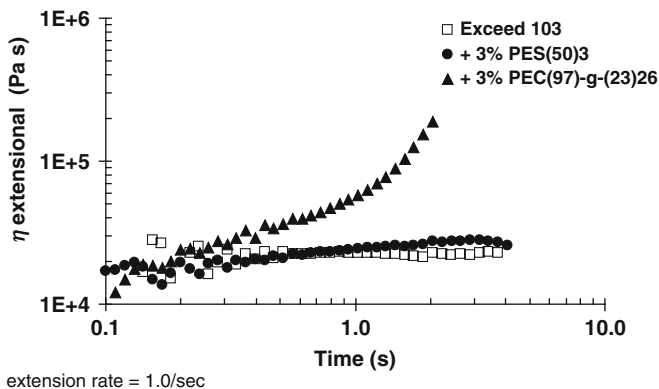
Fig. 16 η_{ext} for a linear polyethylene (Exceed 103) and blends of that linear polymer with a star (PES) or comb (PEC) polyethylene

3GDSPBDG(5,6,5). One can see that the two polymers had nearly identical behavior at high frequencies (short times), reflecting the fact that the outer arms of these molecules, which relaxed first, were identical. But at low frequencies (long times) the distinction between the two became clear, as the interior core of 3GDSPBDG (5,6,5) relaxed well before that of 3GDSPBDG(5,6,32). This allowed for the visualization of three separate plateaus, corresponding to the three branch generations of these molecules. While the presence of more than one plateau can thus be seen as a clear proof of a hierarchy in branching, it is clear that this is a difficult method to use for characterizing commercial polymers that are broadly distributed in the level of branching, as these plateaus will be smeared out. So there is still a need for better means to characterize LCB.

Other methods of rheological characterization have been researched. The nonlinear relaxation of such polymers has been studied using step-strain experiments, and the resulting damping profiles of the polymers used to distinguish various kinds of branching [151, 152]. Other workers are examining the use of large amplitude oscillatory shear (LAOS) rheology for such characterization [178]. Measures of the melt rheology under extension have also been used to characterize LCB [179]. Figure 16 shows some of this data for model polyethylenes [148]. Although all kinds of LCB will enhance the shear thinning of a polymer, as seen above, it has been posited that only polymers with multiple long branches per chain will exhibit thickening in extension [176]. This was tested by looking at linear polymers and several blends of linear and model LCB polymers. (It has proved impossible to measure the extensional rheology of the pure combs, due to their high elasticity.) The linear polymer used here was a commercial metallocene-catalyzed ethylene-hexene copolymer with a melt index of about 1 g/10 min and a density of 0.918 g/cm^3.

From the shear rheology and the assumption of linear viscoelasticity, one can predict what the extensional behavior would be in the limit of small strains, which serves as a baseline for determining the response of the polymer to uniaxial

Fig. 17 Synthesis scheme for random dendritic polymers by anionic condensation
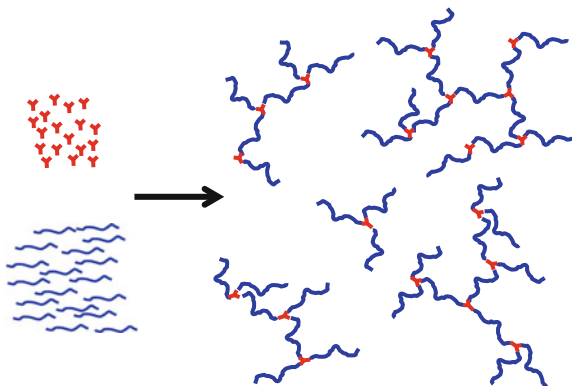
extensional deformation. If the measured extensional viscosity is substantially above the linear viscoelastic limit, then it is said to display extensional thickening. As seen in Fig. 16, both the pure linear polymer and its blend with 3 % of PES(50)3 showed similar behavior. The extensional viscosity was exactly that predicted by linear viscoelasticity from the shear data, so neither sample showed extensional thickening. However, when 3 % of PEC(97)-g-(23)26 was added to the linear polymer, a dramatic rise in η_{ext} was seen, indicating extensional thickening. That this can be seen with such a small addition of comb is remarkable. Thus, extensional rheology is also a powerful technique to characterize LCB, as it can be used to show the presence of low levels of multiple-branched polymers. But by itself it cannot fully characterize the nature of LCB. At this stage, the best recommendation to offer for determining the nature of branching is to use as wide a range of methods as possible to develop as detailed a picture as needed for the application.

Finally, there has been some recent work to make it easier to produce these model polymers with LCB [143, 144]. Typical synthesis routes to dendritic polymers with a very precise architecture require many steps and high vacuum techniques to avoid poisoning [135–142]. The time and care required for such production makes it quite expensive. However, if the requirements for precision in structural control are relaxed slightly, a less demanding method can be used. The new method uses some of the anionic polymerization methods described throughout this book, in a manner that could allow the synthesis of large quantities of saturated polybutadienes with high control of the nature of their branching to be done at much lower cost. This takes advantage of the basic silicon chloride coupling chemistry that has been used to make many star polymers [100, 101], and is illustrated in Fig. 17 where trichlorosilane, $SiCl_3(CH_3)$, is represented by the red Y-shaped unit. The blue lines are polybutadiene chains initiated by dysfunctional initiators to produce chains with Li atoms at each end of the molecule [128]. Instead of using many steps to make a precise dendritic polymer, in the methods described here the dilithium polybutadiene and trichlorosilane are allowed to react randomly to form many kinds of dendritic molecules, in a manner analogous to the condensation polymerization of A_2 and B_3 monomers [180]. By carefully controlling the

ratio of dilithium polybutadiene to trichlorosilane, the majority of the product can have a highly branched structure without producing substantial gel [143, 144]. (The same result can be achieved using dichlorosilane and trilithium polybutadiene.) These polybutadienes can then be saturated in the normal way to make highly branched model polyethylenes. This method may prove to be very useful in future research on branching in polyethylenes.

6   Future Areas of Study

This chapter has shown how the understanding of the basic physical properties of polyolefins has been advanced through the use of models made using the tools of anionic polymerization and hydrogenation. Polymers with a high level of control of molecular parameters such as molecular weight, composition, long-chain branching (as well as the distributions of the parameters), have permitted researchers to discover the physics underlying many measures of performance. This includes the size of polyolefin chains in the melt state, and the way that two of the most important parameters that determine the properties of polyolefins – the degree of entanglement and mutual solubility – are related to the chemical nature of the chains. These models have also shed light on how the details of LCB in polyolefins can be used to control processing and mechanical performance. This understanding has translated into some highly useful tools for designing new materials based on either existing or novel polyolefins. The fact that this research strategy has been successful for parameters such as G_N^0 and X_{12} should give one confidence that a similar degree of understanding can also be achieved for other basic properties. It is known that some mechanical properties, such as yield stress [181] and tensile performance [182] can be related to entanglement. One might also hope to relate other basic properties, such as glass transition temperature, monomeric friction factor [12, 57, 88, 183, 184], crystallization kinetics, and crystal structure back to the chemistry of the chains. These model polymers could also be used to probe the details of the crystalline morphology of polyolefins. Model polymers made by anionic polymerization have proven extremely useful for the advancement of polyolefin physics, and may prove to have even greater uses in the future.

References

1. Lohse DJ (2000) Polyolefins. In: Craver CD, Carraher CE (eds) Applied polymer science – 21st century. Elsevier, New York
2. Fawcett EW, Gibson RO, Perrin MW, Paton JG, Williams EG (1937) Improvements in or relating to the polymerisation of ethylene. Great Britain Patent 471,590
3. Ziegler K, Gellert HG (1953) Verfahren zur polymerisation und mischpolymerisation von olefinen. German Patent 878,560
4. McMillan FM (1979) The chain straighteners. Macmillan, London
5. Sinn H, Kaminsky W (1980) Ziegler-Natta catalysis. Adv Organomet Chem 18:99–149. http://dx.doi.org/10.1016/S0065-3055(08)60307-X
6. Malmberg A, Kokko E, Lehmus P, Löfgren B, Seppälä JV (1998) Long-chain branched polyethene polymerized by metallocene catalysts Et[Ind]$_2$ZrCl$_2$/MAO and Et[IndH$_4$]$_2$ZrCl$_2$/MAO. Macromolecules 31:8448–8454. doi:10.1021/ma980522n
7. Wasserman EP (2010) Metallocenes. In: Kroschwitz JI (ed) Encyclopedia of polymer science and engineering. Wiley, New York
8. Kaminsky W (2004) The discovery of metallocene catalysts and their present state of the art. J Polym Sci Chem 42:3911–3921. doi:10.1002/pola.20292
9. Rachapudy H, Smith GG, Raju VR, Graessley WW (1979) Properties of amorphous and crystallizable hydrocarbon polymers. III. Studies of the hydrogenation of polybutadiene. J Polym Sci Phys 17:1211–1222. doi:10.1002/pol.1979.180170706
10. Carella JM, Graessley WW, Fetters LJ (1984) Effects of chain microstructure on the viscoelastic properties of linear polymer melts: polybutadienes and hydrogenated polybutadienes. Macromolecules 17:2775–2786. doi:10.1021/ma00142a059
11. Xu Z, Mays JW, Chen X, Hadjichristidis N, Bair HE, Schilling FC, Pearson DS, Fetters LJ (1985) Molecular characterization of poly(2-methyl-1,3-pentadiene) and its hydrogenated derivative, atactic polypropylene. Macromolecules 18:2560–2566. doi:10.1021/ma00154a034
12. Ferry JD (1980) Viscoelastic properties of polymers. Wiley, New York
13. Ronca G (1983) Frequency spectrum and dynamic correlations of concentrated polymer liquids. J Chem Phys 79:1031–1043. doi:10.1063/1.445845
14. Lin YH (1987) Number of entanglement strands per cubed tube diameter, a fundamental aspect of topological universality in polymer viscoelasticity. Macromolecules 20:3080–3083. doi:10.1021/ma00178a024
15. Kavassalis TA, Noolandi J (1987) New view of entanglements in dense polymer systems. Phys Rev Lett 59:2674–2677. doi:10.1103/PhysRevLett.59.2674
16. Colby RH, Rubinstein M (1990) Two-parameter scaling for polymers in Θ solvents. Macromolecules 23:2753–2757. doi:10.1021/ma00212a028
17. Fetters LJ, Lohse DJ, Richter D, Witten TA, Zirkel A (1994) Connection between polymer molecular weight, density, chain dimensions, and melt viscoelastic properties. Macromolecules 27:4639–4647. doi:10.1021/ma00095a001
18. Fetters LJ, Lohse DJ, Graessley WW (1999) Chain dimensions and entanglement spacings in dense macromolecular systems. J Polym Sci Phys 37:1023–1033. doi:10.1002/(SICI)1099-0488(19990515)
19. Fetters LJ, Lohse DJ, Milner ST, Graessley WW (1999) Packing length influence in linear polymer melts on the entanglement, critical, and reptation molecular weights. Macromolecules 32:6847–6851. doi:10.1021/ma990620o
20. Rubin RJ (1972) Span of a polymer chain. J Chem Phys 56:5747–5757. doi:10.1063/1.1677112
21. Wignall GD (1987) Neutron scattering. In: Kroschwitz JI (ed) Encyclopedia of polymer science and engineering. Wiley, New York
22. Flory PJ (1969) Statistical mechanics of chain molecules. Interscience, New York

23. Flory PJ (1949) The configuration of real polymer chains. J Chem Phys 17:303–310. doi:10.1063/1.1747243

24. Kirste RG, Kruse WA, Schelten J (1973) Die bestimmung des trägheitsradius von polymethyl-methacrylat im glaszustand durch neutronenbeugung. Makromol Chemie 162:299–303. doi:10.1002/macp.1972.021620128

25. Ballard DGH, Wignall GD, Schelten J (1973) Measurement of molecular dimensions of polystyrene chains in the bulk polymer by low angle neutron diffraction. Eur Polym J 9:965–969. doi:10.1016/0014-3057(73)90059-1

26. Cotton JP, Decker D, Benoit H, Farnou B, Higgins J, Jannink G, Ober R, Picot C, des Cloisseaux J (1974) Conformation of polymer chain in the bulk. Macromolecules 7:863–872. doi:10.1021/ma60042a033

27. Schelten J, Wignall GD, Ballard DGH (1974) Chain conformation in molten polyethylene by low angle neutron scattering. Polymer 15:682–685. doi:10.1016/0032-3861(74)90061-5

28. Lieser G, Fischer EW, Ibel K (1975) Conformation of polyethylene molecules in the melt as revealed by small-angle neutron scattering. J Polym Sci Lett 13:39–43. doi:10.1002/pol.1975.130130107

29. Ballard DGH, Cheshire P, Longman GW, Schelten J (1978) Small-angle neutron scattering studies of isotropic polypropylene. Polymer 19:379. doi:10.1016/0032-3861(78)90241-0

30. Hayashi H, Flory PJ (1983) Configuration of the polyisobutylene chain in bulk and in solution according to elastic neutron scattering. Physica B+C 120:408–412. doi:10.1016/0378-4363(83)90417-5

31. McAlea KP, Schultz JM, Gardner KH, Wignall GD (1985) Molecular dimensions in poly (ethylene terephthalate) by small-angle neutron scattering. Macromolecules 18:447–452. doi:10.1021/ma00145a025

32. Fetters LJ, Graessley WW, Krishnamoorti R, Lohse DJ (1997) Melt chain dimensions of poly (ethylene−1-butene) copolymers via small angle neutron scattering. Macromolecules 30:4973–4977. doi:10.1021/ma961408c

33. Krishnamoorti R, Graessley WW, Zirkel A, Richter D, Hadjichristidis N, Fetters LJ, Lohse DJ (2002) Melt-state polymer chain dimensions as a function of temperature. J Polym Sci Phys 40:1768–1776. doi:10.1002/polb.10231

34. Helfand E, Sapse AM (1975) Theory of unsymmetric polymer-polymer interfaces. J Chem Phys 62:1327–1335. doi:10.1063/1.430632

35. Milner ST, Witten TA (1988) Bending moduli of polymeric surfactant interfaces. J Geophys Res 49:1951–1962. doi:10.1051/jphys:0198800490110195100

36. Lohse DJ (2013) The application of neutron scattering to the relation between chain dimensions and miscibility for polyolefins. Polym J 45:20–25. doi:10.1038/pj.2012.191

37. Fetters LJ, Lohse DJ, García-Franco CA, Brant P, Richter D (2002) Prediction of melt state polyolefin rheological properties: the unsuspected role of the average molecular weight per backbone bond. Macromolecules 35:10096–10101. doi:10.1021/ma025659z

38. Lohse DJ, Graessley WW (2000) Thermodynamics of polyolefin blends. In: Paul DR, Bucknall CB (eds) Polymer blends: formulation and performance. Wiley, New York

39. Schweizer KS, Singh C (1995) Microscopic solubility-parameter theory of polymer blends: general predictions. Macromolecules 28:2063–2080. doi:10.1021/ma00110a046

40. Crist B, Hill MJ (1997) Recent developments in phase separation of polyolefin melt blends. J Polym Sci Phys 35:2329–2353. doi:10.1002/(SICI)1099-0488(199710)

41. Hildebrand JH, Scott RL (1950) The solubility of non-electrolytes. Van Nostrand-Reinhold, Princeton

42. Krishnamoorti R, Graessley WW, Fetters LJ, Garner RT, Lohse DJ (1995) Anomalous mixing behavior of polyisobutylene with polyolefins. Macromolecules 28:1252–1259. doi:10.1021/ma00108a064

43. Reichart GC, Graessley WW, Register RA, Krishnamoorti R, Lohse DJ (1997) Anomalous attractive interactions in polypropylene blends. Macromolecules 30:3036–3041. doi:10.1021/ma9616569

44. Wignall GD, Child HR, Samuels RJ (1982) Structural characterization of semicrystalline polymer blends by small-angle neutron scattering. Polymer 23:957–964. doi:10.1016/0032-3861(82)90393-7

45. Lohse DJ (1986) The melt compatibility of blends of polypropylene and ethylene-propylene copolymers. Polym Engg Sci 26:1500–1509. doi:10.1002/pen.760262106

46. Nicholson JC, Finerman TM, Crist B (1990) Thermodynamics of polyolefin blends: small-angle neutron scattering studies with partially deuterated chains. Polymer 31:2287–2293. doi:10.1016/0032-3861(90)90314-O

47. Rhee J, Crist B (1991) Thermodynamics and phase separation in melt blends of polyethylene and model copolymers. Macromolecules 24:5663–5669. doi:10.1021/ma00020a028

48. Balsara NP, Fetters LJ, Hadjichristidis N, Lohse DJ, Han CC, Graessley WW, Krishnamoorti R (1992) Thermodynamic interactions in model polyolefin blends obtained by small angle neutron scattering. Macromolecules 25:6137–6147. doi:10.1021/ma00049a009

49. Krishnamoorti R, Graessley WW, Balsara NP, Lohse DJ (1994) The structural origin of thermodynamic interactions in blends of saturated hydrocarbon polymers. Macromolecules 27:3073–3081. doi:10.1021/ma00089a026

50. Graessley WW, Krishnamoorti R, Reichart GC, Balsara NP, Fetters LJ, Lohse DJ (1995) Regular and irregular mixing in blends of saturated hydrocarbon polymers. Macromolecules 28:1260–1270. doi:10.1021/ma00108a065

51. Rabeony M, Lohse DJ, Garner RT, Han SJ, Graessley WW, Migler KB (1998) Effect of pressure on polymer blend miscibility: a temperature-pressure superposition. Macromolecules 31:6511–6514. doi:10.1021/ma980723r

52. Alamo RG, Londono JD, Mandelkern L, Stehling FC, Wignall GD (1994) Phase behavior of blends of linear and branched polyethylenes in the molten and solid states by small-angle-neutron scattering. Macromolecules 27:411–417. doi:10.1021/ma00080a014

53. Schipp C, Hill MJ, Barham PJ, Cloke VM, Higgins JS, Oiarzabal L (1996) Ambiguities in the interpretation of small-angle neutron scattering from blends of linear and branched polyethylene. Polymer 37:2291–2297. doi:10.1016/0032-3861(96)85337-7

54. Alamo RG, Graessley WW, Krishnamoorti R, Lohse DJ, Londono JD, Mandelkern L, Stehling FC, Wignall GD (1997) SANS investigations of melt miscibility and phase segregation in blends of linear and branched polyethylenes as a function of branch content. Macromolecules 30:561–566. doi:10.1021/ma961196j

55. Seki M, Nakano H, Yamauchi S, Suzuki J, Matsushita Y (1999) Miscibility of isotactic polypropylene/ethylene-propylene random copolymer binary blends. Macromolecules 32:3227–3234. doi:10.1021/ma981254w

56. Steiner U, Klein J, Fetters LJ (1994) Surface phase inversion in finite-sized binary mixtures. Phys Rev Lett 72:1498–1501. doi:10.1103/PhysRevLett.72.1498

57. Scheffold F, Eiser E, Budkowski A, Steiner U, Klein J, Fetters LJ (1996) Surface phase behavior in binary polymer mixtures. I. Miscibility, phase coexistence, and interactions in polyolefin blends. J Chem Phys 104:8786–8794. doi:10.1063/1.471568

58. Kyu T, Hu S, Stein RS (1987) Characterization and properties of polyethylene blends II. Linear low-density with conventional low-density polyethylene. J Polym Sci Phys 25:89–103. doi:10.1002/polb.1987.090250107

59. Song HH, Wu EQ, Chu B, Satkowski M, Ree M, Stein RS, Phillips JC (1990) Time-resolved small-angle X-ray scattering of a high density polyethylene/low density polyethylene blend. Macromolecules 23:2380–2384. doi:10.1021/ma00210a040

60. Inaba N, Sato K, Suzuki S, Hashimoto T (1986) Morphology control of binary polymer mixtures by spinodal decomposition and crystallization. 1. Principle of method and preliminary results on PP/EPR. Macromolecules 19:1690–1695. doi:10.1021/ma00160a036

61. Chen CY, Yunus WMZW, Chiu HW, Kyu T (1997) Phase separation behaviour in blends of isotactic polypropylene and ethylene propylene diene terpolymer. Polymer 38:4433–4438. doi:10.1016/S0032-3861(96)01039-7

62. Lohse DJ, Fetters LJ, Doyle MJ, Wang HC, Kow C (1993) Miscibility in blends of model polyolefins and corresponding diblock copolymers: thermal analysis studies. Macromolecules 26:3444–3447. doi:10.1021/ma00065a031

63. White JL, Lohse DJ (1999) Spin diffusion analysis of miscibility in an anomalous nonpolar blend. Macromolecules 32:958–960. doi:10.1021/ma981992k

64. Wolak JE, White JL (2005) Factors that allow polyolefins to form miscible blends: polyisobutylene and head-to-head polypropylene. Macromolecules 38:10466. doi:10.1021/ma052162r

65. Krishnamoorti R, Graessley WW, Dee GT, Walsh DJ, Fetters LJ, Lohse DJ (1996) Pure component properties and mixing behavior in polyolefin blends. Macromolecules 29:367–376. doi:10.1021/ma950754b

66. Han SJ, Lohse DJ, Condo PD, Sperling LH (1999) Pressure-volume-temperature properties of polyolefin liquids and their melt miscibility. J Polym Sci Phys 37:2835–2844. doi:10.1002/(SICI)1099-0488(19991015)

67. Lohse DJ (2005) The influence of chemical structure on polyolefin melt rheology and miscibility. J Macromol Sci Rev 45:289–308. doi:10.1080/15321790500304098

68. Dadmun MD (2010) Neutron scattering. In: Kroschwitz JI (ed) Encyclopedia of polymer science and engineering. Wiley, New York

69. Allen G, Gee G, Wilson GJ (1960) Intermolecular forces and chain flexibilities in polymers: I. Internal pressures and cohesive energy densities of simple liquids. Polymer 1:456–466. doi:10.1016/0032-3861(60)90061-6

70. Paul DR, Bucknall CB (2000) Polymer blends: formulation and performance. Wiley, New York

71. Huggins ML (1941) Solutions of long chain compounds. J Chem Phys 9:440–440. doi:10.1063/1.1750930

72. Flory PJ (1941) Thermodynamics of high polymer solutions. J Chem Phys 9:660–662. doi:10.1063/1.1750971

73. Staverman AJ (1941) The entropy of liquid mixtures: II. Deviations from Raoult's law in mixtures containing large, flexible molecules. Recl Trav Chim 60:640–649. doi:10.1002/recl.19410600903

74. Bensason S, Nazarenko S, Chum S, Hiltner A, Bae E (1997) Blends of homogeneous ethylene-octene copolymers. Polymer 38:3513–3520. doi:10.1016/S0032-3861(96)00906-8

75. Yamaguchi M, Miyata H, Nitta KH (1996) Compatibility of binary blends of polypropylene with ethylene-α-olefin copolymer. J Appl Polym Sci 62:87–97. doi:10.1002/(SICI)1097-4628(19961003)

76. Stephens CH, Hiltner A, Baer E (2003) Phase behavior of partially miscible blends of linear and branched polyethylenes. Macromolecules 36:2733–2741. doi:10.1021/ma021621a

77. Kamdar AR, Hu YS, Ansems P, Chum SP, Hiltner A, Baer E (2006) Miscibility of propylene-ethylene copolymer blends. Macromolecules 39:1496–1506. doi:10.1021/ma052214c

78. Bates FS, Fredrickson GH (1994) Conformational asymmetry and polymer-polymer thermo-dynamics. Macromolecules 27:1065–1067. doi:10.1021/ma00082a030

79. Fredrickson GH, Liu AJ, Bates FS (1994) Entropic corrections to the Flory-Huggins theory of polymer blends: architectural and conformational effects. Macromolecules 27:2503–2511. doi:10.1021/ma00087a019

80. Maranas JK, Mondello M, Grest GS, Kumar SK, Debenedetti PG, Graessley WW (1998) Liquid structure, thermodynamics, and mixing behavior of saturated hydrocarbon polymers. 1. Cohesive energy density and internal pressure. Macromolecules 31:6991–6997. doi:10.1021/ma9717552

81. Bates FS, Fetters LJ, Wignall GD (1988) Thermodynamics of isotopic polymer mixtures: poly(vinylethylene) and poly(ethylethylene). Macromolecules 21:1086–1094. doi:10.1021/ma00182a040

82. Yamaguchi M, Nitta KH, Miyata H, Masuda T (1997) Rheological properties for binary blends of i-PP and ethylene-1-hexene copolymer. J Appl Polym Sci 63:467–474. doi:10.1002/(SICI)1097-4628(19970124)

83. Yamaguchi M, Miyata H, Nitta KH (1997) Structure and properties for binary blends of isotactic-polypropylene with ethylene-α-olefin copolymer. 1. Crystallization and morphology. J Polym Sci Phys 35:953–961. doi:10.1002/(SICI)1099-0488(19970430)

84. Nitta KH, Okamoto K, Yamaguchi M (1998) Mechanical properties of binary blends of polypropylene with ethylene-α-olefin copolymer. Polymer 39:53–58. doi:10.1016/S0032-3861(97)00239-5

85. Graessley WW (2004) Polymeric liquids and networks: structure and properties. Garland Science, New York

86. Larson RG, Sridhar T, Leal GH, McKinley GH, Likhtman AE, McLeish TCB (2003) Definitions of entanglement spacing and time constants in the tube model. J Rheol 47:809–818. doi:10.1122/1.1567750

87. de Gennes PG (1974) Remarks on entanglements and rubber elasticity. J Physique Lett 35:133–134. doi:10.1051/jphyslet:01974003509013300

88. Doi M, Edwards SF (1986) The theory of polymer dynamics. Clarendon, Oxford

89. Fetters LJ, Lohse DJ, Colby RH (2007) Chain dimensions and entanglement spacings. In: Mark J (ed) Physical properties of polymers handbook, 2nd edn. Springer, New York

90. García-Franco CA, Lohse DJ, Harrington BA (2005) On the rheology of ethylene-octene copolymers. Rheologica Acta 44:591–599. doi:10.1007/s00397-005-0441-8

91. García-Franco CA, Harrington BA, Lohse DJ (2006) The effect of short chain branching on the rheology of polyolefins. Macromolecules 39:2710. doi:10.1021/ma052581o

92. Graessley WW (1982) Entangled linear, branched and network polymer systems — molecular theories. Adv Polym Sci 47:67–117

93. Wheat WR (1995) Rheological explanations for syndiotactic polypropylene behaviors. ANTEC Proc 2275–2278

94. Eckstein A, Suhm J, Friedrich C, Maier RD, Sassmannhausen J, Bochmann M, Mülhaupt R (1998) Determination of plateau moduli and entanglement molecular weights of isotactic, syndiotactic, and atactic polypropylenes synthesized with metallocene catalysts. Macromolecules 31:1335–1340. doi:10.1021/ma971270d

95. Jones TD, Chaffin KA, Bates FS, Annis BK, Hagaman EW, Kim MH, Wignall GD, Fan W, Waymouth R (2002) Effect of tacticity on coil dimensions and thermodynamic properties of polypropylene. Macromolecules 35:5061–5068. doi:10.1021/ma011547g

96. Fetters LJ, Lee JH, Mathers RT, Hustad PD, Coates GW, Archer LA, Rucker SP, Lohse DJ (2005) The influence of syndiotactic propylene units on the rheological parameters of poly (ethylene-propylene) copolymers. Macromolecules 38:10061. doi:10.1021/ma0509311

97. Ver Strate G, Lohse DJ (1994) Structure characterization on the science and technology of elastomers. In: Mark JE, Erman B, Eirich FR (eds) Science and technology of rubber, 2nd edn. Academic, New York

98. Dahlquist CA (1959) An investigation into the nature of tack. Adhesives Age 2:25

99. Mendelson RA, Bowles WA, Finger FL (1970) Effect of molecular structure on polyethylene melt rheology. I. Low-shear behavior. J Polym Sci Part A-2 8:105–126. doi:10.1002/pol.1970.160080109

100. Graessley WW, Roovers J (1979) Melt rheology of four-arm and six-arm star polystyrenes. Macromolecules 12:959–965. doi:10.1021/ma60071a035

101. Roovers J, Graessley WW (1981) Melt rheology of some model comb polystyrenes. Macromolecules 14:766–773. doi:10.1021/ma50004a057

102. van Ruymbeke E, Kapnistos M, Vlassopoulos D, Huang T, Knauss DM (2007) Linear melt rheology of pom-pom polystyrenes with unentangled branches. Macromolecules 40:1713–1719. doi:10.1021/ma062487n

103. Wagner MH, Rolón-Garrido VH, Hyun K, Wilhelm M (2011) Analysis of medium amplitude oscillatory shear data of entangled linear and model comb polymers. J Rheol 55:495–516. doi:10.1122/1.3553031

104. Wagner MH, Rolón-Garrido VH (2008) Verification of branch point withdrawal in elongational flow of pom-pom polystyrene melt. J Rheol 52:1049–1068. doi:10.1122/1.2957699

105. Rochefort WE, Smith GG, Rachapudy H, Raju VR, Graessley WW (1979) Properties of amorphous and crystallizable hydrocarbon polymers. II. Rheology of linear and star-branched polybutadiene. J Polym Sci Phys 17:1197–1210. doi:10.1002/pol.1979.180170705

106. Raju VR, Rachapudy H, Graessley WW (1979) Properties of amorphous and crystallizable hydrocarbon polymers. IV. Melt rheology of linear and star-branched hydrogenated polybutadiene. J Polym Sci Phys 17:1223–1235. doi:10.1002/pol.1979.180170707

107. McLeish TCB, Allgaier J, Bick DK, Bishk G, Biswas P, Blackwell R, Blottière B, Clarke N, Gibbs B, Groves DJ, Hakiki A, Heenan RK, Johnson JM, Kant R, Read DJ, Young RN (1999) Dynamics of entangled H-polymers: theory, rheology, and neutron-scattering. Macromolecules 32:6734–6758. doi:10.1021/ma990323j

108. van Ruymbeke E, Vlassopoulos D, Mierzwa M, Pakula T, Charalabidis D, Pitsikalis M, Hadjichristidis N (2010) Rheology and structure of entangled telechelic linear and star polyisoprene melts. Macromolecules 43:4401–4411. doi:10.1021/ma902769s

109. Watanabe H, Matsumiya Y, van Ruymbeke E, Vlassopoulos D, Hadjichristidis N (2008) Viscoelastic and dielectric relaxation of a Cayley-tree-type polyisoprene: test of molecular picture of dynamic tube dilation. Macromolecules 41:6110–6124. doi:10.1021/ma800503e

110. Qiao X, Sawada T, Matsumiya Y, Watanabe H (2006) Constraint release in moderately entangled monodisperse star polyisoprene systems. Macromolecules 39:7333–7341. doi:10.1021/ma0616155

111. Rahman MS, Aggarwal R, Larson RG, Dealy JM, Mays J (2008) Synthesis and dilute solution properties of well-defined H-shaped polybutadienes. Macromolecules 41:8225–8230. doi:10.1021/ma801646u

112. Fawcett EW, Gibson RO (1934) The influence of pressure on a number of organic reactions in the liquid phase. J Chemical Soc 386–395. doi: 10.1039/JR9340000386

113. Axelson DE, Levy GC, Mandelkern L (1979) A quantitative analysis of low-density (branched) polyethylenes by carbon-13 Fourier transform nuclear magnetic resonance at 67.9 MHz. Macromolecules 12:41–52. doi:10.1021/ma60067a010

114. Usami T, Takayama S (1984) Fine-branching structure in high-pressure, low-density polyethylenes by 50.10-MHz carbon-13 NMR analysis. Macromolecules 17:1756–1761. doi:10.1021/ma00139a022

115. Vega JF, Muñoz-Escalona A, Santamaría A, Muñoz ME, Lafuente P (1996) Comparison of the rheological properties of metallocene-catalyzed and conventional high-density polyethylenes. Macromolecules 29:960–965. doi:10.1021/ma9504633

116. Quan Z, Cotts PM, McCord EF, McLain SJ (1999) Chain walking: a new strategy to control polymer topology. Science 283:2059–2062. doi:10.1126/science.283.5410.2059

117. Cotts PM, Quan Z, McCord EF, McLain SJ (2000) Novel branching topology in polyethylenes as revealed by light scattering and ^{13}C NMR. Macromolecules 33:6945–6952. doi:10.1021/ma000926r

118. Helmstedt M, Stejskal J, Burchard W (2000) Data evaluation in light scattering from solutions of branched polyethylene. Macromol Symp 162:63–80. doi:10.1002/1521-3900(200012)

119. Randall JC (1989) A review of high resolution liquid ^{13}C nuclear magnetic resonance characterizations of ethylene-based polymers. J Macromol Sci Rev 29:201–317. doi:10.1080/07366578908055172

120. Vega JF, Santamaría A, Muñoz-Escalona A, Lafuente P (1998) Small-amplitude oscillatory shear flow measurements as a tool to detect very low amounts of long chain branching in polyethylenes. Macromolecules 31:3639–3647. doi:10.1021/ma9708961

121. Chai CK (2000) The effect of molecular structure on the extensional melt rheology of conventional and metallocene polyethylenes. ANTEC Proc 1096–1107

122. Wood-Adams PM, Dealy JM, deGroot AW, Redwine OD (2000) Effect of molecular structure on the linear viscoelastic behavior of polyethylene. Macromolecules 33:7489–7499. doi:10.1021/ma991533z

123. Krigas TM, Carella JM, Struglinski MJ, Crist B, Graessley WW, Schilling FC (1985) Model copolymers of ethylene with butene-1 made by hydrogenation of polybutadiene: Chemical composition and selected physical properties. J Polym Sci Phys 23:509–520. doi:10.1002/pol.1985.180230308

124. Masuda T, Ohta Y, Onogi S (1971) Rheological properties of anionic polystyrenes. III. Characterization and rheological properties of four-branch polystyrenes. Macromolecules 4:763–768. doi:10.1021/ma60024a020

125. Zelinski RP, Wofford CF (1965) Synthesis of trichain and tetrachain radial polybutadienes. J Polym Sci Chem 3:93–103. doi:10.1002/pol.1965.100030111

126. Pennisi RW, Fetters LJ (1988) Preparation of asymmetric 3-arm polybutadiene and polystyrene stars. Macromolecules 21:1094–1099. doi:10.1021/ma00182a041

127. Iatrou H, Hadjichristidis N (1992) Synthesis of a model 3-miktoarm star terpolymer. Macromolecules 25:4649–4651. doi:10.1021/ma00044a028

128. Gell CB, Graessley WW, Efstratiadis V, Pitsikalis M, Hadjichristidis N (1997) Viscoelasticity and self-diffusion in melts of entangled asymmetric star polymers. J Polym Sci Phys 35:1943–1954. doi:10.1002/(SICI)1099-0488(19970915)

129. Iatrou H, Siakali-Kioulafa E, Hadjichristidis N, Roovers J, Mays J (1995) Hydrodynamic properties of model 3-miktoarm star copolymers. J Polym Sci Phys 33:1925–1932. doi:10.1002/polb.1995.090331308

130. Hadjichristidis N, Xenidou M, Iatrou H, Pitsikalis M, Poulos Y, Avgeropoulos A, Sioula S, Paraskeva S, Velis G, Lohse DJ, Schulz DN, Fetters LJ, Wright PJ, Mendelson RA, García-Franco CA, Sun T, Ruff CJ (2000) Well-defined, model long chain branched polyethylene. 1. Synthesis and characterization. Macromolecules 33:2424–2436. doi:10.1021/ma991670w

131. Roovers J, Toporowski PM (1981) Preparation and characterization of H-shaped polystyrene. Macromolecules 14:1174–1178. doi:10.1021/ma50006a007

132. Iatrou H, Avgeropoulos A, Hadjichristidis N (1994) Synthesis of model super H-shaped block copolymers. Macromolecules 27:6232–6233. doi:10.1021/ma00099a047

133. Iatrou H, Willner L, Hadjichristidis N, Halperin A, Richter D (1996) Aggregation phenomena of model PS/PI super-H-shaped block copolymers. Influence of the architecture. Macromolecules 29:581–591. doi:10.1021/ma9509063

134. Velis G, Hadjichristidis N (1999) Synthesis of model PS(PI)$_5$ and (PI)$_5$PS(PI)$_5$ nonlinear block copolymers of styrene (S) and isoprene (I). Macromolecules 32:534–536. doi:10.1021/ma9814797

135. Xenidou M, Hadjichristidis N (1998) Synthesis of model multigraft copolymers of butadiene with randomly placed single and double polystyrene branches. Macromolecules 31:5690–5694. doi:10.1021/ma980362f

136. Koutalas G, Lohse DJ, Hadjichristidis N (2005) Well-defined comb, star-comb and comb-on-comb polybutadienes by anionic polymerization and the macromonomer strategy. Macromolecules 38:4996–5001. doi:10.1021/ma047333r

137. Koutalas G, Lohse DJ, Hadjichristidis N (2005) Novel block-comb/graft copolymers by using the macromonomer strategy and anionic polymerization. J Polym Sci Chem 43:4040–4049. doi:10.1002/pola.20891

138. Driva P, Iatrou H, Lohse DJ, Hadjichristidis N (2005) Anionic homo- and copolymerization of double-tailed macromonomers. A route to novel macromolecular architectures. J Polym Sci Chem 43:4070–4078. doi:10.1002/pola.20895

139. Nikopoulou A, Iatrou H, Lohse DJ, Hadjichristidis N (2009) Synthesis of exact comb polybutadienes with two and three branches. J Polym Sci Chem 47:2597–2607. doi:10.1002/pola.23345

140. Orfanou K, Iatrou H, Lohse DJ, Hadjichristidis N (2006) Synthesis of well-defined second (G-2) and third (G-3) generation dendritic polybutadienes. Macromolecules 39:4361–4365. doi:10.1021/ma060231b

141. Nikopoulou A, Iatrou H, Lohse DJ, Hadjichristidis N (2009) Anionic homo- and copolymerization of styrenic triple-tailed polybutadiene macromonomers. J Polym Sci Chem 45:3513–3523. doi:10.1002/pola.22098

142. Driva P, Lohse DJ, Hadjichristidis N (2008) Well-defined complex macromolecular architectures by anionic polymerization of styrenic single and double homo/miktoarm star-tailed macromonomers. J Polym Sci Chem 46:1826–1842. doi:10.1002/pola.22527

143. Lohse DJ, García-Franco CA, Hadjichristidis N (2010) Synthesis and use of well-defined, highly-branched saturated hydrocarbon polymers. US Patent 7,687,580

144. Lohse DJ, García-Franco CA, Hadjichristidis N (2012) Synthesis and use of well-defined, highly-branched saturated hydrocarbon polymers. US Patent 8,168,724

145. Sun T, Chance RR, Graessley WW, Lohse DJ (2004) A study of the separation principle in size exclusion chromatography. Macromolecules 37:4304–4312. doi:10.1021/ma030586k

146. García-Franco CA, Lohse DJ, Robertson CG, Georjon O (2008) Relative quantification of long chain branching in essentially linear polyethylenes. Eur Polym J 44:376–391. doi:10.1016/j.eurpolymj.2007.10.030

147. Ramachandran R, Beaucage G, Rai DK, Lohse DJ, Hadjichristidis N, Sun T, Tsou AH (2012) Quantification of branching in model 3-arm star polyethylene. Macromolecules 45:1056–1061. doi:10.1021/ma2021002

148. Lohse DJ, Milner ST, Fetters LJ, Xenidou M, Hadjichristidis N, Mendelson RA, García-Franco CA, Lyon MK (2002) Well-defined, model long chain branched polyethylene: 2: melt rheological behavior. Macromolecules 35:3066–3075. doi:10.1021/ma0117559

149. Kapnistos M, Koutalas G, Hadjichristidis N, Roovers J, Lohse DJ, Vlassopoulos D (2006) Linear rheology of comb polymers with star-like backbones: melts and solutions. Rheologica Acta 46:273–286. doi:10.1007/s00397-006-0106-2

150. van Ruymbeke E, Orfanou K, Kapnistos M, Hadjichristidis N, Lohse DJ, Vlassopoulos D (2007) Entangled dendritic polymers and beyond: linear rheology of symmetric Cayley-tree polymers and macromolecular self-assemblies. Macromolecules 40:5941–5952. doi:10.1021/ma0706024

151. Lee JH, Orfanou K, Driva P, Hadjichristidis N, Wright PJ, Rucker SP, Lohse DJ (2008) Linear and nonlinear rheology of dendritic star polymers: experiment. Macromolecules 41:9165–9178. doi:10.1021/ma801429k

152. Lee JH, Orfanou K, Driva P, Iatrou H, Hadjichristidis N, Lohse DJ (2009) Damping behavior of entangled comb polymers: experiment. Macromolecules 42:1392–1399. doi:10.1021/ma8022662

153. Kessner U, Münstedt H (2010) Thermorheology as a method to analyze long-chain branched polyethylenes. Polymer 51:507–513. doi:10.1016/j.polymer.2009.11.005

154. Zimm BH, Stockmayer WH (1949) The dimensions of chain molecules containing branches and rings. J Chem Phys 17:1301–1314. doi:10.1063/1.1747157

155. Zimm BH, Kilb RW (1959) Dynamics of branched polymer molecules in dilute solution. J Polym Sci 37:19–42. doi:10.1002/pol.1959.1203713102

156. Berry GC, Orofino TA (1964) Branched polymers. III. Dimensions of chains with small excluded volume. J Chem Phys 46:1614–1621. doi:10.1063/1.1725369

157. Drott EE, Mendelson RA (1970) Determination of polymer branching with gel-permeation chromatography. I. Theory. J Polym Sci A-2 8:1361–1371. doi:10.1002/pol.1970.160080808

158. Drott EE, Mendelson RA (1970) Determination of polymer branching with gel-permeation chromatography. II. Experimental results for polyethylene. J Polym Sci A-2 8:1373–1385. doi:10.1002/pol.1970.160080809

159. Graessley WW, Raju VR (1984) Some rheological properties of solutions and blends of hydrogenated polybutadiene. J Polym Sci Symp 71:77–93. doi:10.1002/polc.5070710109

160. Raju VR (1980) Rheological properties of linear and star-branched hydrogenated polybutadiene with narrow molecular weight distribution. Dissertation, Northwestern

161. Raju VR, Menezes EV, Marin G, Graessley WW, Fetters LJ (1981) Concentration and molecular weight dependence of viscoelastic properties in linear and star polymers. Macromolecules 14:1668–1676. doi:10.1021/ma50007a011

162. Grest GS, Fetters LJ, Huang JS, Richter D (1996) Star polymers: experiment, theory, and simulation. Adv Chem Phys 94:67–163. doi:10.1002/9780470141533.ch2

163. Roovers J (1975) Synthesis and solution properties of comb polystyrenes. Polymer 16:827. doi:10.1016/0032-3861(75)90115-9

164. Roovers J (1979) Synthesis and dilute solution characterization of comb polystyrenes. Polymer 20:843. doi:10.1016/0032-3861(79)90121-6

165. Casassa EF (1971) Gel permeation chromatography and thermodynamic equilibrium. Sep Sci Tech 6:305–319. doi:10.1080/00372367108058964

166. Beaucage G (2004) Determination of branch fraction and minimum dimension of mass-fractal aggregates. Phys Rev E 70:031401. doi:10.1103/PhysRevE.70.031401

167. Carella JM, Gotro JT, Graessley WW (1986) Thermorheological effects of long-chain branching in entangled polymer melts. Macromolecules 19:659–667. doi:10.1021/ma00157a031

168. Pearson DS (1987) Recent advances in the molecular aspects of polymer viscoelasticity. Rubber Chem Tech 60:439–496. doi:10.5254/1.3536138

169. Pearson DS, Fetters LJ, Graessley WW, Ver Strate G, von Meerwall E (1994) Viscosity and self-diffusion coefficient of hydrogenated polybutadiene. Macromolecules 27:711–719. doi:10.1021/ma00081a014

170. Levine AJ, Milner ST (1998) Star polymers and the failure of time-temperature superposition. Macromolecules 31:8623–8637. doi:10.1021/ma980347a

171. Shroff RN, Mavridis H (1999) Long-chain-branching index for essentially linear polyethylenes. Macromolecules 32:8454–8464. doi:10.1021/ma9909354

172. Shroff RN, Mavridis H (2001) Assessment of NMR and rheology for the characterization of LCB in essentially linear polyethylenes. Macromolecules 34:7362–7367. doi:10.1021/ma010573b

173. Van Gurp M, Palmen J (1998) Time-temperature superposition for polymer blends. Rheology Bull 67:5–8

174. Trinkle S, Friedrich C (2001) Van Gurp-Palmen-plot: a way to characterize polydispersity of linear polymers. Rheologica Acta 40:322–328. doi:10.1007/s003970000137

175. Robertson CG, García-Franco CA, Srinivas S (2004) Extent of branching from linear viscoelasticity of long-chain-branched polymers. J Polym Sci Phys 42:1671–1684. doi:10.1002/polb.20038

176. McLeish TCB, Larson RG (1998) Molecular constitutive equations for a class of branched polymers: the pom-pom polymer. J Rheol 42:81–110. doi:10.1122/1.550933

177. Tao H, Lodge TP, von Meerwall ED (2000) Diffusivity and viscosity of concentrated hydrogenated polybutadiene solutions. Macromolecules 33:1747–1758. doi:10.1021/ma991983r

178. Hyun K, Wilhelm M, Klein CO, Cho KS, Nam JG, Ahn KH, Lee SJ, Ewoldt RH, McKinley GH (2011) A review of nonlinear oscillatory shear tests: analysis and application of large amplitude oscillatory shear (LAOS). Prog Polym Sci 36:1697–1753. doi:10.1016/j.progpolymsci.2011.02.002

179. Sentmanat ML (2004) Miniature universal testing platform: from extensional melt rheology to solid-state deformation behavior. Rheologica Acta 43:657–669. doi:10.1007/s00397-004-0405-4

180. Flory PJ (1953) Principles of polymer chemistry. Cornell University, Ithaca

181. Ho J, Govaert L, Utz M (2003) Plastic deformation of glassy polymers: correlation between shear activation volume and entanglement density. Macromolecules 36:7398–7404. doi:10.1021/ma025733d

182. Hiss R, Hobeika S, Lynn C, Strobl G (1999) Network stretching, slip processes, and fragmentation of crystallites during uniaxial drawing of polyethylene and related copolymers: a comparative study. Macromolecules 32:4390–4403. doi:10.1021/ma981776b

183. Pattamaprom C, Larson RG (2001) Predicting the linear viscoelastic properties of monodisperse and polydisperse polystyrenes and polyethylenes. Rheologica Acta 40:516–532. doi:10.1007/s003970100196

184. van Meerweld J (2004) A method to extract the monomer friction coefficient from the linear viscoelastic behavior of linear, entangled polymer melts. Rheologica Acta 43:615–623. doi:10.1007/s00397-004-0358-7

Part V
Future Remarks

Future Remarks

Nikos Hadjichristidis and Akira Hirao

We hope this book has shown the reader the many accomplishments of the polymer chemistry community using anionic polymerization. But the potential for further contributions using these techniques is even greater. For example, the contributors to this volume have demonstrated the unique advantages of anionic polymerization in controlling the architecture and microstructure of polydienes. In the near future post-polymerization reactions on these different structures/microstructures will create novel polymeric materials for many industrial applications. This important topic should be further explored in academia and industry.

Another field that should be fully explored is the combination of anionic with other controlled/living polymerizations. Such techniques hold the promise to produce many novel polymeric materials. In another area, anionic polymerization is generally not the first choice of industry for large-scale production due to its sensitivity to impurities. It is used only when no other industrial method is available (as in the synthesis of triblock copolymers of polystyrene and polydienes for use as thermoplastic elastomers). To increase the commercial use of anionic polymerization simpler and faster polymerization processes should be explored.

N. Hadjichristidis (✉)
Division of Physical Sciences and Engineering, KAUST Catalysis Center (KCC), Polymer Synthesis Laboratory, King Abdullah University of Science and Technology (KAUST), Thuwal, Saudi Arabia
e-mail: Nikolaos.Hadjichristidis@kaust.edu.sa

A. Hirao
Polymeric and Organic Materials Department, Graduate School of Science and Engineering, Tokyo Institute of Technology, 2-12-1, Ohokayama, Meguro-ku, Tokyo 152-8552, Japan

Institute of Polymer Science and Engineering, National Taiwan University, No. 1, Sec.4, Roosevelt Road, Taipei 10617, Taiwan

College of Chemistry, Chemical Engineering and Materials Science, Soochow University, 199 Ren Ai Road, Suzhou Industrial Park, Suzhou 215123, China

The chapters in this book show that anionic polymerization has a lot to offer for the research and development of state-of-the-art materials for high tech applications. For example, advances in nanolithography will require much lower pitch size. This will likely be achieved by employing the potential of anionic polymerization to combine different highly immiscible blocks of low molecular weight and different macromolecular architectures.

This simultaneous control of composition, architecture, and homogeneity of polymeric materials to achieve specific physical, chemical, mechanical, and even optical properties can only be provided by anionic polymerization. There will be an increasing need for such well-defined polymers to meet the new and always demanding applications of polymeric materials. Macromolecules synthesized by anionic polymerization will assist engineers and industrialists in achieving these goals for a long time to come.